Radiocarbon

An International Journal of Cosmogenic Isotope Research

VOLUME 46 / NUMBER 2 / 2004

Proceedings of the 18th International Radiocarbon Conference
Wellington, New Zealand
September 1–5, 2003

Part 2 of 2

Conference Editors
NANCY BEAVAN ATHFIELD
RODGER J SPARKS

Department of Geosciences
The University of Arizona
4717 East Fort Lowell Road
Tucson, Arizona 85712-1201 USA

ISSN: 0033-8222

RADIOCARBON
An International Journal of Cosmogenic Isotope Research

Published by
Department of Geosciences
The University of Arizona

Published three times a year at The University of Arizona, Tucson, AZ 85712-1201 USA.

Subscription rate (2004): $200.00 (institutions), $100.00 (individuals). Foreign postage is extra. A complete price list, including proceedings of international conferences, special publications and back issues, appears on the back pages of this issue. *Advertising rates* available upon request, or see www.radiocarbon.org/adrates.html.

Missing issues will be replaced without charge only if claim is made within three months (six months for India, New Zealand, and Australia) after the publication date. Claims for missing issues will not be honored if non-delivery results from failure by the subscriber to notify the Journal of an address change.

Authors: See our "Information for Authors" document at www.radiocarbon.org/Authors/ for guidelines on manuscript submission and format. All correspondence and manuscripts should be addressed to the Managing Editor, *RADIOCARBON*, Department of Geosciences, The University of Arizona, 4717 East Fort Lowell Road, Tucson, AZ 85712-1201 USA. Tel.: +1 520 881-0857; Fax: +1 520 881-0554; Email: editor@radiocarbon.org.

List of laboratories. Our comprehensive list of laboratories is published annually, and is also available at www.radiocarbon.org/Info/lablist.html. We ask all laboratory directors to provide their laboratory code designation, as well as current telephone and fax numbers, and email addresses. Changes in names or addresses, additions or deletions should be reported to the managing editor. Conventional and AMS laboratories are arranged in alphabetical order by country, and we include laboratories listed by code designation.

RADIOCARBON on the World Wide Web: http://www.radiocarbon.org/

RADIOCARBON is indexed and/or abstracted by the following sources: *Anthropological Index; Anthropological Literature; Art and Archaeology Technical Abstracts; Bibliography and Index of Geology* (GeoRef); *British Archaeological Bibliography; Chemical Abstracts; Chemistry Citation Index; Current Advances in Ecological and Environmental Sciences; Current Contents* (ISI); FRANCIS (Institut de l'Information Scientifique et Technique – CNRS); *Geographical Abstracts; Geological Abstracts; Oceanographic Literature Review; Science Citation Index; Social Sciences Citation Index*.

COMPACT CARBON AMS

Accelerator Mass Spectrometry
Tandem and Single Stage

National Electrostatics Corporation offers a wide variety of compact, low voltage AMS systems for carbon radio isotope ratio measurement. All NEC systems provide high precision and low background. They can be equipped with the high throughput, multi-sample ion source or dual ion source injector for added versatility.

FEATURES INCLUDE:

- **Better than 5 per mil precision**
- **Better than 5 x 10^{-15} background**
- **Throughput of 400 samples/day to 2% precision for modern carbon with the 134 sample source**
- **Gas and solid sample source**
- **All metal/ceramic acceleration tubes with no organic material in the vacuum volume**

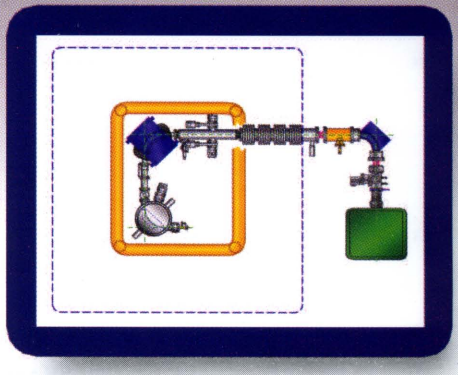

Single Stage AMS

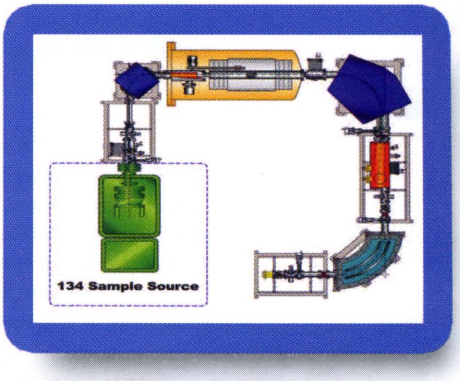

High Through-put Compact Carbon AMS

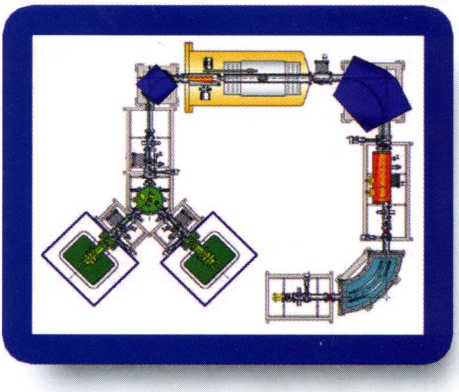

Multi Ion Source Compact Carbon AMS

7540 Graber Road, P.O. Box 620310
Middleton, WI USA, 53562-0310

Phone: 608-831-7600 • Fax: 608-831-9591
nec@pelletron.com • www.pelletron.com

TANDETRON ACCELERATOR MASS SPECTROMETERS

Dedicated and Multi element systems

‘The choice is yours….’

1.0MV, 2.0MV, 3.0MV or 5.0MV

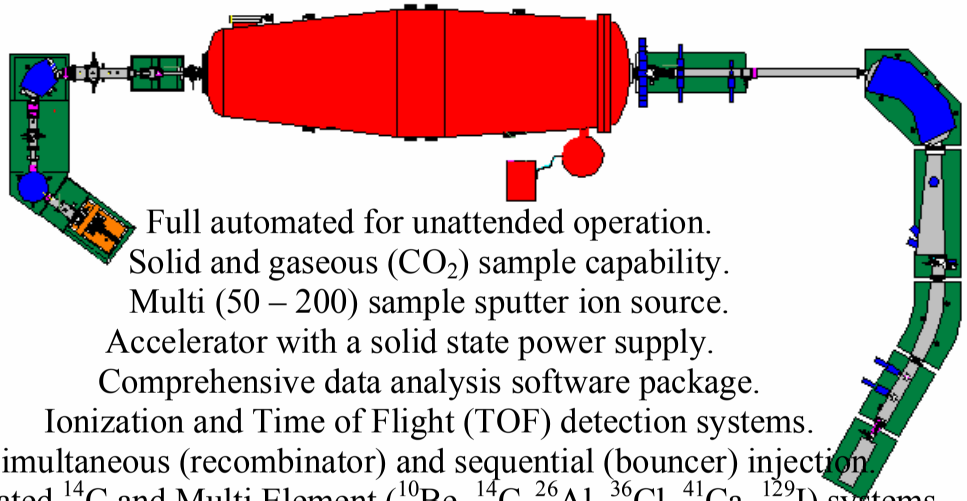

Full automated for unattended operation.
Solid and gaseous (CO_2) sample capability.
Multi (50 – 200) sample sputter ion source.
Accelerator with a solid state power supply.
Comprehensive data analysis software package.
Ionization and Time of Flight (TOF) detection systems.
Simultaneous (recombinator) and sequential (bouncer) injection.
Dedicated ^{14}C and Multi Element (^{10}Be, ^{14}C, ^{26}Al, ^{36}Cl, ^{41}Ca, ^{129}I) systems.

HIGH VOLTAGE ENGINEERING EUROPA B.V.

Amsterdamseweg 63, 3812 RR Amersfoort, P.O. Box 99, 3800 AB Amersfoort, The Netherlands
Phone: +31-33-4619741. Fax +31-33-4615291. Trade register Amersfoort nr. 31014544
E-mail: info@highvolteng.com – Web: www.highvolteng.com

Vol 46, Nr 1–2 **Radiocarbon** 2004

CONTENTS

Sample Processing

Archaeology

Soils

Past Environments

The Modern Environment

RADIOCARBON, Vol 46, Nr 2, 2004, p 497–500

A DIRECT ESTIMATE OF THE INITIAL CONCENTRATION OF ^{14}C IN THE MOUNTAIN AQUIFER OF ISRAEL

Israel Carmi[1,2] • Joel Kronfeld[1] • Yoseph Yechieli[3] • Elisabetta Boaretto[4] • Miryam Bar-Matthews[3] • Avner Ayalon[3]

ABSTRACT. Five radiocarbon analyses were performed on 5 different sources within Soreq Cave, which was used as a model for the Judea Group Aquifer of Israel (pMC_{q0}). The transit time of rainwater through the roof of the cave to sources within it had been determined with tritium. From this information, the year of deposition of rain on the roof of the cave, which later appeared in one of the sources, was estimated and the atmospheric ^{14}C concentration at that time was ascertained (pMC_{a0}). The parameter $Q = pMC_{q0} / pMC_{a0}$ was found to be $Q = 0.60 \pm 0.04$. This makes it possible to calculate the age of water in any well in the Judea Group Aquifer of Israel by measuring its ^{14}C concentration (pMC_{qt}) by use of the decay equation and applying Q.

INTRODUCTION

Water is a scarce commodity in many places in our world. For efficient utilization of this resource, the rate of flow of water in aquifers is of importance and, for this purpose, dating of the groundwater is a useful tool. ^{14}C is a natural candidate for the dating of groundwater and, indeed, the method had been applied routinely to hydrology soon after its introduction by Münnich (1957).

For hydrological dating, the ^{14}C decay equation is

$$A_{qt} = A_{q0} e^{-\lambda t} \quad (1),$$

where q refers to an aquifer, A_{qt} is the ^{14}C concentration at the time of collection of the water sample, A_{qo} was the ^{14}C concentration in the water when the water has just entered the aquifer, λ is the decay constant of ^{14}C, and t is the age of the water.

From the outset, it was realized that the initial level of ^{14}C when the water has just entered the aquifer, A_{q0}, is generally not well known. Its relation to the atmospheric value of $^{14}CO_2$ at the time of deposition of rain on the soil surface, A_{a0}, where a refers to the atmosphere, was defined as

$$Q = A_{q0} / A_{a0} \text{ (Wigley 1975)} \quad (2),$$

where Q is controlled by processes in the unsaturated region which the water traverses on its way to the aquifer.

Many models have been developed to estimate Q and many of them are incorporated into the NETPATH program (Plummer et al. 1991). The program uses the different models and the chemical and isotopic information of the groundwater to calculate its age. Recently, Buckau et al. (2000) applied many of these models to the recharge part of the Gorleben aquifer in Germany and found a conflict between the tritium age of the groundwater, which was <40 yr, and the ^{14}C age of the water, which calculated with these models was 4000 to 8000 yr. Bouhlassa and Aiachi (2002) used a suit of models to estimate A_{q0} for a young aquifer in Morocco (A_{qt} = 76 pMC) and found that the different models yielded very divergent results for A_{q0}, between 22 and 85 pMC.

[1]Department of Geophysics and Planetary Science, Tel Aviv University, Tel Aviv 69978, Israel.
[2]Corresponding author. Email: carmiisr@post.tau.ac.il.
[3]Geological Survey of Israel, 30 Malkei Israel St, Jerusalem 95501, Israel.
[4]Department of Environmental Sciences and Energy Research, Weizmann Institute of Science, Rehovot 76100, Israel.

Proceedings of the 18th International Radiocarbon Conference, edited by N Beavan Athfield and R J Sparks
RADIOCARBON, Vol 46, Nr 2, 2004, p 497–500

We have tried to get a direct estimate of Q for the mountain aquifer of Israel and used dripping water in Soreq Cave as a model for information about the fate of water in the unsaturated zone on its way to the aquifer.

THE MOUNTAIN AQUIFER OF ISRAEL AND SOREQ CAVE

The Judea Group aquifer, several hundreds of meters thick, is of the Upper Cretaceous period. The anticlinal crest of the Judea Mountains dips to the east towards the Rift Valley and to the west towards the Shephela area where Cretaceous rocks are overlain by younger formations.

The karstic Soreq Cave is located within the steep western flank of the Judea Mountains crest, 40 km east of the Mediterranean Sea and 400 m above sea level (Figure 1a). The cave is developed within a 50- to 60-m-thick dolomitic sequence of the Cenomanian Weradim Formation, which is fractured and contains many karstic features. The overlying soil cover is irregular and usually occurs in patches up to 40 cm thick. The thickness of the roof varies between 10 m at the northwestern end to 40–50 m at the southeastern end. The cave ceiling is crossed by 2 main fracture systems in the W-E and NW-SE directions (Figure 1b). The cave is rich with various types of speleothems, straw, conical stalactites, curtains, cave corals, stalagmites, flowstones, etc. The cave is active and drippings of water through the tips of stalactites, through fractures and along the walls, are common and occur throughout the year, but it is more intensive during the winter months. The dripping water accumulates in pools varying in size from several liters to about 500 L.

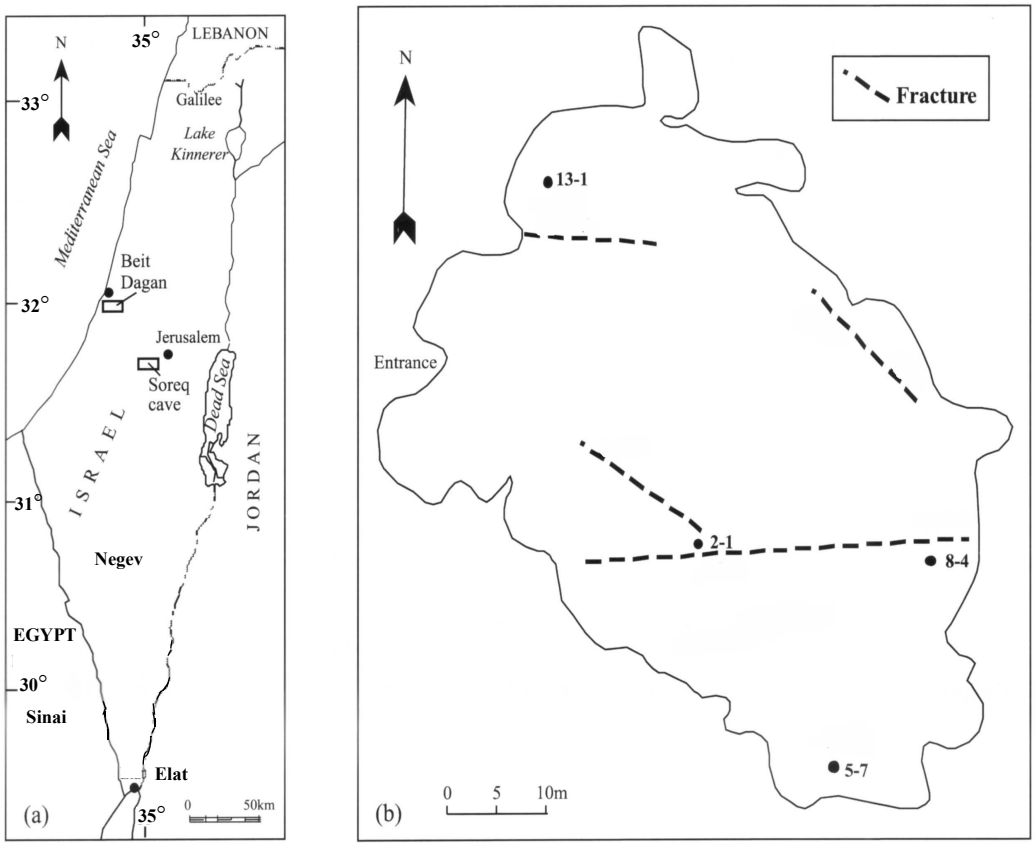

Figure 1 (a) Layout of the Soreq Cave in Israel; (b) sources and fractures in the cave

SAMPLING AND MEASUREMENT

Water drippings from stalactites and from adjoined pools were collected in April 2002 (sampling #59). Extraction of CO_2 from the water and its subsequent graphitization was done in the ^{14}C lab at the Kimmel Center of the Weizmann Institute of Science; AMS measurements were done at the Arizona AMS lab in Tucson; ^{13}C was measured on an aliquot of the extracted CO_2 in the Weizmann Institute of Science. The data of dissolved inorganic carbon (DIC), ^{13}C isotopic composition ($\delta^{13}C$), and the ^{14}C activity in percent modern carbon (PMC), is summarized in Table 1. The sampling sites are shown in Figure 1b. It is assumed that these samples represent A_{q0} for the mountain aquifer of Israel.

Table 1 Water samples collected from Soreq Cave on April 2002, their type (dripping and pool water) and their content of carbon, $\delta^{13}C$ and pMC values.

Source	Type	Lab nr	mg C / l	^{14}C activity (pMC)	$\delta^{13}C$ (‰)
1-8	Drip	4327	52.7	82.6 ± 0.5	–10.4
2-1	Pool	4325	67.3	87.9 ± 0.5	–10.6
5-7	Pool	4321	66.8	108.0 ± 0.6	–13.5
8-4	Pool	4320	40.0	99.9 ± 0.7	–9.5
13-1	Pool	4322	34.4	98.2 ± 0.5	–9.4

CALCULATION OF *Q*

To calculate Q, the parameters A_{a0} and A_{q0} are needed. A_{a0} is the ^{14}C concentration in the atmosphere at the time of deposition of rains on the roof of the cave, which subsequently drips from stalactites. For A_{a0}, we used the atmospheric ^{14}C concentrations measured in Germany (Levin et al. 1985; Levin and Kromer 1997). Their data is adjusted for ^{13}C. We have verified that the international ^{14}C calibration curve is valid for Israel (Carmi, unpublished data) and this justifies the use in Israel of the atmospheric ^{14}C data from Germany.

To derive the value of A_{a0} for water collected from dripping water and pools in the cave, we have calculated the transit times and rates of infiltration of water through the roof of the cave by the use of tritium measurements (Kaufman et al. 2003). In the Kaufman et al. (2003) paper, the tritium data from the cave waters were compared with tritium data in rains from the last 50 yr, which included the thermonuclear era. Tritium measured in drippings and pools in the cave was back-corrected for decay and matched with the rain data until a close fit was found. This defined the year in which the rain fell on the cave. The difference between the year in which the rain fell on the roof of the cave and the year of sampling in the cave gave the transit time of water from the surface to the cave. From this and from the thickness of the roof, the average rate of flow of water through the rock above the cave was calculated. Where temporally-spaced data from the same sources were available, a "wiggle match" on the rain data was done.

To derive the values of A_{a0}, we used the data of the winter and spring months (January to May) because during springtime the most intensive photosynthesis occurs in Israel and the organic matter that is produced is deposited on the ground (Dan Yakir, personal communication).

We neglect the decay of ^{14}C during the movement of rainwater through the unsaturated region and assume that by the time the water reaches the cave, they are saturated with respect to calcium carbonate (Bar-Matthews et al. 1996).

Because the values of A_{a0} that we used are adjusted for ^{13}C, we had to similarly adjust the pMC = A_{q0} of the cave waters from Table 1. The data for the sources that were measured for this study, their ^{14}C concentration adjusted for ^{13}C, the A_{a0} values, and the calculated Q are given in Table 2.

Table 2 Transit time, flow rate of water through the ceiling (inferred for source 1-8), atmospheric (A_{a0}), aquifer ^{14}C concentrations adjusted for ^{13}C (A_{a0}), and calculated Q.

Source	Roof thickness above the cave (m)	Transit (yr)	Deposition (AD)	Flow myr^{-1}	A_{a0}	A_{q0}	Q
1-8	20	~20	1982	~1.0	123.9	80.2 ± 0.5	.65
2-1	30	33	1969	0.9	154.5	85.3 ± 0.5	.55
5-7	40	36	1966	1.1	169.9	105.5 ± 0.6	.62
8-4	40	35	1967	1.1	163.3	96.4 ± 0.7	.59
13-1	20	35	1967	0.6	163.3	95.2 ± 0.5	.58

DISCUSSION

The result of the calculations in Table 2 gives an average value of $Q = 0.60 \pm 0.04$ as a direct estimate for the mountain aquifer of Israel. We compared this result with an estimate based on a mass balance approach with ^{14}C and ^{13}C data from wells in the mountain aquifer of Israel in the Judea Mountains. This study was done by Kroitoru (1987) and the estimate was $Q = 0.62 \pm 0.03$. Thus, the results from the 2 studies, which differ in methods and are from samples that are different both temporally (some 20 yr) and geographically (more than 10 km), are practically identical. Although when water reaches the aquifer further exchange and loss of ^{14}C between it and the matrix of the aquifer may occur, our results suggest that this effect is minimal in this part of the aquifer. The result of our study lends support to the approach that a direct estimate of Q in specific aquifers may help appreciably in dating aquifer groundwater.

ACKNOWLEDGEMENTS

The authors acknowledge the help extended to them in Soreq Cave by the Nature and Parks Authority of Israel. The constructive review of M Stuart is acknowledged with appreciation.

REFERENCES

Bar-Matthews M, Ayalon A, Matthews M, Sass E, Halicz L. 1996. Carbon and oxygen isotope study of the active water-carbonate system in a karstic Mediterranean cave: implications for paleoclimate research in semiarid regions. *Geochimica et Cosmochimica Acta* 60:337–47.

Bouhlassa S, Aiachi A. 2002. Groundwater dating with radiocarbon: application to an aquifer under semi-arid conditions in the south of Morocco (Guelmime). *Applied Radiation and Isotopes* 56:637–47.

Buckau G, Artinger R, Geyer S, Wolf M, Fritz P, Kim JI. 2000. ^{14}C dating of Gorleben groundwater. *Applied Geochemistry* 15:583–97.

Kaufman A, Bar-Mathews M, Ayalon A, Carmi I. 2003. The vadose flow above Soreq Cave, Israel: a tritium study of the cave waters. *Journal of Hydrology* 273: 155–63.

Kroitoru L. 1987. The characterization of flow systems in carbonate rocks defined by the groundwater parameters: Central Israel [PhD dissertation]. Feinberg Graduate School of the Weizmann Institute of Science, Rehovot, Israel.

Levin I, Kromer B, Schoch-Fischer H, Bruns M, Münnich M, Berdau D, Vogel JC, Münnich KO. 1985. 25 years of tropospheric ^{14}C observations in Central Europe. *Radiocarbon* 27(1):1–19.

Levin I, Kromer B 1997. Twenty years of atmospheric $^{14}CO_2$ observations at Schauinsland station, Germany. *Radiocarbon* 39(2):205–18.

Münnich KO. 1957. Messungen des ^{14}C-Gehaltes von hartem Grundwasser. *Naturewissenschaften* 44:32–3.

Plummer LN, Prestemon EC, Parkhurst DL. 1991. NETPATH. *US Geological Survey Water Resources Investigations Report* 91-4078, Reston, Virginia, USA.

Wigley TMI. 1975. ^{14}C dating of groundwater from closed and open systems. *Water Resources Research* 11:324–8.

RADIOCARBON, Vol 46, Nr 2, 2004, p 501–515

TIME-DEPENDENT FACTORS INHERENT IN THE AGE EQUATION FOR DETERMINING RESIDENCE TIMES OF GROUNDWATER USING ^{14}C: A PROCEDURE TO COMPENSATE FOR THE PAST VARIABILITY OF ^{14}C IN ATMOSPHERIC CARBON DIOXIDE, WITH APPLICATION TO THE WAIRAU DEEP AQUIFER, MARLBOROUGH, NEW ZEALAND

Claude B Taylor

28 Wyndrum Avenue, Lower Hutt 6009, New Zealand. Email: sandbagger5@xtra.co.nz.

ABSTRACT. The radiocarbon concentration of dissolved inorganic carbon in groundwater is most logically and completely represented as the product of 5 time-variable factors; these are mutually independent, and all must be considered and evaluated to determine a groundwater residence time. In the case of one factor, the $^{14}C/(^{12}C+^{13}C)$ ratio of atmospheric CO_2, its time variability can be side-stepped by assuming it to be constant at the pre-bomb 1950 value, and assigning an apparent half-life in the radioactive decay term. Apparent half-lives are calculated here for 5 separate periods extending back to 24,000 BP, working from the INTCAL98 atmospheric calibration. This approach can be extended further back in time when the necessary atmospheric calibrations are updated with greater certainty. The procedure is applied to the recently-explored Wairau Deep Aquifer, underlying central areas of the coastal Wairau Plain, Marlborough. The evolution of dissolved inorganic carbon concentration for this river-recharged groundwater is apparent from distinct trends in ^{13}C, and is confirmed by hydrochemical modelling. Extension to the ^{14}C concentrations yields minimum/maximum limits for groundwater residence times to 3 wells. In all 3 cases, the maximum is uncertain due to present uncertainty of the apparent half-life applicable before 24,000 BP. Residence times for the 2 wells closest to the recharge area are at least 17,400 yr, while that for a well further down the aquifer is at least 38,500 yr. Recharge, therefore, occurred during the Otiran glaciation, while the present-day near-surface fluvioglacial deposits of the Wairau Plain were accumulating. Drawdown-recovery records over 3 yr indicate a permeable connection to compensating recharge, enabling limited exploitation for vineyard irrigation.

INTRODUCTION: BASIC EQUATIONS FOR AGE DETERMINATION USING ^{14}C

In applying radiocarbon to determine groundwater residence times, time zero (time of recharge) is assigned when dissolved inorganic carbon (DIC) is no longer exchanging with atmospheric or soil CO_2, i.e. at the open to closed system transition (Taylor 1997). In the strictest sense, groundwater downstream of its recharge area will comprise a spectrum of ages, as a consequence of dispersion and mixing. The concentration of recharged ^{14}C per kg water at a sampling date t_s may be expressed as

$$A(t_s) \times m = \int_{-\infty}^{t_s} F(t)\, dt \qquad (1),$$

where m is the DIC concentration (mmol/kg water), while $A(t_s)$ is the measured isotopic ratio $^{14}C/(^{12}C + ^{13}C) = {}^{14}C/DIC$. $F(t)$ is the residue, after radioactive decay, of the ^{14}C recharged during interval $(t - 0.5dt)$ 6 $(t + 0.5dt)$; it involves 5 time-dependent factors:

$$F(t) = f(t) \times m(t) \times g(t) \times A_a(t) \times exp[-\lambda(t_s - t)] \qquad (2),$$

where $f(t)$ is the weighting function (age spectrum) for water, defined by

$$1 = \int_{-\infty}^{t_s} f(t)\, dt \qquad (3),$$

Proceedings of the 18th International Radiocarbon Conference, edited by N Beavan Athfield and R J Sparks
RADIOCARBON, Vol 46, Nr 2, 2004, p 501–515

depending only on physical factors such as dispersion along the flowpath.[1] *m(t)* was the DIC concentration (mmol.kg^{-1}) of the water fraction *f(t)dt*; $A_a(t)$ was the $^{14}C/(^{12}C+^{13}C)$ ratio of atmospheric CO_2 at time *t*; *g(t)*, called here the transmission factor, is $A(t)/A_a(t)$, where *A(t)* was the $^{14}C/(^{12}C+^{13}C)$ ratio of *m(t)*. Processes determining *g(t)* were outlined in Taylor (1997); the isotopic composition of the groundwater prior to the transition from the open to closed system is the result of a dynamic chemical/isotopic balance between exchange of CO_2 across the atmosphere/water interface and direct addition of CO_2 to the water by plant respiration, decay of organic material, or migration from deeper levels. λ is the radioactive decay constant (half-life is 5730 yr).

Equation 2 is a rigorous expression. If the product $g(t)A_a(t)$ is considered as a single factor, the separate terms on the RHS of Equation 2 are mutually independent. All must be assessed before combining to determine a residence time.

The mean water residence time "(H_2O) is

$$"(H_2O) = \int_{-\infty}^{t_s} t f(t)dt \qquad (4),$$

while the mean residence time "(^{14}C) of recharged ^{14}C is defined by

$$A(t_s) \times m \times "(^{14}C) = \int_{-\infty}^{t_s} t\ F(t)dt \qquad (5).$$

Any calculated residence time is an artifact of the weighting function (Equation 3), the precise form of which is never known or measurable over a timescale of thousands of years. The chosen function must therefore be clearly specified. A frequently-applied simplification assumes that the ^{14}C concentration results from decay of an initial concentration transmitted to the sampling point without dispersion or molecular diffusion (piston flow), and uninfluenced by chemical dilution or retardation mechanisms:

$$A(t_s) = g(t_s–T) \times A_a(t_s–T) \times exp[–\lambda(t_s–T)] \qquad (6),$$

where $A_a(t_s – T)$ applies at the input end, and *T* is the flow (residence) time. Equation 6 is commonly applied to assess the flow time between 2 sample points in a confined aquifer. But there is an inherent danger in this procedure, because it relies on the questionable assumption that the 2 samples had identical ^{14}C concentrations at their times of recharge and reaching the first point.

An exponential age distribution is often applied to cases where aquifer flow lines at different depths converge near points of discharge, causing output tracer concentrations to match those of a well-mixed reservoir receiving steady input (Vogel 1970); the equation for this case is

$$A(t_s) = A(t_s–T)/(1+\lambda T) \qquad (7).$$

As a further complicating factor, addition, removal, or exchange of DIC commonly intervenes during flow under closed conditions. This may occur in several increments m_i, each at time t_i, modifying Equation 1 to

[1] The lower time limit in Equations 1 and 3 is placed at $t = –4$, rather than the time of emplacement of the aquifer matrix, acknowledging the possibility that old water may flow into a younger matrix.

$$(m + \Sigma m_i) \times A_d(t_s) = \int_{-\infty}^{t_s} F(t)\, dt + \Sigma(m_i \times A_i(t_i) \times exp[-\lambda(t_i - t_s)] \quad (8).$$

$A_d(t_s)$ is the measured, dilution-affected $^{14}C/(^{12}C+^{13}C)$ ratio; $A_i(t_i)$ is that of the DIC increment m_i.

The ratio $A_d(t_s)/A(t_s)$ is a chemical dilution factor, usually less than 1, but not necessarily always; it is not easily determined, due to uncertainty about the number, magnitude, timing, and ^{14}C concentrations of the DIC increments. Fortunately, added DIC contributes no ^{14}C in many cases (e.g. carbonate dissolution, addition of magmatic CO_2, CO_2 from microbially-induced decay of very old organic material, or methanogenesis); thus, the second term on the RHS of Equation 8 is often zero. But decay of recent organic material may introduce CO_2 at an early stage, incrementing ^{14}C concentration during closed system flow. In favorable circumstances, dilution factors can be estimated if DIC concentration can be accurately separated into its components m and Σm_i. This can often be achieved by recognizing trends in ^{13}C relative to DIC concentration, or modelling chemical evolution along flow paths (examples in Taylor 1994; Taylor and Fox 1996; Taylor 1997; Taylor and Evans 1999; Taylor et al. 2001). A well-established lack of consistency between earlier approaches/models, when applied to the same set of data, can be ascribed to both misunderstanding of the open system processes (^{14}C concentration at time of recharge) and ineffective identification of the chemical processes after recharge (Taylor 1997).

In summary, the factors to be considered before an estimate of residence time can be undertaken are the following: the likely DIC concentration at time of recharge; chemical processes adding DIC during flow under closed conditions; variations of atmospheric ^{14}C over the period covered by the age spectrum; the $^{14}C/(^{12}C+^{13}C)$ ratio of DIC at time of recharge relative to that of atmospheric CO_2; definition and incorporation of a likely age spectrum.

Modification of Conventional Isotopic Ratios in Groundwater Applications

In accordance with the above considerations, the ratio $^{14}C/(^{12}C+^{13}C) = {}^{14}C/m$, and the equivalent ratio $^{13}C/(^{12}C+^{13}C) = {}^{13}C/m$, should be used routinely in groundwater studies, in preference to the more commonly applied ratios reflecting $^{14}C/^{12}C$ (percent modern carbon = pMC [Stuiver and Polach 1977]) and $^{13}C/^{12}C$ ($\delta^{13}C$ [Coplen 1994]); this allows the trends of both isotopic ratios to be evaluated more precisely in response to changes in m. The modified units ($\delta'^{13}C$ and %MC) are again used here. %MC is a ratio, and it is important to avoid stating or implying that it is a concentration. ^{14}C concentration is proportional to the product %MC.mmol.kg^{-1} and conveniently represented in this format.

ATMOSPHERIC $^{14}CO_2$ CONCENTRATIONS APPLICABLE TO AGE EQUATIONS

Recent and historical records of atmospheric $^{14}CO_2$ underpin interpretations of hydrological data through the product $A_a(t) \times exp[-\lambda(t_s - t)]$ within the function $F(t)$ of Equation 2. Direct measurements of $A_a(t)$ have accumulated since H-bomb testing during the 1950s and early 1960s increased atmospheric concentration levels worldwide; these can be applied when interpreting groundwater recharged since 1950. Here, ^{14}C is an indicator of recent recharge, for which the complementary value of tritium or trace gas measurement should never be ignored. Figure 1 compares records of %MC (corrected from pMC using $\delta^{13}C = -8$) for Europe (Levin et al. 1985; Levin and Kromer 1997) and New Zealand (unpublished measurements); these were constructed from 5-sample averages (incorporating 2 samples to either side of each measurement), in order to smooth out noise due to measurement uncertainties. The European record comprises overlapping periods for the stations

Vermunt (Austria) and Schauinsland (Germany); it begins in 1959, some 4–5 yr after the first H-bomb injections, responds to seasonal injections from the stratosphere in the years following the high-yield Soviet Arctic tests of 1961–62, and subsequently decays exponentially with decay constant 0.0425 ± 0.0005 yr^{-1}. The New Zealand record begins as thermonuclear $^{14}CO_2$ and HTO first reached the Southern Hemisphere via the stratosphere (Taylor 1968). The increase to a peak, due to interhemispheric transfer via both troposphere and stratosphere, is delayed and attenuated relative to the Northern Hemisphere record. The decline is slightly slower, eventually leading to slightly higher ^{14}C concentrations in the Southern Hemisphere, which may reflect greater fossil fuel dilution in the Northern Hemisphere.

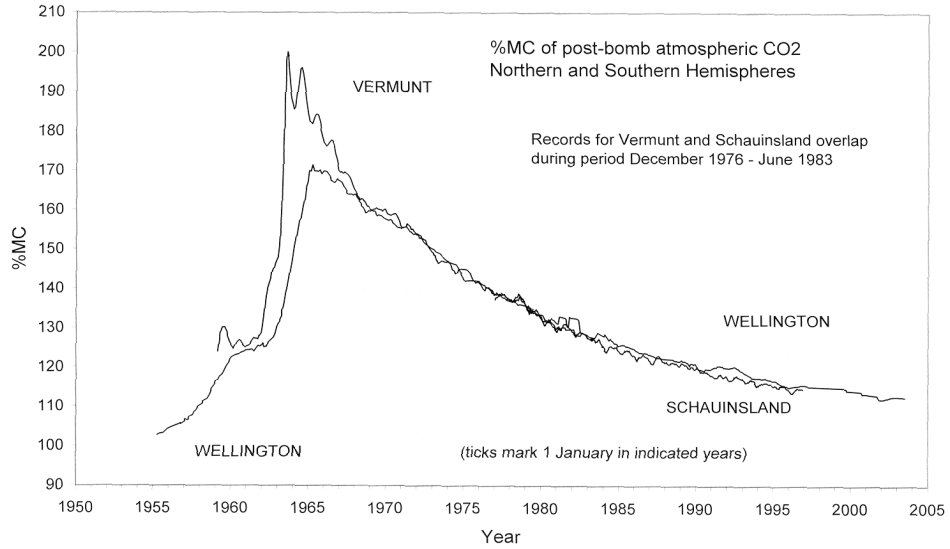

Figure 1 Post-bomb $^{14}C/(^{12}C+^{13}C)$ ratios (as %MC) of atmospheric CO_2 in Europe and New Zealand.

However, most applications of ^{14}C to groundwater dating involve old water recharged long before 1950 (0 BP). Variations of pre-bomb atmospheric $^{14}CO_2$ have been attributed to both geomagnetic effects and significant variation of ocean-atmosphere CO_2 exchange (Björck et al. 1996), and have been established via tree-ring and coral chronology. The irregular curve in Figure 2 shows %MC (modified from pMC, assuming pre-industrial $\delta^{13}C[CO_2] = -7‰$) of atmospheric $^{14}CO_2$ decayed to 1950 [i.e. the term $A_a(t) \times exp\{-\lambda(t_s-1950)\}$ in Equation 2]; this was evaluated from the INTCAL98 ^{14}C age calibration back to 24,000 BP (Stuiver et al. 1998). INTCAL98 was constructed from decadal values of tree rings back to about 11,800 BP, overlap of corals (dated by $^{234}Th/^{230}U$) and marine varves during 11,800–8300 BP, and extension of varve and coral records back to 24,000 BP. The decayed values in Figure 2 are juxtaposed with an exponential curve representing the decayed %MC if $A_a(t)$ had remained constant at the 1950 value throughout the entire period. The true values are less to about 2300 BP, but are significantly greater further back in time.

Due to dispersion, the age spectrum of an old groundwater is unlikely to be narrow. Therefore, the fine details of the INTCAL98 calibration are of little significance. An effective procedure to compensate for the general trends is suggested here: constant $A_a(t) = A_a(1950) \equiv$ %MC = 103.73 is assigned over the entire period (back to 24,000 BP), and coupled with a variable decay constant $\lambda'(t)$, according to the equation

$$A_a(t) \times exp[-\lambda(t_s-t)] = A_a(t=1950) \times exp[-\lambda'(t_s-t)] \quad (9).$$

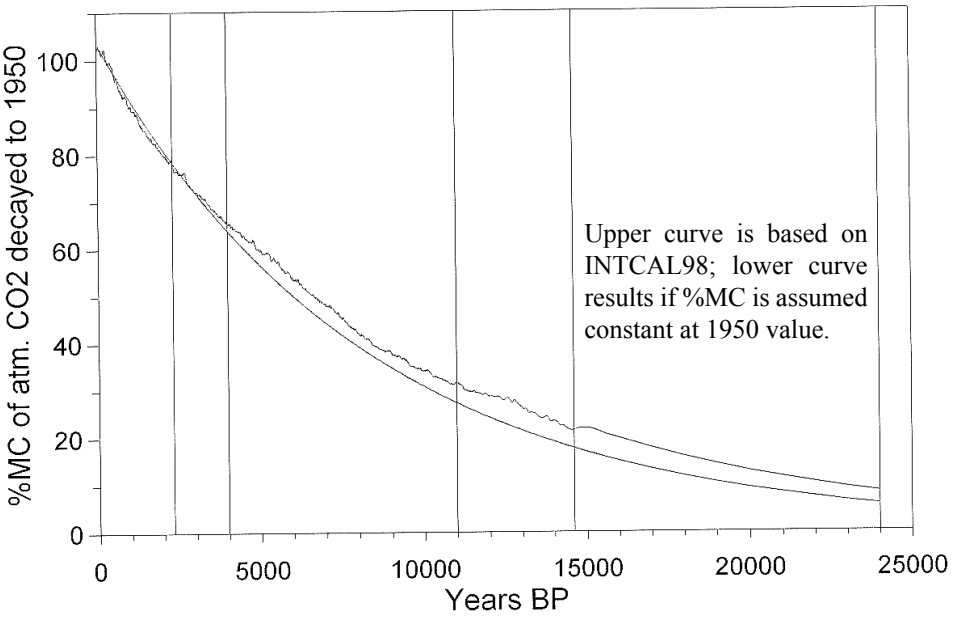

Figure 2 %MC of atmospheric CO_2, decayed to 1950 (calculated from INTCAL98), and compared to values based on unvarying %MC at the 1950 value. The time divisions represent age sections selected for the proposed procedure to adjust for the variations of %MC over the past 24,000 yr.

Figure 2 indicates that an apparent half-life smaller than the true value is required to about 2300 BP, and greater values before then. Various options were tried for $\lambda'(t)$, including continuous linear and exponential functions, but the best result was obtained by assigning discrete values over 5 periods chosen subjectively from the curve $A_a(t) \times exp[-\lambda(t_s-1950)]$, shown in Figure 2. For each period, the apparent half-life was varied until a best least-squares fit was obtained with the decayed curve based on INTCAL98. Figure 3 shows the resulting match and Table 1 the parameters.

Table 1 Apparent ^{14}C half-lives evaluated for indicated age intervals and goodness of fit of modelled distribution to INTCAL98 calibrated values over each interval.

%MC	Age interval BP	Assigned half-life (yr)	Average % difference	Std. dev. %
103.73	0–2300	5385	0.05	0.8
103.73	2300–4000	5905	0.17	0.88
103.73	4000–11,000	6260	–0.10	1.21
103.73	11,000–14,600	6505	–0.02	2.08
103.73	14,600–24,000	6660	–0.09	1.8

The procedure can be revised and extended back in time, after INTCAL98 is updated. Annually-laminated sediments of Lake Suigetsu (Kitigawa and van der Plicht 1998) and a stalagmite in the Bahamas (Beck et al. 2001) provide new information about atmospheric ^{14}C concentrations near the far range of the method (i.e. towards 50,000 BP). Both these studies compared and incorporated less detailed results for marine and terrestrial carbonates, corals, geomagnetic records, ice cores, and other cosmogenic and terrestrial isotopes; the trend of increasing $A_a(t)$ suggested by INTCAL98 back to 24,000 BP appears to continue back in time, but with indications of quite large fluctuations. For groundwater applications, it appears prudent at this time to suggest that the apparent half-life

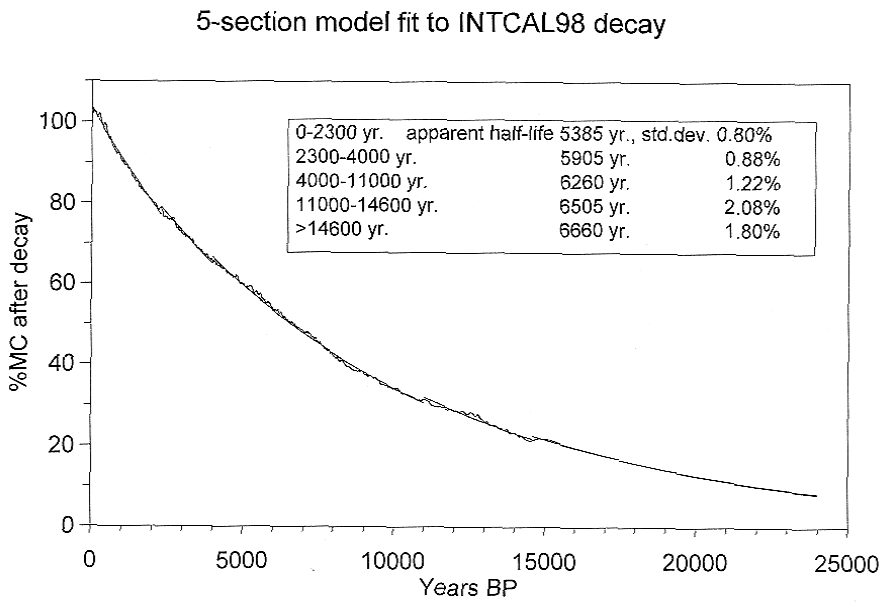

Figure 3 Overlay of the modelled %MC of atmospheric CO_2 decayed to 1950 (based on 1950 value throughout and assigned set of apparent half-life values in Table 1) on the INTCAL98-derived curve of Figure 2, showing also the applied time divisions.

assigned for the age range beyond 24,000 BP should be >6660 yr, thereby yielding minimum residence time estimates.

The procedure provides a practical way to translate measured %MC values to age estimates which are better than those which ignore the temporal variations of $A_a(t)$. Nevertheless, the corrections for the transmission factor and chemical dilution must also be determined; approaches to these aspects were demonstrated in the earlier papers (Taylor 1994; Taylor and Fox 1996; Taylor 1997; Taylor and Evans 1999; Taylor et al. 2001). While measurements in recharge areas may lead to assessment of present-day transmission factors $g(t)$, it must always be recognized that they may have differed at the times of recharge of older samples.

APPLICATION TO THE WAIRAU DEEP AQUIFER

Aquifer Description

The Quaternary alluvial materials (gravel, sand, silt, clay) underlying the coastal Wairau Plain (Figure 4) originate from hill and mountain catchments to the north, south, and west; these are interspersed near the coast with marine deposits (sand, silt, and clay), which accumulated during postglacial marine transgressions (Brown 1981a). The groundwater hydrology to depths no greater than 100 m was reported by Brown (1981b), Rae (1987), Cunliffe (1988), and Taylor et al. (1992). Most groundwater in central areas is recharged by infiltration from the Wairau River, from whose outwash the aquifer gravels derive; the recharge stretch is at the left end of Figure 4. Fan deposits from southern tributary valleys channel some water from the southern hills into gravels underlying southern areas of the Plain. The gravels, weathered to variable degree, are dominantly of greywacke/argillite (from catchments south of the Wairau River) and schist (catchments to the north). Potential sources of DIC after recharge are oxidation of dissolved organic carbon, decay of plant material, carbonate

dissolution (shells) in the marine layers, and methanogenesis; the first 3 of these processes were identified.

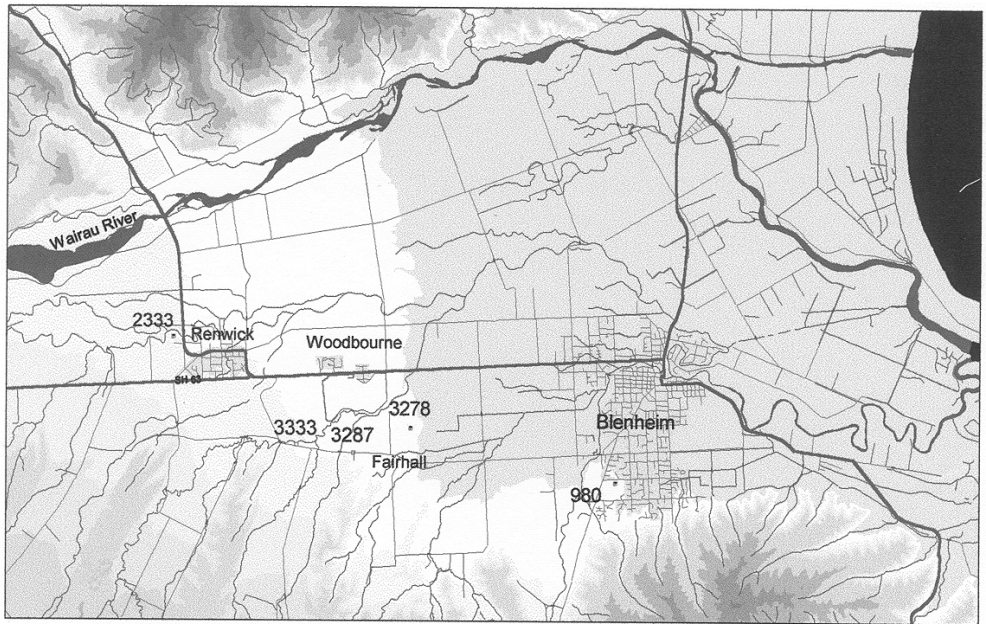

Figure 4 Map of the coastal Wairau Plain showing locations of sampled bores. The area represented is 15.0 × 23.1 km^2.

The Plain and the hills to the south are drought-prone. At Blenheim (the main population center), 92% of years have 100 or more days of moisture deficit. Surfaces between Blenheim and the coast comprise a mix of swamp, beach, and lagoon deposits. Appreciable influence of directly-infiltrated rain was detectable (using ^{18}O) only for shallow groundwater in these deposits in the north of the coastal area (Taylor et al. 1992). Good yields from river-recharged groundwater are the main concern of rural and community users in the central areas. Yields are variable in the southern areas, but generally low. The accelerated development to dominant viticulture over the past 2 decades has led to greatly increased demand for irrigation supply, stimulating exploration to greater depths.

Table 2 summarizes the Quaternary stratigraphic sequence of the area inland of Blenheim. Drilling into the deeper Wairau Gravels in the central area between Renwick and Blenheim commenced during 1997. Bores P28/3293 (at Renwick) and P28/3333 revealed the successive gravel/sand/silt sequences of Table 2, with no intervening marine/estuarine layers. Good water yields were obtained from bore 3333. Proceeding eastwards, bores P28/3287, /3278, and /3291 traverse the full sequence of marine/estuarine layers, encountering artesian pressure with satisfactory water yields from several narrow depth intervals within the Wairau Gravels. While screens were generally placed over quite wide depth intervals, downhole measurements during June 1999 (Waimea Drilling Co.) revealed that most of the water drawn from bores 3333, 3287, and 3278 comes from near-bottom depths (bore details in Table 3).

The nature and timescale of sediment accumulation indicates that the primary source of recharge in the central area of the Plains throughout the timescale of ^{14}C has been the Wairau River. This is confirmed by the ^{13}C patterns and hydrochemistry.

Table 2 Stratigraphic sequence of the Wairau Plains; formations marked with + are found at the surface, those with # are entirely subsurface, while those with * outcrop as remnants on the Plains' southern margins (Brown 1981a; Suggate 1965, 1985).

Formation	Type	Stage/Climate	Age (kyr BP)
Dillons Point + (coastal area)	marine, estuarine, lagoonal and eolian silt; sand; gravel	Aranuian (postglacial)	0–7.5
Rapaura +	fluvial gravels, sand, silt	Aranuian (postglacial)	0–14
Speargrass +	fluvial gravels, sand, silt	Otiran (last) glaciation	14–70
undefined #	marine/estuarine	Kaihinuan glacial retreat	70–120
Tophouse *	glacial outwash, gravel, sand, silt	Waimean glaciation (penultimate)	120–200
undefined #	marine/estuarine	Karoroan glacial retreat	200–250
Manuka*	glacial outwash, gravel, sand, silt	Waimungan glaciation (ante-penultimate)	250–310
undefined # unconformity	marine/estuarine	Scandinavian glacial retreat	310 –350
Wairau Gravels*	undifferentiated gravel, sand, silt, clay	Okehuan to Marahauan	?800–1800

Table 3 Details of sampled bores tapping the Wairau Deep Aquifer.

Bore nr	3333	3287	3278	980
Grid Ref. (NZMS260:P28)	811640	825638	839644	889631
Altitude (m asl)	40	35.6	22.5	10
Total depth (m)	320	255	192	87
Depth to Wairau Gravels (m)	~150	~142	~152	~76
Screen interval (m)	201–318	43–250	100–189	in W. Gravels
Artesian condition	non-flow	flow	flow	flow
Yield on test	50%	95%	almost 100%	not tested
Above yield below depth (m)	260	220	160	
Additional yield information	~20%			
Above yield below depth (m)	295			

Isotopic Data

Measurements (data in Table 4) were performed at the Lower Hutt laboratories of the Institute of Geological and Nuclear Sciences Ltd. Oxygen-18 is reported as $\delta^{18}O$, representing the difference in parts per thousand (‰) between the ratio $^{18}O/^{16}O$ in the water sample (i.e. $H_2{}^{18}O/H_2{}^{16}O$) and that ratio in Vienna Standard Mean Ocean Water (V-SMOW). Precision of the values was reported to be about 0.10. Tritium concentrations are reported as tritium ratios (TR), where TR = 1 corresponds to $^3H/^1H = 10^{-18}$ (Taylor and Roether 1982); quoted measurement errors are 1 standard uncertainty. The carbon measurements were performed on DIC of the groundwater, sampled and measured as described in Taylor and Fox (1996).

Table 4 Isotopic data.

Bore	Date	$\delta^{18}O$	TR(σ)	Date	DIC[a] (mmol/kg)	$\delta'^{13}C$	%MC(σ)
2333				02.06.99	0.875	–16.9	112.3(0.9)
3333	20.08.98	–8.6	0.021(0.015)	02.06.99	2.088	–21.5	6.10(0.16)
3287	21.06.98	–8.8	0.037(0.016)				
3278	13.05.98	–8.8	0.028(0.018)	02.06.99	1.844	–19.6	8.05(0.14)
3278				03.07.01	1.96	–18.8	7.13(0.10)
980	02.06.99	–8.9		03.07.01	2.36	–9.19	0.70(0.06)

[a]Standard measurement uncertainty of DIC concentration is 0.013 mmol/kg.

Preliminary ^{18}O and ^{3}H measurements were made in 1998, for comparison with earlier data for the shallower aquifers (Taylor et al. 1992). While the uniform $\delta^{18}O$ values precisely matched the present-day average of the Wairau River, their significance must be examined after first determining the age of the groundwater. Absence of detectable tritium indicated that groundwater in the deep aquifer had age beyond the detection limit (about 70 yr). A mini-study using carbon isotopes was accordingly conducted, with the expectation that evolution of DIC and its isotopic concentrations would match the patterns found previously in the North Canterbury confined deep aquifers (Taylor and Fox 1996), i.e. a river in equilibrium with the atmosphere at the time of recharge (Taylor 1997), followed by addition of DIC due to decay of organic carbon. The only difference contemplated was the possible influence of marine carbonate beyond the point where confinement by marine layers occurs. Shallow bore 2333 (Grid Ref. NZMS260 P28:781666, screen 14–18 m), situated between the deep aquifer bores and the Wairau River, was chosen as a likely chemical/isotopic match for shallow precursors of the deep groundwater, i.e. a very young, river-recharged groundwater already augmented by DIC from decay of recent organic material. This bore, together with deep bores 3333 and 3278, was sampled in June 1999. Bore 980 (Blenheim Hospital) was sampled in July 2001, after realizing that this very old bore (drilled in 1918) was probably drawing from the deep aquifer, and bore 3278 was re-sampled to check whether any change had occurred as the result of test extraction for irrigation during the intervening period. Bore 3287, although in the area of interest, was not considered for carbon isotopes because of its very long screen length (drawing also from shallower depths, with indication of detectable tritium concentration in 1998). Figure 5 compares relevant bore details (altitude, depth, screen range, extent of Wairau Gravels to the bottom, depths of confining layers).

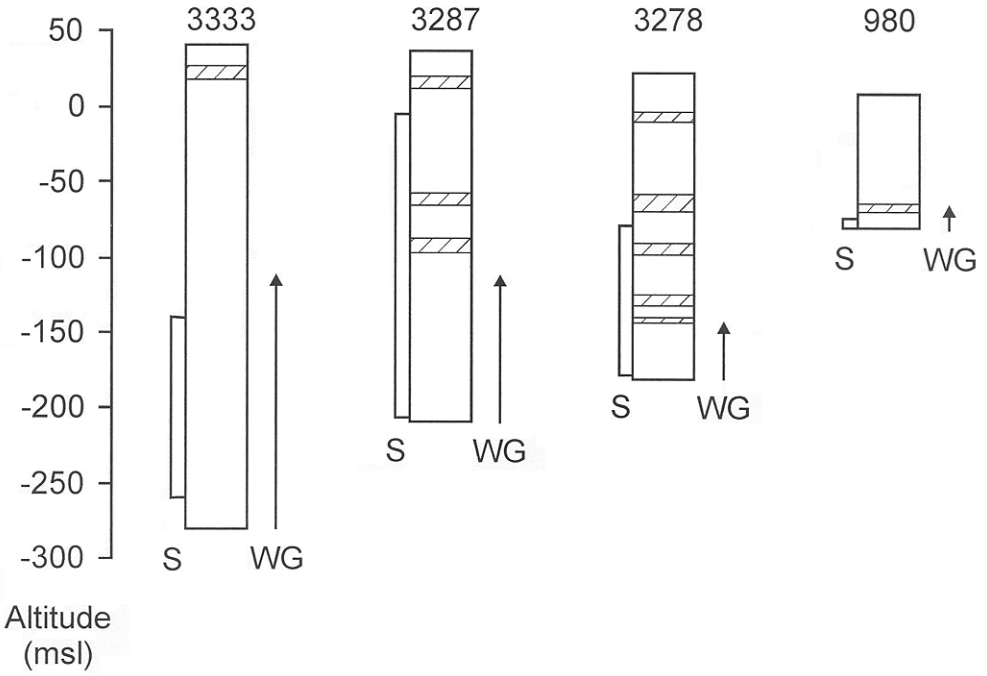

Figure 5 Details of sampled Wairau Deep Aquifer wells (altitude in msl, s = screen interval, WG = Wairau Gravels, shaded bars are marine layers).

Isotopic Evidence of Chemical Evolution of DIC from River to Deep Aquifer

The ^{13}C patterns are consistent with river recharge. Figure 6 ($\delta'^{13}C$ versus 1/DIC) illustrates the evolution of DIC concentration from river to deep old groundwater, via shallow groundwater, represented by bore 2333. Water leaves the river with DIC concentration within the indicated range of variability (based on results for other New Zealand rivers). More DIC is acquired by organic material decay ($\delta'^{13}C$. –24.7), with the trend to the point shown for bore 2333 deriving from an average river composition. Bore 3333 reveals continuation of this process. The 2 points for bore 3278, situated just within the inland extension of a confining marine layer, suggest a minor contribution due to calcite dissolution (^{14}C-free shell material); these points overlap closely, indicating that no significant change occurred following abstraction during the intervening period. The point for bore 980 shows much greater DIC increase due to calcite dissolution.

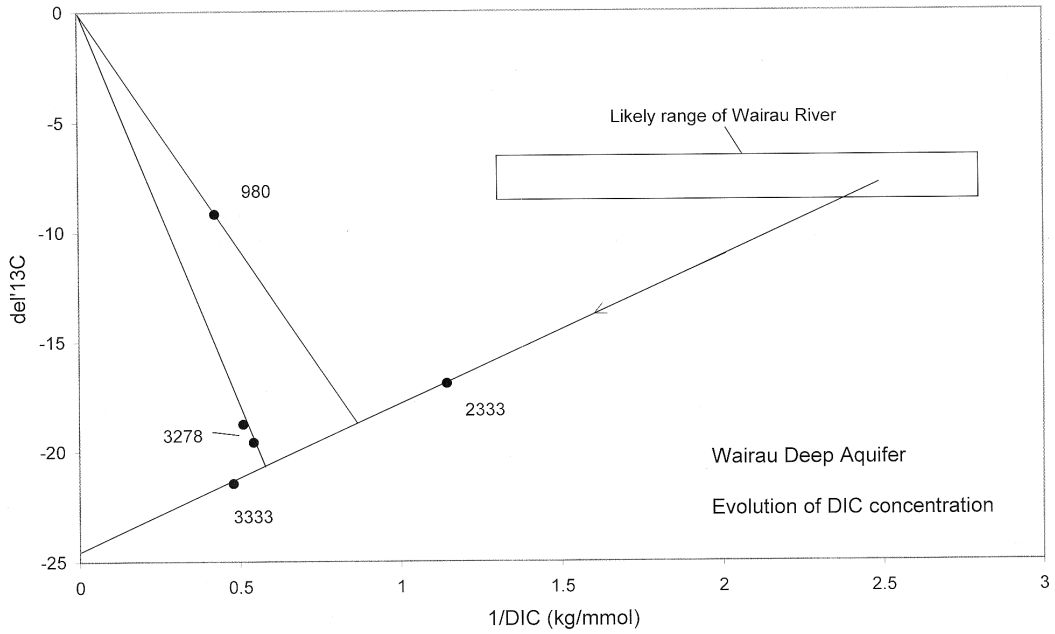

Figure 6 $\delta'^{13}C$ versus 1/DIC diagram reveals the evolution of DIC concentration from river to deep wells.

Consistency between Isotopic Interpretation of Chemical Evolution and Chemical Modelling

To check consistency with the chemical evolution deduced from ^{13}C (Figure 6), chemical data for Wairau River and the bores were modelled using NETPATH (version 2.13; Plummer et al. 1994). Two data sets for major chemical elements at bore 980 yielded slightly higher values of DIC concentration than the isotope sample. Such inconsistency is not unusual; for reliable process identification using the isotope diagrams, the accurately measured DIC concentrations of the isotope samples have proved much superior to less precise chemical values. But the chemical DIC values were nevertheless applied in this modelling. Table 5 lists the chemical data, including repeat analyses of bores 3278 and 980 (samples collected on the carbon isotope 2001 dates). The small sulphate and iron concentrations were ignored, leaving 6 model constraints from the list in Table 5. The phases applied were the following: exchange (sodium replacing calcium, often important during long residence times); albite dissolution (sodium source); anorthite dissolution (alternative calcium source);

CH_2O (source of DIC due to decay of organic material); NaCl (marine); potassium source; magnesium source; calcite dissolution.

Table 5 Chemical concentrations (mmol.l^{-1}) applied for modelling by NETPATH 2.13.

Bore→	River	2333	3333	3278(99)	3278(01)	3287	980(99)	980(01)
C	0.481	0.836	2.649	1.966	2.295	1.967	2.999	2.951
S	0.01	0.044	0.05	0.019	0.018	0.04	0	0
Ca	0.152	0.152	0.349	0.424	0.449	0.21	0.399	0.449
Mg	0.06	0.07	0.202	0.029	0.019	0.107	0.276	0.273
Na	0.157	0.209	2.959	4.351	3.871	3.046	4.787	4.785
K	0.01	0.022	0.02	0.018	0.013	0.01	0.025	0.025
Cl	0.1	0.037	1.58	3.104	2.821	0.988	3.669	3.949
Fe	0	0.052	0.01	0.001	0	0	0.01	0.013

The following transitions were assessed: mean Wairau River → shallow bore 2333; bore 2333 → deep aquifer bore 3333; bore 2333 → deep aquifer bore 3278 (1999); bore 2333 → deep aquifer bore 3287; bore 2333 → deep aquifer bore 980. The 2001 chemical sets for bores 3278 and 980 were not modelled because they had not changed much relative to the 1999 values. Chemical speciation revealed that bores 3278 and 980 were both calcite-saturated. But bore 3333 is undersaturated, consistent with the well logs and indications of the ^{13}C diagram (Figure 6) that this groundwater has not encountered calcite.

Reasonable outcomes are listed in Table 6; other outcomes were rejected, being unrealistic for reasons other than inconsistency with the isotope findings. The only significant change between average river and shallow bore 2333 is (as expected for the very short residence time) DIC increase due to decay of organic material. The outcome of small dissolution of albite is not significant because the mean river concentrations in Table 5 may not be very accurate representative values. Gains of NaCl are obviously related to the presence of marine/estuarine sediments. The outcomes for deep bores 3333 and 3278 are entirely consistent with the isotopic evidence (Figure 6). However, neither of 2 listed outcomes for bore 980 appears satisfactory at first sight. The first delivers a contribution from calcite dissolution more consistent with the ^{13}C evidence, but the absence of weathered sodium makes this outcome unrealistic. The second outcome restores that sodium, but the added calcite component then becomes quite small; the reason might be sought in the apparent large increase from CH_2O. NETPATH cannot distinguish here between this organic source and DIC gained as CO_2 from other processes. Figure 6 shows that calcite dissolution is the main contributor to the higher DIC concentration in the groundwater. The absence of an equivalent gain of Ca in the groundwater may indicate that it is not easily released from the marine layers; the DIC increase in the groundwater may result from gas migration in the form of CO_2 (dissolved), which is likely to be of higher concentration in the acidic environment of the marine layers.

Determination of Residence Times from ^{14}C Concentrations

For interpretation of ^{14}C, applying Equations 6 (piston flow assumption, $g = 1$ for river recharge) and 8 (split of DIC into value at recharge + added amounts during closed system flow), DIC concentration is divided into 3 components: (a) that of the river water plus DIC from decay of recent organic material; (b) further DIC derived from organic material decay, but with unknown %MC; (c) DIC derived from calcite dissolution with %MC = 0. The DIC concentration of component (a) is taken as that measured for bore 2333, which determines the DIC contribution of component (b).

Table 6 Model outcomes (as added components in mmol.l^{-1}) of chemical evolution (X indicates a phase excluded from model to gain this outcome).

\ Phase	Riv.-2333	2333–3333	2333–3278	2333–3287	2333–980	2333–980
CH_2O	0.356	1.813	1.213	1.409	1.443	1.916
NaCl	0	1.543	3.008	0.892	3.632	3.632
Exchange	0	X	X	X	0.473	X
Albite	0.111	1.207	1.186	1.997	X	0.946
Anorthite	X	0.197	X	X	X	X
K-source	0.01	0	0	0.001	0.003	0.003
Mg-source	0.012	0.132	c. 0	c. 0	0.206	0.206
Calcite	0	X	0.272	0.057	0.72	0.247

Component (c) is judged from the ^{13}C diagram (Figure 6). The uncertainty associated with %MC of component (b) is unavoidable, producing a range of possible values for the estimated residence times.

Figure 7 shows ^{14}C concentrations (%MC.mmol/kg) as a function of DIC concentration, and illustrates the interpretation for bore 980. Recharge from the river bears DIC in equilibrium with atmospheric CO_2, i.e. with %MC differing only by parts per thousand (within measurement uncertainty); therefore, $g(t) \approx 1$. Bore 2333 connects towards the origin via a line of gradient not detectably different from that of very recent atmospheric $^{14}CO_2$. The added DIC between river and this shallow bore is, thus, entirely of recent organic origin, matching the finding in a similar situation in North Canterbury (Taylor and Fox 1996). Applying the procedure proposed in Equation 8 (constant %MC of atmospheric CO_2 equivalent to 1950 at all times), a shallow precursor of the 3 deep groundwaters with DIC concentration equal to that at bore 2333 would lie at point C′ on a line AB whose gradient is %MC of 1950.

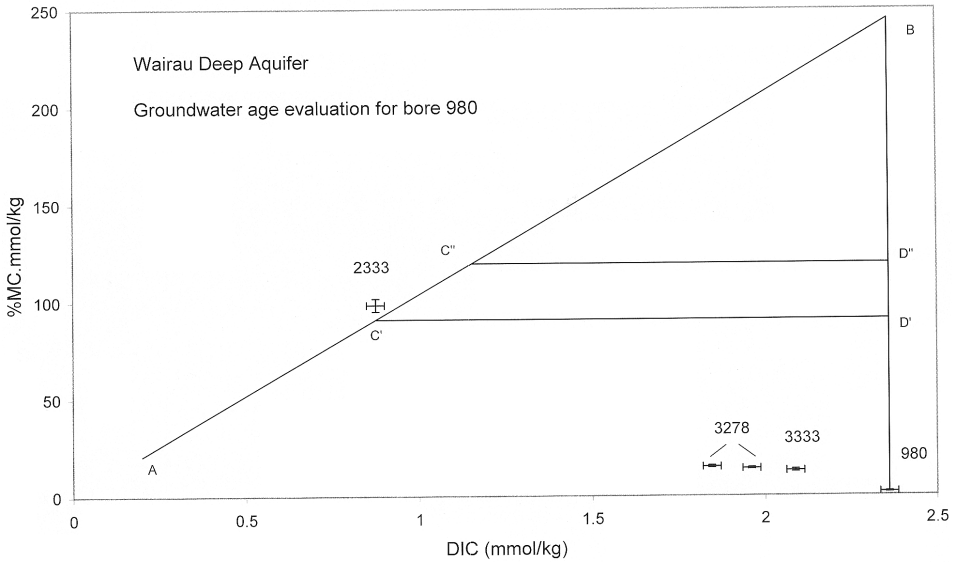

Figure 7 ^{14}C concentrations (%MC.mmol.kg^{-1}) of sampled wells as a function of DIC concentration, illustrating the procedure to deduce residence time for bore 980.

The ^{14}C concentration associated with component (c) is always zero; for bore 980, the DIC concentration added by calcite dissolution is equivalent to the line C′′D′′. The added ^{14}C concentration associated with component (b) is uncertain; it could be any part of the distance D′D′′, which determines the uncertainty in the calculated residence time. Similar scenarios were constructed for bores 3333 (no calcite dissolution) and 3278 (small calcite dissolution). Residence time estimates (rounded to 10 yr) and applied apparent half-lives are in Table 7. The maxima are "greater than" values, resulting from the presently uncertain apparent half-life greater than 6660 yr.

Table 7 Residence time estimates for 3 Wairau Deep Aquifer bores.

Bore	3333	3278(1999)	3278(2001)	980
^{14}C concentration (%MC.mmol.kg^{-1})	12.74	14.84	13.97	1.65
Evolution pattern (Organic, Calcite)	O	O + C (small)	O + C (small)	O + C
Applied half-life (yr)	6660	6660	6660	>6660
Minimum residence time (yr)	18,870	17,390	17,980	>38,470
Applied half-life (yr)	>6660	>6660	>6660	>6660
Maximum residence time (yr)	>27,230	>24,560	>25,730	>48,000

The results are consistent with locations and depths of the bores. Although bore 3333 is closer to the recharge area than bore 3278, it draws from greater depth; the slightly longer residence time is therefore not unreasonable. The calculation has assumed that the first (dispersed or mixed age spectrum) and fifth (exponential decay) factors on the RHS of Equation 2 combine and integrate to match an undispersed flow with the evaluated residence time. No reliable assumption of age spectrum breadth can be made here, but the presence of substantially younger water is very unlikely.

SIGNIFICANCE OF RESULTS FOR AQUIFER MANAGEMENT

The modelled residence times indicate that natural discharge from the Wairau Deep Aquifer is very slow. The likely mechanism is that suggested by multi-disciplinary evidence for shallower confined aquifers closer to the coast, i.e., slow discharge upwards through confining layers (Taylor et al. 1992). These long residence times under natural flow demonstrate that the feasibility of long-term abstraction for irrigation in the Fairhall area depends on the existence of an adequately-permeable connection to the present-day river. This can be assessed from drawdown-recovery records maintained since 1998. The record for bore 3333 (Figure 8) reveals recovery in the winter seasons, although it is incomplete after stronger withdrawal in summer 1999–2000. A permeable connection to a recharge source is indicated, but with obvious limitation on the allowable extent of withdrawal.

SIGNIFICANCE OF $\delta^{18}O$ VALUES IN THE DEEP AQUIFER

The deduced residence times indicate recharge during the Otiran glaciation (about 14,000–70,000 BP), when the highest areas of the Wairau River's mountain catchments were glaciated (Suggate 1965, 1985). During this period, average $\delta^{18}O$ in the catchment's precipitation might have been significantly more negative than today. Statistical analyses of stable isotope concentrations of New Zealand precipitation (Taylor 1990) revealed that the gradient $\delta^{18}O$/temperature in central and southern New Zealand is close to –0.20/EC. According to the estimates of Salinger (1988), New Zealand's average temperature at about 20,000 BP was about 3 °C cooler than today. $\delta^{18}O$ of the groundwater now tapped at wells 3333 and 3278 might therefore have been about –0.6, relative to recent river-recharged groundwater in the shallower aquifers. But no detectable difference is apparent. A likely reason for this would be the enrichment of ocean water by an equivalent amount during

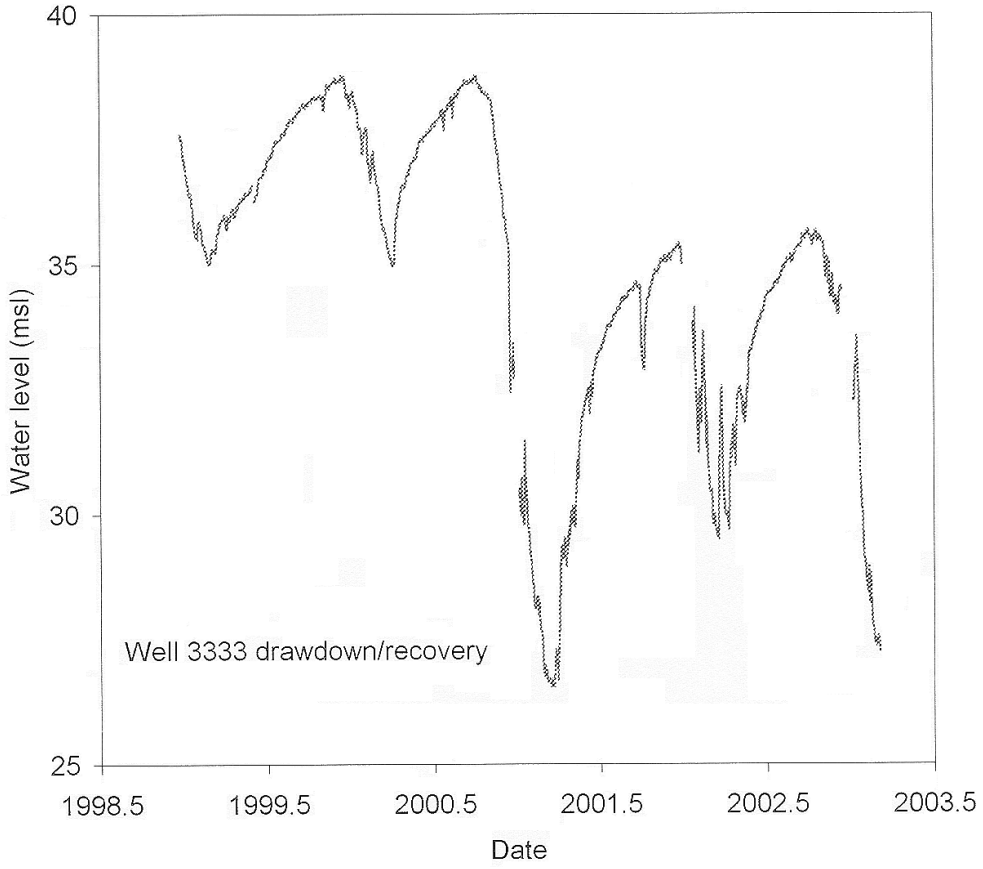

Figure 8 Drawdown/recovery record for bore 3333 shows that recovery occurs over winter following summer irrigation seasons, suggesting permeable connection to river-recharge, but only partial recovery if withdrawal is too great.

glaciation (Craig 1965). Interception of precipitation with the most negative $\delta^{18}O$ by glaciers in the highest catchment areas might also have caused catchment drainage to derive mainly from lower altitudes.

ACKNOWLEDGEMENTS

I gratefully acknowledge the close collaboration of Peter Davidson (Marlborough District Council) in the Wairau Deep Aquifer study and the agreement of the Council to use the data in support of the interpretation procedures proposed in this paper. Overall understanding of the area's hydrogeology owes much to the work of my valued colleague L J Brown.

REFERENCES

Beck JW, Richards DA, Edwards RL, Silverman BW, Smart PA, Donahue DJ, Herrara-Osterheld S, Burr GS, Calsoyas L, Jull AJT, Biddulph D. 2001. Extremely large variations of atmospheric ^{14}C concentration during the last glacial period. *Science* 292:2453–8.

Brown LJ. 1981a. Late Quaternary geology of the Wairau Plain, Marlborough, New Zealand. *New Zealand Journal of Geology and Geophysics* 24:477–90.

Brown LJ. 1981b. Water well data, Northern Marlborough. *New Zealand Geological Survey Report* NZGS93. 126 p.

Coplen TB. 1994. Reporting of stable hydrogen, carbon and oxygen abundances. *Pure and Applied Chemistry* 66:2423–44.

Craig H. 1965. The measurement of oxygen isotope paleotemperatures. In: Tongiorgi E, editor. *Stable Isotopes in Oceanographic Studies and Paleotemperatures*. Pisa: Consiglio Nazionale delle Recherche, Laboratorio di Geologia Nucleare, Pisa. p 161–82.

Cunliffe JJ. 1988. *Water and Soil Resources of the Wairau*. Water Resources Vol. 2. Blenheim: Marlborough Catchment Board and Regional Water Board. 107 p.

Kitigawa H, van der Plicht J. 1998. Atmospheric radiocarbon calibration to 45,000 yr BP: late glacial fluctuations and cosmogenic isotope production. *Science* 279:1187–90.

Rae SN, editor. 1987. *Water and Soil Resources of the Wairau*. Water Resources Vol. 1. Blenheim: Marlborough Catchment Board and Regional Water Board. 301 p.

Salinger MJ. 1988. New Zealand climate: past and present. In: *Climate Change—The New Zealand Response*. Proceedings of a workshop in Wellington, 29–30 March 1988. New Zealand Ministry for the Environment. p 17–24.

Stuiver M, Reimer P, Bard E, Beck JW, Burr GS, Hughes KA, Kromer B, McCormac G, van der Plicht J, Spurk M. 1998. INTCAL98 radiocarbon age calibration 24,000–0 cal BP. *Radiocarbon* 40(3):1041–83.

Stuiver M, Polach HA. 1977. Reporting of ^{14}C data. *Radiocarbon* 19(3):355–63.

Suggate RP. 1965. Late pleistocene geology of the northern part of the South Island, New Zealand. *New Zealand Geological Survey Bulletin* 77. 91 p.

Suggate RP. 1985. The glacial/interglacial sequence of north Westland, New Zealand. *New Zealand Geological Survey Record* 7. 22 p.

Taylor CB. 1968. A comparison of tritium and strontium-90 fallout in the Southern Hemisphere. *Tellus* 20:559–76.

Taylor CB, Roether W. 1982. A uniform scale for reporting low-level tritium measurements in water. *International Journal of Applied Radiation and Isotopes* 33: 377–82.

Taylor CB. 1990. Stable isotopic concentrations of monthly precipitation samples collected in New Zealand and Rarotonga. *Physical Sciences Report 3, Department of Scientific and Industrial Research, Lower Hutt, New Zealand*. 92 p.

Taylor CB, Brown LJ, Cunliffe JJ, Davidson PW. 1992. Environmental tritium and oxygen-18 applied in a hydrological study of the Wairau Plain and its contributing mountain catchments, Marlborough, New Zealand. *Journal of Hydrology* 138:269–319.

Taylor CB. 1994. Hydrology of the Poverty Bay flats aquifers, New Zealand: recharge mechanisms, evolution of the isotopic composition of dissolved inorganic carbon and ground water ages. *Journal of Hydrology* 158:151–85.

Taylor CB, Fox VJ. 1996. An isotopic study of dissolved inorganic carbon in the catchment of the Waimakariri River and deep ground water of the Canterbury Plains, New Zealand. *Journal of Hydrology* 186:181–90.

Taylor CB. 1997. On the isotopic composition of dissolved inorganic carbon in rivers and shallow groundwater: a diagrammatic approach to process identification and a more realistic model of the open system. *Radiocarbon* 39(3):251–68.

Taylor CB, Evans CM. 1999. Isotopic indicators for groundwater hydrology in Taranaki, New Zealand. *Journal of Hydrology* 38:237–70.

Taylor CB, Trompetter VJ, Brown LJ, Bekesi G. 2001. The Manawatu aquifers, North Island, New Zealand: clarification of hydrogeology using a multidisciplinary tracer approach. *Hydrological Processes* 15: 3269–86.

Vogel JC. 1970. Carbon-14 dating of groundwater. In: *Isotope Hydrology*. Vienna: International Atomic Energy Agency, Vienna Symposium Proceedings. p 225–39.

RADIOCARBON, Vol 46, Nr 2, 2004, p 517–529

PALEOGROUNDWATER IN THE MOUTERE GRAVEL AQUIFERS NEAR NELSON, NEW ZEALAND

Michael K Stewart[1,2] • Joseph T Thomas[3] • Margaret Norris[1] • Vanessa Trompetter[1]

ABSTRACT. Radiocarbon, ^{18}O, and chemical concentrations have been used to identify groundwater recharged during the last ice age near Nelson, New Zealand. Moutere Gravel underlies most of the Moutere Depression, a 30-km-wide system of valleys filled with Plio-Pleistocene gravel. The depression extends northwards into Tasman Bay, which was above sea level when the North and South Islands of New Zealand were connected during the last glaciation. The aquifers are tapped by bores up to 500 m deep. Shallow bores (50–100 m) tap "pre-industrial" Holocene water (termed the "modern" component) with ^{14}C concentrations of 90 ± 10 percent modern carbon (pMC) and $\delta^{18}O$ values of –6.8 ± 0.4‰, as expected for present-day precipitation. Deeper bores discharge water with lower ^{14}C concentrations and more negative ^{18}O values resulting from input of much older water from depth. The deep end-member of the mixing trend is identified as paleowater (termed the "glacial" component) with ^{14}C concentration close to 0 pMC and more negative ^{18}O values (–7.6‰). Mixing of the modern and glacial components gives rise to the variations observed in the ^{14}C, ^{18}O, and chemical concentrations of the waters. Identification of the deep groundwater as glacial water suggests that there may be a large body of such water onshore and offshore at deep levels. More generally, the influence of changing sea levels in the recent past (geologically speaking) on the disposition of groundwaters in coastal areas of New Zealand may have been far greater than we have previously realized.

INTRODUCTION

Groundwater in the Moutere Valley is an important resource for horticulture. Deep bores revealed the hitherto unknown water resource in the early 1980s, after shallow bores were found to provide limited and unreliable supplies. The present work uses isotope and chemical measurements in conjunction with other data (Thomas 1989) to improve understanding of the system (Stewart and Thomas 2002).

The term "paleowater" refers to groundwater that can be clearly identified by means of its radiocarbon date, and/or by another isotopic or noble gas signature, as originating in the colder climatic conditions of the late Pleistocene (Edmunds 2001). The objectives of this paper are to establish the deep Moutere Gravel groundwater as "paleo" water, and to consider some implications for New Zealand groundwaters.

Hydrogeology

The Moutere Depression is a 30-km-wide system of valleys between the Tasman Mountains and the ranges of east Nelson at the top of the South Island (Figure 1a). Voluminous Plio-Pleistocene gravels (including Moutere Gravel) are preserved in the depression and have been incised by the Motueka, Moutere, and Waimea Rivers (Rattenbury et al. 1998). Geophysical interpretation of seismic data and petroleum bores indicate that the depression reaches depths of 2500 m on the eastern side (Lihou 1992). The depression formed in the Pliocene-Pleistocene during uplift of the Tasman Mountains and the east Nelson Ranges.

Moutere Gravel is a uniform yellow-brown, clay-bound gravel, with deeply weathered clasts almost entirely of Torlesse-derived sandstone and semi-schist. Well-rounded, quartzofeldspathic sandstone clasts in a brown weathered muddy sand matrix comprise the bulk of the gravel.

[1]Institute of Geological & Nuclear Sciences, Private Bag 30368, Lower Hutt, New Zealand.
[2]Corresponding author. Email: m.stewart@gns.cri.nz.
[3]Tasman District Council, Private Bag 4, Richmond, New Zealand.

Proceedings of the 18th International Radiocarbon Conference, edited by N Beavan Athfield and R J Sparks
RADIOCARBON, Vol 46, Nr 2, 2004, p 517–529

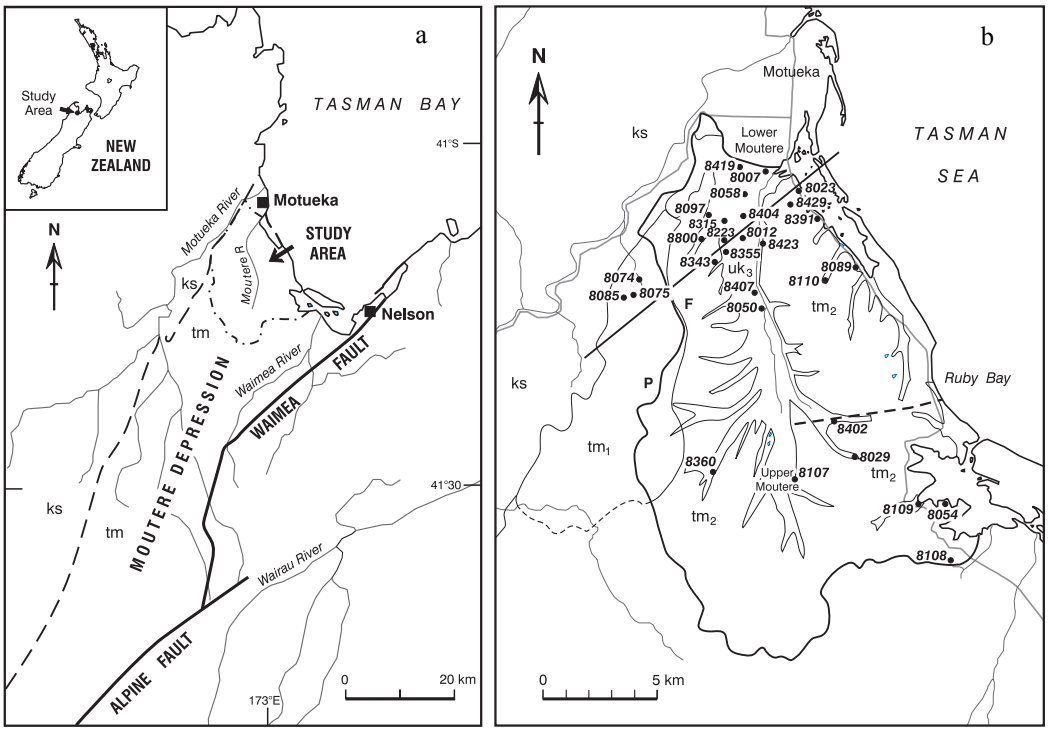

Figure 1 (a) Geology of the Moutere Depression, northwest Nelson. The contact with Separation Point Granite (ks) defines the western boundary, while the eastern boundary is against the upward-faulted east Nelson Ranges. (b) Geological setting of the Moutere Valley showing bore locations. Fine lines show the surface geology comprising Separation Point Granite (ks) to the northwest and Moutere Gravel (units tm_1 and tm_2) to the southeast. The valley floor contains reworked Moutere Gravel (uk_3).

The Moutere Valley lies south of Motueka (Figure 1b). Most of the Moutere River catchment comprises Moutere Gravel (marked tm). The catchment is underlain by a north-east trending basinal structure in which Moutere Gravel reaches a maximum depth of about 600 m (Figure 2). A basement high running through Ruby Bay forms the southern flank of the basin. Basement granite then descends south of Ruby Bay to the Waimea Fault on the east side of the Waimea Plains reaching 2500 m. Groundwater in Moutere Gravel south of the Ruby Bay high is largely unexplored.

The floor of the Moutere Valley has a Quaternary infilling (uk) which derives from reworked Moutere Gravel (Figures 1b, 2). Shallow bores (<20 m) draw limited and often unreliable supplies of water from the valley infill, showing that permeabilities are low. Shallow bores on the Moutere Hills also tend to have low yields and unreliable supplies. Rainfall is the main recharge source of these supplies, with possibly variable contributions from local streams (Thomas 1989).

The hydrogeology has been described by Thomas (1989, 1991, 1992, 2001). Significant groundwater resources are found in deep Moutere Gravel aquifers. The 3 aquifers in vertical succession are the Shallow Moutere Aquifer (SMA), Middle Moutere Aquifer (MMA), and Deep Moutere Aquifer (DMA) (Figure 2). Intervening leaky clay layers containing carbonaceous material constrain the aquifers. Groundwater heads are generally higher and yields improve significantly with depth. Many deep bores (>50 m) are artesian. The deep bores are cased to 30–50 m depth and then are generally screened or open to the bottom, so that they are likely to draw on water from several depths. Thomas (1989) has identified feed zones in several bores from downhole measurements.

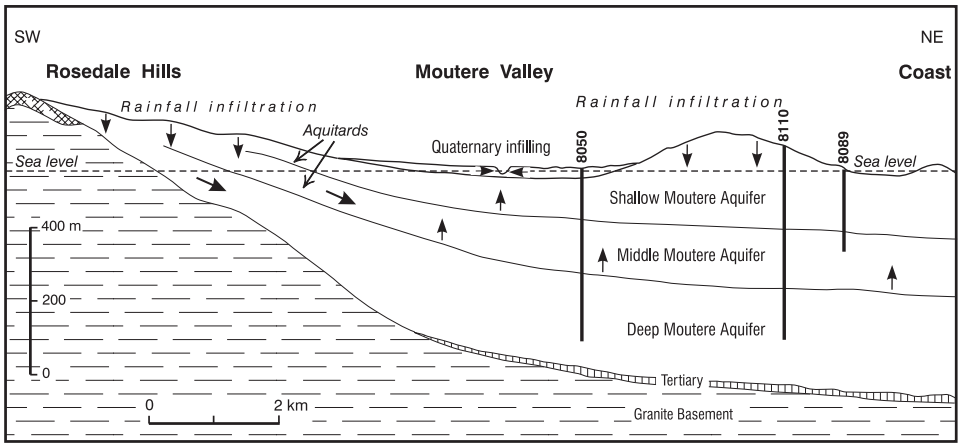

Figure 2 Cross-section showing the structure of the basin underlying the Moutere Catchment. The trace of the cross-section is parallel to the fault in Figure 1b. Inferred recharge patterns for the Moutere aquifers are shown (Stewart and Thomas 2002).

The Moutere groundwater resource north of the Ruby Bay basement high is divided into 2 zones (the western and eastern zones) by a major fault (Figure 1b). Pressure communication between bores is limited across this barrier. These zones are used for management of the resource (Thomas 2001). A third groundwater zone (southern) is defined south of the Ruby Bay high for discussion purposes.

Recharge to the aquifers is believed to occur by infiltration of rainfall where the Moutere Gravels outcrop. Two units have been identified by geological mapping, a lower unit (tm_1) and an upper unit (tm_2). The lower unit outcrops only in the southwest of the area (Figures 1b and 2), dips gently northeast into the Moutere Valley, and correlates with the DMA and MMA. The upper unit correlates with the SMA. Thomas (1989, 1992) proposed a recharge model in which rainfall infiltrated only where the lower unit outcrops in the Rosedale Hills area. This was revised to include recharge from both outcropping units of Moutere Gravel (Figure 2, Stewart and Thomas 2002). However, such recharge only applies to the "modern" component because conditions would have been very different during recharge of the "glacial" component. And no modern recharge (i.e. tritium or CFC-bearing water) has yet been observed in the bores within the valley, despite groundwater levels generally recovering from their summer drawdown during the subsequent winter and spring.

SAMPLING AND METHODS

Sampling

Groundwater bores were purged of at least 3 casing volumes before samples were taken. Bottles were flushed with the water to be sampled, emptied, refilled with water and allowed to overflow, then carefully sealed to prevent evaporation. Samples of water were collected in 28-mL glass bottles for ^{18}O, 500-mL bottles for carbon isotopes, and 1.1-L bottles for tritium. The carbon isotope samples were collected air-free. Bore locations are shown in Figure 1b. (More details on the bores are given in Stewart and Thomas 2002.)

Rafter Radiocarbon Seawater Line Method

The 150-mL samples were extracted using the Rafter Radiocarbon standard seawater method. A seawater vessel is prepared before each extraction. Four mL of ortho-phosphoric acid is added to the

side arm of the flask, and a magnetic stirrer and anti-bumping granules added to the bottom of the flask. The flask and contents are "tared" on a 2 decimal place balance. The 150-mL portion of water to be processed was removed using a plastic syringe from each groundwater sample. The water was transferred to the bottom of the glass seawater vessel using the syringe. The water was added carefully so the acid and water did not mix. Care was taken not to expose the water samples to atmospheric air as much as possible, by flushing the vessel with N_2 gas through a thin plastic hose placed into the spout of the vessel during addition of the sample. The sample bottle was sealed and weighed. The sample and acid were shaken together for approximately 1 min to mix, and attached to the seawater vacuum line. Room air was pumped from the connection between the seawater vessel and the vacuum line to a desirable vacuum. Two dry ice ethanol dewars are placed on the first 2 traps to collect water vapor, and 2 liquid nitrogen dewars are placed on the following 2 traps to collect carbon dioxide. The water sample in the seawater vessel is stirred throughout the transfer with a magnetic stirrer to aid transfer of the gas. The water bubbles vigorously during the vacuum transfer and the extraction is carried on until the bubbling has completely ceased and the vacuum line has again reached the baseline vacuum, which takes approximately 20 min.

The carbon dioxide gas is vacuum-distilled twice to further dry and purify it before measurement of the pressure. The amount of CO_2 gas collected is measured in a known volume, and the amount of dissolved inorganic carbon in the sample calculated. The carbon dioxide gas is made into a graphite target for measurement of ^{14}C by AMS. ^{14}C concentration is expressed as percent modern carbon (pMC), where the activity of "modern carbon" is taken as 95% of the activity of the NBS oxalic acid standard in 1950. Errors depend on concentration, ranging from ±0.07 pMC for near zero to ±0.8 pMC for 100 pMC concentrations.

Part of the gas is retained for measurement of ^{13}C by mass spectrometry. ^{13}C concentrations are expressed as δ values with respect to VPDB (Vienna PDB, the international standard). The measurement errors are ±0.1‰.

^{18}O and Tritium

For ^{18}O measurement on the waters, 2 mL of the water is isotopically equilibrated with CO_2 gas at 29 °C for 2 hr, and then the CO_2 is analyzed in a stable isotope mass spectrometer (Hulston et al. 1981). ^{18}O concentrations are given as δ values with respect to VSMOW (Vienna SMOW, the international standard). Measurement errors are ±0.1‰.

Tritium samples are distilled, enriched in tritium using electrolysis by a factor of about 80, and are then counted in a Quantalus low-background liquid scintillation counter for several weeks (Taylor 1994). Tritium concentrations are given as tritium units (TU), where 1 TU is 1×10^{-18}. Detection limits (errors for near-zero concentrations) are ±0.003 TU.

Chemical Data

Water samples have been collected from groundwater bores in the Moutere Valley by Tasman District Council hydrologists for a number of years. Samples for cations were field filtered and acidified with high-purity nitric acid. Samples for anions were field filtered and kept below 4 °C until analyzed, and bicarbonate samples were collected unfiltered, kept below 4 °C, and analyzed within 48 hr of collection. Samples were analyzed by the Cawthron Institute in Nelson. Methods for cation analyses include Atomic Adsorption and ICP-OES, and for anion analyses include auto titrator, auto analyzer, and ion chromatography.

RESULTS

Carbon Isotope Compositions

The ^{13}C concentrations in dissolved inorganic carbon (DIC) from Moutere are plotted against the reciprocal of the bicarbonate concentration (1/bicarbonate) in Figure 3a. The ^{13}C values are remarkably uniform around the values –20 to –24‰ (except for 1 sample, see below). This range shows that all of the carbon is sourced from organic matter within the soil or aquifers. Waters gain dissolved CO_2 by plant respiration and oxidation of organic matter as they pass through the soil, where CO_2 partial pressures are commonly 10 to 100 times those in the atmosphere. A second source of CO_2 is from carbonaceous matter within the aquifers, in this case from the intervening clay layers between the aquifers. Oxidation of such matter produces CO_2 if chemical and/or microbiological conditions are suitable (bacteria are needed to catalyze redox reactions between water and organic matter). The dissolved CO_2 reacts with rocks to become neutralized to HCO_3^- and CO_3^{2-} ions (Clarke and Fritz 1997). Bicarbonate is the dominant form of carbonate in the present waters.

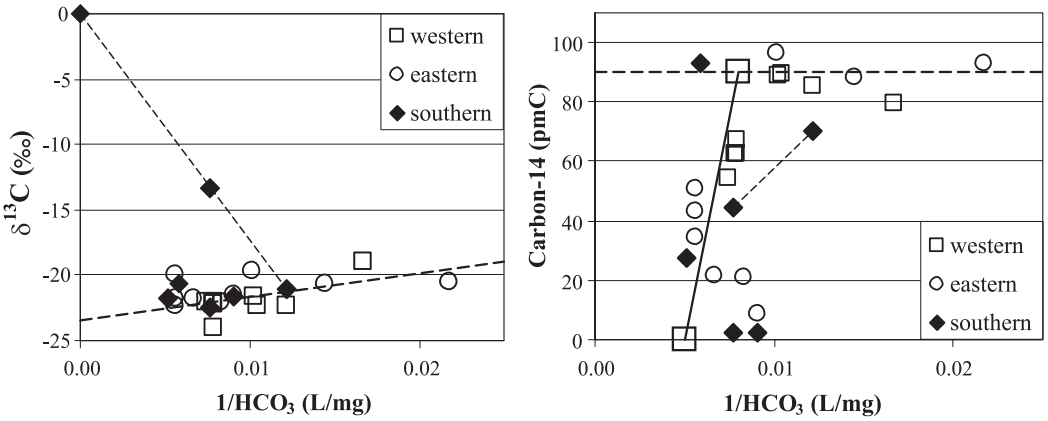

Figure 3 (a) $\delta^{13}C$ values versus $(HCO_3)^{-1}$ for bore waters; (b) ^{14}C values versus $(HCO_3)^{-1}$ for bore waters. The line connects the glacial (zero ^{14}C, 200 mg/L bicarbonate) and modern (90 pMC ^{14}C, 125 mg/L bicarbonate) end-members.

Only 1 sample has ^{13}C outside the range of –20 to –24‰, namely, 8107 with ^{13}C of –13.3‰. This sample is likely to have reacted with marine carbonate, which has the effect of moving the sample towards the ^{13}C value of such carbonate (approximately 0‰). The dotted line in Figure 3a shows the effect of reaction with marine carbonate. Carbon from carbonate rock would have zero ^{14}C; hence, it would have a diluting effect on the ^{14}C concentration. The short dotted line in Figure 3b shows the effect of reaction with carbonate on this sample.

Groundwater dating by ^{14}C is complicated by changes in ^{14}C activity in the atmosphere during the late Pleistocene and Holocene, and by dilution of ^{14}C in groundwater by dead carbon derived from soils and rocks when carbon-bearing solutions penetrate underground. Most of the ^{14}C in groundwater is gained from the soil, where CO_2 accumulates by root respiration and decay of vegetation, as noted above. The ^{14}C in DIC is susceptible to reaction and dilution with dead carbon from carbonate, other minerals, and organic matter in the soil and groundwater zones. A dilution factor q is used to account for the resulting dilution of ^{14}C (Clarke and Fritz 1997). The age equation is written

$$t = (1/\lambda) \,.\, \ln(q \,.\, a_o/a_t) \qquad (1),$$

where a_o is the initial ^{14}C activity ($q.a_o$ the diluted initial activity in the groundwater), a_t is the ^{14}C activity in groundwater after time t (i.e. when measured), and λ is the ^{14}C decay constant ($1/\lambda = T_{½}/\ln 2 = 8267$ yr). The apparent simplicity of this equation is deceptive. Numerous methods have been proposed for estimating q, based on the chemical and ^{13}C composition of the groundwater (a summary of methods is given in Clarke and Fritz [1997]).

Figure 3b shows ^{14}C concentrations plotted against $1/HCO_3$. The ^{14}C concentrations show a wide range of values, from almost 0 to 100 pMC. Shallow bores have ^{14}C concentrations in the range of 90 ± 10 pMC; this is taken as the initial ^{14}C activity. (None of the waters have concentrations high enough to indicate the presence of ^{14}C from nuclear weapons testing and hence are "pre-bomb"; i.e., they were all recharged before the early 1950s.)

The low ^{14}C concentrations in the deep bores along with the low ^{13}C values (which indicate absence of marine carbonates) show that the waters have had long residence times in the deep aquifer. None of the waters have zero ^{14}C concentration (the lowest are 8.6 pMC [western and eastern zones] and 2.4 pMC [southern zone]), but the waters are mixtures because the bores are open to the aquifer from 50 m down to as much as 500 m depth. This allows water from several depth levels to contribute to the discharges. The ^{14}C, ^{18}O, and some chemical constituents show variations consistent with such mixing; Figure 4a shows the mixing line between ^{14}C and $\delta^{18}O$.

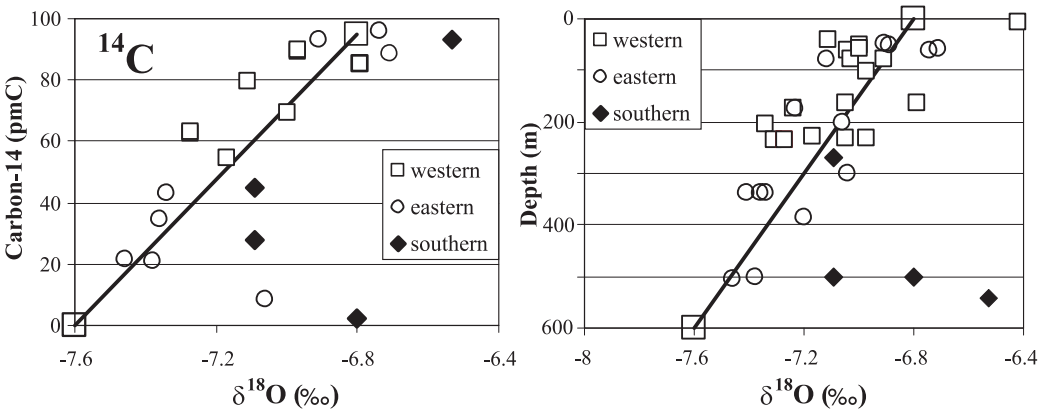

Figure 4 (a) ^{18}O versus ^{14}C for bore waters; the older waters (low ^{14}C) have more negative ^{18}O values. (b) ^{18}O values versus bore depths. A line is fitted to the points and connects deep (–7.6‰, 600 m) and shallow (–6.8‰, 0 m) end-members.

The data have been interpreted in terms of mixing between 2 types of water, a shallow component with ^{14}C concentration of 90 ± 10 pMC and a deep component with 0 pMC. The shallow component is designated "modern," but it has zero tritium and CFC concentrations and, therefore, is "pre-industrial" water with age in the hundreds of years (Stewart and Thomas 2002).

The deep component was recharged during the last glaciation and is the "glacial" component. A minimum mean age can be estimated using Equation 1. We assume that the ^{14}C activity of the deep water is less than 1 pMC, and that of the shallow water is 90 pMC. The bicarbonate concentrations in the deep and shallow waters are 200 and 60 mg/L, respectively (Figure 5a); hence, the dilution factor (q) is 60/200. These give a mean age greater than 27,000 yr. This is probably an underestimate, but an age within the glacial period is what is important, not the precise age.

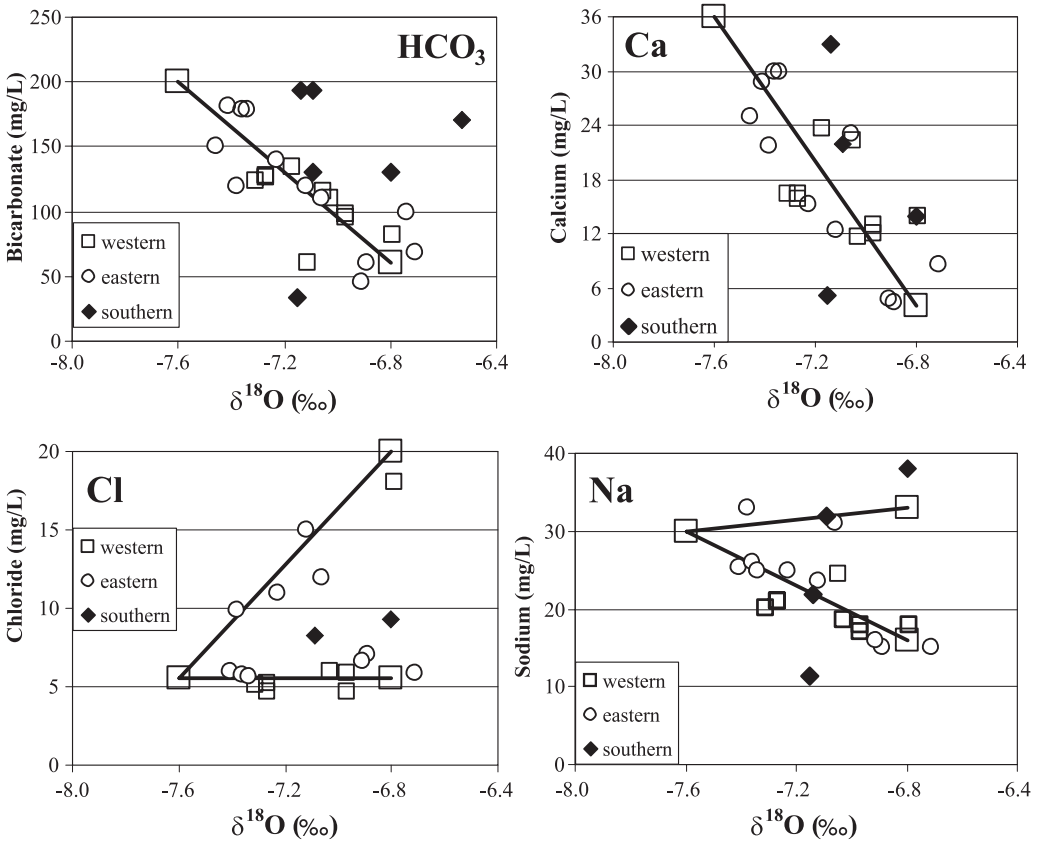

Figure 5 (a–d) ^{18}O versus HCO_3, Ca, Cl, and Na concentrations. Lines connect end-members at ^{18}O values of –7.6‰ (glacial water) and –6.8‰ (modern water).

^{18}O Concentrations

$\delta^{18}O$ values give information on the source and conditions of recharge to the groundwater because there is generally a relationship between the location of recharge and its ^{18}O value (Stewart and Morgenstern 2001). ^{18}O concentrations in water are expressed as δ values with respect to VSMOW (Vienna Standard Mean Ocean Water).

The mean $\delta^{18}O$ value of precipitation at Moutere is discussed in Stewart and Thomas (2002). They conclude that precipitation-recharged groundwater in the region under present-day conditions will have mean $\delta^{18}O$ values in the range of -6.8 ± 0.4‰. This comes from analysis of monthly samples of precipitation from several nearby sites and from locally-fed springs and shallow bores.

Estimation of the mean ^{18}O value of precipitation during the last glaciation is more problematical. The values will have been affected by at least 3 competing processes: 1) the sea would have been enriched in ^{18}O because low-^{18}O ice would have been locked up in ice sheets worldwide, leading to higher mean ^{18}O values; 2) the atmospheric temperature would have been lower, leading to greater isotopic fractionation between atmospheric water vapor and precipitation, and, therefore, to lower mean ^{18}O values; and 3) the sea would have been far from its present position (by up to several hundred km for Moutere), leading to a more continental climate and, therefore, to lower mean ^{18}O val-

ues. Evidence suggests that glacial age groundwater at Moutere would have been more negative than late Holocene groundwater by about 1‰. (e.g., The $\delta^{18}O$ value of calcite deposited on stalactites near Hamilton, New Zealand, was 0.95‰ lower during the last glacial maximum than present deposits [Hendy and Wilson 1968]. This difference would have been mainly due to the $\delta^{18}O$ difference in the waters flowing over the stalactite at these times [Hendy and Wilson 1968].)

The ^{18}O values of the groundwaters were found to be in the range of –6.4 to –7.5‰, except for 1 bore in the southern zone with ^{18}O of –8.3‰. This is a wider range than expected for Holocene waters in the area. The ^{18}O values also show relationships with bore depth (Figure 4b), with lower ^{18}O values at depth, and with ^{14}C as seen above. These observations support the idea of 2 types of water (modern and glacial). The ^{18}O of the glacial component is found to be –7.6‰ from the mixing diagrams.

Hence, the favored explanation is that there are 2 types of water in the Moutere aquifers. The first is a body of "fossil" water, occupying deeper levels of the Moutere aquifers, which has lower ^{18}O values because it was recharged during the last glacial period (in the Pleistocene). Above this is "modern" water, recharged in the last few hundred years of the Holocene, and with ^{18}O values much the same as today. These 2 end-member compositions are shown by the large hollow squares in the figures; the line connecting them shows the effect of mixing of these waters. (Older Holocene water may also be present in the modern component.)

The southern zone bores do not draw on a consistent deep component, unlike the deep bores in the western and eastern zones, and show much more scatter. Part of the reason may be that deep permeabilities are not so high in the south and, consequently, the southern bores draw more water from higher levels in the aquifers than in the western and eastern zones.

Chemical Compositions

The chemical compositions of the western and eastern zone waters are affected by mixing of the 2 water types. The glacial water at depth appears to have a nearly uniform composition, whereas the modern water at shallow depths has a more varied composition. This section looks at data for 4 of the chemical constituents, which show patterns representative of many of the other chemical constituents (Stewart and Thomas 2002).

Bicarbonate and calcium (Figures 5a, b) are readily affected by reaction with soil and rock, and the deep component has higher concentrations of these constituents than the shallow component (the compositions of the end components are indicated by the large squares in the plots). The pattern is of increasing concentration with decreasing $\delta^{18}O$ value, which is indicative of a mixing process. This is consistent with the deep (glacial) component having had much greater interaction with the rock because of its much longer residence time.

Chloride concentrations in groundwater often reflect marine influence on rainfall (i.e. rainout of seasalt particles in the atmosphere) because it is often an unreactive solute underground (Edmunds 2001). For rainfall-recharged groundwater, evapotranspiration causes enrichment of chloride while passing through the soil. A third influence is seawater trapped within parts of the aquifer during past higher sea level stands, or present-day intrusion of seawater. The plot of chloride versus ^{18}O (Figure 5c) shows glacial water (Cl ~ 5.5 mg/L, ^{18}O ~ –7.6‰) mixing with modern water containing a range of chloride values (5.5 to 18 mg/L, ^{18}O ~ –6.8‰). The graph has 2 limbs. Most of the western and eastern bores have chloride near 5.5 mg/L. However, bores on the seaward side of the Moutere Valley (8110, 8423, 8391, and 8089) plot on the upper limb with higher chloride concentrations. This is

considered to reflect their location near the sea, where they receive rainfall that has higher chloride concentrations from Tasman Bay. If so, this shows that the recharge has occurred locally. The lower limb chloride concentration is very low (5.5 mg/L), and probably reflects a continental effect during both glacial and modern times due to the presence of the high Tasman Mountains west of Moutere, which lie at right angles to the prevailing westerlies. Hence, it appears that the input of chloride to groundwater in this region might have been much the same in glacial times as it was in pre-industrial (late Holocene) times.

Sodium (Figure 5d) has similarities to chloride but is more affected by interaction with aquifer rocks. Seawater influence is shown by higher sodium concentrations in 8050 and 8007 (not plotted). The plot with ^{18}O shows 2 limbs as with chloride, but the upper limb values are more scattered (although it still includes 2 of the same bores, i.e., 8110 and 8089). Most of the samples lie on the lower limb, forming a trend towards higher sodium at depth because of increased water/rock interaction in the deep component.

The southern zone points do not generally conform to the patterns shown by the western and eastern zone points, although they are within the same range of values. As before, this is tentatively attributed to lower permeability at depth in the southern zone, leading to more input of waters from higher levels.

Tritium and CFCs

Tritium and CFC concentrations have been measured for a number of the bores (Stewart and Thomas 2002). The results show that the bore waters did not contain detectable tritium or CFC concentrations when first measured (as expected) and continue to show none. (If anything, ^{14}C concentrations appear to be decreasing rather than increasing since 1988.) On the other hand, groundwater levels, which are drawn down during the summer, generally recover during the subsequent winter and early spring. Thus, recharge is occurring, but this new water (which is seen in shallow bores in the hilly Moutere Gravel outcrop areas) must be near the surface in the recharge areas and has not yet found its way to the aquifers tapped by the deep bores, or younger water is slowly penetrating into the deep aquifers, but dilution with old water has been sufficient to keep concentrations at less than detectable levels up to now.

DISCUSSION

^{14}C and ^{18}O concentrations give linear relationships with depth and with each other in the western and eastern zones, showing that 2 types of water are present. Shallow groundwater has ages of hundreds of years and $\delta^{18}O$ values like present-day rainfall (around –6.8‰). The deep component has low ^{14}C concentration and ^{18}O of –7.6‰. These are the modern and glacial water types identified above. The western and eastern bores discharge either modern or mixtures of modern and glacial water, none discharge pure glacial water. The glacial water is believed to have been recharged during part of the last glaciation (20–50,000 yr ago).

This is the first time that the $\delta^{18}O$ shift between modern and glacial groundwaters has been reported for a New Zealand system. The measured difference of –0.8‰ can be compared with differences of +0.5‰ (Portugal), –1.3‰ (France), –1.9‰ (England), and –2.5‰ (Poland), measured in coastal regions of Europe (from Figure 7 in Loosli et al. 2001).

The late Quaternary covers a period of strong climatic changes in the New Zealand landscape brought about by the last glaciation. So much ice was locked up in ice sheets that the sea level was about 130 m lower than at present at the last glacial maximum (LGM). This resulted in large

increases in the New Zealand land area during which time new hydrogeological systems were established offshore from the present coastline. Flow within deep aquifers would have been much more active because of the much greater heads due to lower sea level. The warmer climate during the Holocene saw the sea level rise rapidly to its present level as the ice sheets melted. This caused water tables in groundwater systems to rise and hydraulic heads to diminish, causing profound changes in flow regimes. In particular, flow at deep levels would have become much more sluggish. The present-day configuration of groundwaters in coastal areas is, therefore, to a large extent the result of circulation of freshwater to deeper levels in response to the lower sea level during the last glaciation (Edmunds 2001). The Holocene flow patterns have been superimposed on top of the glacial flow patterns of 10,000 yr and more ago.

Figure 6a shows the eustatic sea level curve for the last 140,000 yr (Edmunds et al. 2001, after Shackleton 1987). Until 7000 yr ago, the sea had not been at its present level for 100,000 yr; it was much lower for most of that time (especially for the last 50,000 yr of it). The minimum level was reached about 18,000 yr ago (at the LGM). Between 14,000 and 7000 yr ago, the sea level rose rapidly (with fluctuations), and in New Zealand is believed to have reached levels 2–3 m above the present level by 4000 yr ago (Stevens 1990). The level has since declined to the present level.

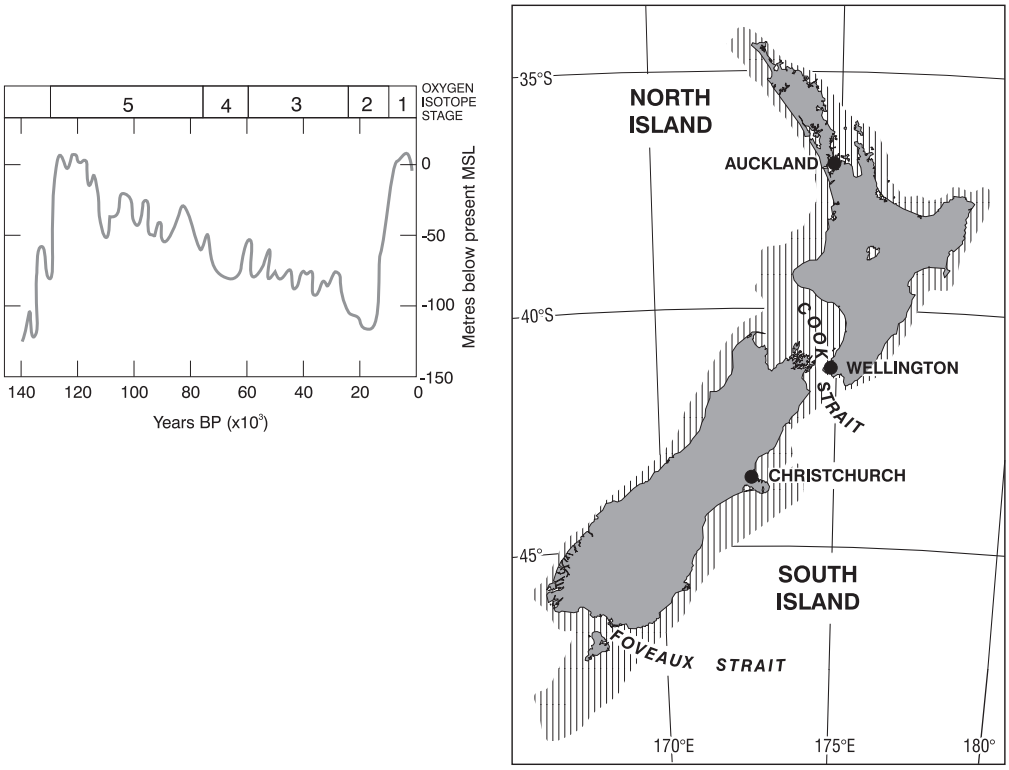

Figure 6 (a) Eustatic sea level curve for the past 140,000 yr; (b) New Zealand shoreline in the last glacial maximum (about 18,000 yr ago).

Figure 6b shows the inferred New Zealand shoreline during the LGM (Stevens 1990). The New Zealand land mass was doubled and the main islands of New Zealand were joined by a large plain. Moutere was an inland location, hundreds of km from the nearest sea. A considerable amount of the

former Pleistocene freshwater body (detected in this work) could now be present extending under Tasman Bay. It is probable that there is very little natural flow through the deep aquifer (i.e. little natural flow towards outlets under the sea). The lack of ^{14}C indicates that no substantial Holocene recharge has taken place into this water body. Some of the water is evidently now being extracted by the deep Moutere bores, causing marked drawdowns in water levels during the late summer. However, levels recover during the winter. Hence, recharge is occurring and there must be a tendency for shallow water to penetrate deeper as the deep water is extracted.

Where repeated measurements have been made (bores 8404 and 8407), there appears to be a trend towards ages becoming older due to exploitation. This suggests that more of the deep water is being extracted because permeabilities at depth allow more efficient recovery (i.e. water flows more rapidly in the deep aquifer).

Ice age groundwaters have been observed in deep aquifers in other parts of New Zealand. Two of them are in basins in the North Island bordering Cook Strait (see Figure 7). Taylor and Evans (1999) reported a ^{14}C age of 31,000 yr for groundwater at a depth of 238.4–241.4 m in the Whenuakura Formation near Hawera. Another deep groundwater at Shannon was reported as having a ^{14}C age of 40,000 yr (CB Taylor, personal communication; see also Taylor et al. 2001). Both bores are in sedimentary formations.

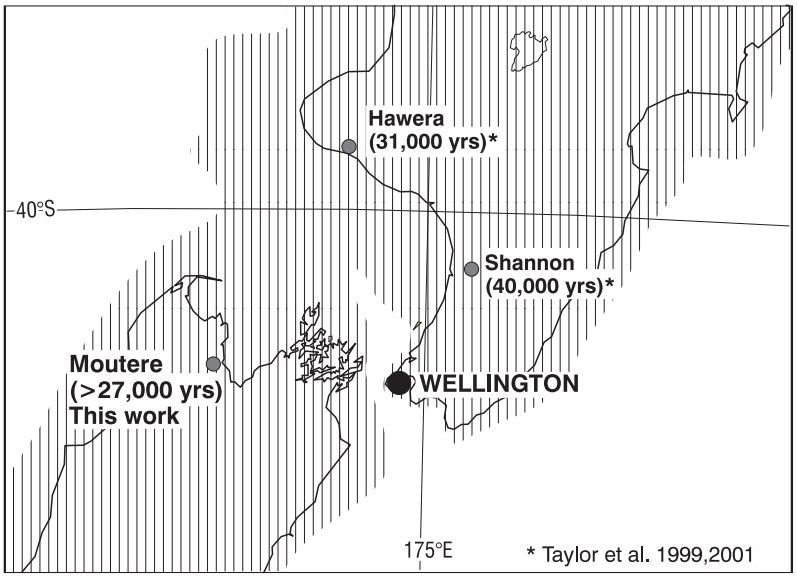

Figure 7 Shoreline in the Cook Strait region during the last glacial maximum and ^{14}C ages of some deep groundwaters.

These observations again suggest circulation of freshwater to deeper levels in response to the lower sea level during the last glaciation. The influence of changing sea levels in the recent past (geologically speaking) on the disposition of groundwaters in coastal areas of New Zealand may have been far greater than we have previously realized, and New Zealand may be surrounded by a "skirt" of pristine paleo-groundwaters at deep levels.

CONCLUSIONS

^{14}C, ^{18}O, and chemical concentrations have been used to identify groundwater in the Moutere Gravel aquifers that was recharged during the last ice age. The aquifers are tapped by bores up to 500 m deep. Shallow bores (50–100 m) tap pre-industrial Holocene water (termed the "modern" component) with ^{14}C concentrations of 90 ± 10 pMC and ^{18}O values of –6.8 ± 0.4‰, as expected for present-day precipitation. Deeper bores discharge water with lower ^{14}C concentrations and more negative ^{18}O values resulting from input of much older water from depth. The deep end-member of the mixing trend is identified as paleowater (termed the "glacial" component) with ^{14}C concentration close to 0 pMC and more negative ^{18}O values (–7.6‰). Mixing of the modern and glacial components gives rise to the variations observed in the ^{14}C, ^{18}O, and chemical concentrations of the waters.

Identification of the deep groundwater as glacial water suggests that there may be a large body of such water onshore and offshore at deep levels. This water would have been caught by rising sea levels that greatly reduced the rate of flow in the aquifer. More generally, the influence of changing sea levels in the recent past (geologically speaking) on the disposition of groundwaters in coastal areas of New Zealand may have been far greater than we have previously realized.

ACKNOWLEDGEMENTS

This work was funded by the New Zealand Foundation for Research, Science and Technology as part of the Integrated Catchment Management Programme of Landcare Research (via a Subcontract to the Institute of Geological and Nuclear Sciences) and the Understanding Groundwater Resources Programme of the Institute of Geological and Nuclear Sciences.

REFERENCES

Clark ID, Fritz P. 1997. *Environmental Isotopes in Hydrogeology.* New York: Lewis Publishers. 328 p.

Edmunds WM. 2001. Palaeowaters in European coastal aquifers—the goals and main conclusions of the PALEAUX project. In: Edmunds WM, Milne CJ, editors. *Palaeowaters in Coastal Europe: Evolution of Groundwater Since the Late Pleistocene.* London: Geological Society, Special Publications 189:1–16.

Edmunds WM, Buckley DK, Darling WG, Milne CJ, Smedley PL, Williams AT. 2001. Palaeowaters in the coastal regions of southern and eastern England. In: Edmunds WM, Milne CJ, editors. *Palaeowaters in Coastal Europe: Evolution of Groundwater Since the Late Pleistocene.* London: Geological Society, Special Publications 189:71–92.

Hendy CH, Wilson AT. 1968. Palaeoclimatic data from speleothems. *Nature* 216:48–51.

Hulston JR, Taylor CB, Lyon GL, Stewart MK, Cox MA. 1981. Environmental isotopes in New Zealand hydrology. Part 2. Standards, measurement techniques and reporting of measurements for oxygen-18, deuterium and tritium in water. *New Zealand Journal of Science* 24:313–22.

Lihou Joanne C. 1992. Reinterpretation of seismic reflection data from the Moutere Depression, Nelson region, South Island, New Zealand. *New Zealand Journal of Geology and Geophysics* 35:477–90.

Loosli HH, Aeschbach-Hertig W, Barbecot F, Blaser P, Darling WG, Dever L, Edmunds WM, Kipfer R, Purtschert R, Walraevens K. 2001. Isotopic methods and hydrogeological context in the investigation of palaeowaters. In: Edmunds WM, Milne CJ, editors. *Palaeowaters in Coastal Europe: Evolution of Groundwater Since the Late Pleistocene*. London: Geological Society, Special Publications 189:193–212.

Rattenbury MS, Cooper RA, Johnston MR, compilers. 1998. Geology of the Nelson Area. Institute of Geological and Nuclear Sciences 1:250,000 geological map 9. (1 sheet + 67 p) Lower Hutt, New Zealand.

Rosen MR. 2001. Hydrochemistry of New Zealand's aquifers. In: Rosen MR, White PA, editors. *Groundwaters of New Zealand*. Wellington: New Zealand Hydrological Society Inc. p 77–110.

Shackleton NJ. 1987. Oxygen isotopes, ice volume and sea level. *Quaternary Science Reviews* 6:183–90.

Stevens GR. 1990. Rugged landscape: the geology of central New Zealand, including Wellington, Wairarapa, Manawatu and the Marlborough Sounds. Wellington: DSIR Publishing. 286 p. (*DSIR information series, ISSN 0077-9636*:169).

Stewart MK, Dicker MJI, Johnston MR. 1981. Environmental isotopes in New Zealand hydrology. Part 4. Oxygen isotope variations in subsurface waters of the

Waimea Plains, Nelson. *New Zealand Journal of Science* 24:339–48.

Stewart MK, Morgenstern U. 2001. Age and source of groundwater from isotope tracers. In: Rosen MR, White PA, editors. *Groundwaters of New Zealand.* Wellington: New Zealand Hydrological Society, Inc. p 161–83.

Stewart MK, Thomas JT. 2002. Moutere Valley groundwater: nature and recharge from isotopes and chemistry. *Institute of Geological and Nuclear Sciences Science Report 2002/22*. 28 p.

Taylor CB. 1994. The relationship between electrolytic deuterium and tritium separation factors, and attainment of improved accuracy in radiometric low-level tritium measurement. *Journal of Applied Radiation and Isotopes* 45(6):683–92.

Taylor CB, Evans CM. 2000. Isotopic indicators for groundwater hydrology in Taranaki, New Zealand. *Journal of Hydrology (NZ)* 38(2):237–70.

Taylor CB, Trompetter VJ, Brown LJ, Bekesi G. 2001. The Manawatu aquifers, North Island, New Zealand: clarification of hydrogeology using a multidisciplinary environmental tracer approach. *Hydrological Processes* 15:3269–86.

Thomas JT. 1989. Hydrogeology of the Moutere Valley, Nelson, New Zealand [Unpublished MSc Eng. Geol. Thesis]. Department of Geology, University of Canterbury, New Zealand.

Thomas JT. 1991. Moutere Valley groundwater investigations 1989/1990. Unpublished Nelson Marlborough Regional report. 81 p.

Thomas JT. 1992. Hydrogeology of the Moutere Valley with emphasis on groundwater recharge. Unpublished Tasman District Council report. 8 p.

Thomas JT. 2001. Groundwater resources of the Tasman Region. In: Rosen MR, White PA, editors. *Groundwaters of New Zealand*. Wellington: New Zealand Hydrological Society, Inc. p 411–25.

RADIOCARBON, Vol 46, Nr 2, 2004, p 531–537

RADIOCARBON RESERVOIR AGE VARIATIONS IN THE SOUTH PERUVIAN UPWELLING DURING THE HOLOCENE

Michel Fontugne[1] • Matthieu Carré[2] • Ilhem Bentaleb[2] • Michèle Julien[3] • Danièle Lavallée[3]

ABSTRACT. In Quebrada de los Burros in coastal southern Peru (Tacna department), human settlements containing shells and charcoal deposits have been excavated since 1995. The sea surface ^{14}C reservoir ages, estimated by calculating the difference of ^{14}C age between marine shells and terrestrial organic materials, exhibit high values during the lower and middle Holocene and decrease abruptly after 4000 cal BP. The increase of reservoir age at around 7000–8000 cal BP suggests an enhancement of Peruvian coastal upwelling intensity and changes in ocean circulation at intermediate depth.

INTRODUCTION

Recent studies in paleo-oceanography and paleoclimate focused on the radiocarbon reservoir age (R) of surface seawaters since they could provide indications on oceanic circulation both for surface and/or deep-intermediate waters (Siani et al. 2000, 2001; Reimer and McCormac 2002; Southon et al. 2002). The classical approach consists in measuring the ^{14}C age difference between a terrestrial organic vegetal sample and a contemporaneous marine shell. Such a conjunction of samples is not often encountered except in coastal archaeological sites.

Here, we present new results from the southern Peruvian coast which provide some information about the upwelling system variability and its relation with El Niño events.

MATERIAL AND METHODS

Sample Location

Samples were collected at Quebreda de los Burros (18°1′S; 70°50′E) and neighboring sites (Cañon site and Inca site) both located in the Tacna department in the northern Atacama Desert (Figure 1). Quebrada de los Burros is a narrow valley oriented roughly north/south. This valley is about 150 m above mean sea level and the archaeological site is located less than 1 km from the shore (see Lavallée et al. 1999a, b, for details; Fontugne et al. 1999). All the shells and organic matter samples come from a narrow area restricted to the gully and excavations (about 400 m × 50 m). At the mouth of Quebrada, on a marine terrace 10 m above present sea level, we collected also charcoal, wood, and shells in an Inca site. The Cañon site is located 500 m from the Quebrada de los Burros sites in a larger and parallel valley at the same elevation. Only in Quebrada, springs occur(red) that created wetlands in very restricted areas and water availability for prehistoric people (Fontugne et al. 1999).

Sampling Procedures

Reservoir ages are generally estimated by calculating the difference of ^{14}C age between marine shells and terrestrial organic materials supposed to be contemporaneous. However, many problems in estimation of marine reservoir ages have been due to problematical associations. In order to illus-

[1]Laboratoire des Sciences du Climat et de l'Environnement, UMR 1572-CEA/CNRS, Domaine du CNRS, F-91198-Gif sur Yvette cedex, France. Corresponding author. Email: Michel.Fontugne@lsce.cnrs-gif.fr.
[2]Institut des Sciences de l'Evolution de Montpellier, UMR 5554, Place Eugène Bataillon CC064 F-34095 Montpellier cedex 5, France.
[3]Archéologie des Amériques, CNRS, Maison de l'Archéologie et de l'Ethnogie, 21, Allée de l'Université, F-92023-Nanterre cedex, France.

Proceedings of the 18th International Radiocarbon Conference, edited by N Beavan Athfield and R J Sparks
RADIOCARBON, Vol 46, Nr 2, 2004, p 531–537

Figure 1 Location of the Quebrada de los Burros site

trate this difficulty, we used results of dating previously obtained at different locations of the archaeological site during different excavation campaigns. Associations were based on stratigraphical correlations or on archaeological interpretation attributing each settlement level to a cultural phase. Results reported in Table 1 led us to perform a specific sampling in order to avoid problems of the samples' location, and in interpretation of sedimentology and stratigraphy units in the site.

Paired samples of charcoals and marine shells (*Concholepas concholepas, Mesodesma donacium*) stratigraphically associated were selected in different archaeological levels. They were strictly in connection (charcoals were within the shell). We tried to select shells without any visible trace of alteration. Dating was performed on shell that contained micro-charcoals (less than 1 mm) using both β-counting and accelerator mass spectrometry (AMS) techniques.

Others samples were collected within 3 cross-sections in a gully within the Quebrada. These cross-sections have been already described by Fontugne et al. (1999) and Usselman et al. (1999). They contain mollusk shells eaten by man, associated with organic layers containing a mixture of plant detritus, with probably aquatic terrestrial plant remains and also charcoal powder, as revealed by pollen analyses. Here, too, samples were collected in connection. Results are in reported in Table 2.

Table 1 ^{14}C conventional ages of marine shell and terrestrial organic samples, calibrated ages, and shell reservoir ages at Quebrada de los Burros, southern Peru. Samples were collected during different excavation campaigns and were not strictly in connection.

Laboratory nr	Sample nr	Unit nr	Nature	Conventional age	$\delta^{13}C$ (‰)	Calibrated age	Cal BP (yr) range	Reservoir age
Gif-10634	5087	QLB 3	Organic layer	8040 ± 105	–19.7	8996	9254–8592	275 ± 121
Gif-11453	—	QLB23	Shell	8315 ± 60	0.0	—	—	—
GifA 97289	5092	A3 NIV 2B	Charcoal	6630 ± 70	–20.5	7548	7611–7336	215 ± 76
Gif-10689	5158	N2B	Shell	6845 ± 30	–0.2	—	—	—
Gif-10635	5066	QLB4	Organic layer	7320 ± 80	–14.9	8150	8326–7944	–10 ± 94
Gif-11450	—	QLB 20	Shell	7310 ± 50	–0.9	—	—	—
Gif-10636	5067	QLB5	Organic layer	6940 ± 60	–16.3	7725	7921–7615	155 ± 78
Gif-11451	—	QLB21	Shell	7095 ± 50	0.0	—	—	—
GifA 97287	5056	B3 NIV2A	Charcoal	6460 ± 60	–15.6	7416	7432–7252	350 ± 100
GifA 97288	5057	C1 NIV 2A	Charcoal	6510 ± 60	–22.0	7424	7552–7270	400 ± 100
Gif-10399	5021	N2a	Shell	6110 ± 80	–3.0	—	—	—

Table 2 ^{14}C conventional ages of marine shell and terrestrial organic samples collected strictly in connection, calibrated ages, and shell reservoir ages at Quebrada de los Burros, southern Peru.

Laboratory nr	Sample nr	Unit nr	Nature	Conventional age	$\delta^{13}C$ (‰)	Calibrated age	Cal BP (yr) range	Reservoir age
Gif-10633	5086	QLB2	Organic layer	8160 ± 70	–15.0	9030	9399–8781	700 ± 148
Gif-10400	5035	—	Shell	8860 ± 130	–1.0			
Gif-10634	5087	QLB3	Organic layer	8040 ± 105	–19.7	8996	9254–8592	740 ± 126
Gif-10401	5031-2	—	Shell	8780 ± 70	0.3			
Gif-10648	5088	QLB17	Organic layer	3700 ± 40	–15.0	4057	4146–3874	745 ± 57
Gif-10404	5011	—	Shell	4445 ± 40	0.3			
GifA 99341	5323	D9/2inf	Charcoal	6090 ± 80	–25.3	6894	7179–6690	980 ± 113
GifA 99509	5323	D9/2inf	Shell	7070 ± 80	0.6			
GifA 99576	5292	E9/2sup	Charcoal	6560 ± 90	–17.9	7430	7573–7272	920 ± 120
GifA 99510	5295	E9/2sup	Shell	7480 ± 80	0.6			
Gif-10643	5080	QLB12	Organic layer	7390 ± 50	–15.3	8175	8330–8030	735 ± 58
Gif-10646	5083	QLB15	Shell	8125 ± 30	0.5			
Gif-10645	5082	QLB14	Organic layer	6595 ± 75	–13.6	7234	7415–7278	565 ± 110
Gif-10647	5084	QLB16	Shell	7160 ± 80	0.7			
Gif-10629	5074	Cañon	Charcoal	3120 ± 80	–25.3	3341	3473–3065	475 ± 120
Gif-10722	5074	Cañon	Shell	3595 ± 90	0.0			
GifA 100347	5406	E5-6N4	Charcoal	6500 ± 80	—	7422	7558–7254	1290 ± 144
GifA 100348	5406	E5-6N4	Shell	7790 ± 120	—			
Gif-11457	—	Site Inca/QLB31	Wood	375 ± 30	–22.9	455	484–313	675 ± 42
Gif-11456	—	Site Inca/QLB 31C	Shell	1050 ± 30	–0.5			
GifA 100142	5373	DE9/fond N2	Charcoal	6090 ± 110	—	6894	7231–6670	550 ± 121
Gif-10649	5061	N2a	Shell	6640 ± 50	–0.4			
Gif-10642	5079	QLB11	Organic layer	8650 ± 70	–13.4	9550	9888–9490	1075 ± 114
Gif-11452	—	QLB22	Shell	9725 ± 90	–0.1			
GifA 100343	5383	B0C5/N4 5383	Charcoal	7360 ± 100	–16.5	8167	8349–7963	520 ± 135
GifA 100342	5383	B0C5/N4 5383	Shell	7880 ± 90	–0.4			

Hardwater or Old Wood Effects

Hardwater effect and/or old wood effect are common problems in estimation of marine reservoir ages. In Quebrada, the hardwater effect could influence the aquatic plants, possibly contributing to these organic layers, and would result from dissolution of old carbonate and contamination by old bicarbonate or dissolved CO_2 that could be used by the plant through photosynthesis processes. This effect is highly improbable in a hyper-arid region and, secondly, because the volcanic origin of the substratum (Formacion Chocolate) covered by sand sediment, is devoid of carbonate.

Taking into account these observations and the coherence of these dates with those obtained for paired charcoal and shell in similar levels in the archaeological site, we admit that no aging due to hardwater effect occurs. Inversely, if we consider that such an aging would have occurred for these organic layers, it would imply a younger actual age and, consequently, a larger increase of sea surface reservoir age than we found. Such results would be hardly compatible with literature data or with other data obtained with charcoals and shells in Quebrada. Similarly, secondary alteration or recrystallization of shell carbonate would lead to the fixation of younger carbon and younger ages, meaning that our calculations of reservoir effect were underestimated.

The "old wood" problem results from the hyper-arid conditions in this region that promote long-term preservation of organic material which could be used by people. This effect gives low or negative *R* values like those observed by Kennett et al. (2002) in the same region. It does not apparently occur at Quebrada de los Burros.

Whatever we consider, if hardwater or old wood effects or shell recrystallization have affected one or both paired samples, it would lead to an actual marine reservoir age that would be higher than we estimate. *R* values reported in Table 2 have to be considered as minimal values.

Analytical Procedures

^{14}C dating was performed using beta-counting gas proportional counter and AMS facilities at Gif sur Yvette. Shells were cleaned using either dilute HCl (β-counting samples) or sandblaster followed by acid treatment for AMS samples (Tisnérat et al. 2001) in order to remove the superficial part of the shell that might have been re-crystallized (Vita-Finzi and Roberts 1984). Charcoals and organic layers were prepared using classical treatments. Results are expressed as conventional ages (Stuiver and Pollack 1977) and calibrated age according to Stuiver et al. (1998).

RESULTS AND DISCUSSION

Results of the first study are reported in Table 1. All *R* values are smaller than the mean ocean reservoir age (400 yr) and are not compatible with an upwelling pattern that always prevailed in this region during the Holocene period. This illustrates that sampling needs to be performed very carefully; moreover, in order to study reservoir ages variations, a specific sampling would be recommended. Comparison of dates obtained by long distance correlation between different archaeological levels at different places in these sandy excavations is very confusing. The Quebrada de los Burros site presents a low sedimentation rate and archaeological levels that are not very thick. In this context, a possible penetration of shell in the underlying archaeological level is probable.

All the results of the second sampling are reported in Table 1 and Figure 2. The chronology is derived from ^{14}C conventional ages of terrestrial organic origin and extends from the Inca period 375 ± 30 ^{14}C BP to 8650 ± 70 ^{14}C BP (455–9550 cal BP). No human settlements or organic deposits could be found between 375 and 3200 ^{14}C BP. During the early- and mid-Holocene, differences between ^{14}C ages of shell and charcoal (*R* values) are high, ranging between 700 and 1230 yr. The "old wood" problem, giving low or negative *R* values like those observed by Kennett et al. (2002) in the same region, do not apparently occur at Quebrada de los Burros. Nevertheless, lower *R* values were observed around 6090 and 6595 and 7390 and 7360 ^{14}C BP. Between 3000 ^{14}C BP and the present, reservoir ages dropped down to low values (less than 700 yr), in good agreement with modern values 590 ± 40 yr and in agreement with Stuiver and Braziunas (1993) and Owen (2002). The large variations observed for reservoir age imply that for dating archaeological sites, the use of modern ^{14}C reservoir age correction (as it is done generally) could introduce uncertainties greater than 500 yr.

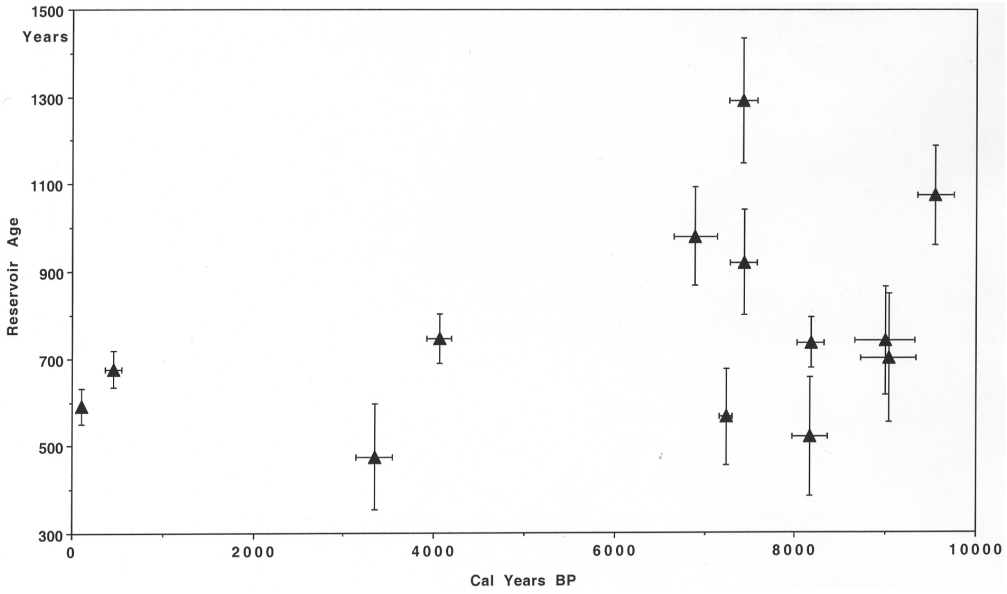

Figure 2 Variation of reservoir age of surface seawater versus time (^{14}C cal BP). The errors quoted are 1 σ.

The increase of reservoir age in upwelling areas is generally interpreted as an enhancement of upwelling intensity which brings deeper waters to the surface. Such an interpretation corroborates the hypothesis developed by Fontugne et al. (1999). They suggest that reinforced upwelling would generate more fogs condensing at mid-altitude (600–1000 m) in the Andes. This precipitation provides enough humidity to insure vegetation growth and food for guanaco hunted by fisher-gatherer/hunter people living on the coast (Lavallée et al. 1999a, b). The increased fog production was certainly the origin of water resources in Quebrada. Conversely, when reservoir ages are low and upwelling is weak, no human settlements are found. Paleo-oceanographic reconstructions in equatorial upwelling and the Peru-Chile current give arguments supporting these observations (see references). Data obtained in Quebrada suggest lower sea surface temperatures during the early mid-Holocene period and agree with this hypothesis. Fish consumed by man at that period belong to a fauna colder than that observed today (Lavallée et al. 1999b), and the $\delta^{18}O$ values of shell carbonate that depend on sea surface salinity and temperature were also higher, indicating colder temperatures (salinity is assumed to be more or less constant) (Carré et al., forthcoming). Finally, Schrader and Snorkes (1991), Lyle et al. (1992), Farrell et al. (1995), and Marchant and Hebbeln (1999), notice higher organic carbon contents in marine early mid-Holocene sediment, related to an increased productivity as a result of the enhancement of upwelling strength. However, the doubling of reservoir age at around 7000–8000 cal BP appears much too important to result from an enhancement of upwelling alone because it would imply that upwelled waters had too deep an origin. Two hypothesis could be proposed: 1) the upwelled waters were older, or 2) the origin of waters was different, implying that Antarctic intermediate water ($\Delta^{14}C$ = –120‰, pre-bomb value) were replaced during the upper Holocene by South Antarctic Mode Water ($\Delta^{14}C$ = –72‰, pre-bomb value) that are upwelled today in the Peru-Chile current (Toggweiller et al. 1991). Whatever the cause of the change in reservoir age was, it corresponds to a major change in the circulation of the south Pacific Ocean around 7000–9000 cal BP. Our results agree with Van Beek et al. (2002) that show higher reservoir ages in the Southern Ocean at the beginning of the Holocene and with reconstruction of surface water pH and pCO_2 variations in the western equatorial Pacific Ocean,

which suggests an important CO_2 degassing as a result of the increased intensity of upwellings at that time (Palmer and Pearson 2003).

The enhancement of upwelling that is associated with strong trade winds and lower sea surface temperature suggests that the La Niña phenomenon would have been the prevailing situation during the early Holocene. This implies that El Niño events were less frequent and certainly less strong than during the upper Holocene and the present period, which is in good agreement with what we observe in sedimentological records at Quebrada de los Burros in coastal southern Peru.

ACKNOWLEDGEMENTS

Thanks are due to Martine Paterne for helpful discussions and Maurice Arnold for AMS measurements. Dr A J T Jull and an anonymous reviewer are acknowledged for suggestions in order to clarify the manuscript. Thanks are due to C Noury for sample preparations. This study was supported by the Franco-Peruvian archaeological project "Pérou-Sud" and the CONCHAS project (PNEDC, CNRS), LSCE contribution nr 1106.

REFERENCES

Carré M, Bentaleb I, Fontugne M, Lavallée D. Forthcoming. Strong El Niño events during early Holocene: stable isotope evidence from Peruvian sea shell. *The Holocene*.

Farrell JW, Pedersen TF, Calvert SE, Nielsen B. 1995. Glacial-interglacial changes in nutrient utilization in the equatorial Pacific ocean. *Nature* 377:514–7.

Fontugne M, Usselmann P, Lavallée D, Julien M, Hatté C. 1999. El Niño variability in the coastal desert of southern Peru during the mid-Holocene. *Quaternary Research* 52:171–9.

Kennett DJ, Ingram BL, Southon J, Wise K. 2002. Differences in ^{14}C age between stratigraphically associated charcoal and marine shell from archaic period site of kilometer 4, southern Peru: old wood or old water? *Radiocarbon* 44(1):53–8.

Lavallée D, Julien M, Béarez P, Usselmann P, Fontugne M, Bolaños A. 1999a. Pescadores-recollectores arcaicos del extremo-sur peruano. Excavaciones en la Quebrada de los Burros (Tacna, Perù): primeros resultados 1995–1997. *Bulletin Institut Français Etudes Andines* 28(1):13–52.

Lavallée D, Bearez P, Chevalier A, Julien M, Usselmann P, Fontugne M. 1999b. Paleoambiente y ocupacion prehistorica del litoral extromo-sur del Peru: las ocupaciones del arcaico en la Quebrada de los Burros y alrededores (Tacna, Peru). In: Kaulicke P, editor. "El periodo arcaico en el Peru: hacia una definition de los origines," *Boletin de Arqueologia PUCP* 3:393–416.

Lyle MW, Prahl FG, Sparrow MA. 1992: Upwelling and productivity changes inferred from a temperature record in the central equatorial Pacific. *Nature* 355: 812–5.

Marchant M, Hebbeln D. 1999. High-resolution planktic foraminiferal record of the last 13,300 years from the upwelling area off Chile. *Marine Geology* 161:115–28.

Owen BD. 2002. Marine reservoir age estimates for the far south coast of Peru. *Radiocarbon* 44(3):701–8.

Palmer MR, Pearson PN. 2003. A 23,000-year record of surface water pH and pCO_2 in the western equatorial Pacific Ocean. *Science* 300:480–2.

Reimer PJ, McCormac FG. 2002. Marine radiocarbon reservoir corrections for the Mediterranean and Aegean Seas. *Radiocarbon* 44(1):159–66.

Schader H, Sorknes R. 1991. Peruvian coastal upwelling: late Quaternary productivity changes revealed by diatoms. *Marine Geology* 97:233–49.

Siani G, Paterne M, Arnold M, Bard E, Metivier B, Tisnérat N, Bassinot F. 2000. Radiocarbon reservoir ages in the Mediterranean Sea and Black Sea. *Radiocarbon* 42(2):271–80.

Siani G, Paterne M, Michel E, Sulpizio R, Sbrana A, Arnold M, Haddad G. 2001. Mediterranean sea surface radiocarbon age changes since the last glacial maximum. *Science* 294:1917–20.

Southon J, Kashgarian M, Fontugne M, Metivier B, Yim WWS. 2002. Marine reservoir corrections for the Indian Ocean and Southeast Asia. *Radiocarbon* 44(1): 167–80.

Stuiver M, Polach H. 1977. Discussion: reporting of ^{14}C data. *Radiocarbon* 19(3):355–63.

Stuiver M, Reimer PJ, Bard E, Beck WJ, Burr GS, Hughen KA, Kromer B, McCormac G, van der Plicht J, Spurk M. 1998. INTCAL 98 radiocarbon age calibration, 24,000–0 cal BP. *Radiocarbon* 40(3):1041–83.

Stuiver M, Braziunas TF. 1993. Modelling atmospheric ^{14}C influences and ^{14}C ages of marine samples to 10,000 BC. *Radiocarbon* 35(1):137–89.

Tisnerat-Laborde N, Poupeau JJ, Tannau JF, Paterne M. 2001. Development of a semi-automated system for routine preparation of carbonate samples. *Radiocarbon* 43(2A):299–304.

Toggweiller JR, Dixon K, Broecker WS. 1991. The Peru upwelling and the ventilation of the South Pacific thermocline. *Journal of Geophysical Research* 96(C11):20,467–97.

Usselmann P, Fontugne M, Lavallée D, Julien M, Hatté C. 1999. Estabilidad y ruptura dinamicas en el Holoceno de la costa surperuana/el Valle de la Quebrada de los Burros (Departamento de Tacna). *Bulletin Institute Française Etudes Andines* 28 (1): 1–11.

Van Beek P, Reyss JL, Paterne M, Gersonde R, Van Der Loeff MR, Kuhn G. 2002. ^{226}Ra in barite: absolute dating of Holocene southern sediments and reconstruction of reservoir ages. *Geology* 30(8):731–4.

Vita-Finzi C, Roberts N. 1984. Selective leaching of shells for ^{14}C dating. *Radiocarbon* 26(1):54–8.

RADIOCARBON, Vol 46, Nr 2, 2004, p 539–550

RADIOCARBON AGES AND ISOTOPE FRACTIONATIONS OF BEACHROCK SAMPLES COLLECTED FROM THE NANSEI ISLANDS, SOUTHWESTERN JAPAN

Kunio Omoto

Department of Geography, College of Humanities and Sciences, Nihon University, 24-40, 3 Chome, Sakurajosui, Setagaya-ku, Tokyo 156-8550, Japan. Email: omoto@chs.nihon-u.ac.jp.

ABSTRACT. A total of 294 beachrock samples were collected from 116 sites on 15 islands in the Nansei Islands chain, southwestern Japan, and were radiocarbon dated. The beachrocks began to form at about 6900 BP and some are still under development in the islands. Values of isotope fractionations of different materials making up the beachrocks ranged between +9.4‰ and –5.7‰. Isotope fractionations outside the range of 0 ± 2‰ suggest that these beachrocks were strongly influenced by underground water and running freshwater when they were cemented. The sea level during the late Holocene has remained the same for at least the past 5000 yr, except for several uplifted coasts.

INTRODUCTION

Beachrocks are observed frequently on the tropical and subtropical sandy beaches where the soft beach sediments, including fossil shells, fragments of corals, and other biocarbonates, are well cemented within the intertidal zone by calcium carbonate (Figure 1). Therefore, they are not only good indicators of the past sea level, but they also provide good sample material for radiocarbon dating. The beachrocks occur in thin beds dipping seaward at less than 15 degrees.

Figure 1 Beachrock observed at Tuha, Ohgimi Village, Okinawa Prefecture, central part of the Nansei Islands

The Nansei Islands (Ryukyu Retto) are a chain of islands consisting of more than 300 smaller islands between Kyusyu and Taiwan, extending about 1200 km parallel to the eastern edge of the Asian plate. The Nansei Islands are divided into 3 major island groups from north to south: the Amami Islands, Okinawa Islands, and Sakishima Islands, respectively (Figure 2). They are subject to the influence of Kuro Shio (warm current), which originates from the North Equatorial Current, forming many coral reefs.

Proceedings of the 18th International Radiocarbon Conference, edited by N Beavan Athfield and R J Sparks
RADIOCARBON, Vol 46, Nr 2, 2004, p 539–550

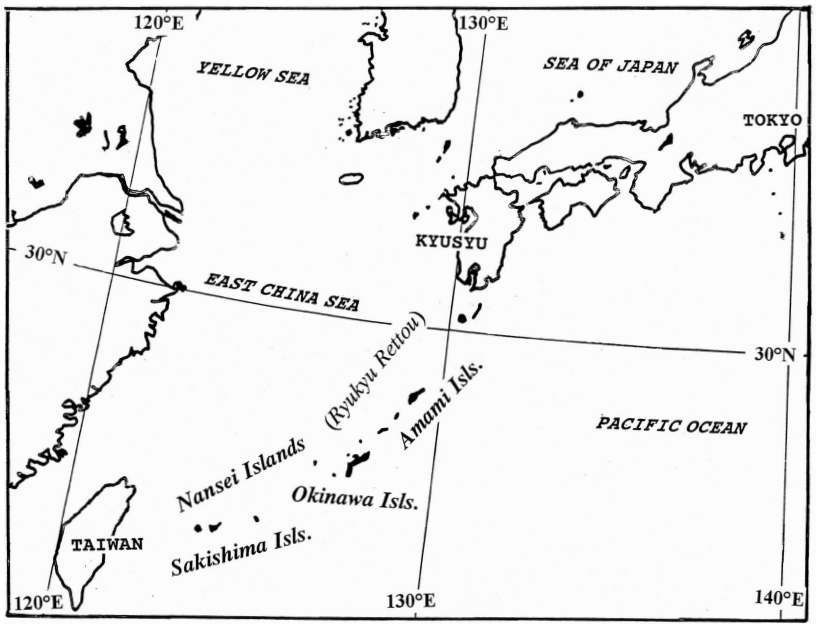

Figure 2 Index map of the surveyed islands

These islands consist of Paleozoic rocks, metamorphic rocks, volcanic rocks, and Quaternary raised coral limestones (Kawana 1988). The coastal geomorphology is characterized most often by rocky coasts, but in other places marine terraces develop at several levels which indicate evidence of Pleistocene or Holocene emergence. On the sandy beaches of the Nansei Islands, beachrocks are observed frequently within the range of the intertidal zone.

Yonetani (1963) was the first geographer to introduce the term "beachrock" in Japan. Since that time, many geomorphologists and geologists have shown interest in the distribution and characteristics of beachrocks found in the Nansei Islands. A number of beachrocks have been ^{14}C dated by numerous scientists (Omoto 1976; Omoto et al. 1976; Takahashi and Koba 1980; Kawana 1981; Ota et al. 1985; Kawana and Pirazzoli 1985; Tanaka 1986, 1990; and others). Takahashi and Koba (1980) and Tanaka (1986) attempted to compile statistics of them. However, great portions of them have not yet been corrected by isotope fractionation. Therefore, the author could not include a great deal of the ^{14}C dates reported previously.

The ^{14}C ages of beachrock samples collected from the Nansei Islands have previously been reported by the author without isotope fractionations (Omoto 1994–2001a), and later with isotope fractionations (Omoto 2001b–2003b; Omoto et al. 2003; Omoto 2003c, 2004).

Locations of each sampling site were determined either by GPS or calculations based on a 1:25,000 scale map. Elevations of each sampling site of beachrocks, beach profiles, and local tide changes were measured with a Nikon Laser Level or a Nikon Total Station. ^{14}C datings and analyses of isotope fractionations for beachrock samples were carried out by the author at the Radiocarbon Dating Laboratory of Nihon University. ^{14}C dates have been corrected for isotope fractionations ($\delta^{13}C$), then 400 yr (Stuiver and Braziunas 1993) were subtracted due to the ocean reservoir effect.

The aim of this paper is to determine the age of beachrock formations and to reconstruct the late Holocene sea-level changes and/or tectonic movements in the Nansei Islands. Another purpose is to

identify the origin of calcium carbonate which cemented soft marine carbonates to beachrock, based on the isotope analysis. In order to accomplish these aims, 294 beachrock samples were collected from 116 sampling sites on 15 islands in the Nansei Islands.

COLLECTION OF BEACHROCK SAMPLES AND RESULT OF ISOTOPE ANALYSES

Samples Collected from Amami Islands

The Amami Islands are located in the northern part of the Nansei Islands. A total of 87 beachrock samples were collected from 4 islands, namely Amami Oshima Island (28°20′N, 129°30′E), Tokuno Island (27°45′N, 128°58′E), Okinoerabu Island (27°22′N, 128°35′E), and Yoron Island (27°02′N, 128°26′E). They consist of 41 calcarenite samples, 26 fossil coral samples, and 20 fossil shells (Table 1).

Table 1 The items of beachrocks collected from the Nansei Islands. Data were compiled from Omoto (1994–2004).

Island name	Calcarenite[a]	Coral	Shell	Total	Nr of sites
Amami Islands					
Amami-Oshima Island	11	8	5	24	10
Tokuno Island	6	4	6	16	4
Okinoerabu Island	11	10	5	26	11
Yoron Island	13	4	4	21	12
Subtotal	**41**	**26**	**20**	**87**	**37**
Okinawa Islands					
Okinawa Island	4	12	15	31	18
Izena Island	3	1	3	7	4
Aguni Island	4	1	1	6	4
Ie Island	14	2	11	27	6
Zamani Island	2	1	10	13	6
Kume Island	15	10	10	35	4
Subtotal	**42**	**27**	**50**	**119**	**42**
Sakishima Islands					
Iriomote Island	5	3	4	12	5
Ishigaki Island	9	13	9	31	12
Miyako Island	11	5	9	25	14
Yonakuni Island	3	2	2	7	3
Hateruma Island	3	2	8	13	3
Subtotal	**31**	**25**	**32**	**88**	**37**
Total	**114**	**78**	**102**	**294**	**116**

[a]Calcirudite samples are included.

All samples were ^{14}C dated and reported without isotope correction (Omoto 1999d, 1999f, 2000a, 2000d). Therefore, the values of the isotope fractionations of the 87 samples gave later measurements and ranged between 4.77‰ and –3.28‰ (Table 2).

Table 2 Statistical data of isotope fractionations of beachrocks collected from the Nansei Islands. Data were compiled from Omoto (1994–2004).

	Calcarenite[a]				Coral				Shell				Total		
Island	nr	max	min	aver	nr	max	min	aver	nr	max	min	aver	max	min	aver
Amami Islands															
Amami-Oshima Island	11	2.05	–2.06	0.26	8	1.79	–0.15	0.74	5	1.51	–0.02	1.02	2.05	–2.06	0.45
Tokuno Island	6	2.62	–3.28	1.26	4	1.68	1.03	1.3	6	4.67	2.74	3.67	4.67	–3.28	2.16
Okinoerabu Island	11	3.18	0.15	2.34	10	4.28	–0.94	2.11	5	4.77	3.33	4	4.77	–0.94	2.57
Yoron Island	13	3.82	1.52	2.62	4	3.09	1.34	2.28	4	4.27	2.77	3.42	4.27	1.34	2.71
Subtotal	**41**	**3.82**	**–3.28**	**1.71**	**26**	**4.28**	**–0.94**	**1.54**	**20**	**4.77**	**–0.02**	**3.04**	**4.77**	**–3.28**	**1.96**
Okinawa Islands															
Okinawa Island	4	5.63	1.78	3.07	12	2.48	–5.97	–0.61	15	4.06	–4.67	0.63	1.42	–5.15	–0.54
Izena Island	3	1.59	1.18	1.32	1	–0.16	–0.16	–0.16	2	3.42	2.72	3.07	3.42	–0.16	1.66
Aguni Island	3	1.42	0.53	1.02	1	–3.49	–3.49	–3.49	3	1.15	–5.15	–1.13	6.03	0.15	2.28
Ie Island	14	2.89	0.15	1.9	2	3.51	0.63	2.07	11	6.03	0.95	2.79	5.63	–5.97	0.46
Zamani Island	2	3.15	2.28	2.72	1	2.74	2.74	2.74	10	5.07	1.18	3.32	5.07	1.18	3.18
Kume Island	15	3.42	0.17	1.82	10	2.31	–2.08	0.44	10	3.37	0.52	2.1	3.43	–2.08	1.49
Subtotal	**41**	**5.63**	**0.15**	**1.386**	**27**	**3.51**	**–5.97**	**0.001**	**51**	**6.03**	**–5.15**	**1.554**	**6.03**	**–5.97**	**1.46**
Sakishima Islands															
Miyako Island	11	4.72	–2.54	1.46	5	2.66	0.42	1.21	9	5.41	1.36	3.44	5.41	–2.54	2.12
Ishigaki Island	9	9.4	–2.54	5.39	13	7.04	–1.1	2.14	9	9.4	1.92	5.07	9.4	–1.1	4.03
Iriomote Island	5	8.4	–0.37	3.28	3	2.44	0.51	1.68	4	8.37	3.5	5.46	8.4	–0.37	3.93
Hateruma Island	3	3.3	2.48	2.83	2	1.81	1.4	1.61	8	4.45	2.09	3.48	4.45	1.4	3.04
Yonakuni Island	3	2.35	0.92	3.33	2	3.57	0.1	1.79	2	6.7	2.3	4.5	6.7	0.1	2.37
Subtotal	**31**	**9.4**	**–2.54**	**2.948**	**25**	**7.04**	**–1.1**	**1.817**	**32**	**9.4**	**1.36**	**4.879**	**9.4**	**–2.54**	**3.11**
Total	**113**	**9.4**	**–3.28**	**1.71**	**78**	**7.04**	**–5.97**	**1.54**	**103**	**9.4**	**–5.15**	**3.04**	**9.4**	**–5.97**	**2.112**

[a]Includes calcirudite.

Samples Collected from Okinawa Islands

The Okinawa Islands are located in the middle part of the Nansei Islands. A total of 119 beachrock samples were collected from 39 sites among 5 islands, namely, Okinawa Island (26°30′N, 128°00′E), Aguni Island (26°35′N, 127°14′E), Ie Island (26°43′N, 127°47′E), Zamami Island (26°13′N, 127°19′E), and Kume Island (26°20′N, 126°47′E). They consist of 42 calcarenite samples, 27 fossil coral samples, and 50 fossil shells (Table 1). An additional 7 dates (Ushikubo 2002) obtained from Izena Island (26°56′N, 127°56′E) were added to this paper. They consist of 3 calcarenites, 1 fossil coral, and 3 fossil shell samples.

The isotope fractionations of the 119 samples ranged between 6.03‰ and –5.97‰ (Table 2).

Samples Collected from Sakishima Islands

The Sakishima Islands are located in the southernmost part of the Nansei Islands. A total of 36 newly analyzed beachrock samples were added to the former report (Omoto 2001). A total of 88 beachrock samples were collected from Iriomote Island (24°20′N, 123°50′E), Ishigaki Island (24°24′N, 124°11′E), Miyako Island (24°27′N, 125°21′E), Yonakuni Island (24°27′N, 123°00′E), and Hateruma Island (24°03′N, 123°47′E). They consist of 31 calcarenite samples, 25 fossil coral samples, and 32 fossil shells (Table 1).

The isotope fractionations of the 88 samples ranged between 9.40‰ and –2.54‰ (Table 2).

DISCUSSION

Isotope Fractionations of Beachrock

Isotope fractionations of 294 beachrocks ranged between 9.40‰ and –5.97‰ (Table 2). The average value of isotope fractionation over the 15 Nansei Islands was 1.95‰. It is noticeable that the average values of isotope fractionations of 11 islands (191 samples) were outside the range of 0 ± 2‰ (Table 2). In the Amami Islands, the value of isotope fractionation decreases gradually from the southern Yoron Island (2.71‰) to the northern Amami Oshima Island (0.45‰).

The maximum and minimum values of isotope fractionation for calcarenite samples in the Nansei Islands were 9.40‰ and –3.28‰, respectively, while the average value was 1.71‰ (Table 2). The maximum and minimum values of isotope fractionation for coral samples were 7.04‰ and –5.97‰, respectively, and the average value was 1.54‰. In addition, the maximum, minimum, and average values of isotope fractionation for fossil shell samples were 9.40‰, –5.15‰, and 3.04‰, respectively (Table 2).

Figure 3 shows the relationship between ^{14}C ages and isotope fractionations of beachrocks collected from the Nansei Islands.

Formative Ages of Beachrocks

The sample materials used in ^{14}C dating are primarily marine carbonates and organisms. Marine organisms such as corals and shells embedded in the beach materials were carried from their original habitats to the intertidal zone by ocean waves, deposited on the beach, cemented by calcium carbonate and then became beachrock. Therefore, the age would indicate only the time of death of the marine organisms, not the formative age of the beachrock.

Kawana and Pirazzoli (1984) posited that the *Tridacna squamosa* (Lamarck) in the beachrocks collected from Miyako Island is not much older than the formation of the beachrocks themselves. The

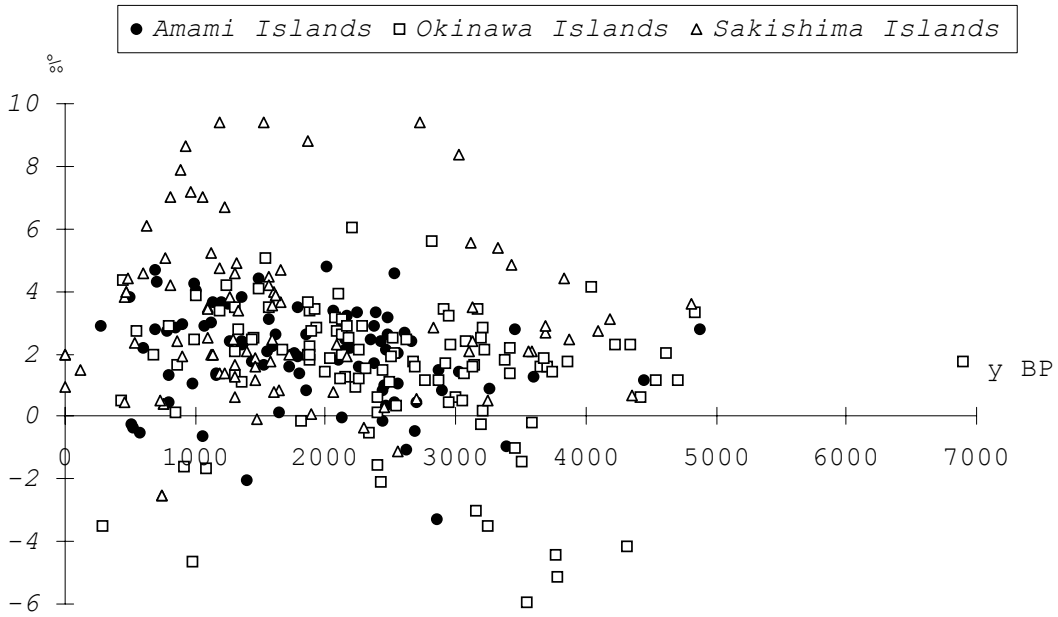

Figure 3 ^{14}C ages versus isotope fractionations of beachrocks collected from the Nansei Islands. Data were compiled from Omoto (1994–2004).

cemented strata of beachrocks have the same seaward slope as the nearby beach. The landward slabs are considered to have been formed earlier than the seaward slabs. Therefore, samples for ^{14}C datings were often collected from the landward slabs. When the seaward width of the beachrock exceeded 50 m, not only the top layer of the beachrock but also the middle and seaward specimens were collected to check the growth rate of the beachrock. Kawana and Pirazzoli (1984) reported that the seaward growth of beachrock was 4.2 cm/yr at Miyako Island. Omoto (1999c) measured the vertical growth rate of beachrock at Agui Island and recorded an average growth rate of 0.15 cm/yr. Based on these figures, beachrocks formed within a rather short timespan.

The author also tried to collect 3 different types of sample materials—fossil shell, fossil coral, and calcarenite (or calcirudite) samples—from each sampling site in order to compare their ages. Whenever the ^{14}C ages coincided within the range of the $\pm 3\ \sigma$ error, the author used whole data to estimate the age of beachrock formation. But the author excluded an age from the discussion when it differed greatly from other dates or outside the range of the $\pm 3\ \sigma$ error.

Whole ^{14}C dates of beachrock samples collected from the Nansei Islands are shown in Figure 4. According to the ^{14}C dates obtained from the Amami Islands, the beachrock began to form at about 4500 BP and the last formation was ~400 BP. The ages of beachrock formation differs according to the islands surveyed; however, beachrocks formed continuously between 3600 and 400 BP.

The ^{14}C age of 6890 ± 90 BP given to a calcarenite sample collected from Bise Point, west coast of Okinawa Island, was the oldest age among the 294 beachrock samples collected from the Nansei Islands (Omoto et al. 2003). The ^{14}C dates obtained indicate that beachrock from the Okinawa Islands began to form at ~6900 BP and the last formation was approximately 400 BP. The ages of beachrock formation differ by surveyed islands, but beachrocks in the Okinawa Islands were formed continuously between 4800 BP and ~400 BP.

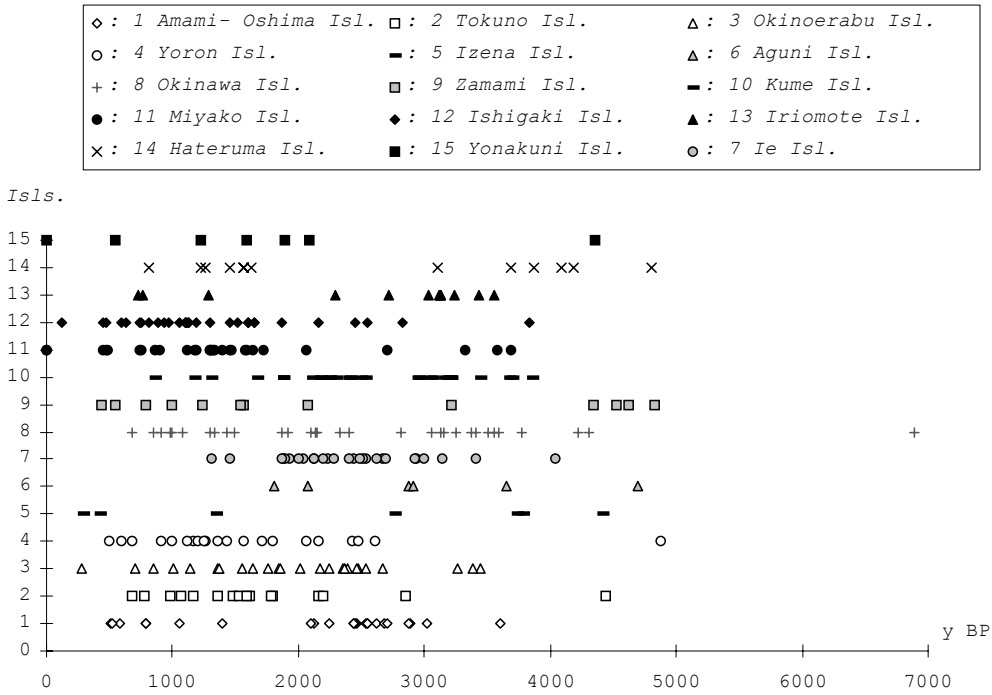

Figure 4 Correlation of ^{14}C ages of beachrocks collected from the Nansei Islands. Data were compiled from Omoto (1994–2004). The islands expressed with figures from 1 to 4, 5 to 10, and the figures from 11 to 15 belong to the Amami, Okinawa, and Sakishima Islands group, respectively.

The beachrocks began to form at 4800 BP in the Sakishima Islands, but there was an intermittent period after which beachrock formations have continued since 4300 BP.

In the Nansei Islands, beachrock began to form at about 6900 BP and is still forming now on some islands. Several time differences among the islands surveyed may be seen in Figure 4.

Late Holocene Sea-Level Change

The marine terrace surfaces that develop at several levels provide good evidence for the emergence of an island. In the Nansei Islands, other researchers have reported on the distribution, elevations, formative ages, Holocene sea level, and tectonic movements of Tokuno Island, Okinoerabu Island, Okinawa Island, Aguni Island, Ie Island, Kume Island, Miyako Island, Hateruma Island, and Yonakuni Island (Koba et al. 1982; Koba 1983; Kawana and Pirazzoli 1984; Kawana 1985; Kan et al. 1991; and others). However, marine terrace surfaces develop poorly in Amami Oshima Island, Zamami Island, Ishigaki Island, and Iriomote Island. The former islands indicate that they have been under active tectonic movements, while the later islands were under a rather stable or submerged environment at least through the Holocene period. Numerous geomorphologists and geologists have reported on the neotectonic movements in the Nansei Islands (Konishi et al. 1974; Nakata et al. 1979; Ota and Hori 1980; Ota et al. 1982; Kawana 1985; Ota and Omura 1992; and others). The results were compiled and summarized recently by Machida et al. (2001).

Beachrock is believed to have formed within the intertidal zone, and is, therefore, a good indication of the past sea level. By using the ^{14}C age and elevation of beachrock, it is possible to reconstruct

past sea-level change. Almost all of the beachrocks observed in the surveyed area were situated within a range corresponding to the present intertidal zone (about ±1 m). But in several islands such as Okinoerabu Island, the west coast of Okinawa Island, Ie Island, the southeast coast of Kume Island, and Hateruma Island, beachrocks were obvious on a higher place above the present high tide level. These facts indicate that the islands have been uplifted by local tectonic movements (Omoto 1999c, 1999d, 2000c, 2003a, 2003b; Omoto et al. 2003), otherwise these beachrocks were formed in a different environment.

The latter cause may be explained as follows: Beach materials were influenced by freshwater or underground water, the calcium carbonate of which cemented the soft beach materials and then formed beachrock (Omoto 2000c, 2003a).

Figure 5 shows the relationship between ^{14}C dates and elevations of whole beachrock samples collected from the Nansei Islands. The sea level seems higher than the present sea level, but we must consider the amount of tide change reaching 1 m.

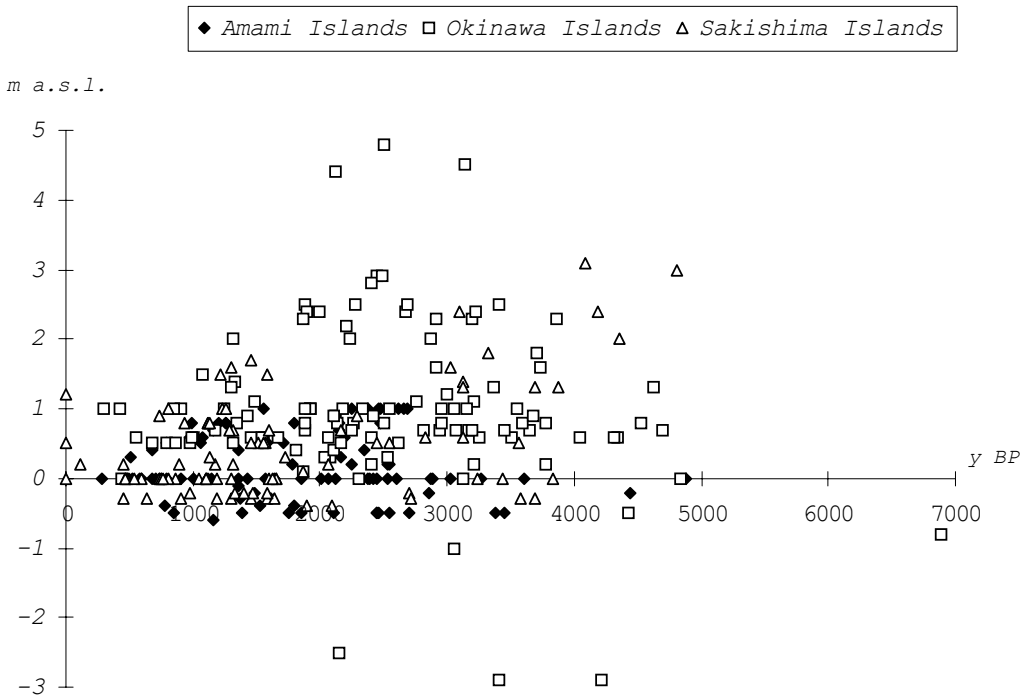

Figure 5 ^{14}C ages versus elevations of beachrocks collected from the Nansei Islands. Data were compiled from Omoto (1994–2004).

Based on these pieces of evidence, the past sea level that existed was similar to the present one; that is, it has maintained nearly the same level since at least 5000 BP, except for several uplifted coasts.

Origin of Calcium Carbonate Cemented Beachrock

Since Russel (1962 and 1963) suggested the origin of calcium carbonate came from underground water, many scientists have tried to identify the origin of the calcium carbonate that cemented beach sediments and formed beachrock. Yet, no one has succeeded in obtaining indisputable evidence in

spite of carrying out several experiments and analyses (Yonetani 1964, 1966; Takenaga 1965; Hori et al. 1972, 1973; Stoddart and Cann 1965). The author proposes that the isotope fractionation of beachrock may give us a key to solving the problem. That is, if the calcium carbonate originates in seawater, it must indicate nearly the same value of marine organisms. If it differs from the average value of marine organisms, then the origin of calcium carbonate is underground water or freshwater. Therefore, the figure of isotope fractionation is a key in solving the origin of calcium carbonates.

The average value of isotope fractionation ($\delta^{13}C$) of marine organisms and carbonates has been reported by Vogel and Ehhalt (1963), Stuiver and Polach (1977), Geyh and Schleicher (1990), and Stuiver and Braziunas (1993). Geyh and Schleicher (1990) reported that the value was within the range of 0 ± 2‰. Although the average isotope fractionation of beachrock samples collected from the Nansei Islands was 1.95‰, the average isotope fractionations of 11 islands were outside the range of 0 ± 2‰ (upper limitation of marine organisms and biocabonate). In addition, the maximum value of isotope fractionations ($\delta^{13}C$) showed +9.40‰ (Table 2). The values for the figure are 4 times larger than those reported by the above authors.

The author considers that the materials making up the beachrocks were obviously affected by different origins of calcium carbonate provided when they were cemented in the intertidal zone. One of the pieces of evidence is the influence of freshwater and underground water. The author often observed that the sand beaches where beachrocks developed were eroded by several streams and spring water flows at low tide level. Further evidence is the existence of submarine limestone caves along the islands. The caves were formed when the sea level dropped during the last glaciations. In such caves, running water flowed down and became underground water. When the waters reached the saltwater area, upwelling might have occurred. Thus, they influenced the growth of marine inhabitants nearby. However, the author needs further evidence to demonstrate the relationship as to the cause of higher isotope fractionation.

SUMMARY

A total of 294 beachrock samples were collected from 116 sites on 15 islands in the Nansei Islands chain (Table 1). The samples were ^{14}C dated and their isotope fractionations were measured (Table 2). The result of this study is summarized as following:

1. Isotope fractionation ($\delta^{13}C$) of all beachrock samples range between +9.40‰ and –5.97‰, with an average of 1.95‰.
2. Figures for isotope fractionation decrease from the southern Sakishima Islands to the middle Okinawa Islands. In Amami Islands, the decrease is gradual from the southern Yoron Island towards the northern Amami Oshima Island.
3. Among 11 islands, the average value of isotope fractionation was outside the range of 0 ± 2‰. This fact suggests that when beachrock was being formed, beach sediments were influenced by an obviously different origin of calcium carbonate, from underground water or freshwater.
4. In the Nansei Islands, beachrocks were formed within the range of the intertidal zone between approximately 6900 BP and the present day. However, several time differences in the formative period of beachrocks exist among the islands surveyed.
5. In the tectonically stable islands, there is no evidence indicating prominent upheaval throughout the late Holocene. Therefore, the elevations and ^{14}C ages of the beachrock samples in those islands would indicate past sea level change. Judging from the evidence, the late Holocene sea level has remained similar to the present one since at least the past 5000 BP, except for several uplifted coasts.

ACKNOWLEDGEMENTS

Sincere thanks go to Professor Motoharu Koba of Kansai University, who identified coral samples. Professor Toshio Kawana of Ryukyu University provided the author with useful comments on the beachrocks. I also thank Miss Wakana Koreeda, who helped with chemical assays. I am grateful to Dr Gordon Cook, SUERC, Scotland; and Prof William D Patterson, Department of English Literature, College of Humanities and Sciences, Nihon University, for their useful suggestions and improvements on the manuscript. Field surveys, ^{14}C dating, and analyses of isotope fractionations were supported by a Scientific Grant in Aid from Nihon University.

REFERENCES

Geyh MA, Schleicher H. 1990. *Absolute Age Determination.* New York: Springer-Verlag. 503 p.

Hori N, Araki T, Terai M, Horiuchi K. 1972. Mechanism of beachrock formation and its geomorphic significance. *Proceedings of the General Meeting of the Association of Japanese Geographers*. p 51–2. In Japanese.

Hori N, Horiuchi K, Araki T, Terai M. 1973. Development of beachrock and its cause: an example of Yoron Island. *Proceedings of the General Meeting of the Association of Japanese Geographers*. p 16–7. In Japanese.

Kan H, Takahashi T, Koba M. 1991. Morpho-dynamics on Holocene reef accretion: drilling results from Nishimezaki Reef, Kume Islands, the central Ryukyus. *Geographical Review of Japan* 64(Series B)2:114–31.

Kawana T. 1981. Radiocarbon ages of the beach rocks on Okinawa, Miyako and Ishigaki Islands, the Ryukyus, Japan. *Bulletin of College of Education, University of the Ryukyus* 25:245–9.

Kawana T, Pirazzoli PA. 1984. Late Holocene shorelines and sea level in Miyako Island, the Ryukyus, Japan. *Geographical Review of Japan* 57(Series B):135–41. In Japanese.

Kawana T, Pirazzoli PA. 1985. Holocene coastline changes and seismic uplift in Okinawa Island, the Ryukyus, Japan. *Zeitschrift für Geomorphologie* Supplement Bd. 57:11–31.

Kawana T. 1985. Holocene sea-level changes and seismic crustal movements in a marginal coral reef area: the central and south Ryukyu Islands (Japan). In: Hopley D, Pirazzoli P, editors. *Proceedings of the Fifth International Coral Reef Congress*. Tahiti, Papeete Antenne Museum-EPHE, Moreea, French Polynesia 3:205–10.

Kawana T. 1988. Geomorphology of the Ryukyus. In: *Series of the Nature of Okinawa*. Naha, Okinawa: Sinsei Tosyo Syuppan Press. 127 p. In Japanese.

Koba M, Nakata T, Takahashi T. 1982. Late Holocene eustatic sea-level changes deduced from geomorphological features and their ^{14}C dates in the Ryukyu Islands, Japan. *Palaeogeography, Palaeoclimatology and Palaeoecology* 39:231–60.

Koba M. 1983. Late Holocene relative sea-level changes and crustal deformation in the Ryukyu Island, Japan. *Gekkan Chikyu* 5(12):722–33. In Japanese.

Konishi K, Omura A, Nakamachi O. 1974. Radiometric coral ages and sea-level records from the late Quaternary reef complex of the Ryukyu Islands. In: *Proceedings of the Second International Coral Reef Symposium 2.* Brisbane, Australia. Brisbane: Great Barrier Reef Committee p 595–613.

Machida H, Ota Y, Kawana T, Moriwaki H, Nagaoka S, editors. 2001. *Regional Geomorphology of the Japanese Islands, Volume 7, Geomorphology of Kyushu and the Ryukyus.* Tokyo: University of Tokyo Press. p 219–325.

Nakata T, Takahashi T, Koba M. 1978. Holocene emerged coral reefs and sea-level changes in the Ryukyu Islands. *Geographical Review of Japan* 51(2): 87–108.

Nakata T, Koba M, Wharyong JO, Imaizumi T, Matsumoto H, Suganuma T. 1979. Holocene marine terraces and seismic crustal movement. *Science Reports of the Tohoku University, 7th series (Geography)* 29(2):195–204.

Omoto K. 1976. Tohoku University radiocarbon measurements V. *Science Reports of the Tohoku University 7th Series (Geography)* 26(1):135–57.

Omoto K, Nakata T, Koba M. 1976. Tohoku University radiocarbon measurements V. *Science Reports of the Tohoku University 7th Series (Geography)* 26(2):29–310.

Omoto K. 1994. Radiocarbon ages of beachrock samples collected from Hateruma Island, Nansei Islands, southwest of Japan. *Annals of the Geography The Chiri Shiso* 35(2):69–71. In Japanese.

Omoto K. 1995a. Radiocarbon ages of beachrock samples collected from Miyako Island, southwest of Japan. *Annals of the Geography The Chiri Shiso* 36(2): 18–20. In Japanese.

Omoto K. 1995b. Radiocarbon dating reports of Nihon University No. 4. *Proceedings of the Institute of Natural Sciences Nihon University* 31:13–37. In Japanese.

Omoto K. 1997a. Radiocarbon ages of beachrock samples collected from Tarama Islamd, Sakishima Islands, southwest of Japan. *Quarterly Journal of Geography* 49(1):60. In Japanese.

Omoto K. 1997b. Radiocarbon ages of beachrock sam-

ples collected from Kuroshima, Sakishima Islands, southwest of Japan. *Annals of the Geography The Chiri Shiso* 39(1):24–32. In Japanese.

Omoto K. 1998a. Radiocarbon dating reports of Nihon University No.5. *Proceedings of the Institute of Natural Sciences Nihon University* 33:1–41. In Japanese.

Omoto K. 1998b. Radiocarbon ages of beachrock and fossil coral samples collected from the east of Kume Island, Ohha Island and Hatenohama, Nansei Islands, Japan. *Quarterly Journal of Geography* 50(1):85–6. In Japanese.

Omoto K. 1998c. Radiocarbon dates of beachrock samples collected from Ie Island, Okinawa prefecture, Japan: Especially on the beachrocks collected from limestone cave of Nyaty Gama. *Proceedings of the Annual Meeting of The Japanese Coral Reef Society.* p 46. In Japanese.

Omoto K. 1998d. Formative age of beachrock samples collected from southern part of Nansei Islands, southwest of Japan. *Quarterly Journal of Geography* 50(3): 221–2. In Japanese.

Omoto K. 1999a. Radiocarbon ages of beachrock samples collected from Zamami Island, Kerama Islands chain, Japan. *Quarterly Journal of Geography* 51(1): 56–7. In Japanese.

Omoto K. 1999b. Radiocarbon ages of beachrock and fossil coral samples collected from Aguni Island, southwestern part of Japan—Chronological view on the Late Holocene sea-level change of Aguni Island. *Annals of The Geography The Chiri Shiso* 40(2):15–28. In Japanese.

Omoto K. 1999c. Radiocarbon ages of beachrock samples collected from Yoron Island, Nansei Islands, southwest of Japan. *Quarterly Journal of Geography* 51(3):237–8. In Japanese.

Omoto K. 1999d. Radiocarbon dates of beachrock samples collected from Miyako Island, southern Ryukyu Islands. *Proceedings of the Annual Meeting of The Japanese Coral Reef Society.* p 17. In Japanese.

Omoto K. 1999e. Radiocarbon ages of beachrock samples collected from Okinoerabu Island, southwest of Japan. *Proceedings of the General Meeting of the Association of Japanese Geographers* 56:104–5. In Japanese.

Omoto K. 2000a. Radiocarbon ages of beachrock samples collected from Tokunoshima Island, southwest of Japan. *Annals of the Geography The Chiri Shiso* 41(1–2):15–30. In Japanese.

Omoto K. 2000b. Radiocarbon dating reports of Nihon University No.7. *Proceedings of the Institute of Natural Sciences Nihon University* 35:35–81. In Japanese.

Omoto K. 2000c. Radiocarbon ages of beachrock samples collected from Iriomote Island, southwest of Japan (A preliminary report). *Annals of the Geography The Chiri Shiso* 42(1):17–30. In Japanese.

Omoto K. 2000d. Radiocarbon ages of beachrock samples collected from northern part of Amamiohshima Island, southwest of Japan. *Proceedings of the General Meeting of the Association of Japanese Geographers* 58:62–3. In Japanese.

Omoto K. 2001a. Radiocarbon dating reports of Nihon University No.8. *Proceedings of the Institute of Natural Sciences Nihon University* 36:22–45. In Japanese.

Omoto K. 2001b. Radiocarbon age correction for beachrock samples based on isotope fractionations (A preliminary report). *Quarterly Journal of Geography* 53(3):192–3. In Japanese.

Omoto K. 2001c. Radiocarbon ages of beachrocks and Late Holocene sea-level changes in the southern part of the Nansei Islands, southwest of Japan. *Radiocarbon* 43(2):887–98.

Omoto K. 2002. Corrections of radiocarbon ages of beachrock samples based on $\delta^{13}C$ values—A case study of beachrock samples collected from Yorn Island, Okinoerabu Island, Tokunoshima Island and Amami Oshima Island: (A preliminary report). *Proceedings of the General Meeting of the Association of Japanese Geographers* 62:131. In Japanese.

Omoto K. 2003a. Radiocarbon ages and $\delta^{13}C$ values of beachrock samples collected from Yonakuni Island and Hateruma Island, southwestern part of Nansei Islands, southwest of Japan. *Proceedings of The Institute of Natural Sciences Nihon University* 38:1–17. In Japanese.

Omoto K, Chigono S, Kanno K. 2003. Radiocarbon ages and $\delta^{13}C$ values of beachrock samples collected from west coast of Okinawa Island. *Proceedings of the General Meeting of the Association of Japanese Geographers* 64:125. In Japanese.

Omoto K. 2003b. Radiocarbon ages and $\delta^{13}C$ values of beachrock samples collected from Ishigaki Island, southwest of Nansei Islands, southwest of Japan. In: *Preprint for Annual Meeting of The Japanese Coral Reef Society.* p 37. In Japanese.

Omoto K. 2004. Radiocarbon ages and $\delta^{13}C$ values of beachrock samples collected from Kume Island, Oh Island and Hateno-hama (beach), west of Okinawa Island. *Proceedings of the Institute of Natural Sciences Nihon University* 39:15–31.

Ota Y, Machida H, Hori N, Konishi K, Omura A. 1978. Holocene raised coral reefs of Kikai-Island (Ryukyu Islands): an approach to Holocene sea-level study. *Geographical Review of Japan* 51(2):109–30.

Ota Y, Hori N. 1980. Late Quaternary tectonic movement of the Ryukyu Islands, Japan. *Daiyonki Kenkyu (The Japanese Quaternary Research)* 18:221–40. In Japanese.

Ota Y, Hori N, Omura A. 1982. Age and deformation of marine terraces of Hateruma Island, Ryukyu Islands, southwestern Japan. *Abstract of XI INQUA Congress, Moscow* 2:232.

Ota Y, Pirazzoli PA, Kawana T, Moriwaki H. 1985. Late Holocene coastal morphology and sea level records on three small islands, the south Ryukyus, Japan. *Geographical Review of Japan* 58 (Series B)2:185–94.

Ota Y, Omura A. 1992. Contrasting styles and rates of tectonic uplift of coral reef terraces in the Ryukyu and Daito Islands, southwestern Japan. *Quaternary International* 15/16:17–29.

Russel RJ. 1962. Origin of beach rock. *Zeitschrift für Geomorphologie Neue Folge Supplementbände* 6:1–16.

Russel RJ. 1963. Beach rock. *The Journal of Tropical Geography* 17:24–7.

Stoddart DR, Cann JR. 1965. Nature and origin of beach rock. *Journal of Sedimentary and Petrology* 35:243–7.

Stuiver M, Polach HA. 1977. Discussion reporting of ^{14}C data. *Radiocarbon* 19(3):355–63.

Stuiver M, Braziunas TF. 1993. Modeling atmospheric ^{14}C influences and ^{14}C ages of marine samples to 10,000 BC. *Radiocarbon* 35(1):137–89.

Takahashi T, Koba M. 1980. Age of beachrock along the coast of Japan. *Geological Studies of the Ryukyu Islands* 5:125–31. In Japanese.

Takenaga K. 1965. Beach rock and lagoon on Yoron Island, Ryukyu Archipelago. *Geographical Review of Japan (Chirihaku-Hyouron)* 38(12):739–55. In Japanese.

Tanaka Y. 1986. Distribution and ages of beachrock in Japanese Islands. *Hyogo Chiri* 31:16–30. In Japanese.

Tanaka Y. 1990. A sand beach changed into stone beach beachrock. In: *Atsui Shizen* (Hot Physical Environment) *Coral Reef and its Environment*. p 137–151. In Japanese.

Ushikubo R. 2002.*Coastal geomorphology of Izena Island (Island)* [Graduate thesis]. Nihon: Nihon University. 50 p.

Vogel JC, Ehhalt D. 1963. The use of the carbon isotopes in groundwater studies. In: *Proceedings of the Symposium on the Application of Radioisotopes in Hydrology.* Tokyo, Japan. Vienna: IAEA. p 383–95.

Yonetani S. 1963. A preliminary study on beach rock in northern part of Amami Oshima. *Geographical Review of Japan (Chirigaku Hyouron)* 36(9):519–27. In Japanese.

Yonetani S. 1964. The beach rock on the south-west of Japan. *The Bunka Hokoku, Shigaku-hen, Kagoshima University* 12:83–94. In Japanese.

Yonetani S. 1966. The beach rock and its analogous landforms. *Geographical Review of Japan (Chirigaku Hyouron)* 39(4):240–50. In Japanese.

RADIOCARBON, Vol 46, Nr 2, 2004, p 551–566

PAIRED ^{14}C AND $^{230}Th/U$ DATING OF SURFACE CORALS FROM THE MARQUESAS AND VANUATU (SUB-EQUATORIAL PACIFIC) IN THE 3000 TO 15,000 CAL YR INTERVAL

Martine Paterne[1,2] • Linda K Ayliffe[1,3] • Maurice Arnold[1,4] • Guy Cabioch[5] • Nadine Tisnérat-Laborde[1] • Christine Hatté[1] • Eric Douville[1] • Edouard Bard[6]

ABSTRACT. Paired radiocarbon and $^{230}Th/U$ dating was performed on 13 surface corals from submerged reefs in the Marquesas and from raised terraces in Vanuatu. The absolute ages of the corals analyzed ranged from 3000 to 15,000 cal yr. Estimates of the difference between the absolute and ^{14}C ages of these corals are in agreement with previous determinations up until 11,500 cal yr. The resulting mean sea surface reservoir age *R* is determined at 390 ± 60 yr for the Marquesas region (9°S), which is slightly higher than the *R* value at 280 ± 50 yr for the Tahiti Islands (18°S). Multiple ^{14}C analyses of 2 corals from the Marquesas present scattered ^{14}C ages at ~12,000 and ~15,100 cal yr. This could be attributed to rapid changes of the ^{14}C content of surface waters around the Marquesas Islands or to a subtle submarine diagenesis.

INTRODUCTION

Radiocarbon and/or $^{230}Th/U$ dating of surface corals have mainly been used to quantify the timing and amplitude of sea-level fluctuations, and also to estimate the deviation between the ^{14}C and calendar ($^{230}Th/U$) ages. Superimposed on the long-term ^{14}C variation over the past 40,000 cal BP (Stuiver et al. 1998; Edwards et al. 1993; Bard et al. 1990a, 1993, 1998; Voelker et al. 1993; Burr et al. 1998; Hughen et al. 1998, 2000; Kitagawa and van der Plicht 1998, 2000; Beck et al. 2000), short-term fluctuations have been recorded in both terrestrial and marine materials and are considered to be linked to changes of solar activity and of the global carbon cycle (Stuiver et al. 1998). In the marine environment, the modern oceanic circulation controls mixing of "old" waters from the deep ocean with surface ocean waters. This leads to latitudinal variations of the sea surface reservoir ages, *R* (Bard 1988). As the oceanic circulation has changed in the past, so have the *R* values at mid- to high latitudes (Bard et al. 1994; Sikes et al. 2000; Siani et al. 2001). Modern surface corals record seasonal to centennial ^{14}C changes of some 20–40‰, related to both the atmospheric ^{14}C and oceanic circulation changes (Druffel 1997; Burr et al. 1998; Guilderson and Schrag 1998). Substantial local intra-ocean variations in *R* were also recently suggested at similar latitudes for the Pacific Ocean (in Stuiver et al. 1998; Goslar et al. 2002).

We present here the results of coupled ^{14}C and $^{230}Th/U$ dating of surface corals, collected from raised terraces from Vanuatu (Cabioch and Ayliffe 2000) and from submerged reefs around the Marquesas Islands (Figure 1). The absolute ages obtained for these corals by $^{230}Th/U$ dating ranged from 3000 to ~15,000 cal yr. The difference between the absolute and ^{14}C ages of these corals are compared to those found in previous studies (Figure 2) (Stuiver et al. 1998; Bard et al. 1990a, 1993, 1998; Edwards et al. 1993; Burr et al. 1998; Hughen et al. 1998, 2000). *R* estimates from the Marquesas and Tahiti are directly compared in the time interval of 9000–11,000 cal yr.

[1]Laboratoire des Sciences du Climat et de l'Environnement, Domaine du CNRS, Avenue de la Terrasse, F-91198 Gif sur Yvette, France.
[2]Corresponding author. Email: Martine.Paterne@lsce.cnrs-gif.fr.
[3]Present address: Department of Geology and Geophysics, University of Utah, Salt Lake City, Utah 84112, USA.
[4]Unité Mixte de Service UMS 2572, CEA Saclay, F-91198 Gif sur Yvette, France.
[5]IRD (Institut de Recherche pour le Développement), B.P. A5, 98848 Nouméa cedex, New Caledonia.
[6]CEREGE, Université d'Aix-Marseille III, CNRS UMR-6635, Europôle de l'Arbois, BP80, 13545 Aix-en-Provence cdx4, France.

Proceedings of the 18th International Radiocarbon Conference, edited by N Beavan Athfield and R J Sparks
RADIOCARBON, Vol 46, Nr 2, 2004, p 551–566

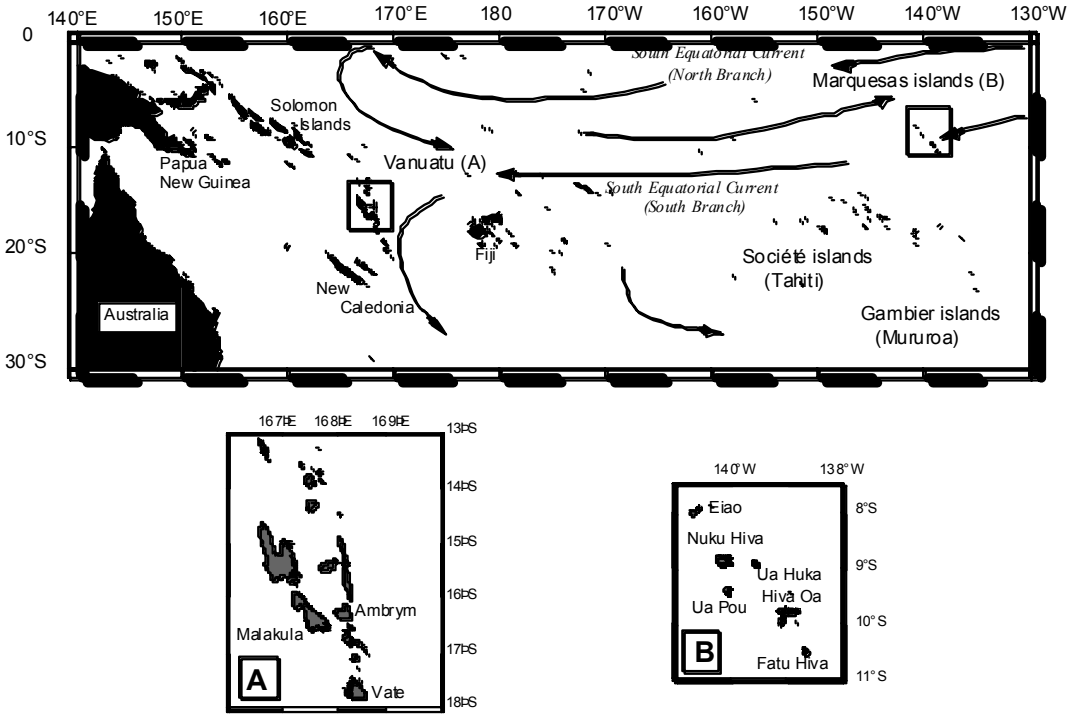

Figure 1 Sample locations; surface currents are also represented

MATERIAL AND METHODS

The surface corals (*Porites sp.*) were collected in the Marquesas Islands (6°S; 140°W) by dredging of submerged coral reefs in water depths greater than 86 m during the cruise conducted by the IRD in 1997 (Musorstom and Paleomarq), and in Vanuatu (20°S; 170°E) by direct sampling of emerged marine terraces raised by tectonic uplift (Figure 1). The corals from the Marquesas have been submerged in seawater since the time of their formation and have as a result most likely been preserved from major recrystallization/dissolution processes.

Coral specimens were cut into small slabs with cross-sectional areas between 4–6 cm^2 and thickness of ~0.1 to 0.2 cm. The shortest axis of these slabs were oriented parallel to the direction of growth. Growth bands were visible and continuous in the corals sampled. The slabs cut from each specimen probably represent some 1 to 15 yr in time, given the range of possible growth rates documented by Priess (1997) of ~2 to 40 mm per yr for the *Porites* species. Each coral slab was then subsampled for X-ray diffractometry (XRD), ^{14}C, and $^{230}Th/U$ analyses. Coral samples having a magnesian calcite or pure calcite content lower than 2% were selected for dating with 1 exception (Table 1).

$^{230}Th/U$ Dating

The U/Th age determination follows the procedure by Cabioch and Ayliffe (2000). Exterior surfaces of corals samples were initially cleaned by physical abrasion with a dental drill bit. The coral samples were then further cleaned by ultrasound treatment and several rinses with quartz distilled (QD) water. U and Th fractions were extracted and purified from coral samples using standard ion exchange chemistry as described by Stirling et al. (1995). The purified U and Th separates were loaded onto zone-refined Re filaments between 2 layers of colloidal graphite. Isotopes of U and Th

Table 1 $^{230}Th/U$ and ^{14}C ages on surface corals from the Marquesas and Vanuatu. Columns referred to (1) the AMS ^{14}C laboratory code GifA, (2) the dredge code (and water depth in m) for Marquesas corals and the altitude in m relative to sea level for Vanuatu corals (Cabioch and Ayliffe 2000), and (3) coral code and the number of measured Fe-C targets. The ^{14}C ages are expressed in conventional ages and are not corrected for reservoir ages. ^{14}C ages for samples 17b marked by * and $ were used to calculate the weighted mean and error similarly noted. The underlined χ^2 values are larger than the $P_{0.95}$ values (3.841 n = 2; 5.991 for n = 3; 7.815 n = 4). The $\Delta^{14}C = (A_{sample}/A_{calendar\ age} - 1) \times 1000$ correspond to the marine values and the atmospheric $\Delta^{14}C$ values in parentheses are calculated using the reservoir age correction of 400 yr.

(1)	(2)	(3)	U conc (ppm)	2 σ	$\delta^{234}U_{initial}$	2 σ	[230/232]	2 σ	$^{230}Th/U$ cal yr	2 σ (yr)	^{14}C age (BP)	2 σ (yr)	^{14}C age* (BP)	2 σ (yr)	χ^2	$\Delta^{14}C$ (‰)	2 σ (‰)	R (yr)	2 σ (yr)	Aragonite %
Marquesas																				
100449	DW1281c	78a 1	3.895	0.002	146.4	2.6	2330	30	3230	30	3420	100				–35 (15)	13	390	110	99.2
100450	DR1261 (850 m)	68a 1	3.984	0.003	145.5	2.4	4770	40	3260	30	3480	100				–38 (11)	13	420	110	98.7
100451	DW1281d	79a 1	2.992	0.002	146.6	2.3	7720	40	9450	70	8750	180				56 (110)	25	360	190	98
100435	DW1281	09b 1	3.139	0.002	147.0	2.2	4920	20	10,230	70	9520	260	9500	110	0.430	57 (111)	17	410	260	100
100452	(450–455 m)	09b 1									9460	160						350	170	
100737		09b 1									9540	200						430	200	
100453	DW1281a	76a 2	3.205	0.002	145.9	2.4	8120	60	10,320	80	9530	140	9590	115	1.940	57 (111)	18	340	150	97.8
100738		76a 1									9700	200						510	210	
100454	DW1281b	77a 2	3.108	0.002	144.7	2.7	7400	30	10,940	80	9960	140	9950	115	0.060	88 (143)	19	370	150	96.3
100739		77a 1									9930	200						340	210	
100455	DW1281	75a 2	3.362	0.002	144.1	2.7	14,330	90	11,470	90	10,600	140	10,540	100	1.725	78 (134)	18	570	150	98
100740		75a 2									10,470	140						440	150	
100456	DR1183(2)	81a 1	3.533	0.002	141.8	2.4	370	2	11,990	90	11,220	220			<u>10.377</u>	55 (109)	31			100
100741	(86–120 m)	81a 2									10,800	140				111 (168)	23			

Table 1 ^{230}Th/U and ^{14}C ages on surface corals from the Marquesas and Vanuatu. Columns referred to (1) the AMS ^{14}C laboratory code GifA, (2) the dredge code (and water depth in m) for Marquesas corals and the altitude in m relatively to sea level for Vanuatu corals (Cabioch and Ayliffe 2000), and (3) coral code and the number of measured Fe-C targets. The ^{14}C ages are expressed in conventional ages and are not corrected for reservoir ages. ^{14}C ages for samples 17b marked by * and $ were used to calculate the weighted mean and error similarly noted. The underlined χ^2 values are larger than the $P_{0.95}$ values (3.841 n = 2; 5.991 for n = 3; 7.815 n = 4). The $\Delta^{14}C = (A_{sample}/A_{calendar\ age} - 1) \times 1000$ correspond to the marine values and the atmospheric Δ^{14}C values in parentheses are calculated using the reservoir age correction of 400 yr. *(Continued)*

(1)	(2)	(3)	U conc (ppm)	2 σ	$\delta^{234}U_{initial}$	2 σ	[230/232]	2 σ	^{230}Th/U cal yr	2 σ (yr)	^{14}C age (BP)	2 σ (yr)	^{14}C age* (BP)	2 σ (yr)	χ^2	Δ^{14}C (‰)	2 σ (‰)	R (yr)	2 σ (yr)	Aragonite %
Marquesas																				
100437	DR1183	17b 2	3.429	0.001	143.7	2.1	2570	20	15,050	120	12,830*	180			29.166					100
100457		17b 2									13,410$	200								
100742		17b 1									13,560$	260	12,920*	150	3.364	236 (298)	25			
100743		17b 1									13,120*	260	13,470$	160	0.836	155 (214)	24			
100458	DR1183(1)	80a 1	3.653	0.003	143.7	2.6	2980	20	15,100	120	13,360	240			13.086	178 (238)	36			98.8
100744		80a 1									12,720	260				276 (341)	42			
Vanuatu																				
100434	13	15a 1	2.360	0.001	149.8	2.2	1750	10	6400	60	6000	160				28 (93)	22	385	165	100
100471	6	74a 2	2.938	0.002	143.5	2.8	18,730	90	8390	70	8060	140	8020	91	0.5765	17 (81)	15	415	95	100
100771		74a 2									7990	120								
100472	15	73a 2	2.945	0.002	147.7	2.4	920	10	8500	60	8010	120				32 (97)	17	270	130	100

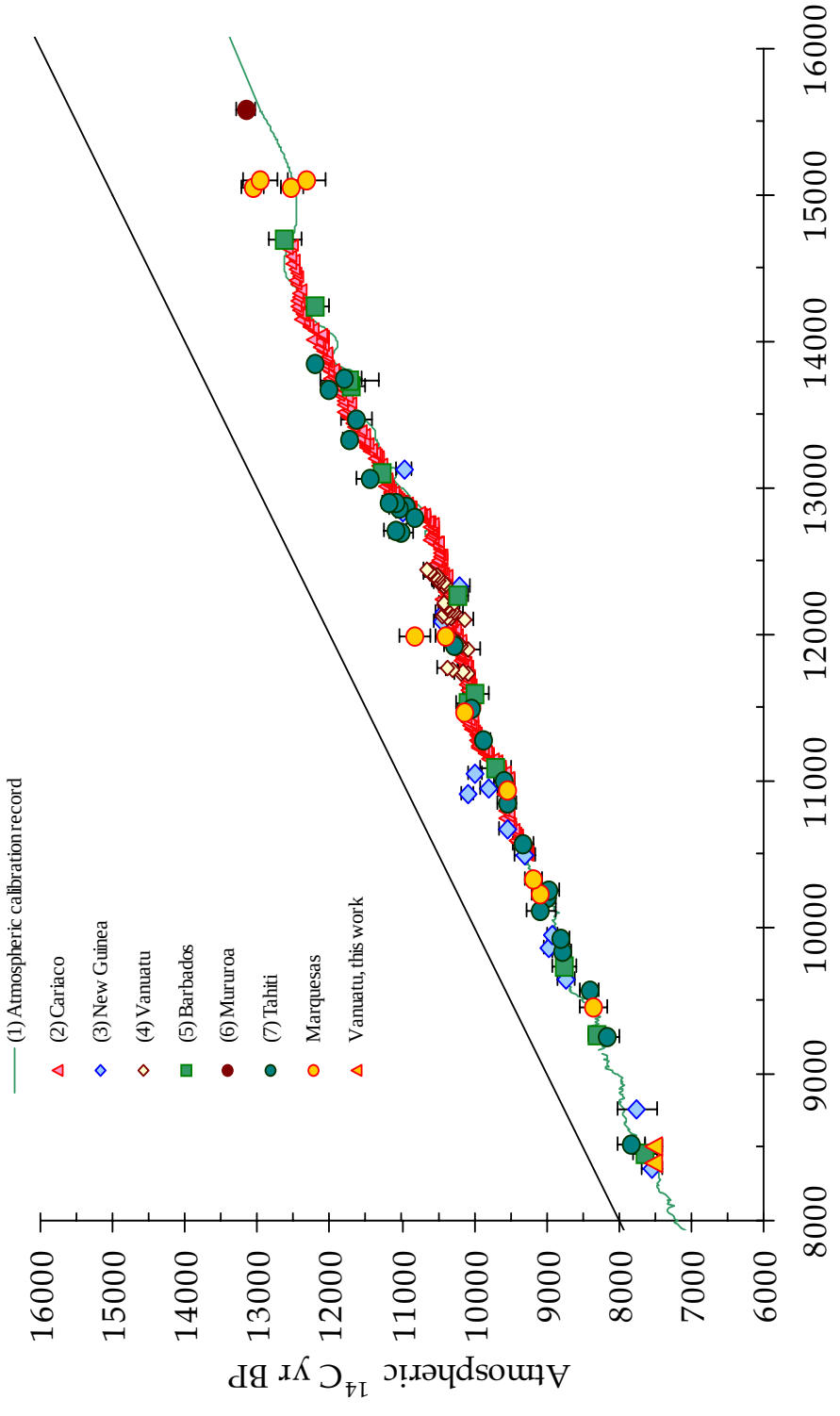

Figure 2 Atmospheric ^{14}C ages (error bars at 2 σ) as a function of calendar ages (error bars not represented). Calendar ages refer to $^{230}Th/U$ dating. (1) Stuiver et al 1998; (2) Hughen et al. 2000; (3) Edwards et al. 1993; (4) Burr et al. 1998; (5, 6, 7) Bard et al. 1993, 1998. The ^{14}C ages of the Marquesas and Vanuatu corals were corrected for a reservoir age of 400 yr.

were measured with a Finnigan MAT 262 solid-source mass spectrometer using a peak jumping routine with a secondary electron multiplier. Repeated analyses of the uraninite standard HU-1 containing ^{238}U, ^{234}U, and ^{230}Th in radioactive equilibrium yielded an average [$^{234}U/^{238}U$] activity ratio of 1.0015 ± 0.0032 (N = 9) (= $^{234}U/^{238}U$ atomic ratio of $54.98 \pm 0.18 \times 10^{-6}$) and a [$^{230}Th/^{238}U$] activity ratio of 1.0004 ± 0.0044 (N = 9). Decay constants used in the age calculations were $\lambda^{230}Th = 9.1954 \times 10^{-6} \pm 7.19 \times 10^{-8}$ yr^{-1} and $\lambda^{234}U = .8349 \times 10^{-6} \pm 5.7 \times 10^{-9}$ yr^{-1}. The reported $^{234}U/^{238}U$ and $^{230}Th/^{232}Th$ activity ratios of all the dated corals were corrected for machine biases by normalization to the corresponding ratios determined for HU-1.

^{14}C Dating

Secondary crystallization in skeleton pores of corals or surface contaminants are usually eliminated by strong acid or stepwise leaching procedures (Bard et al. 1990b; Burr et al. 1992; Yokoyama et al. 2000). Such procedures are time consuming due to the partial dissolution of the sample in several aliquots and then accordingly to the increase of the number of ^{14}C measurements to check cleaning efficacy (Burr et al. 1992; Yokoyama et al. 2000). In this study, coral samples (~20 mg in size) were first pre-cleaned by sand blasting until the elimination of micrite forms around skeleton pores (Figure 3), which can be carefully controlled under a microscope. Under this procedure, coral samples lose between 20–60% of their initial weight. Next, the abraded coral sample is rinsed and ultrasonically cleaned and then crushed in an agate mortar. About 10 mg of the fine powder is then immediately introduced into 1 side of a reaction vessel with 2 side arms. The coral powder is then leached in a 2-cm^3 solution of HNO_3 (0.01N) for 15 min and then rinsed to neutral pH. The second arm of the reactor is then filled with 1 cm^3 of H_3PO_4 and the vessel containing the wet powder is immediately attached to the vacuum line and evacuated as suggested by Schleicher et al. 1998. After hydrolysis of the coral powder by reaction with the H_3PO_4 *in vacuuo*, the evolved CO_2 is trapped into an ampoule. The CO_2 is then reduced into graphite according to the procedure of Arnold et al. (1989).

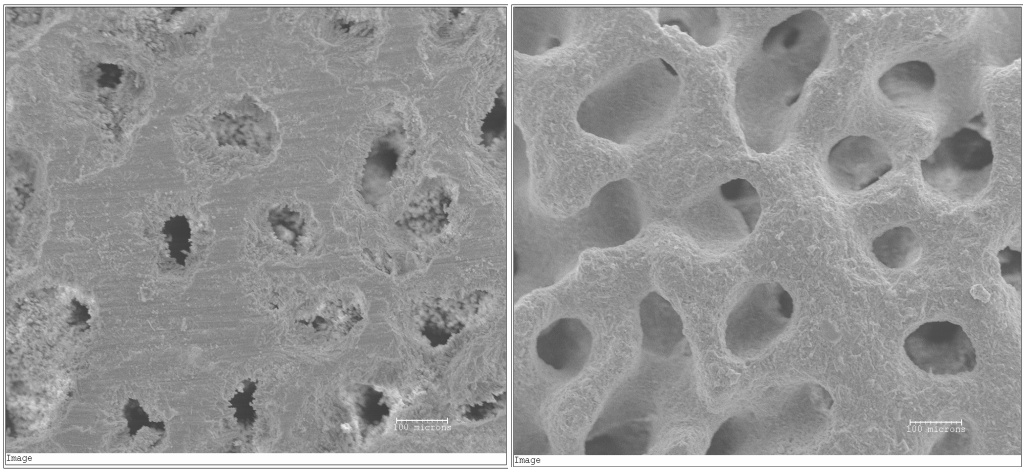

Figure 3 Scanning electron microprobe photographs of coral DR 1183 (17b) before (left) and after (right) cleaning. The sample on the right corresponds to an adjacent piece of coral treated for ^{14}C dating.

Two sub-samples were randomly picked from different parts of each coral slab and prepared independently. Given the range of growth rates observed for *Porites sp.* corals (Priest 1997), it is quite likely that the 2 sub-samples taken from each coral specimen grew during different seasons or years. Two targets of Fe-C powder were made from each graphite preparation in order to increase the pre-

cision of the ^{14}C ages by accelerator mass spectrometry (AMS) at the Gif-sur-Yvette Tandétron facility (Arnold et al. 1987).

RESULTS AND DISCUSSION

Evaluation of Cleaning Procedure of Corals

The efficacy of our cleaning procedure was initially assessed through ^{14}C analyses of old corals (Table 2). In addition, we also proceeded to new ^{14}C dating of corals from Tahiti and Mururoa, previously dated by Bard et al. (1993, 1996, 1998) (Table 3).

Blank values were assessed from 3 corals from Mururoa (Bard et al. 1993), Vanuatu (Cabioch and Ayliffe 2000), and the Marquesas, determined by $^{230}Th/U$ dating to be beyond the limit of the ^{14}C dating method (Table 2). Although the mean and standard deviation obtained for the corals from the Marquesas and Vanuatu (0.21 ± 0.05 pMC: apparent age: 49,350 ± 1900 BP) are slightly higher than those obtained for 1 coral (Irene 30) from Mururoa (0.16 ± 0.02 pMC; apparent age: 51,800 ± 1050 BP), they are nevertheless statistically indistinguishable from one another. The mean and standard deviation for the old ^{14}C-depleted corals using this cleaning procedure are 0.20 ± 0.05 pMC (apparent age 50,100 ± 2070 BP) and are similar to slightly lower than those previously measured (Bard et al. 1990b; Burr et al. 1992; Yokoyama et al. 2000). The AIEA-C1 marble, currently used to assess the full procedural blank of the AMS ^{14}C dating method of our laboratory, has a value of 0.08 ± 0.02 pMC (n = 7; apparent age 57,280 ± 2000 BP). As for the old ^{14}C-depleted foraminifera reported by Schleicher et al. (1998) and Nadeau et al. (2001), the mean blank value of the old corals is larger than that of the geological C1 marble, which is thus inappropriate for ^{14}C age calculation of young biological materials.

Corals from Tahiti and Mururoa, previously dated between 11,000 and 17,000 cal yr (Bard et al. 1990, 1993, 1998), were subjected to our new cleaning procedure and also to that previously introduced by Bard et al. (1990b), which involved a strong HCl leach (Table 3). The χ^2 tests for the ^{14}C ages obtained using the previous and new cleaning procedures suggest no significant differences (at the 95% confidence level) between any of them. Therefore, it appears that our new cleaning treatment is as efficient as the previous one for removing surface contaminants from such corals.

Comparison of the Marine Reservoir *R* Ages from the Tahiti and Marquesas Corals in the Time Interval 9000–11,000 cal yr

The ^{14}C and absolute ages of the coral sub-samples are reported in Table 1. By subtraction of the ^{14}C ages of the corals from Vanuatu and Marquesas from the corresponding atmospheric ^{14}C ages documented in the INTCAL98 tree-ring record, we estimate a reservoir age of ~400 yr for the surface of the central Pacific Ocean prior to 9000 cal yr (Table 1). Using a similar approach between 9000 to 11,000 cal yr, we determine a weighted mean *R* value of 390 ± 60 yr (weighted 2 σ error; n = 8) for the Marquesas corals, which is close to the mean global ocean value (Stuiver et al. 1998) (Figure 4). For the same time period, a slightly lower *R* of 280 ± 50 yr (weighted mean and 2 σ error; n = 8) is determined from the Tahiti corals. This small difference, as previously observed (Stuiver et al. 1998; Bard et al. 1998; Goslar et al. 2000), may be attributed to the location of these islands with respect to the Pacific surface water currents. While the Tahiti Islands are located in the well-ventilated South Pacific gyre, the Marquesas Islands are situated within the South Equatorial westward drift (Figure 1). The likely more extensive vertical mixing of surface waters with underlying ^{14}C-depleted waters due to the Eastern Tradewinds in this region may account for the slightly older Marquesas *R* value.

Table 2 Fraction of modern carbon determined from 3 old ^{14}C-depleted surface corals: Irène 30 (Favidae) from Mururoa (Bard et al. 1993); Marquesas (CP1262: Porites); Vanuatu (undetermined) (Cabioch and Ayliffe 2000). Sample GifA100489 underwent a strong HCl (0.5N) leach. The blank values for these old corals do not show any obvious relationship with species, location, and time of preparation.

Lab code GifA	Dredge	Coral code	Date of preparation	C µg	pMC	1 σ (%)	Apparent age (BP)	1 σ (yr)	$^{230}Th/U$ cal yr	1 σ (yr)	Site
100443		Ir30	26/6	680	0.20	0.03	50,020	1100	259,000*	6000	Mururoa
100445			27/6	1350	0.17	0.03	51,400	1230			Mururoa
100489*			28/9	2000	0.15	0.02	52,470	1340			Mururoa
100499			2/10	2130	0.16	0.02	51,920	1230			Mururoa
100500			9/10	1790	0.15	0.02	52,470	1350			Mururoa
100768			24/11	1150	0.16	0.02	51,920	1230			Mururoa
100769			24/11	1240	0.14	0.02	53,070	1250			Mururoa
100469	CP1262(1)	83a	7/7	1420	0.22	0.03	49,220	1080	63,860	260	Marquesas
100469			7/7	1420	0.17	0.02	51,400	1190			Marquesas
100470	CP1262(2)	14a	10/7	1810	0.25	0.03	48,140	990	64,410	260	Marquesas
100470			10/7	1810	0.25	0.03	48,140	870			Marquesas
100756		83a	14/11	1540	0.27	0.04	47,500	1040			Marquesas
100757		14a	21/11	1700	0.23	0.03	48,840	990			Marquesas
100473	np11 (+59)	44a	3/7	1384	0.26	0.03	47,820	970	66,980	290	Vanuatu
100473			3/7	1384	0.29	0.03	46,910	870			Vanuatu
100764		44a	23/11	1450	0.22	0.03	49,220	970			Vanuatu
100764		44a	23/11	1450	0.20	0.03	50,020	1080			Vanuatu
100474	Mallicolo	13a	3/7	1494	0.10	0.02	55,180	1490	107,580	540	Vanuatu
100474	(204 m) d		3/7	1494	0.17	0.02	51,400	1130			Vanuatu
100765		13a	16/11	1930	0.20	0.03	50,020	1080			Vanuatu
100764		44a	23/11	1450	0.22	0.03	49,220	970			Vanuatu
100766	Espiegle(1)	45a	24/11	1860	0.17	0.02	51,400	1150	121,270	580	Vanuatu
			Mururoa		0.16	0.02	51,840	1040			
			Marquesas		0.23	0.04	48,780	1260			
			Vanuatu		0.20	0.06	49,810	2320			
			Total		**0.20**	**0.05**	**50,100**	**2070**			

Table 3 Comparison of the ^{14}C ages of corals, obtained from different pre-cleaning procedures; M = mechanical sand blasting. The ^{14}C ages are given in conventional yr BP uncorrected for the reservoir age. Samples noted by an asterisk were published in Bard et al. 1998. All samples have a carbon content higher than 500 µg, except sample GifA100494* (340 µg). The χ^2 values for $P_{0.95}$ are 3.841 for n = 2; 5.991 for n = 3; and 7.815 for n = 4.

Sample code	Lab code GifA	Nr of targets	$^{230}Th/U$ (cal yr)	2 σ (yr)	^{14}C age (BP)	2 σ (yr)	^{14}C age (weighted mean)	2 σ (yr)	χ^2 test	Comment
P7-8	95647*	2	11,280	30	10,100	140	10,160	90	1.293	HCl
P7-8	100480	2			10,200	160				HCl
P7-8	100490	2			10,210	180				M
P7-9	95648*	2	11,495	30	10,280	140	10,330	100	1.542	HCl
P7-9	100481	2			10,300	320				HCl
P7-9	100491	2			10,410	160				M
P7-11	95649*	2	12,875	40	11,130	140	11,230	90	5.215	HCl
P7-11	100482	2			11,240	160				HCl
P7-11	100492	2			11,390	180				M
P7-12	95650*	2	12,800	30	11,100	160	11,130	90	5.448	HCl
P7-12	100483	2			11,270	160				HCl
P7-12	100493	2			11,010	160				M
P8-1	95654*	1	12,905	30	11,510	220	11,480	90	2.942	HCl
P8-1	96092*	2			11,540	140				HCl
P8-1	100487	2			11,350	180				HCl
P8-1	100497	2			115,00	180				M
P8-2	95653*	2	13,335	30	11,970	160	12,030	80	4.209	HCl
P8-2	96091*	2			12,000	140				HCl
P8-2	100486	2			12,190	180				HCl
P8-2	100496	2			11,980	180				M
P8-3	95652*	2	13,665	35	12,250	160	12,260	90	3.113	HCl
P8-3	96090*	2			12,350	140				HCl
P8-3	100485	2			12,170	180				HCl
P8-3	100495	1			12,180	240				M
P8-4	95651*	2	13,850	35	12,570	160	12,490	90	6.202	HCl
P8-4	96087*	2			12,560	140				HCl
P8-4	100484	2			12,350	200				HCl
P8-4	100494	1			12,280*	280				M
Mu-8-30-315	95656*	2	17,170	40	14,860	180	14,790	120	1.274	HCl
Mu-8-30-315	100488	1			14,690	280				HCl
Mu-8-30-315	100498	1			14,750	200				M

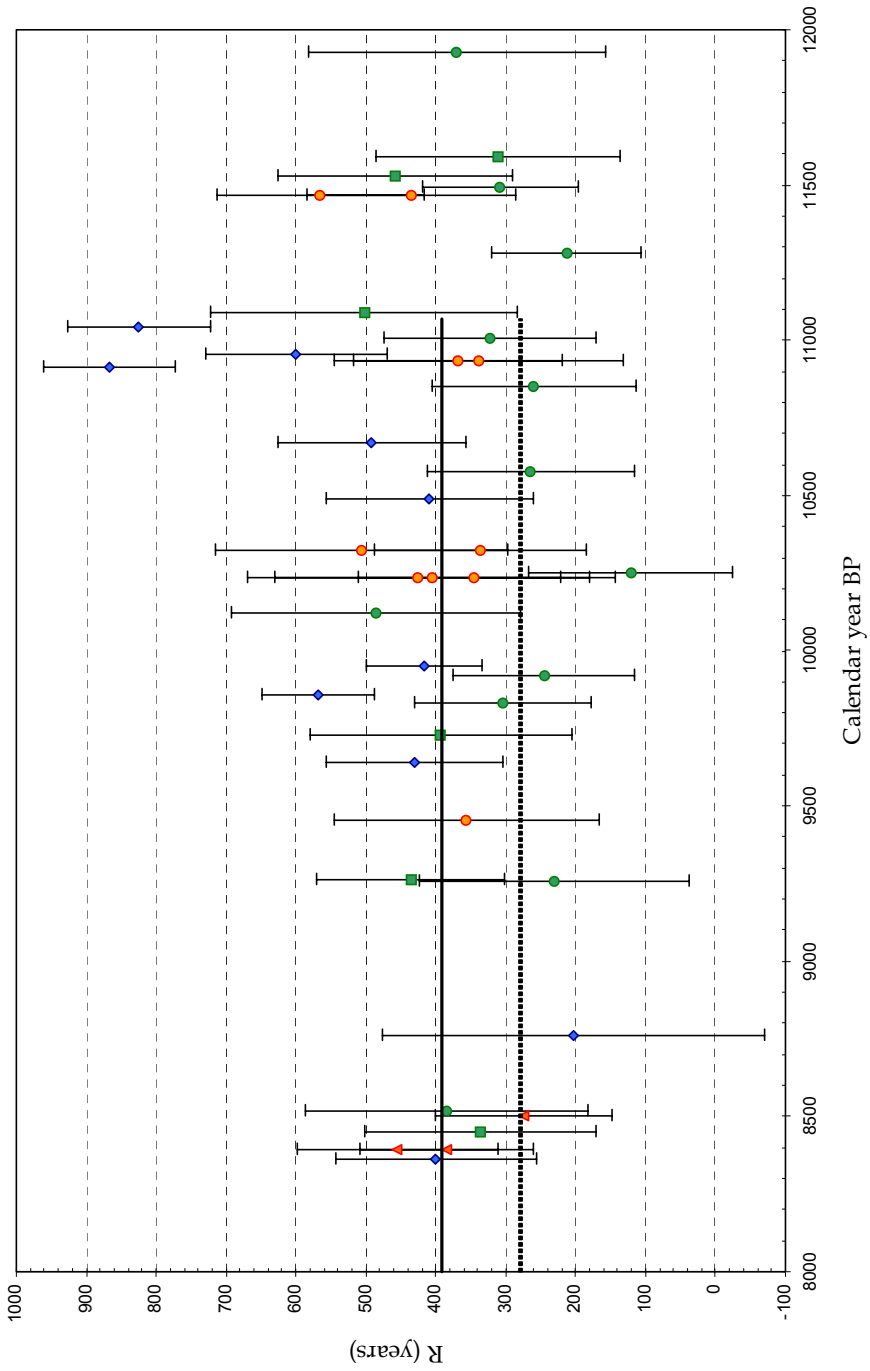

Figure 4 Sea surface reservoir ages (difference between coral and atmospheric ^{14}C ages [Stuiver at al. 1998] of similar calendar ages). Black and dotted lines correspond to the weighted mean *R* value of the Marquesas and Tahiti corals. Same references as Figure 2.

Comparison of the ^{14}C Ages and $\Delta^{14}C$ Values from the Marquesas and Vanuatu with Previous Marine and Atmospheric ^{14}C Record

Between 3000 cal yr and 11,500 cal yr, the ^{14}C ages are very reproducible within each coral (Table 1). Using an *R* value of 400 yr, the estimates of the difference between the absolute and ^{14}C ages are in agreement with previous determinations (Stuiver et al. 1998; Burr et al. 1998; Edwards et al. 1993; Bard et al. 1993, 1998) (Figures 2, 5, 6). Beyond 11,500 cal yr, 2 corals dated at 12,000 and ~15,100 cal yr, however, present scattered ^{14}C values.

The 2 sub-samples of coral specimen DR1183(2) dated at 12,000 cal yr gave significantly different ^{14}C ages at the 95% confidence level (Table 1), with the marine or atmospheric $\Delta^{14}C$ values of these 2 sub-samples varying by some 50‰. Two slabs from a single coral specimen (DR 1183 and DR 1183[1]) were dated each at ~15,100 cal yr by the $^{230}Th/U$ method and were sub-sampled for the ^{14}C dating (Figure 7). While the 2 $^{230}Th/U$ dates are very similar, the ^{14}C dates by contrast are highly scattered (Figures 2, 5, 6; Table 1). The ^{14}C ages of the sub-samples within each slab present the same range of variations from approximately 12,800 to ~13,400 yr, corresponding to marine $\Delta^{14}C$ values of 250 ± 35‰ to 160 ± 55‰ (2 σ), respectively. They are all within error (2 σ) of the marine and atmospheric INTCAL98 values (Stuiver et al. 1998) (Figures 5, 6). Only the upper $\Delta^{14}C$ values at ~310‰, corresponding to the youngest ^{14}C ages, are consistent with those of the atmospheric ^{14}C record from Lake Suigetsu (Kitagawa and van der Plicht 2000) (Figures 2, 4, 5). Similarly, at 12,000 cal yr, only the largest $\Delta^{14}C$ value (Figures 5, 6) agrees well with those of the ^{14}C INTCAL98 calibration record (Stuiver et al. 1998) and with those from the Lake Suigetsu ^{14}C record (Kitagawa and van der Plicht 2000). Therefore, the addition of modern carbon either during the different steps of AMS ^{14}C dating procedure and/or during recrystallization processes with seawater seems unlikely. This is also attested by the very low content of magnesian (Mg) calcite in the corals. The initial $^{234}U/^{238}U$ ratios of all the corals analyzed are very similar to that of sub-modern corals at ~145‰ (in Delanghe et al. 2002) and within ±5‰ of the modern seawater values (Henderson et al. 1999; Delanghe et al. 2002) (Table 1). The detrital Th contents are very low. Thus, little post-depositional alteration or recrystallization of the primary coralline aragonite has taken place. In-situ dissolution processes alone may also be ruled out, as the U concentrations of these 2 corals, DR1183(2) and DR1183(1)/DR1183, are among the largest of the measured ones (Table 1). Therefore, the $^{230}Th/U$ dates may be considered as most likely valid.

The anomalous ^{14}C data at ~12,000 and ~15,000 cal yr would be the low $\Delta^{14}C$ values, and thus the old ^{14}C ages when compared to the determined atmospheric ones from Lake Suigetsu (Kitagawa and van der Plicht 2000) (Figures 2, 6). This may be related to a subtle submarine diagenesis, which would include here dissolution of old carbonates and secondary Mg-calcite precipitation. Due to organic matter degradation, coral pore waters have a lower pH than that of open reef waters (Enmar et al. 2000) that may favor dissolution of carbonates. Secondary precipitation of aragonite and/or Mg-calcite micrites or needles of some 10 μm often fill voids in skeleton pores of sub-marine fossil corals (Enmar et al. 2000) (Figure 3). A 10% result in weight of secondary crystallization deriving from old ^{14}C-depleted carbonates would account for the anomalously old ^{14}C ages at 15,100 cal yr and 5% at 12,000 cal yr. Such a parallel contamination by "old" marine uranium with $^{234}U/^{238}U$ activity of 1.1, close to the value found in last interglacial corals at the time of deposition, would lead to a slight decrease of the $\delta^{234}U_{initial}$ from the value of 149 to ~144‰. This may explain the slightly lower $\delta^{234}U_{initial}$ values of these 2 corals with respect to those of the other corals, although the difference is not significant at the 95% confidence level (Table 1). However, this represents a very extreme case, and in the marine environment, the diagenetic changes in corals with recrystallization and secondary aragonite or Mg-calcite precipitation within seawater are usually related to increasing $\delta^{234}U_{initial}$ values (Bar-Matthews et al. 1993).

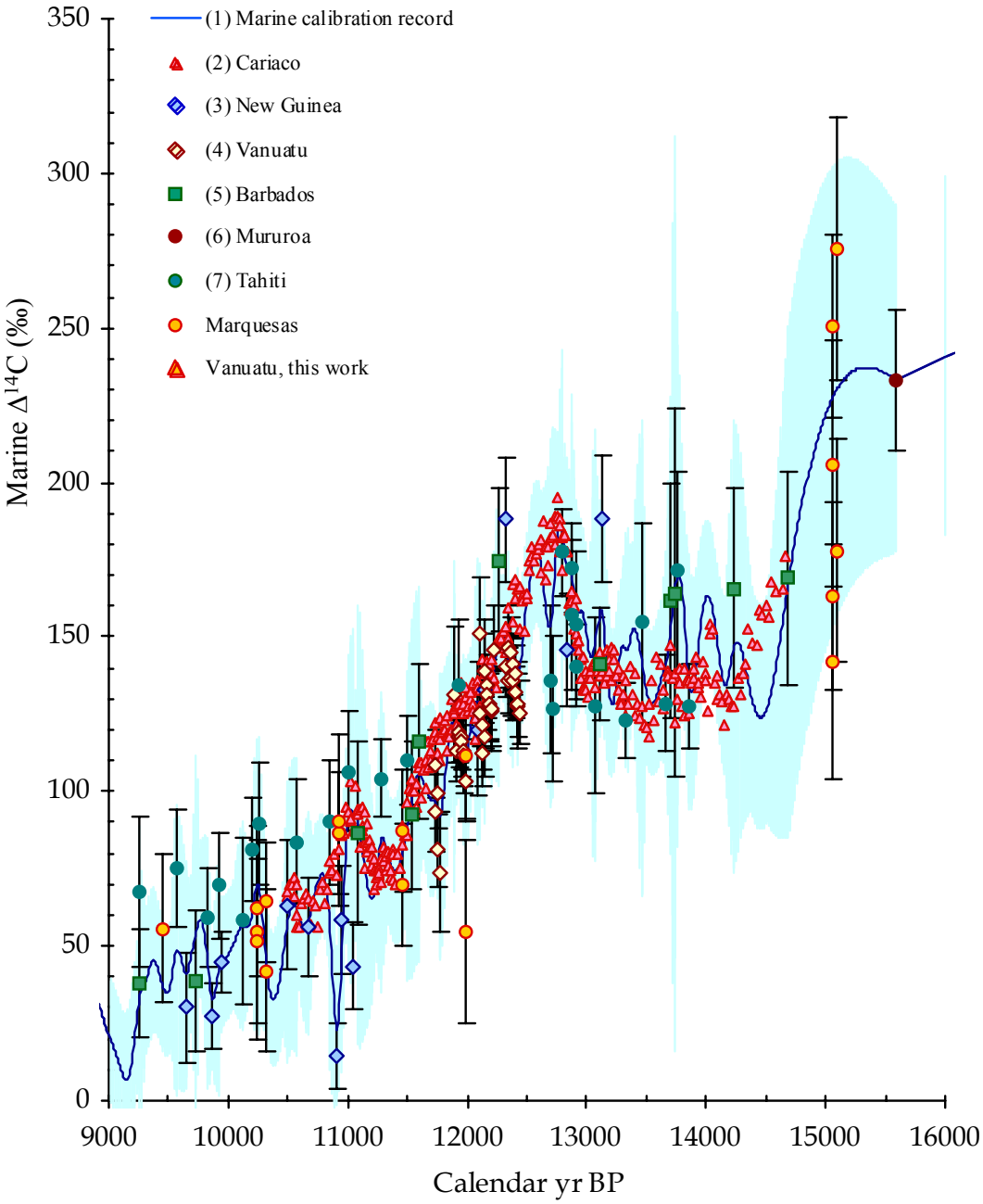

Figure 5 Marine $\Delta^{14}C$ changes at the 2-σ confidence level as a function of calendar ages. The blue envelope figured out the 2-σ error of the marine INTCAL98 $\Delta^{14}C$ values. (1) Stuiver et al 1998; (2) Hughen et al. 2000; (3) Edwards et al. 1993; (4) Burr et al. 1998; (5, 6, 7) Bard et al. 1993, 1998. Same references as Figure 2.

The corals dated at ~12,000 and ~15,100 cal yr were sampled in the same dredge (DR1183: 8°45.5′S; 140°03.8′W) and would reflect local and brief changes of the seawater chemical composition in the vicinity of Marquesas. Seasonal to annual variability of ^{14}C ages, which can be

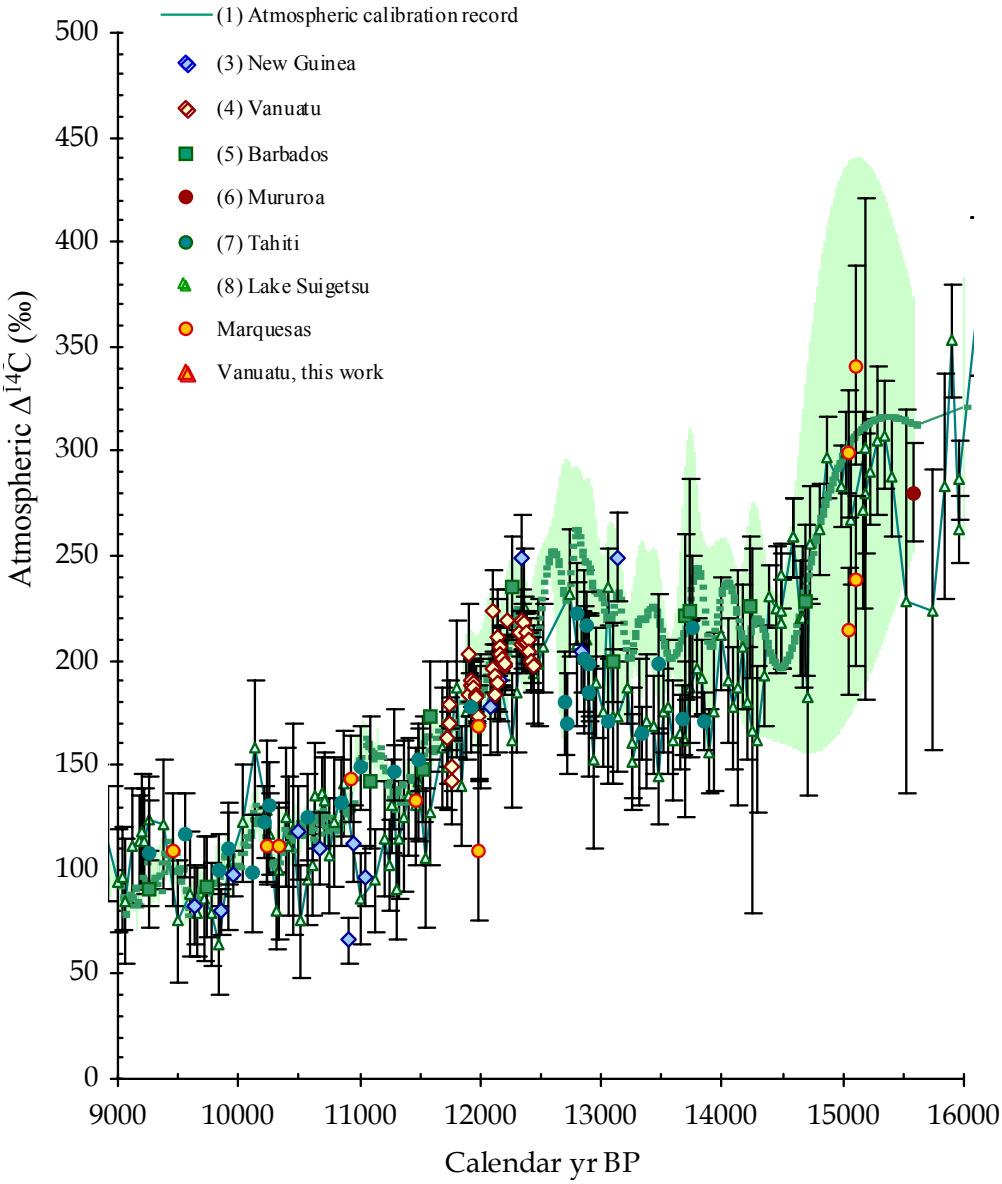

Figure 6 Atmospheric $\Delta^{14}C$ changes at the 2-σ confidence level as a function of calendar ages. The green envelope figured out the 2-σ error of the atmospheric INTCAL98 $\Delta^{14}C$ values. (8) Lake Suigetsu record (Kitagawa and van der Plicht 2000). Same references as Figure 2.

approached from our random sampling, was observed in modern banded coral samples from the Pacific Ocean (Brown et al. 1993; Druffel and Griffin 1993; Guilderson and Schrag 2001). Such variability was attributed to changes in the extent and intensity of the equatorial Pacific upwelling. However, this natural ^{14}C variability did not exceed 10–15‰ (Druffel and Griffin 1993), which is significantly lower than the $\Delta^{14}C$ changes we observed in the fossil Marquesas corals. Thus, causes of the variation of the ^{14}C ages in these corals remain a puzzling question.

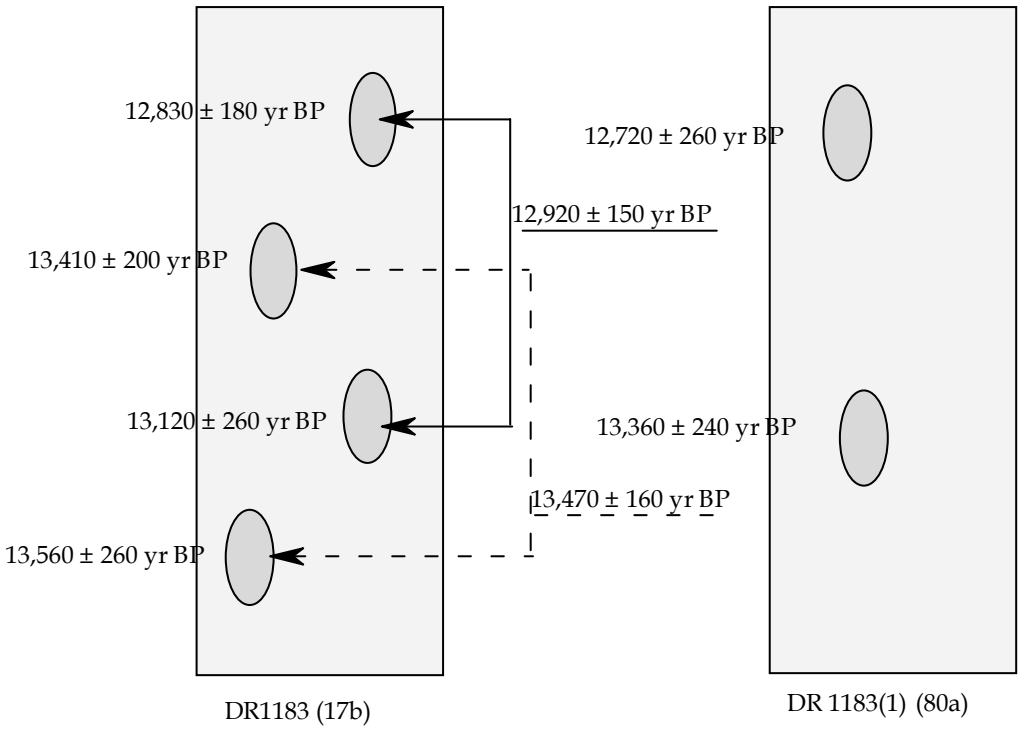

Figure 7 Sketch of 2 slabs, DR1183 and DR1183(1), of the same coral which was sub-sampled for AMS ^{14}C dating. The weighted mean of the ^{14}C ages and the weighted 2 σ from DR1183 (Table 1) are underlined.

CONCLUSION

Paired ^{14}C and $^{230}Th/U$ dating of corals from the Marquesas and Vanuatu provide additional estimates of the difference between the absolute and ^{14}C ages of marine biogenic materials. These estimates are in agreement with those determined in previous studies between 3000 and 11,500 cal yr (Edwards et al. 1993; Stuiver et al. 1998; Bard et al. 1990a, 1993, 1998; Burr et al. 1998; Hughen et al. 2000; Kitagawa and van der Plicht 2000). Over this time interval, the reservoir age of the surface waters from the Marquesas differ by 100 yr from *R* values of corals from Tahiti. This is compatible with previous suggestions that variations of *R* exist in the Pacific Ocean (Stuiver et al. 1998; Goslar et al. 2002).

Among all the corals analyzed, 2 of them from the Marquesas dated at ~12,000 and ~15,000 cal yr present scattered ^{14}C ages during the period of coral growth. Such variability may be related to rapid changes of the ^{14}C content of the surface waters around the Marquesas or to a subtle submarine diagenesis. Additional coupled ^{14}C and $^{230}Th/U$ dating of corals from the Pacific should refine our knowledge of the extent and magnitude of these rapid changes in surface ^{14}C in this region, and will be important in understanding the underlying mechanism responsible for such fluctuations.

ACKNOWLEDGEMENTS

We acknowledge M Fontugne, L Turpin, JL Reyss, N Frank, and E Michel for helpful comments and S Bondevik for his helpful review. This work received the financial support of the Commissariat à l'Energie Atomique and of the Centre National de la Recherche Scientifique, and partly from the

INSU- Eclipse program. L Ayliffe received financial support from the CNRS and the CEA. We wish to thank the captain, R Proner, and the crew of the R/V IRD *Alis* for their efficiency during the cruise in Marquesas. Our thanks are extended to S Caquineau and H Boucher (IRD Bondy) for X-ray diffractometry analysis. This is LSCE contribution 1100.

REFERENCES

Arnold M, Bard E, Maurice P, Duplessy JC. 1987. C-14 dating with the Gif sur Yvette Tandetron accelerator: status report. *Nuclear Instruments and Methods in Physics Research B* 29:120–3.

Arnold M, Bard E, Maurice P, Valladas H, Duplessy JC. 1989. ^{14}C dating with the Gif-sur-Yvette Tandetron accelerator: status report and study of isotopic fractionation in the sputter ion source. *Radiocarbon* 31(3): 284–91.

Bard E. 1988. Correction of accelerator mass spectrometry ^{14}C ages measured in planktonic foraminifera: paleoceanographic implications. *Paleoceanography* 3: 635–45.

Bard E, Arnold M, Fairbanks RG, Hamelin B. 1990a. Calibration of the ^{14}C timescale over the past 30,000 years using mass spectrometric U-Th ages from Barbados corals. *Nature* 345:405–10.

Bard E, Hamelin B, Fairbanks RG, Zindler A, Arnold M, Mathieu G. 1990b. U/Th and ^{14}C ages of corals from Barbados and their use for calibrating the ^{14}C timescale beyond 9000 years BP. *Nuclear Instruments and Methods in Physics Research B* 52:461–8.

Bard E, Arnold M, Fairbanks RG, Hamelin B. 1993. ^{230}Th-^{234}U and ^{14}C ages obtained by mass spectrometry on corals. *Radiocarbon* 35(1):191–9.

Bard E, Arnold M, Mangerud J, Paterne M, Labeyrie L, Duprat J, Mélières M, Sonstegaard E, Duplessy JC. 1994. The North Atlantic atmosphere-sea surface ^{14}C gradient during the Younger Dryas climatic event. *Earth and Planetary Science Letters* 126:275–87.

Bard E, Arnold M, Hamelin B, Tisnerat-Laborde N, Cabioch G. 1998. Radiocarbon calibration by means of mass spectrometric $^{230}Th/^{234}U$ and ^{14}C ages of corals: an updated database including samples from Barbados, Mururoa and Tahiti. *Radiocarbon* 40:1085–92.

Bar-Matthews M, Wasserburg GJ, Chen JH. 1993. Diagenesis of fossil coral skeletons: correlation between trace elements, textures and $^{234}U/^{238}U$. *Geochemica et Cosmochimica Acta* 57:257–76.

Beck JW, Richards DA, Edwards RL, Silverman BW, Smart PL, Donahue DJ, Hererra-Osterheld S, Burr GS, Calsoyas L, Jull AJT, Biddulph D. 2001. Extremely large variations of atmospheric ^{14}C concentration during the Last Glacial period. *Science* 292:2453–7.

Burr GS, Edwards RL, Donahue DJ, Druffel ERM, Taylor FW. 1992. Mass spectrometric ^{14}C and U-Th measurements in coral. *Radiocarbon* 34(3):611–8.

Burr GS, Beck WJ, Taylor FW, Recy J, Edwards LR, Cabioch G, Corrège T, Donahue DJ, O'Malley JM. 1998. A high-resolution radiocarbon calibration between 11,700 and 12,400 calendar years BP derived from ^{230}Th ages of corals from Espiritu Santo island, Vanuatu. *Radiocarbon* 40(3):1093–1105.

Cabioch G, Ayliffe LK. 2001. Raised coral terraces at Malakula, Vanuatu, southwest Pacific, indicate high sea level during marine isotope stage 3. *Quaternary Research* 56:357–65.

Druffel ERM, Griffin S. 1993. Large variations of surface ocean radiocarbon: evidence of circulation changes in the southwestern Pacific. *Journal of Geophysical Research* 98:20,249–59.

Edwards RL, Beck JW, Burr GS, Donahue DJ, Chappell JMA, Bloom AL, Druffel ERM, Taylor FW. 1993. A large drop in atmospheric $^{14}C/^{12}C$ and reduced melting in the Younger Dryas, documented with ^{230}Th ages of corals. *Science* 260:962–8.

Enmar R, Stein M, Bar-Matthews M, Sass E, Katz A, Lazar B. 2000. Diagenesis in live corals from the Gulf of Aqaba. I. The effect on paleo-oceanography tracers. *Geochimica et Cosmochimica Acta* 64:3123–32.

Franck N, Paterne M, Ayliffe L, van Weering T, Henriet JP, Blamart D. 2004. Eastern North Atlantic deep-sea corals: tracing upper intermediate water $\Delta^{14}C$ during the Holocene. *Earth and Planetary Science Letters* 219:297–309.

Goslar T, Arnold M, Tisnérat-Laborde N, Hatté C, Paterne M, Ralska-Jasiewiczona M. 2000. Radiocarbon calibration by means of varves versus ^{14}C ages of terrestrial macrofossils from Lake Gościąż and Lake Perespilno, Poland. *Radiocarbon* 42(3):335–48.

Guilderson TP, Schrag DP. 1998. Abrupt shift in subsurface temperatures in the tropical Pacific associated with changes in El Niño. *Science* 281:240–3.

Henderson GM, Slowey NC, Haddad GA 1999. Fluid flow through carbonates platforms: constraints from $^{234}U/^{238}U$ and Cl- in Bahamas pore-waters. *Earth and Planetary Science Letters* 169:99–111.

Hughen KA, Overpeck JT, Lehman SJ, Kashgarian M, Southon J, Peterson LC, Alley R, Sigman DM. 1998. Deglacial changes in ocean circulation from an extended radiocarbon calibration. *Nature* 391:65–8.

Hughen KA, Overpeck JT, Lehman SJ, Kashgarian M, Southon J, Peterson LC. 1998. A new ^{14}C calibration data set for the last deglaciation based on marine varves. *Radiocarbon* 40(1):483–94.

Kitagawa H, van der Plicht J. 1998. Atmospheric radiocarbon calibration to 45,000 yr BP: Late Glacial fluctuations and cosmogenic isotope production. *Science* 279:1187–90.

Kitagawa H, van der Plicht J. 2000. Atmospheric radiocarbon calibration beyond 11,900 cal BP from Lake Suigetsu laminated sediments. *Radiocarbon* 42(3): 369–80.

Nadeau MJ, Grootes PM, Voelker A, Bruhn F, Duhr A, Oriwall A. 2001. Carbonate ^{14}C background: does it have multiple personalities? *Radiocarbon* 43(1):169–76.

Priess K. 1997. La croissance des *Porites spp.* du groupe lobata-lutea-solida (scléractiniaires massifs) dans le lagon de Mayotte (NO Canal de Mozambique). Etude sclérochronologique [PhD dissertation]. Université de la Méditerranée. 170 p.

Schleicher M, Grootes PM, Nadeau MJ, Schoon A. 1998. The carbonate ^{14}C background and its components at the Leibniz AMS facility. *Radiocarbon* 40(1):85–93.

Siani G, Paterne M, Michel E, Sulpizio R, Sbrana A, Arnod M, Haddad G. 2001. Mediterranean sea surface radiocarbon reservoir age changes since the Last Glacial Maximum. *Science* 294:1917–20.

Sikes E, Samson CR, Guilderson TP, Howard WR. 2000. Old radiocarbon ages in the southwest Pacific Ocean during the last glacial period and deglaciation. *Nature* 405:555–9.

Stirling CH, Esat TM, McCulloch MT, Lambeck K. 1995. High-precision U-series dating of corals from Western Australia and implications for the timing and duration of the last Interglacial. *Earth and Planetary Science Letters* 135:115–30.

Stuiver M, Reimer PJ, Bard E, Beck WJ, Burr GS, Hughen KA, Kromer B, McCormac G, van der Plicht J, Spurk M. 1998. INTCAL98 radiocarbon age calibration, 24,000–0 cal BP. *Radiocarbon* 40(3):1041–83.

Voelker AHL, Sarnthein M, Grootes PM, Erlenkeuser H, Laj C, Mazaud A, Nadeaeu MJ, Schleicher M. 1998. Correlation of marine ^{14}C ages from the Nordic Seas with the GISP2 isotope record: implications for ^{14}C calibration beyond 25 ka BP. *Radiocarbon* 40(1):517–34.

Yokoyama Y, Esat TM, Lambeck K, Fifield LK. 2000. Last ice age millennial scale climate changes recorded in Huon Peninsula corals. *Radiocarbon* 42(3):383–401.

RADIOCARBON, Vol 46, Nr 2, 2004, p 567–581

OCEANIC RADIOCARBON AND TRITIUM ON A TRANSECT BETWEEN AUSTRALIA AND BALI (EASTERN INDIAN OCEAN)

Viviane Leboucher[1] • Philippe Jean-Baptiste[1,2] • Elise Fourré[1] • Maurice Arnold[1] • Michèle Fieux[3]

ABSTRACT. Results are presented of radiocarbon and tritium measurements along a transect between the Australian continental shelf and the Indonesian coast of Bali. The stations lie in the easternmost part of the Indian Ocean, close to the sills over which the Indonesian throughflow (ITF) makes its way to the Indian Ocean. The present data, obtained as part of the Java-Australia Dynamics Experiment (JADE) in August 1989, complement the WOCE ^{14}C and tritium data set on both sides of the Indonesian archipelago and give us the opportunity to discuss the origin of the water masses and timescale of the throughflow. Both tracers point to a north equatorial Pacific origin of the waters. The comparison of the tritium inventories in the Pacific North Equatorial Current and along the JADE transect suggests a minimum transit time of the waters across the Indonesian seaways of the order of 5 to 6 yr, corresponding to a throughflow $<18 \times 10^6$ m^3/s.

INTRODUCTION

The invasion of bomb radiocarbon in the ocean has been used for several decades to study ocean circulation and ventilation processes. However, very few measurements exist for the Indonesian throughflow (Broecker et al. 1986a). Here, we report ^{14}C and tritium measurements at the exit of the Indonesian throughflow (ITF) on a transect between Australia and Bali in the easternmost part of the Indian Ocean (Figure 1). The section crosses all the water masses coming from the western Pacific through the Indonesian seas. Therefore, it represents an open window on the ITF, which constitutes a major return path for the warm North Pacific tropical waters to the Atlantic, and plays an important role in the global ocean circulation and climate regulation (Gordon and Fine 1996).

The samples were taken during the JADE-89 cruise (Java-Australia Dynamics Experiment) in August 1989, about a decade after the end of the GEOSECS Indian Ocean program and a few years prior to the start of the World Ocean Circulation Experiment (WOCE). On the Pacific side, recently available data from the WOCE sections in the western Pacific (Key et al. 2002; Schlosser 2002; Jenkins 2002; Kumamoto et al. 2002) represent an extremely valuable data set in the context of our study. On the Indian side, the eastermost WOCE sections (Schlosser 2002; Jenkins 2002) do not extend beyond 111°E. Owing to its position closer to the passages by which the Indonesian waters enter the Indian Ocean, the JADE-89 transect represents a unique link between the Indian and Pacific data sets.

HYDROGRAPHY AND WATER MASSES CHARACTERISTICS

The main hydrographic characteristics of the water masses along the JADE transect have been described in detail by Fieux et al. (1994) using the distribution of potential temperature, salinity, and dissolved oxygen. At the surface, a wedge of low salinity/high temperature layer (Figure 2a,b), which is more pronounced in the northern part of the section, marks the influx of water of Indonesian origin flowing out of the Savu and Timor Seas. The low salinity results both from the characteristics of the incoming Indonesian waters and from local excess of precipitation over evaporation, which is typical of this region of the Indian Ocean under the Inter-Tropical Convergence Zone

[1]Laboratoire des Sciences du Climat et de l'Environnement, IPSL, CEA-CNRS, CEA/Saclay, F91191-Gif/Yvette cedex, France.
[2]Corresponding author. Email: pjb@lsce.saclay.cea.fr.
[3]Laboratoire d'Océanographie Dynamique et de Climatologie, Université Paris VI, F75252 - Paris cedex 05, France.

Proceedings of the 18th International Radiocarbon Conference, edited by N Beavan Athfield and R J Sparks
RADIOCARBON, Vol 46, Nr 2, 2004, p 567–581

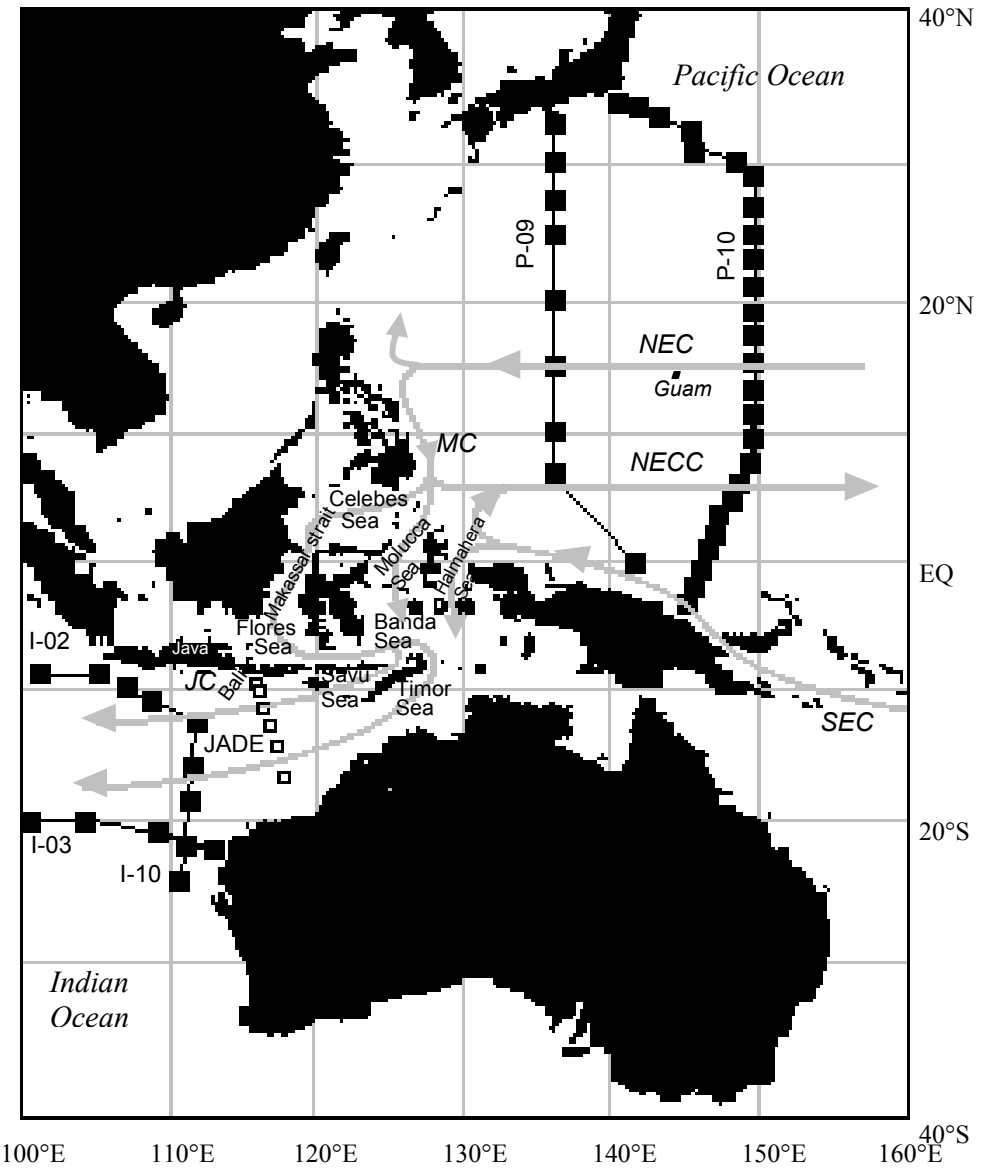

Figure 1 Location of the hydrographic stations with available ^{14}C measurements on both sides of the Indonesian throughflow (the WOCE cruises and JADE-89 transect are indicated by solid and open squares, respectively), and schematic diagram of major currents. *NEC*: North Equatorial Current, *NECC*: North Equatorial CounterCurrent, *SEC*: South Equatorial Current, *MC*: Mindanoa Current, *JC*: Java Current.

(ITCZ). Next to Bali, all the isolines slope upwards due to the presence of a strong coastal upwelling. This upwelling is created by the sustained easterly winds during this phase of the monsoon. These winds also generate a strong westward surface current along the coast, the Java current, which reverses with the monsoons. Below the thermocline, the characteristics of the water masses reveal a sharp front at 13°30′S. South of this front, the salinity maximum between 150 m and 450 m identifies the South Indian Ocean subtropical water (Figure 2b). North of the front, the lower salinity is representative of the waters originating from the Indonesian seas.

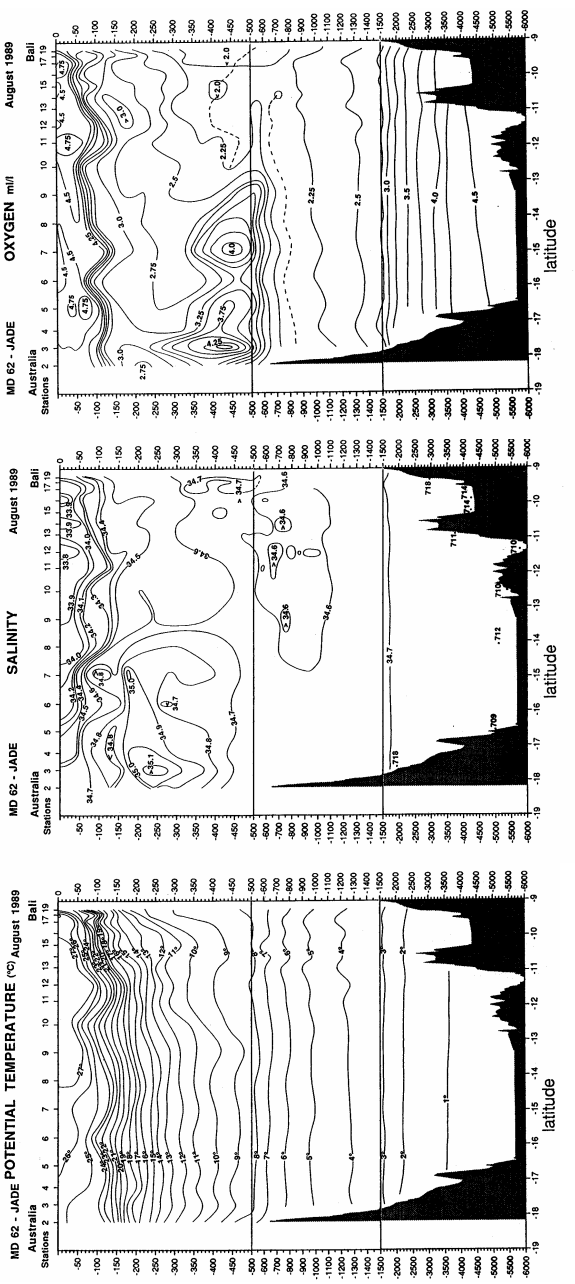

Figure 2 Temperature (a), salinity (b), and dissolved oxygen (c) sections between the Australian continental shelf and the Indonesian coast of Bali during the JADE cruise, August 1989 (from Fieux et al. 1994).

Between 350 m and 600 m, the sharp oxygen maximum in the southern part of the section (Figure 2c) traces the Indian Ocean central water, also named Subantarctic Mode Waters (Warren 1981; McCartney 1982). In the north, trapped along the coast, appears a water mass characterized by a higher salinity S > 34.7 psu and lower oxygen content O_2 < 89 µmol/kg (=2.0 mL/l), which corresponds to northern Indian Ocean waters originating from the Arabian Sea (Fieux et al. 1994).

Between 750 m and 1000 m, north of 15°S, the weak salinity minimum (S < 34.6 psu) points to the presence of the Banda Intermediate waters. This deep Indonesian throughflow is also well depicted by its sharp ^{3}He anomaly, which is characteristic of the Pacific waters (Jean-Baptiste et al. 1997; Top et al. 1997).

From the temperature and salinity data, Fieux et al. (1994) calculated at the time of the JADE cruise a net geostrophic transport of 18.6×10^6 m^3/s directed towards the Indian Ocean. Seventy percent of this flow occurs in the 0–200 m layer, between the coast of Bali and the 13°30–15°S frontal zone, thus representing the core of the Pacific-Indian throughflow.

EXPERIMENTAL METHODS

The ^{14}C samples were treated according to the procedure described by Bard et al. (1987) and Leboucher et al. (1999). Seawater was collected in 12-L Niskin bottles. For each sample, 500 mL of water was transferred to a glass bottle and poisoned with 1 mL of saturated $HgCl_2$ solution. In the laboratory, CO_2 was extracted by adding 2 mL of 15N H_3PO_4 to a 100-mL seawater aliquot in a vacuum-tight system sparged by helium gas (flow rate 80 mL/min); the extraction required 1 hr. Water was removed by a trap at –80 °C and CO_2 was trapped at –180 °C using liquid nitrogen. Then, CO_2 was reduced to graphite by hydrogen at 850 °C during 6–8 hr in the presence of iron powder. Three targets were made from the carbon-iron mixture for accelerator mass spectrometry (AMS). The ^{14}C measurements were performed at the Tandetron AMS facility in Gif-sur-Yvette. The data (Table 1) are expressed as Δ^{14}C. Two targets per sample were analyzed to obtain the required precision of ±3‰.

Samples were also taken for tritium (^{3}H) analysis. Since ^{14}C and ^{3}H were released together by the atmospheric nuclear detonations of the late 1950s and early 1960s, both isotopes constitute complementary tracers for oceanographic studies. The ^{3}H measurements were performed at the helium isotope facility in Saclay using the ^{3}He ingrowth method (Jean-Baptiste et al. 1992). Briefly, the seawater samples were stored in 500-mL Pyrex bottles. In the laboratory, the water was degassed under high vacuum to remove the naturally dissolved ^{3}He, and sealed in a Corning 1724 glass bulb. The bulbs were stored at –20 °C to minimize ^{3}He diffusion through the walls during the storage period (Jean-Baptiste et al. 1989). After 12 to 18 months, the ^{3}He produced by the decay of tritium was measured on a MAP 215-50 mass spectrometer, permitting the determination of the tritium content of the water. The data are expressed in Tritium Unit (TU) at the date of sampling (1 TU corresponds to a T/H ratio of 10^{-18}). The precision on the tritium concentration is better than 0.01 TU.

RESULTS

Vertical Profiles and Sections

The ^{14}C and tritium results are summarized in Table 1. The vertical profiles are plotted in Figure 3. Below the shallow mixed layer, both transient tracer concentrations decrease sharply. Deeper than 1000 m to 1500 m, tritium and ^{14}C concentrations fall to their natural background.

The Δ^{14}C and ^{3}H vertical sections along the Australia-Bali transect are displayed in Figure 4. Surface and intermediate depth isolines are nearly horizontal, following those of temperature. The

Table 1 JADE august 1989 $\Delta^{14}C$ and tritium results.

Depth (m)	Tritium (TU)	$\Delta^{14}C$ (‰)	Depth (m)	Tritium (TU)	$\Delta^{14}C$ (‰)	Depth (m)	Tritium (TU)	$\Delta^{14}C$ (‰)
Station 5: 16°35′S / 117°23′E			Station 8: 14°08′S/116°42′E			Station 10: 12°31′S / 116°16′E		
2.5	—	97	3.0	1.83	96	3.9	1.96	104
29.5	1.69	102	28.8	—	118	28.8	1.76	102
47.7	1.51	93	48.5	2.10	93	48.3	1.93	94
67.3	1.95	79	69.3	1.98	84	67.2	1.90	84
98.2	1.78	86	98.1	1.61	79	99.1	1.66	76
150.0	1.88	56	148.5	1.66	80	148.6	1.65	26
199.2	1.80	65	201.3	1.54	56	198.1	1.39	18
298.8	1.24	3	298.0	1.33	11	298.8	1.01	–33
449.8	0.58	–20	398.5	0.76	–20	398.0	0.79	–73
499.7	0.42	–58	600.4	0.24	–119	601.3	0.34	–116
600.4	0.27	–114	798.5	0.07	–156	797.3	0.16	–152
798.0	0.19	–162	998.4	0.08	–161	998.0	0.07	–173
901.3	0.13	–161	2001.6	0.001	–200	1998.2	0.005	–200
997.7	0.09	–173	4199.0	0.002	–188	4193.8	0.001	–187
Station 12: 11°23′S / 115°57′E			Station 16: 9°55′S / 115°32′E			Station 19: 9°14′S / 115°14′E		
3.2	—	103	2.4	1.73	104	—	—	—
28.2	1.82	111	29.9	1.83	90	25.9	1.98	68
49.6	1.93	100	49.8	1.55	87	44.2	1.54	64
68.0	1.57	111	68.2	1.74	77	66.4	1.65	66
99.1	1.79	94	100.6	1.60	30	99.8	1.71	39
125.2	—	70	149.6	1.43	11	150.1	0.89	–61
199.9	—	21	200.0	1.34	0	200.3	0.8	–89
299.2	0.95	–46	301.6	0.96	–54	299.9	0.59	–91
422.4	0.41	–83	401.7	0.65	–80	400.1	0.30	–101
500.4	0.27	–112	604.5	0.23	–128	499.8	0.22	–122
604.4	0.27	–134	896.6	0.10	–170	599.7	0.29	–125
798.8	0.10	–152	1096.5	0.02	–194	794.5	—	–194
906.2	—	–153	1996.3	0.01	–194	895.5	—	–175
997.4	0.07	–173	3798.9	0.003	–182	997.4	—	–188

upwelling that takes place along the coast of Bali clearly affects both tracer vertical distributions by bringing toward the surface waters from deeper levels, less tagged with ^{14}C and ^{3}H. At deeper levels (below 1500 m), ^{3}H concentrations drop below detection limit (<0.01 TU), while ^{14}C concentrations reach their natural level, between –180 and –200‰. The $\Delta^{14}C$ minimum at 2000 m depth is typical of the oldest waters in the Indian basin, whereas bottom waters, influenced by the more recently ventilated Antarctic Bottom Waters (AABW), display slightly higher values.

Surface $\Delta^{14}C$ and Origin of the Throughflow

The $\Delta^{14}C$ values in the mixed layer are in the range of 100–110‰, except at station 19 located off Bali ($\Delta^{14}C$ = 68‰) which is influenced by the coastal upwelling. These surface $\Delta^{14}C$ are in marked contrast with Indian Ocean data further west at the same latitude, which are in the range of 65–75‰ (Figure 5). The spatial distribution of ^{14}C in the surface ocean, determined in the 1970s thanks to the GEOSECS program, shows a strong gradient between middle latitudes and the 5°S–5°N belt, the

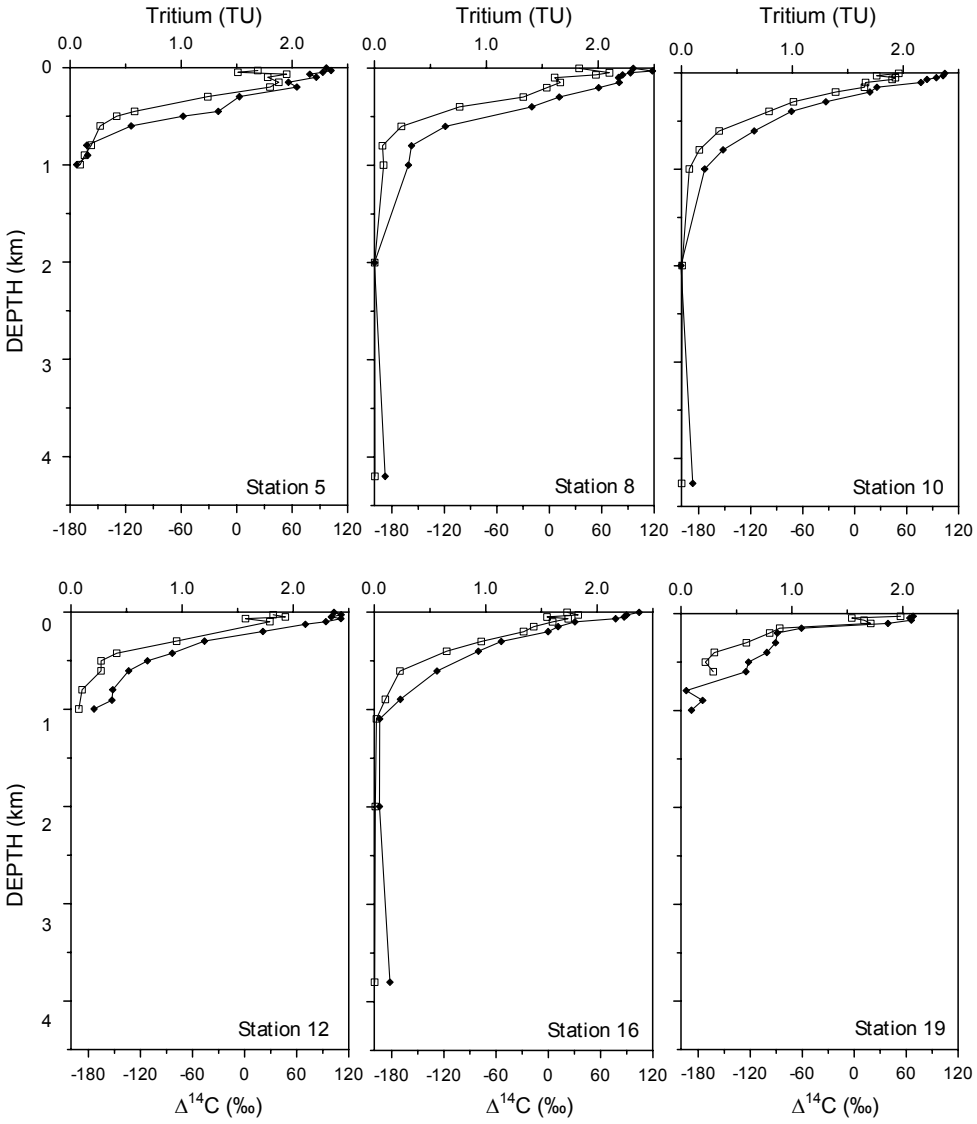

Figure 3 JADE-89 $\Delta^{14}C$ (black diamonds) and tritium (open squares) vertical profiles (stations 5, 8, 10, 12, 16, and 19).

$\Delta^{14}C$ of which is lowered by the equatorial upwelling (Broecker et al. 1985). This latitudinal trend is still present in the WOCE data set (Figure 5), although not so strong, since the initial bomb signal is progressively smoothed by advection and mixing of the water masses. $\Delta^{14}C$ surface values comparable to those observed along the JADE transect are found in the 10°N–15°N latitudinal belt of the Pacific Ocean, which corresponds to westward-flowing North Equatorial current (NEC).

Pacific waters that enter the Indonesian archipelago follow 2 different routes (Gordon and Fine 1996). The westernmost route, which is the main pathway, enters the Celebes Sea from the NEC-fed Mindanoa Current and proceeds through the Makassar Strait towards the Flores Sea before reaching the Banda Sea (Figure 1). The eastern route reaches the Banda Sea directly through the Halmahera and Molucca Seas. There, the waters from both routes mix before entering the Indian Ocean through

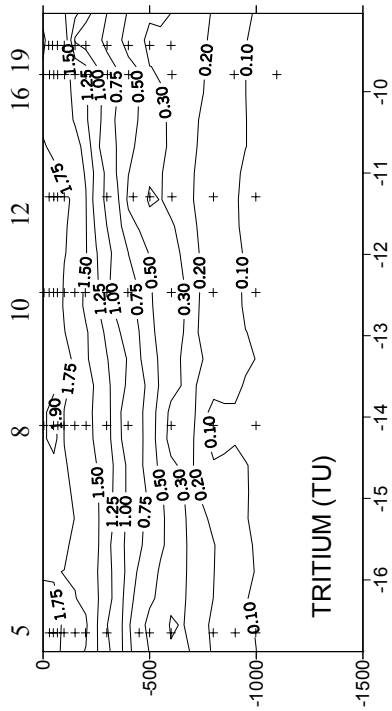

Figure 4b

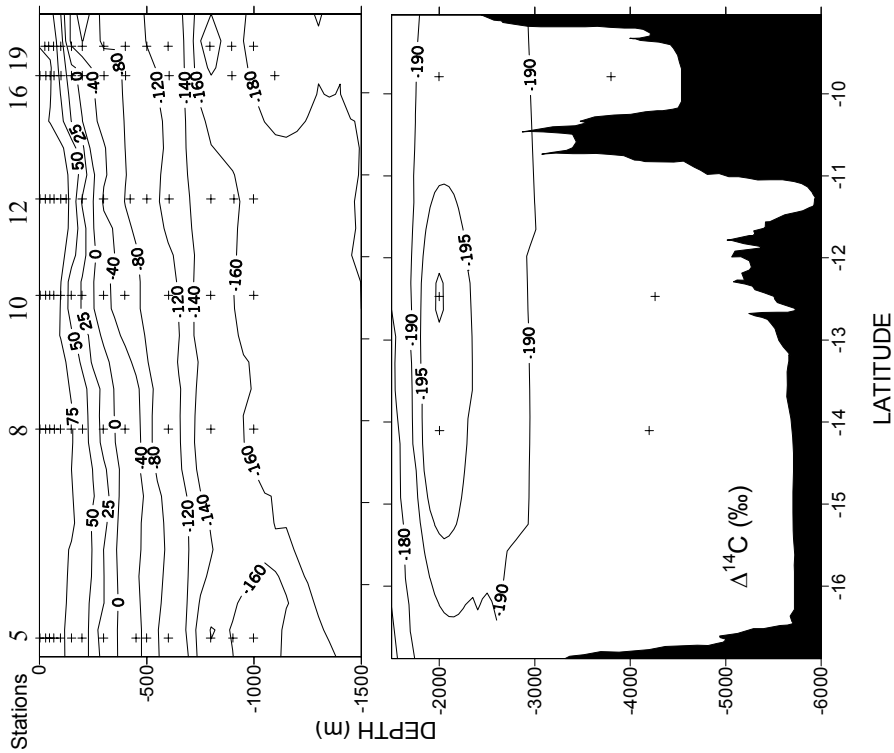

Figure 4a

Figure 4 $\Delta^{14}C$ and tritium vertical sections along the JADE-89 Australia-Bali transect

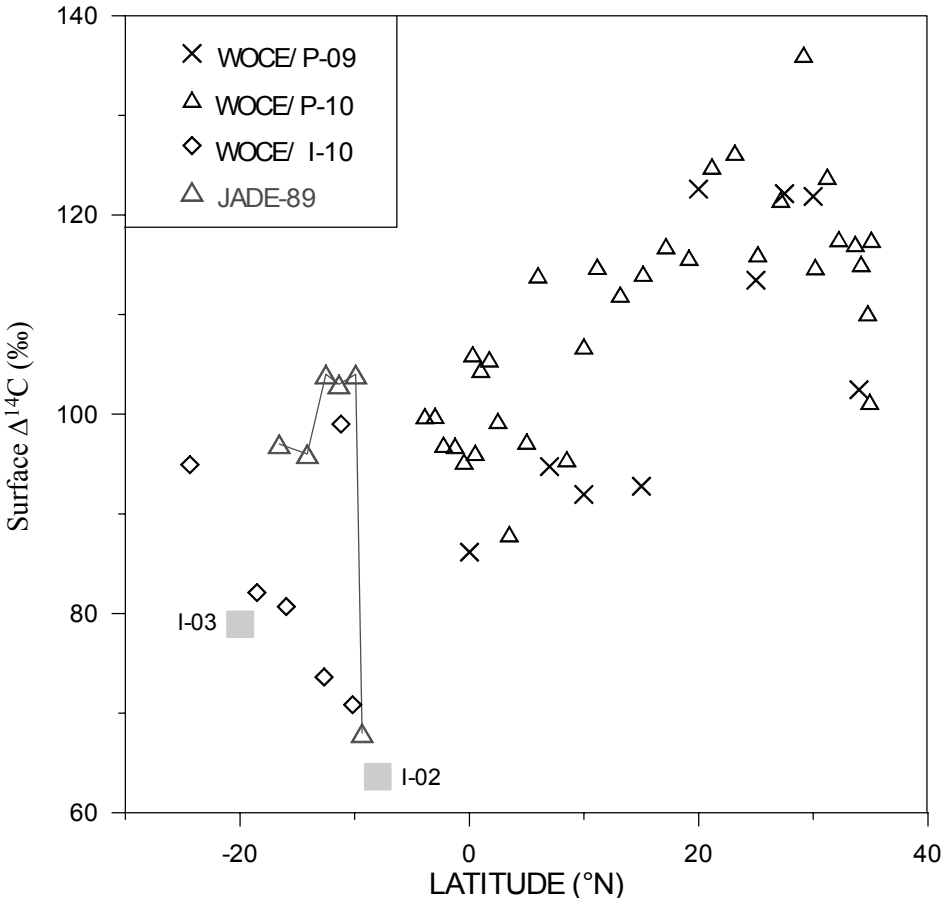

Figure 5 Plot of the WOCE (I-10, P-09, P-10) and JADE-89 $\Delta^{14}C$ surface concentrations as a function of latitude (the grey squares represent the mean value of the 2 zonal sections I-02 and I-03).

the Savu and Timor Seas (Figure 1). By looking at the ^{14}C of corals from the Makassar Strait, Moore et al. (1997) have shown that their $\Delta^{14}C$ are 60‰ higher than in corals from Canton Island, located in the Pacific South Equatorial Current (SEC), and identical to those of Guam, bathed by the NEC (lat. 13°30′N). These findings strongly support the hydrographic observations (Fine 1985; Gordon 1986) which point to a northern Pacific origin of the waters following the western route. The origin of the waters taking the eastern route is less certain, with a possible contribution of the SEC (Field and Gordon 1992; Gordon and Fine 1996). The high $\Delta^{14}C$ surface values measured along the JADE track do not favor any appreciable contribution of the South Pacific component to the waters crossing the Australia-Bali transect. However, the rather large scatter of the surface $\Delta^{14}C$ from the WOCE western Pacific data set (Figure 5) prevent us to derive any precise figure concerning the upper limit of the South Pacific component. This scatter is due to the seasonal and interannual variability of the surface circulation and local upwellings, in relation to the various phases of the monsoon and to the ENSO phenomenon (Druffel 1987; Moore et al. 1997).

Table 2 WOCE (I-02, I-03, I-10, P-09, P-10) and JADE-89 bomb ^{14}C inventories ($\Sigma^{14}C_{bomb}$), defined as $\Sigma^{14}C_{bomb} = [(\Delta^{14}C_{total}-\Delta^{14}C_{natural}) \times \Delta z]$ (Unit: 10^3‰×m).

Stations	Latitude	Longitude	$\Sigma^{14}C_{bomb}$	Stations	Latitude	Longitude	$\Sigma^{14}C_{bomb}$
JADE-89				1067	11°12′S	108°55′E	55.5
5	16°35′S	117°23′E	61.8	1071	10°11′S	107°17′E	42.2
8	14°08′S	116°42′E	64.7	WOCE P-09			
10	12°31′S	116°16′E	53.1	3	34°00′N	136°59′E	59.4
12	11°23′S	115°57′E	53.1	21	30°00′N	137°00′E	136.3
16	9°55′S	115°32′E	45.1	26	27°30′N	137°00′E	146.3
19	9°14′S	115°14′E	32.2	31	25°00′N	137°00′E	114.5
WOCE I-02				41	20°00′N	137°01′E	114.5
1078	9°00′S	105°38′E	48.1	51	15°01′N	137°00′E	68.9
1084	9°07′S	102°00′E	37.9	61	10°00′N	137°00′E	41.1
1090	8°00′S	98°00′E	30.6	70	7°00′N	137°00′E	29.1
1096	8°00′S	94°00′E	37.6	93	0°01′N	142°00′E	37.2
1100	8°00′S	91°20′E	28.9	WOCE P-10			
1104	8°00′S	89°22′E	35.0	3	3°53′S	144°54′E	66.2
1111	6°20′S	88°25′E	25.7	6	3°00′S	145°17′E	58.7
1115	8°00′S	88°00′E	14.2	9	2°15′S	145°30′E	47.8
1120	11°00′S	88°02′E	28.6	13	1°15′S	145°47′E	50.3
1126	10°23′S	88°25′E	24.3	16	0°28′S	146°00′E	49.7
1133	8°00′S	83°20′E	57.8	18	0°17′N	146°09′E	54.7
1143	8°00′S	76°40′E	44.3	20	0°30′N	146°17′E	56.3
1150	8°00′S	72°49′E	43.0	22	1°00′N	146°26′E	48.8
1155	8°00′S	71°02′E	49.2	25	1°45′N	146°39′E	54.3
WOCE I-03				28	2°30′N	146°52′E	50.0
449	22°04′S	112°49′E	82.0	31	3°29′N	147°14′E	38.1
452	21°40′S	111°22′E	76.7	34	5°00′N	147°51′E	37.5
455	20°50′S	109°26′E	70.4	36	6°00′N	148°17′E	39.6
461	20°00′S	104°53′E	68.8	41	8°30′N	149°20′E	32.3
465	20°00′S	101°21′E	94.6	45	10°00′N	149°20′E	39.4
469	20°00′S	97°50′E	93.9	47	11°10′N	149°20′E	44.1
476	20°00′S	92°21′E	97.0	50	13°10′N	149°20′E	59.4
483	20°00′S	89°28′E	100.5	53	15°10′N	149°20′E	69.0
491	20°00′S	85°18′E	105.0	56	17°10′N	149°20′E	77.6
495	20°00′S	82°44′E	111.4	59	19°10′N	149°20′E	93.9
501	20°00′S	78°21′E	100.7	62	21°10′N	149°20′E	115.1
505	20°00′S	75°27′E	106.0	65	23°10′N	149°20′E	118.1
507	20°00′S	74°10′E	101.2	68	25°10′N	149°20′E	112.9
512	20°00′S	71°42′E	101.4	71	27°10′N	149°20′E	117.4
517	20°00′S	69°22′E	113.2	74	29°10′N	149°20′E	124.2
526	20°11′S	64°25′E	115.2	76	30°11′N	148°03′E	139.5
531	20°22′S	61°38′E	117.0	78	31°13′N	146°46′E	138.1
535	20°22′S	59°13′E	113.8	80	32°14′N	145°28′E	140.6
550	20°00′S	53°20′E	103.5	83	33°40′N	143°40′E	142.6
557	20°00′S	50°04′E	84.3	85	34°11′N	142°43′E	134.2
WOCE I-10				88	34°45′N	141°39′E	77.2
1015	24°23′S	110°35′E	112.9	90	34°56′N	141°12′E	56.1
1045	18°32′S	111°05′E	89.7	92	35°05′N	140°54′E	66.8
1051	15°58′S	111°18′E	80.4				
1059	12°41′S	111°35′E	52.4				

^{14}C Water Column Inventories

^{14}C inventories are indicated in Table 2. The inventory of bomb ^{14}C at a given location is the amount of ^{14}C in excess of the natural prebomb concentrations. It is obtained by subtracting the natural ^{14}C component from the total ^{14}C water column inventory. We calculated the natural component using the classic empirical formula of Broecker et al. (1995), which links the natural Δ^{14}C to the dissolved silica concentration (SiO_2):

$$\Delta^{14}C‰ = -70‰ - SiO_2 ,$$

where silica concentrations are expressed in μmol/kg (as alkalinity-based estimates are not available for the JADE cruise, this method was preferred to the Palk method of Rubin and Key [2002] for the sake of consistency).

The bomb ^{14}C inventories are plotted as a function of latitude in Figure 6a. Geographical patterns of the bomb ^{14}C inventory at the scale of the main ocean basin reflect the spatial distribution of the surface Δ^{14}C; however, it is also strongly affected by the spatial pattern of the penetration depth of the tracer. Systematic latitudinal variations were first revealed by the GEOSECS program, with subtropical maxima in both hemispheres and an equatorial minimum (Broecker et al. 1985). This latitudinal pattern is the consequence of the input function structure of oceanic ^{14}C, determined by the exchange of $^{14}CO_2$ at the air-sea interface, and of the large-scale redistribution of the tracer by the ocean circulation (Toggweiler et al. 1989). This latitudinal trend is also apparent in the WOCE data set (Figure 6a). However, as far as the origin of the throughflow waters is concerned, Figure 6a shows that both the NEC and SEC display bomb ^{14}C inventories in the same range. Therefore, ^{14}C inventories do not permit to discriminate between the 2 sources.

Tritium Water Column Inventories

The tritium inventories at the JADE stations and at the WOCE stations on both sides of the ITF are summarized in Table 3. In order to remove the influence of the radioactive decay, which is significant even over short periods of time due to the relatively short tritium half-life of 12.4 yr, all the inventories were decay-corrected to 1 January 1991 (notation TU 91). The geographical pattern of the tritium inventories is characterized by a large contrast between the 2 hemispheres (Broecker et al. 1986b). This is due to the fact that most bomb atmospheric detonations and subsequent tritium fallout occurred in the Northern Hemisphere and to the short residence time of water in the atmosphere (Weiss and Roether 1980). The maximum tritium delivery is observed at middle latitudes. In Figure 6b, the plot of the tritium inventories as a function of latitude reveals that the JADE data points are well above the values typical of the SEC, again strongly suggesting a northern Pacific origin of the waters.

DISCUSSION

The average tritium inventory along the JADE transect (excluding station 19 next to the coast of Bali because of the perturbation by the upwelling) is about 25% below the North Pacific endmember, which is in the range 780–1080 TU91×m (Figure 6b). *A priori*, this 25% change can be due to some mixing with the low-tritium South Pacific component, or simply to the aging of the North Pacific waters during their transit across the Indonesian archipelago, or to a combination of both processes. In Figure 7, the diagram representing the surface Δ^{14}C against tritium inventories suggests that the JADE domain is best explained by a simple aging process of the NEC waters, with no significant contribution from the SEC component.

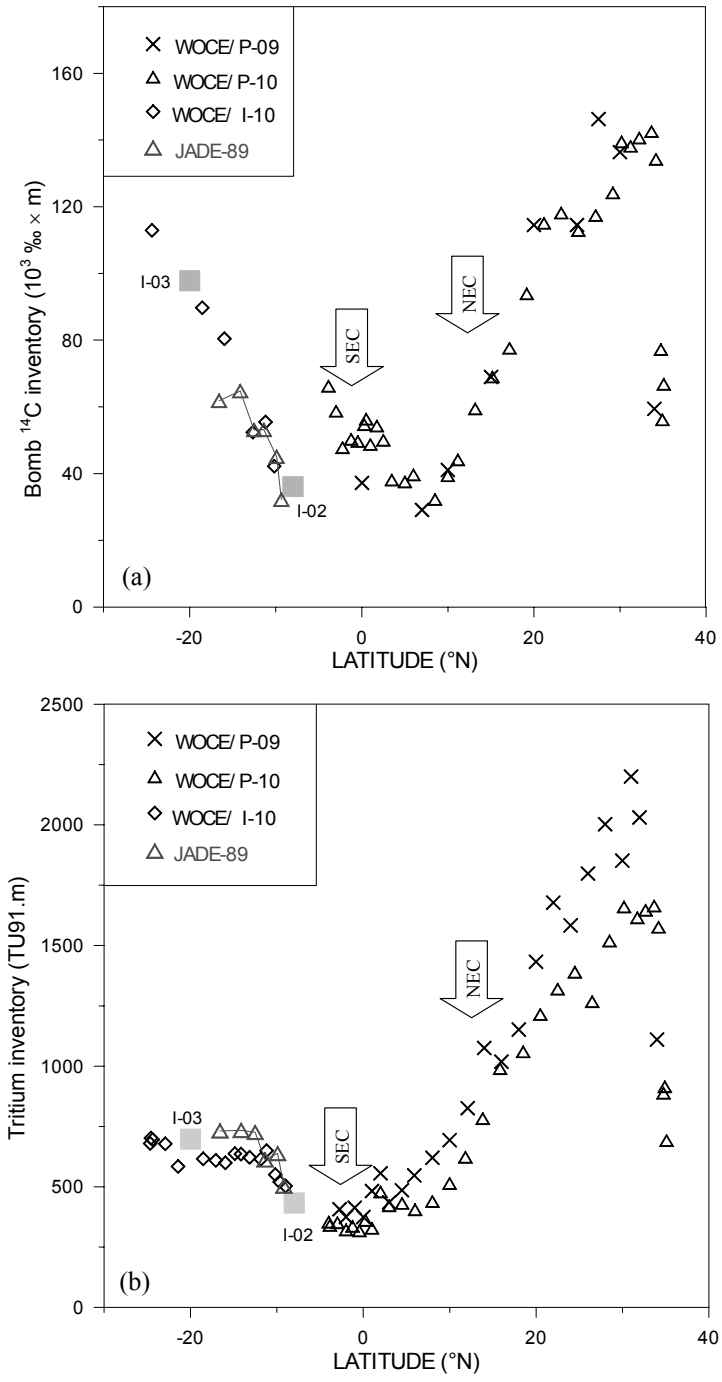

Figure 6 Plot of the WOCE and JADE-89 bomb ^{14}C (a) and tritium (b) inventories as a function of latitude (the grey squares represent the mean value of the 2 zonal sections I-02 and I-03). The 2 arrows signal the core of the NEC when approaching the bifurcation at the Philippines coast (Toole et al. 1990) and the branch of the SEC materialized at this latitude by the New Guinea Coastal Current (Fine et al. 1994).

Table 3 WOCE (I-02, I-03, I-10, P-09, P-10) and JADE-89 tritium inventories (Σ^3H_{91}), decay-corrected to 1 January 1991 (Unit: TU91×m).

Stations	Latitude	Longitude	Σ^3H_{91}	Stations	Latitude	Longitude	Σ^3H_{91}
JADE-89				1039	21°27′E	110°50′E	584.0
5	16°35′S	117°23′E	731.9	1045	18°32′E	111°05′E	615.6
8	14°08′S	116°42′E	733.8	1048	17°04′E	111°13′E	609.1
10	12°31′S	116°16′E	725.6	1051	15°58′E	111°18′E	599.1
12	11°23′S	115°57′E	611.7	1054	14°52′E	111°24′E	637.4
16	9°55′S	115°32′E	638.1	1056	14°09′E	111°27′E	635.1
19	9°14′S	115°14′E	503.6	1058	13°10′E	111°32′E	621.8
WOCE I-02				1062	11°52′E	111°22′E	614.3
1078	9°00′S	105°38′E	514.3	1067	11°12′E	108°55′E	649.2
1079	9°07′S	105°10′E	448.8	1071	10°11′E	107°17′E	550.2
1081	9°07′S	104°00′E	472.6	1073	9°40′E	106°27′E	520.2
1087	8°34′S	100°00′E	436.8	1075	9°00′E	105°38′E	502.5
1094	8°00′S	95°20′E	372.7	WOCE P-09			
1102	8°00′S	90°00′E	364.7	3	34°00′N	136°59′E	1110.4
1106	6°00′S	88°29′E	357.6	15	31°59′N	137°00′E	2031.1
1110	5°31′S	88°30′E	352.6	18	31°00′N	137°00′E	2200.6
1116	10°02′S	88°00′E	548.5	21	30°00′N	137°00′E	1851.5
1120	11°00′S	88°02′E	585.1	25	28°00′N	137°00′E	2002.6
1130	8°00′S	85°20′E	395.7	29	26°00′N	137°00′E	1798.0
1138	8°00′S	80°00′E	399.8	33	24°00′N	137°00′E	1583.3
1145	8°00′S	75°20′E	373.5	37	22°00′N	137°24′E	1677.9
				41	20°00′N	137°00′E	1432.6
WOCE I-03				45	18°00′N	137°00′E	1151.5
445	22°13′S	113°42′E	638.2	49	16°00′N	136°58′E	1018.1
446	22°12′S	113°36′E	638.1	53	14°00′N	137°00′E	1075.2
448	22°08′S	113°10′E	649.4	57	12°05′N	137°00′E	825.7
449	22°05′S	112°49′E	645.8	61	10°00′N	137°00′E	692.9
451	21°50′S	111°54′E	615.9	66	8°00′N	137°00′E	620.3
454	21°09′S	110°09′E	668.6	73	5°55′N	138°04′E	547.0
459	20°00′S	106°37′E	622.1	77	4°28′N	139°35′E	485.6
464	20°00′S	102°14′E	643.9	81	3°01′N	141°07′E	435.4
469	20°00′S	97°50′E	686.4	85	2°02′N	142°03′E	555.7
480	20°00′S	90°17′E	708.8	89	1°01′N	142°00′E	482.4
490	20°00′S	85°56′E	703.8	93	0°00′N	142°00′E	374.4
496	20°00′S	82°00′E	717.8	97	1°00′S	142°02′E	413.0
501	20°00′S	78°22′E	728.4	101	2°00′S	142°00′E	374.8
507	20°00′S	74°10′E	718.2	104	2°45′S	142°15′E	406.8
515	20°00′S	70°15′E	744.2	WOCE P-10			
523	20°00′S	65°59′E	739.5	1	4°01′S	144°49′E	353.8
530	20°22′S	62°15′E	784.0	3	3°53′S	144°53′E	340.1
537	20°22′S	58°09′E	789.4	6	3°00′S	145°17′E	351.4
549	20°00′S	53°53′E	764.2	10	2°00′S	145°34′E	321.6
554	20°00′S	51°18′E	762.1	13	1°15′S	145°47′E	336.5
557	20°00′S	50°04′E	673.8	16	0°28′S	146°00′E	317.8
WOCE I-10				19	0°15′S	146°13′E	360.9
1015	24°23′S	110°35′E	695.6	22	1°00′N	146°26′E	328.2
1020	24°40′S	112°12′E	679.6	26	2°00′N	146°43′E	479.0
1030	24°34′S	111°39′E	701.9	30	3°00′N	147°00′E	421.4
1036	22°55′S	110°43′E	678.0	33	4°30′N	147°39′E	431.3

Table 3 WOCE (I-02, I-03, I-10, P-09, P-10) and JADE-89 tritium inventories (Σ^3H_{91}), decay-corrected to 1 January 1991 (Unit: TU91×m). *(Continued)*

Stations	Latitude	Longitude	Σ^3H_{91}	Stations	Latitude	Longitude	Σ^3H_{91}
WOCE P-10				67	24°30′N	149°20′E	1390.0
Continued				70	26°30′N	149°20′E	1267.5
36	6°00′N	148°16′N	405.3	73	28°30′N	149°20′E	1518.8
40	8°00′N	149°10′N	439.5	76	30°11′N	148°03′E	1659.9
45	10°00′N	149°20′N	514.0	79	31°43′N	146°07′E	1615.3
48	11°50′N	149°20′N	622.6	81	32°41′N	144°54′E	1646.5
51	13°50′N	149°20′N	782.7	83	33°40′N	143°40′E	1663.9
54	15°50′N	149°20′N	989.8	85	34°11′N	142°43′E	1576.2
58	18°30′N	149°20′N	1059.8	88	34°45′N	141°39′E	888.5
61	20°30′N	149°20′N	1214.5	90	34°55′N	141°12′E	914.8
64	22°30′N	149°20′N	1319.5	92	35°06′N	140°54′E	692.0

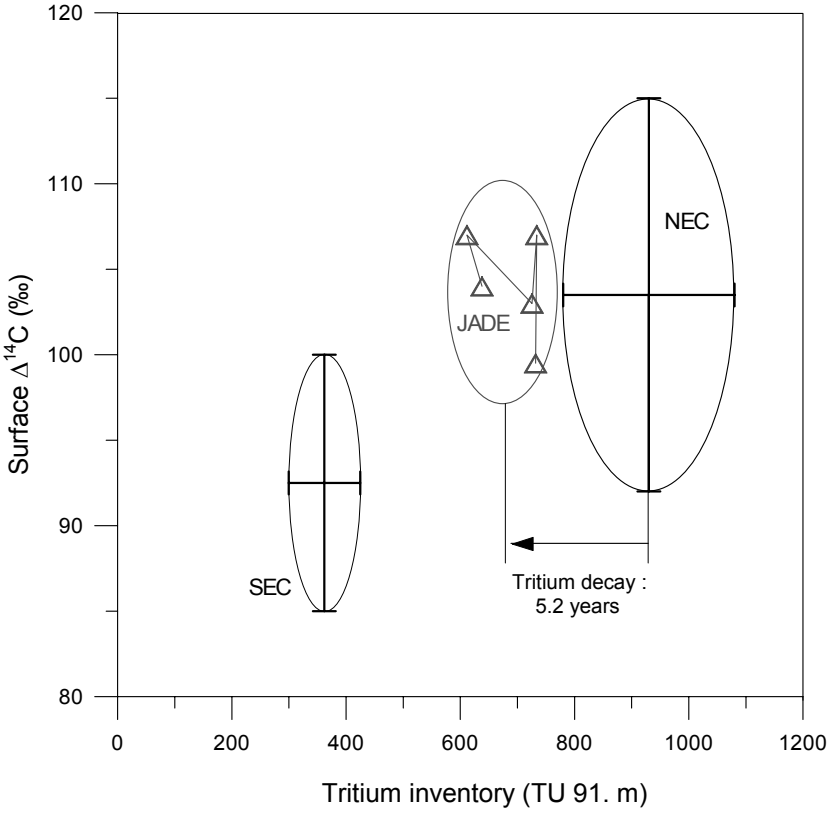

Figure 7 Diagram of the JADE-89 surface $\Delta^{14}C$ versus tritium inventory. The 2 Pacific end-members (NEC and SEC) are also indicated with their respective uncertainty.

The corresponding bulk residence time τ of North Pacific waters in the Indonesian seas is given by $\tau = -\lambda^{-1}\ln(0.75)$, where λ is the decay constant for tritium, leading to a residence time of 5.2 yr. This estimate is certainly a lower limit since it neglects the tritium added by rain and water-vapor exchange at the air-sea interface. This residence time τ can be related in a simple manner to the value of the throughflow Φ by the equation: $\tau = V / \Phi$, where V is the volume of the Indonesian waters

involved in the Pacific-Indian water transport. This volume roughly corresponds to the average surface area of the Indonesian seas ($\approx 2 \times 10^6$ km^2; GEBCO 1984) multiplied by the mean depth of the sills crossed by the Indonesian waters entering the Indian Ocean. Taking an average depth of 1500 m (Gordon et al. 2003), the 5.2 yr minimum residence time translates into an upper value of throughflow $\Phi \sim 18 \times 10^6$ m^3/s. This value is in surprisingly good agreement with the geostrophic transport calculated by Fieux et al. (1994) for August 1989: 18.6×10^6 m^3/s. This agreement may be somewhat fortuitous considering the experimental uncertainties and the crudeness of the above calculation. However, it strongly supports our interpretation of the tritium and ^{14}C data, which discards any significant involvement of the South Pacific waters in the Pacific-Indonesian throughflow at the time of the JADE-89 cruise.

CONCLUSION

The ^{14}C and ^{3}H measurements performed in the framework of the Java-Australia Dynamics Experiment (JADE) in August 1989, on a transect between Australia and Bali, bridge the gap between the western Pacific and the Eastern Indian Ocean tracer data. The results complement the data on both sides of the Indonesian throughflow obtained during the WOCE program in 1993/1995 and are fully consistent with the WOCE tracer results.

The Indonesian throughflow has been the focus of numerous studies, including hydrographic work, tracer data, drifters tracks, and circulation models. Most of these studies point to a mainly North Pacific origin of the waters that cross the Indonesian seaway from the Pacific to the Indian Ocean. The present tracer data fully support these conclusions. Furthermore, our results indicate that, at least at the time of the JADE survey, the south Pacific component was virtually absent from the tracer signal recorded at the exit of the throughflow.

ACKNOWLEDGEMENTS

This work was carried out under the French-Indonesian cooperation program led by A G Ilahude (LIPI) and M Fieux (CNRS-INSU). We acknowledge the support of the Indonesian BPPT and the Terres Australes et Antarctiques Françaises (TAAF). We also thank R Key (Princeton University) for his review and insightful comments.

REFERENCES

Bard E, Arnold M, Maurice P, Duplessy JC. 1987. Measurements of bomb radiocarbon in the ocean by means of accelerator mass spectrometry: technical aspects. *Nuclear Instruments and Methods in Physics Research B* 29:297–301.

Broecker WS, Peng TH, Östlund G, Stuiver M. 1985. The distribution of bomb radiocarbon in the ocean. *Journal of Geophysical Research* 90:6953–70.

Broecker WS, Patzert WC, Toggweiler JR, Stuiver M. 1986a. Hydrography, chemistry and radioisotopes in the Southeast Asian basins. *Journal of Geophysical Research* 91:14,345–54.

Broecker WS, Peng TH, Östlund G. 1986b. The distribution of bomb tritium in the ocean. *Journal of Geophysical Research* 91:14,331–44.

Broecker WS, Sutherland S, Smethie W, Peng TH, Östlund G. 1995. Oceanic radiocarbon: separation of the natural and bomb components. *Global Biogeochemical Cycles* 9:263–88.

Druffel ERM. 1987. Bomb radiocarbon in the Pacific: annual and seasonal timescale variations. *Journal of Marine Research* 45:667–98.

Ffield A, Gordon AL. 1992. Vertical mixing in the Indonesian thermocline. *Journal of Physical Oceanography* 22:184–95.

Fieux M, Andrié C, Delecluse P, Ilahude AG, Kartavseff A, Mantisi F, Molcard R, Swallow JC. 1994. Measurements within the Pacific-Indian Oceans throughflow region. *Deep-Sea Research* 41:1091–130.

Fine RA. 1985. Direct evidence using tritium data for throughflow from the Pacific into the Indian Ocean. *Nature* 315:478–80.

Fine RA, Lukas R, Bingham FM, Warner MJ, Gammon RH. 1994. The western equatorial Pacific: a water mass crossroads. *Journal of Geophysical Research* 99: 25,063–80.

GEBCO (General Bathymetric Chart of the Oceans, Department of Fisheries and Oceans). 1984. Canadian Hydrographic Chart Distribution Office, Canadian Government Publishing Center, Ottawa, Canada.

Gordon AL. 1986. Interocean exchange of thermocline water. *Journal of Geophysical Research* 91:5037–46.

Gordon AL, Fine RA. 1996. Pathways of water between the Pacific and Indian Oceans in the Indonesian seas. *Nature* 379:146–9.

Gordon AL, Giulivi CF, Ilahude AG. 2003. Deep topographic barriers within the Indonesian seas. *Deep-Sea Research* 50:2205–28.

Jean-Baptiste P, Andrié C, Lelu M. 1989. Helium diffusion through glass. *Glass Technology* 30:228–30.

Jean-Baptiste P, Mantisi F, Dapoigny A, Stievenard M. 1992. Design and performance of a mass spectrometric facility for measuring helium isotopes in natural waters and for low-level tritium determination by the helium-3 ingrowth method. *Applied Radiations and Isotopes* 43:881–91.

Jean-Baptiste P, Fieux M, Dapoigny A, Ilahude AG. 1997. An eastern Indian Ocean ^{3}He section from Australia to Bali: evidence for a deep Pacific-Indian throughflow. *Geophysical Research Letters* 24:2577–80.

Jenkins WJ. 2002. World Ocean Circulation Experiment (WOCE) one-time cruises data [internet]. http:/whpo.ucsd.edu/data/onetime.

Key RM, Quay P, Schlosser P, McNichol AP, Von Reden KF, Schneider RJ, Elder KL, Stuiver M, Ostlund HG. 1996. WOCE radiocarbon IV: Pacific Ocean results; P10, P13N, P14C, P18, P19 & S4P. *Radiocarbon* 38(2):239–392.

Kumamoto Y, Murata A, Saito C, Honda M, Kusakabe M. 2002. Bomb radiocarbon invasion into the northwestern North Pacific. *Deep-Sea Research II* 49: 5339–51.

Leboucher V, Orr J, Jean-Baptiste P, Arnold M, Monfray P, Tisnerat-Laborde N, Poisson A, Duplessy JC. 1999. Oceanic radiocarbon between Antarctica and South Africa along WOCE section I6 at 30°E. *Radiocarbon* 41(1):51–73.

McCartney MS. 1982. The subtropical recirculation of mode waters. *Journal of Marine Research* 40:427–64.

Moore MD, Schrag DP, Kashgarian M.1997. Coral radiocarbon constraints on the source of the Indonesian throughflow. *Journal of Geophysical Research* 102: 12,359–65.

Rubin SI, Key RM. 2002. Separating natural and bomb-produced radiocarbon in the ocean: the potential alkalinity method. *Global Biogeochemical Cycles* 16: 1105–24.

Schlosser P. 2002. World Ocean Circulation Experiment (WOCE) one-time cruises data [internet]. http:/whpo.ucsd.edu/data/onetime.

Toggweiler JR, Dixon K, Bryan K.1989. Simulations of radiocarbon in a coarse-resolution world ocean model: distributions of bomb-produced carbon-14. *Journal of Geophysical Research* 94:8243–64.

Toole JM, Millard RC, Wang Z, Pu S. 1990. Observations of the Pacific north equatorial current bifurcation at the Philippines coast. *Journal of Physical Oceanography* 20:307–18.

Top Z, Gordon A, Jean-Baptiste P, Fieux M, Ilahude AG, Muchtar M. 1997. Helium-3 in Indonesians seas: inferences on deep pathways. *Geophysical Research Letters* 24:547–50.

Warren BA. 1981. Transindian hydrographic section at Lat. 18°S: Property distributions and circulation in the South Indian Ocean. *Deep-Sea Research* 28:759–88.

Weiss W, Roether W. 1980. The rate of tritium input to the world oceans. *Earth and Planetary Science Letters* 49:435–46.

RADIOCARBON, Vol 46, Nr 2, 2004, p 583–594

RADIOCARBON IN THE WATER COLUMN OF THE SOUTHWESTERN NORTH PACIFIC OCEAN—24 YEARS AFTER GEOSECS

Pavel P Povinec[1,2] • Takafumi Aramaki[3] • George S Burr[4] • A J Timothy Jull[4] • Laval Liong Wee Kwong[1] • Orihiko Togawa[1,3]

ABSTRACT. In the framework of the Worldwide Marine Radioactivity Studies (WOMARS) project, water profile samples for radiocarbon measurements were taken during the IAEA'97 cruise at 10 stations in the southwestern North Pacific Ocean. While ^{14}C concentrations were rapidly decreasing from the surface ($\Delta^{14}C$ about 100‰) down to about 800 m at all visited stations ($\Delta^{14}C$ about –200‰), the concentrations below 1000 m were almost constant. Some stations were in proximity to the GEOSECS stations sampled in 1973; thus, ^{14}C profiles could be compared after a 24-yr interval. Generally, ^{14}C concentrations had decreased in surface waters (by 50–80‰) and increased (by about the same amount) in intermediate waters when compared with GEOSECS data. In deep waters (below 1000 m), the observed ^{14}C concentrations were similar to GEOSECS values. The bomb-produced ^{14}C inventory had increased by more than 20% over the 24 yr from 1973 to 1997 and was estimated to be about $(32 \pm 5)\ 10^{12}$ atom m^{-2}, with an annual ^{14}C flux of $(1.3 \pm 0.3)\ 10^{12}$ atom $m^{-2}\ yr^{-1}$. The results suggest that bomb-produced ^{14}C has been advected northwards by the Kuroshio Current and the Kuroshio Extension and stored in the intermediate layer as North Pacific Intermediate Water.

INTRODUCTION

From 1995 to 2002, the International Atomic Energy Agency's Marine Environment Laboratory (IAEA-MEL), Monaco, in collaboration with 35 institutes, carried out a research project entitled Worldwide Marine Radioactivity Studies (WOMARS). The main objectives were the following:

- To identify the major sources of anthropogenic radionuclides in the world's oceans and seas;
- To develop present knowledge of concentrations and distributions of the key radionuclides—^{3}H, ^{14}C, ^{90}Sr, ^{129}I, ^{137}Cs, and Pu isotopes—in water and sediment of the world's oceans and seas;
- To study the changes in radionuclide concentrations in the oceans with time using good quality historical data (e.g. from the Geochemical Ocean Sections Programme [GEOSECS] of the mid-1970s) and new data sets collected recently.

In the framework of the WOMARS project, in November 1997, IAEA-MEL organized a research cruise (IAEA'97 Pacific Ocean Expedition) to sample seawater, sediment, and biota in the southwestern North Pacific Ocean. The objectives of this expedition were to develop an understanding of the present open ocean distribution of radionuclides for comparison with data sets obtained in an earlier (GEOSECS) and a more recent (World Ocean Circulation Experiment [WOCE]) international survey of radionuclides in the same region and, specifically, to trace global fallout radionuclides and radionuclides produced during nuclear weapons tests (local fallout) carried out at the Marshall Islands (Povinec and Togawa 1999; Povinec et al. 2003).

Background Oceanography

Specific circulation patterns in the southwestern North Pacific Ocean make radionuclide tracers particularly useful. In the equatorial region, the North Equatorial Current (NEC) is the dominant surface current which flows westward at the southern boundary of the survey area (around Pohnpei),

[1]International Atomic Energy Agency, Marine Environment Laboratory, Monte-Carlo, MC 98012 Monaco.
[2]Corresponding author. Email: p.povinec@iaea.org.
[3]Japan Atomic Energy Research Institute, Marine Research Laboratory, Mutsu, Aomori-ken, Japan.
[4]University of Arizona, NSF Arizona AMS Facility, Tucson, Arizona, USA.

Proceedings of the 18th International Radiocarbon Conference, edited by N Beavan Athfield and R J Sparks
RADIOCARBON, Vol 46, Nr 2, 2004, p 583–594

and on reaching the island of Honshu, merges into the Kuroshio Current. The Kuroshio Current leaves the Japanese coast at between 36°N and 39°N and meets the Oyashio Current (subarctic gyre). The Kuroshio Extension bifurcates at around 155°E into the main current and a northern branch (Kawabe and Taira 1998).

The dominant water masses in the North Pacific are the North Pacific Tropical Waters (NPTW), the North Pacific SubTropical Mode Waters (NPSTMW), and the North Pacific Intermediate Waters (NPIW). NPTW are composed of saline surface water produced in the central region of the North Pacific, while NPSTMW and NPIW are generated in the western North Pacific. NPSTMW are defined as a voluminous water mass in an isothermal layer around 16.5 °C and a layer of potential vorticity minimum $<2 \times 10^{-12} cm^{-1} s^{-1}$, which is formed by deep vertical convection in winter just south of the Kuroshio Current and the Kuroshio Extension (Suga et al. 1989). NPIW exist in the intermediate minimum salinity layer at isopycnal 26.8 σ_θ (potential density) and at isopycnal 27.28 σ_θ, respectively (Reid 1965). NPIW are formed in the region where subtropical waters mix with subarctic waters and then extend to the subtropical gyre (Talley 1993). The deep waters in the investigated area are composed of North Pacific Deep Waters (NPDW).

^{14}C in the Water Column of the Southwestern North Pacific

Radiocarbon enters the ocean through air-sea CO_2 gas exchange, with an equilibration time of 7 to 10 yr. It mainly exists as dissolved inorganic carbonic acid in seawater. Due to its radioactive decay, dissolved inorganic ^{14}C ($DI^{14}C$) in the ocean decreases from the time it enters the ocean, allowing $DI^{14}C/^{12}C$ ratios in seawater to be used to calculate the "age" of seawater (Tsunogai 1981). In the 1950s and 1960s, atmospheric testing of nuclear weapons released large amounts of ^{14}C into the atmosphere, approximately doubling the pre-bomb levels (Levin et al. 1985). Subsequently, surface water in the ocean containing ^{14}C originating from these tests gradually spread deeper into the ocean. Thus, the ^{14}C of bomb origin has provided a means to study air-sea gas exchange and trace intermediate and deep water circulation in the oceans over the last few decades (e.g. Broecker et al. 1985). Broecker et al. (1995) found a relationship between ^{14}C concentration and silicate contents in deep water where no effects of bomb tests were observed, and proposed a method for separation of natural and bomb components of observed vertical $\Delta^{14}C$ profiles. Their method is widely used for estimating the bomb-^{14}C inventory in the ocean (Peng et al. 1998; Leboucher et al. 1999; Watanabe et al. 1999).

In this paper, we present and discuss ^{14}C data obtained for the water column of the southwestern North Pacific Ocean sampled during the IAEA'97 Pacific Ocean Expedition. Some of the northern stations were located close to GEOSECS stations, and preliminary results have been published by Aramaki et al. (2001). In the current paper, we present the complete results and discuss the behavior of bomb ^{14}C in the southwestern North Pacific, including the bomb-produced ^{14}C inventory, over the 24-yr interval between 1973 and 1997.

METHODS

Sampling

In 1997 (21 October–20 November), seawater profile samples for ^{14}C measurements were collected at 10 stations in the southwestern North Pacific during the "IAEA'97 Pacific Ocean Expedition" on board the research vessel "Bosei Maru" (Tokai University, Japan) (Figure 1). Four IAEA stations (IAEA-2, 2B, 3, and 4) were close to GEOSECS stations (GEOSECS-223, 225, 226, and 227) sampled in 1973. IAEA Station 1 was located between GEOSECS Stations 224 and 223. IAEA Stations

6 and 7 were located close to the Bikini and Enewetak Atolls, respectively. IAEA Stations 5, 8, and 9, located north of the Marshall Islands, were chosen in order to trace radionuclides released as local fallout from the nuclear weapons tests.

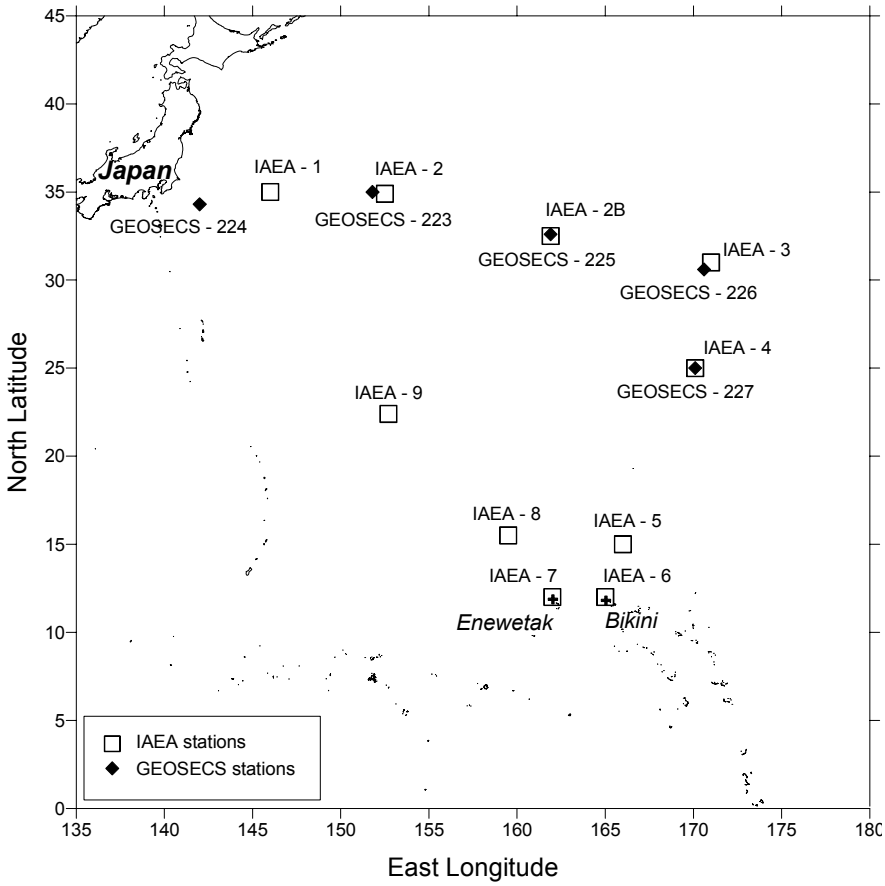

Figure 1 Sampling stations for ^{14}C measurements of the IAEA'97 Pacific Ocean Expedition and GEOSECS stations (1973)

Seawater samples for ^{14}C measurements were collected at each station using a CTD/RMS system equipped with Niskin bottles. Collected samples were stored in 500-mL glass bottles with hermetic stoppers mixed with 100 µL of saturated $HgCl_2$ solution to poison the sample.

Sample Preparation and ^{14}C Measurements

^{14}C measurements of samples taken at 6 stations (1, 2B, 4, 5, 8, and 9) were carried out at the Japan Atomic Energy Research Institute's Marine Research Laboratory in Mutsu, Japan (JAERI-MRL), and measurements of samples from the other 4 stations (2, 3, 6, and 7) were carried out at the University of Arizona's Accelerator Mass Spectrometry (AMS) facility in Tucson, Arizona. The seawater samples were prepared for the measurement of the $^{14}C/^{12}C$ or $^{14}C/^{13}C$ ratios in dissolved inorganic carbon (DIC) by both JAERI-MRL and the University of Arizona, using each laboratory's specific methods.

In the JAERI-MRL measurements, the DIC in the sample was extracted as CO_2 gas by adding 4 mL of 100% H_3PO_4, stripped using pure N_2 gas, and cryogenically collected in a vacuum (Aramaki et

al. 2000). The CO_2 gas was reduced to graphite with pure H_2 gas over an Fe catalyst at 650 °C (Kitagawa et al. 1993; Aramaki et al. 2000). Graphite was pressed into targets for AMS ^{14}C measurements. The stable isotopic composition of sub-samples of the CO_2 gas was measured in a Finnigan mass spectrometer, DELTA^{plus}. The ratio of ^{14}C to ^{12}C was measured by a Tandetron AMS (HVEE, model 4130-AMS) at JAERI-MRL. The ^{14}C activity in seawater samples has been expressed as $\Delta^{14}C$ (Stuiver 1980; Aramaki et al. 2001).

In the University of Arizona measurements, the DIC in seawater was extracted by acidification of the sample to pH 3 and the CO_2 released was cryogenically extracted in a flow of high-purity O_2 gas. The CO_2 gas was reduced to graphite over an Fe catalyst, following the procedure described by Donahue et al. (1990a). Graphite was pressed into targets for AMS ^{14}C measurements. The stable isotopic composition of sub-samples of CO_2 gas was measured in an Optima mass spectrometer. The ratio of ^{14}C to ^{13}C was measured at the NSF Accelerator Facility for Radioisotope Analysis at the University of Arizona. The ^{14}C activity in seawater samples is expressed by the $\Delta^{14}C$ value (Stuiver 1980; Donahue et al. 1990b).

Intercomparison measurements were carried out on seawater samples collected at Station 1 which showed good agreement between both laboratories (Liong et al., these proceedings).

RESULTS AND DISCUSSION

^{14}C Vertical Profiles

^{14}C vertical profile measurements are presented in Figure 2 and Table 1 (only data from the University of Arizona [Stations 2, 4, 6, and 7] are given in the table, as the JAERI-MRI data were published by Aramaki et al. 2001). All profiles have similar curves, although differences can be observed at surface and sub-surface water depths. Generally, the $\Delta^{14}C$ values below 1000 m are the same within uncertainties, except for Station 7 which shows the lowest observed $\Delta^{14}C$ values (at the surface and 1000–2500 m water depths) in contrast to the other radionuclides measured (Povinec et al. 2003). We do not understand at present the reason for this offset, since there are not available comparable data from GEOSECS and WOCE. Surface concentrations (in top 150 m) differ for different stations, and as shown in Figure 3, there is still a visible latitudinal effect, although it probably differs from the original global fallout input. A similar trend was observed for other radionuclides as well (Povinec et al. 2003).

Comparison with WOCE and GEOSECS Data

A very comprehensive $\Delta^{14}C$ data set for the Pacific Ocean has been published recently by the WOCE collaboration (Key et al. 2002). Although the WOCE stations in the southwestern Pacific (sampled in 1993) differ from the WOMARS stations, a comparison presented in Figure 4 for stations in similar latitudinal belts (IAEA Stations 1, 2B, and 3 versus WOCE Stations 78 and 80) shows that WOMARS data are comparable to WOCE data.

A comparison of our $\Delta^{14}C$ profiles with GEOSECS results (Ostlund and Stuiver 1980) are presented in Figure 5 (only stations situated in the northwest Pacific could be compared, as there are no GEOSECS data for stations in the southwest). At Stations 2B, 3, and 4, our $\Delta^{14}C$ values in the surface layer (<200 m) are lower than the GEOSECS values (by up to 50–80‰) but higher (by up to about 60‰) in the sub-surface layer (200–800 m). As other recent ^{14}C measurements in the subtropical western North Pacific also indicate an increase of $\Delta^{14}C$ values in intermediate waters (Gamo et al. 1987; Watanabe et al. 1999; Aramaki 2002; Key et al. 2002), our results are consistent with their observations.

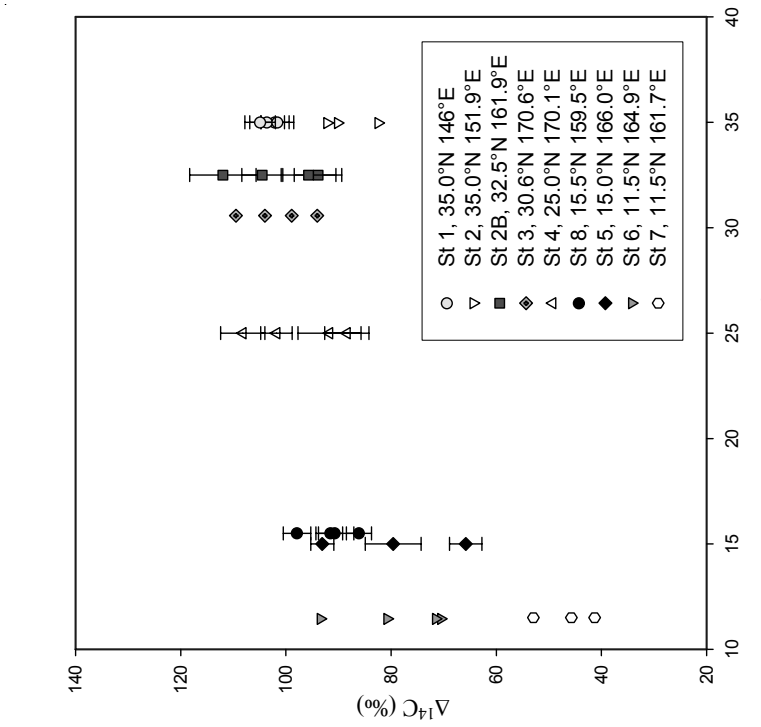

Figure 3 $\Delta^{14}C$ in surface water (top 150 m) as a function of latitude

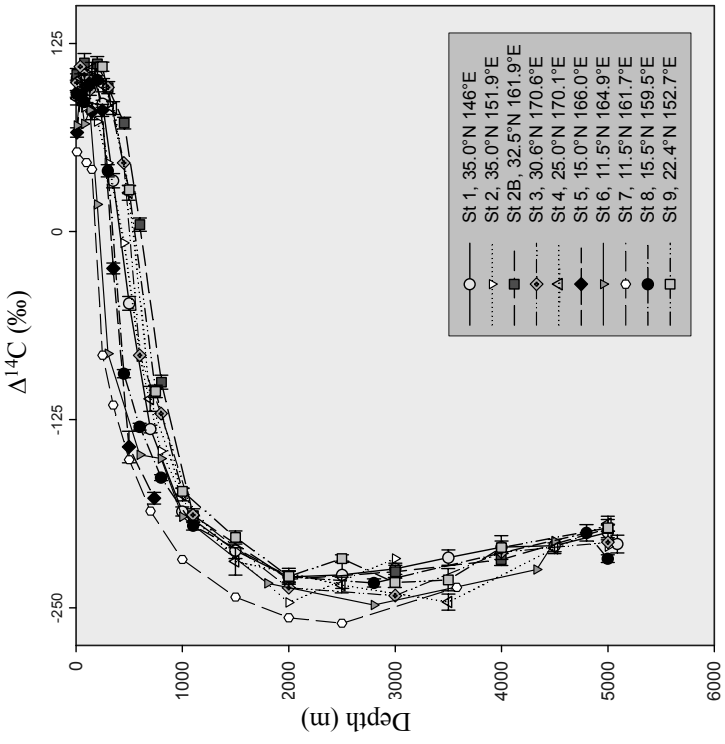

Figure 2 Vertical $\Delta^{14}C$ profiles observed at IAEA'97 stations

Table 1 $\Delta^{14}C$ data for IAEA'97 Stations 2, 3, 6, and 7.

Location	Depth (m)	$\Delta^{14}C$ (‰)	Location	Depth (m)	$\Delta^{14}C$ (‰)
Station 2			**Station 6**		
34.97°N,151.89°E	10	92.2 ± 5.1	11.45°N, 164.88°E	10	70.5 ± 4.1
	40	90.2 ± 5.0		40	93.4 ± 5.2
	80	82.5 ± 4.2		80	71.5 ± 4.2
	130	—		130	80.7 ± 4.6
	200	73.0 ± 4.1		200	18.1 ± 2.9
	300	45.7 ± 2.9		300	–81.1 ± –4.4
	450	–7.6 ± –3.0		450	—
	600	–83.3 ± –4.3		600	–148.3 ± –7.5
	800	–145.9 ± –7.5		800	–150.8 ± –8.0
	1100	–191.2 ± –10.0		1000	–189.6 ± –9.7
	2000	–246.5 ± –12.0		1800	–233.7 ± –12.1
	3000	–217.3 ± –11.0		2800	–248.2 ± –1.2
	4000	—		4330	–224.5 ± –11.5
	5000	–209.4 ± –10.6		4500	–205.9 ± –10.7
Station 3			**Station 7**		
30.57°N, 170.62°E	10	98.9 ± 5.5	11.5°N, 161.74°E	10	53.0 ± 3.4
	40	109.5 ± 5.8		100	45.7 ± 2.9
	80	104.0 ± 5.7		150	41.3 ± 2.9
	130	94.0 ± 5.3		250	–82.2 ± –4.8
	200	—		350	–115.3 ± –6.6
	300	95.8 ± 5.3		500	–151.7 ± –8.1
	450	45.6 ± 2.8		700	–185.8 ± –9.6
	600	–82.2 ± –4.3		1000	–217.9 ± –11.1
	800	–121.0 ± –6.4		1500	–242.9 ± –12.1
	1100	–188.3 ± –9.8		2000	–256.6 ± –13.0
	2000	–236.7 ± –12.0		2500	–260.3 ± –13.0
	3000	–241.9 ± –12.1		3580	–236.5 ± –1.2
	4000	–213.1 ± –11.3		—	—
	5000	–206.5 ± –10.5		—	—

On the other hand, at Stations 1 and 2, the $\Delta^{14}C$ values are lower (by up to 50‰) in the layer above 1500 m. At these stations, the differences between our and GEOSECS observations are found in vertical salinity profiles as well, and this may be caused by the influence of the saline Kuroshio Extension waters in the sampling region (Aramaki et al. 2001). Furthermore, Station 1 lies about 500 km to the east of GEOSECS Station 224 (see Figure 1). Thus, the differences in $\Delta^{14}C$ vertical profiles at these stations are due to the presence of different water masses at the time of the 2 sampling missions, and it is difficult to directly compare data from Stations 1 and 2 with data from GEOSECS Stations 224 and 223, respectively. In Figure 6, $\Delta^{14}C$ values at Stations 1 and 2 are plotted against density (σ_θ), and compared with GEOSECS Stations 224 and 223, respectively. Our $\Delta^{14}C$ values above 25.5 σ_θ (250 m at Station 1 and 170 m at Station 2) are lower than the GEOSECS values, but higher in the intermediate water layer with 25.5–27.0 σ_θ (27.0 σ_θ = 680 m at Station 1 and 27.0 σ_θ = 700 m at Station 2). Stations 2B, 3, and 4 show a similar tendency, confirming that at least at Station 2, water masses have changed since the GEOSECS mission.

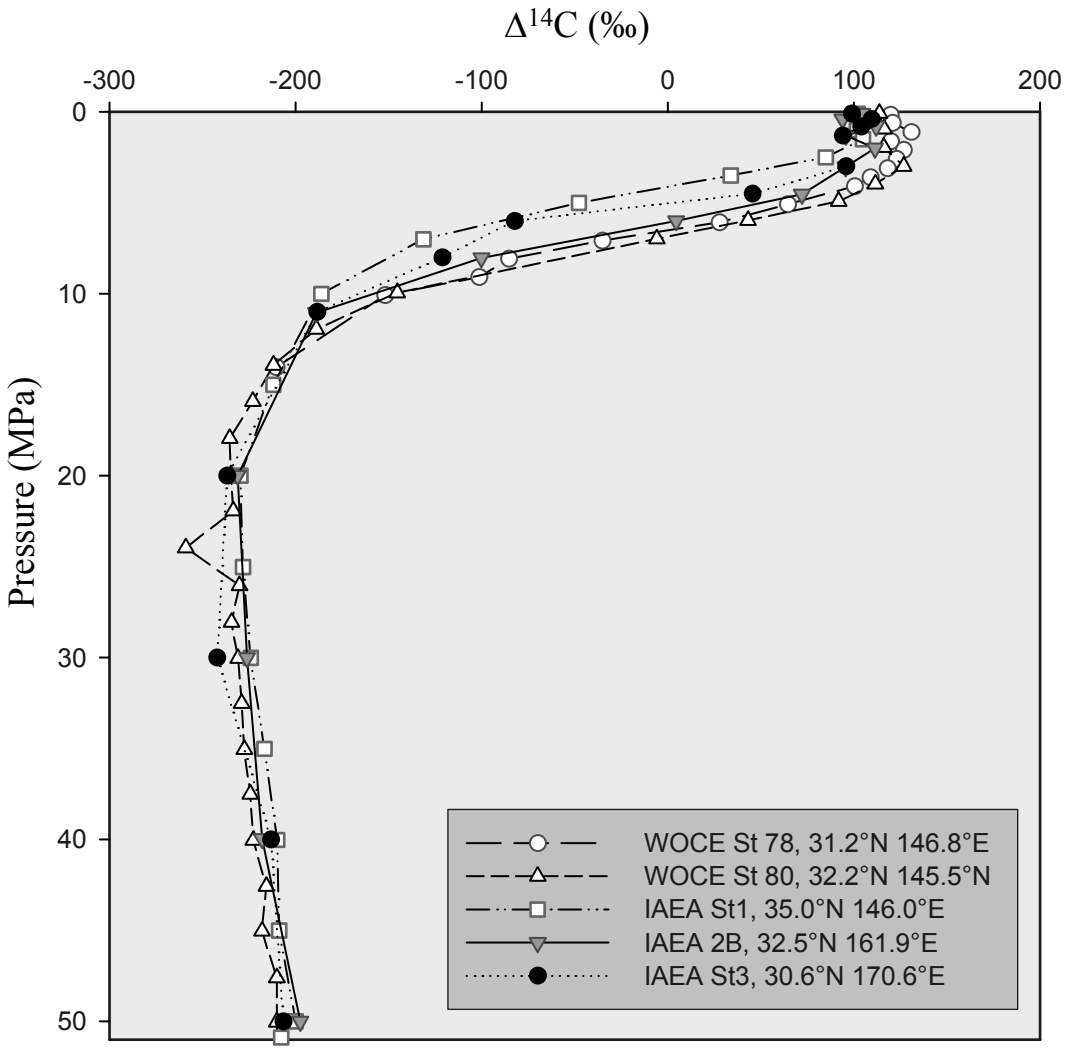

Figure 4 Comparison of vertical $\Delta^{14}C$ profiles observed at IAEA'97 and WOCE (1993) stations

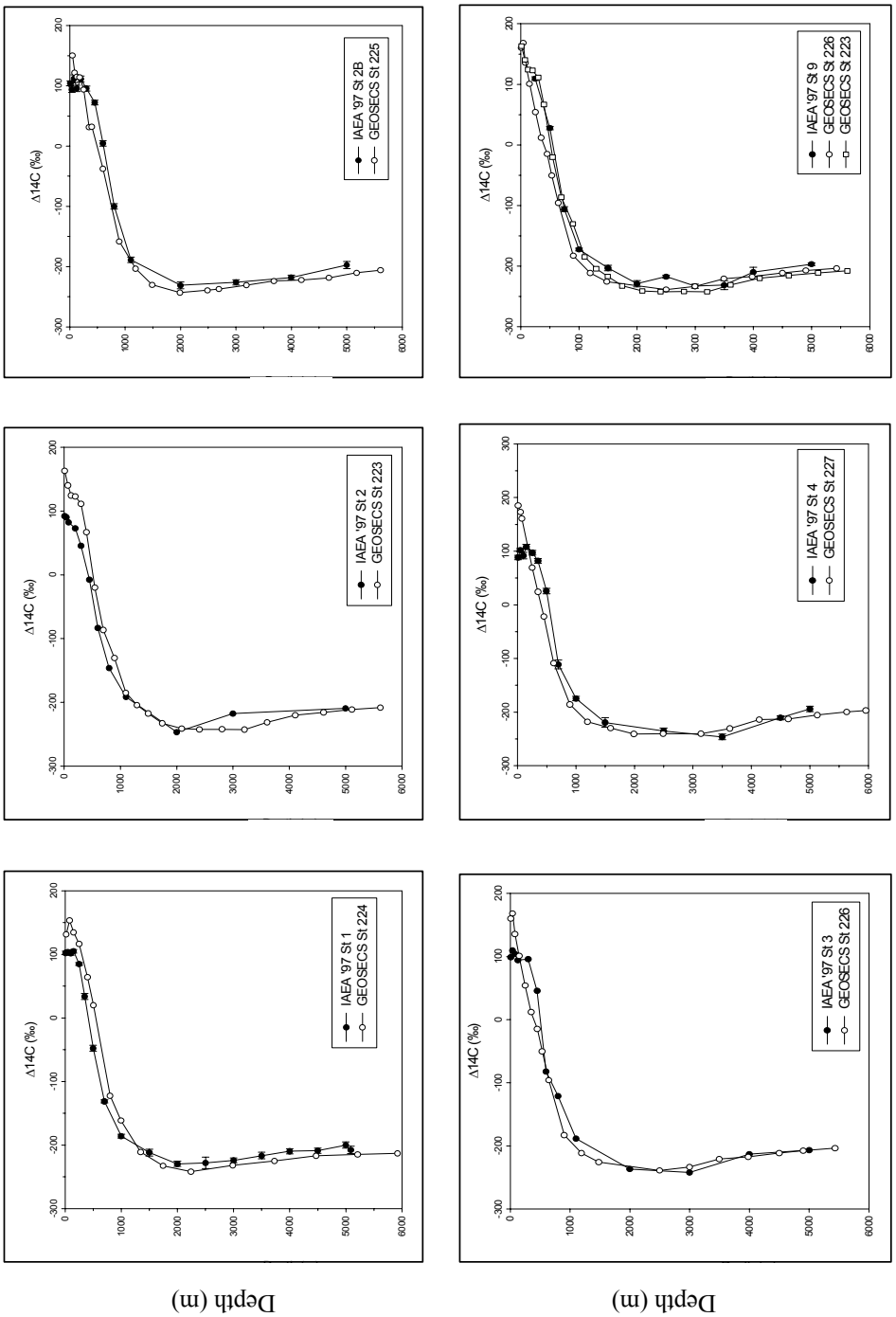

Figure 5 Comparison of IAEA'97 and GEOSECS vertical $\Delta^{14}C$ profiles

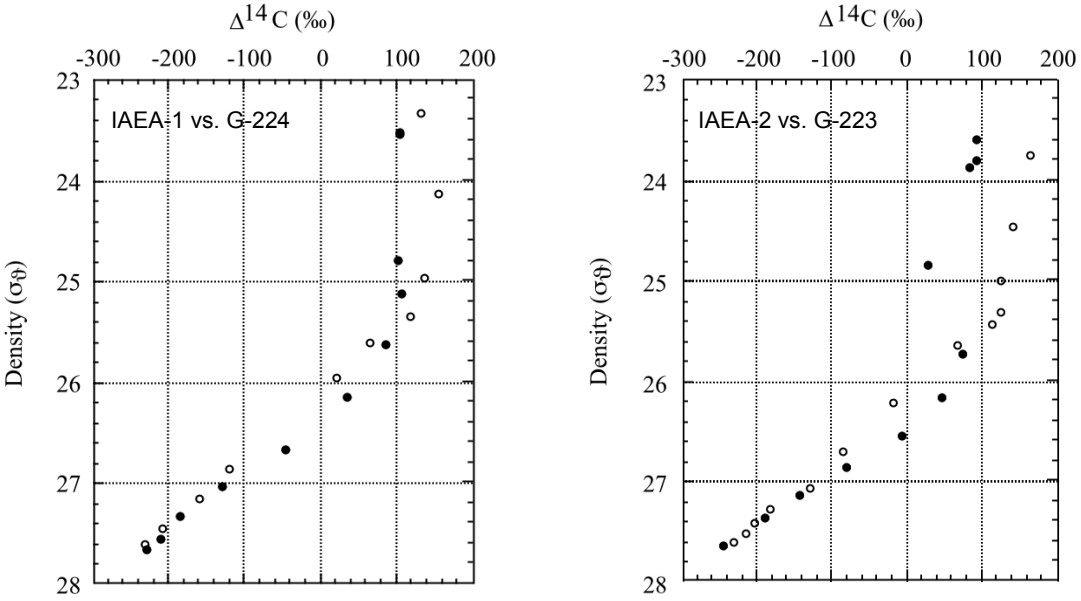

Figure 6 Comparison of $\Delta^{14}C$ vertical profiles against density (σ_θ) between IAEA (dots) and GEOSECS (open circles) stations.

Bomb ^{14}C Behavior in the Southwestern North Pacific

Two sets of vertical profiles (this work and GEOSECS) are used to analyze the behavior of bomb ^{14}C in the southwestern North Pacific over the 24-yr period between 1973 and 1997. The bomb ^{14}C content ($^{14}C_{bomb}$) is expressed as

$$^{14}C_{bomb} = (\Delta^{14}C_{obs} - \Delta^{14}C_{nat}) \times \alpha \times \Sigma CO_2 \quad (1),$$

where $\alpha = 1.176 \times 10^{-12}$ is the ratio of $^{14}C/^{12}C$ at $\Delta^{14}C = 0‰$, and ΣCO_2 is the total carbonate content in mole kg^{-1}, at the time of "observation" and "natural." Both ΣCO_2 at the same depth are regarded as approximately similar values. Therefore, we can calculate the bomb ^{14}C inventory (I_{bomb}), integrating $^{14}C_{bomb}$ from the surface to the lower limit of the bomb ^{14}C penetration depth (z, m) by the following equation:

$$\Delta I_{bomb} = \int_0^Z {}^{14}C_{bomb}\,dz \times \rho \times N_A \quad (2),$$

where ρ and N_A are the density of seawater in kg m^{-3} and Avogadro number ($= 6.02 \times 10^{23}$), respectively. The variability (ΔI_{bomb}) of I_{bomb} in each water column during the last 24 yr is expressed as follows:

$$\Delta I_{bomb} = I_{1997} - I_{1973} \quad (3).$$

By substituting equations (2) at 1973 and 1997 for equation (3), we can obtain the following equation:

$$\Delta I_{bomb} = \int_0^Z {}^{14}C_{1997-1973}\,dz \times \rho \times N_A \quad (4),$$

where $^{14}C_{1997-1973}$ is defined as

$$^{14}C_{1997-1973} = (\Delta^{14}C_{1997} - \Delta^{14}C_{1973}) \times \alpha \times \Sigma CO_2 \quad (5).$$

The calculated ΔI_{bomb} inventories at Stations 2B, 3, and 4 are given in Table 2, where we assume the following: (i) surface water is seawater above 25.5 σ_θ of which the average depth is 200 m; (ii) intermediate water is a water mass of 25.5–27.0 σ_θ; and (iii) deep water is seawater below 27.0 σ_θ (830 m), as defined by Reid (1965), see also Figure 6. At Stations 1 and 2, ΔI_{bomb} cannot be calculated because of the presence of different water masses at the time of the 2 expeditions (this work and GEOSECS). An average value of total of ΔI_{bomb} was (31.9 ± 5.0) × 10^{12} atom m^{-2}. The annual flux of bomb ^{14}C in the southwestern North Pacific from 1973 to 1997 is (1.3 ± 0.3) 10^{12} atom $m^{-2}yr^{-1}$, and is consistent with a previous study in the western North Pacific (Watanabe et al. 1999). The amount of bomb ^{14}C in surface water decreased by (9.4 ± 3.0) 10^{12} atom m^{-2} (0.4 × 10^{12} atom $m^{-2}yr^{-1}$); conversely, the amount of bomb ^{14}C in intermediate water increased by (41.3 ± 3.4) 10^{12} atom m^{-2} (1.7 × 10^{12} atom $m^{-2}yr^{-1}$). On the other hand, in deep water, no variability of I_{bomb} over the 24-yr period was found, suggesting that no bomb ^{14}C had been transported into deep water up to the time of sampling in 1997.

Table 2 The variability of the bomb ^{14}C inventory (ΔI_{bomb}) in the water column, 1973–1997.

		ΔI_{bomb} (× 10^{12} atom m^{-2})			
Station	Location	Total	above 25.5 σ_θ	25.5–27.0 σ_θ	below 27.0 σ_θ
IAEA-2B G-225	32.5°N 161.9°E	37.5	–7.3	44.9	0
IAEA-3 G-226	30.6°N 170.6°E	30.1	–8.0	38.1	0
IAEA-4 G-227	25.0°N 170.1°E	28.2	–12.8	40.9	0
Average:		31.9 ± 5.0	–9.4 ± 3.0	41.3 ± 3.4	0

Annual flux: 1.3 × 10^{12} atom/m^2 yr

The increase of bomb ^{14}C in the water column can be considered to be equal to the increase in the intermediate layer. Atmospheric $\Delta^{14}C$ increased substantially during the 1960s, and then decreased from the late 1960s to the present (Levin et al. 1994). The main input of atmospheric bomb ^{14}C was absorbed into surface water over the whole Pacific Ocean between the 1960s and the 1970s. At the same time, excess bomb ^{14}C in surface water was transported northward by advection by the Kuroshio Current and/or Kuroshio Extension Current. Bomb ^{14}C absorbed into surface water in subarctic areas was carried to the intermediate layer by strong vertical mixing. The excess bomb ^{14}C in the intermediate layer in subarctic areas was transported to the subtropical area by North Pacific Intermediate Water (NPIW) (Mahadevan 2001; Aramaki 2002).

CONCLUSIONS

In the framework of IAEA-MEL's project on Worldwide Marine Radioactivity Studies (WOMARS), water profile samples were taken during the IAEA'97 Pacific Ocean cruise at 10 stations in the southwestern North Pacific Ocean. Some stations were in proximity to the GEOSECS stations sampled in 1973; thus, ^{14}C profiles could be compared over the 24-yr interval. The following conclusions were drawn from the present work:

- ^{14}C concentrations had decreased in surface waters (by 50–80‰) and increased (by about the same amount) in intermediate waters. In deep waters (below 1000 m), the observed ^{14}C concentrations were similar to GEOSECS values (except for Station 7). While a rapid decrease in ^{14}C concentrations was observed from the surface (^{14}C approximately 100‰) down to 1000 m (^{14}C approximately –200‰), the concentrations below 1000 m were almost constant. The bomb-produced ^{14}C inventory had increased by more than 20% over the 24-yr period studied.
- The variability of bomb ^{14}C inventories in the water column over the 24-yr period (ΔI_{bomb}) was estimated at $(32 \pm 5)\ 10^{12}$ atom m^{-2}. The amount of bomb ^{14}C in surface water had decreased to $(9.4 \pm 3.0)\ 10^{12}$ atom m^{-2}; conversely, the amount of bomb ^{14}C in intermediate water had increased to $(41 \pm 4)\ 10^{12}$ atom m^{-2}. However, no variation of I_{bomb} was found in deep water over the period. The average annual flux of bomb ^{14}C has been estimated to be $(1.3 \pm 0.3)\ 10^{12}$ atom $m^{-2}\ yr^{-1}$.
- The results suggest that excess bomb ^{14}C in surface water of the southwestern Pacific Ocean was transported northward by advection by the Kuroshio Current and Kuroshio Extension and then transported into the intermediate layer by North Pacific Intermediate Water (NPIW), which flows southward from the subarctic area to the tropics.

ACKNOWLEDGEMENTS

The WOMARS project and the IAEA '97 Pacific Ocean Expedition were conducted thanks to the generous support provided by the Science and Technology Agency of Japan (presently the Ministry of Education, Culture, Sports, Science, and Technology). The authors are indebted to their colleagues and the crew of the R/V Bosei Maru for their kind cooperation during the field work. We also wish to thank colleagues at JAERI-MRL and the University of Arizona for sample preparation and ^{14}C AMS measurements. IAEA-MEL operates under a bilateral agreement between the IAEA and the Government of the Principality of Monaco.

REFERENCES

Aramaki T. 2002. Study on seawater circulation in the western North Pacific and its marginal seas in the viewpoint of distribution of radiocarbon in seawater [PhD dissertation]. Sapporo, Japan: Hokkaido University.

Aramaki T, Mizushima T, Mizutani Y, Yamamoto T, Togawa O, Kabuto S, Kuji T, Gottdang A, Klein M, Mous DJW. 2000. The AMS facility at the Japan Atomic Energy Research Institute (JAERI). *Nuclear Instruments and Methods in Physics Research B* 172: 18–23.

Aramaki T, Mizushima T, Kuji T, Povinec PP, Togawa O. 2001. Distribution of radiocarbon in the southwestern North Pacific. *Radiocarbon* 43(2B):857–68.

Broecker WS, Peng T-H, Ostland G, Stuiver M. 1985. The distribution of bomb radiocarbon in the ocean. *Journal of Geophysical Research* 90:6953–70.

Broecker WS, Sutherland S, Smethie W, Peng T-H. 1995. Oceanic radiocarbon: separation of the natural and bomb components. *Global Biogeochemical Cycles* 9: 263–88.

Donahue DJ, Linick TW, Jull AJT. 1990a. Isotope-ratio and background corrections for accelerator mass spectrometry radiocarbon measurements. *Radiocarbon* 32(1):135–42.

Donahue DJ, Jull AJT, Toolin LJ. 1990b. Radiocarbon measurements at the University of Arizona AMS facility. *Nuclear Instruments and Methods in Physics Research B* 52:224–8.

Gamo T, Horibe Y, Kobayashi H. 1987. Comparison of oceanic $\Delta^{14}C$ data with those of GEOSECS: vertical profiles in 1973 and 1980 at 30°N 170°E in the northwestern Pacific Ocean. *Radiocarbon* 29(1):53–6.

Kawabe M, Taira K. 1998. Water masses and properties at 165°E in the western Pacific. *Journal of Geophysical Research* 103:12,941–58.

Key RM, Quay PD, Schlosser P, McNichol AP, von Reden KF, Schneider RJ, Elder KL, Stuiver M, Ostlund HG. 2002. WOCE radiocarbon IV: Pacific Ocean results; P10, P13N, P14C, P18, P19 & S4P. *Radiocarbon* 44(1):239–392.

Kitagawa H, Masuzawa T, Nakamura T, Matsumoto E. 1993. A batch preparation method of graphite targets with low background for AMS ^{14}C measurements. *Radiocarbon* 35(2):295–300.

Leboucher V, Orr J, Jean-Baptiste P, Arnold M, Monfray P, Tisnerat-Laborde N, Poisson A, Duplessy J-C. 1999. Oceanic radiocarbon between Antarctica and

South Africa along WOCE section 16 at 30°E. *Radiocarbon* 41(1):51–73.

Levin I, Kromer B, Schoch-Fischer H, Bruns M, Munnich M, Berdau D, Vogel JC, Munnich KO. 1985. 25 years of tropospheric ^{14}C observations in Central Europe. *Radiocarbon* 27(1):1–19.

Levin I, Kromer B, Schoch-Fischer H, Bruns M, Munnich M, Berdau D, Vogel JC, Munnich KO. 1994. $\Delta^{14}CO_2$ records from sites in Central Europe, Trends '93. In: Boden TA, Kaiser DP, Sepanski RJ, Stoss FW, editors. *A Compendium of Data on Global Change*. Oak Ridge: ORNL/CDIA-65. p 203–22.

Liong Wee Kwong L, Povinec PP, Jull AJT. 2004. Preparation of graphite targets from small marine samples for AMS radiocarbon measurements. *Radiocarbon*, these proceedings.

Mahadeva A. 2001. An analysis of bomb radiocarbon trends in the Pacific. *Marine Chemistry* 73:273–90.

Ostlund HG, Stuiver M. 1980. GEOSECS Pacific radiocarbon. *Radiocarbon* 22(1):25–53.

Peng T-H, Key RM, Ostlund HG. 1998. Temporal variations of bomb radiocarbon inventory in the Pacific Ocean. *Marine Chemistry* 60:3–13.

Povinec PP, Togawa O. 1999. Marine radioactivity studies in the world oceans (MARS). Marine Pollution: Proceedings of the International Symposium, Monaco, 5–9 October 1998. *International Atomic Energy Agency TECDOC-1094*:262–7.

Povinec PP, Livingston HD, Shima S, Aoyama M, Gastaud J, Goroncy I, Hirose K, Huynh-Ngoc L, Ikeuchi Y, Ito T, La Rosa J, Liong Wee Kwong L, Lee SH, Moriya H, Mulsow S, Oregioni B, Pettersson H, Togawa O. 2003. IAEA'97 expedition to the NW Pacific Ocean—results of oceanographic and radionuclide investigations of the water column. *Deep-Sea Research II* 50:2607–37.

Reid JL. 1965. Intermediate waters of the Pacific Ocean. *Johns Hopkins Oceanographic Studies 2*. 85 p.

Stuiver M. 1980. Workshop on ^{14}C data reporting. In: Stuiver M, Kra R, editors. Proceedings of the 10th International ^{14}C Conference. *Radiocarbon* 22(3):964–6.

Suga T, Hanawa K, Toba Y. 1989. Thermostad distribution in the North Pacific subtropical gyre: the central mode water and the subtropical mode water. *Journal of Physical Oceanography* 27:140–52.

Talley LD. 1993. Distribution and formation of North Pacific Intermediate Water. *Journal of Physical Oceanography* 23:517–37.

Tsunogai S. 1981. A method for chronology of the Pacific and Atlantic deep water and its application. *Chikyukagaku* 15:70–6. In Japanese with English abstract.

Watanabe YW, Ono T, Harada K, Fukasawa M. 1999. A preliminary study of oceanic bomb radiocarbon inventory in the North Pacific during the last two decades. *Journal of Oceanography* 55:705–16.

RADIOCARBON, Vol 46, Nr 2, 2004, p 595–601

INTERANNUAL ^{14}C VARIATIONS DURING 1977–1998 RECORDED IN CORAL FROM DAYA BAY, SOUTH CHINA SEA

C D Shen[1,2] • W X Yi[1] • K F Yu[3] • Y M Sun[1] • Y Yang[1] • B Zhou[1]

ABSTRACT. Twenty-two annually banded samples of coral from 1977 to 1998 were collected from Daya Bay, South China Sea, and bomb ^{14}C concentrations were determined. The interannual variation of coral $\Delta^{14}C$ is controlled mainly by oceanic factors. In ENSO years, the coastwise upwelling current of the South China Sea has been intensified; hence, the coral $\Delta^{14}C$ displays its minimum value. The interannual variation curve of $\Delta^{14}C$ in coral bears a relationship with the Southern Oscillation Index (SOI) curves: the correlation coefficient between $\Delta^{14}C$ and $(SOI)_w$ is 0.43 and the correlation coefficient between $\Delta^{14}C$ and $(SOI)_y$ is 0.27. The coral $\Delta^{14}C$ has no remarkable response to the variation of solar radiation energy. In the past 20 yr or so, the general situation and oceanic thermal structure of the South China Sea are still stable even though interannual variations in atmosphere-sea interaction and upwelling current driven by the tropical energy have occurred.

INTRODUCTION

Radioactive isotope tracers such as radiocarbon, ^{3}H, ^{222}Rn, and ^{226}Ra are widely applied in oceanological research simply because these radioactive isotopes can be indicative of some extremely slow processes occurring in seawater, which may include offshore vertical mixing (and its rate), deep-water mixing (and its rate), thermocline vertical mixing (and its rate), upwelling current, oceanic transverse mixing, and so on (Broecker 1974). The conventional oceanological methods are usually useless in the study of these extremely slow processes. Natural ^{14}C and bomb ^{14}C are also the most ideal isotope tracers when studying the interaction processes and their exchange rates between the atmosphere and the oceans (Nydal 2000; Levin et al. 2000).

It is usually considered that carbon isotopes in coral skeletons have attained equilibrium with the inorganic carbon isotopes in ambient seawater (Druffel 1982). Therefore, the ^{14}C variation in annual bands of coral can be used to reveal the interannual variation of ^{14}C in the dissolved inorganic carbon in surface seawater during the growing period of coral. The $\Delta^{14}C$ record of tropical coral from the Atlantic Ocean, the Pacific Ocean, and the Indian Ocean can undoubtedly yield important information about ocean current circulation. Based on the $\Delta^{14}C$ record of coral growing during the 1960s to 1970s from the Sargasso Sea area in the Atlantic Ocean, Druffel et al. (1983, 1986) pointed out that the renewal rate of water mass in this area decreased gradually. Druffel et al. (1989, 1993) also contended, based on the seasonal and annual variations of bomb ^{14}C in coral from middle Pacific Ocean, that the "transequatorial transport of surface currents" characterized by seasonal variations is the dominant factor that controls bomb ^{14}C variation. Research by Toggweiler et al. (1991) on coral ^{14}C in the temperate and tropic zones of the Pacific Ocean before nuclear weapon testing demonstrates that the thermocline seawater in the South Pacific Ocean is characterized by a low $\Delta^{14}C$ value (just like the Subantarctic mode water mass, the 13 °C water mass in the Equator, and the Peruvian upwelling current). This is simply attributed to the fact that the Subantarctic mode water mass with a low ^{14}C value is injected into the thermocline from the northern margin of the Antarctic circumpolar current (Guilderson and Schrag 1998). Recently, Guilderson et al. (1998) have conducted research on ^{14}C of coral from the Galapagos Islands in the East Pacific Ocean, indicating that the $\Delta^{14}C$ and the surface seawater temperature (SST) tend to increase in the seasons with upwelling

[1]Guangzhou Institute of Geochemistry, Chinese Academy of Sciences, Guangzhou 510640, China.
[2]Institute of Earth Environment, Chinese Academy of Sciences, Xi'an 710054, China. Corresponding author.
Email: cdshen@gig.ac.cn.
[3]South China Sea Institute of Oceanology, Chinese Academy of Sciences, Guangzhou 510301, China.

Proceedings of the 18th International Radiocarbon Conference, edited by N Beavan Athfield and R J Sparks
RADIOCARBON, Vol 46, Nr 2, 2004, p 595–601

(July to September) since 1976. The synchronous variation of ^{14}C and SST implies that a change in thermal structure has taken place in a vertical direction in the tropical East Pacific Ocean after 1976. This change could be the main factor responsible for the increased frequency and intensity of the occurrence of ENSO (Guilderson et al. 1998).

This study is mainly focused on *Platygyra* collected from Daya Bay in the South China Sea. The interannual ^{14}C variations in coal samples collected annually are discussed to reveal the characteristics of atmosphere-sea gas exchange and the rules governing the evolution of related climatic events in this sea area.

SAMPLES, METHODS, AND RESULTS

The coral samples examined in this study were collected from Daya Bay in the South China Sea. The sampling sites are about 1.5 km from the thermal effluent outlet of the Daya Bay Nuclear Power Station, and about 10–15 m from the sandy beach (coast). Figure 1 is a map showing the geographical position of Daya Bay and the sampling location. The samples were *Platygyra* sp. collected in October 1998 (Yu et al. 2002). One of our co-authors, Kefu Yu, provided a sectioned slice of the original coral measured at 1 cm thickness, together with its X-radiograph film chart. Annual bands were scored according to the growth lines shown on the sectioned coral sample, and a total of 22 specimens of annual bands from 1977 to 1998 were taken for ^{14}C measurement. All the specimens are composed of spotlessly white crystallized $CaCO_3$-aragonite.

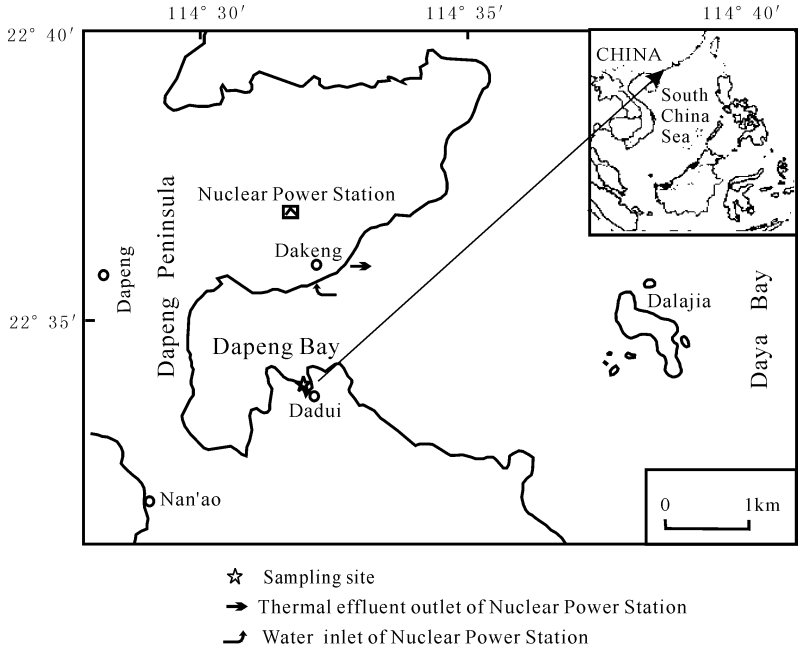

Figure 1 Map showing the geographical position of Daya Bay in the South China Sea

From each annual band, specimens of 5–10 g were taken out, rinsed with deionized water in a supersonic water bath, then acidified with 10% HCl in a glass reactor linked with a vacuum system to derive CO_2. CO_2 gas was repeatedly purified in a series of "liquid nitrogen-dry ice + acetone-liquid nitrogen" traps in the vacuum system, and was finally used to synthesize Li_2C_2 in a stainless steel

reactor under high temperature (900 °C) and vacuum conditions. In succession, Li_2C_2 was hydrolyzed into acetylene (C_2H_2), which was then used to synthesize benzene (C_6H_6) with catalysts. ^{14}C determination for all samples was accomplished on a 1220 Quantulus liquid scintillation counter with extremely low background at the Guangzhou Institute of Geochemistry, the Chinese Academy of Sciences. The results are listed in Table 1, together with the average thickness of the annual growth layer of coral samples, as well as the 1977–1997 atmospheric temperature and 1977–1998 precipitation recorded by the local meteorological observation station (Pan and Wang 1998). In order to conduct a comparative study, the atmospheric ^{14}C data, as recorded in North European tree rings in the Northern Hemisphere on a corresponding timescale (Nydal 2000), are also listed in Table 1. It can be seen from Table 1 that the $\Delta^{14}C$ values of annual bands of the coral samples from 1977–1998 are all greater than zero, which clearly suggests that the contribution of bomb ^{14}C could not be ruled out.

Table 1 ^{14}C measurement results for coral from Daya Bay, South China Sea.

Field code	Lab code	Year	Average thickness of annual growth layer (cm a^{-1})	Atmospheric temperature (°C)	Precipitation (mm)	Atmospheric $\Delta^{14}C$ (‰)	Coral $\Delta^{14}C$ (‰)
DYW-08-1	GC-00081	1977	1.69	22.1	1458.5	335	240
DYW-08-2	GC-00082	1978	1.67	21.8	1930.2	335	230
DYW-08-3	GC-00083	1979	1.56	21.8	2530.0	299	120
DYW-08-4	GC-00084	1980	1.64	22.0	1736.4	271	220
DYW-08-5	GC-00085	1981	1.71	21.9	1986.7	260	190
DYW-08-6	GC-00086	1982	1.69	21.9	1761.3	244	200
DYW-08-7	GC-00087	1983	1.25	21.7	2583.7	223	100
DYW-08-8	GC-00088	1984	1.34	21.4	1438.6	209	160
DYW-08-9	GC-00089	1985	1.54	21.8	1762.2	200	240
DYW-08-10	GC-00090	1986	1.41	21.9	1961.2	186	250
DYW-08-11	GC-00091	1987	1.38	22.7	2038.2	183	160
DYW-08-12	GC-00092	1988	1.33	21.8	1609.7	169	190
DYW-08-13	GC-00093	1989	0.93	22.3	1704.8	159	190
DYW-08-14	GC-00094	1990	0.96	22.5	1469.3	149	200
DYW-08-15	GC-00095	1991	1.29	22.8	1728.3	138	230
DYW-08-16	GC-00096	1992	1.05	22.0	1888.8	134	100
DYW-08-17	GC-00097	1993	1.06	22.3	1843.5	126	140
DYW-08-18	GC-00098	1994	1.03	22.0	2075.5	120	220
DYW-08-19	GC-00099	1995	0.91	21.4	1656.0	112	200
DYW-08-20	GC-00100	1996	0.99	21.8	1716.9	104	250
DYW-08-21	GC-00101	1997	1.33	21.8	2474.6	—	190
DYW-08-22	GC-00102	1998	1.37	—	2081.0	—	230

DISCUSSION

The Response of Coral $\Delta^{14}C$ to Atmospheric ^{14}C Annual Variation

Generally, ^{14}C finds its way into surface seawater with atmospheric CO_2 through the atmosphere-sea gas exchange mechanism. The dissolution process of CO_2 in seawater is described as follows:

$$CO_2 + H_2O <=> H_2CO_3$$

$$H_2CO_3 <=> HCO_3^- + H^+$$

$$HCO_3^{-1} <=> CO_3^{2-} + H^+$$

As viewed from ^{14}C tracing of the atmosphere-sea gas exchange process, one can see that in seawater there are a variety of forms of carbon, such as carbonate, bicarbonate, and dissolved CO_2; their summation is referred to as the total carbon dioxide (ΣCO_2). The concentrations of various carbon components in seawater can be calculated in terms of its temperature, salinity, pH value, total alkalinity, etc. (Broecker 1974). The total CO_2 in seawater at Daya Bay is comprised mainly of HCO_3^{-1} (about 89%), and subordinately of CO_3^{-2} (about 11%), and dissolved CO_2 (about 0.5%) (Han 1998). Based on the gas exchange of CO_2 between air and sea, as well as chemical reactions in the seawater, the coral ^{14}C has attained equilibrium with the dissolved inorganic carbon (DIC) in ambient seawater, i.e., $\Delta^{14}C_{coral} = \Delta^{14}C_{DIC}$ (Druffel 1982).

Figure 2 illustrates the interannual variation curve of $\Delta^{14}C$ from 1977–1998 for the Daya Bay coral samples, together with the interannual variation curve of atmospheric $\Delta^{14}C$ from 1977–1996, as reflected by the north European tree rings. The small block diagram in the upper right presents the variation curve of atmospheric $\Delta^{14}C$ on an even longer timescale, i.e., since the early 1950s, as reflected by the north European tree rings. It can be seen from the small block diagram that due to the atmospheric nuclear weapon testing, the atmospheric ^{14}C concentrations had rapidly increased year by year in the period from the early 1950s to the early 1960s, and reached the maximum of 900‰ in 1963 (Nydal 2000). After the treaty banning atmospheric nuclear weapon testing went into effect, the atmospheric $\Delta^{14}C$ decreased slowly, and $^{14}CO_2$ found its way into the ocean through atmosphere-sea gas exchange and oceanic vertical mixing. Figure 2 is actually a magnification of the dashed block inside the small block diagram, and it can be seen that the 2 curves are completely different: the tree-ring ^{14}C displays noticeable exponential attenuation, i.e., 80% decrease in about 20 yr, while the coral ^{14}C fluctuates in large amplitude around the mean value of 200‰. Since coral ^{14}C attained equilibrium with dissolved inorganic carbon ^{14}C in its ambient seawater, and the $^{14}CO_2$ that was input into the ocean is directly proportional to the $^{14}CO_2$ concentration gradient between the atmosphere and surface seawater, the variation of ^{14}C concentration in the coral annual layers with time can be expressed as:

$$\frac{^{14}C_s}{dt} = \frac{D}{ZM}(^{14}C_S - {}^{14}C_A),$$

where $^{14}C_S$ is the ^{14}C concentration in surface seawater, $^{14}C_A$ is the ^{14}C concentration of atmospheric CO_2, Z is the diffusion thickness and M is the depth of seawater where coral grows.

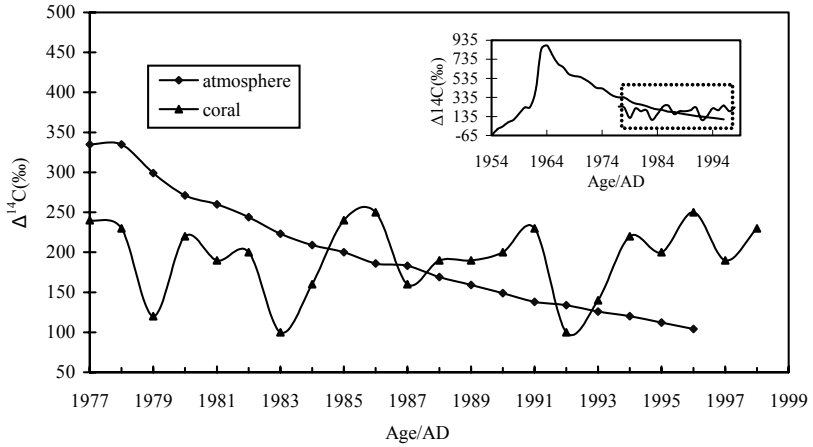

Figure 2 $\Delta^{14}C$ interannual variations of coral samples from Daya Bay and those of the atmosphere

The $\Delta^{14}C$ of annual bands of coral from Daya Bay during 1977–1998 varies from 100‰ to 250‰, which is larger than the $\Delta^{14}C$ value range of 70‰–110‰ in coral from the northwest Pacific for the same period (Morimoto et al. 2004). Perhaps because the sample localities are distributed near the coast, the ^{14}C concentrations of surface seawater ($^{14}C_S$), and hence the coral ^{14}C concentrations, could be influenced by terrestrial freshwater.

Response of Coral $\Delta^{14}C$ to ENSO

It is well known that ENSO—an abnormal phenomenon of climatic change resulting from a complex interaction between the tropical Pacific Ocean and the atmosphere—is the strongest signal of interannual climatic change so far discovered by meteorologists. During an ENSO event, the SST of the western Pacific will be at least 0.5 °C higher than the average value and the duration will be half a year or even longer (McCreary 1983; Huang 2001). The so-called SOI (Southern Oscillation Index) refers to the sea level atmospheric pressure difference between the Darwin and Tahiti areas, which is used as a primary measure of the state of the ENSO system. The available studies have shown that there is a close relationship between SOI and ENSO (Troup 1965; Rasmusson and Wallace 1983). The interannual variation curve of $\Delta^{14}C$ in coral from Daya Bay (Figure 3) can be compared with the SOI curves. $(SOI)_y$ and $(SOI)_w$ represent the monthly average for the entire year and in winter, respectively. The 3 curves display a correlated tendency of variation: the correlation coefficient between $\Delta^{14}C$ and $(SOI)_w$ is 0.43 and the correlation coefficient between $\Delta^{14}C$ and $(SOI)_y$ is 0.27. Ropelewski (1992) points out that during the ENSO years, the precipitation is relatively low and the atmospheric temperature is slightly higher during winter in the South China Sea region, presenting warm-dry climate environmental characteristics. Studies of coral samples taken from the subtropical northwestern Pacific have shown that $\Delta^{14}C$ variation reaches the maximum annual extent in winter season, higher than the average by 20% (Morimoto et al. 2004). The above studies and this work have revealed that there is a better correlation between $\Delta^{14}C$ and $(SOI)_w$. In light of the data on precipitation and atmospheric temperature listed in Table 1, a statistical treatment was carried out. Obviously, from the regression analysis in the 20-yr period from 1977 to 1996, the temperature tends to increase, while precipitation tends to decrease. As a matter of fact, comparison of the average values in the former 10 yr (1977–1986) with those in the latter 10 yr (1987–1996) provides evidence that the atmospheric temperature has risen by 0.40 °C and the precipitation has decreased by 140 mm, showing a tendency of warm-dry climatic change.

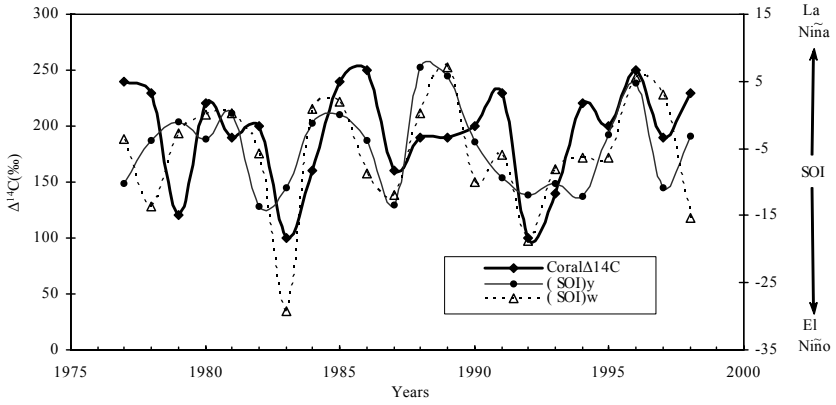

Figure 3 Interannual $\Delta^{14}C$ variations in the coral from Daya Bay and the variation trends of SOI

It is worth noting that the years during which great decreases in $\Delta^{14}C$ occur (for example, 1978–1979, 1982–1983, 1986–1987, 1991–1992, and 1996–1997) correspond precisely to or are within 1 yr of ENSO events. The southwestern monsoon is very prevalent in summer along the coast in eastern Guangdong, and the gale usually results in the offshore movement of surface seawater, causing the deep-layer seawater to upwell for replenishment and forming an upwelling current along the coast. The upwelling current is characterized by low temperature, high salinity, and low ^{14}C radioactivity, which is reflected in the coral record. On the contrary, based on coral $\Delta^{14}C$ variation, one can see that the upwelling current in the South China Sea intensified during ENSO years.

Response of Coral $\Delta^{14}C$ to Solar Radiation

The South China Sea, which is located in a low-latitude area, is a tropical sea and is subject to plenty of solar radiation energy. There is an obvious latitudinal difference for the solar radiation energy to be received by the earth's surface (including the land surface and the ocean surface). Driven by the tropical energy, the water vapor over the South China Sea will be conveyed toward the continent; in fact, the water vapor brought about by summer monsoon in China mainly comes from the South China Sea. Willson (1997) pointed out that the year with the minimum total radiation for the 21st solar activity cycle is 1986/1987, while that for the 22nd solar activity cycle is 1996/1997. Between these 2 yr featuring minimum total radiation, the total solar radiation increased by 0.036%. Table 1 shows atmospheric temperature data recorded in the past 20 yr from 1976 to 1997 by a local meteorological observation station (Pan et al. 1998). It can be estimated from Table 1 that in the 2 decades from 1977 to 1986 and from 1987 to 1996, the 10-yr average atmospheric temperature increased by 0.40 °C from the first decade to the second decade, corresponding to the increasing trend of total solar radiation mentioned above. It also can be seen from the atmospheric $\Delta^{14}C$ variation curve as shown in Table 1 and Figure 2 that in the 2 decades from 1977 to 1986 and from 1987 to 1996, the average atmospheric $\Delta^{14}C$ decreased from 256.2‰ for the first decade to 139.4‰ for the second decade. There are 2 obvious causes for the $\Delta^{14}C$ decrease: 1) the ever increasing consumption of fossil fuels results in further dilution of the atmospheric ^{14}C concentrations by ^{14}C-free CO_2; 2) the atmospheric nuclear weapon testing-derived ^{14}C continues to be absorbed by the vast ocean. Figure 2 shows that for coral from Daya Bay, the average $\Delta^{14}C$ value is 195.0‰ in the first decade and 207‰ in the second decade, respectively, i.e., almost no obvious change has ever taken place in the 10-yr average value of $\Delta^{14}C$, which demonstrates that the $\Delta^{14}C$ value of coral does not respond noticeably to the variation of solar radiation energy. It is apparent that, although apparent interannual variations occur in atmosphere-sea interaction and upwelling activity as driven by the tropical energy, no big fluctuation has ever occurred for the $\Delta^{14}C$ of South China Sea water during the 2 decades, from which we can conclude that the general situation and the oceanic thermal structure of the South China Sea are relatively stable. Nevertheless, whether various changes observed in solar radiation equilibrium in the 2 recent 10-yr time periods were caused by natural variability or by those factors that are well known to be closely associated with global change needs further study (Wielicki et al. 2002).

CONCLUSIONS

From the study of interannual variation of bomb ^{14}C in coral *Platygyra* from Daya Bay, some preliminary conclusions can be drawn as follows:

1. The coral $\Delta^{14}C$ interannual variation is controlled mainly by a series of oceanic factors, such as atmosphere-sea exchange, upwelling, etc. In the years of ENSO, upwelling in the South China Sea is intensified and the coral absorbs the seawater with low ^{14}C radioactivity, which has been brought upward to surface layers by the upwelling current, leading to a decrease in coral $\Delta^{14}C$.

2. The interannual variation curve of $\Delta^{14}C$ in coral from Daya Bay bears a relationship with SOI curves: the correlation coefficient between $\Delta^{14}C$ and $(SOI)_w$ is 0.43 and the correlation coefficient between $\Delta^{14}C$ and $(SOI)_y$ is 0.27.
3. Coral $\Delta^{14}C$ does not show any apparent response to the solar radiation energy in the past 20 yr from 1977 to 1997. Although interannual variations occur in atmosphere-sea interaction and upwelling activity driven by the tropical energy, the general situation and the oceanic thermal structure of the South China Sea still remain unchanged.

ACKNOWLEDGEMENTS

This work was supported jointly by grants from Chinese NKBRSF(G1999043401), CAS Knowledge Innovation Project (KZCX2-SW-118), and the National Science Foundation of China (Grant nr 40231015, 40231009). The authors are indebted to Dr Yongliang Yang for discussion and suggestion in the preparation of this manuscript. We are also grateful for the constructive comments of anonymous reviewers.

REFERENCES

Broecker WS. 1974. *Chemical Oceanography.* New York: Harcourt Brace Jovanovich, Inc. p 120–9.

Druffel ERM. 1982. Banded coral: changes in oceanic carbon-14 during the Little Ice Age. *Science* 218(4567):13–9

Druffel ERM, Suess HE. 1983. On the radiocarbon record in banded corals: exchange parameters and net transport of $^{14}CO_2$ between atmosphere and surface ocean. *Journal of Geophysical Research* 88(C2): 1271–80.

Druffel ERM. 1996. Post-bomb radiocarbon records of surface corals from the tropical Atlantic ocean. *Radiocarbon* 38(3):563–72.

Druffel ERM, Griffin S. 1993. Large variations of surface ocean radiocarbon: evidence of circulation changes in the southwestern Pacific. *Journal of Geophysical Research* 98(C10):20,249–59.

Druffel ERM. 1989. Decade timescale variability of ventilation in the north Atlantic: high-precision measurements of bomb radiocarbon in banded corals. *Journal of Geophysical Research* 94(3):3271–85.

Guilderson TP, Schrag DP. 1998. Abrupt shift in subsurface temperatures in the tropical Pacific associated with changes in El Niño. *Science* 28:240–3.

Han Y. 1998. *Oceanic Chemistry of South China Sea*. Beijing: Science Press. p 180–6.

Huang R, Zhang R, Yan B. 2001. Dynamical effect of the zonal wind anomalies over the tropical western Pacific on ENSO cycles. *Science in China* (Series D) 44(12):1089–98.

Levin I, Hesshaimer V. 2000. Radiocarbon—a unique tracer of global carbon cycle dynamics. *Radiocarbon* 42(1):69–80.

McCreary JP. 1983. A model of tropical ocean-atmosphere interaction. *Monthly Weather Review* 111:370–87.

Morimoto M, Kitagawa H, Shibata Y, Kayanne H. 2004. Seasonal ^{14}C variation of the surface seawater recorded in a coral from Kikai Island, subtropical Northwestern Pacific. *Radiocarbon*, these proceedings.

Nemani RR, Keeling CD, Hashimoto H, Jolly WM, Piper SC, Tucker CJ, Myneni RB, Running SW. 2003. Climate-driven increases in global terrestrial net primary production from 1982 to 1999. *Science* 300:1560–3.

Nydal R. 2000. Radiocarbon in the ocean. *Radiocarbon* 42(1):81–98.

Pan JP, Wang ZD. 1998. *Annual report of Daya Bay Marine Biology Experiment Station*. Beijing: Science Press. p 102–12. In Chinese.

Rasmusson EM, Wallace JM. 1983. Meteorological aspects of the EI Niño/Southern Oscillation. *Science* 222:1195–202.

Ropelewski CF. 1992. Predicting EI Niño events. *Nature* 356:476–7.

Toggweiler JR, Dixon K, Broecker WS. 1991. The Peru upwelling and the ventilation of the South Pacific thermocline. *Journal of Geophysical Research* 96 (C11):20,467–97.

Troup AJ. 1965. The Southern Oscillation. *Quarterly Journal of the Royal Meteoritical Society* 91:456–90.

Wielicki BA, Wong T, Allan RP, Slingo A, Kiehl JT, Soden BJ, Gordon CT, Miller AJ, Yang SK, Randall DA, Robertson F, Susskind J, Jacobowitz H. 2002. Evidence for large decadal variability in the tropical mean radiative energy budget. *Science* 295:841–4.

Willson RC. 1997. Total solar irradiance trend during solar cycles 21 and 22. *Science* 277:1963–5.

Yu K, Chen T, Lian J. 2002. Yearly variation of heavy metals in *Platygyra* coral from the Daya Bay and its oceanic environmental implications. *Quaternary Research* 22(3):230–5. In Chinese.

RADIOCARBON, Vol 46, Nr 2, 2004, p 603–610

MARINE RESERVOIR CORRECTION FOR THE COCOS (KEELING) ISLANDS, INDIAN OCEAN

Quan Hua[1,2] • Colin D Woodroffe[3] • Mike Barbetti[4] • Scott G Smithers[5] • Ugo Zoppi[1] • David Fink[1]

ABSTRACT. Known-age corals from the Cocos (Keeling) Islands, Indian Ocean, have been analyzed by accelerator mass spectrometry (AMS) for radiocarbon to determine marine reservoir age corrections. The ΔR value for the Cocos (Keeling) Islands is 66 ± 12 yr based on the analyses undertaken for this study. When our AMS and previously published dates for Cocos are averaged, they yield a ΔR of 64 ± 15 yr. This is a significant revision of an earlier estimate of the ΔR value for the Cocos (Keeling) Islands of 186 ± 66 yr (Toggweiler et al. 1991). The (revised) lower ΔR for the Cocos (Keeling) Islands is consistent with GEOSECS ^{14}C data for the Indian Ocean, and previously published bomb ^{14}C data for the Red Sea, Gulf of Aden, and Cocos Islands. The revised ΔR is also close to values for the eastern Indian Ocean and adjacent seas. These suggest surface waters that reach the Cocos Islands might be partly derived from the far western Pacific, via the Indonesian throughflow, and might not be influenced by the southeast flow from the Arabian Sea.

INTRODUCTION

Exchanging with the atmosphere and the radiocarbon-depleted deep ocean, the surface ocean has a ^{14}C level intermediate between these 2 reservoirs. This causes an age offset between marine samples, which source their carbon at the surface ocean, and contemporaneous terrestrial samples. This age offset is known as the marine reservoir age (R) and can be several hundred years. To calibrate a ^{14}C age for a marine sample, one needs to know its marine reservoir age (Stuiver and Reimer 1986). Alternatively, the regional variation from the global marine model age for that sample, defined as ΔR, is required (Stuiver and Braziunas 1993; Stuiver et al. 1998). The ΔR value, which is also known as the regional marine correction, accounts for regional deviations in ^{14}C due to variations in ocean circulation and air-sea exchange of CO_2. The latter method is generally preferred for age calibration (Reimer and Reimer 2001) and ΔR values are typically determined by dating pre-bomb known-age marine carbonates (Southon et al. 2002).

The Cocos (Keeling) Islands (12°S, 97°E) are an isolated Australian atoll in the eastern Indian Ocean. An annual band chronology has recently been established for corals from this atoll, which covers most of the 20th century (Smithers and Woodroffe 2000, 2001). The corals were *Porites* microatolls and were collected alive in 1991 and 1992 from 2 reef-flat sites on the southern and eastern sides of Cocos that are freely connected to the open ocean. These Cocos corals offer the possibility of examining regional variability of ^{14}C in the surface waters of the eastern Indian Ocean during the past century. Here, we report ΔR measurements on 5 known-age coral bands and a known-age museum specimen of *Porites* coral. Our new data, in conjunction with previously published ^{14}C data for the atoll (Toggweiler et al. 1991; Woodroffe et al. 1994), can be used to determine a reliable mean ΔR marine correction for Cocos. This is important not only for reliably dating marine fossils of the Cocos Islands by ^{14}C, but also to improve our knowledge of ocean circulation around the Cocos Islands and the eastern Indian Ocean.

[1]Australian Nuclear Science and Technology Organisation (ANSTO), PMB 1, Menai, New South Wales 2234, Australia.
[2]Corresponding author. Email: qhx@ansto.gov.au.
[3]School of Geosciences, University of Wollongong, Wollongong, New South Wales 2522, Australia.
[4]NWG Macintosh Centre for Quaternary Dating, Madsen Building F09, University of Sydney, New South Wales 2006, Australia.
[5]School of Tropical Environment Studies and Geography, James Cook University, Townsville, Queensland 4811, Australia.

Proceedings of the 18th International Radiocarbon Conference, edited by N Beavan Athfield and R J Sparks
RADIOCARBON, Vol 46, Nr 2, 2004, p 603–610

MATERIALS AND METHODS

For this study, we used microatoll PP30, collected on the eastern side of the atoll from a reef-flat site that is freely connected to the open ocean (see Figure 1), for ^{14}C analysis. The coral was sampled alive in 1992 and no recrystallization has occurred. Five single annual bands, which grew in 1906, 1926, 1933, 1941, and 1950, were split for ^{14}C analysis using a dental drill. In addition, a museum specimen of *Porites* coral from Cocos, which was collected alive by Charles Darwin in 1836, was measured in this study to investigate possible changes in ΔR over the past 150 yr. This specimen (sample number 42.12.14.24) is deposited in the Department of Zoology, The Natural History Museum, London.

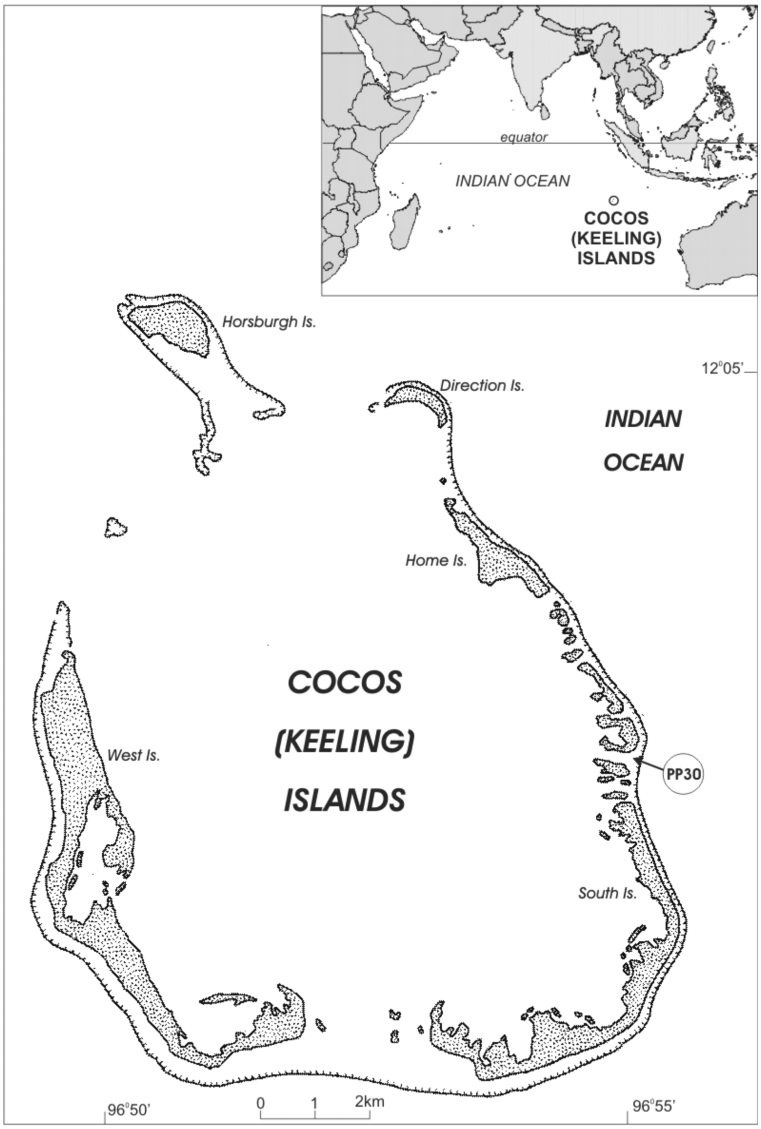

Figure 1 The Cocos (Keeling) Islands, showing location of open reef-flat microatoll PP30

The samples were cleaned with deionized water in an ultrasonic bath 3 times for 20 min each to remove any surface contamination. They were then dried in an oven at 60 °C for 2 days before hydrolysis. The cleaned samples were hydrolyzed to CO_2 using 85% phosphoric acid. The CO_2 samples were then converted to graphite using the Zn/Fe method. The technical aspects of these methods have been described in Hua et al. (2001). The mass of graphite was typically 4 mg. A small portion of graphite from each sample was employed for the determination of $\delta^{13}C$ using the Micromass IsoPrime Elemental Analyser/Isotope Ratio Mass Spectrometer (EA/IRMS) at ANSTO. AMS ^{14}C measurements were performed using the ANTARES facility at ANSTO (Lawson et al. 2000; Fink et al. 2004) with a precision of 0.3–0.4%.

RESULTS

The results of AMS ^{14}C measurements of the coral samples for this study are shown in Table 1. The regional marine correction ΔR (Stuiver and Braziunas 1993) is determined as the difference between the conventional ^{14}C age for each sample after correction for $\delta^{13}C$ (Stuiver and Polach 1977) and the global marine model age for the year of collection or growth. To be compatible with the online marine reservoir correction database (Reimer and Reimer 2001), we used the 1998 marine calibration data set, Marine98 from Stuiver et al. (1998), as the model age of global ocean for the calculation of ΔR.

Table 1 ΔR values for the Cocos (Keeling) Islands, derived from corals. Note: [W-J] - Museum specimen collected by F Wood-Jones; [G-H] - Museum specimen collected by C A Gibson-Hill; [D] - Museum specimen collected alive by C Darwin. This specimen (sample number 42.12.14.24) is kept in the Department of Zoology, The Natural History Museum, London; and [S-W]- Annual coral band from open reef-flat microatoll PP30 (Smithers and Woodroffe 2000, 2001).

Laboratory code	Coral species	Year of growth or collection	$\delta^{13}C$ (‰)	Conventional ^{14}C age (yr BP)	Model age[a] (yr BP)	ΔR (^{14}C yr)
Previous studies						
L-DGO-1657	—	1941	—	652 ± 66[b]	466 ± 8	186 ± 66
ANU-6151	*Acropora scherzeriana* [W-J]	1906	—	370 ± 60[c]	452 ± 5	–82 ± 60
ANU-6152	*Montipora foliosa* [W-J]	1906	—	670 ± 60[c]	452 ± 5	218 ± 60
ANU-6153	*Porites nigrescens (=P. cylindrica)* [W-J]	1906	—	410 ± 60[c]	452 ± 5	–42 ± 60
ANU-7638	*Montipora ramosa* [G-H]	1941	—	510 ± 70[c]	466 ± 8	44 ± 70
ANU-7639	*Montipora lobulata* [G-H]	1941	—	480 ± 60[c]	466 ± 8	14 ± 61
This study						
OZG553	*Porites arenaceae* [D]	1836	–2.8	586 ± 29	494 ± 5	92 ± 29
OZG956	*Porites* [S-W]	1906 ± 2[d]	–2.8	485 ± 21	452 ± 6[e]	33 ± 22
OZF535	*Porites* [S-W]	1926	–2.0	530 ± 25	456 ± 4	74 ± 25
OZF536	*Porites* [S-W]	1933	–3.5	565 ± 25	460 ± 5	105 ± 25
OZF537	*Porites* [S-W]	1941	–3.0	510 ± 25	466 ± 8	44 ± 26
OZF538	*Porites* [S-W]	1950	–4.1	540 ± 25	472 ± 13	68 ± 28

[a]Estimated value from decadal Marine98 data (Stuiver et al. 1998) by linear interpolation.

[b]Calculated from $\Delta^{14}C$ data from Toggweiler et al. (1991).

[c]Data reported in Woodroffe et al. (1994).

[d]Estimated uncertainty in age of growth band reflects the occurrence of zones of ambiguous growth band definition within the coral skeleton (Smithers and Woodroffe 2001).

[e]Estimated model age for AD 1906 ± 2.

In addition, ^{14}C data for the Cocos (Keeling) Islands from previous studies (Toggweiler et al. 1991; Woodroffe et al. 1994) are presented in Table 1. A summary of the ΔR marine correction values for Cocos from previous studies and this investigation are plotted in Figure 2.

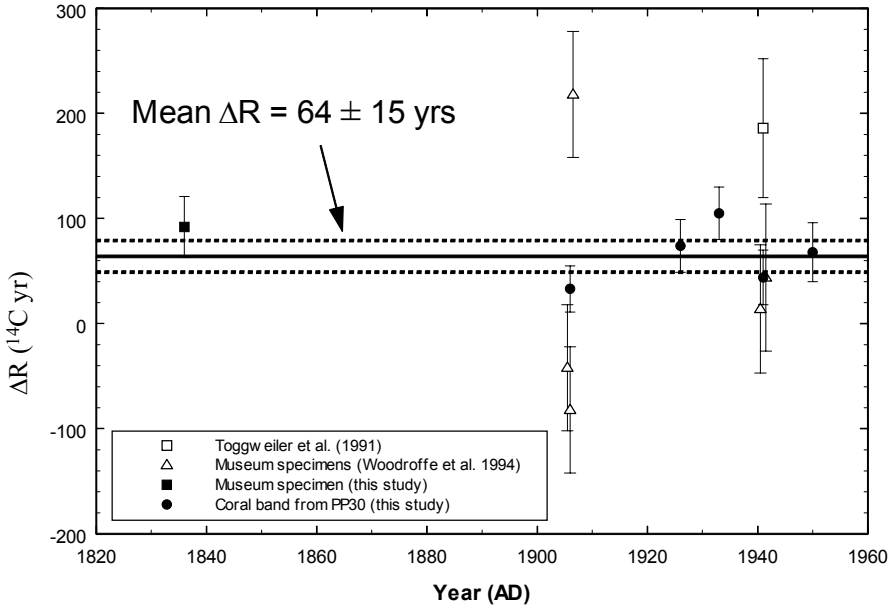

Figure 2 ΔR marine corrections for the Cocos (Keeling) Islands from previous studies and this investigation. The error-weighted mean value of ΔR for Cocos is 64 ± 15 yr.

DISCUSSION

The marine corrections for the Cocos (Keeling) Islands from this study show a small variation ranging from 33 to 105 yr (Table 1 and Figure 2). This variation in our data may indicate the temporal variability in ^{14}C of surface ocean waters around the Cocos Islands for the past 150 yr. The average ΔR marine correction value for the Cocos Islands is 66 ± 12 yr based on the analyses undertaken for this study. To be compatible with the online marine reservoir correction database (Reimer and Reimer 2001), the uncertainty associated with an error-weighted mean ΔR was chosen as the larger of the error of the mean and the standard error. When compared with the previously published ^{14}C data for Cocos, our ΔR value for 1941 (44 ± 26 yr) is in good agreement with those (44 ± 70 yr and 14 ± 61 yr) of Woodroffe et al. (1994), but all these 3 ΔR values are significantly lower than that of Toggweiler et al. (1991) (186 ± 66 yr). For the 1906 data from Woodroffe et al. (1994), the first (*Acropora scherzeriana*) and third (*Porites nigrescens*) ΔR values overlap within 1 σ uncertainty, but they are significantly lower than the second ΔR (*Montipora foliosa*; see Table 1, Figure 2). Our ΔR value for 1906 (33 ± 22 yr) overlaps with their third ΔR value (–42 ± 60 yr) within 1 σ uncertainty, but is significantly different from their first (–82 ± 60 yr) and second (218 ± 60 yr) ΔR values.

The large spreads in ΔR values (300 yr for 1906 and 170 yr for 1941) of the previously published data may be due to the spatial variability within the Cocos lagoon. However, the location of the museum specimens collected by Wood-Jones [W-J] and Gibson-Hill [G-H] (see Table 1), which were presumably collected alive, is largely unknown. Several of the specimens are likely to have been collected from the lagoon, such as *Montipora foliosa*, *Porites nigrescens*, and *Montipora lob-*

ulata (Wells 1950). In addition, no details of sample species and location for Toggweiler et al.'s sample of 1941 were reported. On the other hand, the lagoon of the Cocos (Keeling) Islands, which is enclosed by 26 islands and covers a surface area of 190 km^2, is well connected with the open ocean through tidal currents, indicated by a short flushing time of the lagoon between 5.4 and 2.3 days for neap and spring tidal conditions, respectively (Kench 1994). One may argue that the large spreads in the previously published data are simply due to experimental scatter. However, a scatter of this magnitude (170 to 300 yr) is too large to be accounted for in normal ^{14}C analyses, leaving the excessive ΔR spreads for 1906 and 1941 samples unexplained. When our AMS and previously published dates for Cocos are averaged, they yield a ΔR marine correction of 64 ± 15 yr. This is a significant revision of an earlier estimate of the ΔR value for Cocos of 186 ± 66 yr (Toggweiler et al. 1991), which has recently been restated in the literature (Southon et al. 2002).

The ^{14}C data for the Indian Ocean from the Geochemical Ocean Section Study (GEOSECS) program during 1977–1978 showed that bomb ^{14}C appears less abundantly in the west Indian Ocean than in the east Indian Ocean (Stuiver and Östlund 1983). In other words, ^{14}C levels in surface waters of the western Indian Ocean are generally lower than those of the eastern Indian Ocean, resulting in ΔR values that are higher in the western Indian Ocean than those for the eastern Indian Ocean. This is due to the intense monsoon-driven upwelling which takes place off the Somali and southern Arabian coasts and to a lesser extent off Pakistan and India (Southon et al. 2002 and references therein). Our revised ΔR value of 64 ± 15 yr for the Cocos (Keeling) Island is consistent with the above GEOSECS ^{14}C data as it is lower than the ΔR values of the tropical southwest Indian Ocean (135 ± 24 yr), western Arabian Sea (207 ± 30 yr), and eastern Arabian Sea (187 ± 25 yr) (see Table 2 and Figure 3).

Table 2 ΔR values for the Indian Ocean and adjacent seas from previous studies. All ΔR values were calculated using the 1998 marine calibration data set (Marine98; Stuiver et al. 1998) as the model age of global ocean. The first 9 ΔRs are regional marine corrections. The last 4 ΔRs are marine corrections for a site or a small region. The first 8 regional ΔRs were reported in Reimer and Reimer (2001).

Region or Location	Latitude	Longitude	References	ΔR (^{14}C yr)
Western Arabian Sea (N=8)	11–24°N	43–58°E	—	207 ± 30
Eastern Arabian Sea (N=16)	7–25°N	66–80°E	—	187 ± 25
Bay of Bengal (N=6)	9–13°N	78–94°E	—	64 ± 55
Northwest Australia - Java (N=9)	7–18°S	106–132°E	—	64 ± 24
Northeast Australia (N=5)	10–12°S	141–143°E	—	50 ± 31
Tropical southwest Indian Ocean (N=12)	6–21°S	39–56°E	—	135 ± 24
South Africa (N=2)	30–34°S	18–31°E	—	218 ± 38
South China Sea (N=10)	1–17°N	99–121°E	—	–17 ± 17
Southwest Australia (N=4)	32–35°S	115–117°E	Gillespie (1977) Gillespie and Polach (1979) Bowman and Harvey (1983) Bowman (1985)	66 ± 46
Raffles Bay, N. Australia (N=1)	11°S	132°E	Southon et al. (2002)	58 ± 40
Pelebuhanratu, S. Java (N=1)	7°S	107°E	Southon et al. (2002)	40 ± 70
Port Sudan, Red Sea (N=3)	20°N	37–38°E	Cember (1989) Southon et al. (2002)	120 ± 28
Djibouti, Gulf of Aden (N=5)	11–13°N	43–45°E	Toggweiler et al. (1991) Southon et al. (2002)	193 ± 36

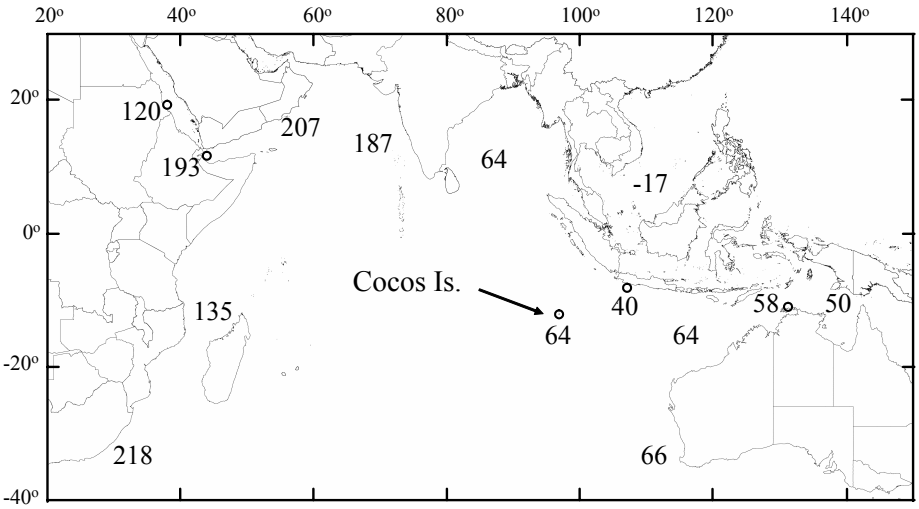

Figure 3 ΔR marine corrections for the Indian Ocean and adjacent seas with our revised ΔR value for the Cocos (Keeling) Islands. ΔR for a region is shown by its value in the middle of the region. ΔR for a site or a small region is shown by its value with an open circle indicating the location of the site or small region. The details of these ΔR marine corrections are given in Table 2.

Published bomb ^{14}C data derived from corals from the northwestern Indian Ocean—Port Sudan (20°N, 37°E, the Red Sea; Cember 1989) and Djibouti (11°N, 43°E, Gulf of Aden; Toggweiler et al. 1991)—compared to those from the Cocos (Keeling) Islands (Toggweiler et al. 1991) are shown in Figure 4. We have also measured ^{14}C in annual bands of corals from the Cocos (Keeling) Islands for 1955–1985 (the bomb pulse period). There is a good agreement between our preliminary results and the data from Toggweiler et al. (1991) for 1970–1976. However, reporting and discussing our bomb ^{14}C results for Cocos are beyond the scope of this paper. Bomb ^{14}C for the Cocos Islands is higher than that for Port Sudan, which, in turn, is higher than bomb ^{14}C for Djibouti. These bomb ^{14}C data also support the revised ΔR value for the Cocos Islands as it (64 ± 15 yr) is lower than the ΔR of Port Sudan of 120 ± 28 yr, which, in turn, is lower than that of Djibouti of 193 ± 36 yr (see Table 2 and Figure 3). Like other parts of the northwest Indian Ocean, the Gulf of Aden is a region of monsoon-driven seasonal upwelling (Cember 1989). This explains why there are high ΔR and low $\Delta^{14}C$ values for Djibouti (Gulf of Aden) and, consequently, medium-high ΔR and medium-low $\Delta^{14}C$ values for Port Sudan as surface waters of the Red Sea are partly derived from those of the Gulf of Aden through the Straits of Bab-el-Mandeb (Cember 1989).

When compared with the marine corrections for the east Indian Ocean (Table 2 and Figure 3), the revised ΔR of 64 ± 15 yr for the Cocos (Keeling) Islands is close to values for the eastern Indian Ocean, e.g., 40 ± 70 yr for Pelebuhanratu (South Java; Southon et al. 2002) and 64 ± 24 yr for northwest Australia and Java (Reimer and Reimer 2001). The Cocos ΔR value is also similar to those for Raffles Bay, northern Australia (58 ± 40 yr; Southon et al. 2002) and Torres Strait and northeastern Australia (50 ± 31 yr; Reimer and Reimer 2001), but significantly higher than that for the South China Sea (–17 ± 17 yr; Reimer and Reimer 2001). In addition, the Cocos ΔR value is significantly lower than those for the western Indian Ocean as discussed above. These suggest surface waters that reach the Cocos Islands might be partly derived from the far western Pacific, flowing through the Indonesian seas (Fieux et al. 1994; Moore et al. 1997), and might not be influenced by the southeast flow from the Arabian Sea as suggested by Southon et al. (2002).

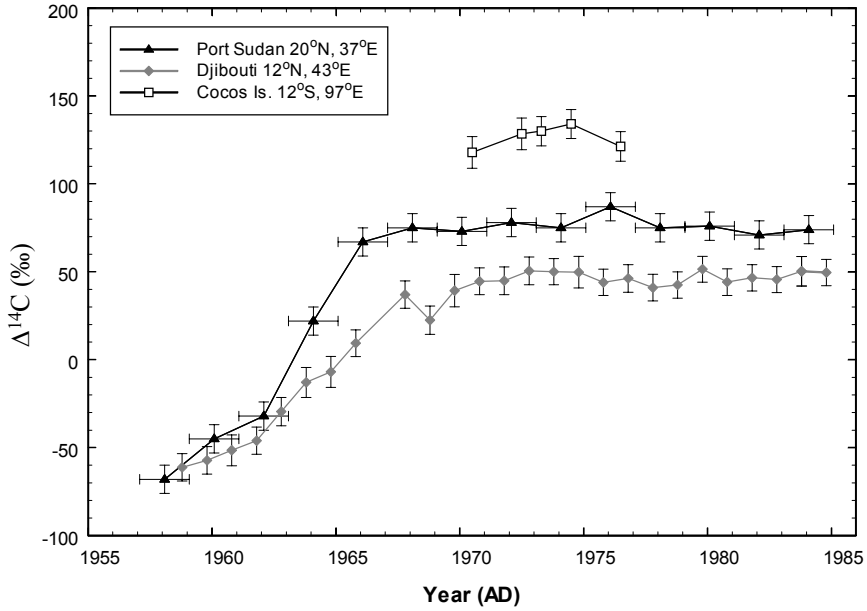

Figure 4 Published bomb ^{14}C data from corals from Port Sudan (the Red Sea; Cember 1989), Djibouti (Gulf of Aden; Toggweiler et al. 1991), and the Cocos (Keeling) Islands (Toggweiler et al. 1991). Djibouti and Cocos records consisted of annual data, meanwhile Port Sudan data were biannual data.

ACKNOWLEDGEMENTS

The authors wish to thank Brian Rosen (Department of Zoology, The Natural History Museum, London) for the supply of a museum specimen of *Porites* coral collected by Charles Darwin (sample number 42.12.14.24). We would like to thank Holly Yeatman for helping with sample preparation and Alan Williams for $\delta^{13}C$ measurements, both at ANSTO. The authors also thank John Southon (Earth System Science Department, University of California, Irvine) for his useful comments which helped improve the manuscript. We gratefully acknowledge funding from the Australian Institute of Nuclear Science and Engineering (AINSE) for AMS ^{14}C measurements (grants 01/207 and 02/150P).

REFERENCES

Bowman GM. 1985. Revised radiocarbon oceanic reservoir correction for southern Australia. *Search* 16:164–5.

Bowman GM, Harvey N. 1983. Radiocarbon dating marine shells in South Australia. *Australian Archaeology* 17:113–23.

Cember RP. 1989. Bomb radiocarbon in the Red Sea: a medium scale gas exchange experiment. *Journal of Geophysical Research* 94:2111–23.

Fieux M, Andrie C, Delecluse P, Ilahude AG, Kartavtseff A, Mantisi F, Molcard R, Swallow JC. 1994. Measurements within the Pacific-Indian oceans flowthrough region. *Deep Sea Research* 41:1091–130.

Fink D, Hotchkis MAC, Hua Q, Jacobsen GE, Smith AM, Zoppi U, Child D, Mifsud C, van der Gaast HA, Williams AA, Williams M. Forthcoming. The ANTARES AMS Facility at ANSTO. *Nuclear Instruments and Methods in Physics Research B*.

Gillespie R. 1977. Sydney University natural radiocarbon measurements IV. *Radiocarbon* 19:101–10.

Gillespie R, Polach HA. 1979. The suitability of marine shells for radiocarbon dating of Australian prehistory. In: Berger R, Suess HE, editors. *Radiocarbon Dating. Proceedings of the 9th International ^{14}C Conference*. Berkeley: University of California Press. p 404–21.

Hua Q, Jacobsen GE, Zoppi U, Lawson EM, Williams AA, Smith AM, McGann MJ. 2001. Progress in radiocarbon target preparation at the ANTARES AMS Centre. *Radiocarbon* 43(2A):275–82.

Kench P. 1994. Hydrodynamic observations of the Cocos

(Keeling) Islands Lagoon. *Atoll Research Bulletin* 408:1–21.

Lawson EM, Elliott G, Fallon J, Fink D, Hotchkis MAC, Hua Q, Jacobsen GE, Lee P, Smith AM, Tuniz C, Zoppi U. 2000. AMS at ANTARES—the first 10 years. *Nuclear Instruments and Methods in Physics Research B* 172:95–9.

Moore MD, Schrag DP, Kashgarian M. 1997. Coral radiocarbon constraints on the source of the Indonesian throughflow. *Journal of Geophysical Research* 102(C6):12,359–65.

Reimer PJ, Reimer RW. 2001. A marine reservoir correction database and on-line interface. *Radiocarbon* 43(2A):461–3. URL: http://www.calib.org/.

Smithers SG, Woodroffe CD. 2000. Microatolls as sea-level indicators on a mid-ocean atoll. *Marine Geology* 168:61–78.

Smithers SG, Woodroffe CD. 2001. Coral microatolls and 20th century sea level in the eastern Indian Ocean. *Earth and Planetary Science Letters* 191:173–84.

Southon J, Kashgarian M, Fontugne M, Metivier B, Yim W. 2002. Marine reservoir corrections for the Indian Ocean and Southeast Asia. *Radiocarbon* 44(1):167–80.

Stuiver M, Braziunas TF. 1993. Modelling atmospheric ^{14}C influences and ^{14}C ages of marine samples to 10,000 BC. *Radiocarbon* 35(2):137–89.

Stuiver M, Östlund HG. 1983. GEOSECS Indian Ocean and Mediterranean radiocarbon. *Radiocarbon* 25(1): 1–29.

Stuiver M, Polach HA. 1977. Discussion: reporting of ^{14}C data. *Radiocarbon* 19(3):353–63.

Stuiver M, Reimer PJ. 1986. A computer program for radiocarbon age calibration. *Radiocarbon* 28(2B): 1022–30.

Stuiver M, Reimer PJ, Braziunas TF. 1998. High-precision radiocarbon age calibration for terrestrial and marine samples. *Radiocarbon* 40(3):1127–51.

Toggweiler JR, Dixon K, Broecker WS. 1991. The Peru upwelling and the ventilation of the South Pacific thermocline. *Journal of Geophysical Research* 96(C11):20,467–97.

Wells JW. 1950. Reef corals from the Cocos-Keeling Atoll. *Bulletin of Raffles Museum* 22:29–52.

Woodroffe CD, McLean RF, Wallensky E. 1994. Geomorphology of the Cocos (Keeling) Islands. *Atoll Research Bulletin* 402:1–33.

RADIOCARBON, Vol 46, Nr 2, 2004, p 611–620

HOLOCENE VARIATIONS IN THE SCOTTISH MARINE RADIOCARBON RESERVOIR EFFECT

Philippa L Ascough[1,2,3] • Gordon T Cook[2] • Andrew J Dugmore[1] • John Barber[4] • Elaine Higney[2] • E Marian Scott[5]

ABSTRACT. We assessed the evidence for variations in the marine radiocarbon reservoir effect (MRE) at coastal, archaeological Iron Age sites in north and west Scotland by comparing AMS measurements of paired marine and terrestrial materials (4 pairs per context). ΔR values were calculated from measurements on material from 3 sites using 6 sets of samples, all of which were deposited around 2000 BP. The weighted mean of the ΔR determinations was -79 ± 17 ^{14}C yr, which indicates a consistent, reduced offset between atmospheric and surface ocean ^{14}C specific activity for these sites during this period, relative to the present day (ΔR = ~0 ^{14}C yr). We discuss the significance of this revised ΔR correction by using the example of wheelhouse chronologies at Hornish Point and their development in relation to brochs. In addition, we assess the importance of using the concepts of MRE correction and ΔR variations when constructing chronologies using ^{14}C measurements made on materials that contain marine-derived carbon.

INTRODUCTION

One of the most fundamental assumptions in radiocarbon dating theory is that there is global uniformity in the specific activity of ^{14}C in living organisms. The short residence time (1–2 decades) and rapid mixing of carbon in the atmosphere (Levin et al. 1980) mean that the assumption is valid for the well-mixed atmosphere and the terrestrial flora and fauna that atmospheric carbon supports, provided due corrections are made for the degree of isotopic fractionation that takes place during ^{14}C transfer through the food chain. Consequently, the record of atmospheric ^{14}C variations (from production rate changes and changes in the carbon cycle) may be measured directly through analysis of annually formed samples such as tree rings.

The residence time of carbon in the deep oceans is of the order of 1000 yr (Sigman and Boyle 2000). This reflects the average length of time that a carbon atom remains in this reservoir before returning to the atmosphere by exchange. Therefore, the deep oceans are depleted in ^{14}C relative to the atmosphere because of the ^{14}C decay that occurs while the deep water is out of contact with the atmosphere. The surface oceans are intermediate in ^{14}C specific activity between the deep oceans and the atmosphere because this reservoir is a mixture of "new carbon" from the atmosphere via gaseous exchange and "old carbon" from the deep oceans.

This depletion of surface waters relative to the atmosphere would not be a major problem if the world's oceans were uniformly mixed, since a global age correction factor could be employed. However, circulation and mixing within the oceans are comparatively slow processes, leading to significant geographical and depth variations in the degree of ^{14}C depletion. These will depend upon factors such as the stratification of water masses, rates of current movement, the length of time that a body of water is in contact with the atmosphere, and the locations of water mass convergence and upwelling (Gordon and Harkness 1992).

[1]Institute of Geography, University of Edinburgh, Edinburgh EH8 9XP, United Kingdom.
[2]Scottish Universities Environmental Research Centre, Scottish Enterprise Technology Park, Rankine Avenue, East Kilbride, Glasgow G75 OQF, United Kingdom.
[3]Corresponding author: Email: pasc@geo.ed.ac.uk.
[4]AOC Archaeology Group, Edgefield Road, Loanhead EH20 9SY, United Kingdom.
[5]Department of Statistics, University of Glasgow, Glasgow G12 8QQ, United Kingdom.

Proceedings of the 18th International Radiocarbon Conference, edited by N Beavan Athfield and R J Sparks
RADIOCARBON, Vol 46, Nr 2, 2004, p 611–620

Therefore, the reservoir age R(t), which is defined as the difference in conventional ^{14}C yr between samples grown contemporaneously in the terrestrial and surface marine reservoirs, varies spatially. R(t) will also vary temporally as a result of changes in reservoir size and input and output fluxes.

Estimates of temporal ^{14}C variations in the surface marine environment are based on models that employ the atmospheric ^{14}C data as input to produce a separate calibration curve for samples containing marine derived carbon (Stuiver and Braziunas 1993). Identification of spatially dependent ^{14}C variations have relied on studies performed in specific geographical areas (Stuiver et. al. 1986).

The aim of this research was to examine variations in the marine ^{14}C reservoir effect (MRE) in northeast Atlantic surface waters during the Scottish Iron Age (about 2000 BP). An accurate quantification of the MRE is crucial to constructing effective environmental chronologies when using material that incorporates ^{14}C from a marine source.

Spatial Dimensions of ΔR/MREs

The marine calibration curve provides an averaged correction for the MRE between the global surface oceans and the atmosphere through time. This correction value does not allow for geographic variations in the surface ocean ^{14}C content and the fact that local MREs may vary through time to significantly different extents from the global average (Stuiver and Braziunas 1993). Due to the short time interval required for tropospheric air masses to circulate globally (Levin et al. 1980), the atmospheric/terrestrial reservoir is relatively homogeneous with respect to ^{14}C. However, the complex circulation patterns of the global ocean reservoir operate at much slower individual rates, producing a wide variation in the ^{14}C concentration of water masses at different depths and in different regions. The ^{14}C age offset of a local surface ocean area may, therefore, be significantly offset from the global marine calibration curve, depending upon local climate and oceanic variables. This positive or negative deviation in ^{14}C age is described as a ΔR value. In areas where deep, ^{14}C-depleted water is upwelled, the ^{14}C content of surface ocean water is reduced, and local MRE offsets increase, producing a positive ΔR value (Silar 1980; Goodfriend and Flessa 1997). Negative ΔR values (and therefore decreased local MRE offsets) are recorded where a strong inflow of water that is more thoroughly equilibrated with the contemporary atmosphere exists (Silar 1980). In addition to ocean circulation, climatic changes can heavily influence ΔR values, these being primarily ocean-atmosphere gas exchange rates and factors of wind speed, sea-ice cover, and temperature (Liss and Merlivat 1986; Broecker et. al. 1985; Stocker and Wright 1996; Barber et. al. 1999).

Temporal Dimensions of MREs/ΔR

ΔR is usually assumed to be time independent in a given location. However, there is a growing body of evidence for large and rapid changes in MRE during known periods of extreme climatic change, including the transition from the last glacial maximum to the Bølling/Allerød (~13,000 BP) and between the Younger Dryas and the start of the Holocene warm period (~10,000 BP). Such variations have been observed in the Atlantic Ocean using data from benthic corals (Adkins et al. 1998), planktonic foraminifera (Siani et al. 2001), and mollusc shells (Austin et al. 1995), and are identifiable over decadal to centennial timescales. These variations have been linked to changing ocean circulation patterns, especially to changes in ocean ventilation rates and in the age and depth of the source waters to various study sites. Investigation into whether MRE change is also visible over human timescales (i.e. the Holocene) is limited. Because climate changes on the scale of a glacial/interglacial transition do not occur in the mid to late Holocene, we assume that identification of the correspondingly smaller ΔR variations during this time would require a comprehensive and intensive sampling methodology, designed to pick up changes at a higher resolution.

METHODOLOGY

Three main methods have been developed in response to the problem of quantifying reservoir ages and local ΔR values. Firstly, it is often possible to obtain samples of marine organisms (generally marine mollusc shells) from an area where the pre-1950 calendar date (and location) of collection was recorded; museum archives often prove a useful source of this material (Mangerud and Gulliksen 1975). ΔR is then calculated from the offset between the global marine model age at the time of collection and the measured ^{14}C content of the marine sample (Stuiver and Braziunas 1993; Dutta et al. 2001). However, since museum collections are confined to the recent past, any temporal study would be severely limited.

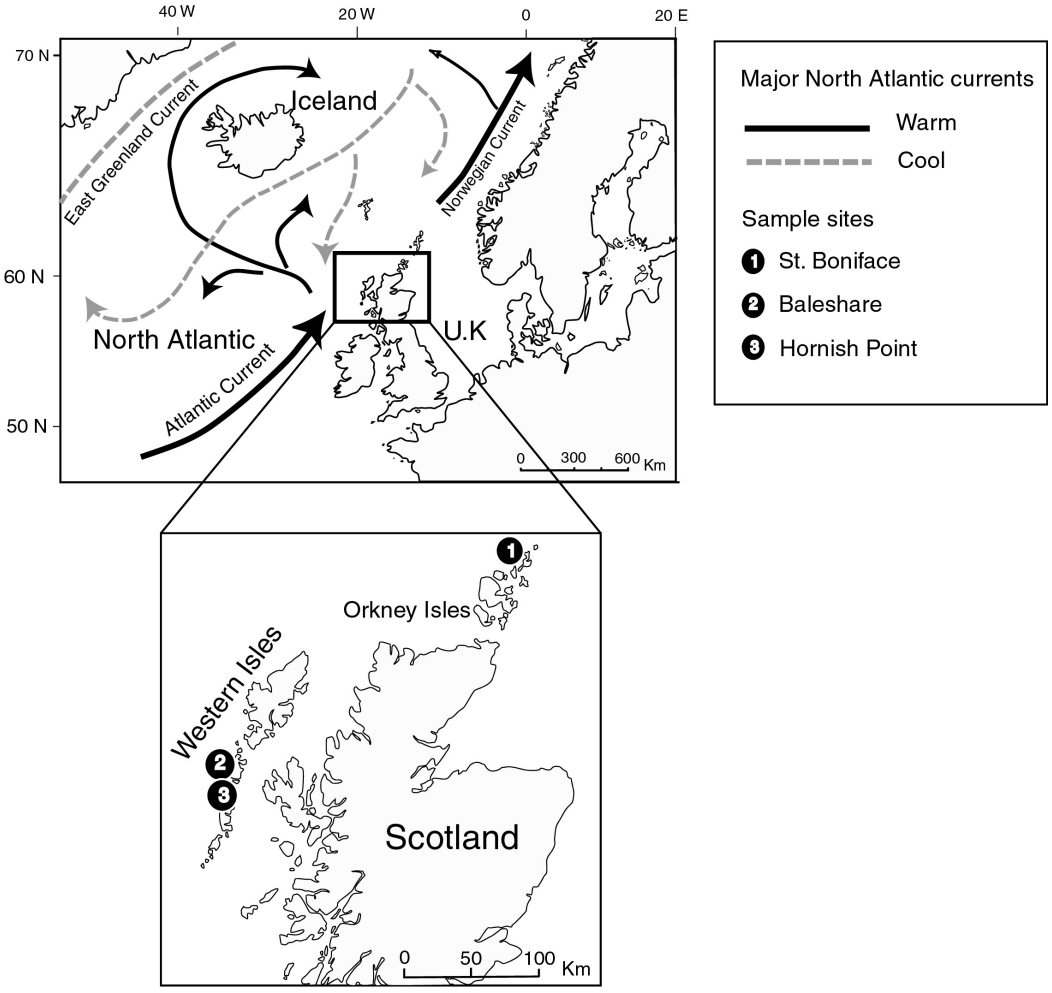

Figure 1 The study area showing investigated sites in Scotland: The study sites are coastal, bordering well-mixed oceanic waters. Major North Atlantic Ocean currents are shown, cold currents as grey, broken lines and warm currents as solid black lines. A well-developed northward flowing warm current (the North Atlantic Current) affects the Atlantic coast of Scotland, which tends to suppress MREs in the region. Climatic change can be expressed in a strengthening and weakening of the flow and related changes in ΔR.

Secondly, the rapid and virtually instantaneous deposition of volcanic ash (tephra) in onshore and offshore deposits allows its use as a marker horizon. It is assumed that marine and terrestrial organisms in close association with the same tephra layer share an equivalent age of death, and the local MRE at the time of tephra deposition is calculated using the offset in their measured ^{14}C ages (Haflidason et al. 2000; Bondevik et al. 2001). Potential difficulties with this approach center upon varying sediment accumulation rates and sediment mixing prior to final incorporation into the deposit.

Finally, it is possible at many coastal archaeological sites to identify a deposit that contains domestic refuse including both marine and terrestrial material, which was gathered at the same time and is contemporaneous. A ^{14}C age measurement made on the terrestrial material can be converted to a global model marine age, which can then be compared with the measured ^{14}C age of the marine material to determine ΔR (Reimer et al. 2002).

The results we present here were obtained through a comparison of paired marine and terrestrial material from a range of Scottish archaeological sites (Figure 1). This methodology was selected as the most promising on the basis of a critical analysis of the advantages and limitations involved. The use of available known-age samples would have limited the possible spatial and temporal study parameters to previously collected material, restricting the opportunity to perform multiple or repeat measurements, a feature which we felt would be central to the accuracy of our calculated ΔR values. The archaeological deposits we used each contained a large amount of suitable material, the nature of which allowed AMS measurement of single organisms. Suitable sampling sites were abundant in the study area, enabling us to apply strict selection criteria and discard-protocols for each individual deposit that was sampled. These were applied through close consultation with the excavators of each site and after examination of the excavation reports. At each site, an individual deposit or deposits were identified; where examination revealed a high likelihood that the deposit had not been disturbed since deposition and represented a period of rapid sediment accumulation, we extracted 4 samples of carbonized cereal grain and 4 samples of marine mollusc shell for AMS analysis (Figure 2).

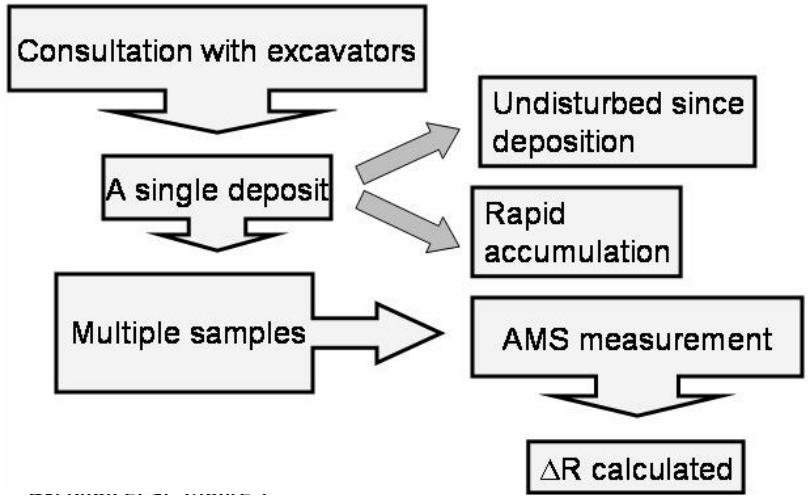

Figure 2 Outline of the paired sample methodology used in this study

To calculate ΔR values, we used the method of Reimer et al. (2002). The maximum and minimum atmospheric ^{14}C ages for an individual deposit (derived from the weighted mean ^{14}C age of the grain

samples) were used to calculate the modelled marine ^{14}C age range. The midpoint of the modelled marine ^{14}C age was then compared with the measured ^{14}C age of the marine shells to establish the size of the offset (ΔR value), from the global average, for this particular set of samples.

RESULTS

The ΔR values were calculated using material around 2000 yr old from 3 sites: Hornish Point and Baleshare on South Uist and St. Boniface on the Orkney Isles (Figure 1). Samples were taken from 3 separate deposits at Baleshare, two at St. Boniface, and one at Hornish Point, thereby allowing 6 assessments of ΔR to be made. Within the group of ΔR determinations, a low level of variation exists, all values being statistically the same at 95% confidence, on the basis of a χ^2 test. This increases our confidence in the integrity of the determinations. The range of values is from –97 to –57, with a weighted mean value for the whole group of –79, and a standard deviation of ±17 ^{14}C yr (Figure 3). This compares to commonly used values of ΔR = ~0 ^{14}C yr for UK waters, e.g. 14 ± 9 ^{14}C yr (Reimer et al. 2002), and a MRE [R(t)] for the region of 405 ^{14}C yr BP (Harkness 1983). The results from these sites, therefore, indicate a suppression of the MRE and, consequently, an elevation of the ^{14}C content in surface ocean waters around the sample sites at about 2000 BP.

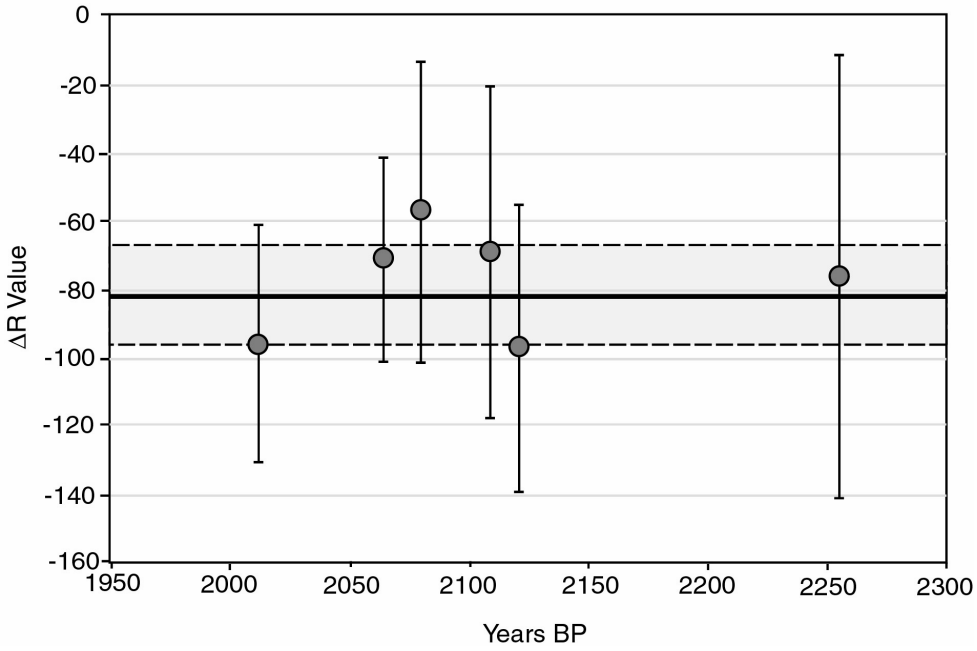

Figure 3 ΔR values from 6 deposits at Baleshare, Hornish Point, and St. Boniface, dated to about 2000 BP, showing the weighted mean ΔR of –79 yr (solid back line) and standard deviation ± 17 yr (shaded area) for the sample group. A ΔR of 0 yr is commonly applied to British waters.

DISCUSSION

Chronological Implications of a Revised ΔR Value

A revised ΔR correction at 2000 BP has significant implications for chronologies constructed using measurements of ^{14}C from marine organisms. These are widely used in Scotland to test theories of human-environment developments and interactions. Because activity periods at a single archaeolog-

ical site are often separated by less than 100 ^{14}C yr, a 79-yr marine correction would affect the perceived chronological relationship of material on an inter-site level. This has particular relevance where events at 1 site are placed into wider patterns of cultural and environmental change. Within a Scottish context, such changes are highly complex, as a wide range of physical landscapes exist within a relatively small land area. As specific developments are adapted to local conditions, to avoid looking at 1 site in isolation, a series of events must be placed upon an absolute timescale, and by linking these environmental and archaeological chronologies, a history of human-environment interactions can be established. The date of about 2000 BP lies within the Scottish Iron Age period, conventionally defined as lasting from about 800 BC to about AD 800 (Armit and Ralston 2003), when environmental changes coincided with extensive cultural changes, including architectural developments. The timing of rapid transitions between several distinct building styles in different regions is currently far from clear, as is the extent to which a cultural change in settlement practice was a response to environmental variations. Two of the architectural styles in question are "brochs" and "wheelhouses." The term "broch" is traditionally used to define a group of prehistoric drystone-built roundhouses with a range of characteristic internal features, including hollow walls, intramural stairs, and galleries (Armit 2003). Some of them are tower-like and, for example, Mousa in Shetland is over 13 m high, but most are now ruinous and the tower-like structures may always have been exceptional (Fojut 1981). Wheelhouses, in contrast, are architecturally much less impressive. While they often enclose spaces that are as large as those found within brochs, they are often dug into the landscape, especially into sandy deposits and were visually unimpressive. Both site types had complex internal subdivision, usually radially arranged, and this became the dominant feature of the wheelhouse where radial dividing walls suggest the spokes of a wheel, giving rise to the site-type designation. The traditional interpretation is that the construction of wheelhouses post-dates that of the brochs; however, an accurate chronology of these architectural forms across the region is needed to determine whether the developments were part of an ordered sequence progression or a more complex regional pattern of co-existence. The impact of a 79-yr ΔR correction to these questions may be illustrated using previously derived ^{14}C data from one of the study sites, Hornish Point (Barber 2003).

Human occupation at Hornish Point is estimated to span no more than 330 ^{14}C yr. The activity consists of a complicated and intensive series of building phases, where later structures often involved the use of material from earlier buildings and several wheelhouses were constructed, occupied, and abandoned over a short period. Ten previously derived radiometric ^{14}C measurements made on bulk samples of mollusc shells from these phases were calibrated using the marine INTCAL98 curve, first using a ΔR of 0 yr, and then using the revised ΔR of -79 ± 17 ^{14}C yr. The shift in calibrated age ranges of the measurements when the revised ΔR is applied is shown in Figure 4. Because the majority of ^{14}C determinations at the site were made on marine mollusc shells, the assessment of the relative duration and age of phases on this individual site should not change radically through application of a revised ΔR value. However, the position of various activity phases at Hornish Point on an absolute timescale, relative to that of many other sites (including broch and wheelhouse structures), is significantly altered.

The Effective Application of MREs and ΔR Values to Chronological Constructions

Our study highlights the importance of applying a correct ΔR value when calibrating marine samples, particularly when the measurement results are to be compared with data from other sites. The use of AMS to analyze single entities with short life spans (e.g. single cereal grains and shells from marine organisms such as limpets, as presented here) has greatly increased our ability to determine accurate ΔR values and has reduced much of the uncertainty previously associated with radiometric

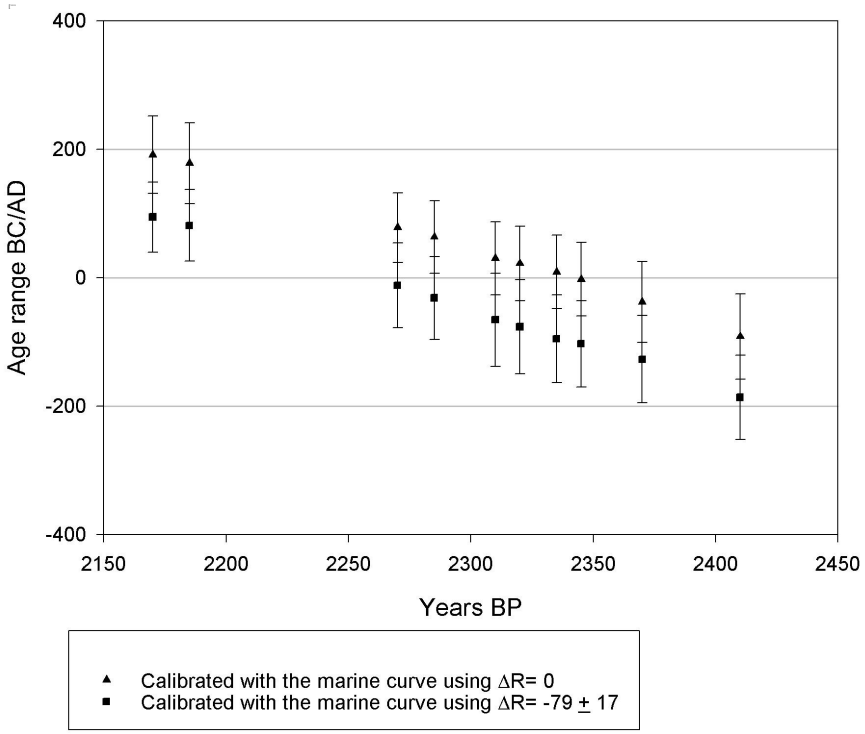

Figure 4 Comparison of the range of calibrated ages for 10 samples from the wheelhouse phases at Hornish point obtained using a ΔR of 0 yr (triangles) and a ΔR of –79 ± 17 yr (squares).

^{14}C dating of bulk samples. Radiometric analysis often involved the use of bulk charcoal samples and, therefore, the potential to introduce an "old wood" effect. In addition, individual contexts often contained insufficient material, which led to a potential compromising of results by bulking material from different contexts, accepting material from less than optimum contexts (e.g. contexts with signs of disturbance) and extrapolation of ^{14}C results between contexts (Barber 2003). All of these factors have affected previous interpretations. One example of this is an earlier assessment of the MRE at Hornish Point (Barber 2003). The methodology used involved a comparison of the ^{14}C age BP of 6 radiometric measurements on terrestrial material (either carbonized plant material or large animal bones) with equivalent marine shell samples. The sample pairs were obtained from both Hornish Point (2 samples) and the nearby site of Baleshare (4 samples). Due to the large volume of material required for each age measurement, it was only possible to obtain marine and terrestrial material from the same deposit in one instance, and other comparisons were made using samples from deposits that were in close proximity. In two instances, the terrestrial sample was composed of material from several adjacent deposits, again due to the sample masses required. In these cases, the equivalent shell age was calculated by interpolating between 2 measurements made on marine shells from deposits directly above and below the bulk of the terrestrial sample, assuming a known sedimentation rate for all deposits.

Using this methodology, the calculated differences between the marine and terrestrial ^{14}C ages of the 6 sample pairs ranged from +121 to –405 yr. Using the Student's *t* test, the differences, taken as a group, were not found to be significantly different from zero at 95% confidence. On the basis of these results, the authors elected to calibrate all ^{14}C measurements in the report using the standard

atmospheric INTCAL98 curve, and consequently, the range of calibrated ages from the Hornish Point wheelhouse phases appear substantially older than those obtained using the marine calibration curve (Figure 5). These ages could imply that the wheelhouses were being constructed and used at the same time as some of the earliest brochs in Scotland. Determination of ΔR using radiometric age measurements produces values between –773 ± 460 and –189 ± 123 due to a high likelihood that a range of entities of different ages were included in the measurement and a reduced likelihood of contemporaneous marine and terrestrial samples due to the restrictions imposed by the required sample masses discussed above. Through the use of AMS single entity dating, we were able to use sample material reliably of a single age and with a high likelihood that the marine and terrestrial material was contemporaneous. The revised data, re-calibrated with the marine curve and a ΔR of –79 ± 17, indicates that the Hornish Point wheelhouses were constructed during a later period. The revised ΔR has important implications for our understanding of the nature of the relationship between both monument types when the ages are calibrated using the marine curve. The chronology of the wheelhouses at Hornish Point, based on a ΔR of 0, places these sites in a chronological span ranging from about 158 BC to AD 252—at the extremes of the calibrated ranges. However, using the revised ΔR of –79 ± 17, this range is revised to 252 BC to AD 149. Traditionally, wheelhouses were viewed as humble successors that evolved, or perhaps, devolved from brochs at a time when the latter were effectively extinct, albeit that some brochs, especially those in the south of Scotland, persisted in use and indeed in construction into the 1st century AD. The Hornish Point dates imply that there is a significant overlap in construction dates of brochs and wheelhouses. This implies sophistication in the social landscape with impressive structures of several types being built, perhaps for personages of differing social grades or for other functions.

This re-interpretation of data from Hornish Point highlights the key issues inherent in applying different calibration methods to material from different locations, which is then fitted into one chronological framework.

Environmental Mechanisms for ΔR Variations

The fact of variation in ΔR demands some consideration of possible mechanisms for this change. A variety of climatic and oceanographic mechanisms could explain observed ΔR variations through time. Paleoenvironmental data from the North Atlantic during the Holocene period indicates the potential for abrupt and intense oscillations in climate and oceanography, with both an overall long-term apparent cooling and evidence for the cyclicity of warming and cooling events (Bond et al. 1997). The key factor in MRE variation may prove to be ocean circulation patterns, as changes in the relative rate and size of flow of prevailing currents at different depths affect the concentration of ^{14}C in the local surface ocean water. On a Holocene timescale, these effects can be seen through evidence such as variation in ice-rafted debris inputs within North Atlantic Ocean sediments to the north of Scotland (Bianchi and McCave 1999).

CONCLUSION

The use of paired marine and terrestrial samples from onshore deposits is an effective way to quantify ΔR values when used with strict controls and multiple analyses on single entities. If the sampling protocol does not ensure a high degree of accuracy, precision, and reproducibility within samples, then the relevance of the calculated ΔR values is compromised. By using the methodology outlined here, the results we have obtained indicate observable deviation from a ΔR value of 0 at sites in the north and west of Scotland around 2000 BP. These results are important for both the calibration of samples containing marine carbon and construction of environmental and archaeological

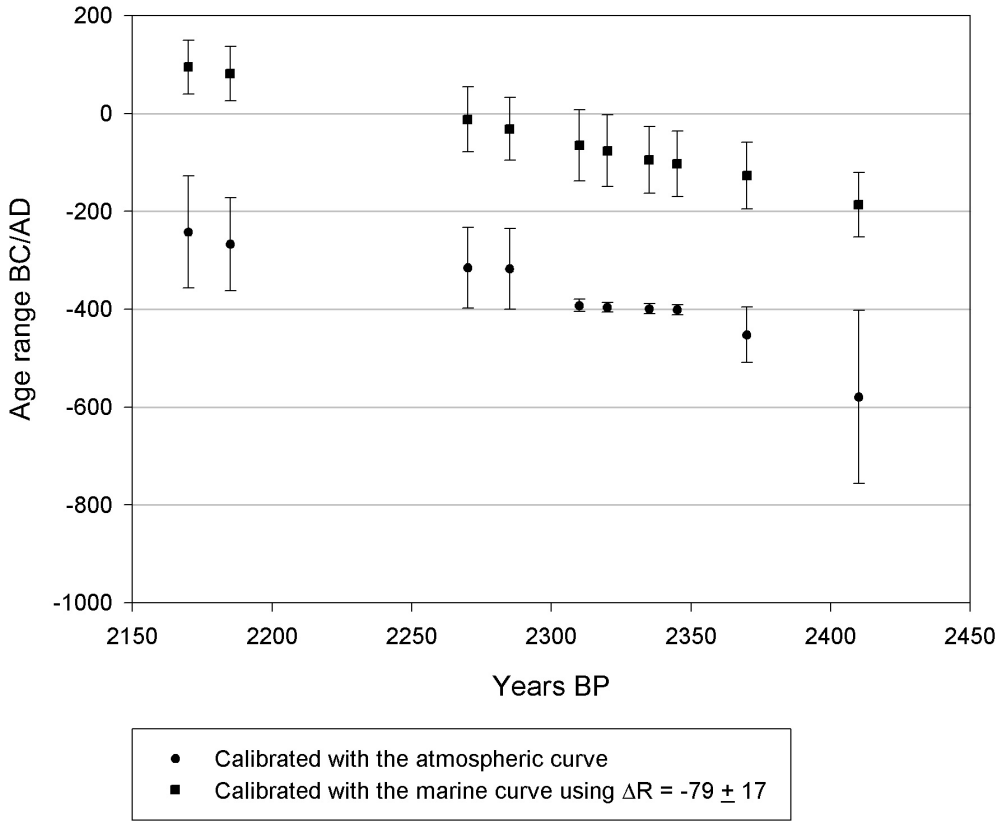

Figure 5 Comparison of the published age ranges for 10 samples from the wheelhouse phases at Hornish Point, where the INTCAL98 atmospheric calibration was applied (circles), with cal age ranges using the marine calibration curve and a ΔR of –79 ± 17 (squares).

chronologies, particularly where data from 1 site are used in relation to that of other sites, on an absolute timescale. It appears important to quantify an appropriate ΔR correction for a given location and time period in situations where the accuracy and precision of measurements is crucial for interpretations. This is especially relevant when interpreting rapid changes over short timescales. Our work highlights the need for a wider understanding among users of current concepts of MREs and ΔR values and how to use this information effectively when formulating interpretations based upon data from marine material. Finally, consideration should be given to the wider environmental mechanisms that underlie temporal variations in ΔR. It may be possible to link marine reservoir effects coherently to both regional paleocirculation changes, and also to local factors of circulation, climate, and coastal topography.

ACKNOWLEDGEMENTS

The authors gratefully acknowledge the support of Historic Scotland in funding this research. We also thank the researchers and excavators who kindly provided sample material for the ^{14}C measurements used to determine ΔR values, Paula Reimer for the provision of data and Fortran coding that enabled us to calculate the ΔR values, the staff of the University of Arizona and SUERC AMS Laboratories for ^{14}C measurements, and Patrick Ashmore (Historic Scotland) for many helpful discussions.

REFERENCES

Adkins JF, Cheng H, Boyle EA, Druffel ERM, Lawrence Edwards R. 1998. Deep sea coral evidence for rapid change in ventilation of the deep North Atlantic 15,400 years ago. *Science* 280:725–8.

Armit I. 2003. *Towers in the North; The Brochs of Scotland*. Gloucestershire: Tempus Publishing.

Armit I, Ralston IBM. 2003. The Iron Age. In: Edwards KJ, Ralston IBM. *Scotland After the Ice Age: Environment, Archaeology and History 8000 BC–AD 1000*. Edinburgh: Polygon. 184 p.

Austin WEN, Bard E, Hunt JB, Kroon D, Peacock JD. 1995. The ^{14}C age of the Icelandic Vedde ash; implications for younger Dryas marine reservoir age corrections. *Radiocarbon* 37(1):53–62.

Barber DC, Dyke A, Hillaire-Marcel C, Jennings AE, Andrews JT, Kerwin MW, Bilodeau G, McNeely R, Southon J, Morehead MD, Gagnon J-M. 1999. Forcing of the cold event of 8,200 years ago by catastrophic draining of Laurentide lakes. *Nature* 400: 344–8.

Barber J. 2003. Bronze Age farms and Iron Age farm mounds of the Outer Hebrides. Scottish Archaeological Internet Reports (SAIR) 3, The Society of Antiquaries of Scotland. URL: http://www.sair.org.uk/sair3/index.htm. Last updated 13 May 2003. Accessed 6 October 2003.

Bianchi GG, McCave IN. 1999. Holocene periodicity in North Atlantic climate and deep ocean flow south of Iceland. *Nature* 397:515–7.

Bond G, Showers W, Cheseby M, Lotti R, Almasi P, deMenocal P, Priore P, Cullen H, Hajdas I, Bonani G. 1997. A pervasive millennial-scale cycle in North Atlantic Holocene and Glacial climates. *Science* 278: 1257–66.

Bondevik S, Mangerud J, Gulliksen S. 2001. The marine ^{14}C age of the Vedde ash bed along the west coast of Norway. *Journal of Quaternary Science* 16(1):3–7.

Broecker WS, Peng TH, Ostlund G, Stuiver M. (1985). The distribution of bomb radiocarbon in the ocean. *Journal of Geophysical Research* 90:6953–70.

Dutta K, Bhushan R, Somayajulu BLK. 2001 ΔR correction values for the Northern Indian Ocean. *Radiocarbon* 43(2A):483–8.

Fojut N. 1981. Is Mousa a broch? *Proceedings of the Society of Antiquaries of Scotland* 111:220–8

Goodfriend GA, Flessa KW. 1997. Radiocarbon reservoir ages in the Gulf of California: roles of upwelling and flow from the Colorado river. *Radiocarbon* 39(2): 139–48.

Gordon JE, Harkness DD. 1992. Magnitude and geographic variation of the radiocarbon content in Antarctic marine life: implications for reservoir correction in radiocarbon dating. *Quaternary Science Reviews* 11: 697–708.

Haflidason H, Eiriksson J, Van Kreveld S. 2000. The tephrochronology of Iceland and the North Atlantic region during the middle and Late Quaternary: a review. *Journal of Quaternary Science* 15(1):3–22.

Levin I, Münnich KO, Weiss W. 1980. The effect of anthropogenic CO_2 and ^{14}C sources on the distribution of ^{14}C in the atmosphere. *Radiocarbon* 22(2):379–91.

Liss PS, Merlivat L. 1986. Air-sea gas exchange rates: introduction and synthesis. In: Buat-Menard P, editor. *The Role of Air-Sea Exchange in Geochemical Cycling*. Dordrecht: D Reidel Publishing Co. p 113–27.

Mangerud J, Gulliksen S. 1975. Apparent radiocarbon ages of recent marine shells from Norway, Spitsbergen and Arctic Canada. *Quaternary Review* 5:263–73.

Reimer PJ, McCormac FG, Moore J, McCormick F, Murray EV. 2002. Marine radiocarbon reservoir corrections for the mid- to late Holocene in the eastern subpolar North Atlantic. *The Holocene* 12(2):129–35.

Siani G, Paterne M, Michel E, Sulpizio R, Sbrana A, Arnold M, Haddad G. 2001. Mediterranean sea surface radiocarbon reservoir age changes since the last glacial maximum. *Science* 294:1917–20.

Sigman DM, Boyle EA. 2000. Glacial/interglacial variations in atmospheric carbon dioxide. *Nature* 407:859–69

Silar J. 1980. Radiocarbon activity measurements of oolitic sediments from the Persian Gulf. *Radiocarbon* 22(3):655–61.

Stocker TF, Wright DG. 1996. Rapid changes in ocean circulation and atmospheric radiocarbon. *Paleoceanography* 11:773–96.

Stuiver M, Pearson GW, Braziunas T. 1986. Radiocarbon age calibration of marine samples back to 9000 cal yr BP. *Radiocarbon* 28(2B):980–1021.

Stuiver M, Braziunas TF. 1993. Modelling atmospheric ^{14}C influences and ^{14}C ages of marine samples to 10,000 BC. *Radiocarbon* 35(1):137–89.

RADIOCARBON, Vol 46, Nr 2, 2004, p 621–626

RADIOCARBON RESERVOIR AGES FROM FRESHWATER LAKES, SOUTH GEORGIA, SUB-ANTARCTIC: MODERN ANALOGUES FROM PARTICULATE ORGANIC MATTER AND SURFACE SEDIMENTS

Steven G Moreton[1] • Gunhild C Rosqvist[2] • Sarah J Davies[3] • Michael J Bentley[4]

ABSTRACT. Lake sediments have the potential to preserve proxy records of past climate change. Organic material suitable for radiocarbon dating often provides age control of such proxy records. Six shallow freshwater lakes on the sub-Antarctic island of South Georgia were investigated for carbon reservoir effects that may influence age-depth profiles from lake sediment records in this important region. Paired samples of particulate organic matter (POM) from the water column and surface sediment (bulk organic carbon) were analyzed by accelerator mass spectrometry ^{14}C. POM in 4 lakes was found to be in equilibrium with the atmosphere (~107% modern), whereas 2 lakes showed significant depletion of ^{14}C. In each lake, the surface sediment ages were older than the paired POM age. Surface sediment ages showed a much greater range of ages compared to the equivalent POM ages, even for lakes located in close proximity. We conclude that sediment disturbance during coring, bioturbation, and periodic resuspension of sediments are likely factors causing the difference in the apparent age of surface sediments.

INTRODUCTION

Radiocarbon dating is a useful tool for providing a chronological framework for Late Pleistocene–Holocene paleoenvironmental studies. However, the application of ^{14}C dating to Antarctic sediments is complicated by the difficulty of establishing the temporal and spatial variability of the carbon reservoir effect in that region. Gordon and Harkness (1992) produced an invaluable review and summary of Antarctic marine reservoir corrections, but as yet, no equivalent review exists for Antarctic freshwater environments. Many studies of sediments from freshwater lakes in Antarctica have yielded older than expected ^{14}C ages (Zale and Karlén 1989; Björck et al. 1991a; Ingólfsson et al. 1992; Hjort et al. 1997; Doran et al. 1999; Takahashi et al. 1999; Hall and Henderson 2001). Explanations for the "old" ages depend on sample type and lake location, although the erroneous ages are most commonly attributed to the input of ^{14}C-depleted glacial meltwater, contamination by marine water or marine sediment, restricted gaseous exchange due to ice cover, and disturbance of sediments by ice. Other factors that may influence the apparent age of core top sediments are mixing of sediment due to bioturbation, resuspension of sediments by wind-driven circulation, and possible loss of surface material during core recovery.

None of the previous investigations of lake sediments from South Georgia produced ^{14}C ages for lake water, microbial mats, water-borne particulate organic matter (POM), or surface sediments. Ages from core-top sediments were not reported due to disturbance of the poorly consolidated upper sediment during core recovery or due to insufficient carbon for radiometric dating (Birnie 1990; Rosqvist et al. 1999; Rosqvist and Schuber 2003). The aim of our study is, therefore, to provide an estimate of the potential local carbon reservoir effect influencing age determinations on lake sediments from South Georgia.

Here, we report contemporary ^{14}C ages from POM and surface sediments from 6 freshwater lakes on South Georgia ahead of a more detailed chronology and multi-disciplinary paleoenvironmental

[1]NERC Radiocarbon Laboratory, Scottish Enterprise Technology Park, East Kilbride, G75 0QF, United Kingdom. Corresponding author. Email: S.Moreton@nercrcl.gla.ac.uk.
[2]Department of Physical Geography, Stockholm University, S-106 91 Stockholm, Sweden.
[3]Institute of Geography and Earth Sciences, University of Wales Aberystwyth, Llandinam Building, Aberystwyth, SY23 3DB, United Kingdom.
[4]Department of Geography, University of Durham, Science Site, South Road, Durham, DH1 3LE, United Kingdom.

Proceedings of the 18th International Radiocarbon Conference, edited by N Beavan Athfield and R J Sparks
RADIOCARBON, Vol 46, Nr 2, 2004, p 621–626

investigation of sediment cores recovered from those lakes. All samples were collected in the austral summer 2002–2003.

The sub-Antarctic island of South Georgia is ideally situated to investigate the chronology of climate change as it lies between the current maximum extent of winter sea ice and the Antarctic Convergence Zone, where warm temperate and cold Antarctic waters meet (Figure 1). Climatically induced changes in the position of these boundaries profoundly impact the environment and are recorded in the sediment by proxy signals (e.g. diatom and pollen assemblage, oxygen isotopes of biogenic silica, carbon and nitrogen isotope ratios of the organic material, and physical parameters, such as grey-scale density, grain size, and magnetic susceptibility). Recent paleolimnological evidence from South Georgia indicates that substantial parts of the island were ice-free by 18,600 calendar BP (Rosqvist et al. 1999), strongly suggesting that deglaciation commenced there much earlier than had been previously thought. Many paleoenvironmental records from other Antarctic and sub-Antarctic islands do not extend beyond the Holocene (e.g. Wasell and Håkansson 1992; Björck et al. 1991a, 1991b, 1996; Jones et al. 2000), which emphasizes the importance of South Georgia in providing long terrestrial paleoclimatic records for the Antarctic region.

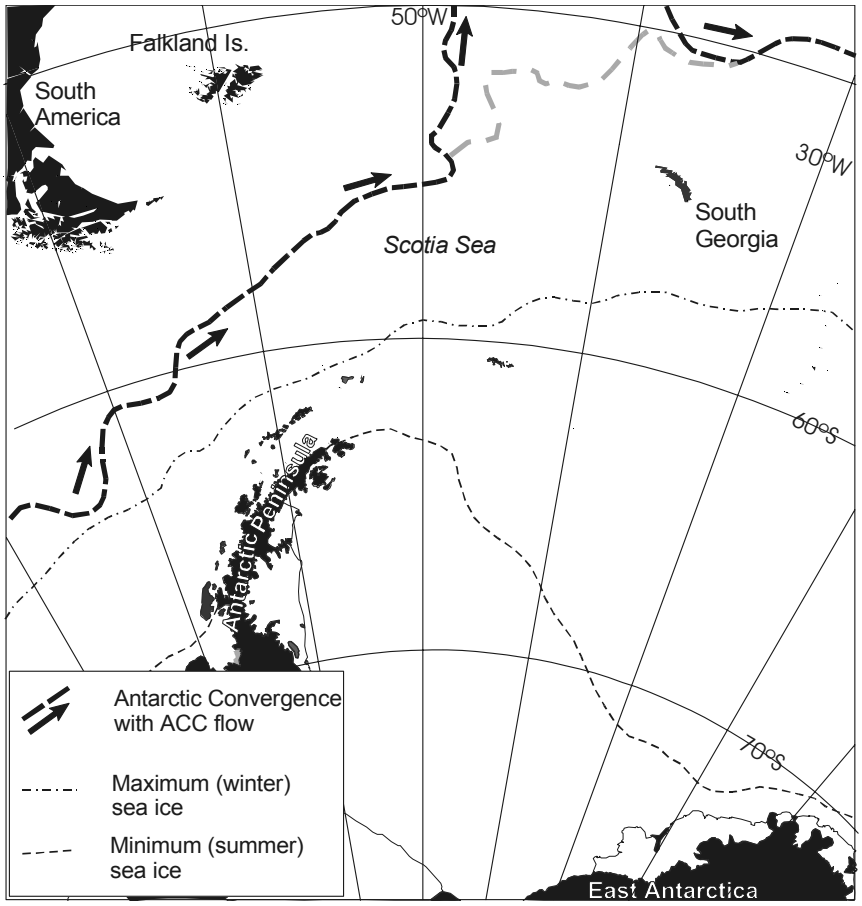

Figure 1 South Atlantic sector of the Southern Ocean showing current positions of the Antarctic Convergence and sea-ice limits. Migrations of these boundaries in response to climatic changes profoundly affect the environment and glacier extent on sub-Antarctic islands.

Site Locations

Six freshwater lakes in a range of geographical and topographical settings on the relatively ice-free eastern side of the island were sampled as part of a sediment coring program which aims to investigate the timing and spatial continuity of the glacier retreat after the Last Glacial Maximum (LGM) and the paleoenvironmental history of South Georgia since the LGM (Figure 2). All lakes are small with surface areas between 3000 m^2 and 60,000 m^2 and a maximum depth of 6.0 m. The presence of overflow channels and low embankments around one or more sides of each lake means that the lakes were close to, or at, their maximum depth at the time of sample collection. In situ roots of terrestrial plants were not observed in recovered sediment cores, indicating that the lakes have not been prone to prolonged desiccation. The lakes are ice-covered for 4–5 months per year but thoroughly mixed when ice-free. Restricted gaseous exchange is not thought to be a major problem for causing $^{14}CO_2$ disequilibrium. Salinity, temperature, and pH profiles indicate that at the time of sampling, all of the lakes were thoroughly mixed (S Davies, unpublished data). Only 1 lake, Block Lake (BLC), is fed by glacial meltwater and receives substantial inputs of mineral material. The steep gradient and length (~1.5 km) of the meltwater stream flowing into Block Lake is sufficient to allow thorough mixing of the water and $^{14}CO_2$ equilibration with the atmosphere (Stuiver et al. 1981). Because all of the POM samples consist of primary or secondary productivity, we expected ^{14}C concentrations close to modern atmospheric $^{14}CO_2$ levels.

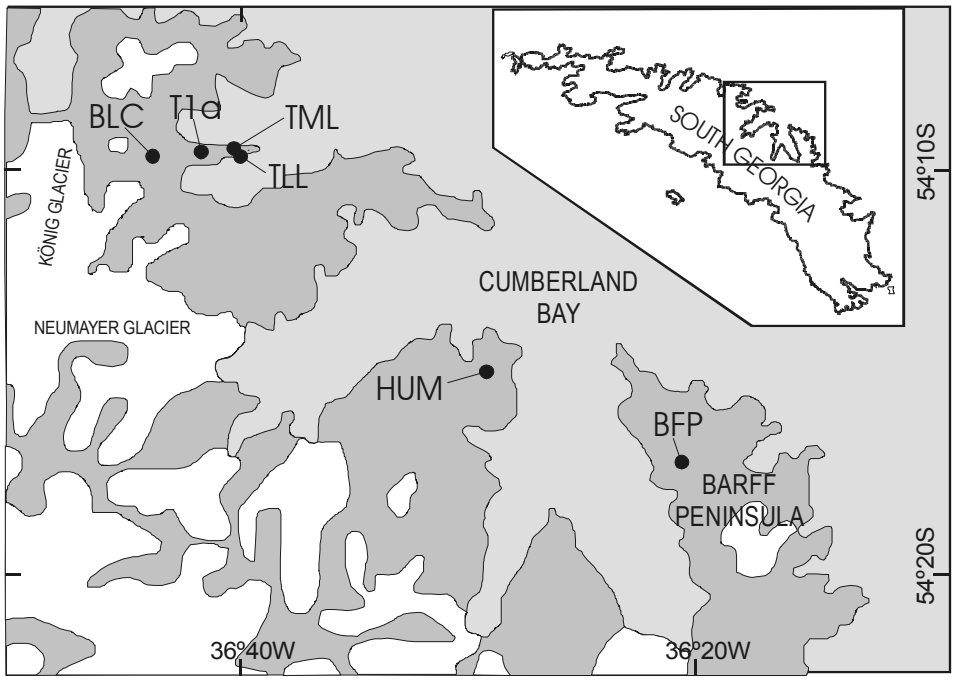

Figure 2 Map showing the location of the 6 freshwater lakes sampled for this study. There is no discernible spatial trend in the ages of either the POM or surface sediments in these lakes.

Most lake names presented are unofficial names and the following codes have been used for brevity: Tønsberg Lake T1 (T1a), Tønsberg Middle Lake (TML), Tønsberg Lower Lake (TLL), Block Lake (BLC), Barff Peninsula Lake (BFP), Humic Lake (HUM).

Sample Collection

The POM was collected from the water column by trawling with a hand-held 30-µm mesh plankton net. Most of the organic material collected was zooplankton, with lesser amounts of phytoplankton, aquatic insects, and insect larvae.

Samples of the uppermost 1 cm of sediment were sampled to compare with the ages of core-top sediment (which will be analyzed in the near future). The poorly consolidated nature of the sediment leads to suspicions that some core-top material might be lost during core recovery and direct comparison between surface sediment and core-top ages will allow the amount of sediment lost to be quantified. A plastic scoop on a 1.5-m pole was used to collect the surface sediment. Direct observation of the sampling operation in clear water ensured that only the topmost 1 cm of sediment was sampled. One lake (TML) was too deep for this method and a core-top sample from a "mini Kullenberg corer" was dated instead.

Particulate organic matter samples were acid washed in 1M HCl for 2 hr at 80 °C, surface sediment samples were acid washed in 2M HCl for 2 hr at 80 °C. All samples were rinsed free from mineral acid with de-ionized water, dried, and homogenized. The total organic carbon in a known weight of pretreated sample was recovered as CO_2 by heating with CuO in a sealed quartz tube. The CO_2 was converted to graphite by stepped Fe/Zn reduction. Sample pretreatment was completed at the Natural Environment Research Council Radiocarbon Laboratory, East Kilbride, UK. Graphite targets were analyzed at the Scottish Universities Environmental Research Centre (SUERC) accelerator mass spectrometry facility, East Kilbride, UK.

RESULTS AND DISCUSSION

Particulate Organic Matter

Four of the 6 POM samples (TML, TLL, BFP, HUM) show ^{14}C enrichment of >100% modern (106.71–109.04 absolute percent modern carbon [pMC]; Table 1). The ^{14}C enrichment values for these 4 lakes lie close to a current (2002–2003) atmospheric ^{14}C concentration of ~107 pMC, extrapolated from the Northern Hemisphere atmospheric $^{14}CO_2$ trend of Levin and Kromer (1997). This indicates that the dissolved $^{14}CO_2$ in these lakes is in equilibrium with the atmosphere and there is no carbon reservoir effect influencing the age of the autochthonous sediments in these 4 lakes.

Two lakes (T1a and BLC) produced POM ^{14}C values <100 pMC, indicating that the lake water is not in equilibrium with the atmosphere. In order to acquire a conventional ^{14}C age, the POM must be diluted with enough "old" carbon to swamp the enriched atmospheric $^{14}CO_2$ signal. With the limited data currently available, it is not possible to definitively calculate the magnitude of the reservoir age for these lakes. However, based on the POM pMC values of 96.60 ± 0.47 (T1a) and 93.76 ± 36 (BLC), we estimate the age offset to be approximately ~850 and ~1100 ^{14}C yr too old, respectively. It is not known at this stage what is producing these age offsets, nor whether the offset has remained constant over time. Hardwater error has been discounted, as the Cumberland Bay region comprises mainly quartzose greywackes, volcanic greywackes, slates, and igneous intrusions in which calcite is absent or present at very low quantities (Skidmore 1972). Contamination by marine water can also be ruled out as the lakes are fresh, conductivity in each is <100 us cm^{-1} (S Davies, unpublished data), and analyses of $\delta^{18}O$ and δD of the lake and through flow water indicate the lakes are replenished by local precipitation, and isotopic enrichment due to evaporation is insignificant (Rosqvist et al. 1999; unpublished data). Relict $^{14}CO_2$ in glacial meltwater has been discounted for the reasons outlined above. At this stage, not enough is known about the hydrology of South Georgia to be able

Table 1 ^{14}C concentrations and conventional ^{14}C ages for POM and surface sediment in 6 freshwater lakes, South Georgia, sub-Antarctic.

Publication Code	Lake code	Absolute % modern ± 1 σ	Conventional ^{14}C age (BP ± 1 σ)	$\delta^{13}C_{PDB}$ ‰ ± 0.1 σ	Carbon content (% by wt)
Particulate Organic Matter					
SUERC-592	T1a	96.60 ± 0.47	226 ± 39	–30.1	27.3
SUERC-593	TML	109.05 ± 0.49	> modern	–27.1	65.2
SUERC-594	TLL	106.64 ± 0.33	> modern	–28.4	59.2
SUERC-595	BLC	93.76 ± 0.36	466 ± 30	–23.7	29.4
SUERC-596	BFP	108.30 ± 0.38	> modern	–25.7	21.6
SUERC-597	HUM	107.66 ± 0.40	> modern	–23.7	54.0
Surface Sediment					
SUERC-598	T1a	85.62 ± 0.27	1196 ± 26	–22.5	14.4
SUERC-603	TML	83.42 ± 0.52	1405 ± 50[a]	–25.5	28.2
SUERC-600	TLL	105.37 ± 0.70	> modern	–25.7	34.4
—	BLC[b]	—	—	—	—
SUERC-604	BFP	94.34 ± 0.84	417 ± 71	–20.6	13.3
SUERC-605	HUM	96.63 ± 0.50	224 ± 41	–27.7	39.2

[a]Core top sample.
[b]No data available.

to establish whether groundwater might play a part in introducing ^{14}C-depleted water in to the lakes. One possible source of old ^{14}C in the POM samples is resuspended sediment. We consider this to be the most likely source given the poorly consolidated nature of the sediments and the shallowness of these lakes.

Surface Sediments

In all lakes, the pMC is greater in the POM than in the surface sediment. However, there was considerable variation in the surface sediment ages between lakes. The 2 lakes in closest proximity to each other (TML and TLL) showed the greatest difference in surface age. One possible cause of this discrepancy might be the need to use a core-top sample from TML rather than directly sampled surface sediment. The sediments in all the lakes are poorly consolidated and the deployment of the trigger operated "mini Kullenberg corer" in TML might have been sufficient to dislodge the uppermost sediment, leaving an incomplete sediment record. Further investigation of down-core ^{14}C and ^{210}Pb profiles will help to clarify this issue. The apparent older surface sediment ages in the other lakes is most likely due to a combination of bioturbation and periodic resuspension and settling of sediment.

CONCLUSIONS

For the majority of lakes studied, POM in the water column is in equilibrium with the atmosphere, indicating that no carbon reservoir effect influences the age of these autochthonous sediments. However, 2 lakes (T1a and BLC) yield reservoir ages. Therefore, the previous chronology produced for sediments from Tønsberg Lake T1 (Rosqvist et al. 1999) might have over estimated the age of deglaciation by about 850 ^{14}C yr, assuming that present-day conditions also existed in the past, as no carbon reservoir/dilution effect was taken into account when producing the age model. Likewise, the age model used in the Block Lake record showing millennial-scale climate change (Rosqvist and Schuber 2003) might also need correction by about 1100 ^{14}C yr.

We have shown that surface sediment ages are highly variable, even from lakes in close proximity. Therefore, studies of modern analogues from POM and surface sediments are necessary before presenting climate change chronologies based on ^{14}C results. The choice of coring method is critical to obtain an undisturbed sediment-water interface of unconsolidated surface sediments.

ACKNOWLEDGEMENTS

We thank the main sponsors of the *SCOTIA* Centenary Antarctic Expedition (2002–2003) to South Georgia: The Royal Scottish Geographical Society, The Carnegie Trust for the Universities of Scotland, The National Geographic Society, the Royal Swedish Academy of Sciences, The Binks Trust, The Brownington Foundation, and The Government of South Georgia and the South Sandwich Islands. We also gratefully acknowledge the help of numerous individuals, including those in the British Antarctic Survey and the captains and crews of *HMS Endurance* and *Ocean Tramp* and all the participants of the *SCOTIA* Centenary Antarctic Expedition. The ^{14}C dating was funded by the Natural Environment Research Council (allocation number 14.45).

REFERENCES

Birnie J. 1990. Holocene environmental change in South Georgia: evidence from lake sediments. *Journal of Quaternary Science* 5:171–87.

Björck S, Håkansson H, Zale R, Karlén W, Jönsson BL. 1991b. A Late Holocene lake sediment sequence from Livingston Island, South Shetland Islands, with palaeoclimatic implications. *Antarctic Science* 3(1):61–72.

Björck S, Hjort C, Ingólfsson Ó, Skog G. 1991a. Radiocarbon dates from the Antarctic Peninsula region—problems and potential. *Quaternary Proceedings* 1:55–65.

Björck S, Olsson S, Ellis-Evans C, Håkansson H, Humlum O, de Lirio JM. 1996. Late Holocene palaeoclimatic records from lake sediments on James Ross Island, Antarctica. *Palaeogeography, Palaeoclimatology, Palaeoecology* 121:195–220.

Doran PT, Berger GW, Lyons WB, Wharton Jr RA, Davisson ML, Southon J, Dibb JE. 1999. Dating Quaternary lacustrine sediments in the McMurdo Dry Valleys, Antarctica. *Palaeogeography, Palaeoclimatology, Palaeoecology* 147:223–39.

Gordon JE, Harkness DD. 1992. Magnitude and geographic variation of the radiocarbon content in Antarctic marine life: implications for reservoir corrections in radiocarbon dating. *Quaternary Science Reviews* 11:697–708.

Hall BL, Henderson GM. 2001. Use of uranium-thorium dating to determine past ^{14}C reservoir effects in lakes: examples from Antarctica. *Earth and Planetary Science Letters* 193:565–77.

Hjort C, Ingólfsson Ó, Möller P, Lirio JM. 1997. Holocene glacial history sea-level changes on James Ross Island, Antarctic Peninsula. *Journal of Quaternary Science* 12(4):259–73.

Ingólfsson Ó, Hjort C, Björck S, Smith RIL. 1992. Late Pleistocene and Holocene glacial history of James Ross Island, Antarctic Peninsula. *Boreas* 21:209–22.

Jones VJ, Hodgson DA, Chepstow-Lusty A. 2000. Palaeolimnological evidence for marked Holocene environmental changes on Signy Island, Antarctica. *The Holocene* 10(2):43–60.

Levin I, Kromer B. 1997. Twenty years of atmospheric $^{14}CO_2$ observations at Schauinsland Station, Germany. *Radiocarbon* 39(2):205–18.

Rosqvist GC, Rietti-Shati M, Shemesh A. 1999. Late glacial to middle Holocene climatic record of lacustrine biogenic silica isotopes from a Southern Ocean island. *Geology* 27:967–70.

Rosqvist G, Schuber P. 2003. Millennial-scale climate changes on South Georgia, Southern Ocean. *Quaternary Research* 59(3):470–75.

Skidmore MJ. 1972. The geology of South Georgia: 3. Prince Olav Harbour and Stromness Bay areas. *British Antarctic Survey Scientific Reports* 73:50.

Stuiver M, Denton GH, Hughes TJ, Fastook JL. 1981. History of the marine ice sheet in west Antarctica during the last glaciation, a working hypothesis. In: Denton GH, Hughes TH, editors. *The Last Great Ice Sheets*. New York: Wiley-Interscience. p 319–436.

Takahashi HA, Wada H, Nakamura T, Miura H. 1999. ^{14}C anomaly of freshwater algae in Antarctic coastal ponds and lakes. *Polar Science* 12:248–57.

Wasell A, Håkansson H. 1992. Diatom stratigraphy in a lake on Horseshoe Island, Antarctica: a marine-brackish-freshwater transition with comments on the systematics and ecology of the most common diatoms, *Diatom Research* 7:157–94.

Zale R, Karlén W. 1989. Lake sediment cores from the Antarctic Peninsula and surrounding islands. *Geografiska Annaler* 71(A):211–20.

RADIOCARBON, Vol 46, Nr 2, 2004, p 627–631

VARIABILITY OF MONTHLY RADIOCARBON DURING THE 1760s IN CORALS FROM THE GALAPAGOS ISLANDS

Ellen R M Druffel[1] • Sheila Griffin • Jeomshik Hwang • Tomoko Komada • Steven R Beaupre • Kevin C Druffel-Rodriguez • Guaciara M Santos • John Southon

Department of Earth System Science, University of California, Irvine, California 92697, USA.

ABSTRACT. Radiocarbon ($\Delta^{14}C$) measurements of monthly samples from a Galapagos surface coral are among the first data sets from the new Keck Carbon Cycle Accelerator Mass Spectrometry laboratory at the University of California, Irvine. An average $\Delta^{14}C$ value of –62‰ is obtained for 144 measurements of samples from monthly coral bands that lived from about AD 1760–1771 (±6 yr). High $\Delta^{14}C$ values were found during January through March, when upwelling was weak or absent at the Galapagos Islands. Low $\Delta^{14}C$ values were obtained mid-year during strong upwelling. The average seasonal variability of $\Delta^{14}C$ was 15–25‰, which is greater than that at other tropical and subtropical locations in the Pacific Ocean because of intense seasonal upwelling at this site. Periods of sustained high $\Delta^{14}C$ values were found during 1762–1763 and 1766. A spectral analysis revealed that the spectral density for the $\Delta^{14}C$ data displays most of its variance at the 5-yr cycle, which is reflective of El Niño periodicity during the 20th century.

INTRODUCTION

Data from banded corals show that the radiocarbon (^{14}C) "age" of pre-bomb, non-polar surface ocean ranges from 620 ^{14}C yr (–72‰) in the eastern tropical Pacific to 340 ^{14}C yr (–40‰) in the mid-gyre regions of the Pacific Ocean (Druffel 1987; Druffel et al. 2001). These non-contemporary reservoir ages of surface dissolved inorganic carbon (DIC) are due mainly to vertical and advective mixing of subsurface water having even "older" ^{14}C ages because of radioactive decay during isolation from the atmosphere. Because ^{14}C has a long turnover time (10 yr) in the atmosphere with respect to the transfer to the sea surface, $\Delta^{14}C$ of DIC in surface seawater is a tracer of circulation patterns and thermocline depth. Records of upper ocean circulation changes during the past are essential for understanding present and future climate changes.

Corals reflect the $\Delta^{14}C$ in surface DIC and provide time histories of $\Delta^{14}C$ on timescales of months to millennia. Records of $\Delta^{14}C$ in the surface ocean reveal past variability of surface-subsurface mixing and horizontal current shifts. We report monthly $\Delta^{14}C$ measurements from a Galapagos coral representing the 11-yr period AD 1760–1771 (±6 yr). We show that $\Delta^{14}C$ is high during the beginning of the year, when trade winds and upwelling were weak, and low $\Delta^{14}C$ values during the rest of the year, when wind-driven upwelling was strong.

OCEANOGRAPHIC SETTING AND SAMPLE COLLECTION

The coral sequence was collected by Drs Rob Dunbar, Mitch Colgan, and Gerard Wellington from a dead, massive head of *Pavona clavus* in Urvina Bay on the west coast of Isabela Island (0°15′S, 91°22′W) in the Galapagos archipelago in 1986 (see Dunbar et al. 1991 for details). The coral site was directly in the path of the cold, nutrient-rich Peru Current and the Equatorial Counter Current (Cromwell Current), which brings subsurface water eastward. The coral and the shoreline of the central coast of Urvina Bay was raised above sea level in March 1954 because of the intrusion and upward movement of magma below the surface (Richards 1957).

[1]Corresponding author. Email: edruffel@uci.edu.

Proceedings of the 18th International Radiocarbon Conference, edited by N Beavan Athfield and R J Sparks
RADIOCARBON, Vol 46, Nr 2, 2004, p 627–631

METHODS

Dunbar et al. (1991) cleaned, X-rayed, and developed an age model for this coral sequence using high-density bands that accrete from about January to April of each year. Based on preliminary ^{230}Th mass spectrometric analyses performed by Bruno Hamelin (LDEO), Dunbar et al. (1991) estimated an uncertainty of ±10 yr for ages at the base of the section (AD 1583), which translates to ±6 yr for our samples during the 1760s (assuming the uncertainty is linear).

We performed Δ^{14}C measurements on coral samples that had been ground off with a diamond-tip dremel tool to a width of 1 mm each from a vertical strip of coral (10 mm wide and 7 mm thick). The sequence was 144 mm long and spanned the time period from late 1760 to mid-1771; the average sampling frequency was 13 samples/yr.

Sub-samples (8 mg each) were converted to CO_2 in evacuated Vacutainers® with 85% phosphoric acid, then to graphite on Co catalyst with H_2 gas as the reducing agent (Vogel et al. 1987). All of the samples were analyzed for $^{14}C/^{12}C$ using accelerator mass spectrometry (AMS) at the Keck Carbon Cycle AMS Laboratory at UC Irvine. Background subtraction was applied using ^{14}C-free spar calcite. The Δ^{14}C measurements had a total uncertainty (counting statistics and laboratory reproducibility) of ±4–5‰ (1 σ). Radiocarbon measurements are reported as Δ^{14}C values (for geochemical samples with known age) according to Stuiver and Polach (1977). The Δ^{14}C results were corrected using δ^{13}C values measured either by the AMS or on CO_2 splits prior to graphitization.

RESULTS

The average of 144 monthly Δ^{14}C measurements (duplicate analyses and splits of the same CO_2 were averaged to a single point) from the Urvina Bay coral is –62 ± 6 (sd)‰. The range of the individual values is large (33‰), from –80‰ in early 1765 to –47‰ in mid-1770 (Figure 1). A least-squares fit of all monthly Δ^{14}C measurements reveals no significant trend with time.

Seasonal cycles are apparent in the Δ^{14}C data during most years (Figure 1), though these cycles are not well defined. The highest Δ^{14}C values (large grey circles) are at the base of the high-density bands (vertical lines in Figure 1), which are formed when surface waters are warm and upwelling is weak or absent (January through March) (Druffel 1981). The average of these 10 high Δ^{14}C values is –53 ± 3‰. Most of the lowest Δ^{14}C values (large black circles) were from samples in the middle of the bands. The average of the 11 low Δ^{14}C values is –71 ± 5‰. A least-squares fit of the low Δ^{14}C values reveals a 6‰ decrease over the 11-yr time period, that for the high Δ^{14}C values is not significant.

DISCUSSION

There appears to be an interannual fluctuation of the Δ^{14}C values in this record. The Δ^{14}C values for 1765 and 1769 were lower than those for other years. Six to 7 consecutive high Δ^{14}C values were found for 1766 and 1770 (average –54‰ for both). A smoothed line of the monthly data is shown in Figure 1 using a Stineman function and suggests that, based on Δ^{14}C data alone, El Niño events occurred during 1762–1763, 1766, and possibly 1770. During 1762–63, Δ^{14}C values increased during the upwelling season relative to other years, similar to Guilderson and Schrag's (1998) Δ^{14}C increase in Galapagos coral after the climate shift of 1976.

Periodicities within the monthly Δ^{14}C record were investigated by spectral analysis using Spectral software provided by Phil Howell (personal communication, 2000). The spectral density for the Δ^{14}C data displays a small amount of variance at the 1-yr cycle and most of its variance at the 5-yr

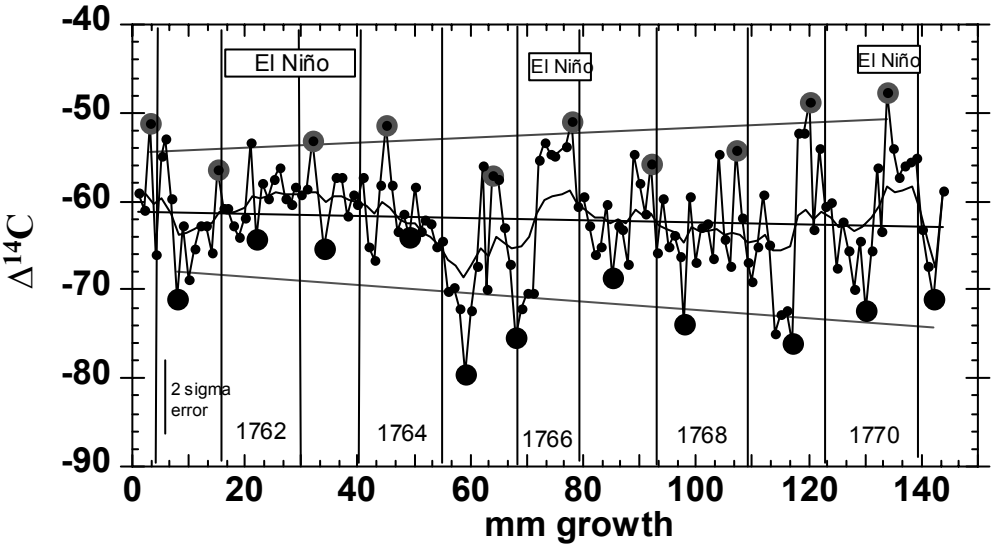

Figure 1 $\Delta^{14}C$ measurements of monthly coral bands from Urvina Bay, Galapagos, during the period 1760 to 1771. The uncertainty of the age assignments in this age range is ±6 yr. Duplicate analyses of separate aliquots from the same coral sample and splits of the same CO_2 were averaged to a single point. Large grey points represent the highest $\Delta^{14}C$ values for each year (lowest upwelling) and large black points represent the lowest $\Delta^{14}C$ values for each year (most intense upwelling). Vertical lines mark the base of the high-density bands, which are generally formed when upwelling is low. Horizontal lines (grey) are the least-squares fits of the high and low ^{14}C values, and that (black) for all of the monthly results. The smoothed line of the monthly data is obtained using a Stineman function, which suggests that El Niño events occurred during 1762–63 and possibly 1766.

cycle (significant to the 95% confidence level). The 5-yr cycle, however, is close to the nyquist frequency of 5.5 yr (11 yr total record/2), so the significance of this result is questionable. Nonetheless, a 5-yr cycle is similar to the frequency of El Niño events during the 20th century, which would suggest that, within the limits of this short data set, El Niño (high $\Delta^{14}C$) events during the 1760s were not different in frequency from those that were observed during recent times.

The average seasonal amplitude of $\Delta^{14}C$ values for the Galapagos coral during the 1760s was 15 to 25‰ (Figure 1), whereas those reported for recent corals from other Pacific sites are significantly lower (3–4‰ for Hawaiian coral, Druffel et al. 2001; 10–15‰ for Raratonga coral, Guilderson et al. 2000; 10–15‰ for Fanning Island coral, Grottoli et al. 2003). Seasonal upwelling at the eastern tropical Pacific is strong during the months of July through September, when the southeast trade winds are strongest. During this period, cold (18–20 °C), nutrient-rich water upwells into the Peru Current and Equatorial Counter Current, both of which lave the Galapagos Islands. The lowest pre-bomb $\Delta^{14}C$ values of any non-polar surface location are found at the Galapagos (Druffel 1981; Toggweiler et al. 1991) because of its proximity to intense equatorial and coastal upwelling.

A comparison of average pre-bomb $\Delta^{14}C$ values for corals from several Pacific locations reveals that the monthly Galapagos record for the 1760s (–62 ± 6‰) and the annual Galapagos record for 1930–1941 (Druffel 1989; –70 ± 6‰) were the lowest. Monthly samples from a Fanning Island coral (4°N, 159°W) have an average $\Delta^{14}C$ value of –55 ± 5‰ (n = 217) between 1922 and 1947 (Grottoli et al. 2003). In the western Pacific, Guilderson et al. (1998) determined the average of monthly $\Delta^{14}C$ values at Nauru (1°S, 166°E) was –58‰ between 1947 and 1956. An average of all Hawaiian bimonthly $\Delta^{14}C$ analyses for the time period 1920.8–1923.0 was –46.4 ± 2.3‰ (Druffel

et al. 2001). A coral from the subtropical South Pacific (Rarotonga, 21°S, 160°W) had a pre-bomb, average $\Delta^{14}C$ value of –52‰ for the 1950s (Guilderson et al. 2000). These sites have higher $\Delta^{14}C$ levels because their mixed layers are more stable and there is little or no upwelling compared to the intense upwelling conditions in the eastern equatorial Pacific (Toggweiler et al. 1991).

The physical mechanism that causes temporal variability of climate and $\Delta^{14}C$ on an interannual timescale is El Niño/Southern Oscillation (ENSO). ENSO is caused by interaction of the tropical ocean and atmosphere (Bjerknes 1969). ^{14}C has been shown to increase in Galapagos coral bands that grew during El Niño events of the past 40 yr because upwelled waters no longer reached the sea surface (Druffel 1981; Brown et al. 1993), especially during mid-year (Guilderson and Schrag 1998). These events were generally coincident with warm waters that laved the region. Therefore, in the case of El Niño events, high $\Delta^{14}C$ measurements reflect a cessation of local upwelling, the presence of high ^{14}C surface water advected eastward along the Equator from the western warm pool, and transport of off-equatorial water masses due to the southward migration of the ITCZ during El Niño events. We suggest that these conditions prevailed during 1762–63, 1766, and part of 1770.

CONCLUSIONS

Radiocarbon ($\Delta^{14}C$) measurements of monthly samples from a Galapagos surface coral show an average $\Delta^{14}C$ value of –62‰ for samples that lived during ~1760–1771. Periods of sustained high $\Delta^{14}C$ values were found for the years 1762–63 and possibly 1770. Spectral analysis of the $\Delta^{14}C$ data shows that the spectral density has most of its variance in the 5-yr cycle, reflecting the El Niño cycle; some variance is seen for the annual cycle. The 5-yr cycle is similar to the frequency of El Niño events during the 20th century, which would indicate that El Niño (high $\Delta^{14}C$) events during the 1760s occurred at a frequency similar to that during the last 100 yr. The seasonal variability of $\Delta^{14}C$ during the 1760s, though not well defined, had a higher amplitude range than at other sites in the Pacific because of the strong seasonal upwelling that is unique to the eastern tropical Pacific.

ACKNOWLEDGEMENTS

We thank Rob Dunbar, Jerry Wellington, and Mitch Colgan for sharing their monstrous coral with us. We thank Xiaomei Xu, Shuhui Zheng, and Sue Trumbore for shared equipment and support, Phil Howell for shared software, Tom Guilderson for helpful comments on the manuscript, Mark McClure for editorial support, and Betty Leidel for her help with the Keck proposal. We thank the W M Keck Foundation for their generous support that allowed us to purchase and set up the Keck Carbon Cycle AMS Laboratory. We acknowledge the NSF Chemical Oceanography Program (to ERMD), the UCOP Marine Sciences for support (to JH), and the Dreyfus Foundation for support (to ERMD and TK).

REFERENCES

Bjerknes J. 1969. Atmospheric teleconnections from the equatorial Pacific. *Monthly Weather Review* 97:163–72.

Brown T, Farwell G, Grootes P, Schimidt F, Stuiver M. 1993. Intra-annual variability of the radiocarbon content of corals from the Galapagos Islands. *Radiocarbon* 35(2):245–51.

Druffel EM. 1981. Radiocarbon in annual coral rings from the eastern tropical Pacific Ocean. *Geophysical Research Letters* 8:59–62.

Druffel ERM. 1987. Bomb radiocarbon in the Pacific: annual and seasonal timescale variations. *Journal of Marine Research* 45:667–98.

Druffel ERM, Griffin S, Guilderson T, Kashgarian M, Schrag D. 2001. Changes of subtropical North Pacific radiocarbon and correlation with climate variability. *Radiocarbon* 43(1):15–25.

Dunbar R, Wellington G, Colgan M, Glynn P. 1991. Eastern tropical Pacific corals monitor low latitude climate of the past 400 years. In: Betancourt J, Tharp V, editors. Seventh Annual Pacific Climate (PACLIM) Workshop. California Department of Water Re-

sources. Interagency Ecological Studies Program. p 183–98.

Grottoli A, Gille S, Druffel ERM, Dunbar R. 2003. Decadal timescale shift in the radiocarbon record of a central equatorial Pacific coral. *Radiocarbon* 45(1):91–9.

Guilderson T, Schrag D. 1998. Abrupt shift in subsurface temperatures in the tropical Pacific associated with changes in El Niño. *Science* 281:240–3.

Guilderson T, Schrag D, Goddard E, Kashgarian M, Wellington G, Linsley B. 2000. Southwest subtropical Pacific surface water radiocarbon in a high-resolution coral record. *Radiocarbon* 42(2):249–56.

Guilderson T, Schrag D, Kashgarian M, Southon J. 1998. Radiocarbon variability in the Western Equatorial Pacific inferred from a high-resolution coral record from Nauru Island. *Journal of Geophysical Research* 103(C11):24,641–51.

Richards AF. 1957. Volcanism in eastern Pacific Ocean basin, 1954–1955. *International Geological Congress, Mexico, Proceedings X* 1:19–31.

Stuiver M, Polach HA. 1977. Discussion: reporting of ^{14}C data. *Radiocarbon* 19(3):355–63.

Toggweiler JR, Dixon K, Broecker WS. 1991. The Peru upwelling and the ventilation of the South Pacific thermocline. *Journal Geophysical Research* 96: 20,467–97.

Vogel JS, Southon JR, Nelson DE. 1987. Catalyst and binder effects in the use of filamentous graphite for AMS. *Nuclear Instruments and Methods in Physics Research B* 29:50–6.

RADIOCARBON, Vol 46, Nr 2, 2004, p 633–642

RADIOCARBON IN POREWATER OF CONTINENTAL SHELF SEDIMENTS (SOUTHEAST MEDITERRANEAN)

O Sivan[1,2,3] • B Lazar[1] • E Boaretto[4] • Y Yechieli[2] • B Herut[5]

ABSTRACT. In this study, we aim to characterize the main processes controlling $^{14}C_{DIC}$ concentrations in porewater at the shallow shelf (water depth less than 120 m) off the Mediterranean coast of Israel. At these water depths, we expected to find evidence for seawater penetration toward the coast, since this area was flooded by seawater only some 18,000 yr ago (the end of the Last Glacial period).

Measurements of the chemical composition ($^{14}C_{DIC}$) and stable carbon isotopic composition ($\delta^{13}C_{DIC}$) were performed in several sediment cores (40–250 cm long) at water depths between 6 and 115 m. At water depths of 60 m, represented by a 2.5-m-long sediment core, the porewater $^{14}C_{DIC}$ levels (85–87 pMC) were lower than the corresponding sediment values in each layer (92–95 pMC), mainly due to the oxidation of relatively old organic matter (about 70 pMC) with no evidence to advection. In contrast, sediment cores from water depths shallower than 50 m showed only slight anaerobic oxidation and high $^{14}C_{DIC}$ values of approximately 100 pMC, indicating possible downward advection. These geochemical observations support the perception that the penetration of seawater into the coastal aquifer occurs at the shallow water zone (<50 m), while further verification by deeper cores is required.

INTRODUCTION

Radiocarbon dating of groundwater and marine sediment porewater is subjected to alterations due to several diagenetic-biogeochemical and transport (advection/diffusion) processes. While several studies stressed the need for correction schemes for diagenetic processes affecting $^{14}C_{DIC}$ levels of fresh groundwater (e.g. Mook 1980; Geyh 2000), it was only recently shown that in deep-sea sediments, diffusion of $^{14}C_{DIC}$ from the bottom water into the sediments is the main process altering porewater $^{14}C_{DIC}$ levels (Sivan et al. 2001, 2002). This process accounted for the gradual "rejuvenation" of porewater (up to 70% increase in $^{14}C_{DIC}$ concentrations) compared to their hosting sediment. An opposite trend of "aging" $^{14}C_{DIC}$ concentrations was observed in saline groundwater attributed to diagenetic processes (e.g. Mook 1980; Geyh 2000; Sivan et al. 2004).

This research aims to present the main processes affecting $^{14}C_{DIC}$ concentrations in porewater at the shallow shelf (water depth less than 120 m) off the Mediterranean coast of Israel. In contrast to the conditions in the deep sea, this area is subjected to heterogenic sediment composition, relatively high sedimentation rates, and possible advection. It is assumed that the potential zone of seawater penetration into the sediments (advection) toward the coastal aquifer is located in this region. This area was flooded by seawater some 18,000 yr ago (the end of the Last Glacial period), and seawater has intruded into coastal aquifers since then (e.g. Fairbanks 1989; Chappell et al. 1996). Examination of the diagenetic processes and $^{14}C_{DIC}$ characteristics in this environment can help in assessing potential areas of seawater penetration. Moreover, such information may add to a better understanding of the chemical evolution and $^{14}C_{DIC}$ values of the saline groundwater in the Israeli Mediterranean coastal aquifer (60–70 pMC at about 100 m from the shoreline and 50 m below sea level [Sivan et al. 2004]).

[1]Institute of Earth Sciences, Hebrew University, Jerusalem 91904, Israel.
[2]Geological Survey of Israel, Jerusalem 95501, Israel.
[3]Current address: Department of Earth and Planetary Sciences, Harvard University, 20 Oxford Street, Cambridge, Massachusetts 02138, USA. Email: sivan@fas.harvard.edu.
[4]Radiocarbon Dating Laboratory, ESER Dept. Weizmann Institute of Science, Rehovot 76100, Israel. Corresponding author. Email: elisabetta.boaretto@weizmann.ac.il
[5]Israel Oceanographic and Limnological Research, National Institute of Oceanography, Haifa 31080, Israel.

Proceedings of the 18th International Radiocarbon Conference, edited by N Beavan Athfield and R J Sparks
RADIOCARBON, Vol 46, Nr 2, 2004, p 633–642

In order to examine the biogeochemical processes, measurements of the chemical composition, $^{14}C_{DIC}$, and stable carbon isotopic composition ($\delta^{13}C_{DIC}$) were performed in several sediment cores (40–250 cm long) at water depths between 6 and 115 m. As far as we know, this preliminary study contains the first set of data that combines $^{14}C_{DIC}$ and major ion composition from short and intermediate cores in these shallow seawater sediments.

METHODS

Sediment cores (40–250 cm long) were collected at the shallow Mediterranean Israeli shelf (location in Table 1) at water depths between 6 and 115 m. The cores were collected with a Benthos piston corer and a box corer (Ocean Instruments model 700 AL) for the relatively deeper sediments (>40 m water depth), and in shallower waters by scuba divers using a Perspex mini-corer specially designed for this research. The cores were immediately sectioned and centrifuged under argon atmosphere to avoid contamination with atmospheric CO_2, except the core at 46 m water depth, which was centrifuged in the laboratory. At shallower depths, the corer was designed to enable a fast separation into closed 10-cm compartments immediately after coring. Each compartment was connected to an argon tank and pressurized to squeeze the water out into a sealed syringe. Seawater samples were collected using Niskin or plastic bottles from about 1 m above the sea floor.

Seawater samples were analyzed for their chemical composition, $^{14}C_{DIC}$, $\delta^{13}C_{DIC}$, and tritium activity. One surface seawater sample was analyzed for ^{14}C in the dissolved organic carbon ($^{14}C_{DOC}$). Due to the low volume of porewater samples, they were not always analyzed for all parameters. The porewater sample was split for major ion analysis (about 2 mL) and ^{3}H (only the large samples). Then, 20 mL was filtered using 0.45-µm Nuclepore polycarbonate filters directly into plastic syringes containing $HgCl_2$ powder for analyses of DIC (1 mL), A_T (1 mL), $\delta^{13}C_{DIC}$, and $^{14}C_{DIC}$. The water samples were kept at 4 °C until the measurements.

Some of the sediment samples were dried at 30 °C and then picked for shell and other inorganic carbonate material. In particular, well-preserved spines of sea urchin (*Paracenstratus lividus*) were identified and analyzed for stable and radioactive carbon isotopes composition ($\delta^{13}C_{urc}$ and $^{14}C_{urc}$). Analysis by scanning electron microscopy (SEM) showed that the sea urchin spines from the core were in a very good state of preservation.

Analytical Methods

Major ions were analyzed using standard methods with precision of less than 3%. DIC was measured in a newly developed system, designed by Sass and Lazar (the Hebrew University, Israel, unpublished), which is able to analyze small volumes (1 mL) at an accuracy better than 1%. The water samples were acidified with concentrated HCl to transform total inorganic carbon to CO_2 gas, which was measured by an NDIR analyzer (LiCor 6252). Total alkalinity was measured on 0.50-mL samples by Gran titration (Stumm and Morgan 1996) using a micro-pH electrode (Orion 9863BN). The error, calculated by averaging numerous duplicate samples, was ±0.03 meq L^{-1}.

^{3}H (tritium) was analyzed by a LKB 1220 Quantulus scintillation counter in the Weizmann Institute. Tritium concentrations are expressed in tritium units (1 TU = 1 atom of ^{3}H per 10^{18} atoms of hydrogen [Faure 1986]), and the counting error was ±0.3 TU. $\delta^{13}C_{DIC}$ and $^{14}C_{DIC}$ analyses were performed on inorganic CO_2 extracted from each water sample (Boaretto et al. 1998). A fraction of the extracted CO_2 was used for $\delta^{13}C_{DIC}$ measurement by conventional mass spectrometry. Another fraction was converted to graphite for $^{14}C_{DIC}$ determination at the Weizmann Institute according to Boaretto et al. (1998). ^{14}C measurements were performed at the Accelerator Mass Spectrometry

(AMS) Radiocarbon Dating Lab at Aarhus University (Denmark) and at the NSF-AMS Laboratory, Tucson (Arizona). $^{14}C_{DOC}$ was performed on organic CO_2 extracted and measured in Tucson according the procedure of Burr et al. (2001). The analyses of $^{14}C_{urc}$ were also performed in Tucson. $\delta^{13}C$ is reported on the PDB scale and its precision is ±0.1‰. The activity of ^{14}C is given in pMC (percent Modern Carbon) according to the international convention (Stuiver and Polach 1977). The precision of the measurement is ±0.5 pMC.

RESULTS AND DISCUSSION

The chemical and the isotopic compositions of the bottom seawater and the porewater samples are given in Table 1.

Here, we test only the results from the upper 250-cm sediments in order to compare the different sites. The chemical profiles of Cl^-, Na^+, and Mg^{2+} in porewater slightly varied between sites, but in general, showed conservative behavior with respect to the bottom seawater concentrations (Figure 1). On the other hand, SO_4^{2-}, total alkalinity, DIC, Ca^{2+}, and Sr^{2+} showed non-conservative behavior along the cores (Figure 2). Ca^{2+} and Sr^{2+} (Figure 2a and 2b, respectively) were constant along the core in some sites and in the others showed slight decrease or slight increase with sediment depth (with no correlation to water depth), indicating precipitation/dissolution of $CaCO_3$. SO_4^{2-} slightly decreased in porewater at shallow water depths (<50 m), where the sediment is composed mainly from sand and silt. In deeper water depths (62-m core), where the sediments are composed mainly by clay, the gradient was much steeper (Figure 2c). In this case, SO_4^{2-} decreased by 30 meq/L along the top 250 cm (Figure 2c). The decrease was probably due to anaerobic oxidation of organic matter by sulfate reduction and maybe involved also other processes as well. The anaerobic oxidation is supported by the increase in the alkalinity and DIC (Figure 2d, e). The close values of total alkalinity and DIC indicate that the alkalinity is mostly from carbonates. The ratio between the alkalinity and DIC (Figure 3) is between 1 (in the 62-m core) to 1.5 in other cores. This indicates that the main process is sulfate reduction, resulting in a 1:1 ratio (aerobic oxidation would increase only the DIC without changing the alkalinity) combined with minor $CaCO_3$ precipitation/dissolution, giving a 2:1 ratio. Other processes might be involved in the sediments at about 60 m water depth, since the increase of the DIC and the alkalinity by 15 mM (and 15 meq/L if the alkalinity is mainly carbonatic) is not balanced by the decrease of the SO_4^{2-} by 30 meq/L. The processes might involve other diagenetic processes and different diffusion fluxes of these parameters.

The stable isotopic composition of the inorganic carbon ($\delta^{13}C_{DIC}$) at the 62-m core became lighter with depth of sediment to a value of –15‰ PDB at the bottom of the core (Figure 4a). These values are close to the levels of organic matter ($\delta^{13}C_{SOC}$) in deep-sea sediments (Sivan et al. 2002). The porewater $\delta^{13}C_{DIC}$ values are consistent with intensive anaerobic oxidation. The addition of 15 mM DIC from the decomposition of organic matter of –16‰ PDB to 2.5 mM DIC of seawater origin (0‰ PDB) would yield DIC with about –14‰ PDB [$2.5 \times (0‰) + 15 \times (–16‰) = 17.5 \times (–14‰)$], similar to the values measured in the deep porewater (Figure 4a). The $\delta^{13}C$ values of the carbonate ($\delta^{13}C_{urc}$) were close to the seawater values as expected (Figure 4a).

Tritium was sampled in 4 sites at the top 20 cm of the sediments (Table 1). The values show that the age of the porewater at the top of the sediments is the same as present-day seawater. The $^{14}C_{DIC}$ profiles (Figure 4b) support this conclusion. The top 50 cm of all cores had $^{14}C_{DIC}$ levels similar to present-day seawater (around 100 ± 10 pMC). Below 50 cm, the $^{14}C_{DIC}$ values were different at the 2 long cores (62 m and 46 m). $^{14}C_{DIC}$ values were high and similar to seawater values all along the 46-m core; whereas, in the 62-m core, they decreased with depth to 85 pMC at the bottom of the

Table 1 Chemical and isotopic composition of shallow sediments' porewater. Dashes = not analyzed; BW = bottom water.

Sample name	Sampling date	Lat N (°)	Long E (°)	Water depth (m)	Mean depth in sediment (cm)	Depth range (cm)	Na (meq/L)	Cl (meq/L)	Ca (meq/L)	Sr (meq/L)	SO_4 (meq/L)	Mg (meq/l)	Alkalinity (meq/L)	DIC (mM)	$\delta^{13}C_{DIC}$ (PDB)	$^{14}C_{DIC}$ (pMC)	^{3}H (TU)	RE (%)
SW	25/3/98	32 16.30	34 50.00	4	0.0	0.0	—	620	23.0	0.192	—	—	—	—	0.00	—	—	
SW2	27/7/98	32 16.30	34 50.00	0	0	—	496	633	22.0	0.196	60.1	112.0	2.75	2.26	0.00	101.6	2.2	–4.0
W1-4	14/5/98	32 23.07	34 41.01	115	0.0	0.0	502	630	22.6	0.192	58.0	120.5	2.93	1.97	—	—	—	–2.6
W1-5	14/5/98	32 23.07	34 41.01	115	BW	—	501	631	22.6	0.192	57.8	120.3	0.00	—	—	—	2.1	–2.6
W1-2	14/5/98	32 23.07	34 41.01	115	3.1	3.1	504	636	22.6	0.194	57.5	118.8	2.82	1.79	—	108.6	—	–2.9
W1-1	14/5/98	32 23.07	34 41.01	115	16.2	10.0	507	648	23.3	0.196	58.2	121.2	4.76	2.89	—	—	2.0	–3.6
P01-BW	30/8/01	32 19.55	34 43.70	62	0.0	0.0	529	633	23.0	0.177	65.9	118.5	2.57	2.41	—	—	—	–1.5
P01-3	30/8/01	32 19.55	34 43.70	62	21.0	5.0	528	621	22.0	0.175	61.4	115.2	5.55	—	—	—	—	–0.8
P01-5	30/8/01	32 19.55	34 43.70	62	37.0	5.0	537	620	21.7	0.175	55.7	116.0	7.04	—	—	—	—	0.3
P01-9	30/8/01	32 19.55	34 43.70	62	72.0	5.0	539	630	19.0	0.163	48.9	113.6	9.92	—	—	—	—	–0.4
P01-11	30/8/01	32 19.55	34 43.70	62	92.0	5.0	539	671	19.5	0.166	46.8	115.2	10.60	—	—	—	—	–3.0
P01-13	30/8/01	32 19.55	34 43.70	62	112.0	5.0	531	619	20.5	0.166	44.9	115.2	12.55	—	—	—	—	0.1
P01-15	30/8/01	32 19.55	34 43.70	62	132.0	5.0	539	630	21.0	0.168	41.6	114.4	13.87	13.38	–13.56	88.6	—	0.2
P01-17&18	30/8/01	32 19.55	34 43.70	62	152.0	5.0	529	636	21.2	0.170	39.3	113.6	14.66	14.22	–13.90	87.6	—	–1.1
P01-20	30/8/01	32 19.55	34 43.70	62	168.0	5.0	526	632	17.0	0.150	36.8	111.9	15.72	15.36	–14.50	87.4	—	–1.3
P01-22	30/8/01	32 19.55	34 43.70	62	187.5	5.0	526	620	18.0	0.156	33.5	114.0	16.76	16.45	—	86.5	—	–0.1
P01-24	30/8/01	32 19.55	34 43.70	62	207.0	5.0	522	619	18.5	0.156	31.0	113.6	17.25	17.39	–14.90	85.7	—	–0.2
P01-26	30/8/01	32 19.55	34 43.70	62	227.0	5.0	520	615	19.0	0.159	28.9	114.4	18.40	18.60	–15.15	85.4	—	0.1
P01-27	30/8/01	32 19.55	34 43.70	62	238.5	6.5	531	621	19.2	0.163	28.7	114.0	17.40	17.74	–15.25	85.7	—	0.7
V1-5	14/5/98	32 20.06	34 45.22	49	BW	—	495	637	22.5	0.190	57.2	119.2	0.00	—	—	—	—	–3.5
V1-4	14/5/98	32 20.06	34 45.22	49	0.0	0.0	—	621	21.2	0.178	54.3	112.3	2.90	1.94	—	—	—	–5.5
V1-1u	14/5/98	32 20.06	34 45.22	49	3.0	3.0	498	—	22.7	0.192	58.4	118.8	3.16	2.10	—	—	—	—
V1-1b	14/5/98	32 20.06	34 45.22	49	13.0	7.0	—	637	21.2	0.180	54.4	112.1	2.97	2.06	—	—	—	–6.3
VII-1	1/7/99	32 23.40	34 47.50	46	105.0	5.0	—	630	22.7	0.219	57.5	115.8	4.28	3.09	—	108.6	—	–4.8
VII-2	1/7/99	32 23.40	34 47.50	46	205.0	5.0	—	623	23.7	0.269	52.7	112.3	5.57	3.92	—	103.6	—	–5.4
U1-4	14/5/98	32 17.89	34 48.16	31	0.0	0.0	492	619	22.8	0.190	57.4	119.0	2.98	1.96	—	—	—	–2.6
U1-1	14/5/98	32 17.89	34 48.16	31	4.3	4.3	512	—	22.6	0.198	58.7	122.8	3.20	2.12	—	—	—	—
P1-5	24/5/98	32 16.91	34 49.31	18	0.0	0.0	490	673	22.4	0.188	57.4	118.5	3.01	2.01	—	—	—	–6.7
P1-1	24/5/98	32 16.91	34 49.31	18	9.0	9.0	508	628	23.1	0.198	59.0	121.8	3.36	2.13	—	—	—	–2.0
Polegs12-B1	8/1/00	32 17.00	34 49.30	12	13.0	8.0	522	—	23.7	0.184	66.6	121.0	2.78	—	—	—	—	—
tt-BW	6/11/01	32 17.00	34 49.30	12	0.0	0.0	499	641	21.2	0.173	68.0	114.0	—	—	—	—	—	–4.7
tt-b	6/11/01	32 17.00	34 49.30	12	24.5	5.5	500	641	22.1	0.179	65.3	114.4	3.36	—	—	—	—	–4.6
tt-m	6/11/01	32 17.00	34 49.30	12	11.5	7.5	—	—	—	—	—	—	3.04	—	—	105.8	—	—
L1-5	24/5/98	32 16.72	34 49.79	6	0.0	0.0	501	629	23.0	0.192	58.7	120.2	3.07	1.96	—	96.7	1.7	–2.7
L1-2	24/5/98	32 16.72	34 49.79	6	32.0	10.0	504	650	22.8	0.196	57.8	120.2	3.81	2.51	—	18.3	—	–3.9
L1-1	24/5/98	32 16.72	34 49.79	6	11.0	11.0	512	631	23.2	0.199	59.2	122.4	3.40	2.23	—	—	—	–1.8
Polegs8-B	8/1/00	32 17.00	34 49.50	8	14.0	9.0	526	—	24.2	0.186	66.6	125.5	3.09	—	—	—	—	—
q-BW	6/11/01	32 17.00	34 49.80	6	0.0	0.0	497	629	20.7	0.173	68.0	114.0	2.76	2.53	—	108.0	—	–4.3
q-b	6/11/01	32 17.00	34 49.80	6	36.0	6.0	509	652	21.3	0.179	70.7	116.0	2.85	—	—	113.6	—	–5.0
q-m	6/11/01	32 17.00	34 49.80	6	20.0	10.0	497	647	20.8	0.175	67.4	114.0	2.73	2.49	—	109.2	—	–5.5
s-BW	6/11/01	32 17.00	34 49.80	6	5.0	0.0	502	629	21.4	0.175	65.1	116.0	—	—	—	—	—	–3.2
s-b	6/11/01	32 17.00	34 49.80	6	44.0	6.0	500	631	21.8	0.177	63.9	114.4	3.82	—	—	101.5	—	–3.9
s-m	6/11/01	32 17.00	34 49.80	6	31.0	7.0	499	636	21.2	0.177	65.1	115.2	3.64	3.32	—	104.0	—	–4.3
s-u	6/11/01	32 17.00	34 49.80	6	12.0	12.0	503	638	20.8	0.175	67.0	114.0	2.66	2.50	—	99.9	—	–4.3

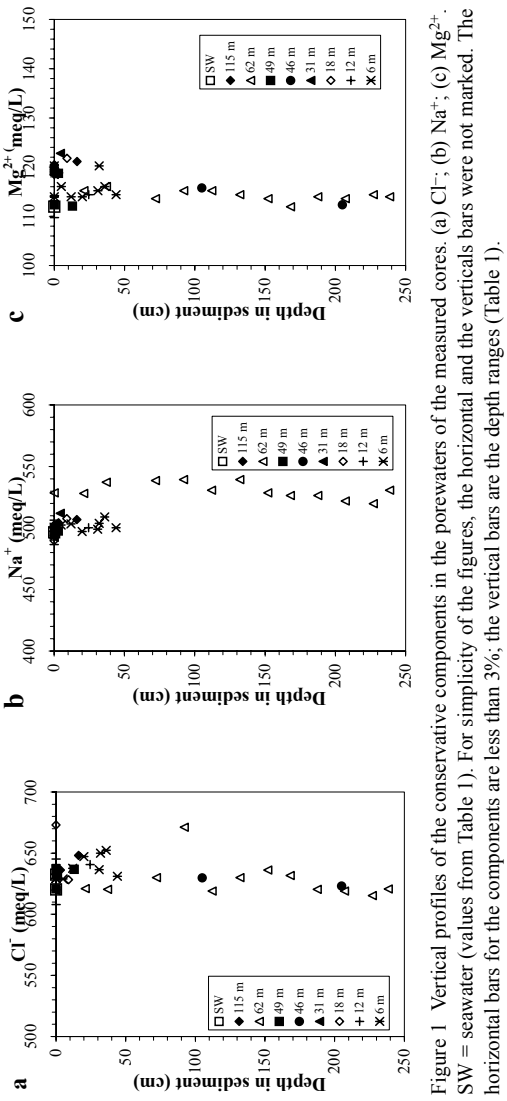

Figure 1 Vertical profiles of the conservative components in the porewaters of the measured cores. (a) Cl^-; (b) Na^+; (c) Mg^{2+}. SW = seawater (values from Table 1). For simplicity of the figures, the horizontal and the verticals bars were not marked. The horizontal bars for the components are less than 3%; the vertical bars are the depth ranges (Table 1).

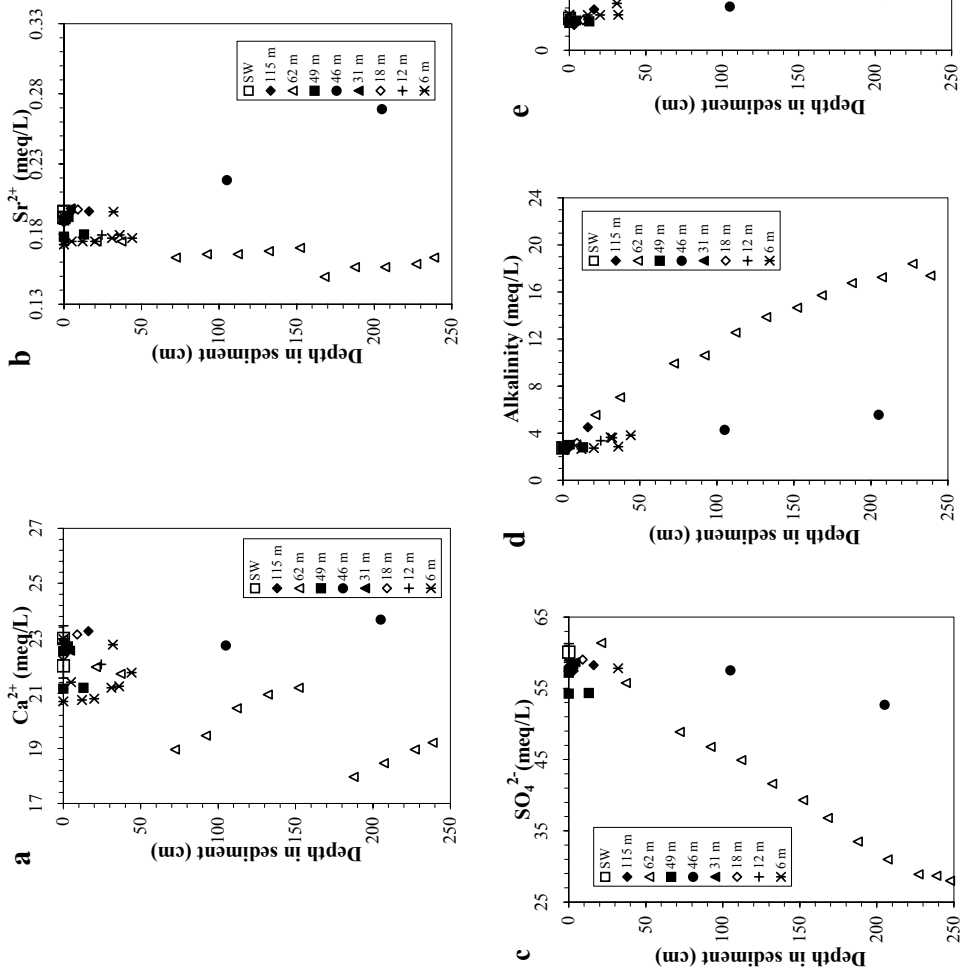

Figure 2 Vertical profiles of the non-conservative components in the porewaters of the measured cores. (a) Ca^{2+}; (b) Sr^{2+}; (c) SO_4^{2-}, (d) total alkalinity; (e) DIC (dissolved inorganic carbon). SW = seawater (values from Table 1). For simplicity of the figures, the horizontal and the verticals bars were not marked. The horizontal bars for Ca^{2+}, Sr^{2+}, SO_4^{2-} are less than 3% for the alkalinity 0.03 meq L^{-1} and for the DIC 1%; the vertical bars are the depth ranges (Table 1).

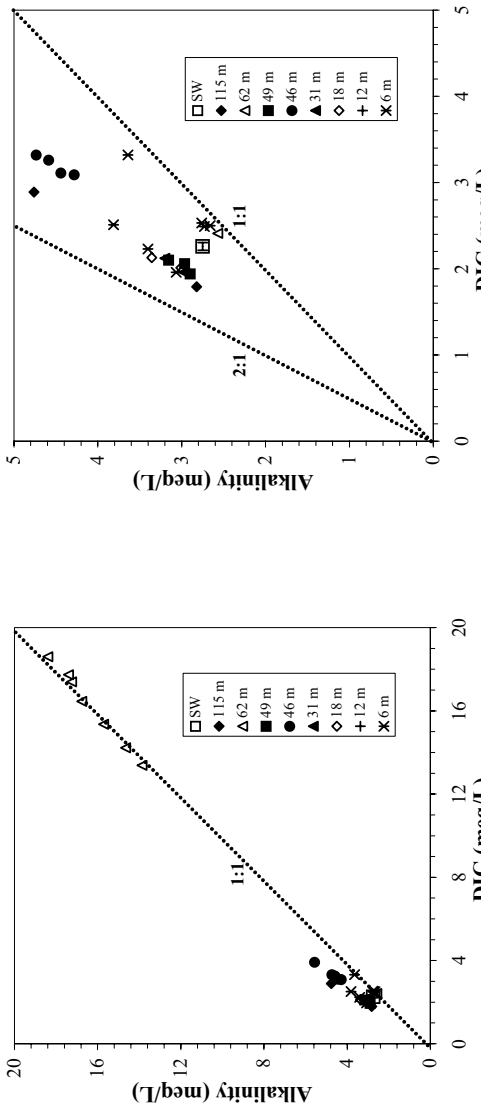

Figure 3 Alkalinity versus DIC in the measured cores at different scales. The dashed lines are the 1:1 and 2:1 ratios between alkalinity and the DIC. The 62-m core fits to 1:1 ratio, indicating that there the major diagenetic process was anaerobic oxidation by sulfate reduction. Most of the cores' samples lie on about 1.5:1 ratio, indicating that $CaCO_3$ dissolution/precipitation is also significant (2:1 ratio) process beside sulfate reduction in those cores.

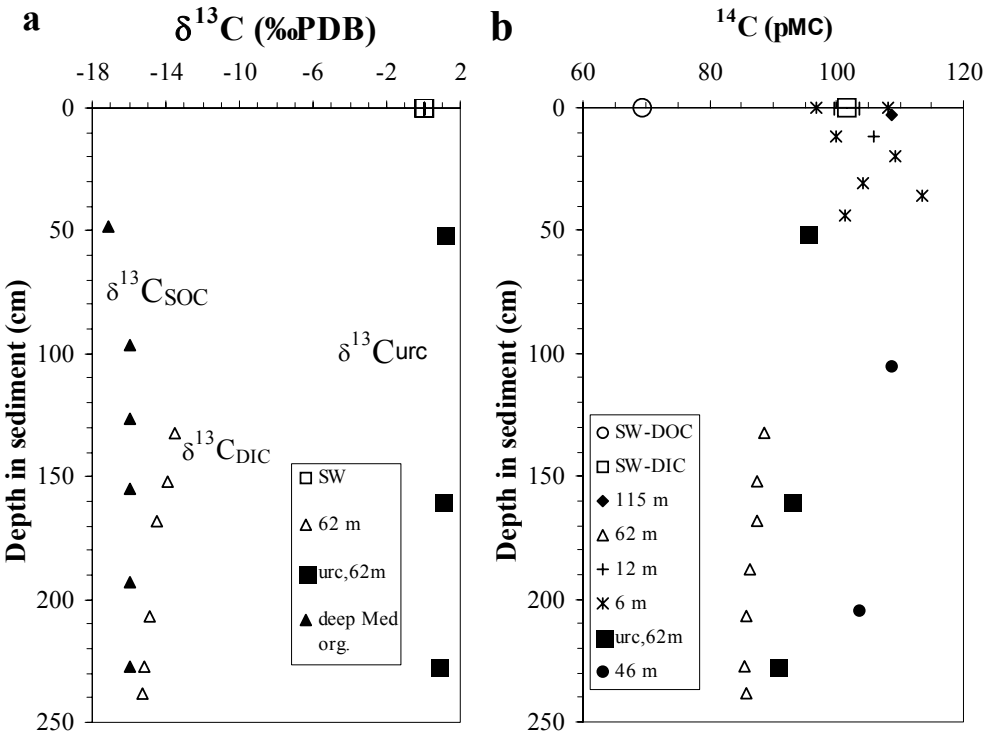

Figure 4 (a) Vertical profile of $\delta^{13}C_{DIC}$ and $\delta^{13}C_{urc}$ (sea urchin spine) at the 62-m water depth core. A vertical profile of $\delta^{13}C_{SOC}$ (SOC-sediments' organic carbon) in the deep Mediterranean is also presented (data from Sivan et al. 2002) as well as the values of $\delta^{13}C_{DIC}$ of the seawater (SW, Table 1). (b) $^{14}C_{DIC}$ profiles at the measured cores and $^{14}C_{urc}$ at the 62-m water depth core. Also, the surface seawater values of $^{14}C_{DIC}$ (black square) and the $^{14}C_{DOC}$ (grey square) are presented. In both graphs, the horizontal bars are smaller than the symbols and the vertical bars (not marked) are the depth ranges (Table 1).

core. The present-day porewater $^{14}C_{DIC}$ levels at the 46-m core indicate that the slight anaerobic oxidation of organic matter with values lower than 100 pMC (assumed value, not measured due to technical problems) and the slight $CaCO_3$ dissolution had a minor effect on $^{14}C_{DIC}$ values. According to Sivan et al. (2002), diffusion alone is not capable of enhancing the $^{14}C_{DIC}$ to values measured at the core bottom (250 cm). We speculate that such relatively high $^{14}C_{DIC}$ values indicate advection of seawater into the sediment at this site.

On the other hand, at the 62-m site, porewater $^{14}C_{DIC}$ levels (85–87 pMC) were lower than seawater values and the corresponding sediment carbonate ($^{14}C_{urc}$) in each layer (92–95 pMC, Figure 4b). The shift of $^{14}C_{DIC}$ values in porewater to values lower than their sediment host probably resulted from the anaerobic oxidation of relatively old organic matter (about 70 pMC, calculated from a rough mass balance). The organic matter was not analyzed for ^{14}C as mentioned above, but $^{14}C_{DOC}$ in seawater in this area was measured as about 70 pMC. This value might be correlated to the organic matter values; the correlation between $\delta^{13}C_{DIC}$ and $^{14}C_{DIC}$ (Figure 5) supports the possibility. It seems that DIC derived from the oxidation of organic matter reduces both $^{14}C_{DIC}$ and $\delta^{13}C_{DIC}$ values. We would like to mention that the values of the sediments (92–95 pMC) probably represent the true ages of the layers. The good preservation of the sea urchin spine suggests that the spine was deposited shortly after the death of the animal. On the other hand, the shells fragments can be much older than the sediment layer. For example, shells collected from some Israeli beaches can be several thousand years older (E Boaretto, personal communication).

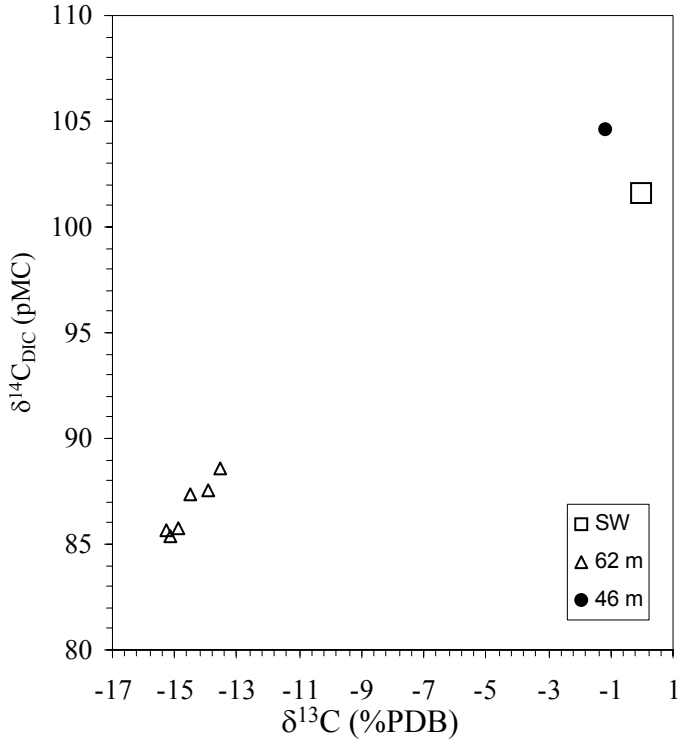

Figure 5 $^{14}C_{DIC}$ versus $\delta^{13}C_{DIC}$ at the 46-m and the 62-m water depth cores and in the seawater (SW). The horizontal and vertical bars are smaller than the symbols.

In general, the porewater $^{14}C_{DIC}$ characteristics showed a threshold between ~45 to ~60 m water depth. In the 62-m area, there is evidence of intensive anaerobic oxidation of organic matter (with ^{14}C values of 70 pMC) by sulfate reduction and slight $CaCO_3$ precipitation with no evidence of advection. The shallower sites showed much less anaerobic oxidation of organic matter and no or even slight dissolution of $CaCO_3$. In the 46-m site, there might be an evidence for fast advection of seawater into the sediments. In order to better validate this evidence, further study is suggested in this shallow sediment system by deeper coring and hydrological modeling.

The above results contribute to a better understanding of the saline groundwater age in the Israeli Mediterranean coastal aquifer. The saline waters in this aquifer contain relatively low $^{14}C_{DIC}$ values (60–70 pMC), mainly attributed to slightly DIC enrichment from the anaerobic oxidation of "dead" organic matter (Sivan et al. 2004). We think that these groundwaters are originated from porewater that has penetrated the aquifer from the shallow water zone (<50 m depth), where indeed there is evidence for advection and slight oxidation of organic matter, and its $^{14}C_{DIC}$ value is reduced only below the young marine (post-glacial) sediments, when it reaches the Pleistocene aquifer.

ACKNOWLEDGEMENTS

This work was supported by the Israel Science Foundation Grant 674/97, and partially by the Israeli Ministry of Infrastructure. We are grateful to the crew of the R/V Shikmona for their work at sea. We would like thank Y Gertner and Y Bishop from the Israel Oceanographic and Limnological Research and H Hemo from the Geological Survey for their help in carrying out the sampling at sea.

Thanks to D Gil from the Geological Survey for collecting one of the cores (46 m) and to O Yoffe and D Stiber from the Geological Survey for the chemical analyses. Special thanks to S Weiner from the Weizmann Institute for the SEM analysis of the *Paracenstratus lividus* and to G Mintz for the ^{14}C preparation and ^{3}H analyses at the Weizmann Institute.

REFERENCES

Boaretto E, Thorling L, Sveinbjörnsdóttir AE, Yechieli Y, Heinemeier J. 1998. Study of the effect of fossil organic carbon on ^{14}C in groundwater from Hvinningdal, Denmark. *Radiocarbon* 40(2):915–20.

Burr GS, Thomas JM, Reines D, Jeffrey D, Courtney C, Jull AJT, Lange T. 2001. Sample preparation of dissolved organic carbon in groundwater for AMS ^{14}C analysis. *Radiocarbon* 43(1):183–90.

Chappell J, Omura A, Esat T, McCulloch M, Pandolfi J, Ota Y, Pillans B. 1996. Reconciliation of late Quaternary sea levels derived from coral terraces at Huon Peninsula with deep sea oxygen isotope records. *Earth and Planetary Science Letters* 141:227–36.

Fairbanks RG. 1989. A 17,000-year lacio-eustatic sea level record: influence of glacial melting rates on the Younger Dryas event and deep-ocean circulation. *Nature* 342:637–42.

Faure G. 1986. *Principles of Isotope Geology*. New York: John Wiley & Sons.

Geyh MA. 2000. An overview of ^{14}C analysis in the study of groundwater. *Radiocarbon* 42(1):99–114.

Mook WG. 1980. Carbon-14 in hydrogeological studies. In: Frits P, Fontes J Ch, editors. *Handbook of Environmental Isotope Geochemistry. Volume 1. The Terrestrial Environment*. New York: Elsevier Scientific Publishers. p 49–74.

Sivan O, Lazar B, Yechieli Y, Boaretto E, Heinemeier J, Herut B. 2002. ^{14}C excess in deep-sea sediments porewater driven by diffusion—southeast Mediterranean. *Limnology and Oceanography* 47:565–70.

Sivan O, Herut B, Yechieli Y, Lazar B. 2001. Radiocarbon dating of porewater—correction for diffusion and diagenetic processes. *Radiocarbon* 43(2B):765–71.

Sivan O, Yechieli Y, Herut B, Lazar B. 2004. Geochemical evolution and timescale of seawater intrusion into the coastal aquifer of Israel. *Geochimica et Cosmochimica Acta*. (submitted).

Stuiver M, Polach HA. 1977. Discussion: reporting of ^{14}C data. *Radicarbon* 19(3):355–63.

Stumm W, Morgan JJ. 1996. *Aquatic Chemistry*. New York: John Wiley & Sons.

RADIOCARBON, Vol 46, Nr 2, 2004, p 643–648

SEASONAL RADIOCARBON VARIATION OF SURFACE SEAWATER RECORDED IN A CORAL FROM KIKAI ISLAND, SUBTROPICAL NORTHWESTERN PACIFIC

Maki Morimoto[1,2] • Hiroyuki Kitagawa[1] • Yasuyuki Shibata[3] • Hajime Kayanne[4]

ABSTRACT. A coral radiocarbon ($\Delta^{14}C$) investigation with a high time-resolution is crucial for reconstructing secular and seasonal $\Delta^{14}C$ changes in the surface seawater which potentially reflect ocean circulations and dynamic ocean-atmosphere interactions. The $\Delta^{14}C$ values of a modern coral (*Porites* sp.) from Kikai Island, southern Japan, in the subtropical northwestern Pacific, were determined for the period of 1991–1998 at a monthly resolution. A coral $\Delta^{14}C$ time series for the 8 yr indicated seasonal cycles superimposed on a secular decreasing trend of 3.8‰ per yr. The seasonal amplitude of the coral $\Delta^{14}C$ was about 18‰ on the average, and the minimum $\Delta^{14}C$ was observed in late spring and summer. The $\Delta^{14}C$ changes were tentatively explained by horizontal oceanic advections around Kikai Island or over the wide range of the equatorial and subequatorial Pacific.

INTRODUCTION

The radiocarbon concentration (represented by $\Delta^{14}C$, which includes a normalization for mass dependent fractionation and decay) of the dissolved inorganic carbon (DIC) in seawater is influenced by several oceanographical factors; these factors include air-sea CO_2 exchange and vertical and horizontal water-body mixing. Investigating seasonal and secular $\Delta^{14}C$ changes of the DIC in the surface water provides valuable information on ocean circumstances.

The coral annual bands can record the past $\Delta^{14}C$ changes of DIC of the surrounding surface seawater during the skeletal accretion. Some massive-type corals living in shallow seawater grow for tens to hundreds of years at rates of more than 1 cm per yr while making annual skeletal density bands. Thus, corals can provide long-term histories with an exact time axis, as opposed to the snapshot views of $\Delta^{14}C$ distributions that accrue from occasional observations made by big projects such as the Geochemical Oceans Sections Study (GEOSECS) and the World Ocean Circulation Experiment (WOCE). ^{14}C measurements across coral density bands have revealed the lowering of $\Delta^{14}C$ at the ocean surface from the late 1800s through to 1955, which was mostly due to the uptake of anthropogenic ^{14}C-free CO_2 emission to the atmosphere by burning of fossil fuels, as well as a sudden increase in the atmospheric testing of nuclear weapons in the 1950s and 1960s (Druffel and Linick 1978; Nozaki et al. 1978). Recent investigations on the coral $\Delta^{14}C$ variations with sub-annual resolution give a new insight of intra-annual decadal variability of the ocean circulations in surface and subsurface water and air-sea CO_2 exchange (Druffel 1989; Guilderson et al. 1998). Based on high, dense ^{14}C measurements of coral bands from Kikai Island, we report here on seasonal and secular $\Delta^{14}C$ variations during 1991–1998 in the subequatorial northwestern Pacific.

SAMPLES AND ANALYTICAL METHODS

Kikai Island (28°16′ to 28°22′N, 129°55′ to 130°02′E) is located in the central part of the Ryukyu Islands of Japan in the northwestern Pacific (Figure 1). The Central and Northern Ryukyu Islands are situated near the northern boundary of a coral reef formation in the subtropical climate zone. Kikai Island consists of several uplifted terraces of Quaternary coral reefs that have experienced a

[1]Graduate School of Environmental Studies, Nagoya University, Nagoya 464-8601, Japan.
[2]Corresponding author. Email: morimoto@ihas.nagoya-u.ac.jp.
[3]National Institute for Environmental Studies, Tsukuba 305-8506, Japan.
[4]Department of Earth and Planetary Science, University of Tokyo, Tokyo 113-0033, Japan.

Proceedings of the 18th International Radiocarbon Conference, edited by N Beavan Athfield and R J Sparks
RADIOCARBON, Vol 46, Nr 2, 2004, p 643–648

high uplift rate of 1.8 m/kyr over the past 120 kyr BP (Ota and Omura 1992). The modern coral reef of Kikai Island is not well developed and has been growing without a reef crest or moat on the outer side of Holocene Terrace IV, which is estimated to have uplifted most recently after 2600 cal BP (U/Th age) (Webster et al. 1998).

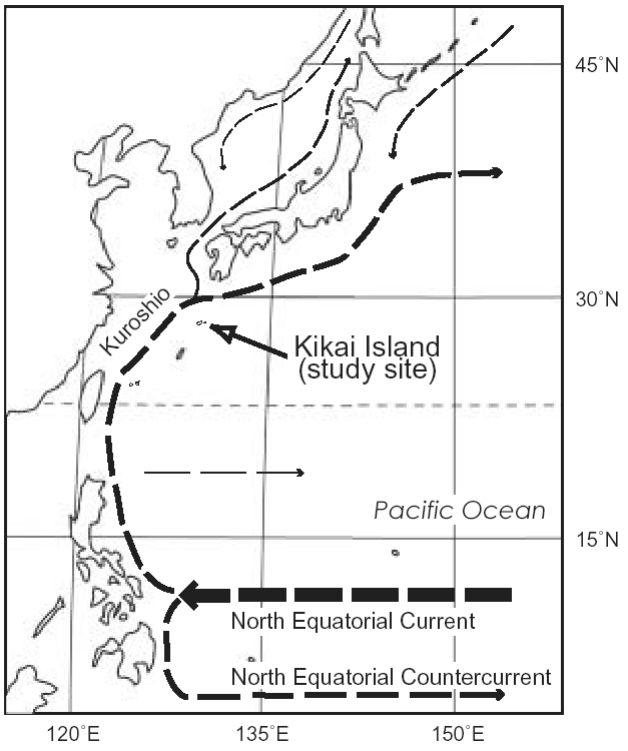

Figure 1 Location of Kikai Island and major surface currents in the northwestern Pacific. A modern coral colony of *Porites* sp. was collected off the southwestern coast of Kikai Island in the central part of the Ryukyu Islands, southern Japan.

A 25-cm-diameter modern, massive colony of *Porites* sp. was collected at the water depth of 2.9 m at Araki on the southwestern coast of Kikai Island in July 1998. The coral colony was cut to a 5-mm-thick skeletal slab parallel to the growth axis. Based on the observation of the X-radiograph image, a sampling line along the growth axis was determined. After cleaning the slab in an ultrasonic bath, samples were drilled out from the slab at 1.2-mm intervals for $\delta^{18}O$ measurements and at 1.5-mm intervals for $\Delta^{14}C$ measurements.

$\delta^{18}O$ analysis of 40- to 70-µg aliquots was performed on a Finnigan MAT252 isotope ratio mass spectrometer equipped with an automated carbonate reaction device (Kiel III) at the University of Tokyo. All measurements are reported relative to V-PDB; external precision for samples of the laboratory carbonate standard was 0.03‰ for $\delta^{18}O$ in general.

Approximately 7 mg of coral powder was dissolved under a vacuum with 85% phosphoric acid, and the carbon dioxide was converted to graphite by means of hydrogen reduction with an iron catalyst. ^{14}C measurements were conducted at the National Institute for Environmental Studies (NIES-TERRA), Japan. $\Delta^{14}C$ (‰) with decay collection are calculated according to standards defined by Stuiver and Polach (1977).

RESULTS AND DISCUSSION

$\delta^{18}O$ and $\Delta^{14}C$ of Kikai Island's Coral

Figure 2 shows $\delta^{18}O$ and $\Delta^{14}C$ variations as a function of depth from the coral surface and the X-radiograph image of a modern coral (Lab nr: KK-Ar-m1) from Kikai Island. The $\delta^{18}O$ values depict seasonal changes of about 1.8‰ on amplitude. The coral $\Delta^{14}C$ values demonstrate seasonal fluctuations superimposed on a secular decreasing toward the present.

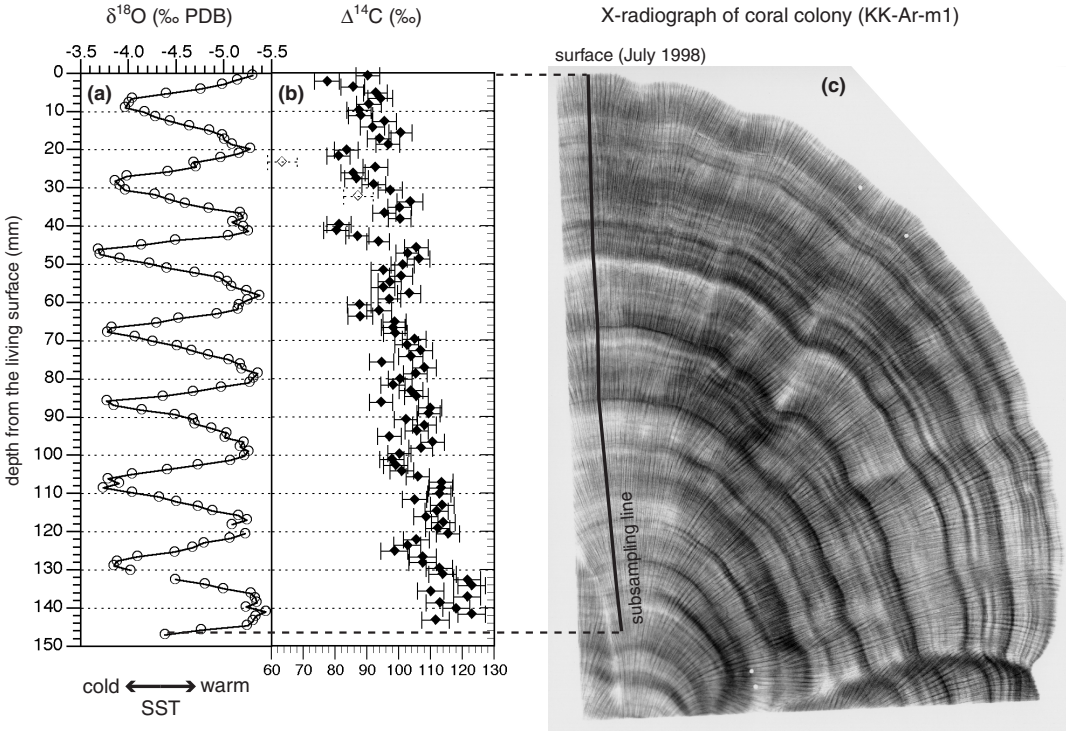

Figure 2 (a) $\delta^{18}O$ and (b) $\Delta^{14}C$ results from a modern coral colony (KK-Ar-m1) from Kikai Island as a function of depth from the living surface. (c) An X-radiograph of the coral is also shown. The subsampling line is indicated as a thick line along the growth axis. Error bars (1 σ) of $\Delta^{14}C$ are also indicated. Two $\Delta^{14}C$ data (shown as open squares) were rejected because total ^{14}C counts for these samples during AMS measurements were less than half of those for other samples.

Determination of Seasonal $\delta^{18}O$ and $\Delta^{14}C$ Fluctuation

Coral $\delta^{18}O$ is controlled by both sea surface temperature (SST) and seawater oxygen isotope ($\delta^{18}O_{sw}$) (e.g. Weber and Woodhead 1972). At Kikai Island, the influence of SST on coral $\delta^{18}O$ changes would be much larger than that of $\delta^{18}O_{sw}$. Observed $\delta^{18}O_{sw}$ at the Kikai Island's coast was relatively constant in a range of less than 0.2‰ (SMOW), without an apparent seasonality, during the 2 yr from 1999 to 2000 (Morimoto 2002). The amplitude of the seasonal SST variations is 8 °C on average at least for the last 20 yr from IGOSS NMC data (http://ingrid.ldeo.columbia.edu/). Maximum and minimum SST is 28–29 °C in July or August and 20.0–21.5 °C in February or March, respectively. Annual SST amplitude of 8 °C is transformed to a $\delta^{18}O$ change of about 1.6‰. The $\delta^{18}O$-based estimation of SST agreed well with the observed SST. The regression between esti-

mated and observed SST showed a high correlation, $r^2 = 0.84$, suggesting that coral $\delta^{18}O$ at Kikai Island is likely controlled by SST.

The SST-$\delta^{18}O$ relationship was applied for determining the chronology with a monthly resolution. Coral $\delta^{18}O$ peaks, both in summer and winter, were fitted to the dates of 3-week-averaged SST maximums and minimums from IGOSS NMC data. For the sections between summer and winter SST peaks, we interpolated assuming linear growth rates between $\delta^{18}O$ peaks to determine the time axis. The coral $\delta^{18}O$ and $\Delta^{14}C$ changes on the time axis as well as monthly SSTs are shown in Figure 3. The $\Delta^{14}C$ time series has a time resolution of 12–15 subsamples per yr during 1991–1998.

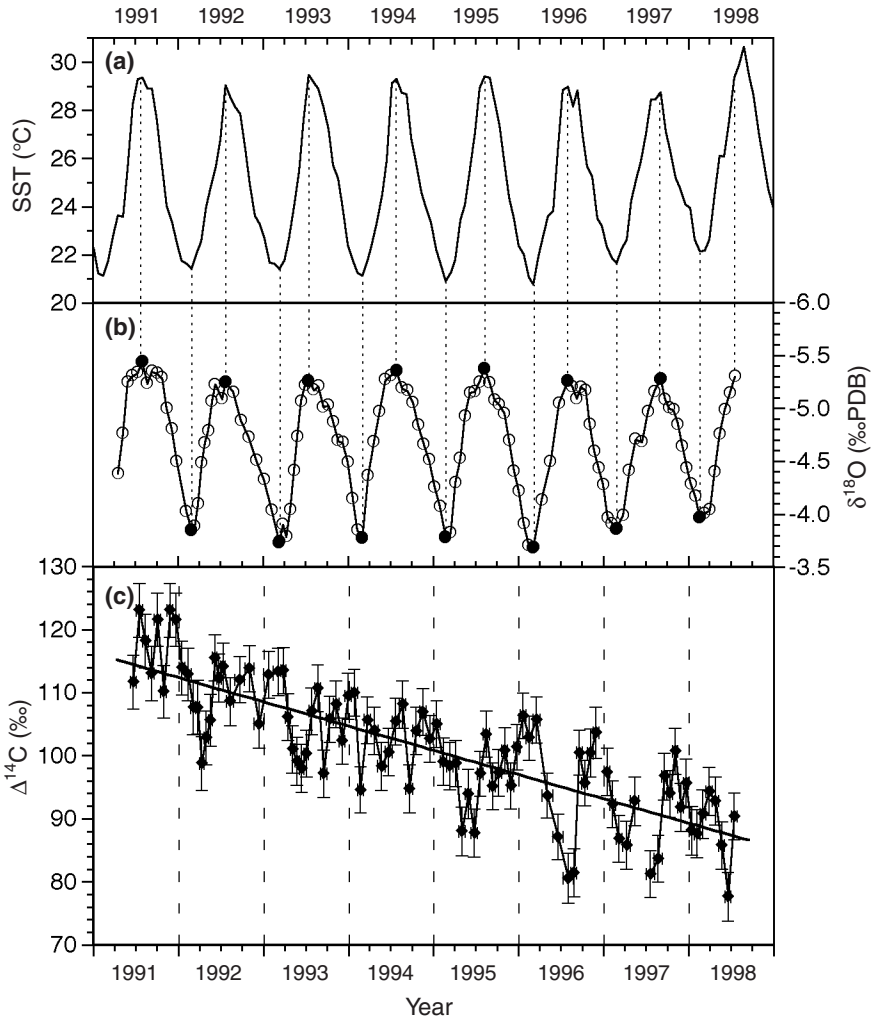

Figure 3 (a) Three-week mean SST (from IGOSS NMC data), (b) coral $\delta^{18}O$, and (c) $\Delta^{14}C$ time series. The timescale for the coral was determined from the SST-$\delta^{18}O$ relationship using summer and winter peak data (fittings are shown as dotted lines). Coral $\delta^{18}O$ peaks are indicated as solid circles. The $\Delta^{14}C$ time series for 1991–1998 shows seasonal and interannual variability. A linear $\Delta^{14}C$ decreasing trend of 3.8 ‰/yr is drawn as a thick line. Vertical error bars are standard errors (±1 σ) of the weighted mean $\Delta^{14}C$, and horizontal bars indicate periods contained in each coral subsample.

Secular and Seasonal Changes of $\Delta^{14}C$ for 1991–1998

The coral $\Delta^{14}C$ values at Kikai Island decreased from 123 to 78‰ during the 8 yr of 1991–1998 (Figure 3). A $\Delta^{14}C$ decreasing trend of 3.8 ‰/yr was obtained from a linear fitting for all data. Measurements from Europe over the last 2 decades provide evidence for a strong continental Suess effect, with fossil fuels driving down $\Delta^{14}C$ in atmospheric CO_2 (Levin et al. 1989; Meijer et al. 1995; Levin and Kromer 1997). The $\Delta^{14}C$ secular decreasing from coral is similar to the atmospheric ^{14}C changes in the 1990s observed at wide range of the Northern Hemispheric stations.

The seasonal amplitude of coral $\Delta^{14}C$ at Kikai Island exceeded 18‰ for the period of 1991–1998, with a minimum in late spring or summer and a maximum in winter (Figure 3). The minimum month of residual $\Delta^{14}C$ differs from year to year after subtracting the linear decreasing trend; February in 1994, April in 1992, May in 1995, June in 1993, July in 1997, and August in 1996. Among these seasonal changes, a drop of 25‰ in 1996 from March to August is the largest decrease in the period.

For the equatorial Pacific, a few previous studies have shown sub-annual variability of coral $\Delta^{14}C$ in the term after atmospheric nuclear bomb testing. Coral $\Delta^{14}C$ at Nauru Island (0.5°S, 166.9°E) is characterized mainly by large interannual variability, in concert with ENSO-associated trade wind changes as well as atmospheric $\Delta^{14}C$ changes. After 1960, only some years have shown a clear seasonal cycle of 20‰ (Guilderson et al. 1998). At the Galapagos Islands in the eastern Pacific, coral $\Delta^{14}C$ reveals large seasonal cycles ranging from 20–100‰ during the period 1957–1983. This phenomenon can be explained by an upwelling signal related to ENSO and atmospheric $^{14}CO_2$ changes (Guilderson and Schrag 1998). In the equatorial western Pacific, large interannual and seasonal coral $\Delta^{14}C$ variability of 15–60‰ in the Indonesian Seaway is observed during the period 1970–1985. This variability has been mostly related to contribution changes of source waters to the strait throughflow (Moore et al. 1997). From $\Delta^{14}C$ annual variations of Kikai Island and these previous studies, there are apparent seasonal $\Delta^{14}C$ cycles of DIC in the surface seawater over the wide range of the equatorial and subequatorial Pacific.

Moore et al. (1997) summarized potential sources of seasonal $\Delta^{14}C$ variability of the surface ocean, such as an invasion of CO_2 from the atmosphere, regional seawater mixing due to an upwelling, and horizontal advection. The phase of seasonal $\Delta^{14}C$ cycles in atmospheric CO_2 with minimum values in winter somewhat differs from that of coral $\Delta^{14}C$ cycles from Kikai Island. The amplitudes of atmospheric $\Delta^{14}C$ changes in this term are 5–30‰ in Europe, not markedly larger than those of coral $\Delta^{14}C$ (Meijer et al. 1995; Levin and Kromer 1997). Therefore, seasonal $\Delta^{14}C$ changes of DIC in the surface ocean cannot be explained only by direct effect of atmospheric ^{14}C. Furthermore, Kikai Island is not located in a region that is influenced by a local upwelling. The seasonality of $\Delta^{14}C$ may indicate a larger-scale oceanic phenomenon.

The spatial distribution of the sea-surface DIC-$\Delta^{14}C$ in the Pacific was revealed by the GEOSECS and WOCE programs. In the equatorial region, modeling studies have estimated that seasonally varying lateral advections are the dominant mechanism for $\Delta^{14}C$ variability of the surface waters (Rodgers et al. 1997). The seasonal $\Delta^{14}C$ cycle observed in this study is potentially explained by horizontal advections, for example, of the North Equatorial Current and the Kuroshio Current.

The present and future investigation of coral-based $\Delta^{14}C$ reconstructions of surface water DIC make it possible to understand seasonal cycles of horizontal advections of the ocean, together with CO_2 exchanges between atmosphere and ocean over the last several decades to centuries.

ACKNOWLEDGEMENTS

The authors would like to express their gratitude to T Kobayashi and R Suzuki of the NIES-TERRA for the AMS ^{14}C measurements, to A Muramoto of the University of Tokyo for support with $\delta^{18}O$ measurements, and to K Yamazaki of the Marine Expedition Club at the University of Tokyo for assistance with coral sample collection at Kikai Island.

REFERENCES

Druffel ERM. 1989. Decade timescale variability of ventilation in the North Atlantic: high-precision measurements of bomb radiocarbon in banded corals. *Journal of Geophysical Research* 94(C3):3271–85.

Druffel EM, Linick TW. 1978. Radiocarbon in annual coral rings from Florida. *Geophysical Research Letters* 5(11):913–6.

Guilderson TP, Schrag DP. 1998. Abrupt shift in subsurface temperature in the tropical Pacific associated with changes in El Niño. *Science* 281:240–3.

Guilderson TP, Schrag DP, Kashgarian M, Southon J. 1998. Radiocarbon variability in the western equatorial Pacific inferred from a high-resolution coral record from Nauru Island. *Journal of Geophysical Research* 103(C11):24,641–50.

Levin I, Kromer B. 1997. Twenty years of atmospheric $^{14}CO_2$ observations at Schauinsland station, Germany. *Radiocarbon* 39(2):205–18.

Levin I, Schuchard J, Kromer B, Münnich KO. 1989. The continental European Suess effect. *Radiocarbon* 31(3):431–40.

Meijer HA, van der Plicht J, Gislefoss JS, Nydal R. 1995. Comparing long-term atmospheric ^{14}C and ^{3}H records near Groningen, the Netherlands with Fruholmen, Norway and Izaña, Canary Islands ^{14}C stations. *Radiocarbon* 37(1):39–50.

Moore MD, Schrag DP, Kashgarian M. 1997. Coral radiocarbon constraints on the source of the Indonesian throughflow. *Journal of Geophysical Research* 102(C6):12,359–65.

Morimoto M. 2002. A high time-resolution calibration of coral oxygen isotope records and mid-Holocene climate in the northwestern Pacific from corals [PhD dissertation]. Tokyo: University of Tokyo. 209 p.

Nozaki Y, Rye DM, Turekian KK, Dodge RE. 1978. A 200-year record of carbon-13 and carbon-14 variations in a Bermuda coral. *Geophysical Research Letters* 5(10):825–8.

Ota Y, Omura A. 1992. Constructing styles and rates of tectonic uplift of coral reef terraces in the Ryukyu and Daito Islands, southwestern Japan. *Quaternary International* 15/16:17–29.

Rodgers KB, Cane MA, Schrag DP. 1997. Seasonal variability of sea surface $\Delta^{14}C$ in the equatorial Pacific in an ocean circulation model. *Journal of Geophysical Research* 102(C8):18,627–39.

Stuiver M, Polach HA. 1977. Discussion: reporting of ^{14}C data. *Radiocarbon* 19(3):355–63.

Weber JN, Woodhead PMJ. 1972. Temperature dependence of oxygen-18 concentration in reef coral carbonates. *Journal of Geophysical Research* 77:463–73.

Webster JM, Davies PJ, Konishi K. 1998. Model of fringing reef development in response to progressive sea level fall over the last 7000 years—(Kikai-jima, Ryukyu Islands, Japan). *Coral Reefs* 17:289–308.

RADIOCARBON, Vol 46, Nr 2, 2004, p 649–655

TEMPORAL CHANGES IN RADIOCARBON RESERVOIR AGE IN THE DEAD SEA-LAKE LISAN SYSTEM

Mordechai Stein[1] • Claudia Migowski[2] • Revital Bookman[3] • Boaz Lazar[3]

ABSTRACT. The Holocene Dead Sea and the late Pleistocene Lake Lisan were characterized by varying radiocarbon reservoir ages ranging between 6 and 2 ka in the Dead Sea and between 2 ka and zero in Lake Lisan. These changes reflect the hydrological conditions in the drainage system as well as residence time of ^{14}C in the mixed surface layer of the lake and its lower brine. Long-term isolation of the lower brine led to ^{14}C decay and an increase in the reservoir age. Yet, enhanced runoff input with atmospheric ^{14}C brings the reservoir age down. The highest reservoir age of 6 ka was recorded after the sharp fall of the Dead Sea at ~8.1 ka cal BP. The lower reservoir age of zero was recorded between 36 and 32 ka cal BP, when the Lake Lisan mixed layer was frequently replenished by runoff.

INTRODUCTION

Radiocarbon dating of the Dead Sea shallow and deep water masses, as well as its carbonate sediments, depends on the evaluation of the "reservoir age" (RA) of the water, which requires an understanding of the fate of ^{14}C during the runoff evolution that is the main dissolved inorganic carbon (DIC) input into the lake. Waters flowing over carbonate terrains, like the Judean Mountains west of the Jordan-Arava Valley, or percolating through carbonate aquifers, may contain substantial amounts of "dead" carbon in their DIC. This DIC gets incorporated into the "new" precipitated carbonates, causing an apparent increase in the ^{14}C ages.

Analyses of fresh and saline waters from the Dead Sea drainage area show that runoff waters are characterized by a high percent of modern carbon values (~100 pMC), while springs that percolate throughout the Cretaceous carbonate aquifers are characterized by significantly lower values (~50 pMC, cf. Talma et al. 1997). Most of the annual bicarbonate supply for aragonite precipitation in the Dead Sea-lacustrine system comes from freshwater, while the Dead Sea brine supplies calcium (Stein et al. 1997; Barkan et al. 2001). Therefore, aragonite layers deposited in the Dead Sea may contain various amounts of ^{14}C depending on the proportions of water types entering the lake and the nature of their relative mixing with Dead Sea brine (besides possible age effects). The combined effect of these mechanisms determines the reservoir age of the Dead Sea.

The Holocene Dead Sea is a remnant water body after the significantly larger, deeper, and relatively less saline Lake Lisan that existed in the Dead Sea basin during the Last Glacial period (Neev and Emery 1967; Begin et al. 1974; Katz et al. 1977; Stein 2001). The annual nature of sedimentation in the lake (Migowski et al. 2004) and the possibility to obtain both ^{14}C ages from the aragonite laminae and from associated organic debris opens a way to resolve secular changes in the ^{14}C RA in the lake. In this paper, we summarize the available ^{14}C RA data from the late Pleistocene Lake Lisan (for the time interval of 36 to 17 ka BP) and the Holocene Dead Sea (past 10 ka), and discuss their relation to the hydrological-limnological history of the lake system.

[1]Geological Survey of Israel 30 Malkhe Yisrael Street, Jerusalem 95501, Israel.
Corresponding author. Email: motis@vms.huji.ac.il.
[2]GeoForschungsZentrum Potsdam, Sec. 3.3 Climate Dynamics and Sediments, Telegrafenberg, D-14473 Potsdam, Germany.
[3]Institute of Earth Sciences, The Hebrew University of Jerusalem, Givat Ram, Jerusalem 91904, Israel.

Proceedings of the 18th International Radiocarbon Conference, edited by N Beavan Athfield and R J Sparks
RADIOCARBON, Vol 46, Nr 2, 2004, p 649–655

LAKE LISAN AND THE DEAD SEA LIMNOLOGICAL SYSTEMS

Lake Lisan existed between ~70 and 14 ka BP (Kaufman 1971; Haase-Schramm et al. 2004). During the time of highest water level (>170 meters below mean sea level [m bmsl]), the lake extended over about 300 km from the Sea of Galilee in the north to the Hazeva area in the south. The Lisan Formation, which was deposited within the lake and its surrounding fan deltas, consists mainly of chemical precipitates, aragonite and gypsum, and clastic material transported by floods. The aragonite appears in thin (~0.5–1 mm thick) laminae alternating with detrital laminae of similar or larger thickness. The aragonite precipitated most likely from the surface water and is preserved in its primary state due to the dry climate in the Dead Sea basin and the high Mg/Ca ratio of interstitial soluble salts (remnants of the former porewater; Katz and Kolodny 1989; Stein et al. 1997).

The excellent preservation and high U concentrations (~3 ppm) of Lisan aragonite make it useful for ^{234}U-^{230}Th dating (Kaufman 1971; Schramm et al. 2000; Haase-Schramm et al. 2004). The U-Th ages established by TIMS on aragonites from the Perazim Valley (PZ1) section lie in the range of ~70 to 14 ka BP (Haase-Schramm et al. 2004).

The average rate of aragonite precipitation during the Lisan period was 1.5 m eq HCO_3 per $cm^2\ yr^{-1}$, which is 4 to 5 times higher than the rate of the present Dead Sea (Barkan et al. 2001). Such a high precipitation rate required a substantial supply of bicarbonate to the lake, which was furnished by the incoming freshwater that most likely stratified the water column (Stein et al. 1997). The lower density surface layer reached aragonite saturation.

At ~13 ka cal BP, Lake Lisan receded rapidly, arriving to its minimum level of below 500 m bmsl (Stein 2002). The lake (now termed the "Dead Sea") recovered at the beginning of the Holocene, when it stabilized around the elevation of 400 m bmsl with a few fluctuations of up to 30 m (Ken-Tor et al. 2002; Bookman et al. 2004; Migowski et al. 2004). The sedimentary lacustrine section of the Holocene Dead Sea resembles that of Lake Lisan, where sequences of aragonite and silty detritus alternate with thicker sandy and gypsum layers. During the past several hundred years, the Dead Sea has stabilized as a 2-layered meromictic lake, which was disrupted by the 1978 overturn (Stiller and Chung 1984).

^{14}C RESERVOIR AGES IN LAKE LISAN-DEAD SEA ARAGONITES

The RAs in the late Pleistocene Lake Lisan and the Holocene Dead Sea are evaluated by subtracting the U-Th calendar age of Lisan aragonite or the ^{14}C age (ka BP) of organic debris (such as wood remains, leaves, twigs) from the measured ^{14}C age (ka BP) of the aragonite laminae in the same stratigraphic horizon (Table 1). Samples were collected in the Perazim Valley section (PZ1, described by Haase-Schramm et al. 2004), Massada section (beneath the archaeological site, see Bartov et al. 2002), and in the Ze'elim gully (Bookman et al. 2004), and were recovered from a sedimentary core drilled in Ein Gedi spa (Migowski et al. 2004). ^{14}C data are listed in Table 1 and are illustrated in Figure 1 against the level chronology of the lakes. During the Holocene, the RA displays temporal decrease from an elevated value of 6 ka at ~7.6 ka cal BP (after the Dead Sea sharp fall at 8.1 ka cal BP) to 2.2 ka at present. One pair that was sampled below the high RA peak, at 9.1 ka cal BP, yielded a lower RA of 3.3 ka. It appears that the brine carried an older ^{14}C memory from the earlier stages of the Holocene and the post-glacial period (when the lake level was at its minimum stand; Stein 2002). When the first aragonite deposited at ~7.6 ka cal BP, the mixed layer accommodated a significant contribution of old carbon from the brine.

Table 1 Lake levels and ^{14}C ages on aragonite and organic matter and U-Th ages data from Lake Lisan and the Holocene Dead Sea.

Sample ID	Location	Lake level (m bmsl)[a]	Sample type	Measured ^{14}C age (ka BP)	±	RA (ka)	Calibrated ^{14}C age (cal ka BP)	Calendar U-Th age (ka BP)	Data source[b]
Lake Lisan									
PZ1-2290	Perazim	280	aragonite	32.8[c]	1.1	~0[a]	—	37	1
PZ1 2236-W			wood	35.9	2.7		—	—	
PZ1 2450	Perazim	280	aragonite	30.6	0.6	~0[b]	—	34	1
PZ1 2450-L			leaf	32.6[d]	1.1		—	—	
PZ-1 2558	Perazim	280	aragonite	30.5	0.3	0	—	33	2
			wood	30.5	0.3		—	—	
MS-410	Massada	180	aragonite	24.0	0.2	1.5	—	24	3
			wood	22.5	0.2		—	—	
MS-405	Massada	180	aragonite	24.0	0.2	1.7	—	24	3
			wood	22.3	0.2		—	—	
M-2375	Massada	180	aragonite	22.7	0.2	2.0	—	24	1
M-2374 W			wood	20.7	0.2		—	—	
ID 455	Perazim	200	aragonite	22.0	0.1	1.3	—	23	2
			wood	20.7	0.1		—	—	
MS-179	Massada	200	aragonite	19.5	0.1	1.4	—	21	3
			wood	18.2	0.1		—	—	
MS-218	Massada	200	aragonite	19.0	0.1	2.0	—	19	3
			wood	17.0	0.1		—	—	
PZ1-3649	Perazim	200	aragonite	14.5	0.1	1.6	—	17	1
			debris	12.9	0.2		—	—	
Dead Sea									
	EG[e] core	400	aragonite	2.38	0.07	2.2	0.1	—	4
			twigs	0.16	0.03			—	
	EG core	400	aragonite	2.97	0.07	2.2	0.2	—	4
			twigs	0.80	0.03			—	
	EG core	400	aragonite	3.86	0.07	2.3	1.1	—	4
			plant fiber	1.56	0.03			—	
	EG core	370	aragonite	6.09	0.04	2.4	4.1	—	4
			twigs	3.68	0.03			—	
	EG core	400	aragonite	7.92	0.07	2.6	6.2	—	4
			twigs	5.28	0.04			—	
	EG core	400	aragonite	9.85	0.07	3.4	7.4	—	4
			twigs	6.46	0.07			—	
	EG core	<450	aragonite	12.7	1.2	6.0	7.7	—	4
			twigs	6.73	0.04			—	
	EG core	400	aragonite	11.5	1.2	3.3	9.1	—	4
			twigs	8.20	0.04			—	

[a] m bmsl= meters below mean sea level.

[b] Data sources: 1=Haase-Schramm et al. 2004; 2=van der Borg et al. 2004; 3=Prasad et al., forthcoming; 4=present study.

[c] The ^{14}C age was obtained on aragonite from a stratigraphically younger layer; thus, considering short transport time of the wood and the large error on sample PZ1-2236-W, the estimated RA at 2236 is about zero.

[d] The leaf is slightly older than the aragonite; therefore, the reservoir age was estimated to be about zero.

[e] EG denotes Ein-Gedi.

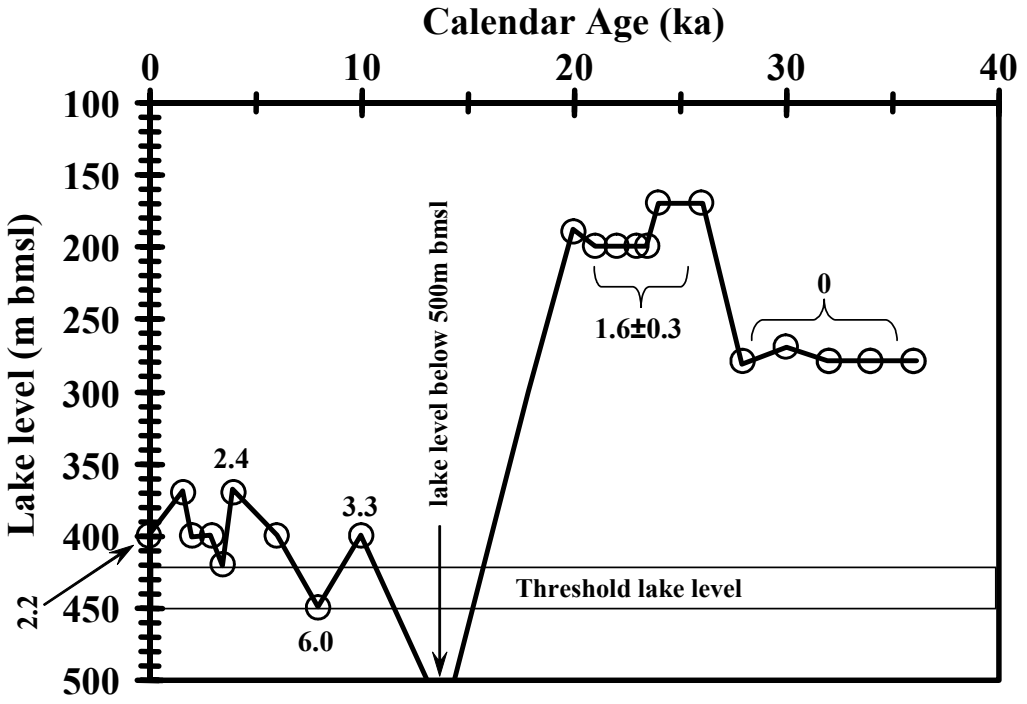

Figure 1 Reservoir ages (RA in ka units) during various water levels of the Last Glacial Lake Lisan and the Holocene Dead Sea. Lake-level data are from Bartov et al. 2002, 2003; Bookman et al. 2004; Migowski et al. 2004.

During the Lisan period (considering the time intervals where aragonite-organic debris pairs are available), the RAs cluster around 2 values: (1) about zero between 36 and 32 ka BP; and (2) 1.6 ± 0.3 ka, between 24 and 20 ka BP. Figure 2 displays the RAs at various lake-level conditions. It appears that the RA is related in a complicated way to the lake level, which is the most prominent hydrological indicator in the lake system. While the early Holocene Dead Sea shows RAs that are significantly higher than Lake Lisan, the mid-late Holocene Dead Sea (past 4000 yr) RAs are not much different from the high-stand Lake Lisan (2.3 ± 0.1 ka compared with 1.6 ± 0.3 ka, respectively). More surprising is the zero RA recorded by Lake Lisan at its "typical" elevation of ~280 m bmsl. These observations indicate that the RA is not a simple function of freshwater bicarbonate supply to the lake, and other factors such as ^{14}C decay in the water body are involved.

DISCUSSION

Residence Time of ^{14}C in the Modern Dead Sea

The dynamics of the carbonate system of the Dead Sea were investigated after unusually high rainfall and enhanced runoff in the winter of 1991/92, which came after years of continuous retreat mainly due to anthropogenic interference (Barkan et al. 2001). The intense flooding formed a shallow pycnocline that divided the water column into 2 dissolved inorganic carbon (DIC) reservoirs: the shallow (about 20 m deep) surface mixed layer DIC reservoir opened to the atmosphere, and a large deep water DIC reservoir isolated from the atmosphere. This salinity stratification of the Dead Sea lasted for more than 2 yr. The average DIC value in the Dead Sea is 850 μmol·kg^{-1}, which is much lower than in the freshwater runoff. The measured $P_{CO_2(liquid)}$ was very high, approximately 2000 μatm (compared to the atmospheric value of 355 μatm) at all depths. This high $P_{CO_2(liquid)}$

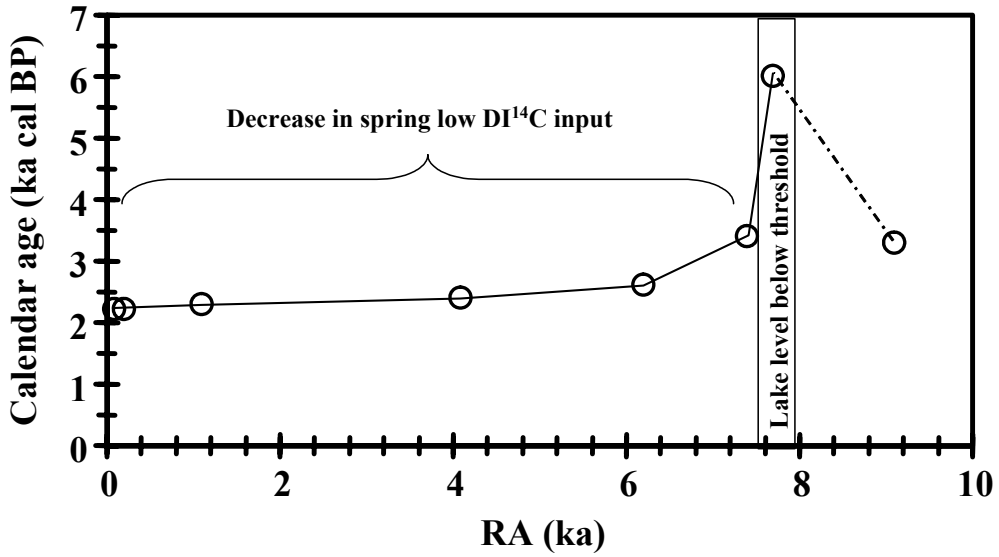

Figure 2 Reservoir age (RA in ka) versus calibrated ^{14}C age in the Holocene core drilled at Ein Gedi shore. Note the fast decrease from the reservoir age peak at 7.6 ka cal BP, and the following moderate decrease in the reservoir age, reflecting the decrease in DIC supply of springs with low DI^{14}C (groundwater DIC source with low ^{14}C content) and the continuous replenishment by runoff water with high DI^{14}C content (atmospheric ^{14}C).

represents a DIC excess (above equilibrium with atmospheric CO_2) of about 300 μmol·kg^{-1}, which is equivalent to 40% of the DIC. The carbon fluxes in the Dead Sea as estimated for the years 1992 to 1994 were (1) HCO_3^- influx with floods of 2.1 mol·m^{-2}·a^{-1}); (2) $CaCO_3$ precipitation of 1.4 mol·m^{-2}·a^{-1} that occurred in the mixed layer; and (3) a large CO_2 escape to the atmosphere of 4 mol·m^{-2}·a^{-1} driven by the high $P_{CO_2(liquid)}$.

The overall DIC balance for the mixed layer suggested a net DIC loss of 3.3 mol·m^{-2}·a^{-1}, which can potentially deplete the mixed layer DIC within 10 yr and the whole water column within about 100 yr. Earlier DIC data (Neev and Emery 1967; Luz et al. 1997) suggested that these conditions of $P_{CO_2(liquid)} >> P_{CO_2(atm)}$ also prevailed in the deep-water column during the several centuries of continuous meromictic stages which prevailed before the 1978 overturn (Stiller and Chung 1984; Barkan et al. 2001). The existence of such high $P_{CO_2(liquid)}$ over a time period that is longer than the calculated residence time of DIC in the deep-water mass of the Dead Sea suggests that the deep DIC reservoir (the main DIC reservoir of the Dead Sea) remained during the whole meromictic stage. Thus, the ^{14}C content of the large deep-water reservoir was several hundred years old when ventilated during the 1978 overturn, increasing the RA of the newly formed mixed layer.

When the lake is stratified during meromictic stages, the ^{14}C content of the surface mixed layer (from which the authigenic carbonate precipitates) may change rapidly. For example, in the modern Dead Sea, the residence time of carbon in the mixed layer is about 8 yr, implying that the RA may approach zero after about 20 yr of continuous stratification. On the other hand, during the holomictic stage (when the lake mixes entirely at least during one period a year), the deep-water column serves as a buffer for abrupt changes in the ^{14}C content of surface water and, hence, the RA of the lake.

Residence Time of ^{14}C in the Old Lakes

The high peak of the RA at 7.6 ka cal BP, when the Dead Sea was at one of its lowest stands ~417 m bmsl (Migowski et al. 2004), and the secular decrease in RA that followed this RA peak are key observations for understanding the behavior of ^{14}C in the old lakes. We suggest that the extremely high RA (6 ka) at 7.6 ka cal BP indicates that i) springs (mainly saline springs having very low ^{14}C) were the main freshwater input into the Dead Sea during its low-stand, while runoff input (with high ^{14}C) was virtually shut down; and ii) the Dead Sea remnant brine that filled the deep basin after the strong retreat at 8.1 ka cal BP could have been isolated for several thousand years (Figure 1), causing additional decrease in ^{14}C content due to decay. When the hydrological system recovered and runoff re-entered the lake, the RA began its continuous decrease towards the present value of 2.2 ka (Figure 2). This decrease is the result of continuous mixing of freshwater with atmospheric ^{14}C with the Dead Sea brine. At ~3.3 ka cal BP, the Dead Sea level dropped again (Bookman et al. 2004; Migowski et al. 2004). Yet, we see no increase in the RA during the time interval of 4.1 to 1.1 ka cal BP. This may indicate that the threshold lake level is between 420 and 450 m bmsl (Figure 1): when the lake level is above this threshold, runoff is the main DIC supply of the lake; and when the lake level is below this threshold, springs (fresh and saline groundwater sources) are the main DIC source of the lake. Apparently, the level decrease at ~3.3 ka cal BP was not accompanied by long brine isolation that could support an additional increase in RA due to ^{14}C decay.

During the Lisan time (70 to 14 ka BP), the RA was significantly lower than the Holocene value (Figure 1 and Table 1), suggesting that the main DIC input was runoff and the brine was never isolated for long periods of time from the mixed layer. The lake level during that period was always above the threshold level (Figure 1). The data shows that Lake Lisan had a zero RA value during the time interval that ended just before the lake reached its highest stand (Figure 1). This zero RA value was measured for the time interval that ends at the dating limit of the ^{14}C method. The lake level at this period was stabilized at 280 m bmsl (Bartov et al. 2002), some 120 m above the present-day level of the Dead Sea. It is possible that the RA of Lake Lisan was zero before its highest stand due to fast replenishment of the surface water with runoff DIC (with high ^{14}C content). The increase in lake area during the high-stand may have added "new" low ^{14}C DIC sources. It is well documented that during the period of maximum stand (26–24 ka cal BP), Lake Lisan converged with the northern Sea of Galilee (Hazan et al., forthcoming). The high-stand was characterized by a stable layered configuration that persisted for several thousand years during which ^{14}C content of the lower brine decreased. Thus, some contribution to RA in the mixed layer could come from the brine. In addition, the aquifers formed during the lake's highest stand may have supplied spring waters with low ^{14}C content, which kept a low RA during the time after the highest stand.

CONCLUSIONS

The Holocene Dead Sea and late Pleistocene Lake Lisan were characterized by varying reservoir ages. In the Holocene Dead Sea, the RA ranges between 2.2 and 6 ka; and in the Lisan, they range from zero to 2.0 ka. These variations reflect the proportions of DIC supplied by freshwater from runoff and springs and periods of brine isolation and mixing with the surface (aragonite precipitating) layer.

The data of the last 36 ka of the lake suggest that the Lisan time was characterized by 2 modes of limnological operation and ^{14}C content: (1) relatively low lake levels, when fast replenishment of the mixed layer occurred, were characterized by zero RA; (2) long high-stand periods, when the lake

developed a stable 2-layer configuration that allowed ^{14}C decay in the lower (brine) layer, and particularly, when areas with enhanced spring activity contributed old carbon to the lakes.

The Holocene low-stand showed the highest RA (6 ka) at lake level lower than about 440 m, indicating that saline springs became an important low ^{14}C DIC source for the lake.

ACKNOWLEDGEMENTS

We thank Nicolas Waldmann and Miryam Freed on help in fieldwork, and separation of aragonite laminae. This study was supported by ISF grant to MS and BL and by GIF grant to MS.

REFERENCES

Barkan E, Luz B, Lazar B. 2001. Dynamics of the carbon dioxide system in the Dead Sea. *Geochimica et Cosmochimica Acta* 65:355–68.

Bartov Y, Stein M, Enzel Y, Agnon A, Reches Z. 2002. Lake-levels and sequence stratigraphy of Lake Lisan, the Late Pleistocene precursor of the Dead Sea. *Quaternary Research* 57:9–21.

Bartov Y, Goldstein SL, Stein M, Enzel Y. 2003. Catastrophic arid episodes in the Eastern Mediterranean linked with the North Atlantic Heinrich events. *Geology* 31:439–42.

Begin ZB, Ehrlich A, Nathan Y. 1974. Lake Lisan, the Pleistocene precursor of the Dead Sea. *Bulletin* 63:1–30.

Bookman R, Enzel Y, Agnon A, Stein M. 2004. Late Holocene lake levels of the Dead Sea. *Geological Society of America Bulletin* 116.

Haase-Schramm A, Goldstein SL, Stein M. 2004. U-Th dating of Lake Lisan aragonite (late Pleistocene Dead Sea) and implications for glacial East Mediterranean climate change. *Geochimica and Cosmochimica Acta* 68:985–1005.

Hazan N, Stein M, Agnon A, Marco S, Nadel D, Schwab M, Negendank J, Neev D. Forthcoming. The late Pleistocene-Holocene history of the Sea of Galilee (Lake Kinneret). *Quaternary Research*.

Luz B, Stiller M, Talma S. 1997. Carbon dynamics in the Dead Sea. In: Niemi TM, Ben-Avraham Z, Gat JR, editors. *The Dead Sea: The Lake and Its Setting*. Oxford Monographs on Geology and Geophysics, Nr 36, Oxford.

Katz A, Kolodny N. 1989. Hypersaline brine diagenesis and evolution in the Dead Sea-Lake Lisan system (Israel). *Geochimica et Cosmochimica Acta* 53:59–67.

Katz A, Kolodny Y, Nissenbaum A. 1977. The geochemical evolution of the Pleistocene Lake Lisan-Dead Sea system. *Geochimica et Cosmochimica Acta* 41:1609–26.

Kaufman A. 1971. U-series dating of Dead Sea basin carbonates. *Geochimica et Cosmochimica Acta* 35:1269–81.

Ken-Tor R, Stein M, Enzel Y, Agnon A, Marco S, Negendank J. 2002. Precision of calibrated radiocarbon ages of earthquakes in the Dead Sea basin. *Radiocarbon* 43(3):1371–82.

Migowski C, Agnon A, Bookman R, Negendank J, Stein M. 2004. Recurrence pattern of Holocene earthquakes along the Dead Sea transform revealed by varve-counting and radiocarbon dating of lacustrine sediments. *Earth and Planetary Science Letters* 222:301–14.

Neev D, Emery KO. 1967. The Dead Sea depositional processes and environments of evaporites. *Israel Geological Survey Bulletin* 41. 147 p.

Prasad S, Vos H, Waldmann N, Goldstein SL, Stein M. Forthcoming. Evidence from Lake Lisan of solar influence on decadal to centennial scale climate variability during MIS 2. *Geology.*

Schramm A, Stein M, Goldstein SL. 2000. Calibration of the ^{14}C timescale to >40 ka by ^{234}U-^{230}Th dating of Lake Lisan sediments (Last Glacial Dead Sea). *Earth and Planetary Science Letters* 175:27–40.

Stein M. 2001. The sedimentary and geochemical record of Neogene-Quaternary water bodies in the Dead Sea basin—inferences for the regional paleoclimatic history. *Journal of Paleolimnology* 26:271–82.

Stein M. 2002. The fall and rise of the Dead Sea during the post-glacial and the Younger Dryas event. *Geochimica Cosmochimica Acta* 12th Annual Goldschmidt Conference. Davos, A738.

Stein M, Starinsky A, Goldstein SL, Katz A, Machlus M, Schramm A. 1997. Strontium isotopic, chemical, and sedimentological evidence for the evolution of Lake Lisan and the Dead Sea. *Geochimica et Cosmochimica Acta* 61:3975–92.

Stiller M, Chung YC. 1984. Radium in the Dead Sea: a possible tracer for the duration of meromixis. *Limnology and Oceanography* 29:574–86.

Talma AS, Vogel JC, Stiller M. 1997. The radiocarbon content of the Dead Sea. In: Niemi TL, Ben-Avraham Z, Gat J, editors. *The Dead Sea: The Lake and Its Setting*. Oxford: Oxford University Press. p 171–83.

van der Borg K, Stein M, de Jong AFM, Waldmann N, Goldstein SL. 2004. Atmospheric ^{14}C at 33 ka close to the AD 1950 level as observed in the high-resolution radiocarbon record from U-Th dated sediment of Lake Lisan. *Radiocarbon*, these proceedings.

RADIOCARBON, Vol 46, Nr 2, 2004, p 657–660

MARINE RESERVOIR CORRECTION IN THE SOUTH OF VIETNAM ESTIMATED FROM AN ANNUALLY-BANDED CORAL

Phong X Dang[1,2,3] • Takehiro Mitsuguchi[3,4] • Hiroyuki Kitagawa[2,5] • Yasuyuki Shibata[4] • Toshiyuki Kobayashi[4]

ABSTRACT. We measured radiocarbon in an annually-banded coral core collected from Con Dao Island, Vietnam, 90 km from the mouth of the Mekong River, and estimated the regional correction of the marine reservoir age (ΔR value). Twelve samples were continuously taken from the annual bands (AD 1949–1960) which were clearly identified under UV light (~352 nm) as well as by X-radiography. The ^{14}C content of the samples was determined using an accelerator mass spectrometer at the National Institute for Environmental Studies, Tsukuba, Japan. Results provide a $\Delta^{14}C$ time series showing a relatively steady value of –48.6 ± 4.6‰ for the period of 1949–1955 and an abrupt increase starting from 1956 that indicates a quick response to the atmospheric testing of nuclear bombs. Using the prebomb ^{14}C data, the ΔR value in the south of Vietnam is estimated to be –74 ± 39 yr.

INTRODUCTION

The marine reservoir age (R value), defined as the difference of conventional radiocarbon age between the atmosphere and surface seawater, is essential for ^{14}C dating of marine samples (e.g. coral skeletons, shells) (Stuiver and Braziunas 1993). The global distribution of atmospheric ^{14}C is almost uniform. On the other hand, seawater ^{14}C concentration varies markedly according to region, depth, and water mass because of global ocean circulation, local upwelling, stratification, and freshwater impact (e.g. Ostlund and Stuiver 1980; Stuiver and Ostlund 1983). Thus, the R value differs regionally. The difference between the regional R value and the model-based globally-averaged R value is termed the regional correction of the marine reservoir age (ΔR value) (Stuiver and Braziunas 1993). The ΔR value is equivalent to the difference between the ^{14}C age of regional surface seawater and the model-based globally-averaged marine ^{14}C age. Therefore, the ΔR value is necessary to correct the ^{14}C age of marine samples and contributes to the understanding of regional oceanography. Because the natural equilibrium of global ^{14}C distribution was broken by atmospheric testing of nuclear bombs in the 1950s and the early 1960s, the ΔR value (or regional R value) is generally estimated from ^{14}C measurements of known-age marine samples formed before the early 1950s, when the influence of the atmospheric testing was negligible or nil (i.e. prebomb period). In this study, the ΔR value in the south of Vietnam is estimated through the ^{14}C analyses of annual bands of coral skeletons collected from Con Dao Island.

MATERIALS AND METHODS

In May 2000, a 68-cm-long core (5.5 cm in diameter) was vertically drilled from the top of a living coral colony of *Porites* sp. in Con Dao Island (08°39′36″N, 106°33′07″E), Vietnam, 90 km from the mouth of the Mekong River (Figure 1). This island, lying on the broad shallow continental shelf of the South China Sea, is strongly influenced by the East Asian monsoon, a seasonally-reversing wind system, as well as by the discharge from the Mekong River. These geographical settings suggest

[1]Institute of Geography, Vietnam National Center for Natural Science and Technology, 18 Hoang Quoc Viet, Cau Giay, Hanoi, Vietnam.
[2]Graduate School of Environmental Studies, Nagoya University, Nagoya 464-8601, Japan.
[3]Japan Society for the Promotion of Science.
[4]National Institute for Environmental Studies, Tsukuba 305-8506, Japan.
[5]Corresponding author. Email: kitagawa@ihas.nagoya-u.ac.jp.

Proceedings of the 18th International Radiocarbon Conference, edited by N Beavan Athfield and R J Sparks
RADIOCARBON, Vol 46, Nr 2, 2004, p 657–660

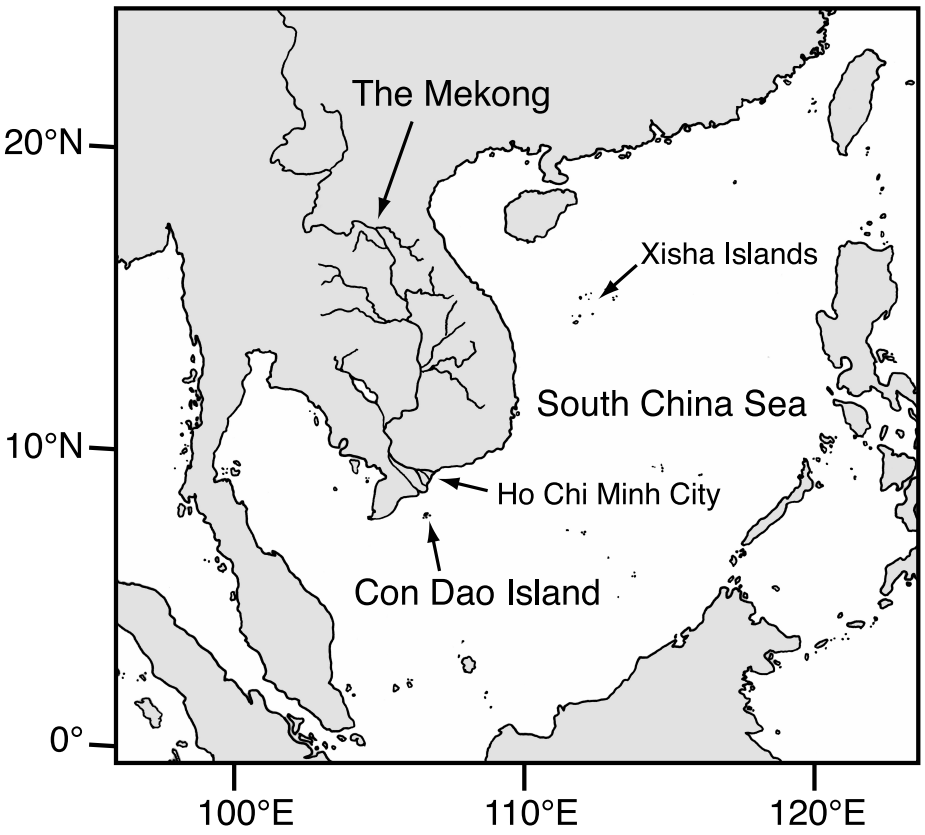

Figure 1 Location map of Con Dao Island, Vietnam (08°39′36″N, 106°33′07″E), where a core sample was drilled from a living coral colony (*Porites* sp.) in May 2000.

considerable influences of the atmosphere and freshwater on surface seawater. The core was cut along its longitudinal axis with a diamond saw to produce 6-mm-thick skeletal slabs. The skeletal slabs were ultrasonically cleaned with a large amount of distilled water renewed repeatedly, dried in a clean plastic box for a week, photographed under long wavelength UV light (~352 nm), and X-rayed. The X-ray photo revealed density banding, while the UV photo showed luminescent banding, both of which were very clear. The total number of the banding patterns in the X-ray photo is exactly the same as that in the UV photo. Average width of the banding patterns is ~12 mm, which is a typical annual growth rate of *Porites* coral skeletons. Thus, we assumed that both of the luminescent and density banding patterns represent annual growth bands. Since Con Dao Island is close to the mouth of the Mekong River, organic content of the coral sample may be relatively high. In order to remove the possible organic contamination, the following chemical treatment procedure was applied to the slabs: (1) cleaning with 5 L of Milli-Q water at room temperature for 1 hr; (2) cleaning with 5 L of 5% H_2O_2 aqueous solution at 50 °C for 30 min; (3) cleaning with 5 L of Milli-Q water at room temperature for 30 min; (4) cleaning with 5 L of 0.5 M NaOH aqueous solution at room temperature for 1 hr; (5) cleaning with 5 L of Milli-Q water at room temperature for 30 min, which was repeated 3 times with Milli-Q water renewed each time; and (6) drying in a clean plastic box at room temperature for 1 week. All of the cleaning steps were achieved with ultrasonic agitation. Twelve subsamples were continuously taken from the annual bands of AD 1949–1960, including the prebomb period (1 subsample per annual band). About 10 mg of coral powder from each subsample was converted to CO_2 in a vacuum line by dissolution in H_3PO_4, then to graphite at ~630 °C on an

iron powder catalyst (1.0 mg) with H_2 gas as the reductant (Kitagawa et al. 1993). The "new" NIST oxalic acid standard (HOxII) and ^{14}C-free $CaCO_3$ were converted to graphite as a standard and a blank material, respectively, in the same vacuum line in the same condition. These graphite materials were individually pressed into a target and measured for $^{14}C/^{12}C$ and $^{13}C/^{12}C$ ratios using an accelerator mass spectrometer at the National Institute for Environmental Studies, Tandem accelerator for Environmental Research and Radiocarbon Analysis (NIES-TERRA). Each target was measured for 10 min per 1 cycle, which was replicated to 11 cycles, resulting in ~100,000–190,000 ^{14}C counts for each subsample.

RESULTS AND DISCUSSION

Results are reported as $\Delta^{14}C$ (‰) and conventional ^{14}C age (yr BP) according to the calculation procedure in Stuiver and Polach (1977) (Table 1). The $\Delta^{14}C$ calculation includes corrections for isotope fractionation to a $\delta^{13}C$ value of –25‰ (relative to PDB) and for radioactive decay between the years of ^{14}C measurement and skeletal formation. These data are not corrected for the Suess effect (the ^{14}C dilution due to fossil fuel CO_2) that is extended into the oceans (Stuiver and Quay 1981; Druffel and Suess 1983; Stuiver and Braziunas 1993). The $\Delta^{14}C$ variation of 1949–1955 shows a relatively steady value of –48.6 ± 4.6‰ (mean ± SD, n=7), followed by an abrupt increase to –10.3‰ in 1960. The abrupt increase starting from 1956 indicates a quick response to the atmospheric testing of nuclear bombs. The $\Delta^{14}C$ time series is compared with the data of the South China Sea reported in Southon et al. (2002) (Figure 2: all the data are not corrected for the Suess effect). Our results are generally in accord with Southon et al. (2002). The data in Ho Chi Minh City (Saigon), located beside the mouth of the Mekong River, is in excellent agreement with our data. On the other hand, the values in Con Dao Island and Ho Chi Minh City seem to be higher than those in the Xisha Islands (by ~10‰), suggesting that the region close to the delta of the Mekong is more influenced by air-sea gas exchange and/or freshwater discharge than the Xisha Islands. The ΔR values are calculated by subtracting the model marine ^{14}C age of 473 BP for 1950 (Stuiver et al. 1998a,b) from the conventional ^{14}C ages of the prebomb data (see Table 1), resulting in ΔR = –74 ± 39 yr (mean ± SD, n=7) in Con Dao Island. Using the Southon et al. (2002) prebomb data in Figure 2 and the same model as we used above (Stuiver et al. 1998a,b), the mean ΔR value in the South China Sea is estimated to be –3 ± 50 yr (mean ± SD, n=9). This value seems to be slightly higher than the value of Con Dao Island, which is consistent with the suggestion that the region close to the Mekong delta is more influenced by air-sea gas exchange and/or freshwater discharge.

Table 1 ^{14}C data of an annually-banded coral sample from Con Dao Island in the south of Vietnam, and calculation of ΔR values.

Year (AD)	$\Delta^{14}C$ (‰)	± 1 σ (‰)	^{14}C age (yr BP)	± 1 σ (yr)	Model age (yr BP)	ΔR (yr)
1960	–10.3	3.9	—	—	—	—
1959	–14.8	3.5	—	—	—	—
1958	–14.5	4.6	—	—	—	—
1957	–27.7	2.6	—	—	—	—
1956	–28.5	3.2	—	—	—	—
1955	–45.4	3.7	370	31	473	–103
1954	–45.3	2.6	370	22	473	–103
1953	–55.6	2.5	458	21	473	–15
1952	–52.1	3.0	429	25	473	–44
1951	–42.4	3.1	348	26	473	–125
1950	–51.0	3.3	422	28	473	–51
1949	–48.5	4.2	401	35	473	–72

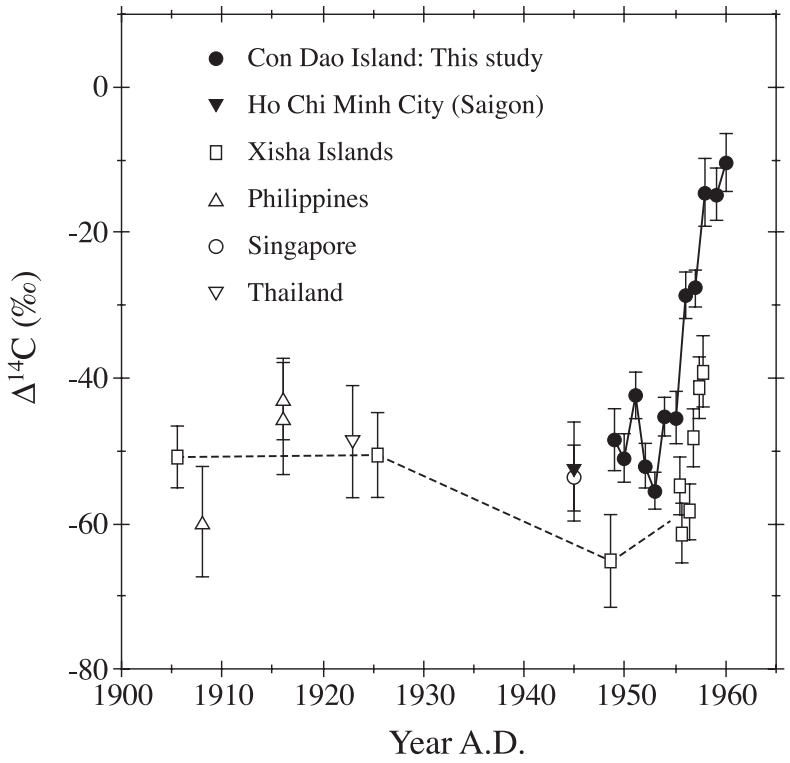

Figure 2 Comparison between $\Delta^{14}C$ results in Con Dao Island (this study) and several sites in the South China Sea (Southon et al. 2002).

ACKNOWLEDGEMENTS

We thank Dr Koichi Watanabe and the staff of the Con Dao National Park for their technical support in drilling the coral core. This work was supported by a Grant-in-Aid from the RONPAKU program of the Japan Society for the Promotion of Science (JSPS) to PXD.

REFERENCES

Druffel ERM, Suess H. 1983. On the radiocarbon record in banded corals. *Journal of Geophysical Research* 88: 1271–80.

Kitagawa H, Masuzawa T, Nakamura T, Matsumoto E. 1993. A batch preparation method for graphite targets with low background for AMS ^{14}C measurements. *Radiocarbon* 35(2):295–300.

Ostlund HG, Stuiver M. 1980. GEOSECS Pacific radiocarbon. *Radiocarbon* 22(1):25–53.

Southon J, Kashgarian M, Fontugne M, Metivier B, Yim WWS. 2002. Marine reservoir corrections for the Indian Ocean and Southeast Asia. *Radiocarbon* 44(1): 167–80.

Stuiver M, Polach HA. 1977. Discussion: reporting of ^{14}C data. *Radiocarbon* 19(3):355–63.

Stuiver M, Quay P. 1981. Atmospheric ^{14}C changes resulting from fossil fuel CO_2 release and cosmic ray flux variability. *Earth and Planetary Science Letters* 53:349–62.

Stuiver M, Ostlund HG. 1983. GEOSECS Indian Ocean and Mediterranean radiocarbon. *Radiocarbon* 25(1): 1–29.

Stuiver M, Braziunas TF. 1993. Modeling atmospheric ^{14}C influences and ^{14}C ages of marine samples to 10,000 BC. *Radiocarbon* 35(1):137–89.

Stuiver M, Reimer PJ, Braziunas TF. 1998a. High-precision radiocarbon age calibration for terrestrial and marine samples. *Radiocarbon* 40(3):1127–51. Data available at http://radiocarbon.pa.qub.ac.uk/calib/.

Stuiver M, Reimer PJ, Bard E, Beck JW, Burr GS, Hughen KA, Kromer B, McCormac G, van der Plicht J, Spurk M. 1998b. INTCAL98 radiocarbon age calibration, 24,000–0 cal BP. *Radiocarbon* 40(3):1041–83. Data available at http://radiocarbon.pa.qub.ac.uk/calib/.

RADIOCARBON, Vol 46, Nr 2, 2004, p 661–681

THE 'STERNO-ETRUSSIA' GEOMAGNETIC EXCURSION AROUND 2700 BP AND CHANGES OF SOLAR ACTIVITY, COSMIC RAY INTENSITY, AND CLIMATE

V A Dergachev[1] • O M Raspopov[2] • B van Geel[3] • G I Zaitseva[4]

ABSTRACT. The analysis of both paleo- and archeomagnetic data and magnetic properties of continental and marine sediments has shown that around 2700 BP, the geomagnetic Sterno-Etrussia excursion took place in 15 regions of the Northern Hemisphere. The study of magnetic properties of sediments of the Barents, Baltic, and White Seas demonstrates that the duration of this excursion was not more than 200–300 yr.

Paleoclimatic data provide extensive evidence for a sharp global cooling around 2700 BP. The causes of natural climate variation are discussed. Changes of the galactic cosmic ray intensity may play a key role as the causal mechanism of climate change. Since the cosmic ray intensity (reflected by the cosmogenic isotope level in the earth's atmosphere) is modulated by the solar wind and by the terrestrial magnetic field, this may be an important mechanism for long-term solar climate variability. The Sterno-Etrussia excursion may have amplified the climate shift, which, in the first place, was the effect of a decline of solar activity. During excursions and inversions, the magnetic moment decreases, which leads to an increased intensity of cosmic rays penetrating the upper atmosphere. Global changes in the electromagnetic field of the earth result in sharp changes in the climate-determining factors in the atmosphere, such as temperatures, total pressure field, moisture circulation, intensity of air flows, and thunderstorm activity. In addition, significant changes in the ocean circulation patterns and temperature regimes of oceans will have taken place.

INTRODUCTION

High-resolution paleoclimatic records provide important information about climate change during the Holocene. Recent paleoclimatic studies have shown that significant natural climate variations occurred on centennial and millennial timescales (e.g. Dansgaard et al. 1993; Magny 1995, 2004; Bond et al. 1997; van Geel et al. 1999; Mann 2000; Johnsen et al. 2001; Esper et al. 2002). The climate can be affected by various types of external forcings which have different spatial and temporal scales of propagation in the climatic system. There is increasing evidence that many of the centennial and millennial climate changes are caused by solar forcing. The best-known example of a solar-climate effect is the cold period between AD 1645 and 1715, which coincides with the Maunder Minimum of solar activity (Eddy 1976).

Several extensive cold intervals occurred during the period between about AD 1450 and 1890 which is known as the Little Ice Age (LIA). Cold events during the LIA coincided with periods of relatively low solar activity. Human communities have always been sensitive to extremes of weather, and there is a great deal of information on weather conditions during the LIA in archived documents, particularly in England and western Europe, extending back to the early Middle Ages, as well as many centuries of records from China, India, and the Near East (Lamb 1995). Many paleoclimatic proxies confirmed that the LIA was a global phenomenon. During the Holocene, there were several similar periods of prolonged cold climatic conditions related to low solar activity (e.g. Dergachev and Chistyakov 1995).

Stratigraphical, paleobotanical, and archaeological evidence points to a change from a dry and warm to a more humid and cool climate in central and northwestern Europe at the boundary from Suboreal

[1]Ioffe Physico-Technical Institute, St. Petersburg, Russia. Corresponding author. Email: v.dergachev@pop.ioffe.rssi.ru.
[2]St. Petersburg Branch of IZMIRAN, St. Petersburg, Russia.
[3]Institute for Biodiversity and Ecosystem Dynamics, University of Amsterdam, the Netherlands.
[4]The Institute for the History of Material Culture RAS, St. Petersburg, Russia.

Proceedings of the 18th International Radiocarbon Conference, edited by N Beavan Athfield and R J Sparks
RADIOCARBON, Vol 46, Nr 2, 2004, p 661–681

to Subatlantic, between 2800–2500 BP (e.g. van Geel et al. 1996). Van Geel et al. (1996, 1998a) also argue that the climatic change affected settlement and land-use activities of European societies. New high-resolution Holocene climatic records provide a more detailed interpretation of cultural shifts in the past. In a recent study, Tinner et al. (2003) compared paleobotanical human impact indicators with independent high-resolution paleoclimatic proxies (oxygen isotopes in ice cores from Greenland and dendroclimatological data) in order to show evidence of the response of prehistoric and historic European cultures to climatic change. The authors suggested that gaps of the archaeological record during 800–650 and 400–100 BC in western and central Europe may indicate climate-driven land-abandonment phases.

There are quite a number of papers describing and interpreting the earth's natural climatic processes on long and short timescales. However, the processes influencing natural climatic change are difficult to understand and to predict. As the Sun is the only effective source of heat reaching Earth, the primary factors causing both short- and long-term climatic changes on the earth's surface are the result of the physical nature of the Sun, and Earth's spatial relationship to the Sun on long-term intervals. As shown in some studies, plausible reasons for changing atmospheric circulation patterns can be changes in the solar activity (e.g. van Geel et al. 1999) or changes in the thermohaline circulation in oceans (e.g. Bond et al. 1997). Bond et al. (2001) suggest a close link between changes in solar activity and past climatic changes over the North Atlantic and Europe. Magny (1993a, 2004) and van Geel et al. (1996, 1998a) argue that Holocene climatic changes affected settlement and land-use activities of prehistoric European societies.

Nevertheless, solar variability remains controversial as a source of climate change, since no causal physical mechanism linking changing solar activity and climate change has been established. From among the assumed factors and mechanisms, the variation of solar irradiance is the most obvious, but there is no direct evidence that the irradiance of the Sun is varying significantly on long timescales. The recent observation of correlations between the galactic cosmic ray intensity and the surface of the earth covered by low clouds (Svensmark and Friis-Christensen 1997) may provide an important clue. Their results demonstrate the high positive correlation of the galactic cosmic ray intensity and cloudiness during long-term cosmic ray modulation in the 11-yr solar activity cycle. An increase of the cosmic ray intensity may lead to an increase in global cloud cover after ionization in the atmosphere by cosmic rays, resulting in an increased aerosol formation and cloud nucleation. Thus, an increase in the global cloud cover may be caused by cooling of the earth during periods of low solar activity.

Since the galactic cosmic ray intensity is modulated by the solar wind, a galactic cosmic ray cloud link could provide a sufficiently amplifying mechanism for solar-climate variability. This would constitute an extra contribution to climate change, in addition to the direct contribution from irradiance changes. Along with solar modulation of the galactic cosmic ray intensity, fluctuations in the geomagnetic field strength are also a cause for variations of the galactic cosmic ray intensity. Earth's magnetic field undergoes a steady-state change and non-periodical short events due to reversals or excursions. The galactic cosmic ray intensity, and subsequently, the cosmogenic production rate in the earth's atmosphere, are increased when the geomagnetic field is less intense. There are a few reports about excursions recorded in lake deposits and marine sediments. The youngest excursion was recorded by Ransom (1973) and has been called the Sterno event (Noel and Tarling 1975) or Sterno-Etrussia event in Russian papers. In the Baltic Sea sediments, Kochegura (1992) observed large variations of the direction of the geomagnetic dipole around 2800 BP. Based on archeomagnetic data from Georgia (Caucasus), Burlatskaya and Chelidze (1990) found that the strength of the geomagnetic field was reduced by 2 to 2.5 times around 2800 BP. A reduction of the geomagnetic

dipole moment would lead to a sharp increase of cosmic ray penetration into the middle and low latitude atmosphere, which would strongly increase the production of cosmogenic isotopes on a global scale. Ultimately, the increase of cosmic rays during the excursion could lead to increased cloud cover and precipitation. Dergachev et al. (2000) and Raspopov et al. (2000) showed that the examination of the combination of external factors (solar activity, cosmic ray enhancement, and fast changes of the geomagnetic field) may contribute to a better understanding of the climate and solar activity as the possible cause of major climatic changes, as well as of breaks in the development of material culture in the past.

The main aims of this study are the following: 1) to present new evidence for the climatic cooling event around 2700 BP, 2) to demonstrate the spatial extension of the Sterno-Etrussia excursion, and 3) to discuss the possible causal connection between galactic cosmic ray intensity and climate.

A Quasi-Cyclical Occurrence of Changing Solar Activity, Cosmic Ray Intensity, and Climate

On the basis of radiocarbon chronologies of mountain glaciers in North America and Europe, Denton and Karlen (1973) established a synchronous and regular millennial-scale pattern of climate variation during the Holocene. Even after 30 yr, the evidence for this long-term regular climate change has not been widely accepted. Based on measurements of soluble impurities in Greenland ice, O'Brien et al. (1995) demonstrated that the Holocene atmospheric circulation above the ice cap was punctuated by a series of millennial-scale cooling events. They established that these increases in soluble impurities probably occurred at times of lowered atmospheric temperatures. The most prominent shifts appeared to correspond with periods of glacial advances (Denton and Karlen 1973).

Bond et al. (1997) carried out detailed investigations of deep-sea sediments (ice-rafted debris: IRD) in the North Atlantic, and established that the North Atlantic's Holocene climate must have undergone a series of abrupt reorganizations, each one with sufficient impact to force concurrent increases in debris-bearing drift ice. Bond et al. showed that cool, ice-bearing waters from the North Atlantic advanced abruptly, synchronous with changes in the atmospheric circulation as recorded in Greenland ice. The IRD events exhibit a quasi-cyclic occurrence with a millennial-scale periodicity through the Holocene. The youngest peaks occurred during the Little Ice Age (LIA) period and about 2800 yr ago. The LIA mode appears to have been the most recent cold phase in the series of millennial-scale cycles. The rafting icebergs are triggered simultaneously from many glaciers, so the driving mechanism must be a common climate forcing mechanism. It points to a trigger that caused air temperatures to drop and induce the release of ice over a large region. For the North Atlantic, the IRD data showed that there has been much more climate change during the Holocene than previously thought. Until recently, the origin of the millennial climate cycle was unknown. Orbital periodicities around the Sun are too long to cause millennial-scale climate cycles. Recent studies (e.g. by Vasiliev et al. [1997] and Vasiliev and Dergachev [2002]) showed that the large maxima of 2300–2400-yr periodicity in atmospheric ^{14}C concentrations may be caused by long-term decreases in solar activity and may be related to cooling climatic periods with Alpine glacier expansions (Denton and Karlen 1973; Rothlisberger 1986) and sharp changes of the Caspian Sea level (Karpychev 1994). The abrupt climate change around 2700 BP is a major event in this series of cool intervals.

Bond et al. (2001) have shown that solar variability is highly correlated with the ice-rafted debris events during the Holocene. As shown in Figure 1a and b, there is good correlation with the galactic cosmic ray intensity (^{14}C record in tree rings). The correlation includes the LIA, the most recent event, and the abrupt climate change around 2700 BP. This rather convincing evidence suggests that solar forcing has caused the long-term climatic cycle during the Holocene. The most pronounced maxima of glacier advance (Maisch et al. 1999) were synchronous with high amplitudes of long-term

variations of ^{14}C rate production (Figure 1c). Magny (1999, 2004) has reconstructed the history of lake levels in the French Jura Mountains. Holocene lake-level fluctuations correlate well (Figure 1d) with the changing galactic cosmic ray intensity (^{14}C record). This implies that the Jura lake levels also correlate with the periods of increased ice-rafted debris in the North Atlantic (Renssen et al. 2000).

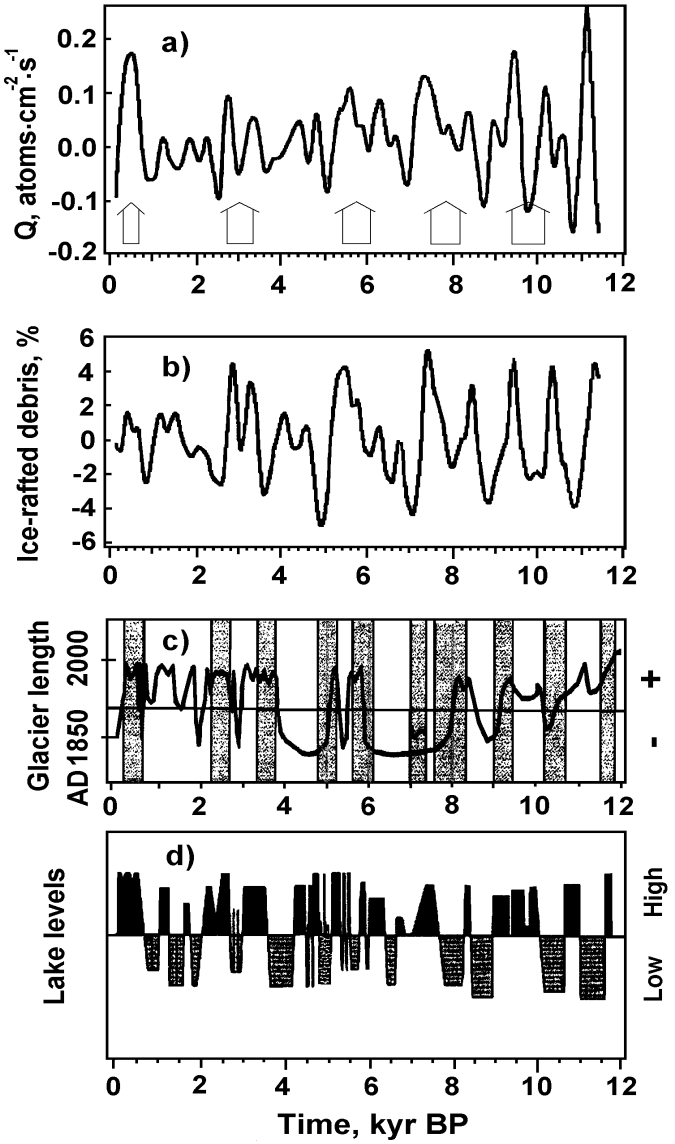

Figure 1 Comparison of (a) cosmic ray variability (Q is smoothed ^{14}C production rate from ^{14}C record of Stuiver et al. 1993); (b) combined ice-rafted debris in the North Atlantic (Bond et al. 2001); (c) estimated length variation of Swiss glaciers (Maisch et al. 1999); cold intervals are indicated by the shaded areas; (d) lake-level fluctuations in the French Jura Mountains (Magny 1999). The arrows show the extrema of the long-term changes of processes considered.

Manifestation of the Sterno-Etrussia Excursion

Information about the youngest geomagnetic excursion was given by Ransom (1973), who mentioned the investigations by G Folgheraiter carried out in AD 1896 and 1899. While performing archeomagnetic studies of Attic and Etruscan vases in Greece and Italy (i.e. at latitudes between ~35 and 45°N and 10 to 25°E), Folgheraiter discovered that the geomagnetic field had the inverse sign during the 8th century BC. The paleomagnetic anomalous changes in declination D and inclination j discovered by Folgheraiter were also observed by Nöel and Tarling (1975) in varved sediments in southern Sweden at around 860 BC. Nöel and Tarling called this excursion "Sterno." Sharp changes in inclination j and declination D (to 90°) dating to the 9th to 6th centuries BC were discovered by Nachasova et al. (1986) and Burlatskaya and Chelidze (1990) in archaeological material from settlements in the western Caucasus (Georgia), and this excursion was called "Etrussia." Nachasova et al. (1986) have shown that the duration of the changes in the geomagnetic field during this excursion was not more than about 100 yr.

Kochegura (1992) described this excursion based on magnetic properties of Baltic and Barents Sea sediments. In recent years, the behavior of the geomagnetic field during the Sterno-Etrussia excursion has been studied in detail by analyzing sediments in the Barents, Baltic, and White Seas. With different degrees of reliability, the excursion was revealed in 15 cores from the bottoms of these seas (Kochegura 1992; Kochegura et al. 1999). In 1998, during the 14th expedition of the research vessel *Academician Sergei Vavilov*, sediment cores were collected in the Barents Sea in order to study their chronostratigraphy and correlation. The Barents Sea is one of the key regions for the investigation of both post-Ice Age climatic history and ocean circulation patterns (Murdmaa and Ivanova 1999). The result obtained is the first information on paleomagnetic properties of Barents Sea sediments for the time interval of the last approximately 30,000 yr. One of the main results of the paleomagnetic investigations of Barents Sea sediments is the discovery of sharp changes of the geomagnetic field inclination j, which could be caused by the geomagnetic excursions Sterno-Etrussia (3000–2200 BP) and Solovki (7000–4500 BP). Figure 2 shows changes in magnetic properties of sediments in boreholes from the Barents Sea bottom. The sediments were dated by the ^{14}C method (Levitan et al. 1999). The core bottom is about 10,000 yr old. The figure shows variations in inclination j (Figure 2a, c), remanent magnetization J_n (Figure 2b), and magnetic declination (Figure 2c). The geomagnetic Sterno-Etrussia excursion shows up as a sharp change of inclination in the time interval 2400–2200 BP. Along with this change, a considerable decrease in J_n is observed against a background of increased J_n, which is the evidence for a decrease in the geomagnetic field during this period. The excursion duration is 100–200 yr. The investigation of magnetic susceptibility has shown that there are no specific mineralogical features during the period of geomagnetic excursion. This indicates that the changes in j and J_n described above are due to changes in geomagnetic field rather than caused by variations in the mineralogical composition of the sediments.

The behavior of the geomagnetic field intensity during the excursion is of fundamental importance for understanding the physical mechanism of climate change. For obtaining data on relative variations, series of experiments were worked out. Re-sedimentation of deposits from a number of cores in which the Sterno-Etrussia excursion had been observed was performed. The results showed that there was a decrease of the geomagnetic field intensity before and during the excursion (Kochegura 1992).

The example of the Sterno-Etrussia excursion discovery in sediments from the upper part of the Ob' River basin (Siberia, Russia) is presented in Figure 3 (Gnibidenko et al. 2000). The changes of dec-

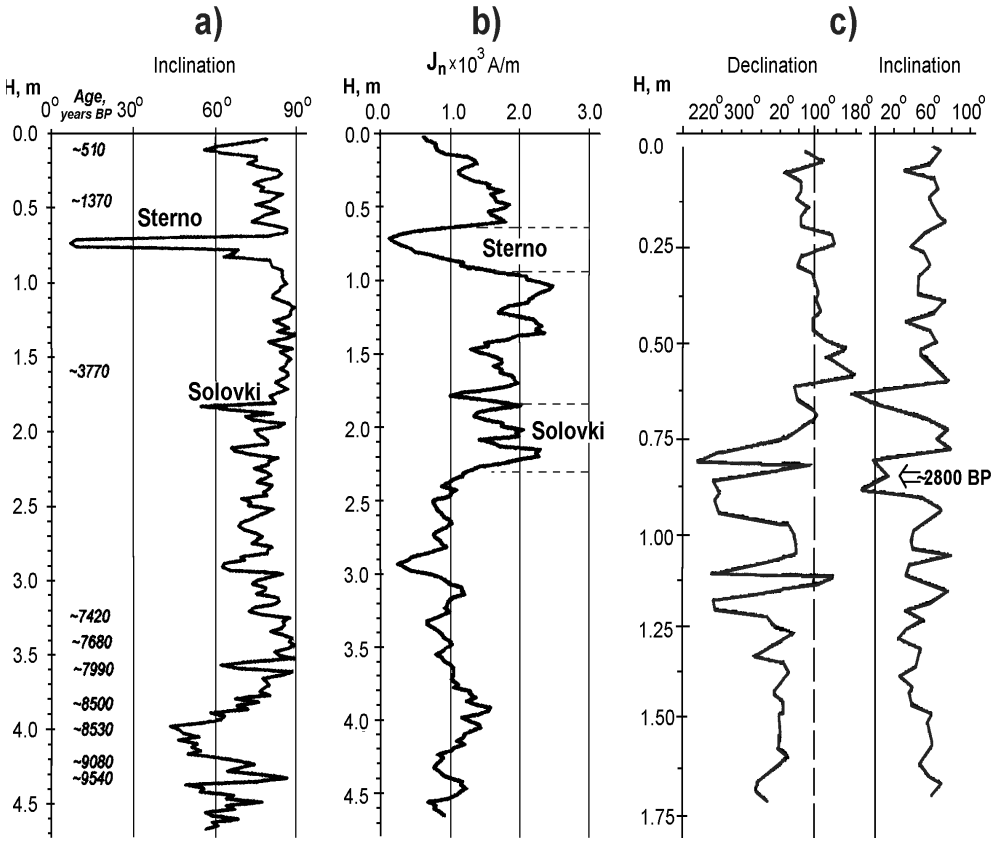

Figure 2 (a) Changes in inclination; (b) remanent magnetization J_n in the Holocene sediments of the Barents Sea; and (c) in declination and inclination of the Baltic Sea sediments as a function of the depth (m).

lination D during the excursion were 147°; the change of inclination j was 60°. Here, it is also noted that the decrease of J_n occurred under equal mean values of magnetic susceptibility κ during the excursion. ^{14}C dating of the layer (3185 ± 50 BP) may serve as a confirmation of the excursion near this date. Wandering of the virtual geomagnetic pole during the period from 2700 to 2340 BP, inferred from studies of volcanic deposits of Mount St. Helens, Washington (Hangstrom et al. 2002), suggests that the excursion occurred during this time interval. The Sterno-Etrussia excursion, as recorded in different investigations, is presented in Table 1. The table reflects the area of paleomagnetic studies in the first place, and it would be premature to conclude about the extension of the Sterno-Etrussia excursion on a global scale. However, it is possible that the excursion was characteristic for the Northern Hemisphere.

Thus, studies of magnetic properties of sediments and archaeological materials during the geomagnetic Sterno-Etrussia excursion lead to the following conclusions. According to different results of dating, the excursion developed in the time interval 2800–2200 BP. Archaeological materials point to the 8th to 4th centuries BC. During the excursion, 1or 2 sharp deviations of inclination j to 0 or negative values occurred, i.e., an abrupt displacement of the geomagnetic pole toward the Equator or its wandering to the Southern Hemisphere took place. The duration of this geomagnetic excursion was rather short, about 100–200 yr.

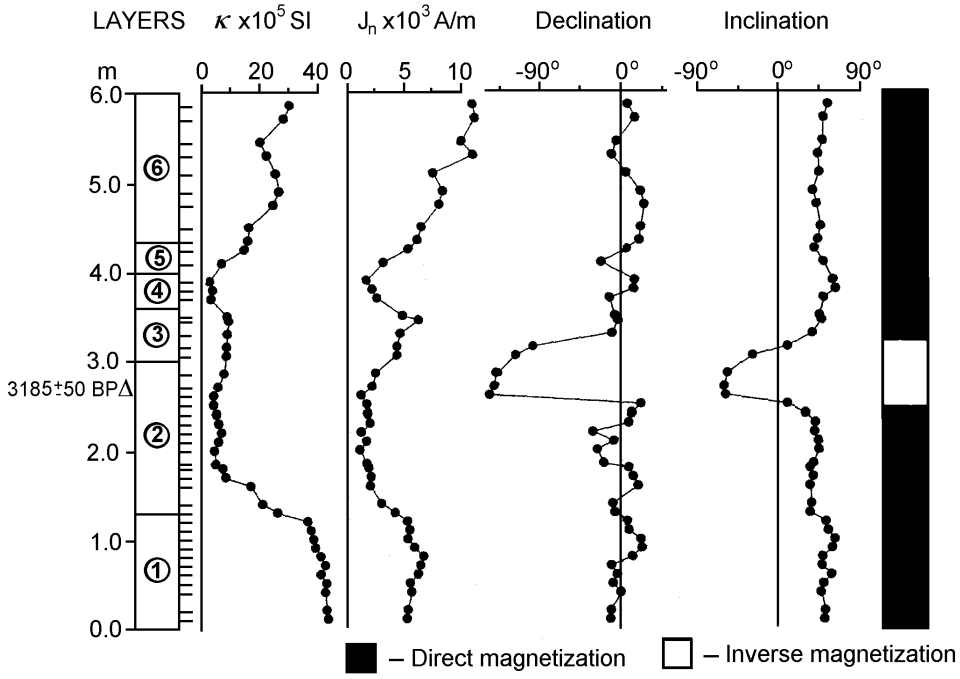

Figure 3 The magnetic characteristics of the Holocene continental sediments in upper part of Ob' River basin (Siberia, Russia): magnetic susceptibility κ, remanent magnetization J_n, declination, inclination, direct, and inverse magnetization (Gnibidenko et al. 2000).

Table 1 List of places where the excursion Sterno-Etrussia was determined.

Nr	Place of the detection	Estimated age	References
1	Creece, Italy	800 BC	Ransom 1973
2	Southern Sweden	860 BC	Nöel and Tarling 1975
3	Georgia	800–700 BC	Nachasova et al. 1986
4	Alaska	3000 BP	Morinaga et al. 1987
5	Yellow Sea	3000–2800 BP	Moqing et al. 1987
6	Northern Sweden	2800–2550 BP	Mörner and Sylvan 1989
7	Ukraine	3000 BP	Tretjak et al. 1989
8	Ural, Russia	2500 BP	Suleimanova et al. 1991
9	Turkmenistan	<4500 BP	Trubikhin et al. 1991
10	Northern coast of Caspian Sea, Russia	3000–2500 BP	Eremin et al. 1992
11	Baltic, Barents, White Seas	3000–2800 BP	Kochegura 1992
12	Karelia, Finland	2500 BP	Saarinen 1994
13	Siberia, Russia	2875 ± 75 BP	Burakov et al. 1996
14	Siberia, Russia	3185 ± 50 BP	Gnibedenko et al. 2000
15	Mount St. Helens, Washington, USA	2700–2340 BP	Hangstrom et al. 2002

Climatic Oscillations Around 2700 BP

Van Geel et al. (1996, 1998a) and Speranza et al. (2002) studied the changing species composition of peat-forming mosses in European Holocene raised bog deposits. They found an abrupt shift at the onset of the sharp rise in the atmospheric ^{14}C concentration (decrease in solar activity) around 850 cal BC, from mosses preferring relatively warm conditions to those preferring colder and wetter

conditions. There is supporting archaeological evidence from the Netherlands. Bronze Age settlements which had been continuously inhabited for more than 1000 yr were suddenly abandoned, presumably because the soil became waterlogged and peat growth started in areas which had been arable land. There is a substantial amount of geological and archaeological information showing that the climate changed abruptly around 2700 BP. We summarize a number of new studies about the abrupt climate change in different regions of the world during this period. We emphasize that the dating precision in some of the studies is rather low (large dating errors, poor sample resolution).

Barber and Langdon (2001) analyzed plant macrofossils in a peat deposit in northern England (Walton Moss) and compared the peatland proxy climate record with a temperature reconstruction based on chironomids in the sediments of a nearby lake. The main long climatic deteriorations identified from these proxy data occur between cal 2900–2830 BP, 2630–2590 BP, 1550–1400 BP; 500–400 BP, and 240–150 BP. Their results indicate that a major temperature decline occurred around 2600 cal BP. Langdon et al. (2003) used a refined plant macrofossil record from Walton Moss and reconstructed the raised mire water tables during the Holocene. They established major climatic deteriorations at about 4410–3990 BP, 3170–2860 BP, and 2320–2040 BP.

Schilman and Bar-Matthews (2001) studied $\delta^{18}O$ and $\delta^{13}C$ in sediments from the southeastern Mediterranean, off Israel, and established humid phases in the time intervals of 3500–3000 and 1700–1000 BP, whereas relatively more arid conditions prevailed in the area between 3000 and 1700 BP and during the last millennium.

Scott and Lee-Thorp (forthcoming) studied different climate proxy records across southern Africa and established marked isotope fluctuations in a cold air cave stalagmite. Climate variability as determined from the stalagmites shows periodic fluctuations in centennial and multi-decadal scales. All stalagmite sequences suggest cooling after 3200 BP, and also increasing development of C4 grasslands, peaking at 2000 BP.

Numerous investigations of postglacial climate in Canada were obtained from proxy records. The "neoglaciation" during 3000–2500 BP has been documented in the Canadian Rocky Mountains (Luckman et al. 1993). Wilson et al. (1997) showed that 3000–2500 BP was a period of downcutting in the Saskatchewan River system of western Canada, reflecting a cooler, moister climate. The proxy records from Harris Lake (Sauchyn and Sauchyn 1991) show that lower temperatures and plant productivity occurred (relatively low percentages of organic matter in the sediments) from 3000–2400 BP. This cool period coincided with a global phase of glacier growth, including the "mid-Neoglacial" advance in the Canadian Rocky Mountains at around 3000–2500 BP (Luckman et al. 1993).

In northern Iceland, the upper limit of tree/shrub birch (*Betula pubescens*) has been used by Wastl et al. (2001) as an indicator of summer temperatures. From the pollen and macrofossil investigations, it was established that there are 2 marked drops in the *Betula pubescens* curve of the Vesturárdalur-Skíðadalur area on the Tröllaskagi peninsula: from about 5000 BP to about 4500 BP and before/around 3000 BP. These variations can be compared to the record of Holocene glacier advances in northern Iceland. One of the glacier advances in the period around 3200–3000 BP, based on ^{14}C dating and tephrochronology, was established by Stötter et al. (1999).

The phenomenon El Niño has had severe consequences for the modern and (historically recorded) inhabitants of Peru, and El Niño events also influenced prehistoric cultural developments. Long-term proxy records for the El Niño-Southern Oscillation (ENSO) events indicate variable recurrence intervals and intensities. The Pacific coast of southern Ecuador and northern Peru is a core region of

ENSO activity, and paleoclimate records there should reflect ENSO history. Peruvian coastal middens contain abundant marine mollusk valves that are proxy indicators for near-shore oceanic conditions (~7–20°S, 70–80°W). Analysis of midden remains from Peru (Sandweiss et al. 2002) suggests an increase in ENSO frequency between about 3200 and 2800 BP. This increase in El Niño frequency is correlated with the abandonment of monumental temples in the region after nearly 3 millennia of uninterrupted development and growth. By 2800 BP, the most warm temperature-sensitive mollusc assemblages (*Choromytilus chorus, Mesodesma donacium*) had disappeared from middens north of 9°S, and over the following centuries, these species were largely replaced by others. Various climatic records support the increased ENSO after 3200 BP: water levels in Lake Titicaca, Peru-Bolivia (Abbott et al. 1997); an increase in lake levels in northern Chile (Betancourt et al. 2000); flood records from Quebrada Tacahuay (17°48′S; Keefer et al. 1998) and Quebrada de los Burros (18°1′S; Fontugne et al. 1999) on the far south coast of Peru, and others.

The Galapagos Islands, located within the core ENSO region, consistently experience positive precipitation and sea surface temperature (SST) anomalies during El Niño events, and possess a number of hypersaline lakes that experience reduced salinity during these periods. Galapagos lake sediment deposits are records of the history of salinity fluctuations, and thus provide a record of ENSO activity. Riedinger et al. (2002) performed lithostratigrahic and mineralogic analyses of sediments from the hypersaline Bainbridge Crater Lake, Galapagos Islands, and provided evidence of past El Niño frequency and intensity. They established that intensity of events increased at about 3000 BP (~3100 cal yr BP).

The Atlantic area demonstrates that marked variations in the distribution of water masses occurred repeatedly through the last 4500 yr (Eiriksson et al. 2002). Of special interest is the exact timing of a marked drop in sea-surface temperature in the area, indicated by ice-rafting debris concentration, which occurred at 2980 cal BP. This appears to predate most records of a general cooling event in NW Europe by a couple of centuries.

A number of periods with climate deterioration have been recorded in the Baltic Sea area and around the North Atlantic during the Holocene. It is possible that periods of increased wetness and reduced evapotranspiration may have increased the freshwater input into the Baltic Sea and decreased the salinity. Gustafsson and Westman (2002) used shore-level data and proxy data (mainly diatoms and shellfish) to evaluate phases of high and low salinity changes. They established a number of phases of decreased salinity, among which are phases coinciding with cold and possibly wet climatic phases in time intervals of 2900–2500 and 500–100 BP.

Estuarine and beach coastal marine deposits in New South Wales, Australia, which might point to an elevated Holocene sea level have been investigated by Bryant et al. (1992). From fossil corals found along the adjacent coast and also based on the elevation and orientation of the raised marine deposits, the authors drew the conclusion that the ocean temperature was higher around 2800 BP by up to 2 °C, and that sea levels from 6000 to 1500 BP were over 1 m higher than at present. The marine deposits show little indication that they were deposited by storms, but the role of tsunami in their formation cannot be ignored.

Columnar stalagmites in caves of the Guadalupe Mountains, southwestern United States, during the late Holocene record a 4000-yr annually resolved climate history. The stalagmite record consistently provides a century and annually resolved history of climate (Polyak and Asmerom 2001). Thicker annual bands in 4 of the 5 stalagmites from ~3000 to 1700 BP indicate significantly greater effective annual moisture than at present. Intervals of increased moisture during the late Holocene in the southwestern United States are reported by numerous studies (e.g. McFadden and McAuliffe 1997;

Wilkings and Currey 1999) supporting an interpretation favoring greater effective moisture during the late Holocene. A 200-yr period of thicker bands from 2800 to 2600 BP in these stalagmites reflects the wettest interval of the late Holocene for this region. This is synchronous with a reported abrupt change to cooler and wetter conditions in the temperate and boreal zones of Europe around 2650 BP (van Geel et al. 1998a). Also, the most notable increase in annual precipitation occurred from 440 to 290 BP during a period of global cooling in the LIA. The period of the LIA was defined by a study of stalagmites from Madagascar as lasting from 425 to 230 BP (Brook et al. 1999) and was reported as beginning at 450 BP on the basis of stalagmites from Nepal (Denniston et al. 2000).

Climate variability on the Yucatan Peninsula during the past 3500 yr is reconstructed by Curtis et al. (1996) from the measurement of $\delta^{18}O$ in monospecific ostracods and gastropods in lake sediments from Punta Laguna, Mexico. From ~3310 to ~1785 BP, low mean $\delta^{18}O$ values indicate relatively wet conditions (i.e. low evaporation to precipitation ratio).

Tinner et al. (2003) performed palynological analysis of ^{14}C-dated sediments from 4 lakes in Switzerland; the main attention was devoted to the period between 2300 BC and AD 800. They also used a series of tree-ring density curves, glacier oscillations, paleobotanical timberline studies, ^{14}C content in tree rings, and compared these with the GRIP and GISP2 climatic record from Greenland. The conclusion was made that, although the general vegetation histories north and south of the Alps are different, climatic fluctuations in both areas are synchronous. Pronounced similarities between fluctuations of human impact indicators (pollen) and climate shifts suggest a common driving factor. Tinner et al. (2003) discussed possible driving factors (independent cultural developments and/or climatic factors). Pollen data suggest that the reduction of agricultural activities (maximum of tree pollen, minimum of Cerealia and *Plantago lanceolata* pollen) north and south of the Alps was accompanied by natural afforestation. Most population discontinuities are considered to be closely related to climatic change.

In 2002 on the eastern side of Lake Bolshoy Turali along the Dagestan coast of the Caspian Sea, field work was carried out with a variety of techniques, including geomorphology, sedimentology, georadar, biostratigraphy, paleoecology, radiochronology, isotope geochemistry, landscape geochemistry, soil science, and process-based modeling. The selection of the site is based on the fact that Caspian Sea level high-stands are reflected in the highest levels reached by coastal barriers moving landwards during transgressions. The most reliable sea level curve for the Caspian Sea so far was given by Rychagov (1977). The first results of the new investigations were communicated during the workshop "Holocene Caspian Sea Level Change" at Delft University in the Netherlands in 2002. Attention was given to the reconstruction of Caspian paleoenvironmental conditions and transgressions. Kroonenberg et al. (2002) stressed that a considerable high-stand of the Caspian Sea around 2600 BP corresponds with a period of low solar activity and high precipitation in the Volga drainage basin. A <500 BP high-stand coincides with the LIA. The data support the correspondence of Caspian high-stands with periods of global cooling.

Gracheva et al. (2002) presented a reconstruction of main regional stages of paleohydrological change and Holocene landscape evolution in the southern part of the Upper Volga Lowlands. At the Suboreal/Subatlantic transition (around 2600 BP), lake levels rose and caused abrupt flooding of soils which led to a collapse of the human economy in all lowland areas bordering the Klin-Dmitrov Heights (lower than 130 m asl). The abrupt hydrological change corresponds to the sudden disappearance of archaeological findings.

DISCUSSION

Apparently, data reported in the preceding sections of this work have demonstrated that sharp climatic changes occurred in the time interval from 3000 BP to 2500 BP. A drastic increase in the galactic cosmic ray (GCR) fluxes, well represented by an increase in the concentration of ^{14}C in tree rings, also took place during this time. Van Geel et al. (1998b, 1999) have drawn attention to this fact and have discussed possible mechanisms of the influence of cosmic rays on climate in the context of modulation of GCR fluxes by solar activity. In particular, they point out that an increase (decrease) of the GCR flux is able to result in attenuation (growth) of the global cloud cover and, therefore, in changes of the solar irradiance flux to low layers of the earth's atmosphere (Dmitriev and Lomakina 1977; Tinsley and Dean 1991; Pudovkin and Babushkina 1992a; Pudovkin and Raspopov 1992; Svensmark and Friis-Christensen 1997). Later, Pallé Bagó and Butler (2000) and Marsh and Svensmark (2000) have shown that variations of the GCR fluxes correlate in general with variations of the density of low cloudiness. Thus, increase of the GCR fluxes might be accompanied by cooling of the near-earth surface.

Tinsley and Dean (1991) have proposed that cosmic rays have an important influence on cloud microphysics. At altitudes from ~3 to 35 km in the earth atmosphere, cosmic rays are the only ionization source (natural radioactivity is an additional source of ionization below ~3 km). Experimental evidence of the plausible impact of galactic cosmic ray ionization on the precipitation efficiency of clouds was reported in Stozhkov et al. (1995). They demonstrate that the precipitation level is increased when the ionization level is increased in response to a higher flux of solar flare protons in the atmosphere. Using visual data from narrow range of latitudes (60°N–64°N), which is consistent with global satellite observations, Pudovkin and Veretenenko (1995) have established a corresponding short-term decrease of cloudiness. They discovered that cloudiness and precipitation are reduced during the periods of high flux of cosmic rays in the atmosphere.

As another consequence of increase of the GCR flux, there might be a change in the ozone concentration in the atmosphere. Shumilov et al. (1992, 1995), Stephenson and Scourfield (1992), and Kodama et al. (1992) showed that solar proton events (SPE), which generate solar cosmic rays, may produce ozone mini-holes at high latitudes (decrease of the total ozone concentration is about 10 to 15%) and they are accompanied by a decrease of temperature in the stratosphere (down to –2.4 °C). Modeling experiments performed by Haigh (1994, 1996) suggest that such ozone depletion and stratospheric cooling could significantly affect the atmospheric circulation. Considering the period between 850 and 760 cal BC, van Geel and Renssen (1998) have inferred from the results of Haigh that stratospheric cooling could have led to a weakening of stratospheric winds and displacement of the tropospheric jet streams toward the Equator. Moreover, they postulated that ultimately it might result in an increase of latitudinal extent of the Hadley Cells and in a weakening of the monsoons.

Thus, as a result of variability of the GCR fluxes, there might be not only changes of optical properties of the atmosphere connected with formation of the clouds cover and aerosol generation in the atmosphere, but there also might be changes in atmospheric circulation. This should substantially affect climatic parameters. The existence of influence of variations of the GCR fluxes on the atmospheric circulation was experimentally confirmed in Tinsley (1988), Pudovkin and Babushkina (1992b), and Cristoforou and Hameed (1997). Tinsley (1988) has shown that a shift in 3–5 degrees of the storm motion trajectory takes place in the Atlantic during solar activity maximum in comparison with solar activity minimum. Cristoforou and Hameed (1997) have obtained similar results for the northern part of the Pacific.

Pudovkin and Babushkina (1992a) and Pudovkin and Raspopov (1992) have reported the results of an analysis of the impact of cosmic ray variation on zonal circulation in the troposphere during the development of strong magnetic storms. Veretenenko and Pudovkin (1993) have shown that decrease of the cosmic ray flux is accompanied by attenuation of the zonal circulation rate and increase of the cosmic ray flux is accompanied by growth of the zonal circulation rate.

Considering climate changes around 2700 BP, one can conclude that drastic increase of the GCR fluxes in this period, which might be connected with solar activity decrease or with influence of the geomagnetic Sterno-Etrussia excursion, should be accompanied by increased transfer of wet Atlantic air to the east—i.e., in Europe. This should result in the formation of cool climate and an increase in the precipitation amount in continental areas, which was actually observed. Note that similar climatic conditions were observed during the Maunder Minimum of solar activity.

Additionally, the papers of Haigh (1994, 1996) have one more important consequence. Displacement of the tropospheric jet stream toward the Equator under the influence of cosmic ray fluxes as well as a decrease of the latitudinal extent of the Hadley Cells means that response of the atmosphere to global perturbation should have a regional character, i.e., growth or weakening of external signal can take place at different latitudes and longitudes.

An ability of the atmospheric system to produce only regional response to a uniformly distributed external impact follows also from more general reasons. The system of atmosphere-ocean-continent, where the redistribution and transport of solar incoming energy takes place, is a non-linear system. Therefore, the spatial distribution of response to any external impact need not exactly follow the spatial distribution of the external forcing. It was also confirmed in model experiments.

A detailed statistical analysis of decadal and multidecadal patterns of the surface temperature response to solar irradiance variations based on analyses of the long-term surface temperature reconstructions during 1650–1850, including the period of the Maunder Minimum, is given in Waple et al. (2002). They estimated the response of surface temperature to solar irradiance variations (SRV) with a period of more than 40 yr and for SRV with a period of 9–25 yr. In the former case, the forcing factor was identified with the century type (Gleissberg) cyclicity of solar activity. The estimates revealed that in the case of Gleissberg cyclicity, the system of atmosphere-ocean-continent, which determines surface temperature, exhibits the highest sensitivity to solar signals with a lag of about 15 yr, which unambiguously suggest a non-linear character of the system. A response of surface temperatures to solar signal demonstrates a high spatial inhomogeneity. For instance, the regions of Scandinavia and Siberia are characterized by a strong positive response to increasing solar irradiance, while the region of western Greenland exhibits a negative response.

As to the impact of cosmic ray fluxes on climatic parameters, Waple et al. (2002) point out that climate response to the GCR fluxes which decrease from the pole to the Equator due to geomagnetic shielding will not follow the law of spatial distribution of GCR but show regional character. Because of differences in conditions of the cloudiness formation in various regions of the globe, the heterogeneity of the spatial atmospheric response to cosmic ray variations will be amplified. The analysis made previously of climatic events around 2700 BP confirmed the idea of regional development of climatic response to external global forcing. Indeed, whereas cooling and precipitation growth occurred in Europe, warm and dry climate occurred on the west coast of Africa, pointing to the blocking of monsoons (Maley and Brenac 1998; Raspopov et al. 1998). Similar spatial structure of climatic processes was observed during the period of the Maunder Minimum of solar activity.

As discussed earlier, van Geel et al. (1998a, 1999) have considered the impact of cosmic ray variations on climate around 2700 BP in the context of solar activity changes. However, a possible influence of the Sterno-Etrussia excursion on the structure of GCR fluxes was not considered in that work. Therefore, let us consider the possible influence of structural change of the geomagnetic field and its configuration (shift of the geomagnetic pole to the Equator) during the excursion on structure of the GCR fluxes and, consequently, on climatic parameters. For this purpose, it is necessary to analyze changes of the magnitude of the geomagnetic dipole (or quadrupole), as well as change of the geomagnetic pole location, making use of paleo- and archaeomagnetic data.

Measurements of magnetic properties of 15 cores from sediments of the Barents, White, and Baltic Seas revealed sharp changes of inclination of the magnetic field at the same age in Holocene deposits. Paleomagnetic characteristics of Holocene-Pleistocene sediments were analyzed in sufficient detail for 9 cores taken from the Barents Sea during the expedition of the research vessel *Academician Sergei Vavilov* in 1998 (Murdmaa and Ivanova 1999; Guskova et al., forthcoming). Recently, the Sterno-Etrussia excursion was revealed with different degrees of reliability in 15 cores in the Holocene shelf sediments of the Baltic, White, and Barents Seas.

One of the main results of paleomagnetic investigations of the Barents Sea sediments is a discovery of sharp changes of the geomagnetic field inclination which might be caused by the geomagnetic excursions Sterno-Etrussia (2200–3000 BP) and Solovki (4500–7000 BP) (Figure 4a). Values of absolute ages for sediments obtained by ^{14}C dating are shown in Figure 4a. The sedimentation rate in the Barents Sea during the Holocene has been estimated making use of this dating, and is 45 cm/1000 yr (Levitan et al. 1999). It is significant that estimates of sedimentation rates can give an approximate timescale. The dating of anomalous values of inclination gave values of ~2200 yr and more than 4000 yr (Figure 4a). Taking into account the obtained sedimentation rate, one can conclude that the inclination change at a depth of 70 cm is connected with this excursion. According to the sedimentation rate, its duration is about 200 yr. Using the paleomagnetic sample, one can derive 3 physical parameters: magnetic susceptibility κ, remanent magnetization J_n, and inclination I. The values of κ are in a narrow range of –0.2 to 0.8 10^{-3} SI, which suggests the uniform distribution of magnetic minerals in sediments during the all the Holocene. Natural remanent magnetization (J_n) strongly varies at a depth of 75 cm. A considerable minimum is observed when J_n decrease from 2.0 to 0.1 10^{-3} A/m. At the 90 cm depth, J_n increases up to 2.5 10^{-3} A/m and oscillates around the mean value of 1.5 10^{-3} A/m up to 230 cm. Inclination I of J_n, averaged over 3 samples, changes sharply from 85 to 5° at the 75 cm depth, and after the 350 cm depth, saw-tooth decreases of inclination are observed. It should be emphasized that the behavior of J_n at the 70 cm depth (Figure 4a) may serve, perhaps, as indirect confirmation of the Sterno-Etrussia excursion at this depth, because J_n decreases under uniform values κ and thus gives information about a decrease of the geomagnetic field intensity during this period rather than about magnetization of minerals.

The existence of the Sterno-Etrussia excursion had been detected earlier in sediments of the Baltic Sea (Figure 4b). For this core, the change of inclination was 80° and the relative change of declination (in the coordinates of drill tube) was 280°. Figure 4c (Gnibidenko et al. 2000) shows the Sterno-Etrussia excursion clearly seen in the Holocene continental sediments from the upper part of the Ob' River basin (Siberia, Russia). The changes of declination during the excursion was 147°; the change of inclination was 60°. The decrease of remanent magnetization J_n, under the equal mean value of magnetic susceptibility κ during the excursion, is also noticeable there. ^{14}C dating of this layer (3185 ± 50 yr) can serve as a confirmation. The time differences of similar inclination variations, recorded at different locations, might be explained by the permanent westward drift of a non-dipole anomaly.

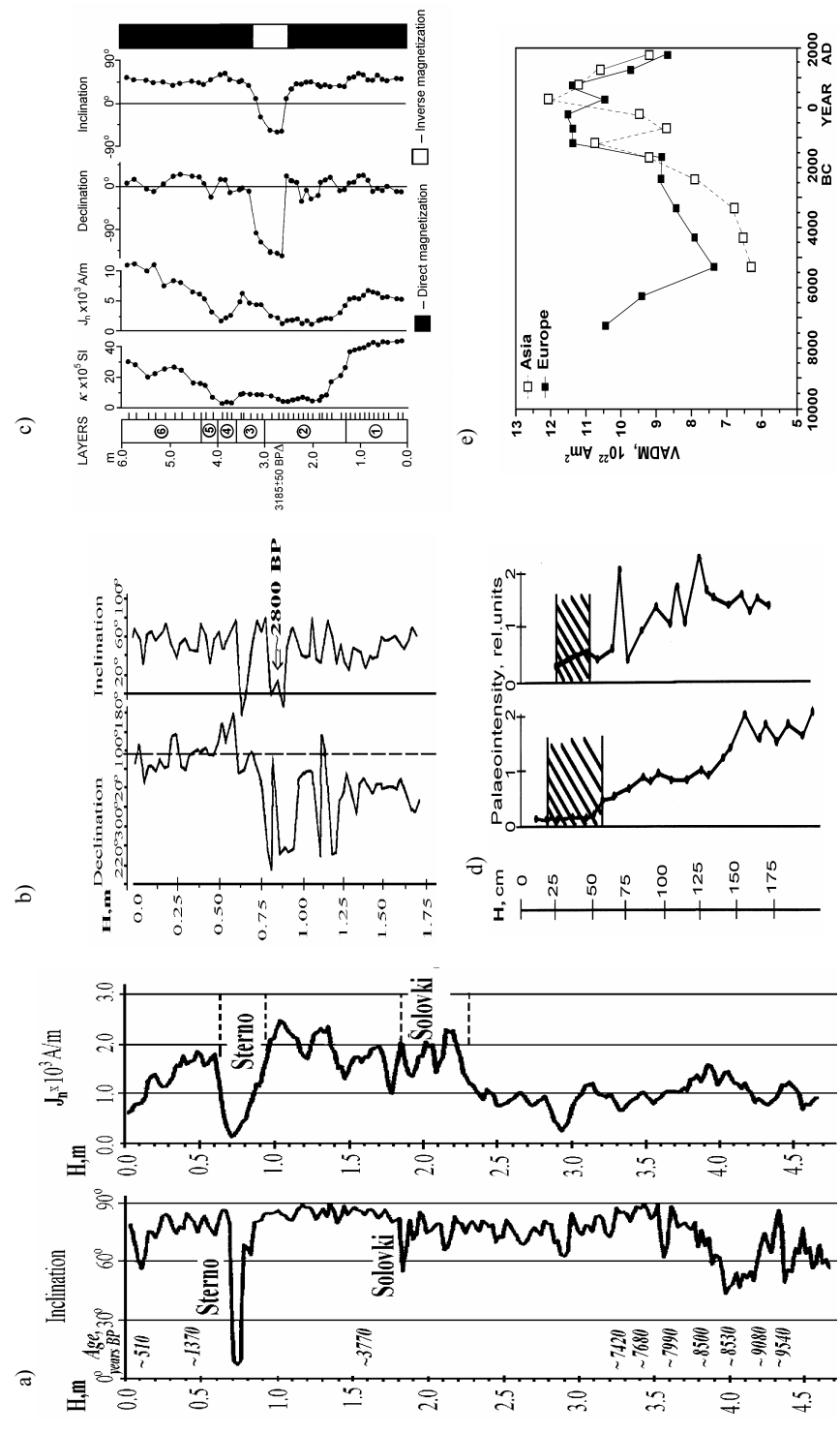

Figure 4 Comparison of changes in parameters of Earth's magnetic field during the Sterno-Etrussia excursion: (a) inclination and remanent magnetization J_n of the Holocene sediments in Barents Sea sediments; (b) declination and inclination in Baltic Sea sediments; (c) magnetic susceptibility κ, remanent magnetization J_n, declination, inclination, direct and inverse magnetization of the Holocene continental sediments in upper part of Ob' River basin from 6 m to 0 m with respect to the water table level (Siberia, Russia) (Gnibidenko et al. 2000); (d) paleointensity in 2 sections from the Baltic Sea where the Sterno-Etrussia excursion was located (Kochegura 1992); (e) comparison of mean virtual axial dipole moment (VADM) values for the European and Asian regions. The archeomagnetic data was averaged over 500 (from AD 2000 to 2000 BC) or 1000 (prior to 2000 BC) yr (Yang et al. 2000).

Data regarding the behavior of geomagnetic field intensity during the excursion are of great interest for understanding the physical mechanism responsible for the excursion. A series of measurements for a number of cores where the Sterno-Etrussia excursion might be recorded have been performed to obtain data on relative variations of sedimentation rate. The results demonstrate that in most cases, this rate decreases before and during the excursion. An example of such a decrease for 2 cores from the Baltic Sea is shown in Figure 4d, taken from Kochegura (1992) and modified in the present work. In sediments of the Baltic Sea, the change in inclination was accompanied by a 3-fold reduction in the geomagnetic field intensity. According to the ^{14}C dating and sedimentation rate estimates, this event occurred between 2300 BP and 3000 BP, and its duration is as short as 100–300 yr. On the basis of the age, one can associate the changes in the magnetic properties of sediments with the geomagnetic Sterno-Etrussia excursion.

There is also other evidence of a sudden drop of the geomagnetic field during the Sterno-Etrussia excursion. Studies of archaeological materials in Georgia (Caucasus) have shown that from the 9th to the 4th century BC, the geomagnetic field strength was approximately 40–60% higher than now (Nachasova and Burakov 2002). This result is consistent with the data of McElhinny and Senenayake (1982) and Yang et al. (2000). However, according to archeomagnetic data from Georgia, during fast changes of the geomagnetic field direction in this excursion, the field magnitude dropped below its present level (Burlatskaya and Chelidze 1987). Based on the virtual axial dipole moment (VADM) model and on archeointensity data, Yang et al.(2000) analyzed the secular variations of the geomagnetic field during the past 12,000 yr. Note that in archeomagnetic data, periods shorter than 1000 yr are usually associated with changes of non-dipole field. Yang et al. (2000) averaged data over 500 and 1000 yr. Comparison of the results from the European and Asian regions is shown in Figure 4e. The authors connected the observed differences between the data sets with strong non-dipole anomalies in Europe. The dipole field increased from its minimum in the vicinity of ~5500 BC, reached its maximum in the vicinity of ~1000 BC, and remained close to this maximum for almost 2000 yr. As can be seen from Figure 4e, the noticeable difference in European and Asian geomagnetic data during this maximum occurred during the time interval from ~1000 BC to ~AD 50, which includes the Sterno-Etrussia excursion. This difference indicates the non-dipolar character of the geomagnetic field.

So far, the evidence of the Sterno-Etrussia excursion has been found in magnetic properties of specimens of marine, lake, and continental sediments, as well as in the directions of magnetized mineral grains in oriented archaeological specimens from 15 widely distributed localities (Table 1). Not all references from Table 1 contain data of the geomagnetic field variation (remanent magnetization) during the Sterno-Etrussia geomagnetic excursion. Nonetheless, the available data covering mainly the European part of Russia, the Baltic and Barents Seas, and the Caucasus region are in favor of a 30–50% drop of the geomagnetic field during such an excursion. This effect should strengthen the fluxes of GCR in this period and, therefore, amplify the effects connected with an increase of the GCR fluxes.

At present, it is difficult to say exactly what was the reason for this excursion: whether it was a decrease of the dipole or the quadrupole component of the geomagnetic field. To establish this fact, additional investigations are needed in various regions of the world. However, in any case, regions of field drops will be over large areas and will significantly affect the integrated values of the GCR flux, having an influence on climatic changes. Another factor influencing the climate might be a shift in latitude of the geomagnetic pole during the excursion and, hence, a spatial movement of the GCR precipitation regions to low latitudes, to the Equator. According to Hagstrom et al. (2002), a virtual magnetic pole moved quickly from the New Land through Scandinavia to Greenland in

2700–2340 BP. Therefore, it was situated 10–15° south of its present location. In that period, the regions of intense GCR precipitation covered not only high latitudes but also middle latitudes and, therefore, might affect considerably the atmospheric circulation.

On the basis of paleomagnetic data, Raspopov et al. (2003) found that during this excursion, the virtual geomagnetic pole (VGP) path during 2800 to 2200 BP moved from high to low latitudes in the longitude sector from 40°E to 30°W. The excursion path reveals not only very rapid movement of the VGP during this time interval, but also a VGP excursion over a considerable distance. Figure 5 shows the virtual magnetic pole position during the excursion for 3 sites of the paleomagnetic investigations: Baltic Sea, Pichori (Caucasus), and West Siberia.

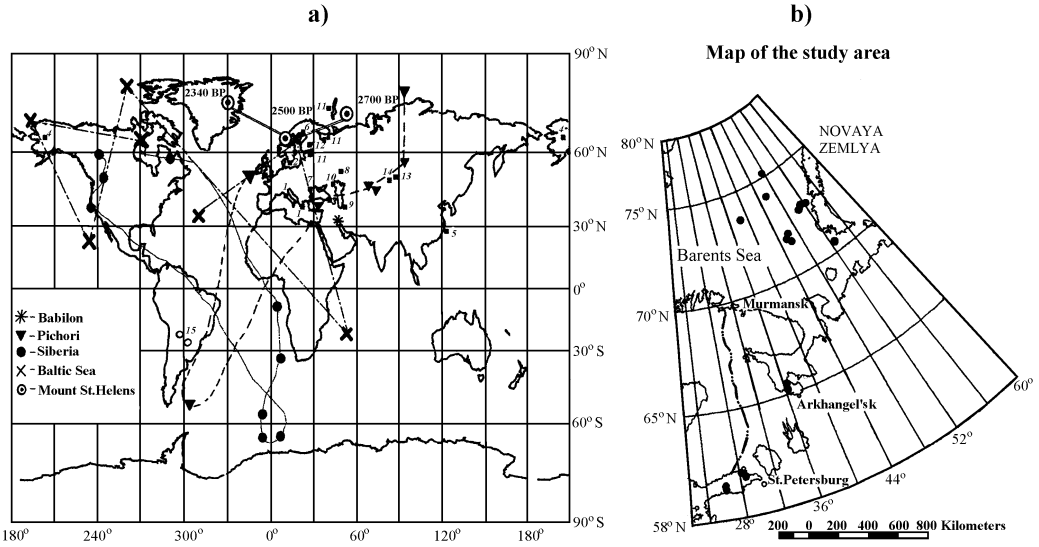

Figure 5 Map showing local sites (filled squares) of the discovered geomagnetic Sterno-Etrussia excursion and the virtual magnetic pole position during the excursion; Numbers 1–14 indicate the regions where the manifestations of the excursion were discovered. The virtual geomagnetic pole path is shown for the archaeological Pichori object (filled triangles), for continental sediments from Siberia (filled circles), and for the Baltic Sea sediments (crosses). The VGP path from 2700 BP to 2340 BP inferred from studies of volcanic sediments from the Mount St. Helens, Washington, is shown by open circles with a dot inside.

In all cases, movement of the VGP happened in the longitudinal interval from 40°E to 30°W. Are there any experimental data confirming this shift of the geomagnetic pole? Apparently, yes. Historical chronicles suggest that optical atmospheric effects similar to the auroras occurred on the latitudes of Ancient Greece and Mesopotamia, that is 30–40°N (Brekke and Egeland 1983; Siscoe et al. 2002). The appearance of auroras supports movement of the geomagnetic pole (and, therefore, the regions of intense influence of CR) to middle and low latitudes. Thus, the development of geomagnetic excursion, promoting increase of the CR fluxes in middle and low latitudes, might noticeably change the structure of atmospheric circulation, as was earlier shown on the example of SPE. First of all, there should be an increase of zonal circulation (transfer of air in the east direction), as well as an increase of precipitation amount, which was actually observed in Europe in the considered interval.

Modern data indicate that variations in cosmic rays controlled by both solar activity and geomagnetic field affect the lower atmosphere and, hence, climate parameters. All these facts show that

investigation of the events in the paleomagnetic data associated with inversions and excursions of the earth's magnetic field is of particular importance. During the reversal of the total magnetic field polarity, the magnetic moment decreases, allowing increased penetration of cosmic rays into the upper atmosphere. Global changes in the electromagnetic field of the earth result in sharp changes in the climate-forming factors in the atmosphere, such as temperatures, total pressure field, moisture circulation, intensity of air flows, and thunderstorm activity. Thus, geomagnetic excursions, which vary the configuration and value of the magnetic field, can affect climatic changes.

CONCLUSION

Sharp climate changes around 2700 BP are well expressed and well dated in a number of different proxy data. Similar events occurred every ~2400 yr, when the intensity of galactic cosmic rays was high. The analysis of paleoenvironmental and archaeological data around 2700 BP supports the idea that external forcing has played a crucial role in sharp climate change during the Holocene. Comparison of fluctuations of the cosmic ray intensity with the detailed proxy record shows that the changing solar activity is a major factor in forcing climate. The sharp shift to cooler, wetter climatic conditions around 2700 BP in the Northern Hemisphere has a parallel with the LIA, which was also related to reduced solar activity. Despite the evidence from the past, solar variability remains controversial as a source of climate change, since the underlying mechanism remains as a puzzle. Changes in solar activity estimated from the instrumental measurements are considered to be too small to cause climate variability.

At present, 3 possible mechanisms of links between solar variability and changes in climate are taken in consideration: 1) changes in total solar irradiance and its influence on the lower atmosphere; 2) changes in solar ultraviolet radiation, related ozone production, and the interaction with the stratosphere and troposphere; and 3) changes in cloud formation related to changes in cosmic ray intensity. It is particularly remarkable that cosmic rays, the flux of which is modulated by the solar wind and geomagnetic field strength, provide the sole source of ions, apart from terrestrial sources of radioisotopes. Solar modulation of cosmic ray intensity could provide an effective initial step by which an energetically weak solar signal (both irradiance and ultraviolet radiation changes are very small) is amplified into a significant climate forcing.

The analysis of paleomagnetic data shows that around 2700 BP, a short and pronounced excursion of the earth magnetic field took place. This Sterno-Etrussia excursion had caused a temporary sharp increase of cosmic ray flux, not only in the northern altitudes but also in the low and middle latitudes. The excursion was contemporaneous with a deep minimum of solar activity around 2700 BP. As a consequence, during the geomagnetic excursion, the zonal circulation and cloudiness increased and it was accompanied by cooling. Precipitation probably was strongly affected and the environmental conditions in the Northern Hemisphere were strongly influenced. The combined effect of external factors (solar activity decay, fast changes of the geomagnetic field, and related cosmic ray enhancement) around 2700 BP triggered abrupt climate change. The available evidence points to an important role of changing cosmic ray intensities in climate change.

ACKNOWLEDGEMENTS

The research was supported by the Netherlands Organisation for Scientific Research (NWO project 047.009.005) and Russian Foundation for Basic Research (project 03-05-65063).

REFERENCES

Abbott MB, Binford MW, Kelts KR. 1997. A 3500 ^{14}C yr high-resolution record of water-level changes in Lake Titicaca, Bolivia/Peru. *Quaternary Research* 47:169–80.

Barber K, Langdon P. 2001.Testing the paleoclimatic signal from peat bogs—temperature or precipitation forcing? *Abstracts, PAGES-PEPIII/ESF-HOLIVAR International Conference: Past Climate Variability Through Europe and Africa*, ECRC/CERegE. p 58–9.

Barber KE, Zolitschka B, Tarasov P, Lotter A. Forthcoming. Atlantic to Urals—the Holocene climatic record of mid-latitude Europe. In: Battarbee RW, Gasse F, editors. *Past Climate Variability Through Europe and Africa*. Dordrecht: Kluwer.

Betancourt JL, Latorre C, Rech J, Quade J, Rylander KA. 2000. A 22,000-year record of monsoonal precipitation from northern Chile's Atacama Desert. *Science* 289:1542–6.

Bond G, Showers W, Cheseby M, Lotti R, Almasi P, deMenocal P, Priore P, Cullen H, Hajdas I, Bonani G. 1997. A pervasive millennial-scale cycle in North Atlantic Holocene and glacial climates. *Science* 278: 1257–66.

Bond GC, Kromer B, Beer J, Muscheler R, Evans MN, Showers W, Hoffmann S, Lotti R, Hajdas I, Bonani G. 2001. Persistent solar influence on North Atlantic climate during the Holocene. *Science* 294:2130–6.

Brekke A, Egeland A. 1983. *The Northern Light*. Berlin, Heidelberg: Springer-Verlag. 170 p.

Brook GA, Rafter MA, Railsback LB, Sheen S-W, Lundberg J. 1999. A high-resolution proxy record of rainfall and ENSO since AD 1550 from layering in stalagmites from Anjohibe Cave, Madagascar. *The Holocene* 9:695–705.

Bryant EA, Young RW, Price DM. 1992. Evidence for Pleistocene and Holocene raised marine deposits, Sandon Point, New South Wales. *Australian Journal of Earth Sciences* 39(4):481–93.

Burakov KS, Nachasova IE, Generalov AG. 1996. Record of geomagnetic field variations in the chemical remanent magnetization of sediments of the archaeological site *Kazachka*. Abstracts. *Paleomagnetism and Magnetism of Rocks*. Moscow: Institute of Earth Physics. p 15–8. In Russian.

Burlatskaya SP, Chelidze ZA. 1987. About change of the geomagnetic field in Georgia from 3rd millennium BC to 1st millennium AD. *Physics of the Earth* 9:102–7. In Russian.

Burlatskaya SP, Chelidze ZA. 1990. The changes of geomagnetic field in Georgia during the last 1500 years BC. *Izvestiya Academii Nauk USSR, Physics of the Earth* 7:84–93. In Russian.

Christoforou P, Hameed S. Solar cycle and the Pacific "centers of action." *Geophysical Research Letters* 24: 293–6.

Curtis JH, Hodell DA, Brenner M. 1996. Climate variability on the Yucatan Peninsula (Mexico) during the past 3500 years, and implications for Maya cultural evolution. *Quaternary Research* 46(1):37–47.

Dansgaard W, Johnson SJ, Clausen HB, Dahl-Jensen D, Gundestrup NS, Hammer CU, Hvidberg CS, Steffensen JP, Sveinbjörnsdottir AE, Jouzel J, Bond G. 1993. Evidence for general instability of past climate from a 250-kyr ice-core record. *Nature* 364:218–20.

Denniston RF, González LA, Asmerom Y, Sharma RH, Reagan MK. 2000. Speleothem evidence for changes in Indian summer monsoon precipitation over the last ~2300 years. *Quaternary Research* 53:196–202.

Denton GH, Karlen W. 1973. Holocene climatic variations—their pattern and possible cause. *Quaternary Research* 3:155–205.

Dergachev VA, Chistyakov VF. 1995. Cosmogenic radiocarbon and cyclical natural processes. *Radiocarbon* 37(3):417–24.

Dergachev VA, van Geel B, Zaitseva G, Alekseev A, Chugunov K, van der Plicht J, Possnert G, Raspopov O. 2000. The earliest records of Scythians in Eurasia and sharp climatic changes around 2700 BP. In: Paraske-Vopoulos KM, editor. *Physics in Culture I*. The Solid State Physics in the Study of Cultural Heritage. Athens: Aristotle University of Thessaloniki. p 208–16.

Dimitriev AA, Lomakina EY. 1977. Cloudiness and solar X-ray emission. In: Rakipova LR, editor. *Solar Activity Effects in the Lower Atmosphere*. Leningrad: Hydrometeoizdat. p 70–5. In Russian.

Eddy E. 1976. The Maunder Minimum. *Science* 192: 1189–202.

Eiriksson J, Knudsen KL, Rytter F. 2002. North Icelandic shelf sediments: Holocene and Lateglacial record of oceanographic events. *32nd International Arctic Workshop.* 14–16 March 2002. Institute of Arctic and Alpine Research, University of Colorado, Boulder, Colorado, USA. *Program and Abstracts*. p 77–8.

Eremin VN, Shadrukhin AB, Molostovskyi EA. 1992. Holocene of north coast of Caspian Sea. *Bulletin of Moscow Society of Nature* 67(6):54–63. In Russian.

Esper J, Cook ER, Schweingruber FH. 2002. Low-frequency signals in long tree-ring chronologies for reconstructing past temperature variability. *Science* 295:2250–3.

Gnibidenko ZN, Volkova VS, Orlova LA. 2000. Climatolomagneto chronology and magnetism of Holocene deposits in upper Ob' region. In: Vaganov EA, Derevyanko AR, Zykin VS, Markin SV, editors. *Problem Reconstruction of Climate and Environment of the Holocene and Pleistocene in Siberia*. Novosibirsk: Nauka. p 110–5. In Russian.

Gracheva R, Sorokin A, Chichagova O, Tishkov A, Vanderbenghe J, Sulerzhitskyi L. 2002. Stages of paleoenvironmental change in the Upper Volga region in the Holocene. *NWO-DUT-MGU-DGU Workshop Ho-*

locene Caspian Sea Level Change, 21–22 October 2002. Delft University of Technology, Department of Applied Earth Sciences. Abstracts. p 9–10.

Guskova EG, Raspopov OM, Piskarev AL, Dergachev VA, Mörner N-A. Forthcoming. The fine structure of the geomagnetic field for the last 30,000 year on the base of Barents Sea sediments. *Geomagnetism and Aeronomy.*

Gustafsson BG, Westman R. 2002. On the causes for salinity variations in the Baltic Sea during the last 8500 years. *Paleoceanography* 17(3):1040.

Fontugne M, Usselmann P, Lavallete D, Julien M, Hatté C. 1999. El Niño variability in the coastal desert of southern Peru during the mid-Holocene. *Quaternary Research* 52:171–9.

Hagstrom JT, Hoblitt RP, Gardner CA, Gray TE. 2002. Holocene geomagnetic secular variation recorded by volcanic deposits at Mount St. Helens, Washington. *Bulletin of Volcanology* 63:545–56.

Haigh JD. 1994. The role of stratospheric ozone in modulating the solar radiative forcing of climate. *Nature* 370:544–6.

Haigh JD. 1996. The impact of solar variability on climate. *Science* 272:981–4.

Johnsen SJ, Dahl-Jensen D, Gundestrup N, Steffensen JP, Clausen HB, Miller H, Masson-Delmotte V, Sveinbjornsdottir AE, White J. 2001. Oxygen isotope and paleotemperature records from six Greenland ice-core stations: Camp Century, Dye-3, GRIP, GISP2, Renland and NorthGRIP. *Journal of Quaternary Science* 16(4):299–307.

Karpychev JuA. 1994. The periodicity of the level of the Caspian Sea on the data of radiocarbon analysis of new Caspian sediments. *Vodnye Resursy* 21(4):415–21. In Russian.

Kochegura VV. 1992. *Use the Paleomagnetic Methods for Geological Mapping of Sea Shelf*. St. Petersburg: VSEGEI. 144 p. In Russian.

Kochegura VV, Piskarev AL, Zhemchuzhnikov EG. 1999. Paleomagnetic study of the Holocene marine sediments in the Barents, White and Baltic Seas. *Abstracts of the EGS Annual Meeting, The Hague, April 1999*. p 134.

Kodama M, Kohmo T, Kanzawa H. 1992. Stratospheric sudden cooling after solar proton event over Syowa Station. *Journal of Geomagnetism and Geoelectricity* 44:361–6.

Kroonenberg SB, Abdurakhmanov GM, Badyukova EN, van der Borg K, Kasimov NS, Rychagov GI, Svitoch AA, Vonhof HB, Wesselingh FP. The 2600 BP and Little Ice Age highstands of the Caspian Sea. *NWO-DUT-MGU-DGU Workshop Holocene Caspian Sea Level Change*, 21–22 October 2002. Delft University of Technology, Department of Applied Earth Sciences. Abstracts. p 20.

Lamb HH. 1995. *Climate, History and the Modern World*. London: Methuen. 433 p.

Langdon PG, Barber KE, Hughes PDM. 2003. A 7500 year peat-based paleoclimatic reconstruction and evidence for an 1100-year cyclicity in mire surface wetness from Temple Hill Moss, Pentland Hills, southeast Scotland. *Quaternary Science Reviews* 22:259–74.

Levitan MA, Duplessy J-C, Khusid TA, Beljaev NA, Bourtman MV. 1999. Holocene sediments of the Southern Novaja Zemlya Trough (the Pechora Sea) and Brunhes history. *IMAGES*, P.P. Shirshov Institute of Oceanology RAS, Moscow. p 11–2.

Luckman BH, Holdsworth G, Osborn GD. 1993. Neoglacial glacial fluctuations on the Canadian Rockies. *Quaternary Research* 39:144–53.

Maisch M, Wipf A, Denneller B, Battaglia J, Benz C. 1999. *Die Gletscher der Schweizer Alpen. Gletscherhochstand 1850, Aktuelle Vergletscherung, Gletscherschwund-Szenarien*. Zürich: Vdf. 373 p.

Magny M. 1993a. Solar influences on Holocene climatic changes illustrated by correlations between past lake-level fluctuations and the atmospheric ^{14}C record. *Quaternary Research* 40:1–9.

Magny M. 1993b. Un cadre climatique pour les habitats lacustres préhistoriques? *Comptes Rendus de l'Academie des Sciences Paris* 316:1619–25.

Magny M. 1995. Successive oceanic and solar forcing indicated by Younger Dryas and early Holocene climatic oscillations in the Jura. *Quaternary Research* 43:279–85.

Magny M.1999. Lake level fluctuations in the Jura and French subalpine regions associated with ice-rafting in the North Atlantic and variations in the polar atmospheric circulation. *Quaternaire* 10:61–4.

Magny M. 2004. Holocene climate variability as reflected by mid-European lake-level fluctuations and its probable impact on prehistoric human settlements. *Quaternary International* 113:65–79.

Maley J, Brenac P. 1998. Vegetation dynamics, paleoenvironments and climatic changes in the forest of western Cameroon during the last 28,000 years BP. *Review of Paleobotany and Palynology* 99:157–87.

Mann ME. 2000. Climate chance—lessons for a new millennium. *Science* 289:253–54.

Marsh N, Svensmark H. 2000. Cosmic rays, clouds, and climate. *Space Science Reviews* 94:215–30.

McElhinny MW, Senenayake WE. 1982. Variations in the geomagnetic dipole–1. The past 50,000 years. *Journal Geomagnetism and Geoelectricity* 34:39–51.

McFadden LD, McAuliffe JR. 1997. Lithologically influenced geomorphic responses to Holocene climate changes in the southern Colorado Plateau, Arizona: a soil-geomorphic and ecological perspective. *Geomorphology* 19:303–32.

Moqing Z, Zongshi G. 1987. Discussion on polarity events of Brunhes normal polarity epoch in the Yellow Sea. *Marine Geology and Quaternary Geology* 7(4): 49–56.

Morinaga H, Morinaga KS, Yaskowa H. 1987. Paleo-

magnetic implication on climatic changes and evidence for excursions recorded in a sediment core from Harding Lake, Alaska. *Journal of Geomagnetism and Geoelectricity* 39(4):229–41.

Mörner N-A, Sylvan CA. 1989. Detailed paleomagnetic record for the last 6300 years from varved lake deposits in northern Sweden. In: Lowes FJ, editor. *Geomagnetism and Paleomagnetism, NATO ASI series,* Series C, Mathematical and Physical Sciences. p 63–70.

Murdmaa IA, Ivanova EV. 1999. After Ice Age sedimentation history in shelf regions of Barents Sea. *Lithology and Minerals* (*Litologiya i Poleznye Iskopaemie*) 6:576–95. In Russian.

Nachasova IE, Burakov KS, Kvirikadze MB. 1986. Paleointensity of geomagnetic field in Georgia in the first millennium BC. *Geomagnetism and Aeronomy* 23(2): 356–8. In Russian.

Nachasova IE, Burakov KS. 2002. Geomagnetic field strength in the 6th century BC–2nd century AD. *Geomagnetism and Aeronomy* 42(2):272–5.

Noel M, Tarling DH. 1975. The Laschamps geomagnetic event. *Nature* 253:705–7.

O'Brien SR, Mayewski PA, Meeker LD, Meese DA, Twickler MS, Whitlow SI. 1995. Complexity of Holocene climate as reconstructed from a Greenland ice core. *Science* 270:1962–4

Pallé Bagó E, Butler CJ. 2000. The influence of cosmic rays on terrestrial clouds and global warming. *Astronomy & Geophysics* 40(4):418–22.

Polyak VJ, Asmerom Y. 2001. Late Holocene climate and cultural changes in the southwestern United States. *Science* 294:148–51.

Pudovkin MI, Babushkina SV. 1992a. Atmospheric transparency variations associated with geomagnetic disturbances. *Journal of Atmospheric and Terrestrial Physics* 54:1135–8.

Pudovkin MI, Babushkina SV. 1992b. Influence of solar flares and disturbances of the interplanetary medium on the atmospheric circulation. *Journal of Atmospheric and Terrestrial Physics* 54:841–6.

Pudovkin MI, Raspopov OM. 1992. The mechanism of action of solar activity on the state of lower atmosphere and meteorological parameters. *Geomagnetism and Aeronomy* 32:593–608. English edition.

Pudovkin MI, Veretenenko SV. 1995. Cloudiness decreases associated with Forbush decreases of galactic cosmic rays. *Journal of Atmospheric and Solar-Terrestrial Physics* 75:1349–56.

Ransom CJ. 1973. Magnetism and archaeology. *Nature* 242:218–9.

Renssen H, van Geel B, van der Plicht J, Magny M. 2000. Reduced solar activity as a trigger for the start of the Younger Dryas? *Quaternary International* 68–71: 373–83.

Raspopov O, Shumilov O, Kochegura V, Dergachev V, van Geel B, van der Plicht J, Renssen H, Maley J. 1998. Dendrochronological and other proxy evidence for climatic cooling around 2700 BP and its heliogeophysical forcing. In: Stravinskiene V, Juknys R, editors. *Proceedings of the International Conference "Dendrochronology and Environmental Trends."* 17–21 June 1998, Kaynas, Lithuania, Vytautas Magnus University, Kaunas. p 113–23.

Raspopov OM, Shumilov OI, Dergachev VA, van Geel B, Mörner N-A, van der Plicht J, Renssen H. 2000. Abrupt climate change around 2700–2800 years BP as example of existence of 2400 year periodicity in solar activity and solar variability. *Proceedings of 1st Solar & Space Weather Euro-Conference, "The Solar Cycle and Terrestrial Climate,"* Santa Cruz de Tenerife, Spain, 25–29 September 2000 (ESA SP-463, December 2000). p 513–16.

Raspopov Oleg M, Dergachev Valentin A, Goos'kova Elena G. 2003. Ezekiel's vision: visual evidence of Sterno-Etrussia geomagnetic excursion? *EOS, Transactions, American Geophysical Union* 84(9) March: 77.

Riedinger M, Steinitz-Kannan M, Last W, Brenne M. 2002. A ~6100 ^{14}C record of El Niño activity from the Galapagos Islands. *Journal of Paleolimnology* 27:1–7.

Rothlisberger F. 1986. *10,000 Jahre Gletscher-geschichte der Erde*. Aarau: Verlag Sauerlande. 384 p.

Rychagov GI. 1997. Holocene oscillations of the Caspian Sea, and forecasts based on paleogeographical reconstructions. *Quaternary International* 41–42:167–72.

Saarinen TJ. 1994. Paleomagnetic study of the Holocene sediments of Lake Päijänne (Central Finland) and Lake Paanjarvi (North-West Russia). *Bulletin of the Geological-Survey of Finland* nr 376. 88 p.

Sandweiss D H, Maasch KA, Burger RL, Richardson III JB, Rollins HB, Clement A. 2001. Variation in Holocene El Niño frequencies: climate records and cultural consequences in ancient Peru. *Geology* 29(7): 603–6.

Sauchyn MA, Sauchyn DJ. 1991. A continuous record of Holocene pollen from Harris Lake, southwestern Saskatchewan, Canada. *Palaeogeography, Palaeoclimatology, Palaeoecology* 88:13–23.

Schilman B, Bar-Matthews M, Almogi-Labin A, Luz B. 2001. Global climate instability reflected by eastern Mediterranean marine records during the Late Holocene. *Palaeogeography, Palaeoclimatology, Palaeoecology* 176(1–4):157–76.

Scott L, Lee-Thorp JA. Forthcoming. Holocene climatic trends and rhythms in southern Africa. In: Battarbee RW, Gasse F, editors. *Past Climate Variability Through Europe and Africa*. Dordrecht: Kluwer.

Shumilov OI, Henriksen K, Raspopov OM, Kasatkina EA. 1992. Arctic ozone abundance and solar proton events. *Geophysical Research Letters* 19:1647–50.

Shumilov OI, Kasatkina EA, Henriksen K, Raspopov OM. 1995. Ozone "mini-holes" initiated by energetic solar protons. *Journal of Atmospheric and Terrestrial*

Physics 57:665–71.

Siscoe GL, Silverman SM, Siebert. 2002. Ezekiel and the northern lights: biblical aurora seems plausible. *EOS Transaction, American Geophysical Union* 83(16): 173, 179.

Speranza A, van Geel B, van der Plicht J. 2002. Evidence for solar forcing of climate change at ca. 850 cal BC from a Czech peat sequence. *Global and Planetary Change* 35:51–65.

Stephenson LAE, Scourfield MWJ. 1992. Ozone depletion over the polar cap caused by solar protons *Geophysical Research Letters* 19:2425–8.

Stozhkov YI, Zullo J, Martin Jr IM, Pellegrino GQ, Pinto HS, Bezerra PC, Bazilevskaya GA, Machmutov VS, Svirzevskii NS, Turtelli Jr A. 1995. Rainfalls during great forbush-decreases *Nuovo Cimento C* 18:335–41.

Stötter J, Wastl M, Caseldine C, Häberle T. 1999. Holocene paleoclimatic reconstruction in Northern Iceland: approaches and results. *Quaternary Science Reviews* 18:457–74.

Stuiver M, Reimer PJ, Braziunas TF. 1998. High-precision radiocarbon age calibration for terrestrial and marine samples. *Radiocarbon* 40(3):1127–52.

Suleimanova FI. 1987. The fine structure of the geomagnetic field in Quaternary deposits on pre-Ural region. In: Sidorov A, editor. *Paleomagnetism in Geology.* Magadan: SVKNIIDVNTS. p 5–14. In Russian.

Svensmark H, Friis-Christensen E. 1997. Variation in cosmic ray flux and global cloud coverage—a missing link in solar-climate relationships? *Journal of Atmospheric and Solar-Terrestrial Physics* 59:1225–32.

Tinner W, Lotter A, Ammann B, Conedera M, Hubschmid P, van Leeuwen JFN, Wehrli M. 2003. Climatic change and contemporaneous land-use phases north and south of the Alps 2300 BC to AD 800. *Quaternary Science Reviews* 22:1447–60.

Tinsley BA, Dean GW. 1991. Apparent tropospheric response to MeV-GeV particle flux variations: a connection via the solar wind, atmospheric electricity and cloud microphysics. *Journal of Geophysical Research* 96:22,283–96.

Tinsley BA. 1988. The solar cycle and the QBO influence on the latitude of storm tracks in the North Atlantic. *Geophysical Research Letters* 15:409–12.

Tretjak AN, Vigilyanskaya LI, Makarenko VN, Dudkin VP. 1989. *Fine Structure of the Geomagnetic Field in the Late Cenozoic*. Kiev: Naukova Dumka. 156 p. In Russian.

Trubikhin VM, Bagin VI, Gender TS, Nechaeva TB, Fein AG. 1991. About the reality of the paleomagnetic record on takyrs. *Abstracts of the IV All-State Meeting for Geomagnetism,* Moscow, Part II. p 49–50. In Russian.

van Geel B, Buurman J, Waterbolk HT. 1996. Archaeological and paleoecological indications of an abrupt climate change in the Netherlands, and evidence for climatological teleconnections around 2650 BP. *Journal of Quaternary Science* 11(6):451–60.

van Geel B, van der Plicht J, Kilian MR, Klaver ER, Kouwenberg HM, Renssen H, Reynaud-Farrera I, Waterbolk HT. 1998a. The sharp rise of $\Delta^{14}C$ ca. 800 cal BC: possible causes, related climatic teleconnections and the impact on human environments. *Radiocarbon* 40(1):535–50.

van Geel B, Raspopov OM, van der Plicht J, Renssen H. 1998b. Solar forcing of abrupt climate change around 850 calendar years BC. In: Peiser BJ, Palmer T, Bailey ME, editors. *Natural Catastrophes During Bronze Age Civilizations.* BAR International Series 728:162–8.

van Geel B, Raspopov OM, Renssen H, van der Plicht J, Dergachev VA, Meijer HAJ. 1999. The role of solar forcing upon climate change. *Quaternary Science Reviews* 18(3):331–8.

van Geel B, Renssen H. 1998. Abrupt climate change around 2650 BP in northwest Europe: evidence for climatic teleconnections and a tentative explanation. In: Issar AS, Brown N, editors. *Water, Environment and Society in Times of Climatic Change.* Dordrecht: Kluwer. p 21–41.

Vasiliev SS, Dergachev VA, Chistyakov VF. 1997. ~2400-year cycle detection in natural radiocarbon level in the atmosphere and the sensitivity of human behavior to the large-scale climatic changes. *Radiocarbon and Archaeology*, St. Petersburg, Institute of the History of Material Culture nr 2:13–35. In Russian.

Vasiliev SS, Dergachev VA. 2002. The ~ 2400-year cycle in atmospheric radiocarbon concentration: bispectrum of ^{14}C data over the last 8000 years. *Annales Geophysicae* 20:115–20.

Veretenenko SV, Pudovkin MI. 1993. Effects of cosmic ray variations on atmospheric circulation. *Geomagnetism and Aeronomy* 33:35–49. In Russian.

Waple AM, Mann ME, Bradly RS. 2002. Long-term patterns of solar irradiance forcing in model experiments and proxy based surface temperature reconstruction. *Climate Dynamics* 18:563–78.

Wastl M, Stötter J, Caseldine C. 2001. Reconstruction of Holocene variations of the upper limit of tree or shrub birch growth in northern Iceland based on evidence from Vesturárdalur-Skíðadalur, Tröllaskagi. *Arctic, Antarctic, and Alpine Research* 33(2):191–203.

Wilkins DE, Currey DR. 1997. Timing and extent of late Quaternary paleolakes in the Trans-Pecos closed basin, west Texas and southcentral New Mexico. *Quaternary Research* 47:306–15.

Wilson SE, Smol JP, Sauchyn DJ. 1997. A Holocene paleosalinity diatom record from southwestern Saskatchewan: Harris Lake revisited. *Journal of Paleolimnology* 17(1):23–31.

Yang S, Odah H, Shaw J. 2000. Variations in the geomagnetic dipole moment over the last 12,000 years. *Geophysical Journal of Interior* 140:158–62.

RADIOCARBON, Vol 46, Nr 2, 2004, p 683–690

THE COSMIC RAY INCREASES AT 35 AND 60 KYR BP

V Florinski[1] • W I Axford[2] • G P Zank[3]

Institute of Geophysics and Planetary Physics, University of California, Riverside, California 92521, USA.

ABSTRACT. Concentrations of ^{10}Be in ice cores and marine sediments exhibit 2 peaks with significant enhancements at 35,000 and 60,000 BP. This radioisotope is produced in the upper atmosphere by spallation of cosmic-ray protons and secondary neutrons on atmospheric nitrogen and oxygen. Previously suggested explanations for the increases include geomagnetic field reversals, a decrease in solar activity, and a supernova explosion. We propose an alternative explanation which involves a change in the galactic environment of the solar system. The structure of the heliosphere is investigated for a period when the Sun enters a cold, dense, unmagnetized interstellar cloud. Under these conditions, the heliosphere contracts to 25% its present size, significantly affecting galactic cosmic ray modulation and increasing anomalous cosmic ray fluxes. A tenfold increase in anomalous cosmic ray flux and a twofold increase in galactic cosmic ray intensity at Earth are possible in this high-density case if heliosheath modulation is reduced. We show that this increase in galactic cosmic ray intensity could be responsible for the peaks in ^{10}Be records.

INTRODUCTION

Paleoisotope records from ice cores and deep-sea sediments offer valuable information about the intensity of cosmic rays fluxes at the top of Earth's atmosphere over tens of thousands of years. A well-publicized feature of the ^{10}Be record is 2 prominent peaks at 35,000–40,000 and 60,000–65,000 BP, first discovered in Antarctic ice cores (Raisbeck et al. 1987). The more recent peak was also detected in ice cores from Greenland (Wagner et al. 2000) and marine sediments (Cini Castagnoli et al. 1995; McHargue et al. 1995; Robinson et al. 1995; Cini Castagnoli et al. 1998). The second peak was also found in sea sediments (McHargue et al. 2000). The duration of the enhanced intensity is of the order of 2 kyr.

^{10}Be is a cosmogenic isotope produced in Earth's upper atmosphere by nuclear reactions of cosmic-ray particles with atmospheric nitrogen and oxygen. Cross-section analysis indicates an energy threshold of 50 MeV for protons. However, the bulk of the production is from secondary neutrons with energies above 10 MeV, produced in atmospheric cascades from primary cosmic rays (Masarik and Beer 1999). The rate of production strongly depends on geomagnetic latitude because Earth's magnetic field prevents lower energy charged particles from reaching the atmosphere.

The global occurrence of the peaks points to the increased production rate and, therefore, an enhanced cosmic-ray flux at the top of the atmosphere, as the cause. Several hypotheses have been suggested to explain the increases in production. The most popular current explanation is that they are caused by geomagnetic field excursions, or incomplete reversals (McHargue et al. 2000; Wagner et al. 2000), when the field intensity was only 10–20% of its present value. The 35 kyr peak (possibly a double peak) appears to correlate with the Mono Lake and Laschamps geomagnetic excursions (Laj et al. 2002). However, the results of Cini Castagnoli et al. (1998) appear to contradict the geomagnetic hypothesis because ^{10}Be in Mediterranean sea sediments starts to increase about 2000 yr *before* the drop in magnetization measured in the same core sample.

The geomagnetic hypothesis largely relies on the assumption that ^{10}Be is distributed evenly across the globe rather than being precipitated locally, i.e., at the latitude it was produced. Latitudinal mix-

[1]Corresponding author. Email: vflorins@citrus.ucr.edu.
[2]Email: ian@axford.org.
[3]Email: zank@ucrac1.ucr.edu.

Proceedings of the 18th International Radiocarbon Conference, edited by N Beavan Athfield and R J Sparks
RADIOCARBON, Vol 46, Nr 2, 2004, p 683–690

ing in the stratosphere, where the isotope spends about a year on average before being deposited, determines whether or not polar ^{10}Be will be sensitive to geomagnetic variations (Beer 2000). Measurements performed in the Northern (Brown et al. 1989) and Southern (Graham et al. 2003) Hemispheres at similar latitudes (~40°) but different longitudes show similar deposition rates, which could imply that mixing is taking place at mid-latitudes. Still, there is no consensus as to whether ^{10}Be deposited near the poles is derived from lower latitudes, and supporting experimental evidence both for (Beer et al. 1990) and to the contrary (Steig et al. 1996) is available.

Several alternative hypotheses have been proposed to explain the peaks. A prolonged decrease in solar activity (i.e. a "Maunder Minimum" lasting 2 millennia) could have caused a reduction in the heliospheric modulation of galactic cosmic rays (GCR). This scenario is considered unlikely in view of the absence of any evidence for such extended periods of negligible solar activity (see Sonett et al. 1987). Another hypothesis involves the interaction of a supernova blast wave with the solar system, carrying with it an increase in shock-accelerated protons (Sonett et al. 1987; Kocharov 1994). The Geminga pulsar at a distance of 160 pc has been suggested as a remnant of the supernova that caused the anomalies (Ramadurai 1995; Ellis et al. 1996). Axford (1981) estimated that the upper limit on the rate of supernova shock passage of any given point in space is only about 4×10^{-7} yr^{-1} for shocks that are capable of producing a twofold increase in GCR pressure. The actual rate will be smaller owing to shock deceleration by the cosmic-ray pressure. It is also worth noting that the concept of a recent nearby supernova explosion contradicts the theory of the origin of the "Local Bubble," where the latter is produced by a sequence of supernova explosions at a much earlier time (Smith and Cox 2001).

A further hypothesis was put forward by Zank and Frisch (1999). They suggested that the solar system may have passed through a relatively small (0.05 parsec), dense molecular cloud, causing the heliosphere to shrink. Binary star system observations show that dense clouds possess structure on scales at and below 0.05 pc, although the data available is not yet sufficient to construct a distribution of these small clouds (Lauroesch and Meyer 1999). Zank and Frisch (1999) estimated that the Sun may enter a region with a higher hydrogen density in 10^4 to 10^6 yr. They also argued that such a condition would result in a decrease of GCR modulation and an increase in anomalous cosmic ray (ACR) flux at Earth. Nevertheless, it remains to be seen to what extent this change in the solar environment could affect ^{10}Be production rates. Here, we calculate the global structure of the heliosphere, including the location of the 3 major discontinuities and the pickup ion intensities, and use this data to estimate the change in cosmic-ray intensities at Earth.

DESCRIPTIVE BACKGROUND

As the solar wind collides with the interstellar plasma flowing past the solar system, an interface is formed consisting of 2 shocks and a contact discontinuity, the heliopause, separating the plasmas. The region inside the heliopause, the heliosphere, is filled with a highly irregular and turbulent magnetic field of solar origin, providing an obstacle for galactic cosmic ray propagation. The process (modulation) is a combination of drift, diffusion, and cooling, or acceleration of the energetic particles in the solar wind region inside the termination shock (TS), and in the heliosheath between the TS and the heliopause. As shown in Florinski et al. (2003), at least half of the total amount of GCR modulation occurs in the heliosheath. Present heliospheric models place the TS at about 90–100 AU from the Sun and the heliopause at about 150 AU in the upwind direction, based on the observed properties of the local interstellar medium (Frisch 2000). The termination shock is also a source of anomalous cosmic rays which are accelerated to tens of MeV per nucleon from a pool of pre-energized pickup ions (see Fichtner 2001 for a review).

In order to estimate GCR modulation in the high-density cloud, we must self-consistently calculate the structure of the heliosphere. We assume the interstellar cloud to have a number density of 8.5 cm^{-3}, which is 40 times that of the total number density of the Local Cloud presently surrounding the solar system (Frish 2000; Lallement 2001). Because of its high density, the cloud is expected to be cold, with a temperature of only 200 K, in order to be in pressure equilibrium with the surrounding warm interstellar medium. This implies that the cloud consists primarily of neutral hydrogen atoms and molecules, i.e., its degree of ionization is close to zero. We chose the relative velocity between the cloud and the solar system to be equal to the Local Cloud velocity of 25 km/s.

Interstellar atoms have a profound effect on the structure of the heliosphere (see Zank 1999 for a review). Atoms can exchange electrons with solar wind ions, producing a new population of ions (pickup ions) and atoms. Because interstellar atoms tend to be less energetic than the solar wind ions, the solar wind loses energy and decelerates. This results in a significant (30–40%) reduction of the distances to the heliospheric boundaries. In the high-density cloud with the LISM neutral hydrogen density some 50 times higher than at present and with no ionized LISM component, one could expect that the solar wind would be drastically decelerated by charge-exchange momentum removal and not undergo a termination shock transition. However, as we show below, pickup ions produced as a result of charge exchange and photoionization provide the missing confining pressure, ensuring that a shock transition still occurs. Moreover, neutral filtration in the outer heliosphere, similar to that predicted by heliospheric models (Baranov and Malama 1993; Pauls et al. 1995; Zank et al. 1996; Fahr et al. 2000), is expected to reduce the density of neutral hydrogen atoms reaching the inner heliosphere.

We use a two-fluid (plasma + neutral) model to describe the flow of partially ionized gas in and around the heliosphere. The present model is based on the work of Florinski et al. (2003) and includes charge exchange and photoionization processes. To estimate the effect of the changed size of the heliosphere on GCR modulation and ACR production, we use a simple one-dimensional model and solve the Parker transport equation for the phase space density $f(r,p)$ using spherical symmetry (p is the particle momentum). We emphasize that the simple spherical model is used only to explore cosmic-ray intensities at 1 AU in a heliosphere that is much smaller in size than at present, rather than to perform a detailed calculation of cosmic-ray density at all heliocentric distances and latitudes. To accomplish the latter, a more detailed model, including the magnetic field geometry and drift effects, should be used (e.g. Jokipii et al. 1993; Steenberg and Moraal 1996).

RESULTS AND DISCUSSION

Figure 1 shows the number density and plasma streamlines in the heliosphere submersed in a high-density interstellar cloud. This result was obtained with a two-fluid plasma-neutral model, taking into account charge exchange and photoionization (Florinski et al. 2003). A similar calculation was performed by Scherer et al. (2002) for a partially ionized cloud with a density 3 times smaller. Our results differ in a significant way from those of Scherer et al. (2002) owing to a difference in our treatment of cosmic-ray propagation.

The heliospheric interface in Figure 1 contains 2 shocks and the heliopause, visible as a surface separating the solar and the interstellar streams. The TS inside the heliopause is greatly elongated in the tailward direction. The heliopause is located at a distance of only 31 AU in the upwind direction, while the bow shock (visible outside the heliopause) is located at 40 AU upstream. Inside the TS, the number density of H atoms decreases monotonically with decreasing heliocentric distance. The neutral hydrogen density inside the TS may be fitted by a power law, such that $n_H = n_{H0}(r/r_0)^b$ with

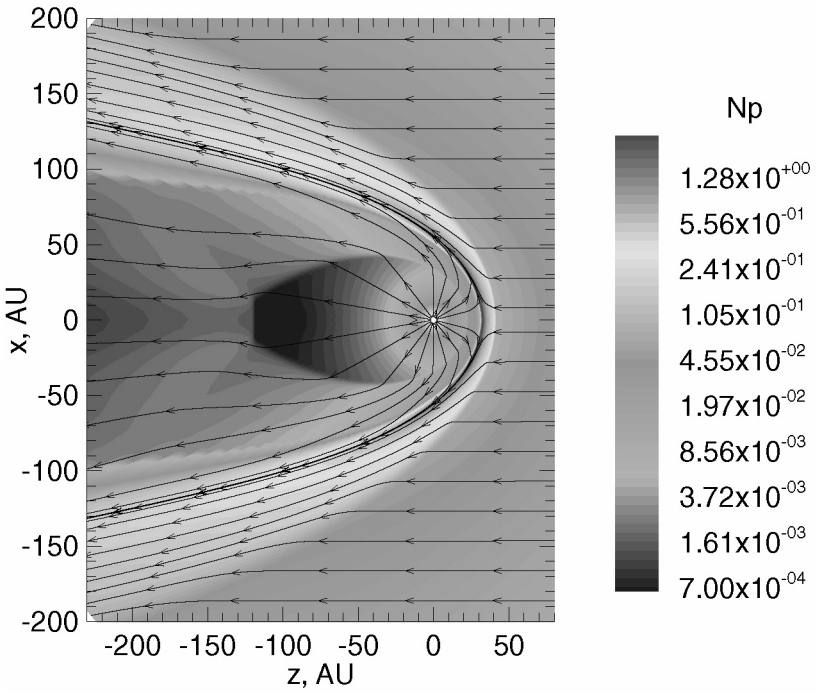

Figure 1 Plasma density (logarithmic scale) and streamlines showing the heliospheric interface in a dense interstellar cloud.

$n_{H0} = 3 \times 10^{-3}$ cm^{-3} and $b = 1.7$. Such a rapid density decrease is caused by a strong deflection of H atoms by the hydrogen wall interaction region between the heliopause and the bow shock, effectively excluding the neutrals from the inner heliosphere. The termination shock is located at 23 AU upwind, 33 AU in the crosswind direction, and at 120 AU in the tail. The solar wind is decelerated from 508 km/s at the inner boundary (1 AU) to 400 km/s just before the TS along the symmetry axis. Our results differ from previous work of Zank and Frisch (1999) in that we did not obtain a highly unsteady solution shown in their work. We also do not observe the twofold decrease in the wind speed as suggested by Scherer et al. (2002). Note that the termination shock in our model is relatively weak as a result of pickup ion heating, with a compression ratio of 3.1 in the upwind direction.

The Parker transport equation for the cosmic-ray phase space density $f(r,p)$ is solved numerically for a radial diffusion coefficient of the form

$$\kappa_{rr} = \kappa_0 \frac{w}{c}\left(\frac{p}{p_0}\right)^{\alpha} \frac{r}{r_0}\left[1 + \left(\frac{r_1}{r} - 1\right)H(r - r_1)\right][1 - (1 - s)H(r - r_s)] \quad (1),$$

where p_0 corresponds to 1 GV rigidity, $r_0 = 1$ AU, w is the particle speed, r_s is the distance to the shock, and H is the Heavyside step function. The radial dependence implies that diffusion increases linearly as a function of r at small heliocentric distances but becomes independent of r beyond r_1. Such a radial dependence may be expected if pickup ion-driven turbulence is present at sufficient levels to compensate for the expansion (Zank et al. 1998). We use $\kappa_0 = 2.2 \times 10^{22}$ cm$^2 s^{-1}$, $\alpha = 1.1$, $r_1 = 19$ AU, and $s = 0.14$ for the present heliosphere. For the high-density case, we reduce the size of the simulation domain by a factor of 4. The small diffusion downstream of the shock simulates the effect of the "modulation wall" bordering the heliopause (Florinski et al. 2003). When used in a

spherical model, the parameters above allow for modeling of the observed ACR (Cummings et al. 2002) and GCR (McDonald 1998) solar minimum fluxes with a reasonable degree of accuracy.

Because of a higher neutral density inside the TS, we would expect elevated turbulence levels and, hence, a reduced diffusion coefficient in the inner heliosphere. To estimate this reduction, we use an incompressible spherically-symmetric MHD turbulence model of Zank et al. (1998) to calculate turbulence generation by pickup ion instabilities. The pickup ion number density n_i may be found from the expression for n_H given above as

$$n_i = \frac{n_{H0} n_{p0} \sigma r_0^{2-b} r^{b-1}}{b+1} \quad (2),$$

where $n_{p0} = 5$ cm^{-3} is the solar wind density at 1 AU and $\sigma = 2.4 \times 10^{-15}$ cm^2 is the cross-section for charge exchange. Our calculations of the turbulent energy density show that it is a factor of 2 to 4 greater in the high-density case than at present. To model the effect of reduced diffusion, we decrease the value of r_1 in Equation 1 to 5 AU for anomalous cosmic rays. However, we leave the diffusion coefficient for the galactic cosmic rays unchanged because this highly energetic population is not likely to be strongly affected by small-scale PUI turbulence. Equation 2 yields $n_i = 1.8 \times 10^{-3}$ cm^{-3} at the TS, which is approximately 20 times that calculated by Fahr et al. (2000) for the present heliosphere. Because the production rate of ACRs is directly proportional to the rate of injection of PUI into the diffusive shock acceleration process, which, in turn, is expected to be proportional to the PUI fluxes through the shock, we increase the injection rate by the same factor of 20.

Figure 2a compares GCR intensities for a high-density cloud and present-day conditions, while Figure 2b shows ACR intensities. The left panel of Figure 2a refers to the present heliosphere with a termination shock at 90 AU and the external boundary at 150 AU, while the right panel shows intensities for a high-density case with a shock at 23 AU and the boundary at 31 AU. This plot demonstrates an intensity enhancement by a factor of 1.5–4 between 100 MeV and 1 GeV (particles which are likely to have the greatest impact on ^{10}Be production) compared with the present heliosphere. This increase is mostly a consequence of the reduced thickness of the "modulation wall," which can be seen by comparing spectra at the termination shock for the 2 cases. Increased GCR intensity implies that ^{10}Be production rates would also increase by the same amount, which is sufficient to explain the peaks. Note that Scherer et al. (2002) calculated a similar GCR enhancement, but without including heliosheath modulation. In their case, the increase was caused by a reduction of the size of the modulation region under the assumption that the diffusion coefficient was nearly independent of radial distance, which is difficult to justify in view of a relatively rapid ($\sim r$ or faster) increase in the particle gyroradius with heliocentric distance.

Anomalous cosmic ray intensities are shown in Figure 2b. In the left panel, corresponding to the present heliosphere, the shock compression ratio was taken to be 3.5 (Florinski et al. 2003).The spectrum shown in the right panel is steeper at lower energy because of the reduced shock compression ratio. The 1 AU intensity at 100 MeV is increased by a factor of 10. Nevertheless, it remains below the GCR intensity shown in the right panel of Figure 2a, especially at higher energies, implying that ACR will have only a small contribution to ^{10}Be production. This result formally agrees with that of Scherer et al. (2002). However, these authors used the same ACR spectra at the TS and diffusion coefficients to obtain both high- and low-density results, in contrast to our analysis.

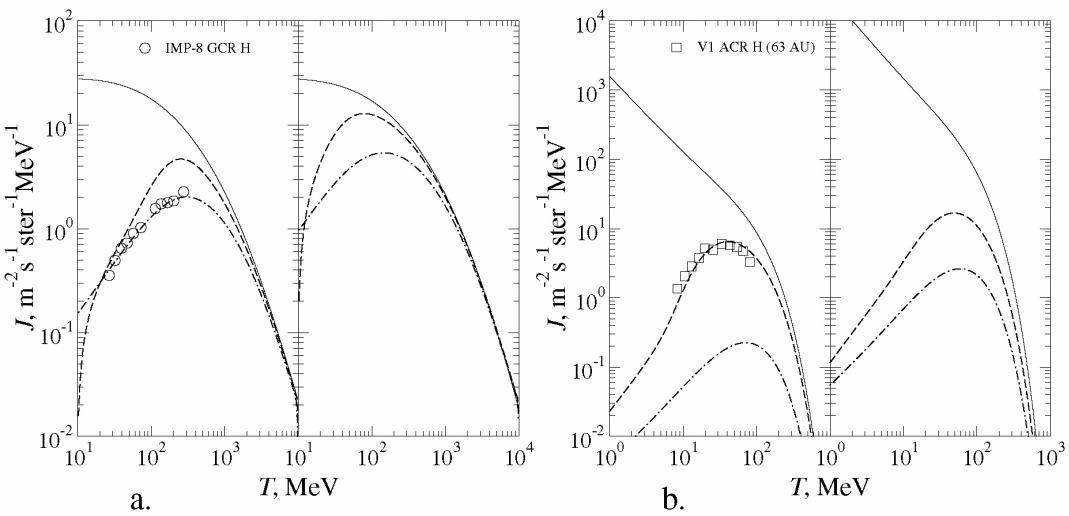

Figure 2 (a) Left panel: present-day GCR intensities at the heliopause (solid line), termination shock (dashed) and Earth (dash-dotted). Right panel: same for the high-density case with the shock at 23 AU and the heliopause at 31 AU. Circles show IMP-8 data from McDonald (1998); (b) Left panel: current anomalous hydrogen intensities at the TS (solid line), 63 AU (dashed) and Earth (dash-dotted). Right panel: same for the high-density case. The dashed line is the intensity at 10 AU. Squares show Voyager 1 data from Cummings et al. (2002).

CONCLUSION

We have examined the possibility of enhancements in cosmic-ray proton fluxes during Earth's history caused by the passage of the solar system through relatively small molecular clouds with a density some 40 times higher than the LISM today. We found that the size of the heliosphere is reduced by a factor of about 4–5 compared to its present state, and that the neutral hydrogen density is increased by a factor of 7 at the termination shock located at 23 AU. Our calculations of anomalous cosmic-ray distribution show a tenfold intensity increase compared to the present heliosphere. Nevertheless, these particles are not very likely to be present in sufficiently high numbers at above the threshold energy for ^{10}Be production. Due to a limitation of our model, we did not consider the possibility of a strongly modified turbulent shock, which requires further investigation. We also found that galactic cosmic ray intensities may be enhanced by a factor of 1.5 to 4 between 100 MeV and 1 GeV. This conclusion depends critically on the amount of modulation inside the "modulation wall" region. The calculated increase in cosmic-ray fluxes at Earth under the conditions inside a dense interstellar cloud is sufficient to explain the twofold increases in ^{10}Be production rate in the past.

ACKNOWLEDGEMENTS

V Florinski and G P Zank acknowledge the support by NSF grant ATM-0296114 and NASA grants NAG5-11621 and NAG5-12903. W I Axford was supported by a Regents Professor appointment at the UC Riverside. Numerical computations were performed on the IGPP/UCR "Lupin" cluster.

REFERENCES

Axford WI. 1981. Acceleration of cosmic rays by shock waves. *Proceedings of the 17th International Cosmic Ray Conference (Paris)* 12:155–204.

Baranov VB, Malama YG. 1993. Model of the solar wind interaction with the local interstellar medium: numerical solution of self-consistent problem. *Journal of Geophysical Research* 98:15,157–63.

Beer J. 2000. Long-term indirect indices of solar variability. *Space Science Reviews* 94:53–66.

Beer J, Blinov A, Bonani G, Finkel RC, Hofmann HJ, Lehmann B, Oeschger H, Sigg A, Schwander J, Staffelback T, Stauffer B, Suter M, Wölfli W. 1990. Use of ^{10}Be in polar ice to trace the 11-year cycle of solar activity. *Nature* 347:164–6.

Brown L, Stensland GJ, Klein J, Middleton R. 1989. Atmospheric deposition of ^{7}Be and ^{10}Be. *Geochimica et Cosmochimica Acta* 53:135–42.

Cini Castagnoli G, Albrecht A, Beer J, Bonino G, Shen C, Callegari E, Taricco C, Dittrich-Hannen B, Kubik P, Suter M, Zhu GM. 1995. Evidence for enhanced ^{10}Be deposition in Mediterranean sediments 35 kyr BP. *Geophysical Research Letters* 22:707–10.

Cini Castagnoli G, Bonino G, Taricco C, Lehman B. 1998. Cosmogenic isotopes and geomagnetic signals in a Mediterranean sea sediment at 35,000 yr BP. *Il Nuovo Cimento* 21:243–6.

Cummings AC, Stone EC, Steenberg CD. 2002. Composition of anomalous cosmic rays and other heliospheric ions. *Astrophysical Journal* 578:194–210.

Ellis J, Fields BD, Schramm DN. 1996. Geological isotope anomalies as signatures of nearby supernovae. *Astrophysical Journal* 470:1227–36.

Fahr HJ, Kausch T, Scherer H. 2000. A 5-fluid hydrodynamic approach to model the solar system—interstellar medium interaction. *Astronomy and Astrophysics* 357:268–82.

Fichtner H. 2001. Anomalous cosmic rays: messengers from the outer heliosphere. *Space Science Reviews* 95: 639–754.

Florinski V, Zank GP, Pogorelov NV. 2003. Galactic cosmic ray transport in the global heliosphere. *Journal of Geophysical Research* 108:1228.

Frisch PC. 2000. The galactic environment of the Sun. *Journal of Geophysical Research* 105:10,279–89.

Graham I, Ditchburn R, Barry B. 2003. Atmospheric deposition of ^{7}Be and ^{10}Be in New Zealand rain (1996–98). *Geochimica et Cosmochimica Acta* 67: 361–73.

Jokipii JR, Kota J, Merenyi E. 1993. The gradient of galactic cosmic rays at the solar-wind termination shock. *Astrophysical Journal* 405:782–6.

Kocharov GE. 1994. On the origin of cosmic rays. *Astrophysical Letters and Communications* 29:227–32.

Laj C, Kissel C, Scao V, Beer J, Thomas DM, Guillou H, Muscheler R, Wagner G. 2002. Geomagnetic intensity and inclination variations at Hawaii for the past 98 kyr from core SOH-4 (Big Island): a new study and a comparison with existing contemporary data. *Physics of the Earth and Planetary Interiors* 129:205–43.

Lallement R. 2001. Heliopause and asteropauses. *Astrophysics and Space Science* 277:205–17.

Lauroesch JT, Meyer DM. 1999. Observations of small-scale interstellar structure in dense atomic gas. *Astrophysical Journal* 519:L181–L184.

Masarik J, Beer J. 1999. Simulation of particle fluxes and cosmogenic nuclide production in the earth's atmosphere. *Journal of Geophysical Research* 104:12,099–111.

McDonald FB. 1998. Cosmic-ray modulation in the heliosphere—a phenomenological study. *Space Science Reviews* 83:33–50.

McHargue LR, Damon PE, Donahue DJ. 1995. Enhanced cosmic-ray production of ^{10}Be coincident with Mono Lake and Laschamp geomagnetic excursions. *Geophysical Research Letters* 22:659–722.

McHargue LR, Donahue DJ, Damon PE, Sonett CP, Biddulph D, Burr G. 2000. Geomagnetic modulation of the late Pleistocene cosmic-ray flux as determined by ^{10}Be from Blake Outer Ridge marine sediments. *Nuclear Instruments and Methods in Physics Research Section B* 172:555–61.

Pauls HL, Zank GP, Williams LL. 1995. Interaction of the solar wind with the local interstellar medium. *Journal of Geophysical Research* 100:21,595–604.

Raisbeck GM, Yiou F, Bourles D, Lorius C, Jouzel J, Barkov NI. 1987. Evidence for two intervals of enhanced ^{10}Be deposition in Antarctic ice during the last glacial period. *Nature* 326:273–7.

Ramadurai S. 1995. Very long time variations of the cosmic ray intensity and their origin. *Advances in Space Research* 15(1):41–8.

Robinson C, Raisbeck GM, Yiou F, Lehman B, Laj C. 1995. The relationship between ^{10}Be and geomagnetic field strength records in central North Atlantic sediments during the last 80 ka. *Earth and Planetary Science Letters* 136:551–7.

Scherer K, Fichtner H, Stawicki O. 2002. Shielded by the wind: the influence of the interstellar medium on the environment of Earth. *Journal of Atmospheric and Solar-Terrestrial Physics* 64:795–804.

Smith RK, Cox DP. 2001. Multiple supernova remnant models of the Local Bubble and the soft X-ray background. *Astrophysical Journal Supplement Series* 134:283–309.

Sonett CP, Morfill GE, Jokipii JR. 1987. Interstellar shock waves and ^{10}Be from ice cores. *Nature* 330: 458–60.

Steenberg CD, Moraal H. 1996. An acceleration/modulation model for anomalous cosmic ray hydrogen in the heliosphere. *Astrophysical Journal* 463:776–83.

Steig EJ, Polissar PJ, Stuiver M, Grootes PM, Finkel RC. 1996. Large amplitude solar modulation cycles of

^{10}Be in Antarctica: implications for atmospheric mixing processes and interpretation of the ice core record. *Geophysical Research Letters* 23:523–6.

Wagner G, Masarik J, Beer J, Baumgartner S, Imboden D, Kubik PW, Synal H-A, Suter M. 2000. Reconstruction of the geomagnetic field between 20 and 60 kyr BP from cosmogenic radionuclides in the GRIP ice core. *Nuclear Instruments and Methods in Physics Research B* 172:597–604.

Zank GP. 1999. Interaction of the solar wind with the local interstellar medium: a theoretical perspective. *Space Science Reviews* 89:413–688.

Zank GP, Frisch PC. 1999. Consequences of a change in the galactic environment of the Sun. *Astrophysical Journal* 518:965–73.

Zank GP, Matthaeus WH, Bieber JW, Moraal H. 1998. The radial and latitudinal dependence of the cosmic ray diffusion in the heliosphere. *Journal of Geophysical Research* 103:2085–97.

Zank GP, Pauls HL, Williams LL, Hall DT. 1996. Interaction of the solar wind with the local interstellar medium: a multifluid approach. *Journal of Geophysical Research* 101:21,639–55.

RADIOCARBON, Vol 46, Nr 2, 2004, p 691–699

HOLOCENE ENVIRONMENTAL CHANGES IN WESTERN HUNGARY

Zsuzsanna Szántó

Institute of Nuclear Research of the Hungarian Academy of Sciences, Laboratory of Environmental Studies, 4026 Debrecen, Bem tér 18/c, Hungary. Corresponding author. Email: aszanto@atomki.hu.

Zsófia Medzihradszky

Hungarian Natural History Museum, Department of Botany, 1087 Budapest, Könyves Kálmán krt. 40, Hungary. Email: medzi@bot.nhmus.hu.

ABSTRACT. We review the reasons for change in paleoecological conditions and their effects on different cultures at the beginning and during the Holocene period in western Hungary using radiocarbon data combined with paleoecological and paleolimnological results. Two sites were investigated in the southern and northern part of the ancient bay of Balaton Lake: Keszthely-Úsztatómajor and Főnyed I. ^{14}C dating of 2 core samples represented a chronology from 11,000 cal BC to 2000 cal BC (10,700 BP to 3700 BP) and from 6200 cal BC to 1200 cal BC (7300 BP to 3000 BP), respectively. A relatively constant inverse sediment accumulation rate was observed in both cases (23 yr/cm and 33 yr/cm, respectively). In the case of Főnyed I, a sharp break was observed in the sedimentation curve around 6000–4800 cal BC (6000 BP). Changes in the vegetation due to human activity were observed in a larger extent only at the end of Late Neolithic, with the most significant changes detected in the landscape coinciding with the presence of Lengyel III culture in the region. The appearance of higher amounts of pollen of cereals at the sites proved the presence of crop cultivation. However, the role of plant cultivation may have been limited for the ancient inhabitants of the Kis-Balaton region due to a limited amount of soil suitable for agriculture and due to the extensive water table. Further changes in vegetation were observed during the Late Copper Age (Baden culture) and the period of Early and Middle Bronze Age, respectively. Signs of forest clearing during the period have not been detected and the increased peak of *Fagus* indicates climatic change. The low intensity of anthropogenic activity should not be attributed to geographic isolation.

INTRODUCTION

Paleoecology, geology, geoarchaeology, and archaeology contribute to various aspects of the spatial and temporal dimension of the human condition (Bradley 1985). Paleoecological techniques and records can be used for reconstructing human communities' environments and human impacts in the ancient ecosystem. Pollen analysis is the primary technique to reconstruct past environmental conditions (Birks and Birks 1980). Pollen grains and spores can be used to reconstruct the vegetation of a region and changes in vegetation composition are used as an indication of variation in environmental conditions (i.e. climate, natural disturbance, or human interference). Combining pollen analysis with radiocarbon dating provides an important tool used for the precise delineation of vegetation shifts and climatic episodes in the region (Pilcher 1993). The development and refinement of ^{14}C dating techniques have allowed palynologists to construct influx pollen diagrams (Maher 1972), and if a reasonably accurate sedimentation rate is available, pollen concentrations may be converted to pollen influx rates. Thus, it is critical for pollen studies to have adequate chronological control such as ^{14}C age determinations.

To determine to what extent human activities in the region have induced changes in the vegetation and to what extent regional vegetation changes are climate-induced, we investigated and attempted to reconstruct the history of vegetation change using analysis of pollen from sediment cores recovered from 2 sites situated in the northern and southern part of the studied region.

STUDY AREA

Two sites of interest in western Hungary are parts of a large mire complex at the ancient bay of Balaton Lake: Keszthely-Úsztatómajor on the northern portion and Főnyed I on the southern portion.

Proceedings of the 18th International Radiocarbon Conference, edited by N Beavan Athfield and R J Sparks
RADIOCARBON, Vol 46, Nr 2, 2004, p 691–699

(Figure 1). Several archeological studies have been done in the area (Sági 1966; Költő and Vándor 1996) and 7 settlements of Middle Neolithic culture were excavated and dated.

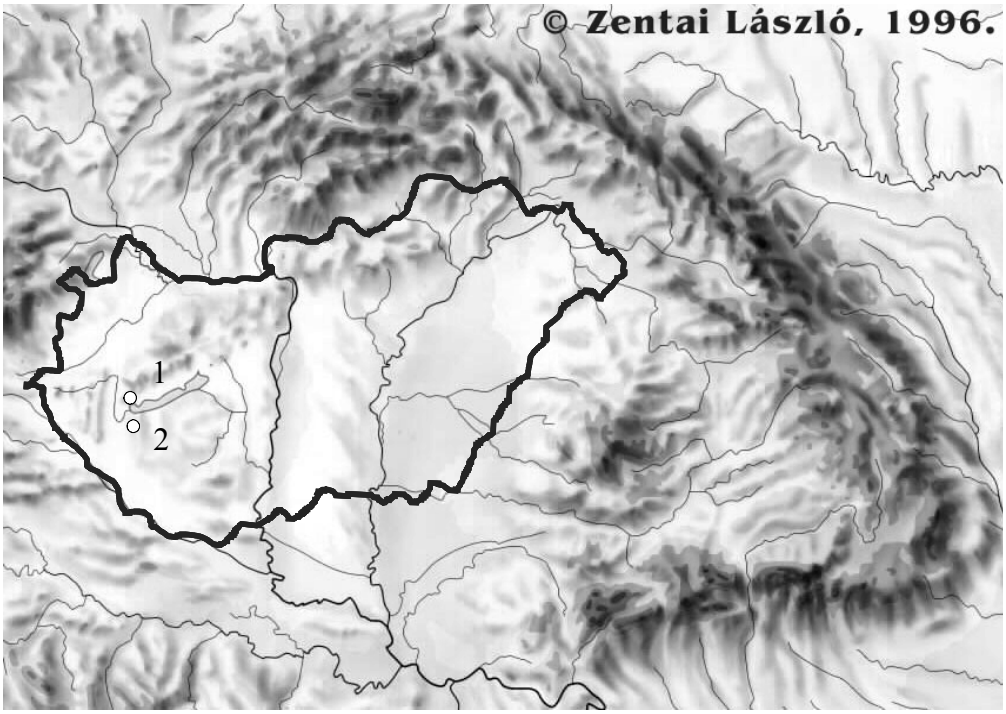

Figure 1 Map showing the location of (1) Keszthely-Úsztatómajor and (2) Főnyed I (❍ = core location).

Keszthely-Úsztatómajor is situated south from Hévíz Lake between the Hévíz and the Úsztatómajor channel. Today, most of the area is uncultivated with a high level of groundwater. Modern vegetation in the area is tall sedge vegetation which is influenced by the thermal water outflow of Hévíz Lake (Medzihradszky 2001a).

Főnyed I is situated west of the village of Főnyed. Today, the site area is covered by 20–50 cm of water. Vegetation is mostly sedge with a small territory areas of planted forest (Medzihradszky 2001b).

MATERIALS AND METHODS

Sample Preparation

The 2 sedimentary sequences were obtained from boreholes 5.8 m and 4.8 m deep, respectively, using a Russian type 5-cm-diameter peat corer. Cores were wrapped in plastic film, aluminum foil, and plastic bags and stored at 4 °C before analysis.

The cores were divided into sections of 10–15 cm. After physical pretreatment and removal of any rootlets or visible contamination, the peat samples were pretreated with the acid/alkali/acid (AAA) method. Samples were leached in 2% HCl at 80 °C for 24 hr, rinsed with distilled water, then heated in 2% NaOH for 24 hr, rinsed again with distilled water, and finally washed with 2% HCl (until pH 3 is reached), filtered, rinsed, and dried. The chemically pretreated sample was combusted to CO_2

in a controlled oxygen stream. Gaseous impurities (like traces of NO_x) and the excess of O_2 unused during combustion were removed by passing the produced CO_2 through a hot copper furnace. The purified CO_2 was trapped into a stainless steel vessel using liquid nitrogen and measured by gas proportional counting (Hertelendi 1979). The multicounter ^{14}C dating system consists of 9 electrolytic copper proportional counters filled with CO_2. The overall precision of the system for modern carbon samples was better than 4‰ after a counting period of 7 days (not including random errors in the process of chemical pretreatment and preparation). The $\delta^{13}C_{PDB}$ value was used to correct ^{14}C activity. Calibration of ^{14}C dates to calendar yr was performed using the Calib 4.0 program (Stuiver and Reimer 1993).

Pollen Analysis

The cores were subsampled at 5-cm intervals and the samples were processed for pollen analysis using standard techniques (Berglund and Ralska-Jasiewiczowa 1986; Erdtman 1943; Stockmarr 1971). Pollen identifications were based on the descriptions and identification keys in Faegri and Iversen (1989), Moore et al. (1991), the pollen atlases of Reille (1992, 1995), and on the reference pollen collection of the W Szafer Botanical Institute of the Polish Academy of Sciences. To reduce statistical error, a minimum of 1000 pollen grains were counted at each stratigraphic level. Pollen abundance was expressed as a percentage of the sum of all pollen grains originating from terrestrial vegetation, namely, the sum of arbor pollen (AP) and the non-arbor pollen (NAP).

RESULTS AND DISCUSSION

Three forms of data were extracted from the sediment cores collected from the 2 sites:

1. Stratigraphic (sediment),
2. Chronostratigraphic (age),
3. Biostratigraphic (pollen).

Stratigraphic results were based on the description of the mineralogical properties of sediments related to their conditions of deposition.

Chronostratigraphic results were based on ^{14}C dates obtained from peat samples separated from sediment cores. Peat is representative of an environment characterized by high biological productivity, low mineral input, and shallow water.

Biostratigraphic results were presented on either relative (percentage) and or absolute (influx) pollen diagrams. In percentage diagrams, the number of grains of each pollen taxon was expressed as a percentage of the total pollen sum for a given sediment sample. A change in the percentage of one of the taxa was assumed to represent a change in vegetation composition.

Lithostratigraphy

The stratigraphy of the sediments within the sites was established analyzing 2 cores of 5.8 m and 4.8 m length, respectively, and described in Table 1.

Chronology

^{14}C dating was made on the 2 core samples of 310 cm and 225 cm length, and represented a chronology from 11,000 cal BC to 2000 cal BC (10,700 BP to 3700 BP) and from 6200 cal BC to 1200 cal BC (7300 BP to 3000 BP), respectively. The data presented here represent the first attempt to provide a ^{14}C-dated record for the Kis-Balaton region. The ^{14}C dating was essential, but as yet only provides the initial measure of sediment ages. ^{14}C dates are presented in Table 2 and Table 3 and were used to derive the age-depth curves (Figure 2).

Table 1 Lithology of the cores from Keszthely-Úsztatómajor and Főnyed I.

Depth (cm)	Keszthely-Úsztatómajor	Főnyed I
0–20	Organic mud	Blackish organic mud, plant fibers and roots, shell debris
30–50		Thin layer of fine sand mixed with shell debris
50–60	Mineralized layer, intermixed with sand grains and mud	
60–70		
70–80	Midbrown fibrous peat	Mixed peat with shell debris
80–100		
100–110		Bright limestone, mixed with mud and visible pieces of plant fibers; peat is missing
135–150		
155–165		Blackish, organic mud
180–190		Fibrous peat
190–200		Black-brown mature peat
205–210		
220–230	Mixed peat with visible plant debris	
240–250		Sandy silt, intermixed with a gravel layer
270–290	Plant debris, loose peat	
290–300	Dark brown fibrous peat, trace of mineralization	
340–350		
360–400	Fine gray sand with carbonate deposition and charcoal pieces	Coarse sand with little organic mud
400–480	Coarse sand with little organic mud	
480–580		

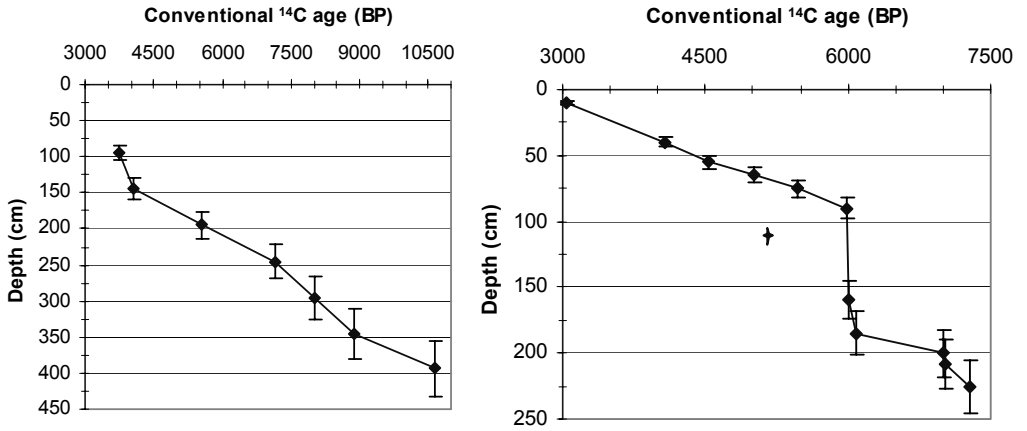

Figure 2 Sediment depth to ^{14}C age relationship for Keszthely-Úsztatómajor (left) and Főnyed I (right). Lines connecting each plotted point are interpolated sediment accumulation rates.

We noted an apparently anomalous date in the Főnyed I site core. The date at 100–110 cm depth was younger than expected and may be due to either humic infiltrates of younger age or the admixture of younger material. The age-depth curve (derived by linear interpolation with the Tilia 2.0 program) also illustrates that the date at 110 cm falls outside the expected range. For the purpose of site chronology, this date has been excluded.

Table 2 ^{14}C and calibrated ages of peat samples from Keszthely-Úsztatómajor.

Depth (cm)	Conventional ^{14}C ages (BP)	Calibrated age (BC) 1 σ (68.3%)	Lab code
90–100	3730 ± 58	2199–2033	deb-5036
135–150	4073 ± 67	2710–2492	deb-5038
190–200	5559 ± 74	4456–4336	deb-5083
240–250	7154 ± 70	6078–5958	deb-5082
290–300	8021 ± 107	7091–6775	deb-5061
340–350	8864 ± 161	8218–7793	deb-5044
390–400	10,657 ± 128	10,948–10,700 10,495–10,458	deb-5085

Table 3 ^{14}C and calibrated ages of peat samples from Keszthely-Úsztatómajor.

Depth (cm)	Conventional ^{14}C ages (BP)	Calibrated age (BC) 1 σ (68.3%)	Lab code
0–20	3030 ± 55	1376–1218	deb-7711
30–50	4085 ± 60	2850–2810 2700–2523	deb-7909
50–60	4530 ± 55	3352–3299 3244–3117	deb-7717
60–70	5010 ± 60	3924–3865 3819–3718	deb-7925
70–80	5475 ± 70	4371–4249	deb-7718
80–100	5980 ± 65	4928–4783	deb-7833
100–110	4890 ± 55	3718–3639	deb-7720
155–165	6000 ± 75	4970–4817	deb-7928
180–190	6080 ± 55	5048–4896	deb-7725
195–205	7010 ± 160	6007–5736	deb-7929
205–210	7030 ± 95	5991–5818	deb-7937
220–230	7275 ± 70	6203–6073	deb-7727

Based on the analysis of ^{14}C dates, the deposition time (inverse sediment accumulation rate) for the 2 cores was determined as 23 yr/cm for Keszthely-Úsztatómajor and 33 yr/cm for Főnyed I. According to the ^{14}C data for Főnyed I, there appeared to be a rapid peat accumulation around 4800 cal BC (6000 BP) with a deposition of approximately 70–75 cm of a sandy layer. This acceleration of sediment accumulation might be associated with some environmental change, possibly flooding. The deposition time for the Főnyed I site was calculated for the upper part of the sedimentation curve before the rapid sedimentation event occurred.

Landscape History

The pollen data covers the time period from 11,000 cal BC to 2000 cal BC (10,700 BP to 3700 BP) for Keszthely-Úsztatómajor and the period from 6200 cal BC to 1200 cal BC (7300 BP to 3000 BP) for Főnyed I. In archaeological terms, this spans the Early Neolithic to Middle Bronze Age. The results from the ^{14}C dating and pollen analysis were plotted versus depth (Figure 3).

Statistical procedures were used to zone the data. In both cases, the pollen diagrams were divided in 4 local pollen assemblage zones (LPAZ) based on the changes in the representation of major arboreals and non-arboreals. The local vegetation changes have been determined during the Holocene as follows:

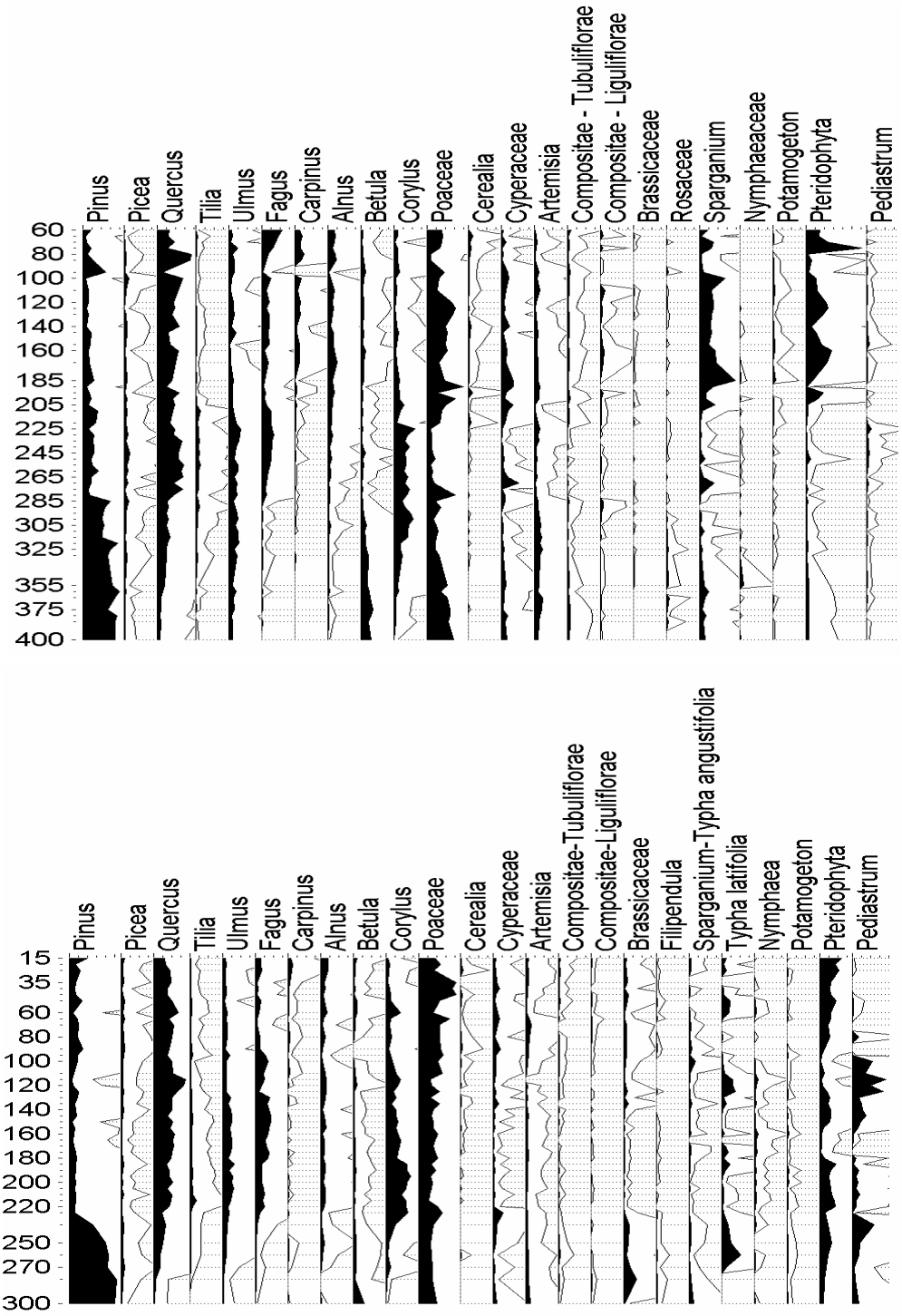

Figure 3 Pollen diagrams for Keszthely-Úsztatómajor (above) and Főnyed I (below)

LPAZ I—10,500–6500 cal BC (10,700–8000 BP)
In this zone, the arbor and non-arbor pollen ratio of the spectra—apart from small variations—was equal, 80–20%. Among the tree taxa, the *Pinus* had a high value, about 30–50%, and *Betula* reached 15%. From the very beginning of the zone, the continuous presence of *Picea* was observed, and the presence of other deciduous trees such as *Quercus*, *Ulmus*, *Tilia*, and a few pollen grains of *Fagus* were detected as well. *Poaceae* is approximately 30% with about 10% *Artemisia*. There were low numbers of the aquatic pollen (e.g. rushes), but some grains of the *Nymphaeaceae* refer to open surface water and higher water level. The presence of hazel was also recorded (25%), a sign of a warm and dry climate.

LPAZ II—6500–4400 cal BC (8000–5500 BP)
The vegetation remained stable until about 8000 BP, when the tree arboreal peak increased and the herbaceous pollen percentages decreased. This zone represented a forestation stage, where the *Quercus*, *Ulmus*, and *Fagus* dominated the forest vegetation, but *Tilia* was also a characteristic element. *Pinus* decreased from 40% to 10%, while *Quercus* reached 30%, *Tilia* about 4–5%, and *Fagus* had an average of 10%. For Főnyed I, an extremely high peak in *Pediastrum* is observed. The forests closed and the first *Cerealia* pollen grains appeared.

LPAZ III—4400–3300 cal BC (5500–4500 BP)
The decreasing AP and increasing NAP pollen peaks were characteristic in this zone. Significant decreases of *Tilia* and *Ulmus* were observable. *Quercus* showed a more or less stable curve at 20%. The percentage of *Carpinus* increased, while the presence of *Fagus* persisted. The *Corylus* pollen curve had a gradual and permanent decrease. The expansion of a wide diversity of herbaceous taxa was observed: an increased percentage of *Sparganium-Typha angustifolia* and ferns was detected. At this time, opening of the forests was observable. In the vegetational spectra, the first considerable *Cerealia* peak was detected.

LPAZ IV—3300–1300 cal BC (4500–3000 BP)
The *Quercus* curve ranged between 20–40% and increased percentages of *Fagus* and *Carpinus* were observed. *Poaceae* had a value of 20–40%. *Cerealia* was constantly present, while *Pediastrum* almost disappeared. The amount and diversity of herbaceous pollen increased substantially.

The vegetation mosaic described above implies that in this region both human activities and climatic changes in the vegetation. We make these assumptions based on the following reasons:

- The analysis of the main components of the tree taxa showed a change in the deciduous trees versus *Pinus* for Keszthely-Úsztatómajor at 285 cm, while for Főnyed I, this ratio changed at 235 cm. In both cases, the process can probably be attributed to climatic changes.
- Agricultural and settlement land-use may create or increase vegetational mosaics, with development of tracks, fields, and so forth, in which different habitat-preferring flora and fauna elements existed. We expected that the results of the research might provide details about ancient life in the Lake Kis-Balaton region, including information on the natural resources in the area and the relationship of the human population to the physical environment and natural resources through time. However, the paleobotanical analyses indicate that in the study area the proof of human-induced vegetation change was scarce, despite the fact that classical primary pollen (*Cerealia*) was present.
- No massive signs in vegetational change due to animal husbandry, plant cultivation, or farming were observed. Although a slight change in the ratio of AP and NAP was distinguished during the Copper Age and the appearance of Lengyel culture (4500/4400 cal BC) in the region (Sági

1996), climatic changes appear to be the driving factor of the vegetation change observed in pollen analysis.
- Signs of forest clearance were not detected during the Neolithic and the Copper Age, but there is a chronological correlation between the increase of *Cerealia* in the core samples and the known increase in the number of settlements in the region during the Bronze Age.

CONCLUSIONS

Sedimentary sequences in 2 peat cores from western Hungary were used to reconstruct the environmental history of the region using ^{14}C data, lithography, and pollen analysis. A relatively constant sediment accumulation rate was observed at Keszthely-Úsztatómajor (23 yr/cm). For Főnyed I, a sharp break was observed in the sedimentation curve around 4800 cal BC (6000 BP). The calculated inverse sedimentation rate was of 33 yr/cm, probably due to flooding followed by a faster sedimentation process, based upon the peak in *Pediastrum* observed in the pollen diagram.

The pollen profiles indicate the vegetation change on a local landscape scale around Lake Kis-Balaton from the Early Neolithic to Middle Bronze Age. Woodland appears to have been maintained for most of this time, although there were repeated declines and recoveries of the principal tree taxa. No significant change in the AP and NAP ratio was observed during the Holocene in the region of Lake Kis-Balaton.

Anthropogenic impact was minimal during the studied period, despite the abundant archaeological evidence found in the region. The Copper Age is characterized by sporadic anthropogenic activity. The appearance of higher amounts of cereal pollen at the sites indicated the presence of crop cultivation and we associate this with the development of the Lengyel III culture in the region.

Further changes in the landscape coincided with the appearance of the Baden culture and the period of Early and Middle Bronze Age. However, the role of plant cultivation may have been limited for the ancient inhabitants of the Kis-Balaton region compared to other areas in Hungary due to the limited amount of soil suitable for agriculture and the extensive water table.

REFERENCES

Berglund GE, Ralska-Jasiewiczowa M. 1986. Pollen analysis and pollen diagrams. In: Berglund BE, editor. *Handbook of Holocene Palaeohydrology*. Chichester: Wiley. p 455–84.

Birks HJB, Birks HH. 1980. Quaternary paleoecology. In: Kaland PE, Moe D, editors. *Quarternary Paleoecology*. Baltimore: University Park Press. p 156–76.

Bradley RS. 1985. Quaternary paleoclimatology: methods of paleoclimatic reconstruction. In: Briggs DE, Crowther PR, editors. *Quarternary Paleoclimatology*. London: Chapman and Hall. 472 p.

Erdtman G. 1943. An introduction to pollen analysis. In: Waltham Verdoorn F, editor. *An Introduction to Pollen Analysis. 4th edition*. Waltham, Massachusetts: Chronica Botanica Company USA. 139 p.

Faegri K, Iverseon J, Krzywinski K, editors. 1989. *Textbook of Pollen Analysis. 4th edition*. New York: John Wiley & Sons. 328 p.

Hertelendi E, Csongor É, Záborsky L, Molnár J, Gál J, Györffi M, Nagy S. 1989. A counter system for high-precision ^{14}C dating. *Radiocarbon* 31(3):399–406.

Költő L, Vándor L. 1996. Évezredek üzenete a láp világából. A Somogy Megyei Múzeumok Igazgatósága és Zala Megyei Múzeumok Igazgatósága Kaposvár-Zalaegerszeg. (Message of the past from the world of the mire. Archaeological investigations of the Kis-Balaton area.) 165 p. In Hungarian.

Maher L. 1972. Nomograms for computing 0.95 confidence limits of pollen data. *Review Palaeobotany and Palynology* 13:85–93.

Medzihradszky Zs. 2001a. The Holocene sequence of the pollen record from Keszthely-Úsztatómajor, Hungary. *Annales Historico-Naturales Musei Nationalis Hungarici* 93:5–12.

Medzihradszky Zs. 2001b. The reconstruction of the vegetation in the Kis-Balaton area during Lengyel period. Preliminary report. In: Regenye J, editor. *Sites and Stones: Lengyel Culture in Western Hungary and Beyond*. Veszprém: Directorate of the Veszprém County Museums. p 143–8.

Moore PD, Webb JA, Collinson ME. 1991. Pollen analysis. In: Turner HJ, editor. *Pollen Analysis*. Oxford:

Blackwell. p 130–96.

Pilcher JR. 1993. Radiocarbon dating and the palynologist: a realistic approach to precision and accuracy. In: Chambers FM, editor. *Climate Change and Human Impact on the Landscape*. London: Chapman and Hall. p 23–32.

Reille M. 1992. Pollen et spores d'Europe et d'Afrique du Nord. *Laboratoire de Botanique Historique et Palynologie*. URA CNRS, Marseille. 520 p.

Reille M. 1995. Pollen et spores d'Europe et d'Afrique du Nord. *Laboratoire de Botanique Historique et Palynologie*. URA CNRS, Marseille. 327 p.

Sági K. 1966. Magyarország régészeti topográfiája I. Veszprém megye. A keszthelyi és tapolcai járás. (Archäologische Topographie Ungarns. Kreise von Keszthely und Tapolca im Komitat Veszprém.) Budapest: Akadémiai Kiadó. 266 p. In Hungarian.

Stockmarr J. 1971. Tablets with spores used in absolute pollen analysis. *Pollen et Spores* 13:615–21.

Stuiver M, Reimer PJ. 1993. Extended ^{14}C database and revised CALIB radiocarbon calibration program. *Radiocarbon* 35(1):215–30.

RADIOCARBON, Vol 46, Nr 2, 2004, p 701–719

CARBON ISOTOPIC COMPOSITION OF TREE RINGS AS A TOOL FOR BIOMONITORING CO_2 LEVEL

Sławomira Pawełczyk • Anna Pazdur[1]

Institute of Physics, Radiocarbon Laboratory, Silesian University of Technology, Krzywoustego 2, 44-100 Gliwice, Poland.

ABSTRACT. Carbon isotopes are widely used as indicators in the study of atmospheric CO_2 variability in space and time. Preliminary results are part of a project investigating ^{13}C and ^{14}C concentration changes during the last 150 yr in Poland, both in industrial and ecologically clean regions, using annual tree rings (*Pinus sylvestris*, *Populus nigra*). The results describe the local Suess effect recorded in the industrial Kraków and Upper Silesia regions compared to changes of background radiocarbon concentration caused by global human activity in a "clean region," Augustów Wilderness. The $\delta^{13}C$ record also shows the influence of the local Suess effect.

INTRODUCTION

$^{14}C/^{12}C$ ($\Delta^{14}C$) and $^{13}C/^{12}C$ ($\delta^{13}C$) ratios in tree rings can reflect corresponding atmospheric CO_2 concentration during their formation and can be used to reconstruct changes in factors influencing these parameters. In particular, $\Delta^{14}C$ and $\delta^{13}C$ could be used as proxies when CO_2 concentrations are unavailable. The carbon isotopic composition of plant material depends on the isotopic composition of CO_2 assimilated during the photosynthesis process. For this reason, $\delta^{13}C$ and $\Delta^{14}C$ determined for plant material can be used as isotopic composition indicators as well as indicators of CO_2 emission caused by fossil-fuel burning and human activity. Many other factors, in addition to isotopic composition of atmospheric CO_2, influence $\delta^{13}C$ and $\Delta^{14}C$. Although the carbon atoms of plant material come from atmospheric CO_2, the $\delta^{13}C$ value is not the same as that of atmospheric CO_2. Diffusion via stomata and carboxylation discriminate against heavier isotopes. Environmental variables, such as temperature, precipitation, humidity, light intensity, and changes in soil moisture, control the degree of fractionation and, thus, $\delta^{13}C$ values. $\Delta^{14}C$ correlates with sun activity and terrestrial geomagnetic variations.

Human activity is another reason for changes in the environment's carbon composition. Changes can have either a global range, which can affect all of nature or a specified reservoir, or a local range covering only a part of reservoirs neighboring the source that caused the changes. Human activity can lead to an increase as well as decrease of ^{14}C concentration in the environment. Anthropogenic changes of radiocarbon concentration are caused by:

- Suess effect;
- Rapid increase of ^{14}C concentration caused by nuclear weapon tests in the atmosphere;
- Production of ^{14}C connected with nuclear reactors and nuclear fuel reprocessing plant activity;
- Release and production of ^{14}C isotope during a nuclear system failure.

Increase of mining and burning of fossil fuels in industrial areas since the 19th century caused the emission of CO_2 to the atmosphere and changes of carbon isotopic composition in both the atmosphere and other carbon reservoirs. Fossil-fuel burning results in the emission of CO_2 to the atmosphere lacking ^{14}C. This decreases the atmospheric ^{14}C concentration and is known as the Suess effect (Awsiuk and Pazdur 1986; Damon et al. 1989; Levin et al. 1989; Levin and Hesshaimer 2000; Rakowski et al. 2001). An increase of ^{14}C concentration in the atmosphere, as a result of nuclear weapon tests in the stratosphere and at the earth surface after the 1950s, made it impossible to eval-

[1]Corresponding author. Email:pazdur@zeus.polsl.gliwice.pl.

Proceedings of the 18th International Radiocarbon Conference, edited by N Beavan Athfield and R J Sparks
RADIOCARBON, Vol 46, Nr 2, 2004, p 701–719

uate the Suess effect directly from measurements of the concentration in the atmosphere and biosphere (Nydal and Lövseth 1983). Such an evaluation is only possible when assuming a mathematical model describing carbon exchange between reservoirs (Oeschger et al. 1975; Siegenthaler and Oeschger 1987).

It can be assumed that lower values of $\delta^{13}C$ in organic material are connected with lower values of ^{13}C concentration in the atmosphere. The depression of $\delta^{13}C$ results from ^{13}C-depleted emission from fossil fuels. In particular, several investigators have tried using $^{13}C/^{12}C$ in tree rings to establish an atmospheric record of this ratio. Nevertheless, many factors may disturb atmospheric CO_2 isotope abundance reconstruction from tree rings, including the choice of a wood constituent for analysis, the effect of respired CO_2, and the influence of climatic factors (Schleser et al. 1999; Tans and Mook 1980).

Marland et al. (2001) estimated fossil-fuel emissions released in successive years from 1751 to 1998. Results of these estimations were used for comparison of values of $\delta^{13}C$ and $\Delta^{14}C$ with estimated CO_2 emission.

Systematic direct observation of Mauna Loa from 1958 and the analysis of air inclusion in Antarctic ice cores shows a continuous increase of CO_2 concentration in the air. We can state that for the period 1000–1800, the CO_2 concentration was at a steady level of 280 ppm, and from 1800–2000, it increased about 80 ppm (Keeling et al. 1989; Levin and Hesshaimer 2000).

The increase in atmospheric CO_2 concentration has been elegantly demonstrated through ^{14}C analyses of tree rings from the last 2 centuries. The first investigation of contemporary tree samples (Suess 1955) proved that their ^{14}C activity was lower than the activity of samples from the middle 19th century. On the basis of $\Delta^{14}C$ determined for tree-ring samples, a rapid decrease of about $\Delta^{14}C = 20‰$ from 1890 to 1950 was observed by Stuiver and Quay (1981).

The $\Delta^{14}C$ depletion in the first half of the 20th century has been shown to be larger in a more polluted area (De Jong and Mook 1982). In such areas, extra CO_2 from the burning of fossil fuels is clearly detectable as $\Delta^{14}C$ depletion relative to background levels. The determination of a local decrease of ^{14}C concentration in the air surrounding urban and industrial areas is important in investigations of the degree of atmosphere contamination, air mass migration, and spread of the contamination (Levin and Hesshaimer 2000).

Representative investigations of local Suess effect were carried out by Levin et al. (1989) in Central Europe, i.e., in Heidelberg, Westerland, Schauinsland, and Jungfraujoch. Levin et al. (1995) used $\Delta^{14}C$ observations to estimate the fossil-fuel contribution in atmospheric CO_2 concentration. Results of those measurements clearly demonstrate decreasing CO_2 from fossil-fuel burning with the increase of distance from the polluted area.

In Poland, investigations of local changes of ^{14}C concentration were performed by Kuc and Florkowski. They observed the depletion of ^{14}C concentration in samples of tree leaves from Kraków. Measurements of atmospheric CO_2 revealed maximum values in December and minimum values in April and May (Kuc 1986).

Investigations of changes of ^{14}C concentration in the boundary of the Upper Silesia region were carried out by Awsiuk and Pazdur (1986). They aimed to determine the range of the Suess effect. The local Suess effect on this area was investigated, in turn, by Rakowski et al. (2001) and Pazdur et al. (1998).

The increase of ^{14}C concentration in the atmosphere as a result of nuclear weapon tests in the stratosphere and on the earth's surface made it impossible to determine the Suess effect directly from mea-

surements of the ^{14}C concentration in the atmosphere and biosphere. However, it is possible to determine the local Suess effect in polluted areas. In this case, ^{14}C concentration in atmospheric CO_2 acquired at sites far from an industrial area can be considered as the ^{14}C of so-called "clean air."

RESEARCH AREA AND TIME RANGE

Investigations were carried out for 3 different areas in Poland (Figure 1). The Upper Silesia region is in the basins of Upper Wisła and Odra in southern Poland. This is the most industrialized area in Poland. Its main natural resources are deposits of coal. Other industrial activities in this area are associated with chemical processing of coal and development of heavy industry utilizing coal as the main source of energy. Spatial distribution of the air pollution is diversified. The largest concentration of pollution in the Upper Silesia region was noted in Zabrze, Ruda Śląska, Bytom, Chorzów, and Gliwice. Due to the prevailing west-south winds, the pollution partly comes from Zagłębie Ostrawsko—Karwińskie in the northern Czech Republic. The towns of Upper Silesia form a specific urban and industrial area between Mysłowice in the east and Gliwice in the west. Sampling sites were at the boundary of Ruda Śląska and Chorzów, but the distance between those places was no more than 5 km. Therefore, they can be considered as 1 site, the center of the Upper Silesia industrial area. Our investigation of Upper Silesia covers the years 1965–1995.

Figure 1 Map of Poland with location of sample collection sites

The second area where investigations were performed was Kraków (50°03′N, 19°03′E). It is one of the biggest Polish cities located in southern Poland and strongly industrialized. Our investigation covers the years 1964–2000.

The third region is Augustów (53°51′N, 22°58′E). It is an ecologically clean region (now a sanctuary) in northeast Poland. Augustów is a town located on the Netta River at the west edge of Augustów Wilderness. The region is the biggest forest complex in Europe. Our investigation covers the years 1861–1968. A minimal impact of anthropogenic effects (mainly the Suess effect) on carbon isotopic composition in tree rings was expected there. The aim of this research was to evaluate the human impact on the environment in this area.

MATERIALS AND METHODS

For investigations of the Upper Silesia region, tree trunks were collected from forests outside of local towns. Annual tree rings of pine (*Pinus sylvestris*), the dominant conifer in Polish forests, constituted the material for isotopic analysis. The choice of tree species was imposed by necessity to unify experimental material, as well as by the fact that pines are commonly used in isotopic studies around the world. An important argument supporting the use of pine for ^{14}C measurements is the fact that pine has a significantly longer vegetation period than deciduous trees. This allows tracking changes of ^{14}C concentration over a longer period. In order to compare changes of ^{14}C concentration in tree rings of deciduous and coniferous trees, the concentration of ^{14}C in tree rings of poplar (*Populus nigra*) was also determined.

In case of the Kraków area, a trunk of pine *(Pinus sylvestris)* was used. That pine grew in the central part of the city.

The investigations performed for Augustów Wilderness were also based on a pine (*Pinus sylvestris*). That tree grew in Augustów in a forest near Necko Lake.

Meteorological data used in the investigation was obtained from meteorological observatories in Warsaw (52°12′N, 21°10′E) and Kaunas (54°88′N, 23°88′E). There is no meteorological data for Augustów, but we did use data from the nearest city. From the cities mentioned above, Kaunas is the nearest one, but the meteorological data set only begins in 1922.

Preparation of samples involved separation of tree rings from the trunk cross-section along edges of the rings. This mechanical operation was performed by cutting the material with a chisel. Samples were cut from individual rings into very small slivers with a scalpel. Then, they were subject to a chemical pretreatment. Wood slivers were refluxed in a Soxhlet apparatus with a 2:1 benzene ethylene mixture to remove resin.

After mechanical processing and resin extraction in the Soxhlet apparatus, the wood samples were converted to Li_2C_2 by combustion with lithium, then to C_2H_2 by adding water, and finally to C_6H_6 in a catalyst process. The detailed procedure is described by Pawlyta et al. (1998). Measurements of $\Delta^{14}C$ were made with the liquid scintillation method using Quantulus 1220.

Values of $\delta^{13}C$ were determined for wholewood and latewood α-cellulose. In the case of several samples from Kraków, $\delta^{13}C$ was determined for earlywood because it was a part of climatic study. The technique for extraction of α-cellulose based upon the sodium chlorite oxidation method of Green (1963) utilizes an ultrasonic bath and small Soxhlet thimbles to prepare α-cellulose from latewood. This technique yields a material with sufficient homogeneity required for isotopic composition measurements (Loader et al. 1997).

The diagram of α-cellulose extraction from latewood samples can be briefly presented as follows (Robertson and Waterhouse 1998):

$$\text{wood} \xrightarrow[CH_3COOH]{NaClO_2} \text{holocellulose} \xrightarrow{NaOH} \alpha\text{-cellulose}$$

For $\delta^{13}C$ wholewood, earlywood and α-cellulose were combusted and the CO_2 cryogenically purified. Isotope ratios were measured using a mass spectrometer and expressed in the conventional δ notation as deviation in permil from the international standard, Vienna PDB (Loader et al. 1997).

RESULTS AND DISCUSSION

Comparison of $\delta^{13}C$ and $\Delta^{14}C$ Results from Different Sites

Data from Kraków are presented in Table 1 and data from Augustów are presented in Table 2. Results of ^{14}C concentration measurements in tree rings from Chorzów and Ruda Śląska are presented by Rakowski et al. (2001).

Table 1 Results of carbon isotopic composition measurements in tree rings (*Pinus sylvestris*) and in atmospheric CO_2 from Kraków (from Kuc and Zimnoch 1998).

Year	$\delta^{13}C$ (±0.1) (‰)	$\Delta^{14}C$ (‰) tree rings	pMC (%)	^{14}S (%)	$\Delta^{14}C$ (‰) atmospheric CO_2
1964	–24.34*[a]	708.91 ± 27.95	170.89 ± 2.79	–8.34 ± 1.55	—
1966	–24.55*	763.86 ± 24.83	176.39 ± 2.48	4.03 ± 1.47	—
1968	–24.94	536.76 ± 27.38	153.68 ± 2.74	–3.48 ± 1.72	—
1970	–25.42	511.04 ± 21.84	151.10 ± 2.18	–2.30 ± 1.42	—
1972	–24.87	423.14 ± 21.18	142.31 ± 2.12	–3.94 ± 1.43	—
1974	–24.42	367.55 ± 19.91	136.76 ± 1.99	–3.66 ± 1.41	—
1975	–24.97*	250.66 ± 20.33	125.07 ± 2.03	–9.89 ± 1.47	—
1977	–24.51	235.34 ± 19.80	123.53 ± 1.98	–7.72 ± 1.48	—
1979	–25.29	208.89 ± 19.94	120.89 ± 1.99	–7.40 ± 1.53	—
1981	–25.49	178.20 ± 19.18	117.82 ± 1.92	–7.32 ± 1.51	—
1983	–23.05*	159.54 ± 20.50	115.95 ± 2.05	–6.08 ± 1.66	225.28 ± 12
1985	–28.04	186.08 ± 18.01	118.61 ± 1.80	–1.52 ± 1.50	175.57 ± 11
1987	–23.20	175.22 ± 18.26	117.52 ± 1.83	–0.37 ± 1.55	163.33 ± 10
1988	–23.88*	153.89 ± 17.47	115.39 ± 1.75	–1.50 ± 1.50	197.00 ± 10
1989	–23.79*	71.29 ± 17.84	107.13 ± 1.78	–7.63 ± 1.54	151.14 ± 10
1990	–23.54	49.49 ± 17.65	104.95 ± 1.77	–9.13 ± 1.53	144.00 ± 10
1991	–23.12	51.38 ± 18.48	105.14 ± 1.85	–7.64 ± 1.63	—
1997	–25.12	24.19 ± 19.26	102.42 ± 1.93	–6.46 ± 1.76	—
1998	–25.89	–2.67 ± 20.08	99.73 ± 2.01	–8.50 ± 1.85	—
1999	–25.60	–13.38 ± 24.11	98.66 ± 2.41	–9.31 ± 2.22	—
2000	–27.07	17.21 ± 19.15	101.72 ± 1.92	–5.81 ± 1.78	—

[a] * = values of $\delta^{13}C$ determined for earlywood.

$\Delta^{14}C$ in the Environment and the Impact of CO_2 Emission

Figure 2 presents annual changes of $\Delta^{14}C$ in tree rings from Augustów, Ruda Śląska, Chorzów, and Kraków, and changes of ^{14}C concentration in the "clean air." Data concerning the concentration in the clean air are taken from the work by Levin and Kromer (1997). They constitute a record of changes of ^{14}C concentration in the atmospheric CO_2 from Schauinsland (48°N, 8°E, 1205 m asl, Black Forest, southern Germany). For the calculation, average values of $\Delta^{14}C$ determined from May

to August for Schauinsland were used. Those changes can be described by the expression $\Delta^{14}C = 417\exp(-0.0625 \times t)$ (‰), where t is time (in yr) counted from 1974.

Table 2 Results of carbon isotopic composition measurements for wholewood and latewood α-cellulose of tree rings (*Pinus sylvestris*) from Augustów.

Year	$\Delta^{14}C$ (‰)	$\delta^{13}C$ for wholewood (±0.1) (‰)	$\delta^{13}C$ for latewood α-cellulose (±0.05) (‰)
1861	–30.41 ± 7.64	–27.02	—
1862	–3.50 ± 6.30	–26.91	—
1863	5.57 ± 6.57	–25.39	—
1864	6.26 ± 6.99	–27.19	—
1865	12.33 ± 6.42	–27.62	—
1866	–9.04 ± 6.39	–27.01	—
1867	–10.42 ± 6.71	–26.59	—
1868	–13.78 ± 7.07	–26.32	—
1869	–4.38 ± 6.73	–26.03	—
1870	6.47 ± 6.79	–27.19	—
1871	–28.02 ± 6.76	–26.82	—
1872	–3.43 ± 5.04	–26.29	—
1873	–42.27 ± 6.25	–26.89	—
1874	0.93 ± 7.42	–26.81	—
1875	–21.00 ± 6.00	–26.13	—
1876	8.16 ± 6.90	–25.32	—
1877	–15.89 ± 6,01	–25.9	—
1878	–10.58 ± 7.24	–25.78	—
1879	–10.64 ± 6.33	–26.60	—
1880	–8.67 ± 6.47	–26.58	—
1881	–1.60 ± 7.37	–26.72	—
1882	–9.55 ± 5.74	–26.21	—
1883	–12.21 ± 9.59	–25.70	—
1884	–20.20 ± 8.92	–25.01	—
1885	–22.87 ± 8.29	–24.90	—
1886	–23.09 ± 9.70	–26.60	—
1887	–12.09 ± 4.24	–25.03	—
1888	–13.90 ± 7.39	–25.91	—
1889	–9.47 ± 6.83	–25.73	—
1890	2.67 ± 6.24	–25.99	—
1891	7.74 ± 6.08	–25.41	—
1892	–0.76 ± 6.51	–25.74	—
1893	2.53 ± 6.61	–26.10	—
1894	–0.54 ± 7.05	–25.32	—
1895	–7.86 ± 7.14	–25.00	—
1896	2.81 ± 6.71	–25.59	—
1897	–6.40 ± 6.44	–25.33	—
1898	–10.42 ± 9.07	–25.00	—
1899	18.10 ± 6.19	–25.66	–25.43
1900	9.62 ± 5.47	–25.06	–24.00
1901	12.44 ± 5.85	–25.76	–24.83
1902	8.23 ± 5.85	–27.26	–25.77
1903	–21.33 ± 5.83	–25.66	–24.80
1904	–3.67 ± 10.91	–25.96	–24.92

Table 2 Results of carbon isotopic composition measurements for wholewood and latewood α-cellulose of tree rings (*Pinus sylvestris*) from Augustów. *(Continued)*

Year	$\Delta^{14}C$ (‰)	$\delta^{13}C$ for wholewood (±0.1) (‰)	$\delta^{13}C$ for latewood α-cellulose (±0.05) (‰)
1905	–0.52 ± 9.42	–25.76	–24.46
1906	5.09 ± 6.44	–25.56	–25.50
1907	–9.16 ± 9.44	–25.76	–25.39
1908	–8.12 ± 5.76	–25.16	–25.20
1909	–23.28 ± 12.44	–25.86	–25.95
1910	–38.50 ± 5.94	–25.86	–24.30
1911	–35.81 ± 7.77	–24.68	–24.62
1912	11.10 ± 6.63	–25.36	–24.36
1913	–41.70 ± 12.41	–25.16	–25.09
1914	–10.90 ± 7.83	–25.96	–24.58
1915	–26.53 ± 8.63	–25.76	–25.78
1916	–0.56 ± 5.60	–26.26	–24.53
1917	31.71 ± 6.81	–25.16	–24.48
1918	–14.72 ± 6.12	–24.96	–25.75
1919	–1.55 ± 6.35	–25.16	–25.02
1920	–4.95 ± 6.03	–23.96	–23.51
1921	–33.11 ± 7.04	–25.36	–24.94
1922	–27.84 ± 7.22	–25.16	–24.68
1923	–4.20 ± 7.13	–25.76	–25.66
1924	32.82 ± 10.78	–25.36	–25.35
1925	33.13 ± 9.76	–25.16	–24.81
1926	34.99 ± 5.44	–25.06	–24.93
1927	18.06 ± 9.56	–24.26	–24.13
1928	12.21 ± 8.76	–25.06	–24.39
1929	38.90 ± 11.99	–25.46	–23.85
1930	5.29 ± 10.19	–24.46	–24.84
1931	25.20 ± 9.90	–25.66	–24.54
1932	36.01 ± 5.88	–25.58	–22.91
1933	21.83 ± 10.40	–26.20	–24.51
1934	–47.33 ± 11.12	–25.82	–25.74
1935	–7.04 ± 10.31	–25.67	–25.56
1936	26.46 ± 6.66	–25.47	–24.22
1937	–84.75 ± 10.39	–26.17	–24.17
1938	4.31 ± 10.16	–26.51	–24.28
1939	–58.72 ± 9.66	–26.76	–22.90
1940	–43.04 ± 11.55	–25.38	–25.82
1941	–20.13 ± 11.35	–25.75	–24.75
1942	–15.61 ± 8.52	–26.05	–24.30
1943	–18.41 ± 5.14	–25.87	–24.94
1944	–26.22 ± 11.99	–27.57	–23.14
1945	–15.85 ± 10.96	–25.51	–25.04
1946	–51.00 ± 12.44	–24.90	–24.12
1947	–14.43 ± 12.35	–26.36	–23.94
1948	–8.50 ± 8.94	–25.22	–24.12
1949	–6.78 ± 10.94	–25.54	–26.18
1950	2.97 ± 11.76	–25.73	–24.85

Table 2 Results of carbon isotopic composition measurements for wholewood and latewood α-cellulose of tree rings (*Pinus sylvestris*) from Augustów. *(Continued)*

Year	$\Delta^{14}C$ (‰)	$\delta^{13}C$ for wholewood (±0.1) (‰)	$\delta^{13}C$ for latewood α-cellulose (±0.05) (‰)
1951	–4.53 ± 9.22	–26.55	–25.99
1952	–9.18 ± 8.56	–26.18	–25.69
1953	–23.42 ± 15.00	–25.39	–24.81
1954	–50.45 ± 11.90	–25.31	–25.53
1955	–26.76 ± 11.09	–25.97	–25.96
1956	2.35 ± 9.32	–26.36	–26.15
1957	10.19 ± 11.47	–26.77	–26.16
1958	129.11 ± 10.37	–26.24	–25.80
1959	247.83 ± 10.87	–27.07	–25.97
1960	209.69 ± 13.23	–27.04	–25.80
1961	264.44 ± 13.74	–28.60	–25.98
1962	459.20 ± 9.21	–25.92	–25.91
1963	—	–27.23	–24.04
1964	—	–27.09	–25.60
1965	—	–26.74	–23.82
1966	—	–26.37	–24.94
1967	—	–25.95	–24.06
1968	—	–26.83	–24.24

We can assume that relations describing changes of this value for data for Chorzów, Ruda Śląska, and Kraków reveal a similar character. The equations take the form of $\Delta^{14}C = exp(-B \times t)$ for Ruda Śląska (*Pinus sylvestris*), parameter A = (680 ± 40)‰ and B = (6.77 ± 0.50) × 10^{-2} 1/yr, and for Chorzów (*Populus nigra*) A = (675 ± 70)‰ and B = (5.91 ± 0.45)‰ 10^{-2} 1/yr, where *t* is time (in yr) counted from 1965; for Kraków (*Pinus sylvestris*), parameter *A* = (198 ± 16)‰ and *B* = (9.70 ± 0.80) × 10^{-2} 1/yr, and for atmospheric CO_2 for Kraków *A* = (156 ± 48)‰ and *B* = (7.60 ± 0.24) × 10^{-2} 1/yr, where *t* is time (in yr) counted from 1964. Time constants of $\Delta^{14}C$ changes are, respectively:

- 14.8 for tree rings from Rudza Śląska,
- 16.9 for tree rings from Chorzów,
- 10.3 for tree rings from Kraków,
- 13.2 for atmospheric CO_2 from Kraków,
- 15.4 for atmospheric CO_2 from Schauinsland.

A local Suess effect can be described by the following value (Florkowski and Kuc 1979):

$$^{14}S = \frac{\Delta^{14}C - \Delta^{14}C_{backgr}}{1000 + \Delta^{14}C_{backgr}} \times 100\,\% \qquad (1),$$

where $\Delta^{14}C$ is the ^{14}C concentration in the sample examined and $\Delta^{14}C_{backgr}$ is the ^{14}C concentration in the clean air.

Figure 3 presents annual changes of ^{14}S determined on the basis of measurements for samples from Chorzów, Ruda Śląska, and Kraków. A decrease of ^{14}C concentration in Kraków caused by emission of ^{14}C-free CO_2 from fossil-fuel burning can be observed. The average value of the Suess effect in Kraków is –5.4 ± 1.6% for 1964–2000. For comparison, the average value of ^{14}S determined for Ruda Śląska is –4.05 ± 1.3% for 1965–1995, and for Chorzów is –1.43 ± 0.9% for 1966–1992.

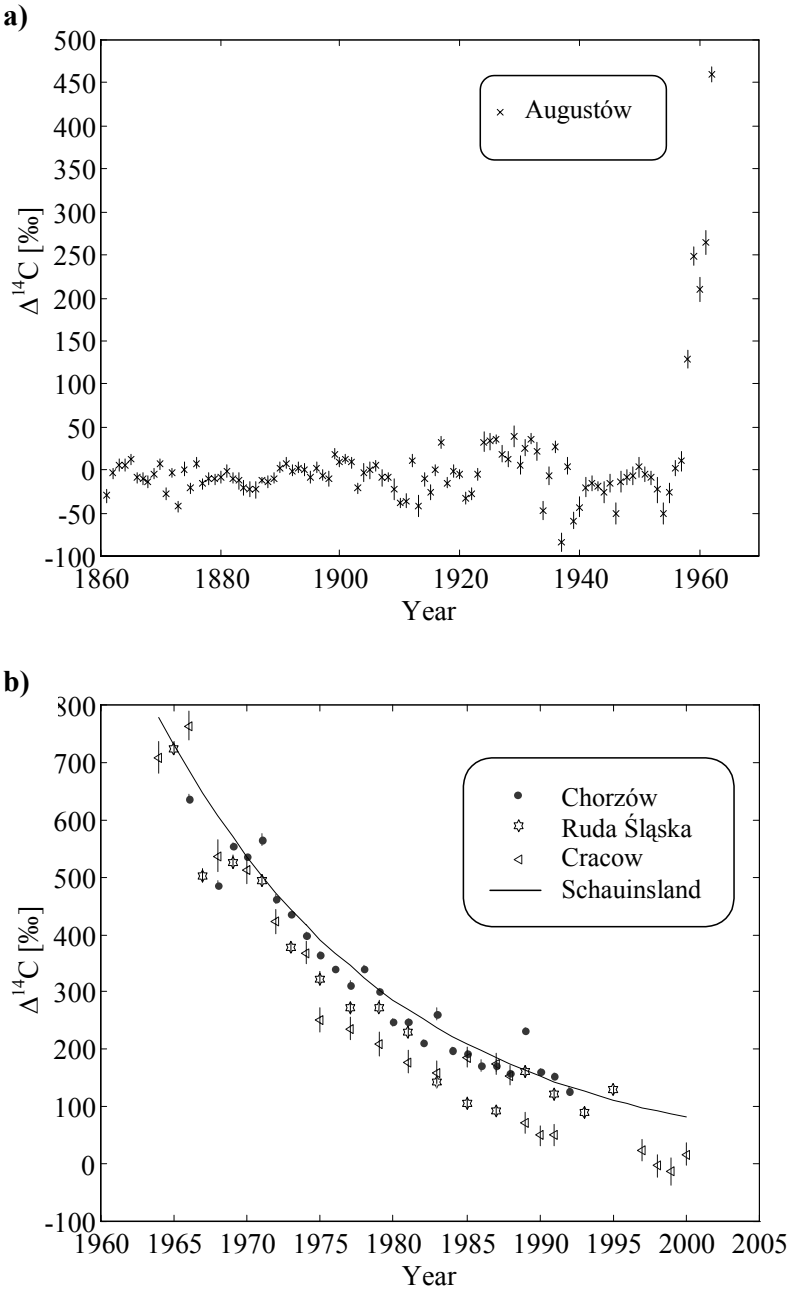

Figure 2 (a) Annual changes of $\Delta^{14}C$ in tree rings from Augustów; (b) Ruda Śląska, Chorzów (from Rakowski et al. 2001), and Kraków.

The values of ^{14}S determined for Ruda Śląska are much lower than corresponding values determined for Chorzów for the same years. The discrepancies result from differences in species of the examined trees. Annual tree rings of pine were used as the samples from Ruda Śląska because the vegetative period in our climatic zone is much longer than that for deciduous trees. Annual tree rings of deciduous poplar were used to determine changes of carbon isotopic composition for Chorzów.

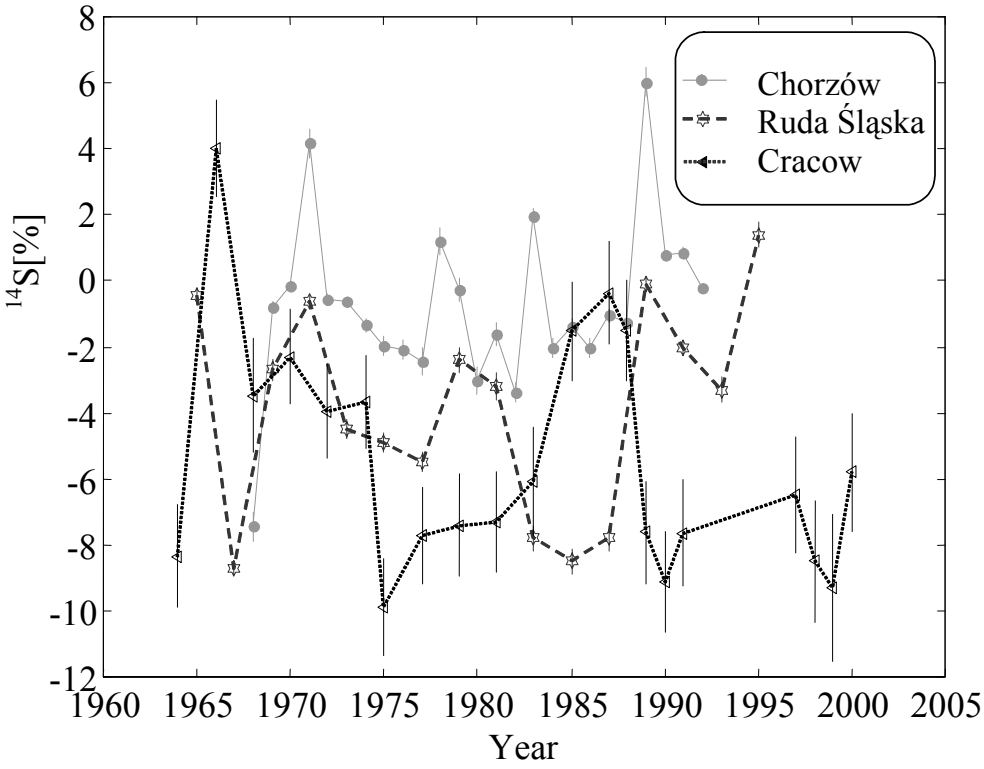

Figure 3 Changes of ^{14}S in tree rings from Ruda Śląska, Chorzów, and Kraków

Coniferous trees, contrary to deciduous trees, begin the assimilation cycle earlier, which allows registration of decreased ^{14}C concentration due to seasonal changes of CO_2 emission originating from fossil-fuel burning.

The value of CO_2 concentration in the atmosphere is a sum of 2 components. Natural changes of CO_2 concentration in the atmosphere and changes due to the global Suess effect are described by C_{backgr}, referred to as the natural component (background concentration). Changes of the concentration due to a local Suess effect are expressed by C_{fossil}, referred to as the emission component (fossil-fuel concentration, Levin et al. 1989). In order to determine the emission component, the following formula is used:

$$C_{fossil} = C_{backgr} \times \left[\left(\frac{^{14}C_{backgr} - {}^{14}C}{^{14}C_{backgr}} \right) \times 100\% \right] \quad (2),$$

where C_{backgr} is the CO_2 concentration in the clean air in (ppmv), $^{14}C_{backgr}$ is the ^{14}C concentration in clean air in (pMC), and ^{14}C is the ^{14}C concentration for the examined region in (pMC).

Values of CO_2 concentration and ^{14}C concentration in the clean air were taken from measurements done in Schauinsland (Levin et. al. 1995; Levin and Kromer 1997). Figure 4 present values of C_{fossil} for tree rings from Kraków, Ruda Śląska, and Chorzów. Negative values of C_{fossil} are not presented in this figure. Such values are contrary to the assumption about ^{14}C concentration in the clean air.

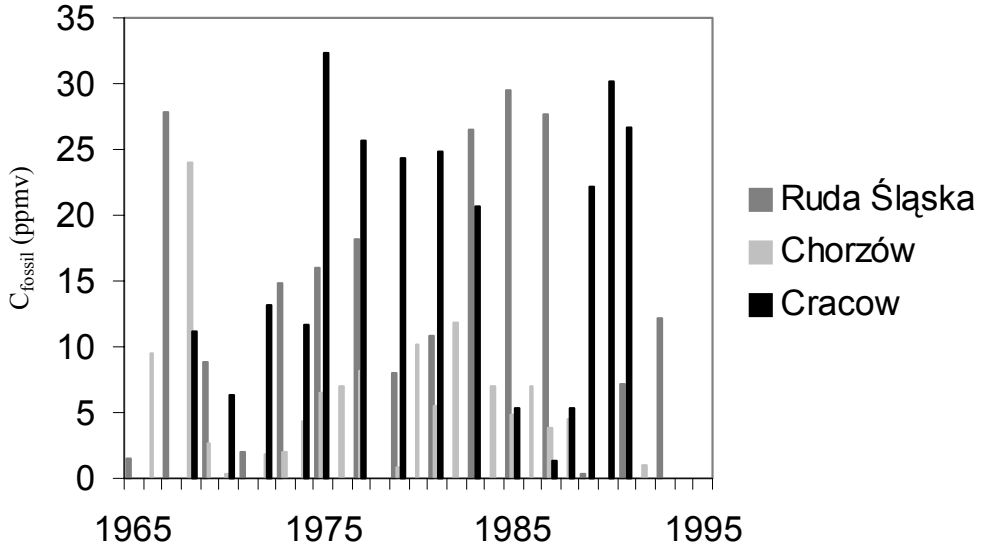

Figure 4 Changes of component value C_{fossil} for Ruda Śląska, Chorzów, and Kraków

A comparison between $\Delta^{14}C$ determined for tree rings and for atmospheric CO_2 from Kraków is presented in Figure 5. The values for atmospheric CO_2 from Kraków were determined on the basis of the average value of $\Delta^{14}C$ for the period from May to August in 1983–1990 (Kuc and Zimnoch 1998). It can be observed that values of $\Delta^{14}C$ in tree rings are lower that in atmospheric CO_2. It is very difficult to explain this effect. It might be connected with natural processes occurring during assimilation of CO_2 by trees. A systematic error between laboratories, however, cannot be excluded.

$\Delta^{14}C$ and $\delta^{13}C$ in a "Clean" Environment in North Poland

Impact of Fossil-Fuel Burning on the Values of $\Delta^{14}C$

Emission of CO_2 from fossil-fuel burning is the reason for ^{14}C concentration depletion. Therefore, ^{14}C concentration was compared with emission of CO_2 for Poland for 1861–1955 as estimated by Marland et al. (2001). Results of that comparison are presented in Figure 6. The correlation coefficient between $\Delta^{14}C$ and average CO_2 emission for 1851–1955 is –0.23 ($n = 95$, $p<0.01$). Analyzing trends of changes reveals that from 1910, an anticorrelation between $\Delta^{14}C$ and average CO_2 emission exists. The correlation coefficient for 1910–1955 is –0.33 ($n = 50$, $p<0.02$).

Generally, the relationship between $\Delta^{14}C$ and CO_2 emission can be described as follows:

$$\Delta^{14}C = a \times e + b \quad (3),$$

where e is CO_2 emission in Poland in tons/yr as estimated by Marland et al. (2001).

Table 3 contains values of parameters a and b, correlation coefficients (r), numbers of samples (n), and significance levels (p) for different periods.

Impact of Anthropogenic Effect on $\delta^{13}C$ Values in Wholewood of Tree Rings

In the case of the trunk from Augustów, the observed decrease of $\delta^{13}C$ values is not absolutely connected with physiological processes occurring in the plant, but it can be anthropogenic. The reason for the decrease can be found in changes of carbon isotopic composition of atmospheric CO_2 for that

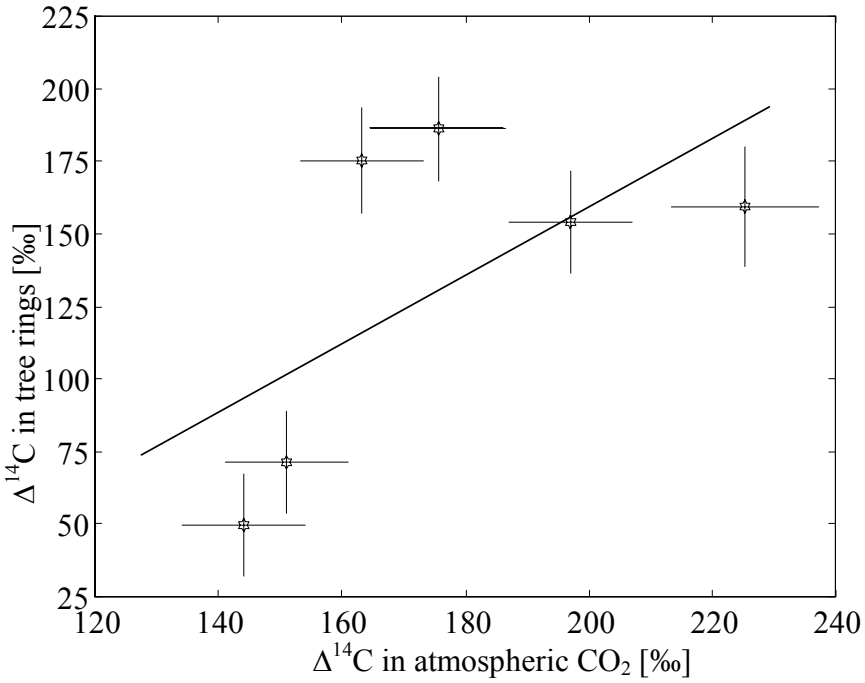

Figure 5 Comparison between $\Delta^{14}C$ determined for tree rings and for atmospheric CO_2 from Kraków

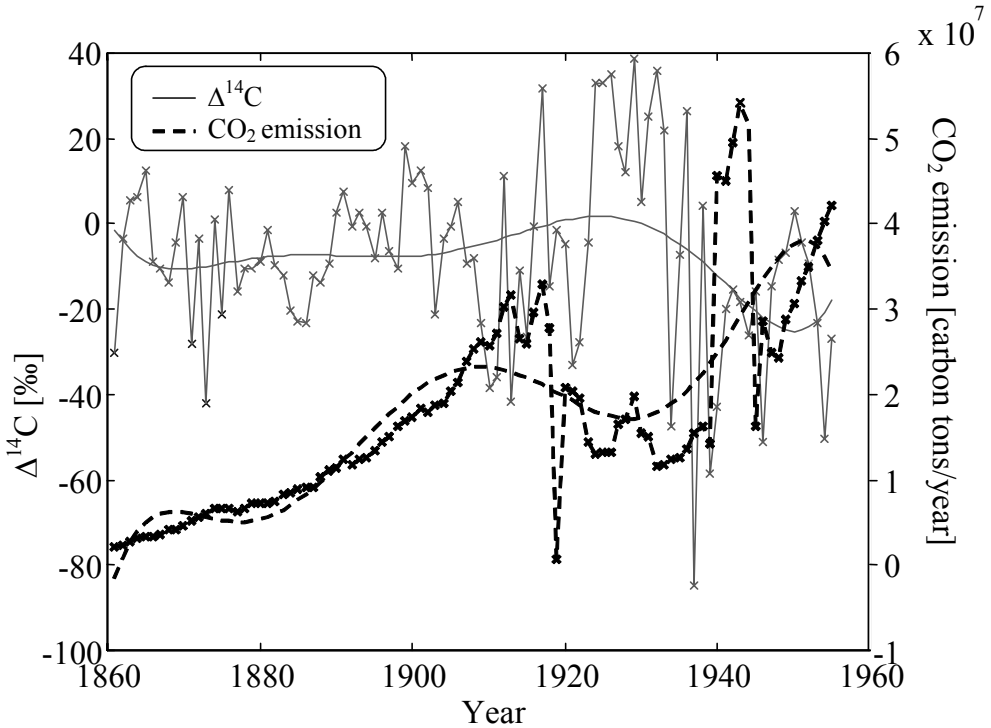

Figure 6 Comparison values of tree ring $\Delta^{14}C$ with estimated CO_2 emission in Poland for years 1861–1955 (Marland et al. 2001)

Table 3 Relationship between $\Delta^{14}C$ in Augustów tree rings and average CO_2 emission estimated for Poland for different periods.

Years	*a*	*b*	*r*	*n*	*p*
1861–1955	-4×10^{-7}	–0.691	–0.23	95	<0.01
1910–1955	-8×10^{-7}	9.965	–0.33	50	<0.02

period. Development of local industry began in the 1950s. It was a source of CO_2 emission from fossil-fuel burning. Such an increase in CO_2 emission throughout Poland since 1949 is evident. Depletion observed after 1950 can be caused by both a local and regional scale increase of CO_2 emission.

Figure 7 presents comparison between $\delta^{13}C$ in wholewood and CO_2 estimated by Marland et al. (2001) for Poland for 1861–1968. Data correlated with CO_2 emission cover the entire year, but wood used for the investigating was formed during a vegetation period. The tree used materials stored in a period before the growth. Analysis by linear regression shows that the average sequence of $\delta^{13}C$ exhibits a higher correlation than $\Delta^{14}C$ with CO_2 emission, $r = -0.24$.

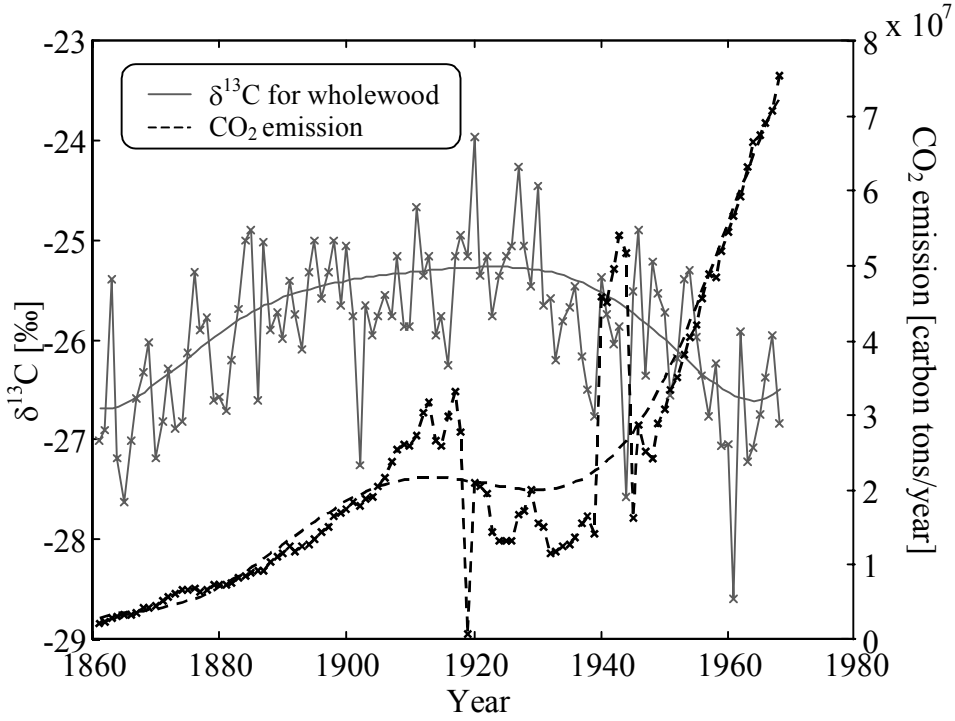

Figure 7 Comparison between $\delta^{13}C$ in Augustów tree rings (wholewood) and emission of CO_2 estimated for Poland for 1861–1968 (Marland et al. 2001).

If values (1861–1889) related to the preliminary stage of growth—"juvenile effect" or "canopy effect" (Sheu et al. 1997)—are eliminated from the curve of $\delta^{13}C$ values, then the correlation coefficient between $\delta^{13}C$ and CO_2 emission is greatly improved, $r = -54$ ($n = 79$, $p<0.001$).

The relationship between $\delta^{13}C$ values of wholewood and CO_2 emission estimated by Marland et al. (2001) can be written as follows:

$$\delta^{13}C = a \times e + b \quad (4),$$

where e is the CO_2 emission in Poland expressed in carbon tons/yr.

Parameters a and b, correlation coefficients (r), numbers of samples (n), and significance levels (p) for different periods are listed in Table 4.

Table 4 Relationship between Augustów $\delta^{13}C$ and CO_2 emission for different periods.

Years	a	b	r	n	p
1861–1968	-9×10^{-9}	–25.724	–0.20	108	<0.02
1890–1968	-2×10^{-8}	–25.116	–0.54	79	<0.001

Impact of Anthropogenic Effect on $\delta^{13}C$ Values in Latewood α-Cellulose

Figure 8 presents a comparison between $\delta^{13}C$ in latewood α-cellulose and CO_2 emission in Poland estimated by Marland et al. (2001) for 1899–1968. A quantitative comparison in this case is complicated because the entire year data is available and CO_2 emission changes seasonally. Higher CO_2 emission is generally connected with the winter time. However, in the case of the investigated material, the strongest impact was probably the local effect due to the development of local industry. If local factories were the main source of CO_2 emission, it can be supposed that this kind of source was not seasonal.

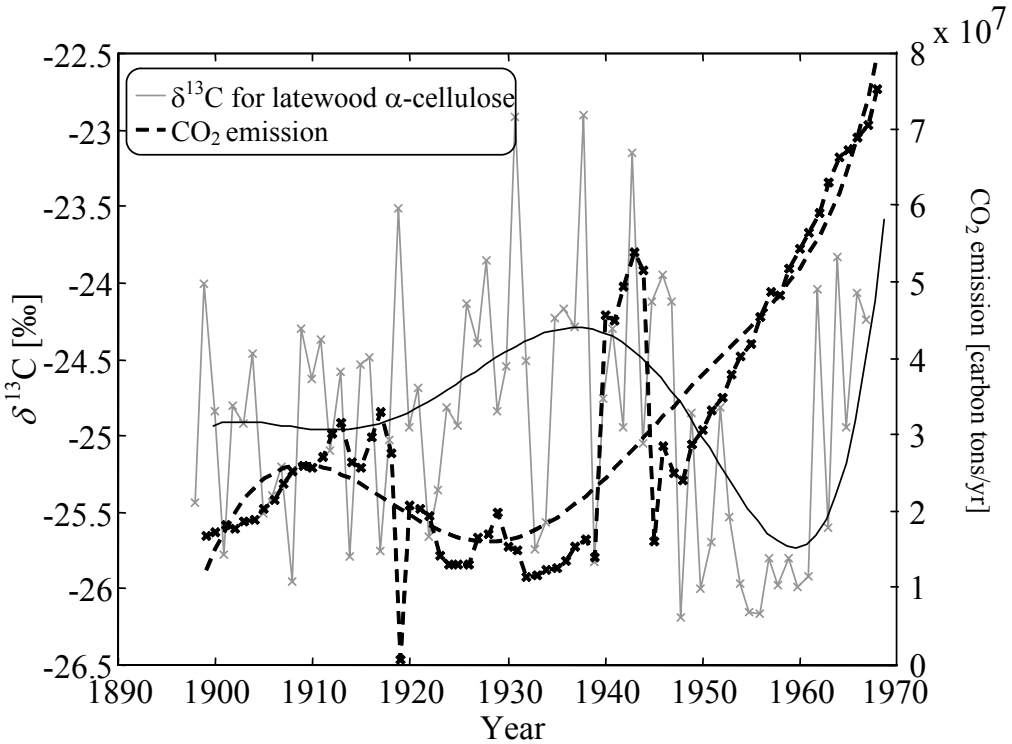

Figure 8 Comparison between $\delta^{13}C$ in latewood α-cellulose of Augustów tree rings and emission of CO_2 estimated for Poland for years 1899–1968.

Values of $\delta^{13}C$ have increased since 1963. Such a behavior can result from the lower hydraulic conductance in vascular systems (Switsur et al. 1996). Considering the impact of anthropogenic and physiological effects on $\delta^{13}C$ values, the period 1963–1968 was ruled out. In this case, the correlation coefficient is –0.36 (n = 64, p<0.005).

Comparing trends in Figure 8, it can be noticed that from 1910 a clear anticorrelation between $\delta^{13}C$ and CO_2 emission exists. The correlation coefficient for 1910–1962 is –0.40 ($n = 53$, $p<0.005$).

On the basis of Equation 4, a relationship between $\delta^{13}C$ in latewood α-cellulose and CO_2 emission estimated for Poland can be described. Parameters *a* and *b*, correlation coefficients (*r*), numbers of samples (*n*), and significance levels (*p*) for different periods are listed in Table 5.

Table 5 Relationship between $\delta^{13}C$ in Augustów α-cellulose and CO_2 emission for different periods.

Years	*a*	*b*	*r*	*n*	*p*
1899–1968	-7×10^{-9}	–24.685	–0.15	70	<0.3
1899–1962	-2×10^{-8}	–24.357	–0.36	64	<0.005
1910–1962	-2×10^{-8}	–24.232	–0.40	53	<0.005

ESTIMATION OF CO_2 CONCENTRATION IN THE ATMOSPHERE ON THE BASIS OF $\Delta^{13}C$ IN LATEWOOD α-CELLULOSE

Values of $\delta^{13}C$ in latewood α-cellulose depend on many factors. By analyzing the impacts of subsequent factors on $\delta^{13}C$, the following partial differential equation can be written:

$$\delta^{13}C = f(y, t, p, e, \rho) \tag{5}$$

$$\frac{\partial \delta^{13}C(y,t,p,e,\rho)}{\partial y} = \frac{\partial \delta^{13}C}{\partial t} \times \frac{\partial \delta^{13}C}{\partial y} + \frac{\partial \delta^{13}C}{\partial p} \times \frac{\partial p(y)}{\partial y} + \frac{\partial \delta^{13}C}{\partial e} \times \frac{\partial pe(y)}{\partial y} + \frac{\partial p(y)}{\partial y} \tag{6}$$

where *y* is the year, $\frac{\partial \delta^{13}C}{\partial y}$ is the partial derivative of $\delta^{13}C$ with respect to time (in yr),

$\frac{\partial \delta^{13}C}{\partial t}$ is the partial derivative of $\delta^{13}C$ with respect to temperature,

$\frac{\partial \delta^{13}C}{\partial p}$ is the partial derivative of $\delta^{13}C$ with respect to precipitation,

$\frac{\partial \delta^{13}C}{\partial e}$ is the partial derivative of $\delta^{13}C$ with respect to CO_2 emission,

$\frac{\partial t}{\partial y}$ is the change of temperature in time,

$\frac{\partial p}{\partial y}$ is the change of precipitation in time,

$\frac{\partial e}{\partial y}$ is the change of CO_2 in time,

$\frac{\partial \rho}{\partial y}$ is the change of $\delta^{13}C$ in time under the influence of additional factors, for example, "potential for growth," carbon flux from biosphere to atmosphere, or an error connected with establishment.

In the analysis using latewood $\delta^{13}C$, constant gradients of $\delta^{13}C$ with respect to temperature, precipitation, and CO_2 emission were assumed.

With the linear regression method, they were found to be:
$\frac{\partial \delta^{13}C}{\partial t} = 0.51‰ / °C$, $\frac{\partial \delta^{13}C}{\partial p} = -0.00217‰ / mm$, $= \frac{\partial \delta^{13}C}{\partial e} = -2 \times 10^{-8}‰ /$ tons carbon (see also the trends). Integrating Equation 6 with respect to time, individual components of $\delta^{13}C$ originating from those factors were obtained (see Figure 9). Defining the following notation:

$$\delta 1(y) = 0.51‰ / °C \times t(y) \quad (7),$$

$$\delta 2(y) = -0.00217‰ / mm \times p(y) \quad (8),$$

$$\delta 3(y) = -2 \times 10^{-8}‰ / \text{tons carbon} \times e(y) \quad (9),$$

it can be written as

$$\delta^{13}C(y) = \delta 1(y) + \delta 2(y) + \delta 3(y) + R \quad (10).$$

In the above equations, R stands for other factors, noted as ρ in Equations 5 and 6 together with errors due to the assumptions made. Figure 9 presents all the components from Equation 10.

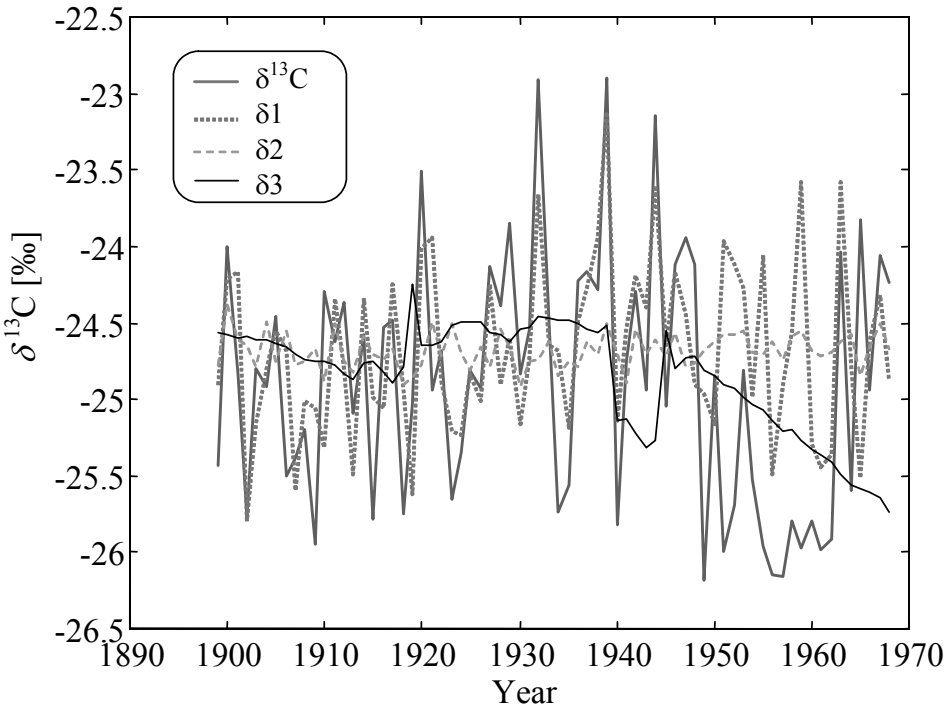

Figure 9 Components of $\delta^{13}C$ due to different factors

The correlation coefficient between $\delta^{13}C$ in latewood α-cellulose and average temperature in July and August (meteorological data for Warsaw) is $r = 0.49$ ($n = 70$, $p < 0.001$).

Considering the impact of anthropogenic and physiological effects on $\delta^{13}C$ values, the period of 1949–1968 was ruled out. In such a case, the correlation coefficient is 0.71, which indicates the significance level is better than 0.001‰.

Because there is no meteorological data for Augustów, values of $\delta^{13}C$ were also compared with average temperatures recorded in Kaunas (for 1922–1968). Correlation coefficients between values of $\delta^{13}C$ in latewood α-cellulose and average temperature for the period of July–August noted in Kaunas are comparable to that obtained for the case of meteorological data for Warsaw ($r = 0.45$, $n = 47$, $p<0.02$). The correlation coefficient for 1922–1948 between $\delta^{13}C$ and the average temperature noted in Kaunas is 0.63 ($n = 27$, $p<0.001$). A simple way to relate $\delta^{13}C$ variations to temperature

is by a coefficient that means carbon isotopes shift per unit temperature change. By analyzing spatial distribution of temperature, it can be noted that $\delta^{13}C$ changes with temperature appear in the range 0.42 – 0.51‰ / °C.

Generally, the relationship between $\delta^{13}C$ in latewood α-cellulose and the average temperature for the period of July–September can be described as follows:

$$\delta^{13}C = a \times t + b \quad (11),$$

where t is average temperature (in °C) for the period of July–September.

Table 6 contains values of parameters a and b, correlation coefficients (r), number of samples (n), and significance levels (p).

Table 6 Relationship between $\delta^{13}C$ in latewood α-cellulose and average temperature in July–August for different periods.

Meteorological data	Years	a [‰ / ºC]	b	r	n	p
Warsaw	1899–1968	0.36	–31.4	0.49	70	<0.001
	1899– 1948 and 1963–1968	0.44	–32.73	0.65	56	<0.001
	1899–1948	0.51	–34.01	0.71	50	<0.001
Kaunas	1922–1968	0.33	–30.66	0.45	47	<0.002
	1922–1948	0.42	–31.97	0.63	27	<0.001

In the case of precipitation, the correlation coefficient between $\delta^{13}C$ in latewood α-cellulose and precipitation in July and August is –0.33 ($n = 27$, $p<0.1$). The poor correlation is due to the distance between the meteorological observatory and Augustów.

A relationship between $\delta^{13}C$, temperature, and precipitation was determined on the basis of meteorological data for Warsaw and for Kaunas for July and August (the time when latewood is formed). However, the relationship between $\delta^{13}C$ and CO_2 emission was determined on the basis of estimations by Marland et al. (2001). CO_2 emission concerns the entire year and whole area of Poland. Local factors had the strongest impact on $\delta^{13}C$ values. It is believed that a similar conclusion can be drawn for CO_2 emission. Therefore, the contribution of CO_2 was excluded (see Figure 10).

Assuming that only temperature, precipitation, and CO_2 from fossil-fuel burning contribute to $\delta^{13}C$, the CO_2 emission can be evaluated as presented in Figure 11. This CO_2 emission data was compared with CO_2 emission evaluated for Poland by Marland et al. (see Figure 11). The comparison can only be done in terms of quality (a general behavior) but not quantity. It is impossible to determine values of local emission and the trend can only be compared.

CONCLUSION

Carbon isotopic composition in tree rings reflects corresponding atmospheric CO_2 concentration during their formation. A decrease of ^{14}C concentration caused by the emission of ^{14}C-depleted CO_2 from fossil-fuel burning was observed in Kraków, Chorzów, and Ruda Śląska. The local Suess effect on the polluted area (Upper Silesia and Kraków) was determined.

An anticorrelation exists between $\Delta^{14}C$ and average CO_2 emission in tree rings from the ecologically clean Augustów Wilderness region. Assuming that only temperature, precipitation, and CO_2 from

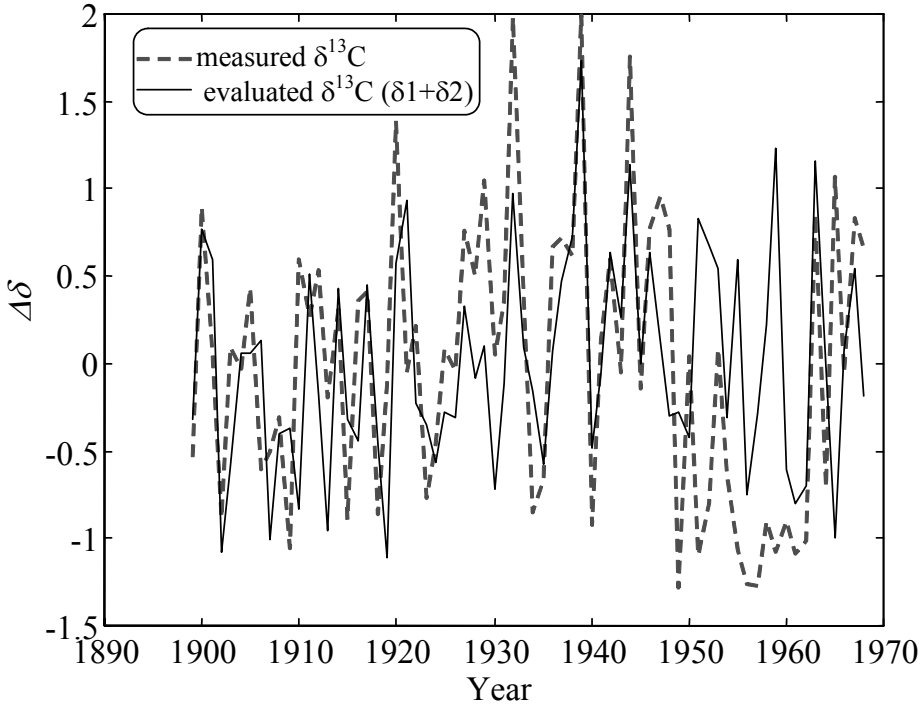

Figure 10 Fluctuating measured and evaluated (δ1 + δ2) $\delta^{13}C$

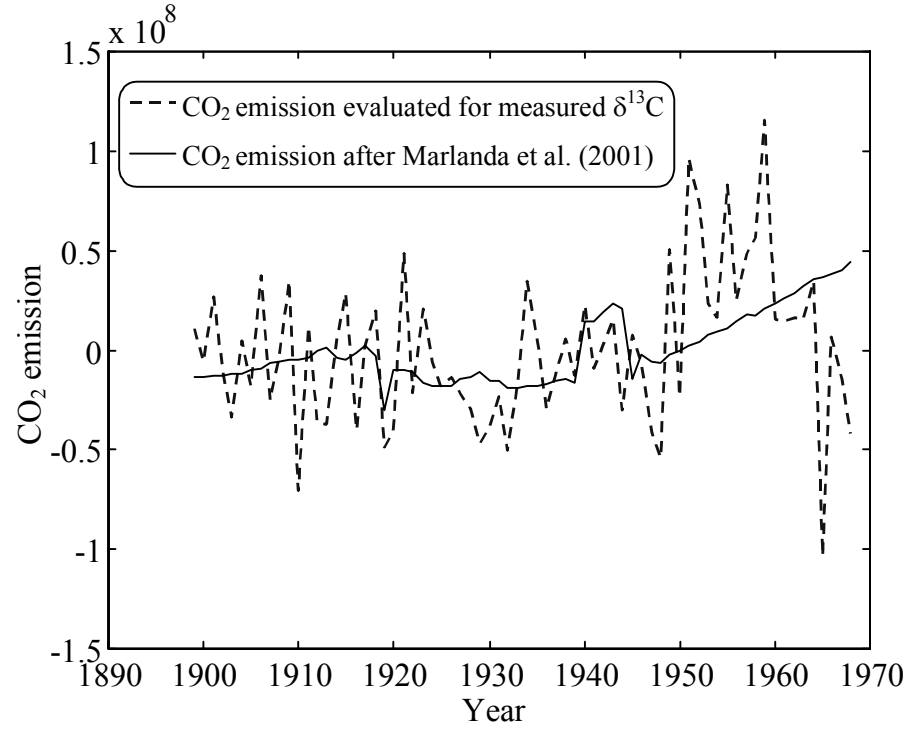

Figure 11 Comparison of evaluated CO_2 emission with that given by Marland et al. (2001)

fossil-fuel burning contributed to $\delta^{13}C$, the CO_2 emission was evaluated. That CO_2 emission data was compared with CO_2 emission evaluated by Marland et al. (2001). The comparison was done only in terms of quality but not quantity.

ACKNOWLEDGEMENTS

The authors express their gratitude to the State Committee for Scientific Research, Poland, which supported the work reported in this article under the grant number 6 P04G 055 20.

REFERENCES

Awsiuk R, Pazdur MF. 1986. Regional Suess effect in the Upper Silesia urban area. *Radiocarbon* 28(2A):655–60.

Damon PE, Cheng S, Linck TW. 1989. Fine and hyperfine structure in the spectrum of secular variations of atmospheric ^{14}C. *Radiocarbon* 31(3):704–18.

De Jong AFM, Mook WG. 1982. An anomalous Suess effect above Europe. *Nature* 298:1–3.

Florkowski T, Kuc T. 1979. Carbon isotopes and sulphur content as indicators of atmospheric pollution from burning fossil fuels. *Environment International* 2: 431–5.

Green JW. 1963. Wood cellulose. In: Whistler RL, editor. *Carbohydrate Chemistry III.* San Diego: Academic Press. p 9–21.

Keeling CD, Bascetow RB, Carter AF, Piper SC, Whorf TP, Heimann M, Mook WM, Roeloffzen H. 1989. A three-dimensional model of atmospheric CO_2 transport based on observed winds: 1. Analysis of observational data. In: Petersen DH, editor. Aspects of Climate Variability in the Pacific and Western Americas. *Geophysical Monographs* 55:165–236.

Kuc T. 1986. Carbon isotopes in atmospheric CO_2 of the Kraków region: a two-year record. *Radiocarbon* 28(2A):649–54.

Kuc T, Zimnoch M. 1998. Changes of the CO_2 sources and sinks in a polluted urban area (southern Poland) over the last decade, derived from the carbon isotope composition. *Radiocarbon* 40(1):417–23.

Levin I, Graul R, Trivett NBA. 1995. Long-term observations of atmospheric CO_2 and carbon isotopes at continental sites in Germany. *Tellus* 47B:23–34.

Levin I, Hesshaimer V. 2000. Radiocarbon—a unique tracer of global carbon cycle dynamic. *Radiocarbon* 42(1):69–80.

Levin I, Kromer B. 1997. Twenty years of high-precision atmospheric $^{14}CO_2$ observations at Schauinsland station, Germany. *Radiocarbon* 39(2):205–18.

Levin I, Schuchard J, Kromer B, Münnich KO. 1989. The continental European Suess effect. *Radiocarbon* 31(3):431–40.

Loader NJ, Robertson I, Barker AC, Switsur VR, Waterhouse JS. 1997. An improved technique for the bath processing of small wholewood samples to α-cellulose. *Chemical Geology* 136:313–7.

Marland G, Boden TA, Andres RJ. 2001. Global, regional, and national fossil fuel CO_2 emissions. In: *Trends: A Compendium of Data on Global Change*. Carbon Dioxide Information Analysis Center, Oak Ridge National Laboratory, US Department of Energy, Oak Ridge, Tennessee, USA. http://cdiac.ornl.gov/ndps/ndp030.html.

Nydal R, Lövseth K. 1983. Tracing bomb ^{14}C in the atmosphere. *Journal of Geophysical Research* 88:3621–42.

Oeschger H, Siegenthaler U, Schotterer U, Gugelmann A. 1975. A box-diffusion model to study the carbon dioxide exchange in nature. *Tellus* 27:169–92.

Pazdur A, Matyja S, Rakowski AZ. 1998. Radiocarbon concentration measurements in contemporary tree rings from Upper Silesia. *RMZ-Materials and Geoenvironment* 45(1–2):255–7.

Rakowski AZ, Pawełczyk S, Pazdur A. 2001. Changes of ^{14}C concentration in modern trees from Upper Silesia region, Poland. *Radiocarbon* 43(2):633–43.

Robertson I, Waterhouse J. 1998. Trees of knowledge. *Chemistry in Britain*. London: Royal Society of Chemistry. p 27–30.

Schleser GH, Helle G, Lucke A, Vos H. 1999. Isotope signals as climate proxies: the role of transfer functions in the study of terrestrial archives. *Quaternary Science Reviews* 18:927–43.

Sheu DD, Kou P, Chiu C-H, Chen M-J. 1997. Variability of tree rings in Taiwan fir: growth effect and response to May–October temperatures. *Geochimica et Cosmochimica Acta* 60(1):171–7.

Siegenthaler U, Oeschger H. 1987. Biospheric CO_2 emmision during the past 200 years reconstructed by deconvolution of ice core data. *Tellus* 39:140–54.

Stuiver M, Quay P. 1981. Atmospheric ^{14}C changes resulting from fossil fuel CO_2 release and cosmic ray flux variability. *Earth and Planetary Science Letters* 53:349–62.

Switsur VR, Waterhouse JS, Field EM, Carter AHC. 1996. Climatic signals from stable isotopes in Oak tree rings from East Anglia, Great Britain. In: Dean JS, Meko DM, Swetnam TW, editors. *Tree Rings, Environment and Humanity.* Tucson, Arizona: Radiocarbon. p 637–45.

Tans PP, Mook WG. 1980. Past atmospheric CO_2 levels and the $^{13}C/^{12}C$ ratios in tree rings. *Tellus* 32:268–83.

RADIOCARBON, Vol 46, Nr 2, 2004, p 721–731

AN AMS ^{14}C POLLEN-DATED SEDIMENT AND POLLEN SEQUENCE FROM THE LATE HOLOCENE, SOUTHERN COASTAL HAWKE'S BAY, NEW ZEALAND

Pamela I Chester

36 Woodland Road, Johnsonville, Wellington, New Zealand. Email: pchester@actrix.co.nz.

Christine A Prior

Rafter Radiocarbon Laboratory, IGNS, PO Box 31–312, Lower Hutt, New Zealand.

ABSTRACT. Hawke's Bay is a region of New Zealand where earliest settlement of indigenous people may have occurred. A sedimentological and palynological study of lake sediments from a small catchment was undertaken to reconstruct erosion, vegetation, and fire histories to determine human environmental impact, and thus add to knowledge of the timing of initial settlement of New Zealand. Precise dating was an essential facet of the research because of the short time span of human occupation in New Zealand. A chronology is proposed based on accelerator mass spectrometry (AMS) radiocarbon dating of palynomorph concentrates. Known-age tephras were used as a check on the validity of the ^{14}C ages obtained using this technique, which is being developed at Rafter Radiocarbon Laboratory. Two episodes of sustained erosion occurred between about 1500 and 1050 BC with a period of ~50 yr at about 1300 BC when no erosion occurred. Five episodes of erosion of very short duration occurred at about 625 BC, 450 BC, 100 BC, AD 950, and AD 1400. Erosion probably resulted from landslides induced by earthquakes or severe storms, with the exception of the last event which coincides with local burning and is probably a consequence of this. A conifer/broadleaved forest surrounded the lake until soon after AD 1075–1300, when a dramatic decline in pollen of forest plants and an increase in charcoal occurred. Forest was replaced by fire-induced scrub, interpreted as a result of anthropogenic burning by prehistoric Polynesians. A further decline in woody vegetation occurred when European-introduced plants appear in the pollen record and extensive pasture was established.

INTRODUCTION

There has been vigorous debate in recent years amongst archaeologists on the time of first human settlement in New Zealand (McGlone 1983; Sutton 1987; Caughley 1988; Anderson 1991; Sutton 1994; Holdaway and Beavan 1999; Anderson 2000; Hedges 2000; Lowe et al. 2000). Three chronologies for first human settlement of New Zealand have emerged from the debate: the short chronology, which suggests that first human settlement occurred no longer than 600 yr ago; the traditional chronology, which suggests that first human settlement occurred about 1000 yr ago; and the long chronology, which suggests that first human settlement occurred at least 1400 yr ago. The shorter chronologies have relied mainly on radiocarbon ages associated with direct archaeological evidence of human presence. Such dates are minimum ages because the site of first settlement may have been missed. Where human occupation has been associated with forest clearance and other disturbance of the vegetation, the palynological signature of these events may be detected in nearby sedimentary deposits without the exact site of disturbance needing to be discovered. Common lines of evidence in these studies, from regions where forest was burnt to clear land for husbandry of domesticated plants, include various combinations of a decline in forest species, an increase in pioneer species, an increase in microscopic charcoal particles, and an increase in the rate of soil erosion (Faegri and Iversen 1992).

In readily datable deposits, the palynological signal of land clearance by burning can provide independent evidence of the time of occupation. A sedimentological and palynological study of lake sediments from a small catchment was undertaken to reconstruct erosion, vegetation, and fire histories to determine human impact, and thus add to the current knowledge of the timing of initial settlement of New Zealand by the indigenous people. Precise dating was an essential facet of the research because of the short time span of human occupation in New Zealand. Accelerator mass spectrometry (AMS) ^{14}C dating of pollen and spore concentrates and known-age tephras were used to construct a chronology. The former technique was expected to give a close temporal association between fossil

Proceedings of the 18th International Radiocarbon Conference, edited by N Beavan Athfield and R J Sparks
RADIOCARBON, Vol 46, Nr 2, 2004, p 721–731

pollen and spores preserved in the lake sediments and the contemporary vegetation and to provide more accurate dating of late Holocene vegetation changes interpreted from palynological analyses than techniques formerly used, as it avoids contamination by inwashed soil carbon (McGlone and Wilmshurst 1999).

METHODS

Site Selection

Hawke's Bay (Figure 1) is a region of New Zealand where earliest settlement of indigenous people may have occurred (Fox 1982). It has an equable climate suitable for growing the tropical crops introduced by the first settlers of New Zealand from eastern Polynesia (Bulmer 1989). Round Lake, 39°39′S, 176°58′E, was chosen for the study reported here because it fulfills the criteria necessary for recording a detailed vegetation history of a small geographic area from before (presumed) human settlement in New Zealand to the present (Jacobson and Bradshaw 1981). The lake lies on a Pleistocene terrace of gravels, sands, and silts of the Kidnappers Group (Kingma 1970), about 2 km from the Hawke's Bay coast at about 40 m above sea level, and is likely to have been in such proximity for several thousand years (L Brown, personal communication, 2001). The lake has a diameter of 250 m and an associated small catchment of about 0.2 km^2. Maximum water depth was 7.5 m at the time of sampling. The lake basin is closed with no inflowing or outflowing streams, and is surrounded by extensive pastureland.

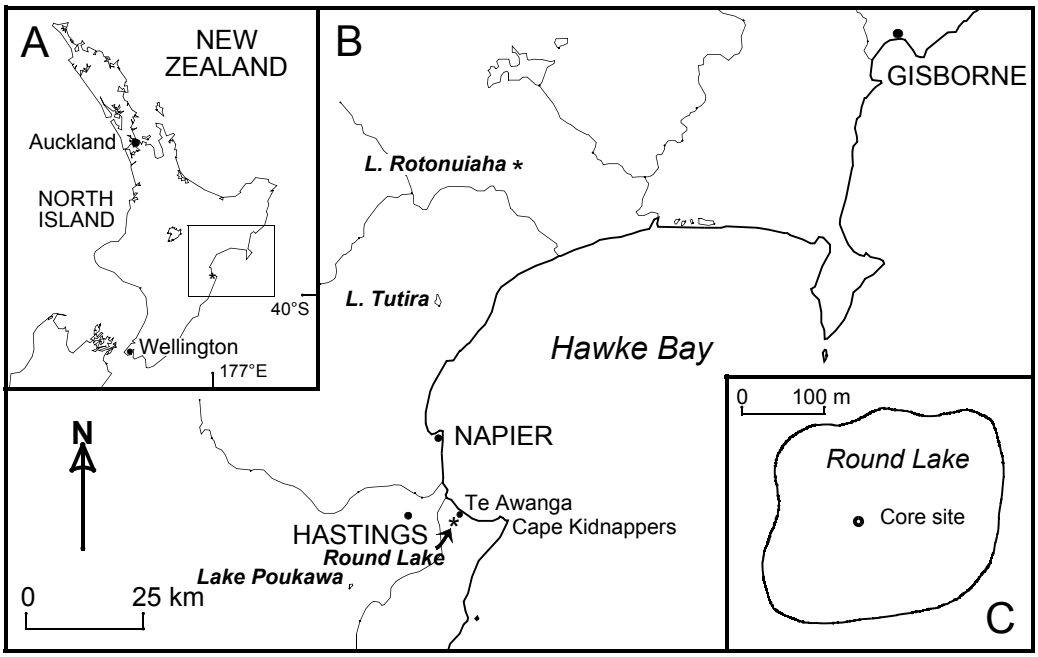

Figure 1 North Island, New Zealand (A), with Hawke's Bay region (B), showing location of places referred to in the text and palynological sampling site (C).

Field and Laboratory Work

A sediment core was collected from near the center of the lake using a hand-operated piston corer. The upper 300 cm were collected as a continuous core. Sampling for dry bulk density, fossil pollen and spores, and charcoal analyses was based on a combination of uniform and structural sampling

principles. Analyses were performed on samples of 1 cm^3 of sediment extracted from the centers of 1-cm slices of core. Dry bulk density was measured using a weight loss technique. Samples with elevated dry bulk density values, containing a high proportion of inorganic matter, were examined under a microscope for presence of glass shards. For correlation with known-age volcanic eruptions, the chemistry of single glass shards was examined using a Jeol-733 Electron Microprobe set at a 10-micron beam, 8 nano amp current and 15 kV accelerating voltage. The glass shards were separated from the bulk sample using sodium polytungstate (2.45 g/cc). At least 10 shards were analyzed for each sample, averages made and compared to the analyst's (Alan Palmer) own database of known rhyolite tephras. A rhyolite glass standard was used for calibration.

A sequence of AMS ^{14}C ages was determined using a pollen separation technique developed at Rafter Radiocarbon Laboratory. ^{14}C dating is the predominant chronological measurement tool for assigning ages to palynological sequences. Generally, ^{14}C ages are obtained on bulk samples of peat or sediment or terrestrial macrofossils. In this study, microfossil pollen and spores extracted from selected palynological samples provide material for ^{14}C dating. This method directly dates the pollen and spore assemblages used to reconstruct the vegetation history of the region, thus eliminating the risk (resulting from contamination by extraneous carbon contained within bulk samples) of a mismatch between chronology and interpreted vegetation. It may still arise, however, that the interpreted vegetation is not contemporaneous with sedimentation if pollen and spores are redeposited. After initially applying standard chemical palynological preparation techniques, with the omission of steps that use organic reagents, a density separation method was used to concentrate pollen and spores (Prior and Chester 2001). This method is superior to that of Brown et al. (1989, 1992) and Richardson and Hall (1994), whose methods failed to remove chemically-resistant non-pollen organic material, and is quicker than hand-picking (Long et al. 1992) or mouth-pipetting (Mensing and Southon 1999).

Fossil pollen and spores and charcoal particles were prepared for microscopic examination using standard palynological techniques (Faegri and Iversen 1989). Tablets containing a known number of *Lycopodium* spores were added to the samples, allowing pollen, spore, and microscopic charcoal particle concentrations to be calculated (Stockmarr 1971). Thus, the more commonly used relative frequencies and influx rates of the pollen rain could be calculated. Palynomorphs were counted until at least 200 grains of terrestrial taxa had been counted (except for 2 samples with very sparse pollen). Charcoal particle analyses were performed on every microscope slide examined for pollen and spores. Individual charcoal particle areas were measured using a semiautomatic computerized image-analyzing system (Raine et al. 1996). Particles were divided into 2 size classes: 400 μm^2 and greater, and smaller than 400 μm^2 (Patterson et al. 1987; Chester 1998).

RESULTS

Sediment Physical Properties

The core sediments comprise mostly a plastic, homogeneous, very fine-grained, highly humified, dark brown to black, highly organic lake mud (gyttja) with 2 clay-rich units near the base of the sequence and thin layers (ranging from 1 to 3 cm thick) of either clay, clay-rich, or sandy material intercalated in the gyttja (Figure 2). Sharp boundaries of the thin layers suggest abrupt environmental changes. With the exception of some thin layers, dry bulk density values are less than 0.4 g cm^{-3} and reflect the organic-rich nature of the sediments. Five thin layers had dry bulk density values greater than 0.4 g cm^{-3} and were found to contain glass shards. Glass chemistry analyses carried out on these samples by A Palmer (personal communication, 2001) indicated that three of these layers represented primary airfall tephras: the Taupo, either the Mapara or Whakaipo (these two are indistinguishable from their glass chemistry unless both are present), and the Waimihia (Figure 2). Thin layers that do not represent primary airfall tephras are sediments eroded from the catchment.

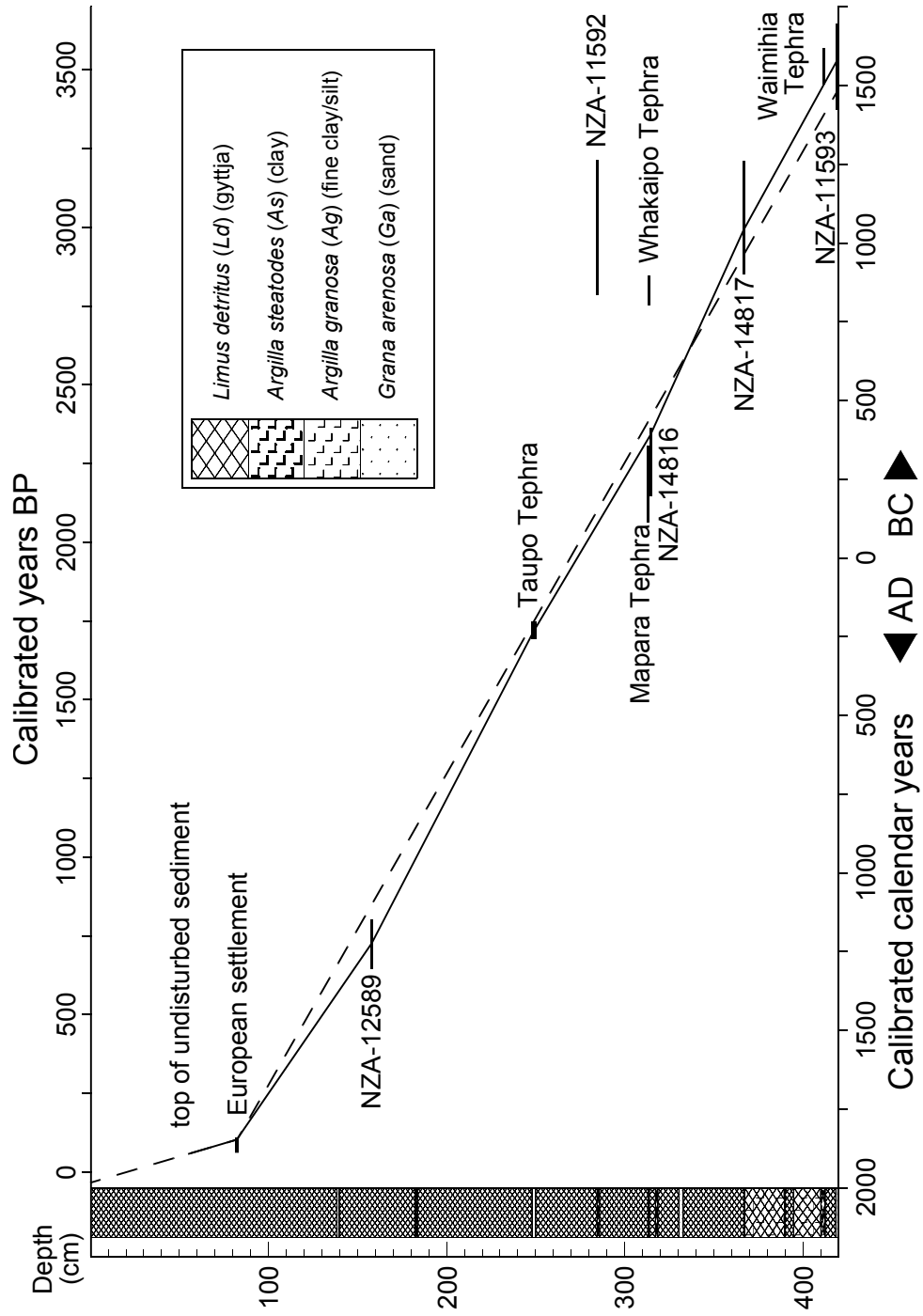

Figure 2 Age/depth plot for Round Lake core. The age/depth function is based on AMS ^{14}C ages of concentrated palynomorphs, ^{14}C ages of tephras identified from glass shard chemistry, and an 1850 date for European settlement placed at first appearance of European plants and a rise in microscopic charcoal content. Length of age bars indicates uncertainty of age measurement. The Taupo tephra age is from Sparks et al. (1995) and has a 1 σ confidence interval. Other tephra ages are derived from the error-weighted mean age and pooled error of Froggatt and Lowe (1990, Table 1). These were calibrated in the same manner as the concentrated palynomorphs and similarly have a 2 σ confidence interval. The solid line is a best-fit age-depth function preferred for the archaeological chronology; for comparison, the dashed line is a linear fit between the extreme dates.

Dating

In the samples prepared for dating by density separation, the density fraction with the greatest concentration of pollen and spores was determined by visual inspection under a microscope. In all samples from Round Lake, it was found that the greatest concentration occurred at a specific gravity of 1.15, so this fraction was chosen for combustion and dating. Carbon yields of this fraction were also significantly higher than that for other fractions (Table 1). The carbon content of that part of pollen and spores that remains after fossilization, the external shell (exine), is higher than that of plant cell walls, the other carbon-containing component remaining after density separation. The primary chemical component of the pollen exine, sporopollenin, is a carbon-rich C_{90} molecule which, although it can vary with taxa, consists of between 60 and 80% carbon (Shaw 1971). Plant cell walls are composed primarily of cellulose. Pure cellulose is about 44% carbon by weight, and when plants, wood, or charcoal are combusted for ^{14}C dating, they typically yield about 50% carbon. High carbon yields are, therefore, also a guide to pollen and spore concentration in the samples.

Table 1 AMS ^{14}C ages on density fractions.

Depth (cm)	Fraction dated (sg[a])	Lab nr NZA-	Carbon yield (%)	^{14}C age[b] (BP)	$\delta^{13}C$ (‰)	Calibrated ages (± 2 σ[c])
158–159	1.15	12589	70.6	786 ± 60	–27.5	AD 1073–1299
284–285	1.15	11636	69.0	2710 ± 60	–27.8	997–795 BC
	1.15	11592	69.0	2866 ± 70	–27.7	1263–838 BC
	1.20	11589	58.0	2794 ± 60	–29.3	1118–818 BC
	1.40	11590	53.3	2850 ± 65	–27.3	1253–835 BC
314–315	<1.20	14816	61.9	2286 ± 50	–24.0	408–202 BC
366–367	1.15	14817	49.7	2882 ± 55	–26.3	1258–907 BC
418–419	1.15	11637	67.7	3201 ± 55	–27.8	1603–1321 BC
	1.15	11593	67.7	3282 ± 60	–27.7	1690–1423 BC
	1.20	11591	61.2	3333 ± 60	–29.5	1747–1459 BC
	1.35	11588	60.1	3243 ± 60	–27.4	1679–1404 BC

[a]sg = specific gravity.
[b]^{14}C age as defined by Stuiver and Polach (1977).
[c]^{14}C ages were calibrated with WINSCAL (Institute of Geological & Nuclear Sciences) using the atmospheric $\Delta^{14}C$ and ^{14}C ages from INTCAL98 (Stuiver et al. 1998).

AMS ^{14}C ages of density fractions are shown in Table 1. In 2 samples (284–285 cm and 418–419 cm), the fraction containing the greatest pollen and spore concentration (1.15 sg) and 2 other fractions containing a greater quantity of other plant remains were dated for comparison. Conventional ^{14}C ages for the 3 fractions from each sample are statistically identical, indicating that the plant remains deposited in the sediment and the palynomorphs are the same age. Reproducibility of ages in this way increases confidence in the contemporaneousness of the dated pollen and spores with the contemporary vegetation that is reconstructed.

^{14}C ages on 2 samples of 1.15 specific gravity from 284–285 cm and 418–419 cm depth were repeated because the first measurements (NZA-11592 and NZA-11593) were made on targets with a low graphite yield. The second ^{14}C age obtained for the fraction from 418–419 cm yielded an age statistically identical to that first obtained, but the second age obtained for the fraction 284–285 cm (NZA-11636) is slightly younger. Since the second measurement was made on a graphite target with

an acceptable reaction yield and conforms better to that expected, we have greater confidence in its reliability. Thus, it is used in the age/depth plot (Figure 2).

The age/depth plot was drawn using various chronological markers. Initially, a series of 3 samples were selected from the pollen-analyzed core for AMS ^{14}C dating. The uppermost sample (NZA-12589) was taken from a pollen sample that showed an increase in the abundance of microscopic charcoal particles. A second sample (NZA-11636), taken near the base of the upper continuous 300 cm of core, was selected for ^{14}C dating because it was contiguous with a layer with elevated dry bulk density suspected of representing either a tephra or eroded sediment. The third sample (NZA-11593) was taken from the base of the entire sequence. Results of these ^{14}C determinations indicated a non-uniform sedimentation rate that did not conform to the results expected from sediment analyses. In addition, the age determined from sample number NZA-11636 did not conform to the known ages of either the Mapara or Whakaipo tephras (Froggatt and Lowe 1990).

A second series of 2 samples from the 314–315 cm and 366–367 cm depths were selected to bracket the lower clay-rich units to provide a rate of deposition for these units, and the tephra identified by glass chemistry as either Mapara or Whakaipo. ^{14}C age measurements on these 2 samples were made on density separation fractions with the highest pollen concentrations. Dating results (NZA-14816 and NZA-14817) indicated that the deposition rate of the clay-rich units was slightly higher than that of the remainder of the sediments which had been deposited almost uniformly, suggesting that the thin intercalated layers of either primary airfall tephra or material eroded from the catchment had been deposited very rapidly. These results match the results of the sediment analyses. A linear age/depth function of best-fit drawn through the chronological markers confirms this. It was also confirmed that the tephra deposited at 313–314 cm was the Mapara; thus, the age of this tephra, 2160 ± 25 BP (Froggatt and Lowe 1990), could be applied to the constructed chronology.

On the basis of this dating, 1 sample, NZA-11636, lies outside the linear age/depth function. This sample was immediately above a thin clay-rich layer (Figure 2). As the layer did not contain glass shards, it must represent sediments eroded from the catchment. The dated sample must have contained reworked palynomorphs and forest litter older than the contemporary vegetation eroded from the catchment; large plant fragments in the 1.40 specific gravity fraction also produced ages that were older than expected. The amount of contamination required by old carbon to increase the age of the ^{14}C age from that expected using the linear age/depth function to that obtained would be small (Caughley 1988). This example demonstrates the necessity of applying multiple lines of evidence to check on the validity of ^{14}C determinations.

Pollen, Spore, and Charcoal Sequence

Only a very few significant taxa of the total taxa counted are discussed here. Pollen spectra are divided into 3 distinct local pollen-assemblage zones based on absolute abundance and relative frequency pollen and spore data and abundance of charcoal particles in the 2 size classes (Figure 3). They are formed to simplify discussion and interpretation of the pollen sequence and facilitate discussion of the vegetational events and comparison with other pollen sequences. The zone boundaries are placed where change in the pollen spectra is most marked, so that the enclosed units are relatively homogeneous and can be juxtaposed with cultural periods.

Zone 3 (420–158 cm) is dominated by tall woody species (mostly *Podocarpus totara* and *Prumnopitys taxifolia*) which represent a conifer/broadleaved lowland forest. A great diversity of small trees was growing close to the lake, but pollen of *Kunzea*/*Leptospermum* is most frequent. Trees of both these genera have high light requirements for growth. They can only establish on bare ground and

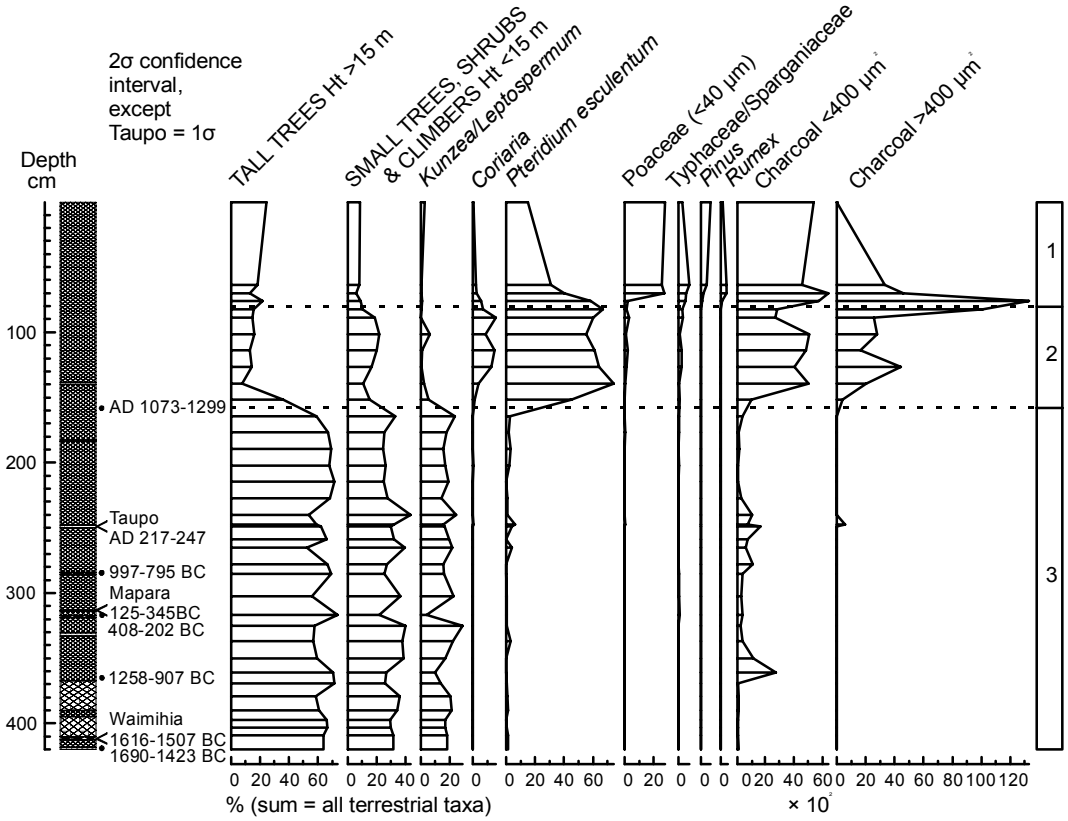

Figure 3 Pollen and charcoal diagram for Round Lake, Hawke's Bay

are not self-perpetuating unless the canopy is open. Their long record suggests that they were growing in an unstable area, perhaps on a flood plain or as a coastal scrub, in swamp and/or perhaps in a damp area close to the lake. *Pteridium esculentum* (the native bracken fern) is sporadic in occurrence, sometimes corresponding to inwashed clay. It is most abundant following the deposition of the Taupo tephra. Charcoal particles in the smaller size class form an almost continuous record but in very low abundance. Particles of the larger size class only occur following the deposition of the Taupo tephra. This may result from a greater frequency of fires in forests of reduced canopy cover and, thus, of greater fire susceptibility.

Zone 2 (158–80 cm) is characterized by a decline in woody taxa, although *Coriaria* and *Pteridium esculentum* increase. Wild grasses (Poaceae pollen with longest axis <40 µm) also increase. *Coriaria*, *Pteridium esculentum*, and grass are light-demanding species, and indicate that the canopy of the lowland forest close to Round Lake was more open. *Coriaria* and *Pteridium esculentum* are also pioneer species and are fire-encouraged. Pollen of Typhaceae/Sparganiaceae also increases, indicating more extensive reeds, probably a response to greater influx of nutrients into the lake. Charcoal particles of both size classes occur in a much greater abundance, indicating a large increase in the frequency and/or intensity of distant and local fires.

Zone 1 (80–0 cm) is characterized by the appearance of the European-introduced *Pinus*, several European-introduced weed taxa (for example, *Rumex*), and an increase in wild grasses. The abundance of the taller woody species remains stable, but the lower woody species decline further.

Typhaceae/Sparganiaceae increases, suggesting that nutrient influx to the lake increases further. A dramatic increase in influx of charcoal in both size classes occurs. This indicates widespread burning both locally and regionally. Notably, the larger size class is not represented in the surface sample; no intentional burning close to Round Lake is known to occur currently.

DISCUSSION

Almost all archaic (earliest) archaeological sites in New Zealand are coastal (McKinnon 1997), so palynological analysis of coastal sites could be expected to better reflect the beginnings of human settlement in the region. Archaic sites have been recorded along the coast of Hawke's Bay (Fox 1982). The oldest dated archaeological site from Hawke's Bay is a rectangular pit, measuring 4 × 2.5 m and 60 cm deep, from a coastal site (Fox 1982). Rectangular pits are the remnants of semi-subterranean food storage houses that were used for the storage of seasonal crops, mostly of kumara (sweet potato), but also for other crops such as yams (Davidson 1984). The pits were roofed with a ridgepole supported on 2 or 3 central upright posts embedded in a dirt floor. A ^{14}C age obtained from the charred remains of a roof-supporting post from the rectangular pit from coastal Hawke's Bay was originally reported as NZ-1914: 1050 ± 90 BP (Fox 1978, appendix 6). Before 1978, ^{14}C age measurements produced by the Rafter Radiocarbon Laboratory (formerly Institute of Nuclear Sciences, DSIR) were calculated using a set of New Zealand reference standards (Rafter et al. 1972) and the Cambridge half-life of 5730 yr. Ages produced since 1978 have been calculated according to the international reporting conventions suggested by Stuiver and Polach (1977), and during the late 1980s, ^{14}C ages in the DSIR database were recalculated to conform to international reporting standards. Conversion of the age of the post to the international reporting conventions of Stuiver and Polach (1977) results in a conventional ^{14}C age of 1009 ± 122 BP (Prior and Chester 2001), which can be calibrated to AD 771–1272 (1179–678 cal BP) at 2 σ confidence interval. The post was made from a tree estimated to be between 75 and 125 yr old based on its diameter and average expected growth rate. There is the possibility that the tree was not freshly cut, so its youngest ^{14}C age could be appreciably older than the date of construction of the storage house (Davidson 1984). However, if the reported age is coeval with the date of construction, this is the earliest known construction of a roofed rectangular food storage house. It can be compared with the date of AD 1170 ± 60 obtained from charcoal on the floor of a rectangular storage pit on the Coromandel Peninsula in the north of New Zealand, where early experiments in the development of this type of storage pit may have been carried out (Davidson 1984). If these 2 dates are an accurate reflection of the time of construction, the development of large roofed rectangular semi-subterranean food storage houses was close to the traditionally accepted date of initial settlement of New Zealand, and there is the possibility that Hawke's Bay was settled early in the original settlement of New Zealand and that it would be palynologically visible.

A widely-known palynological study from the Hawke's Bay region which spans the period of probable initial Polynesian settlement is that from swamps around Lake Poukawa (McGlone 1978, 2002). It was reported that inland central Hawke's Bay was covered with a dense, diverse podocarp-hardwood forest prior to human occupation. Where corresponding pollen percentages were reported to show first signs of the decline of the forest, a ^{14}C determination on a 50-mm-thick slice of peat (0.55–0.60 m) was originally reported as NZ-4162: 1190 ± 70 BP. Another determination on peat, slightly higher in the sequence at 0.40–0.45 m, where forest destruction is more evident, was originally reported as NZ-4163: 980 ± 70 BP. The 2 ^{14}C ages cited by McGlone (1978) have been recalculated to a conventional ^{14}C age of 1156 ± 59 BP (NZ-4162) and 946 ± 59 BP (NZ-4163). These can be calibrated to AD 715–1008 (1235–942 cal BP) and AD 989–1218 (961–732 cal BP) at 2 σ confidence intervals, respectively. Charcoal fragments were found in the swamp sediments and

so the deforestation was assumed to have been caused by fire presumed to have resulted from Polynesian settlement. The upper part of the pollen sequence reflects European settlement and the final conversion of the vegetation to grassland. More recent palynological research studied 2 inland lakes in northern Hawke's Bay (Wilmshurst 1997). The more coastal lake is some 10 km from the coast, beyond the dispersal range of most pollen grains (Tauber 1965 calculated that only 5% of pollen in Denmark reaches distances of 5 to 10 km), and prevailing wind is from the southwest (Tomlinson 1976), so these sites also reflect inland vegetation. ^{14}C dates were rejected for being too old because of contamination, so the sequence was dated by associated tephras. Deforestation is estimated from sedimentation rates to have begun "about 500 calendar years BP" (Wilmshurst 1997).

It is now generally accepted that a rapid loss of forest and coincident rapid rise and sustained abundance in the pioneer plants of *Pteridium esculentum* and wild grass from about 800 to 600 yr ago resulted from anthropogenic burning. This has been interpreted by some authors to be an indication of initial human impact on the environment of New Zealand and first colonization (settlement) of New Zealand. However, Flenley and Todd (2001) have argued that this may not be the palynological signal of initial human impact, but rather represents establishment of the use of the *Pteridium esculentum* rhizome as a staple food, which allowed people to settle areas previously uninhabitable because of the lack of a suitable crop. They proposed that small and sometimes intermittent occurrences of bracken prior to the rapid increase might reflect early establishment of slash-and-burn agriculture that is, small temporary clearings in the forest, used to grow crops for a few years and then abandoned. In this situation, the bracken is a weed in the abandoned gardens, and may disappear as the forest regenerates. They proposed that colonization was a 2-stage process. In the initial stage, colonization was limited to coastal areas and the north because of the need to grow tropical crops. The second stage occurred after the technology to produce the *Pteridium esculentum* rhizome as a crop and safe food resource had been developed. Following this scenario, the small sporadic occurrences of *Pteridium esculentum* spores in the sequence from Round Lake may be indicative of small coastal settlements in Hawke's Bay prior to AD 1075–1300.

CONCLUSION

Dating extracted pollen and spores directly ages the palynomorphs on which the vegetation history is reconstructed and avoids contamination by inwashed soil carbon. However, in this study, there is not complete agreement between AMS ^{14}C ages of concentrated palynomorphs and ^{14}C ages of identified tephras, probably as a result of a dated sample containing reworked palynomorphs. A most probable solution, using selected dates of both dating methods, has been used in construction of the following site history.

Between about 1600 BC to AD 1200, a diverse conifer/broadleaved forest with either a closed canopy and smaller marginal trees and/or a discontinuous upper story with a lower story of smaller trees existed on the Hawke's Bay lowlands. With the exception of the effect of the deposition of the Taupo tephra, when forest taxa decline and abundance of charcoal particles increases, evidence for disturbance of this forest is minimal with *Pteridium esculentum* (which may be indicative of small coastal settlements) occurring sporadically and in low abundance. Two episodes of sustained inwash of sediments from the catchment occurred between about 1500 and 1050 BC with a period of about 50 yr at about 1300 BC when no inwash occurred. Above this, 4 episodes of inwash of catchment sediments of very short duration are recorded at about 650 BC, 450 BC, 100 BC, and AD 950. Inwash of inorganic sediments during this period are not accompanied by deposition of charcoal and probably resulted from slumping within the catchment caused either by storms or tectonic movement, and there was no evident contemporaneous disruption of vegetation. Low abundance of charcoal

particles in the smaller size class probably results from distant infrequent fires, either naturally or anthropogenically induced.

At AD 1200, there is abundant evidence that substantial prehistoric settlement began in the vicinity of Round Lake, a dramatic decline in abundance of forest taxa, coincident with a significant increase in the abundance of charcoal particles, in both size classes. The rapidity, magnitude, and constancy of the increased abundance of charcoal particles suggest that anthropogenic burning occurred in the vicinity of Round Lake. There is a corresponding increase of the pioneer, light-demanding, and fire-encouraged taxa of *Pteridium esculentum* and *Coriaria*, and light-demanding grasses. *Pteridium esculentum* is rapidly suppressed by shrubland and forest regeneration; thus, its persistence in the pollen record represents repeated burning, and the presence of a constantly high influx of charcoal particles confirms this. Erosion occurred within the catchment at about AD 1400 and nutrients into the lake increase. This phase of obvious local human impact, commencing AD 1200, is more recent than the initial anthropogenic destruction noted at the inland site of Lake Poukawa at AD 715–1008 (2 σ confidence level), but may be contemporaneous with the more evident forest destruction at AD 989–1218 (2 σ confidence level). It is earlier than that found at Lakes Tutira and Rotonuiaha, estimated to be about 500 yr ago; it may be contemporaneous with the coastal food storage pit (AD 771–1272). The beginning of this phase occurs within the time period when New Zealand is traditionally thought to have been occupied by immigrants from eastern Polynesia (Davidson 1984).

European settlement began at about AD 1850. A further decline in the lower woody vegetation occurred and European-introduced taxa appear. Charcoal abundance increases dramatically and grass pollen becomes abundant as a result of European land clearance for pasture.

ACKNOWLEDGEMENTS

This research was funded by a post-doctoral fellowship at Massey University, New Zealand. Marsden Grant 99–MAU–010 provided funding for ^{14}C dating. We thank our mentor, John Flenley, for suggesting this research project and giving support throughout the project. For field assistance, we thank David Feek, Tim O'Dea, Kevin Butler, Pip Chrystal, School of People, Environment and Planning, Massey University; and Ian Raine, Institute of Geological and Nuclear Sciences, New Zealand. Thanks are due to Alan Beu, Institute of Geological and Nuclear Sciences, for shell identification. We are greatly indebted to Dennis Eden, private consultant, and Alan Palmer, Institute of Natural Resources, Massey University, who identified tephras.

REFERENCES

Anderson AJ. 1991. The chronology of colonization in New Zealand. *Antiquity* 65:767–95.

Anderson AJ. 2000. Differential reliability of ^{14}C AMS ages of *Rattus exulans* bone gelatin in South Pacific prehistory. *Journal of the Royal Society of New Zealand* 30(3):243–61.

Brown TA, Farwell GW, Grootes PM, Schmidt FH. 1992. Radiocarbon AMS dating of pollen extracted from peat samples. *Radiocarbon* 43(3):550–6.

Brown TA, Nelson DE, Mathewes RW, Vogel JS, Southon JR. 1989. Radiocarbon dating of pollen by accelerator mass spectrometry. *Quaternary Research* 32(2):205–12.

Bulmer S. 1989. Gardens in the south: diversity and change in prehistoric Maori agriculture. In: Harris DR, Hillman GC, editors. *Foraging and Farming: The Evolution of Plant Exploitation*. London: Unwin Hyman. p 688–705.

Caughley G. 1988. The colonisation of New Zealand by the Polynesians. *Journal of the Royal Society* 18(3): 245–70.

Chester PI. 1998. Late Holocene vegetation history of Grevena Province, northwestern Greece [PhD dissertation] Wellington: Victoria University of Wellington.

Davidson J. 1984. *The Prehistory of New Zealand*. Auckland: Longman Paul Ltd.

Faegri K, Iversen J. 1992. *Textbook of Pollen Analysis.* 4th edition (Faegri K, Kaland PE, Krzywinski K, editors). Chichester: John Wiley & Sons Ltd.

Flenley JR, Todd A. 2001. A genome or a memome: the cause of the rise of bracken fern at around 700 BP in New Zealand. In: Jones M, Sheppard P, editors.

Australasian Connections and New Directions. *Proceedings of the 7th Australasian Archaeometry Conference 2001*. p 141–54.

Froggatt PC, Lowe DJ. 1990. A review of the Quaternary silicic and some other tephra formations from New Zealand: their stratigraphy, nomenclature, distribution, volume, and age. *New Zealand Journal of Geology and Geophysics* 33:89–109.

Fox A. 1978. Tiromoana Pa, Te Awanga, Hawke's Bay, Excavations 1974–5. *University of Otago studies in prehistoric anthropology* Volume II (New Zealand Archaeological Association Monograph 8).

Fox A. 1982. Hawke's Bay. In: Prickett N, editor. *The First Thousand Years*. Palmerston North: Dunmore Press. p 62–82.

Hedges REM. 2000. Appraisal of radiocarbon dating of kiore bones (Pacific rat *Rattus exulans*) in New Zealand. *Journal of the Royal Society of New Zealand* 30(4):385–98.

Holdaway RN, Beavan NR. 1999. Reliable ^{14}C AMS dates on bird and Pacific rat *Rattus exulans* bone gelatin, from a $CaCO_3$-rich deposit. *Journal of the Royal Society of New Zealand* 29:185–211.

Jacobson GL Jr, Bradshaw RH. 1981. The selection of sites for paleovegetational studies. *Quaternary Research* 16:80–96.

Long A, Davis OK, De Lanois J. 1992. Separation and ^{14}C dating of pure pollen from lake sediments: nanofossil AMS dating. *Radiocarbon* 34(3):557–60.

Kingma JT. 1970. Sheets N134, Napier and Hastings and N135, Kidnappers. Geological Map of New Zealand 1:63 360. Wellington.

Lowe DJ, Newnham RM, McFadgen BG, Higham TFG. 2000. Tephras and New Zealand archaeology. *Journal of Archaeological Science* 27:859–70.

McGlone MS. 1978. Forest destruction by early Polynesians, Lake Poukawa, Hawke's Bay, New Zealand. *Journal of the Royal Society of New Zealand* 8:275–81.

McGlone MS. 1983. Polynesian deforestation of New Zealand: a preliminary synthesis. *Archaeology in Oceania* 18(1):11–25.

McGlone MS. 2002. A Holocene and latest Pleistocene pollen record from Lake Poukawa, Hawke's Bay, New Zealand. *Global and Planetary Change* 33:283–99.

McGlone MS, Wilmshurst JM. 1999. Dating initial Maori environmental impact in New Zealand. *Quaternary International* 59:5–16.

McKinnon M, editor. 1997. *New Zealand Historical Atlas: ko papatuanuku e takoto nei.* Albany: David Bateman. 290 p.

Mensing SA, Southon JR. 1999. A simple method to separate pollen for AMS radiocarbon dating and its application to lacustrine and marine sediments. *Radiocarbon* 41(1):1–8.

Patterson WAIII, Edwards KJ, Maguire DJ. 1987. Microscopic charcoal as a fossil indicator of fire. *Quaternary Science Reviews* 6:3–23.

Prior CA, Chester PI. 2001. Precision radiocarbon dating of a Late Holocene vegetation history. In: Jones M, Sheppard P, editors. Australasian Connections and New Directions: Proceedings of the 7th Australasian Archaeometry Conference. *Research in Anthropology and Linguistics* 5:285–94.

Rafter TA, Jansen HS, Lockerbie L, Trotter MM. 1972. New Zealand radiocarbon reference standards. In: Rafter TA, Grant-Taylor T, compilers. *Proceedings of the Eighth International Radiocarbon Dating Conference*. Held at Lower Hutt, New Zealand, 18–25 October 1972. Wellington: Royal Society of New Zealand.

Raine JI, Crampton JS, Crouch EM, Hollis CH, St George W, Scott GH. 1996. Manual of digital image capture and processing techniques in Paleontology Section, IGNS. *Institute of Geological & Nuclear Sciences Science Report* 96/20.

Richardson F, Hall VA. 1994. Pollen concentrate preparation from highly organic Holocene peat and lake deposits for AMS dating. *Radiocarbon* 36(3):407–12.

Shaw G. 1971. The chemistry of sporopollenin. In: Brooks J, Grant PR, Muir M, van Gijzel P, Shaw G, editors. *Sporopollenin.* London: Academic Press. p 305–48.

Sparks RJ, Melhuish WH, McKee JWA, Ogden J, Palmer JG, Molloy BPJ. 1995. ^{14}C calibration in the Southern Hemisphere and the date of the last Taupo eruption: evidence from tree-ring sequences. *Radiocarbon* 32(2):155–63.

Stockmarr J. 1971. Tablets with spores used in absolute pollen analysis. *Pollen et Spores* 13:615–21.

Stuiver M, Polach HA. 1977. Discussion: reporting of ^{14}C data. *Radiocarbon* 19(3):355–63.

Stuiver M, Reimer PJ, Bard E, Beck JW, Burr GS, Hughen KA, Kromer B, McCormac FG, van der Plicht J, Spurk M. 1998. INTCAL98 radiocarbon age calibration, 24,000–0 cal BP. *Radiocarbon* 40(3):1041–83.

Sutton DG. 1987. A paradigmatic shift in Polynesian prehistory: implications for New Zealand. *New Zealand Journal of Archaeology* 9:135–55.

Sutton DG, editor. 1994. *The Origins of the First New Zealanders*. Auckland: Auckland University Press.

Tauber H. 1965. Differential pollen dispersion and interpretation of pollen diagrams. *Danmarks Geologiske Undersøgelse*. *Række II 89*.

Tomlinson AI. 1976. Climate. In: Wards I, editor. *New Zealand Atlas.* Wellington: A.R. Shearer Government Printer. p 82–9.

Wilmshurst JM. 1997. The impact of human settlement on the vegetation and soil stability in Hawke's Bay, New Zealand. *New Zealand Journal of Botany* 35:97–111.

RADIOCARBON, Vol 46, Nr 2, 2004, p 733–744

SHAPE ANALYSIS OF CUMULATIVE PROBABILITY DENSITY FUNCTION OF RADIOCARBON DATES SET IN THE STUDY OF CLIMATE CHANGE IN THE LATE GLACIAL AND HOLOCENE

Danuta J Michczyńska[1] • Anna Pazdur

Radiocarbon Laboratory, Institute of Physics, Silesian University of Technology, Krzywoustego 2, 44-100 Gliwice, Poland.

ABSTRACT. We report on a statistical analysis of a large set of radiocarbon dates for reconstruction of paleoclimate. Probability density functions were constructed by summing the probability distributions of individual ^{14}C dates. Our analysis was based on 2 assumptions: 1) The amount of organic matter in sediments depends on paleogeographical conditions; 2) The number of ^{14}C-dated samples is proportional to the amount of organic matter deposited in sediments in the examined time intervals. We quantified how many dates are required to give statistically reliable results. As an example, 785 peat dates from Poland were selected. The dates encompassed the Holocene and Late Glacial period. All dates came from the Gliwice Radiocarbon Laboratory. Results were compared with other paleoenvironmental records. Detailed analysis of the frequency distributions showed that preferential sampling plays an important part in the shape determination. The general rule to take samples from locations where visible changes of sedimentation are apparent (e.g. from the top and the bottom of the peat layer) results in narrow peaks in the probability density function near the limits of the Holocene subdivision.

INTRODUCTION

Since the 1970s, analyses of frequency distributions of radiocarbon-dated samples over restricted timescales have been carried out for several selected geographic regions. Geyh and Streif (1970) used 330 ^{14}C dates of sediments from lagoons and tidal flats in the Netherlands, Niedersachsen, and Schleswig-Holstein to investigate sea-level variations on a regional scale. The basic assumption of their study was that ^{14}C dates could be expected only for periods in which intensive peat formation occurred. In 1980, Geyh presented a Holocene North Sea sea-level history based on a set of 641 ^{14}C dates. In the same article, the limitations of the statistical evaluation of ^{14}C dates using histograms were discussed. Pazdur and Pazdur (1986b) analyzed the frequency distribution of ^{14}C dates between arbitrarily chosen limits of 10 and 15 kyr BP. They used all the ^{14}C dates made before 1985 in the Gliwice Radiocarbon Laboratory for the territory of Poland to construction a cumulative histogram. The authors found prominent maxima corresponding to the interstadials of Bölling and Alleröd, and the minima of the Older and Younger Dryas. Also, the beginning of the Holocene was marked by a sharp increase in the frequency of ^{14}C dates. In turn, Goździk and Pazdur (1987) analyzed the frequency of ^{14}C dates from the territory of Poland in the time interval from 12 to 45 kyr BP based on a set of 193 samples. Although, in the authors' opinion, a significantly larger set of ^{14}C dates was necessary to draw detailed conclusions, the frequency distribution revealed good agreement with conclusions drawn from geological, paleobotanical, and geomorphological evidence and they suggested the dates would be useful in reconstruction of paleoclimate. Pazdur et al. (1995) presented the age distribution of speleothems from the Kraków-Wieluń Upland, southern Poland. The principal period of speleothem deposition fell within the Holocene; in particular, the maximum peak of the probability density approximately fitted the climatic optimum of the Holocene (i.e. Atlantic period). The older dates ranged from 48 to 20 kyr. These boundaries coincided almost exactly with the Interplenivistulian climatostratigraphic unit. ^{14}C dating, which was primarily used simply to determine the age of sediment-containing samples, became an important source of information on the development of some geologic processes in the past. It should be stressed that the analysis of the frequency distribution of results from other dating methods has also been used in paleoclimate study.

[1]Corresponding author. Email: djm@radiocarbon.gliwice.pl.

Proceedings of the 18th International Radiocarbon Conference, edited by N Beavan Athfield and R J Sparks
RADIOCARBON, Vol 46, Nr 2, 2004, p 733–744

Hercman (2000) presented an attempt to utilize the U/Th dates of speleothems as a source of paleoclimatic data. She also presented a detailed review of earlier studies concerning the analysis of growth frequency curves of cave speleothems. The speleothem deposition intensity is influenced by the changing climate, which is reflected in a clustering of dating results in certain time intervals. An example of a frequency distribution of 456 results of TL dating of loess samples was discussed by Singhvi et al. (2001) and Bluszcz and Michczyński (1999).

We report on a statistical analysis of a large set of ^{14}C dates for the reconstruction of the paleoenvironment. Our analysis was based on 2 assumptions:

1. The amount of organic matter in sediments depends on paleogeographical conditions.
2. The number of ^{14}C-dated samples is proportional to the amount of organic matter deposited in sediments in studied time intervals.

When the criteria for including ^{14}C dates in an analyzed set are chosen suitably (Geyh 1980; Goździk and Pazdur 1987; Stolk et al. 1994), fluctuations in the constructed cumulative distribution reflect changes of the investigated geologic phenomenon. The cumulative probability density function (CPDF) is created by superposition of individual Gaussian distributions for each ^{14}C date. Analysis of the shape of the CPDF may allow periods with favorable conditions for sedimentation (peaks of CPDF) or unfavorable conditions (gaps of CPDF) to be determined. But the key question is whether peaks and gaps are the result of environmental changes in the past or statistical and sampling fluctuations. In other words: How does one test accurately if the analyzed CPDF is significantly different from the uniform CPDF? How many dates are required to give reliable results? Geyh discussed such problems for histograms (Geyh 1980) and distinguished 3 kinds of histograms according to the value of the parameter s describing statistical fluctuations:

- Reliable histograms, $s \leq 20\%$
- Common histograms, $50\% < s < 20\%$
- Unreliable histograms, $s \geq 50\%$

In his article, the studied time interval is divided in a number of classes. The number of dates belonging to a certain class l is a random variable. If the number of ^{14}C dates in the studied time interval is large, then this variable can be described by Poisson statistics. In such situations, the statistical fluctuation s, which can be expressed as the ratio of the expected value and dispersion, is easy to calculate.

METHODS

In the case of CPDFs, the situation is a little more complicated. To estimate the range of statistical fluctuation for CPDFs, we carried out a Monte Carlo experiment for different values (N) of the number of ^{14}C dates in the sets (N = 50, 100, 200, 500, 1000, and 2000), and for different values of the mean uncertainties ΔT = 50, 70, 100, 120, 150, and 200 yr. We assumed that the N ^{14}C dates are uniformly distributed in the time range of 0–14 kyr. For simplification, we assumed that all dates have the same uncertainty. Using the Monte Carlo method, we generated 10,000 CPDFs for each pair of N and ΔT values. On the basis of the 10,000 CPDFs, we estimated the fluctuation range as 95% confidence intervals. The results obtained for ΔT = 120 yr and different N values and for N = 500 dates and different uncertainty values are presented in Figure 1. To compare our results with evaluations for histograms, the parameter s_f, which describes statistical fluctuations, was calculated. The results are presented in Figure 2. In comparison with histograms, CPDF is characterized by lower statistical fluctuations, e.g., we need 1530 dates with a mean uncertainty of 115 yr for the time range 0–14 kyr

BP to give reliable (according to the criteria proposed by M Geyh) results for histograms, but we would need about 785 dates for the CPDF. The minimum number of dates for the case ΔT = 120 yr is equal to 125 and for ΔT = 115 yr is equal to 200 dates.

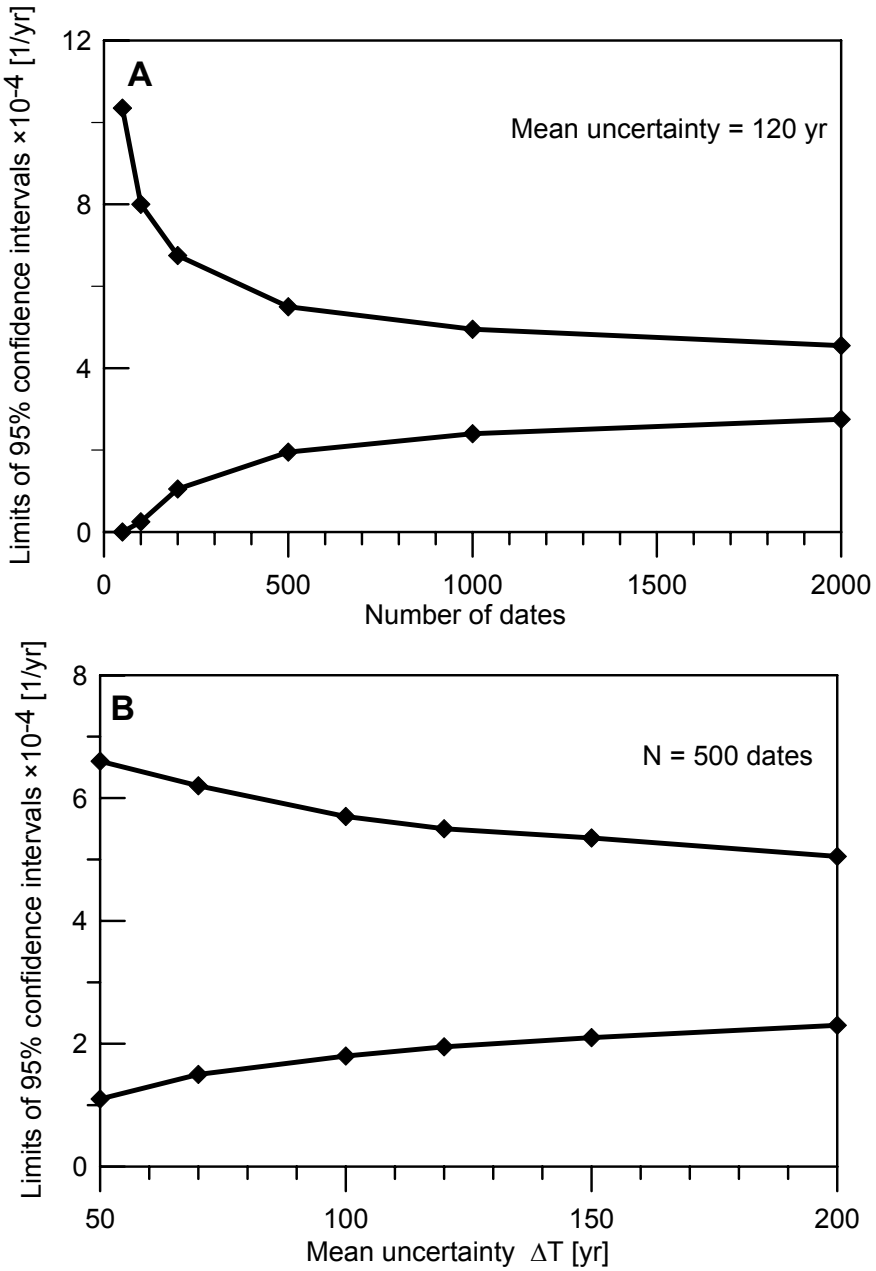

Figure 1 Values of 95% confidence intervals versus number of dates (a) and value of mean uncertainty (b). Part A shows the results for the number of dates N = 50, 100, 200, 500, 1000, and 2000, assumed mean uncertainty 120 yr. Part B presents the results for a set of 500 ^{14}C dates and different values of the mean uncertainty ΔT = 50, 70, 100, 120, 150, and 200 yr.

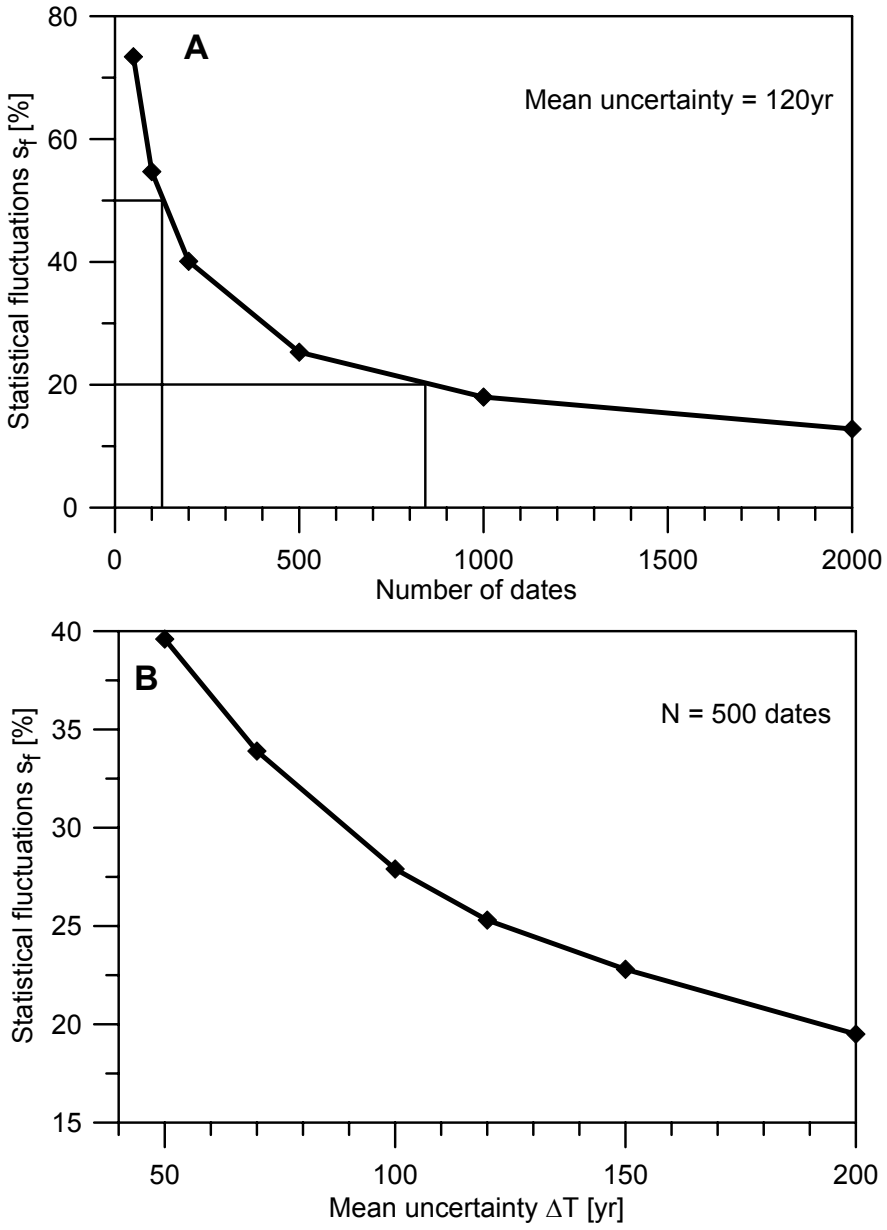

Figure 2 Statistical fluctuations s_f value versus number of dates (a) and mean uncertainty value (b)

In order to estimate the minimum number of dates needed for construction of a reliable CPDF, we did the following:

1. Created a set of 1000 ^{14}C dates (using a random number generator) and calculated the appropriate CPDF;
2. Randomly sampled N_i dates from the set of 1000 dates;
3. Calculated $CPDF_i$ for the selected N_i dates;

4. Calculated the sum of squared deviation between the original (constructed for 1000 dates) CPDF and the secondary (constructed for N_i dates) $CPDF_i$;
5. Repeated steps 2–4 one hundred times and calculated the mean sum of squared deviations MSSD;
6. Repeated steps 2–6 for N_i = 50, 100, 150,...950 dates.

The relationship between the mean sum of squared differences and number of dates is shown in Figure 3. We carried out the experiment for the case mean ΔT = 115 yr. Faster changes of MSSD are characteristic for lower N_i values. The larger the number of dates, the smaller the MSSD value. On the basis of this simulation, we chose N_i = 200 as the minimum number of dates needed for the construction of a reliable CPDF. Hercman (2000) described a similar experiment for the set of $^{230}Th/^{234}U$ dates. She proposed 150 as the minimum number of $^{230}Th/^{234}U$ dates for the analyzed time range 0–200 kyr.

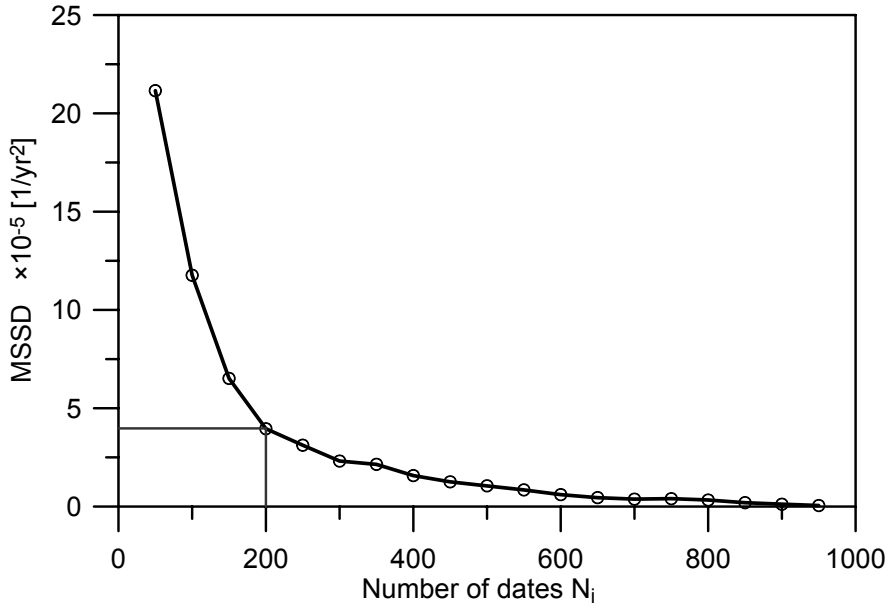

Figure 3 Results of the shape experiment *e*; Mean sum of squared deviations MSSD between the original (constructed for 1000 dates) CPDF and secondary (constructed for N_i dates) $CPDF_i$.

The Monte Carlo experiment provides evidence about how the CPDF constructed for a certain set of ^{14}C dates may differ considerably from the CPDF constructed for the same number of dates but uniformly distributed on a ^{14}C timescale. The experiment gives no information about the significance of particular maxima and minima. This significance could be established by a Monte Carlo experiment using a random number generator with the same distribution as the real distribution of sedimentation of the investigated type of sample. Unfortunately, the real distribution is unknown. To estimate it, the "Bootstrap Method" (Efron and Tibishrani 1993; Hercman 2000) may be used. This method assumes only that the chosen set of dates is representative of the sediment type over the investigated time period. The scheme of the Bootstrap Method algorithm is shown in Figure 4, and illustrative 95% confidence intervals calculated for a set of 785 dates of peat from the territory of Poland (see "Analyzed Material") are shown in Figure 5.

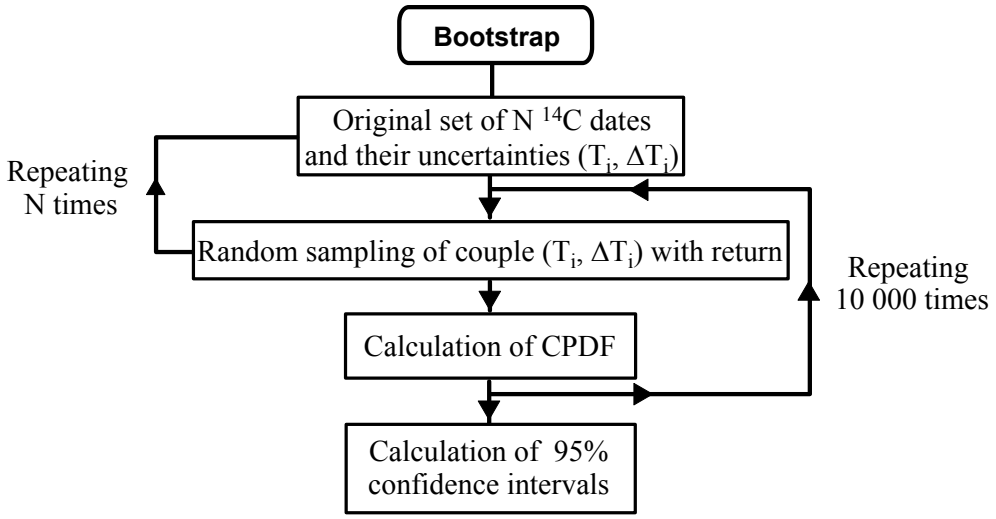

Figure 4 Scheme of the Bootstrap experiment

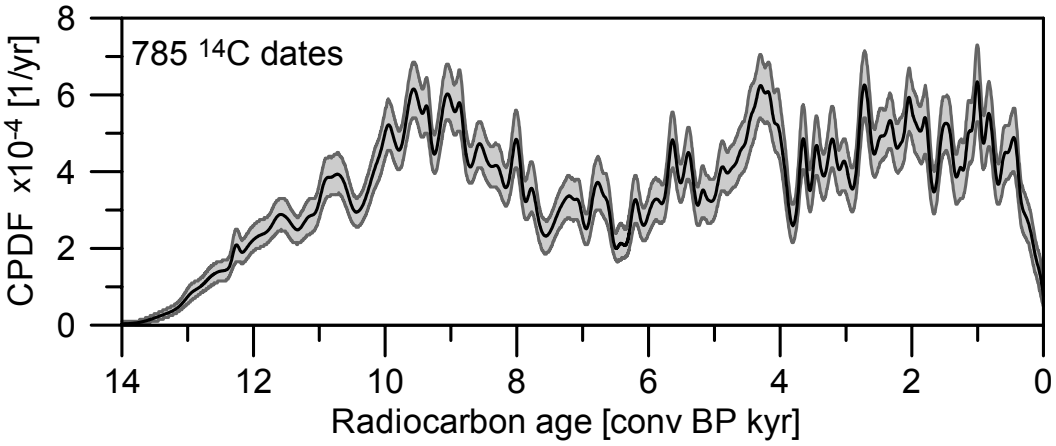

Figure 5 An example of 95% confidence intervals calculated for a set of 785 dates of peat (see "Analyzed Material") on the basis of the Bootstrap Method.

The correct interpretation of the CPDFs depends on the calendar timescale. It is especially important when comparisons with other paleoenvironmental records (e.g. varves) are made (Bartlein et al. 1995). Differences between the ^{14}C and calendar timescale can be the source of misleading impressions of synchronicity of some events or incorrect estimation of the duration of episodes if ^{14}C ages are not calibrated. In order to overcome these difficulties, the method of probabilistic calibration of ^{14}C dates was applied. We used an updated version of the Gliwice Radiocarbon Laboratory Calibration Programme GdCALIB (Pazdur and Michczyńska 1989; Michczyńska et al. 1990). The method of constructing CPDF on the calendar timescale in our program is the same as in OxCal (Bronk Ramsey 1995). We have not used any smoothing. Our earlier study (Michczyńska et al. 2003) shows that the degree of smoothing has no influence on the main peaks and gaps (cf. Figure 6). In the case when only the global changes are the subject of investigation, the degree of smoothing does not play an important role. With the aim of establishing whether the analyzed CPDFs are visibly different to

CPDFs calculated for sets with the same number of dates but for which the dates are uniformly distributed in the calendar timescale, a Monte Carlo experiment (Experiment 2) was performed. Results of the simulations are presented in Figure 7 in the form of 95% confidence intervals for different numbers of dates in the analyzed set (N = 100, 200, and 1000). The influence of the shape of the calibration curve on the 95% confidence intervals is clearly visible.

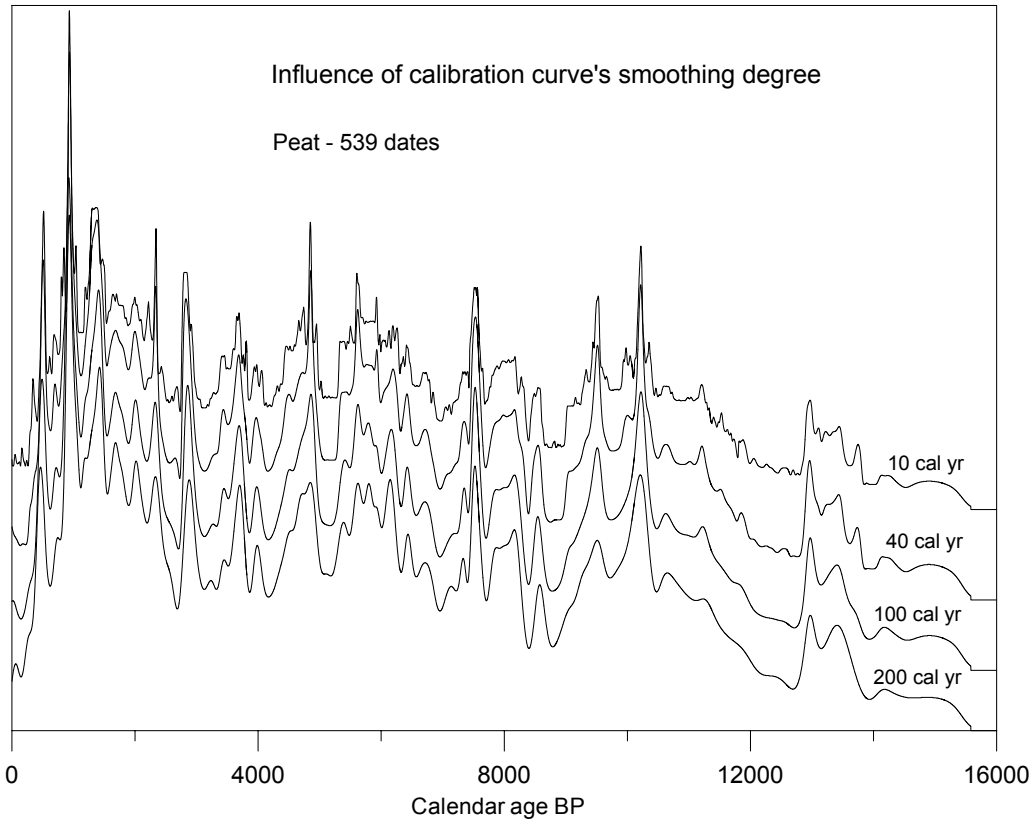

Figure 6 The influence of the calibration curve's smoothing degree on the shape of CPDF. The distributions are constructed for 539 dates of peat samples coming from the whole territory of Poland. Values of the calibration curve's smoothing degree are given in calendar yr; van der Plicht (1993) described details of the smoothing procedure. Particular graphs were vertically separated for higher clarity of the figure (according to Michczyńska et al. 2003).

ANALYZED MATERIAL

A method of statistical analysis for large sets of ^{14}C dates was described with the purpose of identifying environmental changes in the past recorded in the various types of sediment. In this paper, we present the first verification of this method on the basis of ^{14}C dates for peat from Poland. Poland lies in the temperate climate zone of the Northern Hemisphere (latitude 49–55°N, longitude 14–24°E). There are 49,620 peat bogs in Poland (Ilnicki and Żurek 1996). It could be expected that the statistical analysis will show time periods favorable and unfavorable for peat deposition.

For the statistical analysis, 785 dates of peat from Poland were selected. These dates encompassed the Holocene and Late Glacial period (last 14 ^{14}C kyr). The number of ^{14}C dates in particular millennial time periods are shown in Table 1. Dated samples came from Poland, except for those

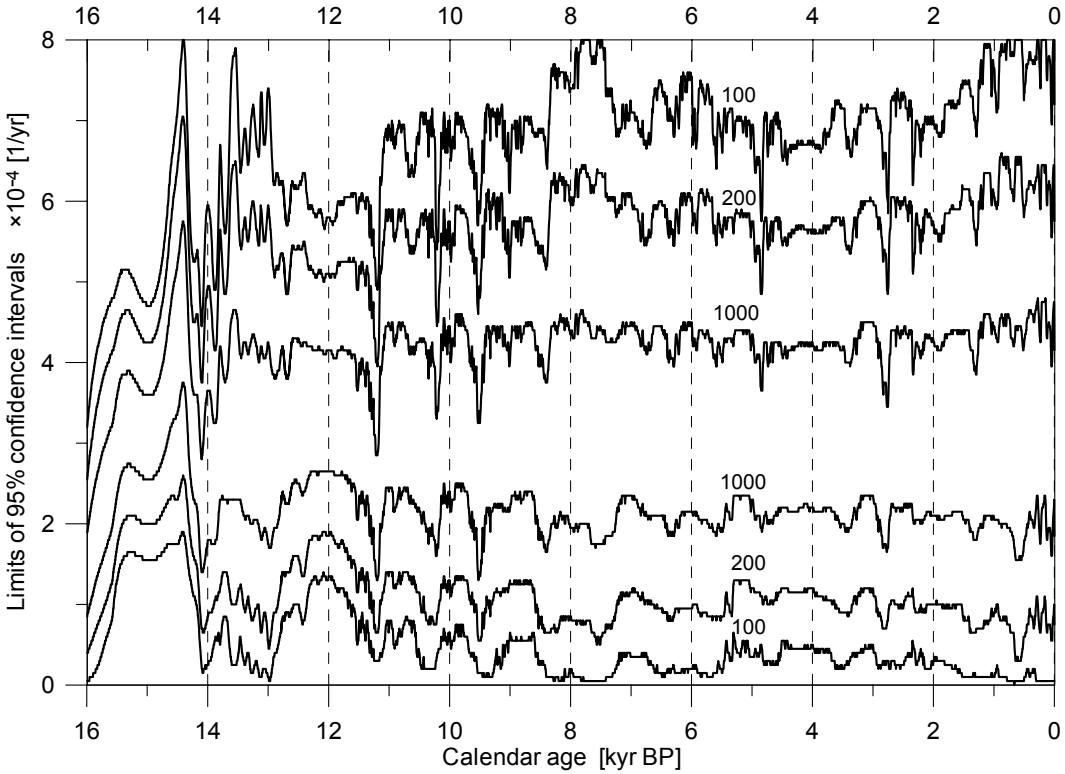

Figure 7 Results of 2nd Monte Carlo experiment. This experiment was executed for N = 100, 200, and 1000. For all simulations, the mean uncertainty was 115 yr.

from part of the Baltic Coast where changes in the Baltic sink range may influence peat deposition. All dates came from the Gliwice Radiocarbon Laboratory. After pretreatment and carbonization, the samples were combusted, and CO_2 was purified by the standard method used in the Gliwice Radiocarbon Laboratory (Pazdur and Pazdur 1986a). Finally, ^{14}C activity measurements were carried out by gas proportional counting (Pazdur et al. 2000). The result of ^{14}C dating is given as measured ^{14}C age T and its uncertainty ΔT ($T \pm \Delta T$). According to the commonly accepted convention (Stuiver and Polach 1977), the ΔT value is calculated only on the basis of statistical analysis of the measurements and properties of the apparatus without taking into account any extra-laboratory factors. Because peat is a typical organic material and often dated using ^{14}C, this type of deposit was chosen for analysis.

RESULTS AND CONCLUSIONS

We constructed a CPDF for the 785 chosen ^{14}C dates. Results in the calendar timescale are presented in Figure 8. The values of the CPDF exceed the 95% confidence intervals (calculated for 785 ^{14}C dates uniformly distributed on the calendar timescale) for 36.5% of the analyzed interval. This figure indicates that the real distribution of dates on the calendar timescale is not uniform.

For the Late Glacial/Holocene transition, there are many paleoclimatic records. Figure 9 presents an example of the comparison of the CPDF with the isotopic composition of authigenic carbonates in the Younger Dryas section of sediments from Lake Gościąż (Kuc et al. 1998), methane concentra-

Table 1 Number of ^{14}C dates of peat samples versus millennial time periods.

Time range conventional BP	Nr of ^{14}C dates
0–1000	60
1000–2000	72
2000–3000	76
3000–4000	62
4000–5000	80
5000–6000	56
6000–7000	40
7000–8000	49
8000–9000	70
9000–10,000	83
10,000–11,000	58
11,000–12,000	40
12,000–13,000	22
13,000–14,000	5

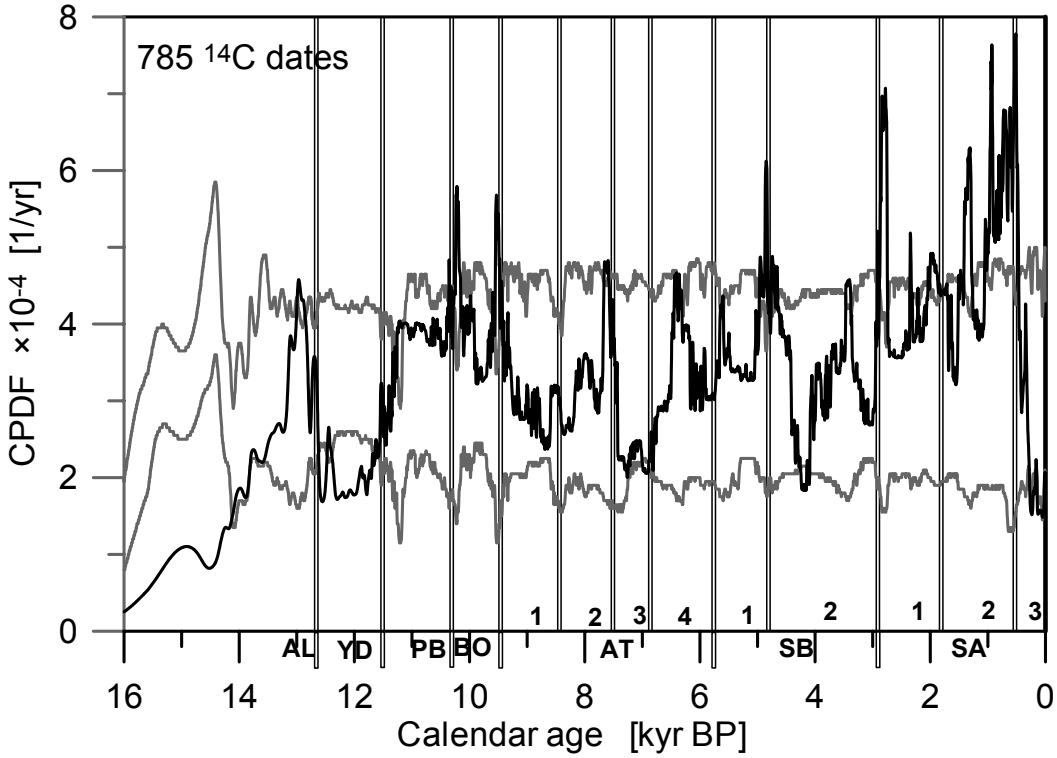

Figure 8 Cumulative probability density function (CPDF) for 785 ^{14}C dates from the interior of Poland is presented as the black curve. The 95% confidence interval is marked in grey based on the uniform distribution on the calendar timescale (cf. experiment Monte Carlo 2). Vertical lines indicate borders of the subdivision of the Late Glacial and Holocene period (Starkel 1999; after calculation on the calendar timescale).

tions in the GRIP ice core (Blunier et al. 1995), and $\delta^{18}O$ composition in the same ice core (Johnsen et al. 1997). Excellent agreement of the shape of CPDF and other environmental records for Late Glacial/Holocene transition testify the validity of basic assumptions of the statistical analysis. We

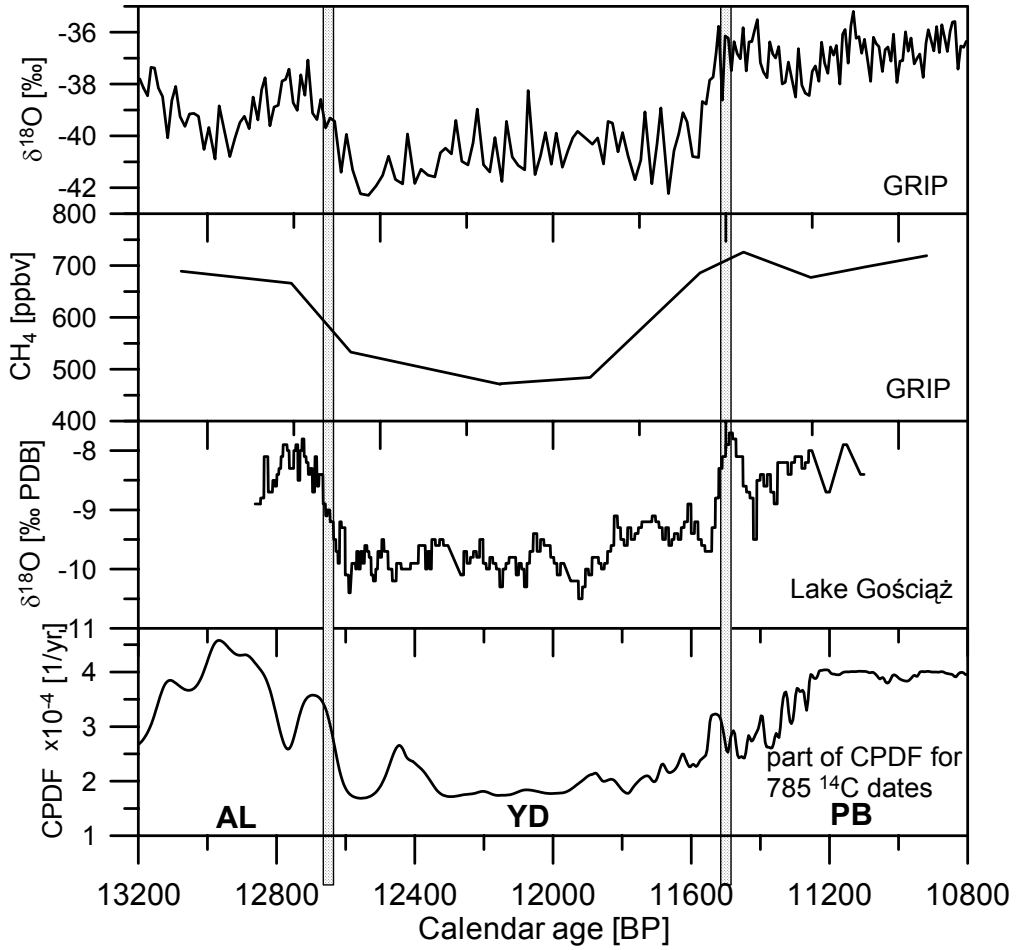

Figure 9 Comparison of part (10,800–13,200 cal BP) of the CPDF constructed for 785 dates and isotopic composition of authigenic carbonates in the Younger Dryas section of the sediments from Lake Gościąż (Kuc et al. 1998), $\delta^{18}O$ in the Greenland ice core (Johnsen et al. 1997),and methane concentration in the Greenland ice core (Blunier et al. 1995). Vertical grey lines indicate transition AL/YD and YD/PB established in studies of Lake Gościąż sediments (Goslar 1998).

have assumed that the random character of dates is preserved in the case of a large set of ^{14}C dates. Dates came from a large territory, and different investigators interested in various scientific disciplines collected them. However, the shape of the CPDF constructed for the 785 dates is strange. We observed narrow peaks; such narrow peaks are characteristic only for the real CPDF. They are absent for the CPDFs generated in Monte Carlo experiments. We could expect essential changes in the shape of CPDFs at those time periods where changes in environment were present, but the narrow peaks are unexpected. We suppose that their presence near the border of the Holocene subdivisions (cf. Figure 8; Starkel 1999, after calculation on calendar timescale) may be the result of the sampling methodology. Samples for ^{14}C dating are frequently collected only from selected horizons which are of special interest from the point of view of investigator. Because of economic reasons, only a limited number of organic layers can be dated. The general rule of taking samples from places of visible sedimentation changes (e.g. from the top and bottom of the peat layer) may be the reason that samples from the border of the Holocene subdivisions are collected essentially frequently. On

the one hand, preferential sampling hampers analysis, but on other hand, it may be useful to establish the border of the Holocene subdivision on the calendar scale for the analyzed geographical area.

The authors intend to repeat the research, basing it only on ^{14}C dates received for peat samples coming from raised bogs. These type of peat bogs supply all of the moisture from the atmosphere; therefore, the humidity in the upper peat layers depends essentially on precipitation, temperature, and evaporation.

We made the following conclusions from our analysis:

- 200 is the minimum number of dates required for the time interval 0–14 kyr;
- The first Monte Carlo experiment showed that CPDFs have lower statistical fluctuations than histograms;
- The first Monte Carlo experiment showed that the CPDF for 785 dates with a mean uncertainty of 115 yr in the range of 0–14 kyr BP is reliable according to the criteria proposed by Geyh (1980); for histograms, 1530 dates from the same time interval would be required;
- Calculated 95% confidence intervals in Monte Carlo Experiments 1 and 2 allow us to state that the CPDF constructed for the real 785 ^{14}C peat dates from Poland are visibly different than the curve constructed for dates uniformly distributed on the ^{14}C timescale and on the calendar timescale;
- Excellent shape agreement of the CPDF with other environmental records for the Late Glacial/Holocene transition indicate the validity of the basic assumptions of the statistical analysis;
- Along with the assumed proportionality between the number of ^{14}C dates and the amount of deposited organic matter in the studied time intervals, the influence of preferential sampling is visible. The general rule to take samples for ^{14}C dating where changes in sedimentation are observed or from a point in the profile where important changes in pollen are apparent, results in narrow peaks in the CPDF near the climatostratigraphic subdivision.

ACKNOWLEDGEMENTS

This study was supported by the Polish Committee for Scientific Research through the grant nr 3 PO4E 055 24.

REFERENCES

Bartlein PJ, Edwards ME, Shafer SL, Barker ED. 1995. Calibration of radiocarbon ages and the interpretation of paleoenvironmental records. *Quaternary Research* 44:417–24.

Blunier T, Chappellaz JA, Schwander J, Stauffer B, Raynaud D. 1995. Variations in atmospheric methane concentration during the Holocene epoch. *Nature* 374: 46–9.

Bluszcz A, Michczyński A. 1999. Statistical methods in chronostratigraphy. In: Pazdur A, editor. *Geochronology of Upper Quaternary in Poland*. Wojewoda: Wind J. p 71–9. In Polish.

Bronk Ramsey C. 1995. Radiocarbon calibration and analysis of stratigraphy: the OxCal program. *Radiocarbon* 37(2):425–30.

Efron B, Tibshirani RJ. 1993. *An Introduction to the Bootstrap*. New York: Chapman and Hall. 436 p.

Geyh MA. 1980. Holocene sea-level history: case study of the statistical evaluation of ^{14}C dates. *Radiocarbon* 22(3):695–704.

Geyh MA, Streif H. 1970. Studies on coastal movements and sea-level changes by means of the statistical evaluation of ^{14}C-data. *Proceedings of the "Symposium on Coastal Geodesy."* Münich, 20–24 July 1970. p 599–611.

Goslar T, Arnold M, Pazdur MF. 1998. Variations of atmospheric ^{14}C concentrations at the Pleistocene/Holocene transition, reconstructed from the Lake Gościąż sediment. In: Ralska-Jasiewiczowa M, Goslar T, Madeyska T, Starkel L, editors. *Lake Gościąż, Central Poland. A Monographic Study.* p 162–71.

Goździk J, Pazdur MF. 1987. Frequency distribution of ^{14}C dates from Poland in the time interval 12–45 kyr BP and its palaeogeographical implications. *Zeszyty Naukowe Politechniki Śląskiej, s. Matematyka-Fizyka, z. 56, Geochronometria* 4:27–42.

Hercman H. 2000. Reconstruction of paleoclimatic changes in Central Europe between 10 and 200 thousand years BP, based on analysis of growth frequency of speleothems. *Studia Quaternaria* 17:35–70.

Ilnicki P, Żurek S. 1996. Peat resources in Poland. In: Lappalainen E, editor. *Global Peat Resources*. Jyväskylä: International Peat Society, Geological Survey of Finland. p 119–25.

Johnsen SJ, Clausen HB, Dansgaard W, Gundestrup NS, Hammer CU, Andersen U, Andersen KK, Hvidberg CS, Dahl-Jensen D, Steffensen JP, Shoji H, Sveinbjörnsdóttir AE, White JWC, Jouzel J, Fisher D. 1997. The $\delta^{18}O$ record along the Greenland Ice Core Project deep ice core and the problem of possible Eemian climatic instability. *Journal of Geophysical Research* 102:26,397–410.

Kuc T, Różański K, Duliński M. 1998. Isotopic indicators of the Late Glacial/Holocene transition recorded in the sediments of Lake Gościąż. In: Ralska-Jasiewiczowa M, Goslar T, Madeyska T, Starkel L, editors. *Lake Gościąż, Central Poland. A Monographic Study.* p 158–62.

Michczyńska DJ, Michczyńsky A, Pazdur A, Żurek S. 2003. ^{14}C dates of peat for reconstruction of environmental changes in the past. *Geochronometria* 22:47–54.

Michczyńska DJ, Pazdur MF, Walanus A. 1990. Bayesian approach to probabilistic calibration of radiocarbon ages. In: Mook WG, Waterbolk HT, editors. Proceedings of the 2nd International Symposium ^{14}C and Archaeology. Strasburg. *PACT* 29:69–79.

Pazdur A, Michczyński A, Pawlyta J, Spahiu P. 2000. Comparison of the radiocarbon dating methods used in the Gliwice Radiocarbon Laboratory. *Geochronometria* 18:9–14.

Pazdur A, Pazdur MF. 1986a. Aparatura pomiarowa Laboratorium ^{14}C w Gliwicach. Doświadczenia konstrukcyjne i eksploatacyjne (The measuring equipment of the Gliwice Radiocarbon Laboratory. Experience gathered in the construction and exploitation). *Zeszyty Naukowe Politechniki Śląskiej, seria Matematyka-Fizyka, z.46, Geochronometria* 1:55–69.

Pazdur A, Pazdur MF. 1986b. Radiocarbon chronology of the Late Glacial period in Poland. *Acta Interdisciplinaria Archaeol*ogy 4:61–71.

Pazdur A, Pazdur MF, Pawlyta J, Górny A, Olszewski M. 1995. Paleoclimatic implications of radiocarbon dating of speleothems from Cracow-Wieluń Upland, S Poland. *Radiocarbon* 37(2):103–10.

Pazdur MF, Michczyńska DJ. 1989. Improvement of the procedure for probabilistic calibration of radiocarbon dates. In: Long A, Kra RS, Srdoć D, editors. Proceedings of the 13th International ^{14}C Conference. *Radiocarbon* 31(3):824–32.

Singhvi AK, Bluszcz A, Bateman MD, Someshwar Rao M. 2001. Luminescence dating of loess-paleosol sequences and coversands: methodological aspects and paleoclimatic implications. *Earth Science Reviews* 54: 193–211.

Stolk A, Törnqvist TE, Hekhuis KPV, Berendsen HJA, van der Plicht J. 1994. Calibration of ^{14}C histograms: a comparison of methods. *Radiocarbon* 36(1):1–10.

Stuiver M, Polach HA. 1977. Discussion: reporting of ^{14}C data. *Radiocarbon* 19(3):355–63.

van der Plicht J. 1993. The Groningen radiocarbon calibration program. *Radiocarbon* 35(1):231–7.

RADIOCARBON, Vol 46, Nr 2, 2004, p 745–754

RADIOCARBON CHRONOLOGY OF THE LATE PLEISTOCENE–HOLOCENE PALEOGEOGRAPHIC EVENTS IN LAKE BAIKAL REGION (SIBERIA)

Sergey K Krivonogov[1] • Hikaru Takahara[2] • Yaroslav V Kuzmin[3] • Lyobov A Orlova[4] • A J Timothy Jull[5] • Toshio Nakamura[6] • Norio Miyoshi[7] • Kimiyasu Kawamuro[8] • Elena V Bezrukova[9]

ABSTRACT. New radiocarbon dates obtained from Late Pleistocene and Holocene deposits of the southern, eastern, and northern shores of Lake Baikal in 1995–2001 are presented, and the most important results of paleoenvironmental studies based on ^{14}C data are discussed. The following paleogeographic events were verified with the help of ^{14}C dating: 1) first Late Pleistocene glaciation (Early Zyryan); 2) Middle Zyryan interstadial; 3) loess formation during the Late Zyryan (Sartan) deglaciation; 4) warm and cold events in the Late Glacial; and 5) vegetation changes and forest successions during the Late Glacial and Holocene.

INTRODUCTION

The international research program being conducted in the Lake Baikal region since 1993 (Baikal Drilling Project) concerns mainly the sedimental and environmental records in the lake cores. In addition, some projects dealt with the surroundings of Lake Baikal. One of these was a joint Russian-Japanese project, "The climate and vegetation changes in the Lake Baikal area during the last 15,000 years" (1995–2001). The project's main task was to investigate bogs and small lakes around Lake Baikal in order to obtain detailed paleoenvironmental information for the Late Glacial and Holocene, and to compare these results with those from the lacustrine sediments of Lake Baikal.

The principal results of the project were recently published in a series of articles (Bezrukova et al. 1998, 2000, 2002; Kataoka et al. 2003; Krivonogov and Takahara 2003; Takahara et al. 2000, 2001). We discovered that the climate and vegetation history of the region is better represented in the bog and small lake sediments surrounding Lake Baikal, rather than in Lake Baikal itself. The reasons for this are 1) greater thickness of the Late Glacial and Holocene sediments allows higher temporal resolution of environmental reconstructions; and 2) high biogenic content of the sediments provide good possibilities for ^{14}C dating. For example, the sedimentation rate in Lake Baikal (Akademichesky Ridge) in the Holocene was about 40 mm/1000 yr (Kuzmin et al. 2000), and in the surrounding small lakes and bogs, it was up to 500 mm/1000 yr according to our research. This permits a 10 times better resolution of paleoclimatic events. In this paper, we present a series of ^{14}C dates and discuss their importance for determining the age of paleogeographic events.

[1]United Institute of Geology, Geophysics, and Mineralogy, Siberian Branch of the Russian Academy of Sciences, Koptyug Ave. 3, Novosibirsk 630090, Russia. Corresponding author. Email: carpos@uiggm.nsc.ru.
[2]Kyoto Prefectural University, 1-5 Hangi-cho, Shimogamo, Sakyo-ku, Kyoto 606-8522, Japan.
[3]Pacific Institute of Geography, Far Eastern Branch of the Russian Academy of Sciences, Radio St. 7, Vladivostok 690041, Russia.
[4]Institute of Geology, Siberian Branch of the Russian Academy of Sciences, Koptyug Ave. 3, Novosibirsk 630090, Russia.
[5]NSF-Arizona AMS Facility, University of Arizona, Tucson, Arizona 85721-0081, USA.
[6]Center for Chronological Research, Nagoya University, Chikusa, Nagoya 464-8602, Japan.
[7]Okayama University of Science, 1-1 Ridai-cho, Okayama 700-0005, Japan.
[8]Kansai Research Center, Forestry and Forest Products Research Institute, Kyoto 612-0855, Japan.
[9]Limnological Institute, Siberian Branch of the Russian Academy of Sciences, Ulanbatorskaya St. 3, Irkutsk 664033, Russia.

Proceedings of the 18th International Radiocarbon Conference, edited by N Beavan Athfield and R J Sparks
RADIOCARBON, Vol 46, Nr 2, 2004, p 745–754

MATERIALS AND METHODS

The area of our investigation covers the southern, eastern, and northern shores of Lake Baikal (Figure 1). In total, 25 boreholes were drilled and a few dozen outcrops were also investigated. Boreholes and outcrops with ^{14}C dates are shown in Figure 1. Fifty-one ^{14}C dates have been generated from several boreholes and outcrops (Table 1). Some outcrops have large series of ^{14}C dates with up to 15 values. Dates mainly correspond to the last 14,000 ^{14}C yr (the Late Glacial and Holocene). Earlier ^{14}C dates, about 46,000–23,000 BP, were obtained from the 2 deepest boreholes, Duliha and Bolshaya Rechka.

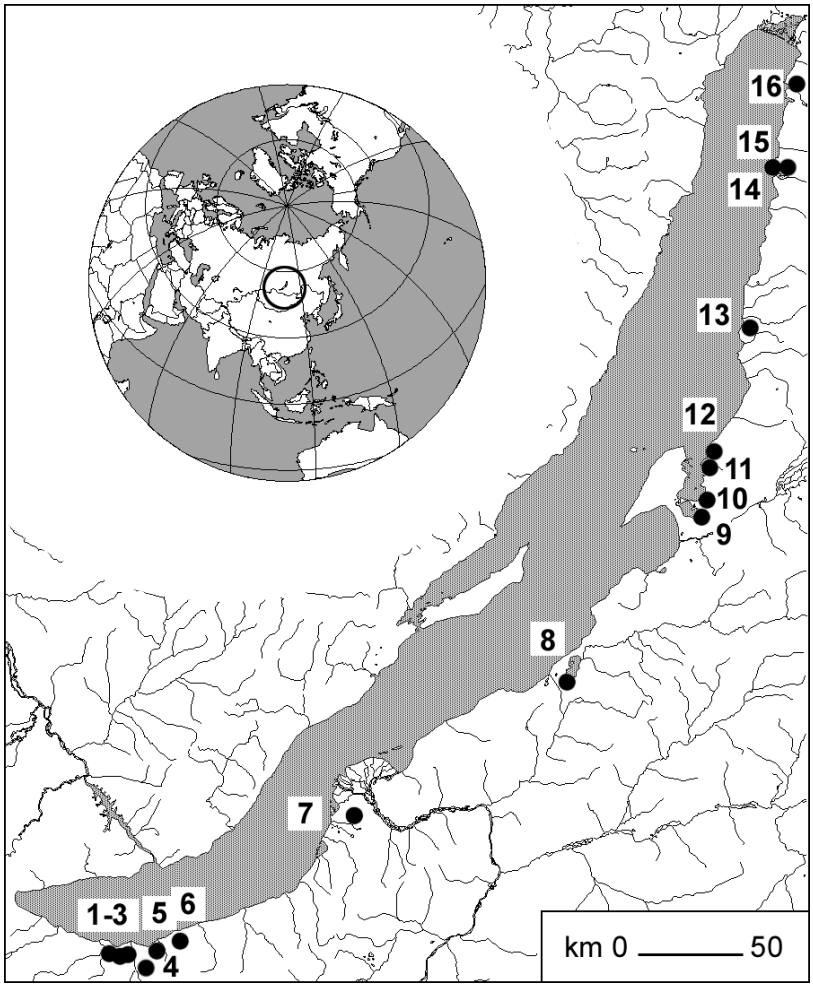

Figure 1 The area under investigation: location of the ^{14}C-dated sites (numbers correspond to those in Table 1).

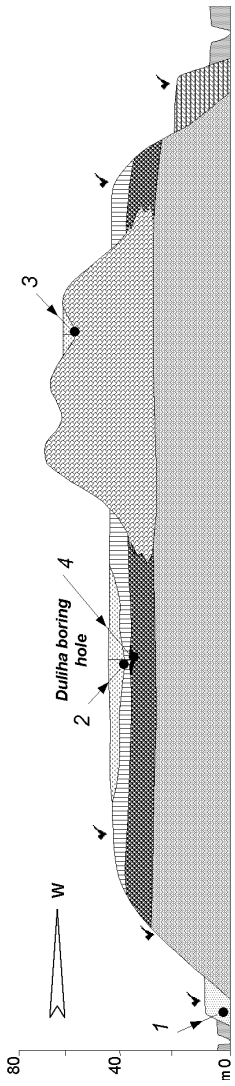

Figure 2 Generalized geological section of the Tanhoi Plain watershed. 1 – the Tanhoi group (N_1): clay, coal, sand; 2 – denudation cover (Q): boulders, pebbles; 3 – end moraine ($Q_{3/1}$); 4 – peat ($Q_{3/2}$); 5 – loess ($Q_{3/3}$); 6 – fluvioglacial terrace ($Q_{3/3}$): boulders, pebbles; 7 – peat (Q_4); 8 – high floodplain (Q_4): sand, peat; 9 – low floodplain (Q_4): sand, pebbles; 10 – exposures; 11 – ^{14}C dates verifying stratigraphic units: *1* – 4590 ± 70 BP (Beta-88092), Pankovka; *2* – 11,110 ± 120 BP (NUTA-5616), Duliha; *3* – 11,400 ± 200 BP (KEEA-170), Krivoe Lake; *4* – 46,700 ± 2800 BP (AA-37975) and 29,820 ± 710 BP (Beta-098423), Duliha.

Table 1 ^{14}C dates obtained by the joint Russian-Japanese expedition in the Lake Baikal area.

Site name and coordinates	Type[a], nr from Figure 1	Depth (cm)	Material dated	Lab code and nr	^{14}C date (BP)
Pankovka River	S, 1	90–92	peat	Beta-88090	1520 ± 60
51°28′N, 104°30′E		187–190	seeds	NUTA-4749	2950 ± 60
		302–305	peat	Beta-88091	4000 ± 70
		393–398	peat	Beta-88092	4590 ± 70
Bolshoe bog	Bh, 2	238–240	peat	NUTA-4781	5330 ± 70
51°28′N, 104°30′E					
Yanvarskoe bog	Bh, 3	268–269	peat	NUTA-4750	5680 ± 70
51°27′N, 104°30′E					
Tabachnye Lakes bog	Bh, 4	187	plant fragment	Beta-149297	7070 ± 40
51°29′N, 104°53′E					
Krivoe Lake bog	Bh, 5	50	seed (*Pinus sibirica*)	NUTA-5444	1655 ± 140
51°29′N, 104°50′E		210	seed (*Pinus sibirica*)	NUTA-5455	8060 ± 115
		235–245	peat	KEEA-169	8520 ± 120
		301–304	seed	NUTA-5616	9260 ± 120
		341–351	peat	KEEA-170	11,400 ± 200
Duliha bog	Bh, 6	300–302	seeds	NUTA-5615	7620 ± 115
51°31′N, 105°00′E		399	peat	AA-37974	9185 ± 55
		474–475	peat	NUTA-6038	11,110 ± 120
		612–613	peat	NUTA-6039	35,890 ± 945
		618	wood	AA-37975	46,700 ± 2800
		663	wood	AA-37976	35,740 ± 850
		679–680	peat	Beta-098423	29,820 ± 710
		682	wood	AA-37977	30,110 ± 360
Bolshaya Rechka bog	Bh, 7	71–73	wood	NUTA-5450	940 ± 70
51°57′N, 106°20′E		508–510	peat	Beta-098421	8380 ± 40
		745–746	peat	Beta-098422	22,810 ± 280
Cheremushuka bog	Bh, 8	366–367	peat	Beta-115297	12,100 ± 60
52°45′N, 108°05′E					
Arangatui bog	Bh, 9	474	wood	Beta-113968	9400 ± 60
55°32′N, 109°08′E					
Chivyrkui Bay, exposure 1[b]	S, 10	35–40	peat	SOAN-3803	1450 ± 75
53°40′N, 109°12′E		75–80	peat	SOAN-3804	3720 ± 185
		115–120	peat	SOAN-3805	3500 ± 90
		155–160	peat	SOAN-3806	4795 ± 80
		195–200	peat	SOAN-3807	5400 ± 125
		215–220	peat	SOAN-3808	6605 ± 130
Chivyrkui Bay, exposure 2	S, 10	185–190[c]	peat	SOAN-3809	5645 ± 85
53°40′N, 109°12′E		165–170	peat	SOAN-3810	6105 ± 220
		145–150	peat	SOAN-3811	7025 ± 230
		105–110	peat	SOAN-3812	8340 ± 300
		65–70	peat	SOAN-3813	9165 ± 150
		25–30	peat	SOAN-3828	9600 ± 130
		0–5	peat	SOAN-3829	10,810 ± 150
	Bh, 10	–25 to –50[d]	peat	SOAN-3830	10,420 ± 200
Chivyrkui Bay	Bh, 10	–50	wood	Beta-113969	9700 ± 70
53°40′N, 109°12′E					
Krohalinaya Bay bog	Bh, 11	260	peat	AA-37976	8550 ± 70
53°46′N, 109°12′E		426	peaty clay	AA-37968	10,980 ± 65
Bolshoi Chivyrkui River bog	Bh, 12	365–366	peat	Beta-136811	9650 ± 40
53°49′N, 109°12′E					
Duguldzeri River bog	Bh, 13	90	wood	AA-37969	4515 ± 40
54°27′N, 109°32′E		193	seed	AA-37970	8020 ± 45
		323	gyttja	AA-37971	11,295 ± 55
		378	gyttja	AA-37972	12,950 ± 90
Tompuda bog	Bh, 14	273–274	peat	Beta-136813	10,150 ± 40
55°08′N, 109°46′E		515–516	gyttja	Beta-136814	14,090 ± 50
Tompuda end moraine	S, 15		woody peat	SOAN-4266	9875 ± 45
55°09′N, 109°42′E					
Froliha River	S, 16	170	wood	AA-37973	8010 ± 70
55°30′N, 109°55′E					

[a] S – section; Bh – borehole.
[b]For the detailed description of the sampling scheme for the sites of the Chivyrkui Bay, see Kataoka et al. (2003).
[c]Elevation above the Lake Baikal level.
[d]Negative value indicates the sample position below the Lake Baikal level.

Palynological and plant macrofossil analyses were conducted according to standard procedures (cf. Berglund and Ralska-Jasiewiczowa 1986). The ^{14}C liquid scintillation dating (SOAN Lab, Novosibirsk, Russia; and KEEA Lab, Fukuoka, Japan) follows the general procedure for peat samples (cf. Taylor 1987; Orlova and Zykina 2003). The ^{14}C accelerator mass spectrometry (AMS) dating (Beta Lab, Miami, Florida, USA; NUTA Lab, Nagoya, Japan; and AA Lab, Tucson, Arizona, USA) was carried out according to general pretreatment and measurement protocols (cf. Tuniz et al. 1998).

Paleogeographic Events in the Lake Baikal Region and Their ^{14}C Ages

The ^{14}C dates were used as geochronological markers for stratigraphical and palynological analyses. Except for the directly dated levels, the age of paleoenvironmental boundaries and palynozones was estimated by linear interpolation between ^{14}C-dated levels. The following paleogeographic events have been verified using ^{14}C dates: 1) the first Late Pleistocene glaciation (Early Zyryan, corresponding to the Early Weichselian in Europe and Early Wisconsin in North America); 2) the Middle Zyryan interstadial (corresponding to the Middle Wisconsin); 3) loess formation in the Tanhoi Plain, southern Lake Baikal shore, in the Late Zyryan (Sartan in Siberia, or Late Wisconsin in North America) deglaciation period; 4) warm and cold events in the Late Glacial; and 5) vegetation changes and forest successions during the Late Glacial and Holocene.

The glacial events in the northern, northeastern, and southern mountainous surroundings of the Lake Baikal region are recorded in broadly distributed end moraines. A wide range of ^{14}C dates generated by previous investigators was described by Back and Strecker (1998) as evidence of asymmetric and asynchronous glaciation of the Lake Baikal mountain system. Moraines of the eastern shore were created by glacier advances at more than 50,000 BP; 40,000–35,000 BP; and 26,000–13,000 BP. Careful examination of the moraine exposures revealed a lack of any organic matter, such as wood and peat, in the basal and supraglacial layers. We interpret this as an indication that temperatures were too cold during glacial times in Siberia for tree growth, and, thus, glacial tongues did not reach the tree belt in the piedmonts and did not incorporate any wood into moraines. Nevertheless, one can find wood and peat in the uppermost and distal parts of the moraine ridges. For example, the end moraine of the Tompuda Valley (Figure 1, #15) has a ^{14}C date of 39,240 ± 1780 BP (Mats et. al. 2001). We also found a woody peat layer in the northern part of this outcrop which was dated to 9875 ± 45 BP (SOAN-4266). Neither of these dates can be correlated with any significant glacial events. We suggest that the dated layers represent a drift of the post-glacial thermokarst flows which resulted from the reworking of frozen moraines or dead-ice massifs. Thus, such dates can only indicate that the glaciation itself is older; we assume it is of Early Zyryan age, older than about 39,000 BP. More obvious evidence that it is of the Early Zyryan end moraines was found on the southern shore of Lake Baikal on the Tanhoi Plane. The end moraine ridge of the Duliha River (Figure 1, #6) is related to the surrounding sediments, as shown in Figure 2. ^{14}C dates of 46,000–30,000 BP (Table 1) were obtained for the peat that lies stratigraphically above the glacial sediments, and their age is, therefore, older than approximately 46,000 BP.

The presence of the Middle Zyryan interstadial (about 50,000–21,000 BP) in the sediments of the Lake Baikal region is still questionable. We occasionally found peat of this age at 2 sites, Duliha and Bolshaya Rechka bogs (Figure 1, #6 and #7). In the Duliha bog (Figure 2), the Middle Zyryan peat, dated to about 46,700–30,100 BP, lies on the layer of outwash pebbles which correlate with the end moraine ridge situated at a distance of 300 m from the drilling site. The peat is lens-shaped with a width of less than 10 m and a maximum thickness of about 0.5 m according to the drilling tests. We suggest that this lens occupies a small depression on the intersection of 2 melted ice wedges (tundra polygons). This allows us to explain the age differences and inversions of the ^{14}C dates (about

30,110 BP on the bottom versus about 35,900 BP and about 46,700 BP on the top) as a result of subsidence or collapse of the peat during the long time development of the ice wedge system. Pollen analysis indicates a cool but relatively mild climate typical for the Middle Zyryan in southern Siberia (Bezrukova et al. 2000).

The loess sediments, atypical for the Lake Baikal region, were found in the western part of the Tanhoi Plain (Figure 2). The different Pleistocene sediments shown in Figure 2 are labeled as Q, Q_3 (Late Pleistocene), and Q_4 (the Holocene). The nearest extensive loess deposits are situated on the Irkutsk-Cheremkhovo Plain, west of Irkutsk City and at least 150 km NW of the Tanhoi Plain. The age of the Tanhoi Plain loess is estimated as Late Zyryan, older than about 11,000 BP and younger than about 30,000 BP, based on the ^{14}C ages of underlying and overlapping biogenic sediments (Table 1, Duliha borehole). Specific "wind-shadow" conditions may have permitted loess accumulation in the piedmonts of the Khamar-Daban Range and deterred erosion.

Some boreholes drilled into the lacustrine and underlying soil layers revealed ^{14}C ages of about 14,000–11,000 BP. Different events, corresponding to the warm and cool phases of the Late Glacial, were established in these boreholes using pollen data. Unfortunately, we do not have a continuous record for this period; the younger events are better represented then the older ones. Thus, the basal layer of the Duliha peat bog at a depth of about 5 m—characterized by pollen of deciduous trees and steppe-and-meadow grasses and dated to about 11,100 BP—corresponds to the end of the Allerød warming. In contrast, paleosol at the bottom of the Krivoe Lake bog core (Figures 1, #5), situated in the depression on the top of the Vydrinnaya end moraine ridge, contains many *Betula nana* L. *s.l.* seeds and indicates cold conditions. Considering that the date of about 11,400 BP shows correspondence of this layer to the middle of the Allerød, this discrepancy might be evidence of a "compression" of the Older Dryas and Allerød events in the paleosol. Our only other conclusion would be that the Older Dryas vegetation survived in the Krivoe Lake depression at the Allerød. Based on these fragmentary data, we would conclude that the post-Last Glacial Maximum forest vegetation began to spread in the Lake Baikal area already at the end of the Late Glacial, and the periglacial tundra and forest tundra formations were rapidly replaced by forest formations.

Regularities in the vegetation changes and migration of the plant zones can be revealed by comparison of the data obtained at different localities. The appearance and predominance of major forest tree species since the Late Glacial, according to Bezrukova et al. (forthcoming), is shown in Figure 3. We can clearly observe the succession of larch (*Larix*) and spruce (*Picea*) assemblages by fir (*Abies*) and Siberian pine (*Pinus sibirica*) in the Boreal period of the Holocene. These formations were replaced by pine (*Pinus sylvestris*) in the post-Atlantic. Correlation of the pollen zones between the main localities for the last 30,000 yr is shown in Figure 4 (Takahara et. al. 2001).

DISCUSSION

The majority of the ^{14}C dates obtained are in good agreement with the sedimentation sequences and paleogeographic interpretations. However, at 2 sites we have inversions of the dates. The lowermost member of the Duliha core was accumulated in the specific conditions described above. The fluvioglacial plain of the Duliha site was developed as a tundra and forest tundra landscape over a long time, from the end of the Early Zyryan glaciation to the beginning of the Late Zyryan one. The formation and melting of ice wedges could have occurred over a prolonged period of time, resulting in mixing of the younger and older parts of the peat layer, downward migration of the organic material, and so on. An apparent inversion occurs in the upper part of the peat layer in the Chivyrkui Bay 1 outcrop: 3720 ± 185 BP (SOAN-3804) at a depth of 75–80 cm versus 3500 ± 90 BP (SOAN-3805)

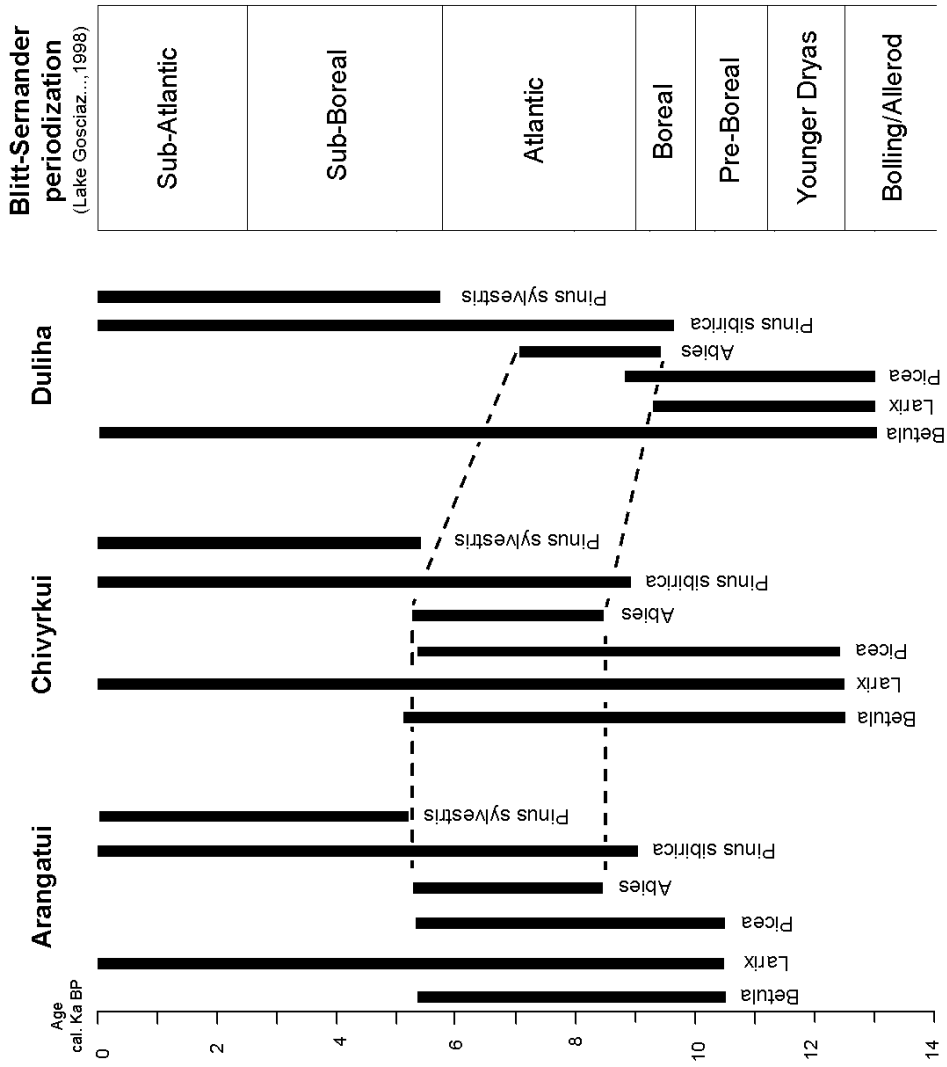

Figure 3 Expansion of the main forest trees and their predominance in the southern and eastern shores of Lake Baikal in the Late Glacial and the Holocene

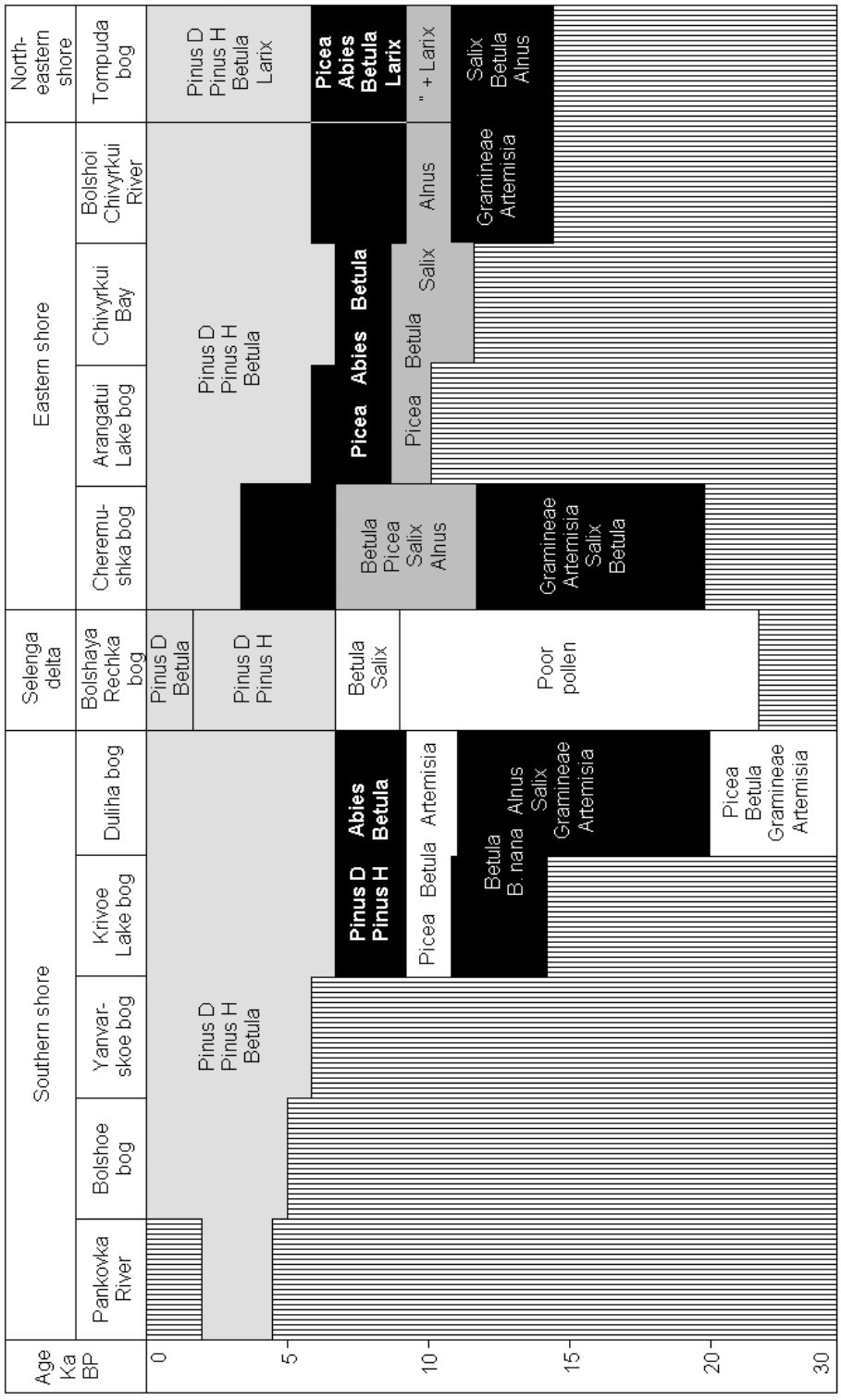

Figure 4 Correlation of the pollen assemblage zones in the cores from the Lake Baikal shore

at a depth of 115–120 cm. This bog is located in the permafrost area; erosion by the Lake Baikal waves causes melting of the exposed sediments and cracking and shifting of the peat blocks which would introduce the suggested migration. As a result, the maximum disturbance of sediments would have occurred only in the upper part of the exposure. In addition, the top of the bog is strongly influenced by the seasonal freeze-and-thaw processes up to a depth of 1 m.

We can only suggest what may cause the large difference between ^{14}C dates from the bottom layer of the Chivyrkui outcrop, exposure 2: 10,810 ± 150 BP (SOAN-3829), from peat collected at a height of 0–5 cm above the Lake Baikal shoreline versus 10,420 ± 200 BP (SOAN-3830) from peat at a depth of 25–50 cm below the Lake Baikal level. Both dates were obtained by the liquid scintillation technique. The AMS date of the wood fragments found at the depth of 50 cm below the lake level, 9700 ± 70 BP (Beta-113969), showed an even larger inversion. Several factors, such as redeposition, post-depositional contamination, and differences between labs using conventional and AMS methods, may be responsible for such differences.

CONCLUSION

Paleogeographic events of the Late Glacial and Holocene recorded in the terrestrial sediments around Lake Baikal are much more detailed (to at least one order of magnitude) compared with the records from the bottom sediments of Lake Baikal. Nevertheless, the phases of significant vegetation changes observed in the palynological analysis have a minimum duration of 150–250 yr. We consider that this is a technical limitation of the resolution of the environmental reconstructions in the palynological record within the last 12,000–10,000 yr. The topmost Holocene peat layers were investigated in a wide territory, and this allowed us to make reliable spatial environmental reconstructions. As for the Late Pleistocene events, such possibilities are significantly smaller.

ACKNOWLEDGEMENTS

We are grateful to colleagues and students who participated in the drilling expeditions. Special thanks go to the staff of the radiocarbon laboratories, and to Dr S G Keates for grammar polishing. This investigation was funded by the Science and Technology Agency of Japan, the Russian Foundation for Basic Research, and the US National Science Foundation. Finally, we are grateful to Drs M McGlone and N Beavan Athfield for useful comments on the earlier version of this manuscript.

REFERENCES

Back S, Strecker MR. 1998. Asymmetric Late Pleistocene glaciations in the north Baikal basin, Baikal rift, Russia. *Journal of the Geological Society of London* 155:61–71.

Berglund BE, Ralska-Jasiewiczowa M, editors. 1986. *Handbook of Holocene Palaeoecology and Palaeohydrology.* Chichester: John Wiley. 869 p.

Bezrukova EV, Krivonogov SK, Takahara H, Abzaeva AA, Vershinin KE, Miyoshi N, Nakamura T, Morita Y, Kawamuro K, Shinomiya T, Krapivina SM. 2002. Rekonstruktsia landshaftno-klimaticheskih uslovii vostochnogo poberezhya ozera Baikal v golotsene po rezultatam kompleksnogo issledovaniya skvazhiny "Arangatui" [Reconstruction of the landscape and climate conditions of the eastern shore of the Baikal in the Holocene resulted from the complex investigation of the "Arangatui" borehole]. In: Vaganov EA, Grachev MA, Derevianko AP, Zykin VS, editors. *Osnovnye zakonomernosti globalnyh i regionalnyh izmenenii klimata i prirodnoi sredy v pozdnem kainozoe Sibiri. Volume 1*. Novosibirsk: Institute of Archaeology and Ethnography Press. p 36–47.

Bezrukova EV, Krivonogov SK, Takahara H, Miyoshi N, Morita Y, Takehara A, Noi X, Shinomiya T. 1998. Izmeneniya prirodnoi sredy, rastitelnosti i klimata Pribaikalya v pozdnem pleistotsene i golotsene [Changes of the environments, vegetation and climate in the Lake Baikal area during the Late Pleistocene and the Holocene]. In: Vaganov EA, Grachev MA, Derevianko AP, Zykin VS, editors. *Problemy rekosntruktsii klimata i prirodnoi sredy golotsena i pleistotsena Sibiri.* Novosibirsk: Institute of Archaeology and

Ethnography Press. p 46–50.

Bezrukova EV, Krivonogov SK, Takahara H, Vershinin KE, Miyoshi N, Nakamura T, Abzaeva AA, Morita Y, Kawamuro K, Shinomiya T, Krapivina SM. 2000. Letopis pozdnepleistotsenovoi i golotsenovoi istorii yugo-vostochnogo poberezhya oz. Baikal po materialam skvazhiny Duliha [Record of the Late Pleistocene and Holocene history of south-east bank of the Lake Baikal by data from the Duliha borehole]. In: Vaganov EA, Grachev MA, Derevianko AP, Zykin VS, editors. *Osnovnye zakonomernosti globalnyh i regionalnyh izmenenii klimata i prirodnoi sredy v pozdnem kainozoe Sibiri. Volume 2*. Novosibirsk: Institute of Archeology and Ethnography Press. p 36–47.

Bezrukova EV, Krivonogov SK, Abzaeva AA, Vershinin KE, Orlova LA, Letunova PP, Takahara H, Miyoshi N, Nakamura T, Krapivina SM, Morita Y, Kawamuro K, Shinomiya T. Forthcoming. Landshafty i klimat Pribaikalya v pozdnelednikovie i golocene po rezultatam kompleksnogo issledovaniya torfyanikov na yuznom i vostochnom beregakh oz. Baikal [Landscapes and climate of the Lake Baikal area in the Late Glacial and Holocene resulted from the complex investigation of the peat sediments of the southern and eastern shores of the Lake Baikal]. *Geologiya i geofizika*.

Kataoka H, Takahara H, Krivonogov SK, Bezrukova EV, Orlova LA, Krapivina S, Miyoshi N, Kawamuro K. 2003. Pollen record from the Chivyrkui Bay outcrop on the eastern shore of Lake Baikal since the Late Glacial. In: Kashiwaya K, editor. *Long Continental Records from Lake Baikal*. Berlin: Springer-Verlag. p 207–18.

Krivonogov SK. 2003. Levels of the Baikal and Hovsgol lakes in Holocene and Pre-Holocene time. In: Kamata N, editor. *Proceedings of the International Symposium of the Kanazawa University: 21st Century COE Program. Volume 1*. Kanazawa: Kanazawa University. p 123–7.

Krivonogov SK, Takahara H. 2003. Late Pleistocene and Holocene environmental changes recorded in the terrestrial sediments and landforms of Eastern Siberia and Northern Mongolia. In: Kamata N, editor. *Proceedings of the International Symposium of the Kanazawa University: 21st Century COE Program. Volume 1*. Kanazawa: Kanazawa University. p 30–6.

Kuzmin MI, Williams DF, Kawai T. 2000. Baikal drilling project. In: Minoura K, editor. *Lake Baikal. A Mirror in Time and Space for Understanding Global Change Processes*. Amsterdam: Elsevier Health Sciences. p 1–14.

Mats VD, Ufimtsev GF, Mandelbaum MM. 2001. Kainozoi Baikalskoi riftovoi vpadiny: stroenie i geologicheskaya istoriya [The Baikal Rift basin in the Cenozoic: structure and geologic history]. Novosibirsk: GEO Publ. 252 p.

Orlova LA, Zykina VS. 2003. Radiocarbon dating of buried Holocene soils in Siberia. *Radiocarbon* 44(1): 113–22.

Takahara H, Krivonogov SK, Bezrukova EV, Miyoshi N, Morita Y, Nakamura T, Hase Y, Shinomiya Y, Kawamuro K. 2000. Vegetation history of the southeastern and eastern coasts of Lake Baikal from bog sediments since the Last Interstadial. In: Minoura K, editor. *Lake Baikal. A Mirror in Time and Space for Understanding Global Change Processes*. Amsterdam: Elsevier Health Sciences. p 108–18.

Takahara H, Ogura A, Krivonogov SK, Bezrukova EV, Miyoshi N, Hase Y, Kawamuro K, Nakamura T, Morita Y, Shichi K, Shinomiya Y, Takehara A, Uchiyama T. 2001. History of dark and light taiga forests around Lake Baikal since the Last Glacial period. In D Tomurhuu, H Takahara, editors. *Abstracts of 2001 International Workshop for the Baikal and Hovsgol Drilling Project in Ulaanbaatar.* Ulaanbaatar, Mongolia, 4–7 October 2001. Ulaanbaatar: Mongolian Academy of Sciences. p 45–6.

Taylor RE. 1987. *Radiocarbon Dating: An Archaeological Perspective*. Orlando, Florida: Academic Press. 212 p.

Tuniz C, Bird JR, Fink D, Herzog GF. 1998. *Accelerator Mass Spectrometry: Ultrasensitive Analysis for Global Science*. Boca Raton, Florida: CRC Press. 371 p.

RADIOCARBON, Vol 46, Nr 2, 2004, p 755–764

CHANGES IN SEDIMENT ACCUMULATION RATE IN AN OXBOW LAKE FOLLOWING LATE 19TH CENTURY CLEARING OF LAND FOR AGRICULTURAL USE: A ^{210}Pb, ^{137}Cs, AND ^{14}C STUDY IN MISSISSIPPI, USA

Gregg R Davidson[1,2] • Meredith Carnley[1] • Todd Lange[3] • Stanley J Galicki[4] • Andrew Douglas[5]

ABSTRACT. Sediment cores were collected from 2 sites in the forested fringe of an oxbow lake surrounded by land that was converted from forest to agricultural use in the late 19th century. The 2 sampling areas were selected to represent areas of high (West site) and low (East site) current sediment accumulation rates, based on distance from a perennially discharging stream. Modern (post settlement and land clearing) sediment accumulation rates were calculated using ^{210}Pb and ^{137}Cs on bulk sediment samples from 2 cores from each site. Two additional cores were collected from each site for radiocarbon analysis of twig cellulose with the assumption that most twigs in the sediment within the forested fringe fell from overhead and are contemporaneous with the sediment. Only the West site, however, yielded sufficient identifiable twig material for analysis. Modern sediment accumulation rates based on ^{210}Pb and ^{137}Cs fall between 0.2–0.4 cm/yr at the East site, and 0.7–1.3 cm/yr at the West site (nearest the stream inlet), with approximate agreement between the ^{210}Pb and ^{137}Cs methods. Modern sediment accumulation rate based on bomb-pulse ^{14}C activity of twigs from cores from the West site is approximately 1.0 cm/yr, in agreement with the ^{210}Pb and ^{137}Cs results. Historic sediment accumulation rates were estimated at the West site using twigs from deeper intervals with pre-bomb ^{14}C activity. Sediment covering approximately 1000 yr of pre-settlement sediment accumulation exhibited evidence of minor bioturbation or in-washing of reworked material, but with a clearly lower accumulation rate of less than 0.1 cm/yr.

INTRODUCTION

A common method of assessing erosion within a watershed is to measure the modern rate of sediment accumulation in a reservoir or lake that receives runoff from the area of interest (e.g. Dendy and Boulton 1976; Ritchie et al. 1983; Hai et al. 1999). Using this approach, many studies have documented higher rates of erosion in watersheds within cultivated land than from comparable watersheds containing less cultivated acreage (Ursic and Dendy 1965; Ritchie et al. 1974; Ritchie et al. 1986). In a few studies, changes in the calculated rate of sediment accumulation in a reservoir or lake over a period of several decades has been attributed to changes in agricultural practice (e.g. Ritchie et al. 1986), but little data exists on rates of erosion or sedimentation prior to cultivation within a specific watershed.

An ideal site for quantifying historical lacustrine sediment accumulation rates before and after surrounding land was cleared and cultivated would be a lake meeting the following criteria: (1) a uniform rate of deposition prior to clearing, (2) no scouring or bioturbation of deposited sediment, (3) a several decade history of sediment accumulation following clearing, and (4) the presence of contemporaneous, identifiable, and datable material throughout the sediment profile. These conditions are approximately met in the numerous oxbow lakes on the ancestral floodplain of the lower Mississippi River, where large-scale clearing began just over a century ago.

[1]Department of Geology and Geological Engineering, University of Mississippi, Carrier 118, University, Mississippi 38677, USA.
[2]Corresponding author. Email: davidson@olemiss.edu
[3]NSF-Arizona AMS Facility, Department of Physics, University of Arizona, Physics Building, 1118 East Fourth St., P.O. Box 210081, Tucson, Arizona 85721, USA
[4]Geology Department, Millsaps College, 1701 N. State St., Jackson, Mississippi 39210, USA.
[5]Department of Biology, University of Mississippi, University, Mississippi 38677, USA.

Proceedings of the 18th International Radiocarbon Conference, edited by N Beavan Athfield and R J Sparks
RADIOCARBON, Vol 46, Nr 2, 2004, p 755–764

STUDY SITE

Sky Lake is an oxbow lake located 10 km north of Belzoni, Mississippi, USA (Figure 1). Sky Lake is believed to have been an ancient channel of the Mississippi River abandoned between 7500 and 10,000 BP (Saucier 1994). Personal records from local residents, many of whom are descendants of the original settlers, indicate that clearing of the forests around the lake began in the late 1880s and continued until all usable lands were under tillage by the 1920s (Mark Simmons, personal communication). A seasonally inundated, forested fringe up to 0.8 km wide still surrounds the lake. The forested fringe is dominated by waterlocust (*Gleditsia aquatica*), water tupelo (*Nyssa aquatica*), and large bald cypress trees (*Taxodium distichum*).

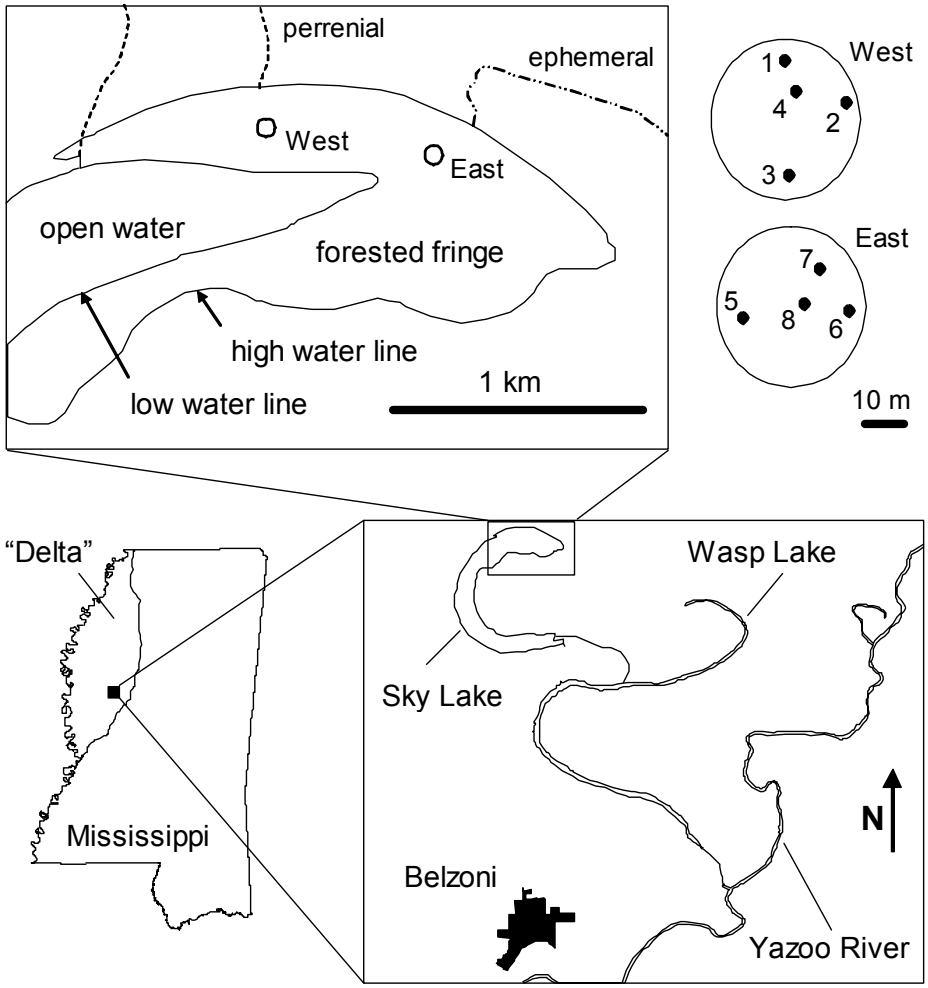

Figure 1 Sky Lake, Humphreys County, Mississippi. The ancestral floodplain of the Mississippi River in the northwestern corner of Mississippi is known as the Delta region. The stream nearest the West sampling site is perennial; the stream nearest the East site is ephemeral. Enlargements of the West and East sites are shown to the right with core numbers identifying the relative location of each core within the sampling site.

The surface area draining into Sky Lake consists of approximately 1860 ha of agricultural land. Runoff from precipitation and irrigation reaches the lake through diffuse overland flow and through several small, low-energy streams. The flow is normally southward with discharge through Wasp Lake into the Yazoo River. During seasonal flooding, the Yazoo River backflows through Wasp Lake into Sky Lake. Both backflow and stream inflow are low velocity events, resulting in a predominance of clay size particles entering the lake. Historically, Sky Lake could completely drain during prolonged dry periods, but surface outflow is now limited by a flow control structure installed in 1980.

METHODS

Site Selection

Two areas within the northern vegetated fringe in Sky Lake were selected based on visual observations of varying sedimentation regimes (Figure 1). The West site is located near the mouth of a low-energy perennial stream. Water entering the wetland from the stream is typically turbid, and tree litter on the wetland floor is coated with fine grained sediment. The East site is more isolated from perennial stream inlets. Water entering the wetland here following storm events is generally clear and surface tree litter is not coated with sediment. Bark and leaf litter in all sediment cores showed no visible sign of reworking by scour or bioturbation. Redox measurements on sediment cores collected from the same areas by Galicki (2002) indicate that the sediment is oxygen poor during much of the year, which should limit the persistence of burrowing organisms.

Sample Collection

Four sediment cores were collected from each of the 2 sites. The West site is represented by Cores 1 through 4, and the East site by Cores 5 through 8 (Table 1). Cores 1 and 5 were collected in 1998 for ^{210}Pb and ^{137}Cs analysis and reported by Galicki (2002). Three additional cores were collected from each site in 2002, two at each site for ^{14}C analysis, and one at each site for additional ^{210}Pb and ^{137}Cs analyses. Sediment cores were collected by manual insertion of a 10-cm PVC pipe to a depth of up to 2 m. Compaction during coring was tracked by recording the thickness of the sediment core inside the core barrel every 10 cm of penetration (Morton and White 1995). The core was extruded in the laboratory using a calibrated threaded rod and cut into intervals ranging from 0.9 to 5 cm thick depending on the estimated deposition rate and intended use (Table 1). Additional compaction during extrusion was insignificant (based on comparison of the length of the core prior to extrusion with the sum of each sectioned interval following extrusion). The outer 0.6 cm of each wafer was cut away and discarded. Water content was determined by weighing before and after drying at 60 °C.

Table 1 Core information.

Location	Core[a]	Intended application	Core depth (cm)[b]	Interval thickness (cm)	n[c]
West site	1	^{210}Pb, ^{137}Cs	70	5.0	10
	2	^{210}Pb, ^{137}Cs	67	3.0	18
	3	^{14}C	170	2.3	31
	4	^{14}C	186	2.3	8
East site	5	^{210}Pb, ^{137}Cs	70	5.0	7
	6	^{210}Pb, ^{137}Cs	35	3.0	8
	7	^{14}C	85	0.9	16
	8	^{14}C	85	0.9	0

[a]Cores 1 and 5 are upper portion of cores 3 and 4, respectively, in Galicki (2002).

[b]Corrected for compaction during core collection.

[c]Number of intervals analyzed for ^{210}Pb and ^{137}Cs, or for ^{14}C.

Sediments typically become more compact with depth, requiring normalization of sediment thickness based on dry bulk density or water content to allow direct comparison of recent and ancient sedimentation rates (Martin and Rice 1981). Compaction at Sky Lake, however, is apparently not significant within the upper 2 m. Water content, dry bulk density, and organic content show no consistent trend with depth (Galicki 2002), and normalization was not required.

^{210}Pb and ^{137}Cs Analysis

^{210}Pb and ^{137}Cs activities were determined at the University of South Carolina on powdered, bulk sediment samples using a low-energy planar germanium detector calibrated using NIST soil samples (Dukat and Kuehl 1995). The supported level of ^{210}Pb was determined by monitoring the level of ^{226}Ra gamma peaks. Corrections were made for self-absorption of low-energy gamma rays (Cutshall et al. 1983). Sedimentation rates based on ^{210}Pb assumed a constant rate of sediment accumulation and rate of atmospheric ^{210}Pb fallout.

^{14}C Analysis

Samples from the cores for ^{14}C analysis were separated into 3 fractions: (1) large organic material retained on a 710-µm sieve (#25), (2) fine, mostly organic debris retained on a 250-µm sieve (#60), and (3) a predominantly clay fraction that passed through the 250-µm sieve. A binocular microscope was used to identify woody plant stems (twigs), representing 1 to 2 yr of growth, from the largest fraction. Wood fragments derived from larger branches or tree trunks were selected from several depths for comparison purposes.

Tree-ring samples were collected from a single 1.3-cm-diameter core taken from a 100-yr-old bald cypress tree growing in the vicinity of sediment core collection. The tree rings were dated by cross-correlation with cores taken from over 70 different trees in the same wetland. Individual annual rings were separated using a stainless steel razor blade and stored dry prior to chemical pretreatment.

Woody material was pretreated using an AAA-bleach procedure for removing potential contaminants and extraction of holo-cellulose (adapted from Hoper et al. 1998). Intact samples (all <3 mm in diameter) were placed sequentially in 1 M HCl for 2 hr at 60 °C; 0.5 M NaOH at 60 °C for 1 hr (repeated until solution was clear); 1 M HCl for 1 hr at 60 °C; and a bleaching solution of 0.3 M $NaClO_2$ and 0.07 M HCl at 60 °C until the material turned white (typically 4–8 hr). Samples were rinsed with distilled water between each step. A few very small samples received shortened wash times to prevent complete dissociation and are identified in the discussion of results and figures.

Organic debris samples collected on the 250-µm sieve were consistently lost when applying the full AAA pretreatment (without the bleach solution). Necessity of the pretreatment for this fraction was tested on split samples from three depths from Core 3. A split from each depth was pretreated as above but with only 1 hr in each solution and a single NaOH wash. The second split was untreated. The ^{14}C activities of untreated and pretreated material differed by less than 1%. The remaining intervals were analyzed without pretreatment.

Prepared samples were combusted in Vicor® or quartz tubing with excess CuO over an open propane flame. Evolved gases were passed through hot Cu and Ag wire to convert nitrogen oxide gases to N_2 and to remove residual halides. CO_2 was purified cryogenically and split into fractions for δ^{13}C and ^{14}C analyses. Graphite targets for ^{14}C analysis were prepared by conversion of CO_2 to graphite in the presence of powdered Zn and Fe, and analyzed by accelerator mass spectrometry (AMS) at the NSF-Arizona AMS facility. Calibrated ages for pre-bomb samples were determined using CALIB 4.4 (Stuiver et al. 1993; revision 4.4: http://radiocarbon.pa.qub.ac.uk/calib/).

RESULTS AND DISCUSSION

^{210}Pb and ^{137}Cs Results

Sediment accumulation rates since clearing of the land around Sky Lake were calculated for 2 cores from each site using ^{210}Pb and ^{137}Cs activities (Figure 2). Agreement between cores and methods in the East site was relatively good. The ^{137}Cs-based sediment accumulation rates calculated from Cores 5 and 6 overlap at approximately 0.3 cm/yr. Variability in the magnitude of each range given in Figure 2a is a reflection of the uncertainty in the exact location of the ^{137}Cs peak within the 3- or 5-cm interval analyzed. The same cores yield ^{210}Pb-based sediment accumulation rates of 0.37 and 0.23 cm/yr, respectively (Figure 2b).

Post land-clearing sediment accumulation rates calculated for the West site are approximately 3 times higher than for the East site. The ^{137}Cs-based sediment accumulation rates from Cores 1 and 2 overlap at approximately 0.9 cm/yr, with a ^{210}Pb-based rate of 1.0 cm/yr for Core 2, and a slightly higher rate of 1.3 cm/yr for Core 1. Deviations from linearity on the ^{210}Pb plots suggest that some bioturbation or variation in sediment influx has occurred, but a clear trend in the excess (unsupported) ^{210}Pb is evident to depths of approximately 55 cm in cores from the West site, and 30 cm in cores from the East site. The depth of datable sediment represents the last 50 to 100 yr of deposition.

Sediment accumulation rate calculations using ^{137}Cs are based on the assumption that peak ^{137}Cs fallout occurred in 1964 following the heaviest period of atmospheric testing of nuclear weapons (Perkins and Thomas 1980), a constant sediment accumulation rate in the ensuing years, and no post-depositional migration of Cs (e.g. Krishnaswamy et al. 1971; Goodsite et al. 2001). The sharp ^{137}Cs peaks in 3 of the 4 cores (Cores 2, 5, and 6) and relative agreement with the ^{210}Pb-based rates suggests that Cs migration has not been significant at these locations since deposition (Figure 2a). The more diffuse peak in Core 1 might result from localized migration of Cs, from dilution of the peak ^{137}Cs activity by under or overlying sediment in the large (5 cm) sample interval, or from minor bioturbation. The ^{210}Pb activity from Core 1 (Figure 2b), however, shows minimal evidence of reworking.

The modern sediment accumulation rates calculated for Sky Lake are significantly lower at both sites than reported in an earlier study of adjacent Wasp Lake. Ritchie et al. (1979) reported sedimentation rates based on ^{137}Cs measurements that ranged from 2.5 to 7.7 cm/yr in Wasp Lake. Higher sediment accumulation rates may be caused by closer proximity to the Yazoo River (Figure 1). It is also possible that sediment discharge to these lakes has decreased in the last 25 yr, though no slope change is evident in the ^{210}Pb plots from Figure 2b.

^{14}C Results

Small branches in lake sediments typically represent material that was washed into the lake after some residence time on the terrestrial forest floor. When dating ancient sediments, a delay of a few years does not represent a significant error (Björck and Wohlfarth 2001), but the error may be more significant when dating modern sediments utilizing bomb pulse activities. In forested wetlands, however, twigs are likely to be buried soon after they fall and should yield a ^{14}C age that is nearly contemporaneous with the date of deposition. Leaf stems detach annually from bald cypress and deciduous wetland trees, and a large percentage of small branches (representing 1 to 2 yr of growth) are shed within the same year of death. Tests of 10 sample sets from different depths demonstrated that the ^{14}C activity of twig samples was consistently higher than the activity of undefined wood fragments (from decomposed tree trunks or larger branches) and the activity of miscellaneous organic debris collected on a 250-μm sieve (Figure 3).

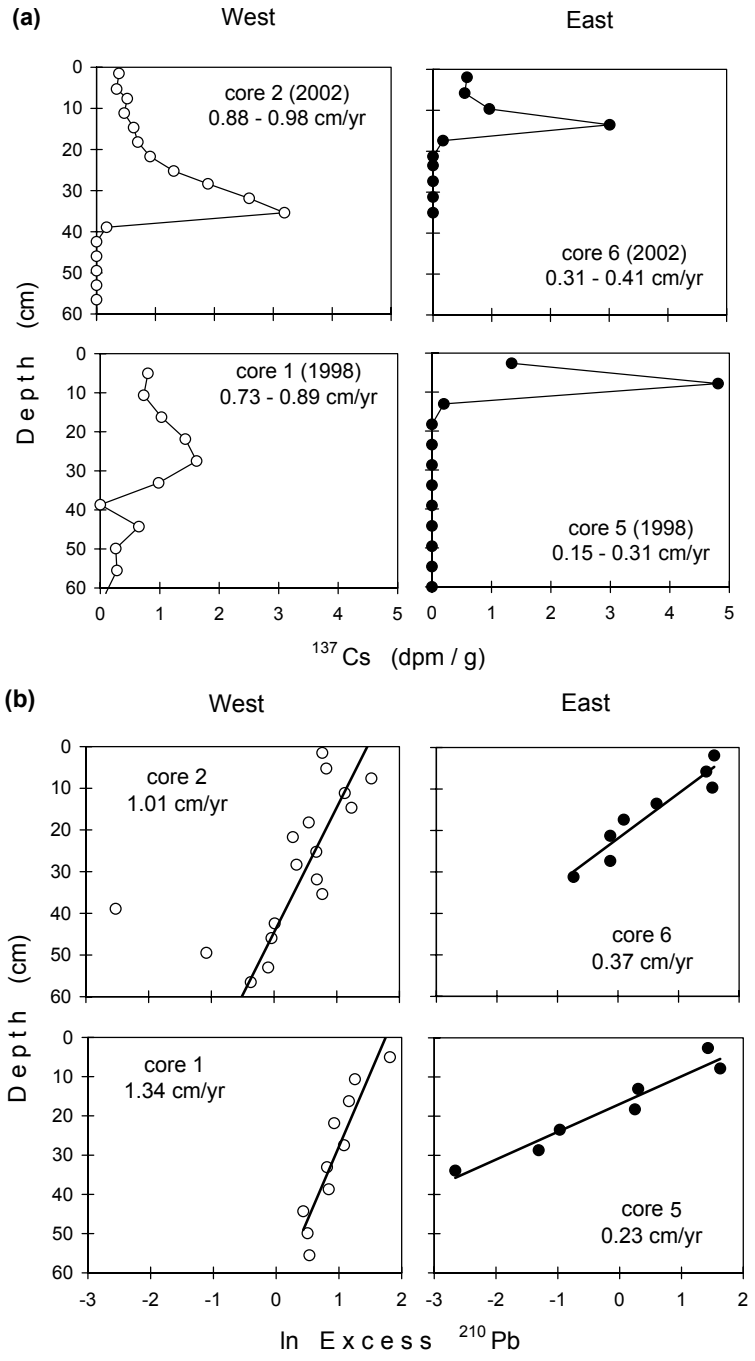

Figure 2 (a) ^{137}Cs activity and (b) ln excess ^{210}Pb activity in sediment samples with depth. The dates given in (a) refer to the year the cores were collected. Data for Cores 1 and 5 are from Galicki (2002). The thickness of each sample interval was 5 cm for Cores 1 and 5, and 3 cm for Cores 2 and 6 (Table 1).

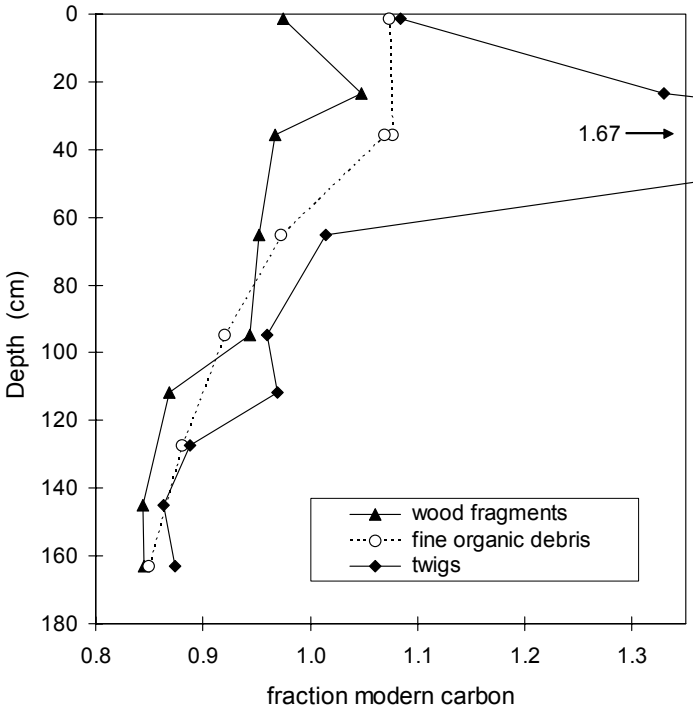

Figure 3 ^{14}C activity of wood fragments, fine organic debris (710–250 μm), and twig samples from the same depths from Core 3 (West site). Analytical uncertainty for ^{14}C activity (1 σ) is equal to or smaller than the size of the data markers.

Post land-clearing sediment accumulation rates were determined for Cores 3 and 4 in the West site using bomb-pulse ^{14}C activity of twig cellulose. The bald cypress tree-ring activity for the years 1950–2000 was aligned with the post-bomb sediment data to achieve the best fit (Figure 4). The tree-ring activity curve shown in Figure 4 is consistent with the annualized atmospheric ^{14}C activities reported by Goodsite et al. (2001) for the Northern Hemisphere (mid to high latitudes). The 2 sediment cores were sectioned into intervals of equivalent thickness, but a much higher number of intervals from Core 3 were analyzed for ^{14}C (Table 1).

Of the 17 sediment samples from the 2 cores with post-bomb ^{14}C activity (13 from Core 3 and 4 from Core 4), 13 align well with the atmospheric ^{14}C curve represented by the tree-ring data, with a clearly identifiable maximum during 1963–1964 (Figure 4). The 4 points that fall significantly off the curve, all from Core 3, may represent evidence of minor bioturbation, introduction of reworked material, or a long delay between death of a twig and separation from the tree. Based on the general fit to the atmospheric bomb-pulse, the ^{14}C profile indicates a sediment accumulation rate of 1.0 cm/yr, and is consistent with the ^{210}Pb and ^{137}Cs results for samples reflecting the last 50 yr of sedimentation at the West site.

The pre-bomb data shows a generally decreasing trend with depth, but the data does not fall neatly along a linear depth versus calibrated age curve (Figure 5). Variability may be due to an occasional influx of reworked material from the surrounding forest (present until the last century) or due to bioturbation, though the data from Figure 3 suggests that the sediment is not highly mixed. Thorough mixing should result in a more random relationship between the ^{14}C activity of wood fragments, fine organic debris, and twigs. The generally intermediate activity of organic debris shown in Figure 3 is

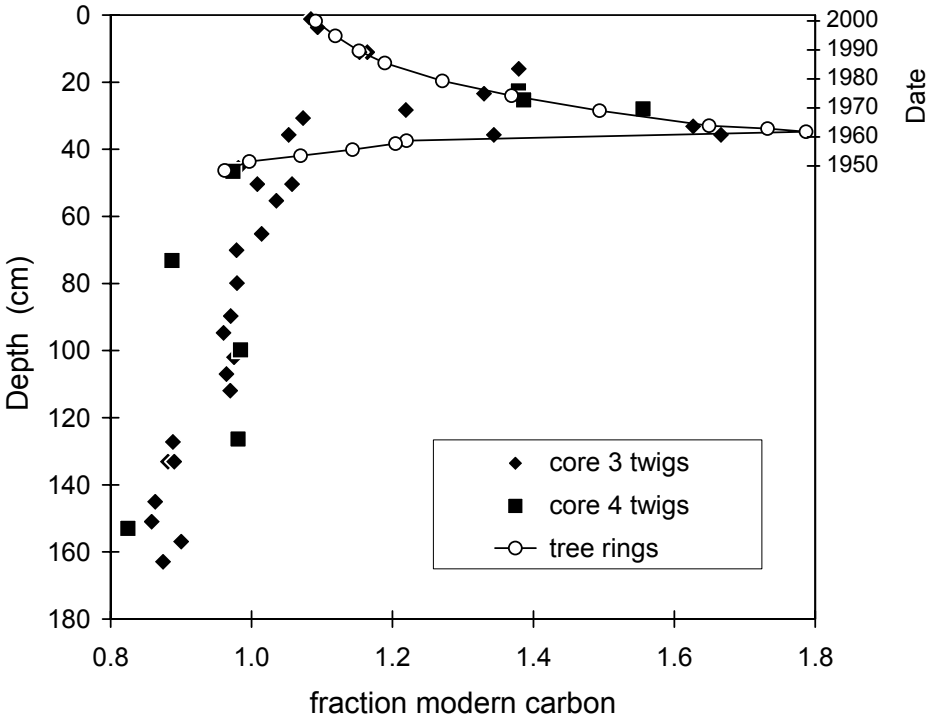

Figure 4 ^{14}C activity of twig samples collected from Cores 3 and 4 from the West site, and of individual tree rings collected from a bald cypress tree growing nearby. The calendar year of tree-ring growth is shown on the right axis and aligned with the peak activity observed in the sediment samples. Analytical uncertainty (1 σ) is equal to or smaller than the size of the data markers.

more consistent with in-place decomposition of older wood and younger twigs, plants, and insect remains resulting in finer organic debris of mixed activity.

In spite of the variability in the pre-bomb data, it is clear that the average pre-settlement sedimentation rate was much less than the current rate (Figure 5). A best-fit line through the data below 60 cm, using the median points of dates assigned the highest probability, yields an average sedimentation rate of 0.07 cm/yr for the 1000 yr preceding clearing. Indeed, even a highly biased line through the data favoring higher sedimentation rates does not exceed 0.1 cm/yr.

Twig samples proved to be much more difficult to find in cores collected from the East site. Twigs from these cores were smaller and harder to differentiate from small roots. The small size also precluded thorough pretreatment, further increasing the uncertainty associated with the results. (No recoverable sample remained after full AAA-bleach pretreatment.) Analyzed samples were pretreated for shorter time periods in each solution, typically no more than 1 hr. Nearly all samples from Core 7 yielded post-bomb ^{14}C activities with no discernible pattern, possibly reflecting accidental selection of small roots instead of twigs. Identifiable twig material was equally difficult to find in Core 8 and no ^{14}C analyses were performed. The relative scarcity of identifiable twig material at this site is probably due to the fact that the leaf and branch litter is not coated as quickly with clay. The organic debris is more aerated and decomposition should be more rapid. However, measurements of organic carbon (based on loss on ignition) did not show a significant difference in the total organic content in sediment cores from the 2 sites (Galicki 2002).

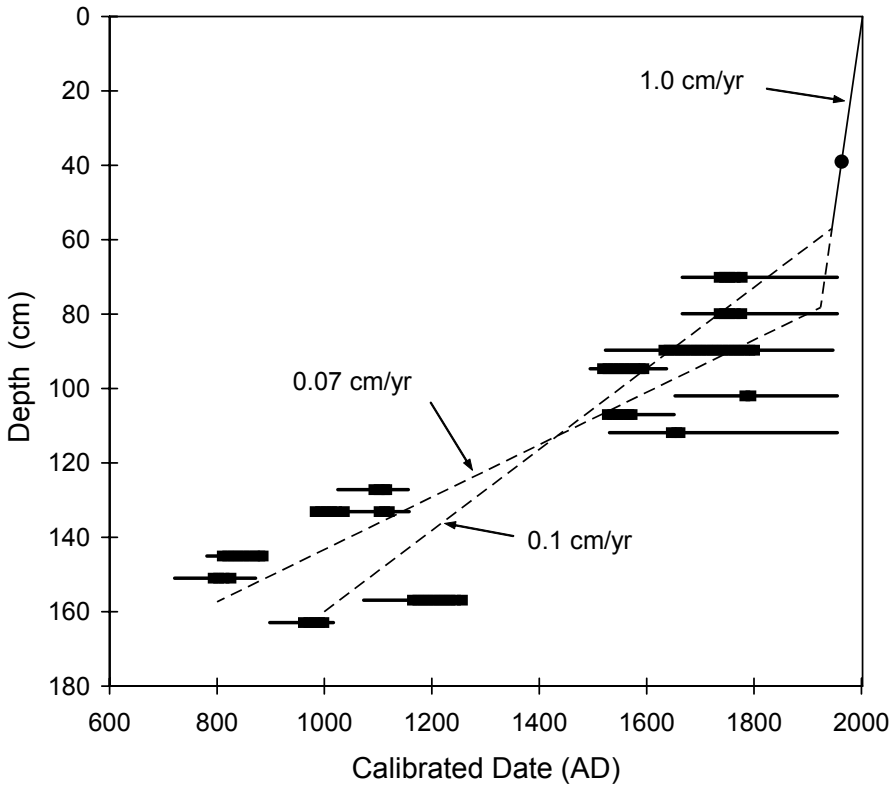

Figure 5 Calibrated dates for pre-bomb twigs in sediment from Core 3 only (West site) versus depth. The single filled circle marks the depth of the peak atmospheric ^{14}C activity observed in the tree rings and sediment in Figure 4, and corresponds to a sediment accumulation rate of 1.0 cm/yr (the remaining post-bomb data are not plotted). The horizontal lines represent the range of possible dates (1 σ) for the pre-bomb samples, with the range of highest probability shown as a thicker line. A linear regression through the highest probability ranges yields a line with a slope of 0.07 cm/yr. A line representing an arbitrary sediment accumulation rate of 0.1 cm/yr is plotted for comparison.

CONCLUSIONS AND SUMMARY

Sediment accumulation rates were determined for multiple sediment cores collected from two different locations at Sky Lake in northwestern Mississippi. Estimates using ^{210}Pb and ^{137}Cs activities measured in bulk sediment and ^{14}C activity in twig cellulose gave comparable results of approximately 1.0 cm/yr at the West site (near stream inlet) during the last 50 to 100 yr. The sedimentation rate prior to clearing the land for agriculture was an order of magnitude less based on ^{14}C activities alone. Erosion rates from the surrounding fields should be proportional to the rate of sediment accumulation in the lake, which means it is likely that erosional losses around Sky Lake were also an order of magnitude less when the surrounding land was still forested. At the East site, more isolated from perennial stream inlets, comparisons were only possible using ^{210}Pb and ^{137}Cs. The 2 methods gave comparable results for modern sediment accumulation rates of approximately 0.2–0.4 cm/yr. Estimates using ^{14}C activity may still be possible using either more sediment from each depth, or by selecting different material for dating.

ACKNOWLEDGEMENTS

Thanks to Jared Holland and John Hart for assistance with sample processing and $\delta^{13}C$ analysis, and to the NSF-Arizona AMS laboratory for advise and ^{14}C analyses. Partial funding for this work was obtained from the USDA-ARS National Sedimentation Laboratory, Oxford, Mississippi.

REFERENCES

Björck S, Wohlfarth B. 2001. ^{14}C chronostratigraphic techniques in paleolimnology. In: Last WM, Smol JP, editors. *Tracking Environmental Change Using Lake Sediments. Volume 1: Basin Analysis, Coring, and Chronological Techniques*. Dordrecht, the Netherlands: Kluwer Academic Publishers. p 205–45.

Cutshall NH, Larson IL, Olsen CR. 1983. Direct analysis of ^{210}Pb in sediment samples: self absorption correction. *Nuclear Instruments and Methods in Physics Research B* 206:309–17.

Dendy FE, Boulton GC. 1976. Sediment yield-runoff-drainage area relationships in the United States. *Journal of Soil and Water Conservation* 31:264–6.

Dukat DA, Kuehl SA. 1995. Non-steady-state ^{210}Pb flux and the use of $^{228}Ra/^{226}Ra$ as a geochronometer on the Amazon continental shelf. *Marine Geology* 125:329–50.

Galicki SJ. 2002. Bald cypress dendrochemistry and sediment geochemistry in a lake fringe wetland, Sky Lake, Mississippi [PhD dissertation]. Oxford: University of Mississippi, USA. 190 p.

Goodsite ME, Rom W, Heinemeier J, Lange T, Ooi S, Appleby PG, Shotyk W, van der Knaap WO, Lohse C, Hansen TS. 2001. High-resolution AMS ^{14}C dating of post-bomb peat archives of atmospheric pollutants. *Radiocarbon* 43(2B):495–515.

Hai PS, Son PN, Dien NN, Tan VH, Hien PD. 1999. Assessment of erosion and accretion in catchment areas based on ^{210}Pb and ^{137}Cs contents in soil and sediment. In: Stevenson NR, editor. *Isotope Production and Applications in the 21st Century.* Proceedings of the 3rd International Conference on Isotopes, Vancouver, Canada, 6–10 September 1999. World Scientific, New Jersey. p 415–8.

Hoper ST, McCormac FG, Hogg AG, Higham TFG, Head MJ. 1998. Evaluation of wood pretreatments on oak and cedar. *Radiocarbon* 40(1):45–50.

Krishnaswamy S, Lal D, Martin JM, Meybeck M. 1971. Geochronology of lake sediments. *Earth and Planetary Science Letters* 11:407–14.

Martin EA, Rice CA. 1981. Sampling and analyzing sediment cores for ^{210}Pb geochronology. *United States Geological Survey, Open-File Report* 81–983.

Morton RA, White WA. 1995. Characteristics of and corrections for core shortening in unconsolidated sediments. *Journal of Coastal Research* 13:761–9.

Perkins RW, Thomas CW. 1980. Worldwide fallout. In: Hansen WC, editor. *Transuranic Elements in the Environment*. Springfield, Virginia, USA: Technical Information Center. p 53–82.

Ritchie JC, Cooper CM, McHenry JR. 1979. Recent accumulation of sediment in lakes in the Bear Creek watershed in the Mississippi Delta. *Southern Geologist* 20:173–80.

Ritchie JC, Cooper CM, McHenry JR. 1986. Sediment accumulation rates in lakes and reservoirs in the Mississippi River Valley. In: Wang SY, editor. *Third International Symposium on River Sedimentation*, The University of Mississippi, 31 March–4 April 1986. p 1357–65.

Ritchie JC, Cooper CM, McHenry JR, Schiebe FR. 1983. Sediment accumulation in Lake Chicot, Arkansas. *Environmental Geology* 5:79–82.

Ritchie JC, McHenry JR, Gill AC. 1974. Fallout ^{137}Cs in the soils and sediments of three small watersheds. *Ecology* 55:887–90.

Saucier RT. 1994. Geomorphology and Quaternary geologic history of the lower Mississippi valley. *United States Army Corps of Engineers, Vicksburg, Vol. II*.

Stuiver M, Reimer PJ. 1993. Extended ^{14}C data base and revised CALIB 3.0 ^{14}C age calibration program. *Radiocarbon* 35(1):215–30. Revision 4.4: http://radiocarbon.pa.qub.ac.uk/calib/.

Ursic SJ, Dendy FE. 1965. Sediment yields from small watersheds under various land uses and forest covers. *U.S. Department of Agriculture, Miscellaneous Publication* 970. p 47–52.

RADIOCARBON, Vol 46, Nr 2, 2004, p 765–774

LATE HOLOCENE ENVIRONMENTAL RECONSTRUCTION OF ST. MICHIEL SALINE LAGOON, CURAÇAO (DUTCH ANTILLES)

Bogumila B Klosowska[1,2] • Simon R Troelstra[1] • Jan E van Hinte[1] • Dirk Beets[1] • Klaas van der Borg[3] • Arie F M de Jong[3]

ABSTRACT. Two sediment cores collected from the saline lagoon St. Michiel on Curaçao (Dutch Antilles) preserve a ~5000-yr record of environmental change. Investigation of radiocarbon-dated sections by accelerator mass spectrometry (AMS) is based on faunal assemblage analyses, sediment mineralogy, and the interpretation of sedimentary facies. The cores recovered from different parts of the lagoon demonstrate different development. Initially, in the proximal part of the lagoon (core STM-2), the sediment accumulated in a coastal, semi-protected bay with strong marine influence, whereas the distal part (STM-1) was dominated by chemical precipitation (gypsum, aragonite). By about 3500–3400 BP, connection with the open sea became very limited due to the gradual formation of a coral rubble barrier at the coastline. Subsequently, the record reveals undisturbed sedimentation in the highly restricted shallow lagoon. Around 1100–1000 BP, biological and sedimentological records indicate a change to less evaporitic conditions. Stages of increased salinity are intercalated with intervals of episodic freshening due to increased runoff and precipitation. The authors demonstrate that since permanent human settlements were established on the island about 1100 BP, the watershed has undergone intensive deforestation, especially during the European colonization at the beginning of the 16th century. Deforestation resulting from agriculture and construction caused increased erosion, which was translated to increased sediment accumulation rates and a shift in lagoon sedimentation from almost entirely endogenic to mostly detrital.

INTRODUCTION

Saline lagoons are common features in arid and semi-arid areas. They respond quickly to environmental change; therefore, their sedimentary record can provide a very sensitive archive of past fluctuations in water chemistry, hydrology, and drainage basin characteristics. In this study, we investigate the late Holocene sedimentary sequence of a saline lagoon of Curaçao, one of the Leeward Islands of the Dutch Antilles. It is based on faunal assemblage analyses, sediment mineralogy, and the interpretation of sedimentary facies of 2 shallow cores.

St. Michiel salina is one of a number of shallow (<2 m average depth) coastline lagoons of Curaçao, separated from the open sea by an approximately 50-m-wide, slightly elevated ridge of coral debris (Figure 1). A very narrow canal (2–3 m wide) cuts the ridge and connects the lagoon with the Caribbean Sea. Bedrock in the area consists of Cretaceous volcanic rocks and Neogene and Quaternary limestones (Beets 1972; De Buisonjé 1974; Klaver 1987; Fouke 1994). The northern parts of the lagoon, most distant from the sea, overlie deeply weathered hyaloclastites and dolerites of the Curaçao Lava Formation, which in a seaward direction are unconformably overlain by more resistant calcareous and dolomitized rocks of the Seroe Domi Formation (Figure 1).

The saline lagoons of Curaçao are essentially shallow remnants of former inland bays. Formation of these coastal embayments is related to eustatic sea-level rise after the last glaciation. In the Pleistocene, when the sea level was lower than today, systems of erosional drainage basins were formed which, in the periods of postglacial transgression, developed into inland bays and lagoons (De Buisonjé 1974).

[1]Faculty of Earth and Life Sciences, Department of Paleoecology and Paleoclimatology, Vrije Universiteit, de Boelelaan 1085, 1081HV Amsterdam, the Netherlands.
[2]Corresponding author. Email: klob@geo.vu.nl.
[3]Robert J van der Graaff Laboratorium, University Utrecht, Box 80.000, 3508 TA Utrecht, the Netherlands.

Proceedings of the 18th International Radiocarbon Conference, edited by N Beavan Athfield and R J Sparks
RADIOCARBON, Vol 46, Nr 2, 2004, p 765–774

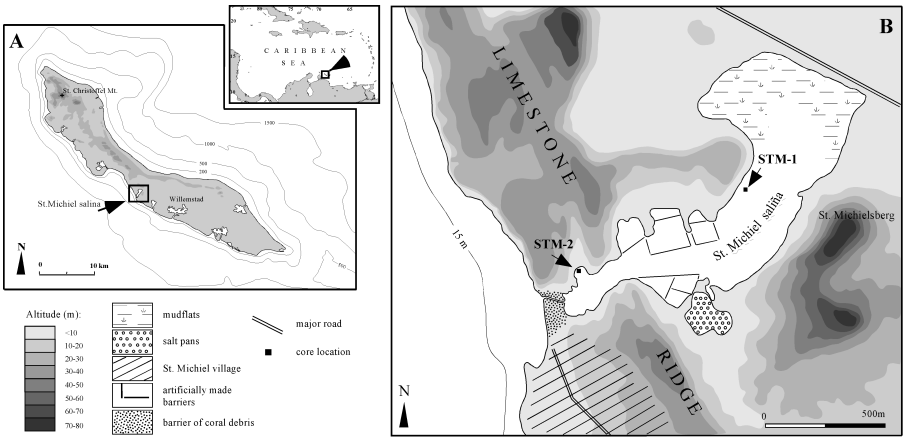

Figure 1 a) Map of Curaçao and the location of saline lagoon St. Michiel. Bathymetry in meters. b) Map of St. Michiel saline lagoon and surroundings with the coring sites. Elevated terrains consist of more resistant limestones of Seroe Domi Formation.

The area experiences a semi-arid climate with a mean yearly temperature of about 27 °C; the mean relative air humidity is about 75% and mean annual precipitation is around 550 mm, although there is usually large variability between years (Martis et al. 2002). Curaçao is situated in the belt of trade winds from the east and east-northeast. Although the island is located south of the Atlantic hurricane belt, occasionally tropical storms pass within 200 km of the island and cause heavy damage in the shallow coastal areas (Meteorological Service: http://www.meteo.an). The average daily tidal range on Curaçao is approximately 30 cm. However, due to its restricted connection to the sea, the lagoon is an area of limited tidal flow. Salinity of the water in the lagoon is primarily controlled by the balance between rainfall and evaporation, by the inflow through the canal, and by seepage. The salinity fluctuates on an irregular basis depending on the amount of rainfall, from brackish conditions after heavy rainfall to hypersaline conditions after prolonged drought.

The pre-colonization history of the island is poorly known, but archaeological evidence indicates the presence of permanent settlements in the area about 1100 BP (Versteeg and Rostain 1997). The original inhabitants were Caquetíos Indians who migrated from the coastal regions of the South American continent. They lived primarily from fishing and agriculture. Since the arrival of Europeans in AD 1499, Curaçao was subjected to 1 century of Spanish rule and came under Dutch control in AD 1634. Rapid growth of the population, woodcutting for private use and commerce, land-cultivation, and the introduction of domestic animals have seriously influenced the environment of the island.

METHODOLOGY

Three cores (STM-1, STM-2, and STM-3) from different parts of the saline lagoon St. Michiel were collected in April 2000. The cores were recovered in 1-m sections using a hand corer. It is important to note that for this coring technique, there is a risk of contamination due to caving, especially at the base of each 1-m section. The diameter of the recovered cores is 4 cm. Sediment samples, weighing on average 10 g and taken every ~5 cm along the entire length of core STM-1 and the 3 upper sections of core STM-2, were gently washed over a 63-µm sieve. The residue was dried and examined under a stereomicroscope. Core STM-3 was not further considered for this study.

The mineralogical composition of bulk sediments was semi-quantitatively determined by X-ray diffraction. X-ray diffraction analyses were obtained at the Institute of Earth Sciences in Barcelona (CSIC, Barcelona) using a Bruker Difractometer, Model D-5005, with a Cu tube, wave-length l =1.5405, Graphyte Secondary Monochromator, KV=40 and mA=30 as working conditions. Mineralogical information obtained from X-ray diffractions were used for semiquantitative determination of mineral phases present in the studied samples. The carbonate content, determined as the $CaCO_3$ weight percentage, was measured at the Vrije Universiteit Amsterdam.

Radiocarbon samples were measured at the R. J. Van de Graaff Laboratory at the Utrecht University, the Netherlands.

RESULTS

Sediment Lithology and Composition

Core STM-1, from near the center of the lagoon, terminated at 500 cm below the sediment surface in weathered basement rocks and, thus, contains the entire sedimentation history in this part of the lagoon. Additionally, the presence of volcanic gravel and the characteristic bluish color of the sediment at the base of the core imply closeness to the "basement," the old volcanic valley floor. Core STM-2, taken close to the entrance, bottomed without reaching the basement at 550 cm and reached the depth limit of the coring equipment. Based on lithological characteristics and the sediment composition each core recovered from the St. Michiel lagoon can be subdivided into stratigraphic units (Figure 2).

Core STM-1

Unit 4 (500–260 cm) consists of mostly laminated sediments. Fine-grained laminae, 3–10 mm thick, are composed of concentrations of light-colored evaporites (gypsum) alternating with dark-grey aragonitic silt with some organic matter. Unit 3 (260–175 cm) is characterized by dark-grey aragonitic silt, very rich in charred plant remains, with locally occurring lenticular, 1–1.5-mm-large gypsum crystals (possibly of interstitial growth). At some levels, abundant gypsum crystals are present, many showing evidence of dissolution and mechanical wear and seem to be reworked. Horizons rich in fecal pellets of crustaceans are common throughout this unit. A 1–2-cm-thick layer, rich in fragments of bivalves, gastropods, and ostracod shells, accompanied by angular volcanic lithoclasts, occurs at 233 cm. Unit 2 (175–70 cm) is composed of grey siliciclastic silt with gastropod-rich horizons at 150 cm, 138 cm, and 105 cm. Unit 1 (70–0 cm) is formed of violet, homogeneous, silt- to sand-sized siliciclastic sediment with a gastropod-rich horizon at 45 cm.

Core STM-2

Unit 6 (550–300 cm) consists of light-grey bioclastic sand containing predominantly fragments of the calcareous algae *Halimeda*, as well as coralline algae, various gastropods and bivalves, echinoid spines, diverse foraminifera, and ostracod species. Above 400 cm, the sediment grains show some abrasion of sharp edges and become darker. Unit 5 (280–250 cm) is composed of grey, bioclastic sand. Sediment is much finer than in the underlying unit and the faunal assemblage consists entirely of abundant fragments of fragile tellinid bivalves and ostracods. Unit 4 (250–190 cm) is characterized by light-grey carbonate silt to sand; in the lower part of this unit, a fine (milimetric), light-grey lamination occurs with some lithified carbonate crusts. Unit 3 (190–140 cm) is formed of yellowish-grey to dark-grey carbonate silt to sand. Unit 2 (140–60 cm) consists of dark-grey, clay- to silt-sized siliciclastic sediment. Gastropod-rich horizons occur at 122 cm and 85 cm. In the lower part of this unit, there are darker layers which are rich in organic detritus and some charred plant remains. Unit 1 (60–0 cm) is composed of yellowish carbonate sand.

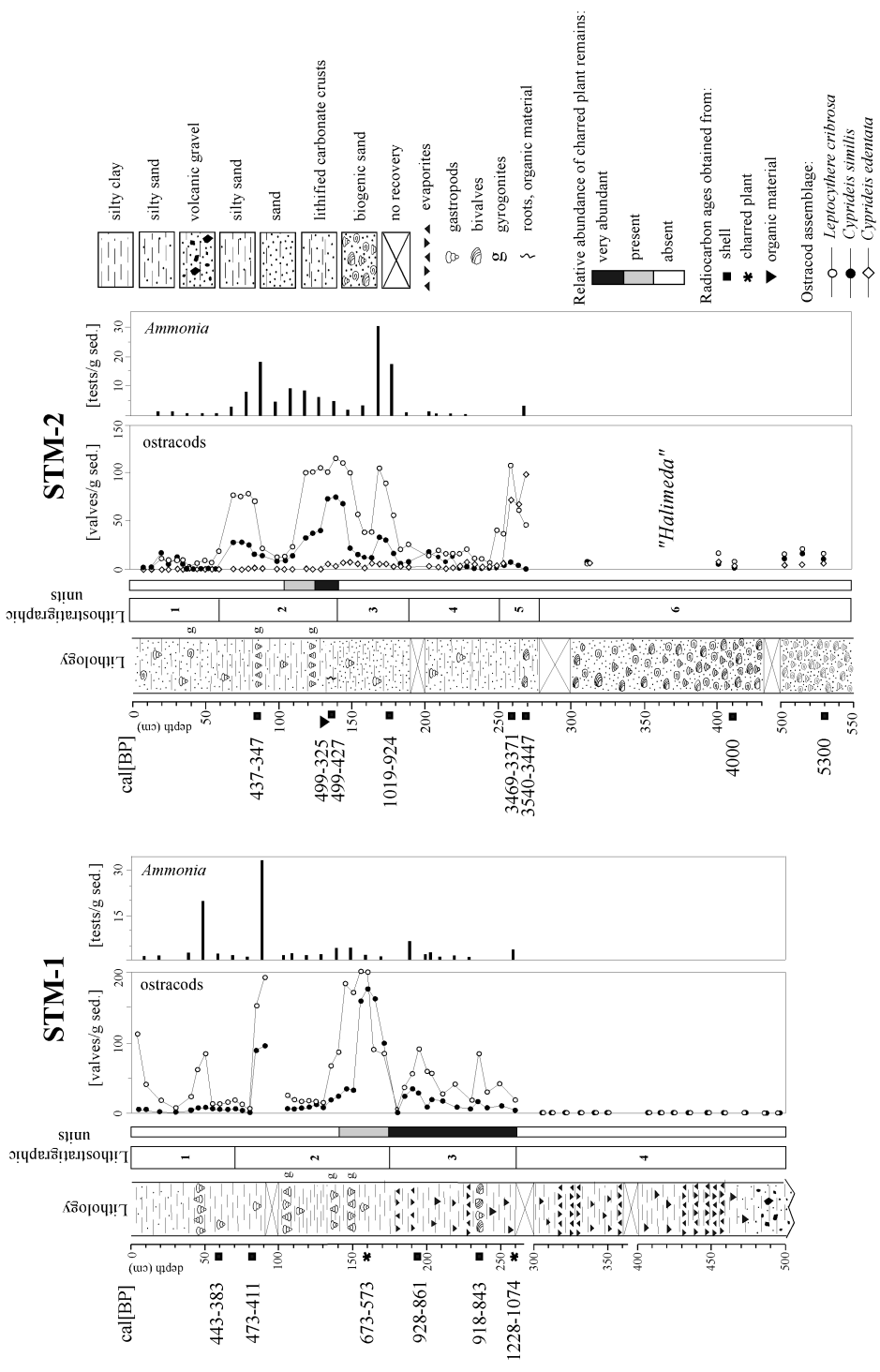

Figure 2 Lithology, abundances of ostracod and foraminiferal assemblages, and ^{14}C dates in cores STM-1 and STM-2

The biota represented in both cores (with exception of Unit 6 in core STM-2) include delicate, smooth, thin-shelled molluscs, as well as foraminifers and ostracods. All species are benthic forms known as euryhaline taxa. Amongst the gastropods, species such as *Pyrgophorus parvulus* (Guilding), *Pyrgophorus* (cf. *trabeata* Weisbord 1962), *Cerithidea costata* (da Costa 1778), and *Henrya morrisoni* (Bartsch 1847) are the most common. Occasionally, landmolluscs as *Ceciliodes* sp. and *Gastrocopta* sp. are also present. Single gyrogonites, calcified oogonia of charophytea (macrophytic algae), occur occasionally in Units 1 and 2.

Mineralogy

Figure 3 shows the variation in the total amount of carbonate as well as calcite, aragonite, and dolomite from cores STM-1 and STM-2. The non-carbonate fraction of each sample corresponds to gypsum, siliciclastics, and clay minerals, which can only be expressed qualitatively from the XRD data. The detrital (allogenic) fraction is derived from weathering and erosion of drainage basin bedrock. It includes plagioclase and clay minerals, mainly smectites. Since the bedrock on Curaçao is formed of quartz-free rocks, it appears that quartz found in the studied cores is a result of atmospheric deposition. Examination under a stereomicroscope shows that calcite in core STM-2 is largely detrital in origin from locally reworked carbonates (limestone debris), especially at the upper part of the core. Other mineralogical components of the sediment comprise aragonite, gypsum, zeolites, and Ca-dolomite. Aragonite can occur as a product of direct precipitation from the seawater or as a detritus of the hard parts of certain organisms (e.g. corals, some molluscs). In core STM-1, aragonite occurs as granular aggregates, up to 1–1.5 mm in size, of very fine-grained crystals and, thus, is interpreted to be primary in origin, precipitated in response to supersaturated conditions in the water column. In core STM-2, however, examination under a stereomicroscope suggests that at least part of the aragonite can refer to biogenic carbonate debris. Zeolites occur as metamorphic minerals in the basalts of the basement (Klaver 1987), suggesting a detrital component, but they are also known to form from the alteration of silicic volcanic glass and tuffs in lacustrine deposits, particularly highly saline and alkaline environments (Deffeyes 1959; Mariner and Surdam 1970). Although Ca-dolomite is present in the surrounding limestones of the Seroe Domi Formation (Fouke 1994), the stratigraphically restricted occurrence in core STM-2 would suggest it to be primary, precipitated directly from the lagoon water or interstitial porewater, or from alteration (dolomitization) of a precursor carbonate mineral.

The most obvious changes identified in the sediments' composition of the cores is the increase in siliciclastic components—as plagioclase, quartz, and smectites—in varying degrees, from being absent or rare in the lower parts of the profiles to being very abundant in the upper part of the profiles (Units 1 and 2; Figure 3). Gypsum and aragonite content of the sediment shows significant inverse correlation with the siliciclastic components.

^{14}C Chronology

The chronology for the St. Michiel salina is based on accelerator mass spectrometry (AMS) ^{14}C dates of 11 well-preserved shells of gastropods, bivalves, and ostracods, one of organic material and two of charred plant remains (Table 1). The age-depth relation plot (Figure 4) shows obvious changes in sediment accumulation rates. In core STM-2, the reduction from ~2.5 mm/yr to ~0.3 mm/yr prior to about 3500–3400 BP is thought to be due to an increased isolation or maybe even closure of the lagoon, which had a major impact on its hydrology. The period that follows is characterized by low accumulation rates, possibly with intervals of non-deposition. Around 1000 BP, the accumulation rate increases to 0.7 mm/yr, and at about 450 BP, dramatically exceeds

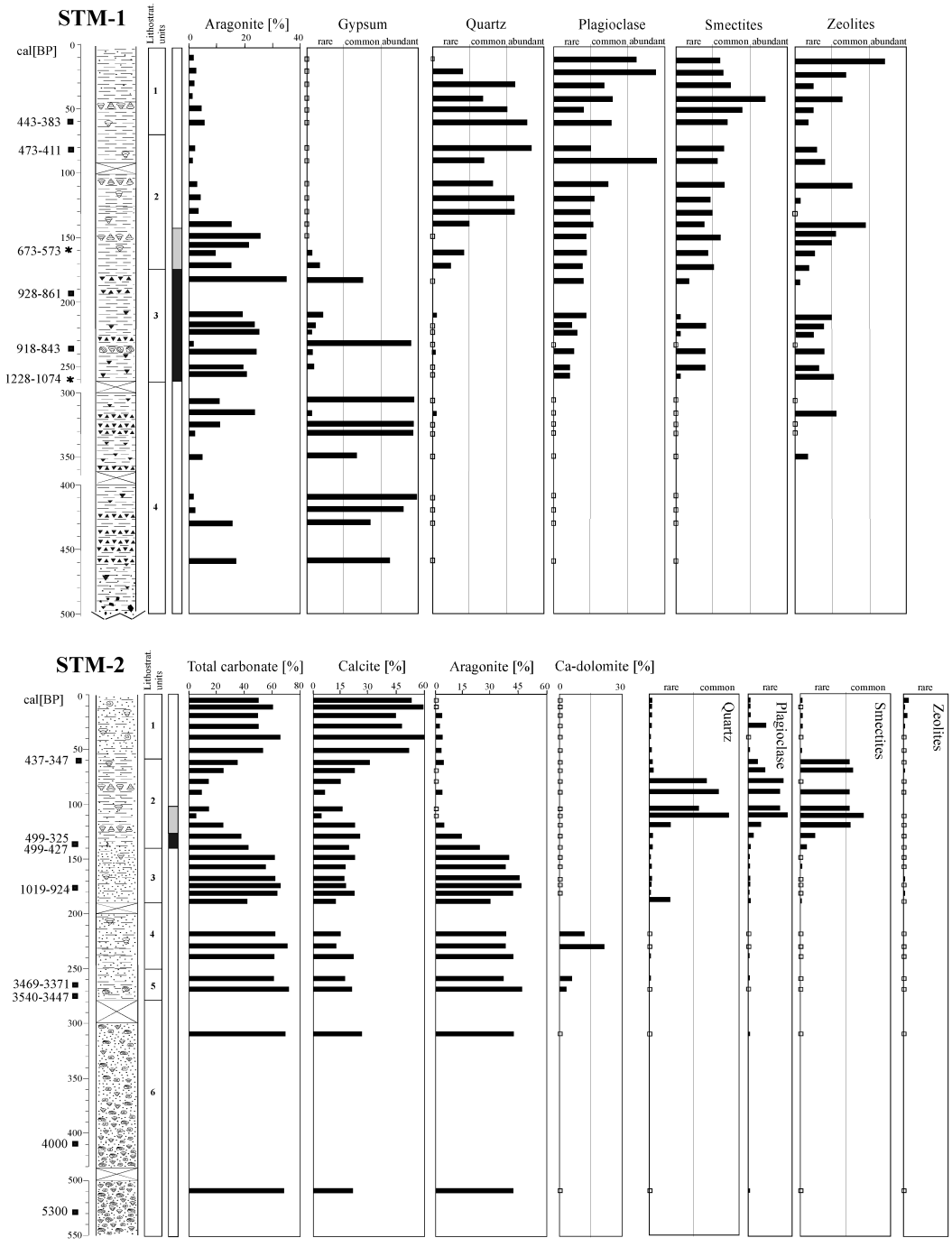

Figure 3 Stratigraphic variation in relative proportions of mineral phases in cores STM-1 and STM-2. Open squares represent absent data.

3 mm/yr. In core STM-1, the lack of suitable material for ^{14}C dating does not allow us to provide a chronology for the lower part of the record. If we assume that the site STM-1 is flooded when the sea level reaches –5 m (the base of the core), then sedimentation rates of the lower 2 m of the core must be low, on average, ~0.3 mm/yr. The detailed chronology of the upper 3 sections of this core yields fairly uniform, high accumulation rates of ~2.4 mm/yr from about 1200–1100 BP. However, two of the ^{14}C dates plot out of sequence, occurring too young to their stratigraphic position (Figure 4; Table 1). Since down-mixing of younger carbon is highly possible in our material due to the coring technique, the dates are considered less reliable age indicators. The base of Unit 3 in both cores is chronologically equivalent, dated to about 1100–1000 BP. ^{14}C ages of charred plant remains from core STM-1, from the interval of abundant charred plants, gives ages of about 1100 and 600 BP and, thus, are evidence of eroded soil and forest clearing by Indians.

Table 1 ^{14}C and carbon isotope data for samples from St. Michiel lagoon. $\delta^{13}C$ [‰]: abundance of ^{13}C relative to ^{12}C with respect to PDB reference. ^{14}C age [BP]: ^{14}C age (Before Present), as calculated from measured abundance (normalized to $\delta^{13}C = –25‰$). Calendar age [cal BP]: intervals (1 σ probability) using the program Calib3 (Stuiver and Reimer 1993) for the atmospheric environment (default), or (indicated by *) for the marine environment with 402 yr of reservoir age. Conversion to cal AD/cal BC according to the relation cal AD = 1950 – cal BP, or cal BC = cal BP – 1950.

Sample	Material	Depth [cm]	$\delta^{13}C$ [‰]	^{14}C age [BP]	Calendar age [cal BP]
Core STM-1					
STM-1/56	gastropods	56	–2.4	759 ± 31	443–383*
STM-1/80	gastropods	80	–4.7	790 ± 36	473–411*
STM1/2/4	gastropods	140	–0.6	686 ± 36	369–286*
SM160	charred plants	160	–14.3	704 ± 32	673–573
STM-1/195	ostrac., gastr.	195	–5.5	1343 ± 58	928–861*
STM1/2	gastropods	210	–2.9	900 ± 80	582–448*
STM-1 3/5	bivalves	235	–1.2	1332 ± 35	918–843*
SM255	charred plants	255	–16.6	1227 ± 39	1228–1074
Core STM-2					
STM-2/85	gastropods	85	–2.9	751 ± 36	437–347*
STM2/2	organic mater.	135	–30	373 ± 38	499–429, 364–325
SE 135	gastropods	135	–5.3	824 ± 49	499–427*
STM-2/2/3	bivalve, ostrac.	175	1.2	1430 ± 50	1019–924*
STM2/3	gastropods	260	–3.2	3549 ± 48	3469–3371*
STM-2/3/5	ostracods	265	–3.3	3601 ± 39	3540–3447*
STM2/5/1	gastropods	410	–0.7	3996 ± 37	4064–3934*
STM2/6/3	bivalve	530	0.9	4990 ± 60	5432–5279*

DISCUSSION

The coastal embayments on Curaçao are old river valleys flooded during the Holocene sea-level rise. The inlets of all bays of the island are narrow. However, that is insufficient to change these bays into hypersaline lagoons, as seen in the fauna of the Spaanse Water Bay (Klosowska et al. 2002), where the restricted range of salinities signifies the oceanic nature of the bay. Those bays that have developed into salinas are characterized by the presence of a natural barrier in front of the inlet con-

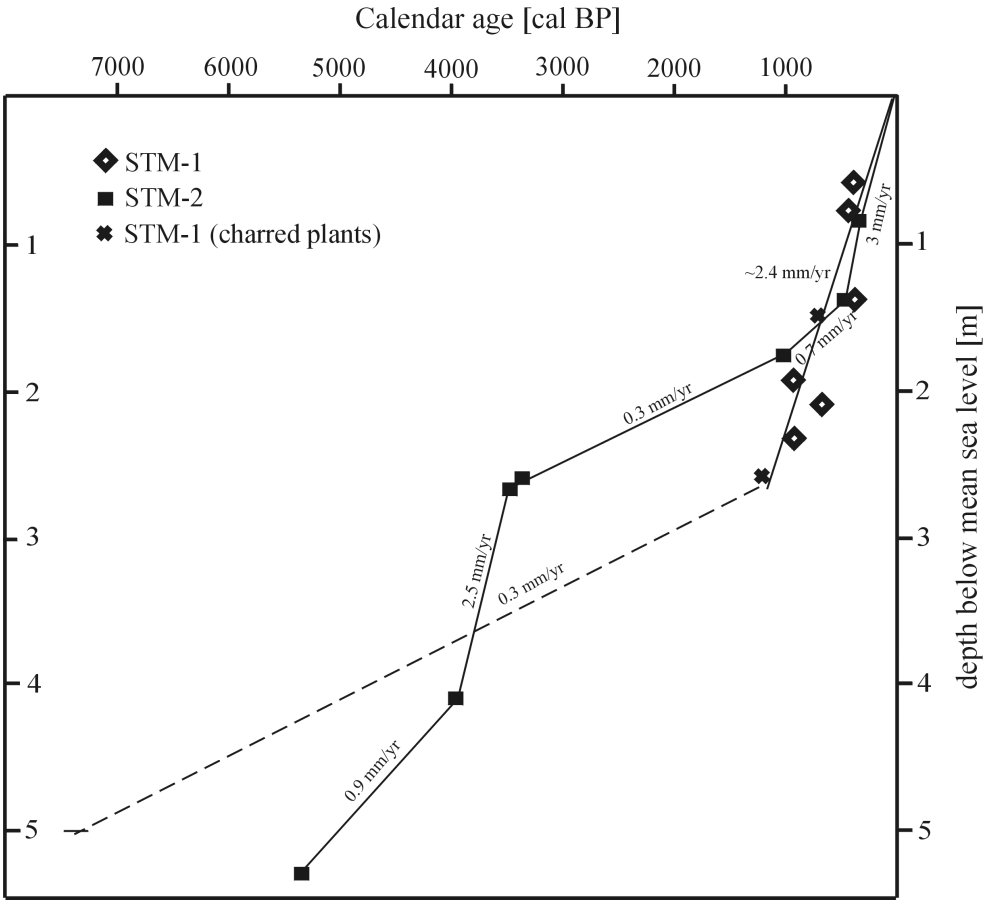

Figure 4 ^{14}C age-depth trend for the 2 cores of the lagoon St. Michiel

sisting of coarse-grained reef debris which severely restricts the connection to the open sea. Evaporites only accumulate in settings where concentrated brines generated by evaporation are not diluted by excessive influx of new solutions, either freshwater or seawater. In a marine setting such as the St. Michiel lagoon, precipitation of evaporites is controlled by evaporation (+outflow) losses exceeding inflow (seawater + rainfall + groundwater).

The STM-1 and STM-2 cores recovered from the St. Michiel lagoon demonstrate the record of a different evolution at different sections of the salina. Core STM-2, situated near the inlet, records the transition from a highly marine to a more restricted, euryhaline environment, whereas core STM-1, situated more inland, shows the reverse. The lower units of core STM-1 were formed in a highly evaporitic environment, changing to a less saline, euryhaline environment, similar to that of STM-2 in the upper units. This difference and the synchronicity of normal marine conditions at STM-2 and hypersaline conditions at STM-1 could be explained by a sill in paleomorphology separating the 2 sites during the earlier history of the bay. Bathymetric data of the St. Michiel salina do not exist, though the morphology of the adjacent areas strongly suggests that the NNW-SSE-running limestone ridge, about 100 m west of STM-2 (Figure 1), could form an efficient barrier/restriction to create a depositional environment suited for evaporite accumulation.

The oldest recovered sediment, the biogenic *Halimeda* sand (Unit 6 of core STM-2) dated to about 5300 BP, was deposited in a coastal, semi-protected bay with a strong marine influence. Similar facies characterize the modern, shallow coastal areas of Spaanse Water Bay (Klosowska et al. 2002). From about 4000 BP onward, accumulation rates notably increased, exceeding the rate of sea-level rise, resulting in shoaling. The sediment grains show abrasion of sharp edges, indicating reworking by waves or currents. At the same time, accumulation of sub-recent coral debris at the seaward margin (Figure 1) formed a natural barrier which increasingly isolated the bay from the open sea influence, and by about 3500–3400 BP, might have even closed the connection. With the closure/isolation, sedimentation changed irreversibly, indicating deposition within a more protected, lower energy setting. Sediment became finer and the initial marine ostracod and foraminiferal assemblage in core STM-2 was replaced by an exclusively euryhaline biofacies (Figure 2). Low faunal diversity and an essentially monospecific foraminiferal assemblage, consisting of *Ammonia tepida*, imply ecological stress. Abundant tellinids and ostracods appear to represent possibly a phase of relatively stronger marine influence (Unit 5 in core STM-2). The distinct reduction of microfauna abundance following this interval suggests that conditions changed and were unfavorable for their survival or preservation, and the lithified carbonate crusts, which were found at some levels, may imply low to non-deposition intervals (Unit 4 of core STM-2).

During the deposition of Unit 6 in core STM-2 and normal marine conditions in this proximal part of the lagoon further inland at site STM-1, evaporites were precipitated (Unit 4 in core STM-1). Precise correlation is difficult due to poor chronology of the evaporite sequence. However, Unit 6 of core STM-2 occurs at the same depth as Unit 4 of core STM-1 and it is highly impossible that when Unit 6 was deposited, Unit 4 was a dry area. As mentioned above, a sill in paleotopography probably separated the 2 sites. Gypsum and aragonite precipitation is induced by increased evaporative concentration of the basin waters. Therefore, abundant evaporite minerals and the presence of laminae composed almost entirely of gypsum in core STM-1 indicate a prolonged period of a negative water balance and are highly suggestive of a very restricted connection to the open sea. The coarse gypsum crystals present in most of the samples imply stable growth in a subaqueous hypersaline environment (Warren 1982; Warren and Kendall 1985). Recorded layering and repeated changes in the relative abundance of aragonite and gypsum in the evaporite sequence result from variations in brine concentrations controlled probably only by climatic factors. Drier, more evaporative phases are recorded by gypsum-rich intervals, while aragonite-rich intervals signify periods with more precipitation. The scarcity of the siliciclastic detritus indicates that surface runoff during the evaporative phase was negligible.

At about 1100–1000 BP in core STM-2, a marked increase in microfauna abundance suggests a change to less extreme and more stable conditions. Similarly, in core STM-1 at the same time, the gradual disappearance of bedded gypsum, frequent occurrence of fecal pellets, and introduction of microfauna define a change to less evaporitic conditions (Figure 2). The presence of some prismatic-lenticular gypsum crystals still indicates stages of salinity increase. Peaks in ostracod and foraminifera abundance in both cores point to less saline intervals due to either fluxes of marine water through a poorly developed barrier and/or increased meteoric input. Episodic freshening of the salina waters associated with periods of increased precipitation and surface runoff may explain the recurrent bands of the gastropod *Pyrgophorus* spp., at times accompanied by angular lithoclasts and the occurrence of characin oogonia (gyrogonites), throughout Units 2 and 1 in both cores.

The lower part of Unit 2 in core STM-2 and the entire Unit 3 in core STM-1 are characterized by a high abundance of charred plant remains (Figure 2) which represent land clearance by forest burning. Practices such as cutting down of trees, charcoal burning, and clearing of land to set up plantations were thought to be most extensive during the Spanish and Dutch colonization of the island

since the beginning of the 16th century (Terpstra 1948; Beers et al. 1997). The dated charred plant material at about 1200 and 600 BP are older than this colonization, and land clearance by burning must have been a common practice of native South American farmers. A small increase in siliciclastic detritus in Unit 3 of STM-1 indicates a higher run-off in comparison to Unit 4 (Figure 3). This is probably also the result of Indian agricultural activities. A higher runoff would explain the change from completely evaporative to partly evaporative sedimentation.

Factors important in the induction of surface erosion of soil are likely due to the changes in drainage basin characteristics. Any disturbance in the drainage basin—as for example, deforestation—changes the fluxes, usually increasing them. Sediments from below Unit 3 in both cores were deposited prior to known permanent human settlements on Curaçao. Reduced rates of supply of clastic material, probably due to stabilization of the slopes, indicate a prolonged period of low-level human activity during which watershed vegetation remained largely intact and soil erosion was minimal. Abundant quartz, plagioclase, and smectites arrive just above the high concentration of charred plants interval (Figure 3), marking enhanced catchment erosion as an effect of land clearance and deforestation. Deforestation practices for agriculture and construction initiated already by Caquetíos Indians and further intensified by the Europeans, especially in the 17th and 18th centuries, destabilized soil cover in the St. Michiel salina's watershed and resulted in remarkably increased runoff of detrital fraction and sediment accumulation rates (Figures 3 and 4).

ACKNOWLEDGEMENTS

We thank Prof Juan Jose Pueyo for help with mineralogical analyses. The research is funded by the Netherlands Institute of Applied Geoscience (TNO-NITG).

REFERENCES

Beers CE, De Freitas J, Ketner P. 1997. Landscape ecological vegetation map of the island of Curaçao, Netherlands Antilles. In: *Natuurwetenschappelijke Studiekring voor het Caraïbisch Gebied* 138:1–54.

Beets DJ. 1972. Lithology and stratigraphy of the Cretaceous and Danian succession of Curaçao. In: *Natuurwetenschappelijke Studiekring voor Suriname en de Nederlandse Antillen* 70:1–153.

De Buisonjé PH. 1974. Neogene and Quaternary geology of Aruba, Curaçao and Bonaire (Netherlands Antilles). In: *Natuurwetenschappelijke Studiekring voor Suriname en de Nederlandse Antillen* 78:1–293.

Deffeyes KS. 1959. Zeolites in sedimentary rocks. *Journal of Sedimentary Petrology* 29:602–9.

Fouke BW. 1994. Deposition, diagenesis and dolomitization of Neogene Seroe Domi Formation coral reef limestones on Curaçao, Netherlands Antilles. *Foundation for Scientific Research in the Caribbean Region* 134:1–182.

Klaver GTh. 1987. The Curaçao Lava Formation, an ofiolitic analogue of the anomalous thick layers 2B of the Mid-Cretaceous oceanic plateau in the western Pacific and central Caribbean. In: *Natuurwetenschappelijke Studiekring voor Suriname and de Nederlandse Antillen* 119:1–163.

Klosowska BB, van Hinte JE, Troelstra SR, Laban C. 2002. Microfacies of Spaanse Water Bay, Curaçao (Netherlands Antilles), with special reference to benthic foraminifera. *Journal of Coastal Research* 18: 316–28.

Martis A, Van Olderborgh GJ, Burgers G. 2002. Predicting rainfall in the Dutch Caribbean—more than El Niño? *International Journal of Climatology* 22:1219–34.

Mariner RH, Surdam RC. 1970. Alkalinity and formation of zeolites in saline alkaline lakes. *Science* 170:977–80.

Meteorological Service of the Netherlands Antilles and Aruba. http://www.meteo.an.

Stuiver M, Reimer PJ. 1993. Extended ^{14}C database and revised Calib 3.0 ^{14}C age calibration program. *Radiocarbon* 35(1):215–30.

Terpstra H. 1948. De boomgroei op de benedenwindse eilanden in vroeger tijd. *Mededelingen van Koninglijke Vereniging van Indisch Instituut* 78:3–19.

Versteeg AH, Rostain S, editors. 1997. The archaeology of Aruba: the Tanki Flip site. Publication of the Archaeological Museum of Aruba 8. *Publication of the Foundation for Scientific Research of the Caribbean Region* 141:1–519.

Warren JK. 1982. The hydrological setting, occurrence and significance of gypsum in late Quaternary salt lakes in South Australia. *Sedimentology* 29:609–37.

Warren JK, Kendall CGStC. 1985. Comparison of sequences formed in marine sabkha (subaerial) and salina (subaqueous) settings—modern and ancient. *American Association of Petroleum Geologists Bulletin* 69:1013–23.

RADIOCARBON, Vol 46, Nr 2, 2004, p 775–784

ON THE EROSIVE TRAIL OF A 14TH AND 15TH CENTURY HURRICANE IN CONNECTICUT (USA) SALT MARSHES

O van de Plassche[1,2] • A J Wright[1] • K van der Borg[3] • A F M de Jong[3]

ABSTRACT. This paper examines if an erosive hiatus found in the peat stratigraphy and marsh-accumulation record from northwest Hammock River Marsh (HRM), Connecticut (CT) can be attributed to a 14th or a 15th century hurricane, each documented by a radiocarbon-dated overwash fan in Succotash Marsh (SM) (Rhode Island) about 90 km to the east. Given that (i) the best estimate age range for the 15th century overwash deposit in SM (1400–1440 cal AD, 2 σ) overlaps entirely with that for first plant growth after erosion at HRM (1390–1450 cal AD, 2 σ), while the best estimate age range for the 14th century overwash deposit (1290–1410 cal AD, 2 σ) overlaps just 10 yr, and (ii) interpretation of the available stratigraphic and sedimentary evidence from HRM suggests that a high-energy event offers the simplest explanation for the observed marsh erosion, we conclude that a plausible link exists between the 15th century hurricane and the marsh erosion in HRM. The best estimate age range for the 14th century hurricane appears to overlap for 91% with the age range for the first plant growth (1290–1400 cal AD, 2 σ) following marsh erosion in East River Marsh (CT), located about 12 km west of HRM. These results imply that erosive boundaries in salt-marsh peat deposits have potential as markers of past hurricane activity.

INTRODUCTION

Salt-marsh deposits along the eastern coast and Gulf Coast of the United States are well known to contain sedimentary records of hurricanes, both as washover deposits behind barriers capped by low dunes, and as thin (mm to cm) beds of sand, silt and/or clay along open coast marshes (e.g. Warren and Niering 1993; Nyman et al. 1995; Donnelly et al. 2001a). In contrast, the literature makes no mention of hurricane-related erosion surfaces preserved in the stratigraphy of salt-marsh deposits. In this paper, we present evidence for salt-marsh erosion and assess if it can be attributed to hurricane activity.

Our study site is located in the northwestern part of Hammock River Marsh (HRM), Connecticut, USA (Figure 1), for which van de Plassche et al. (1998) published a marsh-accumulation record spanning the past 1400 yr. This record is based on paleomarsh-surface estimates obtained by radiocarbon dating preserved sub-surface parts of marsh grasses (e.g. rhizomes, root bulbs, and sub-surface stems) with a known vertical relationship to the marsh surface (i.e. paleomarsh-surface indicators). It shows 2 short (<100 yr) periods of very high (4–8 $mm.yr^{-1}$) rates of marsh accumulation during the past 600 yr, the first beginning around 1425 cal AD (Figure 2) and the second shortly after 1650 cal AD (not shown). On the basis of limited core stratigraphic data, it was claimed that each period of rapid marsh accumulation was preceded by erosion. The possibility that this erosion was hurricane-related is suggested by the fact that the onset of the first period of rapid marsh accumulation (around 1425 cal AD) coincides with a geologically documented hurricane which affected Succotash Marsh (SM), Rhode Island (1411–1446 cal AD) (Donnelly et al. 2001a,b) (Figure 2). Furthermore, the approximate onset of the second period of rapid marsh accumulation (shortly after 1650 cal AD) follows closely on the historically documented hurricanes of AD 1635 and AD 1638, both of which made landfall in southern New England (Boose et al. 2001).

SALT-MARSH SUB-ENVIRONMENTS

New England salt marshes show a tripartite vegetation zonation, generally referred to as the low, high, and upper marsh zones (e.g. Niering and Warren 1980; Bertness 1991). The low marsh zone is

[1]Faculty of Earth and Life Sciences, Vrije Universiteit, De Boelelaan 1085, 1081 HV Amsterdam, the Netherlands.
[2]Corresponding author. Email: orson.van.de.plassche@falw.vu.nl.
[3]R J van der Graaff Laboratory, Universiteit Utrecht, P.O. Box 80.000, 3508 TA, the Netherlands.

Proceedings of the 18th International Radiocarbon Conference, edited by N Beavan Athfield and R J Sparks
RADIOCARBON, Vol 46, Nr 2, 2004, p 775–784

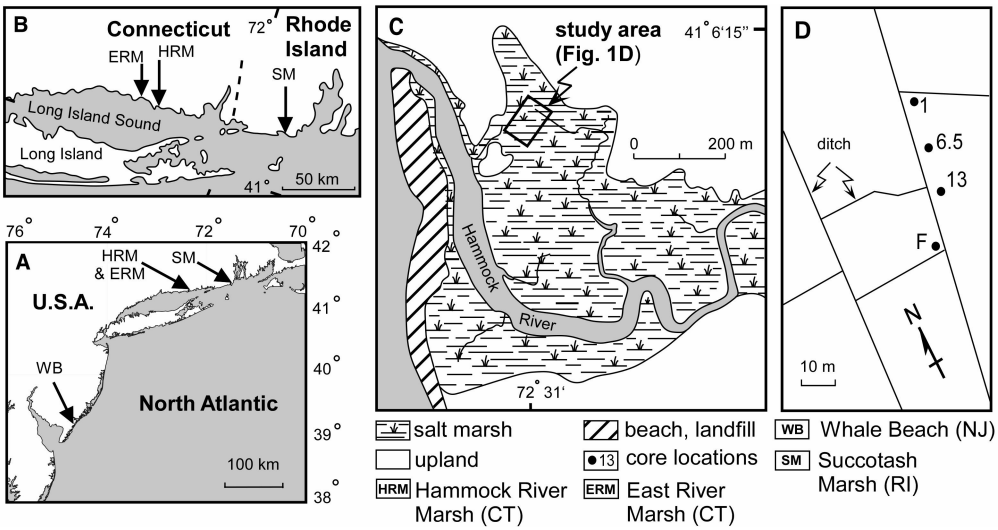

Figure 1 Location of study areas and coring sites mentioned in the text

characterized by pure stands of the tall form of *Spartina alterniflora* (smooth cordgrass). This plant is the first to colonize tidal flats which have reached an elevation between mean sea level and mean high water of neap tides. Low marsh accumulation rates can be quite high owing to the combination of high flooding frequency and sediment trapping by the vegetation. Once the low marsh has accumulated to around mean high water level, grasses such as *Spartina patens* (saltmeadow cordgrass), *Distichlis spicata* (salt or spike grass), and the stunted form of *S. alterniflora* appear to form the high marsh zone. The upper marsh zone, reached only by the highest spring tides, is characterized by, for example, *Scirpus* (sedge) species, *Phragmites australis* (reed), and *Thypha* (cattail) species. Depending on the influx of freshwater into the marsh, upper marsh plants can reach (much) lower into the tidal frame.

WASHOVER DEPOSITS

Donnelly et al. (2001a) discovered 6 overwash fans preserved in the stratigraphy of SM. They used (unspecified) plant fragments sieved from 0.5–1 cm^3 of peat collected from the base of the sand layers (i.e. the very top of the underlying salt-marsh peat) for ^{14}C dating using accelerator mass spectrometry (AMS). Of these 6 fans, only the deepest/oldest two are of relevance here (fans VI and V). Two samples were obtained for the base of fan VI (the deepest) and 6 samples for the base of fan V, all from different cores. The ^{14}C ages were calibrated using the Calib 4.1 program (intercept method) of Stuiver et al. (1998). On the basis of mutual overlap of the calibrated (2 σ) age ranges, Donnelly et al. (2001a) concluded that fan V was deposited between 1411 and 1446 cal AD (or between 1411 and 1433 cal AD if the oldest of the 6 dates is excluded), and that the best estimate age range for the deposition of fan VI is 1295–1407 cal AD. At Whale Beach (WB), New Jersey, Donnelly et al. (2001b) bracketed the age of the only prehistoric overwash fan by AMS dating fragments of *S. alterniflora* collected from the topmost cm of the mud underlying the sand layer and from about 50 cm above the overwash deposit. The 2-σ calibrated age ranges (Calib 4.1, probabilities method) indicate that this fan was deposited after 1278 cal AD and before 1434 cal AD. This age range implies the possibility that the hurricane which deposited this sand layer, and which is inferred to have been very intense, was the same which produced fan VI at SM. However, it is not clear if the peat at the base of the sand layer at WB was eroded, and a meaningful analysis of synchroneity must await additional stratigraphic and ^{14}C data from the study area at WB.

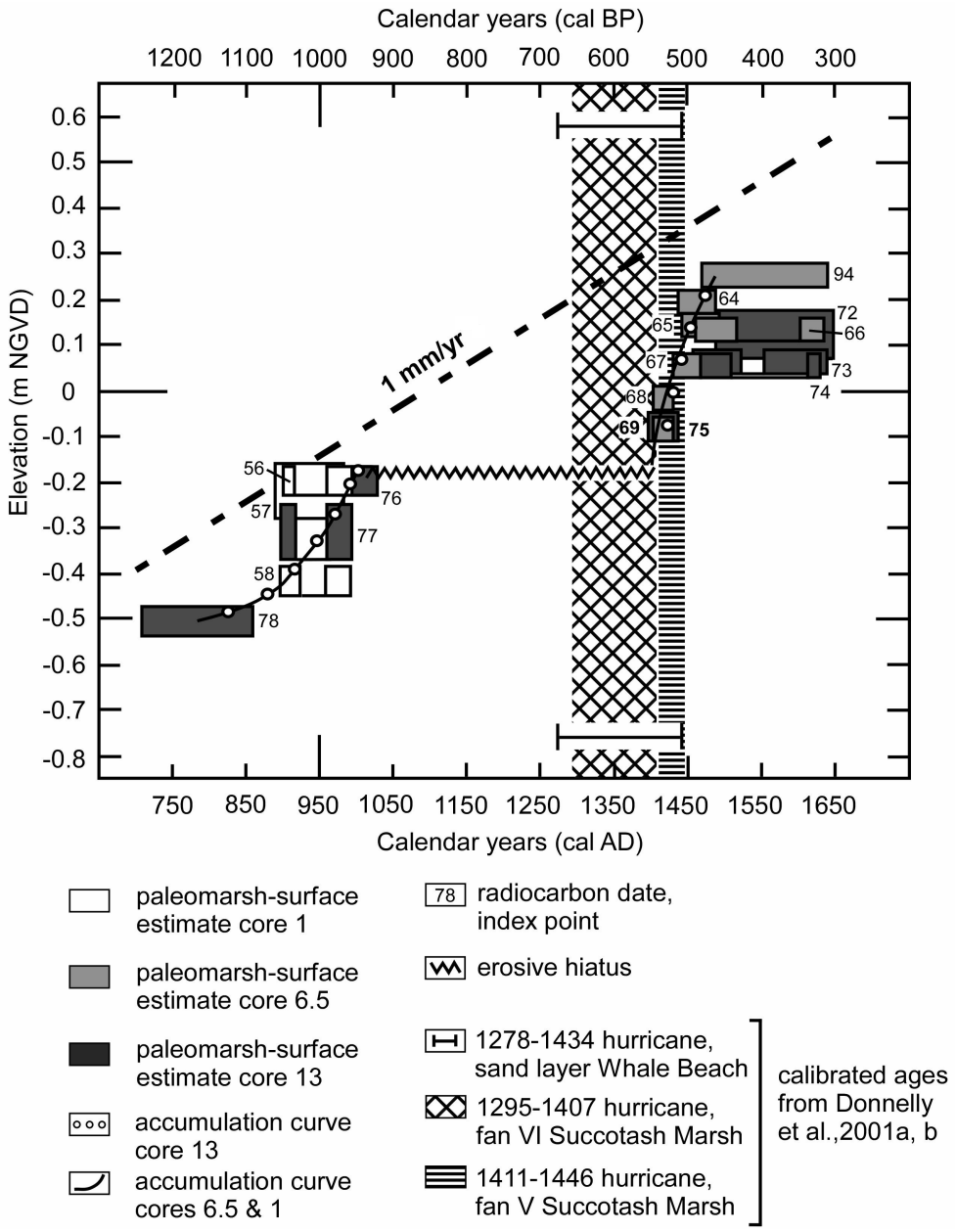

Figure 2 Comparison in time of an erosion-punctuated marsh-accumulation record from the study site at Hammock River Marsh, Connecticut (van de Plassche et al. 1998) with the occurrence of 2 geologically documented hurricanes in Succotash Marsh, Rhode Island, and one at Whale Beach, New Jersey (Donnelly et al. 2001a,b), indicating the possibility that a hurricane was responsible for the marsh erosion at Hammock River Marsh. The error boxes define the calibrated age and estimated elevation ranges of paleomarsh surfaces obtained by ^{14}C dating of paleomarsh-surface indicators (see text) collected from cores 1, 6.5, and 13 (for core locations and in-core position of dated samples, see Figures 1d and 3).

APPROACH AND METHODS

Our approach is to first establish if a link between marsh erosion in HRM and hurricane activity recorded in SM is possible by determining visually the overlap of the best estimate in time (i.e. mutual overlap of calibrated age ranges) for hurricane activity in southern New England and New Jersey, as documented by Donnelly et al. (2001a,b), with that for the onset of first marsh growth following erosion in HRM. Given the result that such a link is possible, we then test its probability by (i) considering (theoretical) alternative explanations for marsh erosion; (ii) assessing available stratigraphical and sedimentological data from HRM in terms of time elapsed between the end of marsh erosion and the onset of recolonization by marsh plants; and (iii) presenting other data from Connecticut suggestive of a link between hurricane activity and marsh erosion.

Because of the very limited stratigraphic database available to van de Plassche et al. (1998) (Figure 3a), we revisited the study area at HRM to verify the presence or absence of erosive hiatuses. Using a 7.5-cm-wide core auger, we reinspected the lithostratigraphy near and between cores 1, 6.5, and 13. The cores were split lengthwise and logged for color, sediment content, and plant macroremains. For the sake of comparability in time of overwash fan formation at WB and SM and of first post-erosion salt-marsh plant growth at HRM, we recalibrated the ^{14}C dates from these study sites using the INTCAL98 data set (Stuiver et al. 1998) and the OxCal program (probabilities method; Bronk Ramsey 1995).

RESULTS

Stratigraphy

In HRM, van de Plassche et al. (1998) found convincing evidence for erosion at a depth of about –0.20 m NGVD (National Geodetic Vertical Datum of 1929) in cores F and 13, and they interpreted the clear lower boundary of a thin bed of rooted clay in core 6.5 to be erosive as well (Figures 3a and 1d). The new stratigraphic information shows conclusively that the erosive boundary present at a depth of about –0.20 m in cores F and 13 can be extended to several meters north of core 6.5 (Figure 3b). The accommodation space created by the erosion was filled in first by a thin (5–10 cm) bed of clayey silt to silty clay and, subsequently, by silty/clayey *S. alterniflora* peat (cores F and 13) and silty/clayey *Sc. robustus* peat with some *D. spicata* (core 6.5). The onset of post-erosion plant growth is approximated by the ages of index points 69 (core 6.5), 75 (core 13), and 83 (core F) (Figures 3b and 2; to avoid clogging, index point 83 is not shown in Figure 2, but it overlaps largely with index point 75). Previously, van de Plassche et al. (1998) overlooked the erosive boundary at the base of the body of sediment-rich *Sc. robustus* peat in core 6.5 because the basal sediment layer is crowded with sub-surface stems, root bulbs, and rhizomes of *Sc. robustus* which first colonized it, and particularly because the sediment had been colored dark brown by humic substances lending the basal deposit the misleading appearance of a muddy *Sc. robustus* peat conformably overlying high marsh peat.

The erosive nature of the base of the thin-rooted clay bed encountered in core 6.5 (at about +0.24 m) could not be confirmed. On the basis of the new stratigraphic data from the vicinity of core 6.5, we now consider the sub-surface stem of *Sc. robustus* which gave index point 63 as belonging to the very top of the bed of *Sc. robustus* peat. It appears that the thin clay layer previously observed in core 6.5 was deposited on the marsh surface without prior erosion.

In conclusion, the studied salt-marsh sequence at HRM contains only 1 unequivocal erosive boundary (Figure 3b).

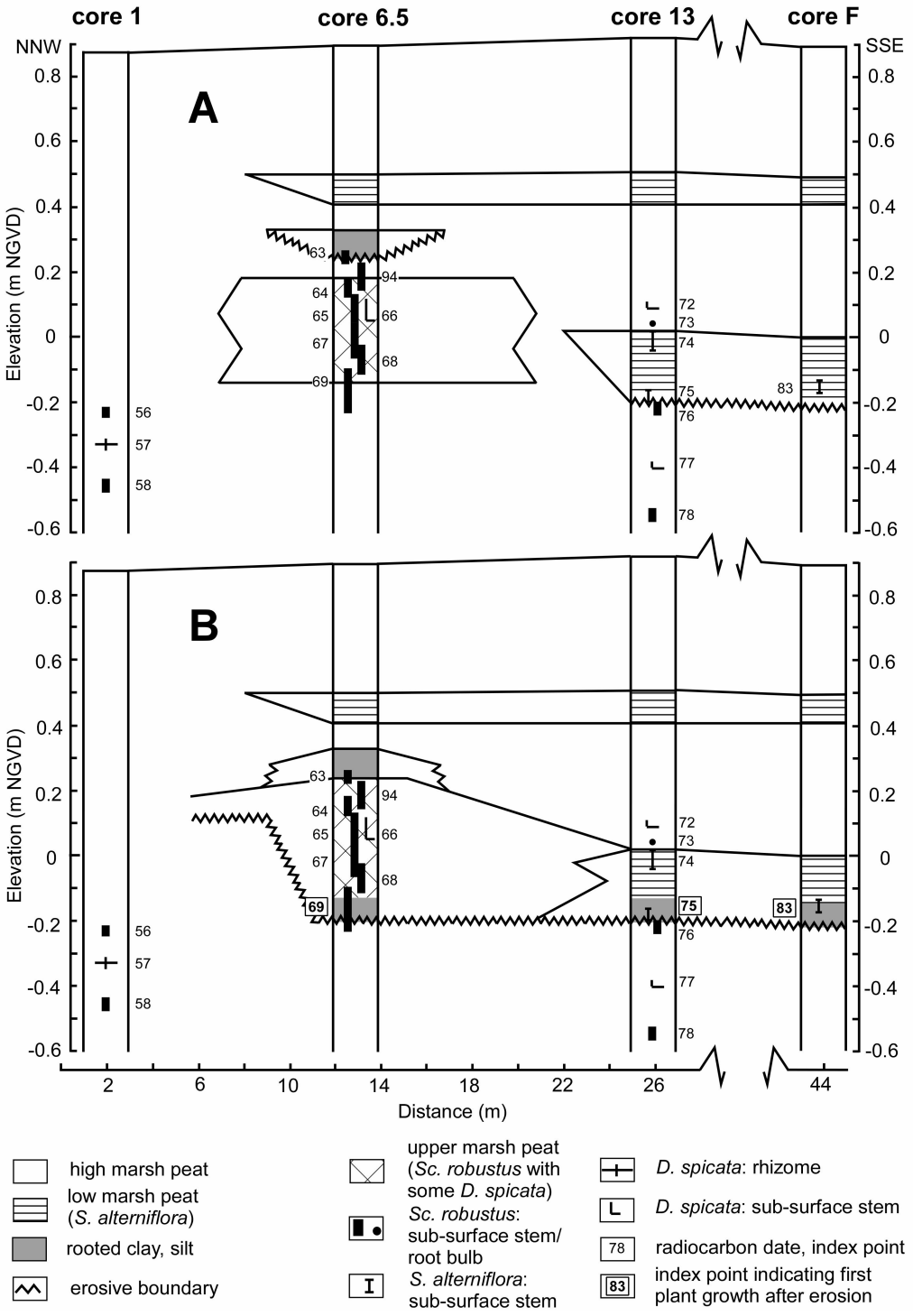

Figure 3 Simplified lithofacies distribution and original depth of (^{14}C-dated) samples in cores from the study site (A: previous [van de Plassche et al. 1998]; B: revised) showing that about 30 cm of high marsh peat was eroded over a distance of at least 34 m and replaced by sediment and silty/clayey low/upper marsh peat.

Age Calibration

The recalibrated ages of the ^{14}C dates used in this paper are listed in Table 1. Donnelly et al. (2001a), using the intercept method for calibration, arrived at a best estimate (i.e. mutual overlap of calibrated age ranges at 2 σ) for the time of deposition of fans VI and V at SM of 1295–1407 cal AD and 1411–1446 cal AD, respectively. The probabilities method yields almost the same best estimates (Figure 4). Minor differences exist also between our calibration result and that of Donnelly et al. (2001b) for the age (pre-)dating the overwash fan at WB (index point 11, Table 1).

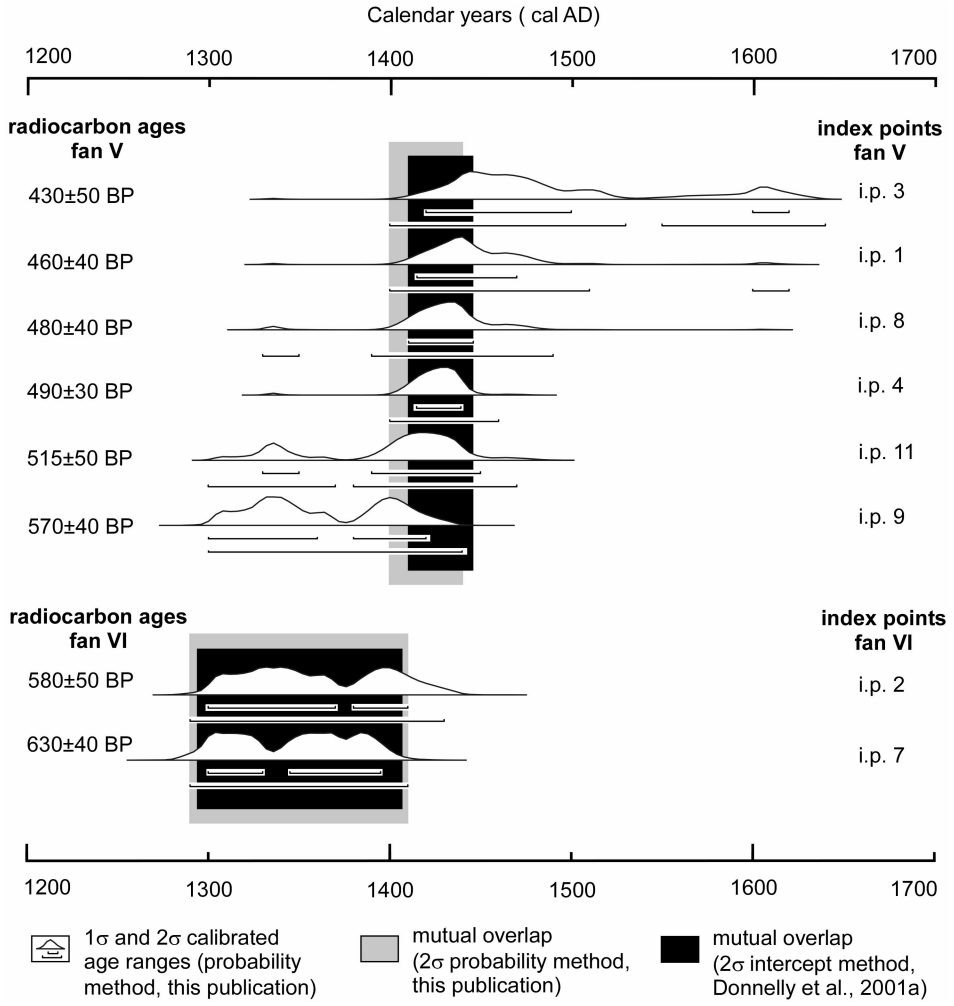

Figure 4 Comparison of best age estimates, based on mutual overlap of 1-σ and of 2-σ calibrated age ranges, for the deposition of overwash fans VI and V at Succotash Marsh, Rhode Island, as obtained with the intercept and the probabilities method of calibration.

Table 1 Age data used in Figures 4 and 5. Numbers in **bold** indicate mutual overlap of calibrated age ranges (see Figures 4 and 5) (HRM: Hammock River Marsh; ERM: East River Marsh; CT: Connecticut; SM: Succotash Marsh; RI: Rhode Island; WB: Whale Beach; NJ: New Jersey).

					Calibrated age ranges (AD), this paper		Calibrated age ranges (AD), Donnelly et al. (2001a)	Calibrated age ranges (AD), this publication	
Study area and sample information	Core nr	Index point	Lab nr	^{14}C age	± 1 σ	± 2 σ	± 2 σ	± 1 σ	± 2 σ
First plant growth after erosion at HRM (CT), van de Plassche et al. (1998)	F	83	UtC-2002	500 ± 30	1413–1436	1330–1340, 1390–1450			
	6.5	69	UtC-2176	520 ± 30	1404–1433	1320–1350, 1390–1450		**1413–1433**	**1390–1450**
	13	75	UtC-2180	520 ± 50	1320–1350, 1390–1450	1300–1370, 1380–1460			
Deposition of overwash fan **V** in SM (RI), Donnelly et al. (2001a)	Succ3	3	Beta-115172	430 ± 50	1420–1500, 1600–1620	1400–1530, 1550–1640			
	Succ2	1	Beta-115171	460 ± 40	1415–1470	1400–1510, 1600–1620			
	Succ1	8	Beta-115174	480 ± 40	1410–1446	1330–1350, 1390–1490			
	Succ4	4	Beta-135397	490 ± 30	1415–1439	1400–1460	**1411–1446**	**1420**	**1400–1440**
	Succ14	11	OS-23293	515 ± 50	1330–1350, 1390–1450	1300–1370, 1380–1470			
	Succ12	9	Beta-115176	570 ± 40	1300–1360, 1380–1420	1300–1440			
First plant growth following erosion at ERM (CT), van de Plassche et al. (2001)	GKR	8	UtC-6820	624 ± 24	1300–1330, 1345–1370, 1380–1395	1290–1400		1300–1330 1345–1370 1380–1395	1290–1400
Deposition of overwash fan **VI** in SM (RI), Donnelly et al. (2001a)	Succ3	2	Beta-103313	580 ± 50	1300–1370, 1380–1410	1290–1430			
	Succ9	7	Beta-115173	630 ± 40	1300–1330, 1345–1395	1290–1410	**1295–1407**	**1300–1330** **1380–1395**	**1290–1410**
(Pre-)dates overwash fan at WB (NJ), Donnelly et al. (2001b)	WB3	11	OS-26451	680 ± 30	1280–1310, 1360–1390	1270–1330, 1340–1400	1278–1319 1353–1389	1280–1310 1360–1390	1270–1330 1340–1400

Hurricane Deposition and Marsh Erosion in Time

Comparison of the best estimate age range for the deposition of fan V at SM with that for first plant growth after erosion at HRM shows that the former falls entirely within the latter (Figure 5; Table 1), indicating a high probability that both events occurred close in time. In contrast, the best age estimates for fan VI and the fan at WB overlap just 12% and 6%, respectively, with the best estimate for the onset of marsh growth after erosion at HRM (Figure 5, Table 1). If a hurricane was responsible for this erosion, it was, therefore, most likely the one that deposited fan V at SM.

DISCUSSION AND CONCLUSIONS

The complete overlap of the best age estimates for the onset of marsh recovery following erosion in HRM with that for the deposition of overwash fan V about 90 km to the east renders it possible that the 2 events are causally related. For the status of this linkage to be upgraded from possible to probable, it is necessary to show or argue that (i) the erosion was, most likely, caused or triggered by high-energy waves and currents, and (ii) little time elapsed between the end of marsh erosion and the recolonization of the site by marsh plants.

With respect to the first point, high-energy wave and current action can result from a hurricane or a tsunami triggered by a seismotectonic event. While minor earthquakes are common in southern New England, relative sea-level data from Connecticut demonstrate conclusively that no seismotectonic crustal movements have occurred during at least the past 3300 yr (van de Plassche et al. 2002). Moreover, Long Island shields the coast of Connecticut from tsunami waves that may have originated off the Atlantic seaboard. Still, one or more of the following 3 other mechanisms, not involving hurricane conditions, may have caused the shallow erosion: (a) mechanical and/or biochemical salt-pan and pond-hole formation, (b) headward erosion of a shallow tidal creek, and (c) lateral expansion of mudflat by marsh-cliff retreat. The absence of organic-rich mud, characteristic of pond-hole deposits, indicates that pond-hole formation is, by itself, not an option to explain the marsh erosion. The presence of shallow pond holes would have enhanced, however, the effectiveness of storm-wave and/or tidal erosion and little or no pond-hole deposit would have been preserved. As for headward erosion of a shallow tidal creek, this process reflects a gradual expansion of the drainage network in response to an increase in tidal prism or an increase in the rate of sea-level rise relative to the rate of marsh accumulation. It is difficult to explain why such a steady dynamic process would end abruptly and give way to rapid infilling of the shallow creek channel with sediment and low/upper marsh peat. Finally, marsh-cliff retreat caused by gradual undercutting would account for the sub-horizontal nature of the erosive boundary, but does not explain why the eroded surface, given its level of just 10–20 cm below local mean high water (Varekamp et al. 1992), was suddenly and simultaneously colonized by *Sc. robustus* (which requires brackish conditions) and *S. alterniflora*. We conclude that hurricane activity, by itself or in combination with pond holes, offers the simplest explanation for the marsh erosion and the subsequent synchronous recolonization by *Sc. robustus* (implying sufficient influx of fresh seepage water) and *S. alterniflora* of the thin layer of sediment deposited on the erosion surface. Mapping of the extent and configuration of the erosive surface over a significant area is likely to yield clues supporting or invalidating this interpretation.

With respect to the second point (rapid establishment of marsh plants following erosion), we infer from the freshness of the peat immediately below the erosive boundary and the absence of crab holes or molluscs in this peat that the erosion surface was not exposed for any length of time. These observations, combined with the fact that (a) the erosion lowered the marsh surface just about 30 cm, i.e., just into the low marsh zone, (b) first plant growth in cores 6.5, 13, and 11 occurred simultaneously, and (c) the rate of subsequent marsh accumulation was very high, lead us to infer that little time elapsed between the erosion and first plant growth.

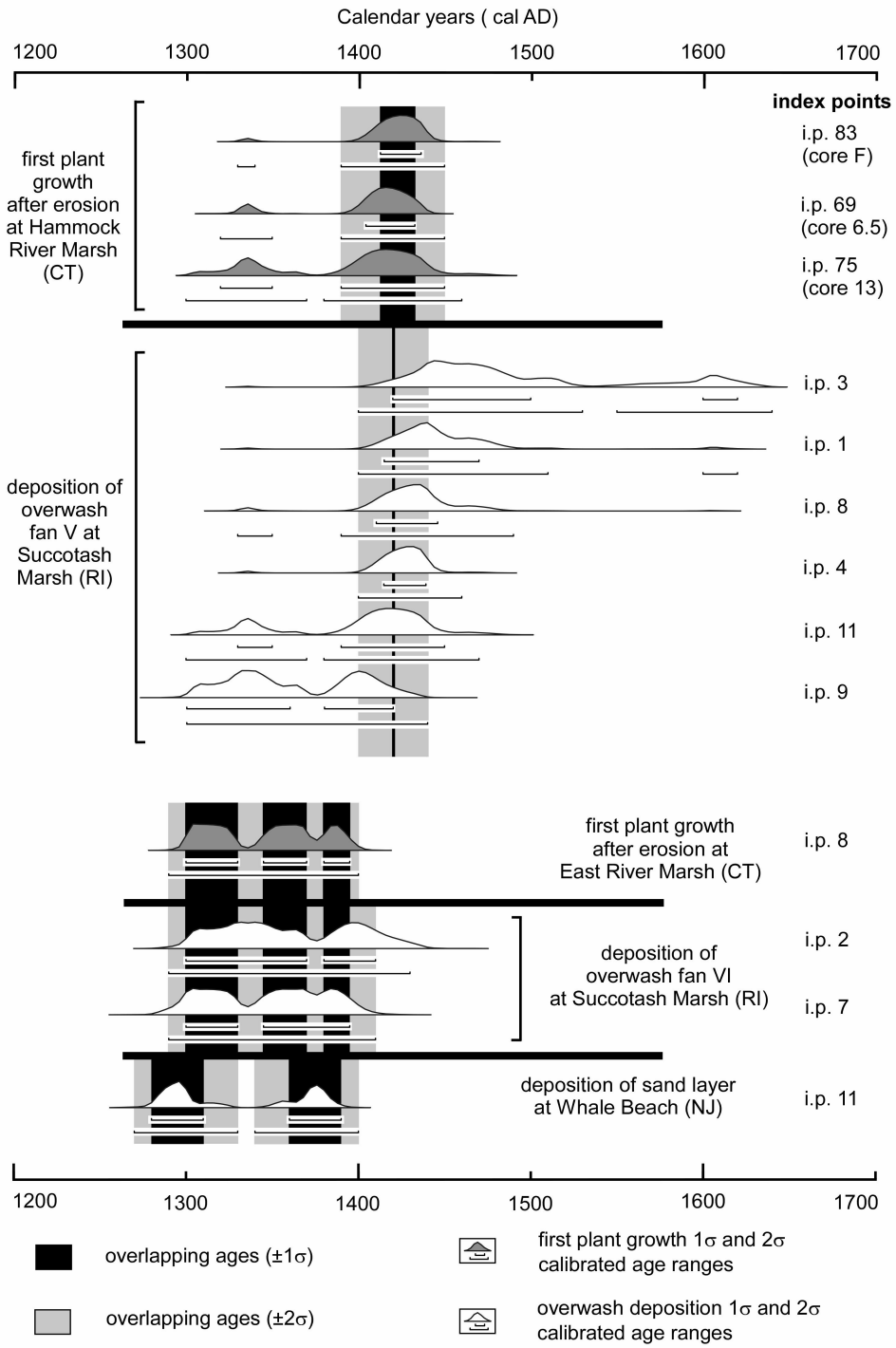

Figure 5 Comparison of best age estimates, based on visual mutual overlap of 1-σ and of 2-σ calibrated age ranges, for deposition of overwash fans VI and V at Succotash Marsh and the overwash fan at Whale Beach with those for first plant growth following marsh erosion in East River Marsh and Hammock River Marsh. (CT: Connecticut; RI: Rhode Island; NJ: New Jersey).

From this evaluation, we conclude that it is plausible that the erosion at HRM is causally linked to the 15th century hurricane which deposited washover fan V at SM. Support for the concept of erosive boundaries in late Holocene salt-marsh deposits serving as paleotempest markers is found in stratigraphic and ^{14}C data from East River Marsh, located about 12 km west of HRM (Figure 1B) (Figure 4 in van de Plassche et al. 2001). Here, the calibrated ^{14}C age (1290–1400 cal AD; Table 1) for first plant growth following shallow marsh erosion to a depth of 0.98 m below the marsh surface overlaps for 91% with the best age estimate for deposition of overwash fan VI at SM. (Figure 5). In the same core from East River Marsh, the wiggle-matched age (1680 cal AD; van de Plassche et al. 2001) for first plant growth after shallow marsh-surface erosion to a depth of about 0.75 m below the marsh surface implies the possibility that the erosion was linked to the historically documented category 2 hurricane of AD 1675 (Boose et al. 2001).

In conclusion, the pre-historical record of hurricane strikes on the southern New England coast is currently based on sedimentary evidence (overwash deposits) only. The data and analysis presented here show that erosive boundaries in salt-marsh deposits deserve attention as potential paleotempest indicators. However, diagnostic criteria to distinguish storm erosion from non-storm erosion need to be defined if this marker is to be used to its full potential. In the absence of such criteria, synchronous first plant growth following erosion in several marshes located many kilometers apart will strengthen the case for hurricane-related erosion.

ACKNOWLEDGEMENTS

We thank Jaap Erkelens and Kim van der Leeuw for field assistance and an anonymous reviewer for thoughtful comments.

REFERENCES

Bertness MD. 1991. Zonation of *Spartina patens* and *Spartina alterniflora* in a New England salt marsh. *Ecology* 72:138–48.

Boose ER, Chamberlin KE, Foster DR. 2001. Landscape and regional impacts of hurricanes in New England. *Ecological Monographs* 71(1):27–48.

Bronk Ramsey C. 1995. Radiocarbon calibration and analysis of stratigraphy: the OxCal program. *Radiocarbon* 37(2):425–30.

Donnelly JP, Bryant SM, Butler J, Dowling J, Fan L, Hausmann N, Newby P, Shuman B, Stern J, Westover K, Webb III T. 2001a. 700 yr sedimentary record of intense hurricane landfalls in southern New England. *Geological Society of America Bulletin* 113(6):714–27.

Donnelly JP, Roll S, Wengren M, Butler J, Lederer R, Webb III T. 2001b. Sedimentary evidence of intense hurricane strikes from New Jersey. *Geology* 29(7): 615–8.

Niering WA, Warren RS. 1980. Vegetation patterns and processes in New England salt marshes. *Bioscience* 30:301–7.

Nyman JA, Crozier CR, Delaune RD. 1995. Roles and patterns of hurricane sedimentation in an estuarine marsh landscape. *Estuarine Coastal and Shelf Science* 40:665–79.

Stuiver M, Reimer PJ, Bard E, Beck JW, Burr GS, Hughen KA, Kromer B, McCormac FG, van der Plicht J, Spurk M. 1998. INTCAL98 radiocarbon age calibration: 24,000–0 BP. *Radiocarbon* 40(3):1041–83.

van de Plassche O, van der Borg K, de Jong AFM. 1998. Sea level-climate correlation during the past 1400 yr. *Geology* 26:319–22.

van de Plassche O, van der Borg K, de Jong AFM. 2002. Relative sea-level rise across the Eastern Border fault (Branford, Connecticut): evidence against seismotectonic movements. *Marine Geology* 184:61–8.

van de Plassche O, Edwards RJ, van der Borg K, de Jong AFM. 2001. ^{14}C wiggle-match dating in high-resolution sea-level research. *Radiocarbon* 43(2A):391–402.

Varekamp JC, Thomas E, van de Plassche O. 1992. Relative sea-level rise and climate change over the last 1500 years (Clinton, CT, USA). *Terra Nova* 4: 293–304.

Warren RS, Niering WA 1993. Vegetation change on a northeast tidal marsh: interaction of sea-level rise and marsh accretion. *Ecology* 74:96–103.

RADIOCARBON, Vol 46, Nr 2, 2004, p 785–795

NEAR-ZERO $\Delta^{14}C$ VALUES AT 32 KYR CAL BP OBSERVED IN THE HIGH-RESOLUTION ^{14}C RECORD FROM U-Th DATED SEDIMENT OF LAKE LISAN

K van der Borg[1,2] • M Stein[3] • A F M de Jong[1] • N Waldmann[4] • S L Goldstein[5]

ABSTRACT. A high-resolution atmospheric radiocarbon record has been obtained for the interval of 17–36 kyr from U/Th-dated aragonite sediment of Lake Lisan. Reservoir age corrections were applied with reservoir ages of 200, 1250, and 2000 yr, which correlate with the different water levels of the lake. The present ^{14}C record for Lake Lisan shows near resemblance with that of Lake Suigetsu: both converge to the value of $\Delta^{14}C$ ~0‰ at 32 kyr cal BP. Both also show significant differences compared to other reported high-resolution ^{14}C records (e.g. Iceland Sea, Cariaco basin, and Bahamas speleothem). This inconsistency should be addressed by re-assessment of the basic assumptions behind the determination of calendar ages of the various records.

INTRODUCTION

The ratio of ^{14}C to ^{12}C in atmospheric carbon dioxide, which is the basis of radiocarbon dating, is not constant but varies due to changes in the ^{14}C production as well as changes in the carbon cycle. Thus, ^{14}C dating requires a calibration curve for transforming ^{14}C ages to calendar years. Many laboratories contributed to the present calibration curve INTCAL98 (Stuiver et al. 1998), which is a detailed record of ^{14}C age versus calendar age for the interval of 0 to 24 kyr cal BP. The interval between 0 to 11.9 kyr cal BP has been established from ^{14}C ages of tree rings identified from dendrochronology, while the portion from 11.9 to 24 kyr cal BP relies mainly on corals and marine sediments. However, while the tree-ring archive yields a direct relation between the ^{14}C age (recorded as the atmospheric ratio of ^{14}C to ^{12}C) versus identified calendar age, other archives are hampered either by problems with reservoir age determination or by incorrect calendar age identification (e.g. sedimentary hiatuses, problems in precise U-Th dating).

Coral samples have been used to derive calendar ages from 7–41 kyr cal BP by combining U/Th dating and accelerator mass spectrometry (AMS) ^{14}C ages (Bard et al. 1998). The atmospheric $^{14}C/^{12}C$ ratio has been deduced from the corals, assuming a constant marine reservoir age of 400 yr. However, the coral data in combination with floating chronologies yield a detailed calibration curve between 11.9 and 16 kyr cal BP, but for the older ages, the coral data are scarce, and for the interval of 16–24 kyr cal BP, INTCAL98 uses a spline function through the coral data points.

Other detailed ^{14}C records with ages >24 kyr cal BP have been reported, but could not be used for INTCAL98 because of lacking consensus on their validity. Figure 1 shows detailed $\Delta^{14}C$ records for the interval of 15–45 kyr cal BP (all with 1-σ errors) from sediments of the Iceland Sea (Voelker et al. 1998), the Cariaco Basin (Hughen et al. 2004), Lake Suigetsu (Kitagawa and van der Plicht 1998), and a Bahamas stalagmite (Beck et al. 2001). Also shown are the coral data (Bard et al. 1998) and the prior data from Lake Lisan (Schramm et al. 2000) with corrected ^{14}C ages in Haase-Schramm et al. (2004). The various records agree reasonably well for the interval of 15–25 kyr cal BP, but for the higher ages, large discrepancies are present. The Lake Suigetsu record shows lower $\Delta^{14}C$ values than the other records, whereas the stalagmite record shows higher $\Delta^{14}C$ values than the

[1]Department of Physics and Astronomy, Utrecht University, Netherlands.
[2]Corresponding author. Email: k.vanderborg@phys.uu.nl.
[3]Geological Survey of Israel, Jerusalem, Israel.
[4]Institute of Earth Sciences, Hebrew University, Jerusalem, Israel.
[5]Lamont-Doherty Earth Observatory of Columbia University, Palisades, New York 10964, USA.

Proceedings of the 18th International Radiocarbon Conference, edited by N Beavan Athfield and R J Sparks
RADIOCARBON, Vol 46, Nr 2, 2004, p 785–795

others. The ^{14}C records, as determined from foraminifera of the Iceland Sea and the Cariaco Basin laminae, are similar, which may be expected as both age scales, has been derived by matching the stable isotope records with the GISP2 ice core. In spite of the large differences between the records, it is remarkable that all agree with coral data. The data points for Lake Lisan (Haase-Schramm et al. 2004) also agree with the coral data and with the data for the Iceland Sea and the Cariaco Basin.

In this paper, we extend the pioneering work of Schramm et al. (2000) with a high-resolution record of Lake Lisan, the Last Glacial Dead Sea, which existed between 14–70 kyr cal BP (Kaufman 1971; Haase-Schramm et al. 2004). During its highest stand (~170 m below mean sea level), the lake covered a large area of the Jordan-Arava Valley from the Sea of Galilee in the north to Hazeva in the south (Begin et al. 1974). The lake deposits consist of millimeter-thin laminae of aragonite and fine silty detritus, plus gypsum and thicker clastic layers. The annually-laminated authigenic aragonite recorded U and ^{14}C and, thus, provides an excellent opportunity to generate a high-resolution ^{14}C record for ages larger than 15 kyr cal BP, which can be compared with the other published ^{14}C records, illuminating the way to achieve consensus among these apparently conflicting records.

METHODS

Samples were taken from the sedimentary section PZ1, located in the Perazim Valley (southwest of the present Dead Sea), which was used to determine the high-resolution U-Th chronology (Haase-Schramm et al. 2004). The lithology and geochemistry of this section has been thoroughly studied and described (Stein et al. 1997; Haase-Schramm et al. 2004). Aragonite samples were prepared from 1–2 individual laminae scratched from individual sediment blocks that were sampled continuously along the PZ1 section. The average spacing between consecutive samples is 7 cm, corresponding to ~100 yr. Two wood pieces were found within the aragonite, allowing for direct comparison between organic and inorganic carbon.

The ^{14}C analysis was performed at Utrecht University (van der Borg et al. 1997). Acid evolution of CO_2 from the carbonate samples was carried out in an evacuated glass line. Wood samples received an HCl wash to remove carbonate traces before they were combusted to CO_2. The collected CO_2 from the samples was then converted into graphite for ^{14}C analysis.

U-Th ages on the PZ1 sedimentary profile were determined by Haase-Schramm et al. (2004), who provided detailed explanation of the analytical and calculation procedures to achieve ^{230}Th-^{234}U of Lisan aragonite. The calendar age of the aragonite samples was obtained using the age-height regression relation $t = 1.400\ h + 68.54$, with h the height in the PZ1 section in meters and t the calendar age in kyr. The 1-σ error in the calendar age was estimated at 400 yr.

RESULTS AND DISCUSSION

The measured ^{14}C ages of the aragonite samples form a record of the bi-carbonate that was provided to the lake by the incoming runoff and spring water (Stein et al. 1997). The corresponding atmospheric ^{14}C record is obtained by correcting the aragonite ages with the reservoir age of the lake at the time the aragonite was deposited. With the 2 samples of wood remains found within the aragonite layers, we assume to derive reservoir ages the corresponding ages. Table 1 shows the ^{14}C ages measured for the wood and aragonite samples. We determine the calendar age of the aragonite samples from the sample position using the above-mentioned U-Th regression. Assuming a negligible age for the wood when it became locked in the sediment, we obtain reservoir ages of 1250 ± 180 yr at 23.0 kyr cal BP and 200 ± 500 yr at 32.7 kyr cal BP. Previous analyses of aragonite-organic debris pairs from the same horizon suggest a higher reservoir age of 1260 to 2000 yr

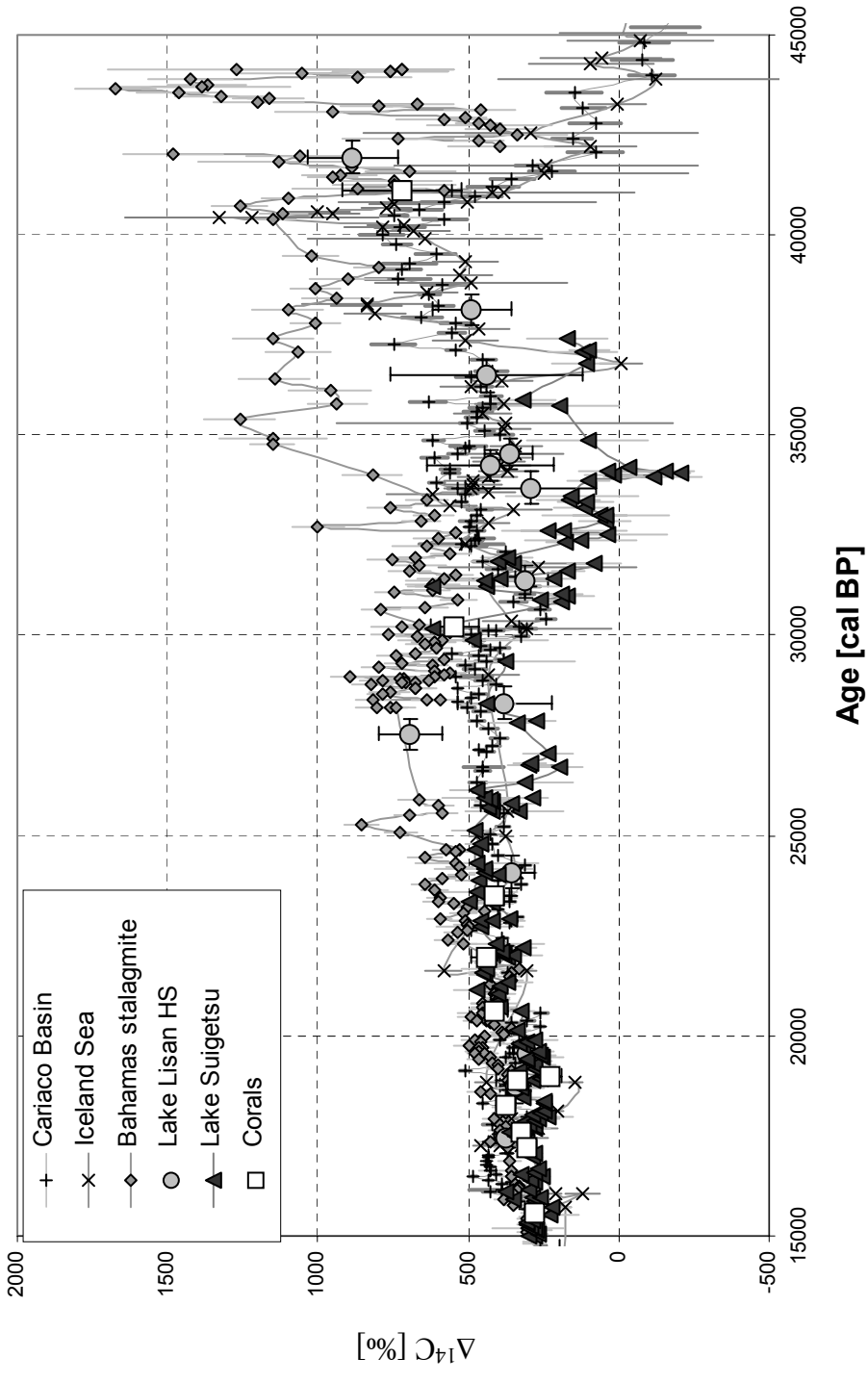

Figure 1 Comparison of high-resolution ^{14}C records versus calendar age from macrofossils of Lake Suigetsu, of sediments of the Iceland Sea and the Cariaco Basin, of a Bahamas stalagmite, of corals, and of aragonite from Lake Lisan.

(average = 1600 ± 250 yr) for the high-stand period of the lake between 19 and 26 kyr cal BP (see data and discussion of the relation between the reservoir ages and the hydrological-limnological conditions in Stein et al., these proceedings).

Table 1 Reservoir age of Lake Lisan from ^{14}C analysis.

Sample name	Height (cm)	U/Th age (cal BP)	Analyzed fraction	$\delta^{13}C$ (‰)	^{14}C age (BP)	Lab code UtC-	Reservoir age (BP)
ID-455w	3247	—	wood	–21.0	20,710 ± 130	12138	—
ID-455a	3247	23,000 ± 400	aragonite	1.6	21,960 ± 130	12172	1250 ± 180
PZ2-2558w	2558	—	wood	–21.9	30,300 ± 400	12278	—
PZ2-2558a	2558	32,700 ± 400	aragonite	1.3	30,500 ± 300	12277	200 ± 500

Using these various reservoir ages, we determine the atmospheric ^{14}C record for Lake Lisan, expressed as $\Delta^{14}C$ values (Table 2). The table includes the height in the section, the calendar age as calculated from the U-series age regression relationship, the estimated reservoir age, and the corresponding $\Delta^{14}C$ values. The uncertainty in the calendar age from U-Th dating for the sample series is smaller than the 400-yr uncertainty deduced from the regression analysis. The average spacing for the samples in the regression analysis was 130 cm, while the average spacing in the high-resolution record is 7 cm. As the regression analysis assumes a constant sedimentation rate, which is likely the largest source of error, the age uncertainty for the sample series is proportional to the spacing, resulting in an average error of 20 yr.

Table 2 Results of the high-resolution ^{14}C analysis for Lake Lisan.

Sample name	Height (cm)	U/Th age (cal BP)	$\delta^{13}C$ (‰)	^{14}C age (BP)	Lab code UtC-	Reservoir age (BP)	$\Delta^{14}C$ (‰)
PZ1-c14	3654.3	17,380	0.4	16,240 ± 80	11265	1250	267 ± 25
PZ1-c13	3652.0	17,412	2.0	15,650 ± 70	11264	1250	368 ± 24
PZ1-c12	3648.6	17,460	1.2	15,580 ± 90	11263	1250	388 ± 31
PZ1-c11	3642.0	17,552	2.0	15,560 ± 80	11262	1250	407 ± 28
PZ1-c10	3639.2	17,591	3.2	15,720 ± 80	11261	1250	386 ± 28
PZ1-c9	3632.5	17,685	1.1	15,890 ± 80	11260	1250	373 ± 27
PZ1-c8	3626.4	17,770	2.3	16,250 ± 80	11259	1250	326 ± 26
PZ1-c7	3620.2	17,857	1.0	16,380 ± 90	11245	1250	319 ± 30
PZ1-c6	3613.8	17,947	2.6	16,410 ± 100	11244	1250	328 ± 33
PZ1-c5	3610.0	18,000	3.3	16,330 ± 90	11243	1250	350 ± 30
PZ1-c4	3609.5	18,007	3.2	16,260 ± 90	11242	1250	363 ± 31
PZ1-c3	3608.8	18,017	1.7	16,220 ± 100	11241	1250	371 ± 34
PZ1-c2	3608.2	18,025	0.7	15,620 ± 90	11240	1250	479 ± 33
PZ1-c1	3607.5	18,035	1.1	15,910 ± 100	11239	1250	428 ± 36
PZ1-c15	3603.8	18,087	2.1	16,460 ± 80	11266	1250	342 ± 27
PZ1-c16	3598.5	18,161	0.6	16,240 ± 80	11267	1250	392 ± 28
PZ1-c17	3593.5	18,231	3.0	16,380 ± 80	11268	1250	380 ± 27
PZ1-c18	3591.8	18,255	3.3	16,420 ± 90	11246	1250	377 ± 31
PZ1-c19	3584.8	18,353	3.3	16,420 ± 90	11269	1250	393 ± 31
PZ1-c20	3579.7	18,424	1.7	16,520 ± 80	11270	1250	388 ± 28
PZ1-c21	3575.2	18,487	1.6	16,870 ± 80	11271	1250	339 ± 27
PZ1-c22	3567.5	18,595	0.7	16,890 ± 90	11272	1250	353 ± 30
PZ1-c23	3562.6	18,664	–0.5	16,890 ± 100	11273	1250	364 ± 34
PZ1-c24	3557.5	18,735	0.1	16,950 ± 100	11274	1250	366 ± 34
PZ1-c25	3552.2	18,809	1.8	16,990 ± 90	11275	1250	371 ± 31
PZ1-c26	3545.6	18,902	0.2	17,050 ± 100	11276	1250	376 ± 34
PZ1-c27	3539.4	18,988	2.7	17,200 ± 90	11277	1250	365 ± 31
PZ1-c28	3533.0	19,078	3.2	17,630 ± 100	11247	1250	308 ± 33

Table 2 Results of the high-resolution ^{14}C analysis for Lake Lisan. *(Continued)*

Sample name	Height (cm)	U/Th age (cal BP)	$\delta^{13}C$ (‰)	^{14}C age (BP)	Lab code UtC-	Reservoir age (BP)	$\Delta^{14}C$ (‰)
PZ1-c29	3528.8	19,137	0.5	17,500 ± 90	11278	1250	339 ± 30
PZ1-c30	3522.3	19,228	1.1	17,440 ± 100	11279	1250	364 ± 34
PZ1-c31	3516.8	19,305	3.5	17,960 ± 100	11280	1250	290 ± 32
PZ1-c32	3510.9	19,387	0.7	18,070 ± 110	11281	1250	286 ± 35
PZ1-c33	3506.6	19,448	0.2	18,010 ± 100	11282	1250	305 ± 32
PZ1-c34	3501.0	19,526	1.3	18,426 ± 100	11283	1250	251 ± 31
PZ1-c35	3495.1	19,609	2.1	18,280 ± 100	11284	1250	286 ± 32
PZ1-c36	3489.4	19,688	1.0	18,100 ± 100	11285	1250	328 ± 33
PZ1-c37	3483.7	19,768	2.4	18,290 ± 100	11286	1250	310 ± 33
PZ1-c38	3477.9	19,849	1.7	18,510 ± 110	11248	1250	287 ± 35
PZ1-c39	3472.2	19,929	1.7	19,070 ± 100	11287	1250	212 ± 30
PZ1-c40	3467.2	19,999	0.6	18,280 ± 110	11288	1250	349 ± 37
PZ1-c41	3462.2	20,069	1.5	18,690 ± 110	11289	1250	293 ± 35
PZ1-c42	3455.4	20,164	5.7	18,990 ± 130	11290	1250	260 ± 41
PZ1-c43	3443.3	20,334	1.3	19,150 ± 130	11291	1250	260 ± 41
PZ1-c44	3438.3	20,404	0.4	18,740 ± 110	11292	1250	338 ± 37
PZ1-c45	3432.1	20,491	1.2	18,950 ± 120	11293	1250	317 ± 39
PZ1-c46	3426.4	20,570	2.2	19,120 ± 110	11294	1250	302 ± 36
PZ1-c47	3420.0	20,660	3.9	18,910 ± 130	11295	1250	351 ± 44
PZ1-c48	3414.4	20,738	3.3	19,270 ± 120	11249	1250	304 ± 39
PZ1-c49	3406.3	20,852	1.9	19,220 ± 120	11296	2000	460 ± 44
PZ1-c50	3398.7	20,958	0.8	19,220 ± 120	11297	2000	479 ± 44
PZ1-c51	3395.3	21,006	1.4	19,820 ± 170	11298	2000	381 ± 58
PZ1-c52	3392.4	21,046	1.8	19,330 ± 130	11299	2000	475 ± 48
PZ1-c53	3387.6	21,114	2.4	19,620 ± 120	11300	2000	434 ± 43
PZ1-c54	3379.1	21,233	1.9	19,660 ± 130	11301	2000	448 ± 47
PZ1-c55	3373.4	21,312	–0.4	19,520 ± 110	11302	2000	487 ± 41
PZ1-c56	3368.2	21,385	2.9	19,810 ± 110	11303	2000	447 ± 40
PZ1-c57	3363.0	21,458	0.3	19,860 ± 120	11304	2000	451 ± 43
PZ1-c58	3357.4	21,536	0.5	19,720 ± 130	11250	2000	491 ± 48
PZ1-c59	3354.5	21,577	0.9	19,520 ± 120	11305	2000	536 ± 46
PZ1-c60	3350.8	21,629	2.9	19,840 ± 120	11306	2000	485 ± 44
PZ1-c61	3346.0	21,696	4.3	19,910 ± 130	11307	2000	484 ± 48
PZ1-c62	3342.0	21,752	0.5	20,030 ± 130	11308	2000	472 ± 48
PZ1-c63	3336.6	21,828	3.1	20,160 ± 120	11309	2000	462 ± 44
PZ1-c64	3331.4	21,900	3.4	20,140 ± 130	11310	2000	478 ± 48
PZ1-c65	3327.3	21,958	0.8	20,340 ± 120	11311	2000	452 ± 43
PZ1-c66	3321.2	22,043	2.5	20,470 ± 120	11312	2000	444 ± 43
PZ1-c67	3312.6	22,164	2.9	20,820 ± 140	11313	2000	402 ± 49
PZ1-c68	3307.0	22,242	1.3	20,810 ± 140	11251	2000	417 ± 49
PZ1-c69	3300.4	22,334	0.8	20,640 ± 140	11314	2000	464 ± 51
PZ1-c70	3292.2	22,449	–0.3	20,890 ± 140	11315	2000	439 ± 50
PZ1-c71	3286.0	22,536	0.0	21,640 ± 130	11316	2000	325 ± 43
PZ1-c72	3280.7	22,610	0.4	21,070 ± 130	11317	2000	435 ± 46
PZ1-c73	3275.5	22,683	–0.3	21,230 ± 140	11318	2000	419 ± 49
PZ1-c74	3270.2	22,757	0.3	21,470 ± 130	11319	2000	390 ± 45
PZ1-c75	3265.6	22,822	1.8	21,080 ± 120	11320	2000	470 ± 44
PZ1-c76	3260.4	22,894	0.4	21,210 ± 140	11321	2000	459 ± 51
PZ1-c77	3256.8	22,945	2.0	21,230 ± 140	11322	2000	465 ± 51
PZ1-c78	3249.1	23,053	2.8	21,480 ± 170	11252	2000	438 ± 61
PZ1-c79	3244.4	23,118	–0.7	22,110 ± 150	11323	2000	341 ± 50
PZ1-c80	3239.0	23,194	0.2	22,350 ± 140	11324	2000	313 ± 46
PZ1-c81	3232.2	23,289	0.5	21,710 ± 160	11325	2000	438 ± 57
PZ1-c82	3226.0	23,376	0.1	21,950 ± 140	11326	2000	411 ± 49
PZ1-c83	3218.1	23,487	0.1	22,010 ± 140	11327	2000	419 ± 49

Table 2 Results of the high-resolution ^{14}C analysis for Lake Lisan. *(Continued)*

Sample name	Height (cm)	U/Th age (cal BP)	$\delta^{13}C$ (‰)	^{14}C age (BP)	Lab code UtC-	Reservoir age (BP)	$\Delta^{14}C$ (‰)
PZ1-c84	3204.7	23,674	1.6	21,850 ± 140	11328	2000	481 ± 52
PZ1-c85	3196.4	23,790	0.2	22,230 ± 140	11329	2000	432 ± 50
PZ1-c86	3188.4	23,902	1.3	22,310 ± 140	11330	2000	438 ± 50
PZ1-c87	3181.6	23,998	1.6	22,310 ± 160	11331	2000	454 ± 58
PZ1-c88	3174.2	24,101	1.1	22,450 ± 170	11253	2000	447 ± 61
PZ1-c89	3167.8	24,191	1.4	22,680 ± 150	11332	2000	422 ± 53
PZ1-c90	3157.9	24,329	1.3	22,680 ± 150	11333	2000	446 ± 54
PZ1-c91	3149.0	24,454	1.8	22,680 ± 160	11334	2000	468 ± 58
PZ1-c92	3141.2	24,563	1.5	22,640 ± 150	11335	2000	495 ± 56
PZ1-c93	3133.1	24,677	1.8	23,070 ± 140	11336	2000	436 ± 50
PZ1-c94	3125.7	24,780	–0.5	23,390 ± 180	11254	2000	398 ± 63
PZ1-c97	3102.4	25,106	1.5	23,420 ± 100	11622	2000	448 ± 36
PZ1-c98	3095.4	25,204	1.4	23,370 ± 120	11623	1250	343 ± 40
PZ1-c99	3084.3	25,360	1.0	23,200 ± 100	11624	1250	398 ± 35
PZ1-c100	3074.4	25,498	–0.2	23,480 ± 110	11625	1250	373 ± 38
PZ1-c101	3063.5	25,651	2.0	23,700 ± 120	11626	1250	361 ± 41
PZ1-c102	3053.5	25,791	1.3	23,640 ± 120	11627	1250	394 ± 42
PZ1-c103	3046.3	25,892	0.8	23,600 ± 120	11628	1250	419 ± 42
PZ1-c104	3038.7	25,998	1.5	23,940 ± 110	11629	1250	377 ± 38
PZ1-c105	3029.7	26,124	0.9	24,380 ± 140	11630	1250	324 ± 46
PZ1-c106	3020.2	26,257	2.1	24,070 ± 110	11631	1250	398 ± 38
PZ1-c107	3010.9	26,387	0.1	24,280 ± 120	11632	1250	384 ± 41
PZ1-c108	2999.7	26,544	1.3	24,630 ± 120	11633	1250	350 ± 40
PZ1-c109	2991.0	26,666	2.6	24,630 ± 120	11634	1250	370 ± 41
PZ1-c110	2982.4	26,786	2.4	25,040 ± 110	11635	1250	321 ± 36
PZ1-c111	2972.9	26,919	2.2	25,000 ± 110	11636	1250	349 ± 37
PZ1-c112	2965.3	27,026	0.2	25,110 ± 110	11637	1250	348 ± 37
PZ1-c113	2959.0	27,114	0.7	25,390 ± 110	11638	1250	316 ± 36
PZ1-c114	2953.3	27,194	1.7	25,220 ± 130	11639	1250	357 ± 44
PZ1-c115	2947.5	27,275	2.0	25,240 ± 130	11640	1250	367 ± 44
PZ1-c116	2940.3	27,376	1.4	25,470 ± 120	11641	1250	345 ± 40
PZ1-c117	2933.0	27,478	3.0	25,480 ± 120	11642	1250	360 ± 41
PZ1-c118	2927.2	27,559	–0.5	26,160 ± 130	11643	1250	262 ± 41
PZ1-c119	2923.1	27,617	0.3	26,210 ± 130	11644	1250	263 ± 41
PZ1-c122	2907.5	27,835	1.8	25,740 ± 120	11647	1250	375 ± 41
PZ1-c120	2906.4	27,850	1.5	26,080 ± 130	11645	1250	320 ± 43
PZ1-c121	2899.7	27,944	0.9	25,840 ± 140	11646	1250	376 ± 48
PZ1-c123	2893.8	28,027	1.6	26,290 ± 130	11648	1250	314 ± 43
PZ1-c124	2884.8	28,153	0.7	26,250 ± 130	11649	1250	341 ± 43
PZ1-c125	2876.6	28,268	1.9	26,380 ± 150	11650	1250	338 ± 50
PZ1-c126	2868.4	28,382	1.3	26,590 ± 130	11651	1250	321 ± 43
PZ1-c127	2863.0	28,458	1.7	26,930 ± 120	11652	1250	278 ± 38
PZ1-c128	2855.4	28,564	1.5	26,860 ± 140	11653	1250	306 ± 46
PZ1-c129	2852.4	28,606	1.2	27,210 ± 140	11654	1250	257 ± 44
PZ1-c130	2841.9	28,753	1.9	26,860 ± 120	11655	1250	336 ± 40
PZ1-c131	2835.2	28,847	1.4	26,880 ± 120	11656	1250	348 ± 40
PZ1-c132	2832.2	28,889	2.0	27,120 ± 120	11657	1250	315 ± 39
PZ1-c133	2828.6	28,940	1.5	27,230 ± 120	11658	1250	305 ± 39
PZ1-c134	2826.7	28,966	2.0	27,160 ± 140	11659	1250	321 ± 46
PZ1-c135	2820.5	29,053	1.3	27,580 ± 150	11660	1250	267 ± 47
PZ1-c136	2818.8	29,077	1.0	27,650 ± 150	11661	1250	260 ± 47
PZ1-c137	2813.4	29,152	0.5	27,700 ± 130	11662	1250	263 ± 41
PZ1-c138	2804.8	29,273	0.4	27,780 ± 130	11663	1250	269 ± 41
PZ1-c139	2796.1	29,395	1.6	27,550 ± 150	11664	1250	325 ± 49
PZ1-c140	2789.4	29,488	3.3	27,600 ± 150	11665	1250	332 ± 50

Table 2 Results of the high-resolution ^{14}C analysis for Lake Lisan. *(Continued)*

Sample name	Height (cm)	U/Th age (cal BP)	$\delta^{13}C$ (‰)	^{14}C age (BP)	Lab code UtC-	Reservoir age (BP)	$\Delta^{14}C$ (‰)
PZ1-c141	2782.4	29,586	1.4	28,040 ± 160	11666	1250	276 ± 51
PZ1-c142	2775.0	29,690	1.7	27,430 ± 120	11692	1250	394 ± 42
PZ1-c143	2767.4	29,796	1.4	28,410 ± 140	11693	1250	250 ± 44
PZ1-c144	2759.3	29,910	1.1	28,720 ± 150	11694	1250	219 ± 46
PZ1-c145	2752.1	30,011	1.5	28,440 ± 140	11695	1250	278 ± 45
PZ1-c146	2743.8	30,127	1.4	28,750 ± 150	11696	1250	247 ± 47
PZ1-c147	2736.8	30,225	2.0	28,750 ± 150	11697	1250	262 ± 47
PZ1-c148	2730.1	30,319	1.8	28,990 ± 150	11698	1250	239 ± 46
PZ1-c149	2724.1	30,403	3.6	29,130 ± 150	11699	1250	230 ± 46
PZ1-c150	2714.6	30,536	2.3	29,260 ± 190	11700	1250	230 ± 58
PZ1-c151	2705.8	30,659	0.5	29,260 ± 160	11701	1250	248 ± 50
PZ1-c152	2699.0	30,754	2.1	29,230 ± 150	11702	1250	267 ± 47
PZ1-c153	2690.1	30,879	1.5	29,410 ± 190	11703	1250	258 ± 60
PZ1-c154	2687.0	30,922	1.5	29,130 ± 150	11704	1250	310 ± 49
PZ1-c155	2680.1	31,019	1.7	29,130 ± 150	11705	1250	325 ± 49
PZ1-c156	2672.2	31,129	2.0	29,630 ± 160	11706	1250	262 ± 50
PZ1-c157	2667.0	31,202	1.8	29,470 ± 160	11707	1250	299 ± 52
PZ1-c158	2661.7	31,276	1.2	30,030 ± 170	11708	1250	222 ± 52
PZ1-c159	2638.7	31,598	0.5	29,800 ± 300	12380	1250	308 ± 98
PZ1-c160	2637.7	31,612	–0.1	29,900 ± 300	12381	1250	294 ± 97
PZ1-c161	2629.7	31,724	–3.9	28,800 ± 300	12382	1250	504 ± 112
PZ1-c162	2621.9	31,833	–0.1	29,700 ± 300	12383	1250	362 ± 102
PZ1-c163	2616.1	31,915	1.0	30,200 ± 300	12384	1250	293 ± 97
PZ1-c164	2613.8	31,947	0.5	29,600 ± 300	12385	1250	398 ± 104
PZ1-c165	2608.0	32,028	2.0	30,700 ± 280	12386	1250	231 ± 86
PZ1-c166	2600.5	32,133	1.9	30,600 ± 280	12387	200	108 ± 77
PZ1-c167	2594.6	32,216	–1.4	31,100 ± 350	12388	200	52 ± 92
PZ1-c168	2588.2	32,305	–1.1	30,600 ± 290	12389	200	131 ± 82
PZ1-c169	2586.7	32,326	2.8	30,700 ± 300	12390	200	120 ± 84
PZ1-c170	2586.2	32,333	1.0	31,300 ± 300	12391	200	40 ± 78
PZ1-c171	2582.8	32,381	–0.5	31,600 ± 300	12392	200	8 ± 75
PZ1-c172	2570.4	32,554	–3.3	31,500 ± 350	12393	200	42 ± 91
PZ1-c173	2567.6	32,594	–1.1	32,000 ± 350	12394	200	–16 ± 86
PZ1-c174	2547.7	32,872	–0.8	31,200 ± 350	12395	200	124 ± 98
PZ1-c175	2544.3	32,920	–0.5	31,600 ± 300	12396	200	76 ± 80
PZ1-c176	2537.6	33,014	–0.7	31,700 ± 300	12397	200	75 ± 80
PZ1-c177	2530.1	33,119	0.9	31,100 ± 300	12398	200	173 ± 88
PZ1-c178	2524.8	33,193	1.6	31,500 ± 300	12399	200	126 ± 84
PZ1-c179	2519.0	33,274	2.4	31,500 ± 300	12400	200	137 ± 85
PZ1-c180	2514.1	33,343	0.4	31,700 ± 300	12401	200	118 ± 84
PZ1-c181	2508.1	33,427	0.6	31,900 ± 350	12402	200	102 ± 96
PZ1-c182	2502.1	33,511	1.7	32,100 ± 350	12403	200	86 ± 95
PZ1-c183	2497.0	33,582	1.8	31,900 ± 350	12404	200	123 ± 98
PZ1-c184	2491.0	33,666	1.4	32,400 ± 350	12405	200	66 ± 93
PZ1-c185	2484.8	33,753	1.0	32,000 ± 350	12406	200	132 ± 99
PZ1-c186	2477.1	33,861	0.7	32,100 ± 400	12407	200	133 ± 113
PZ1-c187	2470.9	33,947	1.0	32,200 ± 400	12408	200	131 ± 113
PZ1-c188	2463.6	34,050	0.7	32,400 ± 400	12409	200	117 ± 111
PZ1-c189	2455.3	34,166	0.6	32,300 ± 400	12410	200	147 ± 114
PZ1-c190	2454.3	34,180	–2.2	32,100 ± 350	12411	200	177 ± 103
PZ1-c191	2447.9	34,269	1.0	32,300 ± 400	12412	200	161 ± 116
PZ1-c192	2439.2	34,391	–1.7	32,400 ± 400	12413	200	164 ± 116
PZ1-c193	2415.2	34,727	–1.0	32,500 ± 400	12414	200	197 ± 119
PZ1-c194	2330.2	35,917	0.8	32,500 ± 400	12415	200	382 ± 138
PZ1-c195	2327.6	35,954	1.8	33,900 ± 400	12416	200	166 ± 116

Figure 2 shows the present $\Delta^{14}C$ record for Lake Lisan corrected for variable reservoir ages (VR). The dashed line indicates the effect in $\Delta^{14}C$ due to deviation from the 1250 yr reservoir age. The present Lake Lisan $\Delta^{14}C$ record agrees with the Lake Suigetsu record until 33 kyr cal BP (the best fit with Lake Suigetsu data is obtained for Lisan reservoir ages of 2000 yr between 20.9 and 25.2 kyr cal BP, and 200 yr between 32.1 and 36.0 kyr cal BP). Structures at 18, 22, 31, and 32 kyr cal BP are recognized in both records. Clearly, the structures at 18 and 22 kyr cal BP are not represented well by the INTCAL98 curve. The close correspondence of the ^{14}C record of lakes Lisan and Suigetsu lends support to the varve counting of the latter in this interval. This means that the $\Delta^{14}C$ ~0‰ observed in the Lake Lisan record at 32 kyr cal BP is confirmed by the ^{14}C record of Lake Suigetsu, where no reservoir age effect plays a role in the ^{14}C data obtained from macrofossils. The new Lake Lisan record agrees with both the coral data, except for the coral data point at 30 kyr cal BP, and the Lake Lisan HS data (Haase-Schramm et al. 2004), except for the data point at 27 kyr cal BP. At 34 kyr cal BP, the Lake Suigetsu record shows a number of different $\Delta^{14}C$ values (Figure 1) which may be indicative of a depositional hiatus. A 2-kyr hiatus would shift the data points to higher ages and higher corresponding $\Delta^{14}C$ values (Figure 2) in agreement with Lake Lisan data.

While the ^{14}C record of Lake Lisan resembles the Lake Suigetsu record, both are different from the $\Delta^{14}C$ values Bard (1998) modeled, based on the paleomagnetic compilation by Guyodo and Valent (1996) and the ^{10}Be production compilation by Frank et al. (1997). The present Lake Lisan record shows a maximum $\Delta^{14}C$ of ~450‰ at 25 kyr cal BP and a minimum $\Delta^{14}C$ of ~0‰ at 32 kyr cal BP, while the model of Bard indicates steadily increasing $\Delta^{14}C$ values toward a maximum $\Delta^{14}C$ of ~350‰ at 30 kyr cal BP. Obviously, other parameters play a role in the ^{14}C record. The $\Delta^{14}C$ ~0‰ at 32 kyr cal BP deduced from lakes Lisan and Suigetsu suggests that the production of ^{14}C was similar at that time to the present day or the same combination of production with the global reservoir carbon exchange prevailed. This matter, which we regard as a fundamental observation, requires further study and modeling.

The similarity of the $\Delta^{14}C$ records of lakes Lisan and Suigetsu lends support to the validity of both calendar chronologies up to 34 cal ka BP, but for ages >25 kyr cal BP, their $\Delta^{14}C$ values are clearly lower than the ^{14}C records of the Iceland Sea, the Cariaco Basin, and the Bahamas stalagmite. In the case of the stalagmite record, the reservoir age of 1450 yr, as derived for the interval of 11–16 kyr cal BP, was assumed for the whole age scale, which may not be justified. However, even zero reservoir age would not be sufficient to reduce the ^{14}C vales sufficiently for matching the other ^{14}C records. Only overestimation of the calendar age record can explain the difference with the Lake Lisan record. Reduction of the calendar age scale of the Iceland Sea and the Cariaco Basin—which were both determined from correlation with the GISP2 core—by 3% and the stalagmite by 5–10%, is sufficient to obtain a reasonable consensus with the present Lake Lisan record (Figure 3). Such a shift could indicate a wrong age assessment for the records of the Iceland Sea and the Cariaco Basin, which both depend on comparison with GISP2 data. In the case of the speleothems, the age assessment depends completely on the assumptions regarding the reservoir age and those related to the presence of initial Th and $^{234}U/^{238}U$ as well as the closed-system condition. The study of the behavior of the U-Th and ^{14}C system in the Lisan aragonite certainly indicated that unlike pristine corals, the initial Th factor can cause shifts in the U-Th calendar ages (Haase-Schramm et al. 2004).

CONCLUSION

We established a high-resolution ^{14}C record for Lake Lisan for the interval of 17–36 kyr cal BP by analyses of authigenic aragonite and application of variable reservoir ages determined by aragonite-organic debris pairs from the same stratigraphic horizons. The calendar ages of the aragonites were determined by U/Th (Haase-Schramm et al. 2004).

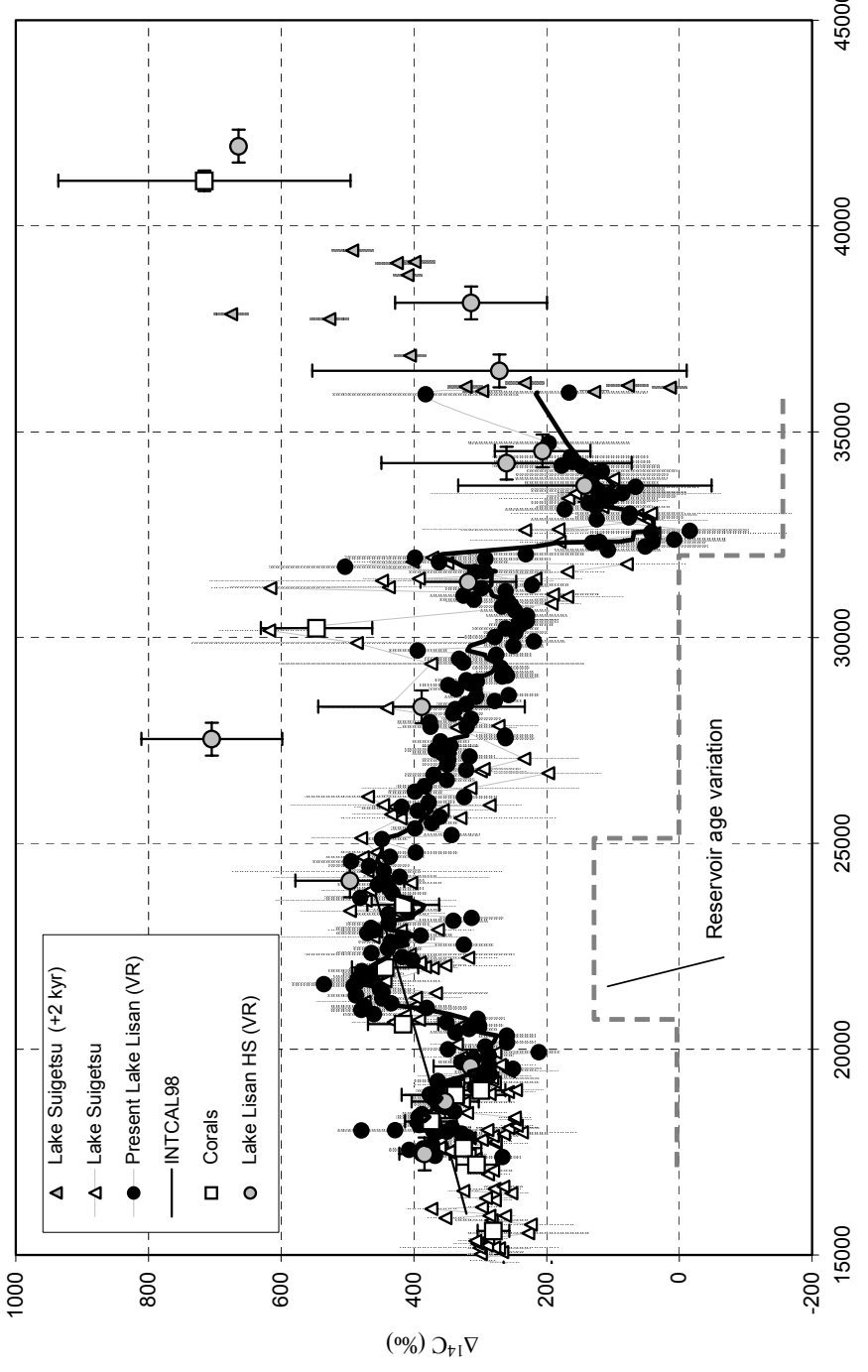

Figure 2 Comparison of the present ^{14}C record of Lake Lisan with that of Lake Suigetsu, and with the data points for Lake Lisan HS (i.e. Haase-Schramm et al. 2004), and with coral data. The present data for Lake Lisan were corrected for a variable reservoir age (VR) with values of 200, 1250, and 2000 yr. The dashed line indicates the difference (expressed as $\Delta^{14}C$ values) with respect to the 1250 yr reservoir age.

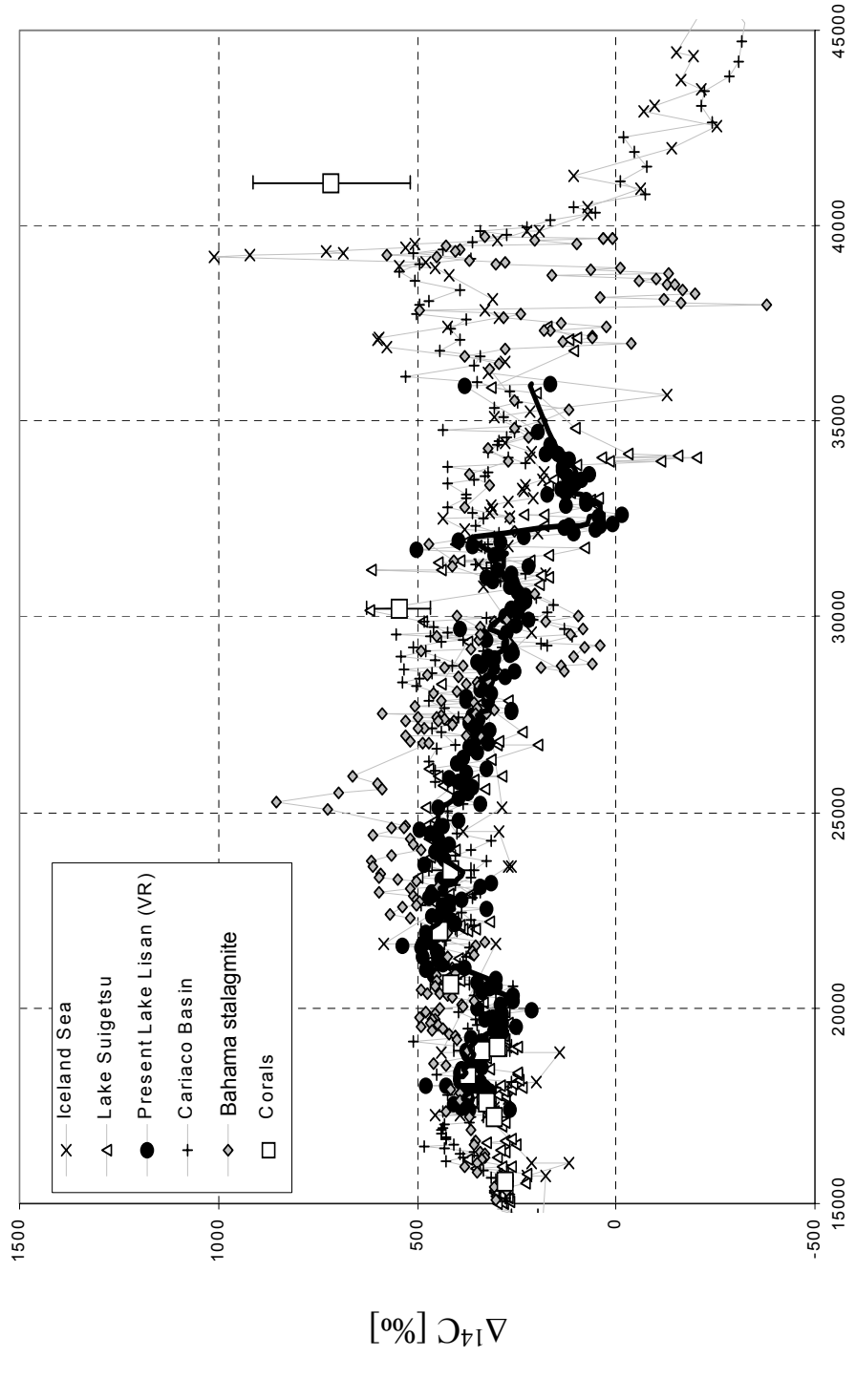

Figure 3 Comparison of ^{14}C records of the lakes Lisan and Suigetsu with the modified ^{14}C records of the Iceland Sea, the Cariaco Basin, and the Bahamas stalagmite. In the modified records, the calendar age scale was modified for ages >25 kyr cal BP by 3% for the records of the Iceland Sea and the Cariaco Basin, and 5–10% for the Bahamas stalagmite.

The present ^{14}C record of Lake Lisan resembles that from Lake Suigetsu. This observation supports both the validity of the varve counting used for the calendar age scale for Lake Suigetsu up to 33 kyr cal BP, and the use of variable reservoir ages in the Lake Lisan record.

Both the Lisan and Suigetsu records converge to $\Delta^{14}C$ ~0 at 32 kyr cal BP, suggesting an atmospheric production rate similar to present-day conditions or the same combination of production with the global reservoir carbon exchange.

The Lake Lisan and Suigetsu records do not show agreement with the modeled ^{14}C record, taking into account the effect of the geomagnetic field on the ^{14}C production. They also do not agree with the ^{14}C records of the Iceland Sea, Cariaco Basin, and the Bahamas stalagmite. However, a reasonable consensus with these other records is obtained by reducing the calendar age scale by 3% for the records of the Iceland Sea and the Cariaco Basin, and 5–10% for the Bahamas stalagmite.

ACKNOWLEDGEMENTS

This work was supported by US-Israel Binational Science Foundation (USIBSF) Grant #2000271 to MS and SLG. Eithan Shelef and Boaz Tatarski helped in field collection and the meticulous work of laminae separation.

REFERENCES

Bard E, Arnold M, Hamelin B, Tisnerat-Laborde N, Cabioch G. 1998. Radiocarbon calibration by means of mass spectrometric $^{230}Th/^{234}U$ and ^{14}C ages of corals: an updated database including samples from Barbados, Mururoa and Tahiti. *Radiocarbon* 40(3):1085–92.

Bard E. 1998. Geochemical and geophysical implications of the radiocarbon calibration. *Geochimica et Cosmochimica Acta* 62(12):2025–38.

Bartov Y, Goldstein SL, Stein M, Enzel Y. 2003. Catastrophic arid episodes in the Eastern Mediterranean linked with the North Atlantic Heinrich event. *Geology* 31:439–44.

Beck JW, Richards DA, Edwards RL, Silverman BW, Smart PL, Donahue DJ, Herrera-Osterheld S, Burr GS, Calsoyas L, Jull AJT, Biddulph D. 2001. Extremely large variations of atmospheric ^{14}C concentration during the last glacial period. *Science* 292:2453–7.

Begin ZB, Ehrlich A, Nathan Y. 1974. Lake Lisan—The precursor of the Dead Sea. *Geological Society Survey Israel Bulletin* 63:1–30.

Frank M, Schwarz B, Baumann S, Kubik PW, Suter M, Mangini A. 1997. A 200-kyr record of cosmogenic radionuclide production rate and geomagnetic field intensity from ^{10}Be in globally stacked deep-sea sediments. *Earth and Planetary Science Letters* 149:121–9.

Guyodo Y, Valet J-P. 1996. Relative variations in geomagnetic intensity from sedimentary records: the past 200,000 years. *Earth and Planetary Science Letters* 143:23–36.

Haase-Schramm A, Goldstein SL, Stein M. 2004. U-Th dating of Lake Lisan aragonite (late Pleistocene Dead Sea) and implications for glacial East Mediterranean climate change. *Geochimica et Cosmochimica Acta* 68(5):985–1005.

Hughen K, Lehman S, Southon J, Overpeck J, Marchal O, Herring C, Turnbull J. 2004. ^{14}C activity and global carbon cycle changes over the past 50,000 years. *Science* 303:202–7.

Kaufman A. 1971. U-series dating of Dead Sea Basin carbonates. *Geochimica et Cosmochimica Acta* 35: 1269–81.

Kitagawa H, van der Plicht J. 2000. A 40,000-yr varve chronology from Lake Suigetsu, Japan: extension of the ^{14}C calibration curve. *Radiocarbon* 42(3):369–80.

Schramm A, Stein M, Goldstein SL. 2000. Calibration of the ^{14}C timescale to >40 ka by ^{234}U-^{230}Th dating of Lake Lisan sediments (Last Glacial Dead Sea). *Earth and Planetary Science Letters* 175:27–40.

Stein M, Starinsky A, Katz A, Goldstein SL, Machlus M, Schramm A. 1997. Strontium isotopic, chemical and sedimentological evidence for the evolution of Lake Lisan and the Dead Sea. *Geochimica et Cosmochimica Acta* 61(18):3975–92.

Stein M, Migowski C, Bookman R, Lazar B. 2004. Temporal changes in radiocarbon reservoir age in the Dead Sea-Lake Lisan system. *Radiocarbon*, these proceedings.

Stuiver M, Reimer PJ, Bard E, Warren Beck J, Burr GS, Hughen KA, Kromer B, McCormac G, van der Plicht J, Spurk M. 1998. INTCAL98 radiocarbon age calibration, 24,000–0 cal BP. *Radiocarbon* 40(3):1041–83.

van der Borg K, Alderliesten C, de Jong AFM, van den Brink A, de Haas AP, Kersemaekers HJH, Raaymakers JEM. 1997. Precision and mass fractionation in ^{14}C analysis with AMS. *Nuclear Instruments and Methods in Physics Research B* 123:97–101.

Voelker AHL, Grootes PM, Nadeau M-J, Sarntheim M. 2000. Radiocarbon levels in the Iceland Sea from 25–53 kyr and their link to the earth's magnetic field intensity. *Radiocarbon* 42(3):437–52.

RADIOCARBON, Vol 46, Nr 2, 2004, p 797–808

HOLOCENE EVOLUTION OF THE OUTER LAKE OF HWAJINPO LAGOON ON THE EASTERN COAST OF KOREA; ENVIRONMENTAL CHANGES WITH HOLOCENE SEA-LEVEL FLUCTUATION OF THE EAST SEA (SEA OF JAPAN)

Jong-Gwon Yum[1,2] • Kang-Min Yu[3] • Keiji Takemura[4] • Toshiro Naruse[5] • Akihisa Kitamura[6] • Hiroyuki Kitagawa[7] • Jong-Chan Kim[1]

ABSTRACT. The evolution of the outer lake of Hwajinpo Lagoon in Korea has been reconstructed using environmental proxies (lithologic, geochemical, and fossil data) with a chronology established using 7 accelerator mass spectrometry (AMS) radiocarbon dates. Grain size, water content, and X-ray analyses from the core of outer coastal lakes (HJ99) were used to reconstruct sedimentary environments by using total organic carbon, C/N, S, and C/S chemical proxies. Assemblages of mollusc remains also provided paleoenvironmental information. The environmental changes of the outer lake of Hwajinpo Lagoon can be divided into 6 depositional phases. The basin of the Hwajinpo was exposed and underwent a weathering process before the Holocene period. The muddy sand layer on the weathered bedrock indicated an estuarine system about 6000 BP. The laminated layer implies that the lagoonal system was anoxic between about 5500–2800 BP. The marl layer implies a relatively oxic lagoonal condition with mollusc presence about 2500 BP. The layer of very low sulfur content indicates a freshwater lake system isolated by a sand barrier about 1700 BP. Beginning about 1000 BP, the river system deposits progress progradation on the marl layer. Two erosional landforms could be related with a high standing sea level span during Holocene. These high-stands are dated at 5700 BP and 2200 BP and are supposed to have formed erosional landforms of about 1.6 amsl and 0.8 amsl, respectively. Environmental changes of the outer lake of Hwajinpo Lagoon are considered due mainly to the lake- and sea-level fluctuation during Holocene.

INTRODUCTION

A lagoonal system can be a useful indicator to understand the history of sea-level change because of its high sensitivity with even small variations of sea level (e.g. Howell et al. 1988; Carter et al. 1989; Eitner 1996; Kirk and Lauder 2000; Li et al. 2001). In addition, a number of sedimentary studies on coastal lagoon systems indicate that the origin and geological histories of coastal lagoons are associated with sea-level changes during the Holocene (e.g. Dominguez et al. 1987; Kraft et al. 1981; Selivanov 1996; Morton et al. 2000).

Holocene sea-level changes of the East Sea (Sea of Japan) have been frequently discussed (Korotkii 1985; Okada 1978; Toyoshima 1978; Tokuoka et al. 1990; Selivanov 1996; Ishiga et al. 2000). They are mostly generated from the western coast of the Japanese Islands, which are known as active blocks. It is essential to compare these data with results from a tectonically stable area such as Hwajinpo Lagoon, in order to confirm overall variation in the East Sea area. A few studies have reported the geologic and environmental aspect of the lagoon. Jung and Park (1976) studied bottom sediment distribution of the Hwajinpo; Park and Kim (1981) investigated sand barrier developments; and Yum et al. (2002) determined recent depositional environment of Hwajinpo Lagoon. Sediment facies of the inner lake of Hwajinpo Lagoon were studied by Yum et al. (2003). Nevertheless, age determination was impossible largely due to difficulties in finding the dating material. Lithological and geochemical analyses with reliable age control using the core from the outer lake of Hwajinpo

[1]AMS Laboratory, National Center for Inter-University Facilities, Seoul National University, Seoul, 151-742, Korea.
[2]Corresponding author. Email: yums@ieg.or.kr.
[3]Department of Earth System Sciences, College of Sciences, Yonsei University, Seoul, 120-749, Korea.
[4]Beppu Geothermal Research Laboratory, Institute for Geothermal Science, Graduate School of Science, Kyoto University, Beppu, 874-0903, Japan.
[5]Department of Geography, Hyogo University of Teacher Education, Hyogo, 673-1494, Japan.
[6]Institute of Geosciences, Faculty of Science, Shizuoka University, Shizuoka 422-8529, Japan.
[7]Institute for Hydrospheric-Atmospheric Science, Nagoya University, Nagoya 464-8601, Japan.

Proceedings of the 18th International Radiocarbon Conference, edited by N Beavan Athfield and R J Sparks
RADIOCARBON, Vol 46, Nr 2, 2004, p 797–808

Lagoon should provide information on the history of the paleoenvironment during the Holocene, and also ascertain sea-level fluctuation.

ENVIRONMENTAL SETTING OF HWAJINPO LAGOON

Hwajinpo Lagoon (38°27′N, 128°28′E) is a large lagoon; it is composed of 2 small brackish-water lakes which are connected to each other by a narrow channel (Figure 1). It has an area of 2.4 km^2 with a maximum water depth of 3.7 m. The basement rock is comprised of the Gyeonggi Gneiss Complex intruded by the Jurassic Daebo granites (Cho et al. 1998). Normally, the lake level approaches near sea level and the tidal range is less than 50 cm. It is difficult to observe ice covered on the lake because of its salinity. The narrow channel between the inner and outer lake is shallow (less than 0.5 m water depth) and the outer lake has a narrow inlet to the sea which connects only during the summer rainy season (the monsoon season) or by seawater inflow due to waves in storms.

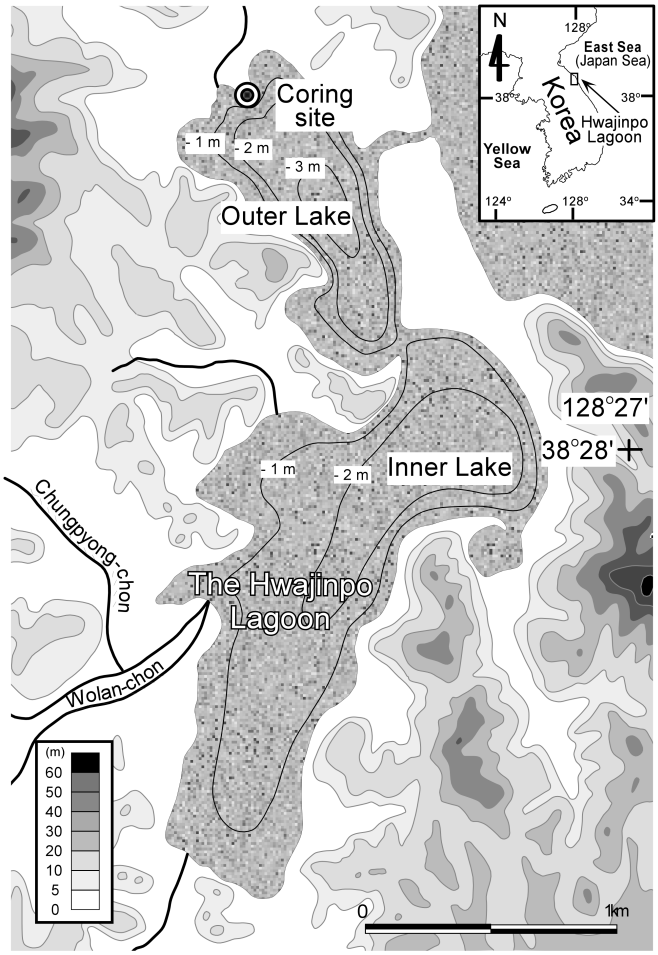

Figure 1 Map showing the location of Hwajinpo Lagoon on the eastern coast of Korea, including the coring site and bathymetry. The largest stream, Chungphyon River, is about 10 m wide near the river mouth.

Hwajinpo Lagoon has relatively well-preserved natural sedimentary records compared to other lagoons in Korea (Park and Kim 1981; Yum et al. 2003). Yum et al. (2002) reported that Hwajinpo Lagoon has been brackish over the last 400 yr. In addition, a halocline has been developed on each lake and is controlled by the flux of freshwater during the monsoon.

Coastal erosional landforms, such as notches, benches, and sea caves, were developed in granite basement rock. Erosional benches, indicating paleo high water level, were developed at 3 different elevations: present bench; about 0.8 m above mean sea level (amsl); and about 1.6 m amsl with a notch. The same levels of 3 platform surfaces were developed in the northern part of the Songjiho Lagoon area, located 25 km south from the study area. According to Yum (2001), these terraces and erosional geomorphologic features (benches, notches, and sea caves) of the Hwajinpo and Songjiho lagoonal areas are categorized into 3 groups summarized in Figure 2: Group I: 1.5~2.0 m (1.6 m) level; Group II: 0.6~0.9 m (0.8 m) level; and Group III: 0 cm present mean sea level.

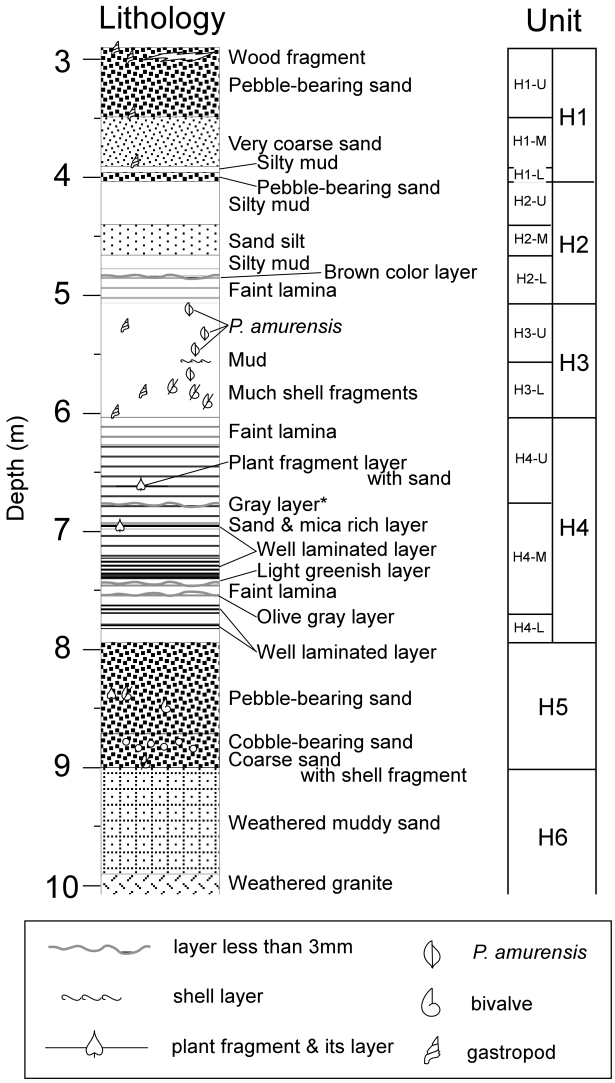

Figure 2 Lithostratigraphic units of the core HJ99 from the outer lake of Hwajinpo Lagoon. Gray layer is determined by X-radiographs.

METHODS

Bathymetrical survey on Hwajinpo Lagoon was conducted by using echo-sounding equipment with DGPS (FEG-770). A 10.1-m-long and 5.5-cm-diameter boring core (HJ99) was collected from Hwajinpo Lagoon (Figure 1). The core was sealed in the field site and stored vertically in order to prevent water loss and disturbance. In the laboratory, it was described and photographed while a X-radiograph was carried out with the acryl slab (1 × 5 × 30 cm). It was then subdivided into 2.5-cm slices. After carefully removing the outer rim of core sample, one-fourth of the remaining slices were dried at 70 °C for 48 hr to calculate sediment water content and for chemical analyses.

Total organic carbon (TOC), total sulfur (TS), and total nitrogen (TN) concentration were measured by an elemental analyzer (EA1108) after removal of carbonates with 1M-HCL (Sampei et al. 1997). Grain size of the sediment was analyzed by a laser-equipped diameter distributor (Mastersizer 2000) after adding enough 10% H_20_2. Each datum, except water content, was taken at 12.5-cm intervals in the core. Water content was measured at 2.5-cm intervals. When the core subdivided, all molluscan shells larger than sand size at every 12.5-cm interval, along with the horizontal plane of core, were collected, identified, and counted. We have obtained 7 ^{14}C ages from wood and plant fragments (Table 1) from the core by the AAA method of Kitagawa (1993) and calibrated the dates using the model of Stuvier et al. (1998).

Table 1 ^{14}C age dating of the core HJ99 from the outer lake of Hwajinpo Lagoon.

Sample	Depth (cm)	Lab code	^{14}C age (BP)
Terrestrial wood fragment	309	HK3129	60 ± 30
Terrestrial wood fragment	348	HK3130	115 ± 30
Terrestrial wood fragment	408	HK3132	1450 ± 40
Terrestrial wood fragment	610	HK3135	2190 ± 110
Terrestrial leaf	685	HK3137	4050 ± 60
Terrestrial plant fragment	707	HK3138	4240 ± 80
Terrestrial wood fragment	794	HK2965	5580 ± 50

RESULTS

Lithologic Units

A 10.1-m-thick core (HJ99) of Hwajinpo lagoonal sediment was divided into 6 major lithologic units based on grain size and sedimentary structure observed by logging and X-radiograph. These units have been named the H1, H2, H3, H4, H5, and H6 units from the top to the bottom (Figure 2). They are subdivided into 11 subunits based on the chemical and biological variations as well as lithologic changes.

Water Contents and Grain Size Analysis

The variation of water content appears to be related to lithologic changes (Figure 3). The upper part of unit H5 displays low water content, and unit H4 shows relatively high water content values compared to the previous unit H5. In subunit H4-L, the values show an increasing trend from 33% to 60%. The water content values in subunit H4-M displayed a slightly increasing trend, and a slightly decreasing trend in subunit H4-U. A diminishing trend from 61% to 45% is shown in the lowermost part of subunit H3-L, and the water content shows a constant value in unit H3 with an average of 44.7%. In all parts of unit H2, water content shows a slightly declining trend from 44% to 31%.

Water content in unit H1, a coarse sand layer, is relatively low. The sand percentage in subunit H4 increased from 2.8% to 6.6%. Yet, rapidly increasing percentage values of sand at the lower part of unit H3 show a decreasing trend. In unit H2, sand percentage increases from 3.5% to 75%. The mean grain size from the bottom of subunit H4-L to subunit H4-M shows a slight increasing trend, though with some fluctuations which range from 5.4 ϕ to 6.3 ϕ. The trend of grain size changes to a decreasing pattern from the boundary between H4-M and H4-U to the topmost of subunit H3-U, ranging from 5.4 ϕ to 6.7 ϕ. Then, grain size becomes coarser in unit H2. A general trend of sorting shows an increase, with fluctuations in the whole core which range from 1.7 ϕ to 2.3 ϕ.

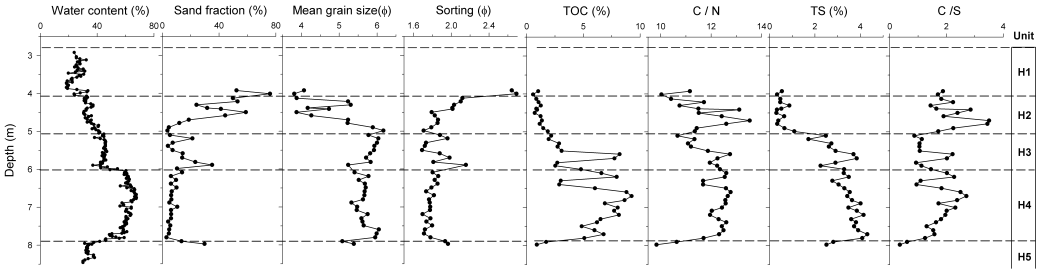

Figure 3 Sedimentology and chemical data from the core of the outer lake of Hwajinpo Lagoon: mean grain size was determined only for muddy units because the high sand contents of H1, H5, and H6 reflected values at the limit of the analyzer; mean grain size and sorting were calculated by Folk's method (Folk and Ward 1957); TOC (total organic carbon contents), C/N (ratio of total organic carbon and nitrogen), TS (total sulfur content), C/S (ratio of total organic carbon and sulfur).

TOC, C/N, TS, and C/S

In subunit H4-L, the TOC content indicates a steep increasing trend, reflecting the lithologic changes from sand to mud (Figure 3). The laminated subunit H4-M demonstrates a higher content of TOC with a slightly increasing trend. In subunits H4-U and H3-L, the value of TOC shows a fluctuation pattern ranging from 2.5% to 9.2%. Subsequently, the value of TOC is <2.7% with a decreasing trend to 0.6% from subunits H3-U and unit H2. The C/N ratio appears to have no significant variation, through the core ranges between 9.8 and 14.8 with fluctuations. In unit H3-U, the C/N ratio displays a downward trend.

The steep TS increase in the boundary between H4 and H5 units reflects the change of grain size; TS from subunit H4-L to unit H3 shows a downward trend ranging from 4.1% to 2.5% with an average value of 3.3%. Unit H2 exhibits very low sulfur content of less than 0.8% with an average value of 0.48%. The C/S ratio through the core ranged from 0.8 to 2.7 with an average of 1.7, except for the subunit H2-L showing a peak shape (maximum value of 3.6).

Mollusca

Figure 4 shows the stratigraphic distributions and relative abundance of molluscan fossils in the core. Nine species of molluscs are present in core HJ99, including 5 unidentified species. They all are shallow estuarine types of mollusc affected by seawater, especially *Potamocorbula amurensis*, which is typically a brackish mollusc found in the coastal areas of Korea (Kwon et al. 1993). Unit H5 contains estuarine molluscs, while units H4 and H2 have no molluscs. On the other hand, Unit H3 contains a large amount of whole molluscs and fragments, including the specific species of brackish mollusc, *P. amurensis.* Unit H1, containing mainly *P. amurensis*, presents the recent condition of Hwajinpo Lagoon (Yum et al. 2002)

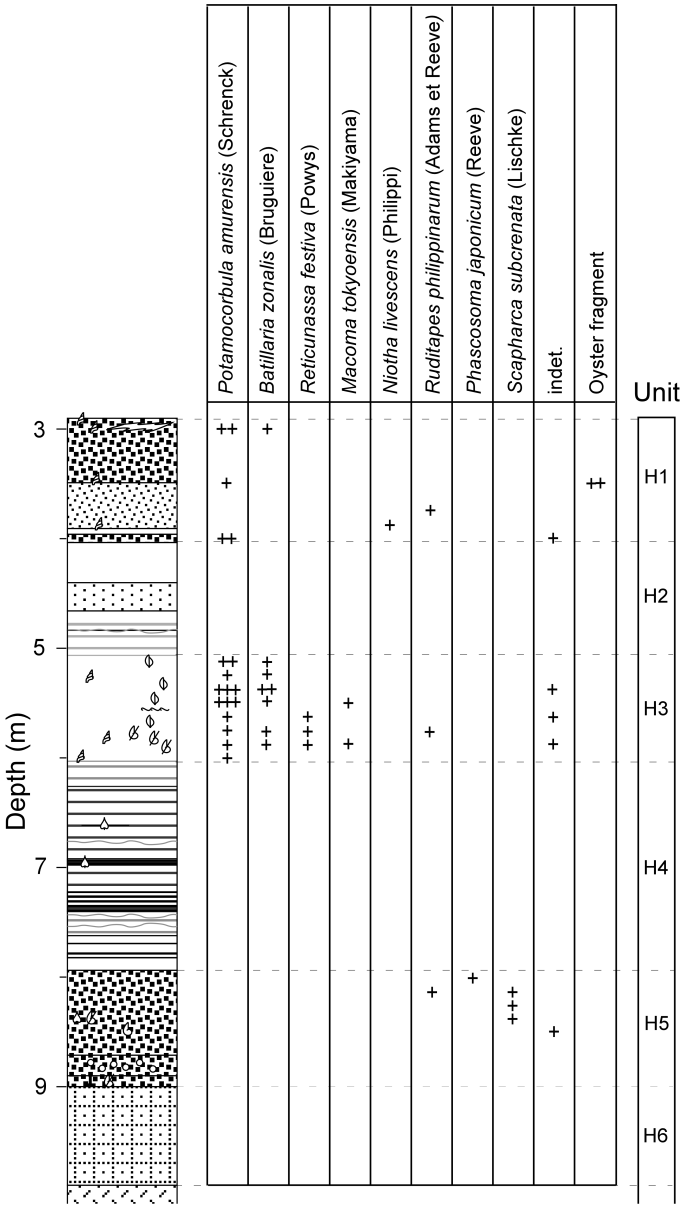

Figure 4 Mollusc abundance in the core HJ99 from Hwajinpo Lagoon; +: 1; ++: 2~3; +++: more than 3 individuals.

Sedimentation Rate

An age-depth model was constructed from 7 AMS ^{14}C dates (Figure 5). The radiocarbon age ranged from 5580 ± 50 BP at the middle part of unit H5 to 60 ± 30 BP in top of unit H1 (Table 1). A straight line was fit between sections of constant sedimentation to construct this age-depth model. In unit H4, the sedimentation rate is calculated to 0.69 mm/yr by linear interpolation. Units H3 and H2 have sedimentation rates of 1.38 mm/yr. In subunit H1-L, the sedimentation rate is 0.47 mm/yr, while in subunit H1-U the rate indicates a very fast depositional environment with a sedimentation rate of 7.02 mm/yr.

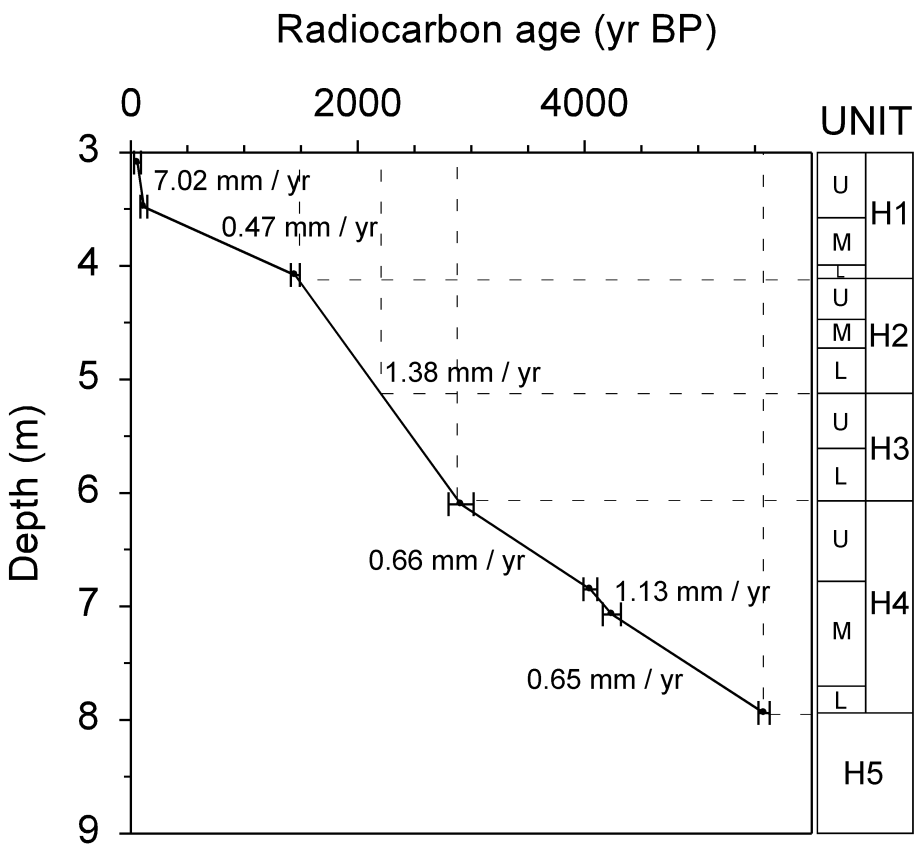

Figure 5 Sedimentation rate in core HJ99 calculated by AMS measurement

DISCUSSION

Criteria for the Reconstruction of Paleoenvironments in Hwajinpo Lagoon

Using the several proxy data from the core, reconstruction of the environment during the Holocene is possible with great clarity and in considerable detail. We applied these useful data as environmental proxy and reconstructed the paleoenvironmental history of the outer lake of Hwajinpo Lagoon. Detailed and basic information of events during the Quaternary can often be obtained from the sedimentary records themselves, even though other data, such as chemical or biological evidence, provide useful insights into past environmental conditions. Based on the criteria for reconstruction of paleoenvironments by Yum et al. (2003), environmental changes for the outer lake of Hwajinpo Lagoon were reconstructed as the following 6 depositional environments.

Environmental Changes of the Outer Lake of Hwajinpo Lagoon

Unit H6 - Weathered Deposit on the Exposed Basement (Before 6800 BP)

The basement rock of the Hwajinpo Lagoon area is comprised of Gyeonggi Gneiss Complex intruded by Daebo granites that have been the most clastic sources of depositional material to Hwajinpo Lagoon. The time that unit H6 was exposed could be prior to the Last Glacial Maximum period, given that the bottom of unit H5 started deposition after 6800 BP (Yum et al. 2003).

Unit H5 - Estuarine Deposit (About 6000 BP)

Unit H5 could be considered tidal inlet sand deposits of estuarine environments during a transgression starting before 5600 BP. The gravel layer in the lower part of this unit was considered a lag deposit which was deposited in the initial time of transgression. Unit H5 displays lower water content related to very poor sorting due to the mixture of sand- and silt-sized grains. The assemblage of estuarine-type molluscs indicates the condition of the outer lake of Hwajinpo Lagoon was an open estuarine system when unit H5 was deposited.

Unit H4 - Stagnant Brackish Lagoonal Deposit (About 5500–2800 BP)

Yum et al. (2002) have suggested that the difference in the bottom conditions is a consequence of monsoon, which may account for the annual variation of precipitation at Hwajinpo Lagoon area. However, the well-laminated structure in unit H4 could remain if the bottom water was stable and/or the absence of bioactivity was absent even after a strong monsoon. The runoff-stagnation model of Howell et al. (1988) by sea-level change explains the development of a well-laminated layer in a brackish lagoonal system. The hypothesis of an isolated basin due to the development of a sand spit in the outer lake of Hwajinpo Lagoon can apply to this model.

Unit H4 shows higher water content values than the previous units H5 and H6. Unit H4 indicates proper sorting and an accordingly stable condition. The sulfur contents are relatively high at the range of about 2.5%, implying a relatively oxygen-poor condition in the bottom sediments. The change of grain size from sand to silt at the boundary between units H5 and H4 might be the result of rapid change in the depositional environment. Unit H4 could be deduced to stagnant bottom and brackish water condition.

The corresponding layer (unit D) of core HJ95 is deposited in the brackish environment, as has been reconstructed from the bases of diatom assemblage (Yum et al. 2003). This unit D layer of HJ95 deposited on the estuarine sand layer dated to about 6000 BP. An overlying layer is a marl deposit with much shell and its fragments, as well as in the unit H4 of HJ99.

Unit H3 - Oxic Condition Marl Deposit (About 2200–2800 BP)

The upward trend of increasingly finer grain size begins in subunit H4-L due to the rising the lake level and continues up to unit H3. The abundance of shells from unit H3 indicates that the condition of the lake was open and had sufficient oxygen and nutrients, in contrast with the previous unit, according to the oxic condition model of Howell et al. (1998). Mollusca, represented by *P. amurensis*, indicates a brackish water condition. We see a constant value for water content and susceptibility, and much shell with their fragments occurred in the same range of this unit H3. This should be the consequence of an active bioturbation. The decrease of shell fragments at the top of unit H3 points to the beginning of environmental change from oxygen-rich to oxygen-poor conditions in Hwajinpo Lagoon. The decreasing trend of TS in the top of unit H3 supports this interpretation, i.e., the sulfur supplied from seawater diminished following oxygen-decreasing phenomena by the isolated Hwajinpo lagoonal system.

Unit H2 - Isolated Lake Deposit Influenced by Freshwater (About 1700 BP)

The low sulfur content of Unit H2 with its higher value of C/S indicates a decrease of seawater influx. The faint lamination in unit H2-L implies a stable and stagnant condition similar to unit H4. This could be due to the decline of sea level, i.e., a sand barrier developed by the rising sea level during the previous stage (unit H3) made the outer lagoon isolated from the sea. Human activity can

also be taken into account for the development of the sand spit when evaluating these phenomena. However, the overall steady trend of grain size indicates that the barrier was not constructed due to sudden unexpected environmental change, such as a typhoon or flood event. The decrease of sea level is a more reasonable factor for explaining the isolation.

The progressive lowering of the lake level influenced the progradation of the river delta near the coring location. This was followed by the sandy silt layer (subunit H2-M) being deposited at the minimum lake-level stage. The use of land by humans can also indicate another explanation to the sand-rich sedimentation; however, TOC and C/N ratios do not show the abrupt change that would be expected by human activities. In subunit H2-U, the lake level recovered and the grain size became finer than in the previous sandy silt layer.

Unit H1 - Prograding River System (Since 1200 BP)

In the final stage, the river system deposit consisting of silt and sand was prograding up to the coring location. The presence of *P. amurensis* in this unit indicates brackish water conditions. The value of C/N for subunit H1-L indicates a high influx of terrestrial material, while the sedimentation rate of unit H1-U implies that it was deposited only during a few centuries (from 150 BP), which can possibly be due to land use by humans and the subsequent weathering rate increase.

Evolution Model of the Outer Lakes of Hwajinpo Lagoon

As a result of our data, we can describe the conceptual evolution model of the outer lake of Hwajinpo Lagoon (shown in Figure 6). The basement rock (Precambrian Gyeonggi Gneiss Complex) was exposed and its surface had been strongly weathered before 6800 BP. Estuarine sediments, including bay-type shells with their fragments, overlie the basement rock. The estuarine deposit on the basement rock was reported in other eastern coasts of Korea. Jo (1980) proposed that the sandy deposits containing molluscs should be related to a rise in sea level during the early Holocene. The age estimated by the depth-age model also suggests a date before 6000 BP. Therefore, it is apparent that the outer lake of Hwajinpo Lagoon became an estuarine system during the same phase of sea-level rise.

Subsequently, the decline of sea level caused the Hwajinpo to be isolated in a brackish condition due to frequent influx of seawater. However, the bottom condition was anoxic and could not support living organisms, and a lamination layer developed in the isolated environment (5500–2800 BP).

The subsequent increase of the sea level again allowed the lake bottom to receive a sufficient influx of seawater containing enough oxygen; thus, many molluscs could live in the higher lake-level conditions (2800–2200 BP). By the resulting slight decreases in sea level, Hwajinpo Lagoon became isolated and like a coastal lake, influenced from freshwater influx (about 1700 BP), or it might have been caused by the role of damming in the development of barriers and/or inlet sand deposit during this high-stand condition of water. Then, with the rising sea level, Hwajinpo Lagoon reached its present condition and the river system was prograding upon the HJ99 coring location.

Sea-Level Fluctuation of the East Sea (Sea of Japan) During the Holocene

The erosional landform near the study area shows high-stand paleosea and/or lake-level conditions above the present sea level (about 0.8 m and 1.6 m abml). The AMS age data from 1.6-m terraces indicate that they were formed during the mid-Holocene stage (Yu et al., forthcoming). Also, other previous studies on the sea level of the East Sea showed that there are more than 2 higher-stand conditions above the present sea level during the Holocene (e.g. Ota et al. 1990; Selivanov 1996;

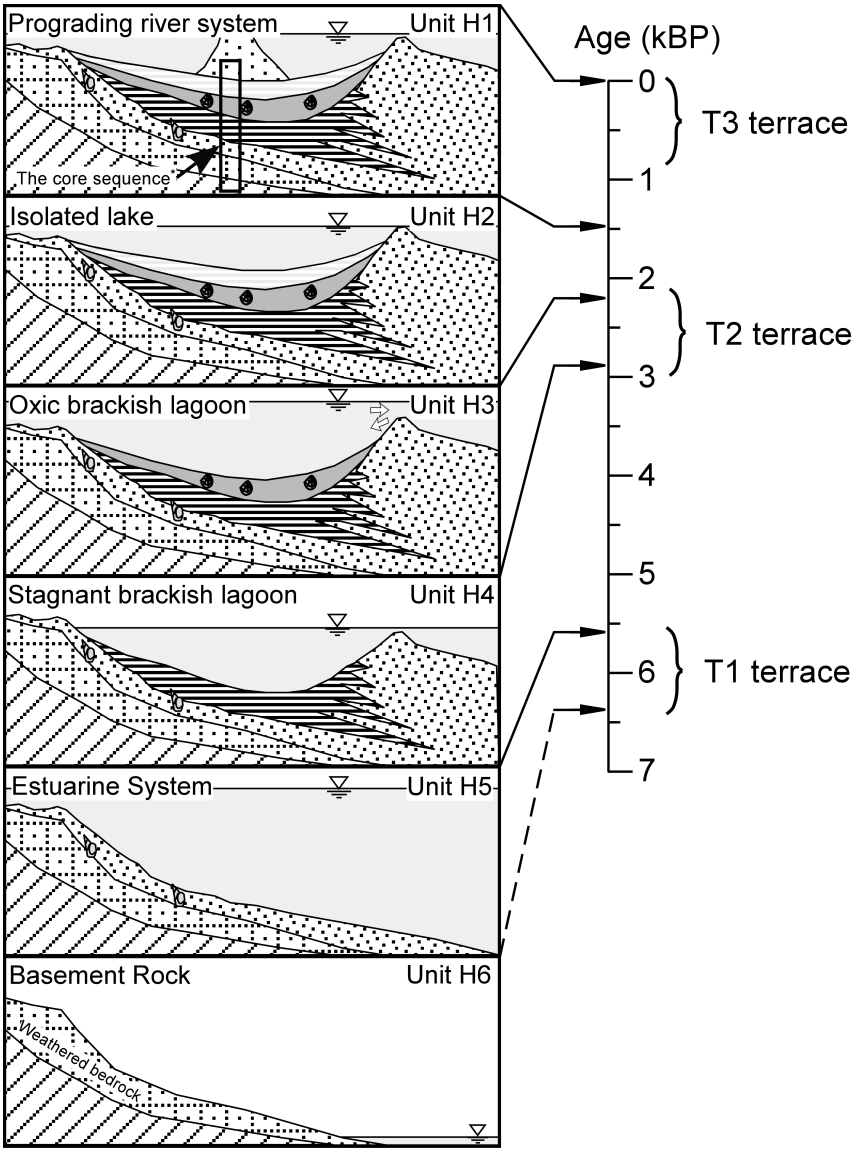

Figure 6 Conceptional evolution model of the outer lake of Hwajinpo Lagoon. The ages are estimated from ^{14}C dating on the hyphothesis of a constant sedimentation rate; the sea-level changes are presented on a relative scale. Core sequence: the upper most part of the core covered with deltaic sand deposits (Unit H1); left side connected to the inner lake and right side connected to the sea side.

Nakamura et al. 2002; Yum 2001). According to Yum's (2001) suggestion, there are 4 high-stand sea levels during the Holocene in the East Sea area, determined by using the changes of sedimentary faces. The oldest high-stand (about 7500 BP) is reported at 10 m below the present sea level, and the fact is concordant with the result of Jo (1980). The youngest high-stand (about 300 BP) is too short a period to form the obvious erosional landform. Therefore, the high-stands aged about 5700 BP and 2200 BP are supposed to have formed erosional landforms of about 1.6 m and 0.8 m level, respectively (Figure 6).

CONCLUSION

A multidisciplinary approach, involving lithologic and chemical as well as paleontological and geomorphological research, allows for the reconstruction of the paleoenvironment. It enables the reconstruction of evolution and sea-level changes of the outer lake of Hwajinpo Lagoon.

The environmental changes of the outer lake of Hwajinpo Lagoon can be divided into the following 6 different depositional phases: 1) Exposed basement rock (Unit H6; before 6800 BP); 2) Estuarine deposit (Unit H5; about 6000 BP); 3) Stagnant brackish lagoonal deposit (Unit H4: 5500–2800 BP); 4) Oxic condition marl deposit (Unit H3; about 2500 BP); 5) Isolated lake deposit influenced by freshwater (Unit H2; about 1700 BP); 6) Prograding river system deposit (Unit H1; beginning about 1000 BP.)

ACKNOWLEDGEMENTS

We are indebted to Professor YJ Lee of Chungbuk National University and Dr JY Kim of the Korea Institute of Geosciences and Mineral Resources for their helpful comments and suggestion. Dr Yum acknowledges work Korea Research Foundation Grant (KRF-2000-042-D00096) for partial financial support.

REFERENCES

Cater RWG, Forbes DL, Jennings SC, Orford JD, Shaw J, Taylor RB. 1989. Barrier and lagoon coast evolution under differing relative sea-level regimes: examples from Ireland and Nova Scotia. *Marine Geology* 88: 221–42.

Cho DL, Hong SH, Chwae U, Lee BJ, Choi P. 1998. Geological report of the Goseong-Ganseong sheet (1: 50,000). Daejeon, Korea: Korea Institute of Geology, Mining and Materials. 12 p.

Dominguez JML, Martin L, Bittencourt ACSP. 1987. Sea-level history and Quaternary evolution of river mouth-associated, beach-ridge plain along the east-southeast Brazilian coast: a summary. In: Nummedal D, Pilkey OH, Howard JP, editors. *Sea-Level Fluctuation and Coastal Evolution*. Tulsa: Society of Economic Paleontologists and Mineralogists, special publication nr 41. p 115–28.

Folk RL, Ward WC. 1975. Brazos River bar: a study in the significance of grain-size parameters. *Journal of Sedimentary Petrology* 27:3–26.

Howell MW, Thunell RE, Tappa E, Rio D, Sprovieri R. 1988. Late Neogene laminated and opal-rich facies from the Mediterranean region: geochemical evidence for mechanisms of formation. *Palaeogeography, Palaeoclimatology, Palaeoecology* 64:265–86.

Ishiga H, Nakamura T, Sampei Y, Tokuoka T, Takayasu K. 2000. Geochemical record of the Holocene Jomon transgression and human activity in coastal lagoon sediments of the San'in district, SW Japan. *Global and Planetary Changes* 25:223–37.

Jo W. 1980. Holocene sea-level changes on the east coast of Korea Peninsula. *Geography Review of Japan* 53: 317–28.

Jung WY, Park YA. 1976. Depositional environments of the recent sediments in the Hwajinpo Lake, Gangweondo, Korea. *Journal of Oceanological Society of Korea* 11:64–70.

Kirk RM, Lauder GA. 2000. Significant coastal lagoon systems in the South Island, New Zealand—coastal processes and lagoon mouth closure. *Science for Conservation* 146:5–47.

Kitagawa H, Masuzawa T, Nakamura T, Matsumoto E. 1993. A batch preparation method of graphite targets with low background for AMS ^{14}C measurements. *Radiocarbon* 35(2):295–300.

Korotkii AM. 1985. Quaternary sea-level fluctuations on the northwestern shelf on the Japan Sea. *Journal of Coastal Research* 1(3):293–8.

Kraft JC, John CJ, Marx PR. 1981. Clastic depositional strata in a transgressive coastal environment: Holocene epoch. *Northeastern Geology* 3:268–77.

Kwon OK, Park SM, Lee JS. 1993. *Coloured Shells of Korea.* Seoul, Korea: Academy Publishing. 446 p.

Li CX, Hang JQ, Fan DD, Deng B. 2001. Holocene regression and the tidal radial sand ridge system formation in the Jiangsu coastal zone, east China. *Marine Geology* 173:97–120.

Morton RA, Ward GH, White WA. 2000. Rates of sediment supply and sea-level rise in a large coastal lagoon. *Marine Geology* 167:261–84.

Nakamura T, Tokuoka T, Onishi I, Sampei Y, Takayasu K, Takehiro F, Ege K, Nishio K, Watanabe M. 1996. Holocene environmental changes and lowland historic sites in eastern part of the Shimane prefecture. *LAGUNA* 3:9–11.

Okada A. 1978. Sea-level change and geomorphic development since the last glacial age in the Wakasa Bay region central west of the Japan Sea coast. *Geographical*

Review of Japan 51(2):131–46.

Ota Y, Umitsu M, Matsushima Y. 1990. Recent Japanese research on relative sea-level changes in the Holocene, and related problems—review of studies between 1980–1988. *The Quaternary Research (Japan)* 29(1):31–48.

Park BK, Kim WH. 1981. The depositional environments of lagoons in the east coast of Korea. *Journal of Geological Society of Korea* 17:241–9.

Sampei Y, Matsumoto E, Tokuoka T, Inoue D. 1997. Changes in accumulation rate of organic carbon during the last 8,000 years in sediments of Nakaumi Lagoon. *Japanese Marine Chemistry* 58:39–50.

Selivanov AO. 1996. Morphological changes on Russian coasts under rapid sea-level changes: examples from the Holocene history and implications for future. *Journal of Coastal Research*12(4):823–30.

Stuiver M, Reimer PJ, Bard E, Beck JW, Burr GS, Hughen KA, Kromer B, McCormac G, van der Plicht J, Spurk M. 1998. INTCAL98 radiocarbon age calibration, 24,000–0 cal BP. *Radiocarbon* 40(3):1041–83.

Tokuoka T, Onish I, Takayasu K, Mitunashi T. 1990. Natural history and environmental changes of Lakes Nakaumi and Shinji. *Memoir of Geological Society of Japan* 36:15–34.

Toyoshima Y. 1978. Postglacial sea-level change along San'in District, Japan. *Geographical Review of Japan* 51(2):147–57.

Yu KM, Takemura K, Yum JG, Naruse T, Nakanish T, Kim HY. Forthcoming. Elevation of two Holocene sea-level high-stands as recorded by terraces and erosional landforms in the Songjiho area, East Sea (Sea of Japan). *Marine Geology.*

Yum JG. 2001. Late Quaternary environmental changes of the Hwajinpo and Songjiho Lagoons on the eastern coast of Korea [PhD dissertation]. Yonsei, Korea: Yonsei University. 145 p.

Yum JG, Sampei T. Tokuoka T, Nakamura T, Yu KM. 2002. Depositional environmental change during the last 400 years in Hwajinpo Lagoon on the eastern coast of Korea. *Journal of Geological Society of Korea* 38:21–32.

Yum JG, Takemura K, Tokuoka T, Yu KM. 2003. Holocene environmental changes of Hwajinpo Lagoon on the eastern coast of Korea. *Journal of Paleolimnology* 29:155–66.

RADIOCARBON, Vol 46, Nr 2, 2004, p 809–826

^{14}C CHRONOLOGY OF MESOLITHIC SITES FROM POLAND AND THE BACKGROUND OF ENVIRONMENTAL CHANGES

Anna Pazdur[1,2] • Mariusz Fogtman[1] • Adam Michczyński[1] • Jacek Pawlyta[1] • Mirosław Zając[3]

ABSTRACT. Mesolithic sites in modern Poland are mainly located in the southern part of the country. Radiocarbon dating of organic material, such as charcoals, wood, and peat, provide a time frame of human settlements in those regions, and dating of speleothems and peat formations provide information on climatic conditions and the timing of climatic change in the region. Here, we present the results of calibrated ^{14}C ages from 3 main Mesolithic sites: Glanów, Chwalim, and Całowanie. Summary probability density distributions of the calendar ages were obtained, and time ranges were ascribed to the cultures in conjunction with archaeological information. These distributions also reveal the changes in human settlement.

INTRODUCTION

At the turn of the IX and VIII millennium BC (Preboreal period), climatic conditions in Poland became similar to the present time. During this early stage of the Holocene, climatic conditions were moderating, as evidenced in the Atlantic maximum level which took place at the V millennium BC. This Pleistocene/Holocene transitional period was characterized by the new ecological circumstances which triggered a movement of human settlements to the northern parts of Poland. The main reason for the migration was probably to search for new resources/food supplies. This new settlement initiated Mesolithic cultures in these regions and defines the Mesolithic for the region as a period that lasted from the beginning of the Holocene to the first appearance of Neolithic people in Poland at the V millennium BC. The onset of the Mesolithic period is also related to the appearance of an entirely new population of reindeer hunters that migrated to Poland from the northwestern part of the European Plain.

The Mesolithic was, generally, a period of cultural stabilization, and cultural differences between individual groups of people were relatively insignificant. The differences were determined on the basis of the technical variety of flint tool production. Mesolithic tools, found mainly in peat bogs, consist of bone, horn, and wood elements. Bones and horns were used in the production of the harpoons, spear points, fishhooks, etc. Wood was used mainly in the production of boats and oars. However, during the Mesolithic, flint tools were becoming less common. Most of the tools were in the form of stone fixed on the top of bone. Other tools present, though rare finds, were designed for scratching and scraping, such as a prototype axe used for cutting and processing trees and wood (Godłowski et al. 1983).

The earliest Mesolithic settlements in Poland associated with the sites studied in this project were connected with 3 successive cultures: Komornica, early Mesolithic to VI millennium (Gąssowski 1985); Janislawice, VII and VI millennium BC to the end of the Mesolithic (Gąssowski 1985); and Chojnicko-Pieńkowska, persisting to the end of the Mesolithic (Gąssowski 1985). These successive cultures specialized in shaved flint tools; in the Janisławice sites, decorations made from wild boar tusks are found in addition to finished tools of flint, horn, and bone. The last successor, the Chojnicko-Pieńkowska culture, specialized in hunting but were also known to fish (Gąssowski 1985).

[1]Silesian University of Technology, Department of Radioisotopes, 44-100 Gliwice, Krzywoustego 2, Poland.
[2]Corresponding author. Email: pazdur@zeus.polsl.gliwice.pl.
[3]Archeological Museum in Kraków, 31-002 Kracow, Senacka 3, Poland.

Proceedings of the 18th International Radiocarbon Conference, edited by N Beavan Athfield and R J Sparks
RADIOCARBON, Vol 46, Nr 2, 2004, p 809–826

During the Mesolithic period, the exploitation of the surrounding environment, which lasted for dozens of millenniums, ended. Cultures were now mainly concentrated on improvements of tools and arms for hunting and defense. The proceeding new Mesolithic economy depended on improved climatic conditions and may have allowed greater cultural development of improved living conditions. This period was marked by the development of clothing production, new building and heating technologies, and more sophisticated food processing (i.e. removal of toxic substances through boiling and roasting), though the significant source of food was still hunting and gathering (Gąssowski 1985).

The least-known issue of the Mesolithic is the character of its social structure. The problem lies in the fact that the Mesolithic cultures were disrupted by subsequent cultures and, thus, there are some problems in identifying true Mesolithic cultural characteristics.

It is thought that the development of these cultures through time was especially dependent upon improving climatic conditions (Godłowski et al. 1983), which we examine in this paper. The Mesolithic period in Poland can be subdivided into 3 climatic stages. The Preboreal (about 9950 BC to 8570 BC) was characterized by a moderately warm climate. Forests were dominated by pine, and mild climatic conditions favored the formation of brown soils (Godłowski et al. 1983). The Boreal (about 8570 BC to 7530 BC) was moderately warm and humid. The black earth and bog soils were formed and the forests were enriched by birch (Godłowski et al. 1983). The Atlantic period, referred to as the climatic optimum of the Holocene (about 7530 BC to about 3960 BC), was warmer than the contemporary climate, with the average annual temperature about 2 °C warmer than the present. These conditions aided the significant growth of vegetation and an increase of the global sea level by up to 2 m (Godłowski et al. 1983). Two climatic eras of the Holocene followed the Mesolithic period. The Subboreal (about 3960 BC to 460 BC) was warm with increased humidity, and the Subatlantic (about 460 BC to AD 1810) had climatic conditions similar to the present climate (Pazdur 1987; Gąssowski 1985).

SITE LOCATIONS AND MATERIALS

The Mesolithic sites in Poland which are included in this study are mainly concentrated in the southern part of the country. The main sites of interest are Glanów, Całowanie, and Chwalim (Figure 1).

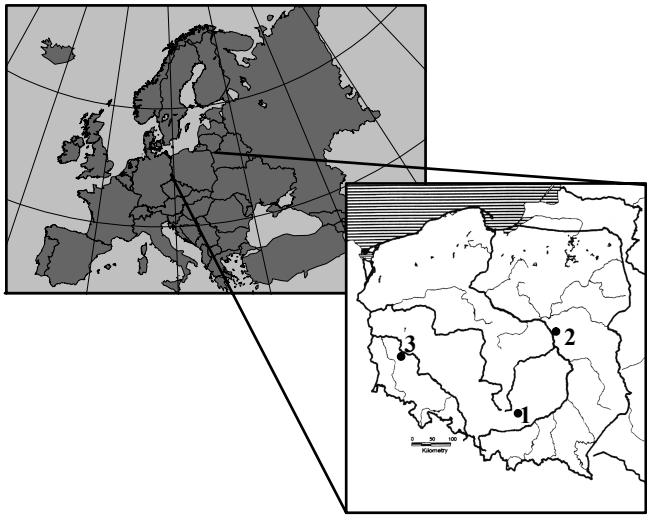

Figure 1 Map of Poland and the location of Mesolithic sites: 1: Glanów 3; 2: Calowanie; 3: Chwalim.

The Glanów site 3 (19°47′W, 50°18′N) is located about 30 km northwest of Kraków. This site is situated on a sandy hill on the left side of the Dłubnia River bank. The study area of Glanów site 3 is about 775 m^2 and is described in detail by Zając (2001), who in 1995–99 lead an archeological excavation of the site. Up to 41 ^{14}C dates have been obtained on charcoal samples, most of which range in age from the Early to Late Mesolithic. These ages are supported by archaeological finds (e.g. flint tools and pottery) corresponding to the Mesolithic. Some additional ^{14}C ages correspond to later cultures such as the Lengyel, Mierzanowice and Lusatian, and the Roman period, which were also in agreement with associated artifacts (Zając 2001).

The Chwalim site (15°46′W, 52°08′N) is situated on the sandy-gravel bed of the Gnila Obra River near Poznań. A preliminary geological stratigraphy of the Chwalim site has been reconstructed by Kobusiewicz et al. (1993) and Kobusiewicz (1999), wherein both a clear stratigraphic section and a section with less distinct layering is described. Several flints and bones of deer, elk, and bison were found in the record with the distinct stratigraphy, and numerous flints, burnt stones, and pottery were present in the section with indistinct layering. Charcoal samples are located together with artifacts in the peat bog. There were 11 charcoal samples, but only three belong to the Mesolithic period (Figure 2). The artifacts found allow one to identify the archaeological cultures. Charcoal samples were dated and the results were compared with the obtained archaeological periods as determined by artifact style. The youngest of the 3 samples came from the palinological profile and had no archaeological significance (Figure 2). The remaining samples belong to Paraneolithic period.

The Całowanie site (21°17′W, 52°01′N) is situated on the sandy island in a peat bog of the Vistula River bed. The area of this site is about 6000 m^2. The distinct geological stratigraphy of the site assisted in the association of the ages of charcoal samples with specific cultural layers. The stratigraphic distinction in the sections at this site was defined by 11 archaeological levels which included artifacts such as flint tools and datable materials such as wood. From this site, 32 samples were dated and correlation between ^{14}C ages and archaeological levels were described by Schild (1975, 1989, 1996, 1998, 2001) and Schild et al. (1999).

All of the samples selected for ^{14}C dating from the Mesolithic sites described above consisted of charcoals and were, except for specific samples, collected by the authors. For Glanów site 3, the charcoal samples were collected by M Zając, who researched this site in 1995–1999. Samples from the Chwalim site were investigated by Kobusiewicz in 1975–1979. In the Całowanie site, charcoals were collected and submitted by Schild.

METHODS

Pretreatment and CO_2 production was done in the Gliwice Radiocarbon Laboratory. Charcoal samples were chemically pretreated with a 1% solution of HCl for 1 hr in 80 °C to remove contamination by carbonates. The sample was then washed in distilled water to neutral pH and dried at 80 °C for 20 hr. In the Gliwice lab, the 0.5 M NaOH treatment for charcoal samples is omitted because of the significant loss of mass that follows a base treatment. Samples were combusted and the resultant CO_2 was purified according to the standard procedure used in the Gliwice lab. The measurement of ^{14}C concentration was carried out in gas proportional counters (Pazdur and Pazdur 1986; Pazdur et al. 2000).

RESULTS

We have collected a total of 84 ^{14}C dates, of which 67 were obtained in the Gliwice lab. These include 41 ^{14}C dates from Glanów site 3, 11 ages from the Chwalim site, and 32 dates from the

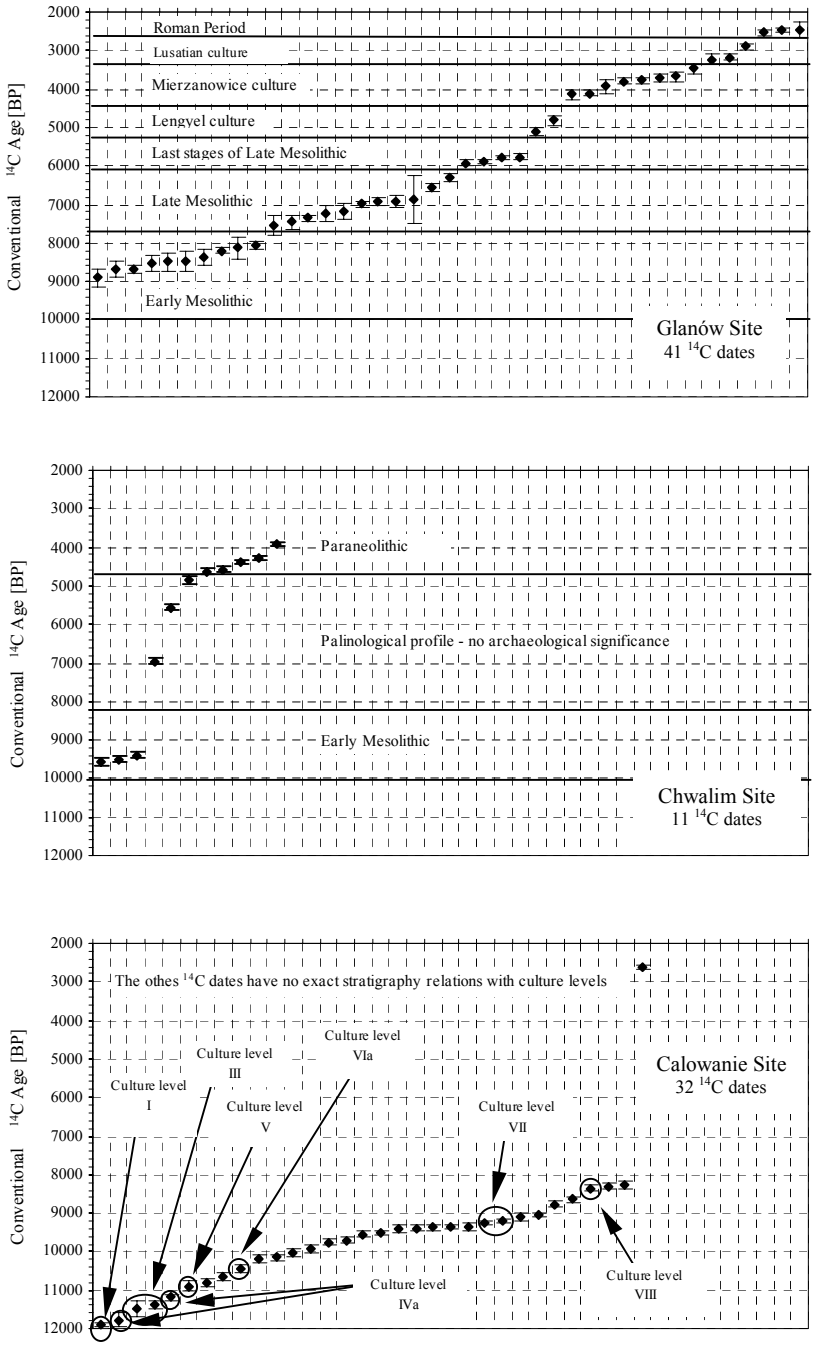

Figure 2 Cumulative probability density distributions of ^{14}C conventional dates from Mesolithic sites in Poland.

Całowanie site (Figure 2). For the 11 samples from the Chwalim site, 4 charcoal samples were dated in the Laboratory of the Zentralinstitut für Alte Geschichte und Archäologie, Akademie der Wissenschaften der DDR in Berlin (Bln). The samples from the Całowanie site were dated at the Center for

Accelerator Mass Spectrometry at Lawrence Livermore National Laboratory (CAMS), USA, the Center of Isotope Research, University of Groningen, the Netherlands (GrN), and at Gliwice. Description of the samples and the ^{14}C dating results from Glanów 3, Chwalim, and Całowanie are given in Tables 1, 2, and 3, respectively, and illustrated in Figure 2.

The ^{14}C dates were calibrated using the OxCal v3.8 calibration program (Ramsey 2002). Results of the calibration procedure, represented by probability intervals with 68% and 95% confidence, are shown (Tables 1, 2, and 3).

FREQUENCY DISTRIBUTIONS OF CALENDAR AGES

The division of ^{14}C dates into archaeological cultures was carried out on the basis of charcoal dating and archaeological determinations based on the cultural style of associated artifacts in each of the sites at Glanów, Chwalim, and Całowanie. Calibration of the dates was then completed for each of the groupings to obtain the calendar age ranges. Figures 3, 4, and 5 show the cumulative probability density distributions of calibrated ^{14}C ages and the assignment of the results into archaeological cultures at the Glanów, Chwalim, and Całowanie sites.

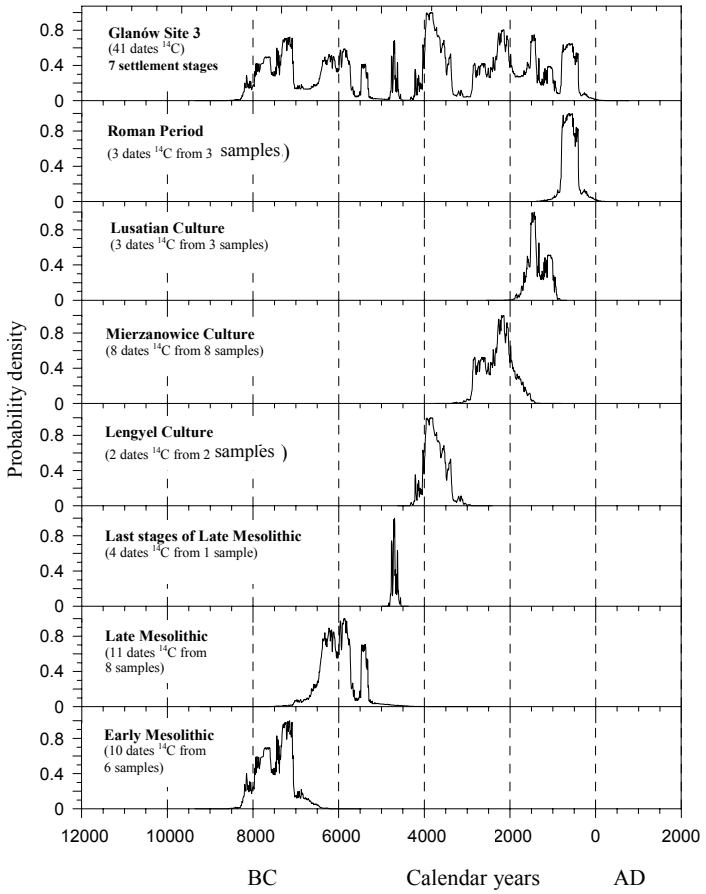

Figure 3 Cumulative probability density distributions of calibrated ^{14}C ages with the division into archaeological cultures from Glanów site 3.

Table 1 Description (name, species [if known], institution, collector, lab nr, aggregation) and conventional and calibrated ages of the samples from Glanów Site 3 (19°47′W, 50°18′N). Age range has been determined with confidence levels of 68% and 95% using the OxCal v3.8 program. The numbers in brackets are the percent of age range in the total probability density distribution of the calibrated age. The system of aggregations on the site are shown in Figure 6.

Name, sample description	Lab nr	Aggregation	^{14}C age (BP)	Age range (68%) (cal AD, BC)	Age range (95%) (cal AD, BC)
1. Glanów G3/97/5948 *Pinus sylvestris*, Archeological Museum in Kraków (Zając 1997)	Gd-17140	NW	8910 ± 250	8300–7650 BC (68.2%)	8800–7400 BC (95.4%)
2. Glanów G3/97/5586 *Pinus sylvestris*, Archeological Museum in Kraków (Zając 1997)	Gd-18160	E	8690 ± 210	8200–7500 BC (68.2%)	8300–7200 BC (95.4%)
3. Glanów G3/97/6133 *Pinus sylvestris*, Archeological Museum in Kraków (Zając 1997)	Gd-10831	NW	8670 ± 110	7940–7930 BC (1.2%) 7920–7900 BC (2.8%) 7880–7860 BC (1.9%) 7830–7580 BC (62.3%)	8200–7500 BC (95.4%)
4. Glanów G3/97/8822 *Pinus sylvestris*, Archeological Museum in Kraków (Zając 1997)	Gd-30016	NE	8530 ± 210	7950–7300 BC (67.4%) 7250–7200 BC (0.8%)	8300–7000 BC (95.4%)
5. Glanów G3/97/5004 *Pinus sylvestris*, Archeological Museum in Kraków (Zając 1997)	Gd-18161	E	8490 ± 220	7950–7150 BC (68.2%)	8300–7000 BC (95.4%)
6. Glanów G3/96/3683 Archeological Museum in Kraków (Zając 1996)	Gd-10749	S	8490 ± 270	7950–7050 BC (68.2%)	8300–6800 BC (95.4%)
7. Glanów G3/97/5303 *Pinus sylvestris*, Archeological Museum in Kraków (Zając 1997)	Gd-17149	E	8360 ± 210	7600–7050 BC (68.2%)	8000–6700 BC (95.4%)
8. Glanów G3/96/3718 *Pinus sylvestris*, Archeological Museum in Kraków (Zając 1996)	Gd-12413	S	8200 ± 80	7320–7070 BC (68.2%)	7480–7050 BC (95.4%)
9. Glanów G3/97/8609 Archeological Museum in Kraków, (Zając 1997)	Gd-13003	NE	8130 ± 280	7500–6700 BC (68.2%)	7800–6400 BC (95.4%)
10. Glanów G3/97/4983 *Pinus sylvestris*, Archeological Museum in Kraków (Zając 1997)	Gd-11413	E	8050 ± 100	7180–7150 BC (3.3%) 7140–6800 BC (62.3%) 6790–6770 BC (2.6%)	7350–6650 BC (95.4%)
11. Glanów G3/96/4035 *Pinus sylvestris*, Archeological Museum in Kraków (Zając 1996)	Gd-16149	S	7550 ± 250	6650–6050 BC (68.2%)	7100–5900 BC (95.4%)
12. Glanów G3/97/7168 *Pinus sylvestris*, Archeological Museum in Kraków (Zając 1997)	Gd-13010	NW	7460 ± 200	6480–6070 BC (68.2%)	6750–5800 BC (95.4%)
13. Glanów G3/97/7744 *Pinus sylvestris*, Archeological Museum in Kraków (Zając 1997)	Gd-11444	E	7360 ± 100	6380–6310 BC (13.9%) 6300–6280 BC (2.1%) 6270–6080 BC (52.2%)	6420–6020 BC (95.4%)
14. Glanów G3/96/3349 *Pinus sylvestris*, Archeological Museum in Kraków (Zając 1996)	Gd-13007	S	7250 ± 210	6380–6310 BC (8.2%) 6300–6280 BC (1.3%) 6270–5970 BC (52.8%) 5960–5910 BC (5.8%)	6500–5700 BC (95.4%)

Table 1 Description (name, species [if known], institution, collector, lab nr, aggregation) and conventional and calibrated ages of the samples from Glanów Site 3 (19°47′W, 50°18′N). Age range has been determined with confidence levels of 68% and 95% using the OxCal v3.8 program. The numbers in brackets are the percent of age range in the total probability density distribution of the calibrated age. The system of aggregations on the site are shown in Figure 6. *(Continued)*

Name, sample description	Lab nr	Aggregation	^{14}C age (BP)	Age range (68%) (cal AD, BC)	Age range (95%) (cal AD, BC)
15. Glanów G3/97/9000 *Pinus sylvestris*, Archeological Museum in Kraków (Zając 1997)	Gd-30015	NE	7180 ± 190	6230–5870 BC (65.9%) 5860–5840 BC (2.3%)	6450–5700 BC (95.4%)
16. Glanów G3/97/8995 *Pinus sylvestris*, Archeological Museum in Kraków (Zając 1997)	Gd-10834	NE	6990 ± 90	5980–5940 BC (12.1%) 5920–5770 BC (56.1%)	6030–5710 BC (95.4%)
17. Glanów G3/97/8611 *Pinus sylvestris*, Archeological Museum in Kraków (Zając 1997)	Gd-15389	NE	6940 ± 110	5980–5950 BC (5.1%) 5910–5720 BC (63.1%)	6020–5630 BC (68.2%)
18. Glanów G3/97/8605 *Pinus sylvestris*, Archeological Museum in Kraków (Zając 1997)	Gd-16148	NE	6930 ± 170	5990–5940 BC (8.2%) 5930–5660 BC (60.0%)	6200–5450 BC (95.4%)
19. Glanów G3/96/3746 *Pinus sylvestris*, Archeological Museum in Kraków (Zając 1996)	Gd-14008	S	6870 ± 640	6500–5000 BC (68.2%)	7300–4300 BC (95.4%)
20. Glanów G3/97/7368 *Pinus sylvestris*, Archeological Museum in Kraków (Zając 1997)	Gd-15394	E	6570 ± 90	5620–5470 BC (66.2%) 5440–5420 BC (2.0%)	5670–5360 BC (95.4%)
21. Glanów G3/97/7387 *Pinus sylvestris*, Archeological Museum in Kraków (Zając 1997)	Gd-11442	E	6300 ± 90	5370–5200 BC (52.2%) 5180–5140 BC (8.5%) 5120–5080 BC (7.5%)	5480–5040 BC (95.4%)
22. Glanów G3/97/7757(1) *Pinus sylvestris*, Archeological Museum in Kraków (Zając 1997)	Gd-12433	E	5920 ± 70	4910–4870 BC (6.5%) 4860–4710 BC (61.7%)	4960–4590 BC (95.4%)
23. Glanów G3/97/7757(2) *Coniferae indet.*, Archeological Museum in Kraków (Zając 1997)	Gd-11658	E	5870 ± 60	4840–4820 BC (2.7%) 4810–4670 BC (60.8%) 4640–4620 BC (4.7%)	4910–4870 BC (1.6%) 4860–4580 BC (91.7%) 4570–4550 BC (2.0%)
24. Glanów G3/97/7757(3) Unidentified, Archeological Museum in Kraków (Zając 1997)	Gd-11659	E	5790 ± 60	4720–4550 BC (68.2%)	4780–4490 BC (95.4%)
25. Glanów G3/97/7790 *Coniferae indet.*, Archeological Museum in Kraków (Zając 1997)	Gd-12432	E	5760 ± 80	4710–4520 BC (66.0%) 4510–4500 BC (2.2%)	4800–4450 BC (94.4%) 4420–4400 BC (1.0%)
26. Glanów G3/97/7292 *Pinus sylvestris*, *Quercus sp.* Archeological Museum in Kraków (Zając 1997)	Gd-10837	NE	5110 ± 110	4040–4020 BC (3.8%) 4000–3770 BC (64.4%)	4250–3650 BC (95.4%)
27. Glanów G3/96/3783 *Pinus sylvestris*, Archeological Museum in Kraków (Zając 1996)	Gd-17147	S	4820 ± 150	3770–3490 BC (53.2%) 3470–3370 BC (15.0%)	4000–3300 BC (92.0%) 3250–3100 BC (3.4%)
28. Glanów G3/97/6594 Pinus sylvestris, *Sambucus sp.*, *Corylus avellana*, Archeological Museum in Kraków (Zając 1997)	Gd-13008	NW	4140 ± 140	2890–2560 BC (64.2%) 2530–2490 BC (4.0%)	3100–2250 BC (95.4%)

Table 1 Description (name, species [if known], institution, collector, lab nr, aggregation) and conventional and calibrated ages of the samples from Glanów Site 3 (19°47′W, 50°18′N). Age range has been determined with confidence levels of 68% and 95% using the OxCal v3.8 program. The numbers in brackets are the percent of age range in the total probability density distribution of the calibrated age. The system of aggregations on the site are shown in Figure 6. *(Continued)*

Name, sample description	Lab nr	Aggregation	^{14}C age (BP)	Age range (68%) (cal AD, BC)	Age range (95%) (cal AD, BC)
29. Glanów G3/97/7174 *Quercus sp.* Archeological Museum in Kraków, (Zając 1997)	Gd-12430	NW	4110 ± 70	2870–2800 BC (16.8%) 2760–2570 BC (50.4%) 2510–2500 BC (1.0%)	2880–2490 BC (95.4%)
30. Glanów G3/97/8112 *Pinus sylvestris*, Archeological Museum in Kraków (Zając 1997)	Gd-30014	NE	3930 ± 170	2850–2800 BC (1.2%) 2700–2100 BC (67.0%)	2900–1950 BC (95.4%)
31. Glanów G3/97/7694 *Pinus sylvestris*, Archeological Museum in Kraków (Zając 1997)	Gd-11445	E	3790 ± 90	2400–2370 BC (3.7%) 2350–2120 BC (55.9%) 2090–2040 BC (8.6%)	2500–1950 BC (95.4%)
32. Glanów G3/97/7177 *Pinus sylvestris*, *Quercus sp.* Archeological Museum in Kraków (Zając 1997)	Gd-10826	NE	3780 ± 70	2330–2320 BC (1.1%) 2310–2120 BC (57.3%) 2090–2040 BC (9.8%)	2460–2020 BC (94.4%) 2000–1980 BC (1.0%)
33. Glanów G3/97/5805 *Quercus sp.* Archeological Museum in Kraków (Zając M 1997)	Gd-15385	NW	3720 ± 90	2290–2250 BC (6.0%) 2240–1970 BC (62.2%)	2500–1800 BC (95.4%)
34. Glanów G3/96/3611 *Pinus sylvestris*, Archeological Museum in Kraków (Zając 1996)	Gd-10754	S	3670 ± 140	2290–1870 BC (66.8%) 1840–1820 BC (1.4%)	2500–1650 BC (95.4%)
35. Glanów G3/97/6548 *Pinus sylvestris*, *Quercus sp.* Archeological Museum in Kraków (Zając 1997)	Gd-14011	NE	3460 ± 130	1950–1600 BC (68.2%)	2150–1450 BC (95.4%)
36. Glanów G3/97/7942 *Pinus sylvestris*, Archeological Museum in Kraków (Zając 1997)	Gd-14013	NE	3240 ± 130	1690–1390 BC (67.4%) 1330–1320 BC (0.8%)	1900–1100 BC (95.4%)
37. Glanów G3/97/7087 *Pinus sylvestris*, *Corylus avellana*, Archeological Museum in Kraków, (Zając 1997)	Gd-10833	NW	3170 ± 70	1520–1380 BC (64.5%) 1340–1320 BC (3.7%)	1620–1260 BC (95.4%)
38. Glanów G3/97/7672 *Pinus sylvestris*, *Corylus avellana*, Archeological Museum in Kraków (Zając 1997)	Gd-12121	E	2900 ± 60	1220–990 BC (68.2%)	1290–910 BC (95.4%)
39. Glanów G3/97/8312 *Pinus sylvestris*, Archeological Museum in Kraków (Zając 1997)	Gd-15383	NW	2530 ± 80	800–750 BC (13.4%) 730–520 BC (54.8%)	810–400 BC (95.4%)
40. Glanów G3/97/6088 *Pinus sylvestris*, Archeological Museum in Kraków (Zając 1997)	Gd-12119	NW	2470 ± 60	770–680 BC (23.0%) 670–610 BC (16.6%) 600–510 BC (22.3%) 470–450 BC (2.6%) 440–410 BC (3.7%)	780–400 BC (95.4%)
41. Glanów G3/97/8533 *Pinus sylvestris*, Archeological Museum in Kraków (Zając 1997)	Gd-13004	NE	2460 ± 210	850–350 BC (67.0%) 300–250 BC (1.2%)	1100 BC–beginning AD

Table 2 Description (name, material, institution, collector, lab nr) and conventional and calibrated ages of the samples from the Chwalim site (15°46′W, 52°08′N). Age range has been determined with confidence levels of 68% and 95% using the OxCal v3.8 program. The numbers in brackets are the percent of age range in the total probability density distribution of the calibrated age.

Name and sample description	Lab nr	^{14}C age (BP)	Age range (68%) (cal AD, BC)	Age range (95%) (cal AD, BC)
1. Chwalim WKT III/79-2, charcoal, PAN in Poznań,Kobusiewicz M, 1979	Gd-1164	9565 ± 90	9150–8790 BC (68.2%)	9250–8600 BC (95.4%)
2. Chwalim WKT I/76-2 charcoal	Bln-1766	9500 ± 75	9120–8990 BC (29.2%) 8910–8870 BC (4.7%) 8860–8720 BC (28.7%) 8710–8690 BC (3.6%) 8660–8640 BC (2.0%)	9200–8600 BC (95.4%)
3. Chwalim WKT III/77-2 wood, PAN in Poznań, Kobusiewicz M 1979	Gd-1165	9385 ± 75	8780–8760 BC (1.7%) 8750–8540 BC (64.7%) 8490–8480 BC (1.7%)	9150–8950 BC (6.3%) 8900–8300 BC (89.1%)
4. Chwalim WKT I/77-2a(1) peat, PAN in Kraków, Wasylikowa 1977 palinological profile	Gd-6342	6950 ± 100	5970–5950 BC (5.2%) 5910–5720 BC (63.0%)	6010–5660 BC (95.4%)
5. Chwalim WKT I/77-2a(2) peat, PAN in Kraków, Wasylikowa 1977 palinological profile	Gd-6366	5550 ± 100	4500–4320 BC (60.9%) 4290–4250 BC (7.3%)	—
6. Chwalim WKT I/77-2a(3) peat, PAN in Kraków, Wasylikowa 1977 palinological profile	Gd-6449	4870 ± 100	3780–3620 BC (49.1%) 3600–3520 BC (19.1%)	3950–3350 BC (95.4%)
7. Chwalim WKT II/79-4,5c charcoal, PAN in Poznań, Kobusiewicz M, 1979	Gd-1176	4630 ± 70	3620–3600 BC (1.8%) 3530–3340 BC (65.0%) 3150–3140 BC (1.3%)	3650–3100 BC (95.4%)
8. Chwalim WKT I/77-4 peat, PAN in Kraków, Wasylikowa K, 1977	Gd-5831	4570 ± 60	3500–3460 BC (7.9%) 3380–3310 BC (22.8%) 3240–170 BC (20.1%) 3160–3100 BC (17.4%)	3520–3410 BC (16.0%) 3390–3080 BC (79.4%)
9. Chwalim WKT I/77-4(1) charcoal	Bln-2018	4375 ± 50	3090–3060 BC (6.2%) 3030–2910 BC (62.0%)	3310–3230 BC (5.2%) 3110–2880 BC (90.2%)
10. Chwalim WKT I/77-4(2) charcoal	Bln-2019	4280 ± 45	3010–2990 BC (2.1%) 2930–2870 BC (61.0%) 2810–2780 BC (5.2%)	3020–2860 BC (80.6%) 2810–2750 BC (11.8%) 2730–2700 BC (3.0%)
11. Chwalim WKT II/76-4 wood	Bln-1767	3900 ± 50	2470–2300 BC (68.2%)	2560–2540 BC (1.0%) 2500–2200 BC (94.4%)

Table 3 Description (name, material, institution, collector, lab nr, culture level) and conventional and calibrated ages of the samples from the Całowanie site (21°17′W, 52°01′N). Age range has been determined with confidence levels of 68% and 95% using the OxCal v3.8 program. The numbers in brackets are the percent of age range in the total probability density distribution of the calibrated age.

Name, sample description	Lab nr	Culture level[a]	^{14}C age (BP)	Age range (68%) (cal AD, BC)	Age range (95%) (cal AD, BC)
1. Całowanie IX/3c charcoal, PAN in Warsaw (Schild)	CAMS-20890	1,*2*,*3*, *4a*,*4b*[1]	11,890 ± 70	12,140–11,850 BC (62.9%) 11,750–11,690 BC (5.3%)	13,300–12,700 BC (11.8%) 12,400–11,500 BC (83.6%)
2. Całowanie IX/5a(1) charcoal, PAN in Warsaw (Schild)	Gd-2882	4a	11,770 ± 160	12,100–11,500 BC (68.2%)	13,300–12,800 BC (7.7%) 12,400–11,200 BC (87.7%)
3. Całowanie X/6(1) charcoal, PAN in Warsaw (Schild 1968)	Gd-4165	3	11,470 ± 200	11,900–11,700 BC (12.5%) 11,650–11,200 BC (55.7%)	12,200–10,900 BC (95.4%)
4. Całowanie X/6(2) charcoal, PAN in Warsaw (Schild)	GrN-5967	3	11,380 ± 95	11,500–11,230 BC (68.2%)	11,850–11,700 BC (10.0%) 11,600–11,050 BC (85.4%)
5. Całowanie IX/5a(2) charcoal, PAN in Warsaw (Schild)	GrN-5410	4a	11,190 ± 65	11,390–11,310 BC (14.2%) 11,260–11,060 BC (54.0%)	11,800–11,750 BC (1.3%) 11,500–10,950 BC (94.1%)
6. Całowanie IX/5c charcoal, PAN in Warsaw (Schild 1969)	Gd-2723	*5*	10,900 ± 130	11,190–11,110 BC (13.6%) 11,100–10,890 BC (54.6%)	11,250–10,650 BC (95.4%)
7. Całowanie VII/6 charcoal, PAN in Warsaw (Schild)	GrN-5253	—	10,820 ± 90	11,050–10,860 BC (56.5%) 10,780–10,710 BC (11.7%)	11,200–10,650 BC (95.4%)
8. Całowanie III/6 charcoal, PAN in Warsaw (Schild)	GrN-4966	—	10,660 ± 100	10,950–10,670 BC (56.9%) 10,520–10,450 BC (11.3%)	11,050–10,350 BC (94.0%) 10,300–10,200 BC (1.4%)
9. Całowanie IX/8 charcoal, PAN in Warsaw (Schild)	GrN-5409	6a	10,455 ± 90	10,850–10,750 BC (5.9%) 10,700–10,350 BC (53.8%) 10,300–10,150 BC (8.5%)	10,900–10,000 BC (95.4%)
10. Całowanie VI/XI/7a charcoal, PAN in Warsaw (Schild 1967)	Gd-5202	—	10,180 ± 100	10,350–10,300 BC (1.1%) 10,200–9600 BC (65.3%) 9550–9450 BC (1.9%)	10,400–9300 BC (95.4%)
11. Całowanie VII/9b(1) charcoal, PAN in Warsaw (Schild 1983)	Gd-1648	*6b, 6c*	10, 140 ± 80	10,050–9400 BC (68.2%)	10,400–9350 BC (95.4%)
12. Całowanie VII/9b(2) wood, PAN in Warsaw (Schild 1983)	Gd-2147	*6b, 6c*	10,030 ± 120	9800–9300 BC (68.2%)	10,400–9200 BC (95.4%)
13. Całowanie III/9a charcoal, PAN in Warsaw (Schild R)	GrN-5254	*6c*	9935 ± 110	9680–9670 BC (0.9%) 9610–9510 BC (17.4%) 950–9240 BC (49.9%)	10,050–9200 BC (95.4%)

Table 3 Description (name, material, institution, collector, lab nr, culture level) and conventional and calibrated ages of the samples from the Całowanie site (21°17′W, 52°01′N). Age range has been determined with confidence levels of 68% and 95% using the OxCal v3.8 program. The numbers in brackets are the percent of age range in the total probability density distribution of the calibrated age. *(Continued)*

Name, sample description	Lab nr	Culture level[a]	^{14}C age (BP)	Age range (68%) (cal AD, BC)	Age range (95%) (cal AD, BC)
14. Całowanie VII/9b(3) wood, PAN in Warsaw (Schild 1983)	Gd-1662	6b, 6c	9750 ± 80	9290–9130 BC (60.0%) 8990–8940 BC (8.2%)	9400–8800 BC (95.4%)
15. Całowanie VII/11b(1) wood, PAN in Warsaw (Schild 1966)	Gd-1717	6c, 7	9700 ± 80	9250–9110 BC (45.1%) 9000–8910 BC (20.4%) 8880–8860 BC (2.6%)	9280–8800 BC (95.4%)
16. Całowanie VI/IX/7a charcoal, PAN in Warsaw (Schild)	GrN-5255	—	9550 ± 85	9140–8980 BC (32.8%) 8940–8780 BC (32.6%) 8770–8740 BC (2.9%)	9250–8600 BC (95.4%)
17. Całowanie 11a(1) charred plants, PAN in Warsaw (Schild)	CAMS-20867	*7, 8*	9510 ± 70	9120–8990 BC (31.1%) 8910–8870 BC (6.3%) 8860–8720 BC (27.7%) 8710–8690 BC (2.3%) 8660–8650 BC (0.8%)	9200–8600 BC (95.4%)
18. Całowanie IX/11b charcoal, PAN in Warsaw (Schild 1969)	Gd-2734	*6a, 6b, 6c, 7, 8*	9410 ± 110	9150–9000 BC (10.5%) 8850–8450 BC (57.7%)	9150–8300 BC (95.4%)
19. Całowanie 9b charred plants, PAN in Warsaw (Schild)	CAMS-20870	*6c*	9390 ± 70	8750–8550 BC (68.2%)	9150–9000 BC (6.1%) 8900–8300 BC (89.3%)
20. Całowanie 11b(1) wood, PAN in Warsaw (Schild 1966)	Gd-1721	*6a, 6b, 6c, 7, 8*	9380 ± 80	8790–8760 BC (2.4%) 8750–8540 BC (63.3%) 8500–8470 BC (2.5%)	9150–8950 BC (6.5%) 8900–8300 BC (88.9%)
21. Całowanie 11b(2) wood, PAN in Warsaw (Schild 1966)	Gd-1719	*6a, 6b, 6c, 7, 8*	9370 ± 60	8740–8550 BC (67.3%) 8490–8480 BC (0.9%)	9100–9000 BC (1.0%) 8800–8300 BC (94.4%)
22. Całowanie 11b(3) wood, PAN in Warsaw (Schild 1966)	Gd-2198	*6a, 6b, 6c, 7, 8*	9350 ± 100	8750–8450 BC (67.4%) 8350–8340 BC (0.8%)	9150–8950 BC (5.3%) 8900–8250 BC (90.1%)
23. Całowanie VII/11b(2) charcoal, PAN in Warsaw (Schild)	GrN-5251	7, *8*	9250 ± 55	8560–8410 BC (51.4%) 8400–8330 BC (16.8%)	8610–8290 BC (95.4%)
24. Całowanie VII/11b(3) charcoal, PAN in Warsaw (Schild)	GrN-5442	7, *8*	9200 ± 75	8530–8500 BC (3.9%) 8480–8290 BC (64.3%)	8610–8270 BC (95.4%)

Table 3 Description (name, material, institution, collector, lab nr, culture level) and conventional and calibrated ages of the samples from the Całowanie site (21°17′W, 52°01′N). Age range has been determined with confidence levels of 68% and 95% using the OxCal v3.8 program. The numbers in brackets are the percent of age range in the total probability density distribution of the calibrated age. *(Continued)*

Name, sample description	Lab nr	Culture level[a]	^{14}C age (BP)	Age range (68%) (cal AD, BC)	Age range (95%) (cal AD, BC)
25. Całowanie 11b(4) wood, PAN in Warsaw (Schild 1983)	Gd-2149	6a, 6b, 6c, 7, 8	9080 ± 100	8520–8510 BC (0.7%) 8480–8200 BC (66.3%) 8040–8020 BC (1.2%)	8600–7950 BC (95.4%)
26. Całowanie VII/11b(4) wood, PAN in Warsaw (Schild 1966)	Gd-3041	6a, 6b, 6c, 7, 8	9030 ± 50	8290–8215 BC (68.2%)	8410–8390 BC (1.1%) 8300–8160 BC (82.3%) 8140–8080 BC (4.1%) 8050–7960 BC (7.9%)
27. Całowanie 11a(2) wood, PAN in Warsaw (Schild 1983)	Gd-1667	*6a, 6b, 6c, 7, 8*	8780 ± 80	8200–8050 BC (4.9%) 8000–7650 BC (63.3%)	8250–7600 BC (95.4%)
28. Całowanie 11a(3) wood, PAN in Warsaw (Schild 1983)	Gd-1668	*6a, 6b, 6c, 7, 8*	8640 ± 80	7760–7580 BC (68.2%)	7950–7540 BC (95.4%)
29. Całowanie IX/11a charcoal, PAN in Warsaw (Schild)	GrN-5966	*7, 8*	8360 ± 75	7530–7320 BC (68.2%)	7580–7290 BC (85.8%) 7270–7240 BC (2.8%) 7230–7180 BC (6.8%)
30. Całowanie 11a(4) wood, PAN in Warsaw (Schild 1983)	Gd-1670	*6a, 6b, 6c, 7, 8*	8300 ± 70	7520–7500 BC (2.6%) 7480–7300 BC (55.8%) 7230–7180 BC (9.8%)	7530–7130 BC (94.0%) 7100–7080 BC (1.4%)
31. Całowanie 11a(5) charred cones, PAN in Warsaw (Schild 1983)	Gd-2146	*6a, 6b, 6c, 7, 8*	8270 ± 100	7480–7170 BC (66.1%) 7160–7140 BC (2.1%)	7530–7070 BC (95.4%)
32. Całowanie 11a(6) wood from post, PAN in Warsaw (Schild 1983)	Gd-2610	younger than 8	2610 ± 40	830–780 BC (65.7%) 775–765 BC (2.5%)	900–870 BC (1.4%) 840–750 BC (83.6%) 690–660 BC (4.2%) 640–590 BC (4.4%) 580–550 BC (1.8%)

[a]Plain numbers: the assignation of ^{14}C date to culture level is certain
Italic numbers: the assignation of ^{14}C date to culture level is uncertain.

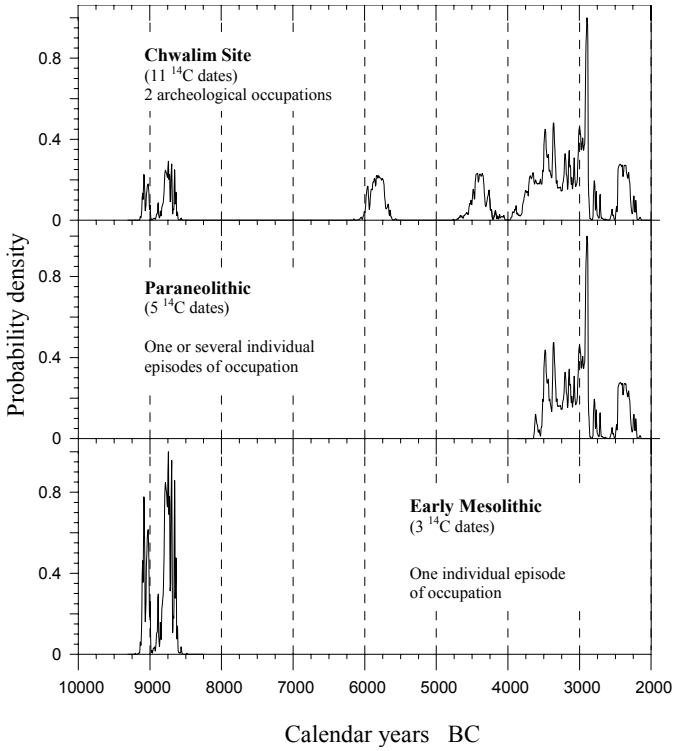

Figure 4 Cumulative probability density distributions of calibrated ^{14}C ages with the division into archaeological cultures from the Chwalim site.

In the case of the Całowanie site, this division was also assisted by the notable stratigraphy found in examined sections. This site has 11 culture levels associated with specific stratigraphic levels. Only 10 from 32 ^{14}C dates fit into the archaeological level from which they were selected (level I: CAMS 20868; level III: Gd-4165, Gd-5967; level IVa: Gd-2882, GrN-5410; level V: Gd-2723; level VIa: GrN-5409; level VII: GrN-5251, GrN-5442; level VIII: GrN-5966) (Table 3). The remaining 22 ^{14}C dates do not fit into the cultural levels precisely and the majority of them fit into several cultural levels simultaneously. The levels without ^{14}C dates are II, IVb, VIb, and VIc. The set of ^{14}C results and associated cultural levels are presented in Table 3.

Additionally, Figure 6 illustrates the cumulative probability density distributions of calibrated ^{14}C ages with the division into Glanów site 3 aggregations. The aggregations were established on the basis of the Mesolithic flint tools. These tools were grouped into 4 clusters (NE, E, NW, S) and each group was archaeologically identified as different (Figure 6a). Only flint tools and charcoals with ^{14}C ages older than 8000 BP were in agreement with archaeological stylistic determinations. Due to the possibility of stratigraphic problems within later levels of Glanów site 3, the aggregations are investigated for the Early Mesolithic only. The resultant distribution indicates the changes in settlement in the Early Mesolithic on Glanów site 3 terrain (Figure 6b, Table 1). The figure shows the probability density distributions of calibrated ^{14}C ages obtained on the basis of the ^{14}C calibration process. For the NE aggregation, 2 dates were calibrated, Gd-30016 and Gd-13003 (see also Table 1); for the E aggregation, 4 dates were calibrated, Gd-18161, Gd-17149, Gd-11413, and Gd-18160; the NW aggregation had 2 dates calibrated, Gd-17140 and Gd-10831; while the S aggregation also had 2 calibrated dates, Gd-10749 and Gd-12413. The comparison of the probability density distri-

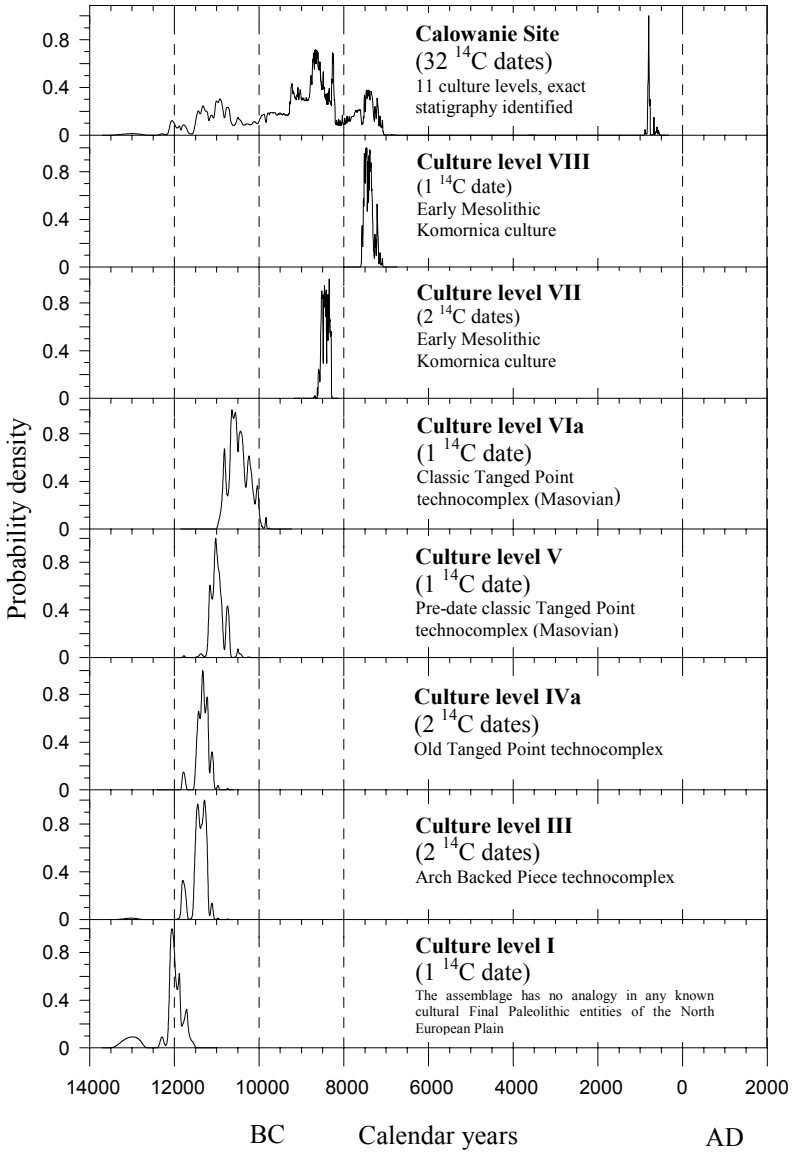

Figure 5 Cumulative probability density distribution of calibrated ^{14}C ages with the division into archaeological cultures from Całowanie Site.

butions of calibrated ^{14}C ages for all 4 aggregations illustrates the changes of settlement on Glanów site 3 terrain. In the age range of about 7940–7550 BC (Figure 6b), settlement activity took place on the NE, E, and NW. On the south part of Glanów site 3 for a similar age range, settlement activity did not occur. Similarly, in the period of about 7450–7050 BC (Figure 6b), human activity on the NE, E, and S aggregations was observed, while the NW aggregation in that age range did not practice husbandry. We also found the probability density distribution of calibrated ^{14}C ages for the NE aggregation shows the continuous settlement activity in all the age range of about 9500–6000 BC (Figure 6b), rising at the beginning and decreasing at the end of that period.

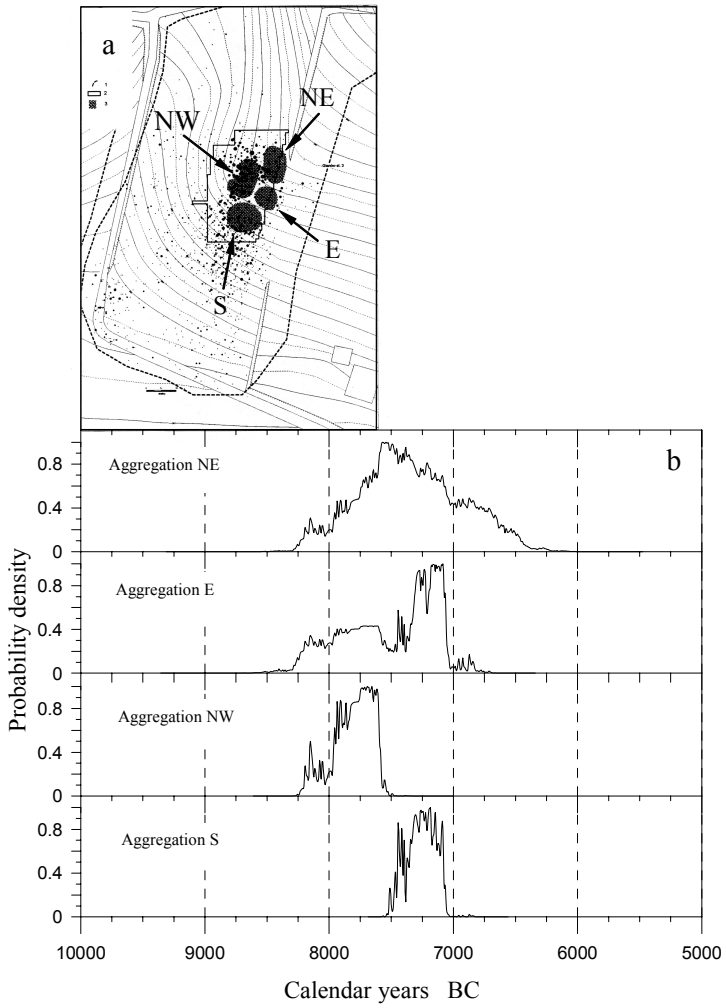

Figure 6 (a) Map of Glanów site 3 with the division into aggregations. The visible aggregations were identified into the Early Mesolithic on the basis of flint tools; (b) Probability distributions of calibrated ^{14}C ages from Glanów Site 3 aggregations. The cumulative probability density distributions show changes of settlement in the Early Mesolithic on this terrain.

SETTLEMENT PERIODS ON THE CLIMATIC BACKGROUND

In order to carry out analysis of climatic conditions, cumulative probability density distributions of calibrated ^{14}C ages from speleothems and peat formations from Poland were calculated. Results of the calculations are shown in Figure 7. The cumulative probability density distribution of calibrated ^{14}C ages from speleothems was done on the basis of 61 ^{14}C dates which belong in the time period ranging from 14,000 BC to AD 1. These dates were obtained from samples that come from caves in the south of Poland, Kraków–Wieluń Upland, where Glanów is situated (Pazdur et al. 1994, 1995).

Prior to calibration using OxCal v3.8, all ^{14}C dates from speleothems were corrected for a reservoir effect of 1350 yr (Pazdur et al. 1994, 1995). The comparison between cumulative probability density distributions of calibrated ^{14}C ages of speleothems and calibrated dates from Glanów site 3 shows

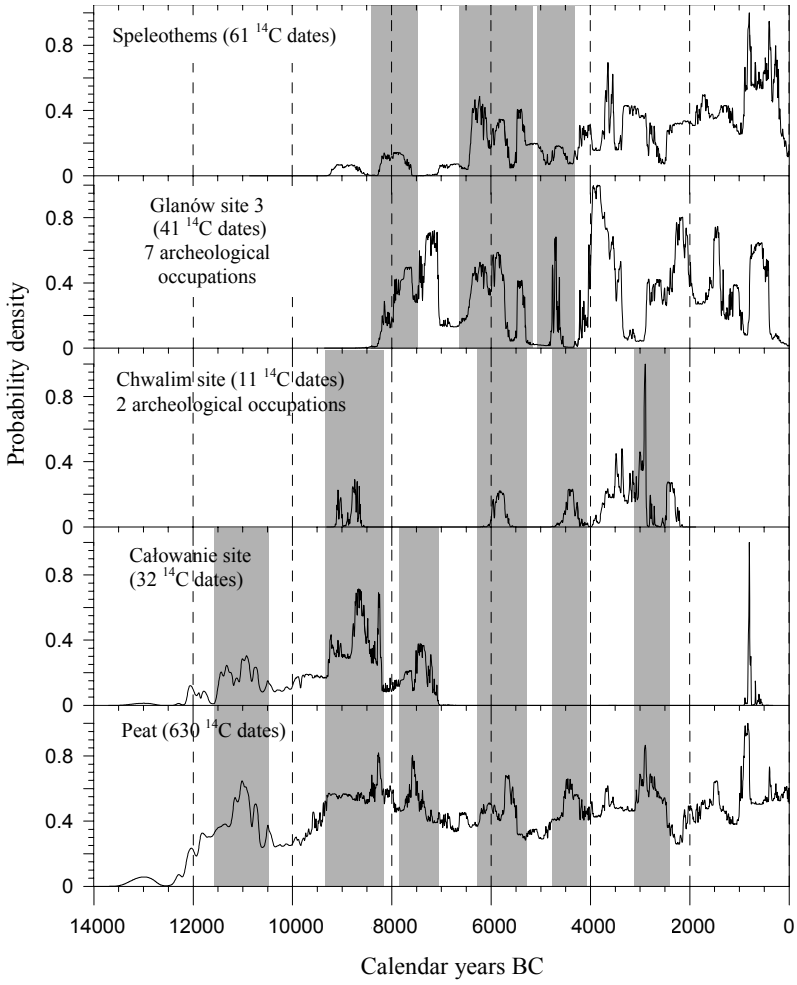

Figure 7 Comparison of probability distributions of calibrated ^{14}C ages from the Mesolithic sites in Glanów 3, Chwalim, and Całowanie. Additionally, the cumulative probability density distribution of calibrated ^{14}C ages from speleothems and peat from Poland are shown respectively on the top and bottom of the figure. These 2 cumulative probability density distributions illustrate the changes in climatic conditions. The grey fields indicate the coincidence between improving climatic conditions and an increase of human activities.

coincidence in the maxima at several Mesolithic time periods (Boreal period, about 8570–7530 BC [Figure 7]; at the beginning of the Atlantic period, about 7000–6500 BC; and in the Atlantic period at 6500–6100 BC, 6100–5500 BC, and 5500–5300 BC). Improving climatic conditions (maxima in the speleothems distributions; Figure 7) coincide with an increase of human activities in Glanów site 3. The increase in human activities creates a greater number of archaeological objects which allow a greater number of samples for each site and a higher number of dates for the sites to be obtained. A similar convergence of improving climatic conditions and an increase in human activities can be shown for the Chwalim and Całowanie sites (Figure 7). At the Całowanie and Chwalim sites, favorable conditions for the formation of peat are used as an indicator of mild climatic conditions. The 630 ^{14}C dates for statistical analysis were taken from peat sites distributed across Poland, with the exception of the Baltic coast (Michczyńska and Pazdur, unpublished data). The cumulative probability

density distribution of calibrated ^{14}C dates from peat indicates periods of humid/dry climatic conditions (Figure 7). Maxima on the distribution are related to the humid climatic conditions and the highest human activity in the site at Całowanie and Chwalim (about 9000–8000 BC, 6000–5500 BC, 4750–4000 BC, 3000–2250 BC for the Chwalim site, and about 11,500–10,500 BC, 9250–8250 BC, 7750–7250 BC for the Całowanie site; Figure 7), while minima (the dry climatic conditions; Figure 7) coincide with lower human activity.

CONCLUSIONS

This study reviewed the results of ^{14}C dating from 3 Mesolithic sites in Poland and the cumulative probability density distributions of calibrated ^{14}C ages. Archaeological cultural determinations and site stratigraphy (where appropriate) were used to fit the time ranges into appropriate cultural associations. Additionally, correlation between formation of speleothems and peat as indicators of the climatic conditions and the development of human settlements was investigated. Comparison of the cumulative probability density distributions of settlements with cumulative probability density distributions from speleothems and peat bogs shows systematic relations between these distributions and the correlation between the initiation and growth of settlements and climatic conditions.

ACKNOWLEDGEMENTS

This study was sponsored by the Silesian University of Technology through grant BW/RMF1/2003.

REFERENCES

Gąssowski J. 1985. *Kultura Pradziejowa na ziemiach polski. Zarys* (Primeval culture on the Polish land. Outline). Chapter 2. p 49–67. In Polish.

Godłowski K, Kozłowski JK. 1983. *Historia starożytna ziem polskich* (Ancient history of the Polish land). Chapter 1 and 3. p 5–17 and 23–57. In Polish.

Goslar T, Hercman H, Pazdur A. 2000. Comparison of U-series and radiocarbon dates of speleothems. *Radiocarbon* 42(3):403–14.

Kobusiewicz M, Kabaciński J. 1993. Chwalim. Subboreal hunter-gathers of the Polish plain. Poznań: IAiE PAN. p 76–9.

Kobusiewicz M. 1999. Ludy łowiecko-zbierackie północno-zachodniej Polski (Hunter-gathers on the northwestern part of Poland). Poznań: Prace Komisji Archeologii19, PTPN. In Polish.

Michczyńska JD, Pazdur A. Forthcoming. Shape analysis of cumulative probability density function of radiocarbon dates set in the study of climate change in the Late Glacial and Holocene. *Radiocarbon*, these proceedings.

Pazdur A, Pazdur MF. 1986. Aparatura pomiarowa Laboratorium ^{14}C w Gliwicach. Doświadczenia Konstrukcyjne i Eksploatacyjne (The measuring equipment of the Gliwice Radiocarbon Laboratory. Experience gathered in the construction and exploitation). *Zeszyty Naukowe Politechniki Śląskiej, Geochronometria* 1:55–69. In Polish.

Pazdur A, Pawlyta J, Spahiu P. 2000. Comparison of the radiocarbon dating methods used in the Gliwice Radiocarbon Laboratory. *Geochronometria* 18:9–13.

Pazdur A. 1987. Skład izotopowy węgla i tlenu holoceńskich martwic wapiennych. (Isotopic composition of carbon and oxygen in Holocene limestones). *Zeszyty Naukowe Politechniki Śląskiej, Geochronometria* 3:1–93. In Polish.

Pazdur A, Pazdur MF, Hercman H, Gorny A, Olszewski M. 1994. Wstępne wyniki badań nad chronologią powstawania nacieków w jaskiniach Wyżyny Krakowsko-Wieluńskiej, *Zeszyty Naukowe Politechniki Śląskiej, Ser. Mat.-Fiz., Z. 71*, *Geochronometria* 10: 61–79.

Pazdur A, Pazdur MF, Pawlyta J, Górny A, Olszewski M. 1995. Paleoclimatic implications of radiocarbon dating of speleothems from the Kraków-Wieluń Upland, southern Poland. In: Cook GT, Harkness DD, Miller BF, Scott EM, editors. Proceedings of the 1994 Radiocarbon Conference. *Radiocarbon* 37(2):103–10.

Pazdur A, Goslar T, Pawlyta M, Hercman H, Gradziński M. 1999. Variations of isotopic composition of carbon in the karst environment from southern Poland, present and past. *Radiocarbon* 41(1):81–97.

Ramsey CB. 2002. OxCal Program v3.8. University of Oxford Radiocarbon, Accelerator Unit. <http:/www.rlaha.ox.ac.uk/orau/06_01.htm>.

Schild R. 1975. Późny paleolit (Late Paleolithic). In: Chmielewski W, Hensel W, editors. *Prahistoria ziem polskich. Paleolit i mezolit* 1:159–338. In Polish.

Schild R. 1989. Datowanie radiowęglowe otwartych stanowisk piaskowcowych późnego paleolitu i mezolitu. Czy mezolit w Europie trwał do drugiej wojny światowej? (Radiocarbon dating of the Paleolithic and

the Mesolithic open-air sandy sites. Did the Mesolithic in Europe last until World War Two?). *Zeszyty Naukowe Politechniki Śląskiej*, *Geochronometria* 6: 153–63. In Polish.

Schild R. 1989. The formation of homogeneous occupation units ("Kshemenitsas") in open-air sandy site and its significance for the interpretation of Mesolithic flint assemblages. In: Bonsall C, editor. *The Mesolithic in Europe. Papers presented at the Third International Symposium. Edinburgh 1985*. p 89–98.

Schild R. 1996. Radiochronology of the Early Mesolithic in Poland. In: Larsson L, editor. The Earliest Settlement of Scandinavia and its Relationships with Neighboring Areas. *Acta Archaeologica Lundensia* 24(8): 285–95.

Schild R. 1998. The perils of dating open-air sand sites of the North European Plain. In: Zvelebil M, Domanska L, Dennell R, editors. *Harvesting the Sea, Farming the Forest. The Emergence of Neolithic Societies in the Baltic Region.* p 71–6.

Schild R. 2001. Three reasons why it is likely that Early Mesolithic population in Poland was not aboriginal. In: Ginter B, Drobniewicz B, Kazior B, Nowak M, Połtowicz M, editors. *Problemy epoki kamienia na obszarze starego świata. Księga Jubileuszowa dedykowana Profesorowi Januszowi K. Kozłowskiemu* (Problems of Stone Age on the Old World Area. Jubilee Tome dedicated to J K Kozłowski). p 229–34.

Schild R, Tobolski K, Kubiak-Martens L, Pazdur MF, Pazdur A, Vogel JC, Stafford Jr TW. 1999. Stratigraphy, palaeocology and radiochronology of the site of Całowanie. In: Kobusiewicz M, Kozłowski JK, editors. *Post-Pleniglacial Re-Colonisation of the Great European Lowland. Folia Quaternaria* 70:239–68.

Zając M. 2001. Zabytki Mezolityczne w zbiorach Muzeum Archeologicznego w Krakowie i ich znaczenie dla poznania mezolitu strefy wyżynnej w Polsce (The Mesolithic monuments in Archeological Museum in Kraków). *Materiały Archeologiczne* XXXII: 19–36. In Polish.

RADIOCARBON, Vol 46, Nr 2, 2004, p 827–830

^{14}C SOURCES AND DISTRIBUTION IN THE VICINITY OF LA HAGUE NUCLEAR REPROCESSING PLANT: PART I—TERRESTRIAL ENVIRONMENT

M Fontugne[1,2] • D Maro[3] • Y Baron[4] • C Hatté[1] • D Hebert[2] • E Douville[2]

ABSTRACT. COGEMA-La Hague nuclear reprocessing plant in the Cotentin Peninsula (northwest France) releases in the atmosphere about 19 TBq.yr^{-1} of radiocarbon. Three experiments in a terrestrial environment with sampling of a bio-indicator like furze were performed in 1997, 1998, and 1999, and additional air samples in the chimney plume were measured. Results presented here establish the ^{14}C distribution in the La Hague environment and suggest that a part of the ^{14}C content in the vegetation near the coast results from a $^{14}CO_2$ degassing of seawater supplied with the liquid waste from the nuclear plant.

INTRODUCTION

The COGEMA-La Hague nuclear reprocessing plant is located in the northwest part of the Cotentin Peninsula near Cherbourg, France. This nuclear plant releases radioelements in the atmosphere and in the English Channel. Radiocarbon is released to the environment as CO_2 through a 100-m-high chimney, and as liquid waste a few km off the shore, west of the reprocessing plant. Atmospheric ^{14}C releases are estimated to be 19 TBq.yr^{-1} (COGEMA data 2000).

The carbon dioxide is assimilated by plants through photosynthetic processes. Consequently, the ^{14}C activity of vegetation constitutes an integrated record of emissions from COGEMA-La Hague during the vegetative period (spring to fall). The aim of this study is to present the distribution of ^{14}C in the vicinity of the La Hague reprocessing plant.

MATERIALS AND METHODS

During 3 yr (1997–1999), the spring growth of furze was collected by the Laboratoire d'Etudes Radioécologiques de la Façade Atlantique (LERFA) and the Groupe d'Etudes Atomiques (GEA) at 70 stations (Figure 1). Twenty stations were chosen each year for ^{14}C analyses. The samples were prepared using classical methods (Delibrias 1985). The ^{14}C activity was measured by ß-counting in CO_2 proportional gas counters at the Laboratoire de Sciences du Climat et de l'Environnement (LSCE) at Gif/Yvette for years 1997 and 1998 and by benzene liquid scintillation at the University of Georgia (USA) for 1999 samples.

In the COGEMA-La Hague reprocessing plant, atmospheric releases of CO_2 through the chimney are not continuous and occur only during the opening of the nuclear fuel casing, about 10 to 15 times a day. Each release lasts for 30 to 40 min. CO_2 air samples were collected in the COGEMA plant downwind of the chimney plume at Digulleville (Eperons Mount), 1000 m north of the chimney, and at sea, southwest of the plant during the TE-SEA cruise (June 2000). Collection of air samples was done at ground level or 2 m above sea level. The chimney plume is detected by continuously measuring the ^{85}Kr activity (Maro et al. 2001), another gas released by COGEMA-La Hague.

CO_2 in a few liters of air was trapped by bubbling air in sodium hydroxide prepared a few hr before sampling to avoid contamination by sodium carbonate generally present within sodium hydroxide

[1]Laboratoire des Sciences du Climat et de l'Environnement, UMR 1572-CEA/CNRS, Domaine du CNRS, F-91198-Gif sur Yvette cedex, France.
[2]Corresponding author. Email: Michel.Fontugne@lsce.cnrs-gif.fr.
[3]Laboratoire de Radioécologie de Cherbourg-Octeville (IRSN/DEI/SECRE/LRC) F-50130 Cherbourg-Octeville, France.
[4]Marine Nationale, Groupe d'Etudes Atomiques (GEA), BP 34 F-50115-Cherbourg Naval, France.

Proceedings of the 18th International Radiocarbon Conference, edited by N Beavan Athfield and R J Sparks
RADIOCARBON, Vol 46, Nr 2, 2004, p 827–830

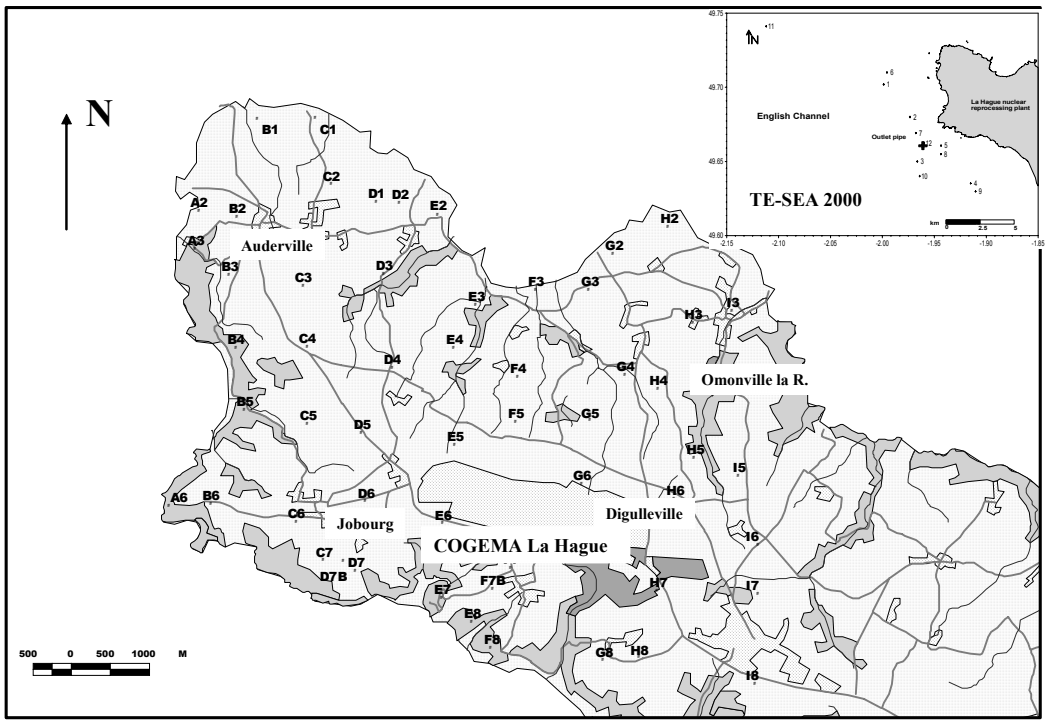

Figure 1 Location of the sampling points in the Cotentin Peninsula and during the TE-SEA cruise (June 2000)

tablets. During 30 min, bigger samples were also collected using a compressor that filled a 50-L bottle. Later, air in the bottle was bubbled in sodium hydroxide.

In the laboratory, barium hydroxide was added to the sodium hydroxide solution to get a precipitate of barium carbonate. This carbonate was then rinsed with degassed distilled water and dried at 50 °C before reaction with orthophosphoric acid under vacuum to evolve CO_2. Water used to prepare the solution was previously degassed. Precipitation, filtration of precipitate, and rinsing were performed under a controlled nitrogen atmosphere. The blank was determined following this procedure on the same solution used for sampling. Very active samples were mixed meticulously with dead carbonate before acid reaction and measurement by ß-counting. Samples were analyzed for ^{14}C activity using accelerator mass spectrometry (AMS) at the Gif AMS facilities or by ß-counting.

Results are expressed in Bq.kg^{-1} C (100 pMC = 226 Bq.kg^{-1} C). The standard deviation varies between 0.5 and 2% for Gif measurements and between 1.3 and 4.4% for the University of Georgia.

RESULTS AND DISCUSSION

^{14}C Activity in the Influence of the Chimney Plume

Results are reported in Table 1. Four samples near the chimney show ^{14}C activity ranging from 4700 to 9800 Bq.kg^{-1} C, with a mean value of 7200 Bq.kg^{-1} C. At sea, 4 to 6 km southwest of the plant, ^{14}C activity ranges between 426 to 908 Bq.kg^{-1} C. Outside the plume influence, the activity ranges between 257 to 291 Bq.kg^{-1} C, with a mean value of 271 Bq.kg^{-1} C, identical to that found at station 11 far to the northwest of the reprocessing plant (Fontugne et al. 2002). This value is slightly higher

than can be expected for unpolluted air. These results show a rapid dilution of the plume, the activity decreasing by a factor of 10 in a few km.

Table 1 ^{14}C activity (Bq.kg^{-1} C) in the chimney plume.

Sample reference	^{14}C activity (Bq/kg C)
Digullville (near COGEME-La Hague reprocessing plant)	
B1	4767 ± 71
B2	7821 ± 67
B3	6518 ± 23
B4	9783 ± 61
TE-SEA cruise	
6	428.9 ± 2.5
7	468.7 ± 2.7
8	435.1 ± 2.7
9	908.1 ± 3.2
10	426 ± 2.7
11[a]	271.1 ± 2.7

[a]Value for sea air samples outside the influence of the chimney plume.

^{14}C Activity in Furze

Results are reported in Table 2. ^{14}C activity varies between 250.5 and 587.1 Bq.kg^{-1} C. Reference samples were collected in Brittany, 300 km southwest from La Hague, and gave values between 252.6 and 254.3, in good agreement with ^{14}C activity in air and plants growing outside areas contaminated by industrial ^{14}C. Samples from La Hague clearly record the influence of the reprocessing plant, the activity varying between 1 to 2 times the reference activity. The ^{14}C distribution is similar for the 3 considered years (1997–1999) and clearly depends on the dominant wind direction, mainly a SW/ENE axis during the vegetative period. However, abnormally high values are found near the coast southwest of the plant at the extreme west of the peninsula, near Auderville and south of Jobourg. This excess of ^{14}C at the coast suggests a marine contribution through degassing from seawater of $^{14}CO_2$ originating from the liquid waste released at the pipe outlet south of the nuclear plant. The pCO_2 measurements in water indicate that the sea was a source of CO_2 for the atmosphere (Keir et al. 2001; Fontugne et al. 2002). Atmospheric ^{14}C values measured at sea outside of the chimney plume that are about 20 Bq.kg^{-1} C higher than atmospheric reference values (1997–1999) support the hypothesis of a marine contribution.

CONCLUSIONS

Measurements of ^{14}C activity in the chimney plume show a rapid dilution, from about 7200 Bq.kg^{-1} C near the chimney to values ranging between 400 and 900 Bq.kg^{-1} C at a distance of 4 to 6 km. Outside periods of release, the ^{14}C residual value is around 270 Bq.kg^{-1} C. Vegetation around the nuclear plant records these periods of release, concentration in bio-indicators ranging between 1 to 2 times the present atmospheric background. Higher ^{14}C concentrations are observed at the coast, suggesting a supplementary marine contribution though the degassing of the ^{14}C excess supplied by the liquid releases of the nuclear plant. This contribution has been estimated for year 2002 (Maro et al., these proceedings).

Table 2 ^{14}C activity (Bq.kg^{-1} C) in furze during years 1997, 1998, 1999.

1997		1998		1999	
A2	262.8 ± 2.6	A2	281.4 ± 1.4	A2	255.3 ± 8.0
A6	263.3 ± 2.6	A6	279.1 ± 1.7	A6	265.0 ± 7.8
B1	275.7 ± 2.8	B1	258.8 ± 1.8	B1	250.5 ± 3.3
C3	262.4 ± 2.6	C3	261.3 ± 1.0	C6	273.2 ± 12.0
C5	256.7 ± 2.6	C5	259.7 ± 1.6	D7	360.5 ± 6.2
C6	288.8 ± 2.9	C6	304.0 ± 2.4	E6	398.2 ± 9.3
C7	464.7 ± 4.6	C7	455.2 ± 4.6	E7	376.0 ± 12.7
E2	265.8 ± 2.7	D7	469.2 ± 2.3	F3	332.8 ± 8.8
E8	388.7 ± 3.9	E2	262.4 ± 0.8	F5	352.3 ± 7.0
F3	416.3 ± 4.2	E6	525.2 ± 3.7	G5	530 ± 8.8
F5	378.6 ± 3.8	E8	334.0 ± 2.3	G8	317.3 ± 8.5
G8	315.5 ± 3.2	F3	401.6 ± 1.2	H2	294.8 ± 11.5
H2	290.9 ± 2.9	F5	338.5 ± 2.0	H4	339.0 ± 11.2
I5	396.9 ± 4.0	G5	587.1 ± 4.7	I5	338.5 ± 11.0
I8	269.8 ± 2.7	G8	265.1 ± 1.6	I8	275.0 ± 8.0
ANSE CULERON	271.4 ± 2.7	H2	316.9 ± 1.6		
D7	461.5 ± 4.6	H4	272.1 ± 2.2	**Reference sample**	
E6	407.0 ± 4.1	I3	302.4 ± 1.5	ash leaves	243.7 ± 8.2
G5	365.0 ± 3.6	I5	353.2 ± 1.8		
H4	383.0 ± 3.8	I8	269.2 ± 1.1		
I3	299.2 ± 3.0				
		Reference samples			
		PEN MARC'H, furze	252.7 ± 1.3		
		LE CONQUET, oak	252.9 ± 1.0		
		A2-31/3/99	254.3 ± 2.5		

ACKNOWLEDGEMENTS

Thanks are due to Martine Paterne for helpful discussions, Rodger Sparks for reviewing the manuscript, and Maurice Arnold for AMS measurements of TE-SEA cruise samples. We thank Mr Le Bourhis and Mr Henri, captains of the crew of the R/V "Côtes de la Manche." TE-SEA and TRANSAT cruises were supported by CNRS.LSCE contribution nr 1101.

REFERENCES

COGEMA. 2000. Surveillance trimestrielle de l'environnement de la Hague. Rapport Hag. 055000120013. 84 p.

Délibrias G. 1985. Le carbone 14. In: Roth E, Poty B, editors. *Méthodes de Datation par les Phénomènes Nucléaires Naturels: Application*. Paris: Coll. CEA, Masson. p 421–58.

Fontugne M, Maro D, Baron Y, Hatté C, Hébert D, Douville E. 2002. Identification of sources and distribution of radiocarbon in the vicinity of La Hague nuclear reprocessing plant. *Radioprotection* 37(C1):1271–6.

Keir RS, Rehder G, Frankignoulle M. 2001. Partial pressure and air-sea flux of CO_2 in the Northeast Atlantic during September 1995. *Deep Sea Research Part II: Topical Studies in Oceanography* 48(14–15):3179–89.

Maro D, Crabol B, Germain. P, Baron Y, Hebert D, Bouisset P. 2001. A study of the near field atmospheric dispersion of emission at height: comparison of Gaussian plume models (Doury, Pasquill-Briggs, Caire) with krypton-85 measurements taken around La Hague nuclear reprocessing plant. *Radioprotection* 37(C1): 1277–82.

Maro D, Fontugne M, Hatté C, Hebert D, Rozet M. 2004. Source and distribution of radiocarbon in the vicinity of La Hague nuclear reprocessing plant: part II—marine environment. *Radiocarbon*, these proceedings.

RADIOCARBON, Vol 46, Nr 2, 2004, p 831–839

^{14}C SOURCES AND DISTRIBUTION IN THE VICINITY OF LA HAGUE NUCLEAR REPROCESSING PLANT: PART II—MARINE ENVIRONMENT

D Maro[1,2] • M Fontugne[3,4] • C Hatté[3] • D Hebert[1] • M Rozet[1]

ABSTRACT. Carbon dioxide partial pressure and radiocarbon activity were measured in air and seawater in the Bay of Seine and around the COGEMA-La Hague nuclear reprocessing plant (northwest France) during 3 cruises in 2000 and 2002. Results clearly show that the sea is a source of CO_2 and ^{14}C to the atmosphere. High ^{14}C concentrations in air and water related to the La Hague liquid waste are clearly recorded. For the restricted area of the Bay of Seine, CO_2 carbon and ^{14}C fluxes were estimated, indicating that less than 3% of the liquid ^{14}C release is introduced in the atmosphere.

INTRODUCTION

The COGEMA-La Hague nuclear reprocessing plant is located in the northwest of the Cotentin Peninsula, near Cherbourg (France). This nuclear plant releases radioelements in the atmosphere and in the English Channel. About 8.5 TBq.yr^{-1} of radiocarbon is released as liquid waste through a pipe a few km off the shore, west of the reprocessing plant (COGEMA data 2000). Recent studies in the peninsula (Fontugne et al., this issue) show anomalously high ^{14}C contents in vegetation near the coast which suggest a supplementary marine contribution through the degassing of the ^{14}C excess supplied by the liquid release of the nuclear plant.

The aim of this study is to estimate the ^{14}C fluxes between seawater and atmosphere in the northwest part of the Cotentin Peninsula and in the Bay of Seine.

MATERIALS AND METHODS

Methods

In order to estimate $^{14}CO_2$ fluxes across the surface seawater and the atmosphere interface, the partial pressure of carbon dioxide (pCO_2) was calculated using measurements of the total alkalinity and pH of water. According to Henry's law, the difference between pCO_2 in air and water indicates if seawater is a source of CO_2 to the atmosphere.

Carbon dioxide fluxes were calculated using Equation 1:

$$\Phi\ (CO_2)\ (\text{mole.m}^{-2}.\text{s}^{-1}) = K.\ S.\ \Delta pCO_2 \qquad (1),$$

where K (m.s^{-1}) is the CO_2 transfer coefficient between seawater and the atmosphere, S is solubility of CO_2 (mole.m^{-3}.atm^{-1}), and ΔpCO_2 (atm) is the difference between partial pressure in water and air. pCO_2 in air was considered as a constant mean value of 367 µatm according to values published by Copin-Montégut (1996), Boehme et al. (1998), Frankignoulle and Borges (2001), and Keir et al. (2001). K is a parameter depending on wind speed; its values are available in Liss and Merlivat (1986), Tans et al. (1990), or Wanninkhof and McGillis (1999). As these K values are slightly different in these 3 studies, we present the 3 CO_2 flux estimates.

[1]Laboratoire de Radioécologie de Cherbourg-Octeville (IRSN/DEI/SECRE/LRC), F-50130 Cherbourg-Octeville, France.
[2]Email: denis.maro@irsn.fr.
[3]Laboratoire des Sciences du Climat et de l'Environnement, UMR 1572-CEA/CNRS, Domaine du CNRS, F-91198-Gif sur Yvette cedex, France.
[4]Corresponding author. Email: Michel.Fontugne@lsce.cnrs-gif.fr.

Proceedings of the 18th International Radiocarbon Conference, edited by N Beavan Athfield and R J Sparks
RADIOCARBON, Vol 46, Nr 2, 2004, p 831–839

The exchange of CO_2 between the atmosphere and the surface seawater is an equilibrium process; the net CO_2 flux is the difference between gas going from water to air and gas going from air to water. Both these fluxes carry ^{14}C at concentrations appropriate to the medium from where they originate, and the net ^{14}C flux is, once again, the difference. The expression for the net ^{14}C flux from the ocean surface to the atmosphere is given in Equation 2:

$$\Phi(^{14}C) = [^{14}C]_O \, \Phi_{OA}(CO_2) - [^{14}C]_A \, \Phi_{AO}(CO_2) \quad (2).$$

Regarding the constant factor due to the use of appropriate units, ^{14}C fluxes were calculated following Equation 3:

$$\Phi(^{14}C)\ (Bq.km^{-2}.d^{-1}) = 10^9\ ([^{14}C]_O \, .\Phi_{OA} - [^{14}C]_A \, \Phi_{AO}) \quad (3),$$

where $[^{14}C]_O$ and $[^{14}C]_A$ are the ^{14}C concentrations ($Bq.Kg^{-1}C$) in the surface ocean and air, respectively, and Φ_{OA} and Φ_{AO} are the CO_2 fluxes ($mole.m^{-2}.s^{-1}$) from ocean to air, and air to ocean, respectively.

Sampling and Analytical Procedures

Seawater and air samples were collected simultaneously during 3 cruises (TE-SEA cruise, 1–4 June 2000; TRANSAT 1 cruise, 24–28 February 2002; and TRANSAT 2 cruise, 27–31 August 2002) around the northern Cotentin Peninsula and the Bay of Seine (Figure 1). During these cruises, krypton-85 (^{85}Kr) was measured continuously at a frequency of 1 measurement.s^{-1} (Maro et al. 2002). The detection of ^{85}Kr emitted from the chimney of the reprocessing plant allows air to be sampled for ^{14}C measurements free of direct contamination coming from the plume of the chimney. CO_2 in a few liters of air was trapped by bubbling air in sodium hydroxide solution. Sodium hydroxide was prepared a few hours before sampling to avoid contamination by sodium carbonate, generally present within sodium hydroxide tablets. In the laboratory, barium hydroxide was added to a sodium hydroxide solution to get a precipitate of barium carbonate. This carbonate was then rinsed with degassed distilled water and dried at 50 °C before reaction with orthophosphoric acid under vacuum to evolve CO_2. Water used to prepare the solution was previously degassed. Precipitation, filtration of precipitate, and rinsing were performed under a controlled nitrogen atmosphere. The blank was determined following this procedure on the same solution used for sampling.

Water samples were collected in glass bottles and poisoned with mercury chloride. In the laboratory, total CO_2 (ΣCO_2) was extracted from seawater following the procedure described by Bard et al. (1988) and Leboucher et al. (1999).

The temperature and salinity of seawater were measured using SBE 19-03 Seabird equipment, and wind direction and speed were recorded. For the TRANSAT cruises, CO_2 partial pressure in surface seawater was calculated using the pH and total alkalinity measurements following the "Standard Operating Procedures SOP3 and SOP6" of the US Department of Energy (DOE 1994).

The ^{14}C activity was measured at the Laboratoire de Sciences du Climat et de l'Environnement using the Gif accelerator mass spectrometry (AMS) facilities. Results are expressed in $Bq.kg^{-1}$ C (100 pMC = 226 $Bq.kg^{-1}$ C). The relative precision varies between 0.5 and 2%.

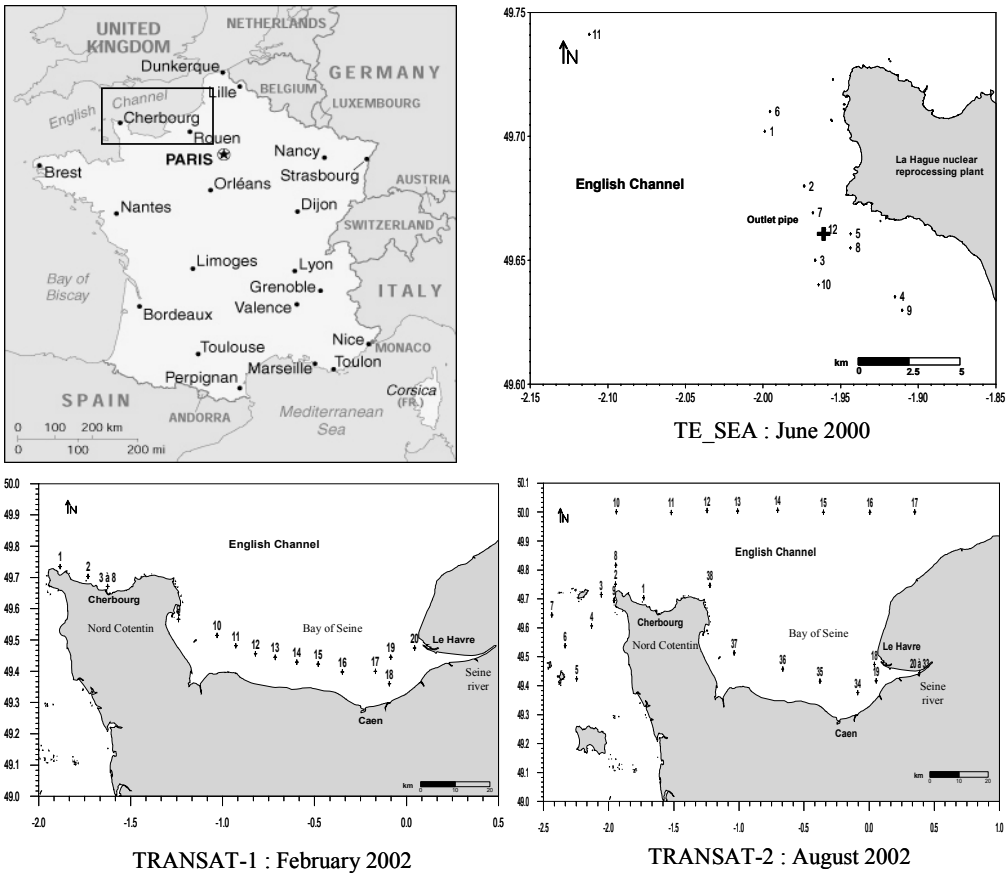

Figure 1 Location of sampling stations during the TE-SEA, TRANSAT 1, and TRANSAT 2 cruises

RESULTS AND DISCUSSION

Carbon Dioxide Flux

pCO_2 values (Figure 2 a, b) vary from 373 to 614 µatm for the TRANSAT 1 cruise data, and between 423 and 1408 µatm for TRANSAT 2 cruise data. pCO_2 measurements in water show similar high values compared to air during the winter and summer cruises and increase toward the Seine River estuary. This indicates CO_2 flux to the atmosphere since the mean atmospheric pCO_2 value is 367 µatm. These results are easily predictable because coastal, shelf, and estuarine areas exhibit high biological activity due to the nutrient input near the river mouths and organic matter recycling in the water column (Savoye et al. 2003). This heterotrophic activity, resulting in high degradation rates at the sediment surface and in the water column, produces high dissolved CO_2 concentrations (April 1999).

CO_2 fluxes to the atmosphere calculated from Equation 1 are reported in Figure 3 a, b. Carbon fluxes range from very few to 911 and 493 kg C $km^{-2}.d^{-1}$ for TRANSAT 1 and TRANSAT 2 cruises, respectively. These values are strongly dependent on the K transfer coefficient chosen (Liss and Merlivat [1986], Tan et al. [1990], or Wanninkhof and McGillis [1999]), the difference between estimations may vary by a factor of 2 or more, especially considering high wind speed.

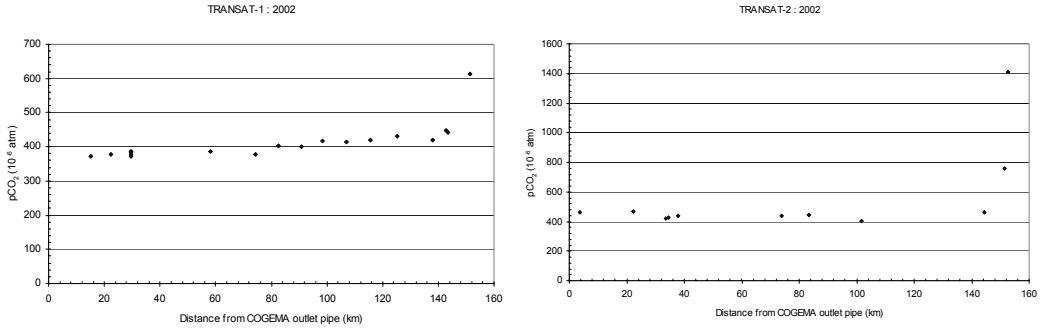

Figure 2 Variation of CO_2 partial pressure in surface seawater versus distance from pipe outlet during TRANSAT 1 and 2 cruises

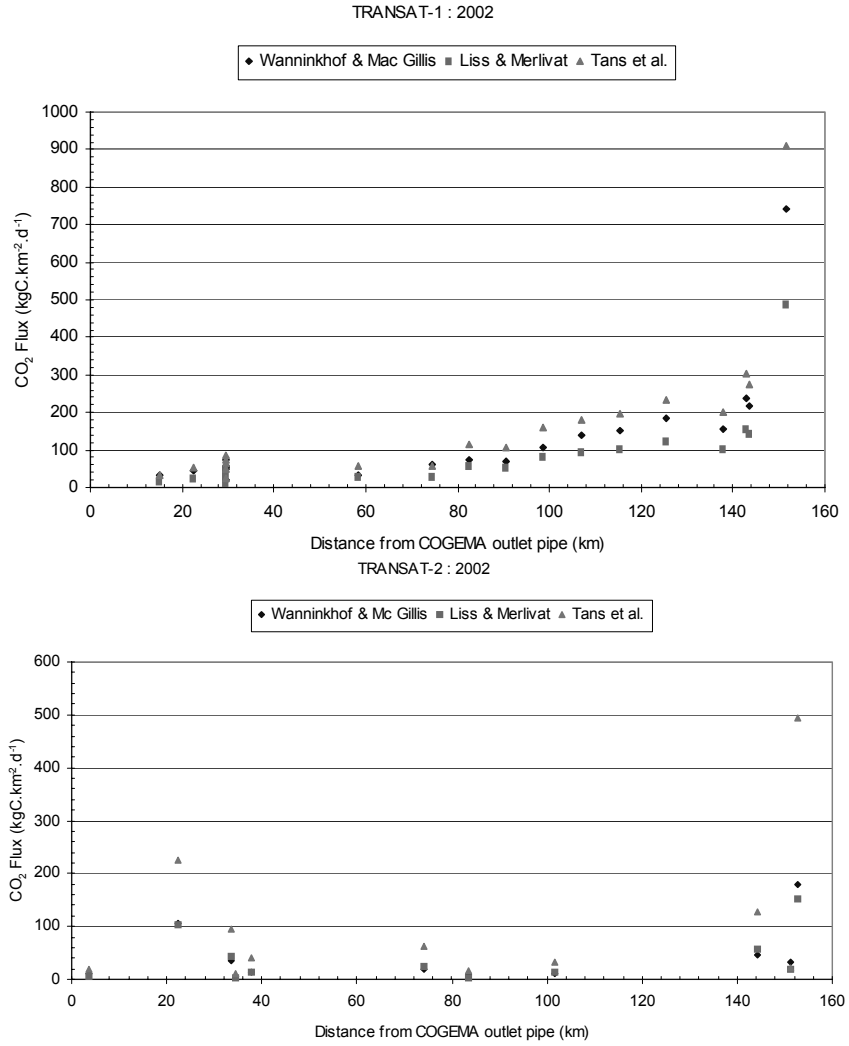

Figure 3 Variations of CO_2 fluxes versus distance from pipe outlet during TRANSAT 1 (above) and 2 (below) cruises

^{14}C Flux

Preliminary experiments performed during the TE-SEA cruise are reported in Table 1 and Figure 4. The ^{14}C activities of ΣCO_2 in seawater vary between 342.2 Bq.kg^{-1} at station 11 in the northwest part of the studied area to 580.8 Bq.kg^{-1} C near the mouth of the pipe. The values (except station 11) range between 479.6 to 580.8 Bq.kg^{-1} C, decreasing from south to north and recording clearly the plume and the dilution of waste. These values are about twice the reference values in 2000 (248 Bq.kg^{-1} C) for modern surface waters measured in Brittany, off Brest. ^{14}C values in air samples are more homogenous, varying between 257.6 to 292.2 Bq.kg^{-1} C. However, these values are higher than the atmospheric reference (248 Bq.kg^{-1} C).

Table 1 Location of sampling, distance from the pipe outlet, ^{14}C activity in seawater and air during the TE-SEA cruise. Shaded rows are under plume influence (see Fontugne et al., these proceedings).

Station TE-SEA	Latitude (N) (°)	Longitude (W) (°)	Distance (km)	^{14}C in water (Bq/kg C)	^{14}C in air (Bq/kg C)
1	49.70	2.00	5.2	480.7	268.5
2	49.68	1.97	2.2	506.0	279.1
3	49.65	1.96	1.5	527.0	257.6
4	49.63	1.92	4.4	562.3	269.8
5	49.66	1.94	1.2	520.3	259.4
6	49.71	2.00	5.9	479.6	428.9
7	49.66	1.97	0.9	539.7	468.7
8	49.66	1.94	1.4	559.6	435.1
9	49.63	1.91	5.1	557.8	908.1
10	49.64	1.96	2.5	506.2	426.0
11	49.74	2.11	14.0	342.2	271.2
12	49.66	1.96	0.0	580.8	292.2

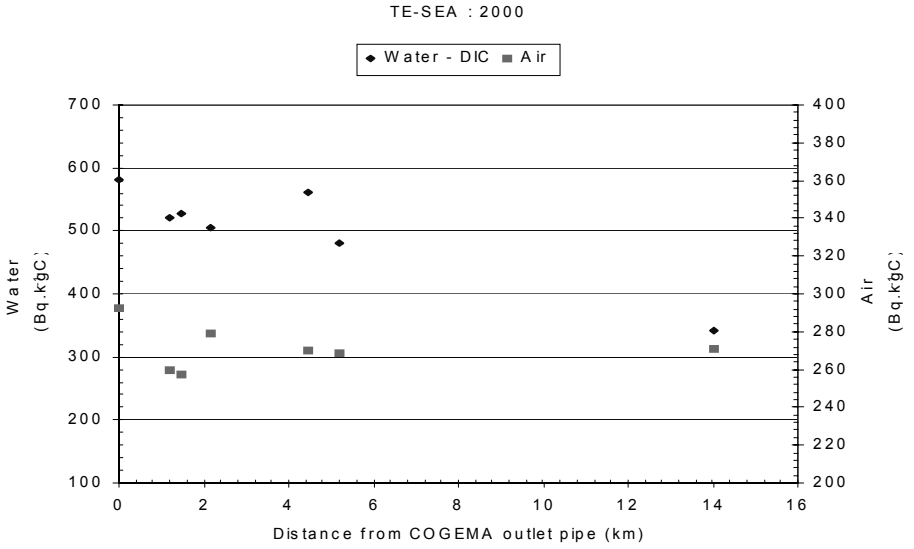

Figure 4 Variations of ^{14}C activities (Bq.kg^{-1} C) in surface seawater and air versus distance from the pipe outlet during the TE-SEA cruise

Table 2 Location of sampling, distance from the pipe outlet, ^{14}C activity in seawater and air, wind speed at 10 m, temperature, salinity, and CO_2 partial pressure in surface seawater during TRANSAT cruises.

Station	Latitude (N)	Longitude	Distance	[^{14}C] water	u10	Temperature	Salinity	pCO_2	[^{14}C] air
TRANSAT 1	(°)	(°)	(km)	(Bq/kg C)	(m/s)	(°C)	(pm)	(µatm)	(Bq/kg C)
1	49.73	1.88W	15.0	587.8	12.0	9.7	33.91	373.4	238.8
2	49.70	1.73W	22.4	—	11.0	9.8	33.86	378.6	—
3	49.67	1.63W	29.4	410.2	12.0	9.5	33.49	377.1	239.4
4	49.67	1.62W	29.6	—	11.0	9.5	33.61	386.3	—
5	49.67	1.62W	29.6	—	10.0	9.6	33.55	384.1	—
6	49.67	1.62W	29.6	—	10.0	9.6	33.42	386	—
8	49.67	1.62W	29.6	—	10.0	9.6	33.63	373.5	—
9	49.57	1.24W	58.3	378.4	8.0	8.7	33.01	387.5	237.1
10	49.51	1.03W	74.4	379.5	12.0	9.2	33.43	378.5	239.3
11	49.48	0.93W	82.5	—	9.0	8.8	33.05	402.8	—
12	49.46	0.82W	90.7	353.3	9.0	8.7	32.88	400.7	236.4
13	49.44	0.71W	98.5	—	9.0	8.6	32.41	416.8	—
14	49.43	0.60W	107.2	331.0	10.0	8.5	32.35	415.3	236.2
15	49.42	0.48W	115.5	—	10.0	8.5	32.31	419.9	—
16	49.40	0.35W	125.4	324.8	10.0	8.5	32.17	430.3	241.3
17	49.40	0.17W	137.9	—	10.0	8.5	32.37	421	—
18	49.39	0.09W	143.6	—	10.0	8.4	31.26	441.2	242.7
19	49.44	0.09W	142.8	—	10.0	8.4	31.65	448.6	—
20	49.47	0.04E	151.5	286.3	10.0	8.1	25.63	613.6	236.2
TRANSAT 2									
1	49.70	1.73W	22.40	342.5	7.3	17.9	34.78	465.7	226.4
5	49.42	2.25W	33.7	270.7	6.2	18.0	35.10	422.7	222.2
7	49.64	2.44W	34.4	—	3.4	16.7	35.10	424.0	—
9	49.69	1.96W	3.6	706.7	3.4	17.8	34.89	462.9	346.4
10	50.00	1.94W	37.7	281.6	4.1	17.1	35.06	438.0	240.9
13	50.00	1.01W	83.4	—	3.4	17.7	34.90	442.5	—
17	50.00	0.35E	175.4	343.6	1.8	18.6	34.56	452.0	262.6
18	49.47	0.04E	151.3	258.3	3.1	19.6	29.01	759.0	243.5
19	49.45	0.05E	152.7	—	5.9	19.5	22.40	1407.6	—
34	49.38	0.09W	144.4	—	5.5	19.4	31.66	464.3	—
36	49.46	0.66W	101.7	—	4.8	19.6	33.30	402.0	—
37	49.51	1.04W	74.0	351.5	4.6	18.7	34.35	441.0	262.2

During the TRANSAT cruises, ^{14}C activities in the surface seawater vary between 258.3 to 706.7 Bq.kg^{-1} C (Table 2). The highest value corresponds to a station within the plume of the liquid waste near the pipe outlet (Figures 5 a,b). All these values are higher than the reference value of 239 Bq.kg^{-1} C (year 2002). During TRANSAT 1, winter cruise atmospheric values are near the reference value mainly due to the stormy meteorological conditions which induce a greater mixing of the atmosphere. During the TRANSAT 2 summer cruise, ^{14}C activities in the air present a positive correlation with ^{14}C in surface water, confirming transfer from the sea.

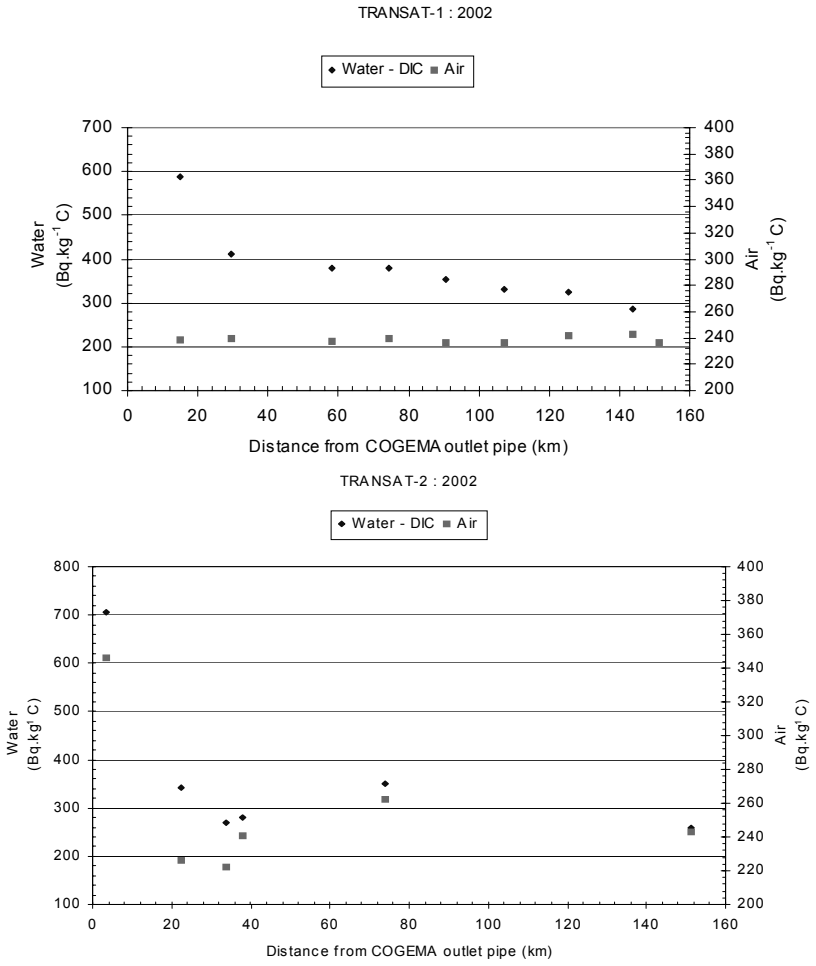

Figure 5 Variations of ^{14}C activities (Bq.kg^{-1} C) in surface seawater and air versus distance from pipe outlet during TRANSAT 1(above) and 2 (below) cruises

For each estimate of carbon dioxide flux, the ^{14}C fluxes were estimated using Equation 3. Maximum fluxes are 6.4 10^5 and 1.7 10^5 Bq.km^{-2}.d^{-1} for TRANSAT 1 and 2, respectively (Figures 6 a,b). During TRANSAT 1, the highest ^{14}C flux is encountered near the city of Cherbourg, and the lowest between Cherbourg and the Seine River estuary. The TRANSAT 2 cruise presents a maximum value near Cherbourg and a minimum value near the Seine River estuary due to lower CO_2 fluxes during these cruises (low wind speed near the Seine estuary). Following estimates derived from the Tans et al. model, the mean flux in the Bay of Seine due to the COGEMA-La Hague liquid waste would

reach 2.3 10^5 and 3.9 10^4 Bq.km^{-2}.d^{-1} for TRANSAT 1 and 2, respectively. A rough annual estimation would give 216 GBq for the 4400 km^{-2} of the Bay of Seine, representing less than 3% of the liquid release from COGEMA-La Hague nuclear reprocessing plant.

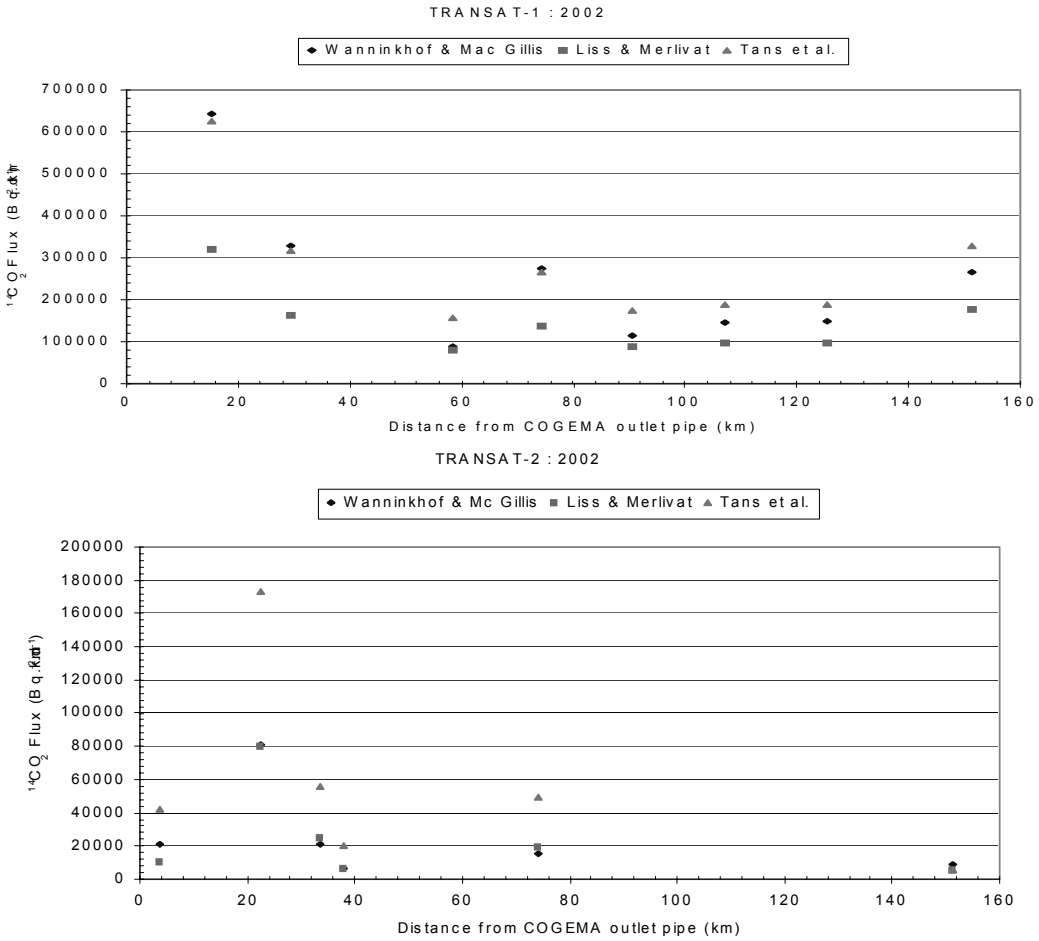

Figure 6 Variations of ^{14}C fluxes versus distance from pipe outlet during TRANSAT 1 (above) and 2 (below) cruises

CONCLUSIONS

Simultaneous measurements of CO_2 partial pressure and ^{14}C activity in air and seawater indicate that the English Channel and Bay of Seine are a source a carbon dioxide to the atmosphere in good agreement with previous studies. ^{14}C activities decrease from the west to the east according to the dilution of the waste plume of the plant. Estimations of CO_2 and ^{14}C flux show that a minor part of the ^{14}C liquid release by industrial activity is recycled to the atmosphere. These estimates are not very accurate due to the variation of CO_2 transfer coefficients proposed by different models. However, the ^{14}C releases in the Bay of Seine could provide a good opportunity to perform new experiments in order to get better estimates of CO_2 transfer coefficients between water and atmosphere.

ACKNOWLEDGEMENTS

Thanks are due to M Paterne for helpful discussions and M Arnold for AMS measurements and S Le Bar and M L Fitament from COGEMA for their help during the cruises. We are very grateful to Rodger Sparks for suggestions and corrections of the manuscript. We thank Mr Le Bourhis and Mr Henri captains of the crew of the R/V "Côtes de la Manche." TE-SEA and TRANSAT cruises were supported by CNRS.LSCE contribution nr 1102.

REFERENCES

Abril G. 1999. Dynamique du carbone dans les estuaires européens: processus de minéralisation et transfert continent-océan-atmosphère [PhD dissertation]. Université de Bordeaux I. p 173–209.

Bard E, Arnold M, Ostlund HG, Maurice P, Monfray P, Duplessy JC. 1988. Penetration of bomb radiocarbon in the tropical Indian Ocean measured by means of accelerator mass spectrometry. *Earth and Planetary Sciences Letters* 87:379–89.

Boehme SE, Sabine CL, Reimers CE. 1998. CO_2 fluxes from a coastal transect: a time-series approach. *Marine Chemistry* 63:49–67.

COGEMA. 2000. Surveillance trimestrielle de l'environnement de la Hague. Rapport Hag. 055000120013. 84 p.

Copin-Montégut G. 1996. *Chimie de l'eau de mer*. Paris: Institut Océanographique. 319 p.

Department of Energy (DOE). Dickson AG, Goyet C, editors. 1994. *Handbook of Methods for the Analysis of the Various Parameters of the Carbon Dioxide System in Seawater*. Version 2. ORNL/CDIAC-74.

Fontugne M, Maro D, Baron Y, Hatté C, Hébert D, Douville E. Sources and distribution of radiocarbon in the vicinity of La Hague nuclear reprocessing plant: part I—terrestrial environment. *Radiocarbon*, these proceedings.

Frankignoulle M, Borges AV. 2001. European continental shelf as a significant sink for atmospheric carbon dioxide. *Global Biogeochemical Cycles* 15(3):569–76.

Keir RS, Rehder G, Frankignoulle M. 2001. Partial pressure and air-sea flux of CO_2 in the Northeast Atlantic during September 1995. *Deep Sea Research Part II: Topical Studies in Oceanography* 48(14–15):3179–89.

Leboucher V, Orr J, Jean-Baptiste P, Arnold M, Monfray P, Tisnerat-Laborde N, Poisson A, Duplessy JC. 1999. Oceanic radiocarbon between Antarctica and South Africa along WOCE section I6 at 30°E. *Radiocarbon* 41(1):51–73.

Liss PS, Merlivat L. 1986. Air-sea exchange rates: introduction and synthesis. In: Buat-Ménard P, editor. *The Role of Air-Sea Exchange in Geochemical Cycling*. Hingham, Massachusetts: D Riedel Publishing Co. p 113–27.

Maro D, Crabol B, Germain. P, Baron Y, Hebert D, Bouisset P. 2002. A study of the near field atmospheric dispersion of emission at height: Comparison of Gaussian plume models (Doury, Pasquill-Briggs, Caire) with krypton-85 measurements taken around La Hague nuclear reprocessing plant. *Radioprotection* 37(C1):1277–82.

Savoye N, Aminot A, Tréguer P, Fontugne M, Naulet N, Kérouel R. 2003. Dynamics of particulate organic matter $\delta^{15}N$ and $\delta^{13}C$ during spring phytoplankton blooms in a microtidal ecosystem (Bay of Seine, France). *Marine Ecology Progress Series* 255:27–41.

Tans PP, Fung IY, Takahashi T. 1990. Observational constraints on the global atmospheric CO_2 budget. *Science* 247:1431–38.

Wanninkhof R, McGillis WR. 1999. A cubic relationship between air-sea CO_2 exchange and wind speed. *Geophysical Research Letters* 26(13):1889–92.

RADIOCARBON, Vol 46, Nr 2, 2004, p 841–851

TESTING THE USE OF BOMB RADIOCARBON TO DATE THE SURFACE LAYERS OF BLANKET PEAT

M H Garnett

NERC Radiocarbon Laboratory, East Kilbride, United Kingdom. Corresponding author. Email: m.garnett@nercrcl.gla.ac.uk.

A C Stevenson

University of Newcastle-Upon-Tyne, Newcastle-Upon-Tyne, United Kingdom.

ABSTRACT. The recently formed surface layers of peatlands are archives of past environmental conditions and can have a temporal resolution considerably greater than deeper layers. The low density and conditions of fluctuating water table have hindered attempts to construct chronologies for these peats. We tested the use of the radiocarbon bomb pulse to date recently accumulated peat in a blanket mire. The site was chosen because the peat profiles contained independent chronological markers in the form of charcoal-rich layers produced from known burning events. We compared chronologies derived from accelerator mass spectrometry ^{14}C analysis of plant macrofossils against these chronological markers. The bomb ^{14}C-derived chronologies were in broad agreement with the charcoal dating evidence. However, there were uncertainties in the final interpretation of the ^{14}C results because the pattern of ^{14}C concentration in the peat profiles did not follow closely the known atmospheric ^{14}C record. Furthermore, samples of different macrofossil materials from the same depth contained considerable differences in ^{14}C. Suggested explanations for the observed results include the following: i) minor disturbance at the site, ii) in-situ contamination of the ^{14}C samples by carbonaceous soot, and iii) differential incorporation of plant material during blanket peat growth.

INTRODUCTION

Peatlands are archives of past biodiversity, climate, and other environmental conditions (Barber 1993). The recently formed surface layers of peatlands are an archive for recent environmental information and offer an opportunity to understand how environmental conditions have been recorded in peat profiles by relating the proxy signals in the peat to recent historical records. Since they have not undergone the same decay and compression, the temporal resolution of surface peats can be considerably higher than deeper layers.

Several techniques are available for dating the surface layers of peats but are frequently hindered due to the low density of the peat and conditions of fluctuating water tables. For example, ^{210}Pb has been used successfully at some peatlands (e.g. Appleby et al. 1997), while at others the technique has failed due to mobility of the Pb (Oldfield et al. 1995). Other radiometric techniques, such as the peak in ^{137}Cs produced by nuclear weapons tests, have similarly proved unreliable due to mobility (Appleby et al. 1997). Although the historical deposition of pollutants such as Pb and Cu has been recorded in peat profiles, these have also been suspected of suffering from post-depositional migration (Clymo et al. 1990); these problems have also affected magnetic profiles (Clymo et al. 1990). The possibility of pollen migration in the low-density surface layers of peats has been demonstrated by Clymo and Mackay (1987), who question the chrono-stratigraphic value of changes in pollen composition in surface peats. Clearly, there is a need for more reliable methods to date the surface layers of peats.

DATING PEATS USING THE ^{14}C BOMB RECORD

Nuclear weapons tests in the 1950s–60s produced enough radiocarbon (bomb ^{14}C) to double the atmospheric content of ^{14}C. Long-term measurements of atmospheric ^{14}C have revealed a distinctive trend with a rapid ^{14}C increase from the late 1950s followed by a peak around 1963 (Levin and Hesshaimer 2000). Subsequently, atmospheric ^{14}C concentrations declined as the isotope dispersed into other components of the C cycle (Levin and Hesshaimer 2000).

Proceedings of the 18th International Radiocarbon Conference, edited by N Beavan Athfield and R J Sparks
RADIOCARBON, Vol 46, Nr 2, 2004, p 841–851

Goodsite et al. (2001) showed the potential of the bomb ^{14}C pulse for dating the surface layers of peats. The technique relies on the fact that stratified peat profiles provide a record of the plants that formerly grew on the mire surface. As the ^{14}C concentration in plant structures reflects the ^{14}C content of the atmosphere at the time of photosynthesis, stratified peat profiles contain a record of past atmospheric ^{14}C concentration. Since large changes in atmospheric ^{14}C occurred as a result of the bomb tests, it should be possible to calibrate the ^{14}C values of the recently formed peat by matching against the record of atmospheric bomb ^{14}C.

Although Tolonen et al. (1992) showed that the bomb ^{14}C pattern was recorded in peat stratigraphy, it was not successfully utilized for chronological purposes until the study on raised mires by Goodsite et al. (2001). No similar study has been performed on blanket peat, yet these peatlands are far more extensive in the UK than raised mires (Immirzi et al. 1992), and provide an important palaeoecological resource. In the present study, we aimed to test whether the bomb ^{14}C pulse could be used to derive chronologies for the surface layers of a blanket peat.

In the test, we compared a bomb ^{14}C-derived chronology with independent chronological markers in the same profile. A site in northern England presented a rare opportunity for this study because suitable independent chronological information had been recorded in the peat profile.

THE HARD HILL EXPERIMENT

The experiment at Hard Hill, Moor House (Figure 1) was established in 1954 to investigate the effects of moorland burning and grazing on the vegetation of mires (for site details, see Garnett et al. 2000). Replicated experimental plots have been treated to different moorland burning regimes for ~50 yr. Since we know the date of all burning events at the site, identification of charcoal layers in the stratigraphy provides an independent dating framework with which to assess the bomb ^{14}C signal.

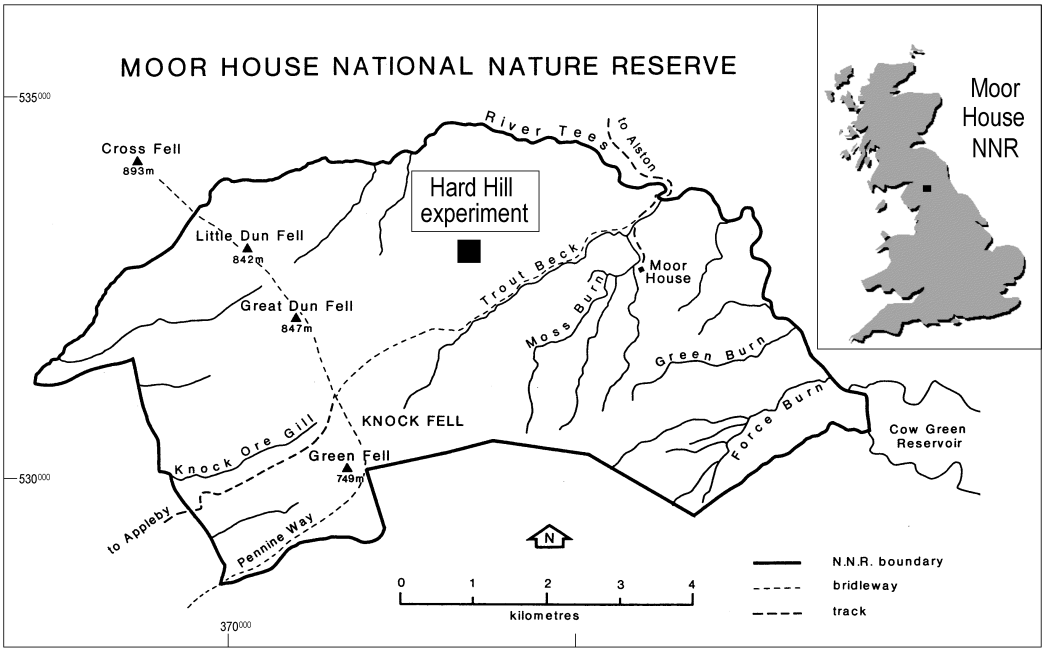

Figure 1 Location of the Hard Hill site within Moor House National Nature Reserve, northern England

All plots at Hard Hill were burnt at the start of the experiment in 1954 and, therefore, all should have a charcoal-rich layer formed as a result of this burning event. Plots which have continued to be burnt at decadal intervals ("burnt" plots) have diminished peat accumulation (Garnett et al. 2000). However, plots which have not been burnt since 1954, and lying adjacent to "burnt" plots, have received pulses of charcoal which have been recorded in the stratigraphy of the surface peat.

METHODS

We recorded the abundance of charcoal fragments in the profiles of 2 plots, one upwind and one downwind (in terms of the prevailing wind) of plots which have been burnt every 10 yr. We also determined the profile of spheroidal carbonaceous particles (SCP). These particles are produced by high temperature combustion of coal and oil and the profile of SCP concentration in sediments reflects regional industrialization; rapid increases in the concentration of SCP have been shown to occur in lake sediments formed in the 1950–60s in this region (Rose et al. 1995). By combining the charcoal and SCP evidence, we determined independent dating points against which we could compare a bomb ^{14}C-derived chronology.

Peat cores were collected in 1997 from 2 lightly sheep-grazed plots which had been burnt in 1954 only. Site A was immediately adjacent and downwind (i.e. to the north-east) of a plot burnt every 10 yr from 1954 and Site B (located ~200 m from Site A) was adjacent but upwind (i.e. to the south-west) of the nearest regularly burnt plot. One short peat core (diameter 10 cm and depth 21 cm) was retrieved from each of the 2 plots, with the coring locations being determined randomly.

The cores were collected by pushing a circular plastic tube into the peat surface and then removing by careful digging. The cores were retained in their tubes, sealed in plastic bags, and returned to the laboratory. A piston device was used to vertically extrude the cores, 1 cm at a time. Each cm of extruded peat was sliced off with a sharp knife, wrapped in aluminium foil, and stored in a refrigerator (~2 °C). A small amount of compression of the peat was observed during coring but was restricted to the surface few cm of the cores.

Rhodes (1998) method was used to quantify charcoal and was performed on sub-samples from each contiguous 1-cm section. After treating the sub-samples, the fragments of charcoal were counted using a microscope (Wild M3Z, Heerbrugg, Switzerland) at 40× magnification. A 10 × 10 square grid graticule was used to group the fragments according to size. SCP were enumerated in the same samples.

Plant macrofossils were selected for ^{14}C analysis at depth intervals which were expected to span the bomb ^{14}C pulse. *Sphagnum* macrofossils were preferentially sought, but where these were scarce, other above-ground plant macrofossils such as seeds and small fragments of heath species (*Erica sp./Calluna vulgaris*) were used. All moss samples were pretreated with a weak acid wash (1 M HCl) and heath fragments subjected to acid-alkali-acid pretreatment (2 M HCl, 1 M KOH, 1 M HCl). All samples were combusted in quartz tubes (900 °C) and prepared as graphite at the NERC Radiocarbon Lab and analyzed using accelerator mass spectrometry (AMS).

RESULTS

Charcoal and SCP Records

Figures 2 and 3 display the profiles of charcoal and SCP concentration in the samples from the study sites. The sites have very different charcoal profiles considered to be a result of Sites A and B being located respectively downwind and upwind of burnt plots; Ohlson and Tryterud (2000) have shown

that by far the greatest charcoal deposition occurs either within or immediately downwind of the area of the burn.

Site A

The top 12 cm of the profile from Site A contained much charcoal, as expected, because the site is adjacent and downwind of a plot burnt every 10 yr from 1954. The profile has distinct and regularly spaced peaks in charcoal. Since the most recent burn to have occurred actually on Site A was in 1954, we consider that this event is represented at 11–12 cm because this depth contains the greatest number of large charcoal fragments (indicating a very local fire). It is more likely that the smaller peaks in charcoal concentration above the 11–12 cm depth were produced by burns located near, but not on, the sampling site because large charcoal fragments were less abundant. We considered that these peaks in charcoal concentration represent the decadal burns of the adjacent plot.

The rapid increase in SCP concentration occurred at 8–10 cm depth, slightly above the 1954 charcoal layer. The SCP results are, therefore, consistent with the charcoal evidence; the rapid increase (1950–60s; Rose et al. 1995) occurs above the 1954 charcoal layer but has ceased at 8 cm, just above the layer interpreted as the 1965 charcoal layer (Figure 2). By combining the charcoal and SCP evidence, we considered that the peat profile at Site A provided 4 independent dating points (Figure 2).

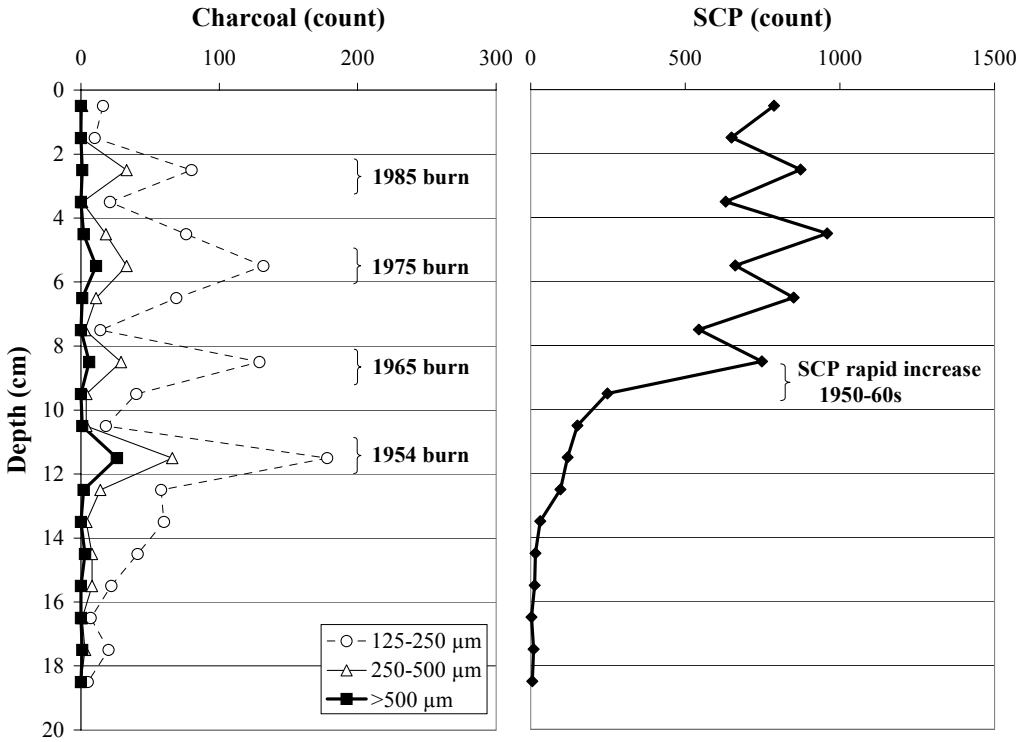

Figure 2 Concentration of different size classes of charcoal fragments and SCP concentration with depth, for Site A

Site B

Depths 9–10 cm and 12–13 cm contained the greatest quantities of large charcoal fragments, indicating a local fire, whereas there was an absence of large fragments above 9–10 cm depth (Figure 3). Since this site was last burnt in 1954, we consider that the most recent layer of large charcoal frag-

ments (9–10 cm) represents the 1954 burn, and that the deeper charcoal-rich layer represents an earlier fire. This interpretation implies that, although the plot was adjacent to sites which have been burnt every 10 yr since 1954, these fires have not been recorded as distinct charcoal layers, probably because Site B lies upwind of the burnt plots.

The SCP concentration at Site B rapidly increased in depths immediately above the 9–10 cm layer, supporting our interpretation that the layer of large charcoal fragments at 9–10 cm represents the 1954 burn. Thus, the peat profile at Site B provided 1 dating point from the charcoal and SCP results (Figure 3).

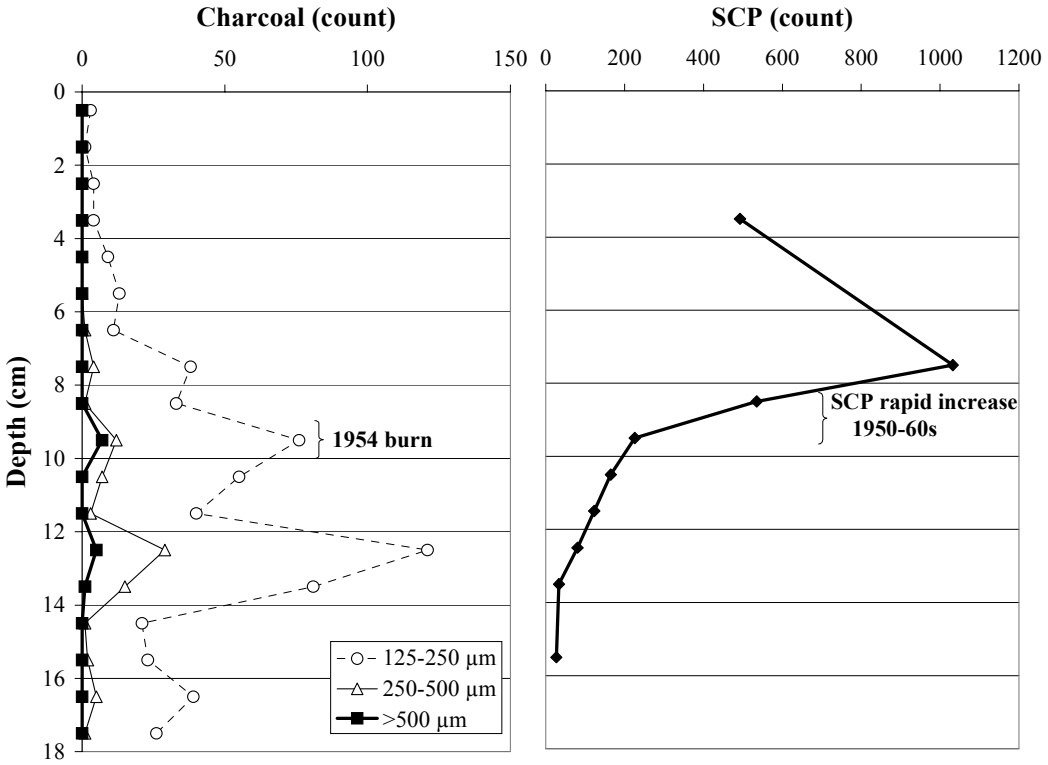

Figure 3 Concentration of different size classes of charcoal fragments and SCP concentration with depth, for Site B

^{14}C Results

Tables 1 and 2 present the ^{14}C results for Sites A and B, respectively. Samples from nearest the peat surface contained bomb ^{14}C (i.e. >100 pMC), whereas samples from below the 1954 charcoal layer had ^{14}C concentrations <100 pMC.

To convert the ^{14}C results to calendar ages, we used a database of atmospheric ^{14}C measurements from the Northern Hemisphere compiled from various sources (Baxter and Walton 1971; Levin and Kromer 1997; Nydal et al. 1980; Walton et al. 1970). We adopted the following calibration procedure: samples with a ^{14}C concentration >100 pMC were matched directly to the atmospheric ^{14}C record. In most cases, this yielded 2 solutions, one either side of the peak in bomb ^{14}C. To determine which of the 2 solutions was more likely, we considered the ^{14}C results for samples from adjacent

Table 1 Details of ^{14}C analyses for Site A.

Publication code	Depth (cm)	Material	^{14}C enrichment (pMC ± 1 σ)	^{14}C age BP ± 1 σ (if applicable)	$\delta^{13}C_{PDB}$ ± 0.1‰
AA-49834	3–4	*Calluna/Erica* leaves/stems	126.83 ± 0.71	—	–27.7
AA-42454	5–6	*Calluna/Erica* fragments	136.16 ± 0.51	—	–28.2
AA-49835	6–7(a)	*Calluna/Erica* leaves/stems	120.92 ± 0.86	—	–28.0
CAMS-91938	6–7(b)	Seeds (95%) and *Calluna/Erica* leaves	101.78 ± 0.35	—	–26.8
AA-42455	7–8	*Calluna/Erica* fragments	135.87 ± 0.55	—	–30.9
AA-42456	9–10	*Calluna/Erica* fragments	112.28 ± 0.48	—	–29.4
AA-42457	11–12	*Calluna/Erica* fragments	96.50 ± 0.44	286 ± 37	–29.1
AA-42458	13–14	*Calluna/Erica* fragments	97.96 ± 0.46	165 ± 38	–28.5

Table 2 Details of ^{14}C analyses for Site B.

Publication code	Depth (cm)	Material	^{14}C enrichment (pMC ± 1 σ)	^{14}C age BP ± 1 σ (if applicable)	$\delta^{13}C_{PDB}$ ± 0.1‰
AA-48953	3–4	Moss leaves	112.33 ± 0.55	—	–28.5
AA-48954	5–6	*Calluna*/*Sphagnum* leaves	136.12 ± 0.58	—	–29.2
CAMS-91936	6–7	Moss leaves and *Calluna*/*Erica* leaves	131.50 ± 0.58	—	–28.7
AA-48955	7–8	*Calluna* leaves and flower heads	130.91 ± 0.57	—	–28.2
AA-48956	9–10	*Sphagnum* leaves/stems	119.76 ± 0.54	—	–27.7
CAMS-91937	10–11	*Sphagnum* leaves	99.40 ± 0.46	50 ± 40	–26.7
AA-48957	11–12	*Sphagnum* leaves	90.95 ± 0.50	762 ± 44	–27.5

depths, and in most cases, could eliminate one of the solutions by assuming that samples from deeper in the peat profile would be older.

Calibration of the 2 samples located nearest the bomb ^{14}C peak was less straightforward. These samples had calibration solutions which fell either side of the bomb peak, and it was not possible to discount one of the solutions simply using the ^{14}C results. In such instances, we considered the rate of peat accumulation which would need to have occurred to result in the alternative calibration solutions. For both sites, only the calibration of these samples shown in Figures 4 and 5 resulted in realistic peat accumulation rates. For example, depths 5–6 cm and 7–8 cm at Site A could be interpreted to be the same age, however, this would imply unrealistic peat accumulation rates of 2 cm yr^{-1}; the only realistic interpretation resulted when the calibrated ages were split either side of the bomb peak.

Three ^{14}C results could not be calibrated against the atmospheric curve when considered with the other samples from the same profile. For Site A, 2 samples of different materials from the same slice of peat (6–7 cm depth) had very different ^{14}C concentrations, both of which were lower than the results for adjacent depths. Calibration of these samples could be performed by independently matching their ^{14}C concentrations to the atmospheric record, giving ages of AD 1960/1984 for the heath fragments and AD 1956 for the seeds. An age of AD 1984 is considered very unlikely for the heath fragments at 6–7 cm since it would make this depth layer younger than layers nearer the surface. Given typical peat accumulation rates of ~10 yr cm^{-1} (Clymo 1991), it is conceivable that different types of macrofossils selected from a 1-cm layer of peat could be at least 4 yr different in age, as in the 6–7 cm layer at Site A. However, when considered in conjunction with the ^{14}C results for the adjacent depths at this site, neither of the samples from depth 6–7 cm could be fitted to the atmospheric record, and, therefore, neither were used in the chronology that we have interpreted for this site.

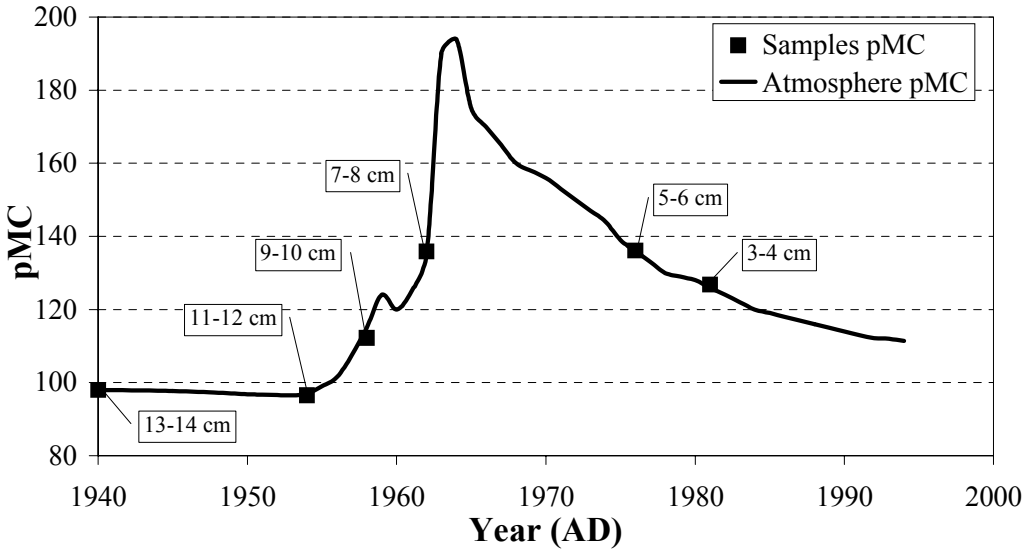

Figure 4 Calibration of ^{14}C AMS results for Site A. The chart shows our best interpretation of the results when matched to the atmospheric ^{14}C record. The symbols are larger than the 2-σ error of the ^{14}C measurements.

For Site B, the samples at depths 7–8 cm and 6–7 cm had very similar ^{14}C concentrations, both of which were lower than the sample at 5–6 cm. To calibrate these results, we again considered peat accumulation rates and chose the interpretation that resulted in more consistent rates of accumulation, rather than an alternative solution which implied very large variations in accumulation rate. Thus, we interpreted the sample at 7–8 cm to be AD 1962, and did not use the result for 6–7 cm in our final chronology (Figure 5). If we had used the result for depth 6–7 cm instead, this would have required much greater changes in peat accumulation rate over the depths between 6–10 cm; we have no stratigraphic evidence to support rapid changes in peat accumulation for this section of the profile.

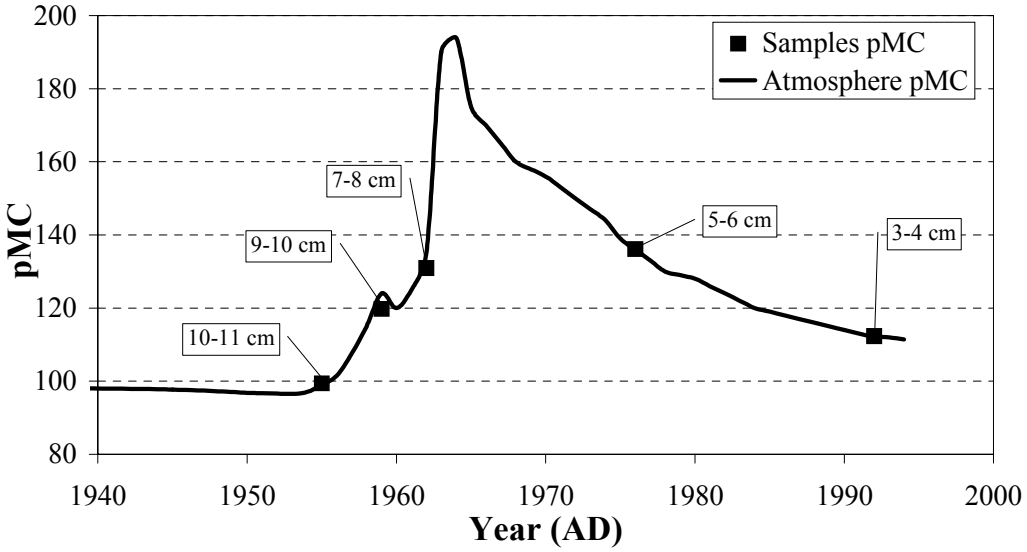

Figure 5 Calibration of ^{14}C AMS results for Site B. The chart shows our best interpretation of the results when matched to the atmospheric ^{14}C record. The symbols are larger than the 2-σ error of the ^{14}C measurements.

We matched samples with ^{14}C concentrations slightly less than 100 pMC to our atmospheric ^{14}C record, but because variations in pre-bomb ^{14}C were small, these calibrations have greater uncertainty. For Site A, the ^{14}C content of the sample from 11–12 cm (96.50 ± 0.44 pMC) best matched with a date of AD 1953 in our ^{14}C database, but was also calibrated using INTCAL98 (Stuiver et al. 1998) to cal AD 1520–1660 (1 σ). Since the ^{14}C concentration of the deeper sample at 13–14 cm [97.96 ± 0.46 pMC; cal AD 1660–1950 (1 σ)] was greater than at 11–12 cm, we consider that the AD 1953 date was the best interpretation for the 11–12 cm layer. Therefore, we consider that the 11–12 cm depth represents the period when the Suess effect had caused greatest depletion of atmospheric ^{14}C, immediately prior to the rapid ^{14}C increases caused by bomb testing. Although we suggest in Figure 4 that the sample at 13–14 cm represents AD 1940 (since this is the best match on our database of atmospheric ^{14}C), we have no evidence to determine whether this date or the INTCAL98 calibrated date is better. The deepest sample from Site B had a much lower ^{14}C concentration than the other samples, and was calibrated using INTCAL98 to cal AD 1220–1290 (1 σ).

Our interpretations of the ^{14}C results are shown in Figures 4 and 5. Although we acknowledge that other interpretations are possible, we consider our interpretations are best when based solely on the ^{14}C results.

DISCUSSION

It is difficult to test new methods for dating surface peats because many of the existing dating techniques which could be used to validate a new technique have themselves been shown to be unreliable. In the present study, the Hard Hill site presented a rare opportunity because it contained suitable independent dating evidence which we consider to be reliable; the large size and distinct peaks in concentration strongly suggests the charcoal is not mobile.

Figure 6 shows the age-depth relationship derived using the bomb ^{14}C chronology for Sites A and B. The independent charcoal-dated layers are also shown to allow comparison of the dating evidence. Our interpretation of the ^{14}C results produced a chronology that closely matched the independent chronology derived from the charcoal record; of the 5 charcoal layers, three were dated to within 1 yr of the known burning event using the bomb ^{14}C-derived chronology (Figure 6). The bomb ^{14}C-derived ages differed from the remaining 2 charcoal-derived ages by only 5 yr. These results show that bomb ^{14}C can be useful for dating the surface layers of blanket peat.

However, there were a number of problems encountered which introduced uncertainty to the results. No sample had a ^{14}C concentration >140 pMC, although atmospheric ^{14}C exceeded 190 pMC (Levin and Hesshaimer 2000). Macrofossils for ^{14}C analysis were picked from 1-cm-thick slices and would contain an average ^{14}C content for the number of years it took for 1 cm of peat to accumulate; Figure 6 indicates that peat growth rates were ~3–5 yr cm^{-1}. Therefore, we expected a greater peak in ^{14}C concentration of the macrofossils. Other causes of a "damped" ^{14}C signal in the peat include possible recycling of "old" carbon from decomposing peat (Tolonen et al. 1992) and contamination with SCP; these particles adhere strongly to macrofossils (Punning and Aliksaar 1997), are fossil fuel derived (would dilute the ^{14}C signal), and were abundant in levels where bomb ^{14}C should have been highest (Figures 2 and 3). ^{14}C analyses of macrofossils by Goodsite et al. (2001) approached 180 pMC; however, the raised mires in their study were more remote from large industrial areas (and therefore SCP sources) and accumulation rates were greater (~2.5 yr cm^{-1}).

Two samples of different macrofossil material were analyzed from depth 6–7 cm at Site A, and neither could be matched to the atmospheric ^{14}C record when considered with the other samples.

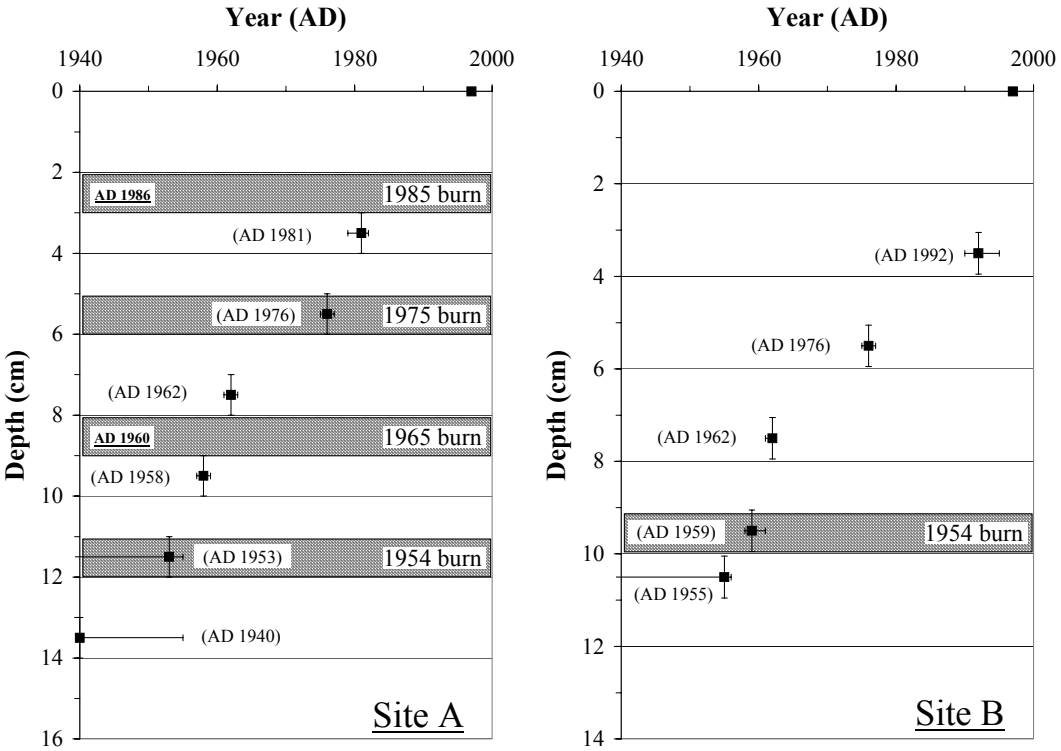

Figure 6 Age-depth relationship for Sites A and B based on the calibration of the ^{14}C results shown in Figures 4 and 5. Shading represents the layers with greatest charcoal concentration which have been dated by reference to the known record of burning. The calibrated ages for the ^{14}C samples are given in brackets. Horizontal error bars are 2-σ age ranges of the calibrated ^{14}C results and vertical error bars represent the sampling resolution (i.e. 1-cm slices). Linear interpolation of the ^{14}C results was used to calculate ages for two of the charcoal-rich layers, which had not been analyzed for ^{14}C (underlined).

Despite being from the same slice of peat, the samples had very different ^{14}C concentrations (~121 and 102 pMC). The ^{14}C differences could have been due to differences in the way the plant materials were incorporated into the accumulating peat at a time when atmospheric ^{14}C concentrations were changing rapidly, or may simply represent plant materials that grew over slightly different years but were ultimately compacted into the same 1-cm layer of peat. Alternatively, there may have been different levels of SCP contamination in the samples since Punning and Aliksaar (1997) found sorption of SCP to *Sphagnum* was (slightly) species dependent; the relative sorption of particles to the entirely different plant materials used in the present study is unknown but could well be greater than the differences between *Sphagnum* species. Also, the other dating results imply this depth relates to the 1960s to the early 1970s, a time when scientific activity at the site was intense; therefore, site disturbance may have been a factor. It is possible that some of the plant macrofossils used for ^{14}C analysis could have been blown in from an upwind disturbed site. However, unless they were from eroding peat, these macrofossils would have a similar ^{14}C concentration to the contemporary vegetation; there were no eroding peat surfaces close to the sampling sites when the cores were collected.

Sphagnum macrofossils were preferentially selected for ^{14}C analysis as recommended by Kilian et al. (1995) but also because *Sphagnum* leaves were considered likely to have a smaller in-built age compared to heath fragments. However, an additional source of uncertainty arose because in some depths the peat was highly decayed and *Sphagnum* macrofossils were scarce, meaning that alterna-

tive materials had to be used for ^{14}C analysis. Where only heath macrofossils were available, we selected fragments which would have the least in-built age. Heath species (e.g. *Calluna vulgaris*) can survive at least 25–30 yr (Hobbs and Gimmingham 1987). Yet, due to the rapid changes in ^{14}C associated with the bomb pulse, it would only require a few years of in-built age for the sample to have a ^{14}C content unrepresentative of the age of the peat layer. Despite taking precautions to avoid analyzing materials with in-built ages, the paucity of suitable dating material in some levels meant that heath fragments were the best material for analysis. The in-built age of these samples may explain some of the difficulties encountered when calibrating the ^{14}C results. However, for the 2 samples from depth 6–7 cm at Site A, it would be expected that the heath leaves/stems (6–7a) would have a greater in-built age than the seeds sample (6–7b), and, therefore, that the leaves/stems would have a ^{14}C content representative of a few years earlier than the seeds. In fact, when these samples were calibrated independently of the others, the results suggested that the seeds were older than the leaves/stems.

The burnt plot adjacent to Site A has been burned on 4 occasions following 1954 (i.e. 1965, 1975, 1985, 1994); however, there are only 3 charcoal peaks (in addition to the 1954 layer) in the charcoal record (Figure 2). Linear interpolation of the ^{14}C-derived chronology for Site A suggests that the charcoal produced in the 1994 burn should be located in the top 1 cm of the profile, but there is no peak in charcoal concentration for this layer (Figure 2). An explanation may be that the surface layer of peat has not yet undergone the same amount of decomposition as deeper layers. Also, whereas the peat decays, the charcoal does not. Therefore, with time, the relative concentration of charcoal will increase in a given weight of peat. Since as much as 90% of the organic matter entering the surface of a peat may be lost through decomposition (Clymo 1984), the effect would be to multiply the charcoal concentration up to a factor of 10. Therefore, as the peat which formed the surface 1-cm layer of the mire in 1997 is buried by subsequent peat growth and progressively decays, a charcoal peak representing the 1994 burn may become evident.

Peat accumulation rates and preservation of macrofossils can be much lower in blanket peats compared to raised mires (e.g. Goodsite et al. 2001). These conditions make blanket peats less suitable for dating using the bomb ^{14}C approach since lower accumulation rates dampen the ^{14}C signal and poor preservation means less suitable macrofossils are available for ^{14}C analysis. Despite these disadvantages, the results of the present study show that the bomb ^{14}C approach can be useful for dating the surface layers of blanket peats.

ACKNOWLEDGEMENTS

We thank Jacky Garnett for fieldwork assistance, John Adamson for discussions, and English Nature for permission to use the Hard Hill site. Part of this work was supported by the University of Newcastle-Upon-Tyne, the former Institute of Terrestrial Ecology (now CEH) and former UK Department of Environment (now DEFRA). The Natural Environment Research Council is acknowledged for providing radiocarbon support.

REFERENCES

Appleby PG, Shotyk W, Fankhauser A. 1997. Lead-210 age dating of three peat cores in the Jura Mountains, Switzerland. *Water Air and Soil Pollution* 100(3–4): 223–31.

Barber KE. 1993. Peatlands as scientific archives of past biodiversity. *Biodiversity and Conservation* 2(5):474–89.

Baxter M, Walton A. 1971. Fluctuations of atmospheric ^{14}C concentrations during the past century. *Proceedings of the Royal Society of London Series A* 321:105–27.

Clymo RS. 1984. The limits to peat bog growth. *Philosophical Transactions of the Royal Society of London B* 303:605–54.

Clymo RS. 1991. Peat growth. In: Shane LCK, Cushing EJ, editors. *Quaternary Landscapes*. London: Bellhaven. p 76–112.

Clymo RS, Mackay D. 1987. Upwash and downwash of pollen and spores in the unsaturated surface-layer of *Sphagnum*-dominated peat. *New Phytologist* 105(1): 175–83.

Clymo RS, Oldfield F, Appleby PG, Pearson GW, Ratnesar P, Richardson N. 1990. The record of atmospheric deposition on a rainwater dependant peatland. *Philosophical Transactions of the Royal Society of London B* 327:331–8.

Garnett MH, Ineson P, Stevenson AC. 2000. Effects of burning and grazing on carbon sequestration in a Pennine blanket bog, UK. *Holocene* 10(6):729–36.

Goodsite ME, Rom W, Heinemeier J, Lange T, Ooi S, Appleby PG, Shotyk W, van der Knaap WO, Lohse C, Hansen T. 2001. High-resolution AMS ^{14}C dating of post-bomb peat archives of atmospheric pollutants. *Radiocarbon* 43(2B):495–515.

Hobbs RJ, Gimingham CH. 1987. Vegetation, fire and herbivore interactions in heathland. *Advances in Ecological Research* 16:87–173.

Immirzi CP, Maltby E, Clymo RS. 1992. *The Global Status of Peatlands and Their Role in Carbon Cycling*. London: Friends of the Earth.

Kilian MR, van der Plicht J, Van Geel B. 1995. Dating raised bogs: new aspects of AMS C-14 wiggle matching, a reservoir effect and climatic change. *Quaternary Science Reviews* 14(10):959–66.

Levin I, Hesshaimer V. 2000. Radiocarbon—a unique tracer of global carbon cycle dynamics. *Radiocarbon* 42(1):69–80.

Levin I, Kromer B. 1997. Twenty years of atmospheric (CO_2)-C-14 observations at Schauinsland station, Germany. *Radiocarbon* 39(2):205–18.

Nydal R, Lovseth K, Skogseth F. 1980. Transfer of bomb ^{14}C to the ocean surface. *Radiocarbon* 22(3):626–35.

Ohlson M, Tryterud E. 2000. Interpretation of the charcoal record in forest soils: forest fires and their production and deposition of macroscopic charcoal. *Holocene* 10(4):519–25.

Oldfield F, Richardson N, Appleby PG. 1995. Radiometric dating (^{210}Pb, ^{137}Cs, ^{241}Am) of recent ombrotrophic peat accumulation and evidence for changes in mass balance. *Holocene* 5:141–8.

Punning JM, Alliksaar T. 1997. The trapping of fly-ash particles in the surface layers of *Sphagnum*-dominated peat. *Water Air and Soil Pollution* 94(1–2):59–69.

Rhodes AN. 1998. A method for the preparation and quantification of microscopic charcoal from terrestrial and lacustrine sediment cores. *Holocene* 8:113–7.

Rose NL, Harlock S, Appleby PG, Battarbee RW. 1995. Dating of recent lake sediments in the United Kingdom and Ireland using spheroidal carbonaceous particle (SCP) concentration profiles. *Holocene* 5:328–35.

Stuiver M, Reimer PJ, Bard E, Beck JW, Burr GS, Hughen KA, Kromer B, McCormac G, van der Plicht J, Spurk M. 1998. INTCAL98 radiocarbon age calibration, 24,000–0 cal BP. *Radiocarbon* 40(3):1041–83.

Tolonen K, Possnert G, Jungner H, Sonninen E, Alm J. 1992. High-resolution ^{14}C dating of surface peat using the AMS technique. *Suo* 42:271–5.

Walton A, Ergin M, Harkness D. 1970. Carbon-14 concentrations in the atmosphere and carbon exchange rates. *Journal of Geophysical Research* 75:3089–98.

RADIOCARBON, Vol 46, Nr 2, 2004, p 853–861

DIFFERENTIATING BONE OSTEONAL TURNOVER RATES BY DENSITY FRACTIONATION; VALIDATION USING THE BOMB ^{14}C ATMOSPHERIC PULSE

Ji Young Shin[1,2] • Tamsin O'Connell[1] • Stuart Black[3] • Robert Hedges[1,4]

ABSTRACT. The density (BSG) of bone increases, at the osteon scale, during lifetime aging within the bone. In addition, post-mortem diagenetic change due to microbial attack produces denser bioapatite. Thus, fractionation of finely powdered bone on the basis of density should not only enable younger and older populations of osteons to be separated but also make it possible to separate out a less diagenetically altered component. We show that the density fractionation method can be used as a tool to investigate the isotopic history within an individual's lifetime, both in recent and archaeological contexts, and we use the bomb ^{14}C atmospheric pulse for validating the method.

INTRODUCTION

Human bones recovered from archaeological sites are an invaluable source for reconstructing paleodiet, paleoenvironment, and other archaeological information. Since remodeling of bone occurs throughout life, information corresponding to times of bone formation is therefore potentially available, provided that the appropriate fraction of bone can be selected. This might enable life-histories to be reconstructed. Such a method would be applicable to fresh as well as archaeological bone. We have developed a density fractionation method, modified from Bell et al. (2001), and here report results which demonstrate its effectiveness in the context of isotopic measurements. An additional benefit is an ability to distinguish bone material which has become hypermineralized through diagenetic action.

We show also that different fractions of human bone correspond to different ages of the individual's lifetime by measuring how the atmospheric nuclear bomb test radiocarbon pulse is incorporated into the bone collagen by diet during the subject's lifetime.

The Specific Gravity of Living Bone

Bone density (specific gravity/BSG) depends on the degree of mineralization resulting from bone formation and maturation. The BSG is controlled by the precipitation of mineral salts, rather than collagen, displacing interstitial water (Figure 1). The BSG increases during lifetime maturation of the bone, and the spatial variation of BSG corresponds to bone packets of different "tissue age" (Lowenstam and Weiner 1989). Macroscopic bone exhibits a variety of growth structures of which the most typical, especially in cortical adult bone, is based on osteons. These functional units are generally axially aligned with diameters of about 150 μm (Fincham 1969). Remodeling involves the replacement of portions or groups of osteons with new, complete osteons. Microscopy of bone sections reveals new osteons as superimpositions; the greater mineralization of the older osteons is also revealed by electron back-scattering SEM. Thus, we expect a density difference between older and younger osteons.

[1]Research Laboratory for Archaeology, University of Oxford, 6 Keble Road, Oxford, UK, OX1 3QJ.
[2]Email: ji.shin@arch.ox.ac.uk.
[3]School of Human and Environmental Sciences, University of Reading, Whiteknights, Reading, PO Box 227, RG6 6AB.
[4]Corresponding author. Email: robert.hedges@archaeology-research.oxford.ac.uk.

Proceedings of the 18th International Radiocarbon Conference, edited by N Beavan Athfield and R J Sparks
RADIOCARBON, Vol 46, Nr 2, 2004, p 853–861

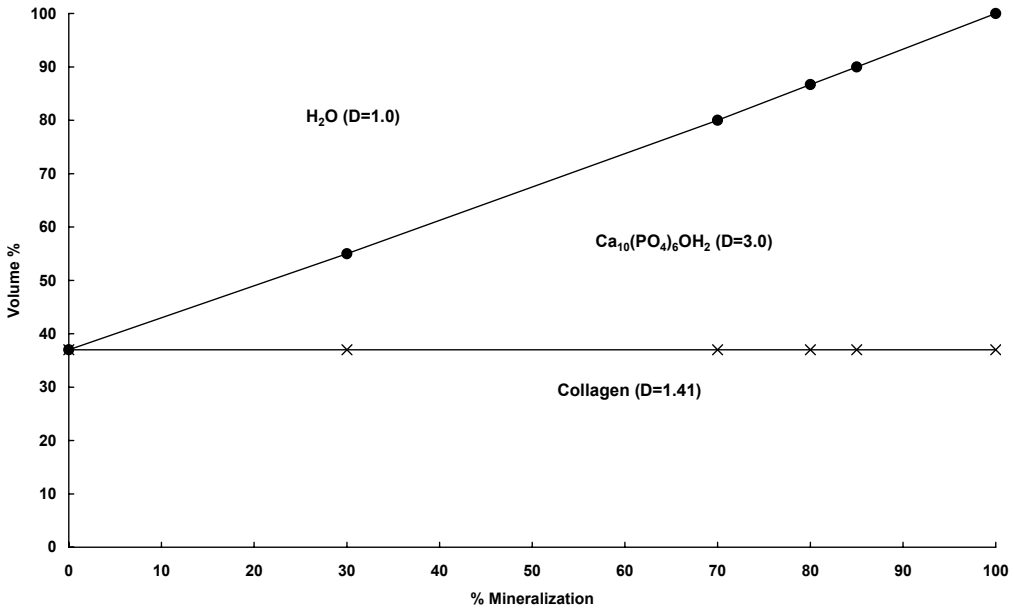

Figure 1 Relative proportion of main components of bone (mineral, collagen, and water) as a function of degree of mineralization. Redrawn from Lowenstam and Weiner (1989).

Bone Turnover

The rate and mode of bone turnover is a vast subject; only the most relevant issues are treated here. In growing bone, the processes of resorption (by osteoclasts) and synthesis (by osteoblasts) occur in quite different locations. In mature bone, remodeling involves the continual replacement of existing bone, both the mineralized and the organic component. The fraction of bone remodeled per yr defines a turnover rate, which is known to vary between skeletal elements, to depend on applied chronic stresses, and to change with age. Estimates of the rate are in the region of 2–8% per yr for cortical bone for adults (Newman and Newman 1958; Frost 1969; Marshall et al. 1973; Stenhouse and Baxter 1979). One source of such estimates is to measure the extent to which the ^{14}C pulse, produced in the atmosphere in the 1960s by nuclear bomb testing and incorporated into the terrestrial biosphere, is taken up in human bone through the diet. We have used this method to verify that different fractions (separated by BSG), which are believed to represent different tissue ages, indeed do correspond to different retention times in bones based on variations in these fractions' ^{14}C bomb pulse.

APPROACH

The development of the BSG method and its potential application to archaeology was first reported by Bell et al. (2001). Methodologically, our approach differs in the grinding technique and in the particle size distribution achieved. We show here that isotopic measurements can be made on different fractions which are consistent with expectation, especially the bulk value, and in particular, can show that different BSG fractions can correspond to different periods of bone formation in an individual.

Since bone is remodeled at an osteonal level of structure, the BSG separation must be carried out on particles that are small compared with an osteon. Therefore, after grinding (see under "Materials and Methods"), we checked the particle size distribution with a laser particle sizer. Fractionation by

BSG separation is achieved by differential flotation in bromoform-methanol mixtures. (We note that we failed to achieve BSG separation on such a fine particle population using sodium polytungstate solutions, probably because of the propensity to flocculate in ionic media.)

We extracted collagen from the separated fractions and compared $\delta^{13}C$ and $\delta^{15}N$ measurements on the fractions with the bulk material to check consistency. Using archaeological bone, which is frequently diagenetically altered by microbial action, we separated lifetime fraction and diagenetic fraction by BSG. Much of the archaeological bone are present in "hypermineralized" form, with loss of its original micromorphology. This altered material, which chemically still corresponds to hydroxyapatite, has a substantially greater BSG, and so can be efficiently removed from unaltered bone by BSG separation. We also made ^{14}C AMS measurements on collagen from the separated BSG fractions from modern bone, so that the effect of the post-1960s atmospheric ^{14}C pulse could be used to compare the relative times of bone formation. This can be used as a direct test that the different BSG fractions correspond to different tissue ages within the same individual.

MATERIALS AND METHODS

Samples were taken from archaeological bones from 2 sites (Greyfriars, Oxford, UK, Late Saxon; Repton, UK, Middle Saxon). Histological examination showed all archaeological bone had some degree of diagenetic alteration. Modern human bone was obtained from forensic and orthopedic studies; these samples were used to test variation in tissue ages by ^{14}C analysis. Modern bone samples were defatted by sequential rinses in chloroform and methanol mixture (2:1), then water. Archaeological bone samples were cleaned by shotblasting. All bone samples were then milled to a size distribution in which over 90% of particles could be calculated as comprising material from 1 osteon only, where mean osteon diameter is assumed to be 150 μm (Fincham 1969). The size distribution was measured by a Coulter Laser Particle Size Analyser (Beckham Coulter LS 230 laser granulometer) within the range of 0.04–2000 μm and confirmed by optical microscopy. The milling was carried out sequentially using a Disc Mill (TEMA, Machinery, Ltd Banbury, Oxon, Laboratory Disc mill) and Micronizing Mill (McCRONE Micronizing mill, McCrone Research Associates Ltd.). In general, it is necessary to have >90% of particles smaller than 9.0 μm in diameter and we note that adequate milling is critical to the success of the method. Fractions were then collected by centrifugation after differential flotation in a sequence of increasing specific gravity mixtures of bromoform and methanol (8–10 ml was added to centrifuge tube) with densities of 1.8, 2.0, 2.1, 2.2, 2.4, and 2.6 g/cm^3.

Following washing in methanol, distilled water, and lyophilization, collagen was extracted by decalcification in 0.5 M aqueous HCl with gelatinization of the insoluble material at pH 3 for 48 hr at 75 °C and subsequent lyophilization of the filtrate. A 3-mg aliquot of the product was then combusted in a continuous-flow isotope ratio mass spectrometer (Carlo Erba carbon and nitrogen elemental analyzer coupled to a Europa Geo 20/20 mass spectrometer) to CO_2, H_2O, and N_2 and measured for C/N, $\delta^{13}C$, and $\delta^{15}N$. The GC-purified CO_2 was retained for ^{14}C measurement by AMS using standard procedures (Hedges et al. 1989; van Klinken and Hedges 1998).

RESULTS

In Table 1, we provide the source, histological condition, and other information on samples selected for this study.

Table 1 Samples used in this study.

Abbreviated sample ID	Site	Sample ID	Bone type	Histological index [a]	Date of birth	Date of sampling
GREY1	Greyfriars	OX69B II4	Femoral shaft	3~4	—	—
GREY2	Greyfriars	OX69B II2-3	Femoral shaft	3~4	—	—
GREY3	Greyfriars	OX69B IV36	Femoral shaft	3~4	—	—
REP1	Repton	R828 6L	Femoral shaft	0~1	—	—
REP2	Repton	R828 718NW14R	Femoral shaft	0~1	—	—
REP3	Repton	R828 718NW43R	Femoral shaft	0~1	—	—
FOR1	Forensic sample	P 10321	Cortical femur	—	1935	1977
FOR2	Forensic sample	P 10323	Cortical femur	—	1947	1966
NOC2	Orthopaedic sample	NOC2	Proximal tibia	—	1915	1998
NOC11	Orthopaedic sample	NOC11	Femoral head	—	1920	1999
NOCX23	Orthopaedic sample	NOCX23	Tibia/femur (compact bone)	—	1964	1999
NOCX24	Orthopaedic sample	NOCX24	Proximal tibia	—	1915	1999

[a]Histological Index scored 0 to 5, where 5 implies very well-preserved bone and 0 indicates poorly preserved bone with hardly any original features (Hedges et al. 1995).

BSG Distributions

The BSG range for fresh bone is rather small and only just sufficient to separate the different minority fractions. We were able to recover sufficient amounts of material in various BSG fractions for our analysis (see Figure 2). However, there is probably scope for improving the method to achieve better resolution. Well-preserved archaeological bone gives a somewhat wider distribution, which is not accounted for by the small variation in collagen content. For archaeological bone where there is a substantial fraction that has been microbially altered (i.e. for bones whose micromorphological structure has largely disappeared as assessed by visible microscopy of thick sections), the BSG distribution tends to an almost bimodal form (see Figure 2). In this case, the heaviest fractions contain relatively little collagen, presumably because of consumption by microbes.

Stable Isotope Results and ^{14}C Results (Fresh Bone Only)

Table 2 presents $\delta^{13}C$ and $\delta^{15}N$ for each BSG fraction and the bulk source of bone. Also, collagen yields (%) and C/N ratios were used to indicate the integrity of the extracted collagen. Generally, for modern bones, collagen yield (%) is about 20%, while in archaeological bone >1% is normally accepted. The C:N ratio, which is derived from C and N content of the extracted "collagen," ranged from 3.2 to 3.6, within the accepted range of 2.9 to 3.6 (Hedges and van Klinken 1992; van Klinken 1999).

BSG fractions from modern bone were analyzed for their bomb carbon content (Table 3). The ^{14}C content is reported as % modern and the results are discussed in the following section.

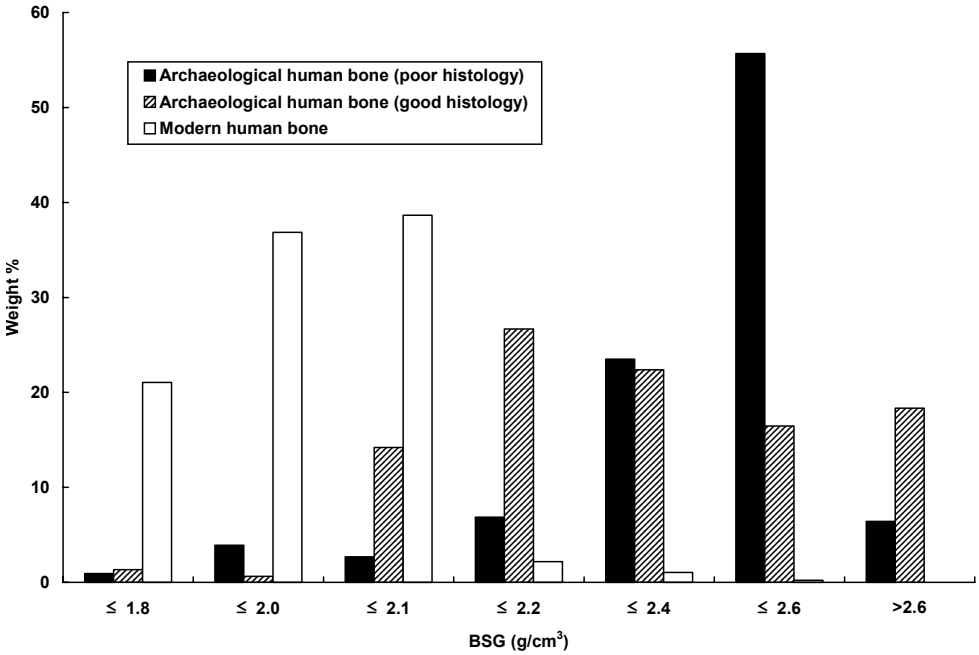

Figure 2 BSG distribution histogram of modern and archaeological human bone. In correlation to Table 1: Archaeological human bone (poor histology): REP1, REP2, REP3; archaeological human bone (good histology): GREY1, GREY2, GREY3; modern human bone: FOR1, FOR2, NOC2, NOC11, NOCX23, NOCX24.

Table 2 Stable isotope analysis results.

BSG Fraction of the sample[a]	$\delta^{13}C$ (‰)[b]	$\delta^{15}N$ (‰)[b]	C/N	Collagen yield (%)[c]
GREY1-C	–18.2	12.6	3.3	13.6
GREY1-D	–18.3	12.4	3.3	12.3
GREY1-E	–18.4	12.6	3.3	8.4
GREY1-F	–18.8	12.6	3.4	2.6
GREY1 bulk	–18.3	12.6	3.3	12.2
GREY2-C	–20.0	13.0	3.3	16.1
GREY2-D	–18.9	12.6	3.3	10.4
GREY2-E	–18.9	12.8	3.3	7.7
GREY2 bulk	–18.9	12.7	3.3	11.1
GREY3-C	–19.8	10.7	3.3	7.2
GREY3-D	–19.7	10.4	3.3	11.7
GREY3-E	–19.5	10.6	3.3	7.8
GREY3-F	–19.8	11.0	3.4	3.9
GREY3 bulk	–19.6	10.5	3.3	12.2
REP1-E	–19.4	11.3	3.4	3.2
REP1-F	–19.9	10.8	3.4	6.0
REP1 bulk	–19.4	10.9	3.3	7.1

Table 2 Stable isotope analysis results. *(Continued)*

BSG Fraction of the sample[a]	$\delta^{13}C$ (‰)[b]	$\delta^{15}N$ (‰)[b]	C/N	Collagen yield (%)[c]
REP2-D	–19.9	11.0	3.4	5.1
REP2-E	–20.5	11.1	3.6	1.6
REP2-F	–20.4	10.9	3.6	1.3
REP2 bulk	–19.8	11.1	3.3	7.5
REP3-D	–20.2	11.4	3.5	2.6
REP3-E	–19.8	11.1	3.4	5.7
FOR1-B	–16.9	11.9	3.4	20.8
FOR1-E+F	–17.2	11.0	3.3	21.7
FOR1 bulk	–17.3	—	—	—
FOR2-B	–18.7	11.6	3.5	23.1
FOR2-C+F	–16.9	11.0	3.3	—
FOR2 bulk	–18.4	—	—	—
NOC2-A	–19.0	12.2	3.4	33.0
NOC2-B	–19.3	12.2	3.3	21.2
NOC2-C	–18.9	12.4	3.2	16.5
NOC2 bulk	–18.9	12.4	3.2	20.3
NOC11-B	–19.8	12.1	3.5	25.8
NOC11-C	–19.1	12.3	3.3	25.2
NOC11 bulk	–19.1	12.2	3.3	16.7
NOCX23-A	–20.2	11.0	3.5	—
NOCX23-B	–19.7	10.9	3.3	28.8
NOCX23-C	–19.3	11.0	3.2	23.8
NOCX23-D	–19.0	11.5	3.2	25.1
NOCX23 bulk	–19.3	11.1	3.3	24.3
NOCX24-A	–19.5	12.6	3.4	36.4
NOCX24-B	–20.4	11.9	3.5	33.3
NOCX24-C	–19.9	12.2	3.2	11.2
NOCX24 bulk	–19.3	12.9	3.2	29.9

[a]Sample code: the specific gravity of each sample is coded as follows: A (≤1.8), B (1.8~2.0), C (2.0~2.1), D (2.1~2.2), E (2.2~2.4), F (2.4~2.6), G (>2.6)

[b]$\delta^{13}C$ and $\delta^{15}N$ values are expressed as ‰ relative to VPDB standard and AIR standard respectively.

[c]Collagen yield are calculated from extracted collagen amount versus amount of bone initially used.

Note that isotopic data were available only from BSG fractions containing more than 50 mg bone.

Table 3 ^{14}C results of modern BSG fractions.

Sample index[a]	OxDate (pMC)	$\delta^{13}C$ (‰)	OxA
FOR1-B	107.0 ± 0.3	–16.9	OxA-X-2021-33
FOR1- E+F	102.2 ± 0.3	–17.2	OxA-X-2022-37
FOR1 bulk	110.2 ± 0.4	–17.3	OxA-9592

Table 3 ^{14}C results of modern BSG fractions. *(Continued)*

Sample index[a]	OxDate (pMC)	$\delta^{13}C$ (‰)	OxA
FOR2-B	124.3 ± 0.3	–18.7	OxA-X-2021-34
FOR2-C+ F	103.6 ± 0.3	–16.9	OxA-X-2022-39
FOR2 bulk	126.0 ± 0.5	–18.4	OxA-9383
NOC2-A	110.3 ± 0.3	–19.0	OxA-X-2042-10
NOC2-B	111.5 ± 0.3	–19.3	OxA-X-2042-11
NOC2-C	114.5 ± 0.3	–18.9	OxA-X-2042-12
NOC2 bulk	113.5 ± 0.3	–18.9	OxA-X-2042-09
NOC11-B	110.2 ± 0.3	–19.8	OxA-X-2042-24
NOC11-C	109.0 ± 0.3	–19.1	OxA-X-2042-25
NOC11 bulk	110.4 ± 0.3	–19.1	OxA-X-2042-22
NOCX23-A	110.5 ± 0.3	–20.2	OxA-X-2042-14
NOCX23-B	110.6 ± 0.3	–19.7	OxA-X-2042-15
NOCX23-C	112.8 ± 0.4	–19.3	OxA-X-2042-16
NOCX23-D	119.2 ± 0.4	–19.0	OxA-X-2042-17
NOCX23 bulk	120.3 ± 0.3	–19.3	OxA-X-2042-13
NOCX24-A	110.0 ± 0.3	–19.5	OxA-X-2042-19
NOCX24-B	107.7 ± 0.3	–20.4	OxA-X-2042-20
NOCX24-C	111.6 ± 0.3	–19.9	OxA-X-2042-21

[a]Density: A (≤1.8), B (1.8~2.0), C (2.0~2.1), D (2.1~2.2), E (2.2~2.4), F (2.4~2.6), G (>2.6).

DISCUSSION

It is important to demonstrate that the complicated processes of grinding, fractionating, and collagen preparation from very fine powder do not incorporate contaminating material. The measurements of collagen (%, C/N, and isotopic composition) from each fraction are generally in accord with that from the "bulk" (unfractionated) bone. In particular, there is no significant change in the isotopic composition between the fractions for samples NOC2; NOC11; NOCX23; NOCX24; GREY1,2,3; REP1,2,3. (i.e. the variance within the delta values is consistent with the errors expected from replicate measurements); this is not the case for FOR1 and FOR2, where a change in dietary history may be indicated.

^{14}C analysis of modern bulk-bone and fractions tested the assumption that different density fractions were metabolized at different times within the subjects lifespan. Figure 3 shows how the lifetimes of 6 subjects are related to the timeline for the northern atmosphere ^{14}C bomb pulse (Goodsite et al. 2001; Levin and Hesshaimer 2000), and, therefore, approximately to the ^{14}C content of terrestrial diet available to the subjects during that timespan. The bulk determinations are roughly consistent with previously published observations (Stenhouse and Baxter 1979; Geyh 2001) for collagen.

When ^{14}C values for different fractions within the same individual are compared (Table 3), we note that the lighter BSG component consistently gives ^{14}C values which correspond to collagen synthesis at a later period along the bomb curve. This is most obvious for samples FOR1 and FOR2, for which the peak of the bomb pulse is later in life, but at an age where bone turnover is still quite active. For sample NOCX23, the bomb pulse occurs very early in life, so that synthesis at a later period of life (the lightest fractions A & B) correspond to relatively low atmospheric excess ^{14}C. Thus, the relationship between ^{14}C value and BSG fraction is opposite to that of FOR1 and FOR2.

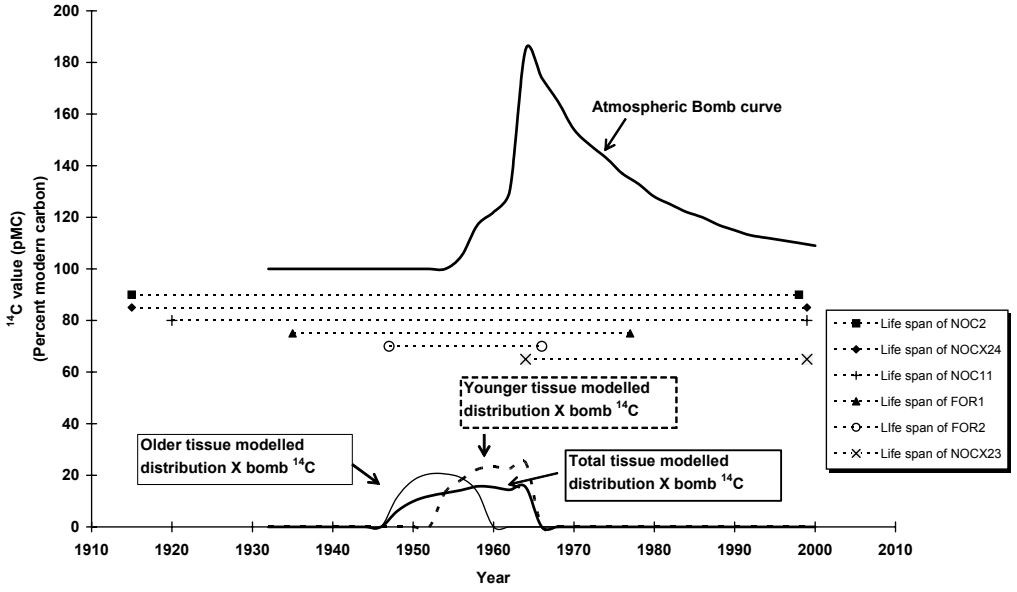

Figure 3 Relationship between the ^{14}C dates and different BSG fractions. The lifespans of the different individuals measured for bone collagen ^{14}C content are shown in relation to the timing of the expected ^{14}C content of their diet. The lower part of the figure shows how an abitrary but feasible model of collagen turnover with age (using the lifespan of FOR2 as an example) can be used to calculate an expected collagen radiocarbon content in different components of the tissue. The turnover model results in an essentially parabolic distribution of tissue age; this distribution, when weighted by the dietary ^{14}C content, gives the curves shown. The more mineralized, higher BSG fraction is modeled as a distribution of tissue age of surviving tissue from deposition during the first 75% of the individual's lifespan, while the less mineralized, lower BSG fraction is modeled as a distribution of surviving deposition during the last 75% of the individual's lifespan. The older (earlier) tissue remains approximately parabolic, since the bomb curve weighting is mainly constant, while the bulk and younger tissue fractions show ^{14}C contents which are weighted towards higher values.

For samples NOC2, NOC11, and NOCX24, all with similar date of birth and age-at-sampling (of >83 yr), the bomb pulse occurs after a biological age of 45, when turnover rate is small. In these cases, there is little apparent difference between the light and heavy fractions, all of which contain roughly 25% of the total integrated bomb-produced ^{14}C. If the light density fractions in these cases do correspond to recent synthesis (i.e. within the 10–20 yr before death), the value of the bomb curve at this point would not be differentiated from the measured BSG fractions synthesized earlier in life. Thus, while the results from these different individual samples are generally similar, it would appear that the bomb curve cannot usefully distinguish between early and later synthesized collagen in this particular situation.

We also note some inconsistencies in the ^{14}C values. These are well outside analytical error, but perhaps record the presence of impurities (such as faster turning-over components from the bone). However, while the results are not entirely error-free, they are unequivocal in showing that the different fractions from a single bone sample give ^{14}C values in qualitative agreement with their "tissue age." To obtain quantitative agreement presupposes a model of tissue turnover, which could only be constructed from a much larger data set. In principle, this method offers a way to investigate some points of the distribution of dates when surviving osteons are laid down in different bones in an individual (providing the bomb curve can be suitably involved).

CONCLUSION

We present evidence here for the validity of a method we have developed to fractionate bone into components of different "tissue age." This can be applied both to archaeological and fresh bone and enables stable isotopic analyses of carbon and nitrogen to be made of the bone collagen (and possibly other components). In particular, we have shown through ^{14}C dating of the collagen that the tissue age of the bone fractions can be qualitatively compared against models of bone turnover using the ^{14}C pulse of the atmospheric bomb curve. The comparison shows, at least for individuals whose age at death is 50 or less, that the lighter fractions contain collagen which was synthesized later in life. We consider the method to have application in investigating tissue age differences in relation to questions of bone physiology, as well as being applicable to studying archaeological material. A side advantage of the method is that diagenetically altered (hypermineralized) bone can be removed by this approach, allowing analysis of biogenic material; this may be its main use in archaeological and paleontological contexts. However, it provides a basis for the validity of measurements which aim to show lifetime changes in individuals as recorded in isotopic or other observations of bone fractions with different ages. We stress that these are initial results and further work should improve the methodology. In particular, the relationship between tissue age and each bone density fraction requires better resolution and clarification.

ACKNOWLEDGEMENTS

The authors would like to thank those who provided samples for this study: Martin Evison of Sheffield University; Hamish Simpson, formerly of the Nuffield Orthopaedic Centre, Oxford, now at the Department of Orthopedics, Edinburgh University; Lauren Gilmour at the Oxfordshire Museums Service; and Martin Biddle and Birthe Kjobye-Biddle of Oxford University. We are grateful to Alistair Pike, Chris Doherty, and Jean-Luc Schwenninger for helping sample preparation and measurement, and the Radiocarbon Accelerator Unit at RLAHA, University of Oxford for ^{14}C dating.

REFERENCES

Bell LS, Cox G, Sealy J. 2001. Determining isotopic life history trajectories using bone density fractionation and stable isotope measurements: a new approach. *American Journal of Physical Anthropology* 116:66–79.

Fincham AG. 1969. The density fractionation of hard tissues; the application of the "Coulter Counter" to the density-volume distribution of dried bone powders. *Calcified Tissue Research* 3:327–39.

Frost HM. 1969. Tetracycline-based histological analysis of bone remodelling. *Calcified Tissue Research* 3: 211–37.

Geyh MA. 2001. Bomb radiocarbon dating of animal tissue and hair. *Radiocarbon* 43(2B):723–30.

Goodsite ME, Rom W, Heinemeier, J, Lange T, Ooi S, Appleby PG, Shotyk W, van der Knaap WO, Lohse C, Hansen TS. 2001. High-Resolution AMS ^{14}C dating of post-bomb peat archives of atmospheric pollutants. *Radiocarbon* 43(2B):495–515.

Hedges REM, Law IA, Bronk CR, Housley RA. 1989. The Oxford accelerator mass spectrometry facility: technical developments in routine dating. *Archaeometry* 31(2):99–113.

Hedges REM, Millard AR, Pike AWG. 1995. Measurements and relationships of diagenetic alteration of bone from three archaeological sites. *Journal of Archaeological Science* 22:201–9.

Levin I, Hesshaimer V. 2000. Radiocarbon—a unique tracer of global carbon cycle dynamics. *Radiocarbon* 42:69–80.

Lowenstam HA, Weiner S. 1989. *On Biomineralization*. Oxford: Oxford University Press. p 162–7.

Marshall JH, Liniecki J, Lloyd EL, Marotti G, Mays CW, Rundo J, Sissons HA, Snyder WS. 1973. Alkaline earth metabolism in adult man. *Health Physics* 24: 125–221.

Newman WF, Neuman MW. 1958. *The Chemical Dynamics of Bone Mineral.* Chicago: University of Chicago Press. p 101–17.

Stenhouse MJ, Baxter MS. 1979. The uptake of bomb ^{14}C in humans. In: Berger R, Suess HE, editors. *Radiocarbon Dating*. Berkeley: University of California Press. p 324–41.

van Klinken GJ, Hedges REM. 1998. Chemistry strategies for organic ^{14}C samples. *Radiocarbon* 40(1):51–6.

RADIOCARBON, Vol 46, Nr 2, 2004, p 863–868

LEVELS OF ^{14}C IN THE TERRESTRIAL ENVIRONMENT IN THE VICINITY OF TWO EUROPEAN NUCLEAR POWER PLANTS

Åsa Magnusson[1] • Kristina Stenström[1] • Göran Skog[2] • Diana Adliene[3] • Gediminas Adlys[3] • Ragnar Hellborg[1] • Agata Olariu[4] • Mohamad Zakaria[5] • Christopher Rääf[5] • Sören Mattsson[5]

ABSTRACT. Radiocarbon is produced in all types of nuclear reactors. Most of the ^{14}C released into the environment is in the form of gaseous emissions. Recent data on the ^{14}C concentration found in terrestrial samples taken in the vicinity of nuclear power plants in Romania and Lithuania are presented. We found increased ^{14}C levels in the surroundings of both power plants. At the Romanian power plant Cernavoda, we found excess levels of ^{14}C in grass within a distance of about 1000 m, the highest ^{14}C specific activity being 311 Bq/kg C (approximately 28% above the contemporary ^{14}C background) found at a distance of 200 m from the point of release (nearest sampling location). At the Lithuanian power plant Ignalina, samples of willow, pine, and spruce showed a ^{14}C excess of similar magnitude, while significantly higher values were found in moss samples. The samples were analyzed at the accelerator mass spectrometry facility in Lund, Sweden.

INTRODUCTION

Radiocarbon is produced in all types of reactors through neutron-induced reactions with isotopes of carbon, nitrogen, and oxygen present in the reactors. Since most of the ^{14}C released into the environment is in the form of gaseous emissions (such as $^{14}CO_2$), terrestrial samples will constitute the primary indicators of increased ^{14}C levels in the surroundings of the nuclear power plant (NPP). Because the food chain starts with plants, measurements of ^{14}C in environmental samples are important for estimates of radiation exposure to the public.

We have investigated the ^{14}C levels in the surroundings of 2 different types of reactors: the Romanian Canadian Deuterium Uranium (CANDU) reactor at Cernavoda and the Lithuanian RBMK (light-water-cooled, graphite-moderated) reactor at Ignalina. These 2 types of reactors are known to release higher amounts of airborne ^{14}C than light-water-moderated reactors. According to UNSCEAR (2000), the mean normalized ^{14}C release to air from 1990–1994 from CANDU reactors was 1.6 TBq/GW_e·yr, and for RBMK reactors, 1.3 TBq/GW_e·yr (estimated). Corresponding values for light-water-moderated pressurized water reactors (PWRs) and boiling water reactors (BWRs) were 0.22 and 0.51 TBq/GW_e·yr, respectively. Published data involving ^{14}C levels in the areas surrounding the Cernavoda and Ignalina NPPs are scarce, which justifies further investigations.

We have collected various vegetation samples in the area surrounding the 2 NPPs. At Cernavoda, we collected grass samples at various distances from the NPP, and from the immediate vicinity of the Ignalina NPP, we collected various vegetation samples.

In this paper, we have included a brief description of the 2 reactor types, as well as a summary of previous measurements involving ^{14}C emission and ^{14}C levels in the area surrounding the 2 NPPs.

[1]Department of Physics, Division of Nuclear Physics, Lund University, Box 118, SE-221 00 Lund, Sweden.
Corresponding author. Email: asa.magnusson@nuclear.lu.se.
[2]Department of Geology, Quaternary Geology, Lund University, Sölvegatan 12, SE-223 62 Lund, Sweden.
[3]Department of Physics, Kaunas Technological University, LT-3031 Kaunas, Lithuania.
[4]National Institute for Physics and Nuclear Engineering, RO-76900 Bucharest, Romania.
[5]Department of Radiation Physics, Lund University, Malmö University Hospital, SE-205 02 Malmö, Sweden.

Proceedings of the 18th International Radiocarbon Conference, edited by N Beavan Athfield and R J Sparks
RADIOCARBON, Vol 46, Nr 2, 2004, p 863–868

SITE DESCRIPTIONS AND PREVIOUS MEASUREMENTS

Cernavoda, Romania

The Cernavoda NPP is located 180 km east of Bucharest and is designed for 5 CANDU-6 (600 MW_e) reactors. So far, only 1 reactor has been built—with a maximum electrical output of 706 MW_e—and this has been in operation since April 1996; a second reactor is under construction. The CANDU-6 reactor is heavy-water-moderated and -cooled and uses natural uranium as fuel. The height of the venting stack is 50 m. About 220,000 people live within 30 km of the site (AECL 2001).

The largest contributor (>95%) to the production of ^{14}C in CANDU reactors is neutron activation of ^{17}O in the heavy-water moderator. Minor quantities are generated in the heat transport system by the annulus gas (CO_2) system (IAEA 2002) and in the fuel elements (Milton 1995).

According to Boss and Allsop (1995) and ACRP (1995), the total ^{14}C production in a CANDU-6 reactor is about 18 TBq/yr (approximately 33 TBq/GW_e·yr, assuming an electrical output of 0.600 GW_e and operation of 90% of the time) and 28 TBq/GW_e·yr, respectively, and it has been estimated that less than 4% is released to the atmosphere (ACRP 1995). Measurements have shown that about 70% of this ^{14}C is released in the form of CO_2 (Cooper 1998).

According to Dubourg (1998), the approximate release rate of ^{14}C with gaseous effluents from a CANDU-6 reactor (assuming operation of 80% of the time) is 4.1 TBq/yr (approximately 8.5 TBq/GW_e·yr, assuming an electrical output of 0.600 GW_e and 80% operation). Baciu et al. (1996) report that "the normal operation source term of ^{14}C in gaseous effluents" from the CANDU-6 at Cernavoda is 5.7 TBq/yr (approximately 11 TBq/GW_e·yr, assuming an electrical output of 0.600 GW_e and 90% operation). However, since these data were reported before the NPP was operational, the value probably refers to typical values for CANDU-6 reactors.

Bobric and Simionov (1999) presented annual ^{14}C emission data from the Cernavoda NPP, measured at the release point, from April 1996 to December 1998. The values are: 0.035 TBq/yr (0.26 TBq/GW_e·yr), 0.18 TBq/yr (0.32 TBq/GW_e·yr) and 0.29 TBq/yr (0.52 TBq/GW_e·yr) for 1996, 1997, and 1998, respectively. They also measured ^{14}C concentrations in terrestrial biota (e.g. vegetables and fruits) within 30 km of the NPP but did not find any detectable amounts with the liquid scintillation counter used.

Tenu et al. (2002) measured ^{14}C in atmospheric CO_2 samples collected monthly from April 1995 to November 1998 at a site close to the Cernavoda NPP. During this period, ^{14}C activities corresponding to values ranging from 210–440 Bq/kg C were recorded, with large fluctuations. Increased ^{14}C levels, compared with the values from the previous year, were found during the same month as the NPP started (April 1996). During 1998, they recorded an increase in ^{14}C activity at the Cernavoda site, from a level corresponding to 250 Bq/kg C in April 1998 to 440 Bq/kg C a month later. The values remained above 280 Bq/kg C until the end of the year.

Ignalina, Lithuania

The Ignalina NPP is located close to the border between Belarus and Latvia and consists of 2 units which were put into operation in 1983 and 1987, respectively. The reactors are graphite-moderated BWRs of channel type (model RBMK-1500) and have a maximum electrical output of 1300 MW_e each. The height of the venting stack is 150 m. About 210,000 inhabitants live within 30 km of the power plant (Almenas et al. 1998).

The emission of ^{14}C from a RBMK-1500 reactor mainly originates from ^{14}C production in the nitrogen-helium mixture that fills the entire reactor space and from ^{14}C production in the coolant. During the initial period of reactor operation, pure nitrogen is used instead of the nitrogen-helium mixture. During this period (approximately 18 months), the formation of ^{14}C is about 10 times higher than during the subsequent normal operation at rated power (Konstantinov 1989). Measurements performed in 1985–1986 of atmospheric ^{14}C release at the high-altitude pipe gave a value of 1.4 ± 0.3 TBq/GW_e·yr (Konstantinov 1989).

Mikhajlov et al. (1999) measured the ^{14}C distribution near the Ignalina NPP, and the highest value found corresponds to a ^{14}C specific activity of 430 Bq/kg C recorded in 2-yr-old pine cones that were collected at a distance of 5 km east of the location. Jakimaviciute-Maseliene et al. (2003) measured the ^{14}C concentration in plants (*Artemisia L.* [stem] and *Alnus L.* [leaves]) in the surroundings of the Ignalina NPP in 1996 and 2001. The highest value they found, within 1 km northwest of the NPP, corresponds to a ^{14}C activity of 400 Bq/kg C (in *Alnus L.* in 2001). From this maximum value, they derived a rough value of the atmospheric ^{14}C release from the Ignalina NPP of 49 TBq/yr (approximately 38 TBq/GW_e·yr, derived from the 2 units mean electrical energy generated during 1996 and 2001).

SAMPLING

Grass samples were collected in 1999 (14 October) and in 2001 (7 September) at various distances (200–4300 m) from the Cernavoda NPP. On the first sampling occasion, 9 samples were collected for ^{14}C analysis, and on the second, 21 samples were collected. The sampling locations and the general wind direction at Cernavoda are shown in Figure 1.

Different types of vegetation samples from trees and moss were collected in the immediate vicinity of the Ignalina NPP on 10 April 2003. All 9 samples were taken within a distance of 400 m from the stack. The approximate sampling locations and the general wind direction at Ignalina can be seen in Figure 2. Additional details are given in Table 1.

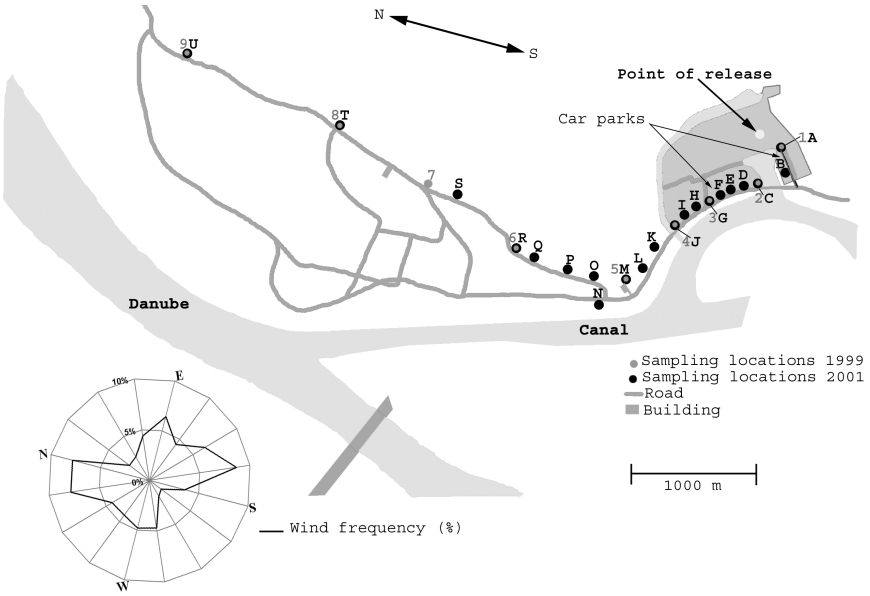

Figure 1 Sampling locations at Cernavoda in 1999 and 2001 and the wind frequency at Cernavoda from March to October 1999.

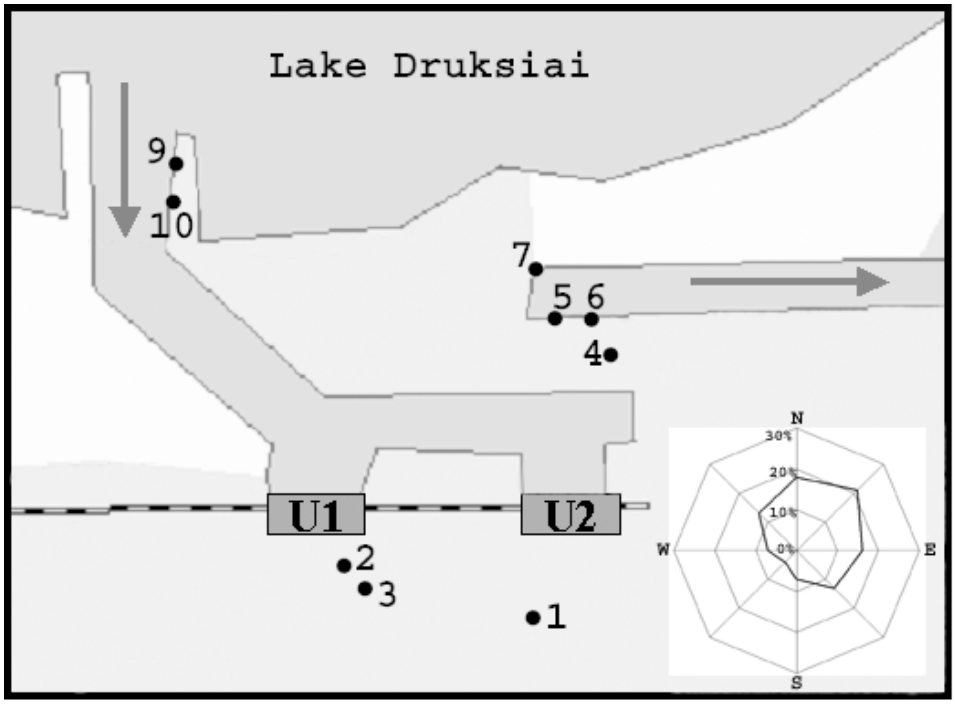

Figure 2 Approximate sampling locations at the Ignalina NPP in April 2003 (additional information is given in Table 1) showing Unit 1 and 2. The wind frequency at Ignalina during 2002 is also shown.

The samples were dried, ground, combusted, and graphitized according to standard procedures at our laboratory (Stenström 1995) and analyzed at the accelerator mass spectrometry facility in Lund, Sweden. The moss samples were fractionated into 1 upper layer (mainly moss) and 1 or 2 lower layers (moss and soil).

RESULTS

Cernavoda, Romania

The results from Cernavoda, which can be seen in Figure 3, show the typical distribution of ^{14}C from a point source. Excess levels of ^{14}C were found within a distance of about 1000 m from the point of release, with a maximum ^{14}C specific activity of 311 Bq/kg C found at the closest sampling location (A, 200 m).

Ignalina, Lithuania

The data given in Table 1 from the Ignalina NPP show similar levels of ^{14}C in willow, pine, and spruce to those found in grass from Cernavoda. The concentration in the moss samples and in the soil is significantly higher.

DISCUSSION

Increased ^{14}C levels were found in the surroundings of both NPPs. At Cernavoda, excess levels of ^{14}C were found in grass up to a distance of about 1000 m. Similar values of ^{14}C excess were found in the samples of leaves, shoots, and twigs from trees and bushes close to the Ignalina NPP. These do not necessarily reflect the maximum levels since they were collected only in the immediate

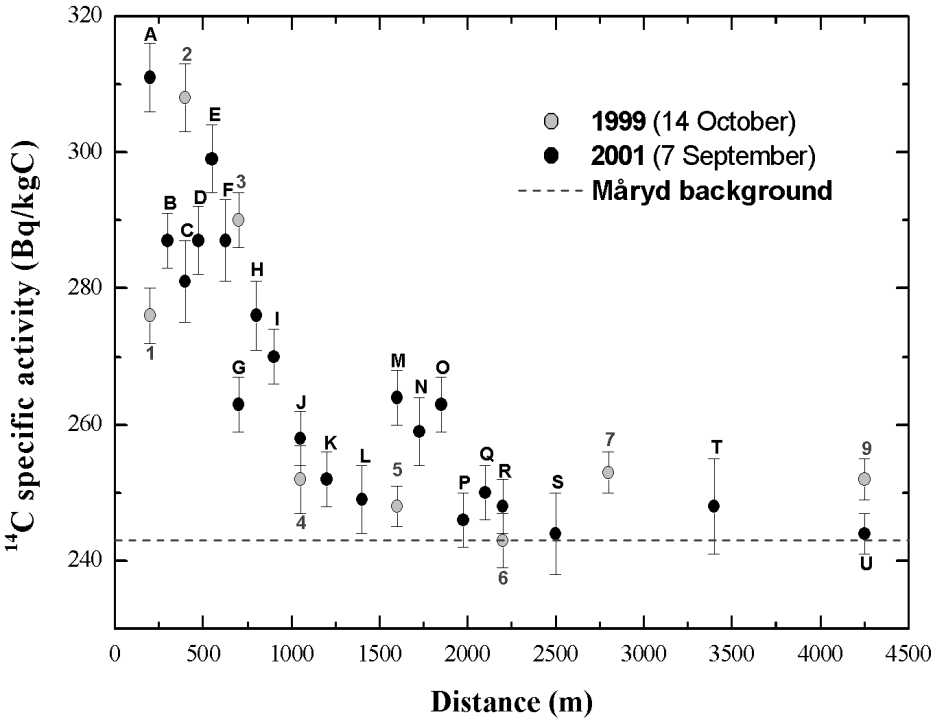

Figure 3 The ^{14}C specific activity (Bq/kg C) found in grass samples collected at various distances from the Cernavoda NPP. The background ^{14}C activity, 243 ± 2 Bq/kg C, measured in rush (*Juncus L*) from Måryd, Sweden, is the mean value for the period 1999–2001. Figures and numbers refer to the sampling times and locations shown in Figure 1.

Table 1 ^{14}C specific activity (Bq/kg C) found in various vegetation samples collected in the immediate vicinity of the Ignalina NPP in April 2003. The sampling locations are indicated in Figure 2. U1 and U2 = Units 1 and 2. The background ^{14}C activity, 241 ± 2 Bq/kg C, measured in rush (*Juncus L.*) from Måryd, Sweden, is the mean value for the period 2002–2003.

Nr	Sample description	Location	Background activity (Bq/kg C)
1	Goat willow (shoot, twig and flower bud)	150 m in front of U2	302 ± 7
2	Pine (shoot and twig)	50–70 m in front of U1	315 ± 7
3	Spruce (shoot and twig)	100 m in front of U1	302 ± 10
4	Goat willow (shoot and twig)	200 m behind U2	309 ± 7
5a	Moss (upper layer of a few cm)	Along outlet canal	362 ± 6
5b	Moss (soil and moss from lower layer)		1960 ± 20
6a	Moss (upper layer of a few cm)	Along outlet canal	370 ± 7
6b	Moss (soil from lower layer)		598 ± 10
7	White willow (shoot and twig)	Beginning of outlet canal	323 ± 7
9	Goat willow (shoot and twig)	Along inlet canal	342 ± 5
10a	Moss (upper layer of a few cm)	Along inlet canal	1020 ± 10
10b	Moss (middle layer of a few cm)		1570 ± 20
10c	Moss (soil and moss from lower layer)		4730 ± 60

vicinity (within 400 m) of the NPP. Because of the considerable height of the venting stack, the maximum ^{14}C concentrations are most likely found at a distance beyond the 400 m. High ^{14}C specific activities were found in the moss samples from Ignalina, with increasing concentrations with increasing depth. As moss grows from the top, the different layers should reflect different time periods, the oldest being the bottom layer. The results obtained may thus indicate that the release of ^{14}C has decreased during the lifetime of the moss. But as the ^{14}C concentrations found in the moss samples are higher than expected, the possibility of airborne ^{14}C particulates must be considered (Marsden et al. 2002; Mikhajlov et al. 1999). According to UNSCEAR (2000), the amount of particulates released with airborne effluents from the Ignalina NPP is considerable. Because of the great number of factors that determine depletion of particulates from a plume, it is extremely difficult to relate the concentration of assumed ^{14}C particulates found on the ground to the emission rate of these particulates.

Further data on moss samples and soil profiles at larger distances (up to ~30 km) from Ignalina NPP will be reported. This study was partly financed by grants from the Swedish Radiation Protection Authority and Carl Tryggers Stiftelse.

REFERENCES

ACRP. 1995. The management of carbon-14 in Canadian nuclear facilities. ACRP-14. Advisory Committee on Radiological Protection.

AECL. 2001. AECL's environmental assessment summary of the Cernavoda nuclear power plant—Unit 2 project. CES-03702-ENA-001, Rev 1. Atomic Energy of Canada Limited.

Almenas K, Kaliatka A, Uspuras E. 1998. Ignalina RBMK-1500, a source book. ISBN 9986-492-35-1. Ignalina Safety Analysis Group, Lithuanian Energy Institute.

Baciu F, Baciu A, Alexandrescu M, Georgescu M, Popescu L, Antone M, Suto E, Dan L. 1996. Environmental radioactivity surveillance of the Romanian CANDU reactor of Cernavoda; normal operation and accident scenarios. *Proceedings of International IRPA Congresess IRPA9-Vienna-April 1996*, Vol. 2. International Radiation Protection Association.

Bobric E, Simionov V. 1999. Environmental monitoring program at Cernavoda nuclear power plant, environmental radiation monitoring data for Cernavoda NPP March 1996 to December 1998. In: Gortnar O, Stritar A, editors. *Nuclear Energy in Central Europe, Portoroz 1999*. Conference of the Nuclear Society of Slovenia.

Boss CR, Allsop PJ. 1995. Radioactive effluents from CANDU 6 reactors during normal operation. AECL-11506. Atomic Energy of Canada Limited.

Cooper EL, Benz ML, Cox JM. 1998. Measurement of low-level airborne $^{14}CO_2$ in the environment using passive sampling. *Applied Radiation and Isotopes* 49(9–11):1307–1311.

Dubourg M. 1998. The carbon-14 cycle. In: Technologies for gas cooled reactor decommissioning, fuel storage and waste disposal. *Proceedings of a Technical Committee Meeting*. IAEA-TECDOC--1043. International Atomic Energy Agency.

IAEA. 2002. Heavy water reactors: status and projected development. *Technical Report Series* no. 407. STI/DOC/010/407. International Atomic Energy Agency.

Jakimaviciute-Maseliene V, Mazeika J, Petrosius R. 2003. Spatial distribution of tritium and radiocarbon in Ignalina NPP region. *Sveikatos Mokslai* (Health sciences) 3:46–9. In Lithuanian.

Konstantinov EA, Korablev NA, Solovev EN, Shamov VP, Fedorov VL, Litvinov AM. 1989. ^{14}C emission from RBMK-1500 reactors and features determining it. *Soviet Atomic Energy* 66(1):77–79.

Marsden BJ, Hopkinson KL, Wickham AJ. 2002. The chemical form of carbon-14 within graphite. Report produced for NIREX. SA/RJCB/RD03612001/R01, Issue 4, 2002.

Mikhajlov ND, Kolkovsky VM, Pavlova ID. 1999. Radiocarbon distribution in northwest Belarus near the Ignalina nuclear power plant. *Radiocarbon* 41(1):75–79.

Milton GM, Kramer SJ, Brown RM, Repta CJW, King KJ, Rao RR. 1995. Radiocarbon dispersion around Canadian nuclear facilities. *Radiocarbon* 37(2):485–496.

Stenström K. 1995. New applications of ^{14}C measurements at the Lund AMS facility. [PhD dissertation]. Lund: Lund University Press.

Tenu A, Davidescu F, Cuculeanu V. 2002. Tropospheric CO_2 in Romania: concentration and isotopic composition measurements. In: Isotope aided studies of atmospheric carbon dioxide and other greenhouse gases, Phase II. IAEA-TECDOC-1269. International Atomic Energy Agency.

UNSCEAR. 2000. Sources and effects of ionizing radiation. UNSCEAR 2000 report to the General Assembly, with scientific annexes, Vol. I.

RADIOCARBON, Vol 46, Nr 2, 2004, p 869–875

SOURCES OF ANTHROPOGENIC ^{14}C TO THE NORTH SEA

P Gulliver[1,2] • G T Cook[1] • A B MacKenzie[1] • P Naysmith[1] • R Anderson[1]

ABSTRACT. The Sellafield nuclear fuel reprocessing plant on the northwest coast of England is the largest source of anthropogenic radiocarbon to the UK coastal environment. In a mid-1990s study of ^{14}C distribution around the UK coast, the pattern of dilution with increasing distance from Sellafield appeared to be perturbed by anomalously high ^{14}C activities in marine biota in the coastal environment of northeast England. This present study was undertaken during 1998 and 1999 to determine whether this ^{14}C enhancement was due to Sellafield or the nuclear power plants on the east coast. Seawater, seaweed (*Fucus* sp.), and mussel (*Mytilus edulis*) samples that were collected from the vicinity of the Torness and Hartlepool advanced gas-cooled reactor (AGR) nuclear power stations were all enhanced above the contemporary regional background activity derived from natural production and atmospheric nuclear weapons testing. We used previously published dilution factors and transfer times for ^{99}Tc between Sellafield and various points on the UK coast to determine likely Sellafield-derived ^{14}C contributions to the activities at the nuclear power plant sites. The results suggest that the activities observed at Torness, which are only marginally enhanced above the natural background activity, are possibly due to discharges from Sellafield; however, the significant ^{14}C enhancements at Hartlepool are not Sellafield-derived. Furthermore, since both reactors have the same fundamental design, the low activities at the Torness AGR imply that the activities at Hartlepool are not from the AGR, suggesting that there is an input of ^{14}C to the marine environment in the vicinity of Hartlepool which is probably non-nuclear-power related. However, there is no other authorized site in the area that could account for the observed ^{14}C enrichments; therefore, further research is required to ascertain the source of this ^{14}C.

INTRODUCTION

A 1995 investigation of ^{14}C activities in the UK coastal marine environment (Cook et al. 1998) analyzed the dissolved inorganic carbon (DIC) component of seawater, seaweed (*Fucus* species), and flesh from mussels *(Mytilus edulis)*, crab (*Cancer pagurus*), flatfish (plaice), and roundfish (cod). The study revealed a pattern of dilution of ^{14}C activity in the DIC with increasing distance from Sellafield (the largest source of anthropogenic ^{14}C to the coastal waters of the British Isles) in a clockwise manner around the British Isles, i.e., in the direction of the prevailing currents. The trend was perturbed by anomalously high ^{14}C activities at Whitby, located on the east coast of the British Isles (Figure 1). As the ^{14}C activities in the north of Scotland were significantly lower than those found at Whitby, Cook et al. (1998) concluded that the net activities found at Whitby were possibly due to releases from the nearby nuclear power producing facility at Hartlepool (Figure 1), which was one of the first advanced gas-cooled reactors (AGR) commissioned in the British Isles.

The use of Sellafield-derived radionuclides as a tracer for water movement is well established, and these studies have shown that the Sellafield discharges are carried north from the Irish Sea, through the North Channel (Figure 1), along the west coast of Scotland, around the north coast of Scotland, and subsequently south along the east coast of the UK (Jefferies et al. 1973, 1982; Prandle 1984; Dahlgaard 1995; Nines 1990; Kershaw and Baxter 1995). Recent studies using Sellafield-derived ^{99}Tc indicate transport times of approximately 9 and 24 months to Pentland Firth and Lowestoft (270 km south of Whitby), respectively (Leonard et al. 1997; McCubbin et al. 2002) (Figure 1). In order to investigate whether or not the activities above ambient background at Whitby were an anomaly or were a common feature close to AGR facilities, this study was carried out to investigate ^{14}C activities in the vicinity of Hartlepool and another AGR facility at Torness (Figure 1) in south-

[1]Scottish Universities Environmental Research Centre, Scottish Enterprise Technology Park, East Kilbride G75 0QF, Scotland.
[2]NERC Radiocarbon Laboratory, Scottish Enterprise Technology Park, East Kilbride G75 0QF, Scotland.
Corresponding author. Email: P.Gulliver@nercrcl.gla.ac.uk.

Proceedings of the 18th International Radiocarbon Conference, edited by N Beavan Athfield and R J Sparks
RADIOCARBON, Vol 46, Nr 2, 2004, p 869–875

east Scotland. Samples were obtained from the immediate vicinity of the Hartlepool AGR in 1998 and 1999, and from the vicinity of the Torness AGR in 1999.

Figure 1 Map of the United Kingdom indicating sampling and other sites referenced in the text

METHODS AND MATERIALS

The following suite of samples was collected from the vicinity of both the Hartlepool and Torness nuclear power plants: DIC extracted from 100 L of water, seaweed (*Fucus* sp.), and mussels (*Mytilus edulis*).

The water samples were acidified, purged with nitrogen, and the CO_2 collected and converted to benzene for radiometric analysis, as described in Gulliver et al. (2001). The seaweed samples were washed thoroughly and then dried. The mussels were boiled briefly to aid removal of the flesh and then freeze-dried. These samples were then combusted and the CO_2 converted to benzene (Gulliver et al. 2001).

At Torness, the samples were collected close to the coolant water outflow pipeline. At Hartlepool, the samples were collected from Parton Rocks, approximately 3 miles from the nuclear plant.

RESULTS AND DISCUSSION

^{14}C activities (Bq kg^{-1} C) for the DIC and biota samples are presented in Table 1 as net activities above the relevant ambient background, which depends on the year of collection and species. The background activities were derived from Burtonport (Figure 1), a site on the west coast of Ireland which is not significantly influenced by discharges from the Sellafield plant (Cook et al. 1998; Gulliver et al. 2001). Also included for reference are net ^{14}C activities (Bq kg^{-1} C) for the samples collected in 1995 from Whitby on the NE coast of England (Cook et al. 1998).

Table 1 Net ^{14}C activities (Bq kg^{-1} C ± 1 σ) in DIC, seaweed, and mussels collected from the vicinity of the Hartlepool and Torness AGRs (1998 and 1999) and from Whitby (1995).

Location	Sampling date	DIC	Mussels	Seaweed
Whitby[a]	1995	23 ± 5	11 ± 3	23 ± 3
Hartlepool	1998	104 ± 4	561 ± 4	55 ± 3
Hartlepool	1999	94 ± 5	913 ± 4	50 ± 4
Torness	1999	16 ± 4	38 ± 3	27 ± 2

[a]From Cook et al. (1998).

The ^{14}C activities of all samples are enhanced above ambient background, while the Hartlepool samples are all more highly enriched than those from either Torness or Whitby. The questions raised by these results are the following:

- What is the source of the enhancements above ambient background at both Torness and Hartlepool?
- Why is there such a difference between the 2 sites?

Based on low ^{14}C activities of samples from northern Scotland, Cook et al. (1998) discounted the influence of Sellafield-derived ^{14}C discharges on the activities found at Whitby in NE England. However, it can be observed from Figure 2 that there was a large increase in ^{14}C discharges from Sellafield in 1994/95, around the time of their study. Sellafield-derived ^{99}Tc has much in common with Sellafield-derived ^{14}C. Both have been discharged since 1952; they have similar, recent discharge histories (Figure 2), including a peak in discharges during 1994/95; they have long half-lives (^{99}Tc has a half-life of 2.3×10^5 yr); and they behave in a conservative manner in the marine environment. In particular, ^{99}Tc has a low K_d in sediments that are low in organic matter, such as those of the Irish Sea. Recent studies using Sellafield-derived ^{99}Tc as a tracer of water movement give transit times of 15–18 months from Sellafield to the east coast of the UK (Leonard et al. 1997; McCubbin et al. 2002). The 1994/95 peak in ^{99}Tc discharge activities and the propagation of this peak through UK coastal waters was studied in detail, with results indicating that the leading edge of the peak had traveled around the north coast of Scotland and as far south as latitude 52° north within 9 months (McCubbin et al. 2002). A further study has shown that the leading edge reached Arctic waters between 1998 and 1999 (Kershaw et al. 2004). If we use transport of Sellafield-derived ^{99}Tc as a proxy for Sellafield-derived ^{14}C transport in UK coastal waters, this implies that the activities found at Torness and Hartlepool in 1998 and 1999 could not be due to the peak in ^{14}C discharges from Sellafield in 1994/1995. In addition, if there was any contribution of ^{14}C to the activities found at Hartlepool or Torness, then it would be from discharges from Sellafield made approximately 15–18 months prior to the collection of samples for this study.

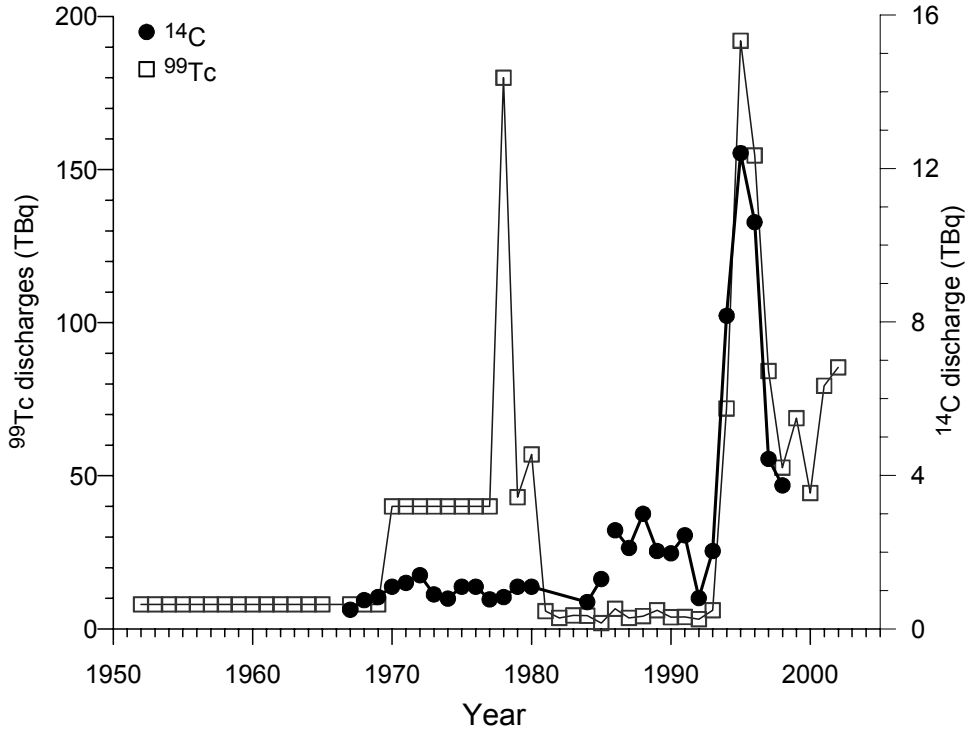

Figure 2 ^{14}C and ^{99}Tc discharges from the Sellafield nuclear fuel reprocessing plant (1952–2000)

From Tables 1 and 3, it can be observed that ^{14}C activities in the vicinity of Hartlepool fall within the range measured at the North Channel. While it is unlikely that transport of ^{14}C in the DIC would not result in dilution, it is hard to be definitive about this without data from an additional site situated between Sellafield and the NE coast of England. Unfortunately, this study did not investigate ^{14}C activities in the marine environment from northern Scotland, unlike the study of Cook et al. (1998). However, estimates of DIC ^{14}C activity at Cape Wrath (Figure 1) can be made using (i) dilution factors between the North Channel and Cape Wrath calculated by McCubbin et al. (2002) for 1993 to 1996 using ^{99}Tc (see Table 2), and (ii) DIC ^{14}C activities from the North Channel collected between August 1997 and July 1999 (Table 3). The North Channel DIC ^{14}C activities reflect discharges from Sellafield made 3–6 months prior to the collection date, and so are representative of Sellafield discharges that would reach Torness and Hartlepool 15–18 months after the date of discharge. Due to variations in current flux and ^{14}C discharge from Sellafield, there are obvious assumptions in using dilution factors for 1993 to 1996 and ^{14}C data for 1997 to 1999; however, neither the dilution factors (4.7 to 12.2) nor the DIC ^{14}C activities at the North Channel (101–271 Bq kg^{-1}) vary greatly over this period. Therefore, the estimates (8.2 to 57.7 Bq kg^{-1} C) (Table 2) based on these data are useful in providing the only probable range of DIC ^{14}C activities for Cape Wrath during this time. The net ^{14}C activity for the DIC at Torness falls within this range, suggesting that at least part of the enhancement above ambient background may be Sellafield-derived. In contrast, the net activities in the DIC at the Hartlepool site are greater than this range. In view of the dilution that ^{14}C undergoes during transport and the fact that Torness is significantly closer to Sellafield than Hartlepool, it would seem unlikely that the enhancements above ambient background at Hartlepool are Sellafield-derived, although some contribution from Sellafield cannot be ruled out. As both the Hartlepool and Torness nuclear plants have the same fundamental design, the low activities at the Torness AGR

imply that the significantly higher activities found at Hartlepool are not from the AGR, although on the evidence available some contribution cannot be ruled out.

Net activities in mussels from Hartlepool were 561 ± 4 Bq kg^{-1} C in 1998 and 913 ± 4 Bq kg^{-1} C in 1999. These activities are significantly higher than those found at the North Channel; indeed, the net mussel activity in 1999 falls within the range of activities found at Nethertown (Table 3), close to Sellafield (Figure 1). Comparison of the Hartlepool data and data from a site very close to Amersham International plc (Cook et al. 1998) indicates certain similarities. The Amersham data had an excess ^{14}C ratio of approximately 10:1 for mussels:seaweed, which was interpreted as indicating a significant organic component in the discharges. The enhancements in mussels relative to seaweed at Hartlepool are 11:1 for 1998 and 18:1 for 1999. These ratios are greater than the Amersham ratio, implying that the discharges close to Hartlepool also have an organic component. The activities in mussels are similar in magnitude at the Amersham and Hartlepool sites, implying a similar sized discharge to Amersham (1–2 TBq during this period), close to the Hartlepool sampling site, or indeed, a greater sized discharge at distance. However, the only other authorized nuclear site in the area was a small test reactor that ceased operations in 1996, and subsequent discharges are under the heading of beta/gamma and ranged from 9.69×10^{-8} to 9.79×10^{-7} TBq between 1996 and 1999 (CEFAS 1997–2000). The magnitude of these discharges is much too small to account for the observed enrichments at Hartlepool. We therefore have no obvious explanation for these anomalously high ^{14}C activities.

Table 2 ^{99}Tc dilution factors between the North Channel and Cape Wrath (from McCubbin et al. 2002) and estimated ^{14}C activities in the DIC fraction of the water column at Cape Wrath.

Survey date	^{99}Tc dilution factor	Estimated ^{14}C activity (Bq kg^{-1} C)
December 1993	12.2	5.5–22.2
December 1994	8.0	8.4–22.9
December 1995	9.1	7.4–29.8
December 1996	4.7	14.3–57.7

CONCLUSIONS

There are ^{14}C enrichments in biota around the Hartlepool and Torness AGRs. Both have the same fundamental design, and so would be expected to have the same ^{14}C formation and discharge pathways; however, the activities around Hartlepool are significantly greater.

Hartlepool is significantly further away from Sellafield than Torness, implying that the activities are not Sellafield-derived.

Using dilution factors for Sellafield-derived ^{99}Tc between the North Channel and Cape Wrath and ^{14}C data from the North Channel, it was possible to calculate likely ^{14}C activities at Cape Wrath. These data demonstrated that the ^{14}C discharges from Sellafield could be a significant contributor to the net DIC activities found in the vicinity of the Torness AGR but are not responsible for the net DIC activities found in the vicinity of the Hartlepool AGR.

The activities in mussels were significantly greater than those in the DIC and seaweed, implying the possibility of an organic ^{14}C discharge in the vicinity of Hartlepool; however, the only other authorized discharge in the area appears too small to account for the activities.

Table 3 Net ^{14}C activities (i.e. above ambient background) in mussels (*Mytilus edulis*) and the DIC fraction of the water column (Bq kg^{-1} C ± 1 σ) collected at Nethertown and the North Channel.

	Nethertown		North Channel	
Collection date	Mussels	DIC	Mussels	DIC
Aug. 97	813 ± 4	440 ± 5	120 ± 4	120 ± 4
Sept. 97	956 ± 7	1012 ± 7	116 ± 4	117 ± 4
Oct. 97	1045 ± 4	2779 ± 9	111 ± 4	116 ± 4
Nov. 97	1104 ± 4	1335 ± 7	118 ± 4	111 ± 4
Dec. 97	1188 ± 5	3283 ± 9	111 ± 4	171 ± 4
Jan. 98	1197 ± 6	2956 ± 10	101 ± 4	271 ± 5
Feb. 98	1210 ± 6	3208 ± 15	117 ± 4	164 ± 4
Mar. 98	1216 ± 5	8057 ± 25	110 ± 5	150 ± 4
Apr. 98	1300 ± 5	2379 ± 9	116 ± 4	109 ± 4
May 98	1983 ± 8	3212 ± 11	108 ± 3	123 ± 4
June 98	1918 ± 8	5807 ± 27	115 ± 4	130 ± 6
July 98	1827 ± 8	4656 ± 15	108 ± 4	136 ± 5
Aug. 98	1812 ± 7	998 ± 5	106 ± 4	126 ± 4
Sept. 98	1596 ± 6	598 ± 5	105 ± 4	122 ± 4
Oct. 98	1569 ± 9	344 ± 4	109 ± 4	101 ± 6
Nov. 98	1555 ± 7	1453 ± 7	102 ± 4	124 ± 4
Dec. 98	1526 ± 10	520 ± 4	102 ± 4	136 ± 4
Jan. 99	1444 ± 7	1400 ± 7	106 ± 4	115 ± 4

It is also unlikely that the Hartlepool AGR is the source of organic ^{14}C as there is no evidence of an organic ^{14}C discharge in the vicinity of Torness and there is no known pathway for a significant production/discharge of organic ^{14}C from these reactors.

A further and more extensive investigation into ^{14}C distributions in the marine environment around Hartlepool is required to determine the location, discharge activities, and impact of the anthropogenic source of ^{14}C in this area.

ACKNOWLEDGEMENTS

We gratefully acknowledge Magnox Electric plc and the Industry Management Committee for their financial support of this study under Contract BL/G/51919/E.

REFERENCES

Begg FH. 1992. Anthropogenic ^{14}C in the natural aquatic environment [PhD dissertation]. Glasgow: University of Glasgow.

Begg FH, Baxter MS, Cook GT, Scott EM, McCartney M. 1991. Anthropogenic ^{14}C as a tracer in western U.K. coastal waters. In: Kershaw PJ, Woodhead DS, editors. *Radionuclides in the Study of Marine Processes*. New York: Elsevier Applied Science. p 52–60.

Begg FH, Cook GT, Baxter MS, Scott EM, McCartney M. 1992. Anthropogenic radiocarbon in the Eastern Irish Sea and Scottish coastal waters. *Radiocarbon* 34(3):707–16.

CEFAS (Centre for Fisheries, and Aquaculture Science). 1997–2000. Radioactivity in Food and the Environment (RIFE). Report to the Food Standards Agency and Scottish Environment Protection Agency.

Cook GT, Mackenzie AB, Naysmith P, Anderson R. 1998. Natural and anthropogenic ^{14}C in the UK coastal marine environment. *Journal of Environmental Radioactivity* 40(1):89–111.

Dahlgaard H. 1995. Transfer of European coastal pollution to the Arctic: radioactive tracers. *Marine Pollution Bulletin* 31:3–7.

Gulliver P, Cook GT, Mackenzie AB, Naysmith P, Anderson R. 2001. Transport of Sellafield-derived ^{14}C from the Irish Sea through the North Channel. *Radiocarbon*

43(2B):869–77.

Gulliver P. 2002. Geochemistry and budgetary considerations of ^{14}C in the Irish Sea [PhD dissertation]. Glasgow: University of Glasgow.

Jefferies DF, Preston A, Steele AK. 1973. Distribution of ^{137}Cs in British coastal waters. *Marine Pollution Bulletin* 4:118–22.

Jefferies DF, Steele AK, Preston A. 1982. Further studies on the distribution of ^{137}Cs in British coastal waters. 1. The Irish Sea. *Deep-Sea Research* 29:713–38.

Kershaw PJ, Baxter A. 1995. The transfer of reprocessing waste from northwest Europe to the Arctic. *Deep-Sea Research II* 42:1413–48.

Kershaw PJ, Heldal HE, Mork KA, Rudjord AL. 2004. Variability in the supply, distribution and transport of the transient tracer ^{99}Tc in the NE Atlantic. *Journal of Marine Systems* 44(1–2):55–81.

Leonard KS, McCubbin D, Brown F, Bonfield R, Brooks T. 1997. Distribution of Technetium-99 in UK coastal waters. *Marine Pollution Bulletin* 34(8):628–36.

McCubbin D, Leonard KS, Brown J, Kershaw PJ, Bonfield RA, Peak T. 2002. Further studies of the distribution of technetium-99 and caesium-137 in UK and European coastal waters. *Continental Shelf Research* 22:1417–45.

Nies H. 1990. The contamination of the North Sea by artificial radionuclides during the year 1987. *Journal of Environmental Radioactivity* 11:55–70.

Prandle D. 1984. A modelling study of the mixing of Cs in the seas of the European continental shelf. *Philosophical Transactions of the Royal Society London, Series A* 310:407–36.

RADIOCARBON, Vol 46, Nr 2, 2004, p 877–883

SELLAFIELD-DERIVED ANTHROPOGENIC ^{14}C IN THE MARINE INTERTIDAL ENVIRONMENT OF THE NE IRISH SEA

G T Cook[1,2] • A B MacKenzie[1] • G K P Muir[1] • G Mackie[1] • P Gulliver[1,3]

ABSTRACT. The intertidal biota from Parton beach, close to the Sellafield nuclear fuel reprocessing plant, were all found to be enriched in radiocarbon relative to ambient background. The degree of enrichment appears to reflect the positions of the biota in the food chain once the dilution in seaweed from atmospheric uptake is taken into account. Close to the low-water mark, the order was mussels > limpets > anemones ≅ winkles > seaweed. The same order was observed close to the high-water mark, except that anemones were absent from this area. The activities in the biogeochemical fractions of the water column reflect the fact that discharges are primarily in the form of dissolved inorganic carbon (DIC), which is subsequently transferred to the particulate organic carbon (POC) and, to a lesser extent, the dissolved organic carbon (DOC), and finally, the particulate inorganic carbon (PIC). Analysis of intertidal sediment suggests that there is likely to be a gradual increase in the specific activity of ^{14}C in the inorganic component of this material as Sellafield contaminated organisms die and their shells are ground down by natural processes.

INTRODUCTION

The Sellafield nuclear fuel reprocessing plant on the Cumbrian coast of NW England (Figure 1) commenced operations in October 1950. The site is operated by British Nuclear Fuels plc (BNFL) and currently hosts a range of operations including magnox and thermal oxide fuel reprocessing, waste management, reactor decommissioning and 4 magnox reactors that form the Calder Hall nuclear power generating facility (BNFL 2002). During reprocessing operations, low-activity waste is discharged to the atmosphere, to sea, or is disposed of as solid waste, either on-site or at the Drigg disposal site to the south of Sellafield. The aquatic discharges which are the subject of this study are via a 2.1 km length pipeline into the NE Irish Sea. The aquatic discharges of most Sellafield-derived radionuclides reached a peak in the early to mid-1970s, and since then, as a result of the introduction of several waste treatment plants, have been reduced by 2 to 3 orders of magnitude from their peak values (MacKenzie 2000). Up to 1984, the reported aquatic ^{14}C discharges were estimated and subsequent to this time, they were measured, typically on a monthly basis. In contrast to most other radionuclides, the reported ^{14}C discharges remained approximately constant at <1–3 TBq per annum until 1994, at which time there were significant increases (BNFL 1997). These were due primarily to a change in discharge policy, whereby discharges previously released to the atmosphere were diverted (as a consequence of introducing a gas scrubber) to the aqueous route, and to a lesser extent, to an increase in reprocessing. This change to the aqueous route also has the positive effect of reducing the radiological impact of the discharges (Begg 1992). Although the total discharges of ^{14}C from Sellafield are small in comparison with many other radionuclides, they are of radiological importance. The marine critical group consists of people in the coastal area of Cumbria who are high consumers of fish and shellfish from the Sellafield area. The most recent BNFL data indicate that ^{14}C accounts for about 4% of the dose to that critical group. However, in terms of the collective dose derived from the aquatic Sellafield discharges, ^{14}C represents the largest contributor to the UK, European, and world populations (BNFL 2002).

A previous study (Begg et al. 1992), which was designed to investigate the biogeochemistry and cycling of ^{14}C in the Sellafield environment, demonstrated that for several tens of km to the north

[1]SUERC, Scottish Enterprise Technology Park, East Kilbride G75 0QF, Scotland.
[2]Corresponding author. Email: g.cook@suerc.gla.ac.uk.
[3]NERC Radiocarbon Dating Laboratory, Scottish Enterprise Technology Park, East Kilbride G75 0QF, Scotland.

Proceedings of the 18th International Radiocarbon Conference, edited by N Beavan Athfield and R J Sparks
RADIOCARBON, Vol 46, Nr 2, 2004, p 877–883

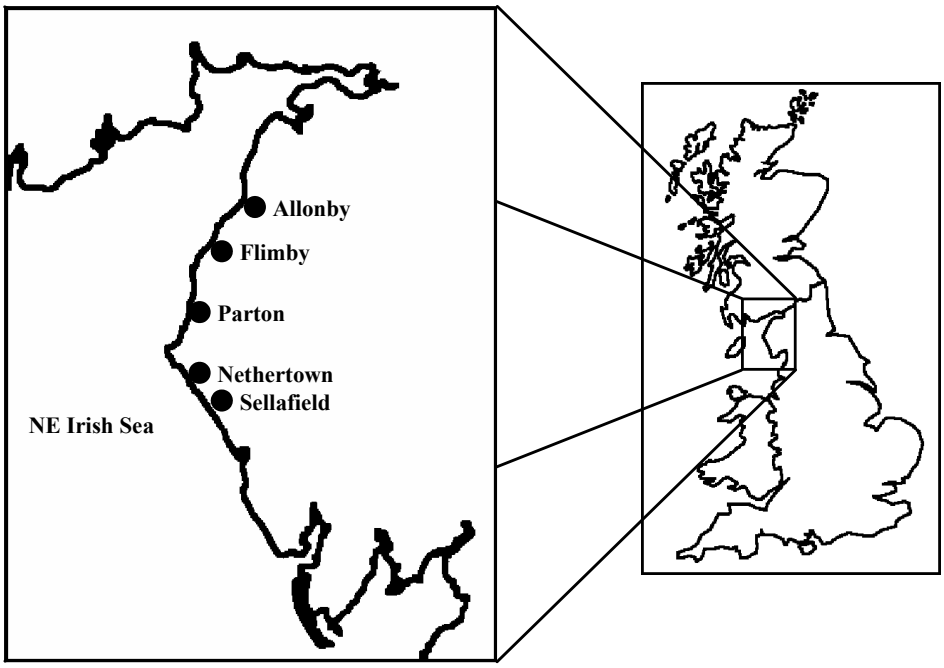

Figure 1 Map of sampling sites

and south of Sellafield, specific activities of ^{14}C were enhanced in a range of biota and that the relative degree of enhancement was always mussels (*Mytilus edulis*) > winkles (*Littorina littorea*) > seaweed (*Fucus* sp.). Begg al. (1992) also confirmed, from analysis of water column samples, that the aquatic ^{14}C discharges were predominantly in the form of dissolved inorganic carbon (DIC). However, the following questions remained unanswered by this study:

- Why did mussels, which are filter feeders, have the greatest ^{14}C enrichments, yet there was no evidence of ^{14}C enrichment in the particulate organic carbon component of the water column?
- Why did seaweed (*Fucus* sp.) have the lowest enhancements when they are primary producers, deriving their carbon directly from the DIC component, which was the only consistently enriched fraction of the water column?

In an attempt to provide a better explanation for these trends, it was decided that we should sample a greater range of intertidal biota, namely, seaweed (*Fucus* sp.), winkles (*Littorina littorea*), mussels (*Mytilus edulis*), anemones (*Actinia equina*), and limpets (*Patella vulgata*), together with water column samples. Also, whenever possible, biota samples were taken for analysis from close to both the low- and high-water marks. Seawater samples were collected periodically from the Sellafield area and ^{14}C analysis was undertaken on the particulate inorganic carbon (PIC), particulate organic carbon (POC), dissolved inorganic carbon (DIC), and dissolved organic carbon (DOC) fractions. Finally, intertidal sediment was collected from a number of locations to assess any potential long-term effects deriving from the breakdown of ^{14}C-contaminated shell from organisms such as winkles, mussels, limpets, etc.

MATERIALS AND METHODS

We collected the biota samples from Parton beach, approximately 20 km north of Sellafield, having chosen this site because of its proximity to the plant and for the range of biota that it supports. All

biota samples were collected in May 2000 and were chosen for their variable feeding habits, in order to explore further the relationship between different feeding behaviors and variations in ^{14}C concentrations within the intertidal environment. Mussels, winkles, seaweed, limpets, and common beadlet anemone were all collected from close to the low-water mark. Close to the high-water zone, the same species were collected with the exception of the anemone, which was completely absent from this zone. We collected approximately 1 kg fresh weight of each invertebrate species, and upon our return to the laboratory, washed them thoroughly in dilute HCl and then in distilled water. We then boiled the mussels, winkles, and limpets for a few minutes to aid removal of the soft tissue from the shell and then re-washed them. We then freeze-dried and homogenized all samples in preparation for analysis. Seaweed samples were washed in dilute HCl, then in distilled water, oven-dried at 60 °C, and then homogenized. Radiometric ^{14}C analysis was carried out according to the method detailed in Begg et al. (1992).

We collected 100-L seawater samples periodically between November 1989 and February 1999 at a location close to the Sellafield plant. The samples were filtered through 0.7-µm glass fiber filters and the filtered particles stored at –22 °C prior to analysis. Where DOC analysis was carried out, the water samples were poisoned with mercuric chloride and stored in the dark at 4 °C prior to analysis. The 4 biogeochemical fractions (PIC, POC, DIC, and DOC) were analyzed according to the methods of Gulliver et al. (2001) and Wolstenholme (1999).

The sediment samples were collected from the intertidal area at 4 locations (Nethertown, Parton, Flimby, and Allonby) as depicted in Figure 1. Large fragments or indeed whole shells (mainly mussel and winkle) lying on the sediment surface were also collected. The sediment was sieved into 2 size fractions, <500 and >500 µm. These fractions and the shells were hydrolyzed with 4M HCl and analyzed for ^{14}C according to the method of Begg et al. (1992)

RESULTS

Figure 2 depicts the ^{14}C activities in intertidal biota from Parton once the contributions from weapons testing fallout and natural production for that year (approximately 248 Bq kg^{-1} C) had been removed (Gulliver 2002). This illustrates that the intertidal biota are all enriched in ^{14}C and that the trend in activity is mussels > winkles > limpets > seaweed, close to the high-water mark, and mussels > limpets > anemone ≅ winkles > seaweed, close to the low-water mark. The trend in ^{14}C activities of mussels > winkles > seaweed is, therefore, the same as that demonstrated by Begg et al. (1992) and applies to biota collected at close to the high- and low-water marks.

Gross ^{14}C activities (i.e. not corrected for natural production and weapons testing fallout) for the 4 geochemical fractions of the water column are presented in Table 1. Gross values are given because the background contribution to the DOC, POC, and PIC activities are difficult to estimate since they are dependent on local variables such as contributions from terrestrial run-off, sediment resuspension, level of primary production, etc. The DIC value for background is not subject to such local variables and is approximately 250 Bq kg^{-1} C (Gulliver et al. 2001). With the exception of 1 sampling date (Feb 1995), the DIC component was always enriched above ambient background. Also, from July 1995 onwards, the POC fraction was consistently enriched above the ambient background for the DIC, which can be taken as a maximum value for any of the geochemical components. The PIC values are highly variable and always depleted relative to the DIC and POC values for the corresponding sampling date. Three samples from 1997 and 1998 certainly are indicative of substantial enrichments above ambient background. DOC values were only measured until November 1996 and the result from this last sampling is certainly indicative of a substantial enrichment.

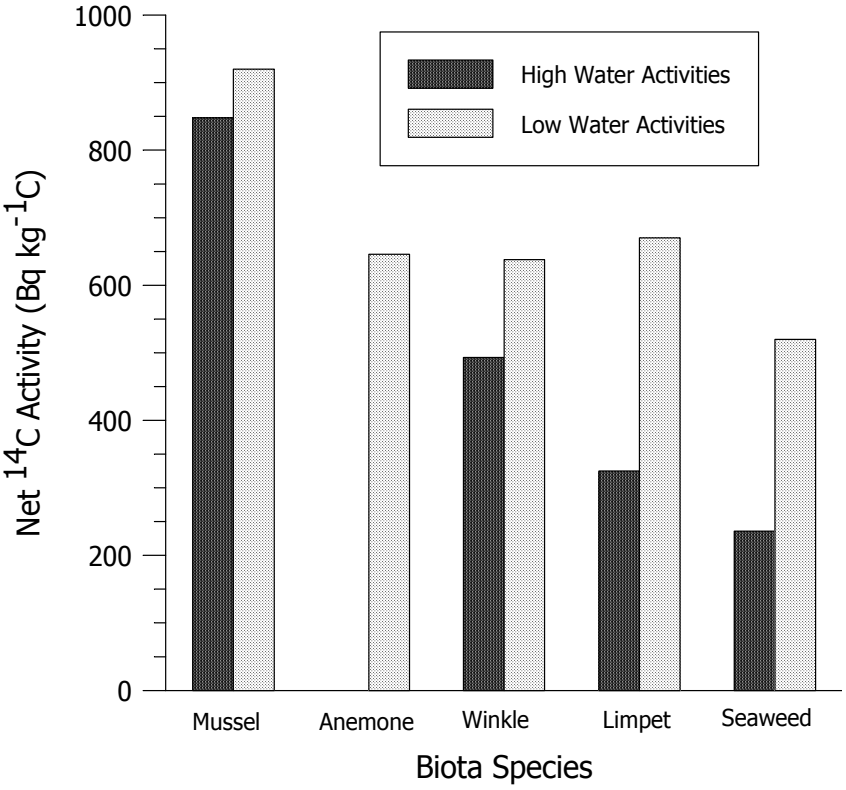

Figure 2 ^{14}C activities in a range of intertidal biota from Parton

Table 1 Gross ^{14}C activities (Bq kg^{-1} C) in the 4 geochemical fractions of the water column from the vicinity of Sellafield.

Collection date	DIC (Bq kg^{-1} C)	POC (Bq kg^{-1} C)	DOC (Bq kg^{-1} C)	PIC (Bq kg^{-1} C)
Dec '89[a]	550 ± 4	165 ± 2	143 ± 2	108 ± 1
Feb '91[a]	452 ± 2	182 ± 3	87 ± 2	134 ± 3
Feb '95[b]	247 ± 3	80 ± 1	218 ± 1	150 ± 2
July '95[b]	1099 ± 7	406 ± 3	107 ± 5	285 ± 3
Nov '95[b]	1538 ± 10	451 ± 2	76 ± 1	145 ± 1
Mar '96[b]	945 ± 4	478 ± 2	132 ± 1	144 ± 1
June '96[b]	1227 ± 5	612 ± 4	183 ± 1	180 ± 1
Nov '96[b]	1677 ± 9	614 ± 3	598 ± 3	201 ± 1
Nov '97	4553 ± 18	3616 ± 12	n/a	796 ± 11
Feb '98	1365 ± 4	631 ± 3	n/a	72 ± 10
May '98	1853 ± 43	1146 ± 4	n/a	860 ± 11
Aug '98	1160 ± 14	1024 ± 4	n/a	579 ± 10
Nov '98	486 ± 5	343 ± 2	n/a	103 ± 11
Feb '99	453 ± 2	296 ± 1	n/a	75 ± 10

[a]Begg 1992.
[b]Wolstenholme 1999.

The results for ^{14}C analysis of intertidal sediments are shown in Figure 3. The <500-µm size fraction data are consistent with sub-tidal inorganic sediment activities, while activities in the >500-µm fraction are consistently higher than the sub-tidal activities (Gulliver 2002). Finally, the whole shells/shell fragments are all significantly enriched with respect to the ambient background activity.

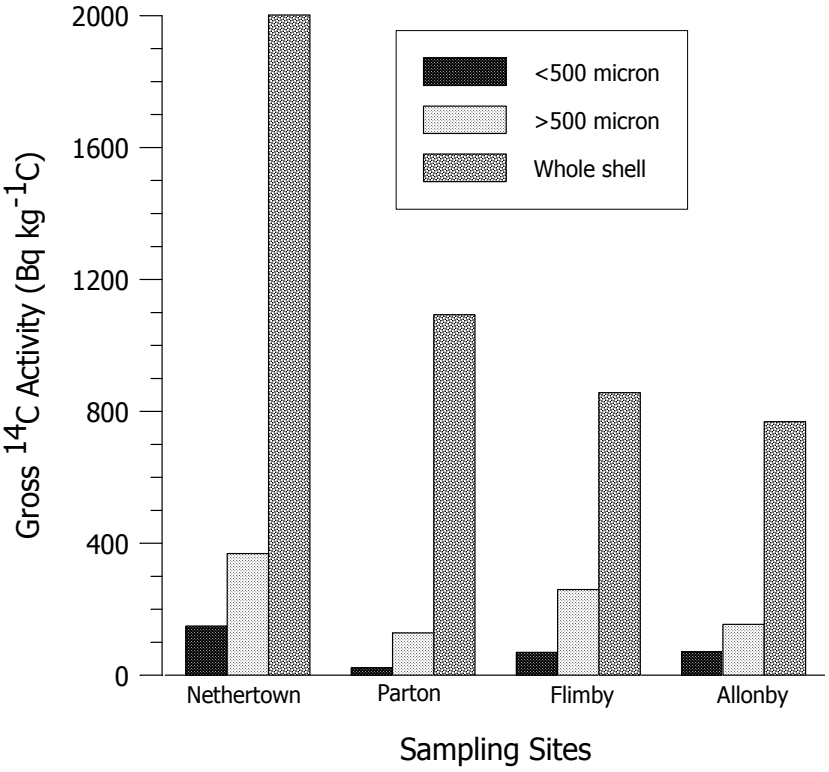

Figure 3 ^{14}C activities in different size fractions of the shell component of intertidal sediments

DISCUSSION

Biota

The explanation for mussels always having the highest activity lies in the fact that they are singularly suspension feeders, trapping fine food particles suspended in the water column. Water flows through an inhalant syphon and over the gills, where food particles in the form of phytoplankton and detritus are trapped on a mucous coating while the filtered water is expelled through an exhalant aperture. Particles that are too large to be digested or are recognized as pseudofeces are ejected (Barnes 1987). As (i) phytoplankton are the primary producers in the marine environment, deriving their carbon from the DIC component of the water, (ii) Sellafield marine ^{14}C discharges are almost entirely in the form of DIC, and (iii) the main food source of mussels is phytoplankton, it is reasonable to assume that the mussels are ingesting relatively active material due to this selective feeding habit as a primary consumer. It can also be noted from Figure 2 that there is little difference in activity between the low-water and high-water mark samples, consistent with mussels being filter feeders.

Seaweed (*Fucus* sp) consistently has the lowest ^{14}C activity of all biota analyzed. Since, like phytoplankton, seaweeds are primary producers that derive their carbon for photosynthesis from the DIC component of seawater, it could be expected that their activities should be similar to those of mussels (primary consumers). However, many seaweed species (including *Fucus*) have the ability to derive carbon from atmospheric CO_2 when they are exposed to the atmosphere. The activity of seaweed relative to mussels must then depend upon (i) the proportion of time that the seaweed is submerged and (ii) the ^{14}C activity of the DIC component of the water column relative to that of the atmosphere, which may be perturbed locally by the atmospheric Sellafield discharges. The fact that the seaweed ^{14}C activities are significantly lower than those in mussels implies that the ^{14}C activity of the atmosphere (Bq kg^{-1} C) is lower than that of the DIC. This can be substantiated by the fact that Isogai et al. (2002) demonstrated that the largest excess ^{14}C activity above ambient background in tree rings from the years 1994 to 1999 was 125 Bq kg^{-1} C in 1995 when the discharges to the atmosphere totalled 4.6 TBq for that year. These data were derived from analysis of a section of oak tree felled in September 1999 at a location 1.5 km east and slightly to the north of Sellafield. In contrast, the intertidal biota samples were collected in 2000 at Parton, which is approximately 20 km northwest from Sellafield, where the excess will undoubtedly be much reduced (the dominant wind direction is roughly from the southwest). Furthermore, the atmospheric discharges in that year totalled 2.9 TBq. Therefore, it can reasonably be assumed that the excess ^{14}C activity in the atmosphere in 2000 at Parton would have been significantly less than 125 Bq kg^{-1} C. It should also be noted from Figure 2 that the seaweed ^{14}C activity close to the low-water mark is approximately double that at the high-water mark, consistent with the fact that seaweed will derive CO_2 from the atmosphere when exposed. The activity of the seaweed close to the low-water mark is still significantly lower than that of the mussels. We would propose that this is because the seaweed close to low water is still exposed to the atmosphere for a significant period of time and also that the integration time of ^{14}C may differ for these 2 forms of biota.

The beadlet anemone feeds on a number of available food sources, including mussel flesh, zooplankton, small crustaceans, and worms. The food is captured on tentacles, paralyzed, and then carried to the mouth. The mussel flesh has been demonstrated here to be highly enriched in ^{14}C, while zooplankton, like mussels, are primary consumers which feed on phytoplankton and are also likely to be highly enriched. In contrast, it can be speculated on the basis of the relatively minor ^{14}C enrichments (and often lack of enrichment) of the organic component of the sediments within this area (Gulliver 2002) that the worms and small crustaceans which live in the surface sediment will show similar minor enrichments. Overall, the data would seem to reflect the position of the beadlet anemone in the trophic food chain as a secondary consumer.

Limpets and winkles can be dealt with together since their feeding behaviors are quite similar. Both species are herbivorous and at high tide they emerge from their protective shells to rasp algae (including *Fucus* sp.) and detritus that cover the rocks. Thus, their activities will reflect those of seaweed and detritus (including plankton); hence, the activities are intermediate between mussels and seaweed. Many of the winkles were collected from tidal pools and this could account for the fact that the high- and low-water activities are similar, i.e., they fed on seaweeds that were covered by seawater for a significant period.

Water Column

The water column results appear to reflect the change in discharge policy that took effect in 1994. After this time, the activities in the 4 biogeochemical fractions are typically greater than pre-1994. The POC component, the food source for mussels, is always depleted in ^{14}C relative to the DIC,

which appears to make the trend in activities of the mussels and seaweed difficult to explain. However, the following 3 factors have to be taken into account as discussed above:

1. Seaweed derive carbon from the atmosphere when not covered by seawater;
2. The activity of ^{14}C in the atmosphere is significantly lower than the DIC of the water column;
3. The mussels are selective feeders that can exclude certain particles. When these factors are taken into account, it becomes possible to understand why the activities in mussels exceed those of seaweed.

Sediment

The results presented in Figure 3 suggest that as contemporary shell is broken down and is incorporated into the sediment, there will be a gradual increase in the ^{14}C activity of the inorganic component of the sediment with time. The current ^{14}C activity of the inorganic component is low, indicating that it is dominantly pre-Sellafield in origin. The rate at which the inorganic sediment ^{14}C activity increases will depend upon future trends in ^{14}C discharges, the mass of Sellafield-era shell material relative to the pre-Sellafield mass, the ^{14}C activity of the Sellafield-era shell material, and the rate at which natural processes break it down into fine material.

CONCLUSIONS

The ^{14}C activities in the biota appear to reflect their positions in the food chain once the dilution in seaweed from atmospheric uptake is taken into account. The activities in the biogeochemical fractions of the water column reflect the fact that discharges are primarily in the form of DIC, which is subsequently transferred to the POC and to a lesser extent the DOC and finally the PIC. Analysis of intertidal sediment suggests that there is likely to be a gradual increase in the specific activity of ^{14}C in the inorganic component of this material as Sellafield contaminated organisms die and their shells are ground down by natural processes.

REFERENCES

Barnes RD. 1987. *Invertebrate Zoology*, 5th Edition. Philadelphia: Saunders College Publishing, International Edition.

Begg FH. 1992. Anthropogenic ^{14}C in the natural aquatic environment [PhD dissertation]. Glasgow: University of Glasgow. 262 p.

Begg FH, Cook GT, Baxter MS, Scott EM, McCartney M. 1992. Anthropogenic radiocarbon in the eastern Irish Sea and Scottish coastal waters. *Radiocarbon* 34(3):707–16.

BNFL. 1997. Annual report on radioactive discharges and monitoring of the environment 1996, Volume 1. British Nuclear Fuels plc, Risley.

BNFL. 2002. Discharges and monitoring of the Environment in the UK—Annual Report 2001. British Nuclear Fuels plc, Risley.

Gulliver P. 2002. Geochemistry and budgetary considerations of ^{14}C in the Irish Sea [PhD dissertation]. Glasgow: University of Glasgow. 263 p.

Gulliver P, Cook GT, MacKenzie AB, Naysmith P, Anderson R. 2001. Transport of Sellafield-derived ^{14}C from the Irish Sea through the North Channel. *Radiocarbon* 43(2B):869–77.

Isogai K, Cook GT, Anderson R. 2002. Reconstructing the history of ^{14}C discharges from Sellafield: 1. Atmospheric discharges. *Journal of Environmental Radioactivity* 59:207–22.

MacKenzie AB. 2000. Environmental radioactivity: experience from the 20th century—trends and issues for the 21st century. *The Science of the Total Environment* 249:313–29.

Wolstenholme A. 1999. The biogeochemistry of ^{14}C within the Irish Sea [PhD dissertation]. Glasgow: University of Glasgow. 182 p.

RADIOCARBON, Vol 46, Nr 2, 2004, p 885–892

SPATIAL AND TEMPORAL IMPACTS OF ^{14}C RELEASES FROM THE SELLAFIELD NUCLEAR COMPLEX ON THE IRISH COASTLINE

Sinead M Keogh[1] • Edward J McGee • Donal Gallagher • Peter I Mitchell

Department of Experimental Physics, University College Dublin, Belfield, Dublin 4, Ireland.

ABSTRACT. The Sellafield nuclear fuel reprocessing plant is estimated to be the largest single source of global anthropogenic radiocarbon discharge. This study addresses the impact of these releases on the Irish coastal marine environment. Spatial trends in the ^{14}C content of seaweed (*Fucus* spp.) were assessed by collecting and analyzing samples from well-distributed locations around the Irish coastline. Temporal trends were studied by comparing ^{14}C concentrations in present-day samples with levels found in archive material collected at the same locations during research campaigns conducted in the mid-1980s and mid-1990s. The impact of ^{14}C discharged from Sellafield was found to be most apparent in seaweeds from the northeastern Irish coast. This indicates that the pattern of residual currents and, in particular, the south to north transfer of water known to predominate in the Irish Sea, largely controls the spatial distribution of ^{14}C releases. Maximum ^{14}C discharge levels to the marine environment from Sellafield (between 12 and 13 TBq yr^{-1}) were mirrored by peak concentrations found in seaweed from the mid-1990s and in present-day samples (highest recorded value of 130.4 pMC). Concentrations of ^{14}C in seaweed from the west coast of Ireland correspond closely with values measured for seaweeds from the Atlantic coast of northwest Spain and do not appear to be significantly affected by Sellafield discharges.

INTRODUCTION

The radiological importance of radiocarbon derives from its long half-life (5730 yr), mobility in the environment, and propensity for entering the food chain. In a global context, the collective dose from world-wide discharges of ^{14}C, integrated over 10,000 yr, comprises about 80% of the collective dose from the complete nuclear fuel cycle (UNSCEAR 2001; Isogai et al. 2002). Data concerning environmental concentrations of ^{14}C are, however, limited, and it is important that ^{14}C be taken into account in estimating the future collective dose commitment to the Irish population, given the proximity of the Sellafield reprocessing plant in the UK.

Sellafield

The Sellafield complex is located on the Cumbrian coast of northwest England, about 120 km from the northeast coast of Ireland, and is operated by British Nuclear Fuels plc. The complex has been identified by UNSCEAR (1993) as the largest single contributor of ^{14}C to the global environment and the vast majority of the ^{14}C discharges from the site result from nuclear fuel reprocessing operations.

Low-level liquid radioactive waste containing ^{14}C has been discharged from Sellafield into the northeastern Irish Sea since operations began in the early 1950s. A decision in the early 1990s to divert ^{14}C waste from the aerial to the liquid effluent stream resulted in an increase in ^{14}C discharges to the marine environment, which is particularly evident in the peak levels of 12.4 and 13 TBq discharged in 1995 and 2002, respectively (BNFL 1995; MAFF 1996; BNFL 2001; FSA/SEPA 2003). Discharges are mainly in inorganic form and are released as aqueous effluent. In this paper, we examine the relationship between the historical record of ^{14}C in liquid discharges and the ^{14}C content of *Fucus* spp. samples from the Irish coastline.

Seaweed as a Bioindicator

Seaweeds of the genus *Fucus* spp. have proved to be extremely useful and practical as bioindicators for monitoring radioactive discharges from nuclear power plants. The advantages of using *Fucus*

[1]Corresponding author. Email: sineadmkeogh@eircom.net.

Proceedings of the 18th International Radiocarbon Conference, edited by N Beavan Athfield and R J Sparks
RADIOCARBON, Vol 46, Nr 2, 2004, p 885–892

spp. are discussed by O'Donnell (1997) and can be summarized as follows: a) sensitivity is greatly increased because of the higher concentrations of radionuclides in the algae relative to the surrounding waters; b) *Fucus* spp. is found in great masses in shallow waters along most marine and brackish water coasts at the latitudes we are investigating; and c) seaweeds are much easier to collect, treat, and store for long periods in comparison to water samples.

A large percentage of the ^{14}C content of aqueous discharge effluent from Sellafield is in the form of carbonate/bicarbonate, and so is immediately incorporated into the dissolved inorganic carbon (DIC) fraction of the water column. Seaweeds, as primary producers, utilize the DIC during photosynthesis and, thus, record a time-integrated ^{14}C value (Cook et al. 1998).

The relevance of using *Fucus* spp. as a bioindicator for monitoring ^{14}C discharges from Sellafield is clearly demonstrated by comparing the measured ^{14}C concentration in seaweed from the Sellafield site with the level of ^{14}C in annual liquid discharges (Figure 1). The superimposed trends are clearly correlated and indicate that the concentrations of ^{14}C in *Fucus* spp. reflect the levels of ^{14}C discharged to the Irish Sea (with a short time lag).

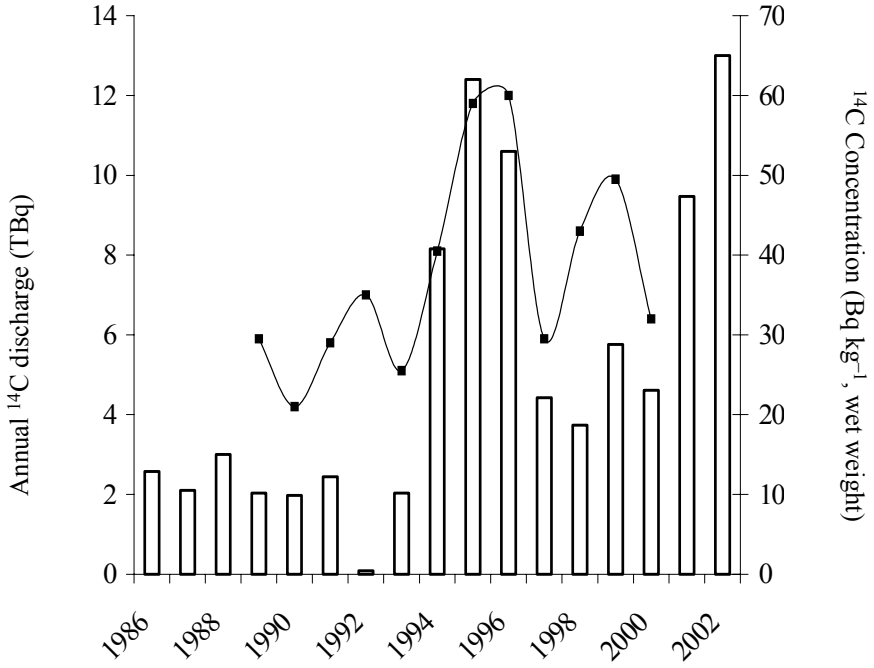

Figure 1 Bar chart showing liquid ^{14}C discharges from Sellafield (Source: FSA/SEPA 2003) and curve showing concentrations of ^{14}C in *Fucus* spp. from the Sellafield shoreline (Source: DEFRA 2002).

METHODS AND MATERIALS

Sample Collection

Seaweeds were sampled from locations selected to provide a representative geographical distribution on all aspects of the Irish coast. The sites were chosen after consulting with the Radiological Protection Institute of Ireland (RPII) in order to coincide with regular monitoring stations for other radionuclides such as ^{137}Cs, ^{99}Tc, and ^{131}I. The locations of these sites are shown in Figure 2.

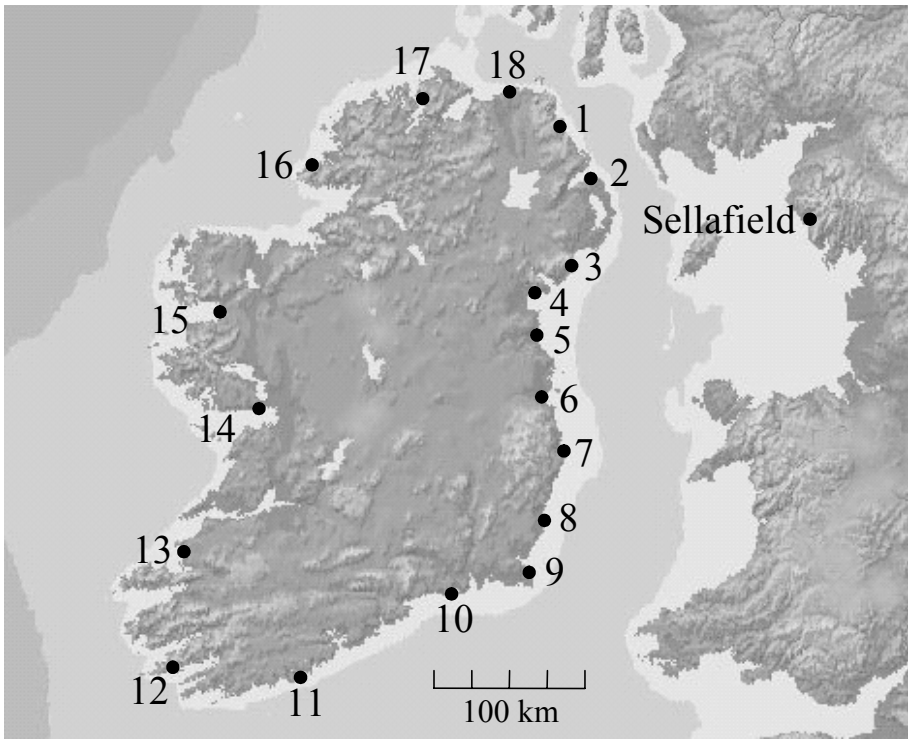

Figure 2 Map of Ireland showing the locations of *Fucus* spp. sampling sites relative to the Sellafield nuclear reprocessing complex in Cumbria, UK.

Seaweed was collected from the intertidal area of each sampling site between November 2002 and August 2003. Archived samples collected between November 1985 and March 1986, and between March 1994 and November 1995 during the course of previous research projects, were sourced from the RPII and the Radiation Physics Research Laboratory of University College Dublin. For convenience, the 3 sets of seaweed samples will hereafter be referred to as relating to 1985, 1994, and 2003, respectively.

Three *Fucus* spp. samples collected near Arosa, Cabo Prior, and Muros (Galician coast, northwest Spain) during 1984 were recovered from our archives. These samples were previously analyzed for plutonium isotopes and showed the ^{238}Pu, ^{239}Pu, and ^{240}Pu concentrations in *Fucus* spp. from this region to be in very good agreement with predicted and reported fallout ratios in mid-latitudes of the Northern Hemisphere (Sanchez-Cabeza 1989).

Fucus spp. samples from both the Irish and Galician coastlines were pretreated and analyzed for ^{14}C as described below.

Sample Analysis

The seaweed was washed thoroughly to remove extraneous material, then oven-dried at 80 °C for 24 hr, ground, and homogenized. Approximately 50 g of each sample was boiled in 1 M HCl for 8 hr to hydrolyze any carbonate and remove surface organic debris. Samples were then rinsed in distilled water and oven-dried again before conversion to benzene via carbon dioxide and acetylene (O'Donnell 1997). The ^{14}C activity of the benzene was measured using low-background liq-

uid scintillation counting (Tri–Carb 2770 TR/SL). The UCD Radiocarbon Age Calculation Program (Gallagher et al. 2002) was used to calculate the ^{14}C concentrations of the seaweeds.

Quality Control

Measurement of the C3 cellulose intercomparison material (IAEA 1998) gave a concentration of 129.8 ± 1.5 (2 σ) percent modern carbon (pMC), which compares very well with the consensus value of 129.41 ± 0.12 (2 σ) pMC and demonstrates the measurement capability of our laboratory. In addition, 8 seaweed samples from the Irish coastline were measured in duplicate to test analytical reproducibility; the resulting data are given in Table 1.

Table 1 Quality assurance data showing values for replicate analyses (#1 and #2) carried out on samples of *Fucus* spp. from selected locations. Quoted uncertainties are ± 2 σ.

		Replicates (pMC)	
Site number	Year	# 1	# 2
3	1985	121.3 ± 1.4	121.7 ± 1.4
3	1994	128.9 ± 1.5	130.4 ± 1.6
4	1994	127.5 ± 1.6	126.6 ± 1.4
4	1985	124.5 ± 1.4	125.8 ± 1.6
5	1985	121.0 ± 1.5	121.4 ± 1.4
12	1994	109.4 ± 1.4	110.6 ± 1.3
15	1985	115.8 ± 1.3	114.2 ± 1.3
16	1985	117.2 ± 1.5	117.2 ± 1.3

RESULTS AND DISCUSSION

Anthropogenic ^{14}C in the Marine Environment

Results are presented as pMC in Table 2. Figure 3a–c reveals enhancements in the pMC value of seaweed taken from the northeast coast of Ireland in 1985, 1994, and 2003 with respect to the pMC value of seaweed taken from the western coast, and indicate that ^{14}C discharged from Sellafield has a measurable impact on Irish marine biota from the north and east coasts. The enhancement along the northeastern coastline appears to reflect the predominantly south to north direction of residual currents of the Irish Sea (Jefferies et al. 1982). These findings concur with previous measurements of ^{14}C enrichments in seawater and biota which revealed a pattern of clockwise water circulation around mainland Britain (Cook et al. 1998).

There is a clear correspondence between the recorded level of ^{14}C in liquid discharges from Sellafield (Figure 4) and the measured concentration of ^{14}C in seaweed from the northeast coast (Figure 3). Peak values of approximately 130 pMC are found in seaweed taken from sites 2 and 3 in 1994 and site 1 in 2003, reflecting the significantly increased discharges from Sellafield in those years relative to 1985.

Ambient Background Levels of ^{14}C

Seaweed from the west coast showed the highest mean concentration of approximately 116 pMC in 1985 with a decrease to 112 pMC in 1994 and a further decrease to 107 pMC in 2003 (Table 3). These measurements concur closely with a previous measurement of ^{14}C activity in seaweed from the west of Ireland in 1995, namely 109.7 pMC (Cook et al. 1998), and show that there has been a decline in ^{14}C activity in North Atlantic surface waters since the mid-1980s.

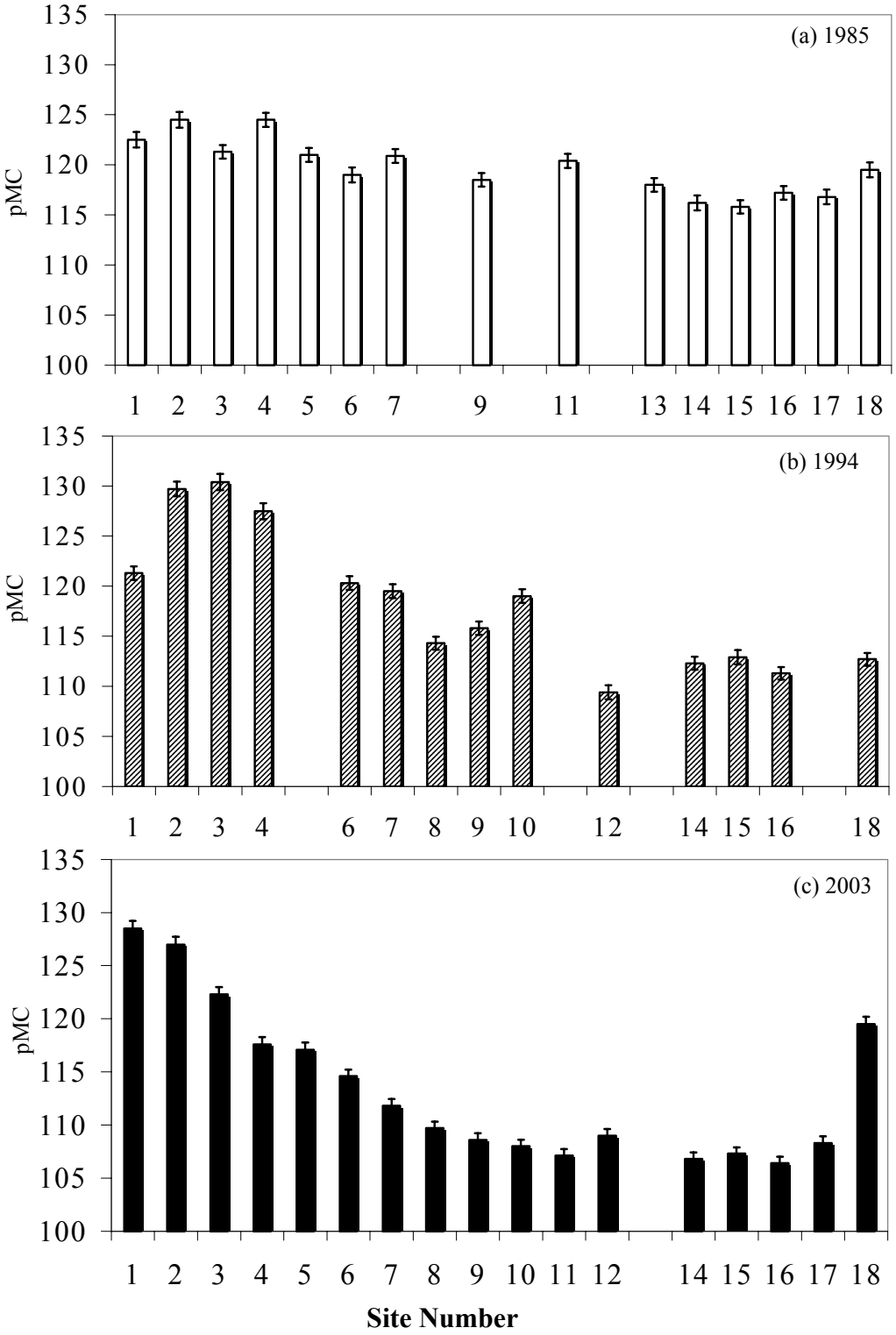

Figure 3 ^{14}C concentrations in *Fucus* spp. from Irish coastal sites taken in (a) 1985, (b) 1994, and (c) 2003. Refer to Figure 2 for locations of site numbers (indicated uncertainties are ±2 σ).

Table 2 ^{14}C concentrations (pMC[a]) in seaweed sampled around the Irish coastline in 1985, 1994, and 2003. Quoted uncertainties are ±2 σ

Site nr	Location	1985	1994	2003
1	Cushendall	122.5 ± 1.5	121.3 ± 1.4	128.5 ± 1.5
2	Bangor	124.5 ± 1.6	129.7 ± 1.5	127.0 ± 1.4
3	Newcastle	121.3 ± 1.4	130.4 ± 1.6	122.3 ± 1.4
4	Carlingford	124.5 ± 1.4	127.5 ± 1.6	117.6 ± 1.3
5	Clogherhead	121.0 ± 1.4	—	117.1 ± 1.3
6	Dublin Bay	119.0 ± 1.5	120.3 ± 1.4	114.6 ± 1.2
7	Wicklow	120.9 ± 1.4	119.5 ± 1.4	111.8 ± 1.3
8	Cahore	—	114.3 ± 1.3	109.7 ± 1.3
9	Rosslare	118.5 ± 1.4	115.8 ± 1.3	108.6 ± 1.2
10	Dunmore East	—	119.0 ± 1.4	108.0 ± 1.2
11	Kinsale	120.4 ± 1.4	—	107.1 ± 1.2
12	Castletownbere	—	109.4 ± 1.4	109.0 ± 1.2
13	Ballyheigue	118.0 ± 1.3	—	—
14	Galway Bay	116.2 ± 1.5	112.3 ± 1.3	106.8 ± 1.2
15	Clew Bay	115.8 ± 1.3	112.9 ± 1.4	107.3 ± 1.2
16	Glen Columcille	117.2 ± 1.3	111.3 ± 1.3	106.4 ± 1.2
17	Lough Swilly	116.8 ± 1.5	—	108.3 ± 1.2
18	Giants Causeway	119.5 ± 1.5	112.7 ± 1.3	119.5 ± 1.4

[a]Note: To convert from pMC to Bq kg^{-1}(carbon) dry weight, multiply by a factor of 2.26.

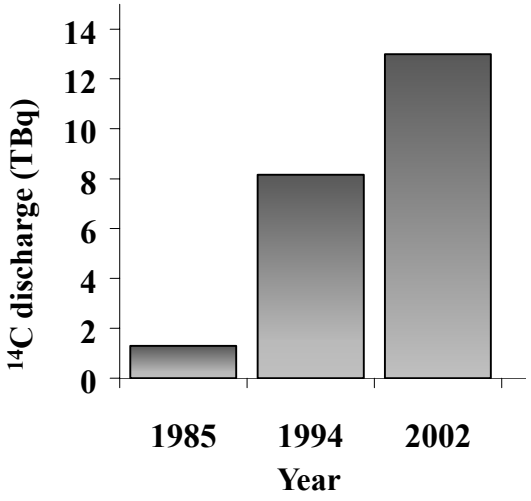

Figure 4 ^{14}C discharged from Sellafield into the Irish Sea during 1985, 1994, and 2002 (UNSCEAR 2001; FSA/SEPA 2003)

It was found that Galician seaweed sampled in 1984 had ^{14}C concentrations that closely correspond with those in *Fucus* spp. sampled along the west coast of Ireland in 1985 (Table 3). This indicates that the ^{14}C activities on the west coast of Ireland are due to a combination of bomb ^{14}C and natural production (ambient background), and accordingly demonstrates that Sellafield discharges have had little impact on the sites west of Ireland.

Table 3 ^{14}C in *Fucus* spp. from the west coast of Ireland and from Galicia. Uncertainties quoted at ±2 σ.

Year	Location (site number)	pMC
1985	West of Ireland (14)	116.2 ± 1.5
	West of Ireland (15)	115.8 ± 1.3
	West of Ireland (16)	117.2 ± 1.3
1994	West of Ireland (14)	112.3 ± 1.3
	West of Ireland (15)	112.9 ± 1.4
	West of Ireland (16)	111.3 ± 1.3
1995	West of Ireland (Burtonport)	109.7 ± 1.4[a]
2003	West of Ireland (14)	106.8 ± 1.2
	West of Ireland (15)	107.3 ± 1.2
	West of Ireland (16)	106.4 ± 1.2
1984	Galicia (Arosa)	116.9 ± 1.3
	Galicia (Cabo Prior)	113.6 ± 1.3
	Galicia (Muros)	115.5 ± 1.3

[a]Converted from 248 ± 2 Bq kg^{-1}(carbon), dry weight (Cook et al. 1998)

CONCLUSIONS

It is clear that levels of ^{14}C found in *Fucus* spp. from the Irish coast are influenced to different degrees by ^{14}C liquid discharges from Sellafield, depending on location, with clear spatial differences found between the ^{14}C content of seaweeds from east and west coasts. Samples from the most westerly locations were found to be unaffected by Sellafield discharges, corresponding closely with global fallout levels, and showing a progressive decrease in concentration from 1985 to 2003.

All data sets show a progressive increase in concentration from the south and west towards the east and north coasts, with maximum values recorded in seaweeds collected along northeastern shorelines. In that region, the lowest ^{14}C concentrations in seaweed were found in samples from 1985, with highest values recorded in 1994 and 2003 (peaking in tandem with Sellafield releases). The spatial patterns observed are attributed to a combination of Sellafield discharges into the northeastern Irish Sea, and the predominantly south to north movement of water through the Irish Sea.

All measurements concur well with data on ^{14}C concentrations in seawater and seaweeds available from other studies (Cook et al. 1998; DEFRA 2002; FSA/SEPA 2003).

ACKNOWLEDGEMENTS

We gratefully acknowledge grant-aid provided by the Marine Institute under the NDP Marine RTDI Networking and Technology Transfer Scheme and a Student Award provided by the Rafter Radiocarbon Laboratory in New Zealand. We also thank the Radiological Protection Institute of Ireland and Alice Lucey for the collection of seaweed samples from around the Irish coast, and Mary and Brendan Keogh for ongoing support provided during the course of the study.

REFERENCES

BNFL. 1995. Annual report on radioactive discharges and monitoring of the environment 1994. Report on Discharges and Environmental Monitoring, Volume 1. British Nuclear Fuels plc., Health and Safety Directorate, Risley, UK.

BNFL. 2001. Discharges and monitoring of the environment in the UK; Annual Report 2001, BNFL, Risley, UK.

Cook GT, Begg FH, Naysmith P, Scott EM, McCartney M. 1995. Anthropogenic ^{14}C marine geochemistry in

the vicinity of a nuclear fuel reprocessing plant. *Radiocarbon* 37(2):459–67.

Cook GT, MacKenzie AB, Naysmith P, Anderson R. 1998. Natural and anthropogenic ^{14}C in the UK coastal marine environment. *Journal of Environmental Radioactivity* 40(1):89–111.

DEFRA. 2002. *UK Strategy for Radioactive Discharges 2001–2020.* United Kingdom Department for Environment, Food & Rural Affairs.

Gallager D, McGee EJ, Mitchell PI. 2002. A radiocarbon age calculation program for windows. *Radiocarbon* 44(1):223–24.

IAEA. 1998. *International Atomic Energy Agency AQCS Catalogue for Reference Materials and Intercomparison Exercises 1998/1999, Vienna, Austria*. http://www.IAEA.org.

Isogai K, Cook GT, Anderson R. 2002. Reconstructing the history of ^{14}C discharges from Sellafield: part 1–atmospheric discharges. *Journal of Environmental Radioactivity* 59:207–22.

Jefferies DF, Steele AK, Preston A. 1982. Further studies on the distribution of Cs in British coastal waters–1. Irish Sea. *Deep Sea Research Part A. Oceanographic Research Papers* 29(6):713–38.

MAFF. 1996. *Radioactivity in Food and the Environment, 1995*. RIFE–1, Ministry of Agriculture, Fisheries and Food, London.

FSA/SEPA. 2003. Radioactivity in Food and the Environment, 2002. RIFE–8, Food Standards Agency and Scottish Environment Protection Agency, London and Stirling.

O'Donnell RG. 1997. The establishment of a radiocarbon dating facility at University College Dublin and its application to a study of paleoecological material from the north Mayo blanket bog and the Ceide fields [PhD dissertation]. Dublin: University College Dublin.

Sanchez-Cabeza JA. 1989. Plutonium in the Irish environment [PhD dissertation]. Dublin: University College Dublin.

UNSCEAR. 1993. Sources and effects of ionizing radiation. *United Nations Scientific Committee on the Effects of Atomic Radiation.* Report to the General Assembly. New York: United Nations.

UNSCEAR. 2001. Sources and effects of ionizing radiation. *United Nations Scientific Committee on the Effects of Atomic Radiation.* Report to the General Assembly. New York: United Nations.

RADIOCARBON, Vol 46, Nr 2, 2004, p 893–900

STEPPED-COMBUSTION ^{14}C DATING OF BOMB CARBON IN LAKE SEDIMENT

J McGeehin[1] • G S Burr[2] • G Hodgins[2] • S J Bennett[3] • J A Robbins[4] • N Morehead[4] • H Markewich[5]

ABSTRACT. In this study, we applied a stepped-combustion approach to dating post-bomb lake sediment from north-central Mississippi. Samples were combusted at a low temperature (400 °C) and then at 900 °C. The CO_2 was collected separately for both combustions and analyzed. The goal of this work was to develop a methodology to improve the accuracy of ^{14}C dating of sediment by combusting at a lower temperature and reducing the amount of reworked carbon bound to clay minerals in the sample material. The ^{14}C fraction modern results for the low and high temperature fractions of these sediments were compared with well-defined ^{137}Cs determinations made on sediment taken from the same cores. Comparison of "bomb curves" for ^{14}C and ^{137}Cs indicate that low temperature combustion of sediment improved the accuracy of ^{14}C dating of the sediment. However, fraction modern results for the low temperature fractions were depressed compared to atmospheric values for the same time frame, possibly the result of carbon mixing and the low sedimentation rate in the lake system.

INTRODUCTION

Accurate ^{14}C dating of lake sediment is complicated by the presence of multiple sources of organic and inorganic carbon fractions. Even after traditional acid/alkali/acid (AAA) pretreatments, radiocarbon dating of lake sediment often leads to inaccurate results because the humin component of the sediment (the fraction of humic substances that is not soluble at any pH value) includes reworked carbon adsorbed to clay minerals. In an earlier research effort, we adapted a stepped-combustion technique developed for ^{14}C dating of smoke-derived versus clay-bound carbon sources in pottery to the problem of dating sediment and paleosols (Delqué Količ 1995; O'Malley et al. 1999; McGeehin et al. 2001). In our 2001 study, we combusted sediment and paleosols at a low temperature (400 °C) to minimize the contribution of the more refractory carbon bound to clay minerals in the samples. The high temperature (900 °C) fraction was also collected and results were compared. ^{14}C ages on the low temperature fraction were in good agreement with macrofossil and humic acid ages, whereas the high temperature fraction gave disparate results.

In this study, we again applied the stepped-combustion method to dating sediment, focusing on post-bomb lake sediments with high clay and silt content, 5–35% and 50–75%, respectively (Bennett and Rhoton 2003). Abbott and Stafford (1996) suggested that in studies of lake sediments, discrete terrestrial plant macrofossils will provide the most accurate ages, followed by aquatic plant macrofossils and humic acids. Lacking sufficient quantities of macrofossils or humic acids, we instead compared ^{14}C activity of the low and high temperature combustion products of our sediment samples to ^{137}Cs bomb profile results made on the same sample material. Above-ground bomb testing during the 1950s and 1960s resulted in elevated concentrations of atmospheric ^{14}C and ^{137}Cs that peaked in 1963–1964 (Levin et al. 1985; Bergan 2002; Figure 1). Both cores taken for this study showed a strong ^{137}Cs bomb peak. We hypothesized that a ^{14}C bomb profile should be present at about the same depth as the ^{137}Cs profile if reworked carbon bound to clay in the sediment could be effectively removed from the activity of the samples.

[1]US Geological Survey, Reston, Virginia, USA. Corresponding author. Email: mcgeehin@usgs.gov.
[2]University of Arizona, Tucson, Arizona, USA.
[3]State University of New York, Buffalo, New York, USA.
[4]National Oceanic and Atmospheric Administration, Ann Arbor, Michigan, USA.
[5]US Geological Survey, Atlanta, Georgia, USA.

Proceedings of the 18th International Radiocarbon Conference, edited by N Beavan Athfield and R J Sparks
RADIOCARBON, Vol 46, Nr 2, 2004, p 893–900

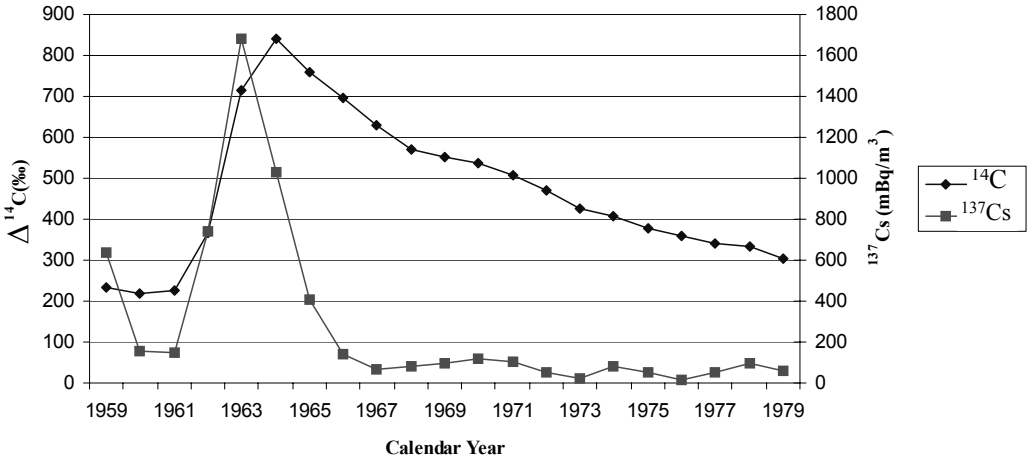

Figure 1 Atmospheric concentrations of bomb ^{14}C and ^{137}Cs

SAMPLE LOCATION

Samples were taken from 2 sediment cores (SB-3 and SB-9) from Grenada Lake, north-central Mississippi (Figure 2). Grenada Lake is a 142-km^2 reservoir formed by the damming of the Yalabusha and Skuna rivers in the year 1954. The 2 cores were taken approximately 7 km apart within the Skuna, or northern, arm of the lake. Both cores were obtained by vibracore with minimal compaction. Core SB-3 was taken under 1 m of water; core SB-9 was taken under 2.9 m of water. Erosion, incision, and channel widening due to channelization of the rivers feeding Grenada lake have increased the sediment load to the lake since its inception. Sediment accumulation and organic content is quite variable depending on the location in the lake.

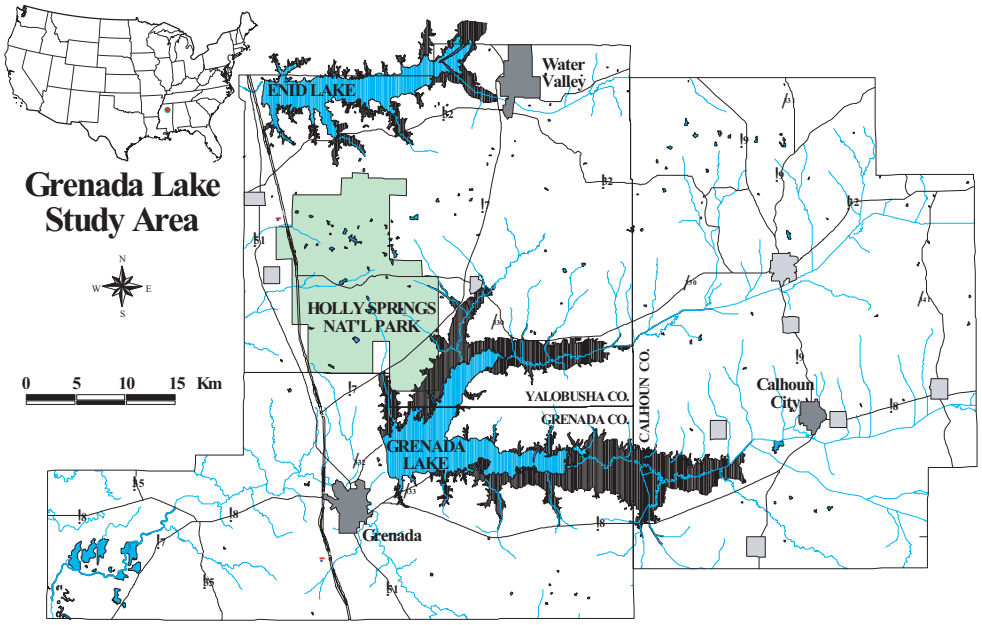

Figure 2 Map of study area, north-central Mississippi

METHODS

^{137}Cs Sample Handling

Sediment samples were cut in 2.5-cm intervals from one-half of the split cores (the other half of each core was used for ^{14}C) and shipped off to the National Oceanic and Atmospheric Administration's Great Lakes Research Laboratory for measurements. Sediment samples were weighed into vials and given a standard geometry. Samples were measured on a gamma detector. Each sample was counted for 1 day or a minimum counting error of 10%, whichever came first. Data was collected for both ^{137}Cs and ^{40}K. The counting errors for the activities of ^{137}Cs in the SB-3 core samples ranged from 3.2% to 3.9% of the reported peak activity values (defined as values with half the maximum ^{137}Cs activity or greater). Counting errors for core SB-9 were 2.9–4.8%.

^{14}C Sample Handling

Pretreatment. Sediment samples were first sieved to <63 μm to collect the silt and clay size fractions of the samples. Collecting only the fine fraction of the sediment incorporated all of the clay-bound carbon and the humic substances associated with the silt fraction, while excluding coarser disseminated fragments of plant rootlets, charcoal, etc. that would further complicate the apparent activity of each sample. The <63-μm fraction of each sediment sample was given an AAA pretreatment consisting of a 1M HCl (2 hr, 60 °C), 0.1M NaOH (overnight, 60 °C), 1M HCl (2 hr, 60 °C). The resultant pretreated sediment is defined here as <63 μm humin.

Stepped-combustion. Samples were placed in 9-mm Vycor combustion vessels and combusted in 0.3 atmosphere ultra-pure O_2 at 400 °C (a diagram of the extraction line is shown in Figure 3). The CO_2 produced at this step is referred to as the low temperature (LT) fraction. After isolating the low temperature CO_2, the remaining sample material was then pumped under a high vacuum, recharged with 0.3 atmosphere ultra-pure O_2, and heated to 900 °C. The CO_2 produced at 900 °C is referred to as the high temperature (HT) fraction. Both the LT and HT CO_2 fractions were individually passed through a platinum trap at 1000 °C to oxidize CO, a copper oxide/silver trap to remove volatile gases, and 2 dry ice/alcohol traps at –78 °C to remove water.

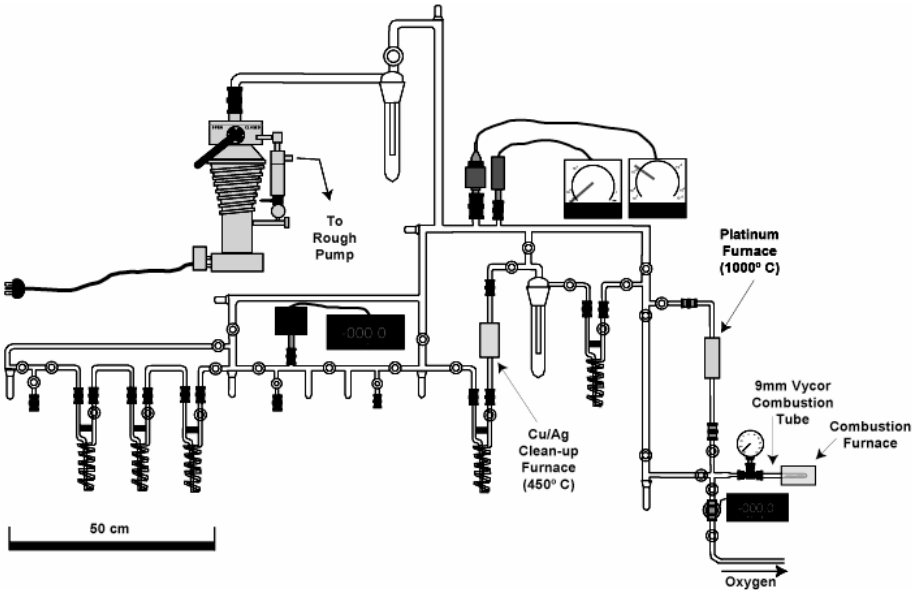

Figure 3 Diagram of the extraction line

Graphitization. Samples were converted to graphite over iron at 575 °C in the presence of ZnO at 425 °C.

AMS Dating. The samples were physically and chemically processed and the ^{14}C activities measured at the NSF-Arizona AMS facility in Tucson, Arizona.

RESULTS AND DISCUSSION

Notation

All of the results in this study are given as fraction modern carbon (F). F is defined as

$$F = (^{14}C/^{13}C)_s / (^{14}C/^{13}C)_{std} \quad (1),$$

where $(^{14}C/^{13}C)_s$ is the sample ratio and $(^{14}C/^{13}C)_{std}$ is the calculated standard ratio at 1950, determined from measurements of NBS oxalic acid standards with both ratios normalized to $\delta^{13}C = -25‰$ (Donahue et al. 1990).

The <63-μm low temperature and high temperature humin samples are referred to and showed graphically as LT and HT, respectively. The combined activity of a sample, which was calculated from the relative input of both the LT and HT fraction modern values, is referred to and shown graphically as "Combined."

Core SB-9

Results for core SB-9 are given in Table 1 and shown graphically in Figure 4a. A strong ^{137}Cs peak is evident in the core at a depth of 74.2 cm. Using the 1963 ^{137}Cs peak as a marker, the sedimentation rate for this site is 1.85 cm/yr. Organic carbon concentrations are low, ranging from 0.12–0.43% in the LT fraction and 0.08–0.28% in the HT fraction. The ^{14}C activity of the stepped-combustion products demonstrate the disparity of results that can occur from fractionating sediment by temperature of combustion. The LT fraction for sediment samples from core SB-9 show a weak but recognizable bomb curve with a peak (F = 1.0946) at 63.4 cm. The HT fraction for samples at all depth intervals have F values well below 1.0. In every case, LT samples have older HT counterparts indicating ^{14}C ages that range from a few hundred to as much as 1800 BP. The Combined activity values for the SB-9 core show a single bomb ^{14}C sample with F = 1.0416 at 63.4 cm.

Core SB-3

Results for core SB-3 are given in Table 1 and shown graphically in Figure 4b. A ^{137}Cs peak is evident in the core at a depth of 23.8 cm. The sedimentation rate of 0.6 cm/yr based on this 1963 peak is considerably lower than with core SB-9. Organic carbon concentrations are very low, ranging from 0.03–0.29% in the LT fraction and 0.02–0.20% in the HT fraction (based on the CO_2 yield of each fraction relative to the total yield). As with core SB-9, the data show a substantial offset between F values for the LT and HT fractions. HT fractions consistently give older results by as much as 7000 ^{14}C yr BP. There is only 1 sample indicating the presence of bomb carbon (F = 1.0612). It occurs in the LT fraction at a depth of 23.8 cm, matching the peak for the ^{137}Cs curve.

The Bomb Profiles

For core SB-9, the 63.4 cm ^{14}C bomb peak in the LT fraction appears to be 10.8 cm shallower than the ^{137}Cs peak at 74.2 cm. The difference may be less if we consider the statistical overlap of ^{14}C F values for samples at the 63.4 cm and 66.1 cm intervals. Core SB-9 has a high sedimentation rate.

Table 1 Results for core SB-3.

Core ID	Core depth midpoint	^{137}Cs		^{14}C activity (F)									% Carbon		
				AMS ID	LT fraction			HT fraction			Combined				
	(cm)	(dpm/g)	+/–		F	+/–	$\delta^{13}C$	F	+/–	$\delta^{13}C$	F	+/–	LT	HT	Combined
SB9-21	55.3	0.818	0.081	AA55361	1.0065	0.0052	–26.4	0.9038	0.0103	–25	0.9736	0.0068	0.4	0.19	0.59
SB9-22	58.0	0.998	0.081	AA55362	1.0502	0.0044	–26.7	0.8958	0.0054	–25	0.9766	0.0049	0.3	0.28	0.58
SB9-23	60.7	1.076	0.083	AA55363	1.0516	0.0045	–26.4	0.7968	0.0060	–25	0.9814	0.0049	0.43	0.16	0.59
SB9-24	63.4	1.577	0.084	AA55364	1.0946	0.0068	–26.6	0.9013	0.0052	–25	1.0416	0.0064	0.31	0.12	0.43
SB9-25	66.1	1.466	0.069	AA54269	1.0818	0.0051	–28.2	0.9142	0.0041	–25.8	1.0069	0.0047	0.14	0.11	0.25
SB9-26	68.8	1.682	0.088	AA54270	1.0579	0.0063	–27.4	0.9189	0.0045	–26.2	0.9964	0.0055	0.15	0.12	0.27
SB9-27	71.5	2.546	0.074	AA54271	1.0061	0.0043	–27.7	0.8749	0.0048	–27.1	0.9607	0.0045	0.12	0.07	0.19
SB9-28	74.2	3.459	0.104	AA54272	0.9170	0.0040	–28.6	0.8543	0.0040	–27.1	0.8816	0.0040	0.16	0.21	0.37
SB9-29	76.9	2.996	0.087	AA54273	0.9727	0.0044	–27.8	0.8946	0.0040	–27.3	0.9290	0.0041	0.23	0.29	0.52
SB9-30	79.6	1.936	0.092	AA54274	0.9132	0.0039	–28.3	0.8231	0.0039	–28.2	0.8636	0.0040	0.14	0.17	0.31
SB9-31	82.3	0.390	0.076	AA54275	0.9443	0.0042	–28.3	0.7898	0.0046	–26.7	0.8852	0.0044	0.13	0.08	0.21
SB3-3	6.3	0.286	0.056	AA55974	0.8252	0.0102	–26.97	0.3479	0.0111	–25	0.7440	0.0104	0.10	0.02	0.12
SB3-4	8.8	0.371	0.066	AA55975	0.8247	0.0127	–27.58	0.4707	0.0084	–25	0.6478	0.0106	0.04	0.04	0.08
SB3-5	11.3	0.449	0.074	AA55976	0.8166	0.0106	–26.06	0.4420	0.0129	–25	0.6930	0.0114	0.06	0.03	0.09
SB3-6	13.8	0.408	0.078	AA55977	0.8612	0.0107	–26.87	0.6137	0.0086	–25	0.7548	0.0098	0.08	0.06	0.14
SB3-7	16.3	0.322	0.077	AA55978	0.7866	0.0121	–27.20	0.3231	0.0091	–25	0.6012	0.0109	0.03	0.02	0.05
SB3-8	18.8	0.675	0.06	AA55979	0.9492	0.0129	–28.01	0.7323	0.0099	–25	0.8559	0.0117	0.12	0.09	0.21
SB3-9	21.3	0.775	0.078	AA55980	0.9141	0.0109	–27.24	0.5143	0.0080	–25	0.7982	0.0100	0.10	0.04	0.14
SB3-10	23.8	2.407	0.094	AA55981	1.0612	0.012	–27.31	0.9113	0.0104	–25	0.9947	0.0113	0.22	0.18	0.40
SB3-11	26.3	2.179	0.069	AA55982	0.9611	0.011	–28.97	0.8363	0.0097	–25	0.8988	0.0103	0.20	0.20	0.40
SB3-12	28.8	0.271	0.069	AA55983	0.923	0.0106	–28.09	0.7956	0.0092	–25	0.8810	0.0101	0.29	0.14	0.43
SB3-13	31.3	0.011	0.078	AA55984	0.9214	0.0108	–27.72	0.8168	0.0104	–25	0.8837	0.0106	0.21	0.12	0.33

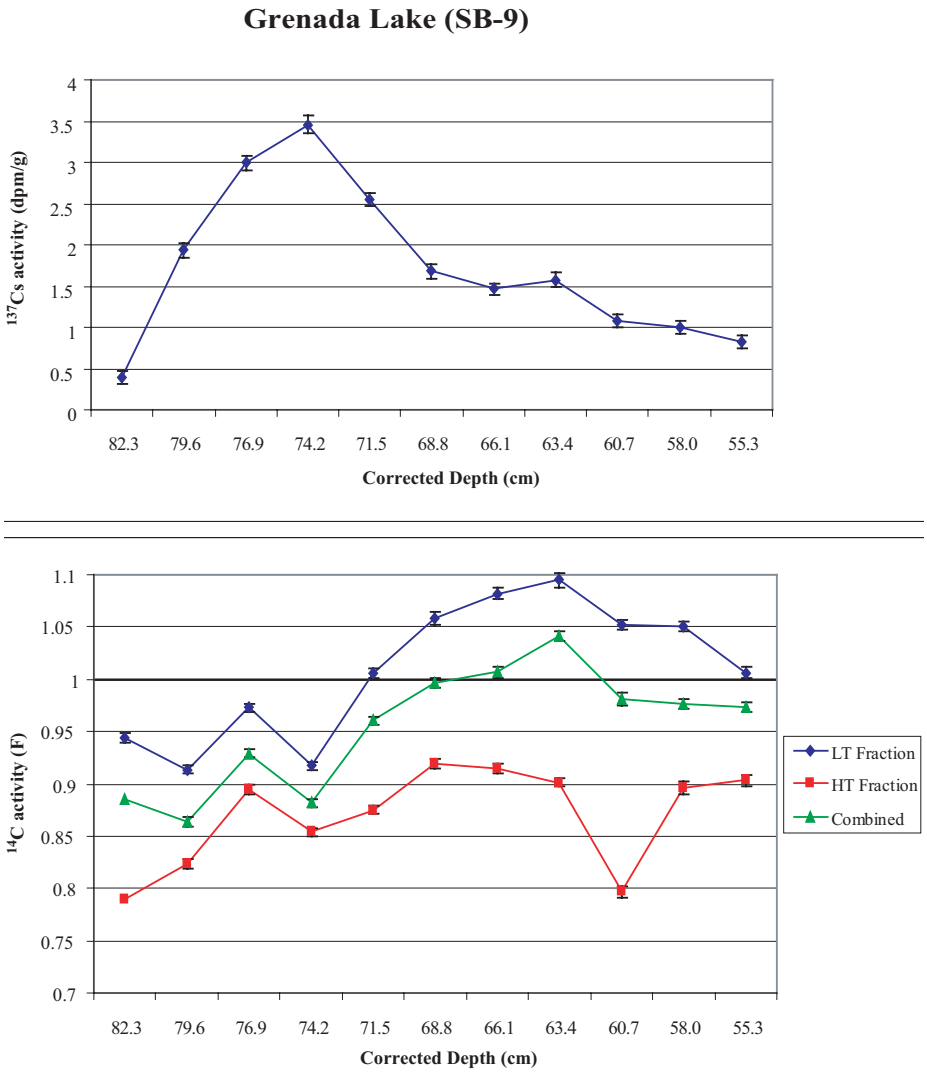

Figure 4a ^{14}C and ^{137}Cs activity versus depth for core SB-9

Using the ^{137}Cs 1963 peak as a marker, sediment is accumulating in the core at a rate of 1.85 cm/yr. This sedimentation rate translates to a offset of 4.5–5.8 yr between the ^{14}C and ^{137}Cs peaks. It is reasonable to assume that the ^{14}C bomb peak would develop somewhat later than the ^{137}Cs peak in lake sediment since cesium is deposited directly through atmospheric fallout, whereas bomb carbon must be incorporated as biomass before being diagenetically altered and deposited as sediment in the lake reservoir.

In core SB-3, the single ^{14}C bomb carbon value in the LT fraction does appear to match up with the ^{137}Cs peak. However, peak values for ^{137}Cs overlap at the 2-σ level for the 23.8-cm and 26.3-cm intervals. With a sedimentation rate of just 0.6 cm/yr, the ^{14}C peak may have developed a few yr later than the ^{137}Cs peak, as with core SB-9.

For both core SB-9 and SB-3, ^{14}C *F* values in the 1950s and 1960s bomb carbon timeframe are significantly depressed relative to atmospheric concentrations of carbon for the same period. The LT

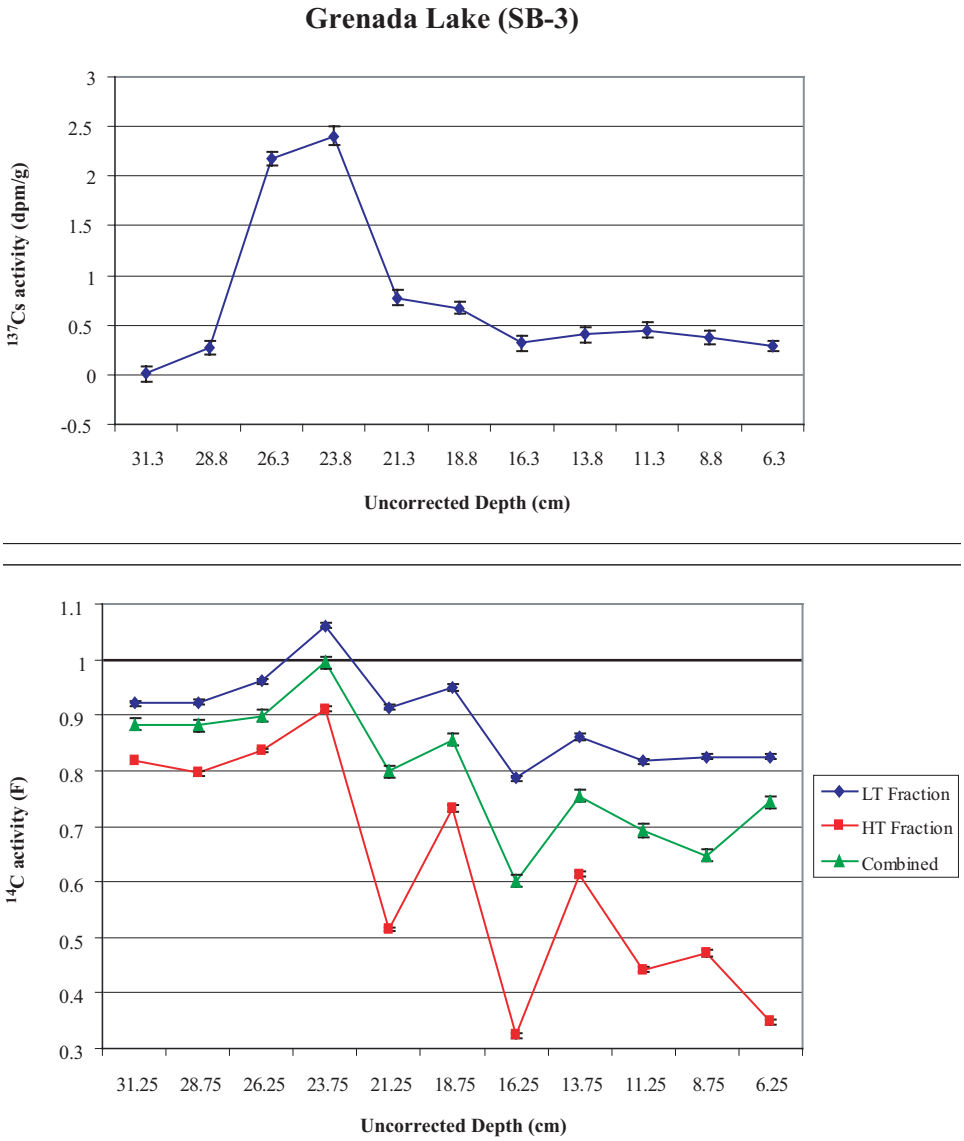

Figure 4b ^{14}C and ^{137}Cs activity versus depth for core SB-3

combustion of these sediments has improved the accuracy of the ^{14}C results. However, ^{14}C *F* values are still too low. This is probably caused by a mixing process where various pools of carbon of differing ages combine, resulting in an apparent age for the sediment. The effect on an apparent age is more pronounced for core SB-3 than SB-9. The low sedimentation rate of core SB-3 means that surface sediment was slow to be buried, likely resulting in greater mixing of carbon and depressed ^{14}C *F* values for the selected samples. ^{137}Cs is not affected by diagenetic forces and, thus, sample activities are unlikely to be affected by the apparent age problem.

By holding the sampling intervals constant for both cores, the low sedimentation rate of core SB-3 relative to SB-9 would also work to reduce ^{14}C *F* values in SB-3. A low sedimentation rate increases the number of years represented in a segment and, as a direct result, the activity measured for that

segment. This effect is also seen for the ^{137}Cs peaks of the cores. The peak ^{137}Cs activity value for core SB-3 is lower than that of SB-9, as it is for ^{14}C.

While the HT fraction is consistently older than the LT fraction in the 2 cores, there appears to be a correlation between the activities of both temperature fractions with depth at various places in the cores. Note the jump in activity for both the LT and HT fractions in core SB-9 at 76.9 cm and the depression of the LT and HT fractions in core SB-3 at 16.3 cm. This may reflect bleeding of carbon from 1 temperature fraction to the other. It is possible that old, reworked carbon is being incorporated into the LT fraction at a lower temperature than expected. Conversely, some of the labile carbon may combust at a slightly higher temperature than the 400 °C of our LT combustions. A more thorough calorimetric study involving additional temperature fractions (e.g. 50 °C intervals) should improve our understanding of temperature effects in the ^{14}C activity of sediment.

CONCLUSIONS

A ^{14}C bomb curve profile in sediment can be a useful tool to help establish sedimentation and carbon sequestration rates, especially when reliable plant macrofossils are absent. However, older reworked carbon adsorbed to clay minerals can mask the true ^{14}C activity of the sediment, unless it can be effectively removed from the sample during processing.

Through the use of a stepped-combustion approach for ^{14}C dating, we have shown that low temperature combustion of sediment improves the accuracy of the results by removing older, reworked carbon bound to clay. Fraction modern values for the LT fraction of these sediments are depressed relative to atmospheric concentrations for the same timeframe. This may reflect mixing of various pools of carbon in the lake environment. Core SB-3 is depressed even more than SB-9, as evidenced by ^{14}C and ^{137}Cs peak activities. This probably reflects the effect of a constant sampling interval on cores with markedly different sedimentation rates.

For cores SB-9 and SB-3, the refractory carbon associated with clay minerals that was isolated during the high temperature combustion was considerably older than the labile carbon fraction associated with the low temperature combustion. Both cores showed evidence of bomb carbon primarily in the low temperature fraction as expected. Peak values of bomb ^{14}C occur stratigraphically at or slightly above the ^{137}Cs peak in both cores, probably reflecting a lag time for incorporation of plant-derived carbon in sediment.

REFERENCES

Abbott MB, Stafford TW Jr. 1996. Radiocarbon geochemistry of modern and ancient arctic lake systems, Baffin Island, Canada. *Quaternary Research* 45: 300–11.

Bennett SJ, Rhoton FE. 2003. Physical and chemical characteristics of sediment impounded within Grenada Lake, MS. *USDA-ARS National Sedimentation Laboratory Research Report No. 36*. 161 p.

Bergan TD. 2002. Radioactive fallout in Norway from atmospheric nuclear weapons tests. *Journal of Environmental Radioactivity* 60:189–208.

Delqué Količ E. 1995. Direct radiocarbon dating of pottery: selective heat treatment to retrieve smoke-derived carbon. *Radiocarbon* 37(2):275–84.

Donahue DJ, Linick TW, Jull AJT. 1990. Isotope-ratio and background corrections for acceleratory mass spectrometry radiocarbon measurements. *Radiocarbon* 32(2):135–42.

Levin I, Kromer B, Schoch-Fischer H, Bruns M, Münnich M, Berdau D, Vogel J, Münnich KO. 1985. Twenty-five years of tropospheric ^{14}C observations in Central Europe. *Radiocarbon* 27(1):1–19.

McGeehin J, Burr GS, Jull AJT, Reines D, Gosse J, Davis PT, Muhs D, Southon JR. 2001. Stepped-combustion ^{14}C dating of sediment: a comparison with established techniques. *Radiocarbon* 43(2A):255–61.

O'Malley JM, Kuzmin YZ, Burr GS, Donahue DJ, Jull AJT. 1999. Direct radiocarbon accelerator mass spectrometric dating of the earliest pottery from the Russian Far East and Transbaikal. In: Evin J, Oberlin C, Daugas J-P, Salles J-F, editors. *^{14}C and Archaeology: 3rd International Conference.* Lyon, France. 6–10 April 1998.

RADIOCARBON, Vol 46, Nr 2, 2004, p 901–910

SEASONAL AND SECULAR VARIATIONS OF ATMOSPHERIC $^{14}CO_2$ OVER THE WESTERN PACIFIC SINCE 1994

H Kitagawa[1] • Hitoshi Mukai[2] • Yukihiro Nojiri[2] • Yasuyuki Shibata[2] • Toshiyuki Kobayashi[2] • Tomoko Nojiri[3]

ABSTRACT. Air sample collections over the western Pacific have continued since 1992 as a part of Center for Global Environmental Research, National Institute for Environmental Studies (CGER-NIES) global environmental monitoring program. The air samples collected on the Japan-Australia transect made it possible to trace the seasonal and secular $^{14}CO_2$ variations, as well as an increasing trend of greenhouse gases over the western Pacific. A subset of CO_2 samples from latitudes of 10–15°N and 23–28°S were chosen for accelerator mass spectrometry (AMS) ^{14}C analysis using a NIES-TERRA AMS with a 0.3–0.4% precision. These $^{14}CO_2$ records in maritime air show seasonal variations superimposed on normal exponential decreasing trends with a time constant of about 16 yr. The $\Delta^{14}C$ values in the Northern Hemisphere are lower those in the Southern Hemisphere by 3–4‰ during 1994–2002. The Northern Hemisphere record shows relatively high seasonality (2.3 ± 1.5‰) as compared with the Southern Hemisphere (1.3 ± 1.2‰). The maximum values of seasonal cycles appear in late autumn and early winter in the Northern and Southern Hemispheres, respectively. Oscillations of 1–10 yr over the western Pacific are found to correlate possibly with the El Niño/Southern Oscillation (ENSO) events.

INTRODUCTION

The tropospheric radiocarbon concentration (represented by $\Delta^{14}C$, which includes a normalization for mass dependent fractionation and decay) has been monitored at islands and continental stations (Nydal and Lovseth 1983; Levin et al. 1980; Vogel 1970; Manning et al. 1990; Meijer et al. 1995; Levin et al. 1989, 1995). It almost doubled from its natural value during the early 1960s due to injection of ^{14}C from thermonuclear bomb testing. At that time, troposphere-stratosphere exchange was a dominant contributor to produce seasonal and latitudinal variations in troposphere $\Delta^{14}C$. After the global moratorium on atmospheric nuclear testing following the Test Ban Treaty in 1963, $\Delta^{14}C$ has decreased mainly through air-sea exchanges of CO_2, transfer to the biosphere, and dilution with fossil-fuel ^{14}C-free CO_2, with an approximate exponential trend. The bomb ^{14}C anomaly in the atmosphere has been used as a transient tracer for studying the global carbon cycle. By the late 1990s, the tropospheric $\Delta^{14}C$ value reflects the distribution of natural and anthropogenic CO_2 source and sinks (Rozanski et al. 1995; Meijer et al. 1995; Levin and Hesshaimer 2000). This information has provided independent information on the global CO_2 source and sinks through the carbon-cycle modeling exercise (e.g. Randerson et al. 2002).

The air collections in the Japan and Australia transect have been made since 1992 as a part of the ongoing studies on a greenhouse gases monitoring program. The $\Delta^{14}C$ changes in maritime air over the western Pacific from latitudes of 10–15°N and 23–28°S were determined for 1994–2002. Here, we made a comparison of those $\Delta^{14}C$ records that could be characterized as "natural background."

METHODS

CO_2 has been continuously collected by an automatic sampler installed on container freighters at the 24 sites on the Japan and Australia transect since 1992. It was started by the Hakuba-maru (NYK line) from 1992. The ship was changed to the Southern Cross-maru (MOL line) in 1996 and again changed to the Golden Wattle (MOL line) in 2001. Air samplings on the Japan and Australia transect

[1]Graduate School of Environmental Studies, Nagoya University, Nagoya 464-8601, Japan. Corresponding author. Email: kitagawa@ihas.nagoya-u.ac.jp.
[2]National Institute for Environmental Studies, Tsukuba, Ibaraki 305-8506, Japan.
[3]Global Environmental Forum, c/o National Institute for Environmental Studies, Tsukuba, Ibaraki 305-8506, Japan.

Proceedings of the 18th International Radiocarbon Conference, edited by N Beavan Athfield and R J Sparks
RADIOCARBON, Vol 46, Nr 2, 2004, p 901–910

were performed at approximately 3° latitude with a frequency of 6–10 times per yr. Air samples were collected in stainless steel containers (3.3 L in volume) at approximately +2.5 atm were picked up when the cargo ships arrived in ports quickly.

In the laboratory, CO_2 was cryogenically separated form about 6 L of air in a vacuum line after the determination of the concentrations of greenhouse gases such as CO_2, CH_4, and N_2O. More than 1000 samples are kept as pure CO_2 in sealed glass tubes for the ongoing measurements of $\delta^{13}C$ and ^{14}C contents. A subset of CO_2 samples collected at the latitudes of 10–15°S and 23–28°N was converted to graphite for accelerator mass spectrometry (AMS) ^{14}C measurements. $^{14}C/^{12}C$ and $^{13}C/^{12}C$ ratios (for the isotope fractionation correction) were determined using the NIES-TERRA AMS. The ^{14}C contents are reported as the permil notation ($\Delta^{14}C$ ‰) following standard convention (Stuiver and Polach 1977) after normalizing to isotope fractionation and correction for decay. Typical 1-σ precision on $\Delta^{14}C$ is about ±5‰.

RESULTS AND DISCUSSION

$\Delta^{14}C$ data from the 2 areas are plotted with CO_2 concentration data (Figure 1). We give the $\Delta^{14}C$ and CO_2 concentration data in the Appendix. The main feature of $\Delta^{14}C$ records is the existence of seasonality superimposed on normal exponential decreasing trends with a decay (or e-folding) time constant (t). To isolate the secular and seasonal components in the $\Delta^{14}C$ time series, the seasonal component is expressed by single harmonic function ($A\ cos\ [2\pi t + \varphi]$, where A and φ are constants), and all the data is fitted to the following formula:

$$\Delta^{14}C_t = \Delta^{14}C_{1994}\ e^{-\Delta t/\tau} + A\ cos\ (2\pi t\ /\ T + \varphi) \quad (1),$$

where $\Delta^{14}C_t$ is the measured value in given time (t) and Δt is the time since 1994 (the base year). The fitting parameters were obtained by the nonlinear least-squares method using a Lebenberg-Marquardt algorithm. The fits are shown in Figure 1, while the fitted parameters are shown in Table 1.

Trend of $\Delta^{14}C$ Over the Western Pacific

$\Delta^{14}C$ values in maritime air over the western Pacific show a gradual decreasing in both hemispheres, corresponding to the exponential decreasing of global $\Delta^{14}C$ trend due to the Suess effect (Levin and Hesshaimer 2000). The average e-fold time constants during 1994–2002 in the Northern and Southern Hemisphere over the western Pacific are, respectively, 15.6 ± 1.3 yr ($\Delta^{14}C$ is 128.4 ± 3.2‰ in January 1994) and 16.4 ± 0.9 yr ($\Delta^{14}C$ is 133.7 ± 2.3‰ in January 1994). The reported e-fold time constant is about 16 yr for the Northern Hemisphere (Levin and Kromer 1997) and about 17 yr for the Southern Hemisphere (Manning et al. 1990). The decreasing trend of $\Delta^{14}C$ over the western Pacific agrees well with that from other area during the 1990s.

Absolute Values

To assess the N-S offset of $\Delta^{14}C$ over the western Pacific, we compared 2 curves shown in Figure 1. As expected, the absolute $\Delta^{14}C$ values in the Northern Hemisphere are lower than those in the Southern Hemisphere by 3.3‰ on average, and they do not show the apparently systematical shift with time for 1994–2002. Surface observation at the globally distributed background stations located between 82°N (Alert, Nunavut, Canada) and 7°S (Neumayer, Antarctica) suggests that the N-S $\Delta^{14}C$ gradient is nearly zero in the early 1990s (Levin and Hesshaimer 2000). The model calculation predicts that the N-S offset will be expanded, with the Northern Hemisphere becoming progressively more ^{14}C-depleted as compared with the Southern Hemisphere in the coming year (Randerson et al. 2002). Our observation supports the model prediction that $\Delta^{14}C$ in the Northern Hemisphere will decrease from the direct input of fossil-fuel emissions with an isotope signal of –1000‰.

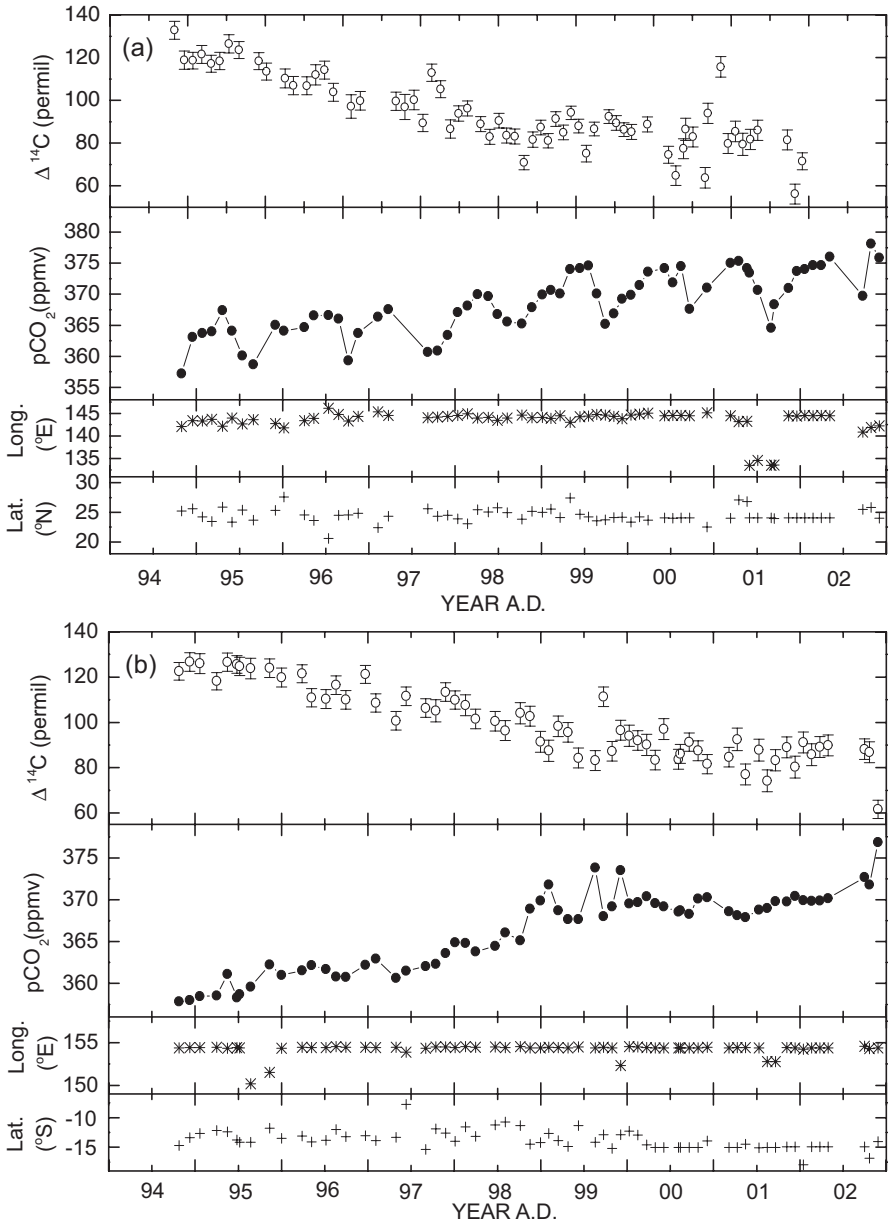

Figure 1 $\Delta^{14}C$ and CO_2 concentration in maritime air collected at the latitudes of 23–28°N (above) and 10–15°S (below) over the western Pacific.

Seasonality

The decreasing trend of the seasonal cycle was assessed using Equation 1. The Northern Hemisphere record shows higher seasonality (2.3 ± 1.5‰) as compared with the Southern Hemisphere (1.3 ± 1.2‰). The larger seasonal variations were reported at observation stations in the Northern Hemisphere, where they are strongly influenced by the anthropologically induced CO_2 emissions (Levin et al. 1989, 1995; Meijer et al. 1995). In remote stations, fossil-fuel emission is little, e.g.,

only <5‰ on peak-to-peak basis at Izana in Canary Island, which is consistent with our results. The $\Delta^{14}C$ data discussed here could be regarded as "natural background."

The amplitudes of the seasonal cycle are close to the $\Delta^{14}C$ measurement error. It should be noted that the estimated phases of seasonal cycles have a margin of error (Table 1). The maximum $\Delta^{14}C$ values appear roughly in October and December in the Northern and Southern Hemispheres, respectively, when the atmospheric CO_2 concentration is lower in the Northern Hemisphere (Figure 1). There seems to be a small N-S difference in phase by about 2 months. Interestingly, the $\Delta^{14}C$ records from the Northern Hemisphere (10–15°N) over the western Pacific are somewhat out of phase with those of Izana, Tenerife Island (28°N) in the Atlantic (with the maximum in middle July [Meyer et al. 1995]).

Table 1 Characteristics of the fitted seasonal and exponential decreasing changes. The $\Delta^{14}C$ measurement series from the Northern and Southern Hemispheres were fitted to the formula, $\Delta^{14}Ct = \Delta^{14}C_{1994}\, e^{-\Delta t/\tau} + A\, cos\, (2\pi t / T + \varphi)$.

Area	$\Delta^{14}C_{1994}$ (‰)	Decay time constant (τ, year)	Amplitude (A, ‰)	Phase (φ, maximum)
23–28°N	128.4 ± 3.2	15.6 ± 1.3	2.3 ± 1.5	Oct 10 (±40 days)
10–15°S	133.7 ± 2.3	16.4 ± 0.9	1.3 ± 1.2	Dec 10 (±50 days)

The seasonality of tropospheric $\Delta^{14}C$ is sensitive to fossil-fuel emissions, ocean-atmosphere exchanges, stratosphere-troposphere mixing, and terrestrial-ecosystem fluxes (Nydel and Lovseth 1983; Enting and Mansbridge 1987). Seasonal cycles in the 1960s were produced by stratosphere-troposphere exchange because stratospheric ^{14}C fluxes are injected into the upper troposphere in April and May in the Northern Hemisphere (Appenzeller et al. 1996). Model analyses of the stratosphere-troposphere exchange could not explain our result for the phase of seasonal cycles (Manning et al. 1990). In later decades, the records from European continental stations show clear seasonal cycles, caused probably by the summer-winter difference in fossil-fuel emissions (Levin et al. 1989; Meijer et al. 1995). The seasonal cycle (with the maximum in middle October and middle December over the western Pacific) is out of phase with that of the European continental stations; the continental stations' maximum occurs during middle July and late August and coincides with the warmest period of summer in the Northern Hemisphere. The direct impact of fossil-fuel ^{14}C-free CO_2 would be a minor contributor to the seasonal cycle over the western Pacific. The phase reverse of $\Delta^{14}C$ and CO_2 concentration cycles in the Northern Hemisphere may be caused by net CO_2 fluxes from terrestrial ecosystems and ocean exchanges, as suggested by model prediction (Randerson et al. 2002).

1–10 Year Oscillations

The residual of $\Delta^{14}C$ ($\Delta^{14}C_{res}$) was calculated as the difference between measured values and each fitted curve (Figure 2). The standard deviation of $\Delta^{14}C_{res}$ values during 1994–2002 is 8.9‰ and 6.2‰ in the Northern and Southern Hemispheres, respectively. $\Delta^{14}C_{res}$ records from 2 areas show a weak coincidence in the general trends. Although more data are needed to verify the presence of the 1–10 year oscillations of $\Delta^{14}C_{res}$, the existence of 1–10 year oscillations of $\Delta^{14}C$ may be a common feature, at least over the tropical western Pacific.

The 1–10 year oscillations of tropospheric $\Delta^{14}C$ during the post- and pre-nuclear era are reported. Spectrum analysis of the annual high-precision ^{14}C time series from tree rings of Washington and Arizona (AD 1511–1954) show periodicities in the 2–6.4 yr ranges, potentially associating with ENSO-related thermohalaine circulation changes (Stuiver and Braziunas 1993). In the post-nuclear

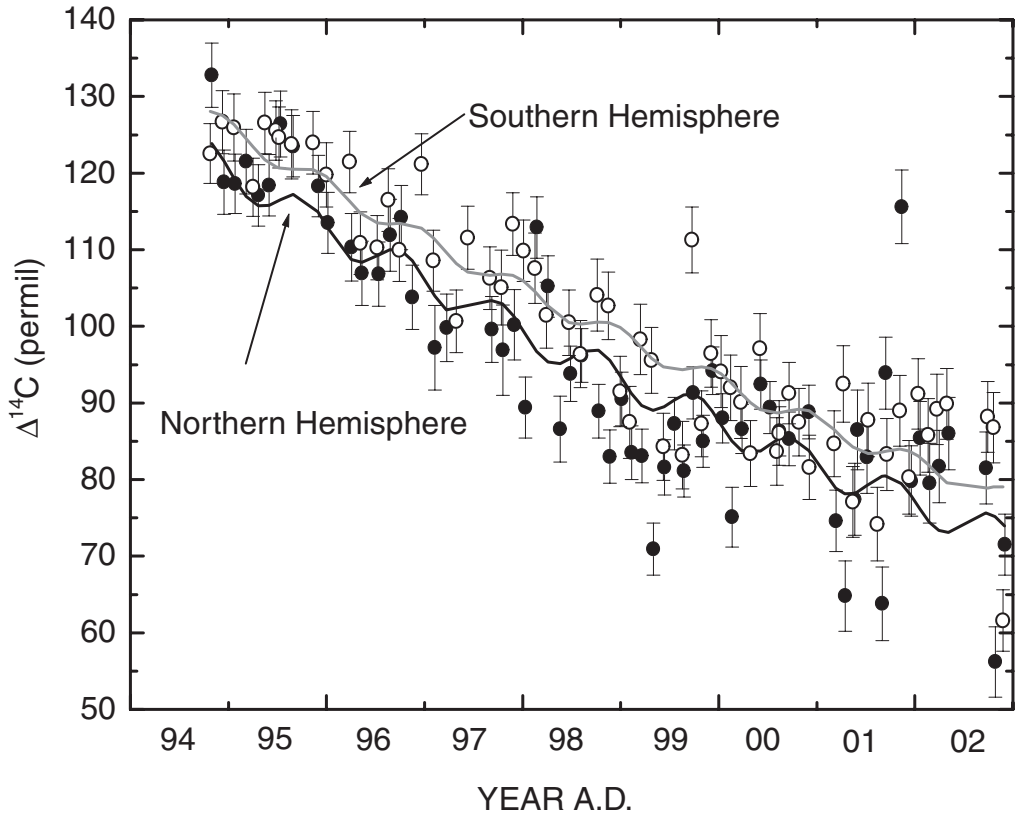

Figure 2 Comparison of $\Delta^{14}C$ records from the Northern and Southern Hemispheric air, fitted with a combined normal exponential and single harmonic curve for the years 1994–2002. Filled and open circles with a ±1-σ error bar are from the Northern and Southern Hemispheres, respectively.

era, $\Delta^{14}C$ changes on a regional scale by ENSO events are also observed in the equatorial Pacific region between 1991–1993 (Rozanski et al. 1995).

In Figure 3, the $\Delta^{14}C_{res}$ over the western Pacific are compared with the Tahiti-Darwin Southern Oscillation (SOI) (Ropelewski and Jones 1987) and the Multi-Variate ENSO index (MEI) (Wolter and Timlin 1998). The overall $\Delta^{14}C_{res}$ trend (relatively high around 1997–1998 and increasing after late 1998) is potentially correlated with the ENSO events.

El Niño events are characterized by anomalously warm sea surface temperature in the equatorial Pacific. The events can cause significant perturbation in the global carbon cycles, such as changes in the ocean-atmosphere CO_2 exchange and terrestrial CO_2 fluxes (Keeling et al. 1995). The weakened thermocline circulation in the equatorial Pacific during El Niño events can generate significant reduction in the upwelling of CO_2-rich deep-water mass and in the sea-air efflux of CO_2 by 30–80% from the normal condition (Feely et al. 1999). In addition, El Niño events are also accompanied by anomalous atmospheric circulation patterns, resulting potentially in enhanced biospheric CO_2 flux due to reduction in rainfall in tropical rainforests (Prentice and Lloyd 1998) and in enhanced transport of stratospheric air with higher $\Delta^{14}C$ (Nakamura et al. 1992) to the troposphere. All these phenomena may be related to the positive anomaly of the $\Delta^{14}C_{res}$ record over the western Pacific during 1997–1998. After the ENSO event, the arid condition in tropical rainforests poten-

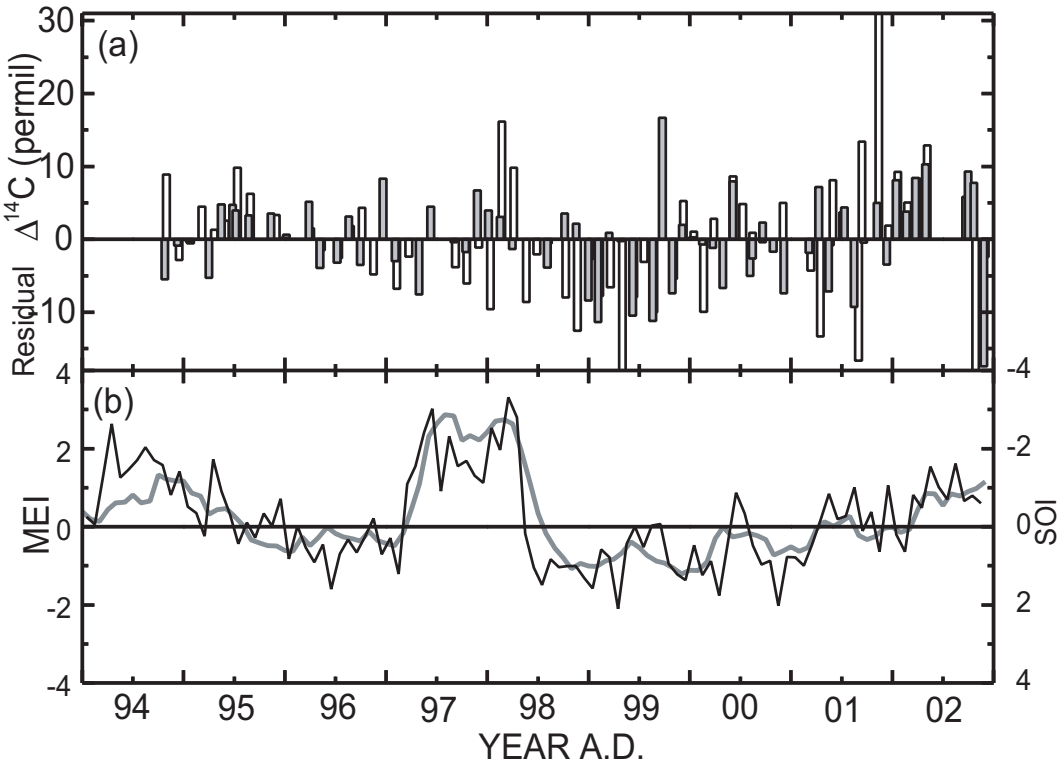

Figure 3 (a) Residual $\Delta^{14}C$ record calculated as the differences between the measured values and fitted curves. The residual $\Delta^{14}C$ values from the Northern and Southern Hemisphere are shown by open and gray bars, respectively; (b) The thick black and thin gray lines are monthly multi-variate ENSO index (MEI) (Wolter and Timlin 1998) and Tahiti-Darwin Southern Oscillation (SOI) (Ropelewski and Jones 1987), respectively. Positive MEI and negative SOI values represent the El Niño condition.

tially can release ^{14}C-rich CO_2 from the fast cycling soil organic matters with a time lag (Payner et al. 1998). The gradual increasing in $\Delta^{14}C_{res}$ after the 1997–1998 ENSO event seems to be related to such a biospheric release of ^{14}C-enriched CO_2.

CONCLUSION

Our observations revealed the 3 timescale changes of $\Delta^{14}C$ of atmospheric CO_2 that could be characterized as "natural background." The ongoing measurements of the samples from the different latitudes on the Japan-Australia transect over the western Pacific will give new insights to quantitatively understand the role of the terrestrial biosphere and ocean as a sink of anthropogenic CO_2 emissions in the past and in the coming years.

REFERENCES

Appenzeller C, Holton JR, Rosenlof KH. 1996. Seasonal variation of mass transport process across the tropopause. *Journal of Geophysical Research* 101(D10): 15,071–8.

Feely RA, Wanninkhof R, Takahashi T, Tans P. 1999. The influence of El Niño on the equatorial Pacific contribution to atmospheric CO_2 accumulation. *Nature* 398: 597–601.

Keeling CD, Whorf TP, Wahlen M, van der Plicht J. 1995. Interannual extrems in the rate of rise of atmospheric carbon dioxide since 1980. *Nature* 398:666–70.

Levin I, Graul R, Trivett NBA. 1995. Long-term observations of atmospheric CO_2 and carbon isotopes at continental sites in Germany. *Tellus* 47B(1/2):23–4.

Levin I, Hesshaimer V. 2000. Radiocarbon—a unique tracer of global carbon cycle dynamics. *Radiocarbon* 42(1):69–80.

Levin I, Kromer B. 1997. Twenty years of atmospheric $^{14}CO_2$ observations at Schauinsland station, Germany. *Radiocarbon* 39(2):205–18.

Levin I, Münnich KO, Weiss W. 1980. The effect of anthropogenic CO_2 and ^{14}C sources on the distribution of ^{14}C in the atmosphere. In: Stuiver M, Kra RS, editors. Proceedings of the 10th International ^{14}C Conference. *Radiocarbon* 22(2):379–91.

Levin I, Schuchard J, Kromer B, Münnich KO. 1989. The continental European Suess effect. *Radiocarbon* 31(3):431–40.

Manning MR, Lowe DC, Melhuish WH, Sparks RJ, Wallace G, Brenninkmeijer CAM, McGill RC. 1990. The use of radiocarbon measurements in atmospheric studies. *Radiocarbon* 32(1):37–58.

Meijer HA, van der Plicht J, Gislefoss JS, Nydal R. 1995. Comparing long-term atmospheric ^{14}C and ^{3}H records near Groningen, the Netherlands with Fruholmen, Norway and Izana, Canary Islands ^{14}C station. *Radiocarbon* 37(1):39–50.

Nakamura T, Nakazawa T, Nakai N, Kitagawa H, Honda H, Itoh T, Machida T, Matsumoto E. 1992. Measurement of ^{14}C concentrations of stratospheric CO_2 by accelerator mass spectrometry. *Radiocarbon* 34(3): 745–52.

Nydal R, Lovseth K. 1983. Tracing bomb ^{14}C in the atmosphere 1962–1980. *Journal of Geophysical Research* 88:3621–42.

Payner PJ, Law RM, Dragaville R. 1998. The relationship between tropical CO_2 fluxes and the El Niño-Southern Oscillation. *Geophysical Research Letters* 26:493–6.

Prentice IC, Lloyd JC. 1998. C-Quest in the Amazon Basin. *Nature* 396:619–20.

Randerson JT, Enting IG, Schuur EAG, Caldeira K, Fung IY. 2002. Seasonal and latitudinal variability of troposphere $\Delta^{14}CO_2$: post-bomb contributions from fossil fuels, oceans, the stratosphere, and the terrestrial biosphere. *Global Biogeochemical Cycles* 16:1112–31.

Ropelewski CF, Jones PD. 1987. An extension of the Tahiti-Darwin Southern Oscillation Index. *Monthly Weather Review* 115:2161–5. http://www.cru.uea.ac.uk/cru/data/soi.htm.

Rozanski K, Levin I, Stock J, Falcon REG, Rubio F. 1995. Atmospheric $^{14}CO_2$ variations in the equatorial region. *Radiocarbon* 37(2):509–15.

Stuiver M, Braziunas TF. 1993. Sun, ocean, climate and atmospheric $^{14}CO_2$: an evolution of causal and spectral relationships. *The Holocene* 3:289–305.

Stuiver M, Polach HA. 1997. Discussion: reporting of ^{14}C data. *Radiocarbon* 19(3):355–63.

Vogel JC. 1970. Groningen radiocarbon dates IX. *Radiocarbon* 12(2):444–71.

Wolter K, Timlin MS. 1998: Measuring the strength of ENSO—how does 1997/98 rank? *Weather* 53:315–24. http://www.cdc.noaa.gov/cru/~kew/MEI/mei.htm.

Appendix ^{14}C data list.

ID		Date	Lat (°N)	Long (°E)	pCO_2 (ppmv)	$\Delta^{14}C$ (‰)	$\Delta^{14}C_{unc}$ (‰)
H06-05	C2	30-Oct-94	25.20	142.12	357.20	132.8	4.2
H06-06	C4	15-Dec-94	25.58	143.40	363.10	118.8	4.2
H06-07	C2	25-Jan-95	24.20	143.30	363.70	118.6	3.9
H06-08	C3	7-Mar-95	23.47	143.67	364.00	121.5	4.2
H07-01	C3	21-Apr-95	25.90	142.17	367.40	117.1	4.0
H07-02	C2	31-May-95	23.37	143.95	364.10	118.4	4.0
H07-03	C4	13-Jul-95	25.40	142.68	360.10	126.4	4.3
H07-04	C1	29-Aug-95	23.68	143.60	358.70	123.5	4.0
H07-06	C3	24-Nov-95	25.30	142.77	365.05	118.3	4.0
H07-07	C6	6-Jan-96	27.57	141.80	364.11	113.5	4.0
H08-01	C5	2-Apr-96	24.58	143.37	364.68	110.3	4.4
H08-02	C4	12-May-96	23.64	143.87	366.56	106.9	4.2
H08-03	C3	13-Jul-96	20.60	146.11	366.62	106.8	4.2
H08-04	C5	24-Aug-96	24.48	144.79	366.05	111.9	4.7
H08-05	C6	5-Oct-96	24.58	143.35	359.30	114.2	4.2
H08-06	C4	16-Nov-96	24.85	144.33	363.73	103.8	4.2
H08-08	C4	8-Feb-97	22.42	145.37	366.35	97.2	5.5
H08-09	C4	23-Mar-97	24.33	144.56	367.57	99.8	4.4
H09-04	C4	7-Sep-97	25.58	144.05	360.69	99.6	4.3
H09-05	C3	18-Oct-97	24.33	144.21	360.89	96.9	5.9
H09-06	C4	30-Nov-97	24.50	144.33	363.42	100.2	4.6
H09-07	C5	11-Jan-98	23.92	144.57	367.07	89.4	4.0
H09-08	C5	22-Feb-98	23.07	144.92	368.12	112.9	4.0
H10-01	C5	5-Apr-98	25.43	143.95	369.96	105.2	4.0
H10-02	C3	20-May-98	25.06	144.08	369.66	86.6	4.3
H10-03	C5	28-Jun-98	25.77	143.46	366.77	93.8	3.6
H10-04	C3	8-Aug-98	24.92	143.96	365.55	96.2	3.5
H10-05	C3	10-Oct-98	23.85	144.58	365.24	88.9	3.5
H10-06	C3	21-Nov-98	25.14	144.03	367.88	83.0	3.5
H10-07	C3	4-Jan-99	24.97	144.13	369.90	90.5	3.5
H10-08	C4	9-Feb-99	25.53	143.87	370.68	83.5	3.5
H10-09	C4	20-Mar-99	24.10	144.50	370.10	83.1	3.5
H11-01	C4	2-May-99	27.43	143.06	374.03	70.9	3.4
H11-02	C3	12-Jun-99	24.69	144.24	374.19	81.6	3.6
H11-03	C3	19-Jul-99	24.22	144.43	374.62	87.3	3.4
H11-04	C2	23-Aug-99	23.57	144.73	370.08	81.1	3.4
H11-05	C3	27-Sep-99	23.71	144.65	365.17	91.3	3.4
H11-06	C4	3-Nov-99	24.09	144.36	366.87	85.0	3.4
H11-07	C4	8-Dec-99	24.17	143.80	369.23	94.2	3.1
H11-08	C4	14-Jan-00	23.32	144.65	369.84	88.0	3.2
H11-09	C4	19-Feb-00	24.21	144.83	371.45	75.1	3.9
H11-10	C3	28-Mar-00	23.66	145.07	373.62	86.6	3.2
H12-02	C4	5-Jun-00	24.04	144.50	374.15	92.4	3.2
H12-03	C4	10-Jul-00	24.03	144.51	371.87	89.4	3.4
H12-04	C4	14-Aug-00	24.04	144.51	374.47	86.3	3.2
H12-05	C4	19-Sep-00	24.04	144.49	367.62	85.3	3.5

Appendix ^{14}C data list. *(Continued)*

ID		Date	Lat (°N)	Long (°E)	pCO_2 (ppmv)	$\Delta^{14}C$ (‰)	$\Delta^{14}C_{unc}$ (‰)
H12-07	C6	2-Dec-00	22.53	145.15	371.03	88.8	3.5
H12-10	C4	12-Mar-01	24.03	144.49	375.01	74.6	4.0
H13-01	C5	16-Apr-01	27.07	143.19	375.31	64.8	4.6
H13-02	C5	21-May-01	26.83	143.28	374.18	77.4	4.7
H13-03	A4	31-May-01	24.04	133.55	373.44	86.5	5.2
H13-04	A4	5-Jul-01	24.05	134.63	370.65	82.9	4.7
H13-05	A4	9-Aug-01	24.04	133.51	364.58	63.8	4.8
H13-06	A4	13-Sep-01	23.95	133.57	368.36	93.9	4.7
H13-07	C4	12-Nov-01	24.05	144.50	370.96	115.6	4.8
H13-08	C4	17-Dec-01	24.06	144.43	373.69	79.8	4.6
H13-09	C4	20-Jan-02	24.05	144.57	374.03	85.4	4.8
H13-10	C4	24-Feb-02	24.06	144.48	374.66	79.5	5.2
H14-01	C4	31-Mar-02	24.05	144.51	374.63	81.7	4.7
H14-02	C4	6-May-02	24.05	144.49	376.03	86.0	4.7
H14-03	C4	22-Sep-02	25.50	140.90	369.72	81.5	4.7
H14-04	C4	27-Oct-02	25.80	141.85	378.10	56.2	4.6
H14-05	C4	1-Dec-02	24.03	142.22	375.85	71.5	4.0
H06-05	A2	24-Oct-94	–14.72	154.37	357.85	122.6	3.9
H06-06	A5	9-Dec-94	–13.38	154.42	357.98	126.7	4.1
H06-07	A4	20-Jan-95	–12.65	154.43	358.47	126	4.4
H06-08	A5	1-Mar-95	–12.18	154.47	358.53	118.2	3.8
H07-01	A4	16-Apr-95	–12.37	154.35	361.10	126.6	4
H07-02	A4	26-May-95	–13.75	154.42	358.31	125.6	3.9
H07-03	A4	7-Jul-95	–14.15	154.37	358.70	124.7	4
H07-04	A2	23-Aug-95	–14.17	150.17	359.58	123.8	4.5
H07-06	A4	19-Nov-95	–11.80	151.52	362.23	124	4.1
H07-07	A6	31-Dec-95	–13.50	154.32	360.98	119.8	4.2
H08-01	A6	27-Mar-96	–13.08	154.47	361.55	121.5	4
H08-02	A5	6-May-96	–14.10	154.41	362.16	110.9	4.1
H08-03	A5	7-Jul-96	–13.80	154.41	361.68	110.3	4.2
H08-04	A6	18-Aug-96	–12.01	154.52	360.81	116.5	4.1
H08-05	A6	29-Sep-96	–13.19	154.46	360.75	110	4.1
H08-07	A5	20-Dec-96	–13.07	154.45	362.20	121.2	4
H08-08	A5	2-Feb-97	–13.88	154.41	362.93	108.6	4
H09-01	A5	28-Apr-97	–13.31	154.44	360.64	100.7	4.1
H09-02	A7	9-Jun-97	–7.76	153.89	361.49	111.6	4.1
H09-04	A5	31-Aug-97	–15.36	154.34	362.05	106.3	4.1
H09-05	A5	13-Oct-97	–11.88	154.50	362.33	105.1	4.9
H09-06	A5	24-Nov-97	–12.59	154.48	363.62	113.4	4.1
H09-07	A6	4-Jan-98	–13.96	154.42	364.87	109.9	4
H09-08	A5	16-Feb-98	–11.57	154.53	364.82	107.6	4.6
H10-01	A5	30-Mar-98	–13.17	154.44	363.78	101.5	4.3
H10-03	A5	22-Jun-98	–11.25	154.50	364.47	100.5	4.3
H10-04	A4	3-Aug-98	–10.71	154.40	366.07	96.4	4.4
H10-05	A4	5-Oct-98	–11.37	154.52	365.12	104.1	4.7
H10-06	A4	15-Nov-98	–14.49	154.37	368.89	102.7	4.4
H10-07	A5	29-Dec-98	–14.21	154.39	369.87	91.5	4.6
H10-08	A5	3-Feb-99	–12.66	154.47	371.79	87.5	4.7

Appendix ^{14}C data list. *(Continued)*

ID		Date	Lat (°N)	Long (°E)	pCO_2 (ppmv)	$\Delta^{14}C$ (‰)	$\Delta^{14}C_{unc}$ (‰)
H10-09	A5	14-Mar-99	–13.85	154.43	368.71	98.3	4.6
H11-01	A4	25-Apr-99	–14.85	154.36	367.64	95.6	4.3
H11-02	A4	7-Jun-99	–11.32	154.51	367.67	84.3	4.4
H11-04	A4	18-Aug-99	–14.17	154.38	373.82	83.2	4.4
H11-05	A5	22-Sep-99	–12.88	154.45	368.01	111.3	4.3
H11-06	A6	28-Oct-99	–15.21	154.39	369.16	87.3	4.3
H11-07	A5	3-Dec-99	–12.88	152.33	373.50	96.5	4.4
H11-08	A6	9-Jan-00	–12.30	154.54	369.52	94.1	4.7
H11-09	A5	13-Feb-00	–12.92	154.51	369.67	92	4.3
H11-10	A4	22-Mar-00	–14.61	154.42	370.38	90.1	4.7
H12-01	A5	26-Apr-00	–15.06	154.39	369.57	83.4	4.3
H12-02	A5	31-May-00	–15.06	154.39	369.16	97.1	4.6
H12-03	A5	5-Jul-00	–15.06	154.39	368.57	83.7	4.4
H12-04	A5	8-Aug-00	–15.06	154.39	368.71	86.1	4.2
H12-05	A5	13-Sep-00	–15.06	154.39	368.28	91.3	4.0
H12-06	A5	20-Oct-00	–15.06	154.38	370.10	87.5	4.4
H12-07	A7	26-Nov-00	–13.92	154.45	370.28	81.6	4.2
H12-10	A5	6-Mar-01	–15.06	154.39	368.58	84.7	4.3
H13-01	A5	10-Apr-01	–15.03	154.40	368.11	92.5	5.0
H13-02	A5	15-May-01	–14.50	154.43	367.89	77.1	4.6
H13-04	C3	11-Jul-01	–15.07	154.39	368.77	87.8	4.8
H13-05	C3	15-Aug-01	–15.06	152.79	368.97	74.2	4.8
H13-06	C3	19-Sep-01	–15.06	152.77	369.79	83.3	4.7
H13-07	A5	6-Nov-01	–14.94	154.40	369.75	89	4.6
H13-08	A5	11-Dec-01	–14.94	154.39	370.42	80.3	4.8
H13-09	A4	14-Jan-02	–17.93	154.23	369.91	91.2	4.6
H13-10	A5	19-Feb-02	–14.94	154.38	369.84	85.8	4.8
H14-01	A5	25-Mar-02	–14.94	154.39	369.89	89.2	4.6
H14-02	A5	30-Apr-02	–14.94	154.38	370.17	89.9	4.6
H14-03	A3	16-Sep-02	–14.92	154.57	372.68	88.2	4.6
H14-04	A3	21-Oct-02	–16.85	154.30	371.79	86.8	4.6
H14-05	A4	26-Nov-02	–14.03	154.38	376.85	61.6	4.0
H06-05	C2	30-Oct-94	25.20	142.12	357.20	132.8	4.2
H06-06	C4	15-Dec-94	25.58	143.40	363.10	118.8	4.2
H06-07	C2	25-Jan-95	24.20	143.30	363.70	118.6	3.9
H06-08	C3	7-Mar-95	23.47	143.67	364.00	121.5	4.2
H07-01	C3	21-Apr-95	25.90	142.17	367.40	117.1	4.0
H07-02	C2	31-May-95	23.37	143.95	364.10	118.4	4.0
H07-03	C4	13-Jul-95	25.40	142.68	360.10	126.4	4.3
H07-04	C1	29-Aug-95	23.68	143.60	358.70	123.5	4.0
H07-06	C3	24-Nov-95	25.30	142.77	365.05	118.3	4.0
H07-07	C6	6-Jan-96	27.57	141.80	364.11	113.5	4.0

RADIOCARBON, Vol 46, Nr 2, 2004, p 911–916

RADIOCARBON CONCENTRATION IN THE ATMOSPHERE AND MODERN TREE RINGS IN THE KRAKÓW AREA, SOUTHERN POLAND

Andrzej Rakowski[1,2,3] • Tadeusz Kuc[4] • Toshio Nakamura[1]• Anna Pazdur[3]

ABSTRACT. New results of radiocarbon concentration in tree rings from the Kraków region covering a growth period of 20 yr have been analyzed, and the relationship between them and ^{14}C concentrations in the atmospheric CO_2 are described. This enabled assessment of the uptake period for pine trees at the regional climatic conditions. Both sets of data show lower ^{14}C concentrations than reported for "clean air" at the reference station, indicating a remarkable input of "dead" CO_2 of fossil fuel origin. Using data of carbon dioxide and ^{14}C concentrations from Schauinsland, summer values of the fossil component (C_f) in carbon dioxide were calculated for the Kraków area. Fitting exponential and linear functions to experimental data, the exchange time was calculated, and expected future ^{14}C concentration in the atmosphere was estimated.

INTRODUCTION

Recently, atmospheric concentration of carbon dioxide has exceeded 370 ppm (Keeling et al. 1995; GLOBALVIEW-CO_2 2003), mainly due to the emission of CO_2 from fossil fuels such as coal, natural gas, and petroleum. This increase has affected global radiocarbon concentration in the atmosphere, as well as in the ocean and biosphere. Due to atmospheric nuclear bomb tests, ^{14}C concentration in atmospheric CO_2 increased rapidly through the 1950s and 1960s to a maximum in 1963, when the measured level was double the natural value (Nydal and Lövseth 1996). Since the atomic test ban treaty was enforced, the concentration of ^{14}C in the atmosphere has slowly decreased; however, in the 1990s, the concentration was still about 10% higher than pre-bomb levels (McNeely 1994; Levin and Kromer 1997). Several laboratories in Europe are continuously monitoring atmospheric CO_2 and/or carbon isotope composition, either directly (Levin and Kromer 1997; NOAA 2001; Necki et al. 2002; Kuc et al. 2003) or in plants (McNeely 1994; Krajcar Bronić et al. 1998; Rakowski et al. 2001). Results show that heavy local emissions of carbon dioxide from fossil fuels cause remarkable disturbances in carbon isotope composition in the local atmosphere and biosphere, and also have an influence on a regional and global scale. This effect is observed not only in heavily industrialized areas but also in urbanized regions where carbon dioxide is emitted from small industrial facilities, vehicles, and other common sources. The magnitude of the effect on ^{14}C concentration is dependent on the distance from the sources of CO_2 emissions (Awsiuk and Pazdur 1986).

Kraków (50°3′N, 19°54′E) is a city of 1 million people, located about 100 km to the north of the Tatra Mountains in southern Poland (Figure 1). Air pollution related to the urban infrastructure, industrial facilities, and a large steel factory (Huta im. Tadeusza Sendzimira) has elevated carbon dioxide levels in the local atmosphere (Kuc et al. 2003). Since 1983, the Department of Environmental Physics, University of Science and Technology in Kraków has monitored carbon isotope compositions in tropospheric CO_2 (Florkowski et al. 1975; Kuc 1991; Kuc and Zimnoch 1998). Samples were taken at biweekly intervals from the Faculty building roof on the university campus, 25 m above ground level. Annual tree rings were also taken from pine trees (*Pinus sylvestris*) growing near the university.

[1]University of Nagoya, Center for Chronological Research, Nagoya, Japan.
[2]Corresponding author. Email: rakowski@zeus.polsl.gliwice.pl.
[3]Silesian University of Technology, Institute of Physics, Radiocarbon Laboratory, Gliwice, Poland.
[4]AGH, University of Science and Technology, Kraków, Poland.

Proceedings of the 18th International Radiocarbon Conference, edited by N Beavan Athfield and R J Sparks
RADIOCARBON, Vol 46, Nr 2, 2004, p 911–916

Figure 1 Map of Poland with the location of Kraków

SAMPLES AND METHODS

In this study, 2 kinds of samples were used: CO_2 separated directly from the air at over sequential 2-week intervals and representing an integrated value over the sampling period, and tree rings obtained from trunks of pine trees (*Pinus sylvestris*) growing near the university.

Atmospheric CO_2 Samples

Samples of atmospheric CO_2 were taken by applying the method of selective sorption in capillary sorbent, as described in Florkowski et al. (1975), Kuc (1991), and Kuc and Zimnoch (1998). ^{14}C measurements were performed with a liquid scintillation spectrometer (Tri-Carb®, Canberra-Packard) after the conversion of purified CO_2 to benzene using a standard procedure and mixing with a scintillation cocktail (b-PBD + b-MSB, Packard). Stable carbon isotope composition was measured using VG Micromass 602 C and Finningan MAT Delta S mass spectrometers at Kraków University.

Tree-Ring Samples

Annual growth rings in pine trees were sampled with a hollow drill. In order to obtain sufficient material for accelerator mass spectrometry (AMS) analysis, 3 core samples were taken from the tree and annual growth rings were separated. Samples were washed in distilled water and prepared following the standard AAA procedure. Each sample was heated at 80 °C in 0.5M HCl for 12 hr, then filtered, rinsed, and heated in 0.1M NaOH (80 °C, 12 hr). The samples were then filtered, rinsed, and heated again in 0.5M HCl (80 °C, 12 hr), then re-filtered, rinsed in distilled water, and dried. Sample residues were combined with cupric oxide, sealed in glass tubes, and evacuated by a rotary pump. The tubes were then placed in an electric furnace for 2 hr at 850 °C. Carbon dioxide produced from the samples was purified in a glass cryogenic vacuum-line system. Water produced during combustion was removed via a trap containing a mixture of methanol and liquid nitrogen at 180 °K. SO_x compounds were removed with an *n*-pentane trap cooled by liquid nitrogen. Pure CO_2 was then condensed in glass tubes at liquid nitrogen temperatures. The prepared CO_2 samples were reduced to graphite using iron powder as a catalyst (Kitagawa et al. 1993). The iron powder was prepared in a

vacuum line containing hydrogen and heated for about 1 hr at 450 °C. The line was evacuated and CO_2 was condensed with the iron powder using liquid nitrogen. Hydrogen was then added and the glass tube was sealed. Reduction was done in an electric furnace at 650 °C for 6 hr. The resulting mixture of graphite and iron powder was dried and pressed into the target holder of the AMS system. The $\Delta^{14}C$ and $\delta^{13}C$ values were measured using a HVEE Tandetron AMS system and a Finningan MAT 252 mass spectrometer, respectively, at the Center for Chronological Research, Nagoya University, Japan (Nakamura et al. 2000).

^{14}C data are reported in terms of $\Delta^{14}C$ (in ‰) deviations from the standard sample, 95% activity of NBS oxalic acid (Stuiver and Polach 1977). Stable carbon isotope data are expressed in δ-notation on the PDB scale (Craig 1957).

RESULTS AND DISCUSSION

^{14}C concentrations in tree rings and atmospheric CO_2 from the Kraków area are shown in Figure 2, together with data from Schauinsland (Levin and Kromer 1997) as reference values. In order to compare results obtained for tree rings and atmospheric CO_2, ^{14}C concentration data in atmospheric CO_2 were averaged for the April to September period of each year, which is the season of vegetative growth and CO_2 uptake in Poland, and corrected to $\delta^{13}C = –25‰$ to provide the $\Delta^{14}C$ notation (Stuiver and Polach 1977). Data from Schauinsland (Levin and Kromer 1997) presented in the $\Delta^{14}C$ notation were fitted to an exponential curve. ^{14}C concentration for 1997–2002 were estimated by extrapolation on the curve. All data show a gradual decrease of ^{14}C activity over time. Decreases of 7.1‰ per yr for tree rings and 9.15‰ per yr for atmospheric ^{14}C were obtained. Atmospheric $\Delta^{14}C$ values measured at 2 stations in Croatia (Zagreb and Plitovice) during the same period decrease at rates of 12‰ and 10.6‰ per yr, respectively (Krajcar Bronić et al. 1998). For the Schauinsland station, decreases of 14.1‰ per yr for the 1983–1985 period and 9.7‰ per yr for 1985–1989 were reported (Levin et al. 1992).

Absolute differences between $\Delta^{14}C$ values from tree rings and atmospheric CO_2 from the Kraków area are presented in bar form in Figure 2. ^{14}C concentrations in atmospheric CO_2 show strong peak-to-peak (~56‰, Kuc and Zimnoch 1998) and seasonal fluctuations that are not recorded in the tree-ring samples. ^{14}C concentrations in both kinds of samples from Kraków are lower than in "clean air" at the Schauinsland station. This is attributed to a local Suess effect. The $\Delta^{14}C$ values in tree rings (108‰, 99‰, and 85‰ for 1994, 1995, and 1996, respectively) are lower than the mean yearly values in atmospheric CO_2 at Schauinsland (117‰, 111‰, and 102‰, respectively; Levin and Kromer 1997) but higher than those measured in Zagreb (81‰, 88‰, and 56‰; Krajcar Bronić et al. 1998) for the same period.

Exponential curves were fitted to the Kraków data for the period of 1983–2002 to determine long-term changes in ^{14}C concentration in the atmosphere and biosphere. These analyses provide time decay constants of 16.7 yr for tree-ring data and 14.3 yr for atmospheric CO_2, which correspond well with ~16-yr estimates reported in the literature (Levin et al. 1995; McNeely 1994; Krajcar Bronić et al. 1998). Carbon isotope ratios calculated from exponential and linear models decrease at rates of 7.1‰ and 6.75‰ per yr, respectively, for tree-ring data, and 7.75‰ and 6.29‰ per yr for atmospheric CO_2 data. According to the linear model, $\Delta^{14}C$ is estimated to equal 0‰ in 2010 for tree rings and 2007 for atmospheric CO_2. The same procedure produces estimates of 2007 for the Schauinsland data (Levin and Kromer 1997) and 2004 for the Groningen data (Meijer et al. 1995).

^{14}C concentration in the atmosphere over large cities is strongly affected by emissions of CO_2 from fossil fuels. Concentrations of carbon dioxide can be divided into 3 components: a background com-

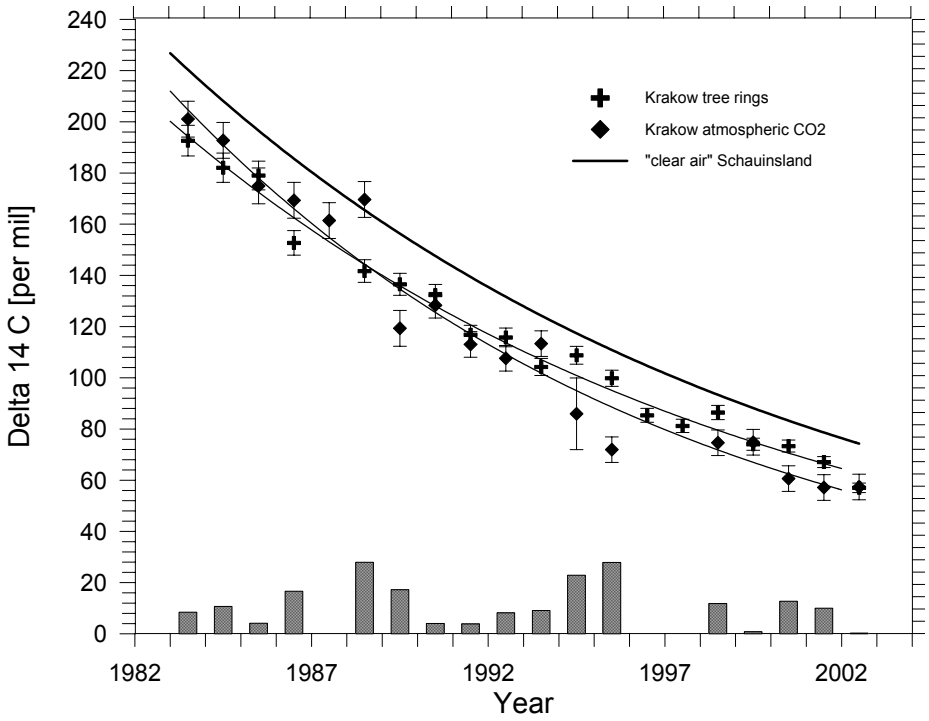

Figure 2 $\Delta^{14}C$ values in tree rings and atmospheric CO_2 samples collected in the Kraków area, southern Poland. The solid line represents ^{14}C concentration in "clear air" at Schauinsland station, estimated from the measurement of atmospheric CO_2 (Levin and Kromer 1997). Bars show absolute differences between atmospheric CO_2 and tree-ring samples for Kraków. All atmospheric data represent mean annual values for the April to September season, expressed as $\Delta^{14}C$.

ponent (C_a), a biogenic component (C_b), and a fossil component (C_f). Mathematical equations that can describe the relationships between each component and carbon isotopic composition are discussed in previous literature (e.g. Levin et al. 1989; Zondervan and Meijer 1996; Kuc et al. 2003), and were used to calculate C_f for the Kraków data. The value of C_f varies seasonally, from ~27.5 ppmv in the winter to ~10 ppmv in the summer during the 1983–1994 period (Kuc and Zimnoch 1998; Kuc et al. 2003). This variation correlates with differences in fossil fuel consumption between the seasons in the Kraków area.

New estimates of C_f using the new Kraków data are presented in Figure 3. Reference values of ^{14}C and CO_2 concentration representing "clean air" were calculated using data from Schauinsland station (GLOBALVIEW-CO_2 2003). Averaging C_f over 2 decades (1983–2003) for the April to September season, values of 5.9 ppmv and 6.5 ppmv were obtained for tree rings and atmospheric CO_2, respectively. Both values are lower than the yearly average obtained for consecutive years by Kuc and Zimnoch (1998); however, the estimates converge over time. Lower values of C_f observed in the Kraków area in recent years are the result of a reduction in fossil fuel consumption, especially in the case of coal.

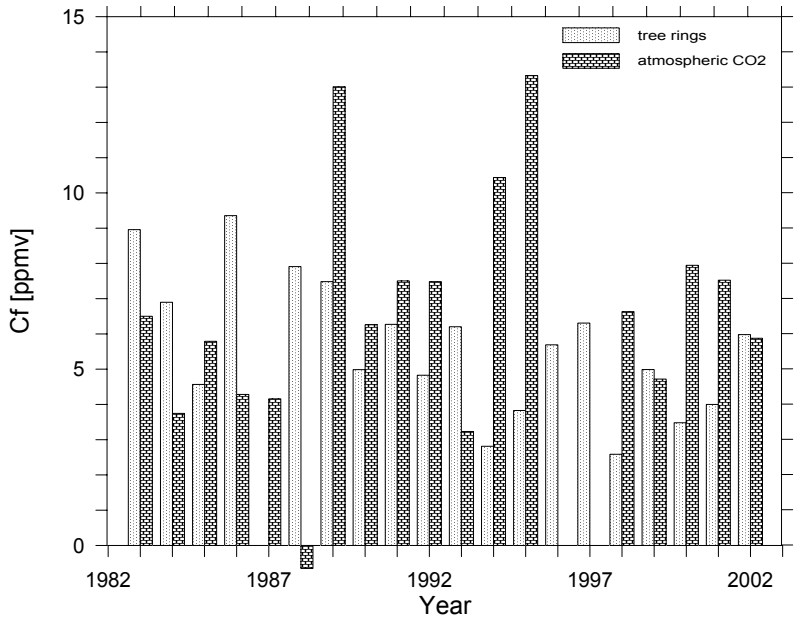

Figure 3 Values of the fossil component C_f calculated using tree-ring and atmospheric CO_2 data from the Kraków sampling site. Data represent mean annual values for the April to September season.

CONCLUSION

^{14}C concentration in samples of tree rings and in atmospheric CO_2, measured in Kraków over last 20 yr, are lower than in "clean air" due to the input of CO_2 from fossil fuels. Decreases in ^{14}C concentration of 7.1‰ per yr for tree rings and 9.15‰ per yr for atmospheric CO_2 were observed. Data fitted to exponential and linear functions provided reliable estimates of rates of decrease in carbon isotope ratios and time decay constants for the sampling area. Isotopic records in tree rings and atmospheric CO_2 collected over long time periods yield information on the local input of anthropogenic CO_2. Moreover, tree rings appear to be a valuable archive of isotopic variations in the local environment over time, albeit in annual increments only. In comparing atmospheric CO_2 and tree-ring data, it is necessary to consider the climatic conditions of central Europe, since the commencement and duration of the vegetative growth (and CO_2 uptake) period can vary from year to year.

ACKNOWLEDGEMENTS

This work was partly supported by Ministry of Education, Sciences, Sport and Culture of Japan and the Polish State Committee for Scientific Research. We express our thanks to all staff of the Center for Chronological Research, Nagoya University for help and especially to Tomoko Ohta for explaining the procedure of sample preparation for the AMS system. The authors also thank Daniel Dunkley for improving the English of the manuscript.

REFERENCES

Awsiuk R, Pazdur MF. 1986. Regional Suess effect in Upper Silesia urban area. *Radiocarbon* 28(2A):655–60.

Craig H. 1957. Isotope standards for carbon and oxygen and correction factors for mass-spectrometric analysis of carbon dioxide. *Geochimica et Cosmochimica Acta* 12:133–49.

Florkowski T, Grabczak J, Kuc T, Różański K. 1975. Determination of radiocarbon in water by gas or liquid

scintillation counting. *Nkcleonika* 20(11–12):1053–66.

GLOBALVIEW-CO_2. 2003. Cooperative Atmospheric Data Integration Project—Carbon Dioxide. CD-ROM, NOAA CMDL, Boulder, Colorado [Also available on internet via anonymous FTP to ftp.cmdl.noaa.gov, Path: ccg/co2/GLOBALVIEW].

Keeling CD, Whorf TP, van der Plicht J. 1995. International extremes in the rate of rise of atmospheric carbon dioxide since 1980. *Nature* 375:666–9

Kitagawa H, Masuzawa T, Nakamura T, Matsumoto E. 1993. A batch preparation method for graphite targets with low level background for AMS ^{14}C measurements. *Radiocarbon* 35(2):295–300.

Krajcar Bronić I, Horvatinčić N, Obelić B. 1998. Two decades of environmental isotope records in Croatia, reconstruction of the past and prediction of future level. *Radiocarbon* 40(1):399–416.

Kuc T. 1991. Concentration and carbon isotope composition of atmospheric CO_2 in southern Poland. *Tellus* 43B:373–8.

Kuc T, Zimnoch M. 1998. Changes of the CO_2 sources and sink in polluted urban area (southern Poland) over last decade, deriving from the carbon isotope composition. *Radiocarbon* 40(1):417–23.

Kuc T, Rozanski K, Zimnoch M, Necki JM, Korus A. 2003. Anthropogenic emissions of CO_2 and CH_4 in an urban environment. *Applied Energy* 75:193–203.

Levin I, Schuchard J, Kromer B, Münnich O. 1989. The continental European Suess effect. *Radiocarbon* 31(3):431–40.

Levin I, Kromer B. 1997. Twenty years of high-precision atmospheric $^{14}CO_2$ observation at Schauinsland station, Germany. *Radiocarbon* 39(2):205–18.

Levin I, Graul R, Trivett NBA. 1995. Long-term observations of atmospheric CO_2 and carbon isotopes at continental sites in Germany. *Tellus* 47B:23–34.

Levin I, Bösinger R, Bonani G, Francey RJ, Kromer B, Münnich KO, Suter M, Trivett NBA, Wölfli W. 1992. Radiocarbon in atmospheric carbon dioxide and methane: global distribution and trends. In: Taylor RE, Long A, Kra RS, editors. *Radiocarbon After Four Decades: An Interdisciplinary Perspective*. New York: Springer-Verlag. p 503–18.

McNeely R. 1994. Long-term environmental monitoring of ^{14}C levels in Ottawa region. *Environment International* 20(5):675–9.

Meijer HAJ, van der Plicht H, Gislofoss JS, Nydal R. 1995. Comparing long-term atmospheric ^{14}C and ^{3}H records near Groningen, the Netherlands with Fruholmen, Norway and Izaña, Canary Islands ^{14}C stations. *Radiocarbon* 37(1):39–50.

Nakamura T, Niu E, Oda H, Ikeda A, Minami M, Takahashi H, Adachi M, Pals L, Gottdang A, Suya N. 2000. The HVEE Tandetron AMS system at Nagoya University. *Nuclear Instruments and Methods in Physics Research B* 172:52–7.

Necki J, Schmidt M, Rozanski K, Zimnoch M, Korus A, Lasa J, Graul R, Levin I. 2002. Six-year record of atmospheric carbon dioxide and methane at a high-altitude mountain site in Poland. *Tellus* 55B:94–104.

NOAA Climate Monitoring and Diagnostics Laboratory. 2001. ftp site: ftp://cmdl.noaa.gov/ccg/ networek.txt.

Nydal R, Lövseth K. 1996. Carbon-14 measurement in atmospheric CO_2 from Northern and Southern Hemisphere sites, 1962–1993. Oak Ridge National Laboratory NDP-057.

Rakowski AZ, Pawełczyk S, Pazdur A. 2001. Changes of ^{14}C concentration in modern trees from Upper Silesia region, Poland. *Radiocarbon* 43(2B):679–89.

Stuiver M, Polach HA. 1977. Discussion: reporting of ^{14}C data. *Radiocarbon* 19(2):355–63

Zondervan A, Meijer AJ. 1996. Isotopic characterization of CO_2 sources during regional pollution events using isotopic and radiocarbon analysis. *Tellus* 48B:601–12.

RADIOCARBON, Vol 46, Nr 2, 2004, p 917–924

WIGGLE-MATCH DATING OF TREE-RING SEQUENCES

Mariagrazia Galimberti[1] • Christopher Bronk Ramsey[1,2] • Sturt W Manning[3]

ABSTRACT. Given the non-monotonic form of the radiocarbon calibration curve, the precision of single ^{14}C dates on the calendar timescale will always be limited. One way around this limitation is through comparison of time-series, which should exhibit the same irregular patterning as the calibration curve. This approach can be employed most directly in the case of wood samples with many years growth present (but not able to be dated by dendrochronology), where the tree-ring series of unknown date can be compared against the similarly constructed ^{14}C calibration curve built from known-age wood. This process of curve-fitting has come to be called "wiggle-matching."

In this paper, we look at the requirements for getting good precision by this method: sequence length, sampling frequency, and measurement precision. We also look at 3 case studies: one a piece of wood which has been independently dendrochronologically dated, and two others of unknown age relating to archaeological activity at Silchester, UK (Roman) and Miletos, Anatolia (relating to the volcanic eruption at Thera).

INTRODUCTION

The use of wiggle-matching for the more precise dating of tree-ring sequences, where dendrochronology is not possible on its own, is not new (e.g. Ferguson et al. 1966; Clark and Renfrew 1972; Clark and Morgan 1983) but is a method which is being performed more and more frequently. The mathematical methods which can be employed (see for example, Christen and Litton 1995; Bronk Ramsey et al. 2001; Pearson 1986) are well worked out. The purpose of this paper is to look at the application of the technique to archaeological material of a form which might be found in archaeological sites. The method has been applied to such materials before (see for example, Friedrich et al. 2001; Lowe et al. 2001; Kilian et al. 2000; Wille et al. 2003; van de Plassche et al. 2001). It has also been applied to long sequences of floating tree-ring chronologies (see for example, Kromer et al. 2001; Manning et al. 2001; van der Plicht et al. 1995; Imamura et al. 1998; Guo et al. 2000; Slusarenko et al. 2001; Vasiliev et al. 2001; Hajdas et al., forthcoming; Slusarenko et al., forthcoming).

Here, we will look at the suitable requirements for a sample for this type of analysis through a process of simulation. We will then look at 3 specific examples to test the accuracy and precision of the technique in fairly typical archaeological contexts. The first of these samples is from a standing building and has actually been dendrochronologically dated, so it is a blind test of the method. The other two are from archaeological sites (Silchester, a Roman site in southern Britain) and Miletos (Late Bronze Age levels of the site in western Turkey). The Silchester sample and standing building sample are both wood (waterlogged in the case of Silchester) and the Miletos sample is charcoal—so these examples cover a range of material types and contexts.

SIMULATIONS

We have conducted a large number of simulations using the calibration program OxCal to see what kind of precision can be obtained through wiggle-matching. In doing this, we use the R_Simulate function of the program and perform each analysis 10 times in order to average over some of the inherent variability in such simulations.

[1]Oxford Radiocarbon Accelerator Unit, University of Oxford, United Kingdom.
[2]Corresponding author. Email: christopher.ramsey@archaeology-research.oxford.ac.uk.
[3]Department of Fine Art, University of Toronto, Canada; Also, Department of Archaeology, University of Reading, United Kingdom.

Proceedings of the 18th International Radiocarbon Conference, edited by N Beavan Athfield and R J Sparks
RADIOCARBON, Vol 46, Nr 2, 2004, p 917–924

Figures 1 and 2 show examples from these simulations directed towards the investigation of what the optimum number of samples are in terms of the measurement precision available for a particular time period. In the particular case shown, good precision (total 95% confidence range of less than 20 yr) can be achieved with only 7 measurements at a measurement precision level of ±35 ^{14}C yr. The sample/precision requirements are very variable depending on the period concerned (essentially due to the details of the shape of the calibration curve). But high precision (20 calendar yr) is often achievable with individual sample precision of ±25 ^{14}C yr and less than a century of wood. The optimum spacing for measurements is usually 10 yr (reflecting the resolution and scale of wiggles in the calibration curve). Note: this work employed INTCAL98; the more smoothed and modeled nature of INTCAL04 will very slightly change conclusions when it is employed (as it lacks some of the largely decadal signal of INTCAL98), but we do not expect significant differences.

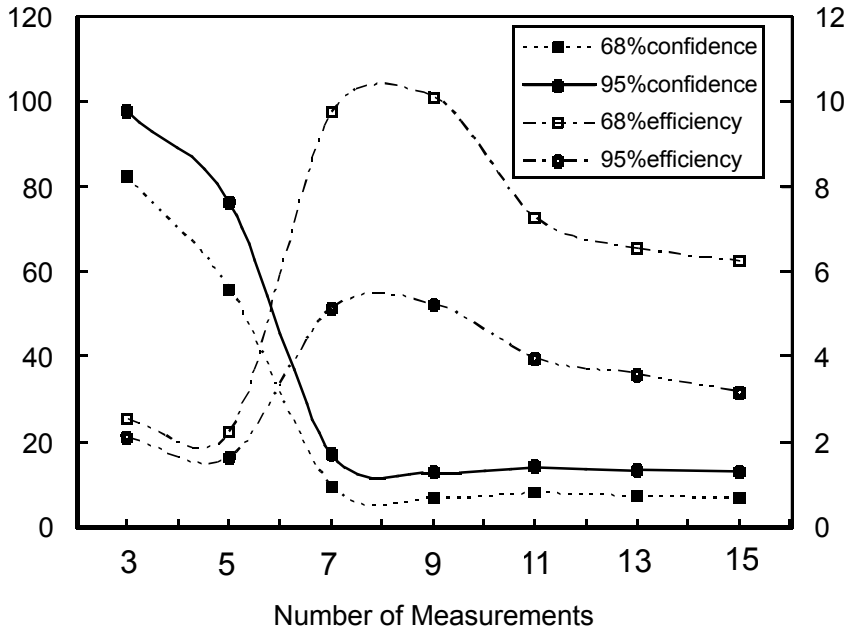

Figure 1 This figure shows the effect of increasing the number of measurements for a particular wiggle-match simulation; the starting date for this simulation was AD 1370; the sample intervals were set to 10 yr; and the precision was set to ±25 ^{14}C yr. The efficiency is defined as being $p^2/(r\ n)$, where p is the precision, r is the range, and n is the number of measurements. Using the efficiency measure or by looking at the ranges, it can be seen that about 7–9 measurements (spanning 70–80 yr) gives high precision for this particular period.

We can define an efficiency quotient (quality/effort) which is proportional to

$$p^2/(r\ n)$$

where r is the calibrated range after the wiggle-match and, therefore, $1/r$ is a suitable quality factor; n is the number of measurements and, therefore, proportional to the measurement effort; and p is the precision of the measurements, and the effort associated with this is assumed to be $1/p^2$.

This efficiency measure can be used to help in the estimation of the optimum number and precision of measurements for any given time range (see Figures 1 and 2).

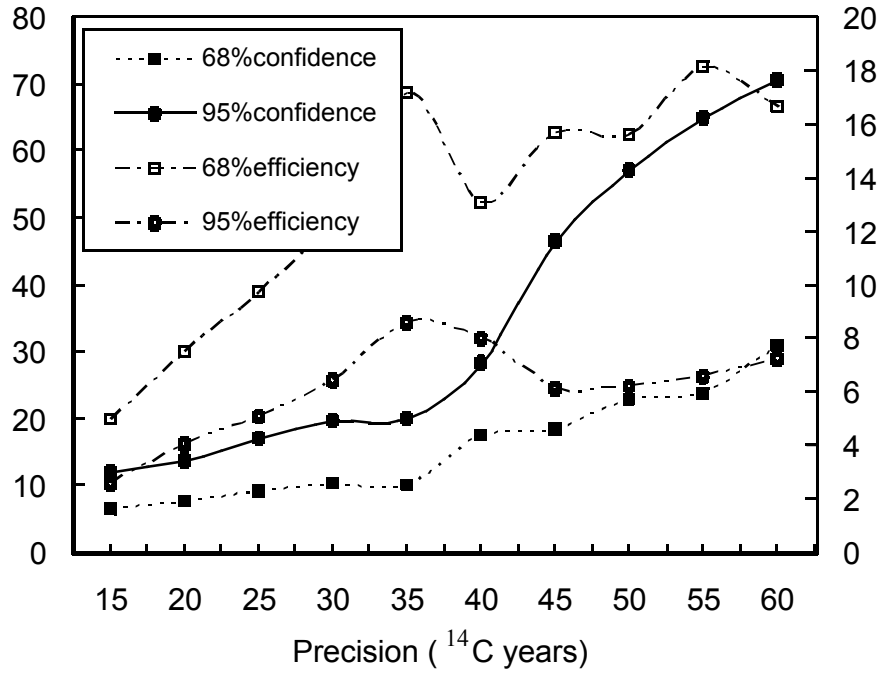

Figure 2 This figure shows the effect of changing the precision of measurements for a particular wiggle-match simulation; the starting date for this simulation was AD 1370; the sample intervals were set to 10 yr; and the number of measurements was fixed at 7. The efficiency is defined as being $p^2/(r\ n)$, where r is the range, n is the number of measurements, and p is the precision of the measurements. Using the efficiency measure or by looking at the ranges, it can be seen that in this case, even a precision of ±35 ^{14}C yr gives high resolution for this particular range.

Dating Methodology

The samples dated here were of wood and charcoal. The methods of sample pretreatment were the standard ones at Oxford for wood and charcoal (Hedges et al. 1989). In each case, we used acid/base/acid treatments. For wood, we followed this with a hypochlorite bleach to minimize the amount of lignin. We did not perform a solvent pre-clean on these samples—though, in retrospect, this might have helped to reduce the scatter in the blind test sample (see below).

All samples were graphitized following the method of Dee and Bronk Ramsey (2000) and the AMS dating followed the procedures described in Bronk Ramsey et al. (2004a).

Blind Test on Dendrochronologically-Dated Wood

This sample (oak) was provided by Dan Miles (Oxford Dendrochronology Laboratory) and had previously been dendrochronologically dated. The results are shown in Figure 3 with the fit to the calibration curve provided by the OxCal program (see Bronk Ramsey et al. 2001 for details of this method; the curve resolution is set to 1 and the INTCAL98 calibration curve used). The fit is good, though some of the later samples are slightly more scattered than one might expect (see comment above regarding pretreatment). Overall, the agreement between the samples and the curve passes a χ^2 test (minimum value 14.507 with 9 degrees of freedom with a threshold of 16.919 for 95% probability). The date for the mid-point of the last dated decade is fitted to 1065–1081 cal AD and, given

the overall tree-ring sequence from the sample, we can deduce from this that the date of the outer ring of the sample should be 1072–1088 cal AD.

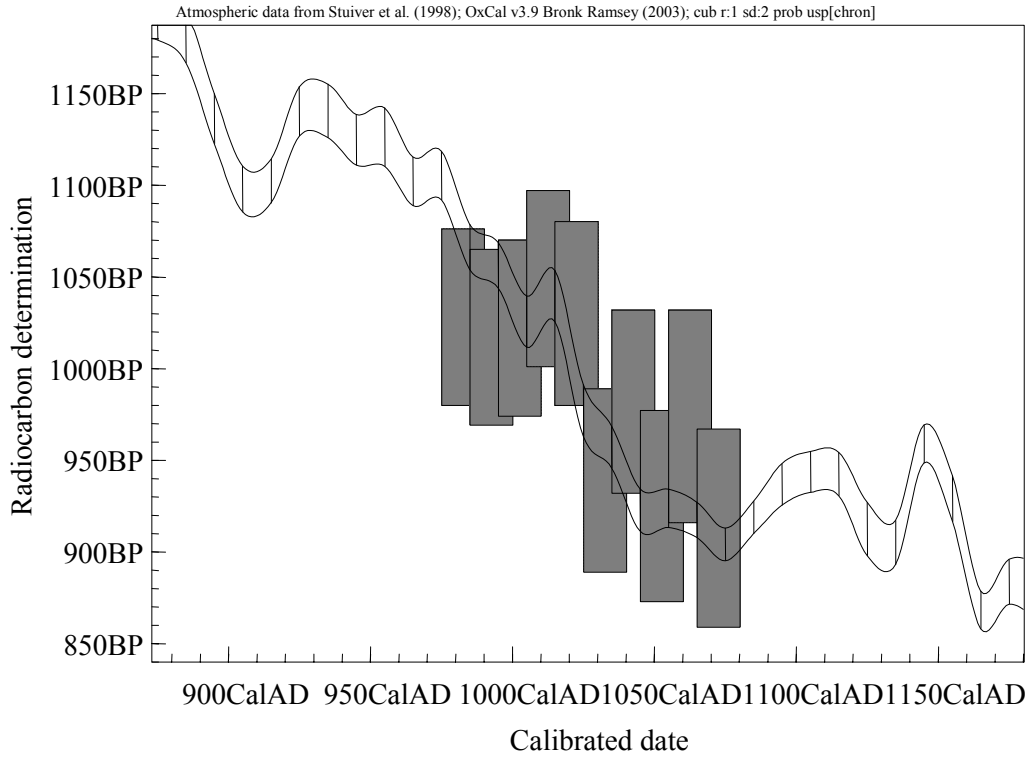

Figure 3 This figure shows the wiggle-match for the sample of dendrochronologically-dated wood which was used as a blind test of the method. The fit to the curve is good, though a little scattered at the right-hand side. The boxes show the 2-σ range of the ^{14}C measurement against the 95% confidence interval of the wiggle-matched sequence. In this case, the sample turned out to be from Salisbury Cathedral (see main text for a discussion of the result).

We subsequently obtained the dendrochronological date for the last ring of the sample, which is from Salisbury Cathedral in southern Britain: AD 1085 (Dan Miles, personal communication). This known dendrochronological age is within the 95% confidence range of the ^{14}C wiggle-match (1072–1088 cal AD).

Dating a Well in Late Roman Silchester

This sample (sill beam N18, oak), from pith through sapwood to a spring cutting date at the start of the 91st year of the sequence, belonged to Well 3011, found in Insula IX at the Late Roman site of Silchester (Clarke and Fulford 2002:143). It was supposed to be contemporaneous to the 3rd phase of the excavations and, thus, to belong to the 2nd–3rd centuries AD. The results of the wiggle-match are shown in Figure 4. The fit is very good for all but 1 sample and the overall agreement with the calibration curve passes a χ^2 test (minimum value 5.897 with 7 degrees of freedom with a threshold of 14.067 for 95% probability). The date for the mid-point of the last dated decade is fitted to 197–235 cal AD and, given the known number of additional rings from here to the terminal ring preserved on the sample, we can deduce from this that the date of the outer ring of the sample should be 202–240 cal AD.

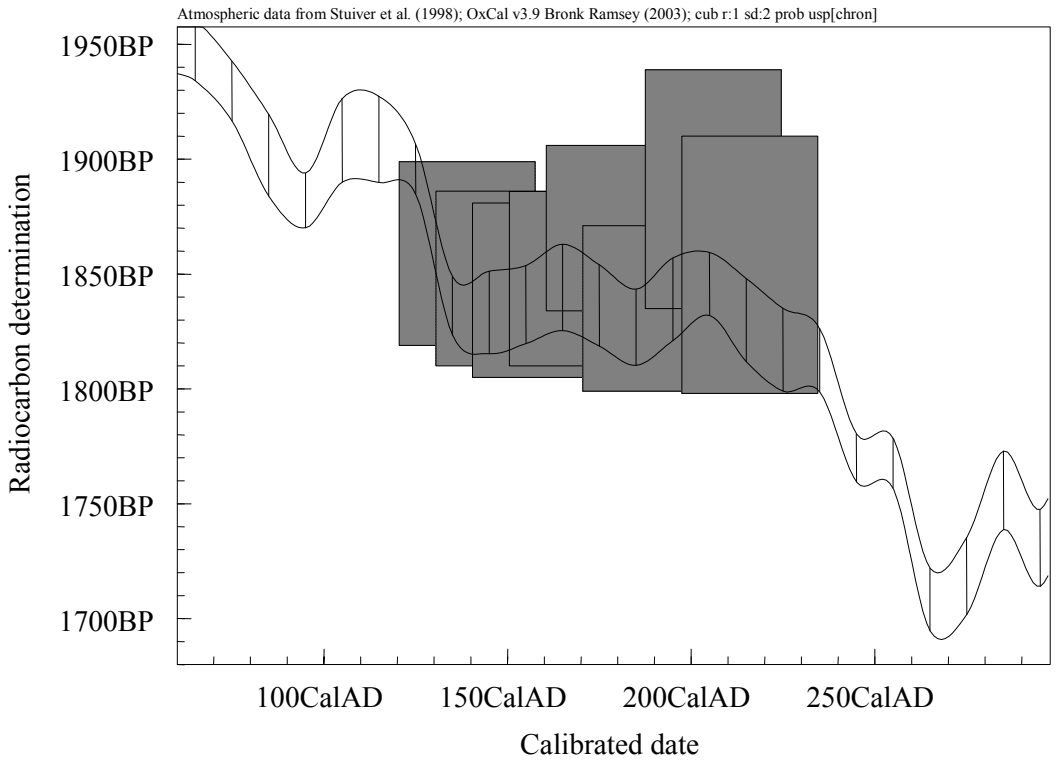

Figure 4 This figure shows the wiggle-match for the wood sample from Silchester. The fit to the curve is good with only the second point from the right being a marginal outlier. The boxes show the 2-σ range of the ^{14}C measurement against the 95% confidence interval of the wiggle-matched sequence.

Dating an Ornate Chair from Late Bronze Age Miletos

This sample (oak) is from an ornate chair found in a room of a sanctuary at Miletos (see also Bronk Ramsey et al. 2004b, these proceedings). Particles of Theran (Minoan) ash (identified by Max Bichler, personal communication) were sticking together with clay on the rim of a conical cup next to the chair. In the destruction deposit covering the burnt chair, there was a patch of ash containing particles of Theran tephra. Pottery, consistent with an LMIA date, was also found.

The dating of this sample offers a *terminus post quem* for the eruption of the volcano of Thera in the Aegean Sea and forms extra evidence to clarify the debate around the chronology of this event and the chronology of the LMIA cultural period in the Aegean. Current research considers the 2 most likely dates for this eruption to be either the mid- to later-17th century BC (Hammer et al. 2003; Manning et al. 1999, 2002; Manning and Bronk Ramsey 2003), or towards the end of the 16th century BC (Warren 1984, 1987, 1988, 1996; Bietak 2003). The results of the wiggle-match are shown in Figure 5. The fit is very good for all samples, and the overall agreement with the curve passes a χ^2 test (minimum value 2.896 with 6 degrees of freedom with a threshold of 12.592 for 95% probability). The date for the mid-point of the last dated decade is fitted to 1674–1651 cal BC; since there are 7 rings from the middle of this decade to the exterior of the sample, we can deduce from this that the date of the outer ring of the sample should be within the range 1667–1644 cal BC (see further in Bronk Ramsey et al. 2004b, these proceedings).

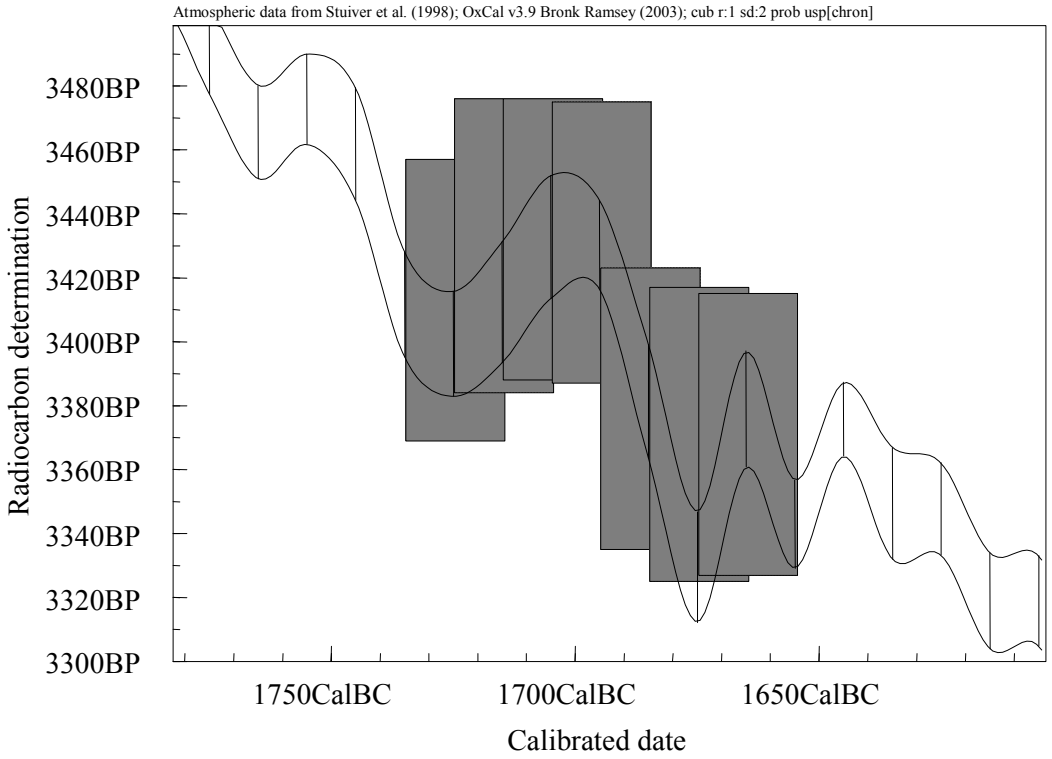

Figure 5 This figure shows the wiggle-match for the charcoal sample from Miletos. The fit to the curve is excellent. The boxes show the 2-σ range of the ^{14}C measurement against the 95% confidence interval of the wiggle-matched sequence.

CONCLUSIONS

We can see from the examples here, and from the simulations performed, that the wiggle-match dating of wood samples from archaeological contexts is a precise and accurate technique of dating, which could, in principle, be more widely applied. Overall 95% confidence ranges can be as short as a few decades. Such time-series wiggle-matching is really the only way to achieve high-precision calendar date estimates through ^{14}C dating. The critical caveat to justify the effort involved is that the dated sample must relate closely and specifically to the associated archaeology. Otherwise, one can have a well-dated piece of wood that serves no purpose.

The method is fairly labor-intensive since a number of ^{14}C determinations are needed for a single date. For this reason, the use of simulations to minimize the amount of work involved is important, and an "efficiency factor" can be used to help to find the optimum strategy.

In many cases, between 5 and 10 measurements at precisions of 25–30 ^{14}C yr are sufficient to achieve an overall 95% confidence range of less than 25 yr. This is many fewer measurements than would be needed to achieve the same precision by dating multiple samples from successive periods in a more general form of Bayesian wiggle-matching (sequence seriation matching, where the absolute time intervals between samples are not known). Thus, if the right material is available in suitable association, this technique should be the method of choice for high-precision dating of archaeological material.

ACKNOWLEDGEMENTS

We would like to thank Dan Miles for the wood from Salisbury and for advice on the dendrochronological aspects of the work. We thank Michael Fulford and Amanda Clark for the samples from Silchester, and Dan Miles again, who had carried out a prior dendrochronological study on them. We thank Wolf-Dietrich Niemeier for the sample from Miletos, and we thank Peter Ian Kuniholm and Maryanne Newton, who carried out the dendrochronological analysis of the sample. Thanks are also due to the staff of ORAU, and in particular to Christine Tompkins and Angela Bowles, who provided invaluable help in the pretreatment of the samples. This work was part of an MSc project and was supported by ORAU and NERC.

REFERENCES

Bietak M. 2003. Science versus archaeology: problems and consequences of High Aegean chronology. In: Bietak M, editor. *The Synchronisation of Civilisations in the Eastern Mediterranean in the Second Millennium BC II*. Proceedings of the SCIEM 2000–EuroConference, Haindorf, 2001, Vienna. p 23–33.

Bronk Ramsey C, Higham TFG, Leach P. 2004a. Towards high-precision AMS: progress and limitations. *Radiocarbon*, these proceedings.

Bronk Ramsey C, Manning SW, Galimberti M. 2004b. Dating the volcanic eruption at Thera. *Radiocarbon*, these proceedings.

Bronk Ramsey C, van der Plicht J, Weninger B. 2001. "Wiggle-matching" radiocarbon dates. *Radiocarbon* 43(2A):381–9.

Christen JA, Litton CD. 1995. A Bayesian approach to wiggle-matching. *Journal of Archaeological Science* 22:719–25.

Clarke RM, Morgan RA. 1983. An alternative statistical approach to the calibration of floating tree-ring chronologies: two sequences from the Somerset levels. *Archaeometry* 25:3–15.

Clarke RM, Renfrew C. 1972. A statistical approach to the calibration of floating tree-ring chronologies using radiocarbon dates. *Archaeometry* 14:5–19.

Clarke A, Fulford M. 2002. The excavation of Insula IX, Silchester: the first five years of the "Town Life" project, 1997–2001. *Britannia* 33:129–66.

Dee M, Bronk Ramsey C. 2000. Refinement of graphite target production at ORAU. *Nuclear Instruments and Methods in Physics Research B* 172:449–53.

Ferguson CW, Huber B, Suess HE. 1966. Determination of the age of Swiss lake dwellings as an example of dendrochronologically-calibrated radiocarbon dating. *Zeitschrift für Naturforschung* 21A:1173–7.

Friedrich M, Kromer B, Kaiser KF, Spurk M, Hughen KA, Johnsen SJ. 2001. High-resolution climate signals in the Bølling-Allerød Interstadial (Greenland Interstadial 1 as reflected in European tree-ring chronologies compared to marine varves and ice-core records). *Quaternary Science Reviews* 20:1223–32.

Guo Z, Liu K, Lu K, Ma H, Li K, Yuan S, Wu X. 2000. The use of radiocarbon dating AMS for Xia-Shang-Zhou chronology. *Nuclear Instruments and Methods in Physics Research B* 172:724–31.

Hajdas I, Bonani G, Seifert M. Forthcoming. Radiocarbon and calendar chronology of Ulandryk 4 and Pazyryk 2 tombs. In: *^{14}C and Archaeology: Proceedings of the 4th Symposium.* Oxford: Oxford University School of Archaeology Monographs.

Hammer CU, Kurat G, Hoppe P, Grum W, Clausen HB. 2003. Thera eruption date 1645 BC confirmed by new ice core data? In: Bietak M, editor. *The Synchronisation of Civilisations in the Eastern Mediterranean in the Second Millenium BC II*. Proceedings of the SCIEM 2000–Euroconference, Haindorf, 2001, Vienna. p 87–94.

Hedges REM, Law IA, Bronk CR, Housley RA. 1989. The Oxford accelerator mass spectrometry facility: technical developments in routine dating. *Archaeometry* 31:99–113.

Imamura M, Sakamotu M, Shiraishi T, Sahara M, Nakamura T, Mitsutani T, van der Plicht J. 1998. Radiocarbon age calibration for Japanese wood samples: wiggle-matching analysis for a test specimen. In: Evin J, Oberlin C, Daugas J-P, editors. 1999. *^{14}C and Archaeology, 3rd International Symposium*. Rennes: Université de Rennes. p 79–82.

Kilian MR, van Geel B, van der Plicht J. 2000. ^{14}C AMS wiggle-matching of raised bog deposits and models of peat accumulation. *Quaternary Science Reviews* 19: 1011–33.

Kromer B, Manning SW, Kuniholm PI, Newton MW, Spurk M, Levin I. 2001. Regional $^{14}CO_2$ offsets in the troposphere: magnitude, mechanism, and consequences. *Science* 294:2529–32.

Lowe JJ, Hoek WZ, INTIMATE group. 2001. Interregional correlation of palaeoclimatic records for the Last Glacial-Interglacial transition: a protocol for improved precision recommended by the INTIMATE project group. *Quaternary Science Reviews* 20:175–87.

Manning WS. 1999. *A Test of Time. The Volcano of Thera and the Chronology and History of the Aegean and East Mediterranean in the Mid-Second Millennium BC*. Oxford: Oxbow Books.

Manning SW, Bronk Ramsey C. 2003. A Late Minoan I-II absolute chronology for the Aegean—combining archaeology with radiocarbon. In: Bietak M, editor. *The Synchronisation of Civilisations in the Eastern Mediterranean in the Second Millennium BC II*. Proceedings of the SCIEM 2000–EuroConference, Haindorf, 2001, Vienna. p 111–33.

Manning WS, Bronk Ramsey C, Doumas C, Marketou T, Cadogan G, Pearson CL. 2002. New evidence for an early date for the Aegean Late Bronze Age and Thera eruption. *Antiquity* 76:733–44.

Manning WS, Kromer B, Kuniholm PI, Newton MW. 2001. Anatolian tree-rings and a new chronology for the East Mediterranean Bronze-Iron Ages. *Science* 294:2532–5.

Pearson GW. 1986. Precise calendrical dating of known growth-period samples using a 'curve fitting' technique. *Radiocarbon* 28(2A):292–9.

Slusarenko IY, Christen JA, Orlova LA, Kuzmin YV, Burr GS. 2001. ^{14}C wiggle-matching of the "floating" tree-ring chronology from the Altai Mountains, southern Siberia: the Ulandryk-4 case study. *Radiocarbon* 43(2A):425–31.

Slusarenko IY, Kuzmin YV, Christen JA Burr GS, Jull AJT, Orlova LA. Forthcoming. ^{14}C wiggle-matching of the Ulandryk 4 (Early Iron Age, Pazyryk Cultural Complex) floating tree-ring chronology, Altai Mountains, Siberia. *^{14}C and Archaeology: Proceedings of the 4th Symposium*. Oxford: Oxford University School of Archaeology Monographs.

van de Plassche O, Edwards RJ, van der Borg K, de Jong AFM. 2001. ^{14}C wiggle-match dating in high-resolution sea-level research. *Radiocarbon* 43(2A):391–402.

van der Plicht J, Jansma E, Kars H. 1995. The "Amsterdam Castle": a case study of wiggle matching and the proper calibration curve. *Radiocarbon* 37(3):965–8.

Vasiliev SS, Bokovenko NA, Chugunov KA, Dergachev VA, Sementsov AA, Sljusarenko JU, Zaitseva GI. 2001. Tree ring, "wiggle-matching" and statistics in the chronological studies of Scythian Age sites in Asia. *Geochronometria* 20:61–8.

Warren P. 1984. Absolute dating of the Bronze Age eruption of Thera (Santorini). *Nature* 308:492–3.

Warren P. 1987. Absolute dating of the Aegean Late Bronze Age. *Archaeometry* 29:205–11.

Warren PM. 1988. The Thera eruption: continuing discussion of the dating. III—Further arguments against an early date. *Archaeometry* 30(1):176–9.

Warren P. 1996. The Aegean and the limits of radiocarbon dating. *Acta Archaeologica* 67:283–90.

Wille M, Hooghiemstra H, van Geel B, Behling H, de Jong A, van der Borg K. 2003. Submillennium-scale migrations of the rainforest savanna boundary in Colombia: ^{14}C wiggle-matching and pollen analysis of core Las Margaritas. *Palaeogeography, Palaeoclimatology, Palaeoecology* 193:201–23.

RADIOCARBON, Vol 46, Nr 2, 2004, p 925–932

RADIOCARBON IN ANNUAL TREE RINGS FROM THAILAND DURING THE PRE-BOMB PERIOD, AD 1938–1954

Quan Hua[1,2] • Mike Barbetti[3] • Ugo Zoppi[1]

ABSTRACT. Annual tree rings from Thailand were analyzed by radiocarbon AMS for AD 1938–1954. The results showed no significant depletion in atmospheric ^{14}C over Thailand during the pre-bomb period, even though the air mass to Thailand during the growing season of tree rings is transported over a potentially significant source of oceanic ^{14}C-depleted CO_2, outgassing in the northern Indian Ocean. When compared with Washington and Chile for different periods from the 17th century to AD 1954, Thailand appears to have the characteristics of Southern Hemisphere ^{14}C. This supports our previous finding that Thailand was strongly influenced by the entrainment of Southern Hemisphere air parcels in the southwest Asian monsoon (Hua et al. 2004). For Thailand, this effect is much stronger than the reduction of atmospheric ^{14}C in association with CO_2 outgassing in the northern Indian Ocean.

INTRODUCTION

In previous work on radiocarbon in annual tree rings from Thailand for the period AD 1952–1975 (Hua et al. 2000), we found a large depletion of ^{14}C for Thailand. This occurred in 1953 and 1954—the period prior to the dominance of bomb ^{14}C in the atmosphere, which started in 1955. We thought that this depletion over Thailand could be partly due to upwelling in the Indian Ocean between 20°N and 5°S. This region is known for persistent upwelling, with excess partial pressure of CO_2 reaching 30 μatm (Keeling 1968; Takahashi et al. 1997) and a low $\Delta^{14}C$ level of surface water [~+100‰ for 1977–1978 compared with ~+140‰ at 30°S (Stuiver and Östlund 1983); –50‰ to –85‰ for 19th to early 20th centuries derived from carbonate samples growing in the surface ocean (Dutta et al. 2001; Southon et al. 2002)]. This upwelling activity might provide a regional source of ^{14}C-depleted CO_2, which mixes with atmospheric CO_2 and is transported over Thailand by the annual southwest monsoon. This phenomenon, a decrease of regional atmospheric ^{14}C in association with the upwelling activity of the oceans, is known for the North Pacific Ocean off the coast of Washington State (Damon et al. 1989).

In the present paper, we present a further investigation of this phenomenon for the period AD 1938–1951, using the same *Pinus kesiya* tree grown in northwestern Thailand (19°N, 99°E). These data are needed for a better evaluation of the above hypothesis—a possible regional reduction of atmospheric ^{14}C in association with upwelling in the northern Indian Ocean.

SAMPLE DESCRIPTION AND AMS ^{14}C ANALYSIS

The same section of *Pinus kesiya* (DIK 235/1) which was employed for examining atmospheric ^{14}C over Thailand for the bomb pulse period (Hua et al. 2000) was used for this study. The cross-section DIK 235/1 with clear annual ring structure and secure cross-dating from AD 1916–1994 is shown in Figure 1. The 1994 ring is incomplete because the tree fell in the middle of the growing season. The outer rings, from AD 1944 onwards, are entirely sapwood and typically 2 mm wide. The sample location was Doi Inthanon National Park in northwestern Thailand at 19°N, 99°E. The site is ~1000 m above mean sea level.

[1]Australian Nuclear Science and Technology Organisation (ANSTO), PMB 1, Menai NSW 2234, Australia.
[2]Corresponding author. Email: qhx@ansto.gov.au.
[3]NWG Macintosh Centre for Quaternary Dating, Madsen Building F09, University of Sydney, NSW 2006, Australia.

Proceedings of the 18th International Radiocarbon Conference, edited by N Beavan Athfield and R J Sparks
RADIOCARBON, Vol 46, Nr 2, 2004, p 925–932

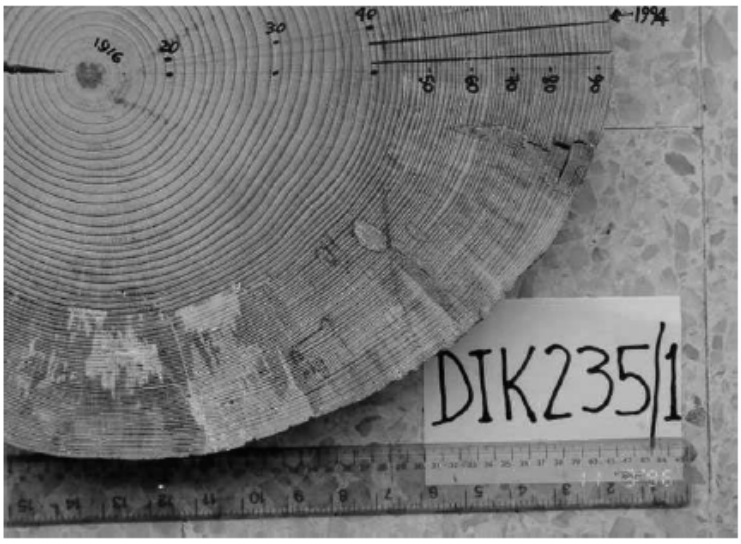

Figure 1 Cross-section of Thai *Pinus kesiya* DIK 235/1 with rings from AD 1916 to 1994, from which a sub-section was used for AMS ^{14}C analysis.

Pinus kesiya is one of very few tree species in the tropics with a clear annual ring structure. It has recently been used for dendroclimatic research due to strong cross-dating between trees from various sites in different regions in Thailand, including Doi Inthanon (Buckley et al. 1995; D'Arrigo et al. 1997). Moisture and temperature are 2 key parameters for the growth of *Pinus kesiya*. During the growing season (the rainy months from May to October), the air mass over the sampling site is from the Indian Ocean carried by the southwest Asian monsoon (Nieuwolt 1978).

Fourteen samples of single tree rings from 1938–1951 were prepared for AMS ^{14}C analysis following the protocols developed by Hua et al. (1999). The samples were pretreated to alpha-cellulose using the method described in Hua et al. (2000). The pretreated material was combusted to CO_2, then converted to graphite using methods described in Hua et al. (2001). AMS ^{14}C measurements were performed using the ANTARES facility at ANSTO (Lawson et al. 2000; Fink et al. 2004) with a precision of 0.25–0.3%. The $^{14}C/^{13}C$ ratio of each sample was measured relative to the NIST standard of oxalic acid I (HOxI; Stuiver 1983). The $\Delta^{14}C$ of each sample was calculated after correcting for (i) backgrounds (accelerator and chemistry), (ii) isotopic fractionation using measured $\delta^{13}C$, and (iii) radioactive decay of both sample and standard. In addition, 2 annual rings, 1953–1954, which had been analyzed previously (Hua et al. 2000), were re-sampled and measured for this study (see below).

AMS RESULTS AND DISCUSSION

The AMS ^{14}C results for Thailand for 1938–1951 expressed in $\Delta^{14}C$ are presented in Table 1 and illustrated in Figure 2. $\Delta^{14}C$ values for Arizona (32°N, 111°W; Damon et al. 1989) and Washington (48°N, 124°W; Stuiver et al. 1998) for the same period are also plotted in Figure 2 for comparison.

^{14}C offsets between Thailand and northern temperate regions for AD 1938–1951 are shown in Table 2. The difference between Washington and Thailand is –0.7 ± 0.9‰ (Thailand is higher). The offset between Arizona and Thailand is 2.4 ± 0.8‰ (Thailand is lower). Note that when compared with Washington (1981 data; Stuiver and Quay 1981), Arizona is ~2.5‰ higher for AD 1930–1954

Table 1 Measured $\Delta^{14}C$ from *Pinus kesiya* DIK-235/1 in Thailand (19°N, 99°E).

Ring formation (year AD)	Laboratory code	$\delta^{13}C$ (‰)	$\Delta^{14}C$ (‰)
1938	OZE647	–25.1	–18.9 ± 2.9
1939	OZE648	–25.4	–20.6 ± 2.7
1940	OZE649	–24.5	–22.7 ± 2.8
1941	OZE650	–24.8	–17.2 ± 2.7
1942	OZE651	–26.3	–16.3 ± 3.0
1943	OZE652	–26.1	–17.6 ± 2.8
1944	OZE653	–25.4	–21.1 ± 2.8
1945	OZE654	–25.7	–24.2 ± 2.9
1946	OZE655	–26.6	–17.1 ± 2.6
1947	OZE656	–27.0	–22.6 ± 2.9
1948	OZE657	–26.0	–24.4 ± 2.8
1949	OZE658	–26.0	–22.5 ± 2.7
1950	OZE659	–25.1	–27.1 ± 2.3
1951	OZE660	–25.5	–25.8 ± 2.4
1952	OZD107	–25.7	–24.9 ± 4.9[a]
1953	OZD108U2	–25.8	–23.5 ± 3.5[b]
1954	OZD109U2	–25.4	–26.8 ± 3.9[b]

[a]Datum reported in Hua et al. (2000).
[b]Data for 1953–1954 are now revised (this paper, cf. Hua et al. 2000).

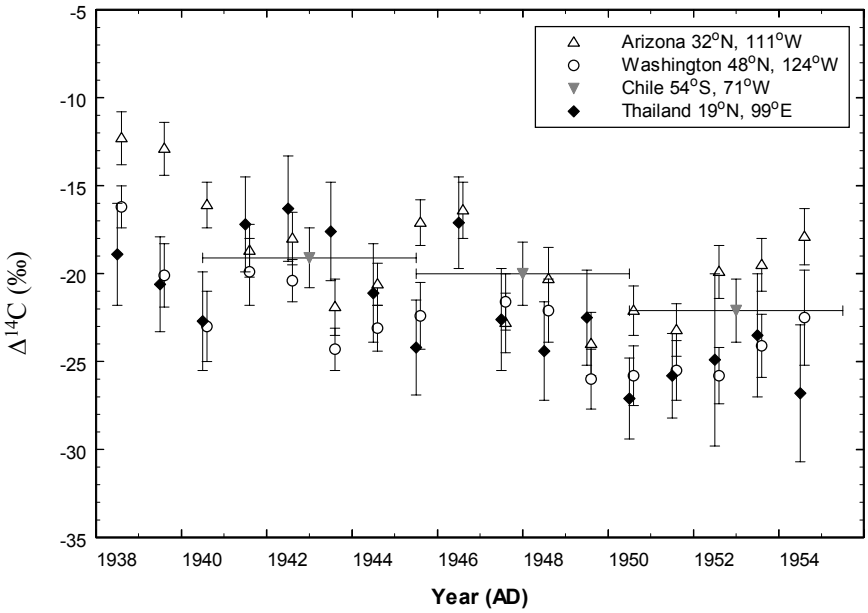

Figure 2 Measured $\Delta^{14}C$ values for Thailand for AD 1938–1954 (from this study and Hua et al. 2000) compared with data for Arizona (Damon et al. 1989), Washington (Stuiver et al. 1998), and Chile (5-ring samples; McCormac et al. 2002).

(Damon et al. 1989). This offset becomes 3.4 ± 0.5‰ when $\Delta^{14}C$ values for Arizona are compared to the revised Washington data (Stuiver et al. 1998). The depletion of Washington (relative to Arizona) for AD 1930–1954 was thought to be due to the oceanic upwelling of the North Pacific Ocean off the coast of Washington State (Damon et al. 1989). The results of this study show that on average, $\Delta^{14}C$ data for Thailand are not lower than those for Washington for AD 1938–1951 (see Table 2). This may imply a no-greater upwelling effect for the northern Indian Ocean (if it exists) compared to that for the North Pacific Ocean off the coast of Washington (see discussion below).

Table 2 ^{14}C offsets between northern temperate sites and Thailand (19°N, 99°E) for AD 1938–1951 (14 yr) and AD 1938–1954 (17 yr). We used Arizona data from Damon et al. (1989) and Washington data from Stuiver et al. (1998).

Sites	Offset relative to Thailand (‰)	Periods (AD)
Arizona	2.4 ± 0.8	1938–1951
(32°N, 111°W)	2.8 ± 0.8	1938–1954
Washington	–0.7 ± 0.9	1938–1951
(48°N, 124°W)	–0.6 ± 0.8	1938–1954

These AMS results for Thailand, which do not show further evidence of intermittent strong upwelling, led us to reexamine the 1953 and 1954 data points. Accordingly, these 2 rings were resampled from the same *Pinus kesiya* section (DIK 235/1), pretreated to alpha-cellulose, and measured by AMS ^{14}C. The $\Delta^{14}C$ values of the new measurements, which are also presented in Table 1, are –23.5 ± 3.5‰ and –26.8 ± 3.9‰ for 1953 and 1954, respectively. The new results (OZD108U2 and OZD109U2; Table 1) differ significantly from those of the first set (–48.5 ± 5.7‰ and –40.8 ± 5.5‰ for 1953 and 1954, respectively; Hua et al. 2000), and show no strong depletion. Given the absence of strong upwelling for the extended period 1938 to 1951 and a subsequent critical evaluation of the concept and likely extent of possible old CO_2 effects downwind of oceanic upwelling localities (Manning et al. 2002), the repeat measurements of the 1953 and 1954 *Pinus kesiya* rings are preferably accepted. Possible reasons for the divergence in the first set of measurements include accidental contamination in the pretreatment and target preparation, and the result of some instability in the measurement system and the accelerator. Before the strongly negative $\Delta^{14}C$ values were published, 2 additional graphite targets were prepared from the old pretreated materials of rings 1953 and 1954, and measured by AMS. Results similar to those of the first set of measurements were obtained. This suggests that the divergence in the first set of measurements was due to accidental contamination of the sample in pretreatment. The earlier measurement for AD 1952 (OZD107; Table 1) did not appear to be affected and was not repeated.

For the pre-bomb period AD 1938–1954, Thailand is 0.6 ± 0.8‰ higher than Washington and 2.8 ± 0.8‰ lower than Arizona (Table 2). Do these offsets imply an oceanic upwelling effect for Thailand similar to that for Washington? In order to answer this question, we have compared published ^{14}C data from Chile (54°S, 71°W; Stuiver and Braziunas 1998; McCormac et al. 2002) with those for Arizona, Washington, and Thailand. Figure 2 also shows $\Delta^{14}C$ values for annual tree rings from Thailand for 1952–1954 (with the new measurements for 1953 and 1954), together with those for Arizona and Washington for the same period. $\Delta^{14}C$ values for 5-ring samples from Chile for 1940–1954 are also included in Figure 2 for comparison. In order to compare ^{14}C data for Arizona, Washington, and Thailand with the 5-ring $\Delta^{14}C$ values for Chile for the overlapping period 1940–1954, we calculated $\Delta^{14}C$ values by averaging the relevant 5 annual data for these

northern temperate and tropical sites. These calculated 5-ring $\Delta^{14}C$ data and measured $\Delta^{14}C$ values for Chile are presented in Table 3. Although 5-ring $\Delta^{14}C$ values calculated from 5 annual measurements and measured $\Delta^{14}C$ values from 5-ring samples are not necessarily identical, the comparison of Arizona, Washington, and Thailand with Chile in Table 3 can give some qualitative indications of their offsets. ^{14}C offsets between northern temperate and tropical regions, and Chile for 1940–1954, are shown in Table 4.

Table 3 Comparison of 5-ring $\Delta^{14}C$, northern temperate and tropical sites versus Chile for AD 1940–1954.

Periods (AD)	Arizona[a] 32°N, 111°W	Washington[b] 48°N, 124°W	Thailand[c] 19°N, 99°E	Chile[d] 54°S, 71°W
1940–1944	–19.0 ± 0.6	–22.3 ± 0.6	–19.0 ± 1.3	–19.1 ± 1.7
1945–1949	–19.6 ± 0.7	–23.0 ± 0.9[e]	–22.0 ± 1.2	–20.0 ± 1.8
1950–1954	–20.6 ± 0.7	–25.1 ± 0.8	–25.9 ± 1.3	–22.1 ± 1.8

[a]Calculated from annual data of Damon et al. (1989).
[b]Calculated from annual data of Stuiver et al. (1998).
[c]Calculated from annual data of this study and Hua et al. (2000).
[d]Data reported for 5-ring samples (McCormac et al. 2002).
[e]Estimated from 4 annual data (1945 and 1947–1949) as no data available for 1946.

Table 4 ^{14}C offsets between northern temperate and tropical regions, and Chile (54°S, 71°W) for AD 1940–1954.

Sites	Offset relative to Chile (‰)
Arizona (32°N, 111°W)	0.6 ± 1.1
Washington (48°N, 124°W)	–3.1 ± 1.1
Thailand (19°N, 99°N)	–1.9 ± 1.3

Figure 3 shows temporal variations in atmospheric $\Delta^{14}C$ for Washington, Thailand, and Chile for the period AD 1600–1954. Washington data are from single-ring samples for 1600–1954 from Stuiver et al. (1998). Thai data are from decadal samples for 1620–1780 (Hua et al. 2004) and from annual samples for 1938–1954 (this study). Meanwhile, data for Chile are derived from 1- to 5-ring samples for 1670–1954 (McCormac et al. 2002). On average, up to AD 1915, the Washington-Chile offset in ^{14}C is positive due to a stronger air-sea exchange of CO_2 in the Southern Hemisphere causing more ^{14}C-depleted CO_2 from the ocean to enter the southern atmosphere compared to the northern (Lerman et al. 1970; Stuiver and Braziunas 1998; McCormac et al. 1998). This north-south offset, however, is significantly reduced and becomes negative after 1915 due to the influence of anthropogenic CO_2 free of ^{14}C entering the atmosphere predominantly in the Northern Hemisphere since the Industrial Revolution (the Suess effect; Suess 1955). The differences between Washington and Chile are 4.9 ± 0.2‰ and –1.8 ± 0.7‰ for AD 1670–1915 and 1916–1954, respectively (Table 5). For AD 1940–1954, a period in which Northern Hemispheric air is strongly influenced by anthropogenic CO_2, the Washington-Chile offset is strongly negative (–3.1 ± 1.1‰, Table 4). The Thailand-Chile offset for AD 1940–1954 is also negative (–1.9 ± 1.3‰; Table 4). This leaves a –1.2 ± 1.7‰ difference between Washington and Thailand with Thailand higher for 1940–1954. The Washington-Thailand offset follows the trend of the inter-hemispheric offset (Washington-Chile), as it is 2.4 ± 0.7‰ for 1620–1780 (Hua et al. 2004), then decreases and reverses to about –1.2 ± 1.7‰ for 1940–1954 (see Figure 3). These results indicate that Thailand follows the trend of the Southern Hemisphere. This supports our previous interpretation that during the latter part of the Little Ice Age

(LIA), the air mass in Thailand during the growing season of tree rings was strongly influenced by the entrainment of Southern Hemisphere air parcels during the southwest Asian monsoon, when the Inter-Tropical Convergence Zone moves to the north of our sampling site (Hua et al. 2004). This implies that for Thailand, the effect of regional oceanic upwelling in the northern Indian Ocean must be small compared to the influence of Southern Hemisphere air during the southwest monsoon.

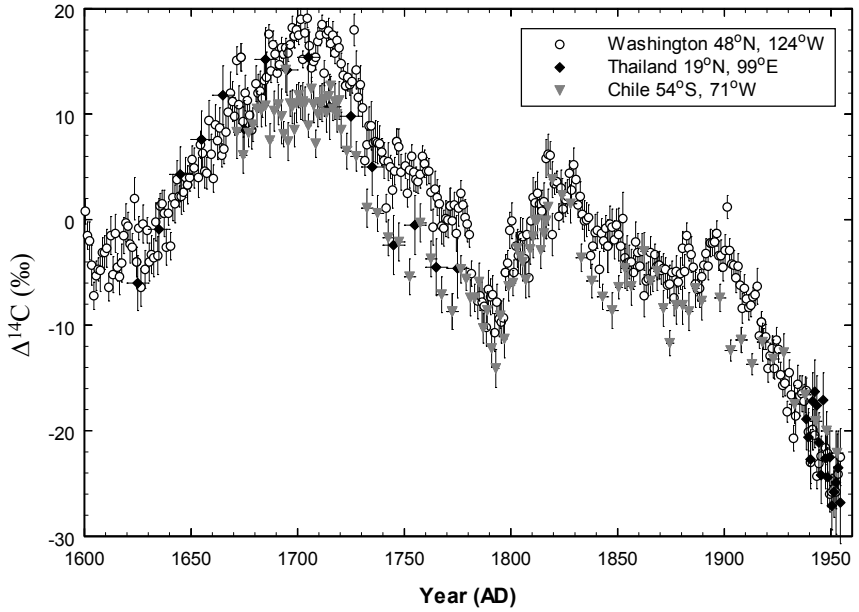

Figure 3 Temporal variations in atmospheric $\Delta^{14}C$ for Washington, Thailand, and Chile for AD 1600–1954. Data are from annual samples for Washington (Stuiver et al. 1998), 1- to 5-ring samples for Chile for 1670–1954 (McCormac et al. 2002), decadal samples for Thailand for 1620–1780 (Hua et al. 2004), and annual samples for 1938–1954 (this study), respectively.

Table 5 ^{14}C offsets between Washington (48°N, 124°W) and Chile (54°S, 71°W) for AD 1670 to 1954. Note: ^{14}C offset for each period of time was an error-weighted mean of the offsets between calculated *n*-ring $\Delta^{14}C$ values from Washington annual data (Stuiver et al. 1998) and measured n-ring $\Delta^{14}C$ values from Chile (McCormac et al. 2002). Note that *n* varies from 1 to 5.

Periods (AD)	Washington-Chile offset (‰)
1670–1915	4.9 ± 0.2
1916–1954	–1.8 ± 0.7

CONCLUSION

Seventeen annual tree rings from Thailand from AD 1938–1954 have now been analyzed by AMS. The results showed no significant depletion in ^{14}C over Thailand during the pre-bomb period, even though the air mass to Thailand during the growing season of tree rings is transported over a potentially significant source of oceanic ^{14}C-depleted CO_2, outgassing in the northern Indian Ocean.

Anthropogenic CO_2 free of ^{14}C has been introduced to the atmosphere due to the combustion of fossil fuel and land clearing, predominantly in the Northern Hemisphere, since the Industrial Revolution. As a result, the Washington-Chile offset was positive for 1670–1915, then decreased and became negative for 1916–1954. The Washington-Thailand offset follows that trend as the offset becomes smaller and reverses to a negative value (–1.2 ± 1.7‰) for 1940–1954 from a measured value of 2.4 ± 0.7‰ for AD 1620–1780. These results indicate that Thailand has the characteristic of Southern Hemisphere ^{14}C and, hence, support our interpretation that Thailand was strongly influenced by the entrainment of Southern Hemisphere air parcels in the southwest Asian monsoon during the latter part of the LIA (Hua et al. 2004) and the pre-bomb period, AD 1938–1954. These results also imply that the effect of the reduction of atmospheric ^{14}C over Thailand in association with upwelling in the northern Indian Ocean must be small compared to the influence of Southern Hemisphere air over Thailand during the southwest monsoon.

ACKNOWLEDGEMENTS

The authors wish to thank P J Krusic, B M Buckley, and R D D'Arrigo (Lamont-Doherty Earth Observatory), and M Watanasak, S Boonchirdchoo, and S Sarutanon (Mahidol University) for their efforts in dendrochronology of *Pinus kesiya*. Mrs A M Macintosh has provided generous financial support for the NWG Macintosh Centre since 1982. We also thank other members of the AMS project (ANSTO) for helping with sample preparation and ^{14}C measurements. We gratefully acknowledge funding from the Australian Institute of Nuclear Science and Engineering (AINSE) for AMS ^{14}C measurements (grant 00/004).

REFERENCES

Buckley BM, Barbetti M, Watanasak M, D'Arrigo R, Boonchirdchoo S, Sarutanon S. 1995. Dendrochronological investigations in Thailand. *IAWA Journal* 16(4):393–409.

Damon PE, Cheng S, Linick TW. 1989. Fine and hyperfine structure in the spectrum of secular variations of atmospheric ^{14}C. *Radiocarbon* 31(3):704–18.

D'Arrigo RD, Barbetti M, Watanasak M, Buckley BM, Krusic P, Boonchirdchoo S, Sarutanon S. 1997. Progress in dendroclimatic studies of mountain pine in northern Thailand. *IAWA Journal* 18(4):433–44.

Dutta K, Bhushan K, Somayajulu BLK. 2001. ΔR correction values for the northern Indian Ocean. *Radiocarbon* 43(2A):483–8.

Fink D, Hotchkis MAC, Hua Q, Jacobsen GE, Smith AM, Zoppi U, Child D, Mifsud C, van der Gaast HA, Williams AA, Williams M. Forthcoming. The ANTARES AMS Facility at ANSTO. *Nuclear Instruments and Methods in Physics Research B*.

Hua Q, Barbetti M, Worbes M, Head J, Levchenko VA. 1999. Review of radiocarbon data from atmospheric and tree ring samples for the period 1945–1997 AD. *IAWA Journal* 20(3):261–83.

Hua Q, Barbetti M, Jacobsen GE, Zoppi U, Lawson EM. 2000. Bomb radiocarbon in annual tree rings from Thailand and Tasmania. *Nuclear Instruments and Methods in Physics Research B* 172:359–65.

Hua Q, Jacobsen GE, Zoppi U, Lawson EM, Williams AA, Smith AM, McGann MJ. 2001. Progress in radiocarbon target preparation at the ANTARES AMS Centre. *Radiocarbon* 43(2A):275–82.

Hua Q, Barbetti M, Zoppi U, Fink D, Watanasak M, Jacobsen GE. Forthcoming. Radiocarbon in tropical tree rings during the Little Ice Age. *Nuclear Instruments and Methods in Physics Research B*.

Keeling CD. 1968. Carbon dioxide in surface ocean waters 4. Global distribution of pCO_2. *Journal of Geophysical Research* 73:4543–53.

Lawson EM, Elliott G, Fallon J, Fink D, Hotchkis MAC, Hua Q, Jacobsen GE, Lee P, Smith AM, Tuniz C, Zoppi U. 2000. AMS at ANTARES–the first 10 years. *Nuclear Instruments and Methods in Physics Research B* 172:95–9.

Lerman JC, Mook WG, Vogel JC. 1970. C14 in tree rings from different localities. In: Olsson IU, editor. *Radiocarbon Variations and Absolute Chronology*. Proceedings, XII Nobel Symposium. New York: Wiley. p 275–301.

Manning SW, Barbetti M, Kromer B, Kuniholm PI, Levin I, Newton MW, Reimer PJ. 2002. No systematic early bias to Mediterranean ^{14}C ages: radiocarbon measurements from tree-ring and air samples provide tight limits to age offsets. *Radiocarbon* 44(3):739–54.

McCormac FG, Hogg AG, Higham TFG, Lynch-Stieglitz J, Broecker WS, Baillie MGL, Palmer J, Xiong L, Pilcher JR, Brown D, Hoper ST. 1998. Temporal variation in the interhemispheric ^{14}C offset. *Geophysical Research Letters* 25(9):1321–4.

McCormac FG, Reimer PJ, Hogg AG, Highham TFG, Baillie MGL, Palmer J, Stuiver M. 2002. Calibration of radiocarbon timescale for the Southern Hemisphere: AD 1850–950. *Radiocarbon* 44(3):641–51.

Nieuwolt S. 1978. *Tropical Climatology—An Introduction to the Climates of the Low Latitudes*. Chichester: John Wiley & Sons.

Southon J, Kashgarian M, Fontugne M, Metivier B, Yim W. 2002. Marine reservoir corrections for the Indian Ocean and Southeast Asia. *Radiocarbon* 44(1):167–80.

Stuiver M. 1983. Business meeting: international agreements and the use of the new oxalic acid standard. *Radiocarbon* 25(2):793–5.

Stuiver M, Braziunas TF. 1998. Anthropogenic and solar components of hemispheric ^{14}C. *Geophysical Research Letters* 25(3):329–32.

Stuiver M, Östlund HG. 1983. GEOSECS Indian Ocean and Mediterranean radiocarbon. *Radiocarbon* 25(1): 1–29.

Stuiver M, Quay PD. 1981. Atmospheric ^{14}C changes resulting from fossil fuel CO_2 release and cosmic ray flux variability. *Earth and Planetary Science Letters* 53:349–62.

Stuiver M, Reimer PJ, Braziunas TF. 1998. Radiocarbon age calibration for terrestrial and marine samples. *Radiocarbon* 40(3):1127–51.

Suess HE. 1955. Radiocarbon concentration in modern wood. *Science* 122:415–7.

Takahashi T, Feely RA, Weiss RF, Wanninkhof RH, Chipman DW, Sutherland SC, Takahashi TT. 1997. Global air-sea flux of CO_2: an estimate based on measurements of sea-air CO_2 difference. *Proceedings of the National Academy of Sciences USA* 94:8292–9.

RADIOCARBON, Vol 46, Nr 2, 2004, p 933–941

TREE-RING RECORDS OF NEAR-YOUNGER DRYAS TIME IN CENTRAL NORTH AMERICA—PRELIMINARY RESULTS FROM THE LINCOLN QUARRY SITE, CENTRAL ILLINOIS, USA

Irina P Panyushkina[1,2] • Steven W Leavitt[1] • Alex Wiedenhoeft[3] • Sarah Noggle[1] • Brandon Curry[4] • Eric Grimm[5]

ABSTRACT. The abrupt millennial-scale changes associated with the Younger Dryas (YD) event ("chronozone") near the dawn of the Holocene are at least hemispheric, if not global, in extent. Evidence for the YD cold excursion is abundant in Europe but fairly meager in central North America. We are engaged in an investigation of high-resolution environmental changes in mid-North America over several millennia (about 10,000 to 14,000 BP) during the Late Glacial–Early Holocene transition, including the YD interval. Several sites containing logs or stumps have been identified and we are in the process of initial sampling or re-sampling them for this project. Here, we report on a site in central Illinois containing a deposit of logs initially thought to be of YD age preserved in alluvial sands. The assemblage of wood represents hardwood (angiosperm) trees, and the ring-width characteristics are favorable to developing formal tree-ring chronologies. However, 4 new radiocarbon dates indicate deposition of wood may have taken place over at least 8000 ^{14}C yr (6000–14,000 BP). This complicates the effort to develop a single floating chronology of several hundred years at this site, but it may provide wood from a restricted region over a long period of time from which to develop a sequence of floating chronologies, the timing of deposition and preservation of which could be related to paleoclimatic events and conditions.

INTRODUCTION

The warming from Late Glacial to Early Holocene was interrupted by an abrupt cold excursion known as the Younger Dryas (YD) event ("chronozone") at about 12,900 to 11,600 cal BP (Mayewski et al. 1993). There is abundant evidence of this event in Europe, but there is less evidence and clarity of its effects in North America, even though events in central North America (melting of the continental ice sheet) may well have been responsible for triggering the YD by slowing thermohaline circulation (Broecker et al. 1989). The Younger Dryas has left a variety of inter-related physical, geochemical, and biological evidence around the world (e.g. Kudrass et al. 1991; Roberts et al. 1993; Denton and Hendy 1994; Goslar et al. 1995; Björck et al. 1996; Benson et al. 1997; Mikolajewicz et al. 1997) from which its characteristics are being pieced together, perhaps with lessons for future world climate change.

We are interested in the YD conditions as expressed in tree-ring growth and characteristics in the Upper Midwest area of North America, focusing on sites where preserved wood samples exist (Figure 1), dispersed over a 4000-radiocarbon yr period (about 10,000 to 14,000 BP) that includes the 1300-yr YD event. One central goal of this project is to develop annual-resolution tree-ring width chronologies from available samples and estimate their variance associated with sample size and sample length. Once chronologies are established with confidence, high-resolution ^{14}C and stable-isotope chronologies will also be developed to infer additional climate/global change/carbon cycle information.

[1]Laboratory of Tree-Ring Research, University of Arizona, Tucson, Arizona 85721, USA.
[2]Corresponding author. Email: panush@ltrr.arizona.edu.
[3]Center for Wood Anatomy Research, USDA Forest Products Laboratory, One Gifford Pinchot Drive, Madison, Wisconsin 53726-2398, USA.
[4]Illinois State Geological Survey, 615 East Peabody Drive, Champaign, Illinois 61820, USA.
[5]Illinois State Museum, Research and Collections Center, 1101 East Ash St., Springfield, Illinois 62703, USA.

Proceedings of the 18th International Radiocarbon Conference, edited by N Beavan Athfield and R J Sparks
RADIOCARBON, Vol 46, Nr 2, 2004, p 933–941

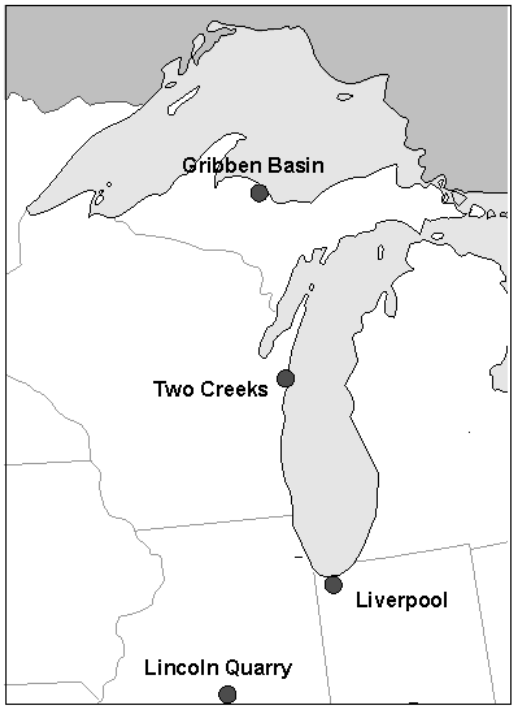

Figure 1 Map of sites from which samples have been recently obtained in this project

We have sampled or obtained samples from 4 sites thus far (Figure 1): Gribben Basin (Upper Peninsula Michigan), the classic Two Creeks site (east-central Wisconsin), Liverpool (northwest Indiana), and Lincoln Quarry (central Illinois). The first 3 of these sites are characterized by spruce (conifer) arboreal flora, all including trees in original growth position. This paper, however, focuses on the Lincoln Quarry site, where a deposit of logs preserved in alluvial sands was discovered at a limestone quarry in central Illinois in the 1980s, for which 2 ^{14}C dates indicating a possible late YD age already existed (10,439 ± 70 BP [ISGS-4397] and 10,160 ± 80 BP [ISGS-4400], unpublished). Our efforts with additional dating, wood identification, and ring-width characteristics have advanced understanding of the wood deposit and its potential for paleoclimate reconstruction.

METHODS

The Lincoln Quarry site is a few km west of the town of Lincoln, Illinois (40°08.272′N, 89°26.858′W), in the Holocene floodplain of Salt Creek. The valley lies in the Illinois Till Plain. End moraines from the last glaciation, also drained by Salt Creek, occur about 20 km to the east. One of us (SWL) visited the quarry on August 10, 2001, and obtained access to available wood. The wood is preserved in gravel-bearing sandy alluvium typically 5 to 10 m thick, sandwiched by 1- to 5-m-thick silty overbank deposits above and mid-Wisconsin deposits below, including the wood-bearing Robein Member of the Roxana Silt that dates at about 26,000 BP. The Quaternary deposits occur above Pennsylvanian limestone.

Specifically, the samples had been excavated out of Yard 10, the area most recently quarried. The original ISGS dates were from wood sampled several years earlier, when the active operation was in a different quarry yard. The wood from Yard 10 was piled on the eastern edge of the excavation, so we do not know the specific location or depth proveniences of the pieces. A few logs were emerging

from the walls of the pit 3–4 m below the surface, but because of safety concerns, we were not able to sample them. We sampled about 30 logs or log fragments in this deposit.

The samples were largely waterlogged, so to reduce cracking, we allowed them to dry out slowly over several months while wrapped in several layers of newspaper. Disks and slices were cut from the dry wood and surfaced to 400 grit. Tree-ring width series were measured with a Henson measurement system (0.01-mm precision) for each cross-section, the total number of rings of which exceeded 45 yr. The tree-ring series were examined for crossdating using the COFECHA program (Holmes 1983) and overlapping plots (TSAP program by RINNTECHenn Co., www.rinntech.com). The main statistics of tree-ring series were calculated with the ARSTAN® program (Cook 1985). Subsamples were taken for wood species identification and for ^{14}C dates.

For ^{14}C dating, 10-yr wood samples were obtained from the inner 50 rings of 4 specimens, ground, and processed to holocellulose. The cellulose samples were combusted to CO_2 with CuO in sealed quartz tubes and then converted to graphite and analyzed on the tandem accelerator mass spectrometer at the University of Arizona NSF Accelerator Facility.

RESULTS AND DISCUSSION

Age

Although the 2 ^{14}C dates (ISGS) obtained before our study were indicative of a late Younger Dryas age, the 4 dates we obtained from Yard 20 showed a wide age range from 6320 to 14,120 BP (Table 1). One of the dates at 9520 BP is most similar to the previous 2 dates, falling about 700 cal yr after the Younger Dryas.

This range of ages is consistent with an alluvial origin and with episodic deposition of the sand, gravel, and wood. Additional studies are necessary to characterize the sediment associated with the logs to determine the periodicity of the flooding, and distance to adjoining paleo-riparian environments, the presumed source of the logs. Our study was hampered by the unstable quarry walls that did not allow close examination of the sediment. If more was known about the stratigraphic distribution and distance from the stream of individual wood samples, it may be possible to make inferences about the size of these floods, which together with the dates might reveal new details about paleoclimate.

Wood Species

The condition of collected timber varied, but preservation was good overall. A few samples were exceptionally well preserved, and contained pith and even fragments of bark. One ash log (LQ-1) showed flattening to an elliptical cross-section, presumably resulting from the weight of overlying sediment. The 14,000 BP date of the sample is consistent with the time when the continental ice sheet would have just retreated northward near the Illinois-Wisconsin border (Hansel and Johnson 1992). No other samples are flattened.

Unlike many of the slightly older wood deposits occurring in the Upper Midwest which contain mostly conifers, primarily spruce, such as the Two Creeks site (Broecker and Farrand 1963; Leavitt and Kalin 1992), the wood from Lincoln Quarry was all from hardwoods, including *Quercus*, *Fraxinus*, *Morus*, *Carya,* and *Ulmus* (Table 1).

Table 1 Wood identification and tree-ring characteristics of Lincoln Quarry samples.

Sample ID	Nr of rings	Species[a]	^{14}C age	Lab nr	Cal BP (1 σ)
LQ-1	104	*Fraxinus*	14,120 ± 120	AA-49148	16,400–17,500
LQ-2	76	*Fraxinus*	9520 ± 120	AA-49149	10,550–11,200
LQ-3	68	*Morus**			
LQ-4		*Carya**			
LQ-5	103	*Quercus*, red or white			
LQ-6	62	*Juglans cinerea*			
LQ-7		*Acer*, soft			
LQ-8		*Quercus*, white group			
LQ-9		*Prunus**			
LQ-10		*Morus**			
LQ-11	54	*Ulmus**			
LQ-12		*Ulmus* sp.			
LQ-13	73	*Quercus*, red or white			
LQ-14		*Morus**			
LQ-15		*Morus**			
LQ-16	52	*Morus**			
LQ-17	69	*Juglans cinerea*			
LQ-18	48	*Morus**			
LQ-19	60	*Ulmus**			
LQ-20	65	*Juglans cinerea*			
LQ-21	60	*Juglans cinerea*			
LQ-22	46	*Celtis**			
LQ-23	56	*Platanus*			
LQ-24	204	*Quercus*, white group			
LQ-25	156	*Quercus*, white group	6320 ± 100	AA-49150	7000–7450
LQ-26	67	*Morus**			
LQ-28		*Platanus**			
LQ-29	111	*Carya*	8926 ± 81	AA-49151	9860–10,200

[a] * = wood identification not certain. [Common name key: *Quercus*=oak; *Ulmus*=elm; *Fraxinus*=ash; *Carya*=hickory; *Prunus*=cherry; *Morus*=mulberry; *Celtis*=hackberry; *Platanus*=sycamore; *Juglans cinerea*=butternut; *Acer*, soft=silver maple, red maple, or boxelder]

The oldest of the dated samples at 14,120 ^{14}C yr BP is *Fraxinus* (ash). The Two Creeks wood dates to about 11,800 BP and is all spruce (Leavitt and Kalin 1992), but Two Creeks occurs much farther north than Lincoln Quarry. In Illinois, *Fraxinus nigra* was common in the late glacial forest (Jacobson et al. 1987; Curry et al. 1999; Williams et al. 2001). *Quercus* and *Carya* at 9000 to 6000 ^{14}C yr BP are consistent with the pollen evidence for the common occurrence of these trees in Illinois at this time (King 1981) which fit other regional macrofossil evidence for these species. Submerged trees in Lake Michigan, 25 km east-southeast offshore at Chicago (Chrzastowski et al. 1991), and buried trees at Kenosha in the southeastern corner of Wisconsin (Schneider et al. 1977) confirm that *Quercus* and *Carya* were firmly entrenched in the region several hundred km north of Lincoln Quarry by 6000 to 8000 BP.

Ring Widths

The logs and wood fragments in our collection had 35 to nearly 200 rings (approximate tree ages are given under the "Nr of rings" column in Table 1). About 80% of the specimens have fewer than 100 yr (distribution of ages in Figure 2), but generally, when trees have ages greater than 50 yr, the potential for crossdating to build tree-ring chronologies is enhanced.

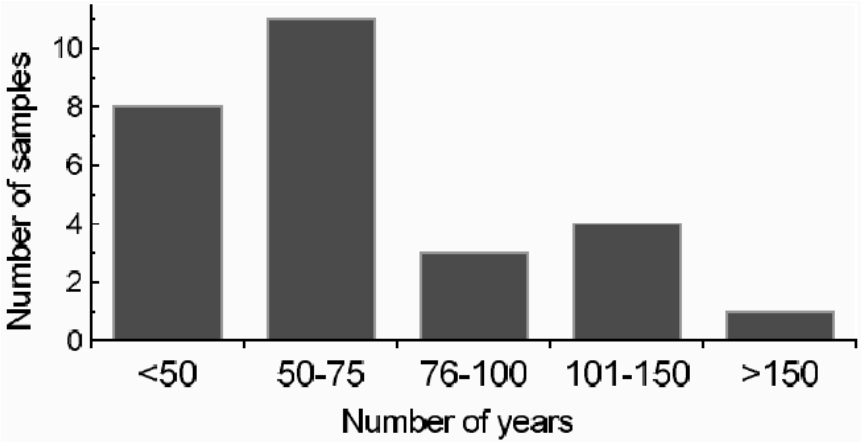

Figure 2 Age distribution of Lincoln Quarry specimens based on number of rings

The raw ring widths and best-fit growth curves of samples that contain pith show a variety of patterns (Figure 3). Some trees, such as LQ-2, 4, 29, and 25, exhibit growth patterns of growth suppression (small rings) early in life, perhaps from competition in a closed-canopy environment. Others, however, such as LQ-6, 1, 20, and 17, grew rapidly in their early years, indicating more open canopy conditions.

By removing age-growth curves from the raw ring widths, it will be eventually possible to develop ring-width indices for use in developing site chronologies. Based on the ^{14}C dating, however, it might be necessary to develop a tree-ring chronology for each of the time periods during which there was presumably an influx of wood. As of now, however, we have not been able to detect any outward physical characteristics that would allow us to group wood samples into the 4 time periods indicated by the ^{14}C dates, although species themselves may be diagnostic for time and may hint at provenience. In the worst case, the wood from the same time cluster could come from a large area, and more than 4 time clusters may exist. Floodplain deposits from Iowa (Chumbley et al. 1990; Baker et al. 1992) and Missouri (Guyette et al. 2003) have yielded wood and macrofossils from throughout the Holocene, and the same situation may exist for Salt Creek in Illinois. Fortunately, with some radiometric dating control (or perhaps species-related dating indicators), a strong response of tree growth to regional climate would help guarantee crossdating of samples even if their source area is large. If so, there is the potential for a single long chronology and certainly for a long series of chronologies over perhaps 8000 ^{14}C yr in central Illinois.

General statistics for tree-ring width measurements (Table 2) indicate that radial growth of trees is quite different. It might be caused by environmental and stand conditions as well as species identities and the young age of trees. *Fraxinus* trees possess the slowest rate of growth and low variance for both the 17,000 and 11,000 cal BP dates. Average tree-ring width is less than 1 mm. *Morus* trees have the highest rate of growth with average tree-ring width around 3 mm. Almost all trees have high autocorrelation (Table 2). This suggests dependency of growth of current year on growth conditions of previous year and, in some cases (*Quercus*, *Morus*, *Fraxinus*, and *Carya)*, 2 previous years.

Particularly promising is that within species groups (see Table 2), the specimens seem to be crossdatable. For example, within *Quercus*, *Juglans*, and *Ulmus* groups there are significant correlation coefficients between overlapped series (Table 2). Five crossdated series of *Quercus* comprise a 204-yr, high-variance chronology (standard deviation is 0.25). The *Juglans* tree group

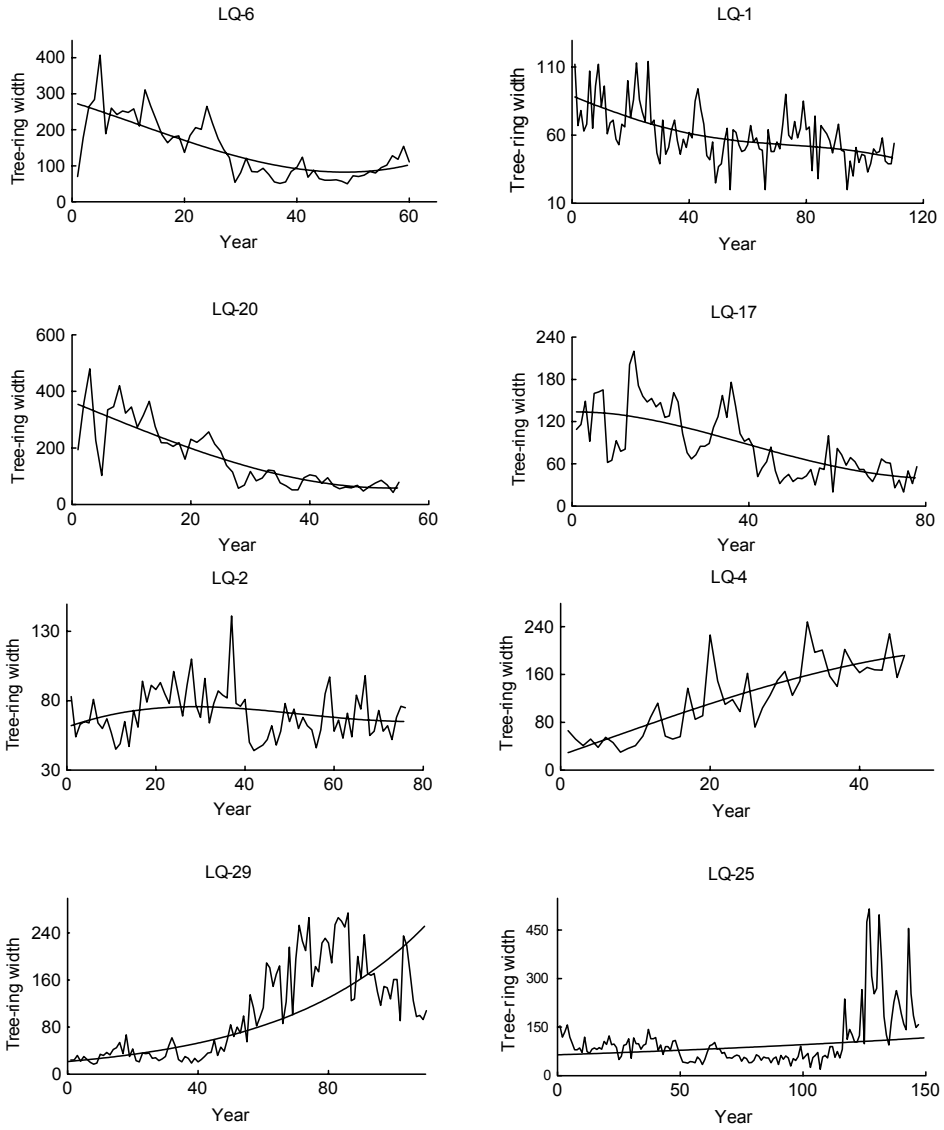

Figure 3 Examples of representative ring-width series (in mm) from Lincoln Quarry specimens

from 45 overlapped samples with length of 97 yr shows the best match (see correlations in Table 2). We also obtained a 60-yr sequence of *Ulmus* and a 75-yr sequences of *Morus*. The *Morus* series has low correlations because of tension wood and, therefore, needs to be verified with a larger sample set. We could not check the crossdating features of *Fraxinus* because two of the available series are from distinct time periods.

Even more interesting, crossdating exists *among* the *Ulmus*, *Juglans*, and *Carya* (LQ-29) series, suggesting they may be the same age. The 7 series of these species combined to make a 111-yr chronology (Figure 4). Because the Carya dates at 10,000 cal BP, the samples from the other 2 species may well be the same age, about 1600 cal yr after Younger Dryas proper.

Table 2 Statistics of measured tree-ring widths (all series >45 yr).

Sample ID	Nr of rings	Mean (mm)	Standard deviation	Autocorrelation Lag 1	Autocorrelation Lag 2	Highest correlation among crossdated series[a]
Fraxinus						
LQ-1	104	0.62	0.18	0.53	0.24	—
LQ-2	76	0.71	0.18	0.40	0.23	—
Morus						
LQ-3	68	1.35	0.45	0.61	0.31	0.22
LQ-16	52	3.10	0.94	0.47	0.20	0.22
LQ-18	48	2.84	0.69	0.45	–0.13	0.33
LQ-26	66	2.90	1.44	0.80	0.12	0.26
Quercus						
LQ-5	103	0.89	0.33	0.63	0.26	0.42
LQ-8	75	0.84	0.24	0.60	0.31	0.38
LQ-13	74	0.91	0.63	0.47	–0.27	0.32
LQ-24	204	1.13	0.35	0.51	0.14	0.35
LQ-25	156	1.02	0.34	0.67	0.13	0.39
Juglans						
LQ-6	62	1.42	0.82	0.79	0.09	0.53
LQ-17	69	0.97	0.39	0.53	0.24	0.45
LQ-20	65	1.34	0.76	0.77	0.07	0.55
LQ-21	60	0.54	0.23	0.60	0.13	0.36
Ulmus						
LQ-11	54	1.21	0.45	0.50	0.04	0.39
LQ-19	60	0.92	0.35	0.63	–0.01	0.39
Misc.						
LQ-22	46	2.10	0.75	0.81	0.15	—
LQ-23	56	1.70	1.08	0.71	0.29	—
LQ-29	111	1.04	0.78	0.86	0.31	—

[a]Coefficients for tree-ring series crossdated only within the species groups.

In conclusion, we suggest that the Lincoln Quarry has good potential for reconstructing environmental changes from the Late Glacial to mid-Holocene. Complications related to unknown provenience of wood might be resolved by dendrochronology and ^{14}C dating. The results of crossdating and the new ^{14}C dates may support a hypothesis of periodic flooding contributing sediments and wood to the Salt Creek floodplain. Further collection of available wood is needed.

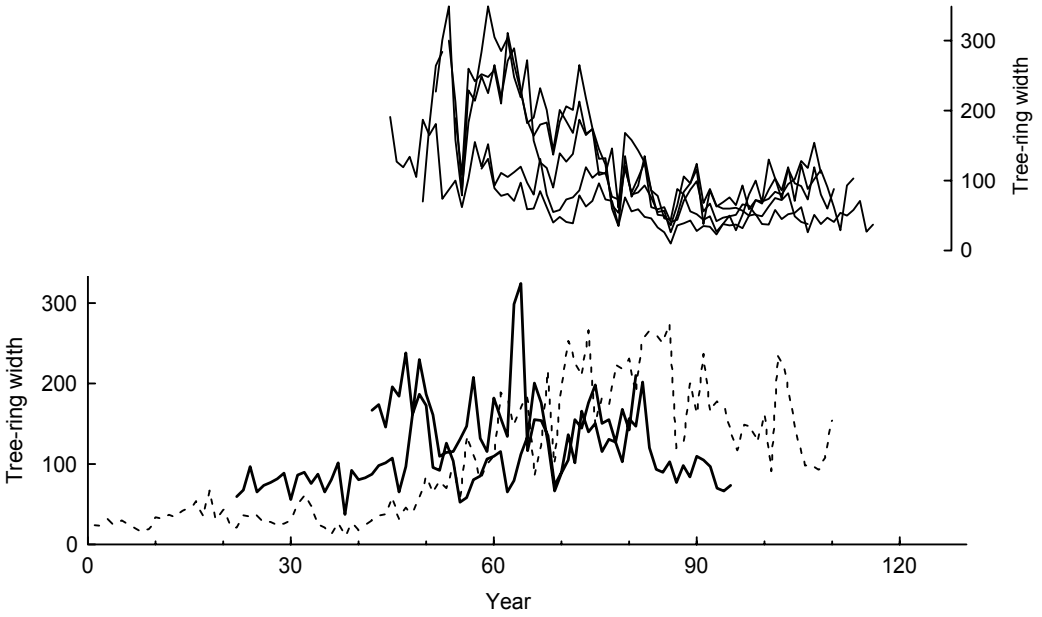

Figure 4 Example of crossdated tree-ring width (in mm) series for 3 species groups: upper 7 curves—*Juglans* (butternut), dashed line—*Carya* (hickory); lower 2 bold lines—*Ulmus* (elm).

ACKNOWLEDGEMENTS

We thank J Bastian and R Brown of Materials Service Corporation for access and assistance in sampling in Lincoln Quarry. F Pranschke and H Leavitt provided help with logistics of transport and shipping. The staff of the Arizona NSF Accelerator Facility provided ^{14}C dating. This research was supported by NSF Grants #ATM-9810474 and #ATM-0213696.

REFERENCES

Baker RG, Maher LJ Jr, Chumbley CA, Van Zant KL. 1992. Patterns of Holocene environmental change in the midwestern United States. *Quaternary Research* 37:379–89.

Benson L, Burdett J, Lund S, Kashgarian M, Mensing S. 1997. Nearly synchronous climate change in the Northern Hemisphere during the last glacial termination. *Nature* 388:263–5.

Björck S, Kromer B, Johnsen S, Bennike O, Hammarlund D, Lemdahl G, Possnert G, Rasmussen TL, Wohlfarth B, Hammer CU, Spurk M. 1996. Synchronized terrestrial-atmospheric deglacial records around the North Atlantic. *Science* 274:1155–60.

Broecker WS, Farrand WR. 1963. Radiocarbon age of the Two Creeks forest bed, Wisconsin. *Geological Society of America Bulletin* 74:795–802.

Broecker WS, Kennett JP, Flower BP, Teller JT, Trumbore S, Bonani G, Wolfli W. 1989. Routing of meltwater from the Laurentide ice sheet during the Younger Dryas cold period. *Nature* 341:318–21.

Chrzastowski MJ, Pranschke FA, Shabica CW. 1991. Discovery and preliminary investigations of the remains of an Early Holocene forest on the floor of southern Lake Michigan. *Journal of Great Lakes Research* 17(4):543–52.

Chumbley CA, Baker RG, Bettis AE III. 1990. Midwestern Holocene paleoenvironments revealed by floodplain deposits in northeastern Iowa. *Science* 249:272–4.

Cook ER. 1985. A time-series analysis approach to tree-ring standardization [PhD dissertation]. Tucson: University of Arizona.

Curry BB, Grimley DA, Stravers JA. 1999. Quaternary geology, geomorphology, and climatic history of Kane County, Illinois. *Illinois State Geological Survey Guidebook 28*. 40 p.

Denton GH, Hendy C. 1994. Younger Dryas age advance of Franz Josef Glacier in the Southern Alps of New Zealand. *Science* 264:1434–7.

Goslar T, Arnold M, Pazdur MF. 1995. The Younger Dryas cold event—Was it synchronous over the North Atlantic region? *Radiocarbon* 37(1):63–70.

Guyette RP, Stambaugh MC, Dey DC. 2003. Holocene oak tree-ring chronology development and analysis in the agricultural landscape of the midwestern United States. *XVI INQUA Congress Programs with Abstracts*. The Desert Research Institute, Reno, Nevada. p 129.

Hansel AK, Johnson WH. 1992. Fluctuations of the Lake Michigan Lobe during the late Wisconsin Subepisode. *Sveriges Geologiska Undersökning*, Series Ca 81. p 133–44.

King JE. 1981. Late Quaternary vegetational history of Illinois. *Ecological Monographs* 51:43–62.

Kudrass HR, Erlenkeuser H, Vollbrecht R, Weiss W. 1991. Global nature of the Younger Dryas cooling even inferred from oxygen isotope data from Sulu Sea cores. *Nature* 349:406–9.

Holmes RL. 1983. Computer-assisted quality control in tree-ring dating and measurement. *Tree-Ring Bulletin* 43:68–75.

Jacobson GL Jr, Webb T III, Grimm EC. 1987. Patterns and rates of vegetation change during the deglaciation of eastern North America. In: Ruddiman WF, Wright HE Jr, editors. *The Geology of North America. Volume K-3. North America During Deglaciation*. Geological Society of America, Boulder, Colorado. p 277–88.

Leavitt SW, Kalin RM. 1992. A new tree-ring width, $\delta^{13}C$ and ^{14}C investigation of the Two Creeks site. *Radiocarbon* 34(3):792–7.

Mayewski PA, Meeker LD, Whitlow S, Twickler MS, Morrison MS, Alley RB, Bloomfield P, Taylor K. 1993. The atmosphere during the Younger Dryas. *Science* 261:195–7.

Mikolajewicz U, Crowley TJ, Schiller A, Voss R. 1997. Modelling teleconnections between the North Atlantic and North Pacific during the Younger Dryas. *Nature* 387:384–7.

Roberts N, Taleb M, Barker P, Damnati B, Icole M, Williamson D. 1993. Timing of the Younger Dryas event in East Africa from lake-level changes. *Nature* 366: 146–8.

Schneider AF, Sander P, Larsen CE. 1977. Late Quaternary buried forest bed in southeastern Wisconsin. *Geological Society of America Abstracts with Programs* 11:256.

Williams JW, Shuman BN, Webb T III. 2001. Dissimilarity analyses of late-Quaternary vegetation and climate in eastern North America. *Ecology* 82:3346–62.

RADIOCARBON, Vol 46, Nr 2, 2004, p 943–948

THE COMPARISON OF ^{14}C WIGGLE-MATCHING RESULTS FOR THE 'FLOATING' TREE-RING CHRONOLOGY OF THE ULANDRYK-4 BURIAL GROUND (ALTAI MOUNTAINS, SIBERIA)

Yaroslav V Kuzmin[1] • Igor Y Slusarenko[2] • Irka Hajdas[3] • Georges Bonani[4] • J Andres Christen[5]

ABSTRACT. Two independent ^{14}C data sets of 10 tree-ring samples from the longest master chronology of the Pazyryk cultural complex were obtained and wiggle-matched to the absolute timescale. The results show very good agreement, within 10–15 calendar yr. The Ulandryk-4 burial ground (mound 1) was dated to about 320–310 cal BC, and this is consistent with wiggle-matching of the Pazyryk burial ground date series.

INTRODUCTION

Recent dendrochronological study of wood from the Iron Age Pazyryk cultural complex in the Altai Mountains, southern Siberia, allow constructing a 415-yr-long "floating" master chronology (Seifert and Slusarenko 1996, 2000). The high-precision ^{14}C dating and consequent wiggle-matching of the results obtained were performed to determine the calendar age of the floating master chronology in particular, and of the Pazyryk complex in general (Slusarenko et al. 2001; Dergachev et al. 2001; Slusarenko et al., forthcoming; Hajdas et al., forthcoming). The longest single tree-ring sequence from the Ulandryk-4 burial ground (which covers 363 yr) was the main object of research. Two independent ^{14}C data sets were obtained, and the results were wiggle-matched to the absolute timescale. In this paper, we present the comparison of the results of parallel ^{14}C dating and wiggle-matching of the same tree-ring sequence.

MATERIALS AND METHODS

The single Siberian larch (*Larix sibirica* Ledebour) dendro sample #19116 (363 tree rings) from burial mound 1, Ulandryk-4 burial ground at the Pazyryk Early Iron Age complex (Altai Mountains, southern Siberia, Russia; 49°42′N latitude, 89°08′E longitude; elevation about 2150 m asl), was used for key study (Figure 1). Mound 1 represents a stone burrow 13 m in diameter, under which a grave pit of 3.6 × 2.85 × 3.05 m was excavated. A rectangular burial chamber of larch logs was found at the bottom of the grave pit (Kubarev 1987). The chamber contains a human skeleton and it was filled with ice; the preservation of archaeological wood is very good.

Sample #19116 was subdivided into 10 annual tree-ring (decadal) sub-samples. Thirty-five consequent sub-samples (U1–U35; tree rings nr 1–350) were ^{14}C dated at the NSF-Arizona AMS facility (University of Arizona, Tucson, Arizona, USA; Lab code AA-). Eighteen sub-samples (Ul1–Ul18), started from tree-ring nr 13 and ended at nr 363, with 10 tree-ring gaps between each sub-sample, were ^{14}C dated at the ETH/AMS facility (Zürich, Switzerland; Lab code ETH-) (Table 1). Thus, 2

[1]Pacific Institute of Geography, Far Eastern Branch of the Russian Academy of Sciences, Radio St. 7, Vladivostok 690041, Russia. Corresponding author. Email: ykuzmin@tig.dvo.ru.
[2]Institute of Archaeology and Ethnography, Siberian Branch of the Russian Academy of Sciences, Lavrentiev Ave. 17, Novosibirsk 630090, Russia. Email: bronza@dus.nsc.ru.
[3]PSI c/o ^{14}C AMS lab, ETH-Hönggerberg, CH-8093, Zürich, Switzerland. Email: hajdas@phys.ethz.ch.
[4]Institute of Particle Physics, ETH-Hönggerberg, CH-8093, Zürich, Switzerland. Email: bonani@phys.ethz.ch.
[5]Instituto de Matematicas, Campus Morelia UNAM, AP 61-3 (Xangari) 58059 Morelia, Michoacan, Mexico. Email: jac@cimat.mx.

Proceedings of the 18th International Radiocarbon Conference, edited by N Beavan Athfield and R J Sparks
RADIOCARBON, Vol 46, Nr 2, 2004, p 943–948

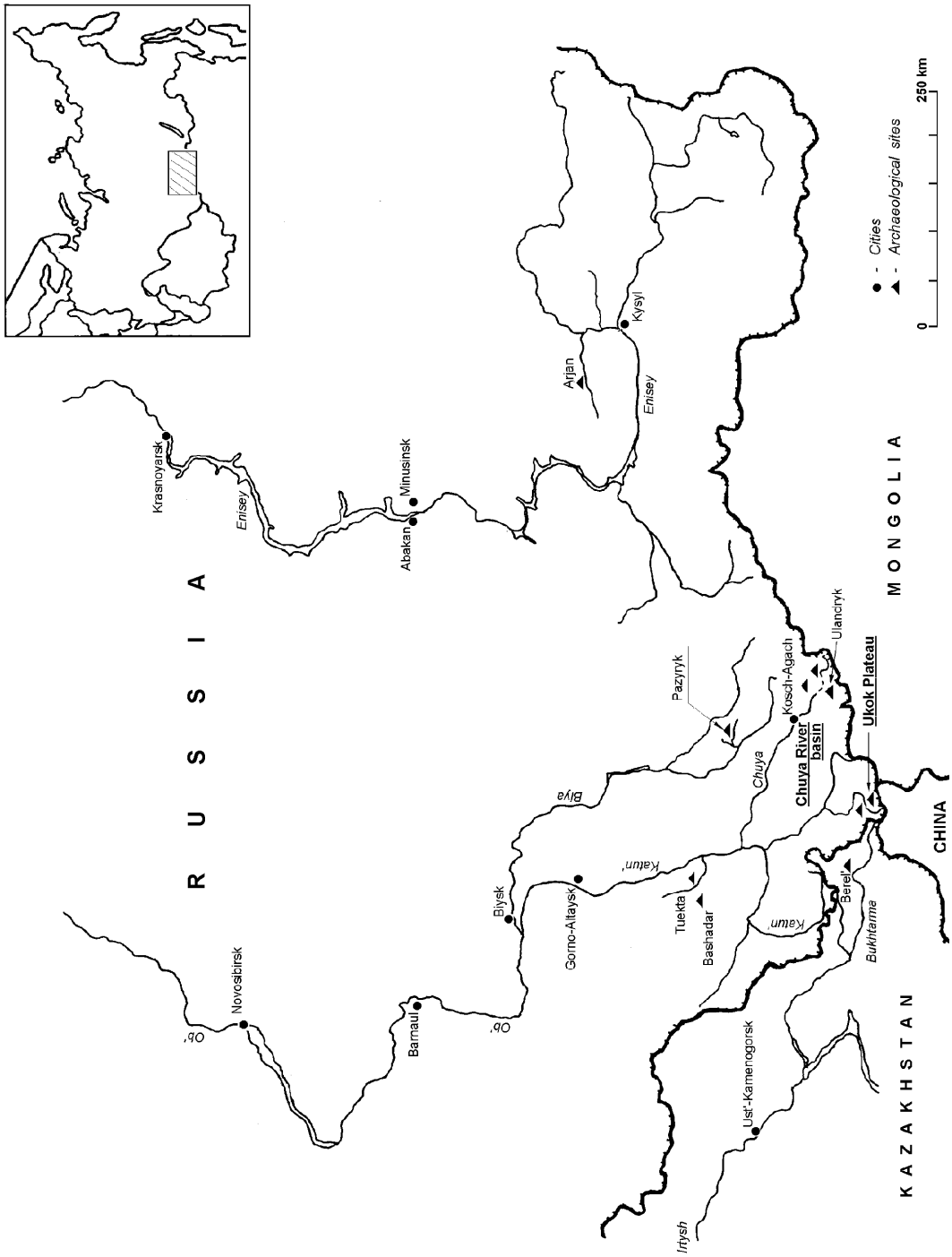

Figure 1 Location of the Ulandryk burial mound and other important Early Iron Age complexes in the Altai Mountains

Table 1 The results of AMS ^{14}C dating of decadal tree-ring samples from Ulandryk-4 (dendro-sample #19116).

Sub-sample (AA-)	^{14}C date	Sub-sample (ETH-)	^{14}C date
U-1 (rings #1–10), 37585	2540 ± 19		
U-2 (rings #11–20), 37586	2440 ± 22	Ul-18 (rings #13–23), 19861[a]	2345 ± 25
U-3 (rings #21–30), 37587	2470 ± 19		
U-4 (rings #31–40), 37588	2470 ± 22	Ul-17 (rings #33–43), 19860[a]	2410 ± 25
U-5 (rings #41–50), 37589	2500 ± 18		
U-6 (rings #51–60), 37590	2490 ± 18	Ul-16 (rings #53–63), 19859	2550 ± 50
U-7 (rings #61–70), 37591	2510 ± 22		
U-8 (rings #71–80), 37592	2525 ± 19	Ul-15 (rings #73–83), 19858	2530 ± 35
U-9 (rings #81–90), 37593	2505 ± 19		
U-10 (rings #91–100), 37594	2520 ± 20	Ul-14 (rings #93–103), 19857	2515 ± 35
U-11 (rings #101–110), 37595	2490 ± 20		
U-12 (rings #111–120), 37596	2480 ± 25	Ul-13 (rings #113–123), 19856	2455 ± 35
U-13 (rings #121–130), 37597	2480 ± 19		
U-14 (rings #131–140), 37598	2435 ± 39	Ul-12 (rings #133–143), 19855	2410 ± 45
U-15 (rings #141–150), 37599	2440 ± 22		
U-16 (rings #151–160), 37600	2470 ± 19	Ul-11 (rings #153–163), 19854	2450 ± 50
U-17 (rings #161–170), 37601	2470 ± 19		
U-18 (rings #171–180), 37602	2470 ± 19	Ul-10 (rings #173–183), 19853	2410 ± 50
U-19 (rings #181–190), 37641	2460 ± 36		
U-20 (rings #191–200), 37642	2410 ± 26	Ul-9 (rings #193–203), 19852	2490 ± 35
U-21 (rings #201–210), 37643	2460 ± 26		
U-22 (rings #211–220), 37644	2435 ± 26	Ul-8 (rings #213–223), 19851	2465 ± 40
U-23 (rings #221–230), 37645	2470 ± 26		
U-24 (rings #231–240), 37646	2395 ± 26	Ul-7 (rings #233–243), 19850	2450 ± 35
U-25 (rings #241–250), 37647	2435 ± 58		
U-26 (rings #251–260), 37648	2450 ± 41	Ul-6 (rings #253–263), 19849	2410 ± 35
U-27 (rings #261–270), 37649	2340 ± 41		
U-28 (rings #271–280), 37650	2270 ± 40	Ul-5 (rings #273–283), 19848	2330 ± 35
U-29 (rings #281–290), 37651	2260 ± 40		
U-30 (rings #291–300), 37652	2280 ± 46	Ul-4 (rings #293–303), 19847	2295 ± 35
U-31 (rings #301–310), 37653	2280 ± 36		
U-32 (rings #311–320), 37654	2205 ± 34	Ul-3 (rings #313–323), 19846	2230 ± 35
U-33 (rings #321–330), 37655	2230 ± 34		
U-34 (rings #331–340), 37656	2260 ± 38	Ul-2 (rings #333–343), 19845	2170 ± 25
U-35 (rings #341–350), 37657	2310 ± 43		
		Ul-1 (rings #353–363), 19844	2215 ± 25

[a]Outliers.

^{14}C decadal data sets were produced for this dendrochronology, which allow a rare chance to compare the results of the wiggle-matching for both data sets.

The Bayesian approach to calibration (Christen and Litton 1995) was used to wiggle-match the Tucson data set, with the help of *Bwigg* software (for more details, see the *Bwigg* web page, http://www.cimat.mx/Bwigg). The χ^2 method was applied to find the best fit to the INTCAL98 curve for the Zürich data set.

RESULTS AND DISCUSSION

The Bayesian approach allows to wiggle-match the Tucson decadal date series (Figure 2). The best match of the end of sequence, including additional 13 tree rings which were not ^{14}C dated, is 2261 cal BP (i.e. ~312 BC) (Slusarenko et al., forthcoming). The interval 2271–2253 cal BP accumulates 96% of the posterior probability for the match. The χ^2 wiggle-match placed the absolute age of the last preserved ring of the construction timber from $312^{+13}/_{-21}$ BC (Figure 3) (Hajdas et al., forthcoming). This is based on the fit which does not include the 2 apparent outliers (ETH-19860 and 19861, Table 1). Thus, both data sets coincide in their matches within some 10–15 yr.

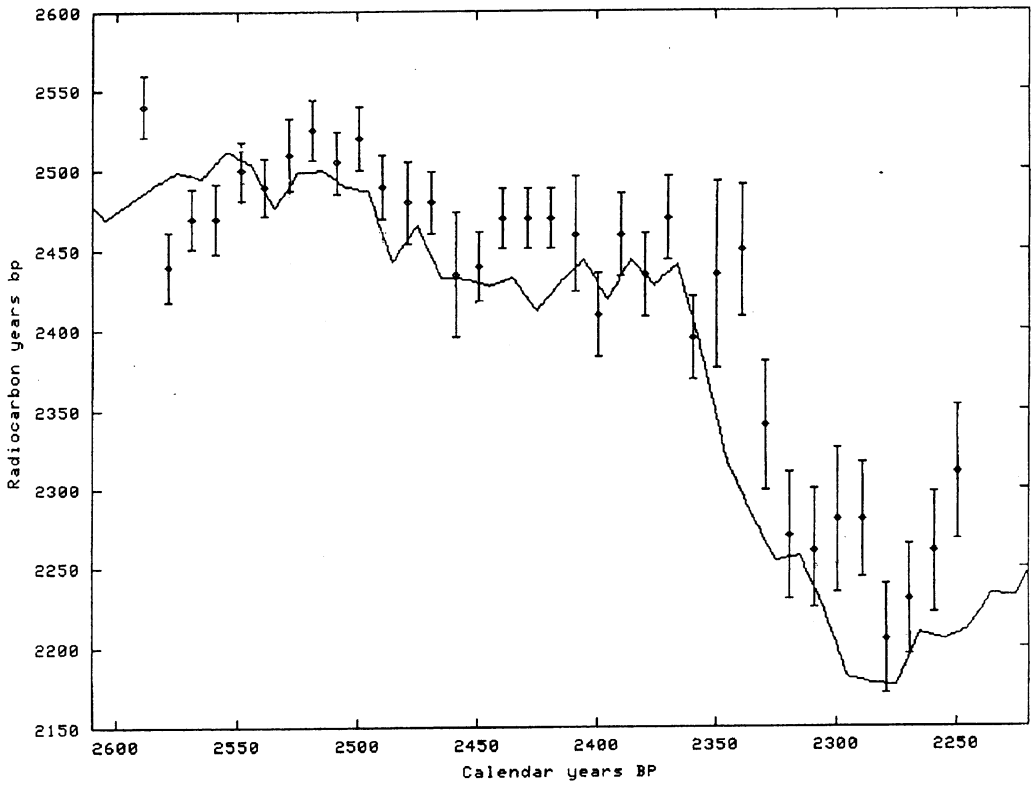

Figure 2 Tucson decadal data set for the Ulandryk-4 series as compared with the INTCAL98 calibration curve

Although it appears that the ^{14}C ages of the 2 earliest tree-ring sub-samples in the Zürich date series are too young when compared with the rest of dates, the repeat measurements on these samples confirm the younger ages, and these are, therefore, included in the calculated mean values (Table 1). We have no explanation for these unexpected ages in comparison with the Arizona date series (AA-37586 and 37588, Table 1); new analyses may be useful to explain them. However, these 2 points have no influence on the final dating result, except for the numeric χ^2 value and overall dating error. If the 2 outliers are included, the dating error is +37/–30 yr, and if rejected, +13/–21 yr (Hajdas et. al., forthcoming).

^{14}C dating for the other key dendroscale, derived from the Pazyryk burial ground, kurgan 2, was performed in 3 different laboratories (St. Petersburg, Zürich, and Belfast). The wiggle-matching of these date series show that the best match is at about 300–290 BC (Dergachev et al. 2001:423;

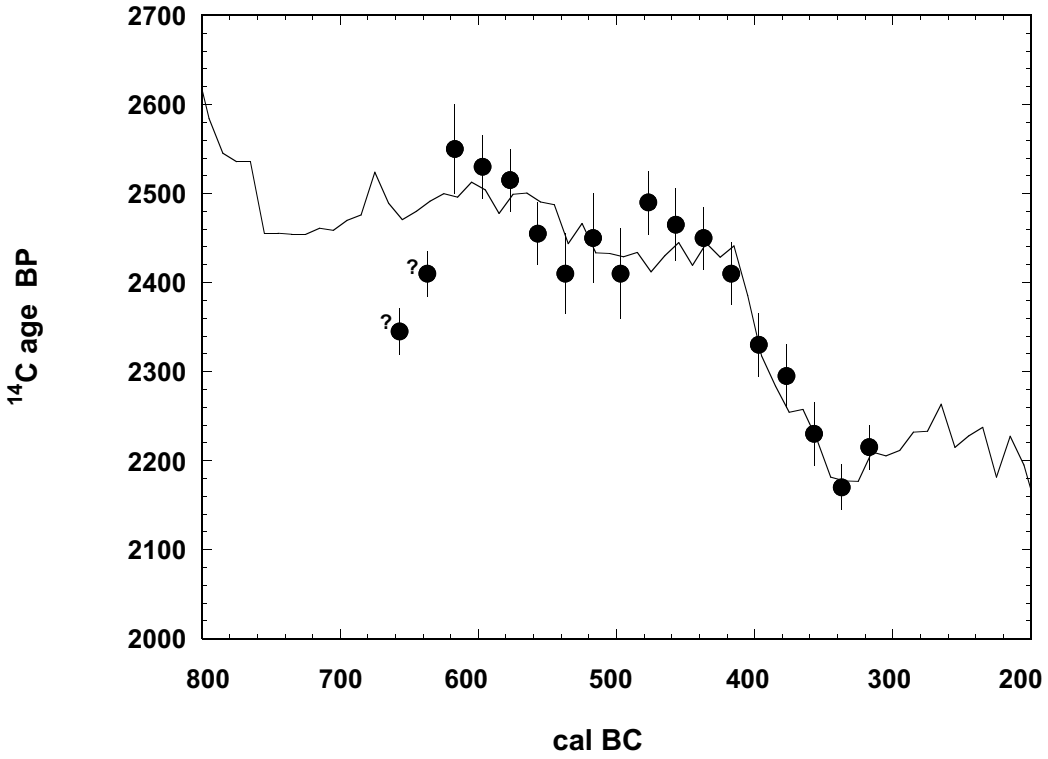

Figure 3 The Zürich decadal data set for the Ulandryk-4 series; the background is the INTCAL98 calibration curve (2 outliers are not included in the fit).

Vasiliev et al. 2001). This is based on a χ^2 fit of the ^{14}C ages previously published by Zaitseva et al. (1998). This result is very consistent with the best matches for the Ulandryk-4 decadal data series. Also, archaeologists who recently excavated the series of the Pazyryk culture burials in southern Altai Mountains, support the age determination of the Pazyryk sites as the end of the 4th to the first part of the 3rd centuries BC (Polos'mak 2001). Therefore, it seems reasonable to assume that the absolute age of the Pazyryk cultural complex in the Altai Mountains is now well established.

CONCLUSION

Two independent data sets, processed by 2 different techniques (Bayesian statistics and χ^2 method), allow us to document firmly the timing of the Pazyryk culture burials in the Altai Mountains, generally dated to the 4th–3rd centuries BC. More research is necessary to establish the calendar chronology of the ancient Bronze and Early Iron Age cultures in southern Siberia and Inner Asia with the help of precise ^{14}C dating and wiggle-matching of the date series. The Altai Mountains are the key region for dendrochronological and ^{14}C studies of archaeological wood.

ACKNOWLEDGEMENTS

We are grateful to colleagues who provided support for this study, Drs A J T Jull and G S Burr. This research was supported in part by grants from the Russian RFFI (00-06-80199) and US NSF (EAR 97-30699).

REFERENCES

Christen JA, Litton CD. 1995. A Bayesian approach to wiggle-matching. *Journal of Archaeological Science* 22:719–25.

Dergachev VA, Vasiliev SS, Sementsov AA, Zaitseva GI, Chugunov KA, Sljusarenko IJ. 2001. Dendrochronology and radiocarbon dating methods in archaeological studies of Scythian sites. *Radiocarbon* 43(2A):417–24.

Hajdas I, Bonani G, Seifert M. Forthcoming. Radiocarbon and calendar chronology of Ulandryk-4 and Pazyryk-2 tombs. In: *Proceedings of the 4th International Symposium "^{14}C and Archaeology" (Oxford, 2002)*. Oxford: Oxbow Books.

Kubarev VD. 1987. *Kurgany Ulandryka* [Kurgans of the Ulandryk]. Novosibirsk: Nauka Publishing. 299 p.

Polos'mak NV. 2001. *Vsadniki Ukoka* [The horse riders of the Ukok]. Novosibirsk: INFOLIO-Press. 334 p.

Seifert M, Sljusarenko IY. 1996. Dendrochronologische daten von graebern der Pazyrik-Kultur (5./4. Jh. v. Chr.) im Altai. *Dendrochronologia* 14:153–64.

Seifert M, Sljusarenko IY. 2000. Dendrokhronologichesky analyz pazyrykskikh pamyatnikov [Dendrochronological analysis of Pazyryk culture sites]. In: Derevianko AP, Molodin VI, editors. *Fenomen altaiskikh mumiy.* Novosibirsk: Izdatelstvo Instituta Arkheologii i Etnografii SO RAN. p 258–64.

Slusarenko IY, Christen JA, Orlova LA, Kuzmin YV. 2001. ^{14}C wiggle-matching of the 'floating' tree-ring chronology from the Altai Mountains, southern Siberia: the Ulandryk-4 case study. *Radiocarbon* 43(2A): 425–31.

Slusarenko IY, Kuzmin YV, Christen JA, Burr GS, Jull AJT, Orlova LA. Forthcoming. ^{14}C wiggle-matching of the Ulandryk-4 (Early Iron Age, Pazyryk cultural complex) floating tree-ring chronology, Altai Mountains, Siberia. In: *Proceedings of the 4th International Symposium "^{14}C and Archaeology" (Oxford, 2002)*. Oxford: Oxbow Books.

Vasiliev SS, Bokovenko NA, Chugunov KA, Dergachev VA, Sementsov AA, Slusarenko IY, Zaitseva GI. 2001. Tree-rings, 'wiggle matching' and statistics in the chronological studies of Scythian age sites in Asia. *Geochronometria* 20:61–7.

Zaitseva GI, Vasiliev SS, Marsadolov LS, van der Plicht J, Sementsov AA, Dergachev VA, Lebedeva LM. 1998. A tree-ring and C-14 chronology of the key Sayan-Altai monuments. *Radiocarbon* 40(1):571–80.

RADIOCARBON, Vol 46, Nr 2, 2004, p 949–955

^{14}C CONCENTRATIONS OF SINGLE-YEAR TREE RINGS FROM ABOUT 22,000 YEARS AGO OBTAINED USING A HIGHLY ACCURATE MEASURING METHOD

Toshiyuki Gandou[1] • Hirohisa Sakurai[1,2] • Wataru Katoh[1] • Yousuke Takahashi[1] • Syuichi Gunji[1] • Fuyuki Tokanai[1] • Hiroyuki Matsuzaki[3]

ABSTRACT. We have measured the radiocarbon concentrations in single-yr tree rings of old wood by accelerated mass spectrometry (AMS) using a multicathode. The ^{14}C concentrations of 10 single-yr tree rings were measured in 100 tree rings at intervals of 10. For each single-yr tree-ring sample, typically 80 measurements of the ^{14}C concentrations were carried out using multicathodes. The sample standard deviations indicated that there are other fluctuations of typically 1.5%, in addition to the fluctuation of the Poisson counting statistics which is typically 3% for each measurement. The average ^{14}C date of the tree rings was 22,130 ± 306 BP for all 624 data of single-yr tree-ring samples measured by the multicathodes. From the calibration data of Lake Suigetsu, the calendar dates of these 100 tree rings were located between 25,400 cal BP and 26,150 cal BP. The ^{14}C dates changed between 21,979 BP and 22,272 BP, with an error of approximately 50 BP, corresponding to a precision of approximately 0.5%. There was a step with a change of approximately 144 BP for each 10 yr in the time profile.

INTRODUCTION

Approximately 20,000 yr ago, radiocarbon concentrations in the atmosphere were about 40% higher than those of the present day (Beck et al. 2001; Kitagawa and Plicht 1998). This difference may be attributed to 2 different causes: one is a change in the production rate of ^{14}C which arose from the variation of geomagnetic fields and/or the variation of the solar modulation of cosmic rays (Beer 2000a; Beer et al. 2000b); the other is an environmental change of the earth which set off a change in the carbon cycle. However, the main cause is unknown. The response of the ^{14}C concentration to the 11-yr solar modulation is a good indicator for investigating the dominant effect (Stuiver and Braziunas 1993, 1998). If the energy spectra of the cosmic rays entering the heliosphere and the solar activities are similar to those during the Holocene, the 11-yr modulation of ^{14}C concentration should increase the amplitude of the modulation corresponding to the decrease in the geomagnetic fields. On the contrary, if the geomagnetic fields are similar to those during the Holocene and the solar activities are different from those during the Holocene, the 11-yr modulation might show a different profile from the 11-yr modulation during the Holocene. Meanwhile, if the increase in ^{14}C concentrations in the atmosphere arises from a change in the carbon cycle, the amplitude and the profile of the 11-yr modulation would be different from those during the Holocene.

^{14}C concentrations in tree rings are indicative of past terrestrial and extraterrestrial environments. Since tree rings record ^{14}C concentrations in chronological order with a time resolution of 1 yr, ^{14}C measurements in single-yr tree rings provide the ^{14}C concentration in the atmosphere for the period of 1 yr. In particular, ^{14}C measurements of the single-yr tree rings of old wood samples are essential for investigating the 11-yr periodicity of solar activity in the past. The expected amplitude in the modulation of the ^{14}C concentrations in the tree rings due to the 11-yr solar cycle is approximately 0.5% to 1%, although the variation of the production rate of ^{14}C is estimated to be approximately 30% based on the observation of the neutron flux at present. The small amplitude in the modulation results from the ^{14}C concentration being reduced to approximately 1/100 by terrestrial carbon circulation in the atmosphere and the ocean (Kocharov et al. 1995; Oeschger et al. 1975; Peristykh and

[1]Department of Physics, Yamagata University, 1-4-12 Kojirakawa, Yamagata 990-8560, Japan.
[2]Corresponding author. Email: sakurai@ksprite.kj.yamagata-u.ac.jp.
[3]Research Center for Nuclear Science and Technology, The University of Tokyo, Tokyo 113-0032, Japan.

Proceedings of the 18th International Radiocarbon Conference, edited by N Beavan Athfield and R J Sparks
RADIOCARBON, Vol 46, Nr 2, 2004, p 949–955

Damon 1998). Therefore, measurements of the ^{14}C concentrations for the single-yr tree rings of old wood are desired with an accuracy of 0.5%.

Accelerator mass spectrometry (AMS) measurement is advantageous for both a small quantity of sample and the simultaneous measurement of a large number of samples. Although the typical measurement accuracy is 0.5% for contemporary carbon, for old samples this accuracy can also be realized by AMS measurement using a multicathode method with graphite samples produced from the same tree-ring samples.

We have measured the ^{14}C concentrations in single-yr tree rings of old wood, of which the ^{14}C date is approximately 22,000 BP using AMS with multicathodes. In order to confirm the usefulness of the multicathode measurement method, the ^{14}C concentrations in 10 single-yr tree rings were measured in 100 tree rings at intervals of 10. We describe the results of the multicathode measurement for the single-yr tree rings and the variation of ^{14}C concentrations in 100 tree rings dating as far back as 22,000 yr ago.

METHODS

The tree rings used in this study are from a sample of old wood that was dug out from the bottom of the river at Kaminoyama City (38°07′N, 140°17′E) in Japan. Many old fallen trees are buried in the geological layers of this area, and the layer from which the sample was dug out was close to, although slightly younger, than that of Aera tephra, which is marked by a volcanic eruption in the vicinity of 23,000 BP. From the appearance of the area, it is considered that many trees were rapidly felled at the same time and were immediately buried.

The number of tree rings was approximately 130 and their typical width was 1 mm. For this experiment, we measured the ^{14}C dates of 10 tree-ring samples (labeled KY10 to KY95). Each tree-ring sample was separated by hand into single-yr intervals in order to measure the concentration of ^{14}C. Because α-cellulose in the cell walls is the most reliable chemical component of wood for measuring the annual concentration of ^{14}C, its chemical extraction was carried out using acid and alkaline solutions. Approximately 1 g of α-cellulose was extracted from 5 g of wood sample for a single-yr tree ring.

For the multicathode measurement of a single-yr tree ring, approximately 10 graphite samples were produced from the α-cellulose by the same process. First, 28 mg of cellulose was burned by chemical reaction with copper oxide (CuO) to produce carbon dioxide (CO_2); sulfur was removed with a silver sheet. Graphite was then produced by hydrogen reduction of the CO_2 in the presence of iron powder (1 mg) as catalyst. The graphite was pressed into the cathode container at 60 PSI using a pressing machine. Because it is important to produce identical graphite samples, we attempted to keep the ratio of graphite to iron at 1:1 by weight. The weight ratios of graphite to 1 mg of iron were between 0.6 and 1.2, which indicates that the graphite samples were similar.

Measurements of ^{14}C in the graphite samples were carried out using the 5 MeV Tandem accelerator at the Micro-Analysis Laboratory, The University of Tokyo (MALT). ^{12}C, ^{13}C, and ^{14}C were injected into the AMS with 6000 cycles of 0.12 sec per cycle by sequential injection. Hereafter, the 6000 cycles are referred to as 1 turn. The injected current of ^{12}C was maintained between 6 and 9 μA.

The ^{14}C dates of each graphite sample were calculated from the measured value of $^{14}C/^{12}C$ for the graphite samples of cellulose and the National Institute of Standards and Technology (NIST) standard samples. In the calculation, the value of $\delta^{13}C$ for cellulose measured with a mass spectrometer was used for the isotope fractionation correction.

RESULTS AND DISCUSSION

The numbers of multicathodes and turns for the measurements are shown in Table 1 for each tree-ring sample. Because the number of ^{14}C in the samples is counted to typically 1000 for 1 turn, the relative statistical error is approximately 3% from Poisson counting statistics. Hence, by measurements using 10 multicathodes with 8 turns, we can obtain the relative statistical error of approximately 0.35% for a tree-ring sample from the total counts of ^{14}C. Strictly speaking, however, the conditions for each multicathode and each turn are not identical, although the multicathodes were produced from the same cellulose and they were measured under similar AMS conditions. Therefore, first of all, the statistical behavior was investigated using the data of the multicathode measurements.

Table 1 Numbers of multicathodes, turns, and measurements for the tree-ring samples.

Tree-ring sample	Nr of multicathodes	Nr of turns	Nr of measurements
KY10	10	8	80
KY20	8	4	32
KY30	8	9	72
KY40	8	9	72
KY50	10	8	80
KY60	8	4	32
KY70	8	9	72
KY80	8	4	32
KY90	10	8	80
KY95	8	9	72

For the measurement of a multicathode, the distribution of counts per turn was statistically investigated. The statistical indicators are as follows:

1. $1/\sqrt{N}$, where N is average count of ^{14}C per turn;
2. The relative sample standard deviation (RSD1) calculated from the concentrations of $^{14}C/^{12}C$ per turn;
3. The relative standard deviation (RSD2), which is the ratio of the σ value to the mean of the Gaussian distribution obtained from the distribution of the concentrations of $^{14}C/^{12}C$ per turn, as shown in Figure 1. (The figure, for instance, shows the distributions of the concentrations of $^{14}C/^{12}C$ per turn measured for the multicathodes for samples KY10 and KY70, respectively. The curves represent the best-fitted Gaussian distribution using a least-squares method.);
4. The reduced χ^2 values for the least-squares fitting of the Gaussian distribution.

These values are listed for each tree-ring sample in Table 2.

The values of $1/\sqrt{N}$ are approximately between 2.7% and 3.1%, and indicate the relative standard deviations (PSD), assuming Poisson counting statistics for the ^{14}C counts. The RSD1s were between 3.2% and 3.5% for each tree-ring sample, except samples KY50 and KY80. By removing 2 data from KY50 and 3 data from KY80, respectively, by the χ^2 test, the RSD1s were determined to be 3.6%. Since the significance levels before and after the removal are from 10^{-11}% to 1.3% for KY50 and from 10^{-3}% to 5% for KY80 in the χ^2 distributions, their data were removed. The RSDs are the same as or greater than the PSDs. This indicates that the RSD1s include other fluctuations of typically 1.5%, in addition to the fluctuation of the Poisson counting statistics. Moreover, we attempted to apply Gaussian fitting to the distributions of the concentrations of $^{14}C/^{12}C$ per turn, although the

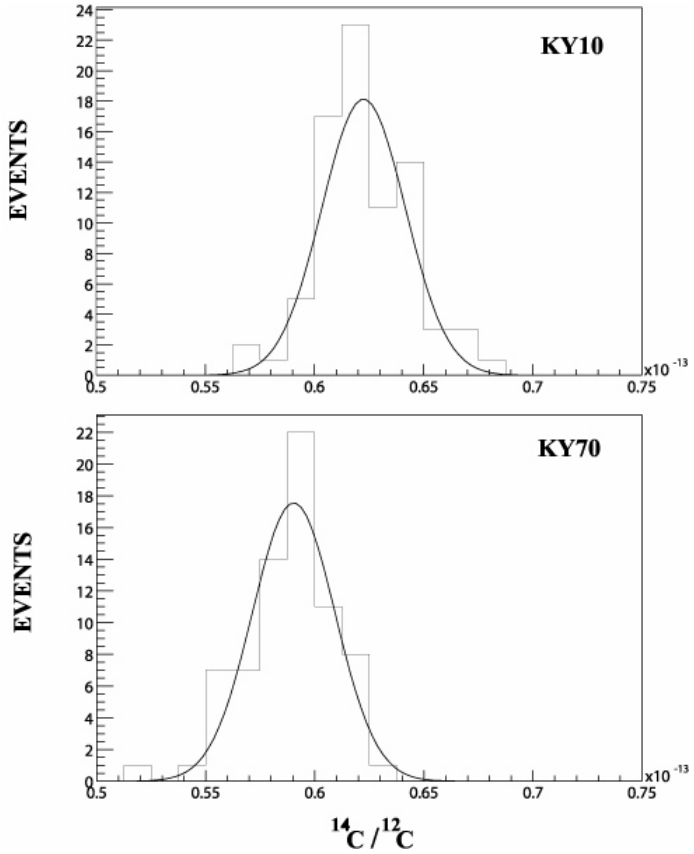

Figure 1 Distributions of the concentrations of $^{14}C/^{12}C$ per turn measured for the multicathodes of single-year tree rings KY10 and KY70. The curves represent the best-fitted Gaussian distribution using a least-squares method.

Table 2 Statistical values obtained from the multicathode measurements of the concentrations of $^{14}C/^{12}C$ for the tree-ring samples (see text).

Tree-ring sample	$\frac{1}{\sqrt{N}}$ (%)	$\frac{SD}{^{14}C/^{12}C}$ (%)	$\frac{\sigma}{mean}GaussFit$ (%)	$\frac{\chi^2}{\nu}$
KY10	3.1	3.5	3.1	1.5
KY20	2.8	2.8	3.4	0.6
KY30	2.8	3.3	3.5	1.5
KY40	2.8	3.2	3.8	1.3
KY50	3.1	5.0 (3.6)	3.2 (3.2)	0.9 (0.9)
KY60	2.8	3.2	3.6	0.1
KY70	2.8	3.4	3.2	1.0
KY80	2.8	4.2 (3.6)	5.5 (4.5)	2.0 (2.0)
Y90	3.1	3.2	3.0	0.7
KY95	2.7	3.3	3.1	0.3

number of events is not large. The RSD2s from the best-fitted Gaussian curves were similar to the RSD1s, indicating that the distributions of the concentrations of $^{14}C/^{12}C$ per turn are not significantly different from the Gaussian distribution, although the reduced χ^2 values scatter from 0.1 to 2.0. On the basis of these results, to determine the estimated error in the average concentration of $^{14}C/^{12}C$ of the multicathode measurement for each tree-ring sample, we used the value of the sample standard deviation divided by the square root of the number of data, which is the mean error of the mean.

Figure 2 shows the ^{14}C dates for all of the turn data of each tree-ring sample. The average ^{14}C date of the tree-ring samples from KY10 to KY95 was 22,130 BP, with the standard deviation of 306 BP from the 624 data obtained from the measurements of multicathodes for the single-yr tree-ring samples. Except for 2 ^{14}C dates of KY50, the ^{14}C dates of 622 data for the tree-ring samples were within 3 standard deviations. The ^{14}C date of an outer portion of the tree ring KY95 was 22,198 ± 31 BP. Moreover, the ^{14}C date of the same tree-ring sample was 22,169 ± 86 BP according to the measurement using the highly accurate liquid scintillation counting system (LSC) at Yamagata University (Suzuki et al. 199; Endo et al. 2000; Sakurai et al. 2003). Results obtained using AMS and those obtained using LSC were consistent with each other, confirming the accuracy of the AMS measurements. From the calibration data of Lake Suigetsu (Kitagawa and Plicht 1998), the calendar dates of these 100 tree rings were located between 25,400 cal BP and 26,150 cal BP. The calibration data showed that the ^{14}C dates varied considerably between the calendar dates.

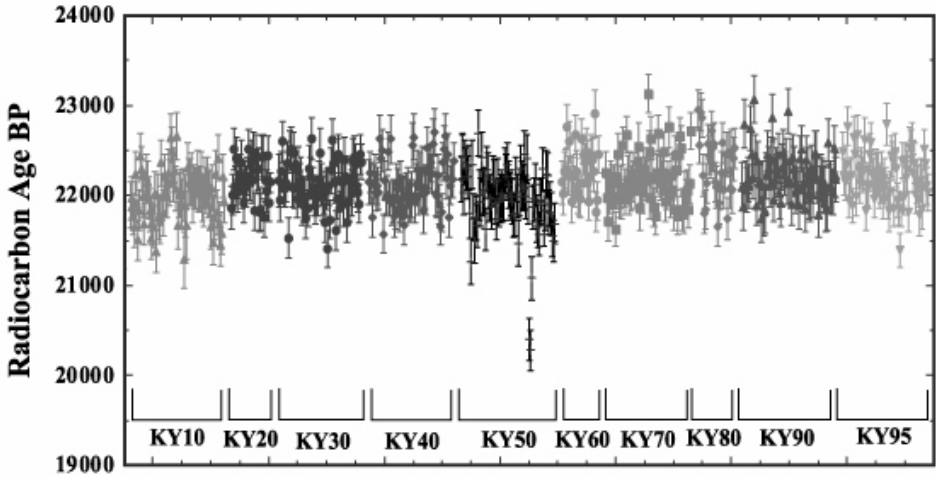

Figure 2 ^{14}C dates for all turn data of each tree-ring sample. The average ^{14}C date of the tree rings from KY10 to KY95 was 22,130 BP, with the standard deviation of 306 BP from the 624 data. Except for 2 ^{14}C dates of KY50, the ^{14}C dates were within the 3 standard deviations.

Finally, Figure 3 shows a time profile of the ^{14}C dates for the tree-ring number. The ^{14}C date for a tree-ring number is derived from the average value of the concentrations of $^{14}C/^{12}C$ per turn obtained by the measurements for the multicathodes of the single-yr tree ring, and the error bar from the mean error of the mean for the concentrations. Two and 3 ^{14}C dates from the KY50 and KY80 samples, respectively, are removed by a χ^2 test with the significance level of 1%. The ^{14}C dates changed between 21,979 BP and 22,272 BP, with an error of approximately 50 BP, corresponding to a precision of approximately 0.5%. As shown in the figure, the average ^{14}C ages between KY10 and KY50 and between KY60 and KY95 were 22,080 BP and 22,224 BP, respectively, indicating a step with a change of 144 BP in the ^{14}C date for a 10-yr period in the vicinity of KY50. Both sample

processing and AMS measurements were carried out in the following order with 4 AMS machine times: KY10, KY50, and KY90 for the 1st; KY20, KY60, and KY80 for the 2nd; KY30, KY40, KY70, and KY95 for the 3rd; and KY50 again for the 4th, respectively. Since the analyzing order is approximately random and the difference between 2 measurements for KY50 was about 40 BP, the possibility of a systematic effect causing the shift of 144 BP is very small. By taking into account the Lake Suigetsu data, which shows a change of 940 BP in ^{14}C date for 7 yr during the calendar dates, the rapid change in the ^{14}C dates for this tree-ring sample implies that the concentrations of $^{14}C/^{12}C$ in that period were highly variable.

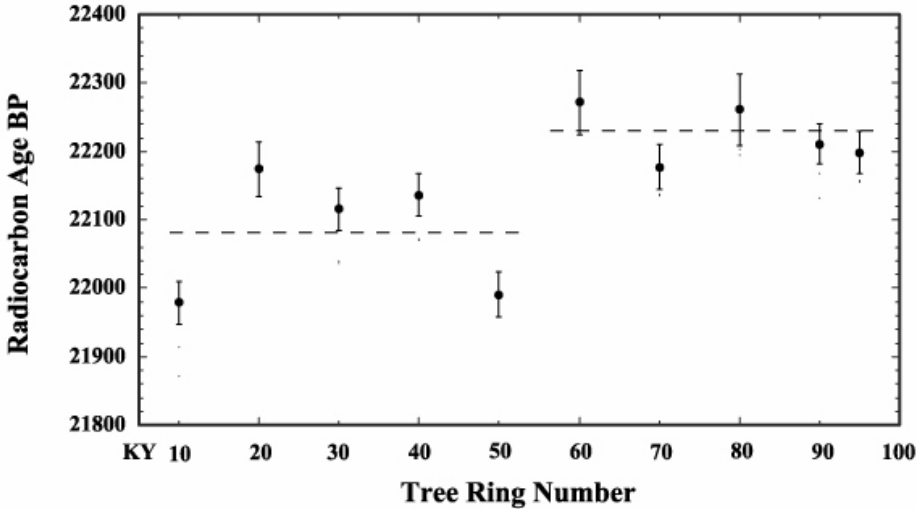

Figure 3 Time profile of ^{14}C dates for the tree-ring number using the mean error mean as the estimated error on average. Dotted lines represent the average ^{14}C dates between KY10 and KY50 and between KY60 and KY95. The ^{14}C dates underwent a change between 21,979 BP and 22,272 BP with the error of approximately 50 BP, corresponding to the precision of approximately 0.5%. As shown in the figure, the average ^{14}C ages between KY10 and KY50 and between KY60 and KY95 were 22,080 BP and 22,224 BP, respectively, indicating a step with a change of 144 BP in the ^{14}C date for a 10-yr period in the vicinity of KY50.

CONCLUSION

We have measured the ^{14}C concentrations in single-yr tree rings of old wood by AMS using a multicathode. The measurement of ^{14}C using a multicathode has 2 advantages. One is an enhancement of the statistical accuracy and, hence, it is expected that the ^{14}C concentrations are measured with high precision. The other advantage is that using a multicathode enables the testing of systematic errors caused by the process of graphite production, and, in turn, this improves the accuracy of the AMS measurement (Sakurai et al. 2004; Guo et al. 2000; Tuniz et al. 1998).

In order to confirm the applicability of the multicathode measurement method, the ^{14}C concentrations in 10 single-yr tree rings were measured in 100 tree rings at intervals of 10. For the multicathode measurement of a single-yr tree ring, approximately 10 graphite samples were produced from its α-cellulose by the same process. For the outer sample of the tree ring, the ^{14}C dates were 22,198 ± 31 BP by AMS and 22,169 ± 86 BP by LSC, respectively, confirming the accuracy of the AMS measurements with the multicathode.

For a single-yr tree-ring sample, typically the ^{14}C concentrations of 80 measurements were obtained using the multicathodes and, hence, we have obtained 624 data in total for the 10 tree-ring samples. The statistical behavior was investigated and compared using Poisson counting statistics for the data set of each tree-ring sample. The sample standard deviations indicated that they include other fluctuations of up to 2%, in addition to the fluctuation of the Poisson counting statistics (Tuniz et al. 1998). From the best-fitted Gaussian curves, the distributions of the concentrations of $^{14}C/^{12}C$ were not significantly different from the Gaussian distribution.

The average ^{14}C date of the tree rings was 22,130 ± 306 BP for all 624 data. From the calibration data of Lake Suigetsu, the calendar dates of these 100 tree rings were located between 25,400 cal BP and 26,150 cal BP.

The time profile of the ^{14}C dates changed between 21,979 BP and 22,272 BP, with an error of approximately 50 BP, corresponding to a precision of approximately 0.5% using the mean error of the mean as the estimated error on average. From these refined measurements using the multicathode, we identified a step with a change of approximately 144 BP in ^{14}C date for a 10-yr period in the vicinity of KY50 in the time profile. Since both sample processing and AMS measurements were carried out by approximately random order with 4 AMS machine times, it is highly possible that the discrete step is regarded as a real shift. By taking into account Lake Suigetsu data between the calendar dates, the rapid change in the ^{14}C dates in the tree rings implies that the concentrations of $^{14}C/^{12}C$ in that period were highly variable.

REFERENCES

Beck JW, Richards DA, Edwards RL, Silverman BW, Smart PL, Donahue DL, Hererra-Osterheld S, Burr GS, Calsoyas L, Jull AJT, Biddulph D. 2001. Extremely large variations of atmospheric ^{14}C concentration during the Last Glacial Period. *Science* 292: 2453–58.

Beer J. 2000a. Long-term indirect indices of solar variability. *Space Science Reviews* 100:1–15.

Beer J, Mende W, Stellmacher R. 2000b. The role of the sun in climate forcing. *Quaternary Science Reviews* 19:403–15.

Endo K, Sakurai H, Sekiguchi H, Gunji S, Kato A, Furusawa S, Inui E, Suzuki A, Hamano M. 2000. ^{14}C measurement of synthesized benzene from old tree rings. *IEEE Transactions on Nuclear Science* 47(6):302–5.

Guo Z, Liu K, Lu X, Ma H, Li K, Yuan S, Wu X. 2000. The use of AMS radiocarbon dating for Xia-Shang-Zhou chronology. *Nuclear Instruments and Methods in Physics Research B* 172:724–31.

Kitagawa H, van der Plicht J. 1998. Atmospheric radiocarbon calibration to 45,000 yr BP. *Science* 279:1187–90.

Kocharov GE, Ostryakov VM, Peristykh AN, Vasil'ev VA. 1995. Radiocarbon content variations and Maunder Minimum of solar activity. *Solar Physics* 159: 381–91.

Oeschger H, Siegenthaler U, Gugelmann A, Schotterer U. 1975. A box diffusion model to study the carbon dioxide exchange in nature. *Tellus* 27:168–92

Peristykh A, Damon PE. 1998. Modulation of atmospheric ^{14}C concentration by the solar wind and irradiance components of the Hale and Schwabe solar cycles. *Solar Physics* 177:343–55.

Sakurai H, Sawaki Y, Matsumoto T, Aoki T, Kato W, Gandou T, Gunji S, Tokanai F. 2003. Characteristics of high-purity Teflon vial for ^{14}C measurement in old tree rings. *Nuclear Instruments and Methods in Physics Research A* 505:454–7.

Sakurai H, Gandou T, Kato W, Sawaki Y, Matsumoto T, Aoki T, Matsuzaki H, Gunji S, Tokanai F. Forthcoming. AMS measurement of C-14 concentration in a single-year ring of a 2500-year-old tree. *Nuclear Instruments and Methods in Physics Research B*.

Stuiver M, Braziunas F. 1993. Sun, ocean, climate and atmospheric $^{14}CO_2$. *The Holocene* 3:289–305

Stuiver M, Braziunas F. 1998. Anthropogenic and solar components of hemispheric ^{14}C. *Geophysical Research Letters* 25(3):329–32.

Suzuki A, Sakurai H, Endo K, Noma M, Gunji S, Inui E, Hamano M. 1999. Pulse-height distribution of β rays in ^{14}C Measurement with liquid scintillation counting system Quantulus. IEEE *Transactions on Nuclear Science* 46(3):302–5

Tuniz C, Bird JR, Fink D, Herzog GF. 1998. *Accelerator Mass Spectrometry*. Boca Raton: CRC Press. 300 p.

RADIOCARBON, Vol 46, Nr 2, 2004, p 957–964

INTERPRETING RADIOCARBON DATES USING EVIDENCE FROM TREE RINGS

Alex Bayliss

English Heritage, 23 Savile Row, London, W1S 2ET, United Kingdom.
Corresponding author. Email: alex.bayliss@english-heritage.org.uk.

Ian Tyers

Sheffield University, West Court, 2 Mappin Street, Sheffield, S1 4DT, United Kingdom. Email: i.tyers@sheffield.ac.uk.

ABSTRACT. Often it is not possible to date a sample of wood from the final growth ring of the tree from which it came. In these cases, an "old-wood offset" is apparent. A number of quantitative approaches for the assessment of this offset are available, dependent on the actual tree rings that have been dated. A range of examples are given, demonstrating how such radiocarbon measurements can be interpreted using additional information from archaeology and dendrochronology.

INTRODUCTION

When dating wood or charcoal, it is frequently impossible to select samples from the final growth ring of the dated tree. The approach needed to estimate the date of this ring, and thus the felling of the tree from which it came, depend upon the number and nature of the rings between the radiocarbon sample and the edge of the tree. This paper demonstrates a number of these approaches. All have been implemented using OxCal v3.5 (Bronk Ramsey 1995, 1998, 2001) and the calibration data of Stuiver et al. (1998).

'WIGGLE-MATCHING' TO BARK EDGE

The simplest case is where we know the exact number of rings between each ^{14}C sample, and between the ^{14}C samples and the outside of the tree. An example of this situation is provided by waterlogged coffin F1790 from Barton upon Humber, Lincolnshire (Rodwell and Rodwell 1982). Two ^{14}C samples were processed from this coffin. Relating the core holes where these samples were taken to the subsequently constructed tree-ring sequence suggests that OxA-2283 (1300 ± 110 BP) consisted of a 30-yr block of rings, the center of which was 161 yr earlier than OxA-2284 (915 ± 80 BP). This also consisted of 30 rings, the center being 46 rings from the outside of the tree.

Using the D_SEQ function of OxCal, a model which combines all this information suggests that coffin F1790 was constructed in cal AD 950–1210 (95% probability; Figure 1). This is consistent with the tree-ring date for this coffin of winter AD 1131/2 (Figure 2).

The absolute dating of this sequence by dendrochronology suggests that OxA-2283 consisted of a 30-yr block centered on AD 924, and OxA-2284 of a 30-yr block centered on AD 1085. OxA-2283 is statistically consistent with the weighted mean of the 3 decadal measurements spanning AD 910–40 from the calibration curve (T'=2.6; T'[5%]=3.8; ν=1; Ward and Wilson 1978), and OxA-2283 is consistent with the 3 measurements spanning AD 1070–1100 (T'=0.0; T'[5%]=3.8; ν=1). These measurements also show good overall agreement with the date suggested by dendrochronology ($A_{overall}$=74.7%; An=40.8%; Bronk Ramsey 1995:429).

SAMPLES ENDING IN THE HEARTWOOD/SAPWOOD BOUNDARY

Another burial at Barton upon Humber, F3564, was placed in a coffin dug out of a single tree trunk. The ^{14}C sample, HAR-6501 (900 ± 70 BP), consisted of a decadal block of wood ending in the heartwood/sapwood boundary. The best estimate for the date of this coffin is, therefore, the calibrated ^{14}C

Proceedings of the 18th International Radiocarbon Conference, edited by N Beavan Athfield and R J Sparks
RADIOCARBON, Vol 46, Nr 2, 2004, p 957–964

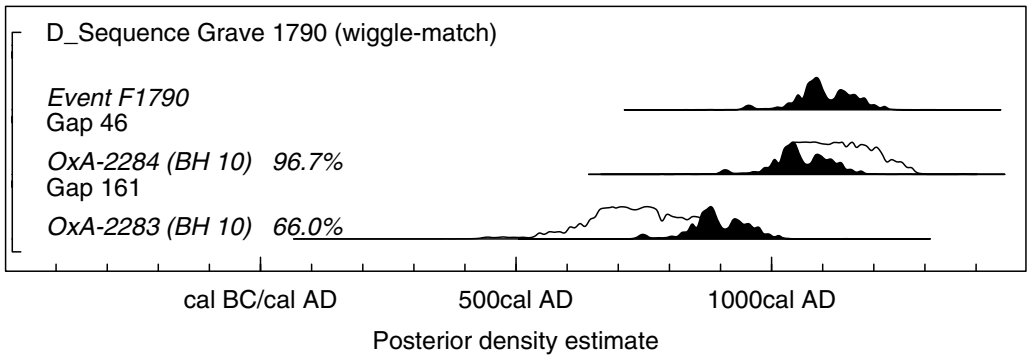

Figure 1 Probability distribution of dates from coffin F1790 at Barton upon Humber. Each distribution represents the relative probability that an event occurs at a particular time. For each ^{14}C date, 2 distributions have been plotted: one in outline which is the result of simple ^{14}C calibration, and a solid one based on the chronological model used. The large square brackets down the left-hand side and the OxCal keywords define the overall model exactly.

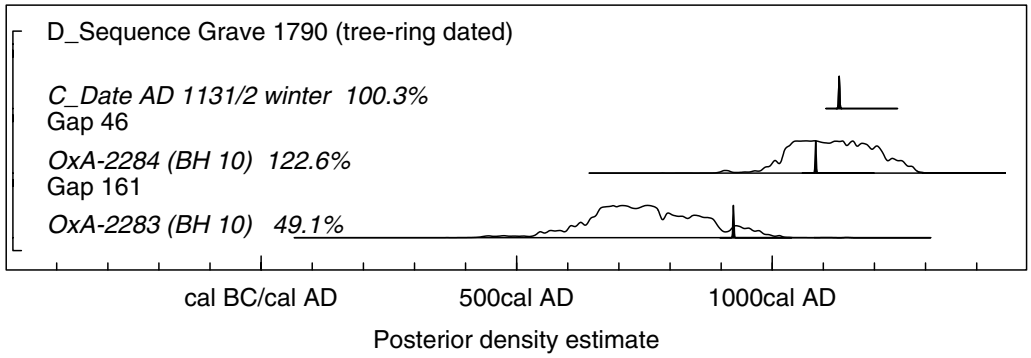

Figure 2 Probability distributions of dates from coffin F1790 at Barton upon Humber, including the absolute dating from dendrochronology (Tyers 2001).

date, offset by the distribution of the number of sapwood rings expected on oak timbers from England (Millard 2002).

This distribution is known empirically from dendrochronology (Figure 3; Table 1). The data set includes timbers from the prehistoric, Roman, medieval, and post-medieval periods (but not modern data), although it is dominated by material of Roman and medieval date. A national estimate has been used in this case because, although there is now some evidence for regionality within the medieval data set (Miles 1997), there is little evidence for this when considering multi-millennial data. In particular, at present there is insufficient data to construct specific sapwood estimates for other periods, and so it is not possible to determine whether there are appropriate regional divisions. Obviously, this position may change as further data are collected.

The sapwood estimate can be applied to the ^{14}C date using the PRIOR and SHIFT functions of OxCal (Figure 4). This model suggests that coffin F3564 dates to cal AD 1035–1290 (95% probability).

The structure that implements this approach in OxCal is shown by the square brackets and keywords down the left-hand side of Figure 4. The sapwood estimate must be placed in a file (*.14d) in the format shown in Table 1. This distribution is invoked as a prior distribution, and then used to shift a previously calibrated ^{14}C measurement. These functions must be used within a part of a model when MCMC is operational (if this is not the case, then the MCMC may be invoked using a "dummy" sequence, as shown in Figure 4).

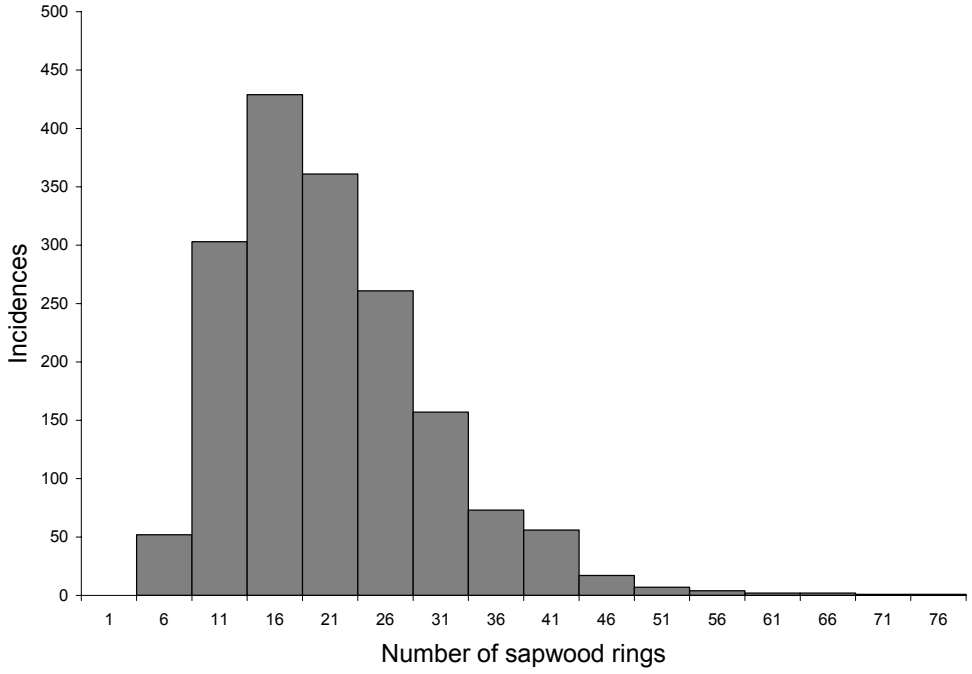

Figure 3 Distribution of the number of sapwood rings present on ancient oak timbers complete to bark edge from England.

Table 1 Distribution of the number of sapwood rings present on ancient timbers complete to bark edge from England, converted to an appropriate format for calculating offsets to calibrated ^{14}C dates in OxCal.

Number of sapwood rings	Occurrences (n = 1726)	OxCal file (sapwood1.14d)	
1–5	0	0	0.000000
6–10	52	5	0.030127
11–15	303	10	0.175550
16–20	429	15	0.248552
21–25	361	20	0.209154
26–30	261	25	0.151217
31–35	157	30	0.090962
36–40	73	35	0.042294
41–45	56	40	0.032445
46–50	17	45	0.009849
51–55	7	50	0.004056
56–60	4	55	0.002317
61–65	2	60	0.001159
66–70	2	65	0.001159
71–75	1	70	0.000579
76–80	1	75	0.000579

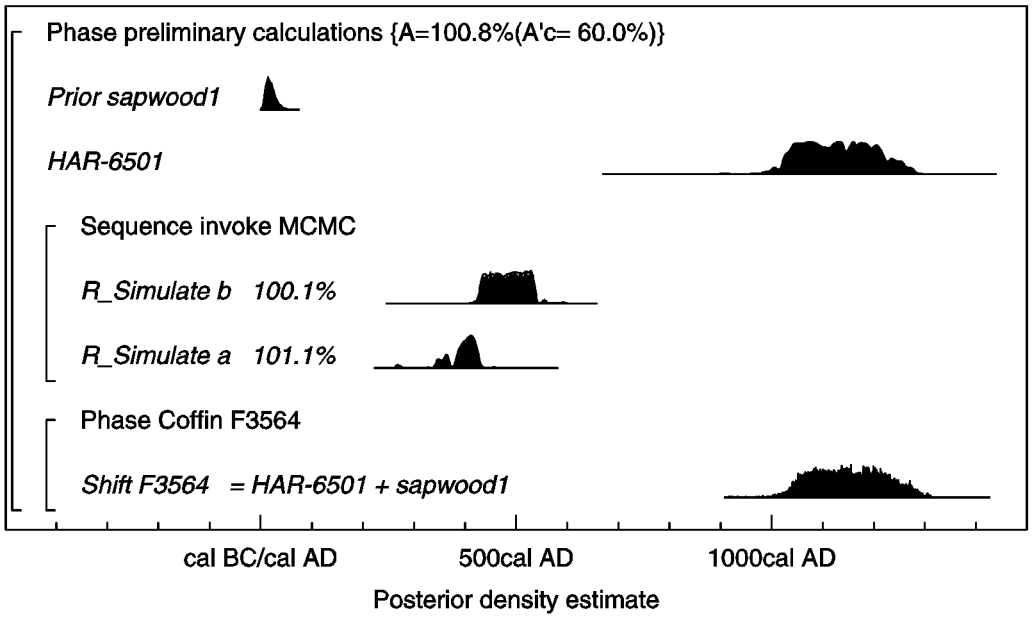

Figure 4 Probability distributions of dates from coffin F3564 at Barton upon Humber, shifting the calibrated ^{14}C date for the decadal sample to the heartwood/sapwood boundary by the expected number of sapwood rings for ancient oak samples in England (see Figure 3).

The skeleton buried within coffin F3564 produced a ^{14}C date of cal AD 1020–1160 (UB-4655; 957 ± 17 BP).

SAMPLES WITH SOME SAPWOOD

Coffin F5045 at Barton upon Humber is another plank-built example. A single ^{14}C sample has been dated from this object (OxA-2286, 1035 ± 80 BP), which consisted of a 40-yr block centered on AD 1015. This result is statistically consistent with the weighted mean of the 3 decadal measurements spanning AD 910–40 from the calibration curve (T'=2.6; T'[5%]=3.8; ν=1; Ward and Wilson 1978), and also shows good overall agreement with the date suggested by dendrochronology ($A_{overall}$ = 60.9%; An=50.0%; Bronk Ramsey 1995:429).

Absolute dating, however, is provided by dendrochronology. Another plank from this coffin has a heartwood/sapwood boundary dated to AD 1051 and 20 surviving sapwood rings (and, thus, a last dated ring of AD 1071). The best estimate for the date of this burial is provided, therefore, by the addition of a truncated sapwood distribution that accounts for the surviving sapwood rings (Figure 5; Table 2). This distribution is applied in a similar manner to previous examples (Figure 6) and suggests that this coffin was built in cal AD 1071–1095 (95% probability).

'WIGGLE-MATCHING' TO A HEARTWOOD/SAPWOOD BOUNDARY

Figure 7 shows the results of the wiggle-matching of a floating tree-ring sequence from Swalecliffe, Kent (Masefield et al. 2003). Six sequential bi-decadal blocks of waterlogged wood were dated, ending 9 yr before the heartwood/sapwood boundary on timber 5124.2<3>. No sapwood survived on this sample, and so the best estimate for the date of this timber is provided by the wiggle-matched ^{14}C sequence offset by the expected number of sapwood rings (Figure 3).

This model suggests that the timber was cut in 730–680 cal BC (95% probability).

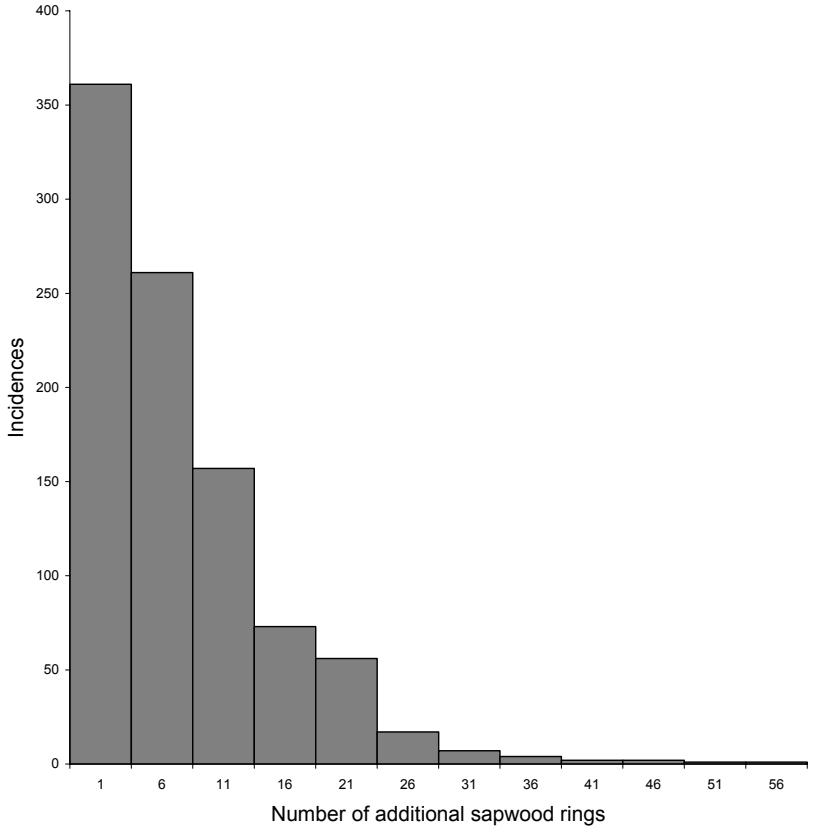

Figure 5 Additional number of sapwood rings expected on an oak sample with 20 surviving sapwood rings (based on Figure 3).

Table 2 Distribution of additional sapwood rings expected when 20 rings are present, converted to an appropriate format for calculating offsets to calibrated ^{14}C dates in OxCal.

Number of additional sapwood rings	Occurrences (n=942)	OxCal file (sapwood1.14d)	
1–5	361	0	0.383227
6–10	261	5	0.277070
11–15	157	10	0.166667
16–20	73	15	0.077495
21–25	56	20	0.059448
26–30	17	25	0.018047
31–35	7	30	0.007431
36–40	4	35	0.004246
41–45	2	40	0.002123
46–50	2	45	0.002123
51–55	1	50	0.001062
56–60	1	55	0.001062

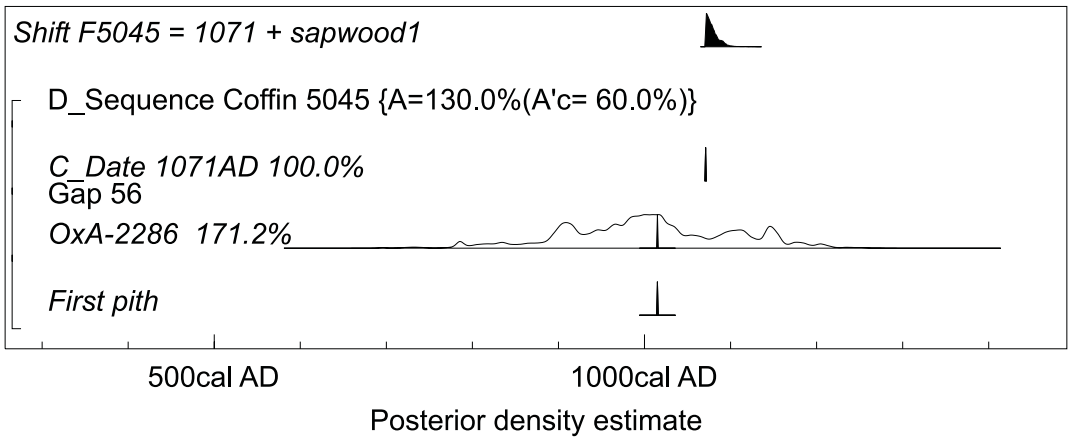

Figure 6 Probability distributions of dates from coffin F5045 at Barton upon Humber, incorporating the relative and absolute dating information known from dendrochronology and including the expected number of additional sapwood rings for ancient oak samples in England for timbers with this amount of sapwood survival (see Figure 5).

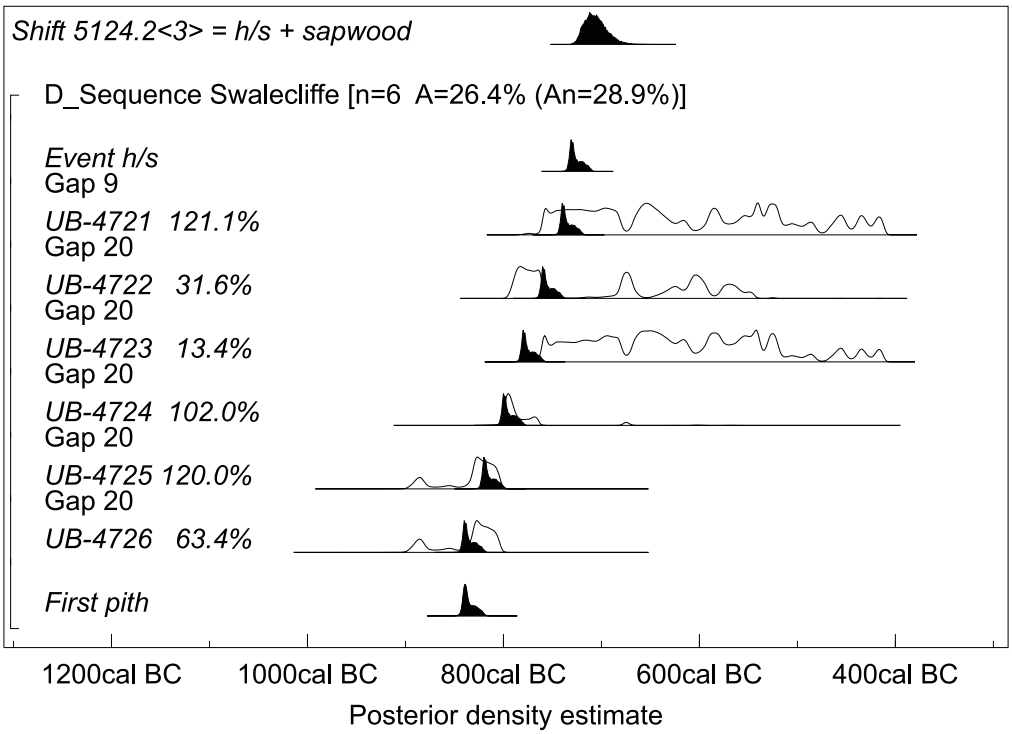

Figure 7 Probability distributions of wiggle-matched sequence from SWALCLF2, shifting the date for heartwood/sapwood boundary of sample 5124.2<3> by the expected number of sapwood rings for oak samples in England (see Figure 3).

'WIGGLE-MATCHING' TO A *TERMINUS POST QUEM*

A rather more complicated example is provided by the wiggle-matching of the timbers from the Dover boat (Bayliss et al. 2003). Here, a sequence of 5 contiguous bi-decadal samples was taken

from a floating tree-ring sequence, with 34 rings to the last heartwood ring undated by ^{14}C. Adding the probability distribution of the number of sapwood rings expected (Figure 3) provides a *terminus post quem* for the samples of short-lived material, which are those closest in date to the actual construction of the boat. These samples were of yew withies that tied the planking of the boat together, and moss which was used as caulking to make the craft watertight.

This model is shown in Figure 8. It suggests that the boat was constructed in 1640–1520 cal BC (87% probability).

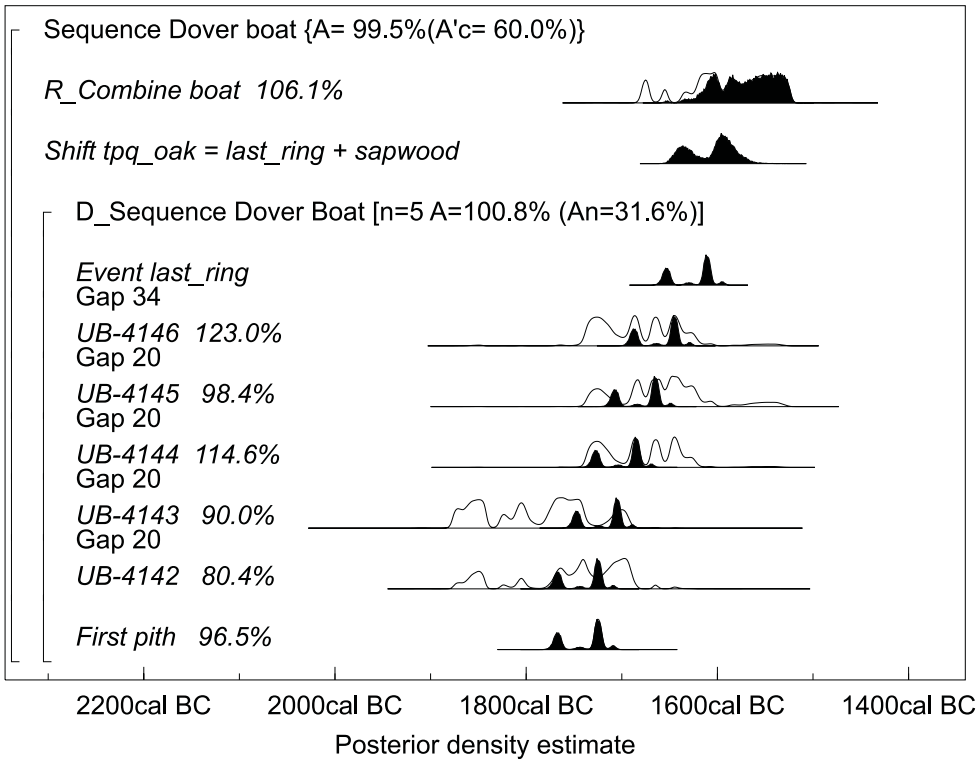

Figure 8 Probability distributions of wiggle-matched sequence from the Dover boat, shifting the date of the last heartwood ring by the expected number of sapwood rings for oak samples in England (see Figure 3). This provides a *terminus post quem* for the samples of short-lived yew withy and moss which were used to tie the boat together and keep it watertight.

CONCLUSIONS

Determining the age of the tree rings contained within a ^{14}C sample is crucial for its interpretation. Quantitative methods for correcting ^{14}C dates for a known or unknown "old-wood effect" have been suggested for many years (e.g. Warner 1990).

The Bayesian approach to interpreting chronological data allows the integration of ^{14}C dating with evidence from tree rings in a quantitative manner. This is particularly important in situations where precise and accurate chronology is required.

ACKNOWLEDGEMENTS

We are grateful to Warwick Rodwell, the Canterbury Archaeological Trust, and RPS Group Plc. for permission to cite data in advance of full publication. English Heritage funded the ^{14}C dating reported here and the tree-ring analysis from Barton upon Humber. The tree-ring dating at Swalecliffe was funded by Southern Water. In addition, the excavation of the Dover Boat was supported by NorWest Holt and the Environment Agency, and that at Swalecliffe by Southern Water.

REFERENCES

Bayliss A, Groves C, McCormac FG, Bronk Ramsey C, Baillie MGL, Brown D, Cook GT, Switsur RV. 2003. Dating. In: Clark P. *The Dover Bronze Age Boat*. English Heritage Archaeological Monograph. p 250–5.

Bronk Ramsey C. 1995. Radiocarbon calibration and analysis of stratigraphy. *Radiocarbon* 36(3):425–30.

Bronk Ramsey C. 1998. Probability and dating. *Radiocarbon* 40(1):461–74.

Bronk Ramsey C. 2001. Development of the radiocarbon calibration program OxCal. *Radiocarbon* 43(2A): 355–63.

Masefield R, Branch N, Couldrey P, Goodburn D, Tyers I. 2003. A later Bronze Age well complex at Swalecliffe, Kent. *The Antiquaries Journal* 83:47–121.

Miles D. 1997. The interpretation, presentation and use of tree-ring dates. *Vernacular Architecture* 28:40–56.

Millard A. 2002. A Bayesian approach to sapwood estimates and felling dates in dendrochronology. *Archaeometry* 44:137–43.

Rodwell W, Rodwell K. 1982. St Peter's Church, Barton-upon-Humber: excavation and structural study 1978–81. *The Antiquaries Journal* 62:283–315.

Stuiver M, Reimer PJ, Bard E, Beck JW, Burr GS, Hughen KA, Kromer B, McCormac G, van der Plicht J, Spurk M. 1998. INTCAL98 radiocarbon age calibration, 24,000–0 cal BP. *Radiocarbon* 40(3):1041–83.

Tyers I. 2001. The tree-ring analysis of coffin timbers excavated at the church of St Peter, Barton upon Humber, North Lincolnshire. *Centre for Archaeology Report* 48/2001.

Ward GK, Wilson SR. 1978. Procedures for comparing and combining radiocarbon age determinations: a critique. *Archaeometry* 20:19–31.

Warner RB. 1990. A proposed adjustment for the "old-wood" effect. In: Mook WG, Waterbolk HT, editors. Proceedings of the Second International Symposium ^{14}C and Archaeology. *PACT* 29:159–72.

RADIOCARBON, Vol 46, Nr 2, 2004, p 965–968

VARIATION OF THE RADIOCARBON CONTENT IN TREE RINGS DURING THE SPOERER MINIMUM

Hiroko Miyahara[1,2] • Kimiaki Masuda[1] • Hideki Furuzawa[1] • Hiroaki Menjo[1] • Yasushi Muraki[1] • Hiroyuki Kitagawa[3] • Toshio Nakamura[4]

ABSTRACT. This paper presents the variation of radiocarbon content in annual tree rings for the period AD 1413–1553, which includes the Spoerer Minimum period (AD 1415–1534). Since the variation of the production rate of ^{14}C is strongly related to solar activity, the variation of ^{14}C content in annual tree rings gives us information on the characteristics of variation of solar activity. We have studied solar activity during the grand solar minima, focusing especially on the stability of the 11-yr cycle. The minima are determined to have been almost free of sunspots. Our results, however, have revealed quite remarkably the existence of the 11-yr cycle for most of the time during the Spoerer Minimum. The 11-yr variation weakened around AD 1460–1510, suggesting that solar activity might have been strongly suppressed during these 50 yr.

INTRODUCTION

Continuous sunspot data are available only after the beginning of the 18th century (Figure 1), immediately following the Maunder Minimum, when the sunspots had almost disappeared and the earth's temperature was lower than usual by 1 to 2 °C. Since then, the sun appears to have followed the "11-yr" cycle rather constantly. However, most of the history of the solar cycle is still unclear and the constancy of its period is a matter of controversy, especially during the period of grand solar minima.

The history of solar activity can be investigated by measuring the abundance of cosmogenic nuclides in layered natural archives such as trees or ice cores. Cosmogenic nuclides such as radiocarbon are mainly produced by incoming galactic cosmic rays (GCR) which are modulated by the solar wind and interplanetary magnetic field. When the sun is active, the flux of incoming GCR decreases, and consequently, the production rate of cosmogenic nuclides decreases, and vice versa. Therefore, the production rate of the cosmogenic nuclides has an anti-correlation with solar activity. ^{14}C produced in the upper atmosphere forms carbon dioxide which circulates within the atmosphere and some is absorbed into tree rings.

About 10,000 yr of decadal data on the ^{14}C content of the atmosphere are available so far. On the other hand, continuous annual ^{14}C data, required to investigate the solar cycle in detail, are available only for the period from AD 1511–1945. Figure 2 shows the decadal variation of the ^{14}C content in tree rings from the 11th century (Stuiver et al. 1998). Decadal-to-centennial variations are mainly caused by the variation of solar activity. Periods of high concentration correspond to the grand solar minima, and it is likely that there were 5 grand minima during the last millennium. The second most recent ^{14}C maximum is the Maunder Minimum, for which sunspot data are available (Figure 1). Prior to this was the Spoerer Minimum, for which neither sunspot data nor annual data of ^{14}C concentration have so far been obtained. We have aimed to measure the ^{14}C content annually in tree rings during the Spoerer Minimum, and have studied the corresponding solar variations, focusing especially on the change of the 11-yr cycle. We have now almost completed measuring all of the annual samples for the Spoerer Minimum. Here, we report the results of the measurement and discuss the characteristics of the variation of ^{14}C concentration during the Spoerer Minimum.

[1]Solar-Terrestrial Environment Laboratory, Nagoya University, Nagoya, Aichi 464-8601, Japan.
[2]Corresponding author. Email: miyahara@stelab.nagoya-u.ac.jp.
[3]Graduate School of Earth and Environmental Sciences, Nagoya University, Japan.
[4]Center for Chronological Research, Nagoya University, Japan.

Proceedings of the 18th International Radiocarbon Conference, edited by N Beavan Athfield and R J Sparks
RADIOCARBON, Vol 46, Nr 2, 2004, p 965–968

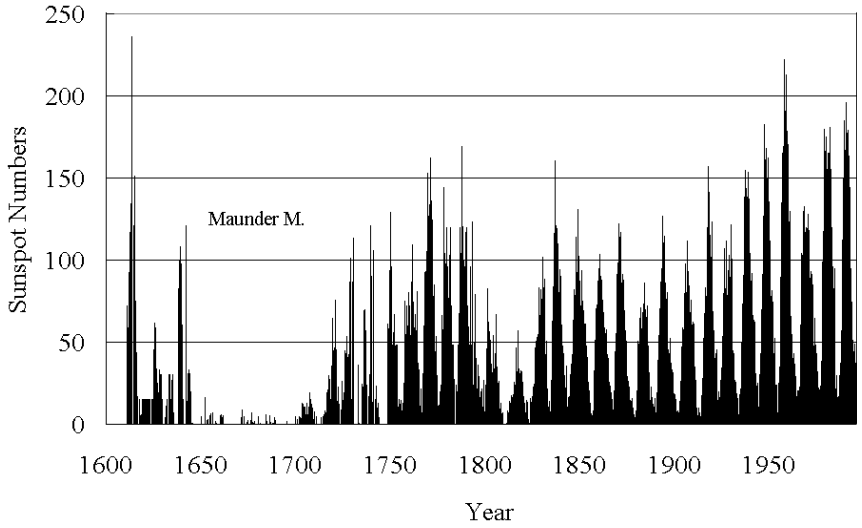

Figure 1 Sunspot numbers from the 17th century (Hoyt and Schatten 1998)

MEASUREMENT

To study the variation of ^{14}C content during the Spoerer Minimum, a 711-yr-old Japanese cedar tree, obtained at 30.18°N, 130.30°E, was used. The tree rings were first dendro-dated and separated annually, and then milled into small pieces. Each piece was then washed with a benzene-ethyl alcohol mixture to remove resins and other constituents which could move between rings. The extracts were subsequently bleached by a $NaClO_2$/HCl solution at 80 °C to remove lignin. They were then boiled and rinsed in distilled water. The resultant celluloses were combusted with CuO to obtain CO_2 gas. After purification, the CO_2 gas was deoxidized to graphite using H_2 gas (Kitagawa et al. 1993). Finally, the samples were pressed into the target holders of the accelerator mass spectrometer (AMS). The concentration of ^{14}C in each graphite sample was measured by using the AMS of Nagoya University in Japan, which achieves an accuracy of 3–5‰.

RESULTS AND DISCUSSION

Figure 3 shows the ^{14}C content in the tree rings from AD 1413 to 1553. The margin of error includes statistical error for ^{14}C counting and the stability of the AMS system. The solid curve is the decadal data shown in Figure 2. Our results are consistent with this curve. Our data, however, reveal more detailed variations that may be caused by solar variations. First, data gaps were replaced using a linear interpolation and the time series was analyzed for periodicity. The power spectrum of the Fourier analysis showed peaks at the periods around 5, 7, 11, and 22 yr. The peak at 11 yr was most prominent, its confidence level being about 2.3 σ. On the other hand, the 22-yr period, which can be considered as the Hale cycle, was relatively insignificant and comparable to the statistical uncertainty. It is notable that the 11-yr Schwabe cycle remained the most dominant during the Spoerer Minimum, although solar activity is considered to have been extremely low and sunspots almost absent at that time.

Next, the data were analyzed by band-pass filtering in order to remove the high frequency noise and the long-term trend. Figure 4 shows the detailed variation of amplitude of the 11-yr Schwabe cycle which was derived from the data with a filter with a bandwidth of 10–12 yr. In the beginning of the

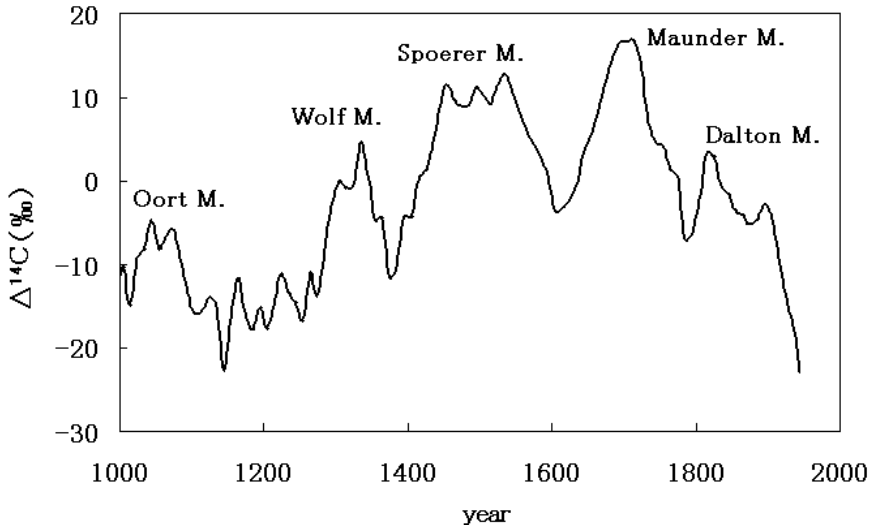

Figure 2 Decadal variation of ^{14}C content in tree rings (Stuiver et al. 1998)

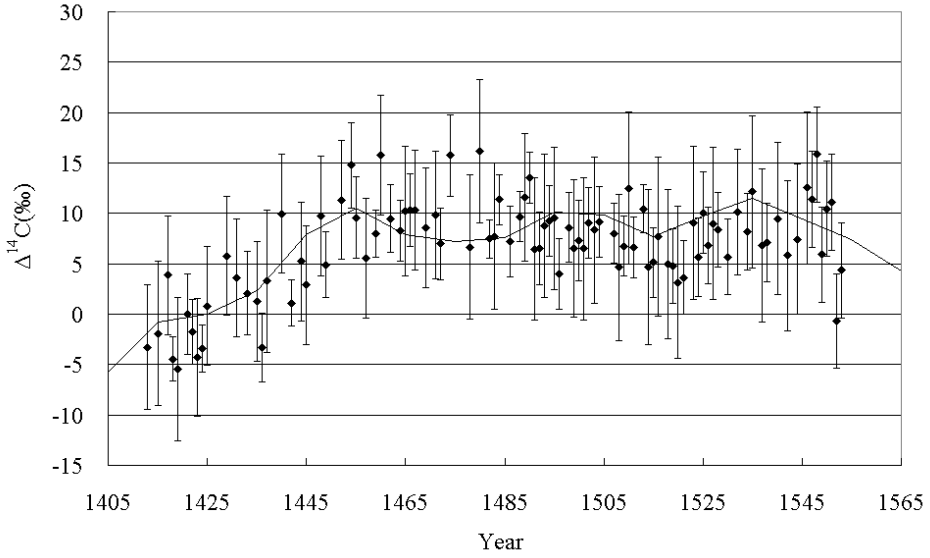

Figure 3 The ^{14}C content in tree rings during the Spoerer Minimum

period, the amplitude of the 11-yr cycle was about 1.5‰ and appeared to be weak around AD 1460–1510. From around AD 1510, the 11-yr Schwabe cycle seems to have recovered, increasing to about 1.5‰. The cosmic ray flux usually varies by 15–20% through a solar cycle with a corresponding variation of the ^{14}C content of the atmosphere of about 1.5–2.0‰, which is consistent with our result. As for the period of AD 1460–1510, when the 11-yr cycle was weak, it appears that the solar activity might have been most absent.

The data were also analyzed using the wavelet transform method in order to investigate more detailed variations of the periodicity. As a result, we found that there is a possibility that the 11-yr

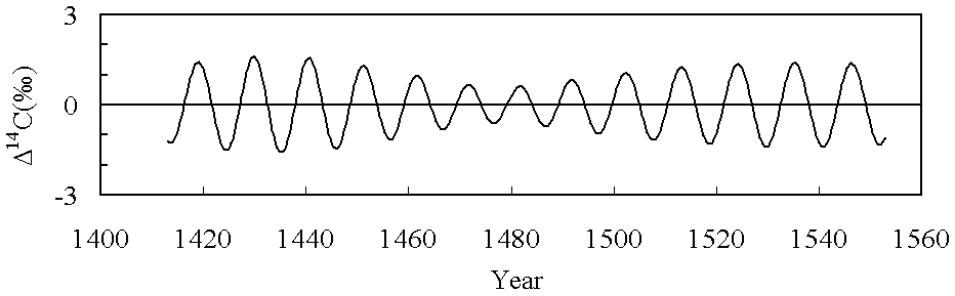

Figure 4 Variation of the amplitude of 11-yr period

Schwabe cycle was stretched by several years during the period when the 11-yr cycle was suppressed. As is well known from sunspot data, the length of the Schwabe cycle and the intensity of solar activity have an anti-correlation (Clough 1905; Baliunas and Soon 1995). This also supports the view that the sun was very quiet during the middle 50 yr of the Spoerer Minimum. The same feature of a lengthened and weakened 11-yr cycle has been also reported for the Maunder Minimum (Peristykh and Damon 1998). This feature might be common to solar activity during the grand minima, though our data for the Spoerer Minimum is as yet incomplete and can be improved. We also have already begun measurements relevant to the Maunder Minimum using a Japanese cedar tree. These comparisons will bring us more information on the characteristics of solar variations during the grand minima.

CONCLUSION

The variation of solar activity during the Spoerer Minimum has been surveyed by measuring the ^{14}C content in annual tree rings. As a result, the existence of the 11-yr cycle with an amplitude around 1.5‰ has been confirmed in the variation of ^{14}C concentration in the beginning and in the end of the Spoerer Minimum. The 11-yr cycle was suppressed around the middle 50 yr of the minimum. During this period, solar activity appears to have been most weakened, and the 11-yr cycle might have been stretched by several years. This feature is similar to that found in the Maunder Minimum. Further measurements will clarify the features of solar activity during these minima in greater detail.

ACKNOWLEDGEMENTS

We would like to thank Prof J Beer for helpful discussions and Prof K Kimura for providing ring-width data concerning dendrochronology. We also thank Sir Ian Axford for his careful reading of the manuscript. This work is supported by a Grant-in-Aid for Scientific Research (B) from the Japan Society for the Promotion of Sciences (JSPS). HM's work is supported by a Grant-in-Aid for JSPS Fellows.

REFERENCES

Baliunas S, Soon W. 1995. Are variations in the length of the activity cycle related to changes in brightness in solar-type stars? *Astrophysical Journal* 450:896.

Clough HW. 1905. Solar rotation and cycle length. *Astrophysical Journal* 22:42.

Hoyt D, Schatten KH. 1998. Group sunspot numbers: a new solar activity reconstruction. *Solar Physics* 181: 491.

Kitagawa H, Masuzawa T, Nakamura T, Matsumoto E. 1993. A batch preparation method for graphite targets with low background for AMS ^{14}C measurements. *Radiocarbon* 35(3):295–300.

Peristykh AN, Damon PE. 1998. Modulation of atmospheric ^{14}C concentration by the solar wind and irradiance components of the Hale and Schwabe solar cycles. *Solar Physics* 177:343.

Stuiver M, Reimer PJ, Bard E, Beck JW, Burr GS, Hughen KA, Kromer B, McCormac FG, van der Plicht J, Spurk M. 1998. INTCAL98 radiocarbon age calibration, 24,000–0 cal BP. *Radiocarbon* 40(3):1041–83.

RADIOCARBON, Vol 46, Nr 2, 2004, p 969–978

A ^{14}C CALIBRATION WITH AMS FROM 3500 TO 3000 BC, DERIVED FROM A NEW HIGH-ELEVATION STONE-PINE TREE-RING CHRONOLOGY

Franz Dellinger[1] • Walter Kutschera[1,2] • Kurt Nicolussi[3] • Peter Schießling[3] Peter Steier[1] • Eva Maria Wild[1]

ABSTRACT. High-precision radiocarbon accelerator mass spectrometry (AMS) measurements of a new high-altitude stone-pine tree-ring chronology from the European Alps were performed for a 500-yr stretch in the second half of the 4th millennium BC. A ^{14}C calibration curve with a typical 1-σ uncertainty of about 20 ^{14}C yr was achieved. Although the general agreement of our data set with INTCAL98 is very good (confirming once more that INTCAL98 is also proper for calibration of samples of extraordinary sites), we found small deviations of 17 ± 5 ^{14}C yr, indicating possible seasonal effects of the delayed growing season at high altitude.

INTRODUCTION

It is well known that ^{14}C calibration with tree rings is an indispensable prerequisite for accurate radiocarbon dating. It provides the absolute time reference for ^{14}C content in the atmosphere during the past 12,000 yr. Although the global uniformity of $^{14}C/^{12}C$ isotope ratios in atmospheric CO_2 is a well-established fact, small deviations from the INTCAL98 calibration curve (Stuiver et al. 1998) have been recently reported (Kromer et al. 2001; Manning et al. 2001; Reimer 2001). In a steep section of the calibration curve between 850 BC and 750 BC, a shift of ~30 yr was obtained by comparing INTCAL98 with a ^{14}C calibration based on a (floating) tree-ring sequence of junipers from Anatolia, Turkey (*Juniperus excelsea* and *Juniperus foetidissima*). Kromer et al. (2001) pointed out that this small shift may have been caused by a regional $^{14}CO_2$ offset linked to the different growing season of junipers as compared to German and Irish oaks used for INTCAL98.

In the present work, we performed high-precision ^{14}C AMS measurements for a new high-altitude tree-ring chronology of stone pines (*Pinus cembra L.*) (Nicolussi and Schießling 2001, 2002). Stone pines are the typical trees one finds at the timberline in the central parts of the European Alps (Figure 1). Our measurements covered the time period from 3500 BC to 3000 BC. On one hand, this time period is interesting since it includes the famous Iceman "Ötzi," who lived around 3200 BC in the same Alpine region where the stone pines were collected. On the other hand, the calibration curve has similar steep sections as the juniper curve mentioned above, and a different growing season of the stone pines, as compared to the low-altitude German and Irish oaks of INTCAL98, suggest another possible observation of a regional $^{14}CO_2$ offset. A prerequisite for such a comparison is a precision of ^{14}C AMS measurements comparable to beta counting. How this could be accomplished at VERA is described separately (Steier et al., these proceedings).

THE STONE-PINE TREE-RING CHRONOLOGY

The basis for our investigations was the new high-elevation stone-pine (*Pinus cembra L.*) tree-ring chronology established at the Institute of High Mountain Research of the University of Innsbruck (Nicolussi and Schießling 2001, 2002). Until recently, absolutely dated multi-millennial chronologies (such as those existing for German and Irish oaks) did not exist in the Alps. The stone-pine

[1]Vienna Environmental Research Accelerator (VERA), Institut für Isotopenforschung und Kernphysik, Universität Wien, Währingerstrasse 17, A-1090 Wien, Austria.
[2]Corresponding author. Email: walter.kutschera@univie.ac.at.
[3]Institut für Hochgebirgsforschung, Universität Innsbruck, Innrain 52, A-6020 Innsbruck, Austria.

Proceedings of the 18th International Radiocarbon Conference, edited by N Beavan Athfield and R J Sparks
RADIOCARBON, Vol 46, Nr 2, 2004, p 969–978

Figure 1 Fully-grown stone pine (*Pinus cembra L.*) near the timberline in the European Alps. (Photo courtesy of W Kutschera, 2003). As seen in this picture, the tree literally grows on a rock, hence the term "stone" pine seems appropriate.

chronology can be used as the dating base for the establishment of Alpine event records (e.g. Holocene glacier fluctuations, avalanche activity) and the reconstruction of summer temperatures (Nicolussi and Schießling 2001), respectively. In the Alps, there is always enough precipitation at timberline sites, and the main limiting factor for tree growth is the summer temperature. Therefore, from the tree-ring-width pattern, the information of the summer temperatures can be extracted.

In the course of several years, about a hundred subfossil logs were collected near the timberline, above 1900 m above sea level (asl). The logs came from 26 sites in the Hohe Tauern, Stubaier Alps, Zillertaler Alps, Ötztaler Alps, and in the Ortler Group. These collecting sites are in the general vicinity of the location where the famous prehistoric Iceman Ötzi was found (Kutschera et al. 2003). Stone pines were collected almost exclusively; the number of spruce (*Picea abies*) was only about 1% of the whole data set.

A continuous chronology was established ranging back more than 7000 yr, from the present day until 5125 BC (Figure 2). The mean replication of this continuous part is approximately 20, although some weaker replicated sections also exist. Including 3 other (floating) sections, the Alpine conifer tree-ring chronologies now cover nearly the entire Holocene (Figure 2).

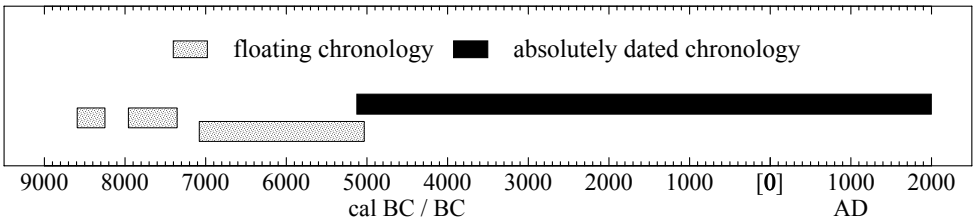

Figure 2 Current state of the central Eastern Alpine tree-ring chronologies. The absolutely dated continuous stone-pine chronology is about 7100 yr long and extends back to 5125 BC. It is based on approximately 430 subfossil logs and also includes more than 300 tree-ring series of living trees and sub-recent logs, respectively, in the latest section. The temporal positions of the floating chronologies have been assessed by wiggle-matching of ^{14}C dates. These 3 chronologies are based on about 50 subfossil logs of the species *Pinus cembra* (stone pine), *Larix decidua* (European larch), and *Picea abies* (Norway spruce).

SAMPLE EXTRACTION, PREPARATION, AND PRETREATMENT

All trunks investigated in the present work originated from sites between 2150 and 2300 m asl (Table 1). The samples were selected at the Institute for High Mountain Research from the inside of the logs (far away from exposed surfaces). Water was used as a contrast amplifier for tree-ring counting, instead of the usual chalk to exclude possible contamination. For each sample, several cubic cm of wood were cut out and sent to the VERA Laboratory. For safe storage, the samples were first vacuum-dried at 60 °C overnight. The dry mass was between 0.6 and 1.4 g. For proper comparison with the INTCAL98 data set (Stuiver et al. 1998), which is given in decadal steps, we used 50 decadal tree-ring sections beginning with 3499–3490 BC until 3009–3000 BC.

Table 1 Characterization of the tree-ring samples from stone pines used in this work.

Tree log identifier	Collection site	Site coordinates	Elevation (m asl)	Tree rings (n)	Tree-ring period (yr BC)	Ring-width range (mm)	Decadal sections used
KRO-2	Krottenlacke Windachtal/Stubaier	46°57′15″N 11°06′05″E	2278	118	3508–3391	0.715–2.103	9
SSM-84	Schwarzsteinmoor Zillertaler Alps	47°01′45″N 11°48′55″E	2150	134	3467–3334	0.136–2.501	6
EBA-47	Ebenalm Ötztaler Alps	47°01′15″N 10°57′55″E	2170	111	3351–3241	0.637–3.353	6
SSM-102	Schwarzsteinmoor Zillertaler Alps	47°01′45″N 11°48′55″E	2150	307	3312–3006	0.124–0.958	10
EBA-46	Ebenalm Ötztaler Alps	47°01′15″N 10°57′55″E	2170	172	3211–3040	0.314–2.733	9
GDM-40	Daunmoränensee Kaunertal/Ötztaler Alps	46°53′40″N 10°43′30″E	2295	355	3188–2834	0.416–1.553	10

From each sample material, a 1-mm-thick slice was cut from the trunk axis by using a fretsaw. The (usually oiled) saw blades were washed in acetone in an ultra-sonic bath for 10 min and then heated for 1 hr at 550 °C in the furnace. A stick of wood was then cut out with a scalpel for tree rings covering exactly 10 yr. A thickness of 1 to 2 mm was chosen so that the mass of the wood stick was slightly above 10 mg (see Figure 3). In this step, care was taken that the chosen wood stick did not contain any visible resin channels.

Our standard acid-base-acid procedure was used for sample pretreatment (1M HCl at 60 °C for 1 hr, 0.1 M NaOH at 60 °C for 1 hr, 1M HCl at 60 °C for 1 hr). Typically, this procedure resulted in a loss of sample weight of a few percent. The good state of preservation of the sample was indicated by the fact that very little humic acids were visible. The pretreated samples were vacuum-dried overnight.

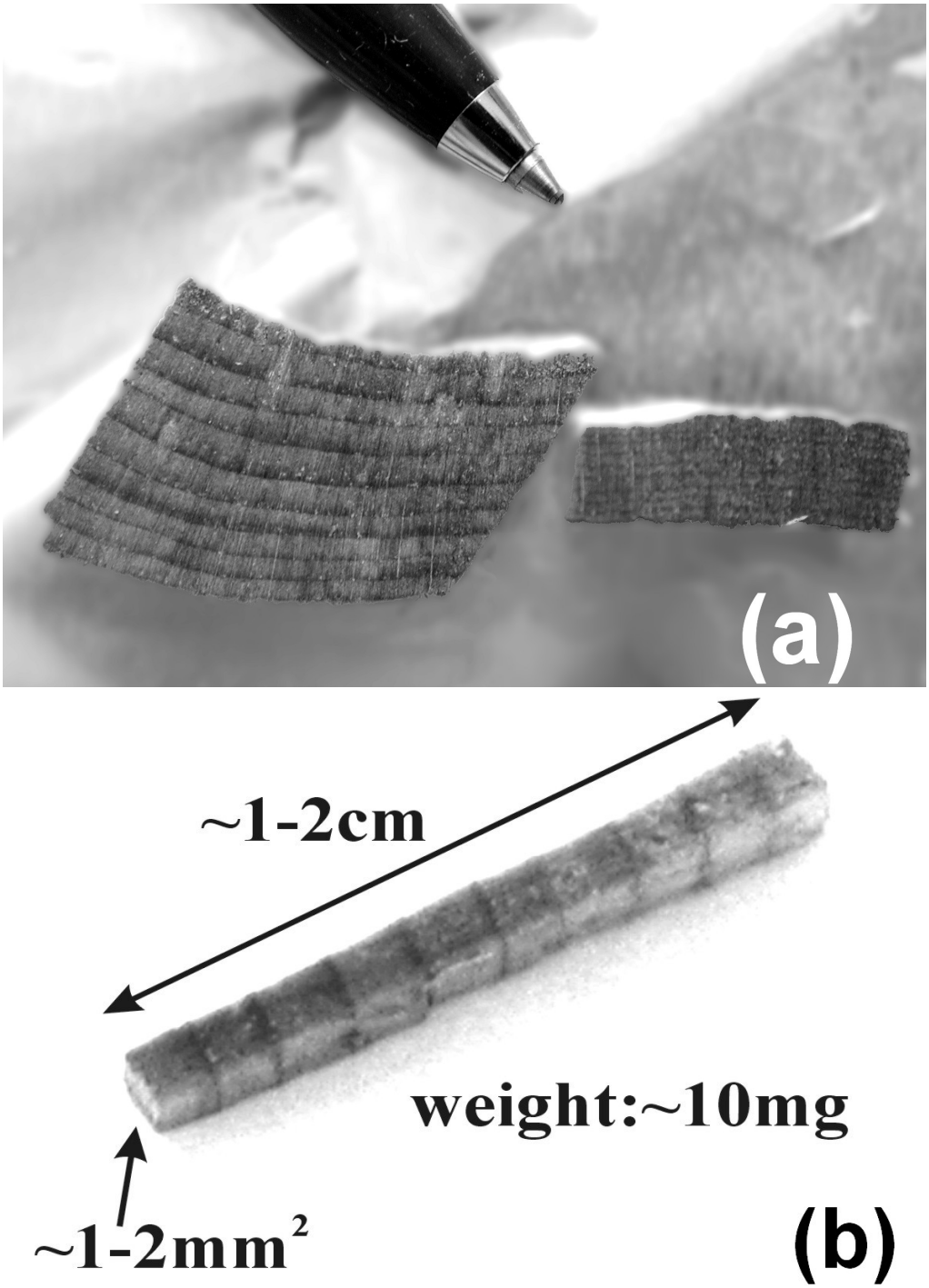

Figure 3 Typical decadal wood samples: (a) 2 pieces of wood with different tree ring widths, from which sticks shown in (b) were cut for sample preparation. The sticks were converted into graphite samples for the AMS measurement. The contribution of the various tree rings to the sample mass depends on the ring width.

The combustion of the sample material took place at 900 °C for 4 hr in a flame-sealed quartz tube containing 1g CuO as oxidant and some silver wire. The sample CO_2 was then reduced to elemental carbon at 610 °C using H_2 and an iron catalyst (Vogel et al. 1984). The mixture of graphite and catalyst was divided and pressed into 2 aluminium target holders suitable for our 40-position MC-SNICS ion source. Both sputter targets were measured.

AMS MEASUREMENTS

The measurement of the stone-pine samples was performed in 5 separate AMS beam times (runs). Run 1 only contained material of the "KRO-2" tree slice, while in run 2, 3, and 4, material of all other tree slices was used. An additional run (run 5) was performed for samples which showed a deviation of more than 2 σ from INTCAL98 in the preliminary evaluation of runs 1 to 4. Samples which got lost in chemical pretreatment were also measured in run 5.

In run 1, IAEA C-3 cellulose (129.41 ± 0.06 pMC) and IAEA C-5 wood (23.05 ± 0.02 pMC) were used as standard materials (Rozanski et al. 1992). It turned out to be advantageous to use wood of 10 tree rings (3239–3230 BC) of the dendro-dated FIRI-D wood as standard material instead of the C-5 wood in the remaining runs. The FIRI-D wood from the Fourth International Radiocarbon Intercomparison (Scott 2003) has a higher pMC value (57.17 ± 0.06) and the wood chips of FIRI-D behave more similar to the actual samples than the powdered C-5 wood. For each run, 2 chemically independent standards were produced from FIRI-D wood and C-3 cellulose, respectively. For the standards, splits from the same graphite were exchanged between the runs to increase the diversity of standard material. After run 2, the idea arose to permute also the doublets of the samples with another wheel. Hence, we decided to mount single samples in the target wheel of run 3 and measure all the doublets in run 4.

Compared to routine measurements which usually take 24 hr, the stone-pine measurements lasted approximately 3 days per run. For such long measurement periods, it is necessary to retune the AMS facility once per day (Steier et al. 2004).

DATA EVALUATION AND RESULTS

Each run is evaluated separately using the present version of the program "EVALGEN" (Puchegger et al. 2000), which is also used for routine measurements. For yet unknown reasons, the quality of the data varied for the different "tunings" of 1 run, judged from the reproducibility of the sample results and from the agreement of the standards with the nominal values. The evaluation program takes this into account by assigning additional uncertainties to the measured isotope ratios. So the final precision may even improve if data from such a tuning are left out. In some cases, the reason for the uncertainty can be identified and a workaround can be found. For example, the first tuning of run 5 could be used after normalizing to the low energy $^{12}C^-$ current instead of the usual $^{12}C^{3+}$ current. Obviously, the accelerator transmission of the $^{12}C^-$ beam was not constant for this setup, but the ^{13}C and ^{14}C were not affected.

From 12 chemically independent ABA pretreatments of the standards, one was rejected as an outlier because all targets of this material showed a consistent deviation of ~50 ^{14}C yr (which is more than 2 σ) in all 3 runs where this graphite was used. We think that contamination during the pretreatment is the most likely reason. Additionally, 1 single standard target was excluded in run 4. The same graphite in run 3 showed regular results. A possible reason for a deviation of 1 single target may be contamination during target pressing.

The exclusion of certain standards is no problem for measurement precision. At least 8 standards are mounted in each target wheel. Even if 2 standards are excluded (run 4), the 6 remaining are sufficient to calculate external uncertainties.

The final results of all stone-pine measurements are listed in Table 2. The dendro date in column 2 is the medium of the respective 10-yr tree-ring section. The ^{14}C ages of run 3 and run 4 are combined by building the weighted mean treated as 1 measurement (run 3+4) in the following.

For most samples, a total 1-σ uncertainty of less than 20 ^{14}C yr could be achieved, corresponding to an overall precision of 2.5‰ for the ^{14}C determination. Compared to routine ^{14}C measurements, this precision is mainly due to longer measurement times and the larger number of standards and their arrangement.

DATA INTERPRETATION AND ANALYSIS

The overall agreement of the stone-pine measurements with INTCAL98 is very good (see Figure 4). However, by taking a closer look at the curve, small offsets in certain sections can be recognized. First, the whole data set of run 1 tends to be shifted to older ^{14}C ages. Second, in the section of approximately 3410–3260 BC (i.e. the steep decline of the calibration curve), the data are shifted to younger ^{14}C ages, independent from the measurement in which they were obtained. For the data of run 5, this trend to younger values remains for the calendar section 3260–3000 BC, while the data points of run 2 and run 3+4 are distributed almost equally to older and younger ages. Although these shifts can be clearly seen, they have to be carefully interpreted. Such offsets may come from systematic errors in the measurements and would then not be meaningful in terms of a paleoclimatic interpretation.

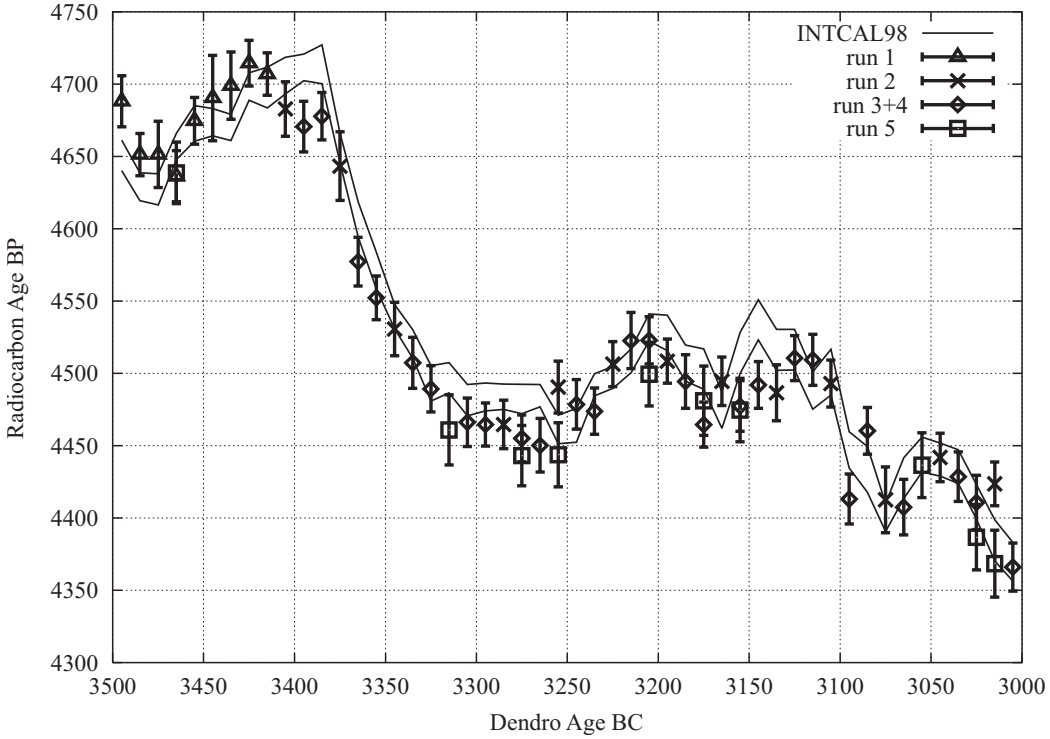

Figure 4 Comparison of the results from the present work (run 1, 2, 3+4, and 5) with the INTCAL98 calibration curve

Table 2 Comparison of the ^{14}C results for stone-pine samples with INTCAL 98.

Dendro data		VERA data				INTCAL 98
Tree log identifier	Date BC	VERA nr	Run #	$\delta^{13}C$ (‰)	^{14}C age (BP)	INTCAL 98 (BP)
KRO-2-1	3495	V2384/1	1	–18.7 ± 0.5	4688 ± 18	4650.7 ± 10.5
KRO-2-2	3485	V2385/1	1	–18.6 ± 0.6	4651 ± 15	4629.1 ± 9.6
KRO-2-3	3475	V2386/1	1	–18.3 ± 0.4	4651 ± 23	4627.2 ± 10.7
KRO-2-4	3465	V2387/1	1	–18.9 ± 0.6	4636 ± 18	4656.8 ± 9.0
KRO-2-4	3465	V2387/2	5	–22.2 ± 0.3	4639 ± 21	4656.8 ± 9.0
KRO-2-5	3455	V2388/1	1	–19.5 ± 0.5	4675 ± 16	4672.9 ± 12.3
KRO-2-6	3445	V2389/1	1	–18.7 ± 0.8	4690 ± 30	4673.7 ± 9.4
KRO-2-7	3435	V2390/1	1	–19.7 ± 1.1	4699 ± 23	4670.0 ± 9.0
KRO-2-8	3425	V2391/1	1	–18.2 ± 0.5	4714 ± 16	4698.4 ± 9.5
KRO-2-9	3415	V2392/1	1	–19.7 ± 0.6	4707 ± 15	4697.6 ± 14.1
SSM-84-1	3405	V2393/1	2	–19.8 ± 0.6	4683 ± 19	4705.8 ± 12.7
SSM-84-2	3395	V2394/1	3+4	–21.8 ± 0.4	4671 ± 18	4711.5 ± 9.2
SSM-84-3	3385	V2395/1	3+4	–22.2 ± 0.3	4678 ± 16	4713.7 ± 13.4
SSM-84-4	3375	V2396/1	2	–22.8 ± 1.0	4643 ± 24	4655.9 ± 10.2
SSM-84-5	3365	V2397/1	3+4	–21.2 ± 0.3	4577 ± 17	4606.4 ± 12.1
SSM-84-6	3355	V2398/1	3+4	–21.6 ± 0.3	4552 ± 15	4571.0 ± 12.6
EBA-47-1	3345	V2399/1	2	–22.7 ± 0.4	4531 ± 18	4539.3 ± 8.4
EBA-47-2	3335	V2400/1	3+4	–21.5 ± 0.3	4507 ± 18	4520.3 ± 9.9
EBA-47-3	3325	V2401/1	3+4	–22.1 ± 0.3	4489 ± 16	4493.1 ± 12.2
EBA-47-4	3315	V2402/1	5	–23.1 ± 0.2	4461 ± 24	4497.0 ± 10.5
EBA-47-5	3305	V2403/1	3+4	–23.0 ± 0.3	4466 ± 17	4481.4 ± 10.8
EBA-47-6	3295	V2404/1	3+4	–22.6 ± 0.3	4465 ± 15	4483.7 ± 9.6
SSM-102-1	3285	V2405/1	2	–23.3 ± 0.2	4465 ± 17	4483.8 ± 8.7
SSM-102-2	3275	V2406/1	3+4	–20.8 ± 0.2	4455 ± 16	4482.2 ± 10.2
SSM-102-2	3275	V2406/2	5	–22.8 ± 0.4	4443 ± 21	4482.2 ± 10.2
SSM-102-3	3265	V2407/1	3+4	–23.4 ± 0.3	4450 ± 19	4484.6 ± 7.7
SSM-102-4	3255	V2408/1	2	–24.3 ± 0.3	4490 ± 18	4461.2 ± 9.9
SSM-102-4	3255	V2408/2	5	–24.7 ± 1.8	4444 ± 22	4461.2 ± 9.9
SSM-102-5	3245	V2409/1	3+4	–21.7 ± 0.3	4479 ± 17	4464.1 ± 11.7
SSM-102-6	3235	V2410/1	3+4	–22.0 ± 0.3	4474 ± 16	4492.1 ± 7.7
SSM-102-7	3225	V2411/1	2	–22.7 ± 0.2	4506 ± 16	4497.2 ± 7.6
SSM-102-8	3215	V2412/1	3+4	–21.2 ± 0.3	4523 ± 19	4508.7 ± 8.2
SSM-102-9	3205	V2413/1	3+4	–22.5 ± 0.3	4523 ± 16	4531.7 ± 9.5
SSM-102-9	3205	V2413/2	5	–22.4 ± 0.2	4499 ± 22	4531.7 ± 9.5
SSM-102-10	3195	V2414/1	2	–22.9 ± 0.5	4508 ± 15	4527.9 ± 12.2
EBA-46-1	3185	V2415/1	3+4	–23.5 ± 0.4	4494 ± 19	4507.1 ± 12.5
EBA-46-2	3175	V2416/1	3+4	–24.6 ± 0.3	4465 ± 16	4503.0 ± 14.0
EBA-46-2	3175	V2416/2	5	–25.5 ± 0.8	4481 ± 24	4503.0 ± 14.0
EBA-46-3	3165	V2417/1	2	–26.1 ± 0.8	4495 ± 19	4474.7 ± 12.6
EBA-46-4	3155	V2418/1	3+4	–24.7 ± 0.3	4477 ± 18	4514.2 ± 14.1
EBA-46-4	3155	V2418/2	5	–24.4 ± 0.5	4475 ± 22	4514.2 ± 14.1
EBA-46-5	3145	V2419/1	3+4	–23.1 ± 0.3	4492 ± 16	4537.0 ± 13.9
EBA-46-6	3135	V2420/1	2	–25.3 ± 0.5	4487 ± 19	4516.3 ± 14.2
EBA-46-7	3125	V2421/1	3+4	–22.0 ± 0.3	4511 ± 16	4516.4 ± 14.1
EBA-46-8	3115	V2422/1	3+4	–24.0 ± 0.4	4509 ± 18	4488.1 ± 12.9
EBA-46-9	3105	V2423/1	2	–24.9 ± 0.4	4493 ± 16	4500.8 ± 15.8
GDM-40-1	3095	V2424/1	3+4	–22.9 ± 0.3	4413 ± 17	4447.1 ± 12.6
GDM-40-2	3085	V2425/1	3+4	–22.1 ± 0.3	4460 ± 16	4433.6 ± 15.8
GDM-40-3	3075	V2426/1	2	–24.6 ± 0.2	4413 ± 23	4400.4 ± 9.7
GDM-40-4	3065	V2427/1	3+4	–23.3 ± 0.3	4407 ± 19	4427.6 ± 14.1
GDM-40-5	3055	V2428/1	5	–23.6 ± 0.8	4437 ± 22	4443.9 ± 12.1
GDM-40-6	3045	V2429/1	2	–22.9 ± 0.2	4442 ± 17	4440.4 ± 11.4
GDM-40-7	3035	V2430/1	3+4	–24.1 ± 0.3	4429 ± 17	4435.5 ± 11.7
GDM-40-8	3025	V2431/1	3+4	–23.1 ± 0.4	4411 ± 19	4411.2 ± 12.0
GDM-40-8	3025	V2431/2	5	–23.6 ± 1.3	4387 ± 23	4411.2 ± 12.0
GDM-40-9	3015	V2432/1	2	–23.5 ± 0.2	4424 ± 15	4384.5 ± 14.2
GDM-40-9	3015	V2432/2	5	–22.2 ± 0.8	4368 ± 23	4384.5 ± 14.2
GDM-40-10	3005	V2433/1	3+4	–21.8 ± 0.3	4366 ± 17	4369.8 ± 13.3

In the statistical analysis, we wanted to investigate the significance of the deviations of the stone-pine data. In the first step, we calculated the difference between every stone-pine data point and the associated INTCAL98 data point. Subsequently, the mean deviation for every run was determined: +15.1 ^{14}C yr for run 1, –0.7 ^{14}C yr for run 2, –15.1 ^{14}C yr for run 3+4, and –25.3 ^{14}C yr for run 5. These offsets may originate in a systematic error which is correlated for all samples in a whole run. This error cannot be reduced by averaging and is the same for each individual sample and for the average of a complete measurement. However, this uncertainty cancels out if the average bias of a run is subtracted from the data points. In the corrected data, it can be explored if there are significant differences between the flat part of the calibration curve and the region with the steep decline. Unfortunately, the samples of run 1 cover only a short calendar period and not even 1 single data point lies in the steep part of the curve. As a consequence, these data could not be utilized in the calculations above.

In Figure 5, the deviation of the offset-corrected data points from the INTCAL98 curve are plotted. The error bars include the internal uncertainty of the stone-pine data points and the uncertainty of INTCAL98. The plot suggests that deviations from INTCAL98 may exist. For a statistical check, we divided the data set into 2 parts. The data points in the steep part between 3410 and 3260 BC generally seem to be located below the average, while in the flatter region from 3260 to 3000 BP, the deviation is slightly positive. The solid lines in the plot are the weighted mean values in the 2 regions. The mean values confirm the visual impression: the resulting difference of the 2 regions of 16.6 ± 4.8 yr is statistically significant at 3.4 σ.

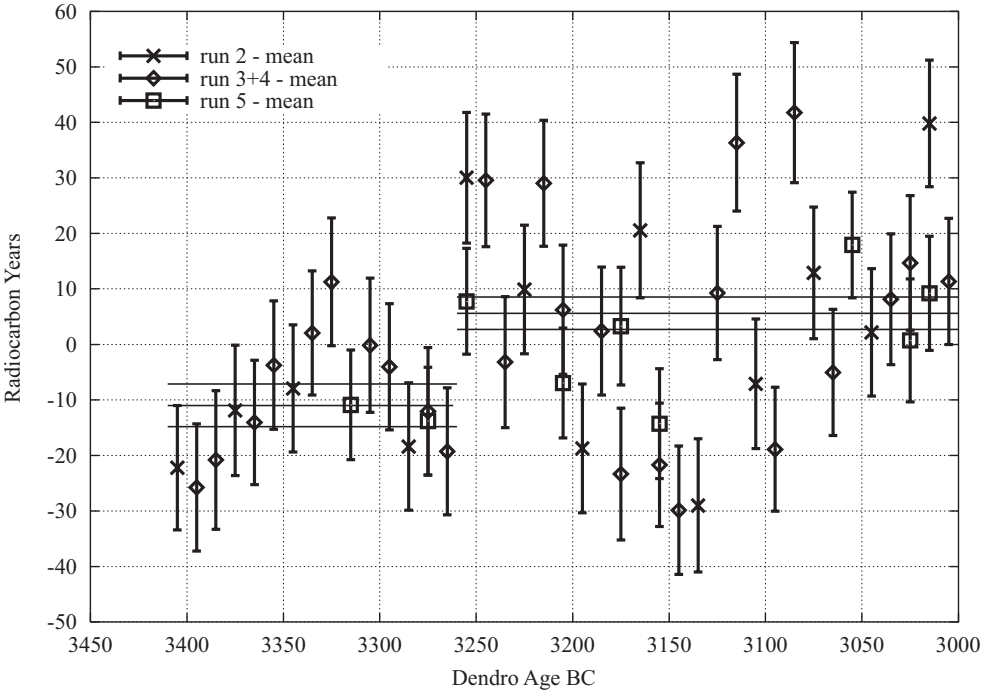

Figure 5 Difference between the ^{14}C calibration from the stone pine and INTCAL98. For details of the procedure for how to arrive at the different offsets indicated by the horizontal lines (±1 σ), see text.

To investigate whether the uncertainties of the data points in each of the 2 regions are realistic, a χ^2 test was performed. For the region 3410–3260 BC consisting of 16 data points, a χ^2 of 5.86 was determined (25.0 is allowed for 95% confidence). Concerning the region 3260–3000 BC, the test resulted in a χ^2 of 39.1 (45.0 is allowed at 95% confidence for 32 data points).

POSSIBLE EXPLANATION FOR THE SMALL SHIFT IN CALIBRATION

Interestingly, similar deviations have been observed by Kromer et al. (2001) and Manning et al. (2001) in Turkish junipers. At a sharp drop of the calibration curve around 800 BC, the data of Turkish junipers were shifted by about 30 yr towards older ^{14}C ages relative to the (mainly) German oaks of INTCAL98. It is argued that the reason for this deviation lies in the seasonal variability of atmospheric ^{14}C. In Figure 6, our understanding of the emerging deviations based on the discussion in Kromer et al. (2001) is illustrated.

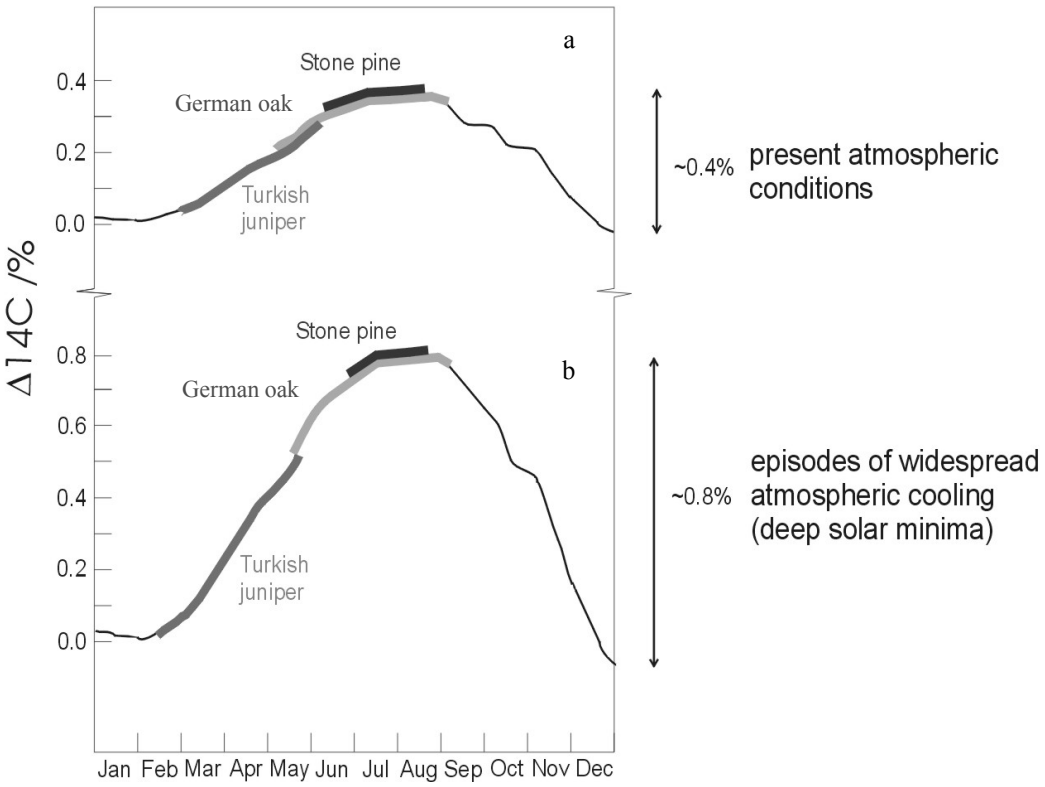

Figure 6 Our understanding of Kromer et al. (2001). The preindustrial/prebomb seasonal variability of ^{14}C is shown for atmospheric conditions similar to the present ones (a), and for deep solar minima which are also episodes of widespread atmospheric cooling (b). The different growth cycles of the various tree species is manifested in the $\Delta^{14}C$. In (b), the seasonal variability is larger and the colder climate causes later growth of the stone pine, whereas higher precipitation allows earlier growth of the Turkish juniper. This increases the differences between the 3 species.

From modeling bomb ^{14}C (Hesshaimer 1997) and from present-day tropospheric ^{14}C monitoring networks (Levin and Hesshaimer 2000), variations of 4‰ between low winter/spring and maximum summer activity have been deduced (Kromer et al. 2001). Depending on the rate of carbon uptake during the growing season and the phase relation of the growing seasons between the different

regions, different parts of this seasonal cycle are seen. Turkish junipers, for instance, start their main wood production earlier in spring than German oaks do. Hence, due to the intra-annual variations of the seasonal cycle, the wood of the Turkish junipers is depleted in ^{14}C compared to the wood of German oaks. As the amplitude of the seasonal cycle is proportional to the ^{14}C influx from the stratosphere, the effect of intra-annual variations should be best observable during times of "deep" solar minima. In these times, the amplitude of the seasonal cycle is supposed to be twice as large as in the average of the 11-yr solar cycle (Kromer et al. 2001; Masarik and Beer 1999). Such periods of enhanced ^{14}C production appear as a steep decline in the calibration curve.

Following the previous argument, the stone pines should be higher in ^{14}C than German oaks and appear younger due to the later growing season at high elevation sites. That agrees with the observed offset in our measurement.

CONCLUSIONS

To our knowledge, this is the first high-altitude calibration curve which has been established by AMS. In our measurements, we achieved a typical 1-σ uncertainty of about 20 ^{14}C yr (2.5‰) at a reasonable increase of effort. The results of the stone-pine measurements confirm once more that INTCAL98 is also proper for calibration of samples of extraordinary sites, such as the timberline in the Alps. Although the agreement of our data set with INTCAL98 is very good, at the edge of statistical analysis we found small deviations of 17 ± 5 ^{14}C yr. Considering the argumentation of Kromer et al. (2001), this shift seems reasonable.

REFERENCES

Hesshaimer V. 1997. Tracing the global carbon cycle with bomb radiocarbon. [PhD dissertation]. Heidelberg: University of Heidelberg.

Kromer B, Manning S, Kuniholm P, Newton M, Spurk M, Levin I. 2001. Regional $^{14}CO_2$ offsets in the troposphere: magnitude, mechanism, and consequences. *Science* 294:2529–32.

Kutschera W, Müller W. 2003. "Isotope language" of the Alpine Iceman investigated with AMS and MS. *Nuclear Instruments and Methods in Physics Research B* 204:705–19.

Levin I, Hesshaimer V. 2000. Radiocarbon—a unique tracer of global carbon cycle dynamics. *Radiocarbon* 42(1):69–80.

Manning S, Kromer B, Kuniholm P, Newton M. 2001. Anatolian tree rings and a new chronology for the East Mediterranean Bronze-Iron Ages. *Science* 294:2532–5.

Masarik J, Beer J. 1999. Simulation of particle fluxes and cosmogenic nuclide production in the earth's atmosphere. *Journal of Geophysical Research* 104D: 12,099–111.

Nicolussi K, Schießling P. 2001. Establishing a multimillennial *Pinus cembra* chronology for the central Eastern Alps, Conference "Tree Rings and People," 22–26 September 2001, Davos, Switzerland. http://www.wsl.ch/forest/dendro2001.

Nicolussi K, Schießling P. 2002. A 7000-year-long continuous tree-ring chronology from high-elevation sites in the central Eastern Alps. *Dendrochronology, Environmental Change and Human History*, Abstracts: 251–252, 6th International Conference on Dendrochronology, Quebec City, Canada, 22–27 August 2002.

Puchegger S, Rom W, Steier P. 2000. Automated evaluation of ^{14}C AMS measurements. *Nuclear Instruments and Methods in Physics Research B* 172:274–80.

Reimer JR. 2001. A new twist in the radiocarbon tale. *Science* 294:2494–5.

Rozanski K, Stichler W, Gonfiantini R, Scott EM, Beukens R, Kromer B, van der Plicht J. 1992. The IAEA ^{14}C intercomparison exercise 1990. *Radiocarbon* 34(3):506–19.

Scott EM. 2003. The Fourth International Radiocarbon Intercomparison (FIRI). *Radiocarbon* 45(2):135–291.

Steier P, Dellinger F, Kutschera W, Rom W, Wild EM. 2004. Pushing the precision limit of ^{14}C measurements with AMS. *Radiocarbon*, these proceedings.

Stuiver M, Reimer PJ, Bard E, Beck JW, Burr GS, Hughen KA, Kromer B, McCormac G, van der Plicht J, Spurk M. 1998. INTCAL98 radiocarbon age calibration, 24,000–0 cal BP. *Radiocarbon* 40(3):1041–83.

Vogel JS, Southon JR, Nelson DE, Brown T. 1984. Performance of catalytically condensed carbon for use in accelerator mass spectrometry. *Nuclear Instruments and Methods in Physics Research B* 5:289–93.

RADIOCARBON, Vol 46, Nr 2, 2004, p 979–985

BAYESIAN PERIODIC SIGNAL DETECTION APPLIED TO INTCAL98 DATA

V Palonen[1] • P Tikkanen

Accelerator Laboratory, P.O. Box 43, FIN-00014 University of Helsinki, Finland.

ABSTRACT. A Bayesian multiple-frequency model has been developed for spectral analysis of data with unknown correlated noise. A description of the model is given and the method is applied to decadal atmospheric INTCAL98 $\Delta^{14}C$ data. The noise of the INTCAL98 data is found to be red, and there seems to be no support for continuous harmonic frequencies in the data.

INTRODUCTION

The discrete Fourier transform (DFT) has been shown to be analogous to a Bayesian one-frequency model with several additional assumptions (Bretthorst 1988). The one-frequency model has been extended to take into account multiple sinusoids (Andrieu et al. 2001; Bretthorst 2003). Already these Bayesian models for spectral analysis have advantages compared to DFT. However, the analysis of proxy data with these models is hard because the models use parametric functions to handle the trend in the data. Their use is also doubtful because the models assume uncorrelated noise.

The power spectrum of uncorrelated noise is uniformly distributed for all frequencies. This is why it is also called white noise. Correlated noise has a power spectrum with more weight in the lower frequencies and is, therefore, called red noise. There is considerable evidence for red noise in the climatic time series (Gilman et al. 1962), as also a glance at power spectra of most proxies will reveal.

Our previous Bayesian model for spectral analysis assumed that the trend is random walk, i.e., we assumed red noise (Palonen and Tikkanen 2004). While it can be argued that this is a good assumption, we cannot be sure that the noise is red either. In this work, we develop a new Bayesian model where the noise color is allowed to vary. As an example of the new model, we analyze the decadal INTCAL98 atmospheric $\Delta^{14}C$ data.

MODEL

Let $\boldsymbol{M} = \{m_1,\ldots, m_N\}$ be the set of N measured data values with the corresponding uncertainties $\boldsymbol{S} = \{s_1,\ldots, s_N\}$ recorded at different times $\boldsymbol{T} = \{t_1,\ldots, t_N\}$. It is assumed that there is no uncertainty in $\boldsymbol{T}$.

We will take the measurements $\boldsymbol{M}$ to consist of a parametric function $g(t, \Theta)$ and noise:

$$m_i = g_i + \varepsilon_i + x_i \quad (1),$$

where $g_i = g(t_i, \Theta)$ and Θ is a vector containing all model parameters. The noise consists of measurement error ε_i, which is taken to be Gaussian white noise with given variances s_i, and of a first-order autoregressive noise x_i. The autoregressive noise represents all else in the data, i.e., the trend. It is given by the following equation:

$$x_i = \alpha x_{i-1} + \nu_i \quad (2),$$

[1]Corresponding author. Email: vesa.palonen@helsinki.fi.

Proceedings of the 18th International Radiocarbon Conference, edited by N Beavan Athfield and R J Sparks
RADIOCARBON, Vol 46, Nr 2, 2004, p 979–985

where ν_i are normally distributed errors and α is the noise correlation coefficient, included as a parameter in the model. This enables analysis of data with noise of unknown color, from uncorrelated white noise ($\alpha = 0$) to heavily correlated red noise ($\alpha = 1$). We assume that only first-order correlations are present and that α is constant for the whole data set. We limit our model to first-order correlations instead of the whole correlation structure matrix in order to keep the model simple and computationally feasible.

Now, we would expect the variance of ν_i to scale linearly with the time step for red noise (random walk), and to remain constant for white noise. We will, therefore, include a linear change from a constant variance to a time-step-scaled variance according to the noise color parameter α:

$$\nu_i \sim N\left(0, \left(\left|\frac{(t_i - t_{i-1})}{\langle t_j - t_{j-1}\rangle_j}\right| \times \alpha + (1-\alpha)\right)\Sigma^2\right) \tag{3},$$

where Σ is the parameter representing the square root of the variance.

In order to model multiple sinusoids, the function g is taken to be:

$$g(t, k, A_{1,\ldots,k}, \phi_{1,\ldots,k}, f_{1,\ldots,k}, m) = \sum_{j=1}^{k} A_j \sin(2\pi f_j t + \phi_j) + m \tag{4},$$

where k is the number of sinusoids, and A_j, ϕ_j, and f_j are the amplitudes, phases, and frequencies of the sinusoids, and m is the mean value of the data.

From Equations 1 and 2, we get:

$$m_i - g_i - \alpha(m_{i-1} - g_{i-1}) = \varepsilon_i - \alpha\varepsilon_{i-1} + \nu_i \equiv \beta_i \tag{5}.$$

The likelihood, namely, the probability of the data with known parameter values Θ, is then:

$$p(\boldsymbol{M}|\Theta, \boldsymbol{S}, \boldsymbol{T}) = \prod_{i=2}^{N} \frac{1}{\sqrt{2\pi\sigma_{i,\text{tot}}^2}} \exp\left\{\frac{-\beta_i^2}{2\sigma_{i,\text{tot}}^2}\right\} \tag{6},$$

where

$$\sigma_{i,\text{tot}}^2 = s_i^2 + \alpha^2 s_{i-1}^2 + \left(\left|\frac{(t_i - t_{i-1})}{\langle t_j - t_{j-1}\rangle_j}\right| \times \alpha + (1-\alpha)\right)\Sigma^2 \tag{7}.$$

The joint posterior probability distribution for the parameters Θ can now be obtained from Bayes' theorem:

$$p(\Theta|\boldsymbol{M}, \boldsymbol{S}, \boldsymbol{T}) = \frac{p(\Theta)p(\boldsymbol{M}|\Theta, \boldsymbol{S}, \boldsymbol{T})}{p(\boldsymbol{M}|\boldsymbol{S}, \boldsymbol{T})} \tag{8},$$

where $p(\Theta)$ is the combined prior for the parameters and $p(\boldsymbol{M}|\boldsymbol{S}, \boldsymbol{T})$ is a normalization constant.

Table 1 shows the prior types and ranges used for each parameter. Normalized priors were used for all parameters. More information on the selection of priors in spectral analysis can be found in Bretthorst (1988).

Table 1 Priors for the parameters.

Parameter	Symbol	Prior type	Prior range
Number of sinusoids	k	uniform	[0, 10]
Noise color parameter	α	uniform	[−0.1, 1.1]
Standard deviation of RW step	Σ	Σ^{-1}	[0.01, 10]
Data mean	m	uniform	[−100, 300]
Amplitude	A_j	uniform	[0, 50]
Phase	ϕ_j	uniform	[0, 2π]
Frequency	f_j	f_j^{-1}	[1/5000, 1/20]

As usual in Bayesian analyses, inference on the parameters Θ from Equation 8 cannot be made analytically and computational methods are needed.

COMPUTATIONAL METHODS

Inference on the posterior in Equation 8 is done with a reversible jump Markov chain Monte Carlo (MCMC) algorithm.

In MCMC, a chain of parameter space points distributed as the posterior distribution is constructed. This is done by using only the previous point Θ (hence the word Markov) in the chain to propose the next point Θ' at random (hence the words Monte Carlo) and then selecting or rejecting the proposed point according to some acceptance probability that is proportional to the posterior (Gilks et al. 1996). Reversible jump MCMC algorithms are capable of jumping between points in different parameter spaces, e.g., from parameter space of 1 sinusoid to parameter space of 2 sinusoids. In the present implementation, a jump to a new point is realized via one of the following 3 moves (Andrieu 2001); birth of a new frequency, death of an old one, or update of all at the moment existing parameters (normal MCMC move). The new point $\Theta' = (k', \boldsymbol{z}')$ is then accepted with an acceptance probability (Green 1995; Waagepetersen and Sorensen 2001):

$$a(\Theta, \Theta') = \min\left(1, \frac{\text{likelihood}(\Theta')}{\text{likelihood}(\Theta)} \frac{\text{prior}(\Theta')}{\text{prior}(\Theta)} \frac{h(\Theta', \Theta)}{h(\Theta, \Theta')} \left|\frac{\partial(\boldsymbol{z}', \boldsymbol{u}')}{\partial(\boldsymbol{z}, \boldsymbol{u})}\right|\right) \quad (9),$$

where the function $h(\Theta, \Theta')$ is a proposal probability of a MCMC jump from Θ to Θ' with the random vector $\boldsymbol{u}$ used in construction of the new point, e.g., electing the amplitude, phase, frequency, and location of the new frequency. The random vector $\boldsymbol{u}'$ is used to construct Θ from Θ'. Our algorithm differs from the one in Andrieu (2001) in that we also select the location of the new sinusoid among the old ones at random, thereby fulfilling the dimension matching requirement. Further details of the birth and death moves are discussed in the appendix.

The above form of the acceptance probability ensures the reversibility of the MCMC chain, and it has been shown that the chain will converge to the posterior, i.e., the points of the chain will be distributed according to the posterior, when the chain is long enough. When this is the case, calculating the expectation values for the parameters from the chain points, integrating over nuisance parameters, and getting the probability density as a histogram of the points is straightforward. An open problem is when the chain has converged. In this work, 7 separate chains starting from different points in the parameter space were simulated in order to strengthen the conclusion for convergence. The chains gave the same result. Trace plots do not show any problems either.

Our analysis on similar but synthetic data also ensured that the method finds frequencies when they are present. The method produces the synthetic frequencies well, but, as expected, smaller frequen-

cies in red noise begin to be less believable even if present in the synthetic data. We also checked the algorithm without data, i.e., with a constant likelihood. In this case, the posteriors for all parameters and the model order parameter k, in particular, were equal to the priors in Table 1.

ANALYSIS OF INTCAL98 DATA

We will analyze the INTCAL98 past atmospheric ^{14}C concentration (Stuiver et al. 1998), shown in Figure 1. ^{14}C concentration is influenced by Earth's magnetic field, cosmic ray flux, solar activity, and various sinks and sources of carbon. Therefore, periodic oscillations in the ^{14}C concentration data are possible and, if present, are important in understanding the complex Sun-Earth system.

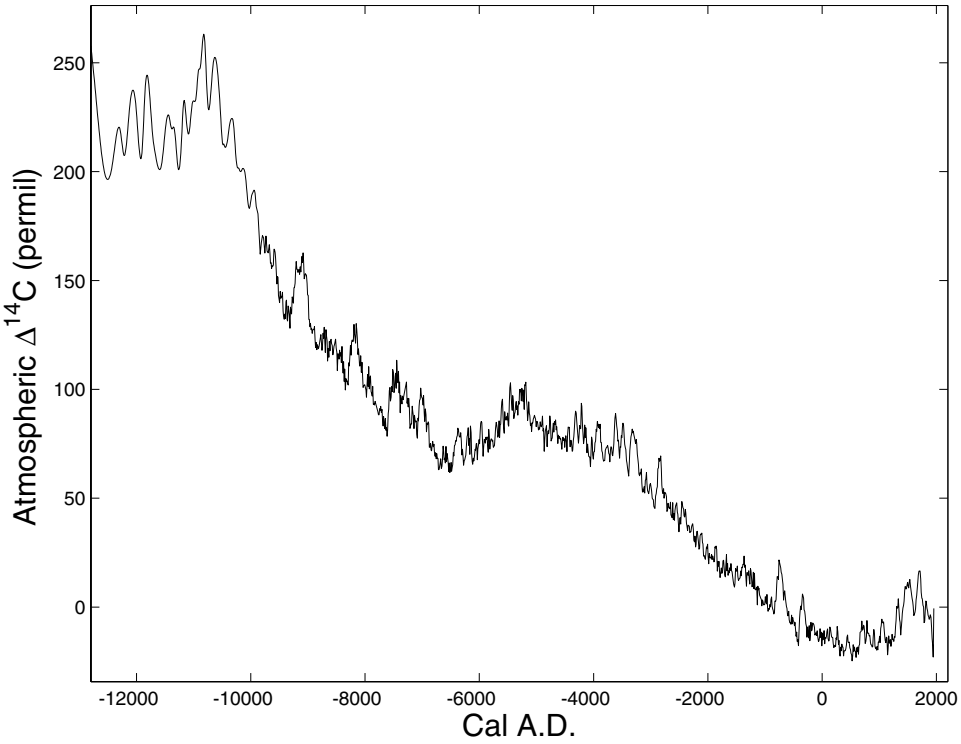

Figure 1 Atmospheric ^{14}C concentration. Vertical units represent a ‰ difference from the AD 1950 value. The data is taken from the INTCAL98 calibration measurements (Stuiver et al. 1998).

We made an MCMC simulation of 10^8 points to obtain a posterior probability distribution of the model parameters for the INTCAL98 $\Delta^{14}C$ data from –9905 to 1955 cal AD. In Figure 2, a discrete probability distribution is shown for the number of sinusoids in the INTCAL98 $\Delta^{14}C$ data. The most probable number of sinusoids in the data is 0. The sinusoids, therefore, do not explain enough of the data to be believable with the present model and priors. This result contrasts with previous studies (Stuiver et al. 1991, 1993; Damon and Peristykh 2000) that used DFT or MEM with no or unspecified confidence levels and reported several frequencies in the INTCAL98 or INTCAL93 data.

A probability density for the noise color parameter α is shown in Figure 3. The noise is highly correlated red noise with $\alpha = 1.0006 \pm 0.0008$. Previous studies with DFT or MEM do not take this into account and, therefore, they probably have incorrect confidence levels, if any. The number of frequencies and the noise color roughly confirm our previous analysis with a random walk model

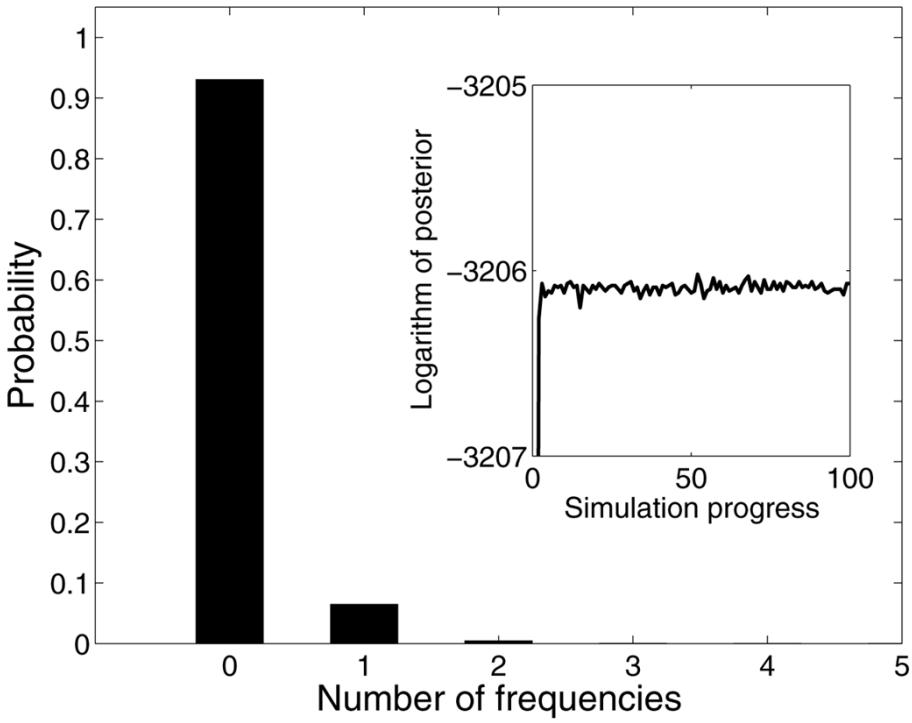

Figure 2 A probability distribution for the number of continuous harmonic frequencies in the INTCAL98 data. Inset shows the logarithm of prior times likelihood.

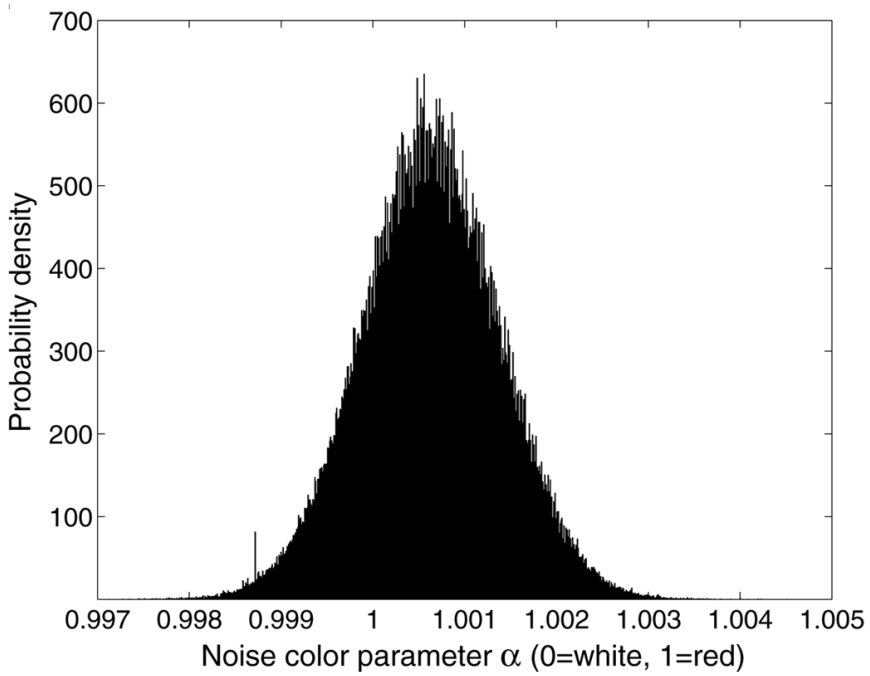

Figure 3 A probability distribution for the noise color parameter α for the INTCAL98 data

(Palonen and Tikkanen 2004) which is equivalent to $\alpha = 1$, although the selection of the prior range for the amplitude has an effect upon the model probabilities.

Probability distribution for period in the case $k = 1$ is shown in Figure 4. Because the distribution is smooth and the peaks are in accord with previous analyses, we conclude that there is sufficient mixing in the present MCMC chain.

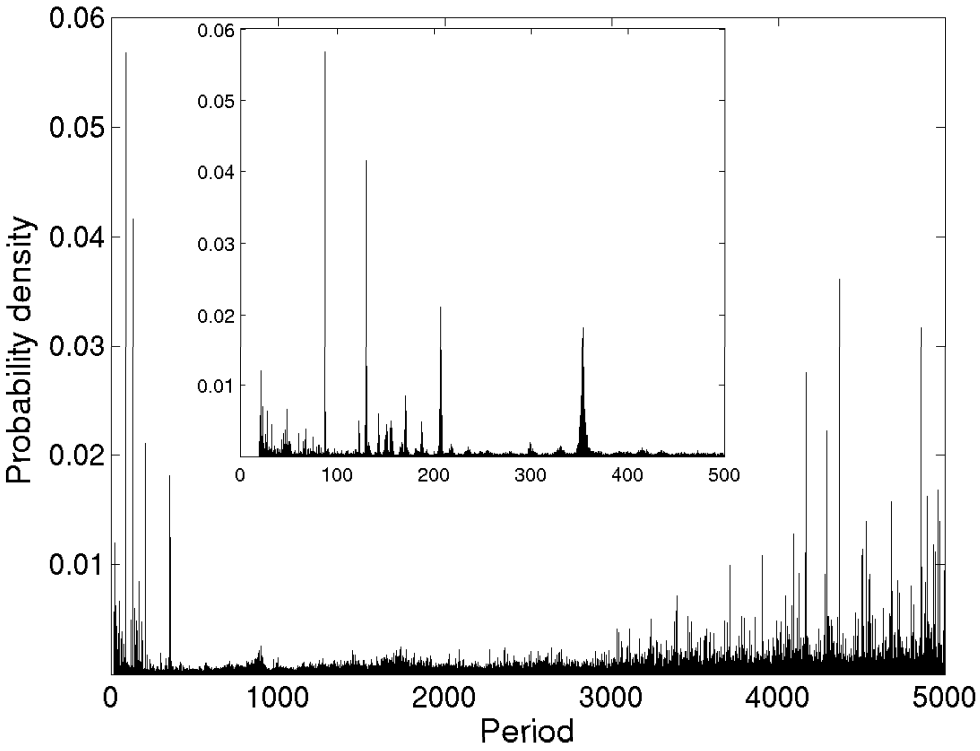

Figure 4 A probabilty distribution for the period assuming there is one frequency in the data ($k = 1$). The inset shows the lower-period part in more detail.

CONCLUSIONS

The noise model in this work uses only first-order correlations. It is the simplest model capable of modeling white, pink, and red noise. The noise model is a step in the right direction—the data should determine the type of noise to be used. The present model also incorporates a simple and effective way to handle the trend. Artificial differentiation between the trend and noise is not needed. A problem of the present method is the computational implementation. For large parameter spaces, there are problems with convergence of the MCMC chain.

Not every peak is a real signal. The present model indicates that there are no believable continuous harmonic frequencies in the INTCAL98 $\Delta^{14}C$ data. However, there are indications that some frequencies in climatic proxies are not continuous (Ogurtsov et al. 2001) and, in these cases, continuous frequency models like the present model, DFT, or MEM are not the best option. Wavelets provide a better option but, like DFT and MEM, they also have a problem with confidence levels and noise color. We are currently working on a Bayesian model with noncontinuous sinusoids.

APPENDIX

The total proposal distribution $h(\Theta, \Theta')$ is a product of the probability of a move from k to k' and the proposal distribution of the new point, $q(\Theta, \Theta')$. Because we use a uniform prior for the model parameter k, the move probabilities take a constant value c, except where new values of k would be out of prior range, in which case the probability is 0. We use independent proposal distributions for the amplitude, phase, and frequency of the new sinusoid. The proposal distributions are uniform and truncated as the prior of the corresponding parameter. Therefore, the acceptance probability in Equation 9 for a birth move is simply:

$$a((k, z), (k+1, z')) = \min\left(1, \frac{p(\Theta'|\boldsymbol{M}, \boldsymbol{S}, \boldsymbol{T})c(k+1)}{p(\Theta|\boldsymbol{M}, \boldsymbol{S}, \boldsymbol{T})c(k+1)\frac{1}{R_A R_\phi R_f}}\right)$$

$$= \min\left(1, \frac{p(\Theta'|\boldsymbol{M}, \boldsymbol{S}, \boldsymbol{T})}{p(\Theta|\boldsymbol{M}, \boldsymbol{S}, \boldsymbol{T})\frac{1}{R_A R_\phi R_f}}\right),$$

where the $(k + 1)$ terms come from the selection of the frequency to be added or removed, and R_A, R_ϕ and R_f are the prior ranges, e.g., $R_A = A_{max} - A_{min}$.

The probability for a remove-move is correspondingly:

$$a((k+1, z'), (k, z)) = \min\left(1, \frac{p(\Theta|\boldsymbol{M}, \boldsymbol{S}, \boldsymbol{T})\frac{1}{R_A R_\phi R_f}}{p(\Theta'|\boldsymbol{M}, \boldsymbol{S}, \boldsymbol{T})}\right).$$

REFERENCES

Andrieu C, Djuric PM, Doucet A. 2001. Model selection by MCMC computation. *Signal Processing* 81:19–37.

Bretthorst GL. 1988. Bayesian spectrum analysis and parameter estimation. *Lecture Notes in Statistics, Vol. 48.* Berlin: Springer Verlag. 209 p.

Bretthorst GL. 2003. Frequency estimation, multiple stationary nonsinusoidal resonances with trend. *AIP Conference Proceedings* 659:3–22.

Damon PE, Peristykh AL. 2000. Radiocarbon calibration and application to geophysics, solar physics, and astrophysics. *Radiocarbon* 42(1):137–50.

Gilks WR, Richardson S, Spiegelhalter DJ, editors. 1995. *Markov Chain Monte Carlo in Practice.* Boca Raton: Chapman & Hall/CRC Press. 512 p.

Gilman DL, Guglister FJ, Mitchell JJM. 1962. On the power spectrum of red noise. *Journal of the Atmospheric Sciences* 20:182–4.

Green PJ. 1995. Reversible jump Markov chain Monte Carlo computation and Bayesian model determination. *Biometrika* 82:711–32.

Ogurtsov MG, Kocharov GE, Lindholm M, Eronen M, Nagovitsyn YA. 2001. Solar activity and regional climate. *Radiocarbon* 43(2A):439–47.

Palonen V, Tikkanen P. Forthcoming. Spectral analysis of the INTCAL98 calibration curve: a Bayesian view. AMS-9 conference proceedings. *Nuclear Instruments and Methods in Physics Research Nuclear Physics B*.

Stuiver M, Braziunas TF, Becker B, Kromer B. 1991. Climatic, solar, oceanic and geomagnetic influences on late-glacial and holocene atmospheric $^{14}C/^{12}C$ change. *Quarternary Research* 35:1–24.

Stuiver M, Braziunas TF. 1993. Sun, ocean, climate and atmospheric $^{14}CO_2$: an evaluation of causal and spectral relationships. *The Holocene* 3:289–305.

Stuiver M, Reimer PJ, Bard E, Beck JW, Burr GS, Hughen KA, Kromer B, McCormac FG, van der Plicht J, Spurk M. 1998. INTCAL98 radiocarbon age calibration, 24,000–0 cal BP. *Radiocarbon* 40(3):1041–83.

Waagepetersen R, Sorensen D. 2001. A tutorial on Reversible Jump MCMC with a view toward applications in QTL-mapping. *International Statistical Review* 69:49–61.

RADIOCARBON, Vol 46, Nr 2, 2004, p 987–995

RADIOCARBON/TREE-RING CALIBRATION, SOLAR ACTIVITY, AND UPWELLING OF OCEAN WATER

F B Knox

900 Ohariu Valley Road, R.D., Johnsonville, Wellington, New Zealand. Email: fbmoknox@actrix.gen.nz.

B G McFadgen

Stout Research Centre for NZ Studies, Victoria University of Wellington, P.O. Box 600, Wellington, New Zealand.
Present address: 99 Sefton Street, Wellington, New Zealand. Email: mcfadgen@actrix.gen.nz.

ABSTRACT. Least-squares fitted smooth curves to radiocarbon versus tree-ring calibration data for the period AD 1140 to 1950 are compared with climatic warming and cooling of the North Atlantic (Little Ice Age), and with recorded sunspot numbers over the period AD 1670 to 1950.

Calibration curves from different parts of the globe are not identical, and appear to be determined by a combination of variable solar activity and variable oceanic upwelling of ^{14}C-depleted water, with the variable upwelling itself partly determined by solar activity.

INTRODUCTION

An optimum smoothing procedure for radiocarbon versus tree-ring age calibration curves (Knox and McFadgen 2001) showed calibration curves from different parts of the globe to be significantly different. Two extreme curves are from western North America (part of the INTCAL98 curve) and curves from New Zealand (Figure 1). Standard deviations for the smoothed curves are better than 10 yr and calendar time resolutions are about 20 yr for the later curves, and 27 and 45 yr for the earlier curves. The average difference between the curves agrees with the recommended 24-yr adjustment between Northern and Southern Hemispheres (Stuiver et al. 1998), but the difference actually varies with time from 0 to 70 yr. In addition, there is a time variable longitudinal difference between the British Isles and western North America of up to 60 yr.

If only the typical ±50-yr accuracy in individual measurements is wanted, then one universal calibration curve may be sufficient. Considering the accuracy now available from the tree-ring calibration *viz.* standard deviations better than 10 yr, there is a family of regional curves to be defined. What is needed to construct the family of regional curves is a set of calibration measurements spread across the globe, together with appropriate interpolation procedures. In order to achieve this, it is necessary to know what factors contribute to the wiggles in the calibration curves.

The purpose of this paper is to explore quantitatively the contribution from the 2 most likely factors: solar activity and upwelling to the sea surface of ^{14}C-depleted water.

CORRELATION OF ^{14}C/C WITH SUNSPOT NUMBER AND CLIMATIC VARIATION

Climatic cooling and warming in the North Atlantic is generally considered to correlate with variation in solar activity, but this is only really known for the Maunder and Dalton periods; prior to the Maunder period, there are no consistently reliable records of sunspot numbers (Royal Greenwich Observatory and SIDC data, in references). It is generally inferred (e.g. Damon et al. 1998) that the Wolf and Sporer periods correlate with solar activity from the observation that the corresponding climatic cooling correlates with the ^{14}C calibration curves in the same way as the Maunder and Dalton periods (Figure 2). Other observations (Damon et al. 1998; Rigozo et al. 2001) support the inference, which we consider valid, but, as we show, the correlation of ^{14}C/C with solar activity is not altogether simple.

Proceedings of the 18th International Radiocarbon Conference, edited by N Beavan Athfield and R J Sparks
RADIOCARBON, Vol 46, Nr 2, 2004, p 987–995

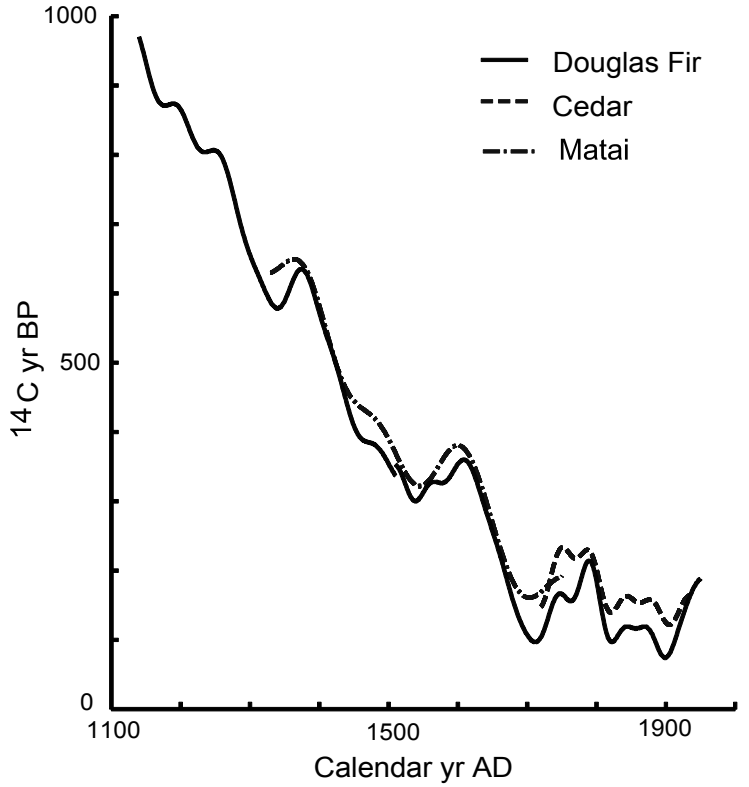

Figure 1 Smoothed calibration curves from the west coast of North America (Douglas fir) and New Zealand (cedar and matai). Standard deviation of early Douglas fir = 8 yr, late Douglas fir = 3 yr, cedar = 8 yr, matai = 9 yr.

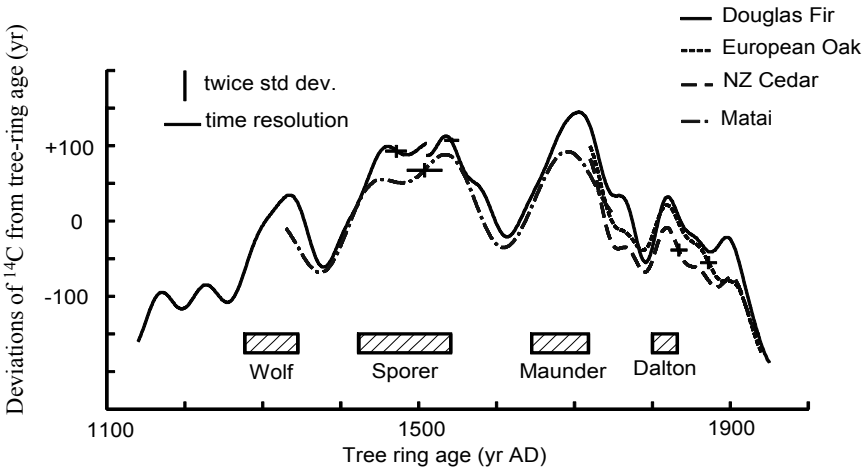

Figure 2 Detrended calibration curves from the west coast of North America (Douglas fir), British Isles (European oak), and New Zealand (cedar) compared with the Wolf, Sporer, Maunder, and Dalton periods of climatic cooling in the North Atlantic (Masarik and Beer 1999; Damon et al. 1998). The calibration curves have been detrended by taking the difference between ^{14}C and tree-ring age, and plotting the difference as deviations of ^{14}C from tree-ring age.

The decadal ^{14}C curves used below all have calendar resolution times close to 20 yr; so to facilitate comparison (Figure 3), the sunspot curve has been decadally averaged and then smoothed with a 5-point binomial digital filter (a weighted running mean with weighting ratios 1:4:6:4:1). This filter applied to decadal data can be shown to give a resolution time close to 20 yr; due to this, the 11-yr cycle does not appear. Sunspot numbers were first reliably and consistently recorded only after AD 1700 (Royal Greenwich Observatory and SIDC data, in references). Prior to AD 1700, well into the Maunder Minimum, we take the sunspot number as zero (Figure 3). Prior to AD 1850, Figure 3 shows that time variation of the $^{14}C/C$ ratio in all 3 calibration curves lags the sunspot variation. The section "Analysis of Calibration Sites" discusses a possible reason for this.

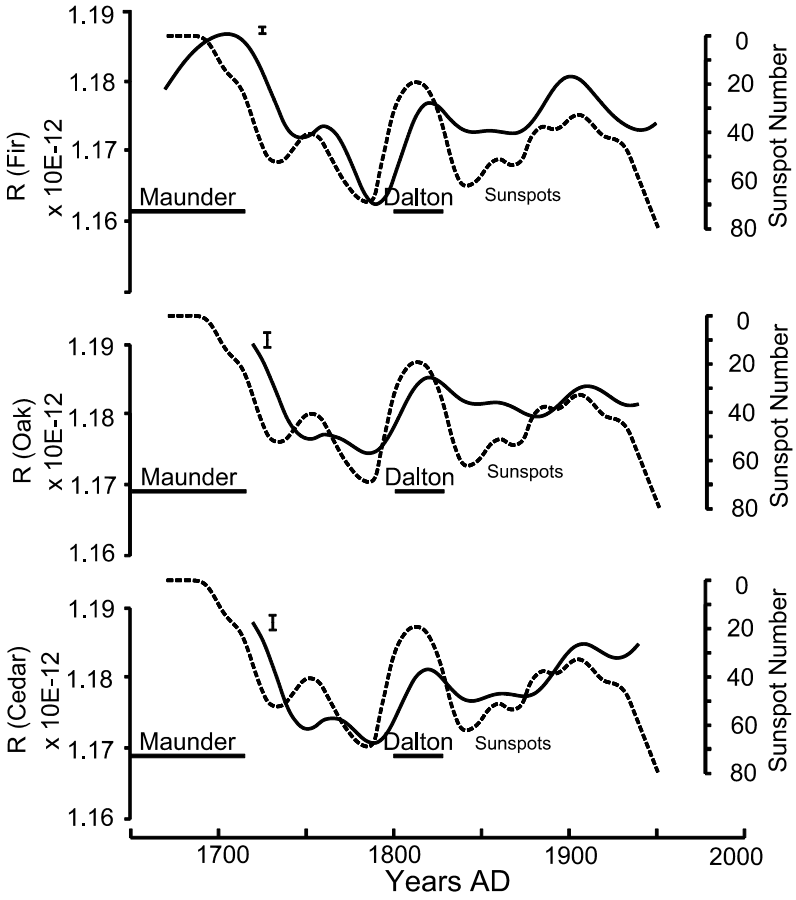

Figure 3 Sunspot number (averaged and smoothed) versus time, compared with the $^{14}C/C$ ratios (R) in fir (western North America), oak (British Isles), and cedar (New Zealand) calibration curves. The curves are approximately corrected for the Suess effect (see text). From AD 1700 onwards, sunspot data was obtained from the web site references. Error bar range is twice standard deviation.

QUANTITATIVE ANALYSIS

To analyze the situation quantitatively, we start by modifying an equation used by Lassey et al. (1990) for the rate of change of the global ^{14}C inventory, ^{14}I:

$$(d/dt)^{14}I = Q - k(1-R_m/R)\ ^{14}I - \lambda^{14}I \quad (1),$$

where Q is the cosmogenic production rate of ^{14}C, the radioactive decay rate $\lambda = 1/(8267\ yr)$, and $k = 1 / [7.2 \times (0.975)^2\ yr]$ is the exchange rate coefficient for the net carbon flux from atmosphere to ocean surface adjusted for fractionation to the mean surface ocean value of $\delta^{13}C = 0$. The variables R_m and R are the $^{14}C/C$ ratios in the upper mixed layer of the ocean and the atmosphere, respectively, corrected for fractionation to $\delta^{13}C = -25‰$.

Let I be the global total carbon inventory for the atmosphere, then R is $^{14}I/I$, and

$$(d/dt)\ ^{14}I = (d/dt)\ (R\ I) = (dR/dt)\ I + R\ (dI/dt) \quad (2).$$

Inserting equation (2) into equation (1) and dividing through by I gives

$$dR/dt = Q / I - (k+\lambda+\sigma)\ R + k\ R_m \quad (3),$$

where σ is (dI/dt) / I.

A best estimate of the ^{14}C production rate per unit area in the stratosphere as a function of sunspot number is taken from Lal (1992: Equation 3) with the variable term increased by 20% (see Lal 1992, section 4). This rate is multiplied by the area of the earth at stratospheric height (equivalent radius 6380 km) and divided by the total carbon inventory to give $Q/I = \alpha - \beta S$, where $\alpha = 4.2 \times 10^{26}$ atom yr^{-1}/I and $\beta = 1.1 \times 10^{24}$ atom yr^{-1}/I and S is the sunspot number. Equation (3) can now be written as

$$(d/dt)R = \alpha - \beta S - (k+\lambda+\sigma)\ R + k\ R_m \quad (4).$$

Next, consider the rate of change of $^{14}C/C$ in the upper mixed layer of the ocean:

$$(d/dt)^{14}I_m = k(1-R_m/R)\ ^{14}I - \lambda^{14}I_m + k_d(^{14}I_d - ^{14}I_m) \quad (5).$$

The term $k(1-R_m/R)^{14}I$, which in equation (1) is the net flux of ^{14}C from the atmosphere to the ocean, becomes in equation (5) the production rate for the ocean. The term $k_d(^{14}I_d - ^{14}I_m)$ represents an unknown depletion rate of ^{14}C due to upwelling of ocean water: $^{14}I_d$ being the global total ^{14}C inventory of depleted ocean water rising and mixing into the surface layer, and k_d an unknown constant.

Proceeding as before,

$$(d/dt)^{14}I_m = (d/dt)\ (R_m\ I_m) = (dR_m/dt)\ I_m + R_m\ (dI_m/dt) \quad (6),$$

and inserting equation (6) into equation (5) and dividing through by I_m gives

$$dR_m/dt = k\ X\ R - (kX+\lambda+\sigma_m)\ R_m + U \quad (7),$$

where I_m is the global total C inventory in the upper mixed layer of the ocean, $X = I/I_m$, $\sigma_m = (dI_m/dt)/I_m$ and $U = k_d(^{14}I_d - ^{14}I_m)/I_m$, the rate of change of $^{14}C/C$ in surface sea water due to upwelling.

Measurements of R_m are not always available in the vicinity of any given calibration tree, but R_m can be eliminated from the calculation. To do this, differentiate equation (4) with respect to time to get

$$d^2R/dt^2 = -\beta(dS/dt) - (d\beta/dt)\ S - (k+\lambda+\sigma)\ (dR/dt) - (d\sigma/dt)\ R + k(dR_m/dt) \quad (8),$$

and substitute dR_m/dt from equation (8), and R_m from equation (4) into equation (7). After rearranging by putting the external driving terms, U and the solar activity terms, on one side of the equation as a driving function, V, this yields

$$U + C_S(\alpha - \beta S) + [(d/dt)(\alpha - \beta S)] / k = V = C_0\, \lambda R + C_1(dR/dt) + (d^2R/dt^2) / k \quad (9),$$

where

$$C_0 = X(1+\sigma/\lambda) + [1+ (\lambda+\sigma) / k)](1+\sigma_m/\lambda) + (d\sigma/dt) / (k\lambda),$$

$$C_1 = 1 + X + (2\lambda+\sigma+\sigma_m) / k \text{ , and } C_S = X + (\lambda+\sigma_m) / k.$$

The above equates the driving function with an expression derived from ^{14}C measurements made entirely in the calibration wood. V expresses the combined effects of variable ocean upwelling and variable $^{14}C/C$ production in the stratosphere, driving the change of $^{14}C/C$ in the troposphere.

The right-hand side of equation (9) is the sum of 3 terms proportional to R (the measured $^{14}C/C$ ratio), to dR/dt (the slope) and to d^2R/dt^2 (the curvature of R), respectively, when plotted against calendar time, and it is this combination which fully measures the combined effects on R of upwelling and variable ^{14}C production.

ANALYSIS OF CALIBRATION SITES

A significant amount of the reduction of the $^{14}C/C$ ratio after about AD 1750 is due to human activity (the Suess effect) (Figure 2). In Figure 3 and subsequent figures, this has been approximately corrected for by letting I, the total carbon inventory, increase exponentially from its value at AD 1750 to 3% more than this value at AD 1950 (Lassey et al. 1990). For this exploratory analysis I, before AD 1750, is assumed to be constant at 3.02×10^{40} atom (Lassey et al. 1996), but a more thorough analysis would also look at the effect of a more generally variable I.

Comparison of ΔV, the variation of V about the local average for the fir (1.6×10^{-16}/yr), oak (1.8×10^{-16}/yr), and cedar (2.4×10^{-16}/yr) is given in Figure 4. The standard deviations for the ΔV are 0.6×10^{-16}/yr for the fir, and 1.6×10^{-16}/yr for both the oak and the cedar. A resolution time of 20 yr over the interval AD 1720 to 1940 is equivalent to the curves being plotted through 11 independent points. χ^2 tests for significance of the differences between the curves show the differences between fir and oak and between fir and cedar to be highly significant, but the difference between oak and cedar to be not significant (Snedecor and Cochran 1967).

With 11 degrees of freedom (11 independent points), the correlation coefficients for fir and oak (0.83), fir and cedar (0.86), and oak and cedar (0.96) are all individually highly significant (Snedecor and Cochran: §7.6), but the differences between the correlation coefficients are not significant (Snedecor and Cochran: §7.7 and §2.13).

The above and Figure 4 together show that between all 3 sites the variation of V is highly correlated, but that the amplitude of the variation for the North American west coast is significantly greater than the amplitudes for either the British Isles or New Zealand. Amplitudes for the British Isles and New Zealand do not differ significantly. This difference may relate to stronger upwelling of water along the North American west coast. More $^{14}C/C$ depletion has been measured in surface water off the North American west coast than in such water in the immediate vicinity of New Zealand or the British Isles (Stuiver and Braziunas 1993).

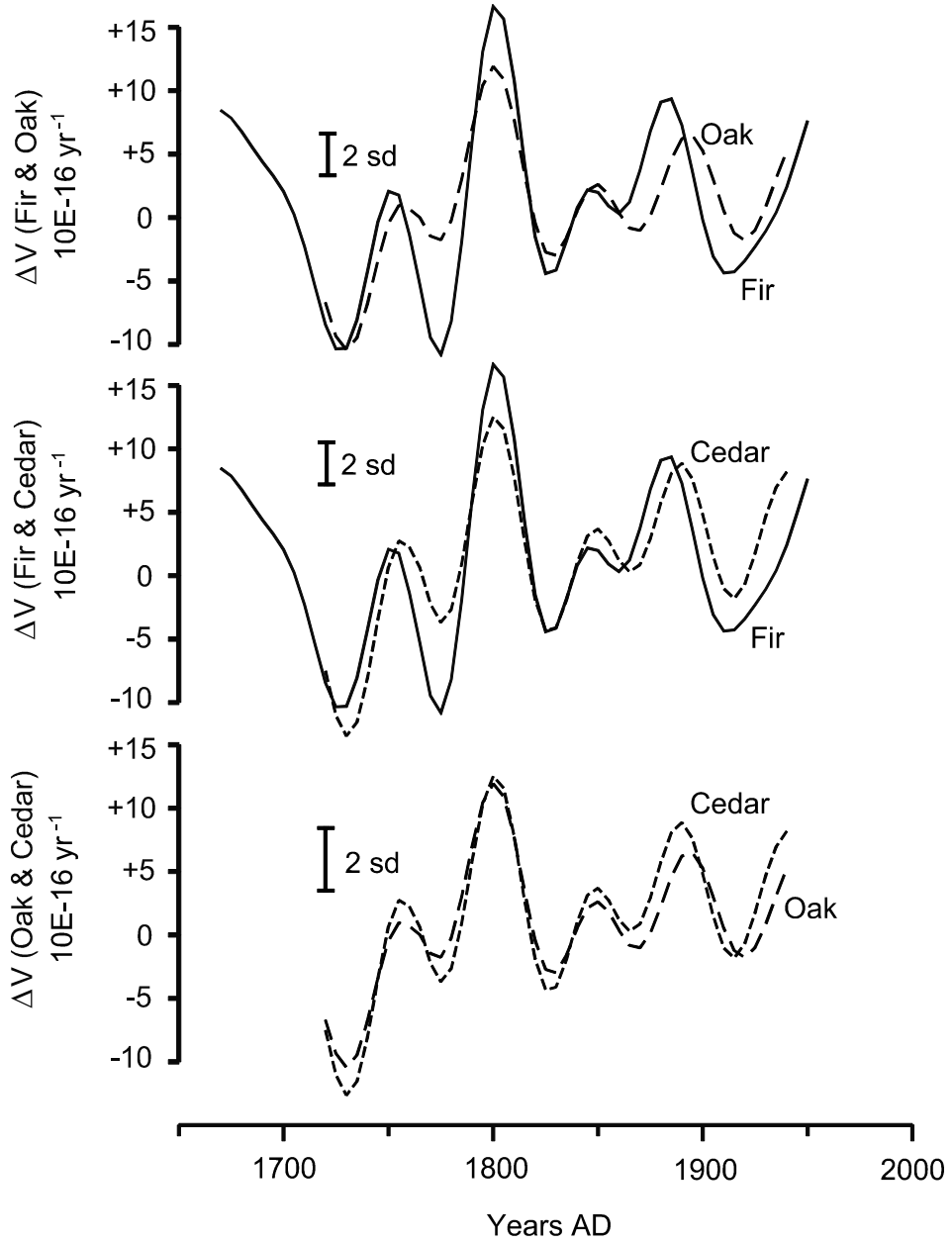

Figure 4 Comparisons of ΔV (yr^{-1}) obtained entirely from tree calibration data for the 3 calibration sites versus time.

There is increasing evidence for correlation of climate with solar activity (Foukal 2003), and we must make allowance for the possibility that solar activity may affect upwelling of ^{14}C-depleted water, through variable heating of the upper layer of the ocean. To examine this, we estimate a quantity ΔT, which is proportional to the solar activity induced fluctuation of sea surface temperature about its average temperature. We then compare at the 3 calibration sites, ΔT with the rate of reduction of $^{14}C/C$ in surface seawater due to upwelling (U) (Figure 5). However, it should be pointed out

that, within existing climate models, the variation of solar heat output found over 2 solar cycles seems to be too small, by a factor of 3 to 5, to account for the correlation (Foukal 2003). We will look at this again later.

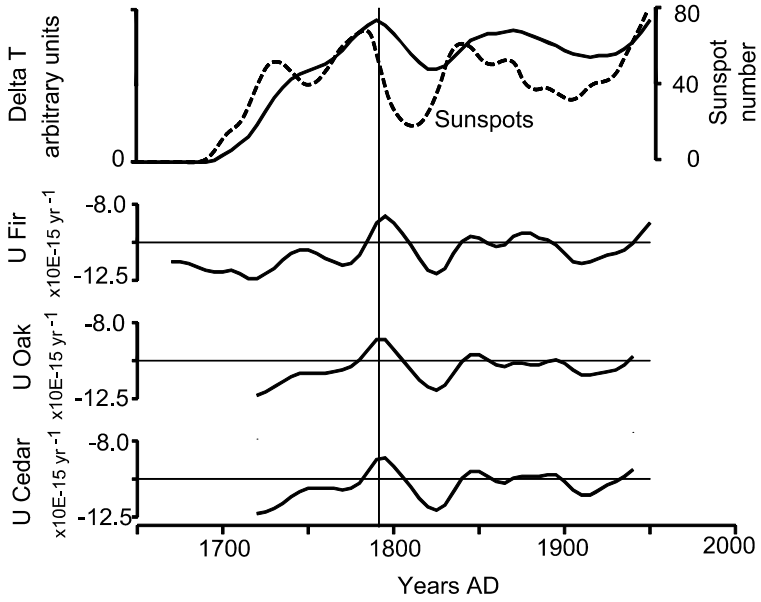

Figure 5 ΔT (for $\tau = 30$ yr), smoothed sunspot number, and U (yr^{-1}) for the 3 calibration sites versus time.

Since the variation in solar heat output is small compared with the average output, then considering the uncertainties, an assumed linear form for the variation of heat output as a function of sunspot number is all that is warranted at this stage. At least it should be more comparable with U than unprocessed sunspot numbers. The underlying assumption is that variable heating, through changing buoyancy of the upper sea surface layer, modulates the effective area of spread of previously deeper cooler ocean water over the surface, where it exchanges ^{14}C directly with the atmosphere.

ΔT, the fluctuation of sea surface temperature about the average temperature, is given by:

$$(d/dt)\,\Delta T = (\text{constant})\,S(t) - (\text{constant})\,\Delta T \qquad (10),$$

where the first term on the right-hand side of equation (10) is the variable heat input to the ocean (assumed proportional to sunspot number), and the second term is the excess heat loss from the surface layer (assumed proportional to ΔT). The solution to this differential equation yields

$$\Delta T \propto \exp(-t/\tau)\int S(t)\exp(t/\tau)dt$$

where τ is a time constant related to how fast excess heat is lost from the surface layer.

ΔT, for $\tau = 30$ yr, is plotted against t and compared with U at the 3 calibration sites in Figure 5. However, some of the terms contributing to U (Equation 9) directly relate to sunspot number, so care is needed in interpreting any correlation of U with ΔT, a quantity derived directly from this number. In the extreme case, if U was not correlated with solar activity the sunspot terms in equation (9) would

all cancel with parts of the calibration tree terms. But if, for example, the expression used for the variation of ^{14}C production with sunspot number was significantly in error, the cancelling would not be exact and a spurious correlation of U with ΔT would emerge.

While it cannot be ruled out that the observed correlation of U with ΔT is spurious, it cannot be entirely so. The correlation makes physical sense. In Figure 5, increasing ΔT leading to increasing buoyancy of the upper surface layer correlates with a decreasing magnitude of U, as the amount of depleted water brought up to and spread out over the sea surface declines.

In Figure 5, the curve ΔT versus t, for finite τ (>0), is smoother than S versus t and is delayed in time. Putting τ = 30 yr yields a ΔT delayed by 9 yr, which synchronizes well with the U. The matching delay in the U cannot be spurious, since no such delay applied to S occurs in equation (9).

The curve ΔT versus t is also smoother than the U curves, and since the U are supposed to correlate directly only with ΔT (not S), it could be construed that the enhanced variation in the U is spurious, but another explanation is possible. If the warmer buoyant sea surface layer has one or more natural oscillatory periods in its motion of covering and uncovering the cooler upwelled water, it may respond to the variable heating as a set of damped harmonic oscillators (Jaeger 1951).

If some external force, in this case the excess buoyancy, induces motion in the layer, the motion will be dominated by broad resonance between the natural periods of the layer and nearby periods in the external force. Thus, the enhanced variation in the U compared with ΔT may be due to resonance with the corresponding muted variation in ΔT, extending back over a long time (to well before the Maunder Minimum) to allow build-up of the resonance.

It is also possible that the periods involved in the resonance will be less than the resolving time (20 yr) of the present smoothed data. In this case, the resonant build-up time could be shorter, with the time variation visible in the figures being some function of a longer-term modulation of the shorter period oscillations.

Resonance between variable upwelling (proportional to U) and variable heating may also be responsible for the previously mentioned enhancement by a factor of 3 to 5 needed in existing climate models to account for the correlation of climate with (so far observed) heating associated with solar activity (Foukal 2003).

CONCLUSION

The reason for ^{14}C versus tree-ring calibration curves from different parts of the globe not being identical appears to be mainly due to exchange of CO_2 between the atmosphere and seawater in which the $^{14}C/C$ ratio is variable. Mixing of variable proportions of upwelled ^{14}C-depleted ocean water into the surface ocean layer brings about variability in the surface layer. Variable solar heating related to solar activity appears to modulate the mixing. The variability brought about by exchange of CO_2 with surface seawater, combined with the variable ^{14}C production in the stratosphere due to changes in solar activity, leads to a complicated, but calculable, correlation of the tropospheric $^{14}C/C$ ratio with sunspot number.

The exploratory analysis in this paper has been carried out on only 3 sites, albeit widely spaced across the globe, but they are all mid-latitude, essentially oceanic sites. A more thorough analysis is required using, in addition, data from low and high latitudes and from inland sites. It would be desirable to extend the analysis back in time beyond the beginning of the Maunder Minimum, if a reliable proxy (other than sunspot number) for solar activity is developed. If this can be achieved, and with

the added advantage of historical accounts, the last 1000 yr of ^{14}C versus tree-ring calibration data, from the medieval maximum through the periods of climatic cooling to the modern maximum, represents a unique opportunity to develop insight into variable solar heating and climate change.

The above would also allow the development of a global family of calibration curves that takes account of spatial as well as temporal variation.

Finally, although R_m in this paper is eliminated between equations (4) and (7), these equations can be differently combined (or kept separate) to make explicit use of R_m as desired.

ACKNOWLEDGEMENTS

For discussions and help, we thank Dr B Carter of the Carter Observatory; Drs W Allan, L Carter, D Lowe, K Lassey, and P Sutton of the National Institute of Water and Atmospheric Research; and Dr R Sparks of the Rafter Radiation Laboratory, Institute of Geological and Nuclear Sciences: Wellington, New Zealand.

REFERENCES

Damon PE, Eastoe CJ, Hughes MK, Kalin RM, Long A, Peristykh AN. 1998. Secular variation of $\Delta^{14}C$ during the medieval solar maximum: a progress report. *Radiocarbon* 40(1):343–50.

Foukal P. 2003. Can slow variations in solar luminosity provide missing link between the sun and climate. Eos, Transactions, American Geophysical Union 84(22):205, 208.

Jaeger JC. 1951. *An Introduction to Applied Mathematics*. Oxford: Clarendon Press. §31:76–82.

Knox FB, McFadgen BG. 2001. Least-squares fitting smooth curves to decadal radiocarbon calibration data from AD 1145 to AD 1945. *Radiocarbon* 43(1):87–118.

Lal D. 1992. Expected secular variations in the global terrestrial production rate of radiocarbon. NATO ASI Series 12:113–26.

Lassey K, Manning MR, O'Brien BJ. 1990. An overview of oceanic radiocarbon: its inventory and dynamics. *Reviews in Aquatic Sciences* 3(2&3):117–46.

Lassey K, Enting IG, Trudinger CM. 1996. The earth's radiocarbon budget. *Tellus* 48B:487–501.

Masarik J, Beer J. 1999. Simulation of particle fluxes and cosmogenic nuclide production in the earth's atmosphere. *Journal of Geophysical Research* 104(D10): 12,099–111.

Royal Greenwich Observatory. Sunspot Record 1874-2004. Space Science Center (NASA). Solar Physics Data. *The Sunspot Cycle. Monthly Averages*. http://science.msfc.nasa.gov/ssl/pad/solar/greenwch_spot_num.txt.

Rigozo NR, Echer E, Vieira LEA, Nordemann DJR. 2001. Reconstruction of Wolf sunspot numbers on the basis of spectral characteristics and estimates of associated radio flux and solar wind parameters for the last millennium. *Solar Physics* 203:179–91.

Solar Influences Data Analysis Center (SIDC). Royal Observatory of Belgium, Brussels, Belgium. *Sunspot Archive. Yearly Sunspot Number*. http://sidc.oma.be/DATA/yearssn.dat.

Snedecor GW, Cochran WG. 1967. *Statistical Methods. 6th edition.* Ames: Iowa State University Press. 593 p.

Stuiver M, Braziunas TF. 1993. Modeling atmospheric ^{14}C influences and ^{14}C ages of marine samples to 10,000 BC. *Radiocarbon* 35(1):137–89.

Stuiver M, Reimer PJ, Braziunas TF. 1998. High-precision radiocarbon age calibration for terrestrial and marine samples. *Radiocarbon* 40(3):1127–51.

RADIOCARBON, Vol 46, Nr 2, 2004, p 997–1004

INFLUENCE OF ^{14}C CONCENTRATION CHANGES IN THE PAST ON STATISTICAL INFERENCE OF TIME INTERVALS

Adam Michczyński

Radiocarbon Laboratory, Institute of Physics, Silesian University of Technology, Bolesława Krzywoustego 2, 44-100 Gliwice, Poland. Email: amichcz@polsl.gliwice.pl.

ABSTRACT. The influence of the calibration curve on the statistical inference of time intervals was investigated. For this purpose, the calculation of the summed probability density function was used. Computer simulations were done for batches of 11 samples, each time uniformly covering 200-yr time intervals. The results show that the calibration curve causes the summed probability density function of a group to cover a wider interval than the real-time interval of the phenomenon. Moreover, the estimated time interval may be often shifted in relation to the real-time interval.

INTRODUCTION

Geologists and archaeologists often face the problem of how to assign time intervals to a phenomenon (geological phase or archaeological culture) based on a group of radiocarbon dates from artifacts associated with this phenomenon. One of the treatment methods for such a group of related ^{14}C dates is to create summed probability density distributions by summing distributions of the relevant calibrated dates. The 50% confidence interval (interquartile range), which corresponds with the conception of the *floruit* of a culture (Aitchison et al. 1991), or the highest probability confidence intervals of this distribution are usually interpreted as the time limits of the phenomenon. However, the changes of ^{14}C concentration in the past represented by the calibration curve cause the relation between the ^{14}C and the calendar (calibrated) date to be ambiguous, and the time intervals estimated by this method may be very different from the actual time intervals in the calendar scale.

The influence of the calibration curve on the statistical inference of time intervals was first mentioned in the late 1980s by Stuiver and Reimer (1989). They showed that in unfavorable circumstances, a large distortion of probability distribution may occur; in their example, the part of the calculated summed probability distribution retained in the original (real) time interval is about 50%. In 1994, McFadgen et al. (1994) discussed the distortion of histograms of calibrated ^{14}C dates from New Zealand. They emphasized that the "calibrated stochastic distortion (CSD)" results from composition of the statistical spread of measured ^{14}C ages and the ambiguous character of the calibration curve. This paper presents a more complex diagnosis of the problem.

METHODS

Analysis was carried out for 200-yr-wide time intervals; i.e., it was assumed that the real timespan of the investigated phenomenon was equal to 200 calendar yr. Because the current work was mainly concerned with the influence of the calibration curve, the following assumptions were made:

- The frequency distribution of the artifacts is uniform for the time interval range of the phenomenon;
- The calendar ages of the collected samples (artifacts) uniformly cover the whole 200 yr of the time interval.

The calculations were performed in the following order:

Proceedings of the 18th International Radiocarbon Conference, edited by N Beavan Athfield and R J Sparks
RADIOCARBON, Vol 46, Nr 2, 2004, p 997–1004

- It was assumed that 11 samples (artifacts) were collected in the 200-yr time interval under investigation. The calendar ages of the samples were uniformly spread across the interval, with the first one falling at the beginning of the interval and the subsequent ones in 20-yr increments.
- For the calendar date of each sample, the corresponding ^{14}C age was determined from the calibration curve.
- Each of the ^{14}C dates was calibrated with the assumption that the error of the ^{14}C date was equal to 25 yr.
- All probability density distributions obtained as a result of the calibration were calculated in order to discern the summed probability density distribution.
- On the basis of this summed probability density distribution, the following intervals were calculated: interquartile range (*floruit*), the highest probability 50% confidence interval, and the highest probability 95% confidence interval.

Calculations were carried out using the revised and updated calibration module of the Gliwice Radiocarbon Laboratory Calibration Program, GdCALIB (Pazdur and Michczyńska 1989; Michczyńska et al. 1990), and the INTCAL98 calibration curve (Stuiver et al. 1998).

RESULTS AND DISCUSSION

Figure 1 shows how the calibration curve may influence the summed probability density function and the intervals estimated using this function. In the ideal case (Figure 1a), the obtained distribution should be similar to the uniform distribution. It would present the frequency distribution of the artifacts, and the calculated intervals would be quite a good estimate of the real-time interval. However, when we take into consideration the influence of the calibration curve (Figure 1b), the results become distorted. In Figure 1b, a few types of distortion of calculated intervals can be seen, namely:

- The highest probability intervals are discontinuous (especially the 50% confidence interval);
- All intervals are distinctly longer than in the ideal case; the 95% interval is much longer than the real-time interval;
- A large part of each interval—even the interquartile range and the highest probability 50% confidence interval—is outside of the real-time interval;
- The interquartile interval is clearly shifted in relation to the real-time interval.

Figure 1c shows a part of calibration curve that corresponds with the time interval considered in Figure 1b. We note that the boundaries of the summed probability distribution presented in Figure 1b are in concordance with the boundaries of the flat and ambiguous part of the calibration curve. This means that the calibration procedure spreads the analyzed time interval and causes the distortion mentioned above. It should be emphasized that these distortions are not a consequence of the calculation method used. Figure 2 shows a comparison of the summed probability density distribution for 11 samples from the time interval 2380–2580 cal BP (the same as in Figure 1b), with the probability distributions of the first and the last event in this group of dates calculated using OxCal v.3.8. It is clearly visible that both methods give the same differences between calculated limits and real limits of the analyzed time interval.

The question remains: How important are these distortions for particular time intervals in the past? In order to answer this question, the 2 factors were calculated for each of the 200-yr time intervals from 0–200 cal BP to 13,800–14,000 cal BP. The factors were defined as follows:

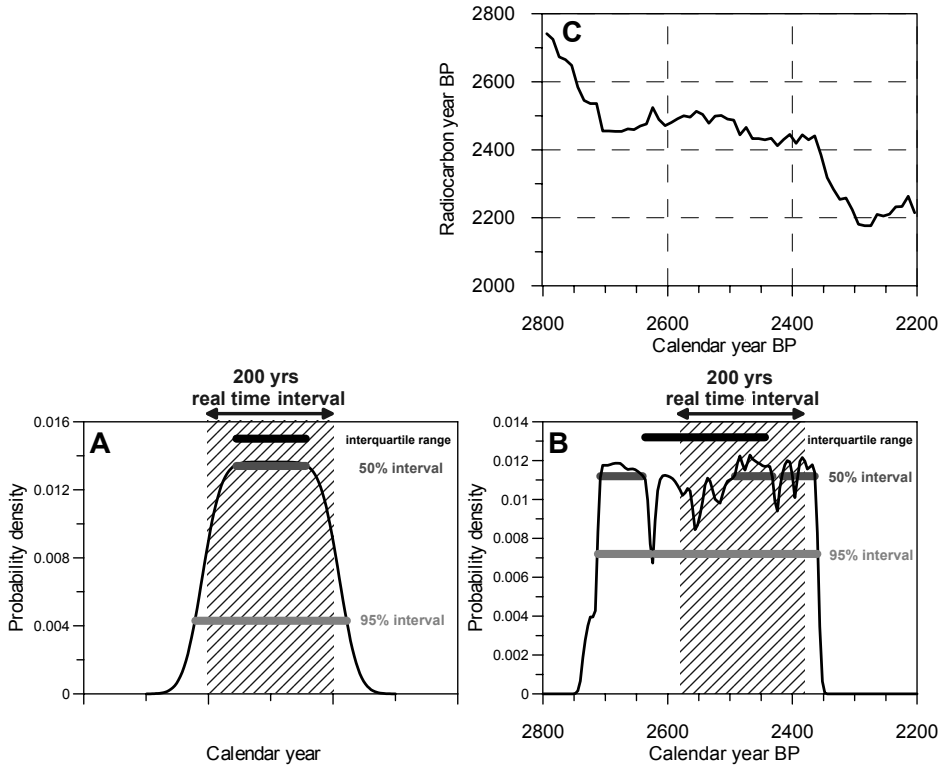

Figure 1 (a) The ideal case: the summed probability density function and the appropriate intervals for 11 samples from the 200-yr time interval obtained by summed Gauss distributions (the influence of the calibration curve was omitted); error of dates = 25 yr; (b) Summed probability density function and appropriate intervals for 11 samples from the time interval 2380–2580 cal BP; error of dates = 25 yr; (c) Part of the calibration curve (Stuiver et al. 1998) that corresponds with the time interval 2380–2580 cal BP.

- *The Common to Input Overlap Factor* (CI Factor) is equal to the length of the common part of the real-time interval (Input Interval) and the calculated interval (Output Interval) divided by the length of the Input Interval (see Figure 3). The CI Factor tells us which part of the real-time interval overlaps with the calculated interval.
- *The Common to Output Overlap Factor* (CO Factor) is equal to the length of the common part of the real-time interval (Input Interval) and the calculated interval (Output Interval) divided by the length of the Output Interval. The CO Factor tells us which part of the calculated interval overlaps with the real interval.

The values of the Overlap Factors for the analyzed interval (CO Factor, CI Factor) should be compared with the values for the ideal case ($CO\ Factor_{ideal\ case}$, $CI\ Factor_{ideal\ case}$) in order to draw conclusions concerning the distortion of the interval. The most important conclusions are the following:

- When the CO Factor < $CO\ Factor_{ideal\ case}$, the calculated interval is wider than the real interval or shifted in relation to the real one;
- When the CI Factor > $CI\ Factor_{ideal\ case}$, the calculated interval is wider than the real interval;
- When the CI Factor < $CI\ Factor_{ideal\ case}$, poor agreement between the calculated and the real interval exists, and the calculated interval may be shifted in relation to the real one.

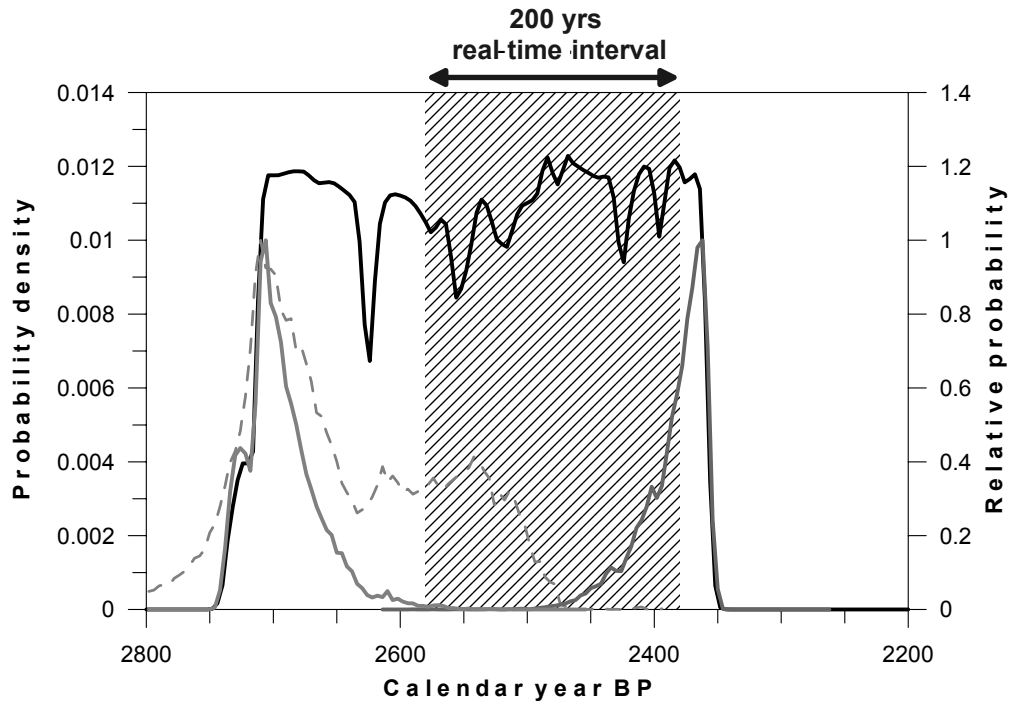

Figure 2 Comparison of the summed probability density distribution for 11 samples from the time interval 2380–2580 cal BP (black line), with the probability distributions of the first and the last event in this group of dates calculated using OxCal v.3.8 (grey, continuous lines). The grey dashed line shows the probability distribution of the last event in the group calculated using the "boundary" option of OxCal v.3.8. It should be emphasized that this distribution comprises the limit of the real-time interval, but the maximum of the distribution is still shifted.

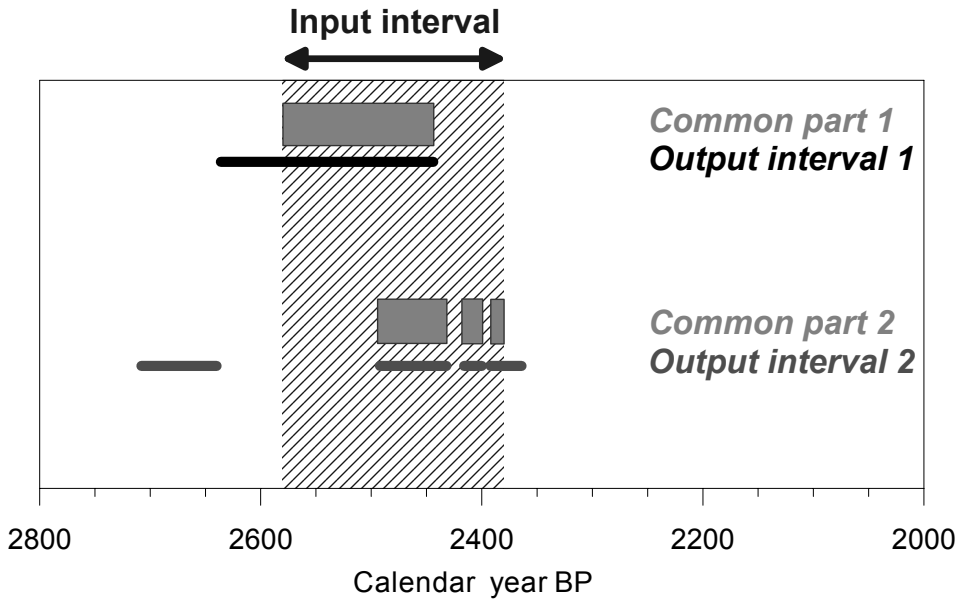

Figure 3 An example of the relationship between the real interval (Input Interval), the interval calculated on the basis of the summed probability density function (Output Interval), and the common part of these intervals.

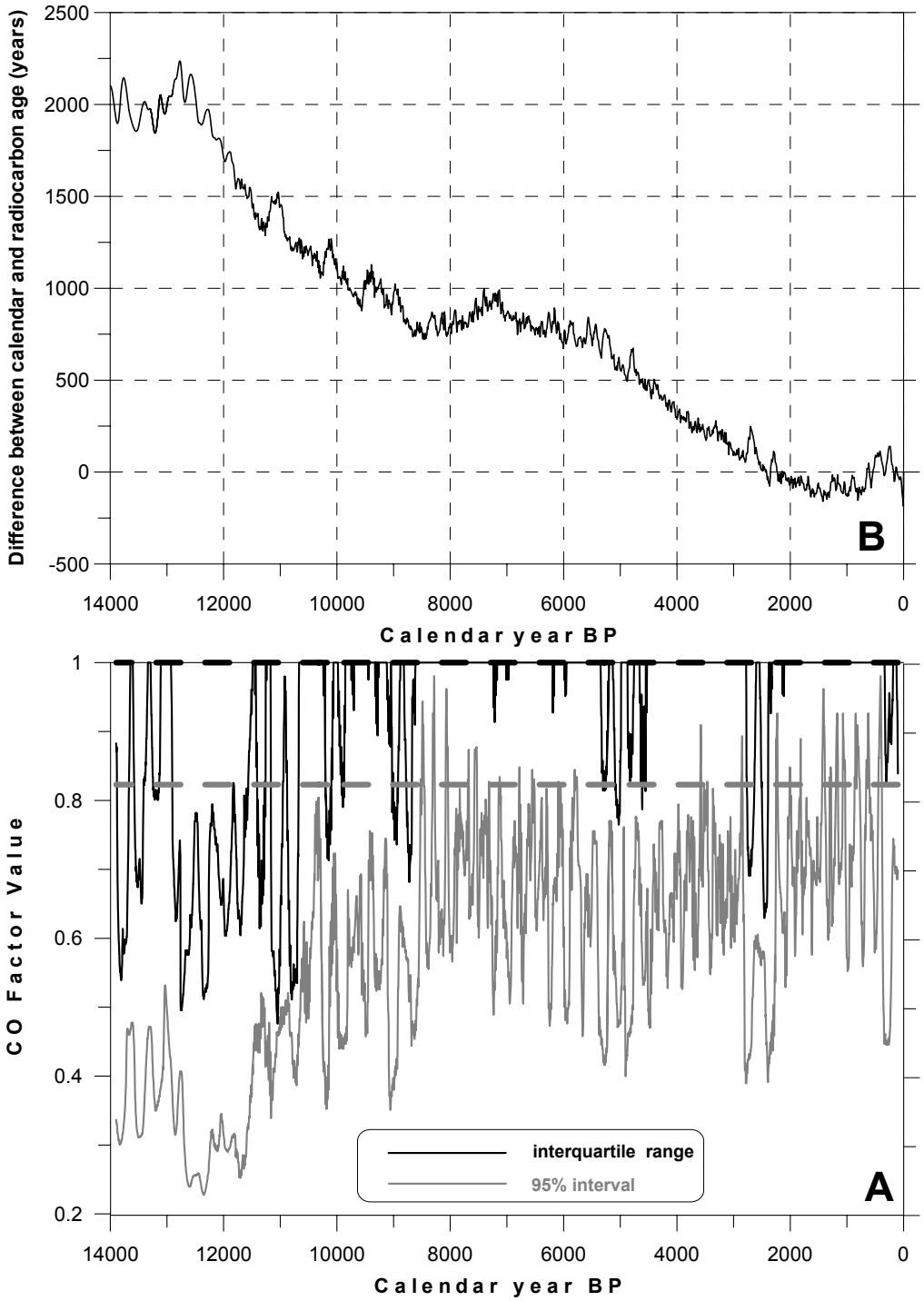

Figure 4 (a) Common to Output Factors for the interquartile range and the highest probability 95% confidence interval calculated for each 200-yr time period from 0–200 cal BP to 13,800–14,000 cal BP. The black and the grey dashed lines show the values of the CO Factor in the ideal case for the interquartile interval and for the highest probability 95% confidence interval, respectively; (b) Values of the difference between calendar age and corresponding ^{14}C age calculated on the basis of the calibration curve.

The results of calculations of Overlap Factors are shown in Figure 4 and Figure 5. The calculated values of the factors for a particular interval were assigned to the middle of that interval—i.e., values assigned, for example, to 2000 cal BP, correspond with time interval 1900–2100 cal BP. Figure 4a shows that for almost the entire 14,000-yr period, the value of the CO Factor for the highest probability 95% confidence interval is lower than in the ideal case. Likewise, the value of the CO Factor for the interquartile interval is often lower than 1 (CO Factor value in the ideal case). It allows us to draw the conclusion that the calibration curve causes the summed probability density function to cover a wider interval than the real-time interval of the phenomenon. Moreover, the low values of the CO Factor for the interquartile range suggest that the calculated intervals are shifted in relation to the real intervals. The relation between the shape of the calibration curve and the value of the CO Factor can be clearly seen when we compare Figures 4a and 4b. Figure 4b presents values for the difference between calendar age and corresponding ^{14}C age calculated on the basis of the calibration curve. We note that the lowest values of the CO Factor correspond with the major wiggles which are characteristic of the ambiguous region of the calibration curve.

In Figure 5, we observe that the values of the CI Factor for the interquartile range are almost always greater than the value of this factor in the ideal case. It confirms that the calibration curve extends the interval comprised by the probability density distribution, and thereby, the intervals calculated on the base of this distribution. On the other hand, the values of the CI Factor for the highest probability 50% confidence interval are, in most cases, greater than the value in the ideal case, and, in some cases, less than this value. Thus, the calculated intervals may be shifted in relation to the real-time interval. It should be emphasized that the CI Factor values for the interquartile range are always greater than for the highest probability 50% confidence interval.

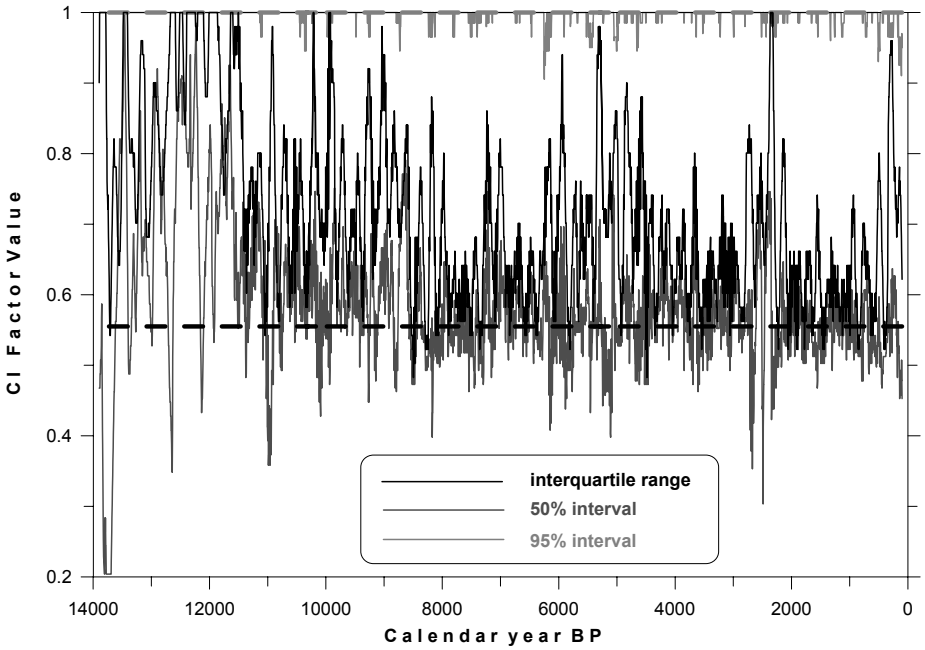

Figure 5 *Common to Input Factors* for the interquartile range, the highest probability 50% confidence interval and the highest probability 95% confidence interval calculated for each 200-yr time period from 0–200 cal BP to 13,800–14,000 cal BP. The black and the grey dashed lines show the values of the CI Factor in the ideal case for the interquartile interval (and the highest probability 50% confidence interval) and for the highest probability 95% confidence interval, respectively.

In order to assign the periods when calculated intervals are shifted in relation to the real-time intervals, the end and beginning values of the interquartile interval were calculated in relation to the beginning of the real interval. Figure 6 presents these values calculated for each of the 200-yr time intervals from 0–200 cal BP to 13,800–14,000 cal BP. It can be seen that for the greater part of the analyzed 14,000-yr period, the interquartile interval is contained in the real interval; therefore, the first may be used as an estimate of the latter. However, for about one-third of the 14,000 yr, we may observe a distinct shift of the interquartile interval (and consequently, the probability density function) in relation to the real interval. This shift is extremely large for the period past 10,500 cal BP.

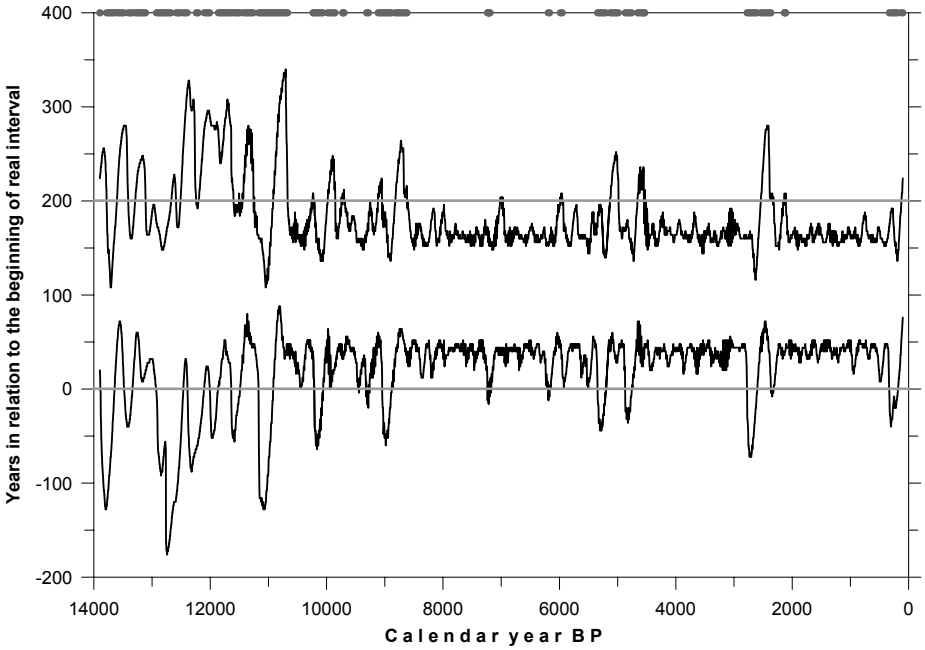

Figure 6 The values of the beginning and the end of the interquartile range shown in relation to the beginning of the real interval calculated for each 200-yr time interval from 0–200 cal BP to 13,800–14,000 cal BP. Grey continuous lines show the limits of the real-time interval. Grey dashed lines on the top of the figure indicate periods when a large shift of the interquartile interval in relation to the real interval is observed.

CONCLUSIONS

This study shows that the influence of the calibration curve on the statistical inference of time intervals is very important. First of all, the calibration curve always causes the summed probability density function of a group of ^{14}C dates associated with a phenomenon to cover a wider interval than the real time period of this phenomenon. Moreover, we may observe a distinct shift of the summed probability density function in relation to the real-time interval for about one-third of the 14,000 yr. The results also show that the interquartile interval estimates the length of the real time period of the phenomenon better than the highest probability 50% confidence interval and the highest probability 95% confidence interval.

REFERENCES

Aitchison T, Ottaway B, Al-Ruzaiza AS. 1991. Summarizing a group of ^{14}C dates on the historical time scale: with a worked example from the Late Neolithic of Bavaria. *Antiquity* 65(246):108–16.

McFadgen BG, Knox FB, Cole TRL. 1994. Radiocarbon calibration curve variations and their implications for the interpretation of New Zealand prehistory. *Radiocarbon* 36(2):221–36.

Michczyńska DJ, Pazdur MF, Walanus A. 1990. Bayesian approach to probabilistic calibration of radiocarbon ages. In: Mook WG, Waterbolk HT, editors. Proceedings of the 2nd International Symposium ^{14}C and Archaeology. Strasburg. *PACT* 29:69–79.

Pazdur MF, Michczyńska DJ. 1989. Improvement of the procedure for probabilistic calibration of radiocarbon dates. In: Long A, Kra RS, Srdoć D, editors. Proceedings of the 13th International ^{14}C Conference. *Radiocarbon* 31(3):824–32.

Stuiver M, Reimer P. 1989. Histograms obtained from computerized radiocarbon age calibration. *Radiocarbon* 31(3):817–23.

Stuiver M, Reimer PJ, Bard E, Beck JW, Burr GS, Hughen KA, Kromer B, McCormac G, van der Plicht J, Spurk M. 1998. INTCAL98 radiocarbon age calibration, 24,000–0 cal BP. *Radiocarbon* 40(3):1041–83.

RADIOCARBON, Vol 46, Nr 2, 2004, p 1005–1014

NEW ΔR VALUES FOR THE SOUTHWEST PACIFIC OCEAN

Fiona Petchey[1] • Matthew Phelan[2] • J Peter White[3]

ABSTRACT. ΔR results of known-age shells from the Solomon and Coral Seas and the northwest coast of New Ireland are presented. The results are too few to be conclusive but indicate that ΔR in this region is variable. An average ΔR value of 370 ± 25 yr is recorded for a range of shell species from Kavieng Harbor, New Ireland, and is primarily attributed to weak equatorial upwelling of depleted ^{14}C due to seasonal current reversals. In contrast, values from the Solomon and Coral Seas are lower (average ΔR = 45 ± 19 yr). Higher ΔR values for some shellfish from these 2 seas is attributed to ingestion of ^{14}C-depleted sediment by deposit-feeding species.

INTRODUCTION

Marine shell is ubiquitous in archaeological sites throughout the Pacific. The ability to accurately calibrate marine shell radiocarbon dates is, therefore, vital to the development of regional chronologies for human colonization (e.g. Spriggs 1996; White and Murray-Wallace 1996; Specht and Gosden 1997; Best 2002). Regionally, the ^{14}C of the ocean surface deviates from the modeled marine curve of Stuiver et al. (1998) due to variations in upwelling, ocean currents, and inter-hemispheric atmospheric ^{14}C (Stuiver and Braziunas 1993). Therefore, when dating marine shells, it is essential to know the difference (ΔR) between the global average [Rg(t)] and the actual ^{14}C activity of the surface ocean at a particular location [Rs(t)]. The ΔR for a specific location(s) can be calculated from known-age shells collected prior to atmospheric bomb testing using the formula: Rs(t) – Rg(t) = ΔR(s) (Stuiver et al. 1998).

Unfortunately, there are few published ΔR results for the southwest Pacific (see Reimer and Reimer 2003). Moreover, marine shell ^{14}C determinations can be difficult to interpret because they may incorporate ^{14}C from a range of carbon reservoirs. High ΔR values are typically produced by the incorporation of dissolved (i.e. hardwater effect) or particulate carbonates derived from calcareous bedrock or the upwelling of ^{14}C-depleted water. Lower values have been attributed to well-mixed water and the incorporation of freshwater—either derived from river-borne dissolved and particulate organic matter or high rainfall (Stuiver and Braziunas 1993; Ingram 1998; Southon et al. 2002). The effect of these varying sources of ^{14}C on shellfish will depend upon the degree of water exchange with the open ocean coupled with peculiarities of habitat and diet (Tanaka et al. 1986; Hogg et al. 1998). Anomalous ΔR values for algae grazers[4] and deposit feeders have been attributed to the intake of detrital matter, which can vary in age depending on local geology (Dye 1994; Spenneman and Head 1998; Hogg et al. 1998). Suspension feeders generally consume suspended phytoplankton and dissolved inorganic carbon from seawater, though some bivalve species will also engage in deposit-feeding activities depending on local circumstances (Snelgrove and Butman 1994). Consequently, anomalous ΔR values could be caused by a hardwater effect or the incorporation of riverine material, while some filter feeders may also be affected by similar sources of error

[1]Waikato Radiocarbon Dating Laboratory, University of Waikato, Private Bag 3105, Hamilton, New Zealand. Corresponding author. Email: f.petchey@waikato.ac.nz.
[2]Aboriginal Affairs Victoria, PO Box 515, East Melbourne, Victoria 3002, Australia.
[3]School of Philosophical and Historical Inquiry, University of Sydney, New South Wales 2006, Australia.
[4]Algae grazers feeding on a living coral substrate should only incorporate very recent carbon, although this could vary where fossil and/or sub-fossil coral are present. Algal grazers that target species restricted to seaweed surfaces should not present this problem.

Proceedings of the 18th International Radiocarbon Conference, edited by N Beavan Athfield and R J Sparks
RADIOCARBON, Vol 46, Nr 2, 2004, p 1005–1014

as deposit-feeding species. Little data is available for carnivorous shellfish, but they are presumed to show an averaging effect depending on the carbon reservoirs of their prey.

This paper presents preliminary results of research undertaken to increase our knowledge of ΔR variation in a region stretching from the Bismarck Archipelago to New Caledonia.

ΔR RESULTS AND DISCUSSION

A total of 16 prebomb age shells have been dated as part of this study (Figure 1). Samples were obtained from collections housed in the University of Auckland and the Auckland Museum in New Zealand, the Australian Museum, and the National Museum of Natural History, Paris. The shellfish were identified as coming from Buka and Bougainville Islands, New Ireland; the Duke of York Islands; New Britain; Malaita, Russell, and Masighe Islands in the Solomon Group; Ambrym Island in Vanuatu; and New Caledonia. ^{14}C measurements were made at either the Waikato Radiocarbon Dating Laboratory at the University of Waikato, New Zealand, or the Australian Nuclear Science and Technology Organization (ANSTO). ^{14}C data and ΔR values are shown in Table 1.

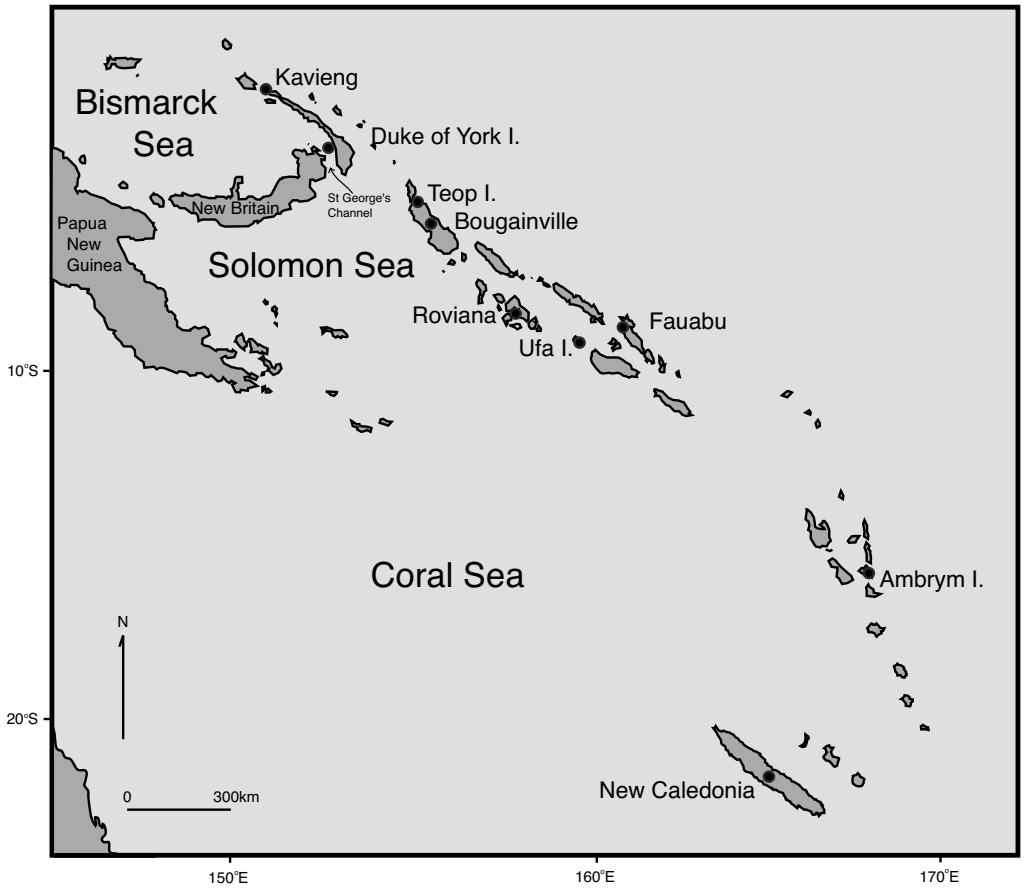

Figure 1 Map of the southwest Pacific Ocean showing location of known-age marine shells collected for this research

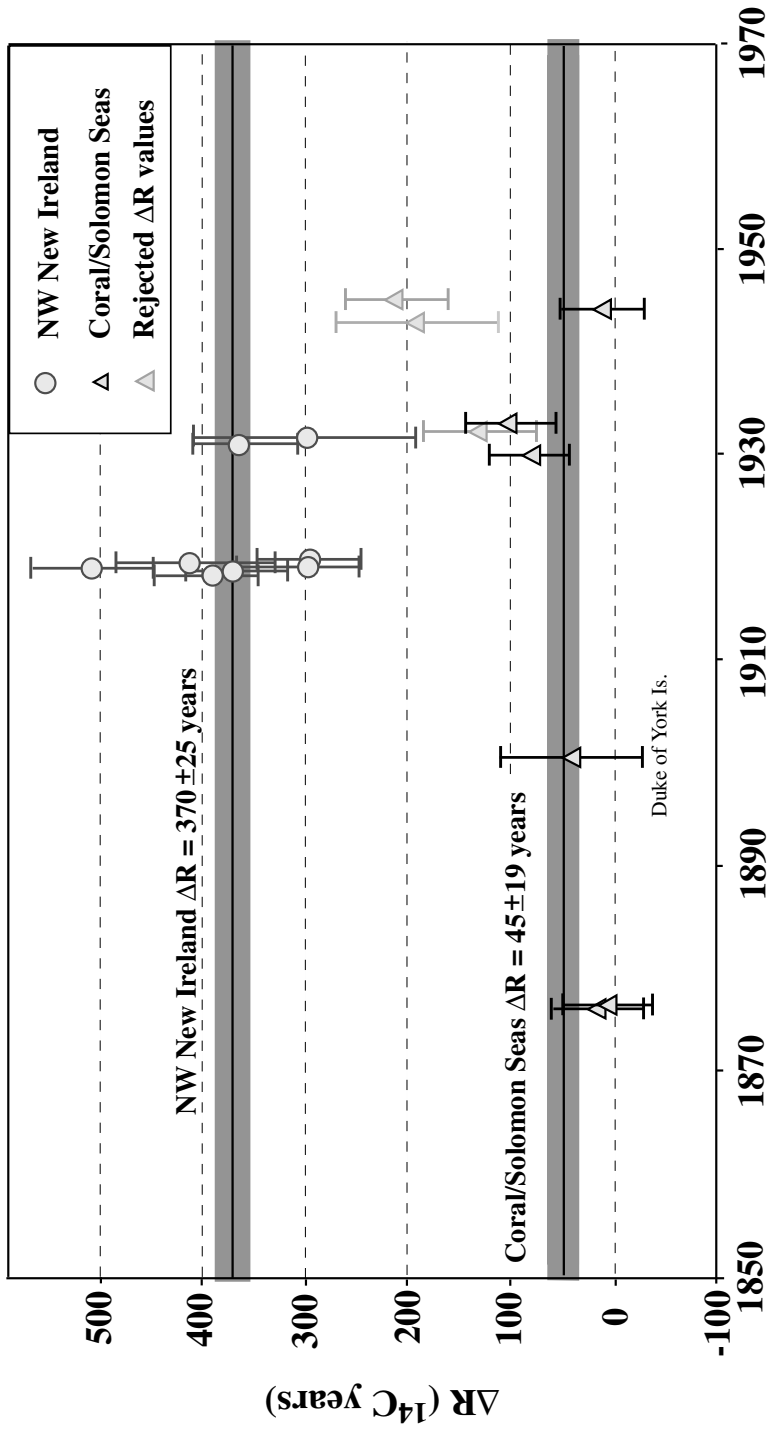

Figure 2 ΔR values obtained from this study for the Coral/Solomon Seas and northwest New Ireland plotted against year of collection. Error bars denote 1 standard deviation from the mean.

New Ireland and Duke of York Islands

Eight shells were collected from Kavieng Harbor (Figure 1) and provide a ΔR weighted mean of 370 ± 21 yr with a 1-σ scatter in the data of 25 yr (Figure 2). The slightly larger scatter sigma indicates an additional uncertainty in ΔR introduced by non-uniform ^{14}C content of the shellfish. Stuiver et al. (1986) recommend the use of the larger standard error to account for this uncertainty.

The shells selected come from 2 species of *Conus*, a carnivorous gastropod: *Nerita plicata*, an algae grazer; and *Barbatia foliata*, a suspension-feeding bivalve. The close proximity of Pleistocene-aged limestone islands to the southwestern edge of the harbor (Hohnen and Cooper 1973a) may be responsible for the elevated ΔR values. Dye (1994) has previously demonstrated that *Nerita* may give unreliable ^{14}C values if living on a limestone substrate (see also Anderson et al. 2001). Similarly, *Conus* sp. could incorporate depleted ^{14}C from prey living on these sands. The ΔR values of *Nerita* (360 ± 50 yr) and *Conus* sp. (range from 298 ± 50 yr to 508 ± 60 yr) are, however, indistinguishable [$T' = 9.42$; $\chi^2_{7:0.05} = 14.07$ (Ward and Wilson 1978)] from *Barbatia* (ΔR = 300 ± 110 yr). The general agreement between all shellfish species suggests this high ΔR value is a true reflection of the surface waters at this location. High values have also been calculated for archaeological terrestrial/marine pairs from Watom Island in the Bismarck Sea (Petchey, unpublished data). Similar ΔR values are found in regions of upwelled deep ocean water [e.g. the east coast of North America (Stuiver and Braziunas 1993) and the Arabian Sea (Southon et al. 2002)].

New Ireland is situated within the northern branch of the South Equatorial Current (SEC). Typically, ΔR values obtained for locations within the SEC are much lower than that for Kavieng Harbor [e.g. Fanning Island (4°N, 159°W) ΔR = 19 ± 21 yr (Druffel 1987); Nauru (0°S, 166°W) ΔR = 6 ± 14 yr (Guilderson et al. 1998)]. This suggests a localized effect is responsible for the elevated ΔR for New Ireland. Ocean circulation within this New Ireland/New Britain region is typified by large seasonal reversals of the major current systems [the northern branch of the SEC and the North Equatorial Counter Current (NECC)] (Figure 3). In summer (June/July), the NECC flows to the northwest. During 1995/96, Kuroda (2000) observed that this intrusion caused a reversal in the sub-surface current that resulted in surface water accumulation along the New Guinea coast and weak Ekman upwelling at the Equator. In winter (January/February), the currents reversed and Kuroda (2000) noted that upwelling occurred along the New Guinea coastline. It seems probable that this summer Ekman upwelling is responsible for elevated ΔR values off the north coast of New Ireland.

Table 1 presents a wide range of $\Delta^{14}C$ values (–88.4 to –111‰) for the Kavieng Harbor shellfish. Variation in $\Delta^{14}C$ of 25–30‰ has also been noted for banded corals in the southwest Pacific (Druffel and Griffin 1993, 1999) and western equatorial Pacific (Druffel 1987; Guilderson et al. 1998). These authors attributed this variation to seasonal differences in climate and currents, with longer term differences possibly associated with El Niño/Southern Oscillation events (ENSO). During normal years, ^{14}C-depleted water upwells in the east and is advected westward at the surface, primarily within the SEC, where it mixes with water from the sub-tropics. During each warm phase (El Niño), upwelling of low-^{14}C water slows in the eastern Pacific and the equatorial trade winds relax or reverse. As a result, $\Delta^{14}C$ values began to increase and subtropical water with higher concentrations of ^{14}C invade the SEC (Guilderson et al. 1998).

A much lower ΔR value was obtained for the Duke of York Islands (39 ± 68 yr), which are located between New Britain and New Ireland (Figure 1). The Duke of Yorks are composed primarily of Pleistocene-age raised corals (Hohnen and Cooper 1973b). A high ΔR value could, therefore, be expected if *Nassarius camelus*, a carnivorous gastropod, fed on animals which had digested this material. However, this is not supported by the ΔR value. Instead, we favor an explanation whereby

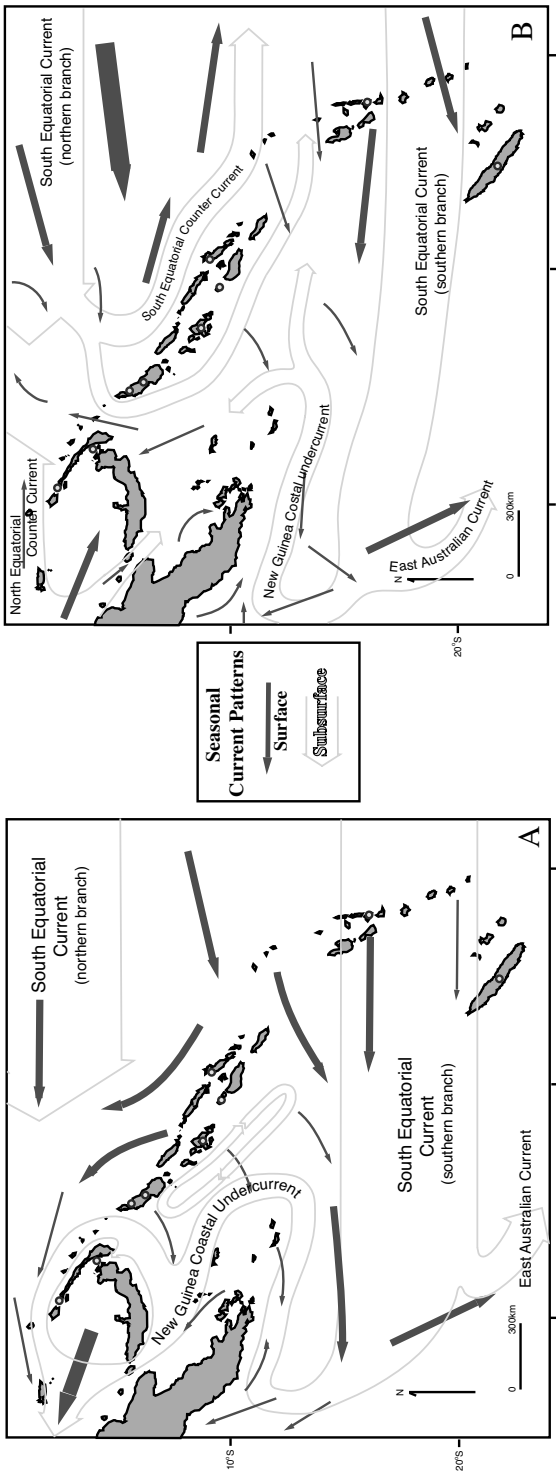

Figure 3 Map of the southwest Pacific Ocean showing major current patterns during 1999/2000 for (a) Summer (June/July); (b) Winter (Jan/Feb) [Current data: AIMS (1998)]

the New Guinea Coastal Undercurrent brings higher $\Delta^{14}C$ waters from the Coral and Solomon Seas (see below) into the St George's Channel (Butt and Lindstrom 1994), shielding the Duke of York Islands from the effects of the upwelling noted above.

The Coral and Solomon Seas

Nine ΔR values have been measured for the Coral/Solomon Sea region (Figure 1 and Table 1).

The high ΔR results from Ufa Island (211 ± 50 yr) and Fauabu, Malaita (130 ± 55 yr) are suspect because they are of a deposit-feeding gastropod (*Asaphis violascens*) collected from areas dominated by calcareous bedrock of Pleistocene, Miocene, and Pliocene age (British Solomon Islands. Dept of Geological Surveys 1969). A lower ΔR value of 82 ± 40 yr was obtained for the carnivore *Chicoreus ramosus* collected from Roviana Lagoon on the southern coast of New Georgia Island. Roviana Lagoon is largely bounded by volcanic bedrock with only minor Pleistocene limestone to the west of the lagoon, and on Rendova Island to the south.

Two ΔR results are available for Bougainville. The ΔR of 100 ± 45 yr for *Anadara* (Wk-8380), a suspension-feeding bivalve collected from Teop Island just off the northern coast of Bougainville, is indistinguishable ($T' = 2.14$; $\chi^2_{1:0.05} = 3.84$) from the ΔR of 12 ± 40 yr for the *Conus* sp. gastropod (Wk-8381). Unfortunately, the exact collection location for Wk-8381 is unknown. The ΔR value does not, however, suggest any influence from Pleistocene-age limestone that is located sporadically around the coast of Bougainville (Blake and Miezitis 1967), though the influence of riverine input cannot be excluded.

Only 1 value is available from Ambrym Island, Vanuatu (ΔR = 192 ± 80 yr). This result is indistinguishable [$T' = 1.52$; $\chi^2_{1:0.05} = 3.84$] from a ΔR of ~94 ± 10 yr obtained by Burr et al. (1998).[5] The possibility that these results are also influenced by incorporation of depleted carbon from limestone bedrock on the island cannot be discounted. Although Ambrym is a basaltic island formed by an active shield volcano, Pliocene and Pleistocene limestone sands from islands 10 km away (British Govt. Ministry of Overseas Development 1976) are available to the deposit-feeding *Tellina linguafelis*. Localized volcanic activity on the island may also affect ^{14}C. The influence of geothermal activity on the ^{14}C content of terrestrial and aquatic plant material is well documented (Rubin et al. 1987; Shutler 1971; Sveinbjörnsdóttir et al. 1992), and the venting of CO_2 and carbonates depleted in ^{14}C (Pichler et al. 1999) could be responsible for localized anomalies in shell ΔR.

Two very similar ΔR values are available for 2 species of Venus shells from New Caledonia (ΔR = 15 ± 45 yr and 5 ± 45 yr). Since *Venerines* are suspension-feeders, it is possible that the low ΔR values are caused by the incorporation of river-borne organic matter. Unfortunately, the collection location for these samples is unknown.

The 9 ΔR results presented here for the Coral and Solomon Seas and Duke of York Islands are highly variable [$T' = 17.83$; $\chi^2_{8:0.05} = 15.51$]. This variation may, in part, reflect peculiarities of ocean circulation within this region (Figure 3). The primary inflow to the Coral Sea is supplied by the west-flowing SEC. This current reaches the western boundary through a complex of islands, resulting in localized eddies and wakes (Coutis and Middleton 1999). The East Australian Current also introduces water with a higher $\Delta^{14}C$ signature than the SEC into the Coral Sea (Rafter 1968), and high

[5] Burr et al. (1998) give a reservoir value of 494 ± 10 yr for the island of Espiritu Santo, Vanuatu, which was calculated from the average of 35 prebomb samples of known age. The ΔR value of ~94 ± 10 yr given here assumes a 400-yr difference from the modeled marine curve (Stuiver et al. 1998).

Table 1 ^{14}C ages and ΔR results for known age shells from the Coral/Solomon Seas and northwest New Ireland.

Location	Lab nr[a]	Species[b]	$\delta^{13}C$‰[c]	Year collected[d]	$\Delta^{14}C$‰[e]	CRA [Rs(t)] + error[f]	Marine modeled age [Rg(t)][g]	ΔR (yr): Rs(t)–Rg(t)
New Ireland								
Kavieng Harbor	Wk-8377	*Nerita plicata* (AG)	1.06	1931	–96.8 ± 5.3	820 ± 50	459 ± 4	360 ± 50
	Wk-8379	*Barbatia foliata* (SF)	0.39		–90.4 ± 12.4	760 ± 110		300 ± 110
	OZB-768	*Conus lividus* (C)	1.94	1919*	–89.2 ± 6.5	760 ± 60	452 ± 4	308 ± 60
	OZB-769	*Conus lividus*	2.62		–111.2 ± 5.9	960 ± 60		508 ± 60
	OZB-770	*Conus lividus*	2.63		–95.7 ± 4.7	820 ± 50		368 ± 50
	OZB-771	*C. sanguinolentus* (C)	1.67		–100.4 ± 8.9	860 ± 80		408 ± 80
	OZB-772	*C. sanguinolentus*	1.96		–88.4 ± 5.1	750 ± 50		298 ± 50
	OZB-773	*C. sanguinolentus*	1.19		–100.7 ± 4.7	850 ± 50		398 ± 50
Solomon Sea/Coral Sea								
Duke of York Is.	Wk-9219	*Nassarius camelus* (C)	2.72	~1905*	–59.4 ± 7.9	492 ± 68	453 ± 5	39 ± 68
Bougainville	Wk-8381	*Conus* sp.(C)	2.12	1944	–57.5 ± 4.7	480 ± 40	468 ± 10	12 ± 40
Bougainville; Teop Is.	Wk-8380	*Anadara antiquita* (SF)	3.13	1933	–67.7 ± 4.9	560 ± 45	460 ± 5	100 ± 45
New Georgia	Wk-7828	*Chicoreus ramosus* (C)	3.83	1930*	–64.7 ± 4.9	540 ± 40	458 ± 4	82 ± 40
Fauabu, Malaita	Wk-8382	*Asaphis violascens* (DF)	–0.96	1932	–71.0 ± 6.2	590 ± 55	460 ± 5	130 ± 55
Ufa Is.; Russel Islands	Wk-8383	*Asaphis violascens*	1.71	1945	–80.7 ± 5.3	680 ± 50	469 ± 10	211 ± 50
Ambrym Is.; Vanuatu	Wk-8384	*Tellina linguafelis* (DF)	2.46	1943	–79.4 ± 8.6	660 ± 80	468 ± 9	192 ± 80
New Caledonia	Wk-8046	*Venus peupera* (SF)	1.66	1876*	–58.9 ± 4.9	490 ± 45	475 ± 4	15 ± 45
	Wk-8047	*Venus reticulata* (SF)	2.46		–57.7 ± 5.2	480 ± 45		5 ± 45

[a]Lab prefixes: Wk = Waikato Radiocarbon Dating Laboratory; OZ = Australian Nuclear Sciences and Technology Organisation (ANSTO).

[b]SF = suspension feeder; DF = deposit feeder; C = carnivore; AG = algae grazer. Diet information from Beesley et al. (1998).

[c]$\delta^{13}C$ reported relative to the PDB standard with a precision of 0.2‰.

[d]Although museum records were not always adequate to indicate if the shellfish were collected live, all shells used were unweathered and bivalves in articulation. Samples are marked with an * where live collection unknown. Wk-9219 was collected prior to 1910 and we have assumed a 1905 date.

[e]$\Delta^{14}C$ calculated following the conventions of Stuiver and Polach (1977).

[f]No Suess correction has been applied to these calculations due to uncertain effect of anthropogenic ^{14}C in the southwest Pacific (Druffel and Griffin 1993).

[g]Marine model age calculated from 1998 marine calibration dataset (Stuiver et al. 1998).

precipitation associated with the winter monsoon and the Southern Oscillation adds a thin layer of freshwater into the ocean north of 17°S (Sokolov and Rintoul 2000). These factors combine to produce inter-annual and seasonal changes that have previously been documented for the Coral Sea (Druffel and Griffin 1993, 1999; Godfrey et al. 2001). However, if ΔR values of deposit-feeders are excluded (i.e. those from Ufa Island, Malaita, and Ambrym Island) the 6 remaining values have a weighted mean of 45 ± 19 yr and a scatter σ in the unweighted mean of 16 yr (Figure 2). This suggests that much of this variability can be attributed to the habitat and dietary preferences of some shellfish species.

CONCLUSIONS

The limited results presented here indicate a wide range of ΔR values for the Coral and Solomon Seas and the northern coast of New Ireland. High ΔR values recorded around Kavieng Harbor, New Ireland are possibly the result of Ekman upwelling caused by seasonal reversals in the SEC and NECC. In contrast, values obtained for the Coral and Solomon Seas are lower. Significant differences in ΔR, especially for shells from Kavieng Harbor, highlight that this entire southwest Pacific region is influenced by ENSO and seasonal climatic variation that will make designation of a specific ΔR difficult. Some variability in ΔR is also attributed to the incorporation of material depleted in ^{14}C by deposit-feeding shellfish, and it is recommended that these species are avoided for dating. Unfortunately, there are too few results currently available to fully evaluate the reliability of different species or the range of ΔR values that can be expected. Moreover, changes to ocean circulation and climate due to anthropogenic influences have been recorded in banded coral records from this region as early as the 1850s (Druffel and Griffin 1993, 1999; Tudhope et al. 1995; Quinn et al. 1993, 1998) and may influence the results presented here.

A range of modern shell species and environmental samples have been collected from Roviana Lagoon as part of ongoing research investigating variation in ΔR, with specific focus on marine, estuarine, sea-grass meadows, and coral reef environs. A change in ocean reservoir effects over time as climatic regimes change and influence rainfall patterns, ocean currents, and upwelling is also likely. To assess the impact of longer term fluctuations in ΔR, paired marine/terrestrial samples have been selected from archaeological sites in Vanuatu, the Reef/Santa Cruz Islands, Babase Island, and New Britain. These data are still to be fully investigated.

ACKNOWLEDGEMENTS

Known-age samples have been acquired from various sources: Roviana Lagoon, Malaita, and Russel Islands (courtesy of Dr Peter Sheppard, University of Auckland); Bougainville and northwest New Ireland (courtesy Auckland Museum); Rabual Harbor and Duke of York Islands (courtesy Australian Museum); and New Caledonia (courtesy Dr Phillipe Bouchet, National Museum of Natural History, Paris). Thanks to Prof Roger Green (University of Auckland) for arranging access to the Auckland Museum collections, Dr Carol Diebel and Noel Garner (Auckland Museum) for assistance in selecting suitable shellfish, Dr Ugo Zoppi (ANSTO) for additional information on the ANSTO date results, and Dr Alan Hogg (University of Waikato) for helpful comments. OZB dates were funded by AINSE grant 95/R142 to White. Wk dates were funded by a Waikato post-doctoral grant to Phelan.

REFERENCES

Australian Institute of Marine Science (AIMS). 1998. Coral Sea Region Billfish Atlas: Currents [Online]. AIMS Research, Australian Institute of Marine Science. Available: http://www.aims.gov.au/pages/reflib/billfish/pages/bf_05.html [Accessed 25 August 2003].

Anderson A, Higham T, Wallace R. 2001. The radiocarbon chronology of the Norfolk Island archaeological sites. *Records of the Australian Museum, Supplement* 27:33–42.

Beesley PL, Ross GJB, Wells A, editors. 1998. *Mollusca: the Southern Synthesis. Fauna of Australia. Volume 5*. Melbourne: CSIRO Publishing.

Best S. 2002. *Lapita: A View from the East*. Auckland: New Zealand Archaeological Association Monograph 24.

Blake DH, Miezitis Y. 1967. *Geology of Bougainville and Buka Islands, New Guinea* Bureau of mineral resources, geology and geophysics. Bulletin No. 93. Canberra, ACT.

British Government Ministry of Overseas Development. 1976. Geology of Pentecost and Ambrym 1:100,000. New Hebrides Geological Survey, Sheet 6.

British Solomon Islands. Department of Geological Surveys. 1969. Geological Map of the British Solomon Islands, 2nd edition. Scale 1:1,000,000. *The British Solomon Islands Geological Record, Vol 111*. Great Britain. Ordnance Survey, London.

Burr GS, Beck JW, Taylor FW, Recy J, Edwards RL, Cabioch G, Correge T, Donahue DJ, O'Malley JM. 1998. A high-resolution radiocarbon calibration between 11,700 and 12,400 calendar years BP derived from ^{230}Th ages of corals from Espiritu Santo Island, Vanuatu. *Radiocarbon* 40(3):1093–105.

Butt J, Lindstrom E. 1994. Currents off the east coast of New Irelands, Papua, New Guinea and their relevance to regional undercurrents in the western equatorial Pacific Ocean. *Journal Geophysical Research* 99: 12,503–14.

Coutis PF, Middleton JH. 1999. Flow-topography interaction in the vicinity of an isolated, deep ocean island. *Deep-Sea Research I* 46(9):1633–52.

Druffel ERM. 1987. Bomb radiocarbon in the Pacific: annual and seasonal timescale variations. *Journal of Marine Research* 45:667–98.

Druffel ERM, Griffin S. 1993. Large variations of surface ocean radiocarbon: evidence of circulation changes in the southwestern Pacific. *Journal of Geophysical Research* 98(C11):20,249–59.

Druffel ERM, Griffin S. 1999. Variability of surface ocean radiocarbon and stable isotopes in the southwestern Pacific. *Journal of Geophysical Research* 104 (C10):23,607–13.

Dye T. 1994. Apparent ages of marine shells: implications for archaeological dating in Hawaii. *Radiocarbon* 36(1):51–8.

Godfrey JS, Hohnson GC, McPhaden MJ, Reverdin G, Wijffels SE. 2001. The tropical ocean circulation. In: Siedler GJ, Church J, Gould J, editors. *Ocean Circulation and Climate: Observing and Modeling the Global Ocean*. International Geophysics Series Vol 77. London, San Diego: Academic Press. p 215–46.

Guilderson, TP, Schrag DP, Kashgarian M, Southon J. 1998. Radiocarbon variability in the western equatorial Pacific inferred from a high-resolution coral record from Nauru Island. *Journal of Geophysical Research* 103(C11):24,641–50.

Hogg AG, Higham TFG, Dahm J. 1998. ^{14}C dating of modern marine and estuarine shellfish. *Radiocarbon* 40(2):975–84.

Hohnen PD, Cooper RD. 1973a. New Ireland and Tabar Islands 1:250,000. Bureau of Mineral Resources, Geology and Geophysics, Department of Minerals and Energy, in co-operation with the Geological Survey of Papua New Guinea. Mercury-Walch Pty Ltd, Australia.

Hohnen PD, Cooper RD. 1973b. *Gazelle Peninsula 1: 250,000.* Bureau of Mineral Resources, Geology and Geophysics, Department of Minerals and Energy, in co-operation with the Geological Survey of Papua New Guinea. Mercury-Walch Pty Ltd., Australia.

Ingram BL. 1998. Differences in radiocarbon age between shell and charcoal from a Holocene shellmound in northern California. *Quaternary Research* 49:102–10.

Kuroda Y. 2000. Variability of currents of the northern coast of New Guinea. *Journal of Oceanography* 56(1):103–16.

Pichler T, Veizer J, Hall GEM. 1999. The chemical composition of shallow-water hydrothermal fluids in Tutum Bay, Ambitle Island, Papua New Guinea and their effect on ambient seawater. *Marine Chemistry* 64: 229–52.

Quinn TM, Crowley TJ, Taylor FW, Henin C, Joannot P, Join Y. 1998. A multicentury stable isotope record from a New Caledonia coral: interannual and decadal sea surface temperature variability in the southwest Pacific since 1657 AD. *Paleoceanography* 13(4): 412–26.

Quinn TM, Taylor FW, Crowley TJ. 1993. A 173-year stable isotope record from a tropical South Pacific coral. *Quaternary Science Reviews* 12:407–18.

Rafter TA. 1968. Carbon-14 variations in nature, Part 3, C14 measurements in the South Pacific and Antarctic Oceans. *New Zealand Journal of Science* 11:551–88.

Reimer PJ, Reimer R. 2003. Marine reservoir correction database [online]. Available: http://calib.org/marine/ [Accessed 25 Aug 2003].

Rubin M, Lockwood JP, Fried I. 1987. Effects of volcanic emanations on carbon-isotope content of modern plants near Kilauea volcano. In: Decker RW, Wright TL, Stauffer PH, editors. *Volcanism in Hawai'i. U.S. Geological Survey Professional Paper No. 50.* Wash-

ington: U.S. Department of the Interior. p 209–11.

Shutler R. 1971. Pacific Island radiocarbon dates, an overview. In: Green RC, Kelly M, editors. *Studies in Oceanic Culture History: Papers Presented at Wenner-Gren Symposium on Oceanic Culture History, Singatoka, Fiji, 1969, V II.* Pacific Anthropological Records No. 12. Honolulu: Bernice Pauahi Bishop Museum. p 13–27.

Snelgrove PVR, Butman CA. 1994. Animal-sediment relationships revisited: cause vs effect. *Oceanography and Marine Biology: An Annual Review* 32:111–77.

Sokolov S, Rintoul S. 2000. Circulation and water masses of the southwest Pacific: WOCE Section P11, Papua New Guinea to Tasmania. *Journal of Marine Research* 58(2):223–68.

Southon J, Kashgarian M, Fontugne M, Metivier B, Yim WW-S. 2002. Marine reservoir corrections for the Indian Ocean and Southeast Asia. *Radiocarbon* 44(1): 167–80.

Specht J, Gosden C. 1997. Dating Lapita pottery in the Bismarck Archipelago. *Asian Perspectives* 36(2): 175–99.

Spenneman DHR, Head MJ. 1998. Tongan Pottery chronology, ^{14}C dates and the hardwater effect. *Quaternary Geochronology* (Quaternary Science Reviews) 17(11):1047–6.

Spriggs M. 1996. Chronology and colonisation in island Southeast Asia and the Pacific: new data and evaluation. In: Davidson J, Irwin G, Leach F, Pawley A, Brown D, editors. 1996. *Oceanic Culture History: Essays in Honour of Roger Green*. Dunedin: New Zealand Journal of Archaeology Special Publication. p 33–50.

Stuiver M, Braziunas TF. 1993. Modeling atmospheric ^{14}C influences and ^{14}C ages of marine samples to 10,000 BC. *Radiocarbon* 35:137–89.

Stuiver M, Polach HA. 1977. Discussion: reporting ^{14}C data. *Radiocarbon* 19(3):355–63.

Stuiver M, Pearson GW, Braziunas TF, 1986. Radiocarbon age calibration of marine samples back to 9000 cal yr BP. *Radiocarbon* 28(2B):980–1021.

Stuiver M, Reimer PL, Braziunas TF. 1998. High-precision radiocarbon age calibration for terrestrial and marine samples. *Radiocarbon* 40(3):1127–54.

Sveinbjörnsdóttir AE, Heinemeier J, Rud N, Johnsen SJ, 1992. Radiocarbon anomalies observed for plants growing in Icelandic geothermal waters. *Radiocarbon* 34(3):696–703.

Tanaka N, Monaghan MC, Rye DM. 1986. Contribution of metabolic carbon to mollusc and barnacle shell carbonate. *Nature* 320:520–3.

Tudhope AW, Shimmield GB, Chilcott CP, Jebb M, Fallick AE, Dalgleish AN. 1995. Recent changes in climate in the far western equatorial Pacific and their relationship to the Southern Oscillation; oxygen isotope records from massive corals, Papua New Guinea. *Earth and Planetary Science Letters* 136:575–90.

Ward GK, Wilson SR. 1978. Procedures for comparing and combining radiocarbon age determinations: a critique. *Archaeometry* 20:19–31.

White JP, Murray-Wallace CV. 1996. Site ENX (Fissoa) and the incised and applied pottery tradition in New Ireland, Papua New Guinea. *Man and Culture in Oceania* 12:31–46.

ERRATUM

There is an error in Figure 8 of Hua et al. "Bomb Radiocarbon in Tree Rings from Northern New South Wales, Australia: Implications for Dendrochronology, Atmospheric Transport, and Air-Sea Exchange of CO_2", *Radiocarbon* 45(3):431–47. The original figure had incorrect latitude and longitude labels; the correct figure is given below. We apologize for this error.

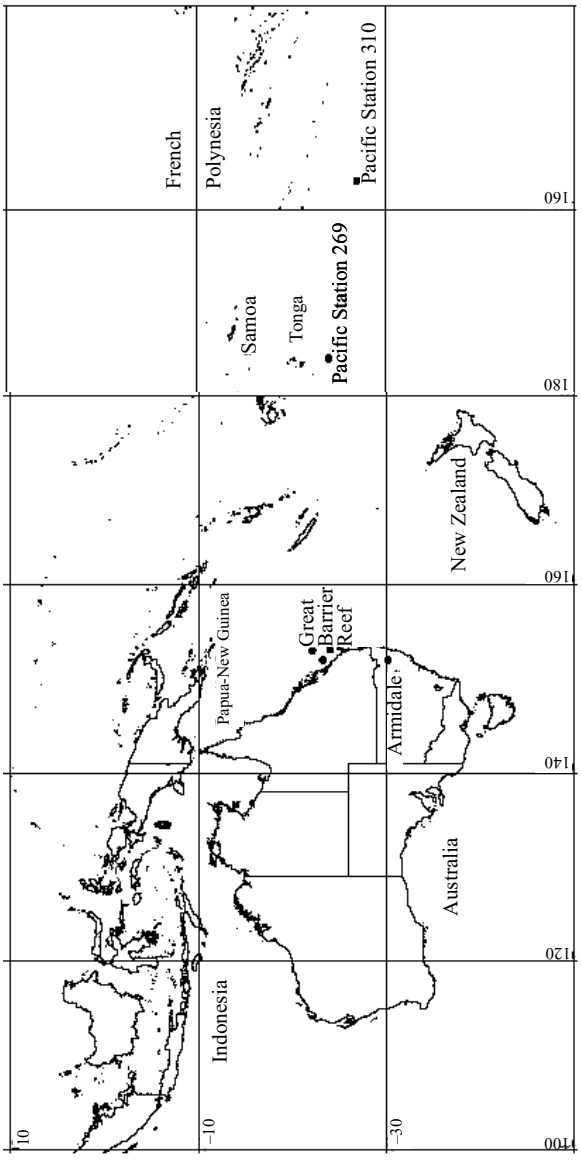

Figure 8 Map of Australia and the Southwest Pacific showing location of the Armidale *Pinus radiata* tree, sites for Great Barrier Reef corals (Heron Island, Abraham Reef, and Lady Musgrave Island), and GEOSECS Pacific stations 269 and 310.

RADIOCARBON UPDATES

Death of Reidar Nydal

We regret to announce the passing of Reidar Nydal, one of the pioneers in the radiocarbon community. We plan to publish an obituary in the next volume of the journal.

INTCAL04

The next issue of *Radiocarbon* is devoted to the findings from the IntCal04 group. Please check our website at http://www.radiocarbon.org for news and updates regarding the issue.

Online Access to the Journal

The journal's internet host, Ingenta, is in the process of reorganizing their website, making it easier for users to access information. Radiocarbon subscribers have free access to the online journal (starting with Volume 42) at http://www.ingenta.com. Subscribers often can access the journal online before they receive their copy of the print issue. If you should have any problems accessing the journal, please email Mark McClure at editor@radiocarbon.org.

Upcoming Conferences

Geological Society of America Annual Meeting

The Geological Society of America (GSA) will hold its annual meeting and exposition in Denver, Colorado, USA, from November 7–10, 2004. The conference is titled "Geoscience in a Changing World." Further information can be found at the conference website, http://www.geosociety.org.

American Geophysical Union Annual Fall Meeting

The 2004 AGU Fall Meeting is expected to draw a crowd of over 10,000 geophysicists from around the world. The meeting will be held in San Francisco, California, USA, from December 13–17, 2004. Abstracts may be submitted electronically. See the meeting's website for instructions and information: http://www.agu.org/meetings/fm04/.

Society for American Archaeology 70th Annual Meeting

The Society for American Archaeology will hold its annual meeting in Salt Lake City, Utah, USA, from March 30th to April 3rd, 2005. Papers may be submitted electronically. For directions, refer to the conference website, http://www.saa.org. *Radiocarbon* will be an exhibitor, so please stop in and see us.

AMS 10th Annual Conference

The Center for Accelerator Mass Spectrometry (CAMS) at the Lawrence Livermore National Laboratory will host the 10th Annual AMS Conference to be held from September 5–10th, 2005, in Berkeley, California, USA. Updates can be found at http://cams.llnl.gov/events.php.

AUTHOR INDEX
VOLUME 46(1–2), 2004

SUBJECT INDEX
VOLUME 46, Nr 1–2

Australian Government

ansto

ANTARES AMS

^{129}I ^{26}Al ^{10}Be ^{14}C ^{236}U

Established at the Australian Nuclear Science and Technology Organisation (ANSTO) in 1991, we offer AMS services and collaborative arrangements to Australian and international researchers in a wide range of applications.

Capabilities

- Designed for Multi-isotope analysis with high precision and high throughput.
- ^{10}Be, ^{14}C, ^{26}Al, ^{129}I and ^{236}U are routinely analysed.
- A suite of chemistry laboratories for sample processing and target preparation for a wide range of sample types.
- Stable isotope analysis ($\delta^{13}C$ and $\delta^{15}N$).

Current Applications

- Radiocarbon dating
- Geological exposure dating
- Nuclear safeguards

We specialise in

- Small radiocarbon sample size
- Atmospheric carbon dioxide analysis
- High sensitivity actinide analysis

To find out more contact

ANTARES AMS Facility
Australian Nuclear Science and Technology Organisation
PMB 1, Menai NSW 2234, AUSTRALIA
antares.ams@ansto.gov.au
www.ansto.gov.au/ansto/environment1/ams

RADIOCARBON

$5 Back Issues Clearance Sale

YEAR	VOL.	Write in the number of copies desired for each issue					
		NR 1	NR 2	NR 2A	NR 2B	NR 3	NR 4
1980	22						
1981	23						
1982	24						
1983	25						
1984	26						
1985	27						
1986	28						
1987	29						
1988	30						
1989	31						
1990	32						
1991	33						
1992	34						

Calculate Payment

____ copies × $5 ea. = $_____

Subtotal: $_____

Shipping via surface mail:
(Contact us for other shipping methods)

Add $2 ea. book for US
Add $3 ea. book outside US

___ copies × $____ea. = $_____

Shipping total: $_____

Total due: $_____

Payment & Shipping Address

❑ MasterCard ❑ Visa
❑ Check enclosed ❑ Please bill me

Name:

Address:

Fax: E-mail:

For Credit-Card Orders

Card number: Expiration date:

Signature: Phone:

For online Contents see: `http://www.radiocarbon.org/Pubs/contents.html`

Prices good while supplies last. Mail or fax this form to:

RADIOCARBON, 4717 East Fort Lowell Road, Room 104, Tucson, Arizona 85712-1201 USA
Phone: +1 520 881-0857; Fax: +1 520 881-0554; orders@radiocarbon.org

Radiocarbon

An International Journal of Cosmogenic Isotope Research

Univ. of Arizona, Dept.of Geosciences
4717 E. Fort Lowell Rd, Rm. 104
Tucson, AZ 85712-1201 USA
Phone +1 520 881-0857
Fax: +1 520 881-0554
E-mail: orders@radiocarbon.org
http://www.radiocarbon.org

2004 PRICE LIST

Proceedings of the 18th International Radiocarbon Conference (Vol 46, Nrs 1 and 2, 2004) *Save $10*	$70.00*
Proceedings of the 17th International Radiocarbon Conference (Vol 43, Nrs 2A, 2B and 3, 2001)	75.00
Proceedings of the 16th International Radiocarbon Conference (Vol 40, Nrs 1 and 2, 1998)	50.00
INTCAL98 (1998 Calibration issue; Vol 40, Nr 3, 1998)	40.00
Calibration 1993 (Vol 35, Nr 1, 1993)	40.00
Proceedings of the 15th International Radiocarbon Conference (Vol 37, Nr 2, 1995)	50.00
Liquid Scintillation Spectrometry 1992 (ISBN: 0-9638314-0-2; 1993)	20.00
Liquid Scintillation Spectrometry 1994 (ISBN: 0-9638314-3-7; 1996)	10.00
Liquid Scintillation Spectrometry 2001 (ISBN: 0-9638314-4-5; 2002)	60.00
Special offer—**LSC 92**, **LSC 94, LSC 2001** package—save $10.00	80.00
Tree Rings, Environment and Humanity (ISBN 0-9638314-2-9; 1996) (Proceedings of the International Tree-Ring Conference, Tucson, Arizona, 1994)	20.00
Late Quaternary Chronology and Paleoclimates of the Eastern Mediterranean (ISBN 0-9638314-1-0; 1994) *Back in print!*	40.00

SUBSCRIPTION RATES **VOLUME 46, Nrs 1–3, 2004** (subscriptions include free online access)	
Institution (US, shipping included)	190.00
Institution (Foreign, shipping included)	205.00
Individual (US, shipping included)	90.00
Individual (Foreign, shipping included)	105.00
Lifetime Subscription—Institutional	2500.00
Lifetime Subscription—Individual	1000.00

BACK ISSUES (except conference proceedings and special issues)	Single issue 40.00
VOLUMES 1–9 each volume	40.00
VOLUMES 10–21 each volume	65.00
VOLUMES 22–45 each volume	100.00
Radiocarbon Conference Proceedings	50.00
SPECIAL FULL-SET OFFER—Volumes 1–45 (1959–2003)	1300.00
Big savings! Includes bound copies of 35 out-of-print issues. Take $50.00 off for each additional set.	

2004 POSTAGE AND HANDLING CHART

	U.S.	Foreign
Subscription	—	$13.00
Single back issue	$3.00	$9.00
Book or Proceedings	$5.00	$15.00
Full set	$72.00	$220.00

Surface mail rates are listed here. Please contact us for airmail or express delivery rates.
Orders must be prepaid. We accept payments by Visa, MasterCard, or AMEX or by check or money order payable in US$ to *Radiocarbon*. Bank funds transfers are also accepted. Please contact us for instructions.

*Postage will be added; see above chart. Subscription rates and book prices are subject to change.